

5/16

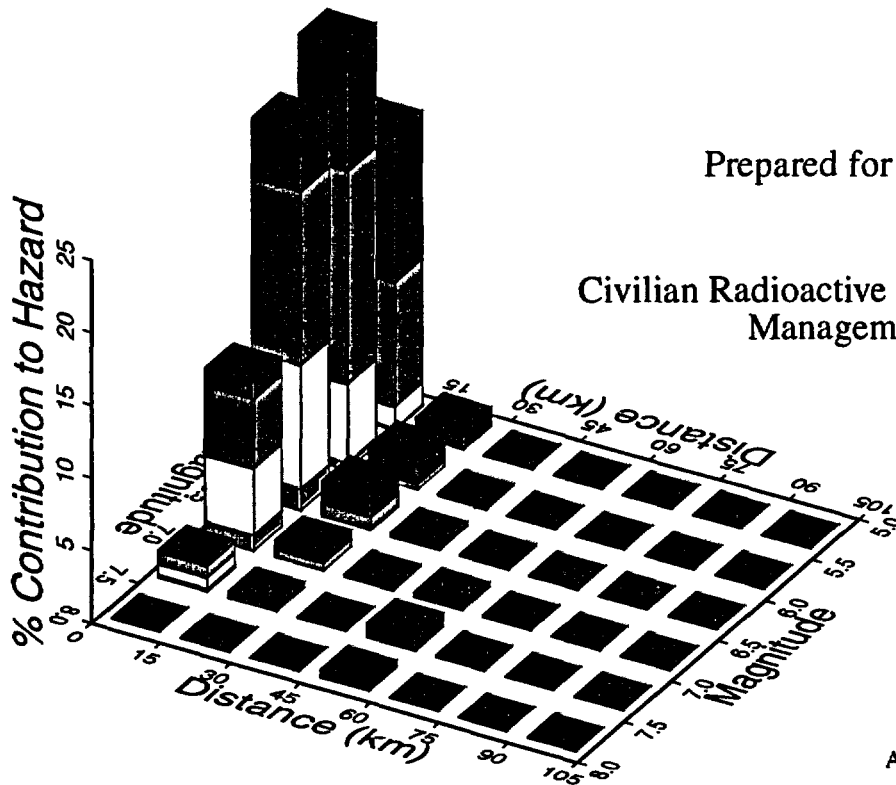
PROBABILISTIC SEISMIC HAZARD ANALYSES FOR FAULT DISPLACEMENT AND VIBRATORY GROUND MOTION AT YUCCA MOUNTAIN, NEVADA

**FINAL REPORT
VOLUME 2
APPENDICES**

Prepared for the U.S. Geological Survey

by the

**Civilian Radioactive Waste Management System
Management & Operating Contractor**



Ivan G. Wong and J. Carl Stepp
Report Coordinators

A report to the U.S. Department of Energy
that fulfills Level 3 Milestone SP32IM3
WBS Number 1.2.3.2.8.3.6

Prepared in cooperation with the U.S. Department of Energy
under Interagency Agreement DE-AI08-92NV 10874
Contract DE-AC04-94AL85000

Oakland, California
23 February 1998

4-1-98

enclosure shelf
FILED IN BINDER V3

DF 03%

9804240209 980223
PDR WASTE
WM-11 PDR

NO LTA ENTRY DOCUMENT

102

WM-11

**PROBABILISTIC SEISMIC HAZARD ANALYSES FOR
FAULT DISPLACEMENT AND VIBRATORY
GROUND MOTION
AT YUCCA MOUNTAIN, NEVADA**

**FINAL REPORT
VOLUME 2 APPENDICES**

Prepared for the

U.S. Geological Survey

by the

**Civilian Radioactive Waste Management System
Management & Operating Contractor**

**Ivan G. Wong and J. Carl Stepp
Report Coordinators**

**A report to the U.S. Department of Energy
that fulfills Level 3 Milestone SP32IM3
WBS Number 1.2.3.2.8.3.6**

**Prepared in cooperation with the
U.S. Department of Energy under
Interagency Agreement DE-AI08-92NV10874
Contract DE-AC04-94AL85000**

**Oakland, California
23 February 1998**

APPENDIX A
BIOGRAPHIES OF EXPERTS

BIOGRAPHIES OF SEISMIC SOURCE AND FAULT DISPLACEMENT EXPERTS

Dr. Jon P. Ake is a seismologist whose recent research interests have been focused primarily on seismic hazard analyses, engineering seismology, and induced seismicity. He received his undergraduate degree in 1979 in geology and physics from Western State College. He then worked at the New Mexico Engineering Research Institute where he conducted research dealing with strong ground motions generated by explosions, the dynamic response of earth media, and the applications of signal analysis techniques to ground shock problems. From 1983 to 1987, Dr. Ake attended graduate school at the New Mexico Institute of Mining and Technology where he received a Ph.D. in geophysics in 1987. His research dealt with the analysis of microearthquake data applied to studies of crustal structure, seismic sources, and near-station effects. From 1987 to 1989 he had responsibility for operating a seismic network focused on assessing seismic hazard in the Colorado Front Range for Denver Water Department facilities. His research involved probabilistic seismic hazard analyses and application of inversion procedures. From 1989 to the present Dr. Ake has been employed by the U.S. Bureau of Reclamation (USBR) as a senior seismologist in the Seismotectonic and Geophysics Group. His duties include seismologic and tectonic fault assessments, estimation of strong ground motions by several techniques, and consultation on engineering geophysics. He has been responsible for review and coordination of seismic hazard and risk analyses and review of contract seismotectonic studies. Additional duties include operation, maintenance, and data analysis from two seismic monitoring networks in western Colorado. Current research involves application of finite source ground motion modeling to engineering analyses, risk-based seismic hazard assessment, and studies of induced seismicity.

Dr. R. Ernest Anderson received his Ph.D. from Washington University, St. Louis in 1962 after which he spent 11 years working on Atomic Energy Commission-sponsored geologic studies (mostly mapping at various scales) in and around the Nevada Test Site (NTS). This NTS background gives him a valuable perspective on a broad range of geologic problems in the Yucca Mountain area. Equally important, he has built on that background to become an expert on the structure and tectonics of the Basin and Range province by his mapping and topical studies in more than 40 mountain ranges throughout the province. For more than 20 years, his studies have dovetailed a broad range of regional and site-specific investigations bearing on seismicity and paleoseismicity including (1) mapping Quaternary fault scarps in

western Utah and developing some of the first quantitative relations of the time dependence of scarp degradation, (2) coordinating U.S. Geological Survey (USGS) paleoseismic studies of the Wasatch fault in Utah, (3) developing an understanding of integrated focal mechanism and fault-slip data in central Utah, (4) evaluating hazards aspects of basaltic volcanism in southern Utah and adjacent Arizona, and (5) advising other agencies such as the USBR and U.S. Soil Conservation Service on seismic hazards aspects of dams in central and southwestern Utah. Dr. Anderson has a strong interest in paleohydrology and has authored papers on the paleohydrology of areas in Clark and Lincoln counties, Nevada, and a paper interpreting the impoundment-related seismicity at Lake Mead in terms of geographic contrasts in hydraulic continuity. His strongest current research interest is in improving understanding of the 3-D aspects of the deformation field in the Basin and Range province and the role of plutonism in shaping that deformation field – two subjects of potentially great importance to understanding the seismotectonics of Yucca Mountain.

Mr. Larry W. Anderson is a geologist with over 17 years of experience in the identification, evaluation, and seismic hazard analysis of active and potentially active faults as applied to engineered facilities. Born in San Francisco, California, Mr. Anderson attended Brigham Young University and the University of Colorado. He received an M.S. degree from the University of Colorado in 1976. From 1977 to 1980, Mr. Anderson was employed by Fugro, Inc., where he worked on geotechnical investigations for major facilities including fault-related studies for several existing or planned nuclear power plants in the western U.S. While at Fugro, he compiled the first Quaternary fault map of the state of Utah. In 1981, Mr. Anderson began work with USBR's Seismotectonic Group. Since that date, Mr. Anderson has personally conducted or been responsible for numerous seismic hazard studies for USBR dams and facilities throughout the western U.S. Many of these studies included detailed fault evaluations such as those for the Ortigalita fault in California, the Pyramid Lake fault zone in Nevada, and the Horseshoe fault in Arizona. Results of these studies have been published in several publications. Since 1992, Mr. Anderson has been the Principal Investigator on the study of "Quaternary Faulting within 100 km of Yucca Mountain, Including the Walker Lane" for the Yucca Mountain Project. The major emphasis for this study has been on evaluating the Quaternary paleoseismic history of the Death Valley-Furnace Creek fault zone and the Bare Mountain fault.

Dr. Walter J. Arabasz graduated summa cum laude from Boston College in 1964 with a B.S. in Geology. He obtained an M.S. and Ph.D. in geology at the California Institute of Technology in 1966 and 1971, respectively (with a minor in geophysics). He was also a Post-Doctoral Research Fellow at the Department of Scientific and Industrial Research in New Zealand (1970-73). He has more than 27 years of experience in conducting research in seismology and tectonics, with current interests focusing on network seismology, earthquake hazard analysis, tectonics and seismicity of the intermountain area, and statistical patterns of earthquake occurrence. He has been the director of the University of Utah Seismograph Stations since 1985 and research professor at the University of Utah since 1983. He is Chair of the Utah Seismic Safety Commission and recently served as Chair of the Council of the National Seismic System (1995-97), as a member of the Board of Directors of the Seismological Society of America (1994-97), and as a member of the National Research Council's Panel on Seismic Hazard Evaluation (1992-96). His experience with regard to Yucca Mountain is extensive, including (1) member of the Peer Review Group for Early Site Suitability Evaluation of the Potential Repository Site at Yucca Mountain (1991), (2) member of the Specialist Panel for the Earthquakes and Tectonics Expert Judgment Elicitation Project (1991-92), and (3) technical reviewer for reports on seismic hazards methodology for Yucca Mountain and on seismic design inputs for the Exploratory Studies Facility (1993-94). He was also a member of the Seismic Hazard Methodology Team for the Electric Power Research Institute's (EPRI) Seismic Hazards Research Program (1984-87).

Dr. Ronald Bruhn received his B.A. in geology from Alaska Methodist University in 1971. He received his Ph.D. in geology from Columbia University in 1976. He is a Professor of Geology in the Department of Geology and Geophysics at the University of Utah, where he has worked since 1976. He teaches courses in physical geology, structural geology, engineering geology, and tectonics. Dr. Bruhn's expertise includes structural geology and tectonics, and the application of structural geology to problems in mining and petroleum geology, and seismic hazards. In earthquake hazards studies, he specializes in the applications of structural geology to infer rupture characteristics, including segmentation of fault zones, fluid flow in fault zones, and earthquake mechanics. He has conducted seismic hazards projects in strike-slip, normal, and reverse faulting regimes in the western U.S., Alaska, Israel, South America, and South Korea. He has extensive experience with both regional and detailed studies of faulting in the Basin and Range province, including the

tectonic evolution of the Mesozoic and Cenozoic Cordillera. He has also completed studies on the seismogenic properties of faults in the Central Nevada Seismic Belt. Currently he is developing new methods to date paleo-earthquakes using cosmogenic isotopes. His research and consulting work is supported by the National Earthquake Hazards Reduction Program, the National Science Foundation (NSF), the Norwegian Petroleum Directorate, the U.S. Department of Energy (DOE), and private firms.

Mr. Craig dePolo received his B.S. degree in geology from California State University, Sacramento and his M.S. degree in geology from University of Nevada, Reno. He is presently a Research Geologist for the Nevada Bureau of Mines and Geology and has been involved with seismic hazard characterization and research for the past 18 years, 12 of which have been studying the Basin and Range province. He has been involved with the seismic hazard characterization of Yucca Mountain, Nevada for the last 9 years. Mr. dePolo has conducted aerial reconnaissance and photographic missions of active faults and historical earthquake ruptures, worked on logging and interpreting trenches, and has, to date, characterized the seismic hazard of several hundred faults. He has worked on fault segmentation theory using historical earthquakes as a data base and a fault slip-rate theory using fault data from Nevada and California. He has mapped out the surface ruptures from the 1932 Cedar Mountain earthquake, and worked on trench studies along these breaks. Recent research has included an analysis of the maximum background earthquake for the Basin and Range province and studies of multiple segment and distributed surface ruptures. He is currently involved in devising and managing an earthquake scenario project in the Reno-Carson City urban corridor. Mr. dePolo is an active participant in the Nevada Earthquake Safety Council, and is the past Chairman and currently serves on the Executive Committee of the Western States Seismic Policy Council.

Dr. Diane Irene Doser obtained her B.S. in applied geophysics from Michigan Technical University. She obtained her M.S. and Ph.D. in geophysics from the University of Utah. She was a Post-Doctoral Fellow at the California Institute of Technology. She has been at the University of Texas at El Paso since 1986 where she now is a professor and the director of the Kidd Memorial Seismic Observatory. Her experience related to seismic sources in the western U.S. is extensive. Both her M.S. and Ph.D. work related to earthquakes of the intermountain west. She has published 16 papers related to source processes of U.S.

intermountain earthquakes, including 4 papers on Nevada earthquakes. She has also published papers on the source processes of earthquakes in other continental rifts (Baikal, east Africa), on southern California-northern Baja California earthquakes, and on papers related to induced seismicity in west Texas oil fields. Additionally, since 1987, Dr. Doser has been Co-Principal Investigator on numerous grants from the Texas Low-Level Radioactive Waste Authority to assess seismic hazards associated with two proposed disposal sites in west Texas, and to operate seismic monitoring networks in these regions.

Dr. Christopher J. Fridrich obtained both his doctorate and masters degrees in geology from Stanford University where he conducted research on the petrology and structure of the Grizzly Peak caldera in Colorado. He also has a bachelor's degree in geological engineering from Michigan Technical University. Dr. Fridrich has extensive mapping experience throughout the western U.S., particularly investigating volcanic deposits. He has been working on the Yucca Mountain project since 1988, including both research, oversight, and coordination duties. He is responsible for geologic mapping of the Crater Flat basin and structural analysis of the map data for the purpose of developing constraints on tectonic models to be used in seismic hazard assessments of the Yucca Mountain site. He is also principal investigator for studies of tectonic effects on the hydrology of Yucca Mountain, which includes hydrogeologic studies, surface and subsurface mapping, and evaluation of several types of geological, geophysical, and hydrologic data. Prior to working on the Yucca Mountain project, Dr. Fridrich was a Research Fellow for the American Museum of Natural History and has several years of experience working in the mineral and oil industries.

Dr. Peter L.K. Knuepfer has worked on paleoseismic and geomorphic studies of active faults in the Basin and Range of the western U.S. throughout his professional career. He received his B.S. in 1976 and his M.A. in 1977 from Stanford University, after which he spent 4 years with Woodward-Clyde Consultants. He was a member of the Woodward-Clyde Consultants team that pioneered trenching of normal faults for paleoseismic analysis along the Wasatch fault in the late 1970s. As a graduate student at the University of Arizona in the early 1980s, he assisted in trenching studies of a low-slip-rate fault, the Santa Rita Piedmont fault, south of Tucson, Arizona, and he worked with Prof. William B. Bull and other students on studies of the 1887 surface rupture and previous breaks along the Pitaycachi fault in northern Sonora, Mexico. He completed his Ph.D. there in 1984. Since joining the faculty of Binghamton

University in 1986, Dr. Knuepfer has studied the paleoseismicity of the Lemhi fault in Idaho with a group of students (jointly with Woodward-Clyde Federal Services and personnel at the Idaho National Engineering Laboratory) and more recently has been a team member and/or reviewer of trenching studies along the southern Lemhi and Lost River faults. This work led to Dr. Knuepfer's inclusion in an expert panel solicitation regarding earthquake hazards at the Idaho National Engineering Laboratory (INEL), under the direction of Lawrence Livermore National Laboratory. Further work in Idaho, in early stages of research, focuses on the temporal relationship and possible strain partitioning between basaltic volcanic eruptions in the Eastern Snake River Plain and faulting on the Lemhi and Lost River faults. Dr. Knuepfer has other extensive experience in active tectonics and paleoseismic studies in California and overseas in Taiwan and New Zealand. Recent research in New Zealand and Taiwan has focused on studies of terraces formed by river incision to deduce rates and styles of uplift during active mountain-building.

Dr. James P. McCalpin is President of GEO-HAZ Consulting, Inc., and is also Research Associate Professor of Geology at Utah State University and Special Graduate Faculty at the University of Colorado, Boulder. He has been performing neotectonic studies since 1976. Dr. McCalpin has developed an international reputation for trenching faults and using numerical dating techniques to reconstruct the magnitude and timing of paleoseismic events. He recently edited the first reference book in paleoseismology ("Paleoseismology," Academic Press, 1996) along with 10 coauthors from government and academia. Between 1982 and 1992, Dr. McCalpin was the Principal Investigator on 10 research grants, funded by the USGS and NSF, to decipher the Quaternary history of faulting on various large normal faults in the western U.S. During these studies, he developed (along with Dr. S.L. Forman) a technique for combined radiocarbon and thermoluminescence dating of fault zone sediments that provides the best dating control yet achieved for many tectonic and climatic settings. His synthesis of the Holocene paleoearthquake history of the Wasatch fault zone, Utah, is the basis for the most up-to-date estimates of future earthquake probability (work with USGS collaborator S.P. Nishenko). More recently he has been an expert reviewer for seismic hazards assessments of two DOE facilities, the Rocky Flats Plant, Colorado, and Los Alamos National Laboratory, New Mexico. His current research involves statistical analysis of paleoseismic data for application to logic trees and probabilistic seismic hazard analyses, particularly with reference to normal faults and the western USA.

Dr. Dennis W. O'Leary has been a research geologist with the USGS since 1972 when he received a Ph.D. in geology from Penn State University. Dr. O'Leary has taken on a wide variety of research tasks in various geologic settings. He has performed bedrock and surficial geologic quadrangle mapping at scale of 1:24,000 in Massachusetts and Connecticut, and conducted remote sensing investigations in the Tonopah, Nevada area, eastern Missouri, the Mississippi embayment, the Paradox Basin in Utah, and eastern Maine, in order to analyze fault and fracture patterns relevant to seismicity, ore mineralization, and bedrock integrity for nuclear waste storage site evaluation. Dr. O'Leary also conducted marine seismic and sidescan sonar surveys (GLORIA) along the U.S. Atlantic coast in order to assess seafloor stability and geological processes within the U.S. Exclusive Economic Zone. Since 1992, Dr. O'Leary has conducted tectonics evaluation studies for the USGS Yucca Mountain Project Branch. Principal tasks include evaluation and formulation of tectonic models for Yucca Mountain and its geologic setting, and characterization of northeast-striking strike-slip faults (chiefly the Rock Valley fault zone). Dr. O'Leary has also consulted on a variety of other tectonic-related problems, including seismic hazards analysis, performance assessment, and history of Neogene and Quaternary faulting in the Yucca Mountain area. His current research specializes in tectonic processes and tectonic effects in the Yucca Mountain region, structural geology of extensional terranes, morphotectonic phenomena, and Neogene and Quaternary tectonostratigraphy.

Mr. Alan R. Ramelli received his B.S. and M.S. degrees in geology from the University of Nevada, Reno. He has held a position as Research Geologist with the Nevada Bureau of Mines and Geology since 1986. He has been involved in research studies of active faulting and paleoseismology in the Basin and Range province and issues related to high-level nuclear waste storage since 1983. From 1983 to 1986, on a consulting basis, Alan conducted active-fault evaluations and reviews of environmental assessments and other documents for the Yucca Mountain, Deaf Smith, Hanford, and Davis Canyon proposed high-level nuclear waste storage sites. From 1986 to 1991, he conducted document reviews and original studies of the Yucca Mountain area, including planning of low-sun-angle aerial photography missions and mapping of faults and Quaternary geology, as part of studies conducted by the State of Nevada. From 1992 to present, under contract to the USGS, he has conducted paleoseismic studies, including exploratory trenching, of the Yucca Mountain area and has held primary

responsibility for studies of the Solitario Canyon fault. Other recent projects involve paleoseismic studies, including exploratory trenching, of the Carson Range fault system in western Nevada and studies of the 1994 Double Spring Flat earthquake.

Dr. Albert M. Rogers is a Director of GeoRisk Associates, Inc., a geological hazards assessment corporation. Dr. Rogers has over 30 years of research experience, scientific publication, and professional project activities in both government and industry that are related to earthquake hazard assessment. He received a Ph.D. in geophysics in 1970 and a B.S. in 1965, both from Saint Louis University. He has conducted research related to earthquake hazard assessment in Nevada, Utah, the west Texas/southern New Mexico region, and the Pacific Northwest. Dr. Rogers was a Senior Scientist at Environmental Research Corporation and Technical Manager at EQE International. In these capacities, he was responsible for ground motion prediction research, site-specific probabilistic seismic hazard assessments of nuclear power plant sites in Finland and Slovakia, and at offshore oil platform sites in Venezuela, Trinidad, Java, and Sumatra. Dr. Rogers has conducted seismicity network studies to assess the seismic hazard to nuclear waste sites at the Waste Isolation Pilot Project in New Mexico, and at the proposed Yucca Mountain site in Nevada; he also led a study of induced seismicity at Lake Mead, Nevada. Dr. Rogers conducted a probabilistic seismic hazard assessment for DOE for the initial proposal for high-level nuclear waste site at NTS, termed the Retrievable Surface Storage Facility. He was an Expert Panel member for the first Tectonics Expert Judgment Elicitation Project for Yucca Mountain in 1991-92. His current research interest concerns earthquake strong motion prediction; this research focuses on prediction of the effect of geologic conditions on earthquake shaking levels, including current studies of vertical strong motion array data in Los Angeles. Dr. Rogers has had collaborative or advisory roles with scientists at the University of Roorkee, India, the Earthquake Engineering Research Institute in Skopje, Macedonia, the University of Costa Rica, and the Engineering Research Institute in Harbin, China. Dr. Rogers served as Branch Chief of the USGS Branch of Geologic Risk Assessment from 1984 to 1988 and during that time was also responsible, as Program Coordinator, for both the internal and external USGS Regional Earthquake Hazards Assessments Programs.

Dr. D. Burton Slemmons has published numerous papers, abstracts, and edited volumes dealing with neotectonics, earthquake hazard evaluation, and paleoseismicity. Dr. Slemmons

received his Ph.D. in geology from the University of California, Berkeley in 1953. While a professor at the University of Nevada-Reno, he supervised more than two dozen theses of graduate students including studies in the Yucca Mountain region, covering Owens, Panamint, Saline, Death, Fish Lake, Amargosa, and Pahrump valleys. He assisted the Lawrence Livermore National Laboratory as a consultant in making high-level nuclear waste assessments of the 11 sites considered by the DOE. From 1985 to 1989, he directed the Yucca Mountain Project of the University of Nevada-Reno. He was one of the seven expert technical specialists selected by Geomatrix Consultants in the EPRI Earthquakes and Tectonics Expert Judgment Elicitation Project for the high-level waste repository at Yucca Mountain. He has consulted for Woodward-Clyde Federal Services in support of TRW from January 1992 to present on the Yucca Mountain Project, including activity as a member of the technical assessment team that prepared the report "Seismic Design Inputs for the Exploratory Studies Facility at Yucca Mountain" in 1994. During the past 25 years, he has also been an expert consultant for the U. S. Nuclear Regulatory Commission (NRC) or industry at more than 12 power plants in the U.S. Since 1984, he has been a technical expert for the International Atomic Energy Agency (IAEA) on missions to assess earthquake hazards at nuclear power plant sites in Armenia, Brazil, Croatia, and Indonesia.

Dr. Kenneth D. Smith obtained his Ph.D. from the University of Nevada in 1991. He holds bachelors degrees in geophysics from Boise State University and in geology from Indiana University. Dr. Smith has been involved in studies of the seismotectonics of the western Basin and Range province for over 10 years. During this time, he has had extensive experience in seismic network operations, portable seismic experiments, and seismic network data management for western Great Basin earthquake activity. Since 1992, these efforts have focused on evaluating the seismicity in and around the Yucca Mountain area. He was a primary author of a study of the source parameters and faulting behavior of the 1992 Little Skull Mountain earthquake and of a study of recent earthquake activity on the Rock Valley fault zone. He participated in the data collection for the Little Skull Mountain earthquake, the 1993 Rock Valley earthquake sequence, and the 1993 Non-Proliferation Experiment refraction survey. Other research activities in the western Basin and Range province have included determining the source parameters and complex faulting geometry of mainshock-aftershock sequences near Mammoth Lakes, California. Currently, he is involved in the

operations and development of the digital upgrade for the southern Great Basin seismic network.

Dr. Robert B. Smith received his B.S. and M.S. in geology from Utah State University in 1960 and 1965, respectively. He received his Ph.D. in geophysics from the University of Utah in 1967. He is a Professor of Geophysics in the Department of Geology and Geophysics where he has worked since 1967. He has also served as a Visiting Professor at the Swiss Federal Institute of Technology and at Cambridge University. Most recently he has taught courses in tectonophysics/elastic waves, earthquake seismology, theoretical seismology, and inverse theory. He has supervised 53 graduate students. Dr. Smith's expertise includes mechanics and processes of earthquakes, the relationship between seismicity and active tectonics, wave propagation, seismicity of the Intermountain seismic belt, Global Positioning satellite measurements of crustal deformation, numerical modeling of fault and volcano processes, and analyses of earthquake hazards. In earthquake hazard, he has specifically worked on geometry and mechanics of normal faulting, scaling relations of surface fault parameters to magnitude, strong ground motion and attenuation of normal faulting earthquakes, and general seismotectonics. He has worked on seismic hazards projects in the Pacific Northwest, the Basin and Range province, and the Intermountain seismic belt. Dr. Smith has been Director and Associate Director of the University of Utah Seismograph Stations and he recently directed studies on the neotectonics of the Teton fault and paleoseismicity of the Intermountain seismic belt. His research and consulting work is supported by the NSF, the USGS National Earthquake Hazards Reduction and the Volcano Hazards programs, the National Park Service, as well as petroleum and mining companies. Smith has served as the President of the Seismology section of the American Geophysical Union, on the NSF Panel on Geophysics, on the NSF Advisory Board in Earth Sciences, on the Advisory Committee of the Southern California Earthquake Center, on the NRC Committee on Seismology, on the Executive Committee of the Seismological Society of America, and was a founding member of Incorporated Research Institutes of Seismology.

Since 1973, **Dr. Frank H. (Bert) Swan** has participated in and directed projects for seismic hazard evaluations for critical facilities, including more than 15 nuclear power plants, and other nuclear-related facilities. He has conducted fault studies in the eastern and western U.S., Alaska, Central and South America, North Africa, the Middle East, Southeast Asia, and

Eastern Europe. From 1978 to 1985, Dr. Swan was the principal investigator for a series of research projects funded by the USGS to investigate recurrence of moderate to-large-magnitude earthquakes associated with past surface faulting along the Wasatch fault zone in Utah and to make a probabilistic assessment of the potential ground motion levels for selected urban areas along the Wasatch Front. From 1987 to 1993, Dr. Swan was Project Manager and principal investigator for a detailed paleoseismic investigation of the Meers fault, Oklahoma for the NRC's Research Division. In 1992, he was a member of IAEA's Geological and Seismic Hazards Safety Review Mission for the Crimea Nuclear Power Plant in the former Soviet Union. In 1993, Dr. Swan provided technical review of a probabilistic seismic hazard analysis of the Krsko Nuclear Power Plant in the Republic of Slovenia. He was principal investigator for studies conducted at NTS in Nevada to assess the potential for surface faulting at the proposed site for the waste-handling facilities where high-level nuclear wastes will be received and packaged prior to their permanent burial in the proposed underground repository beneath Yucca Mountain. From 1990 to 1993, Dr. Swan was a member of the Nuclear Management and Resources Council's Ad Hoc Advisory Committee to review and propose revisions to the NRC guidelines for seismic and geological siting criteria for nuclear power plants. From 1990 to 1994, Dr. Swan was a member of the American Society of Civil Engineers Working Group on Dynamic Analysis and Design Considerations for High Level Nuclear Waste Repositories where he had the primary responsibility for preparing guidelines for investigations to assess the seismic potential of active faults and to assess the potential for fault rupture. Dr. Swan is currently a member of their Subcommittee on Design and Analysis for Seismic Fault Displacements.

Mr. James C. Yount has conducted research in tectonics with the USGS since 1975. He worked on the delineation of the seismotectonic framework of the Puget Sound region, including research on liquefaction phenomena in Seattle area, and identification of youthful faults in offshore regions of Puget Sound from 1975 to 1983. He has been investigating active faulting in the NTS area since 1983. These studies included mapping and trench description of faulting features along the Rock Valley fault system and mapping of youthful faulting features along the Solitario Canyon fault system, the Wahmonie fault, the Mine Mountain fault, and the Cane Spring fault system. Past studies related to neotectonics include investigation of faulting along the Mohawk Valley fault system, northeast California, mapping of ground rupture following the 1979 Imperial Valley earthquake, and mapping of

ground rupture following the 1980 Mammoth earthquake. Mr. Yount obtained his B.S. from the University of Washington in 1968 and his M.S. from the University of Colorado in 1970.

BIOGRAPHIES OF GROUND MOTION EXPERTS

Dr. John G. Anderson is a seismologist and the Associate Director of the Seismological Laboratory at the University of Nevada, Reno. His undergraduate degree was earned in physics from Michigan State University. He received his Ph. D. degree in geophysics from Columbia University in 1976, where he specialized in seismology, and carried out research at the Lamont Doherty Earth Observatory. After earning his degree, Dr. Anderson held positions on the research faculty at the California Institute of Technology, the University of Southern California, and the University of California at San Diego. In 1988, he accepted a position of teaching and research at the University of Nevada. Dr. Anderson's research has included a broad range of studies relating to seismic hazards. He has installed strong motion accelerograph networks in the eastern U. S., in the Los Angeles metropolitan region, and in Guerrero, Mexico. He has carried out a wide variety of analyses of strong motion data: data processing, interpretation of the seismic source, describing and understanding site effects, developing attenuation relations, and preparing complete synthetic seismograms. These studies, combined, have helped to develop an understanding of the dominant effects that control the strong motion seismogram. Dr. Anderson has also been involved in research and applications of probabilistic seismic hazard analysis. One of the critical input parameters to hazard analysis is the seismic activity rate, and Dr. Anderson has studied how this rate can be developed from geological observations. Among other studies, he is currently involved in state-of-the-art studies in ground motion attenuation for the Southern California Earthquake Center. Dr. Anderson has published over 125 research articles and reports describing results of this research. He has some personal experience with the Yucca Mountain project originating from studies of the Little Skull Mountain aftershock sequence and site effects in Midway Valley and the region around the southeastern portion of the NTS. Professional relationships have included membership on two panels for the National Academy of Science (Seismic Risk, and Base Isolation), member and Chair of the Nevada Earthquake Safety Council, and Associate Director and Acting Director of the Seismological Laboratory of the University of Nevada. He has served on advisory panels organized by the USGS and the NSF and the National Earthquake Hazard Reduction Program.

Dr. David M. Boore is a geophysicist with the USGS. He earned his B.S. and M.S. degrees in geophysics from Stanford University and his Ph.D. in geophysics from M.I.T. He is internationally known for his work in developing empirical attenuation relations from strong ground motions. He has acted as an expert consultant to the Lawrence Livermore National Laboratory panels on seismic strong ground motion estimation in the eastern U. S. and on the Senior Seismic Hazard Analysis Committee (SSHAC). Dr. Boore currently also serves as a consultant to the DOE's Tank Seismic Expert Panel and on the Peer Review Panel for the NRC's Ground Motion Guidelines Project. He has chaired and acted as a member of the International Association of Seismology and Physics of the Earth's Interior Commission on Strong Motion Seismology, and is a member of the Panel on Wind and Seismic Effects for the U. S. - Japan Cooperative Program in Natural Resources. Dr. Boore has published over 130 papers, most of which deal with predicting ground motion.

Dr. Kenneth Campbell has professional experience in strong ground motion, seismic hazard evaluation, and engineering seismology, gained in his more than 20 years of research and consulting practice. He obtained his Ph.D. in 1977 in geotechnical and earthquake engineering from the University of California at Los Angeles. Since 1972, he has worked as an earthquake engineering consultant for several engineering firms and has served as a research civil engineer with the National Oceanic and Atmospheric Administration and the USGS. His experience lies in technical management, consulting, and research in the areas of engineering seismology, strong ground motion, seismic hazards evaluation, and geotechnical and lifeline earthquake engineering. He has directed projects throughout the world to develop deterministically and probabilistically defined seismic design and evaluation criteria for the nuclear, oil, utility, and construction industries. He has developed strong ground motion attenuation relationships from empirical data and has evaluated ground motions and seismic hazards for nuclear power plants, nuclear waste repositories, DOE facilities, and other critical facilities. Dr. Campbell has also served as an engineering seismology consultant to the NRC. He has participated on two expert panels for ground motion – for the NRC's seismic hazard estimates of the eastern U. S. and on the SSHAC. Currently, he is a member of the Earth Science Advisory Committee for the Savannah River site and is reviewing ground motion and seismic hazard estimates. He has estimated ground motions and provided testimony for the proposed low-level radioactive waste repository in Hudspeth County, Texas, which is regulated by the NRC. He participated on the seismic hazard

evaluation for the Rocky Flats, Colorado nuclear arsenal performed by Risk Engineering, Inc. Dr. Campbell has also estimated ground motions for the IPEEE at the Palo Verde nuclear power plant in Arizona and at California's San Onofre Nuclear Generating Station and Diablo Canyon Nuclear Power Plant. He testified on his work at San Onofre at a hearing conducted by the Atomic Safety Licensing Board. Using regional strong motion data bases, Dr. Campbell has developed attenuation relationships appropriate for specific regions including Utah in the Basin and Range province and the source region for the 1989 Loma Prieta, California earthquake, among others. He is a recognized expert in this field and has developed near-source relationships for use in specifying seismic design criteria for critical and noncritical facilities. He has published widely on his attenuation studies in various scientific journals and presented his work at professional and technical conferences.

Dr. Arthur F. McGarr, geophysicist, is currently Chief of the Earthquake Geology and Geophysics Section, Earthquake Hazards Team, USGS, Menlo Park, California. His undergraduate degree was earned in physics followed by a M.S. in geophysics from the California Institute of Technology. He received his Ph.D. degree in geology from Columbia University in 1968, having specialized in seismology there. In late 1968, Dr. McGarr accepted the position of Senior Research Officer at the Bernard Price Institute of Geophysics, University of the Witwatersrand, Johannesburg, South Africa. During the next 9 years, he led a team of technical support staff and graduate students in numerous investigations of earthquakes induced by the deep-level gold mining operations of the Witwatersrand. Most of these studies entailed running underground networks of seismic and strain monitoring instrumentation. Broad-band, wide-dynamic range acceleration recorded in boreholes within several hundred meters of the hypocenters of mining-induced earthquakes yielded novel insights about the source processes that give rise to the strong ground motion as well as the response of the nearby mine excavations, at typical depths of 3 kilometers, to these vibrations. In 1978, Dr. McGarr accepted a research position at the USGS in Menlo Park where his primary efforts have included the analysis of strong ground motion in the western U.S., the state of stress in the lithosphere, and further studies of induced and triggered earthquakes. In 1990, for example, he determined the design seismic ground motion for the Sudbury Neutrino Observatory, Ontario, Canada, due to nearby mining-induced earthquakes. Of particular interest here, Dr. McGarr demonstrated how the state of crustal stress and focal depth influence ground motion parameters. In this latter study, a result of key interest for the

Yucca Mountain project is the finding that earthquakes in extensional tectonic regimes yield lower levels of ground motion than their counterparts in compressional regimes, for similar recording circumstances. Dr. McGarr's personal experience with the Yucca Mountain project includes participation in the study that led to the development of the ground motion attenuation model SEA 96 for earthquakes in extensional tectonic regimes, one of the empirical proponent models utilized by the Expert Panel.

Dr. Walter J. Silva is President and Senior Seismologist at Pacific Engineering and Analysis. He holds a B.A. degree in geophysics, an M.A. in geophysics, and a Ph.D. in geophysics all from the University of California, Berkeley. He has over 20 years of experience in seismology with particular emphasis on strong ground motion estimation using both numerical modeling and empirical approaches. He has developed and thoroughly validated a numerical modeling methodology that accurately models strong ground motions at any distance (0-500 km) from small or large magnitude earthquakes. In addition to source modeling, Dr. Silva also specializes in quantifying the effects of site conditions on strong ground motions using empirical and 1- and 2-dimensional modeling techniques. In this context, he has evaluated a number of nonlinear approaches as well as the widely used equivalent-linear methodology in applications to recorded motions. To augment his finite fault modeling to accommodate nonlinear site response in an accurate and computationally attractive manner, he developed and validated a frequency domain random vibration theory equivalent-linear formulation. Dr. Silva has provided ground motion evaluations on a number of both large and small projects on a worldwide basis. He has provided site response predictions for over 30 nuclear power plants and numerous small projects. He has applied strong motion modeling techniques at four DOE facilities and at the Exploratory Studies Facility for the proposed high-level nuclear repository at Yucca Mountain, Nevada. Similar projects include numerous USBR dams. He has developed region-specific attenuation relations for eastern and central North America, Colorado, Idaho, New Mexico, and Spain using the stochastic ground motion model. He has been a state-of-the-art speaker on site effects and continues to do applied research on source modeling and site effects for such agencies as National Earthquake Hazards Reduction Program and DOE.

Dr. Paul G. Somerville received his doctoral degree in geophysics from the University of British Columbia in 1976. He spent 2 years as a Visiting Research Fellow at the Earthquake

Research Institute, Tokyo University, during 1977 and 1978, and since then has participated in post-earthquake reconnaissance activities in Japan, most recently in the 1996 Kobe earthquake. He has 18 years of experience as an engineering seismologist with Woodward-Clyde and is manager of the Pasadena office. He is a member of the National Research Council's Seismology Committee and is a member of the Earthquake Engineering Research Institute and an affiliate member of the Structural Engineers Association of California. Dr. Somerville has participated in earthquake hazard evaluations for a large number and variety of engineering projects in many parts of the world. During the past 10 years, he has developed and applied seismological methods for estimating ground motions for the seismic design of engineered structures, including the use of strong motion simulation procedures to generate realistic ground motion time histories close to large earthquakes, which include near-fault effects such as those due to rupture directivity. These procedures have been used to simulate ground motion time histories for structures such as the California Department of Transportation bridges in Northern and Southern California, and the Metropolitan Water District's Domenigoni Valley Reservoir in Southern California. Dr. Somerville is currently participating with the FEMA/SAC Steel Project by providing ground motion time histories to represent the ground motions experienced by steel moment frame buildings during the Northridge earthquake as well as other possible events. Multiyear projects that Dr. Somerville has directed include a program of numerical ground motion studies for the Long Term Seismic Program for PG&E's Diablo Canyon Power Plant, evaluation of earthquake source and ground motion characteristics in eastern North America for EPRI and NRC, estimation of strong ground motions in the Pacific Northwest from large subduction earthquakes on the Cascadia subduction zone for the USGS, analysis of the characteristics of near-fault ground motions for the USGS, and analysis of the ground motion characteristics of the 1989 Loma Prieta and 1994 Northridge earthquakes for the NSF.

Dr. Marianne C. Walck has been evaluating local-to-near-regional recordings of NTS underground nuclear explosions (UNEs) since 1984. She obtained her A.B. degree in geology-physics from Hope College, Michigan, and both an M.S. and Ph.D. in geophysics from California Institute of Technology, Pasadena, California. Currently the Manager of the Geophysics Department at Sandia National Laboratories, Dr. Walck is a seismologist whose career has focused on seismic array analysis of the structure of the upper mantle. She has used seismic array data to model attenuation parameters and acceleration anomalies using ray

tracing and synthetic seismograms. She has sited acceleration stations on Jackass Flats, analyzed the resulting data for travel times and relative amplitude patterns, and modeled the shallow crustal structure at NTS using both 2-D ray tracing and finite difference synthetic seismogram techniques. Her involvement with the Yucca Mountain project began in 1988 with a study of 2-D crustal structure for three paths at NTS between nuclear testing areas and Yucca Mountain. Using UNE source, she successfully reproduced absolute travel time, relative amplitude, and waveshape data for the three paths, documenting significant crustal structure differences at shallow depths near Yucca Mountain. She has recently been employing propagator matrix techniques to model the very shallow structure at Yucca Mountain using UNE records from four borehole/surface pairs in order to develop a predictive capability at depth near the site of the potential repository. She has also conducted and published research using recordings of nuclear explosion sources at teleseismic and regional distances. The latter used NTS explosions recorded at high-frequency stations in Nevada and California; the former used Soviet Explosions recorded at NORESS to deduce path attenuation. She has published her work on spectral estimates of P-wave attenuation (teleseismic recordings), path attenuation (northern Europe, regional recordings), and attenuation of Asian explosions (teleseismic recordings) in refereed journals and conference proceedings.

APPENDIX C

**SUMMARIES OF
SEISMIC SOURCE AND FAULT DISPLACEMENT
CHARACTERIZATION WORKSHOPS**

SUMMARIES OF SSFDC WORKSHOPS

Summary of Data Needs Workshop	C-1
Summary of Hazard Methodologies Workshop	C-19
Summary of Field Trip and Workshop on Alternative Models and Interpretations	C-35
Summary of Preliminary Interpretations Workshop	C-51
Summary of Feedback Workshop	C-67
Summary of Fault Displacement Workshop	C-83

Note: Workshop summaries were prepared after each workshop and then distributed to workshop participants. See the project files for all figures and attachments referred to in these summaries, including agendas and copies of information distributed to workshop participants both during and after the workshops.

WBS: 1.2.3.2.8.3.6
QA: L

**Civilian Radioactive Waste Management System
Management & Operating Contractor**

**Summary of Data Needs Workshop on Seismic
Source Characterization at Yucca Mountain**

SSC Workshop 1

**Salt Lake City, UT
April 17-19, 1995**

May 25, 1995

Prepared for:

**U.S. Geological Survey
Box 25046, MS-425
Denver Federal Center
Denver, CO 80225**

Prepared by:

**Woodward-Clyde Federal Services of
Civilian Radioactive Waste Management System
Management & Operating Contractor
101 Convention Center Drive
Suite P-110
Las Vegas, NV 89109**

MONDAY, APRIL 17, 1995

A welcome and introductory presentations were given by: 1) the Project Representative for DOE, Tim Sullivan; 2) the Project Director, J. Carl Stepp of Woodward-Clyde Federal Services; and 3) the Team Leader of the Seismic Source Characterization and Fault Displacement Facilitation Team (SSC-FT), Kevin J. Coppersmith of Geomatrix Consultants. Table 1 shows the list of workshop attendees.

Because the DOE has the responsibility of evaluating Yucca Mountain as a potential repository site for the permanent disposal of spent nuclear fuel and high-level radioactive waste, Mr. Sullivan provided an overview of the overall Yucca Mountain Project. His overview included a brief description of proposed facilities and background on the DOE's program approach and general objectives for the PSHA. He emphasized that although the DOE's position was that the database was adequate to begin assessment, data would continue to be gathered, and that this PSHA will provide seismic design parameters for the preclosure period (100 years). The project will also provide seismic hazard estimates that have potential application in evaluating the performance of the repository system during the postclosure period. Dr. Stepp more specifically defined PSHA project objectives and outlined the project plan, including the basic approach, organization, and schedule for the project.

Dr. Coppersmith introduced members of the Expert Panel and SSC-FT, further explained their roles and responsibilities, and specified the guidelines used for selecting experts. He defined ground rules for experts and emphasized their role as informed "evaluators" of various interpretations, rather than "proponents" of a single model, in an intensely interactive but nonhostile process whereby a common understanding of the issues and available data is achieved. He also discussed forthcoming workshops and the project deliverables, including milestones and the final report. Four workshops are scheduled through January 1996, followed by the elicitation process through March, a workshop to provide feedback, final assessments by experts in June, and a final report delivered in September 1996. In addition to the workshops, two field trips were tentatively planned for November.

Dr. Coppersmith also provided background on multiple-expert probabilistic hazard assessments, including an ongoing study of volcanic hazards at Yucca Mountain. He highlighted important aspects of this PSHA, such as: 1) results of the source characterization component of the project will be used to evaluate the probabilities of exceeding both certain levels of vibratory ground motions and certain amounts of fault displacement through the proposed repository; 2) ground motions will be used for design purposes and fault displacements will be used for performance assessment; 3) this project is a hazard rather than risk analysis, although results could become an integral part of a risk analysis; 4) resulting probability distributions should incorporate various types of uncertainties (including expert-to-expert diversity of interpretation, modeling uncertainties, parameter uncertainties, aleatory and epistemic uncertainties); 5) probabilistic treatment should allow for full consideration of

TUESDAY, APRIL 18, 1995

Frank (Bert) H. Swan of Geomatrix Consultants started the morning session with a presentation on technical issues significant to characterizing fault sources at Yucca Mountain. He covered basic concepts and provided insights into both general and site-specific issues for Yucca Mountain, particularly in regard to distributive and secondary faulting that is important to characterizing fault displacements. He also highlighted caveats in using the present geologic database, such as likely subsurface differences and complexities in geometry, absence of Quaternary cover, the incomplete paleoseismic record, and differences between average net slip and observed displacements.

Next, one of the Deputy Directors of the project, Ivan G. Wong of Woodward-Clyde Federal Services, presented technical issues found to be most significant during the preliminary PSHA done for the Exploratory Studies Facility (ESF) at Yucca Mountain. For their preliminary study of vibratory ground motions only and not fault displacement, they considered 24 faults and one background seismic source zone. They found that the background source was the most significant contributor to seismic hazard at the ESF for return periods up to 100,000 years. This finding underscores the importance of how the earthquake catalog is processed and analyzed for use in characterizing background sources at Yucca Mountain. They also found that three local faults, the Paintbrush Canyon, Solitario Canyon, and Fatigue Wash faults, became significant contributors to the peak acceleration hazard at return periods greater than 20,000 years. When asked whether this project should just focus on local faults, Mr. Wong emphasized the limitations of his study, which was not comprehensive and used simple tectonic and fault segmentation models. He cautioned the experts to use the preliminary findings from the ESF study only as guidelines for prioritizing time spent on characterizing sources.

The morning session concluded with a discussion of the significant technical issues highlighted by Drs. Arabasz, Swan, and Mr. Wong, which are shown in Table 2. Also shown in Table 2 are the data identified by project participants as being particularly important to addressing each issue. Dr. Coppersmith facilitated the discussion and Dr. Arabasz served as scribe. Many members of the Expert Panel, Oversight Panel and Project Management Team actively contributed to the discussion.

Mary-Margaret Coates of the USGS began the afternoon session with a brief explanation of the introductory data package sent out to experts prior to the workshop (Table 3) and the data that are scheduled to be forthcoming from the USGS during this, and the next, fiscal years. She described the role of the Data Management Team as a resource to the experts with the objective of providing a consistent database to all experts in a timely fashion that is as comprehensive and up-to-date as reasonably possible. In regard to timeliness, many experts expressed an interest in electronic access to digital data files, such as placing earthquake

series data), and some trenching. The day concluded with the opportunity for questions and comments from observers.

WEDNESDAY, APRIL 19, 1995

The Project Chief, John W. Whitney of the USGS, opened the last day of the workshop with a presentation on available data for local Quaternary faults at Yucca Mountain. He summarized data on geometry, kinematics, and paleoseismic behavior for the seven to eight faults closest to the proposed repository block. He focused on mapping and trenching data and emphasized the closely-spaced, complex trace geometry and the long, but incomplete, paleoseismic record preserved for most of the faults. He also identified data that are scheduled to be available this and next fiscal year, including cooperative studies with the State of Nevada being conducted by Alan R. Ramelli of NBMG and Dr. Brune of UNR.

James B. Paces of the USGS gave the next presentation on available and forthcoming geochronological data for Yucca Mountain. He gave an overview of the multiple-purpose, extensive scope, general problems, and integrated approach for the geochronology program at Yucca Mountain. Although a variety of methods have been applied, including cosmogenic, radiocarbon, tephrochronology, U-series, and thermoluminescence, the effort has been most concentrated toward applying the latter two methods. Dr. Paces then identified new developments in U-series dating that are expanding application opportunities at Yucca Mountain. He also identified extensive problems with U-trend methods such that U-trend ages are no longer deemed reliable by most geochronologists. Finally, he stated that the USGS plans to have a trench-by-trench summary of geochronology data for Yucca Mountain that will be available to the Expert Panel by this autumn.

Christopher J. Potter of the USGS summarized available and forthcoming data from structural geology studies of the proposed repository block. He summarized previous and ongoing work involving geologic mapping, paleomagnetic studies, borehole investigations, fracture studies and 3-D modeling. Fracture studies include 2-D and 3-D mapping of surface fracture networks in cleared pavements, outcrop studies of general orientations and crosscutting relations, and stratigraphic studies of vertical continuity of fractures. Many experts expressed an interest in obtaining map data of the ESF and the ongoing 3-D modeling study, which integrates stratigraphic and structural data and uses a surface handling method. Dr. Potter also highlighted some of the issues surrounding the Sundance fault and ongoing studies to address these issues.

Victoria E. Langenheim of the USGS gave the final presentation on available and forthcoming geophysical databases for Yucca Mountain. She specified available data from numerous potential field, seismic, electrical, borehole, heat flow, geodetic, and hydrofracture studies. Potential field studies included gravity and magnetic data, and seismic studies

TABLE 1
SEISMIC SOURCE CHARACTERIZATION AND
FAULT DISPLACEMENT WORKSHOP

17-19 APRIL 1995
Attendance List

Name	Affiliation
Norm Abrahamson	Consultant
Jon Ake	U.S. Bureau of Reclamation
Ernie Anderson	U.S. Geological Survey
Larry Anderson	U.S. Bureau of Reclamation
Walter Arabasz	University of Utah
Ann Becker	Woodward-Clyde Federal Services
John Bell	University of Nevada at Reno
Ron Bruhn	University of Utah
Jim Brune	University of Nevada at Reno
Bob Budnitz	Future Resources Associates Inc.
Tom Chaney	U.S. Geological Survey
Mary-Margaret Coates	U.S. Geological Survey
Kevin Coppersmith	Geomatrix Consultants
Allin Cornell	Consultant
Tony Crone	U.S. Geological Survey
Craig dePolo	University of Nevada at Reno
Diane Doser	University of Texas at El Paso
Chris Fridrich	U.S. Geological Survey
Tom Hanks	U.S. Geological Survey
Robert Harpster	SAIC
Bakr Ibrahim	U.S. Nuclear Regulatory Commission
Dick Keefer	U.S. Geological Survey
Jerry King	SAIC
Vicky Langenheim	U.S. Geological Survey
Martha Mustard	U.S. Geological Survey
Jim McCalpin	GEO-HAZ Consulting
Steve McDuffie	U.S. Nuclear Regulatory Commission
Robin McGuire	Risk Engineering

TABLE 2
**SIGNIFICANT TECHNICAL ISSUES AND ASSOCIATED DATA NEEDS FOR
CHARACTERIZING SEISMIC SOURCES IN THE YUCCA MOUNTAIN REGION**

Note: This list of issues was not intended to be exhaustive. Rather, it was developed to focus discussion and thought on the types of data that could be used to address several key SSC issues.

Issue 1. What are the candidate seismic sources for the background earthquake and what is the relative importance of volcanic earthquakes.

Data Needed:

- Spatial and temporal relation of volcanic-related events and background seismicity
- Suzette Jackson's compilation of volcanic-related seismicity (analog information)
- Heat flow data
- Comparison of the temporal and spatial patterns of paleoseismic events and volcanic-related events
- Stress field and relation to volcanic features, such as dike injection
- Recurrence information on volcanism near Yucca Mountain

Issue 2. What is size of maximum background earthquake?

Data Needed:

- Compilation by Craig dePolo of minimum magnitudes for surface-faulting earthquakes
- Other evidence of deformation besides surface faulting
- Stability of rupture dimensions with magnitude
- Maximum magnitude of non-surface-faulting earthquakes in other extensional tectonic environments (analog information)

Issue 6. Characterizing fault geometry and kinematics.

Data Needed:

- Mapping
- Subsurface data including drill hole, seismic reflection and refraction, and gravity
- Cross-sections
- Focal mechanisms, focal depths, and aftershock patterns
- Kinematic indicators (distinguish those in bedrock from those in Quaternary deposits)
- Aftershocks of normal-faulting earthquakes worldwide (analog information)

Issue 7. Characterizing distributive faulting.

Data Needed:

- Literature on hangingwall versus footwall deformation
- Analogs of normal-faulting earthquakes and their aftershocks and focal mechanisms
- Historical faulting in the Basin and Range Province
- Mapping of tunnel for superconducting supercollider in Texas
- Oil industry data on normal faults in subsurface
- Geoff King's 3-D boundary element model of Yucca Mountain
- Ron Bruhn's preprint on splay faulting and evolution of normal faults
- Mining industry data to calibrate models

Issue 8. Non-stationary and possible temporal clustering of large earthquakes

Data Needed:

(Data Needs added by SSC-FT after workshop)

TABLE 3

CONTENTS OF THIS PACKAGE

**BACKGROUND INFORMATION ON YUCCA MOUNTAIN
SEISMIC SOURCES AND FAULT DISPLACEMENT**

FIRST MAILING TO EXPERTS / APRIL 7, 1995

Cover letter from John Whitney and Mary-Margaret Coates

Preliminary table of contents: Tectonic characterization studies of Yucca Mountain, Nevada--A potential geologic repository for high-level nuclear waste, U.S. Geological Survey Circular (based on talks presented at a workshop in January 1994)

Summaries, reports, bibliographies, and other material as listed below, by topic. Note that the enclosed U.S. Geological Survey Bulletin 1790 contains several referenced papers.

Faults and Seismic Sources

Summary: Faults and seismic sources

Bibliographies: Detachment faulting
Faulting at Yucca Mountain
Quaternary faulting
Surface faulting

Carr, M.D., and Yount, J.C., eds., 1988, Geologic and hydrologic investigations of a potential nuclear waste disposal site at Yucca Mountain, southern Nevada, U.S. Geological Survey Bulletin 1790, 152 p.

Menges, C.M., Wesling, J.R., Whitney, J.W., Swan, F.H., Coe, J.A., Thomas, A.P., and Oswald, J.A., 1994, Preliminary results of paleoseismic investigations of Quaternary faults on eastern Yucca Mountain, Nye County, Nevada, International Conference, High-Level Radioactive Waste Management, 5th, Proceedings, v. 4, p. 2373-2390.

Pezzopane, S.K., Menges C.M., and Whitney, J.W., 1994, Quaternary paleoseismology and Neogene tectonics at Yucca Mountain, Nevada: U.S. Geological Survey Open-File Report 94-568, p 149-151.

Piety, L.A., (in press), Appendices 2, 3, 4, and 5 of Compilation of known and suspected Quaternary faults within 100 km of Yucca Mountain: U.S. Geological Survey Open-File Report 94-112, text to accompany map, 331 p.

Geophysical Data

Summary: Geophysical data

Bibliographies: Gravity
Magnetic
Seismic reflection and refraction

Carr, M.D., and Yount, J.C., eds., 1988, Geologic and hydrologic investigations of a potential nuclear waste disposal site at Yucca Mountain, southern Nevada, U.S. Geological Survey Bulletin 1790, p. 3-21. Several articles.

Hildenbrand, T.G., Rogers, A.M., Oliver, H.W., Harmsen, S.C., Nakata, J.K., Aitken, D.S., Harris, R.N., and Carr, M.D., Regional geologic and geophysical maps of the southern Great Basin, *in* Carr, M.D., and Yount, J.C., eds., 1988, Geologic and hydrologic investigations of a potential nuclear waste disposal site at Yucca Mountain, southern Nevada, U.S. Geological Survey Bulletin 1790, p. 3-21.

Oliver, H.W., Ponce, D.A., and Hunter, W.C., (in press), Major results of geophysical investigations at Yucca Mountain and vicinity, southern Nevada: U.S. Geological Survey Open-File Report 95-74, 235 p.

Heat Flow

Summary: Heat flow

Bibliography: Heat flow

Sass, J.H., Dudley, W.W., Jr., and Lachenbruch, A.H., (in press), Regional thermal setting, *in* Oliver, H.W., Ponce, D.A., and Hunter, W.C., eds, Major results of regional geophysical investigations of Yucca Mountain and vicinity, Nevada: U.S. Geological Survey Open-File Report 95-74, 235 p.

Seismicity

Summary: Historical and current seismicity

Bibliography: Seismicity

Harmsen, S.C., 1994, The Little Skull Mountain, Nevada, earthquake of 29 June 1992--Aftershock focal mechanisms and tectonic stress field implications, Bulletin Seismological Society America, v. 84, p. 1484-1505

Rogers, A.M., and Harmsen, S.C., 1991, The seismicity of Nevada and some adjacent parts of the Great Basin, *in* The Geology of North America, Decade Map Volume 1, p 153-184

**Civilian Radioactive Waste Management System
Management & Operating Contractor**

**Summary of Seismic Source Characterization
Hazard Methodologies Workshop**

SSC Workshop 2

**Salt Lake City, UT
October 16-18, 1996**

Prepared for:

**U.S. Geological Survey
Box 25046, MS-425
Denver Federal Center
Denver, CO 80225**

Prepared by:

**Woodward-Clyde Federal Services of the
Civilian Radioactive Waste Management System
Management & Operating Contractor
101 Convention Center Drive
Suite P-110
Las Vegas, NV 89109**

November 11, 1996

displacement hazard analysis. SSC is then divided into three components: seismic source location and geometry, maximum earthquake magnitude, and earthquake recurrence assessment. Each of these topics is first introduced by overview presentations that focus on the *methods and approaches* that are available to characterize them. These talks are then followed by a series of talks that describe the available *data bases and data interpretations* that relate to these topics. Although the presentations will undoubtedly entail some interpretations, the next workshop (Workshop #3 Alternative Models and Interpretations) will provide a forum for debating alternative interpretations of the available data.

WEDNESDAY, OCTOBER 16, 1996

Introductory presentations were given by: 1) the Project Representative for DOE, Tim Sullivan; 2) the Project Director, J. Carl Stepp; and, 3) the Team Leader of the SSFD Facilitation Team, Kevin J. Coppersmith. Table 2 shows the list of workshop attendees and their affiliations.

Mr. Sullivan provided an update and overview of developments in the Yucca Mountain program since April 1995. He emphasized that the objectives for the PSHA to provide seismic design parameters for the 1998 Viability Assessment remained the same, and that the viability assessment is a interim step to site recommendation in 2001. He also pointed out that the DOE Topical Report "Methodology to Assess Fault Displacement and Vibratory Ground Motion Hazards at Yucca Mountain" has been accepted by the U.S. Nuclear Regulatory Commission (NRC) pending review of the final results of the PSHA.

Dr. Stepp reviewed changes in the PSHA schedule and project plan. The plan remains mainly the same with one difference being in the change of the Oversight Panel to a Peer Review Panel. This panel will consist of four members, reviewing different project areas according to expertise, and the process will be structured as a participatory peer review.

Dr. Coppersmith outlined the goals and approach of the workshop. He also discussed ground rules for the workshops, roles of project participants, major milestones and key aspects for the SSC component of the project, guidelines used in selecting experts, ground rules for experts and expert teams, and the goal of having a defensible basis for combining team assessments into the final analysis with equal weights. With the aid of hats as props, he emphasized that although the experts are encouraged to play the role of proponent occasionally during the process, their overall role and the role they must ultimately play when they develop their assessment is that of an evaluator.

that were used to help constrain interpretations of the seismic lines. These interpretations suggest a series of east-dipping faults buried in Crater Flat, west of Yucca Mountain and a series of west-dipping faults that are chiefly east of and include the Solitario Canyon fault. All of those faults show relatively minor total offsets and are in the hanging wall of the larger Bare Mountain fault. Beds in the hanging wall overall step down to the west, forming a slight rollover and suggesting a listric geometry for the Bare Mountain fault. However, the Bare Mountain fault appears planar to 6-7 km depth and dips roughly 65° to the east in the seismic lines. Dr. Brocher also emphasized the large uncertainties in the data and models.

Dr. Kenneth Smith presented results from recent studies of seismicity in the vicinity of Yucca Mountain, focusing on location, depth, focal mechanisms, and spatial distributions of sequences. He discussed the 1992 Little Skull Mountain earthquake sequence, the 1993 Rock Valley earthquake sequence, and other small events in the region including the 1995 M 4.2 Timber Mountain earthquake and a sequence of small events south of Lathrop cones. He also discussed 15 very small earthquakes ($M < 1$) detected by the new network at Yucca Mountain that occurred since May 1995, and moment-magnitude scaling relations for the region.

Dr. Coppersmith then wrapped-up the day by asking for questions and comments from observers. Dr. Clarence Allen commented on the increased importance of the PSHA and the SCC due to changes in canister design and emplacement. Dr. Phil Justus presented a list of issues including points of clarification, and themes that needed further consideration, and important aspects of the SCC from the NRC's perspective.

THURSDAY, OCTOBER 17, 1996

Topics on SSC for evaluating ground motions continued to be the focus for Thursday's presentations. Dr. Coppersmith started the day with a presentation on methods for assessing maximum magnitudes, focusing on using fault rupture dimensions to estimate maximum magnitude. He pointed out some of the common pitfalls in determining maximum magnitudes and introduced methods for incorporating uncertainties using logic trees and continuous distributions.

Dr. Silvio Pezzopane gave the next presentation on data (fault length and displacement per event) for determining maximum magnitudes on Yucca Mountain faults. This included using paleoseismic data to assess fault segmentation and fault interdependence so that rupture scenarios could be developed. Surface-faulting earthquake parameters for these rupture

After the break, Dr. Thomas Channey distributed copies of the Quality Management Procedure for scientific expert elicitation (YMP-USGS-QMP-3.16, RO) to each of the experts, and Facilitation and Management Team members

Following Dr. Stamatakos, Dr. Pezzopane discussed results from geodetic studies conducted by the U.S. Geological Survey. He emphasized the questionable data quality of the earlier leveling surveys, particularly the 1907 survey. He pointed out that in contrast to the CNWRA's results, Savage et al. (1994 JGR) found no detectable deformation above the error limits of the network except for a negative elevation change (≈ 2 cm at the surface) associated with the 1992 Little Skull Mountain earthquake.

Mr. Ivan Wong presented results on development of the historical earthquake catalogue for the Yucca Mountain PSHA. He discussed the data sources and statistics of the catalogue and highlighted significant issues related to its use. Dr. Pezzopane then gave a short unscheduled presentation on his analysis of relevant fault sources for Yucca Mountain that is summarized in Chapter 11 of the seismotectonic synthesis report, and follows guidance given by NRC in their report NUREG-1451. Mr. Wong also provided input on faults found to be most significant during their preliminary PSHA for the ESF.

Dr. Coppersmith then announced the SSC teams. Teams were selected by a random process that would ensure that each team contains a seismologist, a regional geologist, and a local geologist/paleoseismologist.

Dr. Coppersmith then closed the day with statements from observers. Dr. Allen commented on the change of the location and shape of the proposed repository block (it now lies entirely west of the ESF and the Ghost Dance fault). Dr. Jerry King commented on his role as providing regulatory oversight to ensure that the needs of the NRC are met. He discussed seismic design parameters of interest from his perspective, including dual design basis earthquakes (with return periods of 1,000 and 10,000 years) and periods of interest (up to 1 second) for the types of facilities being designed. Leon Reiter asked a question regarding the time frame in considering maximum magnitudes and Dr. Coppersmith clarified that these are independent of time with respect to the current tectonic regime. Dr. Stamatakos commented that the CNWRA's report on Type I faults will be available soon.

FRIDAY, OCTOBER 18, 1996

Dr. Robert Youngs gave the first presentation on SSC for fault displacement analysis. He discussed methods for assessing the fault displacement hazard, pointing out differences with assessments for ground motions and differences between fault hazard analysis for design

characterize secondary displacement by analyzing along-strike and across-strike fault displacement distributions. He described the data set, including its uncertainties and limitations. He discussed large variations in the shape of along-strike slip distributions, variations in the width of surface ruptures, the relation between lengths of primary and secondary components of surface-rupturing events, the relation between displacements on primary and secondary faults, and the relation between secondary rupture lengths and secondary displacements.

Dr. Coppersmith wrapped up the workshop by discussing plans for the next workshop and field trip. He then opened up the meeting to comments from observers. Dr. Allen commented on the observations of fracturing in the ESF opening up more issues. Dr. Daniel Soeder clarified the status of availability for certain data sets. Dr. Reiter commented on the difficulty of characterizing fault displacement without a more specific minimum threshold, and he encouraged design engineers to give as much guidance as possible to the SSC experts to help focus their efforts. The workshop was adjourned at about 3:00 pm.

TABLE 1 (Cont.)
BIBLIOGRAPHY OF MATERIAL DISTRIBUTED AT
HAZARD METHODOLOGIES WORKSHOP
(SSC WORKSHOP #2)

- Day, W.C., Potter, C.J., Sweetkind, D.S., and Dickerson, R.P., 1996, Detailed bedrock geologic map of the central block area, Yucca Mountain - implications for structural development of the potential high-level radioactive waste repository area in Nye county, Nevada: Geological Society of America Abstracts with Program, v. 28, no. 7, p. A-248.
- Day, W.C., Potter, C.J., Sweetkind, D.S., Dickerson, R.P., and San Juan, C.A., 1996, Bedrock geologic map of the central block area, Yucca Mountain, Nye County, Nevada: U.S. Geological Survey Administrative Report, prepared in cooperation with the Nevada Operations Office, U.S. Department of Energy.
- Dickerson, R.P., and Drake, R.M., 1995, Source of the rhyolite of Comb Peak, southwest Nevada Volcanic Field, Geological Society of America Abstracts with Program.
- Dickerson, R.P., 1996, Geologic and geophysical evidence for normal faulting in Yucca Wash, Yucca Mountain, Nevada: unpublished abstract.
- Ferrill, D.A., Stamatakos, J.A., Jones, S.M., Rahe, B., McKague, H.L., Martin, R.H., and Morris, A.P., 1996, Quaternary slip history of the Bare Mountain fault (Nevada) from the morphology and distribution of alluvial fan deposits: *Geology*, v. 24, no. 6, pages 559-562 (abstract only).
- Ferrill, D.A., Sims, J., Stamatakos, J.A., and Rahe, B., 1996, Role of ductile detachment horizon in the development of pull-apart basins in physical analog models: American Geophysical Union Abstracts with Programs, Fall 1996, in press.
- Ferrill, D.A., and Stamatakos, J.A., 1996, Structural controls on progressive deformation of the Yucca Mountain (Nevada) region: American Geophysical Union Abstracts with Programs, Fall 1996, in press.
- *Ferrill, D.A., Stirewalt, G.L., Henderson, D.B., Stamatakos, J.A., Morris, A.P., Spivey, K.H.C., and Wernicke, B.P.C., 1996, Faulting in the Yucca Mountain region: Critical review and analyses of tectonic data from the central Basin and Range: Center for Nuclear Waste Regulatory Analyses NUREG/CR-6401, or CNWRA 96-007, Rev.01.
- Morris, A., Ferrill, D.A., and Henderson, D.B., 1996, Slip-tendency analysis and fault reactivation: *Geology*, v. 24, no. 3, p. 275-278 (abstract only).

TABLE 1 (Cont.)
BIBLIOGRAPHY OF MATERIAL DISTRIBUTED AT
HAZARD METHODOLOGIES WORKSHOP
(SSC WORKSHOP #2)

Sweetkind, D.S., Potter, C.J., and Verbeek, E.R., 1996, Interaction between faults and the fracture network at Yucca Mountain, Nevada: EOS, v. 77, no. 17, p. S266.

*U.S. Geological Survey 1996, Seismotectonic framework and characterization of faulting at Yucca Mountain, Nevada: United States Geological Survey administrative report to the U.S. Department of Energy that fulfills Level 3 Milestone 3GSH100M WBS Number 1.2.3.2.8.3.6, variously paginated

TABLE 2 (Cont.)
YUCCA MOUNTAIN SEISMIC SOURCE CHARACTERIZATION
WORKSHOP #2 - HAZARD METHODOLOGIES

Attendance List
OCTOBER 16-18, 1996

Name	Affiliation
31. Perman, Roseanne	Geomatrix
32. Pezzopane, Silvio	USGS
33. Pomeroy, Paul	Advisory Committee on Nuclear Waste
34. Potter, Chris	USGS
35. Quittmeyer, Richard	WCFS
36. Ramelli, Alan	UNR
37. Reiter, Leon	NWTRB
38. Robert Smith	UU
39. Rogers, Al	EQE International
40. Savy, Jean	Lawrence Livermore National Laboratory
41. Schwartz, David	USGS
42. Slemmons, Burt	WCFS
43. Smith, Ken	UNR
44. Soeder, Daniel	USGS
45. Stamatakos, John	CNWRA
46. Stepp, Carl	WCFS
47. Sullivan, Tim	DOE
48. Swan, Bert	Geomatrix
49. Tillson, David	Nevada Agency for Nuclear Projects
50. Toro, Gabe	Risk Engineering
51. Whitney, John	USGS
52. Wong, Ivan	WCFS
53. Youngs, Robert	Geomatrix
54. Yount, Jim	UNR

**Civilian Radioactive Waste Management System
Management & Operating Contractor**

**Summary of Seismic Source Characterization Field Trip
and Workshop on Alternative Models and Interpretations**

SSC Workshop 3

**Amargosa Valley, NV
November 18-21, 1996**

Prepared for:

**U.S. Geological Survey
Box 25046, MS-425
Denver Federal Center
Denver, CO 80225**

Prepared by:

**Woodward-Clyde Federal Services of the
Civilian Radioactive Waste Management System
Management & Operating Contractor
101 Convention Center Drive
Suite P-110
Las Vegas, NV 89109**

December 18, 1996

position, and the associated uncertainties. The field trip included 2½ days of field review and discussion focusing on: 1) the behavior of faults in the Yucca Mountain vicinity; 2) the nature of faulting in the potential repository block; and 3) the behavior of the Bare Mountain fault. The workshop discussions entailed presentations and discussions centered around five key issues of importance to the ground motion and fault displacement hazard: tectonic models, three-dimensional geometry of faults, definition and synchronicity of faulting events, characterization of faulting in the repository, and maximum background earthquakes.

The agenda is included as Attachment 1 and it contains a map showing general locations of most field trip stops. Copies of overhead transparencies shown by presenters and additional material distributed during the workshop are included as Attachment 2. Table 1 is a list of participants and their affiliations.

MONDAY, NOVEMBER 18, 1996

The first day of the field trip covered faults on the west side of Yucca Mountain in Crater Flat. The first stop was at Steve's Pass at the southern end of Crater Flat. Dr. John Whitney, the field trip coordinator, gave a brief introduction and outline of the trip. The itinerary was constructed to highlight major issues in interpreting field data and provide a representative sampling of the range and variability of the data. At all of the sites with trench or natural exposures, excavations were still accessible and participants were given the opportunity to observe exposures first hand throughout the trip. Next, Dr. Christopher Fridrich provided a brief overview of the geology of Yucca Mountain, Crater Flat, Bare Mountain, and Black Marble Hill, including eruption of the nearby Timber Mountain and Silent Canyon calderas.

The second stop was at a trench site along the southern Crater Flat fault. Dr. Emily Taylor presented results from Trenches SCFF1 and SCFF1a, including evidence for three surface-faulting events that caused 24 to 65 cm of total vertical slip during the past 250,000 years. Dr. Taylor pointed out uncertainties and alternative interpretations, particularly for Trench SCFF1. Dr. Whitney pointed out possible structural relationships and coseismic rupture between the southern Crater Flat and Windy Wash faults. He also pointed out that deposits associated with the penultimate event on the southern Crater Flat fault contain basaltic ash and this fault may have ruptured with other faults at Yucca Mountain in addition to the Windy Wash fault, as outlined for Scenario U of the rupture scenarios presented in Chapter 5 of the Seismotectonic Synthesis Report.

The third stop was at the Windy Wash fault where Dr. Whitney discussed long-term net slip rates (with 5:1 vertical to horizontal slip ratios) of 0.027 mm/yr derived from offset of a 3.7 Ma basalt flow. He compared these to shorter-term vertical slip rates determined at trench site CF2, to the north, for the past 300 ka that are 0.011 mm/yr. The differences imply that

The last stop of the day was at Trench T4 on the Solitario Canyon fault. Mr. Ramelli first discussed the trench exposure. Of the two fault traces at this site, only the westernmost trace shows evidence for Quaternary activity, with two fissure fills that are similar to, but smaller than those in Trench T8, indicating that displacement is dying out to the north. Drs. Christopher Potter and Warren Day discussed some of the results of their bedrock mapping along the Solitario Canyon fault. They discussed deformation patterns of block-bounding, intrablock and bridging faults.

After dinner, an evening workshop session on tectonic models and their implications was convened. Dr. Christopher Fridrich presented his data and interpretations on the Late Cenozoic tectonic evolution of the Crater Flat basin. He distributed preprints of two related papers. He defined structural domains in the region and described chronologically the tectonic development of the Crater Flat basin from 13 Ma to the present. He estimated the percent of extension for two tectonic models: a tilted-block model and combination listric fault and tilted-block model. He discussed spatial and temporal patterns of extension rates, and implications for tectonic models from observed deformation patterns.

Next, Dr. Rich Schweickert presented his model for a major strike-slip fault system in the Yucca Mountain region. He proposed that a 250-km-long zone of dextral simple shear extends from Amargosa Valley, through Crater Flat and Yucca Mountain, continuing northwest of the Timber Mountain caldera. He described the fault system and outlined the evidence for it, emphasizing the caveat that the data are only permissive for his model. He proposed a geometry for the fault system after a model originally proposed by Hardyman and Oldow (1991), that kinematically links normal and oblique-normal faults at the surface with a detachment and strike-slip fault at depth. He then highlighted some of the tectonic implications of his model that are relevant to seismic hazards in the region.

The third speaker was Dr. Warren Hamilton, who presented a rolling hinge tectonic model for Yucca Mountain. He first described the model in general, emphasizing that the model explains how low-angle normal faults cutting steeply-dipping beds can evolve from initially high-angle normal faults cutting flat-lying beds. He provided examples of low-angle normal faults in the surrounding region (the Funeral and Whipple Mountains), highlighting characteristics of these fault systems that fit the rolling hinge model. Finally, he described how the rolling hinge model may apply to the Yucca Mountain region and highlighted structural features and aspects of the tectonic history that fit the rolling hinge model.

Next, Dr. John Stamatakos gave Dr. David Ferrill's presentation on their tectonic studies of Bare Mountain and Crater Flat, as Dr. Ferrill was absent on jury duty. Dr. Stamatakos first presented data and interpretations on the uplift and tilting history of Bare Mountain. He then summarized their interpretation of significant Tertiary tectonic events at Bare Mountain,

Visits to surficial exposures on Yucca Mountain started at Trench 14D on the Bow Ridge fault. For Group 2, Dr. Christopher Potter and Dr. Whitney presented results of paleoseismic investigations for Dr. Christopher Menges, who was in the ESF tunnel with Group 1. They presented evidence for at least two, probably three surface-faulting events since before 250,000 to 340,000 years ago, with a total net slip of 60-70 cm, resulting in a slip rate of 0.003 mm/yr. Slickensides rake 47° to 67° SW and displacements are 20 to 25 cm for each event. The most recent event occurred before ~50 ka and the penultimate event occurred between 140 and 150 ka. Dr. Potter also described nearby along-strike variations in the character of the Bow Ridge and small subsidiary faults that they had observed during their mapping.

The next stop was where Split Wash crosses the Ghost Dance fault. Dr. Potter discussed their detailed bedrock mapping in the area, emphasizing differences with previous interpretations by Spengler and others, particularly that Dr. Potter and his colleagues do not interpret the Sundance fault to be a through-going fault that offsets the Ghost Dance fault based on nearby continuous exposures of volcanic tuff beds. Dr. Whitney then presented results from Trenches 4a, 4b and 4c, located in Split Wash across the projection of the Ghost Dance fault. These trenches were excavated to see if older, buried Quaternary deposits in the wash were faulted. Dr. Whitney pointed out that no faults were exposed in Trenches 4b and 4c, only unfaulted late Quaternary alluvium and colluvium; whereas some bedrock fractures that are probably not part of the Ghost Dance fault were exposed in Trench 4a. Uncertainties in interpreting faulting history from the exposures were discussed.

The next stop was at the Antler Ridge pavement, an excavated bedrock surface which exposes the Ghost Dance fault. Dr. Potter described how this exposure in the Tiva Canyon Tuff was made and the characteristics of the Ghost Dance fault. Next, Dr. Whitney presented findings in two nearby trenches (Trench 5 and 5a) excavated in alluvium burying the Ghost Dance fault. Although suggestive evidence for a possible Quaternary fracturing event was found in Trench 5, they found no evidence for Quaternary fracturing in Trench 5a.

The next stop was at a trench exposure on the Ghost Dance fault in bedrock at the top of Whaleback Ridge. Dr. Potter described characteristics of the Ghost Dance fault determined from mapping and next Dr. Whitney presented results from cosmogenic isotope studies of the ridge surface, which suggests that the ridge morphology is about 500,000 years old. He also discussed Dr. Emily Taylor's interpretation of the faulting history based on the trench exposure. They found no evidence for any Quaternary events on the Ghost Dance fault at this site, in contrast to work at this site by Dr. John Bell, who next presented his interpretation. Dr. Bell found suggestive evidence for a possible Quaternary fracturing or small faulting event that occurred after 400 to 500 ka. Just south of Whaleback Ridge, we

Dr. Thomas Brocher gave the next presentation on implications from seismic reflection data for high angle faulting in the shallow crust at Yucca Mountain. He re-emphasized that based on distinctive zones of truncated reflectors, the Bare Mountain fault appears planar to a depth of 6 to 7 km, dipping 65°E. He also emphasized that west-dipping faults at Yucca Mountain appear relatively planar and high-angle, which is in general agreement with interpretations by Lawrence Berkeley National Laboratories (LBNL) in their seismic reflection studies. He then reiterated that a major difference between the USGS and LBNL interpretations was the USGS proposes large offsets of the Tertiary-Paleozoic contact along the Ghost Dance and Solitario Canyon faults based on their interpretation of the seismic data, whereas LBNL interprets the Tertiary-Paleozoic contact to be fairly smooth with only small offsets across these faults based largely on gravity models. Finally, Dr. Brocher discussed implications for a ~12-km depth of the seismogenic crust based on seismic data, seismicity data, thermal constraints, and rheologic models.

After the break, Dr. John Bell presented results and tectonic implications from recent and ongoing fault studies conducted by the Nevada Bureau of Mines and Geology. He discussed the newly recognized east Lathrop Cone fault, the poorly understood West Dune Wash fault and several, small, down-to-the-east faults. He also pointed out how some of their interpretations for the paleoseismic history of the Ghost Dance, Bare Mountain and southern Solitario Canyon-Windy Wash faults differed from other investigators (these differences were discussed in more detail during the field trip). Finally, he highlighted aspects of the 1932 Cedar Mountain earthquake that are significant to seismic source characterization at Yucca Mountain.

Next, Dr. Robert Smith presented his insights into seismotectonic issues for normal faults, focusing on examples from the Basin and Range province and the Intermountain seismic belt. These included: 1) the caveat that many big earthquakes nucleate below the brittle-ductile transition and so we could be underestimating rupture area and seismic moment; 2) the need to consider viscoelastic deformation and long-term behavior because a significant component of the surface deformation we observe may not be coseismic; 3) the need to better understand relationships between volcanism and extensional tectonism; 4) observations of contagion behavior and triggered slip; 5) the need to consider both historic seismicity and geodetic data as contemporary strain indicators; and 6) some issues in using scaling relationships to estimate earthquake magnitudes. He provided abstracts for many references and also gave a brief introduction to application of finite and boundary element modeling to investigate normal fault interactions. This stimulated discussion among the experts of triggered slip on faults.

earthquake. Mr. Ramelli began the session on synchronicity of faulting events with a presentation on basaltic ash exposures and evidence for a distributed late Quaternary surface-faulting event at Yucca Mountain. He discussed the location, character, age, interpretations and implications of ash exposures at several localities along many of the faults (southern Windy Wash, Fatigue Wash, Solitario Canyon, Bow Ridge, Stagecoach Road, and Paintbrush Canyon). He pointed out problems with absolute dating, and uncertainties in interpreting certain exposures and the potential involvement of corresponding faults. He also discussed the implied association of volcanism and faulting, and suggested possible explanations for the interaction of volcanism and faulting. A discussion then followed on any evidence for faulting south of Lathrop Wells and Mr. Ramelli pointed out that he and Dr. Bell were planning to finalize their fault map by the January workshop (a draft map was included with Dr. Bell's presentation package).

Next, Dr. Whitney discussed event rupture scenarios presented in the Seismotectonic Synthesis Report and implications to earthquake recurrence, maximum magnitudes and slip rates. Dr. Whitney outlined nine reasons in favor of distributive faulting at Yucca Mountain. He discussed the effects of various rupture scenarios on the slip rate data, which are generally negligible due to the long-term nature of the data. He also discussed the effect on recurrence and magnitude estimates, highlighting the trade-off between decreasing recurrence values and increasing maximum magnitudes for distributive faulting, depending on how magnitudes are calculated.

Dr. David Schwartz then gave the first presentation in the session on characterization of future faulting in the repository. He discussed various coseismic slip models and various issues in generally characterizing fault displacement, including: 1) observations of slip at a point versus along-strike slip distributions for a fault; 2) precision and uncertainties of surface and trench data; 3) whether single-event displacement measurements at the surface are representative of the slip at depth; 4) complexity of displacement patterns near segment boundaries and where faults overlap; and, 5) variations in displacements at a point for successive events. In regards to the last issue, he presented preliminary findings from a worldwide database that indicate characteristic behavior is dominant but not universal.

Next, Dr. Potter discussed the nature of fault interactions at Yucca Mountain. He first described characteristics and displacement histories for block-bounding faults, focusing on the Bow Ridge and Solitario Canyon faults. He next described interactions between block-bounding faults and northwest-striking faults. He also noted that many of the faults post-dated most of the tilting. Finally, he summarized key points on deformation in the potential repository area.

Next, Dr. Pezzopane gave a presentation on minimum faulting earthquakes and maximum background earthquakes in the Great Basin. He analyzed the geologic effects (except liquefaction) associated with 100 historic earthquakes, including the frequency of surface-faulting and cracking as a function of magnitude. He also developed a model for the average and maximum background earthquake that is dependent on rupture area (both shape and size).

Dr. Coppersmith gave the next presentation for Dr. Robert Youngs on some skeletal advice from the Fault Displacement Working Group regarding methodologies for characterizing fault displacement. He described required products, necessary data and interpretations, possible approaches, and differences between SSC for fault displacement and ground motion. He discussed models for characterizing the length of rupture and amount of displacement within the repository. He also discussed considerations for characterizing displacement at various designated points. Dr. Swan clarified how the Working Group envisioned this might be done to allow assessments for different teams to be easily compared.

The next presentation was by Mr. Wong on assessing the contributions from background earthquakes at Yucca Mountain. He pointed out that his assessment of the background earthquake for the ESF study conflicts with results from studies of precariously-balanced rocks and their assessment may be too conservative due to assumptions and simplifications made in modeling the background earthquake. He highlighted the significant issues and presented results from a recent study for the Waste Handling Building, including sensitivity analyses of recurrence of maximum background earthquakes.

Next, Dr. Allin Cornell gave a brief unscheduled presentation on background earthquakes and uncertainties in the Yucca Mountain region. He discussed problems with using the "standard background model" typically used in western U.S. hazard studies at Yucca Mountain where faults are better known, without consideration as to the resolution and detail of available information. He emphasized considering resolution of the data in developing background earthquake zones for Yucca Mountain.

Mr. Craig dePolo gave the final presentation of the workshop on determining the size of the maximum background earthquake. He clarified his definitions of primary and secondary faulting and discussed magnitudes for some historic Basin and Range earthquakes. He highlighted the observed overlapping magnitude ranges for non-surface rupturing, secondary surface-rupturing, and primary surface-rupturing events.

Finally, Dr. Coppersmith opened the floor to observers for comments and questions. Dr. Leon Reiter had several comments, including: 1) given the new configuration proposed for the repository block, the Nuclear Waste Technical Review Board is concerned with the need

**TABLE 1. YUCCA MOUNTAIN SEISMIC SOURCE CHARACTERIZATION FIELD TRIP
AND WORKSHOP ON ALTERNATIVE MODELS AND INTERPRETATIONS**

November 18-21, 1996

Attendance List

Name	Affiliation
1. Abrahamson, Norm	Consultant
2. Ake, Jon	U.S. Bureau of Reclamation (USBR)
3. Anderson, Ernie	U.S. Geological Survey (USGS)
4. Anderson, Larry	USBR
5. Arabasz, Walter	University of Utah (UU)
6. Bell, John	UNR
7. Biggar, Norma	WCFS
8. Brocher, Tom	USGS
9. Bruhn, Ron	UU
10. Brune, James	UNR
11. Coppersmith, Kevin	Geomatrix
12. Cornell, Allin	Consultant
13. Day, Warren	USGS
14. dePolo, Craig	UNR
15. Doser, Diane	University of Texas, El Paso
16. Fridrich, Chris	USGS
17. Hamilton, Warren	Colorado School of Mines
18. Hanks, Tom	USGS
19. Ibrahim, Bakr	U.S. Nuclear Regulatory Commission (NRC)
20. Justus, Phil	NRC
21. King, Jerry	M&O/SAIC
22. Knuepfer, Peter	State University of New York at Binghamton
23. McCalpin, Jim	GEO-HAZ Consulting, Inc.
24. McGuire, Robin	Risk Engineering
25. Menges, Chris	USGS
26. O'Leary, Dennis	USGS
27. Olig, Susan	Woodward-Clyde Federal Services (WCFS)
28. Parizek, Richard	Technical Review Board
29. Penn, Sue	WCFS
30. Perman, Roseanne	Geomatrix
31. Pezzopane, Silvio	USGS
32. Pomeroy, Paul	Advisory Committee on Nuclear Waste

**Civilian Radioactive Waste Management System
Management & Operating Contractor**

**Summary of Seismic Source Characterization Preliminary
Interpretations Workshop**

SSC Workshop 4

**Salt Lake City, Utah
January 6-8, 1997**

Prepared for:

**U.S. Geological Survey
Box 25046, MS-425
Denver Federal Center
Denver, CO 80225**

Prepared by:

**Woodward-Clyde Federal Services of the
Civilian Radioactive Waste Management System
Management & Operating Contractor
1180 Town Center Drive
Las Vegas, NV 89134-6363**

January 31, 1997

ensure that each team understood the interpretations of others, including the degree to which they were supported by earthquake and faulting process models and observed data, and could then more knowledgeably re-evaluate their own team interpretations. The overall goal is for interpretations given at the upcoming elicitation interviews to be well-reasoned, technically-supported, and complete.

The workshop agenda is included as Attachment 1. Copies of overhead transparencies shown by presenters and additional material distributed during the workshop are included as Attachment 2. Table 1 is a list of participants and their affiliations.

MONDAY, JANUARY 6, 1997

The first day of the workshop included a series of presentations to provide additional information on a variety of specific issues outstanding from previous workshops. Kevin Coppersmith gave an introduction, describing the purpose and approach, and outlining the workshop agenda. He emphasized the overall goal was to prepare for the SSC elicitations such that the expert panel's interpretations were well-reasoned, technically-supported and complete. He also emphasized that team interpretations were still preliminary and experts should: feel free to explore the issues thoroughly, ask questions that will help them during the elicitations, and continually keep in mind the characterization of uncertainties. Miscellaneous questions about developing team assessments, scheduling elicitations, and the status of the historical seismicity catalogue were then discussed.

Next, Christopher Potter gave a presentation on the Sundance fault, reviewing previous studies from a historical perspective and discussing the evolution of interpretations as additional data were collected. In particular, he compared studies by Spengler et al. (1994) with those of Potter et al. (1995), describing in detail differences in scope, approach, products and results. He explained many differences in interpretations with site-specific examples from maps, highlighting one of the most significant differences was that although Spengler et al. (1994) interpreted the Ghost Dance fault to be offset by the Sundance fault by as much as 52 m, Potter et al. (1995) concluded that the Sundance fault did not even intersect the Ghost Dance fault based on mapping of continuous volcanic subunits. He pointed out probable causes for differences in interpretations, including the broader area covered by Potter et al. (1995), their emphasis on a geologic-based rather than engineering-based approach to defining rock units, and their mapping of several zones in the upper Tiva Canyon Tuff that provided good marker beds, which were not identified in the mapping used by Spengler et al. (1994).

Ernie Majer gave the next presentation on geophysical interpretations of the Yucca Mountain vicinity developed by Lawrence Berkeley National Laboratories (LBNL). Due to scheduling

trough. He also discussed the Spotted Range-Mine Mountain fault system, the caldera complex, the Kawich Range faults to the north of the caldera, and a faulted block of rocks on the southern flank of Mid Valley that may be an appropriate structural analog for Yucca Mountain. Dr. O'Leary's presentation stimulated much group discussion, including input from Burt Slemmons, John Whitney, Chris Fridrich, and Alan Ramelli on the southern extent of Yucca Mountain faults and faults east, west, and south of Bare Mountain.

The next presentation was given by Brian Wernicke on whether or not shallow-dipping normal faults (SDNF) generate significant earthquakes. He said his talk would largely follow the outline of a paper he recently published on this topic, and he provided reprints of the paper (Attachment 2). He described the apparent paradox about SDNF, that they are prominent and prevalent crustal-scale features that have accommodated significant amounts of brittle extension, and yet historical seismicity patterns and mechanical considerations suggest that SDNF are not seismically active and are not even capable of producing large earthquakes. He reviewed the limited number of historic, large normal-faulting earthquakes observed worldwide and presented kinematic and mechanical arguments as to why SDNF would have very long recurrence intervals. Thus, he argued that perhaps the general lack of observed large earthquakes on SDNF may be due to the historical record being too short. He also presented paleothermal interpretations for some SDNF in the Basin and Range province that suggest the faults initiated at a shallow dip, implying that they were active at a shallow dip and have not evolved from an active high-angle normal fault to an inactive SDNF. Dr. Wernicke then switched topics to review results from geodetic studies he worked on for the Center for Nuclear Waste Regulatory Analyses, which John Stamatakos had also presented at Workshop #2. At the end of Dr. Wernicke's presentation, there was discussion about the general lack of background seismicity on SDNF and the nature of a possible detachment under Yucca Mountain, which Dr. Wernicke believes is no longer active.

The final presentation of the afternoon was given by James Brune on studies of precarious rocks conducted by him, John Whitney, and associates at UNR, and their implications to paleoseismicity. He presented results from studies in southern California and Nevada of the spatial distribution of precarious rocks and their relation to (i.e. away from) major active faults and the area affected by NTS blasts. He showed examples of the many (~100) precarious rocks they had identified in the Yucca Mountain area and discussed age data that indicates all of the rocks they dated have likely been precariously balanced for longer than 10,000 years. He emphasized that these results have implications for longer recurrence of background earthquakes and the need to allocate some historical seismicity to faults in the area. He pointed out some new developments in thinking about ground motions since their report on precarious rocks was written, which was distributed to SSC experts (Attachment 2).

rotations could lock-up structures, stimulating discussion about whether the stress-field is understood well enough to reliably conclude such structures are inactive.

During the discussion session that followed, Ernie Anderson presented a tectonic model, first proposed by Al Rogers to explain observed seismicity patterns, that relates oblique-slip on north-south-striking fault blocks to southward-directed translation of the blocks rather than dextral shear. As many teams seemed to favor the half-graben/planar fault block model, John Whitney next brought up some information relevant to a question raised earlier regarding whether the sum of late Pleistocene slip rates on Yucca Mountain faults was comparable to the late Pleistocene slip rate observed on the Bare Mountain fault. Dr. Whitney, Dennis O'Leary, and Alan Ramelli all discussed indirect geomorphic and geophysical evidence for additional buried traces of the Bare Mountain fault to the one that is visible and was trenched at the surface. Thus, although this trace has definitely been the most active during the late Quaternary, slip rates determined solely from this trace may still be minimums for the entire fault zone. David Ferrill then reiterated the higher longer-term slip rates that he and his associates have interpreted along the southern Bare Mountain fault based on 30 m of subsidence of a basalt flow inferred to be one million years old. Finally, Dr. Coppersmith reviewed the tectonic models presented and some of the key points that were discussed.

Chris Fridrich gave the first presentation on potential seismic sources, representing the team of Diane Doser, Bert Swan and himself. Dr. Fridrich described five types of seismic sources they had considered: 1) background sources; 2) regional fault sources based on mapped Quaternary faults identified in the Seismotectonic Synthesis Report; 3) local Quaternary faults, including a three-fault segment rupture model; 4) a strike-slip shear zone, which may truncate the southern end of some Yucca Mountain faults; and 5) a detachment fault. They defined seven domains for the background sources within 300 km and three domains within 100 km: the northeastern Walker Lane, the southeastern Walker Lane, and the northern Basin and Range. Bert Swan asked if there were any additional faults other teams had considered and Craig dePolo mentioned the buried fault inferred from the Bouguer gravity gradient bounding the Amargosa trough and buried faults in Crater Flat. Dr. Swan clarified that they considered the latter to be included with background sources and explained that they would zone the maximum magnitude for the background domains using a lower magnitude centered around Yucca Mountain where the resolution for identifying and characterizing potential fault sources is better because of more detailed study.

Jim Yount gave the next presentation on potential seismic sources, representing the team of Larry Anderson, Al Rogers and himself. He began by mentioning some additional buried faults under Jackass Flats that they had wondered about either characterizing explicitly or including them implicitly in the background source. Kevin Coppersmith said that the former

behind their approach. He said they had only looked at closer fault sources so far, which had raised some questions about characterizing uncertainties and concerns about some possible inconsistencies. This initiated discussion about the shortcomings of using their approach for closely-spaced, short faults with long recurrence intervals. Difficulties in assessing displacements with limited data were also discussed, along with apparent discrepancies between short fault lengths and larger than expected displacements. Kevin Coppersmith pointed out that of the three sources of uncertainty (statistical, process, and parameter), the latter was probably the greatest, but all need to be considered.

Craig dePolo gave the next presentation on maximum magnitudes, representing the team of Robert Smith, Chris Menges, and himself. He outlined the different approaches his team would use to estimate maximum magnitudes depending on the type of data available for each seismic source. Types of data included surface and possibly subsurface rupture length, average and maximum displacement, down-dip width (to determine area), and slip rate. He discussed many different regression relations they might use and the factors they would consider in weighting the different relations. Next, he discussed their approach to assessing the maximum background earthquake, which would likely be about M_w 6.3 (+0.3, -0.1). He also discussed the problem of potentially double-counting seismic moment when characterizing fault and background sources in the same area. Finally, Robert Smith brought up concerns about uncertainties in magnitude conversions to M_w , and possible systematic biases introduced during declustering of the seismicity catalogue.

Next, two unscheduled presentations were given by David Ferrill and James Brune. Dr. Ferrill presented results of laboratory deformation studies used as a physical analog for the development of pull-part basins. He discussed similarities and differences of features in the lab experiments to those observed at Yucca Mountain. He also reiterated results from their slip-tendency analysis of Yucca Mountain faults (presented by John Stamatakos at Workshop #2), emphasizing implications for a low-slip tendency on shallow-dipping faults. Dr. Brune also discussed results from laboratory modeling experiments. He pointed out that implications from his foam rubber models are that SDNF are much more mechanically stable than shallow-dipping reverse faults because of different dynamic effects, implying that SDNF are not likely seismogenic. Following the presentations was considerable discussion about complexities in using displacement data to estimate maximum magnitudes.

Diane Doser gave the first presentation on earthquake recurrence, representing the team of Chris Fridrich, Bert Swan and herself. She discussed how they planned to use the seismicity catalogue to calculate earthquake recurrence for their background source zones. She emphasized that there were many issues in preparing the catalogue and making the calculations and she highlighted some of these. Bert Swan then discussed how their team

team of Ernie Anderson, Alan Ramelli, and himself. He outlined premises to their approach and discussed their two types of sources, primary and non-primary. Their approach is to directly use displacement per event data wherever it exists and for other faults to use various scaling relations to estimate slip per event. He pointed out how fault aspect ratios generally observed for moderate to large earthquakes have implications for expected fault rupture lengths at Yucca Mountain, given a certain depth of rupture penetration and vice versa. He discussed scaling relations to estimate slip per event from length and cumulative slip, including some examples developed specifically for Yucca Mountain faults. He said they were considering both recurrence interval and slip rate approaches to incorporate the frequency of displacement events into the assessment. Finally, he mentioned how scaling relations from Chapter 9 of the Seismotectonic Report can be incorporated into the methodology developed by Coppersmith and Youngs (1992) to assess displacement within the repository, particularly various characteristics of secondary displacement.

Next, Alan Ramelli discussed the spatial distribution of faulting within the proposed repository. He focused on issues of how does the potential for secondary faulting vary and what areas of different potential can be defined. Both he and Ernie Anderson described similarities of the Clover Mountain area, which they believe provides a structural analog to Yucca Mountain and may have implications for the shallow depth of penetration of some faults, particularly non-primary faults. Discussion followed about possible problems with using some of the scaling relations in an area where deformation rates are transient and much of the total throw occurred during the Miocene. Finally, Kevin Coppersmith emphasized that the methodologies developed by the experts need to be appropriate for the entire Controlled Area, not just the proposed repository.

Ron Bruhn gave the next presentation on their team's fault displacement methodology, representing the team of Ken Smith, Peter Knuepfer, and himself. He said that there would be two parts to their presentation, he would focus on the displacement aspects and Ken Smith would discuss assessing rates using historical seismicity and paleoseismic data. Dr. Bruhn then outlined the conceptual framework of their approach, which is based on statistical analyses used in mining engineering. He emphasized that their goal was to develop an algorithm for estimating the probability of exceedance of a specified displacement at a point within a rock mass without prior knowledge of the point, but given that certain statistical and structural properties of observed faults in the rock mass are known or can be estimated. He provided details of the technical description of his method in a handout. He outlined the general steps in his talk, highlighting assumptions and the data needed for each of the three steps. He discussed application to an analog repository in Leagerdorf, Germany. Finally, he emphasized they were still working on incorporating recurrence into the assessment and he discussed some of the issues and considerations related to both direct and indirect

April 14-16. After this last workshop, elicitation summaries would be finalized. Dr. Coppersmith emphasized that elicitations and development of the team's interpretations were an ongoing process that would continue until the final summary was written. He then asked for comments from observers. Leon Reiter commented on the need to know the resolution for all types of data and the importance of considering this in the assessments. He also reiterated a point he had made earlier that it would be helpful to the experts if a minimum threshold of engineering concern for displacement could be defined at some level above 0 cm. He believed this would help experts to better focus on characterizing the displacements of main concern to design. Carl Stepp responded that the Management Team advised against doing this because they wanted to avoid any possible conditioning of the experts' interpretations. Kevin Coppersmith then added that in terms of guidance on the distance of interest for SSC characterization for ground motion hazard, experts needed to characterize sources out to 100 km, with detailed characterization of sources out to 50 km from Yucca Mountain.

The final afternoon session was devoted to elicitation training, conducted by Peter Morris. Ivan Wong introduced members of the ground motion panel, who had arrived to also participate in the elicitation training (participants in the Ground Motion Workshop on Methods and Models are not included in Table 1, but will be included in a separate report on the Ground Motion Workshop). Peter Morris referred to the training as a workshop in probability assessment. The topics covered included using probability to quantify uncertainty, representing and manipulating probabilities, and assessing probabilities. The information presented followed his handout closely (Attachment 2), with the addition of many real-life examples and interactive exercises with the experts. The workshop was adjourned after the elicitation training, at about 5:00 pm.

**TABLE 1 (CONT). YUCCA MOUNTAIN SEISMIC SOURCE CHARACTERIZATION
WORKSHOP #4 - PRELIMINARY INTERPRETATIONS**

January 6 to 8, 1997

Attendance List

Name	Affiliation
33. Pomeroy, Paul	Advisory Committee on Nuclear Waste
34. Potter, Chris	USGS
35. Quittmeyer, Richard	WCFS
36. Ramelli, Alan	UNR
37. Reiter, Leon	NWTRB
38. Rogers, Al	EQE International
39. Savy, Jean	Lawrence Livermore National Laboratory
40. Schwartz, David	USGS
41. Sheaffer, Patricia	USGS
42. Slemmons, Burt	WCFS
43. Smith, Ken	UNR
44. Smith, Robert	UU
45. Stamatakos, John	CNWRA
46. Stepp, Carl	WCFS
47. Stuckless, John	USGS
48. Sullivan, Tim	DOE
49. Swan, Bert	Geomatrix
50. Toro, Gabriel	Risk Engineering
51. Wernicke, Brian	Cal Tech
52. Whitney, John	USGS
53. Wong, Ivan	WCFS
54. Youngs, Robert	Geomatrix
55. Yount, Jim	UNR

**Civilian Radioactive Waste Management System
Management & Operating Contractor**

**Summary of Seismic Source Characterization
Feedback Workshop**

SSC Workshop 5

**Salt Lake City, Utah
April 14-16, 1997**

Prepared for:

**U.S. Geological Survey
Box 25046, MS-425
Denver Federal Center
Denver, CO 80225**

Prepared by:

**Woodward-Clyde Federal Services of the
Civilian Radioactive Waste Management System
Management & Operating Contractor
1180 Town Center Drive
Las Vegas, NV 89134-6363**

May 16, 1997

discussion was on understanding the interpretations of others, their technical bases, consistency with data, and expression of uncertainty. Preliminary results and sensitivity analyses were presented for five of the teams, highlighting the most significant sources and parameters to the analyses. Assumptions and simplifications of the teams' assessments that were made for the analyses were clarified and discussed. As interpretations will be finalized shortly after this workshop, emphasis was on the experts gaining a common understanding of each other's interpretations and clarification of any outstanding questions regarding their own assessments.

The workshop agenda is included as Attachment 1. Copies of overhead transparencies shown by presenters and additional material distributed during the workshop are included as Attachment 2. Table 1 is a list of participants and their affiliations.

MONDAY, APRIL 14, 1997

Kevin Coppersmith opened the workshop with an introduction, describing the purpose and approach, and outlining the workshop agenda. He highlighted significant aspects of the key issues to be addressed, encouraged technical challenge and debate during the workshop, and emphasized that the experts need to have been exposed to and consider all of the various proponent views. He also stressed that preliminary seismic hazard results are provided only for sensitivity and information on relative importance, and are not intended as hazard results for any other purpose. He reviewed three issues relevant to the seismic source characterization for Yucca Mountain which were raised in the Nuclear Regulatory Commission's 1996 Annual Progress Report (Chapter 3 of NUREG/CR-6513, No. 1). These include questions regarding: (1) adequate consideration and incorporation of alternative tectonic models in the SSC team interpretations; (2) adequate consideration by the teams of all 52 Type I faults, identified by the NRC, as potential seismic sources that may affect repository design or performance; and (3) possible explanations for the apparent anomalous lengths of certain faults (Bare Mountain, Windy Wash, and Ghost Dance) as suggested by scaling relations between fault length and cumulative throw.

The rest of the afternoon was devoted to covering the issues of characterizing areal seismic source zones and the geometry of local faults. Al Rogers made the first presentation on his team's (Rogers, Yount, Anderson - [RYA]) interpretations of seismic source zones. They defined three zones primarily based on structural domain considerations (Yucca Mountain-Bare Mountain, Basin and Range, Death Valley-Furnace Creek), all with the same maximum moment magnitude (M_{max}) of 6.3 ± 0.3 for background earthquakes (they referred to as background faults). Recurrence rates for background faults were calculated for each zone using declustered versions of the historical seismicity catalog and uncertainties in a- and b-values were included, particularly those resulting from assessing catalog completeness.

tectonic model (with from one to three groups of coalescing faults). He discussed their rules of assessing downdip extent, summarized what their preferred interpretations were, and highlighted some geometries that the cross-sections either preclude or suggest are less likely (e.g., coalescence of the Windy Wash, Solitario Canyon and Paintbrush Canyon into one fault). Discussion then followed about how they handled uncertainties in fault dips and calculated slip rates for the various models.

Peter Knuepfer gave the last presentation of the day, discussing his team's (K. Smith, Bruhn, Knuepfer - [SBK]) interpretations of local fault geometry. As their characterization of fault geometry is dependent on their tectonic models, he began with an overview of their models and the resulting influences or constraints on local fault dips, downdip extent, and lengths. He presented many arguments in favor of steeply to moderately dipping planar faults, including geophysical data, seismicity data, and arguments from stress-drop considerations and slip-length scaling relations. Based on the latter considerations and relations, and the Mammoth Lakes earthquake sequence as an analog for "the ash event" (Scenario U of Pezzopane, 1996), they favor interpreting the ash event as a sequence of multiple event ruptures that were not actually synchronous from a ground-motion viewpoint, but were separate events, on individual faults, that were tightly clustered in time. The expert panel discussed the uncertainties with this interpretation. Next, Dr. Knuepfer explained how his team characterized uncertainties in downdip extent and fault length. Except for the Bare Mountain fault, they interpreted the maximum southern extent of Yucca Mountain faults to be around Lathrop Wells.

This stimulated discussion about how other teams interpreted the southern termination of local faults, given the observed increase of total slip and slip rates to the south. Some had interpreted the Highway 95 (or Carrara) fault as truncating local faults, whereas others had terminated faults at the southern end of the Crater Flat basin structural domain. The panel also discussed implications for uncertainty in some fault lengths (i.e., Bare Mountain, Ghost Dance and Windy Wash faults) from scaling relations between length and total throw. Finally, discussion followed about the evidence both for and against listric fault geometries, and how fault segmentation was variously considered in the analyses.

Dr. Coppersmith asked for comments from observers and Clarence Allen asked for clarification about how the teams had considered the Ghost Dance fault in their assessments. Dr. Coppersmith explained that all teams had included the Ghost Dance fault as a possible source for secondary fault slip in their preliminary fault displacement analyses, but none, so far, had included it as a seismogenic source (an independent generator of earthquakes) in their characterizations for the vibratory ground motion analysis. Leon Reiter asked for clarification on the time frame being considered by the experts. Some had considered both

faults rupturing within 10 seconds of each other. He presented the general structure of their logic tree for local faults, gave examples of simultaneous ruptures considered, and discussed their original basis for assigning a low weight to simultaneous ruptures, although they may re-evaluate this based on geometrical considerations. This stimulated discussion among the panel about the geometries, settings, and characteristics of possible analog earthquakes that have exhibited distributive rupture on multiple faults. Examples discussed included both simultaneous rupture (according to the ASM team definition) and non-simultaneous rupture. Discussion also followed about: considering buried dike systems as a possible source, considering the Yucca Mountain faults as aseismic and dependent on the Bare Mountain fault, expanding uncertainties for synchronous rupture models and the need to clarify how teams are defining terms (such as synchronous rupture, distributive rupture, linked faults, etc.).

Craig dePolo gave the first presentation on M_{max} and recurrence on local faults, representing the SDO Team. His team's approach to characterizing M_{max} included using many different regression relations to scale earthquake size from multiple fault parameters such as length, area, maximum surface displacement, slip rate and seismic moment. He clarified how they would determine certain parameters for different scenarios in their assessment, what relations they would use, and how they would be combined. He reported some preliminary values which ranged greater than M_w 7 for certain scenarios with extreme geometries (e.g., 45° dip and 19 km depth). In terms of earthquake recurrence, he said they were considering using geodetic data, in addition to paleoseismic data, to estimate moment rates. They would also use a recurrence interval approach and he discussed how they were using the available paleoseismic data to determine average recurrence intervals for different rupture scenarios in their assessment.

Walter Arabasz gave the next presentation on M_{max} and recurrence on local faults, representing the AAR Team. He began by pointing out they had considered seismogenic depths in two different ways in their assessment because they were considering depths for Yucca Mountain that were generally larger than the depths included in the development of the empirical relations they were using to estimate M_{max} (Wells and Coppersmith, 1994). Thus, they used seismogenic depths to constrain their physical models (D_{max2}) that did not necessarily equal the seismogenic depths used to estimate M_{max} (D_{max1}), indeed D_{max2} was often greater than D_{max1} . He said they considered flexural rigidity to be a better indicator of seismogenic depth than heat flow and presented their rules for constraining downdip fault widths for their various tectonic models and structural categories. He presented the four empirical relations they had used, how they were weighted and the basis for the weights. Next, he discussed their approaches to estimating recurrence, which included both slip rate (weighted 0.6) and recurrence interval (weighted 0.4) methods, whenever data for the latter

Analyses. The latter is suggested by the work of Richard Schweickert and his colleagues. Dr. Anderson discussed how they characterized these buried sources, the bases, and the uncertainties.

Silvio Pezzopane mentioned that their cross-basin faults may be geomorphically expressed as the down-to-the-east faults of Ramelli and Bell (1996). Discussion followed about the geomorphic and paleomagnetic evidence for possible basin-bounding and cross-basin faults. As part of this discussion, Burt Slemmons then gave an overview of geomorphic and geophysical evidence supporting a fault origin for the Carrara or Highway 95 scarp. He showed slides from his aerial reconnaissance and explained that the fault could not only be important as another potential seismic source but it could truncate the Bare Mountain and Yucca Mountain faults (as for example the AAR Team had interpreted in their pull-apart basin model).

Next, Dr. Coppersmith asked the teams why they had not included either the Ghost Dance or Sundance faults as independent seismic sources. Reasons given included no definitive evidence for Quaternary displacement, too short of length (events would be small and fall into "background" or areal seismic zones), and rates of activity are too low. Craig dePolo said that they may include a low-weighted scenario where the Abandoned Wash and Ghost Dance faults are linked and seismogenic, particularly to account for the uncertainty in possible early Quaternary shearing at Whaleback Ridge. Finally, the issue of why vertical slip rates on the Bare Mountain fault are apparently much lower than total vertical slip rates for Yucca Mountain faults, and what significance this may have to tectonic models, was discussed.

After the break, Frank (Bert) Swan gave a presentation on his team's (DFS) fault displacement methodology. He reviewed their general logic tree, describing their overall approach for faults, and fractures/intact rock. Their methodology uses slip rate, displacement per event, recurrence intervals (wherever available), and an event-to-event displacement variability function to characterize the displacement hazard at a location. They use Quaternary slip rates (weighted 0.7) wherever possible and also use Tertiary slip rates with three different models for behavior. These models include: a uniform slip rate since 12.7 Ma, a uniform slip rate since 11.6 Ma with only 20% of the post-Tiva Canyon slip having occurred since 11.6 Ma, and a decreasing rate such that the Quaternary rate is between 0.3 and 3.9% of the late Miocene rate. He discussed how reduction factors and resulting rates were determined for this last model. He presented the bases for all the models and all the resulting slip rates for each of the structures at the nine specified test locations. Next, he discussed their displacement per event and recurrence estimates. He then explained how they used paleoseismic data to develop a relationship between average and maximum

Finally, Dr. Coppersmith asked for comments from observers. Dr. Allen mentioned evidence from historical earthquakes in California supporting characteristic behavior along faults. Dr. Schwartz added that evidence along the Borah Peak earthquake rupture also supported characteristic behavior. Bakr Ibrahim asked how focal depth distributions were being incorporated into fault displacement assessments and Dr. Coppersmith clarified that these were only relevant for principal faults and were included in the ground motion evaluation. Dr. Reiter urged experts to appropriately match the level of complexity of their models to the available data as simplified models that encompass the data are most defensible. He also encouraged them to consider using multiple methodologies in evaluating fault displacement. Discussion then followed as to whether the present schedule afforded the time necessary for adequate consideration of multiple methodologies.

WEDNESDAY, APRIL 16, 1997

Dr. Coppersmith opened the discussion to miscellaneous issues that had been raised over the past two days. Dr. Brune pointed out many issues related to using a quasi-static fault mechanics approach to evaluating the displacement hazard at Yucca Mountain. These included uncertainties in: the absolute deviatoric stresses in and below the repository, pore pressures at seismogenic depths and how these affect the earthquake cycle, the heat flow paradox, and partial versus total stress drops and the large differences in general between the quasi-static models considered and the actual dynamic conditions of the earthquake rupture process. Speaking as a proponent, he believed that fault displacement methods based on total slip or the more traditional earthquake approach, coupled with empirical relations to characterize distributive faulting, were more credible than any fault mechanics approach that can be developed given our current state-of-knowledge. Next, the difference between the probability of seismogenic slip versus non-seismogenic slip on the Ghost Dance fault was discussed.

Next, Gabriel Toro presented the preliminary results for the probabilistic seismic hazard analysis (PSHA). He prefaced his talk with some assumptions made in the modeling of the site and source geometries. Starting with the AAR Team, he gave an overview of their input (in the form of logic trees and maps), presented preliminary hazard curves for 5 and 20 Hz (without many regional fault sources), and discussed some implications from the analysis of variance for the most significant sources. He also presented the ground motion curves used, explaining the significance of the uncertainties in the curves and generally how they were combined with the SSC input to calculate the hazard curves. Following this same format of input, results, and sensitivity analyses, Dr. Toro presented feedback for each team except the SDO Team because he had just received their input. Throughout his presentation, various questions were discussed by the teams, Dr. Toro, and Bob Youngs; clarifying how some of

will be using results from the PSHA to judge the probability of occurrence of such scenarios over 10,000-year, to 100,000-year, to multiple-100,000 year periods.

Next, Carl Stepp gave the experts guidance, from a regulatory perspective, on the documentation required in their elicitation summaries so that their assessments will be complete. He also discussed the revised schedule, which would allow more time for the experts to develop their fault displacement methodologies and evaluate the methodologies used by others. He said to provide more feedback and interaction on fault displacement methodologies, another one-day workshop would be scheduled for early June. The date would depend on the availability of the experts, and additional funds would be provided for associated travel costs and time.

After the break, Dr. Coppersmith and Norm Abrahamson initiated the joint session between the Ground Motion and SSC Experts. For the benefit of the Ground Motion Panel, Dr. Coppersmith reviewed the SSC issues that were covered over the last three days, emphasizing questions particularly relevant to the ground motion issues. Dr. Abrahamson prefaced his overview with the caveat that much of the SSC models are generalized by the ground motion experts to develop their source models. He then reviewed key aspects of the ground motion characterization, including: types of faults considered, magnitudes and distances that calculations were done for, the ground motion parameters calculated, and how the special cases of detachment faults and synchronous (multiple) rupture of local faults were modeled. Discussion among the panel members centered around what, if any, additional parameters the SSC experts might need to provide (such as directivity of rupture, sense of slip, and primary versus secondary rupture planes for multiple fault ruptures), and if model simplifications made by the ground motion experts were reasonable and most appropriate given the actual geologic conditions at Yucca Mountain. In regard to the latter, the geometries of detachments and synchronous ruptures of multiple local faults were of particular interest. Some discrepancies between the panels' characterizations were also highlighted, such as ground-motions models only extended to a depth of 14 km, but many SSC characterizations included deeper seismogenic depths (as deep as 22 km).

Finally, Dr. Coppersmith asked for comments from observers. Dr. Reiter commented that it would be useful to learn from experts what might occur down the road (new data or event) that would cause them to change their assessment. Responses included: (1) the occurrence of a large earthquake on a low-angle detachment anywhere worldwide; (2) occurrence of observable non-tectonic slip on local faults; (3) occurrence of a Cedar Mountain-type earthquake at Yucca Mountain; (4) obtaining additional along-strike slip data for the Solitario and/or Paintbrush Canyon faults; and (5) obtaining definitive data on deep, downdip fault geometry. Dr. Ibrahim asked how much weight was given to each of the two seismic line

**TABLE 1. YUCCA MOUNTAIN SEISMIC SOURCE CHARACTERIZATION
WORKSHOP #5 - FEEDBACK**

April 14-16, 1997

Attendance List

Name	Affiliation
1. Ake, Jon	U.S. Bureau of Reclamation (USBR)
2. Allen, Clarence	Nuclear Waste Technical Review Board (NWTRB)
3. Anderson, Ernie	U.S. Geological Survey (USGS)
4. Anderson, Larry	USBR
5. Arabasz, Walter	University of Utah (UU)
6. Barnard, Ralston	Sandia National Laboratory
7. Bruhn, Ron	UU
8. Brune, James	UNR
9. Coppersmith, Kevin	Geomatrix Consultants
10. Cornell, Allin	Consultant
11. dePolo, Craig	University of Nevada, Reno (UNR)
12. Doser, Diane	University of Texas, El Paso
13. Fridrich, Chris	USGS
14. Golos, Joyce	USGS
15. Hanks, Tom	USGS
16. Harrington, Charles	Los Alamos National Laboratory
17. Hinze, William	Advisory Committee on Nuclear Waste
18. Ibrahim, Bakr	U.S. Nuclear Regulatory Commission (NRC)
19. Justus, Phil	NRC
20. King, Jerry	M&O/SAIC
21. Knuepfer, Peter	State University of New York at Binghamton
22. Lui, Christiana	NRC
23. McCalpin, Jim	GEO-HAZ Consulting, Inc.
24. McGuire, Robin	Risk Engineering
25. O'Leary, Dennis	USGS
26. Olig, Susan	Woodward-Clyde Federal Services (WCFS)
27. Parks, Bruce	USGS
28. Penn, Sue	WCFS
29. Perman, Roseanne	Geomatrix Consultants
30. Pezzopane, Silvio	USGS
31. Pomeroy, Paul	Advisory Committee on Nuclear Waste

**Civilian Radioactive Waste Management System
Management & Operating Contractor**

**Summary of Seismic Source Characterization
Fault Displacement Workshop**

SSC Workshop 6

Salt Lake City, Utah

June 3, 1997

Prepared for:

**U.S. Geological Survey
Box 25046, MS-425
Denver Federal Center
Denver, CO 80225**

Prepared by:

**Woodward-Clyde Federal Services of the
Civilian Radioactive Waste Management System
Management & Operating Contractor
1180 Town Center Drive
Las Vegas, NV 89134-6363**

June 24, 1997

TUESDAY, JUNE 3, 1997

Kevin Coppersmith opened the workshop with an introduction, describing the purpose and approach for the one-day meeting. He reviewed the workshop ground rules and the key characteristics of the nine demonstration points chosen for analysis of the fault displacement hazard.

Next, Robert Youngs explained the purpose of the fault displacement working paper that was sent out for review before the workshop, and he distributed revised copies of the paper with some minor corrections (see Attachment 2). He emphasized that, as a summary of the alternative approaches being used by the expert teams, the paper was intended to provide the teams with a common understanding of the approaches. He also emphasized that the teams needed to consider and evaluate all the available tools in developing their final fault displacement assessments. He reiterated the input needed, the basic hazard formulation, what the final hazard curves portray, and definitions for various terms. This initiated extensive discussion about the meaning and use of "triggered" slip; it was generally agreed that this term may be problematic for describing distributed slip that occurs on secondary faults associated with (geologically coeval to) principal faulting (where principal faulting is seismogenic slip on the fault with the primary moment-release during an earthquake).

Dr. Youngs then discussed each component of the various approaches in more detail, elaborating with specific examples from the team's assessments and making comparisons between various models and submodels. Throughout his presentation, there was extensive discussion, and experts often contributed responses, explanations, and comments about their individual assessments. Of particular interest were the methods used for estimating displacement event frequency and average displacement per event at locations where faults or fractures are present in Tertiary rocks, but Quaternary paleoseismic data is lacking. Frank (Bert) Swan described how his team estimated recurrence intervals when fault-specific paleoseismic data was lacking and Ronald Bruhn explained how his team used data from the Exploratory Studies Facility (ESF) to constrain curves relating fault length and cumulative displacement. Extensive discussion also focused on the use of data from historical surface-faulting events to develop relations for the likelihood of distributive faulting.

After a break, Dr. Youngs continued his presentation, describing two approaches to estimating the probability of a displacement exceeding a given value, given that a displacement event had occurred. He emphasized that variability in fault slip has two components: along-strike, and event to event variations. Dr. Swan, Alan Ramelli, and James Yount all discussed how they had used displacement data to characterize both types of variations for Yucca Mountain faults. James McCalpin described his fault displacement curves, derived from averaging slip along five normal surface-faulting events in the western

more limited and indirect. Methods for estimating displacement frequency were evaluated and discussed, such as how teams addressed the problems in applying the slip-rate approach when the parameters may have significantly changed as the fault and tectonic regime have evolved through time. The weighting of potential activity was also discussed, including consideration of the slip-tendency of faults in the present stress regime. The advantages and disadvantages of using distributive fault models were also discussed. Dr. Bruhn then described one model his team is considering in which the probability of damage and displacement is assumed to be a function of peak particle velocity at a point. He discussed general constraints on displacement probability provided by observations in underground mining studies. Dr. Brune then urged the experts to consider that the recent stress differences determined from hydrofracture tests implied that appropriately-oriented normal faults at Yucca Mountain may be on the verge of slipping.

Characterizing the frequency and amount of displacement on fractures with no measurable displacement was discussed next. Some experts commented that defendably estimating displacements on such small features is at or beyond the limit of resolution of available data and knowledge, considering the likely small size of the displacement events. Other experts commented that if a fracture showed no measurable offset in 12 million-year-old rock, the probability it would slip in the future was so low as to be negligible in the analysis. Different properties and likely behavior of different types of fractures (such as cooling, tension, shear, open, and sealed) were discussed, along with approaches used to constrain upper bounds of frequency and amounts of slip.

Next, Tim Sullivan provided an update on the ESF excavation. He stated that the tunnel boring machine reached the south portal on April 25, 1997 and provided preliminary cross-sections showing the stratigraphy and larger faults in the last part of the tunnel. Next, John Whitney showed a video of the exposure of the Ghost Dance fault at Alcove #6 in the ESF. He also distributed a one-page summary on the exposure. The exposure revealed a 0.6- to 1.0-m-wide breccia zone with isotropic fabric. There was no apparent mineralization, marker horizons, shear fabric, slickensides or other kinematic indicators. Fracture density did increase significantly within 4 m of the zone, especially in the hanging wall. The west edge of the zone appeared more open and less coherent; otherwise, there was no other evidence of repeated or different age movements. Dr. Whitney pointed out that despite the paleoseismic evidence for three to four late-Quaternary surface-faulting events on nearby faults, there is no evidence for associated secondary slip on the Ghost Dance fault. After the video, Mr. Sullivan explained that DOE plans to excavate another drift next year that will trend southeast from the ESF, intersecting the Solitario Canyon fault. The purpose of the drift is to get a better sample of the repository block to confirm constructability and investigate hydrologic parameters.

**TABLE 1. YUCCA MOUNTAIN SEISMIC SOURCE CHARACTERIZATION
WORKSHOP #6 - FAULT DISPLACEMENT**

June 3, 1997

Attendance List

Name	Affiliation
1. Ake, Jon	U.S. Bureau of Reclamation (USBR)
2. Allen, Clarence	Nuclear Waste Technical Review Board (NWTRB)
3. Anderson, Ernie	U.S. Geological Survey (USGS)
4. Anderson, Larry	USBR
5. Arabasz, Walter	University of Utah (UU)
6. Bruhn, Ron	UU
7. Brune, James	University of Nevada, Reno (UNR)
8. Coppersmith, Kevin	Geomatrix Consultants
9. dePolo, Craig	UNR
10. Doser, Diane	University of Texas, El Paso
11. Harrington, Charles	Los Alamos National Laboratory
12. Hinze, William	Advisory Committee on Nuclear Waste
13. Justus, Phil	U.S. Nuclear Regulatory Commission
14. King, Jerry	M&O/SAIC
15. Knuepfer, Peter	State University of New York at Binghamton
16. McCalpin, Jim	GEO-HAZ Consulting, Inc.
17. Nelson, Priscilla	NWTRB
18. O'Leary, Dennis	USGS
19. Olig, Susan	Woodward-Clyde Federal Services (WCFS)
20. Parizek, Richard	NWTRB
21. Parks, Bruce	USGS
22. Penn, Sue	WCFS
23. Perman, Roseanne	Geomatrix Consultants
24. Pezzopane, Silvio	USGS
25. Quittmeyer, Richard	WCFS
26. Ramelli, Alan	UNR
27. Reiter, Leon	NWTRB
28. Rogers, Al	GeoRisk Associates, Inc.
29. Savy, Jean	Lawrence Livermore National Laboratory
30. Schwartz, David	USGS
31. Slemmons, Burt	WCFS
32. Smith, Ken	UNR

APPENDIX D

**SUMMARIES OF GROUND
MOTION WORKSHOPS**

SUMMARIES OF GROUND MOTION WORKSHOPS

**Civilian Radioactive Waste Management System
Management & Operating Contractor**

Summary of Data Needs Workshop on Ground Motion at Yucca Mountain

**Salt Lake City, UT
April 20 and 21, 1995**

May 25, 1995

Prepared for

**U. S. Geological Survey
Box 25046, MS-425
Denver Federal Center
Denver, CO 80225**

Prepared by

**Woodward-Clyde Federal Services of
Civilian Radioactive Waste Management System
Management & Operating Contractor
101 Convention Center Drive
Suite P-110
Las Vegas, NV 89109**

Under Contract Number

INTRODUCTION

The United States Geological Survey (USGS) is carrying out a probabilistic seismic hazards analysis (PSHA) Yucca Mountain, Nevada as part of the Department of Energy's (DOE) project to characterize this site as a potential geologic repository for high-level radioactive waste. The aim of this study is to provide the annual probability with which various levels of vibratory ground motion and fault displacement will be exceeded at the site. These results will be used as a basis for developing seismic design inputs and in assessing the performance of the site.

The PSHA process involves development by two panels of experts of input interpretations and assessments of uncertainties required by the hazards calculations. One panel addresses characterization of seismic sources and fault displacement, while the other deals with vibratory ground motion. Development of interpretations is being facilitated through a series of structured workshops to evaluate available data, to explore the range of interpretations allowed by the data, to examine critically the interpretations proposed by the experts, and to provide feedback on the implications of various interpretations for the seismic hazard at the site. The goal of this process is to have differences in experts' interpretations be the results of true differences in judgment and not differences in access to data, differences in definition, or differences resulting from a lack of understanding each others' interpretations. This report summarizes the first in the series of structured workshops for characterization of ground motion: the Data Needs Workshop.

The Workshop began with introductory comments including an overview of the DOE's Yucca Mountain project and specifically the PSHA project. Team experts were next briefed on several issues of relevance to the ground motion characterization and existing data bases. This information provided the grounds for a discussion by the experts of additional data required to perform a comprehensive assessment of ground motion attenuation at Yucca Mountain. Each speaker has provided a brief summary of his presentation. These summaries and copies of overhead transparencies are included as an Attachment to this Summary.

The Workshop was attended by a representative of the DOE, Tim Sullivan, and the Project Management Team, John Whitney, Carl Stepp, Ivan Wong, and Jean Savy. All Ground Motion Team experts were present: John Anderson, David Boore, Kenneth Campbell, Art McGarr, Walter Silva, Paul Somerville, and Marianne Walck. Members of the Ground Motion Facilitation Team in attendance were Norman Abrahamson, Ann Becker, and John Schneider. Several members of other Teams organized for the PSHA project were also present: James Brune, Allin Cornell, and Tom Hanks (Project Oversight Panel), Robin McGuire and Richard Quittmeyer (Seismic Design Basis Team), Gabriel Toro (PSHA Calculations Team), and Mary-Margaret Coates (Data Management).

The remaining briefings on the first day covered various technical issues and available seismologic data. Silvio Pezzopane discussed the tectonic and seismologic setting. He showed known and suspected Quaternary faults and provided a comprehensive table summarizing their characteristics. A second table listed a preliminary evaluation of "relevant" (DOE specification) and Type I (U. S. Nuclear Regulatory Commission specification) faults. Data on source parameters, crustal structure (velocity profiles) and attenuation (Q), and site effects were summarized by John Schneider. Variations in stress drop and Q were noted in the results of various studies. Within 5 to 10 km of the planned repository, a variety of geophysical data are available and two current studies will provide information local to the site. The DOE is measuring velocities in several bore holes in the immediate vicinity to depths of 1500 ft and the USGS is evaluating shallow and deep crustal profiles from a seismic refraction and reflection survey. Walter Silva summarized the effect of site conditions on spectra using empirical and theoretical data. The latter were also used to illustrate the potential influence of the uncertainty in the site properties as compared to the potential influence of variability of source properties in terms of the resulting variability of the ground motion.

A key set of seismological data near Yucca Mountain was recorded in the 29 June 1992 Little Skull Mountain main shock (m_b 5.6) and aftershock sequence (Kenneth Smith). The data shown include focal mechanisms and depth sections of aftershocks. Main shock accelerograms were recorded at an array maintained by URS/John A. Blume & Associates for the DOE with epicentral distances of 15 km to 232 km from the main shock. Records are also available from portable arrays of instruments deployed by the USGS and the University of Nevada-Reno (UNR) for the aftershock sequence. A second data set was obtained from the 1993 Rock Valley sequence and an event in Rock Valley triggered by the Little Skull Mountain (LSM) earthquake. This set includes focal mechanisms, event locations, and seismograms. Site response in Midway Valley and Yucca Mountain was assessed by UNR (John Anderson) using a number of earthquakes. Kappa and relative site amplification (as a function of frequency) were estimated at 12 stations from the LSM main shock and various other earthquakes.

Site response effects were also examined by Marianne Walck using underground nuclear explosion (UNE) data. The UNE data indicate strong azimuthal dependence on amplification. The more relevant data were recorded at various sites since 1977. These data have been evaluated for 2-dimensional crustal structure to explain the amplification and transfer functions have been developed for three uphole/downhole station pairs within about 3 m of the perimeter of the planned repository.

The special case of near fault ground motions was presented by Paul Somerville. Few earthquake data are available within about 5 to 10 km a fault rupture. Empirical and synthetic data show a levelling off of ground motion in these distances. Other issues

- Issue 2: What is the range of values of source parameters for earthquakes in this region of the Basin and Range? (These are model dependent.)
- Issue 3: What is the explanation for the apparent aseismic slip in the uppermost few kilometers of crust for earthquakes with rupture that reaches the surface?
- Issue 4: What is the Yucca Mountain specific ground motion attenuation predicted by various numerical ground motion simulations?
- Issue 5: What is the basis for apparent discrepancies in the literature regarding regional attenuation (combined effect of Q and geometrical spreading)?
- Issue 6: What is the explanation for the reported large amplification of motions at Yucca Mountain compared to other NTS sites?

Issues 1, 2, and 6 will be satisfied by obtaining new data or evaluating existing data. Issue 3 arises from Workshop discussions regarding numerical modeling procedures. Numerical models are typically implemented with no slip assigned to the uppermost few kilometers of the rupture surface. This assumption is attributed to two possible physical constraints which the Team believes must be investigated: either low shear modulus characterizes materials in this zone or a long source rise time. Numerical simulations specific to the proposed repository conditions (Issue 4) will be used by the experts to evaluate ground motion predictions by the various models and methods. An investigation into regional attenuation (Issue 5) is required to resolve conflicting research results on geometrical spreading and Q.

During their deliberation, the experts identified data or analyses required to resolve these issues. These specific Data Needs are discussed in detail below and are summarized in Table D-1.

Site Response

To evaluate the site response requires the shear wave velocity profile on rock and alluvium (Midway Valley). Ideally, this profile should extend to 1500' depth, but shallower profiles will also be useful.

In addition to the low strain velocity profiles, standard geotechnical information, in terms of strain dependence of the shear modulus and damping, are also needed for both rock and alluvium.

Action:

Perform a sensitivity study to determine the range of rise-times for shallow slip that can be used and still give reasonable agreement with the recorded data. This will provide a means for including the shallow slip without generating unrealistic ground motions. This work may be performed as part of the scenario ground motion study.

Numerical simulations

Because there is little strong motion data in the Basin and Range, and in particular at Yucca Mountain, numerical simulations will be used to provide the experts with region- and site-specific estimates of the ground motion attenuation.

the stochastic point source should be run at all magnitudes and distances for which the experts will be asked to predict the ground motion. The stochastic point source will serve as a reference model and is selected for this purpose because it is simple and well understood by the experts.

Because the site is located close to the faults, finite-source models should also be used to estimate the ground motion for the larger magnitudes (M 6-7). The following models should be considered:

- Stochastic finite-fault model
- Composite source model
- Empirical source function model
- Hybrid empirical model

All of these models except for the hybrid empirical are being used as part of the scenario ground motion study to predict the ground motion for magnitude 6.4 normal faulting events and magnitude 7.0 strike-slip faults. this study will not consider magnitude 7.0 normal faulting events.

Action:

Compare ground motions for the following cases:

- Stochastic point source model for magnitudes 5 to 7 for distances of 1 to 100 km
- Finite-fault model for a magnitude 7 normal faulting event for distances less than 10 km

Regional Attenuation

Different studies have come to apparently inconsistent conclusions about Q (inelastic attenuation) in the Basin and Range. Some structures have found lower attenuation than in California whereas other studies have found similar attenuation as in California. some of this

**TABLE D-1
GROUND MOTION ESTIMATION DATA NEEDS**

ISSUE 1: SITE RESPONSE CHARACTERISTICS

Data Needed:

Site profile information
Shear velocity of rock and soil (geophysical)
Geotechnical properties (soil and rock)

ISSUE 2: SOURCE PARAMETERS

Data Needed:

Evaluate distribution of stress drop (for each model)
Main shocks and significant aftershocks (USGS data)
Aftershocks (Little Skull Mountain and rock Valley earthquakes)
(Site conditions for Little Skull Mountain main shock recordings)

ISSUE 3: NON-SEISMOGENIC SHALLOW SLIP

Data Needed:

Evaluate research related to effects of shallow slip
SCEC summary
Detailed study of Superstition Hills and Landers (Lucerne records) earthquakes

ISSUE 4: NUMERICAL SIMULATIONS

Data Needed:

Perform numerical simulations
Stochastic point source model (set as reference; run for all distance-magnitude pairs)
Stochastic finite fault model (run for distances less than 10 km at magnitude 7)
Composite source model (run for distances less than 10 km at magnitude 7)
Empirical source function model (run for distances less than 10 km at magnitude 7)
Hybrid empirical model (run for distances less than 10 km at magnitudes 6.4 and)

ISSUE 5: REGIONAL ATTENUATION

Data Needed:

Investigate regional attenuation (existing studies and new data)
Methodological differences in studies on geometrical attenuation and Q?
Investigate Little Skull Mountain data (require instrument site conditions, kappa, processing)

**Civilian Radioactive Waste Management System
Management & Operating Contractor**

**Summary of Methods, Models, and Preliminary Interpretations
Workshop on Ground Motion at Yucca Mountain**

**Salt Lake City, UT
January 9 and 10, 1997**

Prepared for

**U. S. Geological Survey
Box 25046, MS-425
Denver Federal Center
Denver, CO 80225**

Prepared by

**Woodward-Clyde Federal Services of
Civilian Radioactive Waste Management System
Management & Operating Contractor
101 Convention Center Drive
Suite P-110
Las Vegas, NV 89109**

February 4, 1997

vertical surface and normal slip on a moderately dipping fault are to be considered. The site is representative rock with dynamic properties equivalent to the existing conditions at repository level (called "repository outcrop"). The repository outcrop is based on the velocity profile with the top 300 m removed. Horizontal and vertical motions will be estimated for peak ground acceleration, peak ground velocity, and spectral acceleration at frequencies of 0.5, 1, 2, 5, 10, and 20 Hz. The Experts must document in detail the reasoning underlying their interpretations. The median ground motion, aleatory uncertainty, and the epistemic uncertainties of both are to be provided. The importance of quantifying uncertainty was discussed in the context of the elicitation process by an expert in these techniques (Peter Morris, Wednesday joint session with Seismic Source Characterization Team). This was elaborated on (Gabriel Toro, Thursday) and the partitioning of uncertainty as parametric or modeling and (orthogonally) as aleatory or epistemic was discussed. Several relevant examples of the partitioning as it relates to ground motion modeling were presented to thoroughly inform the Experts of the process.

A fundamental question which the Experts must address is whether ground motions at Yucca Mountain differ from the motions represented by the data set which forms the basis for empirical models. Differences could be caused by source effects (extensional vs. compressional regimes and normal vs. strike-slip faulting), path effects (crustal differences), or site effects (site response). It was shown that significant differences in near fault ground motions for normal and reverse faults are observed in foam rubber models (James Brune). The propagating wavefront in dip-slip faulting is greatly affected by normal stresses. In reverse faulting, the surface reflected wave is dilatational and reduces normal stress on the slip surface. Foam rubber models show the reflected wave destabilizes the fault and results in increased particle motions in the hanging wall and at the fault tip. In normal faulting, the reflected wave is compressional, which stabilizes the fault and results in weak motions. Additionally, weak surficial layers were shown to significantly reduce the ground motion from near-surface slip due to increased rise-time. This supports ground motion modeling experience which consistently shows reduced high frequency motion radiated from near-surface layers.

The USGS (Paul Spudich) has compiled a data base of strong ground motion records in extensional tectonic regimes. The criteria for inclusion were that the data were: (1) available in digital form; (2) recorded in the free field or in structures less than 3 stories high; (3) triggered before the S-wave arrival; (4) resulted from earthquakes with moment magnitude at least 5; and (5) recorded at distances no greater than 105 km. Nine normal faulting events in the data base were inverted for stress drop and kappa using a Brune ω^2 spectral form with a single corner frequency (Ann Becker). The median stress drop was about 30 bars for several cases using site transfer functions developed by Silva and about 60 bars using site transfer functions by Boore and Joyner. The median kappa obtained was about 0.04 to 0.06 sec for all sites and the inversion results confirmed that the Little Skull Mountain recording sites have particularly low kappas (about 0.015 sec). This compares with stress drops for western

The empirical data base at Yucca Mountain consists of data recorded from underground nuclear tests. The records have been interpreted by Walck (Workshop #1) for two-dimensional crustal structure. The very shallow blasts result in large surface waves. There are also unusual wave propagation effects observed at some locations in NTS (not Yucca Mountain) which are not well understood (Paul Somerville). Confined shallow sources, such as the blasts, are not common in large earthquakes so the variability from typical earthquake depths may be much less than observed in the blast data.

Existing empirical relationships were next examined. The USGS extensional regime study (Paul Spudich) focused on calculating correction factors for empirical relations to better fit the extensional data, and on developing a new predictive relation derived from the extensional data. The factors include a bias correction and a standard deviation correction for all distances and also for distances less than 20 km. Many of the factors show a period dependence. Spudich also presented the new attenuation relation developed using extensional regime data only. This model should be applicable to Yucca Mountain without changes to the source.

FRIDAY, JANUARY 10, 1997

The second day of the Workshop continued with discussions of proponent models arising from empirical data. The Abrahamson and Silva (1996) relationship was not available at the time of the USGS study; style-of-faulting modification factors were provided (Norman Abrahamson) as well as a discussion of the regression procedure.

An advantage to numerical simulations is the ability to modify input parameters to evaluate the sensitivity of ground motions to the parameters (and thus uncertainties) and compute scaling factors. Walter Silva presented results using the point source RVT model, and Kenneth Campbell for the hybrid empirical model. (The attached notes for Dr. Silva's presentation are not complete; much of his work was performed under separate contract to the DOE and was not authorized for release in print form.) Silva has calibrated the point source model using data from 16 earthquakes. This calibration exercise also provides estimates of the modeling uncertainty term. Silva's point source model will be presented to the experts with variable stress-drop so the experts can select their own estimate of the stress drop in applying the model.

Campbell's approach is to estimate ground motions by scaling existing empirical relationships. He develops the scaling factors from comparisons of California motion estimates to Yucca Mountain motion estimates, both developed using the BLWN RVT point source model. The examples he presented correspond to a postulated M 6.5 earthquake at 10 km distance and considered both strike-slip and normal faulting. The correction factors for peak ground acceleration were presented for three discrete values of stress drop and ranged

the acceleration required to topple these rocks provide physical evidence of the attenuation of motion surrounding an historic earthquake. This information is currently being collated to provide a constraint on ground motion attenuation in the region. Near the repository itself, balanced rocks could be toppled by about 0.3 g accelerations, and semiprecarious rocks by about 0.4 g. Age-dating the rock varnish indicates that they have been precariously positioned for about 40,000 to 80,000 years, suggesting a bound on these acceleration levels.

At the conclusion of the Workshop, the Experts presented trial estimates of median ground motion (and uncertainties) for a M 6.5 earthquake occurring 10 km from both strike-slip and normal faulting earthquakes. The purpose of this exercise was to familiarize the experts with the process and the form of the estimates that they will have to provide. Several of the experts only presented proponent models rather than evaluating the suite of alternative models. As a result there was a large variability in their estimates; their estimates of the median peak ground acceleration varied by about a factor of 2 for the strike-slip case, up to 3 for the hanging wall of the normal case, and over 3 for the footwall.

In the comments by observers, Jerry King indicated that the seismic design will include tall structures whose natural periods are beyond 1.0 sec. It was decided that this observation needed to be verified given the fact that the planned period range to be characterized by the Experts only went to 2.0 sec (0.5 Hz). Attached is a memorandum addressing this issue; the requested period range extends to 3.0 seconds.

**Civilian Radioactive Waste Management System
Management & Operating Contractor**

**Summary of Feedback on Ground Motion Interpretations
Workshop on Ground Motion Characterization at Yucca Mountain**

**Salt Lake City, UT
April 16, 17 and 18, 1997**

Prepared for

**U. S. Geological Survey
Box 25046, MS-425
Denver Federal Center
Denver, CO 80225**

Prepared by

**Woodward-Clyde Federal Services of
Civilian Radioactive Waste Management System
Management & Operating Contractor
1180 Town Center Drive
Las Vegas, NV 89134**

May 12, 1997

motion estimates include deviations from the specified fault dip and depth extent, multiple ruptures on parallel faults, and a subhorizontal detachment fault. The latter two faulting cases may deviate too far from the average models to be covered by aleatory variation. These cases were discussed subsequently during the 3-day meeting. The experts will develop simple scaling rules to make the models applicable to these multiple rupture cases.

THURSDAY, APRIL 17, 1997

Because the focus of the Workshop was feedback and discussion among the experts, the experts each outlined their approach to developing their ground motion estimates. Generally, most experts developed weighting schemes for the proponent models, applied the weights, and evaluated the output. Two experts used approaches different from the other five experts. Marianne Walck developed a method to identify outlier points within the proponent values and eliminated these from consideration. John Anderson implemented three schemes which he then weighted to develop estimates. In the first, he accommodated all relevant proponent models and developed a uniform distribution between the maxima and minima. In the second scheme he emphasized a preferred empirical proponent model, and in the third he emphasized a preferred numerical proponent model. Norman Abrahamson presented results of regression analyses on the experts' preliminary estimates and facilitated discussions of the regressed models.

Preliminary hazard computations were presented by Gabriel Toro. The computations were based on the preliminary models developed by the source characterization teams and the regressions based on the preliminary ground motion point estimates. Large magnitude earthquakes on distant faults dominate the hazard at long period and the contribution from faults and areal sources more local to the site dominates at all other periods. Significant hazard arises from multiple ruptures on parallel faults (faults which coalesce at depth) in those models which incorporate this style of rupture. In general, the results show that the largest contribution to uncertainty in the hazard is the uncertainty in the ground motion models.

Each of the experts employed some means of weighting mean values to compute their estimates. They developed several methods of combining weighted values and some developed different objective schemes to obtain weights, all of which were discussed. Because of the importance of uncertainty, its partitioning as epistemic or aleatory and as parametric or modeling was reiterated by Norman Abrahamson. A standard statistical procedure for evaluating the epistemic uncertainty was agreed to by the experts.

these issues cannot be determined a priori, the experts will address any changes to their point estimates by incorporating additional uncertainty.

Following these discussions, Carl Stepp provided guidance on the level of detail the experts are required to provide to document their work. Data sources and all references must be thoroughly documented.

At the close of the Workshop, each expert briefly described potential changes to their point estimates based on the presentations in the Workshop. None anticipated major modifications to their procedures, but rather refinements based on closer evaluations of various proponent models.

APPENDIX E

SEISMIC SOURCE AND FAULT DISPLACEMENT EXPERT ELICITATION SUMMARIES

The following seismic source and fault displacement team expert interpretations have received review by PSHA Review Panel members in accordance with quality assurance approved PSHA Project Plan requirements but have not been reviewed for conformity with Department of the Interior, U.S. Geological Survey standards.

ELICITATION SUMMARY

WALTER J. ARABASZ, R. ERNEST ANDERSON, AND ALAN R. RAMELLI

TABLE OF CONTENTS

	<u>Page i</u>
1.0	TECTONIC MODELS..... AAR-1
1.1	DEXTRAL SHEAR STRUCTURES.....AAR-3
1.2	LOCAL DETACHMENT.....AAR-4
2.0	DEPTH OF THE SEISMOGENIC CRUST..... AAR-6
3.0	REGIONAL FAULT SOURCES..... AAR-8
3.1	TABULATED PARAMETERSAAR-8
3.2	M_{MAX} APPROACH.....AAR-11
3.3	RECURRENCE APPROACH.....AAR-12
4.0	LOCAL FAULT SOURCES AAR-13
4.1	FAULTS CONSIDERED IN LOCAL ANALYSISAAR-13
4.2	NOTES ON LOCAL FAULT ESTIMATES (TABLE AAR-4).....AAR-19
4.3	UNCERTAINTIES IN LOCAL FAULT ESTIMATESAAR-21
4.4	NOTES ON ESTIMATES FOR BURIED/BOUNDING FAULTS.....AAR-22
4.5	NOTES ON THE 52 FAULTS THAT NRC CONSIDERS IMPORTANTAAR-23
4.6	COMPARISON OF QUATERNARY AND MIOCENE DEFORMATION.....AAR-26
4.7	SYNCHRONOUS RUPTURESAAR-28
4.8	M_{MAX} DIMENSIONSAAR-34
4.9	M_{MAX} APPROACH.....AAR-36
5.0	REGIONAL SOURCES AND LOCAL BACKGROUND SOURCE ZONES..... AAR-38
5.1	CATALOG.....AAR-38
5.2	BACKGROUND SOURCE ZONES COUPLED TO REGIONAL SOURCES.....AAR-39
5.3	BACKGROUND SOURCE ZONE BASED ON SPATIALLY SMOOTHED SEISMICITY.....AAR-39
5.4	HOST ZONEAAR-40
5.5	M_{MAX} FOR BACKGROUND SOURCE ZONES > 20 KMAAR-40
5.6	WEIGHTING OF ALTERNATIVES FOR BACKGROUND SOURCE ZONESAAR-41
5.7	NON-INCLUSION OF A VOLCANIC ZONE.....AAR-41

TABLE OF CONTENTS

Page ii

6.0 FAULT DISPLACEMENT CHARACTERIZATION.....	AAR-43
6.1 GENERAL REMARKS	AAR-43
6.2 THE ISSUE OF TRIGGERING	AAR-44
6.3 ORDER OF PRESENTATION	AAR-46
6.4 NOTATION.....	AAR-47
6.5 SCALING RELATIONS.....	AAR-48
6.6 DISPLACEMENT AT A POINT	AAR-53
6.7 OVERVIEW OF LOGIC TREES.....	AAR-57
6.8 PRINCIPAL FAULTING—EARTHQUAKE APPROACH.....	AAR-58
6.9 PRINCIPAL FAULTING—DISPLACEMENT APPROACH	AAR-60
6.10 DISTRIBUTED FAULTING—POINT-ESTIMATE METHOD	AAR-62
6.11 DISTRIBUTED FAULTING—PRINCIPAL-DISTRIBUTED FAULTING METHOD	AAR-63
6.12 SECONDARY/DISTRIBUTED FAULTING.....	AAR-66
6.13 ASSESSMENTS FOR NINE TEST CALCULATION SITES.....	AAR-69
7.0 REFERENCES	AAR-74

TABLES

Table AAR-1	Seismic source parameters for regional fault sources
Table AAR-2	Source inventories
Table AAR-3	Inventory of Crater Flat domain (CFD) faults
Table AAR-4	Estimates of fault parameters for local fault sources
Table AAR-5	Weights for behavior of local faults depending on tectonic models
Table AAR-6	Weights for linked options given independent behavior
Table AAR-7	Weights for coalesced models given coalesced behavior
Table AAR-8	Weights for M_{\max} approaches—local fault sources
Table AAR-9	Regression relations
Table AAR-10	Displacement Data Used for Figure AAR-11

TABLE OF CONTENTS

Page iii

FIGURES

Figure AAR-1	Logic tree for tectonic models and local faults
Figure AAR-2	Map showing regional faults included in the seismic source model
Figure AAR-3	Map showing local fault sources included in the independent model
Figure AAR-4	Map showing local fault sources included in the coalesced model
Figure AAR-5	Map showing hypothetical fault sources included in the seismic source model
Figure AAR-6	Logic tree: behavior branches for Crater Flat domain
Figure AAR-7	Map showing boundaries of seismic source zones, Scenario 1
Figure AAR-8	Map showing boundaries of seismic source zones, Scenario 2
Figure AAR-9	Map showing boundaries of seismic source zones, Scenario 3
Figure AAR-10a	Logic tree for source zones (top)
Figure AAR-10b	Logic tree for source zones (bottom)
Figure AAR-11	Probability density function (PDF) and cumulative distribution function (CDF) for 80 measurements of single-event displacement, normalized to MD^{\max} for the corresponding fault, from 19 trenches in the Yucca Mountain area
Figure AAR-12	Initial branches of separate logic trees for principal and distributed faulting
Figure AAR-13	Logic tree for principal faulting
Figure AAR-14	Logic tree for principal faulting—earthquake approach (cont'd): estimating potential rupture length, given M
Figure AAR-15	Logic tree for principal faulting—earthquake approach (cont'd)
Figure AAR-16	Logic tree for earthquake approach to principal faulting (cont'd): estimating principal fault displacement, MD
Figure AAR-17	Logic tree for principal faulting—displacement approach
Figure AAR-18	Logic tree for distributed faulting—point-estimate method
Figure AAR-19	Logic tree for distributed faulting—point-estimate method, cont'd
Figure AAR-20	Logic tree for distributed faulting—point-estimate method, cont'd
Figure AAR-21	Logic tree for distributed faulting—principal-distributed faulting method

TABLE OF CONTENTS

Page iv

- Figure AAR-22 Logic tree for distributed faulting—principal-distributed faulting method, cont'd (for site of distributed faulting only)
- Figure AAR-23 Logic tree for distributed faulting—principal-distributed faulting method, cont'd (for site of principal faulting also)

ELICITATION SUMMARY
WALTER J. ARABASZ, R. ERNEST ANDERSON, AND ALAN R. RAMELLI

1.0

TECTONIC MODELS

No single tectonic model yet proposed can serve as a predictive template for seismic hazards assessments at Yucca Mountain. The region comprises several tectonic domains, each having distinctive (and, in most areas, complex) internal structure and contrasting bounding structures (O'Leary, 1996, chapter 8). In our evaluation of tectonic models, we accept that Yucca Mountain is located in a specific tectonic domain, to which we attach fundamental tectonic importance. Following O'Leary (1996, chapter 8), we refer to it as the Crater Flat domain (CFD). Any viable tectonic model must explain the structural development of the CFD, especially its Quaternary structural history. It must also be consistent with contemporary regional tectonics, especially with those of the domains adjacent to the CFD.

Before determining the appropriate tectonic models, we evaluate the processes that control the contemporary tectonics of the CFD. In particular, we distinguish between pure shear and simple shear processes, evaluate whether magmatism should be considered a controlling process, and, similarly, whether regional detachment faulting is a controlling process. We recognize that fault-related tilting is pervasive in the CFD, and that in much of the domain the tilting is complicated by steep-axis rotation. These tilts and rotations are incompatible with pure (irrotational) shear, leaving simple (rotational) shear as the only option leading into the front end of our logic tree (Figure AAR-1).

We recognize that silicic magmatism, and especially caldera-forming processes, may have played an important role in the early development of the CFD. But we conclude that contemporary deformation in the CFD is not controlled by caldera-forming magmatic processes, because there is no evidence that events related to such processes continued into the latest Tertiary and Quaternary. Because there is evidence for both Quaternary basaltic volcanism in the CFD and a temporal association of faulting and volcanism, we recognize

that future earthquakes could be associated with basaltic volcanic processes. In a separate section, we assess that likelihood. Based on the estimated low frequency of basaltic volcanic events and the relatively low magnitude of earthquakes typically associated with basaltic volcanism, we do not include in our logic tree a tectonic model controlled by basaltic volcanic processes.

A separate but related question concerns the percentage of extension across the CFD that might be accommodated by volcanic intrusion. Basaltic intrusions occurring as dike injections, rather than rising along vertical pipes, should accommodate some extension and reduce the occurrence of earthquakes (cf., Parsons and Thompson, 1991). Estimates of Quaternary extension across the CFD come from evidence of surface faulting, so the question is whether surface faulting is caused by extensional stresses induced by intruding dikes (if not, then any extension accommodated by volcanism would occur in addition to that accommodated by earthquakes). Paleoseismic data for the Yucca Mountain faults typically span time frames of hundreds of thousands of years. Over these periods, most faults show evidence of several earthquake cycles (recurrence intervals for the principal faults average about 50 ka). The only evidence of volcanism over this same time span is the Lathrop Wells basalt cone, which formed within a relatively narrow time window (possibly primarily during a single eruptive episode). We do not consider accommodation of extension by volcanism for two reasons: (1) surface faulting occurs much more frequently than volcanism; and (2) surface faulting occurs over a widespread area, with little direct spatial association with the Lathrop Wells cone. If basaltic intrusions that did not reach the surface occurred much more frequently and over a broader area than suggested by the Lathrop Wells cone, this interpretation could bear revision.

We conclude that contemporary deformation in the CFD is not controlled by a regional detachment fault of the type envisioned by Scott (1990) because: (1) extensive geologic mapping of Miocene and pre-Miocene rocks has failed to reveal it; (2) there is no evidence that Miocene volcanic features or cells of Miocene hydrothermal activity have been shifted laterally from their roots; and (3) no detachment-related breakaway zone and tectonically denuded footwall have been identified in areas east of the domain. Also, we do not consider a tectonic model controlled by a deep (12 to 15 km) detachment fault because extensive

geologic evidence (geobarometry on mylonitic rocks) indicates that yielding in subhorizontal high-strain zones at those depths is accommodated by crystal-plastic recrystallization processes. In such cases, seismicity is considered to be generated only from the higher-angle faults feeding into the ductile accommodation zone.

We consider deformation in the CFD to be controlled by a stress field created by superposed stresses of uncertain relative influence, chiefly: (1) WNW-ESE Basin and Range extension, along with possible combinations of (2) NW-SE dextral shear related to Pacific-North American relative plate motion and (3) general N basal traction and/or horizontal compression related to southerly mass movement from an elevated northern Great Basin lithosphere. We conclude that all viable tectonic models for the CFD must include an element of extension.

1.1 DEXTRAL SHEAR STRUCTURES

The first node of our logic tree (Figure AAR-1) addresses whether a NW-SE dextral shear influence is manifested by significant unrecognized or poorly characterized dextral shear structure(s). The branch for "no significant NW-SE dextral shear structure(s)" does not preclude an influence by regional dextral shear. The branch simply indicates that if there is such an influence, it is not manifested by right-slip faults of a size that would produce earthquakes having maximum magnitudes greater than that of our background source zone. We weight the two possibilities equally because the issue is unresolved. Hypothesized dextral shear structures are plausible (in particular, a fault paralleling Highway 95, as proposed by Slemmons, or a cross-basin fault as supported in a presentation by Pezzopane), but (1) their existence has not been established, and (2) they are not characterized sufficiently to conclude that they are potential sources of strong ground motion above a background source.

The nature of plausible NW-SE dextral shear structure(s) is treated at the second node of our logic tree. Here three branches consider the possibility of unrecognized or poorly characterized sources in addition to the CFD faults: a throughgoing regional dextral shear zone; a right-stepping shear zone that produces a pull-apart basin, and a right-stepping shear

zone in which the pull-apart basin is underlain by a cross-basin, right-slip fault. We assign the greatest weight to a pull-apart basin containing one or more bounding dextral faults, because the Highway 95 fault is the only proposed dextral shear structure for which evidence has been described (Slemmons, information distributed to SSC teams by R. Quittmeyer dated 3/4/97). We assign less weight to the existence of a cross-basin fault; such a structure could explain the structural discontinuity of CFD faults, but its existence is based on indirect evidence. We assign a very low weight to the existence of a throughgoing regional shear zone because no direct evidence for such a feature exists and we know of no analogs.

In the absence of significant dextral shear structures, the CFD faults accommodate extension independently, but such accommodation can be accompanied by both dextral shear and southerly directed tectonic displacement. The evidence for such accompanying deformation comes from the earthquake record (Rogers et al., 1991) and the geologic record of strike-slip faulting and steep-axis bending (Fridrich et al., SSC Workshop 3, handout dated 11/1/1996). This model has as its analog the Gale Hills north of Lake Mead, where N- to NE-striking, left-normal faults and the blocks bounded by them bend clockwise as they are traced southward toward the adjacent right-slip Las Vegas Valley shear zone (Sonder et al., 1994). Rather than having formed by drag associated with dextral shear, the faulting and bending are best interpreted as resulting from south-directed tectonic collapse and to have involved distributed basal traction (Anderson et al., 1994).

1.2 LOCAL DETACHMENT

The third node of our logic tree (Figure AAR-1) addresses the existence of a local detachment and outlines credible models in which a local detachment is conditionally favored or permissible. In no case is a detachment fault considered to be a controlling structural element. As interpreted by us, a local detachment fault could be a reactivated thrust or a gently dipping accommodation zone.

The depth of a local detachment is addressed at the fourth node of the logic tree where, conditional on its existence, we consider the probability that the detachment lies at a depth < 3 km, 3 to 10 km, or > 10 km. Based on the geophysical data, we preclude a depth less

than 3 km. We give greatest credibility to the 3- to 10-km depth range, because narrow fault blocks such as the 3- to 5-km-wide major blocks of the CFD are more likely to maintain their structural integrity to depths 1 to 2 times their width than to 3 to 4 times their width. Our assigned distribution for the depth (and relative weighting) of a detachment in the 3- to 10-km depth range is:

4.5 km (0.185), 7.0 km (0.63), 9.0 km (0.185).

Throughout, when we assess a three-point distribution, we follow Keefer and Bodily (1983) in assigning relative weights. Following their guidance for three-point distributions, we consistently attempt to estimate the median (i.e., 50th percentile value) together with either the 5th and 95th percentile values or the 10th and 90th percentile values. The appropriate weights then are 0.185, 0.63, and 0.185 to approximate the 5th, 50th, and 95th percentile values, respectively, and 0.3, 0.4, and 0.3 for 10th, 50th, and 90th percentile values. Thus, our use of these combinations of weights in any three-point distribution implicitly indicates the estimated percentiles to which the weighted values correspond.

If the detachment is deeper than 10 km, we consider its depth to have a uniform probability of being anywhere between 10 km and the maximum depth of the seismogenic crust (discussed in the next section).

We conclude that a local detachment, if it exists, has a low-likelihood of being seismogenic, because the data provide no evidence for earthquakes on such faults in the Basin and Range. Accepting the agreed use of this term in this PSHA project, "seismogenic" is defined as capable of generating earthquakes significant to ground motions ($M \geq 5$). For convenience, we use the notation P[S] for "Probability [Seismogenic]." For a local detachment fault, we attach a low probability, $P[S] = 0.05$, to such a fault being seismogenic.

We concluded that any local detachment beneath the CFD would not be active over the entire domain. It would, for example, be constrained in extent by the downdip projection of the Bare Mountain fault on the west and the downdip projection of the Paintbrush Canyon fault on the east. Our evaluation is the following: In the unlikely case that a local detachment were seismogenic, we account sufficiently for its rare earthquake by our local background

source zone, which has a maximum magnitude of 6.3 ± 0.3 . This range would encompass seismic slip on a detachment having a maximum rupture of 200 km^2 and a larger than normal average displacement of 1 m. Accordingly, we do not include a local detachment in our inventory of seismic source zones.

2.0

DEPTH OF THE SEISMOGENIC CRUST

In assessing the maximum depth of the seismogenic crust, we distinguish between (1) the maximum thickness of the seismogenic layer as a control on downdip width (and hence area) of rupture, particularly for use with regressions of Wells and Coppersmith (1994), and (2) the maximum depth to which seismic rupture (and seismic energy release) may physically reach during larger earthquakes. The latter depth becomes important in estimating rupture area, RA , for use in the moment equation, $M_0 = \mu * RA * \bar{U}$ (see, for example, Youngs and Coppersmith, 1985, equation 2), where μ is the rigidity or shear modulus (assigned the value $3 \times 10^{11} \text{ dyne cm}^{-2}$), and \bar{U} is the average (subsurface) displacement over the slip surface.

Our assessed distribution for the maximum thickness (and relative weighting) of the seismogenic layer, called DMAX1, in the Yucca Mountain region is:

11 km (0.185), 15 km (0.63), 17 km (0.185).

We base our assessment of DMAX1 on the depth distribution of seismicity in the southern Great Basin (K.D. Smith presentation at SSC Workshop 2), the aftershock sequence of the 1992 Little Skull Mountain earthquake (Harmsen, 1994), and a review of how Wells and Coppersmith (1994) measured downdip rupture width, including values for the largest historical normal-faulting earthquakes in the Western United States.

Taking into account the tectonophysics of rupture dynamics (e.g., Yeats et al., 1997, p. 49ff, and references therein) and observational studies of the coseismic slip distribution for the Borah Peak and Landers earthquakes (Mendoza and Hartzell, 1988; Wald and Heaton, 1994; Cohee and Beroza, 1994), we assess a separate distribution, called DMAX2, for the

maximum depth of seismic rupture during some larger earthquakes in the Yucca Mountain region. The depths and their relative weights are:

14 km (0.185), 18 km (0.63), 22 km (0.185).

Simply put, the rupture surfaces of large earthquakes can "reach down" below the seismogenic layer into the brittle-plastic transition zone, resulting in greater rupture width (and area). We interpret descriptions of this phenomenon as implying that seismic moment (and high-frequency seismic radiation) is released from the part of the rupture surface that extends into the transition zone. There, material that behaves plastically at low strain rates fails in a brittle mode at the high strain rates that accompany the dynamic rupture of a large earthquake.

We apply DMAX2 in cases where the expected rupture length is 25 km or greater (discussed presently) and where we also intend to estimate maximum magnitude through rupture area, RA, by using only the moment equation. In our evaluation, there is an important distinction between an estimate of RA for use in the moment equation and one for use in the regression equation of Wells and Coppersmith (1994). In the first case, RA can appropriately be estimated by the product of rupture length and downdip width, constrained by DMAX1 or DMAX2. In the second case, however, Wells and Coppersmith (1994) based the use of RA as an estimator of moment magnitude primarily on the spatial extent of aftershock hypocenters, inherently reflecting the thickness of the seismogenic layer. Thus, when applying their regression equation for moment magnitude using RA, we use DMAX1 as the depth constraint on area, regardless of rupture length.

Our consideration of a buried regional strike-slip fault beneath the CFD was an important factor leading to our evaluation of DMAX2. We chose a rupture length of 25 km as the threshold for applying DMAX2 based on (1) the 26.5-km surface rupture length of the 1959 Hebgen Lake normal-faulting earthquake ($M_w = 7.3$) (Wells and Coppersmith, 1994), and (2) our reasoning that candidate ruptures for penetrating deeper than 15 km would have an aspect ratio of length to width that exceeded 1.5, whether for a vertical strike-slip fault or a 60°-dipping normal fault. Coincidentally, 25 km corresponds to a low point in our density

distribution of expected rupture lengths for local fault sources. Ultimately, DMAX2 is applied to only two local fault sources, each of them a major dextral shear structure (the buried regional strike-slip fault and the Highway 95 fault, discussed in a later section).

3.0

REGIONAL FAULT SOURCES

The surface traces of 19 regional faults having known or suspected histories of Quaternary surface displacement, and trace lengths great enough to classify them as relevant to ground motion considerations at Yucca Mountain, are shown on Figure AAR-2. Fault acronyms correspond to those used by Pezzopane (1996, chapter 11). With the exception of the West Specter Range fault, map traces are generalized from Piety (1996). The trace of the West Specter Range fault is generalized from Anderson et al. (1995a). Also, the southeast limit of the Pahrump fault is extended about 43 km beyond that shown by Piety (1996).

3.1 TABULATED PARAMETERS

Parameters for the seismic source characterization of each regional fault source are given in Table AAR-1. Note that the table includes parameters for two linked regional faults, the Death Valley-Furnace Creek and the Amargosa River-Pahrump. On the basis of a highly preferred rhombochasm tectonic model for Death Valley, where these faults are intimately related, we assign a probability of 0.8 to the linked configuration of the Death Valley-Furnace Creek faults versus 0.2 that they behave independently. For the Amargosa River-Pahrump faults, the probabilities are 0.1 for the linked configuration and 0.9 for independent behavior. This low probability of linkage for the AR/PSV faults is based on a lack of evidence for Quaternary faulting in the 15- to 20-km-long gap between Stewart Valley and the Amargosa Desert (Anderson et al., 1995b).

Where three values for any parameter are entered in Table AAR-1, these indicate estimates corresponding to 10th, 50th, and 90th percentile values, with appropriate weights of 0.3, 0.4, and 0.3, respectively. Further explanation of the table follows.

Total Fault Length

Tabulated values for minimum, preferred, and maximum total fault length (TFL) are scaled from trace lengths on Figure AAR-2. Values for minimum, preferred, and maximum maximum rupture length (MRL) for 14 of the regional faults are the same as the values for TFL. For the remaining five faults, the Rock Valley, West Spring Mountains, Belted Range, Kawich Range, and Pahrump faults, the MRLs are less than the TFLs because the faults are considered segmented. Because little or no paleoseismologic data pertaining to segmented behavior exist, we assume that the maximum rupture length can occupy any portion of the total fault length.

The MRL on the linked Death Valley-Furnace Creek fault is less by about 30 km than the combined TFLs of those two faults because the two faults overlap. If these two faults rupture together, the rupture would likely bypass the southeastern part of the Furnace Creek fault which extends beyond the Death Valley fault. If the overlap area did rupture, we interpret that displacements would be relatively minor and would not significantly contribute to the size of the event. Also, in the Last Chance Canyon area between the Fish Lake Valley fault and the Furnace Creek fault, there is little evidence of Quaternary faulting (Klinger and Piety, 1996) despite the high rates of activity along the major faults that lead away from that area. We interpret this relatively inactive zone as a persistent segment boundary and do not link the Fish Lake Valley fault with the Furnace Creek fault.

Minimum Distance to Repository

Tabulated values were taken from Pezzopane (1996, chapter 11) or measured from Figure AAR-2.

Documented Quaternary Displacement

Quaternary displacement is documented for 14 of the 19 regional faults (indicated by y). Our decision to include some faults that lack documented Quaternary displacement (indicated by y?) is based on various criteria and reasoning. The Mine Mountain and Cane Spring faults are included because they form part of a northeast-trending zone of coherent, active deformation that includes: (1) the Rock Valley fault, which has the highest slip rate of any fault located closer to Yucca Mountain than 50 km (the distance to the Death Valley/Furnace

Creek fault system); and (2) the epicenter of the Little Skull Mountain earthquake. The Keane Wonder fault is included because it is a range-bounding structure at the east margin of the highly active Death Valley region (Klinger and Piety, 1996). The Yucca Lake fault is included because it appears to form the northeast margin of the potentially active Mine Mountain-Wahmoni-Cane Spring fault group. The Oasis Valley fault is included because it is the only fault Anderson et al. (1995a) studied within the relatively stable Goldfield sector of the Walker Lane, for which they equivocated about Quaternary displacement over a significant length of trace.

Style of Faulting

N = normal, L = left lateral, R = right lateral, O = oblique.

Fault Dip

There are no specific subsurface data (such as from mines, drill holes, or aftershock distributions) to constrain the overall dip of any of the regional faults. Minimum, maximum, and preferred dip values are assigned mainly on the basis of known or inferred fault slip characteristics with steep dips assigned to strike-slip faults, and moderate dips to dip-slip faults. For example, preferred dips of 90 degrees are assigned to the Rock Valley, Cane Springs, Amargosa, Pahrump, and Furnace Creek strike-slip faults whereas all of the major range-front normal faults are assigned preferred dips of 65 degrees. Maximum and minimum values are assigned on the basis of reasonable ranges of overall dip of faults typical of each slip-sense category.

Slip Rate and Recurrence Data

Published slip rate and recurrence data are available for only two of the nineteen regional faults: the Death Valley and Furnace Creek faults (Klinger and Piety, 1996). These parameters were estimated for the Rock Valley fault from data in Piety (1996) augmented by more recent thermoluminescence ages (Shannon Mahan, USGS, written communication 2/20/97). For the west Spring Mountains fault, the parameters are estimated by assuming that events equivalent in displacement to the estimated displacement of the most recent surface faulting event were responsible for forming the largest scarp and by estimating an age

range for alluvium on which the largest scarp is formed (Anderson et al., 1995a). For the other regional faults, slip rates are estimated, but recurrence intervals are not.

Some estimates of slip rate are based on geomorphic data (primarily scarp-profile data) combined with an estimate of the age of the surficial deposits or alluvial surfaces that are offset by the fault. An example is the Belted Range fault. Other slip rates are estimated by qualitative comparison of the fault orientation, location, fault-trace geomorphology, and tectonic setting to the faults in the region that have provided constraints on slip rate. For the Mine Mountain and Cane Spring faults, for example, maximum slip rates were taken to be $\frac{1}{3}$ to $\frac{1}{2}$, respectively, of the conspicuously more active Rock Valley fault. The Pahump fault may have tectonic affinities with the strike-slip faults of the Death Valley system, but reconnaissance paleoseismic study shows that it is significantly less active than that system. It was assigned a maximum slip rate twice that of the relatively active Rock Valley fault because of its potential affinity to the Death Valley faults.

Probability of Being Seismogenic, P[S]

All the regional faults having documented Quaternary displacement are considered seismogenic, with $P[S] = 1$. These include the linked regional faults. For faults that lack documented Quaternary displacement, probabilities are assigned based on their orientation, tectonic setting, and relation to other seismogenic faults.

3.2 M_{max} APPROACH

For the regional fault sources, we use three approaches to estimate M_{max} in terms of moment magnitude M : (a) M estimated from surface rupture length SRL, using the relation from Wells and Coppersmith (1994) for all slip types; (b) M estimated from rupture area RA (SRL x downdip rupture width) using the relation from Wells and Coppersmith (1994) for all slip types; and (c) M estimated from SRL and slip rate S , using the relation from Anderson et al. (1996). We assign the following weights to the three approaches:

(a) (0.4), (b) (0.2), (c) (0.4).

Although M and RA are well correlated, we downweight approach (b) because the data Wells and Coppersmith (1994) used for RA were based on aftershock hypocenters; they are not a product of rupture length and width (see earlier section on "Depth of the Seismogenic Crust"). We also recognize the uncertainty in using SRL to estimate subsurface rupture length for calculating RA . Regarding approach (c), most of the preferred slip rates tabulated for the regional faults in Table AAR-1 lie within the range of data regressed by Anderson et al. (1996), and the relation is straightforwardly applicable.

In Table AAR-1, total fault length is the length of the fault that is active, meaning the length along which seismic moment should be distributed given the slip-rate approach to recurrence (discussed below). The parameter used to estimate M_{max} is maximum rupture length (a measure of SRL), estimated in terms of minimum (mi), preferred (p), and maximum (m) values. When either the preferred or minimum value is selected for total fault length, weights for allowable maximum rupture length are renormalized.

3.3 RECURRENCE APPROACH

For the regional fault sources, we use two approaches for recurrence modeling: (1) a slip-rate approach and (2) a recurrence-interval approach. Weighting of these approaches is 0.6 and 0.4, respectively, for all the regional fault sources for which both slip-rate and recurrence-interval data are provided in Table AAR-1. Otherwise, the slip-rate approach is weighted fully.

Fault-specific recurrence relationships are generated from the slip rates using the methodology of Youngs and Coppersmith (1985) assuming constant moment rate. Whether using the slip-rate or recurrence-interval approach, we adopt the characteristic earthquake model with a weight of 0.7 and the "modified exponential" model (Youngs and others, 1987) with a weight of 0.3. The exception is for the Death Valley and Furnace Creek faults. Because of their high slip rates the exponential model would lead us to expect many more moderate-magnitude earthquakes than have been observed. Given this, and the fact that the characteristic model was developed from observations for faults having high rates of activity, we give 1.0 to the characteristic model for the Death Valley and Furnace Creek faults. For

both the characteristic and "modified exponential" models. M_{max} evaluated for a fault is assumed to be uniformly distributed in the range $M_{max} \pm 1/4$ magnitude unit, with $M_{max} + 1/4$ being the upper-bound magnitude, m .

Where recurrence intervals are provided, we use the method of Youngs and Coppersmith (1985) that assumes a constant frequency of earthquakes above some specified size. Given M_{max} for a fault, the cumulative frequency for earthquakes of $M_{max} - 1/4$ is set equal to the inverse of the tabulated recurrence interval, which is interpreted to represent the frequency of characteristic-size events for the fault.

Based on seismicity recurrence calculations provided (Section 3.1 contains a description of the methodology used to calculate seismicity parameters) from diverse regional sources within 300 km of Yucca Mountain, our assessed distribution for the b-value (and relative weighting) for applying the methodology of Youngs and Coppersmith (1985) is:

0.80 (0.3), 1.00 (0.4), 1.20 (0.3).

4.0

LOCAL FAULT SOURCES

4.1 FAULTS CONSIDERED IN LOCAL ANALYSIS

The following faults are considered potential seismic sources within 20 km of Yucca Mountain, and are referred to in our analysis as local faults. Figures AAR-3 and AAR-4 show local faults included in our coalesced and independent models (discussed later in this section).

Paintbrush Canyon Fault (PBC)

PBC connotes the fault zone that bounds the west sides of Alice and Fran Ridges and Busted Butte. Activity extends at least from near Yucca Wash, where PBC has no obvious geomorphic expression (but where trench A1 reveals minor Quaternary offsets), to southwest of Busted Butte, where Holocene alluvium truncates a subtle scarp. Some map depictions

(e.g., Simonds et al., 1995) indicate a left step of about 0.7 km at Fran Ridge, suggesting possible segmentation. We do not segment PBC here because other depictions suggest greater continuity, and data do not require it; in any case, we would give this a low weight and consider it for only some events. Displacement and recurrence parameters for PBC are derived from chapter 4.4 of the Tectonics Synthesis Report (USGS, 1996). With multiple exposures and an extensive record (~700 ka) at Busted Butte, a value was calculated for the average displacement per event (D_{avg}) that is less than the maximum displacement per event (D_{max}).

Stagecoach Road Fault (SR)

As delineated on most maps, SR has a short length (about 4 km), despite prominent geomorphic expression and a relatively high rate of activity. SR commonly is considered linked as a single fault with PBC, with the intervening area masked by young alluvium; we favor this interpretation. At least one depiction suggests that SR could connect with the Mine Mountain fault to the northeast (Maldonado, 1985); this interpretation is not considered here because mid to late Quaternary alluvial surfaces east of Yucca Mountain lack geomorphic evidence of such a connection. The uncertainties in trench data possibly are larger for SR than for other Crater Flat Domain (CFD) faults because of: (1) the predominant loose sand encountered in the trenches, which are difficult materials to work with; (2) dating results that were inconsistent; and (3) significant hanging wall deformation in the trenches. Unless age estimates are grossly in error, which rough agreement suggests is not the case, SR is one of the most active CFD faults during the late Quaternary, although this is based on a relatively short record. Correlation of an 8 Ma tephra across SR (J.W. Whitney presentation at SSC Workshop 2) indicates substantial post-Rainier Mesa offset.

Bow Ridge Fault (BWR)

BWR has weak geomorphic expression of Quaternary activity for < 1 km along Exile Hill, and all data come from one cluster of trenches. Length and displacement thus are poorly constrained, but do not appear significantly underestimated given the lack of geomorphic expression elsewhere. The northward projection of BWR has been depicted alternatively as continuing with a northerly strike to near Yucca Wash (Scott and Bonk, 1984; Day et al., 1996) or curving to the northwest and connecting with the Sever Wash fault (Simonds et al.,

1995). We favor the former interpretation because BWR appears to control a north-trending linear drainage between Exile Hill and Yucca Wash. Trench A/BWR-3, excavated across the projection of BWR north of Exile Hill, showed no evidence of displacement in Q3 gravels (est. 100 to 200 ka), supporting a low rate of activity. BWR commonly is depicted as having a steep dip and connecting with PBC at a depth of a few km; however, projection to the Exploratory Studies Facility (ESF) (cross-section, R.C. Lung presentation at SSC Workshop 2 and handouts at SSC Workshop 3) indicates a dip of about 60 degrees, similar to that of the other block-bounding faults.

Ghost Dance Fault (GD)

There is evidence of minor Quaternary activity on GD, but the evidence is nondefinitive, geomorphic evidence constrains offset to be minor (at a detection threshold), and the possible displacements could be secondary. Map depictions suggest that GD connects with the Abandoned Wash fault, but considering them as a single fault indicates an extremely high aspect ratio (i.e., a long, small displacement fault), and the Abandoned Wash fault shows no evidence of Quaternary activity. GD is considered in the analysis because of its location, but we assign a low weight to the probability that it is seismogenic ($P[S]=0.1$), because activity is unproven and the possible small displacements could reflect secondary slip.

East Lathrop Cone Fault (ELC)

This is a NE-striking fault south of SR and east of the Lathrop Wells basalt cone (Ramelli and Bell, in prep.). It displays a small scarp (< 0.5 m high) in late Quaternary alluvial deposits (A.R. Ramelli presentation at SSC Workshop 3). The fault has not been studied in detail, so estimated parameters are poorly constrained. However, its small scarp, its moderate post-Tiva offset (Frizzell and Shulters, 1990), and its apparent short length all indicate that ELC is a minor fault. The fault is located well south of the controlled area. If considered part of a PBC/SR system (our preferred interpretation), ELC slightly increases the overall length of the system.

Solitario Canyon Fault (SC)

SC is taken to extend along a nearly continuous scarp projecting toward Lathrop Wells cone and the southern end of SR. A possible NE-striking connection between SC and SWW is not

directly included here because of its weak geomorphic expression and unproven activity, but is included in the single west-side coalesced model. The southern end of SC is buried by young alluvium. SC has the longest continuous late Quaternary scarp of any Yucca Mountain fault, but trench results indicate a lower long-term rate of activity than for the other block-bounding faults (e.g., PBC, SR, SWW, SCF). Displacement and rate estimates are based on late Quaternary activity, which is considered more likely to be representative of the next 10^4 to 10^5 years. Our estimate for Davg is less than that for Dmax, based on the multiple trench sites and the fact that relatively large displacements are confined to a short section of the fault.

Iron Ridge Fault (IR)

IR strikes subparallel to SC, and is therefore considered a SC splay that obliquely connects to SR. IR has a nearly continuous bedrock scarp along much of its length. Results from a single trench site (SCF-T2) indicate Quaternary activity. The trench revealed massively cemented gravels (mid-Pleistocene in age) juxtaposed against bedrock, with permissible minor late Quaternary extensional opening. The lack of definitive late Quaternary offset indicates a low rate of activity and precludes significant rupture associated with late Quaternary events on SC or SR.

Fatigue Wash Fault (FW)

The FW scarp originally was referred to as part of the Windy Wash fault but actually connects with Scott and Bonk's (1984) Fatigue Wash fault. FW lies close to and interconnects with the Windy Wash fault, and the two are considered likely to make up a single fault system. This likelihood is incorporated in our linked and coalesced models (discussed below). The northernmost mapped extent of FW has minor bedrock offset and no evidence of Quaternary activity; it therefore is not considered in the analysis. Estimates for FW are based largely on a single, poorly sited trench (CF-1), one of the original trenches excavated for the Yucca Mountain program. CF-1 is adjacent to a drainage that flows parallel to the fault (perpendicular to the trench), providing a cross-sectional view of channelized deposits that form poor stratigraphic markers. The estimate of slip rate is adjusted to account for surface separations where FW crosses the Crater Flat road, as discussed in USGS (1996).

South Windy Wash Fault (SWW)

This fault is considered to be separate from the North Windy Wash fault because the two are not directly connected. To the north, SWW abruptly terminates against the Central Windy Wash fault; its southern end is less well constrained. Paleoseismic data are derived from a trench site at the extreme north end of SWW. Displacements are assumed to be somewhat larger along its central part (south of FW splay), based on a 100-m offset of 3.7 Ma basalt. The trench site is the best along SWW with respect to Quaternary stratigraphy. The best long-term rate for a principal Yucca Mountain fault is provided by offset of 3.7 Ma basalt. Total displacement along the central part of SWW is unknown.

North Windy Wash Fault (NWW)

This is the original Windy Wash fault of Scott and Bonk (1984). A small, nearly continuous bedrock scarp likely reflects some Quaternary activity, but field relations indicate this is largely a fault-line scarp formed by erosion of deposits on the downthrown side of the fault. Late Quaternary activity is minor at most. There are no trench data or other good constraints on activity, which is therefore assumed to be similar to northern SC and the Northern Crater Flat fault.

South Crater Flat Fault (SCF)

Offset of 3.7 Ma basalt on this fault is much smaller than that on SWW (about one-third). The fault projects toward CWW, and is considered a splay of the Windy Wash system. SCF is the best candidate for having activity that extends through the hills south of Crater Flat. Trench data are complicated by uncertain correlations across the fault, but they show progressively downthrown and buried soils, indicating repeated activity.

North Crater Flat Fault (NCF)

As described by the USGS (1996), this fault is a system that includes at least three closely spaced, subparallel faults, each having probable small Quaternary scarps. Two trenches were located across its westernmost trace. Quaternary activity is documented at trench CFF-T2a, but late Quaternary activity is constrained to be minor based on lack of faulting in trench CFF-T2 (USGS, 1996).

Central Windy Wash Fault (CWW)

This down-to-the-east fault is distinguished from the down-to-the-west faults of the Windy Wash system (SWW and NWW); it abruptly truncates the north end of SWW and terminates near the south end of NWW. The scarp of CWW is modified along its central part because of drainage deflection, but unmodified scarps are present along both ends. Displacement and rate estimates are based on vertical separations of late Quaternary alluvial surfaces.

Central Crater Flat (CCF)

This down-to-the-east fault has a similar extent and position as CWW, although it is not as directly connected to down-to-the-west faults. Displacement and rate estimates are the same as for CWW, based on similar surface separations of the same alluvial surfaces.

Black Cone Fault (BC)

This down-to-the-east fault displays a system of NW-trending, mostly down-to-the-east scarps northeast of Black Cone, indicating minor late Quaternary activity. BC is inferred to connect with a north-striking fault southeast of Black Cone. The north-striking fault has a 0.5- to 1-m scarp in alluvium that deflects drainage and possibly offsets 3.7 Ma basalt near drillhole VH-2 (Simonds et al., 1995; Ramelli and Bell, in prep.). Displacement and rate estimates are the same as for CWW and CCF, based on similar surface separations and provide the basis for our preferred rate.

Bare Mountain Fault (BM)

This down-to-the-east fault forms the western boundary of Crater Flat. Its southern end is poorly defined, with bedrock offset extending south into Amargosa Desert, but Quaternary activity apparently is confined to north of Black Diamond. BM has a slightly longer continuous Quaternary trace than does SC. It was the most active fault and had the largest throw within CFD during the Miocene. Its Quaternary rate is similar to the Yucca Mountain faults, suggesting reactivation under different conditions. The postulated higher rate for BM based on alluvial fan size (Ferrill et al., 1996) is incorporated in our upper bound on slip rate, but trench data and surficial mapping are considered better constraints and provide the basis for our preferred rate.

Midway Valley (MWV)

MWV is a north-striking fault inferred from geophysical surveys and shallow borehole data. It is buried by unfaulted mid to late Quaternary alluvium. Estimates for this fault are based on activity at the threshold of resolution.

West Dune Wash #1 (WD1)

WD1 is a left step of about 0.3 km from the Ghost Dance fault. McKague et al. (1996) list it as a Type I fault, and Quaternary activity is suggested by bedrock scarps, vertical CaCO₃-filled fractures, and linear drainage (Simonds et al., 1995). Estimates for this fault are based on activity at the threshold of resolution.

West Dune Wash #2 (WD2)

WD2 is a north-northwest-striking fault listed as a Type I fault by McKague et al. (1996), and Quaternary activity is suggested by bedrock scarps (Simonds et al., 1995). Estimates for this fault are based on activity at the threshold of resolution.

East Busted Butte (EB)

EB is a down-to-the-east fault bounding the eastern sides of Busted Butte and Fran Ridge. Quaternary activity is indicated by arcuate, subtle scarps flanking Busted Butte (Simonds et al., 1995; Ramelli and Bell, in prep.). Estimates for EB are based on small mid to late Quaternary offset reflected in its scarp. Topographic relief suggests extension of this fault along the east side of Fran Ridge, although no evidence of Quaternary activity has been described at that location.

4.2 NOTES ON LOCAL FAULT ESTIMATES (TABLE AAR-4)

Total Active Length

This is the surface length over which a fault has apparent Quaternary activity. It is scaled from mapped depictions and cross-checked against low-sun-angle aerial photographs: minimum = distance over which Quaternary fault scarps or other evidence of activity can be traced; preferred = preferred value from considerations of topography, mapped depictions,

and burial by younger deposits; maximum = upper bound considering map depictions, fault intersections, topographic expression, and relative cumulative displacements.

Style

In the nomenclature used, ln = left-normal (dominantly normal with a left-oblique component). Slip vector is poorly defined for most faults, but available constraints (fault striations, apparent offsets) suggest that most faults are dominantly normal with a left-oblique component. Where not documented, slip is assumed to be related to fault strike.

Fault Dip

For most faults, 60 degrees is the preferred estimate of dip based variously on well-constrained cross sections (e.g., the projection of BWR to the ESF), bedrock fault exposures (e.g., trench exposures along central SC), or geophysical data (e.g., BM). Reported dips from fault trenches and other surface exposures are consistently 10 to 15 degrees steeper and therefore are not used.

Total Displacement

In most cases, this measure is made from offset of the top of the Tiva Canyon member of the Paintbrush Tuff, which is estimated from cross sections or geologic maps (or topographic maps, where necessary). It was estimated for the part of a given fault where it appears largest. It generally is well constrained for faults in the north part of the basin, and less constrained in the southern part, where hanging walls are buried by thicker alluvium.

Displacement Per Event

Using data reported in individual chapters of the Tectonics Synthesis Report (USGS, 1996), the maximum displacement per event (D_{max}) and the average displacement per event (D_{avg}) are estimated for the part of a given fault where displacement appears largest (generally the central part of the fault). Maximum observed displacements, in some cases averaged for multiple events, are taken as best estimates of average displacement for faults for which there are single trench sites or multiple sites in nonrepresentative locations. Averages are derived from the largest displacements along a given fault for which there are multiple trenches deemed to be in representative locations, and/or from records of several events.

Slip Rate

Slip rates are based on data reported in individual chapters of the Tectonics Synthesis Report (USGS, 1996) and are estimated for the part of a given fault where they appear largest. For example, trenches CF-2 & CF-3 (Simonds et al., 1995) are located at the extreme northern end of SWW and north of the intersection of SWW & FW, so a slip rate derived from offset of basalt along the central part of the fault is assumed to be more representative.

Recurrence Interval

This is the average interseismic interval derived from paleoseismic data reported in individual chapters of the Tectonics Synthesis Report (USGS, 1996).

4.3 UNCERTAINTIES IN LOCAL FAULT ESTIMATES

Estimates of activity on local faults at Yucca Mountain involve large epistemic uncertainties. Estimates of length involve difficulties in recognizing remnants of small surface offsets, especially at the ends of ruptures, and they are sometimes complicated by burial by younger deposits. Measuring displacements is uncertain because there is a general lack of piercing points (and hence poorly constrained slip vectors), poor stratigraphic markers, uncertain correlation of units across a fault zone, and the common need to project geomorphic surfaces or stratigraphic units across a broad zone of deformation. Activity rates (slip rates and recurrence intervals) are highly uncertain because they depend on age estimates, which incorporate uncertainties in such things as analytical errors, unknown errors related to poorly understood processes and the experimental nature of most dating techniques, and indirect control (i.e., events typically are bracketed and not directly dated).

Subsurface fault geometry is poorly constrained because depths of fault penetration are unknown and fault dips are uncertain. Interpreting the number of events within the paleoseismic record is complicated by several factors: (1) The nature of fault interactions is uncertain (i.e., distributed events seem likely, but it is beyond our resolution to determine which faults rupture during individual events and how consistent such events have been). (2) Some displacements may have secondary or nontectonic origins. (3) Some events—

especially small, older events—likely are unrecognized, as suggested by plots of event timing (e.g., Pezzopane et al., 1996, chapter 5). (4) Events are not necessarily recognizable at all sites because of factors such as variable offsets, bioturbation, and carbonate overprinting. (5) Not all fault traces have been studied.

Despite these many sources of uncertainty, our estimates of activity of the CFD faults appear to be reasonable and adequately accurate, and are internally consistent and in accord with generally low rates of regional strain. For example, comparing the minimum distances over which fault activity can be traced to conservative upper bounds on length suggests that length estimates are unlikely to be off by as much as a factor of two; displacement measurements are probably rarely off by more than 20% to 30%; and comparisons based on soils and geomorphology suggest that age estimates likely are accurate within factors of two to three.

We consider that current estimates of parameters for the CFD faults are reasonable approximations. To portray their approximate nature, most estimates are rounded to a single significant digit, and no adjustments are made that introduce additional significant digits. For example, cumulative displacements and numbers of events could be reduced to account for possible secondary or nontectonic offsets. However, we would expect such nonprimary displacements to occur as fracturing or small offsets, which generally are difficult to recognize. In no cases have fracturing events lacking discernable offset been factored into earthquake frequency. We estimate the contribution of small offsets to be less than 20% to 25%, and some small offsets may represent primary faulting associated with moderate-sized events or distributed rupture, so a correction factor would be no more than 10% to 15%. Current interpretations include more frequent occurrence of small offsets within relatively recent time periods, strongly suggesting that older small offsets have been obscured and are unrecognizable. To a first approximation, unrecognized small offsets might balance out consideration of a few secondary or nontectonic offsets as seismogenic events. In either case, any adjustment we might make would be a minor fraction of the one-significant-figure estimates.

4.4 NOTES ON ESTIMATES FOR BURIED/BOUNDING FAULTS

Postulated buried or bounding fault sources associated with dextral shear across the CFD (Figure AAR-5) are model-driven; no direct evidence of activity is available. Estimates are thus hypothetical, with bounds deemed to cover reasonable possibilities.

Total Active Length

The following subsurface lengths were deemed reasonable for the postulated structures. For the throughgoing, regional strike-slip fault, min = dimension required to extend beyond CFD and thus qualify as a throughgoing structure; pref = midpoint between min and max; max = approximate comparison to the longest historical strike-slip ruptures in the Basin and Range province (specifically 1872 Owens Valley). For the "Highway 95 fault," length estimates are based on a general comparison to historical Basin and Range surface-faulting events (e.g., 1932 Cedar Mountain) and on constraints posed by postulated segment boundaries (i.e., intersection with the Rock Valley fault and the extensional bend at Oasis Valley). For the cross-basin fault, min = approximate dimension required for a seismic event above the background source; pref = midpoint between min and max; max = constrained by dimensions of the CFD. The north-bounding strike-slip fault is inferred to have similar dimensions and activity as the cross-basin fault.

Style and Fault Dip

As conceptualized, all buried and bounding sources are strike-slip faults assumed to be nearly vertical.

Displacement per Event/Slip Rate

These parameters are based on historical analogs and comparisons to the CFD faults. For the throughgoing, regional strike-slip fault, the slip rate was estimated as that required to be a driving fault (i.e., approximately equal to the sum of slips on CFD faults). For the "Highway 95 fault," we estimated rates required for the fault to be a partially driving fault (i.e., somewhat less than the summed slip on CFD faults). For the cross-basin and north-bounding faults, we used historical analogs and comparison to CFD faults (i.e., approximately equal to CFD faults).

4.5 NOTES ON THE 52 FAULTS THAT NRC CONSIDERS IMPORTANT

The faults listed below, which McKague et al. (1996) included as Type I faults, either were not considered or have designations that could lead to confusion. Reasons for not considering these faults and/or clarifications as to fault designation are given below.

Simonds #1 Fault

Included on Simonds et al. (1995) as a bedrock fault having an unknown age of movement; lack of geomorphic expression in bedrock is unsupportive of significant Quaternary activity; estimated Mw 5.6 (McKague et al. 1996) is less than M_{max} for our background source zone.

Simonds #2 Fault

Included on Simonds et al. (1995) as a bedrock fault having an unknown age of movement; lack of geomorphic expression in bedrock is unsupportive of significant Quaternary activity; estimated Mw 7.28 (McKague et al., 1996) is unsupportably high given the fault's 7-km length and is inferred to be a typographical error; estimated Mw should be less than M_{max} for our background source zone.

Simonds #3 Fault

Included on Simonds et al. (1995) as a bedrock fault having an unknown age of movement; lack of geomorphic expression in bedrock is unsupportive of significant Quaternary activity; estimated Mw 5.9 (McKague et al., 1996) is less than M_{max} for our background source zone.

Simonds #4 Fault

Included on Simonds et al. (1995) as a bedrock fault having an unknown age of movement; lack of geomorphic expression in bedrock is unsupportive of significant Quaternary activity; estimated Mw 5.9 (McKague et al., 1996) is less than M_{max} for our background source zone.

Simonds #5 Fault

Included on Simonds et al. (1995) as a bedrock fault having an unknown age of movement; lack of geomorphic expression in bedrock is unsupportive of significant Quaternary activity; estimated Mw 5.9 (McKague et al., 1996) is less than M_{max} for our background source zone.

Simonds #7 Fault

Included on Simonds et al. (1995) as a bedrock fault having an unknown age of movement; lack of geomorphic expression in bedrock is unsupportive of significant Quaternary activity; estimated Mw 5.9 (McKague et al., 1996) is less than M_{max} for our background source zone.

Simonds #8 Fault

Included on Simonds et al. (1995) as a bedrock fault having an unknown age of movement; lack of geomorphic expression in bedrock is unsupportive of significant Quaternary activity; estimated Mw 6.1 (McKague et al., 1996) is less than M_{max} for our background source zone.

Simonds #9 Fault

Included on Simonds et al. (1995) as a bedrock fault having an unknown age of movement; lack of geomorphic expression in bedrock is unsupportive of significant Quaternary activity; estimated Mw 5.8 (McKague et al., 1996) is less than M_{max} for our background source zone.

Simonds #10 Fault

Included on Simonds et al. (1995) as a bedrock fault having an unknown age of movement; lack of geomorphic expression in bedrock is unsupportive of significant Quaternary activity; estimated Mw 5.9 (McKague et al., 1996) is less than M_{max} for our background source zone.

Simonds #11 Fault

Figure 1-2 of McKague et al. (1996) depicts this fault as one we include as part of the No. Crater Flat fault system, whereas their Appendix A describes this as the Black Cone fault of Piety (1996), which we include as a separate fault.

Simonds #12 Fault

We include this fault as part of the North Crater Flat fault system, consistent with chapter 4.11 of the Tectonics Synthesis Report (USGS, 1996).

Boomerang Point Fault (BP)

Included on Simonds et al. (1995) as a bedrock fault having an unknown age of movement; lack of geomorphic expression in bedrock is unsupportive of significant Quaternary activity; estimated Mw 5.9 (McKague et al., 1996) is less than M_{max} for our background source zone.

Note: For Simonds #13 to #19 faults, there is a discrepancy between Figure 1-2 and Appendix A of McKague et al. (1996), with all faults apparently shifted one number (e.g., fault #13 on Figure 1-2 is fault #14 in Appendix A). The following fault names refer to their Figure 1-2.

Simonds #13 Fault

Simonds et al. (1995) depict evidence of possible Quaternary activity along the fault's southern part; as depicted, it is located within the controlled area; we include this fault as our West Dune Wash #1 fault (WD1).

Simonds #14 Fault

Geomorphic expression suggests possible Quaternary activity on this fault (Simonds et al., 1995; Bell, 1996), and it is located within the controlled area; we include this fault as our West Dune Wash #2 fault (WD2).

Simonds #15 Fault

Included on Simonds et al. (1995) as bedrock fault having an unknown age of movement; lack of geomorphic expression in bedrock is unsupportive of significant Quaternary activity; estimated Mw 5.8? (McKague et al., 1996) is less than M_{max} for our background source zone.

Simonds #16 Fault

We include most of the depicted length of this fault as part of our South Windy Wash fault (SWW). North of where it merges with SWW, it has a length of about 4 km and has

geomorphic expression (bedrock scarps) permissive of Quaternary activity. We interpret this as a secondary fault connecting the SWW and Solitario Canyon faults; we do not include it as a separate source.

Simonds #17 Fault

Included on Simonds et al. (1995) as bedrock fault having an unknown age of movement; lack of geomorphic expression in bedrock is unresponsive of significant Quaternary activity; estimated Mw 5.6? (McKague et al., 1996) is less than M_{max} for our background source zone.

Simonds #18 Fault

This is the South Crater Flat fault, which we include.

4.6 COMPARISON OF QUATERNARY AND MIOCENE DEFORMATION

The plausible tectonic models we consider relevant to Quaternary activity within the CFD (Figure AAR-1) hinge in part on the similarities between Quaternary and Miocene deformation. For example, we consider it likely that an active detachment surface may have existed at shallow depths (i.e., less than 10 km) during the Miocene, when heat flow associated with the caldera systems likely reduced the effective brittle thickness of the crust. The relative deformations of the Paintbrush Tuff (primarily the broadly exposed Tiva Canyon member) and the Timber Mountain Tuff (primarily the Rainier Mesa member) clearly indicate that Quaternary faulting within the CFD generally has occurred along structures that were more active during the Miocene. However, stratigraphic constraints are insufficient to demonstrate whether Quaternary activity represents the waning stages of Miocene activity, as has been suggested by Fridrich (1996), or whether it represents reactivation of preexisting zones of weakness within the past 5 Ma or so (the period marking significant changes in Basin and Range tectonics, including rapid uplift of the Sierra Nevada and formation of Death Valley). Wholesale differences in Miocene and Quaternary deformation in the Sliver Peak area about 100 km northwest of the CFD were documented by Stewart and Diamond (1990), who found no relation between the Miocene Esmeralda basin and the current basin configuration. Although they describe differences between Miocene and Quaternary deformation that are much greater than in the CFD, both areas lie just east of the Death

Valley/Owens Valley region within the Nevada Walker Lane and are likely to have some affinities.

Although difficult to prove, reactivation of Miocene faults during the past 5 Ma seems plausible given the regional tectonic changes, especially onset of major activity in the adjacent Death Valley region, and renewal of basaltic volcanism in the CFD. Aside from rate, Quaternary deformation appears generally similar to Miocene deformation, but several lines of evidence indicate potentially significant differences.

(a) Relative activity of the Bare Mountain and Yucca Mountain faults.

Cumulative throw clearly is much larger on the Bare Mountain fault (BM) than on any of the Yucca Mountain (YM) faults, and estimated uplift rates suggest that BM was considerably more active during the primary phase of Miocene deformation. Paleoseismic data, on the other hand, suggest that at least two YM faults (SWW and SR) have higher Quaternary rates than does BM, and the estimated summed slip across the YM faults is several times that on BM. The apparent discrepancy in Miocene versus Quaternary rates is significantly larger than what we consider reasonable bounds on estimates of Quaternary activity for these faults.

(b) Contrast in deformation of Miocene tuffs and 3.7 Ma basalts along So.

Windy Wash fault. Deformation of the tuffs involved extensive and highly variable tilting, including broad-scale, low-amplitude north-south warps, whereas the basalts are uplifted uniformly. This difference is compatible with the notion of a warmer, thinner, more-ductile crust during the main phase of deformation; it also begs the question as to what extent tilting and displacements are coeval.

(c) Age of formation of hills bounding the south end of Crater Flat. Parts of these hills are capped by slide blocks, which rest on 10.5 Ma basalts; therefore the hills have entirely formed post-10.5 Ma. This contrasts with the topography of Yucca Mountain, which must have largely formed before eruption of the Timber Mountain Tuff (assuming that tilts and major fault displacements were coeval).

(d) Difference in state of stress. From populations of fault striations, extension is interpreted to have rotated in a clockwise direction: it is inferred that during the primary phase of Miocene deformation it was WSW-ENE to nearly east-west, whereas during the Plio-Quaternary it has been NW-SE (Ander, 1984; Frizzell and Zoback, 1987).

- (e) **Relative activity of NE-striking and NW-striking bridging faults.** Northeast-striking, connecting faults show Quaternary activity in several locations, whereas northwest-striking ones rarely do. In one case (the northeast-striking connection between the Fatigue Wash and southern Windy Wash faults), Quaternary scarps trend over a bedrock ridge, producing only minor bedrock offset, which suggests that they are post-Miocene features.

4.7 SYNCHRONOUS RUPTURES

To account for possible distributed (or synchronous) ruptures involving multiple faults, we define various models that group closely spaced and/or interconnected faults into coalesced or linked fault systems. In these models, slip at depth on a defined principal structure results in distributed and/or secondary surface rupture on the faults included in a given system. Linked faults imply along-strike connection of separately defined faults (e.g., a combined Paintbrush/Stagecoach Road fault). Aside from considering combined lengths, linked faults are treated the same as independent faults. Coalesced faults imply upward-splaying fault systems, with interconnection between subparallel faults.

At the outset, we make the following points regarding our consideration of synchronous ruptures.

- Completely independent behavior of the CFD faults (with the exception of the Bare Mountain fault) seems highly unlikely, given their similarities, close cross-strike spacing (generally < 2 km), and high degree of plan-view interconnection.
- The presence of basaltic ash within extensional openings along several faults is possible indication of synchronous rupture. Without such evidence, synchronous ruptures would be more speculative.
- Similarities in timing indicated by paleoseismic data are suggestive, but not compelling, evidence for synchronous ruptures, given many uncertainties.
- Synchronicity of paleo-ruptures is ultimately unprovable. Even under ideal circumstances (e.g., tightly-constrained events based on C14 dating or dendrochronology), synchronicity cannot be distinguished from occurrences close in time, as might occur from short-term triggering.

Two methods for grouping the CFD faults into "predicted" distributed ruptures during future surface-faulting earthquakes are: (1) defining scenarios (as done by Pezzopane et al., 1996, chapter 5) for past ruptures, allowable within the constraints of paleoseismic data; and (2) defining distributed systems that incorporate the principal faults and a surrounding halo of lesser faults. Both methods capture a range of behavior.

Scenarios (Pezzopane et al., 1996, chapter 5) allow the most direct input of paleoseismic data. Assuming that distributed behavior occurs, the data can be viewed as documenting the minimum extent of events if one includes only those faults for which evidence has been described. As defined by Pezzopane (1996), the scenarios can generally be divided into east- and west-side rupture events.

Defined distributed systems, in our judgment, have distinct advantages. They (1) allow grouping of the most directly connected faults; (2) allow inclusion of all faults; (3) are stable (i.e., they don't jump around, thus avoiding open-ended complexity); and (4) are controlled by parameters of the principal structures, with small contributions to displacement by lesser structures.

Methodology for Treating Possible Synchronous Behavior

First, we assign weights (Table AAR-5) to the likelihood of independent versus coalesced behavior (Figure AAR-6) for each of our 11 defined tectonic models depicted on Figure AAR-1. In summary, the tectonic model designations are based on the following structure of our logic tree: A = buried, throughgoing right-slip fault beneath CFD; B = shear couple across CFD with bounding structure(s), but no buried cross-basin fault; C = shear couple with bounding structure(s) and buried cross-basin fault; D = basin extension without significant dextral shear structures; 1 = shallow (3 - 10 km) detachment; 2 = deep (> 10 km) detachment; 3 = no detachment.

Notes:

- (1) Examples: In Model B-1 there is a shear couple with no buried fault and there is a shallow detachment; in Model D-3 there is basin extension with no significant dextral shear structure(s) and without any detachment.

- (2) "Detachment" implies a subhorizontal zone of decoupling, but not necessarily a seismogenic structure.
- (3) For buried sources, we consider only those deemed potential sources of earthquakes larger than the maximum background earthquake of $M 6.3 \pm 0.3$.
- (4) Exception to detachment numbering: Model C-2 involves a buried cross-basin fault without a detachment. (Given a detachment >10 km, we exclude the possibility that a buried cross-basin fault would generate an earthquake larger than the maximum background earthquake.)

With one exception (model C2), the CFD faults are considered much more likely to rupture during distributed (coalesced) events than as completely independent faults (Table AAR-5) for several reasons, including the close fault spacing, anastomosing nature, similar event timing, and historical analogs. In model C2, higher weighting is assigned to independent behavior based on reasoning that an overlapping cross-basin fault likely would segment the CFD faults. Coalesced behavior is considered more likely in models containing a 3- to 10-km detachment, because such a feature would provide a straightforward mechanism for interconnection of overlying steep faults. Because most CFD faults appear to have similar dips, coalesced behavior is considered less likely with increasing depth of penetration; however, no distinction is made between models having ≥ 10 km detachment or no detachment because at those depths ruptures have extended through most of the seismogenic layer and possible mechanisms of interconnection are poorly understood.

We exclude the possibility of a third west-side system associated with an inferred major fault in central Crater Flat, because we have no evidence of Quaternary activity. We also exclude additional coalesced options on a "diminishing-returns" basis; additional options would quickly magnify the complexity of the interpretation without adding to its credibility.

Second, we define various linked and coalesced fault systems. The following CFD faults are considered in our linked and coalesced models:

WEST-SIDE FAULTS	EAST-SIDE FAULTS
SC - Solitario Canyon	PBC - Paintbrush Canyon
IR - Iron Ridge	SR - Stagecoach Road
SWW - So. Windy Wash	ELC - E. Lathrop Cone
FW - Fatigue Wash	MWV - Midway Valley
NWW - No. Windy Wash	BWR - Bow Ridge
SCF - So. Crater Flat	WD1 - West Dune Wash #1
NCF - No. Crater Flat	WD2 - West Dune Wash #2
CWW - Central Windy Wash	EB - E. Busted Butte
CCF - Central Crater Flat	
BC - Black Cone	
BM - Bare Mountain	

For cases of independent fault behavior, we make a further distinction whether some faults may be connected along strike (i.e., linked faults). Based on map patterns, we define two plausible linked systems, PBC/SR and WW/FW (Table AAR-6). PBC/SR is considered a somewhat more likely linked system than WW/FW because PBC/SR involves faults that are on line with each other, there is no obvious discontinuity in the possible linked trace, and coincident rupture during multiple events is suggested by paleoseismic data. WW/FW involves faults that do not have the same continuity, but are closely spaced and have direct splaying relations. In models that include 3- to 10-km detachment, relatively less weighting is assigned to linked behavior because a shallow detachment would result in unusually high aspect ratios (i.e., long ruptures, given their depth of penetration). In model C2, an overlapping cross-basin fault provides a mechanism for segmenting the faults, especially WW/FW, so lower weighting is assigned to linked behavior.

For cases of coalesced behavior, we divide the CFD faults into four coalesced systems (Figure AAR-4) as follows.

- **E-side:** Coalesced system including all faults on the east side of Yucca Mountain. The PBC/SR linked fault, with a slight extension to the south along ELC, forms the principal structure of the system, with all other faults secondary.
- **W-side #1:** Simple coalesced system comprising SC and IR: SC forms the principal structure, and IR is secondary. Paleoseismic studies indicate relatively low long-term rates on these two faults, so this system is the least significant in a three-system model; however, the late Quaternary rate for SC compels inclusion at a similar level.

- **W-side #2:** Coalesced system including all faults on the west side of Yucca Mountain except SC and IR. The linked SWW/FW/CWW/NWW fault forms the principal structure of the system, with all other faults secondary.
- **Bare Mountain fault (BM):** Mostly a singular fault trace, but also includes some possible distributed faulting along its northern part. BM is considered more likely to behave independently because it lacks the close spacing and interconnection of the YM faults.

We then distinguish and assign weights to four models involving rupture of different combinations of the defined coalesced systems (Table AAR-7). The principal structures of the three Yucca Mountain systems appear to have similar fault dips, and therefore are interpreted to extend to sufficient depths to be considered separate seismogenic structures. For models in which multiple coalesced systems rupture synchronously (for example, in response to external forces), they are treated as simultaneous rupture of separate structures.

Weights are assigned on a relative basis, with a higher probability of comprising fewer systems (increased coalescence) assigned to models including: first, a buried dextral fault spanning the CFD (i.e., throughgoing or cross-basin fault), because displacement on such a structure should affect all of the overlying area; and second, a 3- to 10-km detachment, because such a feature would provide a straightforward mechanism for interconnection of steep, overlying faults. Coalescence is thus considered most likely given a buried dextral fault AND 3- to 10-km detachment, less likely given a buried throughgoing fault AND >10-km detachment or no detachment, even less likely given deep or no detachment AND no buried dextral fault, and least likely given a cross-basin fault AND no detachment (i.e., $A1 > C1 > A2 = A3 > B1 = D1 > B2 = B3 = D2 = D3 > C2$).

- **One system**—CFD faults, including BM, comprise a single coalesced system; this possibility is considered only in models that include BOTH a 3- to 10-km detachment AND a buried strike-slip fault (i.e., models A1 and C1).
- **Two system**—All YM faults comprise a single coalesced system, and BM is independent; again, this possibility is considered only in models including BOTH a 3- to 10-km detachment AND a buried strike-slip fault (i.e., models A1 and C1).

- **Three systems (E-W)**-PBC/SR/ELC/BWR/MWV/GD/WD1/WD2/EB comprise an east-side system; SC/IR/SWW/FW/NWW/SCF/NCF/CWW/CCF/BC comprise a single west-side system; and BM is independent.
- **Four systems (E-2W)**-PBC/SR/ELC/BWR/MWV/GD/WD1/WD2/EB comprise an east-side system; SC/IR comprise one west-side system; SWW/FW/NWW/SCF/NCF/CWW/CCF/BC comprise a second west-side system; and BM is independent.

Geometry of Coalesced Systems

The following factors are considered.

- The overall geometry is controlled by the geometries of principal structures,
- In general, we consider 60 degrees our best estimate of dip for the principal structures, as suggested by well-constrained cross sections (e.g., Bow Ridge), bedrock fault exposures (e.g., Solitario Canyon), or geophysical data (e.g., Bare Mountain),
- If fault curvature is considered, deeper penetration would equate to shallower dip, but we eliminate this because of uncertainties (i.e., uncertainty in amount of curvature and insensitivity, given range of estimates),
- Depth of penetration is model-dependent (truncation at detachment, fault intersection, or base of seismogenic zone).

Slip Rates of Coalesced Systems

To assess slip rates for the coalesced systems, we use a simple summation of rates across strike.

4.8 M_{max} DIMENSIONS

For the local fault sources, maximum rupture dimensions basically are constrained by rupture length and downdip rupture width, RW. In some cases, RW is constrained not only from below, but also from above. Measures of maximum rupture length are provided in Table AAR-4 under the heading "active length," meaning the total length along which either

(a) rupture may extend during a single event or (b) seismic moment should be distributed as part of the slip-rate approach to recurrence (discussed below). For each fault source, the three entries for active length represent 10th, 50th, and 90th percentile values, for which corresponding weightings are 0.3, 0.4, and 0.3. When either the 10th or 50th percentile value is selected for fault length, allowable maximum rupture length follows accordingly, and weighting is renormalized.

Constraints on RW for the local fault sources include DMAX1 or DMAX2, aspect ratio (fault length/downdip width), and scenarios of truncation by either a local detachment (if one exists), by the Bare Mountain fault, or by a W-dipping fault in the case of E-dipping faults considered antithetic. For the CFD faults (Table AAR-3), the first general rule is that RW is not allowed to exceed twice the maximum rupture length (i.e., the minimum allowable aspect ratio is 0.5), based on data for earthquake slip-surface aspect ratios (Nicol et al., 1996). The second general rule for these faults is that their downdip extent is limited by a detachment, if one exists; otherwise, the lower limit is DMAX1 or DMAX2—or the plane of the Bare Mountain fault. Rules for the other local fault sources listed in Table AAR-2, including special cases, are described below.

For the "Highway 95 fault," RW is independent of any detachment, and limits on lower and upper depth are provided by DMAX2 and the Earth's surface, respectively. RW for the "No. bounding strike-slip (ss) fault" is also independent of any detachment. For this fault, we allow RW to extend from DMAX1 up to 3 km below the surface, based on the fault's lack of clear surface expression.

Four of the down-to-the-east faults listed in Table AAR-4 are considered to be antithetic to, and hence would have downdip projections truncated by, a nearby west-dipping fault. Specifically, the Black Cone (BC), Central Crater Flat (CCF), and Central Windy Wash (CWW) faults would be truncated by the Fatigue Wash (FW) fault. Similarly, the West Dune Wash 2 (WD2) fault would be truncated by the Paintbrush Canyon (PBC) fault.

Scenarios A-1, A-2, A-3

For the regional ss fault, the lower depth limit of RW, in all cases, is constrained by DMAX2. Its uppermost limit—and the lowermost limit of the other CFD faults—is either the depth of the detachment (scenarios A-1 and A-2) or, where no detachment exists (scenario A-3), a decoupling level for which we assign a depth distribution (and relative weighting) as follows:

4.5 km (0.185), 7.0 km (0.63), 9.0 km (0.185).

Scenarios C-1, C-2

For the cross-basin fault, the lower depth limit of RW is constrained by DMAX1. In scenario C-1, its upper-most limit—and the lowermost limit of the other CFD faults—is the depth of the detachment. In scenario C-2 we allow RW for the cross-basin fault to extend up to 3 km below the surface, based on the fault's lack of clear surface expression. In this scenario, DMAX1 or other general truncating rules constrain the lower depth limit of RW for the CFD faults. We accept the possibility of intersections between the cross-basin fault and the other CFD faults as the former develops under the shear couple.

Multiple-structure Coalesced Systems

In the cases of "multiple-structure coalesced systems" (Table AAR-4), that is, coalesced systems of the local faults that are allowed to rupture simultaneously in parallel, RW is constrained by DMAX1 in all cases. Although the tabulated lengths for these sources is greater than 25 km, we use DMAX1 because the expected value of rupture length for any of the individual coalesced systems is less than 25 km.

4.9 M_{\max} APPROACH

For the local fault sources, using the data in Table AAR-4, we use four approaches to estimate M_{\max} in terms of moment magnitude M : (a) M estimated from the "active length" of a fault, using either the relation for surface rupture length SRL or subsurface rupture length RLD (more below) from Wells and Coppersmith (1994) for all slip types; (b) M estimated from rupture area RA ("active length" x downdip rupture width) using the relation from Wells and Coppersmith (1994) for all slip types; (c) M estimated from fault length and slip

rate S , using the relation from Anderson et al. (1996); and (d) M calculated from seismic moment M_0 , determined from the moment equation. Note that approach (d) was not used for the regional fault sources because necessary information for single-event displacement was not available.

We refer the reader to the section on "Depth of the Seismogenic Crust" for an explanation of the moment equation and other relevant background such as DMAX1, DMAX2, and our perspective on using RA in the moment equation and in the regression equation of Wells and Coppersmith (1994).

In approach (a), we take the "active length" of the local faults (Table AAR-4) to be equivalent to estimates of subsurface rupture length (RLD) in the case of the buried or bounding strike-slip faults and to surface rupture length (SRL) for all the other cases involving the CFD faults in Table AAR-4. The correspondingly appropriate regression relation from Wells and Coppersmith (1994) is then applied. For the moment-equation approach in which RLD must be estimated for the CFD faults, data of Wells and Coppersmith (1994, their Figures 2 and 3) can be used to relate "active length" (i.e., SRL) to RLD, which is expected to have a slightly larger value. For the range of ruptures being considered, we use their mean value of 0.75 for the ratio of SRL to RLD. We consider the extra length in the subsurface (RLD - SRL) to extend symmetrically from the surface trace lengths depicted in Figures AAR-3 and AAR-4.

In approach (b), DMAX1 is used in all cases for the maximum depth constraint on downdip rupture width. In approach (d), we estimate \bar{U} , the average (subsurface) displacement over the slip surface, by $(MD + AD)/2$, where MD and AD are the maximum and average surface displacements per event, respectively, tabulated in Table AAR-4.

Table AAR-8 outlines our weighting used for the M_{max} approaches. The weighting depends on expected rupture length and on the subsurface structure involved in some of the tectonic models. In the case of rupture length, we assign 25 km to be the threshold for large earthquakes whose downdip rupture may extend to DMAX2. Whereas the RA regression of Wells and Coppersmith (1994) is used (along with DMAX1) when expected rupture length is

less than 25 km, it is not used when expected rupture length is 25 km or greater, and its weight is redistributed to the moment-equation approach. We downweight the rupture-length/slip-rate approach because many of the local faults have slip rates lower than the range of data regressed by Anderson et al. (1996). Given a local detachment at 3 to 10 km depth, we downweight the rupture-length approaches and redistribute weight to the moment-equation approach. For the cases of multiple-structure coalesced systems, for which slip-rate information is not available, weight for the rupture-length/slip-rate approach is redistributed to the rupture-length approach.

4.10 RECURRENCE APPROACH

For the local sources, we use two approaches for recurrence modeling: (1) a slip-rate approach and (2) a recurrence-interval approach. These approaches are assigned weights of 0.6 and 0.4, respectively, for all the local fault sources for which both slip-rate and recurrence-interval data are provided in Table AAR-4. Where only slip-rate or recurrence-interval data are provided, the corresponding approach is weighted fully.

Fault-specific recurrence relationships are generated from the slip rates using the methodology of Youngs and Coppersmith (1985) and assuming constant moment rate. Whether using the slip-rate or recurrence-interval approach, we assign the characteristic earthquake model a weight of 0.7 and the "modified exponential" model (Youngs et al., 1987) a weight of 0.3. For both the characteristic and "modified exponential" models, M_{max} for a fault is assumed to be uniformly distributed in the range $M_{max} \pm 1/4$ magnitude unit, with $M_{max} + 1/4$ being the upper-bound magnitude, m .

Where recurrence intervals are provided, we use the method of Youngs and Coppersmith (1985) that assumes a constant frequency of earthquakes above some specified size. Given M_{max} for a fault, the cumulative frequency for earthquakes of $M_{max} - 1/4$ is set equal to the inverse of the tabulated recurrence interval, which is interpreted to represent the frequency of characteristic-size events for the fault.

Based on seismicity recurrence calculations provided (Section 3.1 contains a description of the methodology used to calculate seismicity parameters) from diverse regional area sources within 300 km of Yucca Mountain, our assessed distribution for the b-value (and relative weighting) in applying the methodology of Youngs and Coppersmith (1985) are:

0.80 (0.3), 1.00 (0.4), 1.20 (0.3).

5.0

REGIONAL SOURCES AND LOCAL BACKGROUND SOURCE ZONES

5.1 CATALOG

For all calculations, we place full weight on Version 7 of the Yucca Mountain earthquake catalog, which consists of primary events derived using the declustering algorithm of Veneziano and Van Dyck (1985). We believe their algorithm is statistically rigorous and far superior to declustering approaches that use fixed space-time windows as a function of mainshock size, given that mainshocks are known to generate clusters having characteristics that differ greatly in space, time, and size—even in the same general area. Our judgment here is guided by substantial experience of one team member with the practical problems of declustering earthquake catalogs (W.J. Arabasz presentation at SSC Workshop 2).

Completeness intervals adopted for the 100-km-radius declustered catalog are those proposed by I.G. Wong (handout to team seismologists at SSC Workshop 4), based on the completeness technique of Stepp (1972). We examined "Stepp" plots specifically for the Version 7 catalog before adopting the intervals. The completeness intervals are: 2.5-2.99 (1979 to date), 3.0-3.49 (1979 to date), 3.5-3.99 (1961 to date), 4.0-4.49 (1934 to date), 4.5-4.99 (1934 to date), 5.0-5.49 (1924 to date), 5.5-5.99 (1924 to date), and 6.0-6.49 (1914 to date). Where seismicity is sampled from regions extending beyond 100 km, we gave approval to use the same completeness intervals, recognizing that any incompleteness at the lower magnitude end would simply require selecting a higher minimum magnitude in the recurrence modeling. For the 100-km-radius area, the minimum magnitude we accepted for recurrence modeling was 2.5, with a weight = 0.3, and 3.0, with a weight = 0.7.

To delimit seismicity induced by underground nuclear explosions (UNEs) in the Nevada Test Site, we eliminate from the catalog all seismic events that lie within a zone defined by Rogers et al. (1987, their Figure 2) that occurred post 1950.

5.2 BACKGROUND SOURCE ZONES COUPLED TO REGIONAL SOURCES

We define our background source zones to lie within a radius of 100 km of the repository site. Three alternatives in which background source zones are coupled to regional area sources are depicted on Figures AAR-7 to AAR-9. A fourth alternative, based on spatially smoothed seismicity, is discussed in the next section. For the first three scenarios, large regional sources are defined for capturing seismicity. Seismicity is first gathered from the entirety of each regional source (except the area of exclusion for UNEs and associated seismicity). It is then normalized per unit time and unit area and assigned to the corresponding sector of the area source that lies within 100 km of the repository site—including the 20-km-radius "host zone" (explained below).

In scenario I (Figure AAR-7), we depict three background source zones that form parts of an eastern California shear zone (1), a Nevada Walker Lane belt (2), and the northern Basin and Range (3A), respectively. In scenario II (Figure AAR-8), the Walker Lane belt is not considered distinct from the northern Basin and Range (3B). In scenario III (Figure AAR-9), the southern Nevada transverse zone (3C) (e.g., Rogers et al., 1991) is taken as a distinct subarea of the northern Basin and Range, parts of which lie both to its north and south (forming zone 3D).

5.3 BACKGROUND SOURCE ZONE BASED ON SPATIALLY SMOOTHED SEISMICITY

Given the spatial variability of epicentral density in the declustered Yucca Mountain catalog, we also consider a background source zone based on spatial smoothing of declustered seismicity within 100 km of the repository site. Values for the kernel width, h (i.e., $\frac{1}{2}$ the distance seismicity effectively can be smoothed away from its location), and corresponding

weighting are as follows: 5 km (0.25), 10 km (0.5), 20 km (0.25) (Figure AAR-10b). Where a prior b-value is used, we use the same distribution (and weighting) described for the recurrence modeling of our regional and local fault sources: 0.80 (0.3), 1.00 (0.4), 1.20 (0.3).

5.4 HOST ZONE

We define a local background source region, with an M_{\max} of 6.3 ± 0.3 , as extending in a 20-km radius from the repository site, within which we are confident that we have identified all fault-specific sources capable of generating earthquakes larger than the background. This "host zone" is defined only for assigning its own M_{\max} . Recurrence rates derive from the applicable scenario for the background source zone within which the host zone is embedded. We use data and the results of modeling presented by Pezzopane and Dawson (1996, chapter 9) for the maximum background earthquake to assess the following distribution for M_{\max} of the host zone (with corresponding weighting):

6.0 (0.3), 6.3 (0.4), 6.6 (0.3).

5.5 M_{\max} FOR BACKGROUND SOURCE ZONES > 20 km

Beyond 20 km—and out to 100 km—we admit the possibility that there may be faults (buried, unrecognized, or not included in our inventory of fault sources because of an interpreted lack of Quaternary slip) that may be capable of generating earthquakes larger than $M = 6.3 \pm 0.3$. An example would be the Gravity fault, for which a Quaternary displacement history is not established and which we interpret to be distinct from, but possibly related to, the Ash Meadows fault. Accordingly, we assign a higher M_{\max} to our background source zones from 20 to 100 km radial distance from the repository site to account for these potential sources. The distribution also is used to model seismicity rates for the regional sources.

For our assessment of this M_{\max} we used data from Table AAR-1 for regional fault sources within 100 km of Yucca Mountain (excluding the Death Valley and Furnace Creek faults and the linked case for the Amargosa River/Pahrump faults). From these data we constructed

cumulative distributions of maximum rupture lengths (using preferred and maximum values only) and slip rates. Simply put, we use what can be seen as representative of what cannot be seen or has been missed. (Simultaneously, we considered dimensional arguments for possibly unrecognized intra-basin faults.)

Using the above data and the same weighted M_{\max} approaches used for the regional faults, our resulting distribution for the generic M_{\max} for all background sources > 20 km (with corresponding weighting) is:

6.6 (0.3), 6.9 (0.4), 7.3 (0.3).

5.6 WEIGHTING OF ALTERNATIVES FOR BACKGROUND SOURCE ZONES

Our weighting scheme for alternative background source zones takes into account the stationarity of seismicity vis-à-vis a 10,000-yr time frame. We give higher weight to scenarios in which seismicity rates near the site are similar to those in distinct regional zones in which regional seismicity (mainshocks per unit time and area) is interpreted to be representative of a stationary pattern over thousands of years. Thus, spatially smoothed seismicity, which reflects localization of seismicity from the short instrumental time sample, is down-weighted. In our section on Tectonic Models, we discuss the uncertain relative influence on the regional stress field of WNW-ESE Basin and Range extension, NW-SE dextral shear, and general N-S basal traction and/or horizontal compression. This uncertainty leads us to give equal weight to the three scenarios based on regional seismotectonics. Our weights, then, are:

- 0.3: Scenario I (Zones 1, 2, 3A)
- 0.3: Scenario II (Zones 1, 3B)
- 0.3: Scenario III (Zones 1, 3C, 3D)
- 0.1: Spatially Smoothed Seismicity.

5.7 NON-INCLUSION OF A VOLCANIC ZONE

We considered the need to account for seismicity associated with episodic volcanism in the Crater Flat domain and concluded that it is unnecessary to include a volcanic source zone in

addition to a spatially coincident background source zone. Our reasoning is as follows: An appropriate M_{\max} for volcanic-related seismicity in the Yucca Mountain region is M 5.0 to M 5.5 (Smith et al., 1995, 1996). Given that the project definition of seismogenic implies the generation of earthquakes of $M \geq 5.0$, the question becomes, "How often are volcanic-related earthquakes of M 5.0 to M 5.5 likely to occur in the Crater Flat domain?"

According to (Crowe et al., 1995, p. i), postcaldera basaltic volcanism in the Yucca Mountain region represents "one of the lowest eruptive rates in a volcanic field in the southwest United States." More specifically, estimates of the maximum or worst-case recurrence (minimum interevent time) for volcanic events in the Yucca Mountain region are 8.0×10^{-6} events yr^{-1} ($1/N = 125,000$ yr) using homogeneous Poisson models and 8.4×10^{-6} events yr^{-1} ($1/N = 119,000$ yr) using nonhomogeneous Poisson models (ibid., p. 7-2f).

We examined the recurrence rates for background seismicity in the Yucca Mountain region calculated for DOE's 1994 design study for the ESF (I.G. Wong presentation at SSC Workshop 3). The cumulative annual number of events per km^2 above $M_{\min} = 2.5$ and with $M_{\max} = 6.5$ is given by $\log N = -1.37 - 0.83M$. (We assume equivalency between M_L and moment magnitude for the magnitude range being considered.) From the above, the expected annual number of events per km^2 in the range $5.0 \leq M < 5.5$ is 1.8×10^{-6} events $\text{yr}^{-1} \text{km}^{-2}$.

For comparison, we provisionally considered a volcanic source zone in the southwestern part of the CFD that has an area of approximately $1.4 \times 10^3 \text{ km}^2$ smaller (and hence containing more events $\text{yr}^{-1} \text{km}^{-2}$) than the area of potential volcanism considered by Crowe et al. (1995). The number of background seismic events in the range $5.0 \leq M < 5.5$ within our volcanic source zone would be 1.8×10^{-6} events $\text{yr}^{-1} \text{km}^{-2} * 1.4 \times 10^3 \text{ km}^2$ or 2.52×10^{-3} events yr^{-1} ($1/N = 397$ yr).

From the above, we compared the rate of background seismic events within our volcanic source zone (2.52×10^{-3} events yr^{-1}) to the estimated worst-case rate of volcanic events with which earthquakes would be associated— $(8.0-8.4) \times 10^{-6}$. The rate of volcanic events is two to three orders of magnitude lower than the rate of M5.0 to M5.5 background earthquakes

within our volcanic source zone—beyond the precision with which background seismicity can be estimated.

Thus, we concluded that there is no need to define a volcanic source zone in addition a spatially coincident background source zone. Background earthquakes in the range of M5.0 to M5.5 sufficiently represent, for probabilistic vibratory ground-motion hazard, the rare episodic occurrence of volcanic-related earthquakes in the same magnitude range.

6.0

FAULT DISPLACEMENT CHARACTERIZATION

6.1 GENERAL REMARKS

Our methodology for characterizing the potential for fault displacement at Yucca Mountain has been influenced greatly by the presentations and interactions at SSC Workshops 4, 5, and 6. In order to characterize, in a probabilistic way, the amount, frequency, and variability of future fault displacements at a point, we use two basic approaches: (i) an earthquake approach that builds on our seismic source characterization for ground-motion hazard and (ii) a displacement approach in which the observed geology guides the expectation of the long-term outcome.

From the outset, we have held the view — based chiefly on empirical observations and a substantial literature in structural geology (see, for example, the February-March 1996 Special Issue of the Journal of Structural Geology) — that scaling relationships variously involving single-event slip, fault dimension, and total cumulative displacement on a fault offer a practical way to characterize fault-displacement potential. This applies particularly to a displacement approach.

We recognize that any use of scaling relationships in the context of earthquakes and faulting can be expected to invite scrutiny and concern. There is ongoing debate about the scaling of earthquake slip with source dimensions, particularly as it relates to implications for underlying mechanics and the dynamics of rupture propagation (e.g., Bodin and Brune, 1996,

and references therein). Controversy about scaling relations for large earthquakes is a notable case in point (Romanowicz and Rundle, 1993).

In our final methodology we have taken care to use only scaling relations that are empirically founded and defensible from documented observations in the Yucca Mountain region and/or by supporting reference to the published literature. We specifically avoid assumptions about the underlying physics of fault rupture, and we limit the validity of our empirical scaling relations to the size range and structural framework of faults and fractures at Yucca Mountain. We elaborate in Section 6.2.

6.2 THE ISSUE OF TRIGGERING

Another issue that warrants comment at the outset is the triggering of fault slip and the relative importance of static versus dynamic triggering, an issue raised at SSC Workshops 5 and 6 and a subject attracting considerable attention since the 1992 Landers, California, earthquake (see Gomberg et al., 1997, and references therein). The question here is whether our characterization of fault-displacement potential adequately accounts for the possibility of both types of triggering.

Static triggering refers to seismic slip hypothesized to result from static-stress changes which are caused by fault slip elsewhere and which increase the stress on a fault or fault segment so as to move it closer to a threshold of frictional failure, generally specified by the Coulomb failure criterion (see King et al., 1994, and Simpson and Reasenber, 1994, for overviews). Such static-stress changes can act oppositely to retard failure, but our focus here is on triggering. Dynamic triggering, which also involves frictional instability, refers to the hypothesized initiation of seismic slip by transient stress/strain changes associated with the passage of seismic waves, either from near or distant earthquakes (e.g., Gomberg and Bodin, 1994; Gomberg, 1996; Gomberg et al., 1997).

Gomberg et al. (1997) usefully distinguish two types of potential triggering: in the first, termed a clock-advance type, triggering (static or dynamic) simply advances the time of fault slip that would have eventually happened anyway; in the second, termed a new-seismicity

type, triggering (static or dynamic) induces fault slip that would not otherwise have occurred under a constant background load. Triggering from near earthquakes (tens of kilometers) may result from either static or dynamic stress/strain changes or both, whereas triggering from remote earthquakes (hundreds to thousands of kilometers) would be attributed to dynamic triggering (Gomberg, 1996; Gomberg and Davis, 1996).

For the Yucca Mountain fault-displacement characterization, we can separately consider (a) the triggering of a primary faulting event on one of the principal faults and (b) the triggering of secondary/distributed fault slip on any fault or fracture at Yucca Mountain. For both (a) and (b), instances of clock-advance triggering (static or dynamic) would have no effect on our probabilistic characterization of fault-displacement potential over the long-term because the relative timing of displacement events would be altered, not their average frequency over the long term, and estimates of the amount of displacement would not change.

What about new-seismicity triggering? First, we emphasize that such a hypothesis is still in a formative stage. Observational evidence presented in its support includes the triggering of small-magnitude earthquakes interpreted to be in excess of background seismicity at Long Valley, California, and at The Geysers, California (see Gomberg et al., 1997, p. 302). Gomberg et al. (1997) show qualitatively by using model studies that the new-seismicity hypothesis is plausible under conditions of dynamic triggering, but they caution against using their results to make quantitative interpretations or predictions. Further, the potential for dynamic triggering appears to depend strongly on site characteristics and response (Gomberg, 1996).

For the case of principal faulting, we ask the question, What are the effects on our fault-displacement characterization if triggering (static or dynamic) were to cause surface-rupturing events that otherwise would not have occurred? Logically, this implies surface rupture on a fault not included in our inventory of faults that have a nonzero probability of being seismogenic. Allowing, for the sake of argument, that such new-seismicity triggering is plausible, we reason that its relative long-term probability of occurrence in the future would be similar to that in the past. Because our inventory of principal faults is based on the observed geology, which reflects ample opportunity during

the Quaternary epoch for dynamic or static triggering of surface-rupturing events on potential sources of principal faulting not now accounted for, we consider the probability of triggering new principal faulting to be negligible.

If one pushes the concept of new-seismicity triggering to have it add to the number of surface-rupturing events on our inventoried principal faults, we again reason that its long-term relative probability of occurrence in the future, would be similar to that in the past. As we describe later (see Sections 6.3 and 6.6), our displacement approach to surface displacement on a principal fault effectively accounts for the average relative frequency of any surface displacement, regardless of its cause. In our lower-weighted earthquake approach to principal faulting (Section 6.5), the frequency-magnitude relation of earthquakes on a principal fault is constrained by the average recurrence interval and/or slip rate from paleoseismology, which implicitly accounts for the aggregate long-term history of all displacement events, however they are produced.

Continuing this line of questioning, we examine the case of secondary/distributed fault slip and question what effects new-seismicity triggering (static or dynamic) would have on our characterization. Here too, our displacement approach (Sections 6.3 and 6.7) effectively accounts for all displacements, however they are produced. The last case remaining to be examined is that of our earthquake approach to secondary/distributed faulting on faults and fractures that are not principal faults (Section 6.8). In this case, our method accounts for all earthquakes on identified fault sources and in background source zones out to 100 km that represent opportunities for static or dynamic triggering. Whether or not triggering ensues is assessed probabilistically using empirical approaches. Admittedly, we do not account for plausible new-seismicity triggering by remote earthquakes at distances greater than 100 km. The magnitude of such earthquakes would have to be reasonably large for dynamic stress/strain changes to exceed a triggering threshold (Gomberg and Davis, 1996). Faced with the epistemic uncertainties associated with this particular case, we downweight it in our logic tree.

6.3 ORDER OF PRESENTATION

In the following sections, we first lay the groundwork for our fault-displacement assessment by defining terms and notation, presenting scaling relations, and describing our analysis of variability of slip at a point. We then proceed to describe our separate logic trees for principal and distributed faulting, beginning with an overview followed by sequential description of (1) our earthquake approach to principal faulting, (2) our displacement approach to principal faulting, (3) our point-estimate method (a displacement approach) for distributed faulting, and (4) our principal-distributed-faulting method (an extension of our earthquake approach) for distributed faulting. Finally, we provide the assessments for the nine test calculation sites.

In applying our logic trees, we distinguish between sites subject to principal faulting (on potentially seismogenic faults) and sites subject to distributed faulting only. Sites in the first category are subject to the hazard of both principal and distributed faulting.

6.4 NOTATION

A potential pitfall we encountered in the fault-displacement analysis is the use of ambiguous terms, so we emphasize the importance of careful notation. In the case of "average displacement," for example, there are clear physical distinctions between the average displacement over the slip surface (i.e., the area of a fault engaged in a rupture event), the average displacement at the ground surface along a rupture, and the average displacement at a point on a fault (at or near the surface) over many displacement events at that point.

In our notation, both for fault displacement and ground-shaking hazard, we try to be as consistent as possible with (1) terms defined by Wells and Coppersmith (1994), whose regression relations we frequently refer to, (2) the notation and terms used most recently by R.R. Youngs and the SSC Facilitation Team (presentations at SSC Workshop 6), and (3) notation used in citations to which we refer the reader. In some cases, however, we give preference to special notation needed to emphasize clear thinking about what is being described and analyzed. For example, we use the term \bar{U} for the average displacement over

the slip surface to prevent any possible confusion with other terms for displacement involving the letter D. Following usual convention, a bar over a symbol signifies an average value.

We use superscript notation for some special cases in which the largest value of a parameter has particular importance, in part to avoid confusion with the commonly used suffix "max." (Consider the term "Dmax," which has been used extensively during the SSC Workshops to indicate a maximum displacement, but variously defined.) Some scaling relations involving fault length are only valid for total fault length, which we emphasize by using the term L^{total} . Similarly, the value of maximum surface displacement, MD, that is estimated for the largest displacement event on a fault (generally involving L^{total}) we designate as MD^{max} .

The following is a basic outline of notation used. More complete explanation is given as the terms arise in subsequent discussion.

- AD = average (surface) displacement
- AR = aspect ratio (L/W)
- D or d = general terms for a displacement on a fault
- Dcum = total cumulative displacement (herein meaning post-Tiva Canyon Tuff)
- D_E = single-event displacement on a fault at or near the surface
- \bar{D}_E = average value of D_E at a point on a fault over many displacement events
- L = general term for the length or longest horizontal dimension of a fault or rupture
(equivalent to RLD in the case of a single rupture)
- L^{total} = total length of a fault
- M = magnitude (herein meaning moment magnitude)
- MD = maximum (surface) displacement
- MD^{max} = expected value of MD corresponding to the largest displacement event on a particular fault
- P[C] = probability of being capable of slip (i.e., slip susceptibility) given the contemporary stress field at Yucca Mountain
- P[S] = probability of being seismogenic (i.e., of generating an earthquake of $M \geq 5.0$)
- P[slip|pf] = probability of secondary/distributed faulting, given principal faulting on a nearby fault
- QSR = Quaternary slip rate
- RA = rupture area
- RI = recurrence interval
- RLD = subsurface rupture length (rupture length at depth)

RW = rupture width (downdip dimension)

SR = slip rate

SRL = surface rupture length

\bar{U} = average displacement over a slip surface (i.e., the area of a fault engaged in a rupture event)

W = general term for the width or downdip dimension of a fault

λ_{DE} = frequency at which displacement events occur

6.5 SCALING RELATIONS

In this section we provide a basis for adapting scaling relations that can be used for characterizing fault-displacement potential on structures ranging from small fractures upward to the unsegmented relatively small faults ($L < 25$ km) with relatively small cumulative displacement (< 0.5 km) at Yucca Mountain.

We emphasize that we use only scaling relations that are empirically founded, reasonably robust, and which can be adopted without critical assumptions about the underlying physics of fault rupture. We recognize that some of the scatter in data distributions that control the scaling relations we use undoubtedly arise from the kind of complications in earthquake source mechanics discussed by Bodin and Brune (1996)—such as might be expected, for example, from dynamic rupture propagation with spatially varying stress drops, as opposed to quasi-static constant-stress-drop modeling.

The following logic is used to develop our scaling relations: (1) for the Yucca Mountain faults and fractures to be considered, and based on empirical observations alone, a linear approximation can be justified for the scaling of single-event slip \bar{U} with fault rupture length L ; (2) empirical observations over a wide range of scales show that total cumulative displacement D_{cum} on a fault scales linearly with total fault length L^{total} ; (3) given (1) and (2), \bar{U} should scale linearly with D_{cum} when $L = L^{total}$. We show how knowledge of D_{cum} on a fault or fracture can provide a practical basis for scaling the likely amount of slip on that feature during a future displacement event.

\bar{U} Versus L

Abundant data summarized by Abercrombie (1995, her Figure 11), among others, provide an empirical basis for relating seismic moment to the cube of source dimension—without any assumption about stress drop—over the range from 10 m to at least 10^4 m. The measurements of source dimension are based mostly on corner frequencies from shear-wave spectra, such that each represents the radius r of an equivalent circular fault. Based on the moment equation, the distribution of these data imply that \bar{U} , on average, scales linearly with r , and similarly \bar{U} can be inferred to scale linearly with rupture length L for roughly equidimensional faults in this range of source dimensions. Thus we adopt a relation of the form, $\bar{U} = \alpha * L$, where α is the constant of proportionality.

Let us be clear. We are not arguing for a model-dependent linear scaling of \bar{U} with L (a so-called L model), which we recognize to be controversial, particularly for large earthquakes (Romanowicz and Rundle, 1993; Bodin and Brune, 1996). Rather, we argue that a linear relationship is a reasonable approximation for the fault sizes we are considering—based on the abundant earthquake source data summarized by Abercrombie (1995).

We derived an empirical value of α for the Yucca Mountain local faults using data in Table AAR-4 (preferred values for independent faults, Bare Mountain fault excluded). In order to compile consistently paired values of displacement and rupture length for regression, the data were first corrected in the following way. Values of MD, the maximum surface displacement per event along a fault (labeled Dmax in Table AAR-4), were converted to \bar{U} using Wells and Coppersmith's (1994) modal value 0.76 for the ratio \bar{U}/MD . Also, we converted the tabulated values of total fault length (labeled active length in Table AAR-4), which were originally assessed as estimates of SRL, to RLD using Wells and Coppersmith's (1994) result that the expected ratio of SRL/RLD is 0.75. Applying the latter correction is appropriate insofar as all the SRL values for the independent faults in Table AAR-4 are within the range of data from which the expected ratio was originally estimated (see Wells and Coppersmith, 1994, p. 985).

Given paired values of \bar{U} and L^{total} for 19 faults, we followed guidance from R.R. Youngs of the Facilitation Team to derive an empirical estimate of $3.69 (\pm 1.10) \times 10^{-5}$ m/m for α from the mean value of $\log(\bar{U}/L^{\text{total}})$ (see equation 1, Table AAR-9). This procedure was followed in order to allow the Facilitation Team to estimate aleatory uncertainty in an appropriate form. For comparison, we performed similar calculations using data from Pezzopane and Dawson (1996, chapter 9), who plot Quaternary displacement per event versus maximum fault length for six Yucca Mountain faults (their Figure 9-19). To convert their displacement values to \bar{U} , we interpreted them as estimates of average surface displacement AD and used Wells and Coppersmith's (1994) modal value 1.32 for the ratio \bar{U}/AD . Processing Pezzopane and Dawson's six paired values of displacement and fault length in the form of $\log(\bar{U}/L^{\text{total}})$, α = their values of "maximum fault length" $3.42 (\pm 1.08) \times 10^{-5}$ m/m, taking L to be estimates of SRL.

For our logic tree, we adopt $\alpha = 3.69 \times 10^{-5}$ m/m derived from our own data—both for internal consistency and because of our larger data set. Because the data are specific to the Yucca Mountain faults, we prefer the result to other values found in the literature. Cowie and Scholz (1992c) cite values for α ranging from $\sim 1.5 \times 10^{-5}$ for continental plate boundary earthquakes to $\sim 1.0 \times 10^{-4}$ for intraplate earthquakes, including an estimate of $\sim 2.0 \times 10^{-5}$ for earthquakes in the northern Basin and Range.

Dcum Versus L^{total} , General Relation

The basis for the linear scaling of cumulative displacement Dcum with total fault length are developed at length by Cowie and Scholz (1992a,b,c). More recently, rigorous statistical testing by Clark and Cox (1996) of 11 worldwide data sets of $\log(\text{Dcum})$ versus $\log(L^{\text{total}})$, for fault populations ranging in length from tenths of a meter to hundreds of kilometers, confirm a linear relationship between fault displacement and length within each data set. (See McKague et al., 1996, for evidence of the linear scaling of Dcum with fault trace length for faults in the general Yucca Mountain region.)

Following the conventional analysis of Dcum versus L in log-log space, we seek an empirical relation of the form, $\log(\text{Dcum}) = K + \log(L^{\text{total}})$, where K is a constant. In terms of the alternate scaling factors P (Clark and Cox, 1996) and γ (Cowie and Scholz, 1992 b, c),

$P = 10^{-K} = 1/\gamma$. We derived an empirical value of K for the Yucca Mountain faults using data in Table AAR-4 (preferred values for independent faults, Bare Mountain fault excluded). The values of D_{cum} (labeled total displacement in Table AAR-4) consistently represent total cumulative displacement of the Tiva Canyon Tuff. As we did in relating \bar{U} to L^{total} , values of total fault length were first converted to RLD. The resulting regression of 16 available paired values of D_{cum} and L^{total} yielded a best-fit value of $K = -1.58$ (see Table AAR-9 for regression parameters), equivalent to $P = 38$ or $\gamma = 2.6 \times 10^{-2}$ m/m. We examined, but decided not to regress 6 paired values of D_{cum} and L^{total} presented by Pezzopane and Dawson (1996, chapter 9) in their Figures 9-19 and 9-20 because those data are presented as only preliminary.

D_{cum} Versus L^{total} for Small Faults and Fractures

Available data and well-constrained trends indicate that D_{cum} on small faults and fractures appears to be systematically smaller than that estimated by extrapolating the scaling with length from larger faults (Clark and Cox, 1996; Cowie and Scholz, 1992b). We accept this empirical observation.

Based on data in Clark and Cox (1996, their Figure 1) and the range of our data, we judge that our scaling constant for D_{cum}/L derived in the previous section can be reliably applied only for L greater than about 3 km and D_{cum} greater constant for than about 75 m. For smaller faults and fractures—down to the scale lengths of features possibly of engineering concern in the repository, we use the data of Clark and Cox (1996) to assess the following distribution for the scaling factors (and corresponding weights), where the minimum value of P is that observed from the data set of the Yucca Mountain faults:

$$\begin{aligned} K &= -1.58 [P = 38; \gamma = 2.63 \times 10^{-2}] \text{ (weight = 0.3)} \\ K &= -2.18 [P = 150; \gamma = 6.67 \times 10^{-3}] \text{ (weight = 0.4)} \\ K &= -2.70 [P = 500; \gamma = 2.00 \times 10^{-2}] \text{ (weight = 0.3)} \end{aligned}$$

\bar{U} (and MD^{max}) Versus D_{cum}

Given the relations: (1) $\bar{U} = \alpha * L^{total}$ and (2) $\log(D_{cum}) = K + \log(L^{total})$, straightforward substitution leads to (3) $\log \bar{U} = \log \alpha - K + \log(D_{cum})$ when $L = L^{total}$. This in turn can be expressed in the form $\bar{U} = \beta * D_{cum}$, where $\beta = \log^{-1}(\log \alpha - K)$. For small faults and

fractures. our distribution on K transforms into the following values (and weights) on β (m/m):

$$1.40 \times 10^{-3} (0.3), 5.59 \times 10^{-3} (0.4), 1.85 \times 10^{-2} (0.3).$$

The restriction that $L = L^{\text{total}}$ implies that the assessed value of D_{cum} should be the largest value for the entire fault. Thus, the scaling we have derived is fundamentally tied to maximum values associated with a maximum displacement event, which is equivalent to a maximum-magnitude earthquake on a fault. In both circumstances, expected parameters for smaller-size events are scaled from those of the maximum event using other information.

Because we are concerned with fault-displacement characterization at or near the surface, we use the parameter MD^{max} , the value of MD corresponding to the maximum displacement event on a particular fault, instead of \bar{U}^{max} for that same event. We relate the two using Wells and Coppersmith's (1994) modal value of 0.76 for the ratio \bar{U}/MD such that, for the relatively small-displacement faults at Yucca Mountain ($D_{\text{cum}} < 500\text{m}$), $MD^{\text{max}} = 1.32 * \bar{U}^{\text{max}}$ or, by substitution, $MD^{\text{max}} = 1.32 * \beta * D_{\text{cum}}$.

QSR Versus D_{cum}

In our point-estimate method for distributed faulting, we require estimates of Quaternary slip rate QSR on a secondary fault or fracture, given an observation of D_{cum} . Here, we develop a regression relation between QSR and D_{cum} based on selected paired values in Table AAR-4 for the local Yucca Mountain faults. We use the median values listed for 11 of the 19 independent faults, excluding the Bare Mountain, E. Lathrop Cone, East Busted Butte, Midway Valley, and West Dune Wash (1 and 2) faults. The Bare Mountain fault is excluded because we judge it to be less relevant than the Yucca Mountain faults and it is an extreme outlier if used. Data for the latter five faults are excluded because their slip rates are based on relative comparisons of geomorphology, rather than on direct paleoseismic information.

Using the 11 paired values of QSR and D_{cum} , we performed a linear regression of QSR (mm/yr) on D_{cum} (m), constraining the intercept to be zero, and derived a value of 3.26

$(\pm 1.72) \times 10^{-5}$ mm/yr/m for the slope coefficient. Statistical parameters for the regression are given in Table AAR-9.

6.6 DISPLACEMENT AT A POINT

A key part of the methodology for fault-displacement characterization is assessing the variability of slip at a point—both (1) as a function of position along strike of the fault, given the size of an event, and (2) variability of slip at the same point from event to event. Of the techniques presented and evaluated to date (summarized in presentations by R.R. Youngs at SSC Workshops 5 and 6), we are satisfied with available solutions for (1), but not (2).

The method developed by the Ake, Slemmons, McCalpin (ASM) team is well suited for estimating variable slip along strike, scaled to the maximum surface displacement MD for a given event (see summary of fault-displacement-hazard methodologies by SSC Facilitation Team, SSC Workshop 6, Figure 5; see also Appendix F this volume). The statistical averaging inherent in the method is realistic, and we see no reason to use an alternate approach that is more deterministic. We considered alternate shape functions to the elliptical displacement profile of the ASM model. Cowie and Scholz (1992a), for example, describe a profile predicted to taper gradually toward the fault tip; they also show normalized displacement profiles for faults in Japan and Britain that are relatively linear from fault-center to fault-end. Nicol et al. (1996), on the other hand, show normalized profiles for restricted faults (i.e., those that intersect the surface or closely approach other faults) whose envelope follows the elliptical shape of the ASM profile. In the end, we determined the ASM model is sufficient for the use we make of it in our logic tree (1) in our earthquake approach to principal faulting (Figure AAR-16) and (2) in assessing distributed faulting at sites where principal faulting also occurs (Figure AAR-23). We adopt the statistical relationships to repeat the ASM model presented in Appendix H, Section H.3.1.

In analyzing the problem of variability of slip at a point from event to event, we observed that, in aggregate, the displacement measurements in the many fault trenches at Yucca Mountain, scaled to MD^{max} on each fault, reflect an exponential-like distribution. This appears to be a combined result of both temporal and spatial variability. We proceed to

describe our analysis and use the results as a key basis for assessing the conditional probability for displacement exceedance.

We adapt and extend the approach used by the Doser, Fridrich, Swan (DFS) team (presentation at SSC Workshop 5; see also Appendix H this volume). The DFS team made a composite of displacement data measured in trenches throughout the Yucca Mountain region and summarized by Pezzopane et al. (1996, chapter 5) in their Table 5-1. Each displacement was normalized to the average from its same trench, and data were then pooled from all trenches. We note that the true average slip over many events at the same point is poorly estimated when the number of observations in a single trench is small. We reasoned that a more robust basis for normalizing the displacement measurements would be to compare them to some independent measure, and we selected MD^{max} , the expected value of MD corresponding to the largest displacement event on that fault.

First, we used the same multiple approaches specified in Figure AAR-16 of our logic tree (but using only median parameter values) to get a weighted-average estimate of MD^{max} for each of the nine faults associated with the 19 trench summaries in Table 5-1 of Pezzopane et al. (1996, Chapter 5). Second, we normalized each of 82 available displacement measurements (excluding the Rock Valley fault) to a corresponding value of MD^{max} . Third, we constructed both a probability density function (PDF) and a cumulative distribution function (CDF) for the combined data, shown here in Figure AAR-11. We discuss these results presently. Fourth, as a test, we carefully examined the trench locations with respect to their along-strike location and used data only for nine of the 19 trenches that were unambiguously located along the central half of a fault to construct a separate PDF-CDF combination. Again, distributions similar to those in Figure AAR-11 resulted. For greater robustness, we chose to use the data from all 19 trenches. The data are listed in Table AAR-10.

Regarding Figure AAR-11, one might ask, 'how can the ratio D/MD^{max} exceed 1.0, as plotted on the abscissa?' Note, as described in the preceding paragraph, that MD^{max} for each fault is a weighted-average from different approaches of the expected maximum displacement and that central values were used in the calculations. Thus epistemic uncertainty in the estimate

and randomness in the process allows the observed values of D to exceed the expected value of MD^{\max} estimated for any individual fault. As we have estimated it, MD^{\max} simply provides a basis for normalizing observations for comparison from fault to fault.

The PDF shown in Figure AAR-11 was fit with the function $y = 0.09 \exp(-0.68 D/MD^{\max})$. Regression parameters are listed in Table AAR-9. Following Benjamin and Cornell (1970), we analyze the CDF in terms of the generalized exponential distribution $\lambda e^{-\lambda x}$, whose CDF is $1 - e^{-\lambda x}$. For the generalized PDF, values along the x-axis are numerically plotted as λx . The mean value of D/MD^{\max} , which is 0.83 for the 82 displacement measurements, directly provides the expected value of $1/\lambda$. Hence $\lambda = 1.20$. The variance on λ is approximated by λ^2/n , and the median for the distribution is given by $0.693/\lambda$.

In the CDF in Figure AAR-11 we superpose the curve for $1 - \exp(-1.20 (D/MD^{\max}))$, which shows good agreement with the observed CDF. Importantly, the mean (0.83) of the observed values of D/MD^{\max} gives a key piece of information—namely, a reliable estimate of \bar{D}_E , the average displacement at a point on a fault (at or near the surface) over many displacement events at that point.

The data of Figure AAR-11 were analyzed independently by the Facilitation Team (Appendix H, Section H.2.5), and various statistical distributions were fit to the data. As described in Appendix H, good fits to the data were obtained for an exponential distribution with a mean of 0.83 and for a gamma distribution with two parameters; a slightly better goodness of fit for the gamma distribution is shown to be only marginally statistical significant.

In examining Figure AAR-11, note that a lower limit of resolution is implicit and inescapable. Some would argue that very small, unobserved surface displacements are greatly more numerous than observed ones, but such a hypothesis must be reconciled with observed earthquake statistics and the observed geology, particularly in terms of the cumulative offset implied by having many small unobserved displacement events. For example, if a one-centimeter displacement event is thought to be material, 100 such

unobserved events require one meter of cumulative offset to be accounted for during some time period. and 1,000 such events, 10 m.

In the case of the data used in Figure AAR-11, the smallest bin is centered on $0.1 D/MD^{\max}$. Following conventional rules for rounding, the two smallest observed ratios of 0.04 and 0.05 (rounded to the nearest even integer) fell below the smallest bin. These ratios correspond to one displacement of 5 cm on the Solitario Canyon fault ($MD^{\max} = 112$ cm) and another of 6 cm on the Paintbrush Canyon fault ($MD^{\max} = 112$ cm). The eleven displacement events included in the smallest bin range from 3 to 7 cm.

Based on the data shown on Figure AAR-11, together with the supporting analysis of the Facilitation Team (Appendix H), we adopt the exponential distribution as an appropriate and reasonable empirical predictor for the distribution of displacement at a point — within implied limits of resolution for the ratio of a displacement event to MD^{\max} .

To summarize, MD^{\max} provides a useful basis for scaling and comparing displacement measurements on the Yucca Mountain faults. The result that aggregated values of D/MD^{\max} can be modeled approximately by an exponential distribution has great utility. Not only does the distribution enable a reliable estimate of the average displacement at a point, it also combines both spatial and temporal variability at that point. We interpret the distribution to be a composite effect of event-to-event variability of primary fault ruptures, along-strike variability during ruptures on the same fault, and distributed faulting triggered by static and/or dynamic stress/strain changes. We emphasize that having displacement events at a generalized point on the surface approximate an exponential distribution does not necessarily imply that earthquakes on the primary faults also follow such a distribution. We adhere to our separate assessment of characteristic versus exponential slip events at depth on the principal faults.

6.7 OVERVIEW OF LOGIC TREES

For convenience, we construct separate logic trees for principal and distributed faulting. After evaluating various approaches proposed and discussed at SSC Workshops 4 and 5 for

characterizing fault-displacement potential, we use both an earthquake and a displacement approach for principal faulting. We then assess the potential for distributed faulting using two methods described by R. Youngs (presentation at SSC Workshop 5) as a point-estimate (displacement) method and a principal-distributed faulting (earthquake) method.

For principal faulting, we give a weight of 0.67 to the displacement approach and 0.33 to the earthquake approach. We give greater weight to the former because we are persuaded that, ultimately, the size and frequency of displacements on faults and related features exposed at the surface (or in the repository) must be governed by the budget of what is observed—namely, the record of displacements at or near the surface.

When we assess the potential for distributed faulting, we take different approaches for (1) sites of distributed faulting only and (2) sites where principal faulting also occurs (Figure AAR-12). We do this because at the latter sites the displacement approach for principal faulting simultaneously accounts for distributed faulting at the same point. At such sites, conditional on using the earthquake approach to principal faulting (weight = 0.33), we then use only the principal-distributed faulting method to characterize distributed faulting.

For assessing the potential for distributed faulting at sites of distributed faulting only, we give a weight of 0.33 to our principal-distributed faulting method and 0.67 to our point-estimate method. We downweight the first method for two reasons. First, as discussed earlier in Section 6.2, it does not fully account for plausible new-seismicity triggering by dynamic stress/strain due to remote earthquakes at distances greater than 100 km. Second, we have more confidence in our point-estimate method for characterizing the frequency of slip on a specific secondary fault or fracture.

Throughout our logic tree, whenever we use a regression relation from Wells and Coppersmith (1994), we intend the use of the respective equation for the category of All Data. Our defined sources of principal faulting include those local fault sources in Table AAR-3 which have a probability of being seismogenic, $P[S] > 0$.

6.8 PRINCIPAL FAULTING—EARTHQUAKE APPROACH

In the earthquake approach (Figure AAR-13), our logic tree for ground-shaking hazard provides a starting point at which one is given a frequency-magnitude distribution for a subject fault. Given an event of magnitude M , we proceed to estimate rupture length L , in part as a predictor of maximum surface displacement (MD) and average surface displacement (AD). For later application, we distinguish between surface rupture length, SRL (for cases of rupture at or near the surface), and subsurface rupture length, RLD. Unless specified otherwise, L is implied to be subsurface rupture length.

Estimating RLD

We give equal weights (0.5, 0.5) to two approaches for estimating RLD (Figure AAR-14). The first is the straightforward use of a regression relation between RLD and M from Wells and Coppersmith (1994). In the second approach we follow Nicol et al. (1996), who review data indicating that simple normal faults have an approximately elliptical shape with a subhorizontal major axis. We constructed a cumulative distribution of aspect ratios for 54 earthquake slip surfaces using data from Nicol et al. (1996, their Table 2), from which we assess the following distribution for aspect ratio (and relative weighting):

0.8 (0.3), 1.4 (0.4), 2.5 (0.3).

Given M , we use the regression relation, $\log(RA) = -3.49 + 0.91 M$ (Wells and Coppersmith, 1994) to estimate rupture area RA in units of km^2 . For an elliptical rupture, the major axis = $L/2$, from which it can be shown that $L(\text{km}) = [(4/\pi * \text{aspect ratio} * (RA))]^{1/2}$.

Estimating SRL

Our two approaches to estimating SRL (Figure AAR-14) basically parallel those just described for estimating RLD, and again we assign equal weights (0.5, 0.5). The first approach uses a regression relation between SRL and M from Wells and Coppersmith (1994). In the second approach, we calculate the length dimension of an elliptical rupture area as for RLD, but the difference is that for the range of lengths being considered, SRL is expected to

be less than RLD, and we adopt the ratio 0.75 for SRL/RLD (Wells and Coppersmith, 1994) as a correction factor.

Estimating P[Surface Rupture]

In order to estimate the probability of surface rupture, $P[\text{surface rupture}]$, given an event of magnitude M , we invoke a simulation approach developed for the ground-motion modeling in which the location of a rectangular fault is randomized on the subject fault source (Figure AAR-15). The modeling uses our adopted focal depth distribution for $M \geq 5.0$ (based on one from K. Smith, presentation at SSC Workshop 2, "Depth Distribution—SGB 1979-present"). The distribution of distance from a hypocenter to the top of rupture is calculated by allowing the hypocenter location to be uniformly distributed on the lower 75% of the rupture.

In the randomization analysis, the subsurface dimensions of a rupture for an event of magnitude M are modeled by using, with equal weights, the two methods already described for estimating RLD (see Figure AAR-14). In the first, RLD is determined from a regression relation between RLD and M , and downdip rupture width W follows from an assessed distribution on aspect ratio (Figure AAR-15), which has the following distribution of values and weights, justified earlier: 0.8 (0.3), 1.4 (0.4), 2.5 (0.3). In the second method, RLD and W derive from the rupture area RA of an elliptical rupture (where RA is determined from a regression relation between RA and M) whose aspect ratio has the same distribution specified above.

For realizations of surface rupture, the weighted-average value of surface-rupture length SRL (Figure AAR-14) is used to randomize the along-strike location of surface rupture. For the general case in which SRL is less than the total trace length of a fault, the cases of surface rupture in effect become a one-dimensional randomization in which a rupture of trial length SRL is randomly located along the fault trace. This later enables one to assess the location of any point on the fault with respect to a realized surface rupture in order to apply the ASM model for variability of slip along strike. In any application to a specific fault, the weighted-average value of SRL cannot exceed the total fault length and must be limited to the latter in such cases.

Although this simulation modeling for estimating the probability of surface rupture undoubtedly oversimplifies some complex aspects of faulting, we adopt it for the following reasons. It directly incorporates our subsurface characterization of fault sources at Yucca Mountain and it yields results that are similar to the empirical distributions for the probability of surface rupture derived from samples of historical earthquakes in the Great Basin and surrounding regions of the western U.S. (see Appendix H).

Estimating MD And Variability Along Strike

Given M, SRL, and RLD, we proceed to estimate the expected maximum surface displacement MD on a principal fault (Figure AAR-16).

We focus on estimating the expected value of MD for principal faulting because we adopt the ASM model to assess variability of slip along strike, and that method uses a distribution normalized to MD. Our logic tree outlines three approaches to estimating MD, and we give basically equal weights to each approach. The first two involve regression relations from Wells and Coppersmith (1994) which deliver MD, given SRL or M.

We do not use direct assessments of MD from paleoseismic data tabulated in Table AAR-4 because those values imply rupture of total fault length. Instead, the paleoseismic data for the Yucca Mountain local faults are incorporated into the scaling relation between \bar{U} and RLD, which is our third approach to estimating MD.

6.9 PRINCIPAL FAULTING—DISPLACEMENT APPROACH

Estimating MD^{max}

In our displacement approach to principal faulting (Figure AAR-17), we use three methods to estimate MD^{max}, which provides an underpinning for the recurrence modeling: (1) a fault-length approach (weight = 0.3), (2) a cumulative-displacement approach (weight = 0.3), and (3) a paleoseismology approach (weight = 0.4).

In the fault-length approach, we use (a) an empirical relation between MD and SRL from Wells and Coppersmith (1994) (weight = 0.4) and (b) our empirical scaling relation between

\bar{U} and L^{total} , from which MD^{max} is then scaled from the implicit maximum value of \bar{U} (weight = 0.6). In the first relation, the maximum value of SRL is used to yield MD^{max} .

The cumulative-bedrock-displacement approach, informally referred to as the "Dcum approach" in parts of our logic tree, uses the scaling relations we developed and discussed at length in the section on Scaling Relations. The operative relation is $MD^{max} = 1.32 * \beta * Dcum$, where the scaling factor β depends on the size of the fault being considered (see Figure AAR-19). We described earlier our reasoning for treating larger and smaller faults differently, where the threshold of larger faults is approximately $L^{total} > 3$ km and $Dcum > 75$ m. For the larger faults, which with few exceptions include nearly all the principal Yucca Mountain faults, $\beta = 1.40 \times 10^{-3}$ m/m. For the smaller faults, the values (and weights) for β (m/m), justified earlier (see section on Scaling Relations, \bar{U} [and MD^{max}] Versus $Dcum$), have the following distribution

$$1.40 \times 10^{-3} (0.3), 5.59 \times 10^{-3} (0.4), 1.85 \times 10^{-2} (0.3).$$

In the Paleoseismology approach, we use the values tabulated in Table AAR-4 under $Dmax$ as direct assessments of MD^{max} .

Recurrence Of Displacement Events And Variability At A Point

To estimate the frequency of fault displacement as a function of size, we rely on the exponential distribution we derived (Figure AAR-11) as a basis for recurrence modeling (Figure AAR-17). We originally considered using an approach similar to that of Youngs and Coppersmith (1985) to derive a frequency-displacement recurrence relation using slip-rate information to distribute seismic moment. With our exponential model in hand, however, we consider it appropriate to use the more direct approach of estimating λ_{DE} , the average frequency of slip events, by dividing slip rate by \bar{D}_E , the average displacement at a point over many events. As discussed in our section on "Variability in Displacement at a Point," \bar{D}_E is estimated by $0.83 MD^{max}$. Slip-rate information for the principal faults is provided in Table AAR-4.

6.10 DISTRIBUTED FAULTING—POINT-ESTIMATE METHOD

This method has three basic steps, which we have modified from an approach proposed by the DFS Team at SSC Workshop 5: (1) estimation of slip rate at a point using alternative methods linked to an observed value of Dcum; (2) estimation of the average frequency of slip events at the same point; and (3) estimation of the variability of slip at the point.

In our application of this method (Figure AAR-18), we give zero weight to estimating what we will call Quaternary slip rate QSR by assuming uniform slip on a feature during the last 12.7 Ma (post-Tiva Canyon Tuff), based on abundant evidence for major deformation prior to 11.6 Ma (pre-Rainier Mesa Tuff). We adopt as one approach, however, the possibility of uniform slip during the past 11.6 Ma. In order to assess the fraction of Dcum that accumulated before 11.6 Ma—in a way that is completely independent of paleo-seismological slip-rate information, we did the following. We used data presented by Fridrich et al. (1996) for estimates of extension in Miocene bedrock (based on the amount of stratal tilting as a measure of extension) for the three time periods: 12.7 to 11.6 Ma, 11.6 to 10.5 Ma, and 10.5 Ma to present. For the Controlled Area (of most direct interest to this fault-displacement characterization), we estimated the proportion of the cumulative percent of extension post-dating the 12.7 Ma Tiva Canyon Tuff that occurred from 12.7 to 11.6 Ma. Based on conditional logic reasoning, we then assessed the following distribution for the fraction of Dcum that has occurred during the last 11.6 Ma:

60% (0.3), 40% (0.4), 20% (0.3).

The post-11.6 Ma slip rate in this approach is inferred to approximate the average QSR.

Our second approach to estimating QSR was adapted from one described by J. Yount (presentation at SSC Workshop 5) in which offsets of basalts 3.7 Ma old in the Crater Flat basin are used to estimate the fraction of Dcum post-Tiva Canyon Tuff that has occurred in the past 3.7 Ma. Based on estimated offsets of basalts across the So. Windy Wash and So. Crater Flat faults, and offset tephra across the Stagecoach Road fault, we assessed the following percentages (and weights):

40% (0.3), 16% (0.4), 5% (0.3).

Our third approach is the use of an empirical estimate of QSR as a function of D_{cum} , based on paleoseismic slip-rate data. The regression relation has already been described and is summarized in Table AAR-9. We assign relative weights to the three approaches that are inversely proportional to the duration of the time interval for which uniformity of slip rate is assumed. Accordingly, the weights are 0.1 for uniformity during the past 11.6 Ma, 0.3 for the past 3.7 Ma, and 0.6 for the time span covered by paleoseismic data (approximately ranging from 0.1 to 1 Ma).

In order to estimate MD^{max} on a secondary fault or fracture, we use information on L^{total} , if available, together with D_{cum} (Figure AAR-19). If both length and total-displacement information are available, we give equal weight to estimating MD^{max} from: (1) the scaling relation, $MD^{max} = 1.32 * \bar{U}^{max}$, where $\bar{U}^{max} (m) = 3.69 \times 10^{-5} L^{total} (m)$; and (2) the D_{cum} approach we described above in the section, Principal Faulting—Displacement Approach, Estimating MD^{max} . We then use the same procedures described in that section to estimate λ_{DE} and variability of slip at a point (Figure AAR-20)—except that here, our estimates of QSR come not from paleoseismic information in Table AAR-4, but from the feature-specific estimates of QSR just made.

6.11 DISTRIBUTED FAULTING—PRINCIPAL-DISTRIBUTED FAULTING METHOD

In this method, principal faulting may cause the occurrence of slip on secondary/distributed faults and fractures as well as on other principal fault sources. The frequency-magnitude distribution on the primary seismogenic fault is first determined by the earthquake method for principal faulting (Figure AAR-21). Whether a secondary fault or fracture slips is judged to depend on its slip-susceptibility tendency, the size of the principal faulting event, and distance from the principal fault in either the footwall or hanging-wall direction.

We attempted to invert the magnitude and frequency of principal faulting from our displacement approach using MD^{\max} , but we encountered what we judged to be a fatal flaw. Given a principal fault, we can straightforwardly determine MD^{\max} for the fault, as we did, for example, in our Principal Faulting-Displacement Approach. Given MD^{\max} , our exponential distribution yields the relative frequency of displacement events of size D_E/MD^{\max} . However, this measure is for the displacement at a single point and cannot be transformed into some measure such as AD or MD from which the magnitude of the event can be estimated. Therefore, we assign full weight to the earthquake approach for determining the magnitude and frequency of principal faulting.

Our logic tree for handling secondary/distributed faulting includes two probability terms (Figure AAR-21). First, $P[C]$ is the probability that a feature is capable of slip to produce secondary/distributed displacement, given the contemporary stress field at Yucca Mountain. Second, $P[\text{slip}|pf]$ is the probability that a secondary fault or feature slips to produce secondary/distributed displacement, given principal faulting nearby. Given a principal faulting event, the potential for secondary/distributed displacement on a nearby fault or fracture directly contains the multiplicative terms, $P[C]$ and $P[\text{slip}|pf]$. Rules for assessing $P[C]$ are given in a following section.

In order to apply $P[\text{slip}|pf]$, we invoke a probability distribution function described by R.R. Youngs (presentation at SSC Workshop 6; see also Appendix H this volume) based on data from S. Pezzopane for the density of distributed faulting accompanying historic normal-faulting earthquakes in the extensional western U.S. Cordillera—as a function both of event size and distance in the footwall or hanging-wall direction. We believe such a density function provides a suitable measure of the probability that a secondary fracture undergoes slip which is induced by principal faulting.

For application of the modeling of $P[\text{slip}|pf]$ to our logic tree, we prefer to exclude data points for surface cracking from the 1986 Chalfant Valley, California, and the 1980 Mammoth Lakes, California, earthquakes. In both cases, the structural setting of Quaternary volcanic rocks that are affected by distributed faulting (Pezzopane and Dawson, 1996, chapter 9) arguably confound the composite, two-dimensional frequency-distance

distribution being sought. Also, we prefer that the regression modeling of the data impose a magnitude scaling effect on the hanging wall-footwall relations, which we consider more realistic than having magnitude-invariant relations.

Given that secondary/distributed faulting occurs, our procedures for estimating the amount of displacement and the variability of slip depend on whether the site is one of distributed faulting only (Figure AAR-22) or one where principal faulting also occurs (Figure AAR-23). In the former case, our logic tree uses the same approaches described for the point-estimate method.

At a site where principal faulting also occurs, we chose not to let MD^{\max} be an estimator of the expected secondary displacement. In principle, this could result in secondary displacements on faults with large MD^{\max} that are larger than the displacements on the primary faults. Instead, we use data summarized by Pezzopane and Dawson (1996, chapter 9, Figures 9-15 and 9-22) relating observations of maximum secondary displacement to maximum primary displacement as a function of mainshock magnitude. The data include both (1) their own compilation from a sample of surface-faulting earthquakes in the extensional Cordillera of the western U.S. and (2) an earlier compilation from Coppersmith and Youngs (1992; see Figure 9-22 in Pezzopane and Dawson, 1996). We relied on compilation (1) to estimate a cumulative distribution for the ratio of maximum secondary displacement to maximum primary displacement from which we assessed the following distribution of ratios (and weights):

0.20 (0.3), 0.45 (0.4), 0.70 (0.3).

This distribution is consistent with the assumption by Coppersmith and Youngs (1992) of a uniform distribution between 0.1 and 0.8 for the ratio of maximum secondary displacement to maximum primary displacement (see Figures 9-15 and 9-22 of Pezzopane and Dawson, 1996).

Given a mainshock of magnitude M , we first estimate the maximum primary displacement MD from the regression relation of Wells and Coppersmith (1994) (See Figure AAR-23).

We use the ASM model to estimate the variability of MD on the primary fault. To do this, we assume MD follows the distribution at the midpoint of the fault, which is the most conservative assumption. The maximum secondary displacement is then calculated from its ratio to MD on the primary fault.

6.12 SECONDARY/DISTRIBUTED FAULTING

We spell out 10 rules for characterizing secondary/distributed faulting at the nine test calculation sites. The rules are grouped under the issues of: (1) susceptibility to displacement; (2) the amount, frequency, and variability of displacement; (3) dip and sense of slip; and (4) the width of the zone of displacement. In terms of notation, recall that $P[C]$ is the probability that a feature is capable of slip to produce secondary/distributed displacement, given the contemporary stress field at Yucca Mountain.

Susceptibility to Displacement:

Rule 1. For any fault assigned $P[S] = 1.0$ (Tables AAR-2, AAR-3), $P[C]$ is also 1.0.

Rule 2. Based on slip-tendency analysis of Yucca Mountain faults (Morris et al., 1996; McKague et al., 1996), and using Figures 3-3 and 3-4 of McKague et al. (1996) as a guide for relative scaling, we assign $P[C]$ ranging from 1 for faults with high slip tendency to 0.5 for faults with intermediate slip tendency to 0.1 for faults with low slip tendency, such as the NW-SE striking faults. Although we assigned $P[S] = 0$ to the latter, we allow some possibility that NW-SE striking structures may undergo secondary/distributed displacement; local stresses may be rotated, for example, during principal faulting nearby.

Rule 3. In an underground excavation at Yucca Mountain, we assign $P[C] = 1$ to any shears with about 10 cm of cumulative offset or to fractures with less or no measurable offset—concluding that, in principle, they can participate in local strain accommodation, regardless of orientation. We adopt this interpretation because we think it very likely that the underground excavation disrupts the coherency of the stress field used for the slip-tendency analysis.

Rule 4. For intact rock, $P[C] = 0$.

Secondary displacement of intact rock could occur either by propagation of an existing fault or shear fracture into intact rock or by creation of a new fault. Studies at Yucca Mountain show that existing faults were reactivated during Quaternary deformation. The studies provide no examples of the creation of new faults or of the propagation of existing faults into unbroken rock. There is, therefore, no geologic basis for evaluating the probability that such events may occur.

We consider such displacement may be possible given a condition in which the existing fault or rock block is pre-loaded by regional stress to the point of failure and displacement occurs in response to passage of a transient dynamic stress. We consider such an occurrence at Yucca Mountain to be negligible because: (1) the strength of intact rock is commonly 5 to 10 times greater than that of fault rock (Cowie and Scholz, 1992a), (2) small shear fractures tend to propagate along existing fractures or joints (Segall and Pollard, 1983), (3) the rocks at Yucca Mountain (as revealed in the ESF) are cut by many fractures and faults, some of which (for example, the Ghost Dance fault) are marked by low-strength rock thus providing abundant opportunity for stress release adjacent to intact rock, and (4) there is no indication that the Ghost Dance fault, even with its low strength aspect, has been activated in secondary faulting through several cycles of local Quaternary faulting.

Local evidence for a difference in strength between intact and fractured rock can be interpreted from stress measurements made in the ESF (Sandia National Laboratory, 1997). Table 1 (p. 7) of that report shows a skewed distribution of critical pressures (P_c) measured at different levels in the test hole. Four values are in the range 1.6 to 1.8 and a fifth is 6.4. The high value is suggested to be typical of intact test intervals as opposed to the lower values which are ascribed to pre-fractured conditions (p. 20). Taking these results to be a crude estimate of strength contrasts between intact and fractured rock, we infer that intact rock is 3.8 times stronger than fractured rock. Although less than the factor of 5 to 10 we cite from Cowie and Scholz (1992a), this nonetheless provides local evidence that intact rock is significantly stronger than fractured rock in the ESF.

Amount, Frequency, and Variability of Displacement:

Rule 5. To estimate the expected amount, frequency, and variability of secondary/distributed faulting on any fault or fracture with measurable offset, our logic tree for "Distributed Faulting" should be followed.

Rule 6. For a fracture with no measurable offset, we adopt the logic of our scaling relation for \bar{U} versus L^{total} , requiring an observer to assess a distribution for L^{total} , combined with our exponential distribution for $D_E/\text{MD}^{\text{max}}$. Such a distribution for L^{total} (and weights), for example, might be: 5 m (0.3), 10 m (0.4), 20 m (0.3). For the median value of 10 m, $\text{MD}^{\text{max}} = 1.32 \times 3.69 \times 10^{-5} \text{ m/m} \times 10 \text{ m}$, yielding $4.87 \times 10^{-4} \text{ m}$. The expected value of λ_{DE} is $0.83 * \text{MD}^{\text{max}}$ or $4.0 \times 10^{-4} \text{ m}$. To place a bound on λ_{DE} , the relative frequency of displacement events, one could assume (or assess a distribution otherwise) that "no measurable offset" means $\leq 10 \text{ cm}$ for D_{cum} , in which case the upper bound number of displacement events would be 0.1 m divided by $4.0 \times 10^{-4} \text{ m/event}$ yielding 2.5×10^2 events. Thus, λ_{DE} would be 2.5×10^2 events divided by the age of the rock. For an age of 12.7 Ma , λ_{DE} would be $2.0 \times 10^{-5} \text{ events/yr}$ (recurrence interval = $50,000 \text{ yr}$).

Dip and Sense of Slip:

Rule 7 Begging the obvious, estimating the dip to be expected for displacement at a specific point should clearly rest on either (1) direct observation of the candidate feature and fracturing in its immediate vicinity or (2) inference from either detailed mapping of fractures and faults in the repository excavation similar to mapping in the ESF (e.g., R.C. Lung presentation at SSC Workshop 2) or detailed surface mapping (e.g., presentations by W.C. Day, C.J. Potter, and D.S. Sweetkind at SSC Workshops 3 and 4). Dips of 60° to 90° are well known to predominate.

Rule 8. The sense of slip to be expected on a fault or fracture can reasonably be estimated by relating its 3-D orientation to the 3-D orientations of the contemporary principal stresses at Yucca Mountain (e.g., Stock et al., 1985; Morris et al., 1996; Sandia National Laboratory, 1997). An interactive computer tool developed for application at Yucca Mountain provides a direct way to assess the "relative likelihood and direction of slip on surfaces of all orientations" (Morris et al., 1996; McKague et al., 1996). Such methodologies assume that slip will occur in the absence of strain partitioning involving other faults or fractures in the rock volume under consideration (e.g., Wesnousky and Jones, 1994).

Rule 9. For faults or fractures exposed in an underground excavation at Yucca Mountain, we consider that those with dimensions exceeding roughly twice the dimensions of the excavation will have an expected sense of slip

controlled by the orientation of the contemporary principal stresses (Rule 8). We have little understanding of how stresses will be induced and modified by the excavation, so we have little confidence in assessing the sense of allowable slip on small fractures intersected by the excavation.

Width of the Zone of Displacement:

Rule 10. The width of the zone of displacement (fault zone thickness), interpreted to be the width of the deformation zone within which most of the slip across a fault or fracture has occurred (as distinct from a broader "damage zone" of deformed rock), scales linearly with fault throw (Knott et al., 1996; Power et al., 1988; Hull, 1988). The mean ratio of fault zone thickness to throw (D_{cum}) for natural faults is approximately 0.01, with individual values ranging between 0.1 and 0.001 (Power et al., 1988).

The ratio of fault zone thickness to throw is observed to vary with lithology, and within the same lithology to vary greatly along an individual fault trace (Knott et al., 1996). This ratio for the Yucca Mountain faults, in the absence of a compilation for the local fault population, can reasonably be assessed from global data by the following distribution of values (and weights): 0.001 (0.185), 0.01 (0.63), 0.1 (0.185). For illustration, a fault zone thickness of 0.6 to 1.0 m for the Ghost Dance fault observed in Alcove 6 of the ESF (J.W. Whitney presentation, SSC Workshop 6), divided by a throw of the order of 20 to 40 m, gives a ratio of the order of 0.01 to 0.05.

6.13 ASSESSMENTS FOR NINE TEST CALCULATION SITES

In this final section, we give specific guidance for calculating fault-displacement hazard at the Nine Test Calculation Sites.

Point 1 (Bow Ridge fault):

- Susceptibility to slip: Source of principal faulting. $P[C] = P[S] = 1$
- Amount/frequency/variability of displacement: Logic trees for Principal and Distributed Faulting, respectively (see Table AAR-4 under "total disp." for D_{cum})
- Dip/Sense of Slip: Rules 7, 8
- Width of zone of displacement: Rule 10

Point 2 (Solitario Canyon fault):

- Susceptibility to slip: Source of principal faulting, $P[C] = P[S] = 1$
- Amount/frequency/variability of displacement: Logic trees for Principal and Distributed Faulting, respectively (see Table AAR-4 under "total disp." for Dcum)
- Dip/Sense of Slip: Rules 7, 8
- Width of zone of displacement: Rule 10

Point 3 (Drill Hole Wash fault):

- Susceptibility to slip: Susceptible to secondary/distributed faulting only; $P[C] = 0.75$ (see McKague et al., 1996, Figure 3-4)
- Assessed distribution for L^{total} , in km (and weights): 2.0 (0.3), 5.0 (0.4), 9.0 (0.3); assessed distribution for Dcum, in m (and weights): 20 (0.3), 50 (0.4), 100 (0.3)
- Amount/frequency/variability of displacement: Logic tree for Distributed Faulting
- Dip/Sense of Slip: Rule 7 for dip; Rule 9 for sense of slip in an underground excavation, which reverts to Rule 8 because of the dimension of the fault
- Width of zone of displacement: Rule 10

Point 4 (Ghost Dance fault):

- Susceptibility to slip: Source of principal faulting, $P[S] = 0.1$; however, based on its high slip susceptibility (see McKague et al., 1996, Figure 3-4), we assign $P[C] = 1$ for secondary/distributed faulting,
- Amount/frequency/variability of displacement: Logic trees for Principal and Distributed Faulting, respectively (see Table AAR-4 under "total disp." for Dcum)
- Dip/Sense of Slip: Rule 7 for dip; Rule 9 for sense of slip in presumed underground excavation, which reverts to Rule 8 because of the dimension of the fault
- Width of zone of displacement: Rule 10

Point 5 (Sundance fault W of ESF):

- Susceptibility to slip: Source of secondary/distributed faulting only; $P[C] = 0.8$ (see McKague et al., 1996)
- Assessed distribution for L^{total} , in km (and weights): 0.5 (0.3), 0.75 (0.4), 2.0 (0.3); assessed distribution for D_{cum} , in m (and weights): 5 (0.3), 10 (0.4), 20 (0.3)
- Amount/frequency/variability of displacement: Logic tree for Distributed Faulting
- Dip/Sense of Slip: Rule 7 for dip; Rule 9 for sense of slip in presumed underground excavation, which reverts to Rule 8 because of the dimension of the fault
- Width of zone of displacement: Rule 10

Point 6 (Minor unnamed fault W of Dune Wash):

- Susceptibility to slip: Source of principal faulting, $P[S] = 0.1$; however, based on its high slip susceptibility (see McKague et al., 1996, Figure 3-4), we assign $P[C] = 0.9$ for secondary/distributed faulting
- Amount/frequency/variability of displacement: Logic trees for Principal and Distributed Faulting, respectively. (For fault parameters, see Table AAR-4 for what we call the W. Dune Wash 2 fault, along which Point 6 is located.)
- Dip/Sense of Slip: Rules 7, 8
- Width of zone of displacement: Rule 10

Point 7 (feature 100 m E of Solitario Canyon fault):

(a) Assuming a small fault with 2 meters of cumulative offset not directly identifiable from surface mapping

- Susceptibility to slip: Source of secondary/distributed faulting only; $P[C] = 0.9$ (assuming northerly orientation similar to major fractures in that neighborhood)
- Amount/frequency/variability of displacement: Logic tree for Distributed Faulting

- Dip/Sense of Slip: Rule 7 for slip, Rule 9 for sense of slip in underground excavation, which reverts to Rule 8 because of the inferred length dimension of the fault
- Width of zone of displacement: Rule 10

(b) Assuming a shear with about 10 cm of cumulative offset

- Susceptibility to slip: Susceptible to secondary/distributed displacement only; $P[C] = 1$ (Rule 3)
- Amount/frequency/variability of displacement: Logic tree for Distributed Faulting
- Dip/Sense of Slip: Rule 7 for slip, Rule 9 for sense of slip (uncertain for small fracture in underground excavation)
- Width of zone of displacement: Rule 10

(c) Assuming a fracture with no measurable offset

- Susceptibility to slip: Susceptible to secondary/distributed displacement only; $P[C] = 1$ (Rule 3)
- Amount/frequency/variability of displacement: Rule 6
- Dip/Sense of Slip: Rule 7 for slip, Rule 9 for sense of slip (uncertain for small fracture in underground excavation)
- Width of zone of displacement: Rule 10

(d) Assuming intact rock

- Susceptibility to slip: No expected displacement (Rule 4)
- Amount/frequency/variability of displacement: N/A

Point 8 (Feature midway between Solitario Canyon and Ghost Dance faults):

[Except for not knowing the orientation of the feature, all assessments would be identical to those for Point 7 (a-d). The only factor that might change would be $P[C]$ in assumption (a)—

if the orientation implied higher or lower susceptibility than $P[C] = 0.9$ assigned for Point 7(a).]

Point 9 (Site on alluvium in Midway Valley E of the Bow Ridge fault):

All arguments heretofore assume accessibility to direct observations of a fault or fracture in order to assess MD^{max} . Nevertheless, we can proceed as follows:

- Susceptibility to slip: Figure 3-4 of McKague et al. (1996) indicates faults/fractures in this vicinity with slip tendencies varying from high to low, so we assume uniform probability of $P[C]$ between 0.1 and 1.0

Amount/frequency/variability of displacement: To assess displacement parameters, we can rule out (from earlier site characterization studies) the presence of a shallowly buried principal fault. We then assess that the most significant shallowly buried intrablock feature at that site has D_{cum} as follows:

2 m (5%) 10 m (50%) 20 m (95%)

- Given the above distribution for D_{cum} , follow the logic tree for Distributed Faulting
- Dip/sense of slip: Under the present stress field, the faults most favorably oriented for slip would have strikes of $N0^{\circ}E$ to $N30^{\circ}E$, dips of 60° to 90° , and normal-slip motion with a sinistral component (Morris et al., 1996)
- Width of zone of displacement: Rule 10

- Abercrombie, R.E., 1995, Earthquake source scaling relationships from -1 to 5 M_L using seismograms recorded at 2.5-km depth: *Journal of Geophysical Research*, v. 100, no. B12, p. 24,015-24,036.
- Ander, H.D., 1984, Rotation of Late Cenozoic extensional stresses, Yucca Flat region, Nevada Test Site, Nevada: unpublished Ph.D. thesis, Houston, TX, Rice University.
- Anderson, J.G., Wesnousky, S.G., and Stirling, M.W., 1996, Earthquake size as a function of fault slip rate: *Bulletin of the Seismological Society of America*, v. 86, no. 3, p. 683-690.
- Anderson, L.W. and Klinger, R.E., 1996, Evaluation and characterization of Quaternary faulting - Bare Mountain fault, Nye County, Nevada: Bureau of Reclamation Seismotectonic Report 96-5, Denver, Colorado, prepared for Yucca Mountain Project Activity 8.3.1.17.4.3.4, 78 p., plates and appendices.
- Anderson, R.E., Barnhard, T.P., and Snee, L.W., 1994, Roles of plutonism, midcrustal flow, tectonic rafting, and horizontal collapse in shaping the Miocene strain field of the Lake Mead area, Nevada and Arizona: *Tectonics*, v. 13, p. 1381-1410.
- Anderson, R.E., Bucknam, R.C., Crone, A.J., Haller, K.M., Machette, M.N., Personius, S.F., Barnhard, T.P., Cecil, M.J., and Dart, R.L., 1995a, Characterization of Quaternary and suspected Quaternary faults, regional studies, Nevada and California: U.S. Geological Survey, Open-File Report 95-599, 56 p.
- Anderson, R.E., Crone, A.J., Machette, M.N., Bradley, L.-A., and Diehl, S.F., 1995b, Characterization of Quaternary and suspected Quaternary faults. Amargosa area, Nevada and California: U.S. Geological Survey, Open-File Report 95-613, 41 p.
- Bell, J.W., de Polo, C.M., Ramelli, A.R., Dorn, R.I., Sarna-Wojcicki, A.M., and Meyer, C.E., 1996, Surface faulting and paleoseismic history of the 1932 Cedar Mountain earthquake area, Central Nevada: *Geological Society of American Bulletin*, in review.
- Benjamin, J.R., and Cornell, C.A., 1970, Probability, statistics, and decision for civil engineers: New York, McGraw-Hill Book Company, 684 p.

- Bodin, P., and Brune, J.J., 1996, On the scaling of slip with rupture length for shallow strike-slip earthquakes: Quasi-static models and dynamic rupture propagation: *bulletin of Seismological Society of America*, v. 86, no. 5, p. 1292-1299.
- Carr, M.D. et al., 1986, Geology of drill hole UE25p#1: USGS Open-file Report 86-175.
- Clark, R.M., and Cox, S.J.D., 1996, A modern regression approach to determining fault displacement-length scaling relationships: *Journal of Structural Geology*, v. 18, nos. 2/3, p. 147-152.
- Cohee, B.P., and Beroza, G.C., 1994, Slip distribution of the 1992 Landers earthquake and its implications for earthquake source mechanics: *Bulletin of the Seismological Society of America*, v. 84, no. 3, p. 692-712.
- Coppersmith, K.J., and Youngs, R.R., 1992, Earthquakes and tectonics: in McGuire, R.K. (ed.), *Demonstration of a Risk-Based Approach to High-Level Waste Repository Evaluation: Phase 2*, Electric Power Research Institute, EPRI TR-100384, Palo Alto, California
- Cowie, P. A., and Scholz, C.H., 1992a, Physical explanation for the displacement-length relationship of faults using a post-yield fracture mechanics model: *Journal of Structural Geology*, v. 14, no. 10, p. 1133-1148.
- Cowie, P. A., and Scholz, C.H., 1992b, Displacement-length scaling relationships for faults: data synthesis and discussion: *Journal of Structural Geology*, v. 14, no. 10, p. 1149-1156
- Cowie, P. A., and Scholz, C.H., 1992c, Growth of faults by accumulation of seismic slip: *Journal of Geophysical Research*, v. 97, no. B7, p. 11,085-11,095.
- Crowe, B., Perry, F., Geissman, J., McFadden, L., Wells, S., Murrell, M., Poths, J., Valentine, G.A., Bowker, L., Finnegan, K., 1995, Status of volcanism studies for the Yucca Mountain site characterization project, Los Alamos National Laboratory Report LA-12908-MS.
- Day, W.C., Potter, C.J., Sweetkind, D.S., Dickerson, R.P., and San Juan, C.A., 1996, Bedrock geologic map of the central block area, Yucca Mountain, Nye County, Nevada: U.S. Geological Survey Administrative Report, prepared in cooperation with the Nevada Operations Office, U.S. Department of Energy, 48 p.

- Faulds, J.E., Bell, J.W., Feuerbach, D.L., and Ramelli, A.R. 1994, Geologic map of the Crater Flats area: Nevada Bureau of Mines & Geology Map 101, scale 1:24,000.
- Ferrill, D.A., Stamatakos, J.A., Jones, S.M., Rahe, B., McKague, H.L., Martin, R.H., and Morris, A.P., 1996, Quaternary slip history of the Bare Mountain Fault (Nevada) from the morphology and distribution of alluvial fan deposits: *Geology*, v.24, no. 6, p.559-562.
- Fridrich, C.J., 1996, Tectonic evolution of the Crater Flat basin, Yucca Mountain region, Nevada, in Wright, L. and Troxel, B. (eds.), *Cenozoic basins of the Death Valley region: Geological Society of America Special Paper*, in press.
- Fridrich, C.J., Whitney, J.W., Hudson, M.R., and Crowe, B.M., 1996, Late Cenozoic extension, vertical-axis rotation, and volcanism in the Crater Flat basin, southwest Nevada, in Wright, L. and Troxel, B. (eds.), *Cenozoic basins of the Death Valley region: Geological Society of America Special Paper*, in press.
- Frizzell, V.A., Jr., and Shulters, J., 1990, Geologic map of the Nevada Test Site, southern Nevada: U.S. Geological Survey Miscellaneous Investigations Map I-2046, scale 1:100,000.
- Frizzell, V.A. and Zoback, M.L., 1987, Stress orientation determined from fault slip data in Hampel Wash area, Nevada, and its relation to contemporary regional stress field: *Tectonics*, v. 6, p. 89-98.
- Gomberg, J., 1996, Stress/strain changes and triggered seismicity following the $M_w 7.3$ Landers, California earthquake: *Journal of Geophysical Research*, v. 101, no. B1, p. 751-764.
- Gomberg, J., Blanpied, M.L., and Beeler, N.M., 1997, Transient triggering of near and distant earthquakes: *Bulletin of Seismological Society of America*, v. 87, no: 2, p. 294-309.
- Gomberg, J., and Bodin, 1994, Triggering of the $M_s = 5.4$ Little Skull Mountain, Nevada, earthquake with dynamic strains: *Bulletin of the Seismological Society of America*, v. 84, no. 3, p. 844-853.
- Gomberg, J., and Davis, S., 1996, Stress/strain changes and triggered seismicity at The Geysers, California: *Journal of Geophysical Research*, v. 101, no. B1, p. 733-749.

- Harmsen, S.C., 1994, The Little Skull Mountain, Nevada, earthquake of 29 June 1992: Aftershock focal mechanisms and tectonic stress field implications: *Bulletin of the Seismological Society of America*, v. 84, no. 5, p. 1484-1505.
- Hull, J., 1988, Thickness-displacement relationships for deformation zones: *Journal of Structural Geology*, v. 10, no. 4, p. 431-435.
- Keefer, D.I., and Bodily, S.E., 1983, Three-point approximations for continuous random variables: *Management Science*, v. 26, p. 595-609.
- King, G.C.P., Stein, R.S., and Lin, J., 1994, Static stress changes and the triggering of earthquakes: *Bulletin of the Seismological Society of America*, v. 84, no. 3, p. 935-953.
- Klinger, R.E., and Piety, L.A., 1996, Evaluation and characterization of Quaternary faulting on the Death Valley and Furnace Creek faults, Death Valley, California: Bureau of Reclamation Seismotectonic Report 96-10, Denver, Colorado, prepared for the U.S. Geological Survey for Yucca Mountain Project Activity 8.3.1.17.4.3.2, 98 p.
- Knott, S.D., Beach, Alastair, Brockbank, P.J., Brown, J.L., McCallum, J.E., and Welbon, A.J., 1996, Spatial and mechanical controls on normal fault populations: *Journal of Structural Geology*, v. 18, nos. 2/3, p. 359-372.
- Maldonado, F., 1985, Geologic map of the Jackass Flats area, Nye County, Nevada: U.S. Geological Survey, Miscellaneous Investigations Map I-1519, scale 1:48,000.
- McKague, H.L., Stamatakos, J.A., and Ferrill, D.A., 1996, Type I faults in the Yucca Mountain region: Center for Nuclear Waste Regulatory Analyses CNWRA 96-007, Rev. 01, variously paginated.
- Mendoza, C., and Hartzell, S.H., 1988, Inversion for slip distribution using teleseismic P-waveforms: North Palm Springs, Borah Peak, and Michoacan earthquakes: *Bulletin of the Seismological Society of America*, v. 78, no. 3, p. 1092-1111.
- Menges, C.M., and Whitney, J.W., 1996, Summary of Quaternary faulting on the Paintbrush Canyon, Stagecoach Road, and Bow Ridge faults; Chapter 4.4, Seismotectonic Framework and Characterization of Faulting at Yucca Mountain, Nevada: U.S. Geological Survey, Report to U.S. Department of Energy, p. 4.4-1 - 4.4-35.
- Morris, A., Ferrill, D.A., and Henderson, D.B., 1996, Slip-tendency analysis and fault reactivation: *Geology*, v. 24, no. 3, p. 275-278.

- Nicol, A., Watterson, J., Walsh, J.J., and Childs, C., 1996. The shapes, major axis orientations and displacement patterns of fault surfaces: *Journal of Structural Geology*, v. 18, nos. 2/3, p. 235-248.
- O'Leary, D.W., 1996, Synthesis of tectonic models for the Yucca Mountain area; Chapter 8, *Seismotectonic Framework and Characterization of Faulting at Yucca Mountain, Nevada*: U.S. Geological Survey, Report to U.S. Department of Energy, p. 8-1 - 8-153.
- Parsons, T., and Thompson, G.A., 1991, Coupled processes of normal faulting and dike intrusion in tectonically extended regions: *Geological Society of America, Abstracts with Programs*, v. 23, n. 2, p. 87.
- Pezzopane, S.K., 1996, Relevant earthquake sources; Chapter 11, *Seismotectonic Framework and Characterization of Faulting at Yucca Mountain, Nevada*: U.S. Geological Survey, Report to U.S. Department of Energy, p. 11-1 - 11-44.
- Pezzopane, S.K., and Dawson, T.E., 1996, Fault displacement hazard: A summary of issues and information; Chapter 9, *Seismotectonic Framework and Characterization of Faulting at Yucca Mountain, Nevada*: U.S. Geological Survey, Report to U.S. Department of Energy, p. 9-1-9-160.
- Pezzopane, S.K., Whitney, J.W., and Dawson, T.E., 1996, Models of earthquake recurrence and preliminary paleoearthquake magnitudes at Yucca Mountain; Chapter 5, *Seismotectonic Framework and Characterization of Faulting at Yucca Mountain, Nevada*: U.S. Geological Survey, Report to U.S. Department of Energy, p. 5-1 - 5-100.
- Piety, L.A., 1996, Compilation of known and suspected Quaternary faults within 100 km of Yucca Mountain: U.S. Geological Survey, Open-File Report 94-112, 31 p.
- Power, W.T., Tullis, T.E., and Weeks, J.D., 1988, Roughness and wear during brittle faulting: *Journal of Geophysical Research*, v. 93, no. B12, p. 15,268-15,278.
- Ramelli, A.R., and Bell, J.W., in prep, Known and suspected Quaternary faults Yucca Mountain - Bare Mountain, scale 1:62,500.
- Rogers, A.M., Harmsen, S.C., and Meremonte, M.E., 1987, Evaluation of the seismicity of the southern Great Basin and its relationship to the tectonic framework of the region: U.S. Geological Survey Open-File Report 87-408, 196 p.

- Rogers, A.M., Harmsen, S.C., Corbett, E.J., Priestley, K., and dePolo, D., 1991. The seismicity of Nevada and some adjacent parts of the Great Basin, in Slemmons, D.B., Engdahl, E.R., Zoback, M.D., and Blackwell, D.D. (eds.), *Neotectonics of North America: Boulder, Colorado, Geological Society of America, Decade Map Volume 1*, p. 153-184.
- Romanowicz, B., and Rundle, J.B., 1993, On scaling relations for large earthquakes: *Bulletin of the Seismological Society of America*, v. 83, no. 4, p. 1294-1297.
- Sandia National Laboratories, 1997, Hydraulic Fracturing Stress Measurements in Test Hole ESF-AOD-HDFR#1, Thermal Test Facility, Exploratory Studies Facility at Yucca Mountain: Sandia National Laboratories WBS 1.2.3.2.7.3.4. WA-0065 QA:L, 50 pages.
- Scott, R.B., 1990, Tectonic setting of Yucca Mountain, southwest Nevada, in Wernicke, B.P. (ed.), *Basin and Range extensional tectonics near the latitude of Las Vegas, Nevada: Geological Society of America Memoir 176*, p. 251-282.
- Scott, R.B., and Bonk, J., 1984, Preliminary geologic map of Yucca Mountain, Nye County, Nevada with geologic sections: U.S. Geological Survey Open-File Report 84-494, 9 p., scale 1:12,000.
- Segall, P., and Pollard, D.D., 1983, Nucleation and growth of strike slip faults in granite: *Journal of Geophysical Research*, v. 88, no. B1, p. 555-568.
- Simonds, W.F., Whitney, J.W., Fox, K.F., Ramelli, A., Yount, J., Carr, M.D., Menges, C.M., Dickerson, R., and Scott, R.B., 1995, Map of fault activity of the Yucca Mountain area, Nye County, Nevada: U.S. Geological Survey Miscellaneous Investigations Series Map I-2520, scale 1:24,000.
- Simpson, R.W., and Reasenber, P.A., 1994, Earthquake-induced static-stress changes on central California faults, in Simpson, R.W. (ed.), *The Loma Prieta, California, Earthquake of October 17, 1989—Tectonic Processes and Models: U.S. Geological Survey Professional paper 1550-F*, p. F55-F89.
- Smith, R.P., Jackson, S.M., and Hackett, W.R., 1995, Method for estimating the maximum magnitudes of earthquakes associated with potential dike intrusion and basaltic volcanism in the Yucca Mountain area: Implications for seismic hazards assessment, *Proceedings of the Topical Meeting on Methods of Seismic Hazards Evaluation, Focus '95: American Nuclear Society, Inc., La Grange Park, Illinois*, p. 178-184.

- Smith, R.P., Jackson, S.M., and Hackett, W.R., 1996, Paleoseismology and seismic hazards evaluations in extensional volcanic terrains: *Journal of Geophysical Research*, v. 101, no. B3, p. 6277-6292.
- Sonder, L.J., Jones, C.H., Salyards, S.L., and Murphy, K.M., 1994, Vertical-axis rotations in the Las Vegas Valley Shear Zone, southern Nevada: Paleomagnetic constraints on kinematics and dynamics of block rotations: *Tectonics*, v. 13, p. 769-788.
- Stepp, J.C., 1973, Analysis of completeness of the earthquake sample in the Puget Sound area, *in* Harding, S.T. (ed.), *Contributions to seismic zoning*: U.S. Department of Commerce, NOAA Technical Report ERL 267-ESL 30, p. 16-28.
- Stewart, J.H., and Diamond, D.S., 1990, Changing patterns of extensional tectonics; Overprinting of the basin of the middle and upper Miocene Esmeralda Formation in western Nevada by younger structural basins, *in* Wernicke, B.P. (ed.), *Basin and Range extensional tectonics near the latitude of Las Vegas, Nevada*: Geological Society of America Memoir 176, p. 447-475.
- Stock, J.M., Healy, J.H., Hickman, S.H., and Zoback, M.D., 1985, Hydraulic fracturing stress measurements at Yucca Mountain, Nevada, and relationship to regional stress field: *Journal of Geophysical Research*, v. 90, no. B10, p. 8691-8706.
- U.S. Geological Survey (Whitney, J.W., Coordinator), 1996, Seismotectonic framework and characterization of faulting at Yucca Mountain, Nevada: U.S. Geological Survey report to the Department of Energy that fulfills Level 3 Milestone 3GSH100M WBS Number 1.2.3.2.8.3.6, four volumes variously paginated.
- Veneziano, D., and Van Dyck, J., 1985, Statistical discrimination of "aftershocks" and their contribution to seismic hazard, seismic hazard: *Methodology for Nuclear Facilities in the Eastern United States*, EPRI Research Project No. P101-29, EPRI/SOG Draft 85-1, v. 2, Appendix A-4.
- Wald, D.J., and Heaton, T.H., 1994, Spatial and temporal distribution of slip for the 1992 Landers, California, earthquake: *Bulletin of the Seismological Society of America*, v. 84, no. 3, p. 668-691.
- Wells, D.L., and Coppersmith, K.J., 1994, New empirical relationships among magnitude, rupture length, rupture width, rupture area, and surface displacement: *Bulletin of the Seismological Society of America*, v. 84, no. 4, p. 974-1002.

Wesnousky, S.G., and Jones, C.H., 1994, Oblique slip, slip partitioning, spatial and temporal changes in the regional stress field, and the relative strength of active faults in the Basin and Range, western United States: *Geology*, v. 22, no. 11, p. 1031-1034.

Yeats, R.S., Sieh, K., and Allen, C.R., 1997, *The geology of earthquakes*: Oxford University Press, New York, 568 p.

Youngs, R.R., and Coppersmith, K.J., 1985, Implications of fault slip rates and earthquake recurrence models to probabilistic seismic hazard estimates: *Bulletin of the Seismological Society of America*, v. 75, no. 4, p. 939-964.

Youngs, R.R., Swan, III, F.H., Power, M.S., Schwartz, D.P., and Green, R.K., 1987, Probabilistic analysis of earthquake ground shaking hazard along the Wasatch Front, Utah, in Gori, P.L., and Hays, W.W., (eds.), *Assessment of regional earthquake hazards and risk along the Wasatch Front, Utah*: U.S. Geological Survey Open File Report 87-585, M-1 to M-110.

TABLE AAR-1
SEISMIC SOURCE PARAMETERS FOR REGIONAL FAULT SOURCES
 (p. 1 of 2)

Fault Name	Total Fault Length ¹ (km)	Max. Rupture Length ¹ (km)	Min. Distance to Rep. (km)	Doc. Quaternary Displacement	Style	Dip ¹ (deg.)	Slip Rate ¹ (mm/yr)	Recur. Int. ¹ (ka)	P[S]
Mine Mountain (MM)	20	20	11	y?	LO	50	0.002		0.6
	23	23				70	0.015		
	37	37				90	0.03		
Wahmoni (WAH)	11	11	22	y	NL	50	0.002		1
	14	14				65	0.025		
	17	17				90	0.05		
Ash Meadows (AM)	8	8	24	y	N	50	0.001		1
	42	42				65	0.01		
	72	72				80	0.1		
Oasis Valley (OSV)	8	8	24	y?	N	50	0.001		0.4
	19	19				65	0.005		
	29	29				80	0.01		
Rock Valley (RV)	25	25	25	y	LO	65	0.02	33	1
	33	33				90	0.06	50	
	69	46				90	0.1	180	
Cane Spring (CS)	18	18	29	y?	LO?	65	0.002		0.6
	22	22				90	0.025		
	36	36				90	0.05		
West Specter R. (WSR)	7	7	33	y	N	45	0.001		1
	8	8				60	0.004		
	22	22				80	0.01		
Amargosa R./ Pahrump (AR/PRP)	75	75	34	y	R?	80	0.005		1
	82	82				90	0.07		
	134	110				90	0.2		
Amargosa R. (AR)	13	13	34	y	NR	80	0.005		1
	14	14				90	0.04		
	25	25				90	0.2		
Yucca Lake (YCL)	12	12	36	y?	N	45	0.001		0.5
	14	14				60	0.005		
	24	24				80	0.01		
Eleana Range (ER)	11	11	37	y	N	45	0.001		1
	13	13				60	0.005		
	18	18				80	0.01		

TABLE AAR-1
SEISMIC SOURCE PARAMETERS FOR REGIONAL FAULT SOURCES
 (p. 2 of 2)

Fault Name	Total Fault Length ¹ (km)	Max. Rupture Length ¹ (km)	Min. Distance to Rep. (km)	Doc. Quaternary Displacement	Style	Dip ¹ (deg.)	Slip Rate ¹ (mm/yr)	Recur. Int. ¹ (ka)	P[S]
Yucca Fault (YC)	20	20	40	y	N/RO	50	0.001		1
	25	25				65	0.025		
	31	31				90	0.05		
Keane Wonder (KW)	19	19	43	y?	N	50	0.001		0.6
	23	23				65	0.005		
	32	32				85	0.01		
Furnace Creek (FC)	100	100	50	y	R	80	2.3	0.5	1
	118	118				90	8.0	0.7	
	146	146				90	10.0	1.0	
Death Valley/ Furnace Creek (DV/FC)	154	125	50	y	N/R	50	2.3	0.5	1
	178	150				82	8.0	0.7	
	193	165				90	10.0	1.0	
West Spring Mts. (WSM)	37	23	53	y	N	50	0.02	28	1
	52	37				65	0.05	30	
	66	48				80	0.07	124	
Death Valley (DV)	42	42	55	y	N	50	3.0	0.5	1
	57	57				65	4.0	0.75	
	74	74				90	5.0	1.3	
Belted Range (BLR)	21	21	55	y	N	50	0.02		1
	29	29				65	0.05		
	50	45				80	0.1		
Kawich Range (KR)	20	20	57	y	N	50	0.005		1
	27	27				65	0.03		
	76	45				80	0.07		
Pahrump (PRP)	37	37	68	y	R	80	0.005		1
	45	45				90	0.07		
	107	85				90	0.2		
West Pintwater (WPR)	30	30	76	y	N	45	0.002		1
	48	48				60	0.04		
	57	57				80	0.07		

¹ Three numbers represent minimum, preferred, and maximum values

**TABLE AAR-2
SOURCE INVENTORIES**

Model [?]	Local Seismic Source	P[s] [§]
A-1, A-2, A-3	CFD faults *	*
	Highway 95 fault (H95)	0.5
	Regional ss (subjacent) (T4-SS)	1.0
	Background source zones	1.0
B-1, B-2, B-3	CFD faults *	*
	Highway 95 fault (H95)	0.8
	No. bounding ss fault (T4-PA2)	0.5
	Background source zones	1.0
C-1, C-2	CFD faults *	*
	Highway 95 fault (H95)	0.8
	No. bounding ss fault (T4-PA2)	0.5
	Cross-basin fault (T4-CB)	1.0
	Background source zones	1.0
D-1, D-2, D-3	CFD faults *	*
	Background sources	1.0

[?] Keyed to Figure AAR-1

[§] Probability of being seismogenic

* See Table AAR-3

**TABLE AAR-3
INVENTORY OF CRATER FLAT DOMAIN (CFD) FAULTS**

FAULT	P[s] ⁵
Bare Mountain	1.0
Bow Ridge	1.0
S. Crater Flat	1.0
N. Crater Flat	1.0
W. Dune Wash #1	0.1
W. Dune Wash #2	0.1
Ghost Dance	0.1
Fatigue Wash	1.0
Iron Ridge	1.0
E. Lathrop Cone	1.0
Midway Valley	0.1
Paintbrush Canyon	1.0
Solitario Canyon	1.0
Stagecoach Road	1.0
S. Windy Wash	1.0
N. Windy Wash	1.0
C. Windy Wash	0.6
C. Crater Flat	0.6
Black Cone	0.8
E. Busted Butte	0.4

⁵ Probability of being seismogenic. P[S] for each fault is constant for all the logic tree branches outlined in Table AAR-2 and Figure AAR-1

TABLE AAR-4
ESTIMATES OF FAULT PARAMETERS FOR LOCAL FAULT SOURCES
 (p. 1 OF 3)

fault name	act length ¹ (km)	doc. Quat act?	styl	fault dip ¹ (deg)	total disp. ¹ (m)	disp./event Dmax ¹ (cm)	Davg ¹ (cm)	slip rate ¹ (mm/yr)	rec. int. ¹ (ka)
Independent down-to-west faults									
	17			50	2500	120	80	0.005	200
Bare Mountain (BM)	21	Y	n	60	3000	150	120	0.01	100
	31			70	4000	180	160	0.25	30
	4			50	100	20	20	0.002	200
Bow Ridge (BWR)	8	Y	ln	60	200	40	40	0.003	120
	10			70	300	60	60	0.007	70
	6			50	40	30	30	0.002	150
S. Crater Flat (SCF)	8	Y	ln?	70	300	50	50	0.008	80
	14			80	600	70	70	0.02	40
	5			50	100	30	30	0.001	
N. Crater Flat (NCF)	8	Y	ln?	60	200	50	50	0.003	
	10			70	300	70	70	0.005	
	3			70	50	10	10	0.0001	
W. Dune Wash 1 (WD1)	7	N?	ln?	80	100	20	20	0.0005	
	10			90	200	30	30	0.001	
	2			60	30	5	5	0.0001	
Ghost Dance (GD)	2.5	Y?	ln	70	40	10	10	0.0005	
	7			80	50	15	15	0.001	
	6.5			50	70	30	30	0.003	
Fatigue Wash (FW)	9.5	Y	ln	60	200	50	50	0.009	
	14			70	400	70	70	0.02	
	4.5			50	200	10	10	0.001	
Iron Ridge (IR)	6.5	Y	ln?	60	250	50	50	0.002	
	9			70	400	80	80	0.005	
	1.5			50	50	30	30	0.005	
E. Lathrop Cone (ELC)	4	Y	ln?	65	100	50	50	0.01	
	9			80	200	80	80	0.03	
	3			60	30	10	10	0.0001	
Midway Valley (MWV)	4	N	ln?	70	50	20	20	0.0005	
	8			80	70	30	30	0.001	
	8			50	300	100	40	0.01	200
Paintbrush Cyn (PBC)	12	Y	ln	60	500	150	90	0.015	60
	25			70	700	250	130	0.03	30
	13.5			50	400	70	50	0.005	100
Solitario Cyn (SC)	16	Y	ln	60	700	100	80	0.01	60
	25			70	1000	130	110	0.02	35
	3.5			50	300	50	50	0.01	40
Stagecoach Road (SR)	4.5	Y	ln?	60	500	70	70	0.04	20
	8			70	700	100	100	0.07	5
	8			50	300	50	50	0.01	60
S. Windy Wash (SWW)	9	Y	ln	60	500	70	70	0.03	40
	12			70	700	90	90	0.04	20

TABLE AAR-4
ESTIMATES OF FAULT PARAMETERS FOR LOCAL FAULTS SOURCES
(P. 2 OF 3)

fault name	act length ¹ (km)	doc. Quat act?	styl	fault dip ¹ (deg)	total disp. ¹ (m)	disp./event Dmax ¹ (cm)	Davg ¹ (cm)	slip rate ¹ (mm/yr)	rec. int. ¹ (ka)
<u>Independent down-to-west faults (cont'd.)</u>									
N. Windy Wash (NWW)	7			50	300	30	30	0.001	
	8	Y	ln?	60	400	50	50	0.003	
	10			70	600	70	70	0.005	
<u>Independent down-to-east faults</u>									
Black Cone (BC)	3.5			50		10	10	0.001	
	8	Y	m?	65		30	30	0.003	
	12			80		50	50	0.005	
E. Busted Butte (EB)	1.5			50	200	10	10	0.0005	
	4	Y	n?	60	400	30	30	0.001	
	11			70	600	50	50	0.003	
C. Crater Flat (CCF)	3			50		10	10	0.001	
	6.5	Y	n?	65		30	30	0.003	
	8			80		50	50	0.005	
W. Dune Wash 2 (WD2)	1.5			70	100	10	10	0.0001	
	3	N?	n?	80	150	20	20	0.0005	
	5			90	200	30	30	0.001	
C. Windy Wash (CWW)	4			50		10	10	0.001	
	5	Y	n?	65		30	30	0.003	
	6			80		50	50	0.005	
<u>Linked systems</u>									
PBC/SR	14			50	300	100	40	0.01	120
	18	Y	ln	60	500	150	90	0.04	40
	32			70	700	250	130	0.07	15
SWW/FW/CWW/NWW	21			50	300	50	50	0.01	60
	23	Y	ln	60	500	70	70	0.03	40
	28			70	700	90	90	0.04	20
<u>Coalesced systems</u>									
E-side	22			50	300	100	40	0.01	120
	24	Y	ln	60	500	150	90	0.04	40
	36			70	700	250	130	0.07	15
W-side #1	13.5			50	400	70	30	0.005	100
	16	Y	ln	60	700	100	60	0.01	60
	25			70	1000	130	90	0.02	35
W-side #2	21			50	300	70	70	0.01	60
	23	Y	ln	60	500	110	110	0.04	40
	29			70	700	150	150	0.06	20

TABLE AAR-4
ESTIMATES OF FAULT PARAMETERS FOR LOCAL FAULTS SOURCES
(P. 3 OF 3)

Multiple-structure coalesced systems (length & recurrence)

fault name	act leng ¹ (km)	rec. int. ¹ (ka)
Single	35	100
W-side	39	60
(W-side1+W-side2)	54	35
Single	57	120
YM system	63	60
(E-side+W-Side1+W-side2)	907	35
Single system	74	200
(YM+BM)	84	100
	121	35

fault name	active length ¹ (km)	doc Q actv?	style	fault dip ¹ (deg.)	disp./event Dmax ¹ (cm)	Davg ¹ (cm)	slip rate ¹ (m/ka)
Buried/bounding strike-slip (ss) faults							
	50			70	200	200	0.05
Regional ss fault (T4-ss)	75	N	ri	90	400	400	0.1
	100			90	600	600	0.2
No. bounding ss fault (T4-PA2)	10			70	30	30	0.005
	20	N	ri	90	80	80	0.01
	30			90	130	130	0.05
	20			60	50	50	0.02
Hwy.95 fault (H95)	40	N?	ri	80	150	150	0.05
	60			90	250	250	0.1
	10			70	30	30	0.005
Cross-basin fault (T4-CB)	20	N	ri	90	80	80	0.01
	30			90	130	130	0.05

¹ Three numbers represent minimum, preferred, and maximum values.

**TABLE AAR-5
WEIGHTS FOR BEHAVIOR OF LOCAL FAULTS
DEPENDING ON TECTONIC MODELS**

Behavior	A1	A2	A3	B1	B2	B3	C1	C2	D1	D2	D3
Independent	0.1	0.2	0.2	0.1	0.2	0.2	0.1	0.6	0.1	0.2	0.2
Coalesced	0.9	0.8	0.8	0.9	0.8	0.8	0.9	0.4	0.9	0.8	0.8

**TABLE AAR-6
WEIGHTS FOR LINKED OPTIONS GIVEN INDEPENDENT BEHAVIOR,**

	A1	A2	A3	B1	B2	B3	C1	C2	D1	D2	D3
PBC/SR:											
Independent	0.4	0.2	0.2	0.4	0.2	0.2	0.4	0.5	0.4	0.2	0.2
Linked	0.6	0.8	0.8	0.6	0.8	0.8	0.6	0.5	0.6	0.8	0.8
WW/FW:											
Independent	0.5	0.4	0.4	0.5	0.4	0.4	0.5	0.7	0.5	0.4	0.4
Linked	0.5	0.6	0.6	0.5	0.6	0.6	0.5	0.3	0.5	0.6	0.6

- PBC/SR includes Paintbrush and Stagecoach Road faults.
- WW/FW includes So. Windy Wash, Fatigue Wash, Central Windy Wash, and No. Windy Wash faults. CWW is antithetic to the subparallel FW. Estimates for this linked system are primarily derived from SWW, the most active of the four faults.

**TABLE AAR-7
WEIGHTS FOR COALESCED MODELS
GIVEN COALESCED BEHAVIOR**

Coalesced model	A1	A2	A3	B1	B2	B3	C1	C2	D1	D2	D3
1 system	0.2	0.0	0.0	0.0	0.0	0.0	0.1	0.0	0.0	0.0	0.0
2 systems 0.2	0.0	0.0	0.0	0.0	0.0	0.2	0.0	0.0	0.0	0.0	
3 systems 0.3	0.4	0.4	0.3	0.2	0.2	0.3	0.1	0.3	0.2	0.2	
4 systems 0.3	0.6	0.6	0.7	0.8	0.8	0.4	0.9	0.7	0.8	0.8	

**TABLE AAR-8
WEIGHTS FOR M_{max} APPROACHES—LOCAL FAULT SOURCES**

Expected Rupture Length <25 km:

Approach	Weight
a. Rupture length	0.3
b. Rupture area	0.2
c. Rupture length/slip rate	0.2
d. Moment equation	0.3

Expected Rupture Length \geq 25 km:

Approach	Weight
a. Rupture length	0.3
b. Rupture area	0.0
c. Rupture length/slip rate	0.2
d. Moment equation	0.5

Exception #1: For scenarios A-1, B-1, C-1, and D-1 (local detachment at 3-10 km depth), use these weights for all CFD faults other than the Bare Mountain fault:

Approach	Weight
a. Rupture length	0.1
b. Rupture area	0.2
c. Rupture length/slip rate	0.1
d. Moment equation	0.6

Exception #2: For "multiple-structure coalesced systems" (which have no slip rates provided in Table AAR-4), use these weights:

Approach	Weight
a. Rupture length	0.5
b. Rupture area	0.2
c. Rupture length/slip rate	0.0
d. Moment equation	0.3

**TABLE AAR-9
REGRESSION RELATIONS**

Equation	Number of Data Points	Coefficients and Standard Errors		Standard Deviation	Correlation Coefficient	Range of Variables	
		a (sa)	b (sb)			Independent	Dependent
1. $\log \bar{U} = \log b + \log L^{total}$ [m/m]	19		$\log b = -4.433$ (0.041)	0.18	n.d.	3.3 to 21.3 km	0.08 to 1.14 m
2. $\log (Dcum) = a + b (\log L^{total})$ [m/m]	16	-1.58 (1.37)	1.00*	0.32	0.61	3.3 to 21.3 km	40 to 700 m
3. $QSR = a + b Dcum$ [mm/yr/m]	11	0*	$3.26 (1.72) e-05$	0.01	0.58	40 to 700 m	0.0005 to 0.04 m/yr
4. $PDF = a * \exp (b * D/MD^{max})$	19	0.09 (0.02)	-0.68 (0.16)	1.88	-0.70	0.1 to 2.9	0.01 to 0.14
5. $CDF = 1 - \exp (-\lambda * D/MD^{max})$	82		$\lambda = 1.20 (0.13)$	0.69	n.d.	0.1 to 2.9	0.14 to 1.00

* Constrained

Table AAR-10
Displacement Data Used for Figure AAR-11

FAULT	TRENCH	MD^{max} (cm)	D_{obs} (cm)/ $DIMD^{max}$							
BR	14D	40.92	44 1.08	13 0.32	14 0.34					
NCF	CFF-T2a	46.79	3 0.06	5 0.11	40 0.85	50 1.07	50 1.07			
SCF	CFF-T1a	52.77	18 0.34	10 0.19	20 0.38					
FW	CF 1	49.59	25 0.50	105 2.12	54 1.09					
IR	SCF-T2	46.98	5 0.11	70 1.49	100 2.13	70 1.49				
PB	A1	114.07	6 0.05	39 0.34	7 0.06	100 0.88				
PB	BB4	114.07	44 0.39	28 0.25	47 0.41	167 1.46	142 1.24	105 0.92	94 0.82	
PB	MWV-T4	114.07	20 0.18	62 0.54	98 0.86	40 0.35				
SC	SCF-T1	111.64	10 0.09	70 0.63						
SC	SCF-T3	111.64	10 0.09	80 0.72	35 0.31					
SC	SCF-T4	111.64	5 0.04	30 0.27	20 0.18					
SC	SCF-T8	111.64	10 0.09	120 1.07	30 0.27	50 0.45				
SCR	SCR-T1	66.21	40 0.60	42 0.63	47 0.71	51 0.77				
SCR	SCR-T3	66.21	43 0.65	59 0.89	57 0.86	67 1.01	35 0.53			
WW	CF-2 northwall	30.34	4 0.13	20 0.66	23 0.76	20 0.66	73 2.41	45 1.48	50 1.65	80 2.64
WW	CF-2 southwall	30.34	4 0.13	12 0.40	50 1.65	42 1.38	28 0.92	16 0.53	60 1.98	65 2.14
WW	CF-2.5	30.34	6 0.20	20 0.66	42 1.38	15 0.49				
WW	CF-3 northwall	30.34	4 0.13	33 1.09	87 2.87	35 1.15	65 2.14			
WW	CF-3 southwall	30.34	3 0.10	35 1.15	88 2.90					

Existing Tectonic Framework	Significant NW-SE Dextral Shear Structure(s)?	Dextral-Shear Structure	Local Detachment Beneath Crater Flat Domain?	Depth of Detachment	SOURCE INVENTORY See Table AAR-2, Figure AAR-6
-----------------------------	---	-------------------------	--	---------------------	---

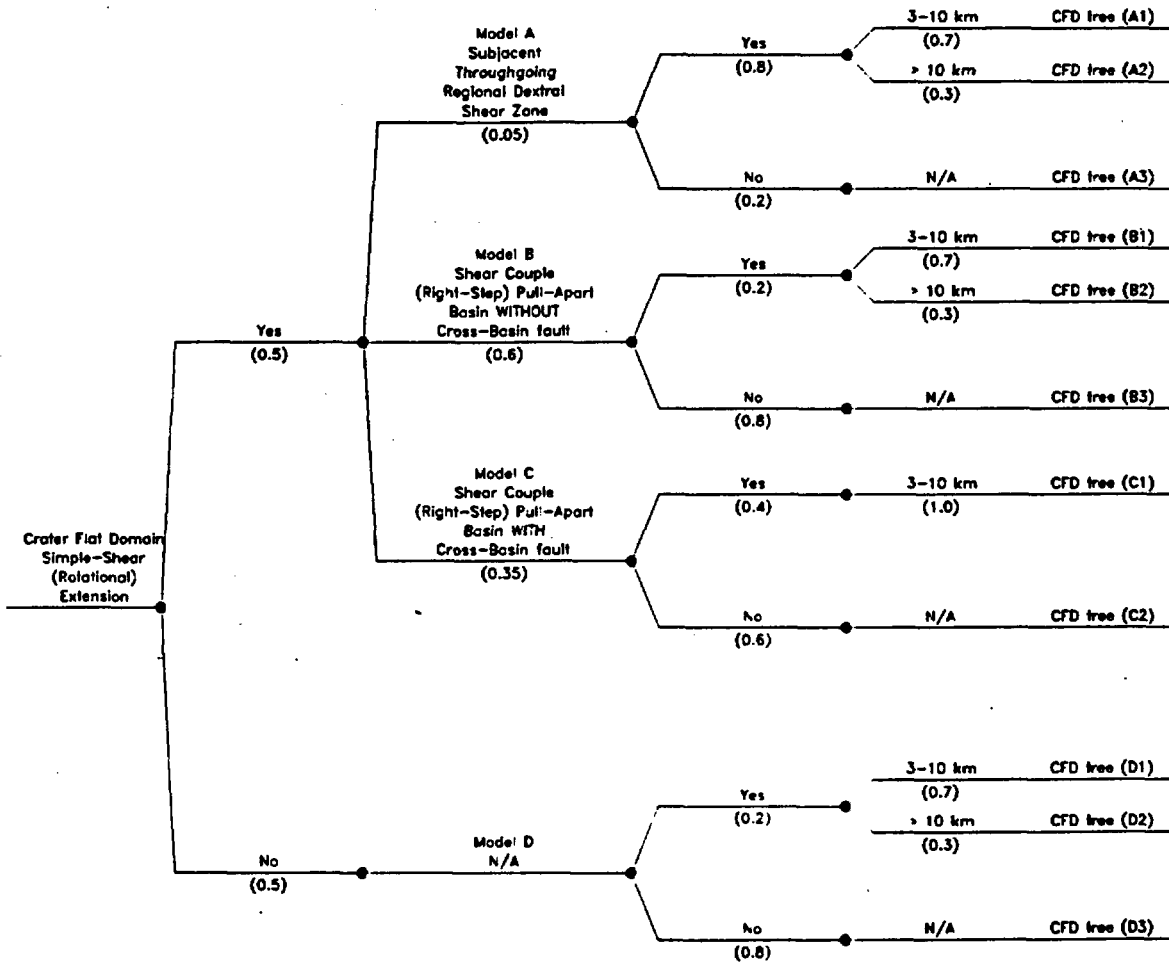
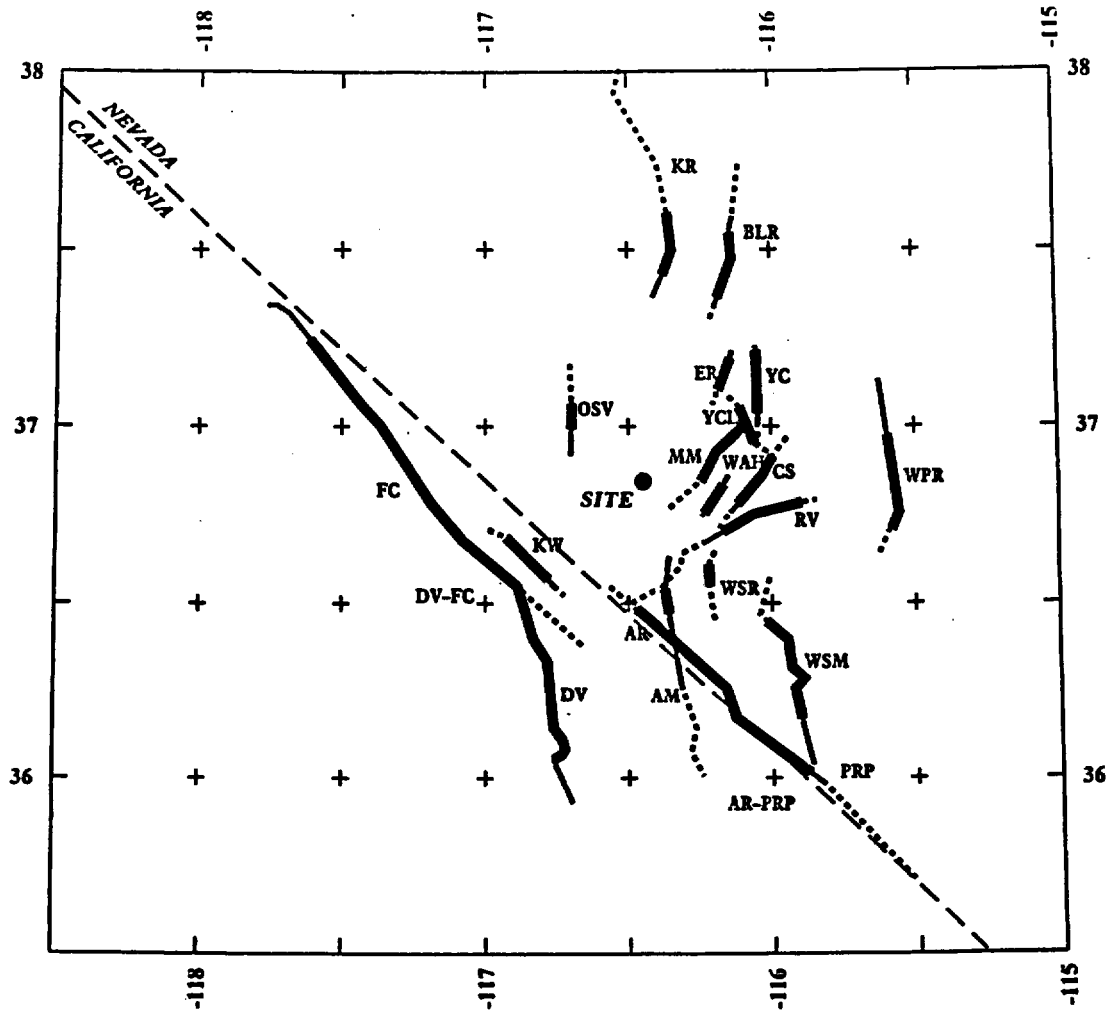


Figure AAR-1 Logic tree for tectonic models and local faults



EXPLANATION

NOTE: Fault names are listed in Table AAR-1

Fault Lengths:

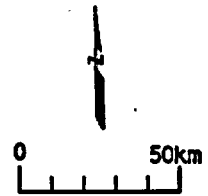
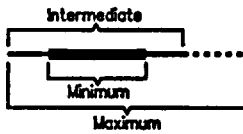


Figure AAR-2 Map showing regional faults included in the seismic source model

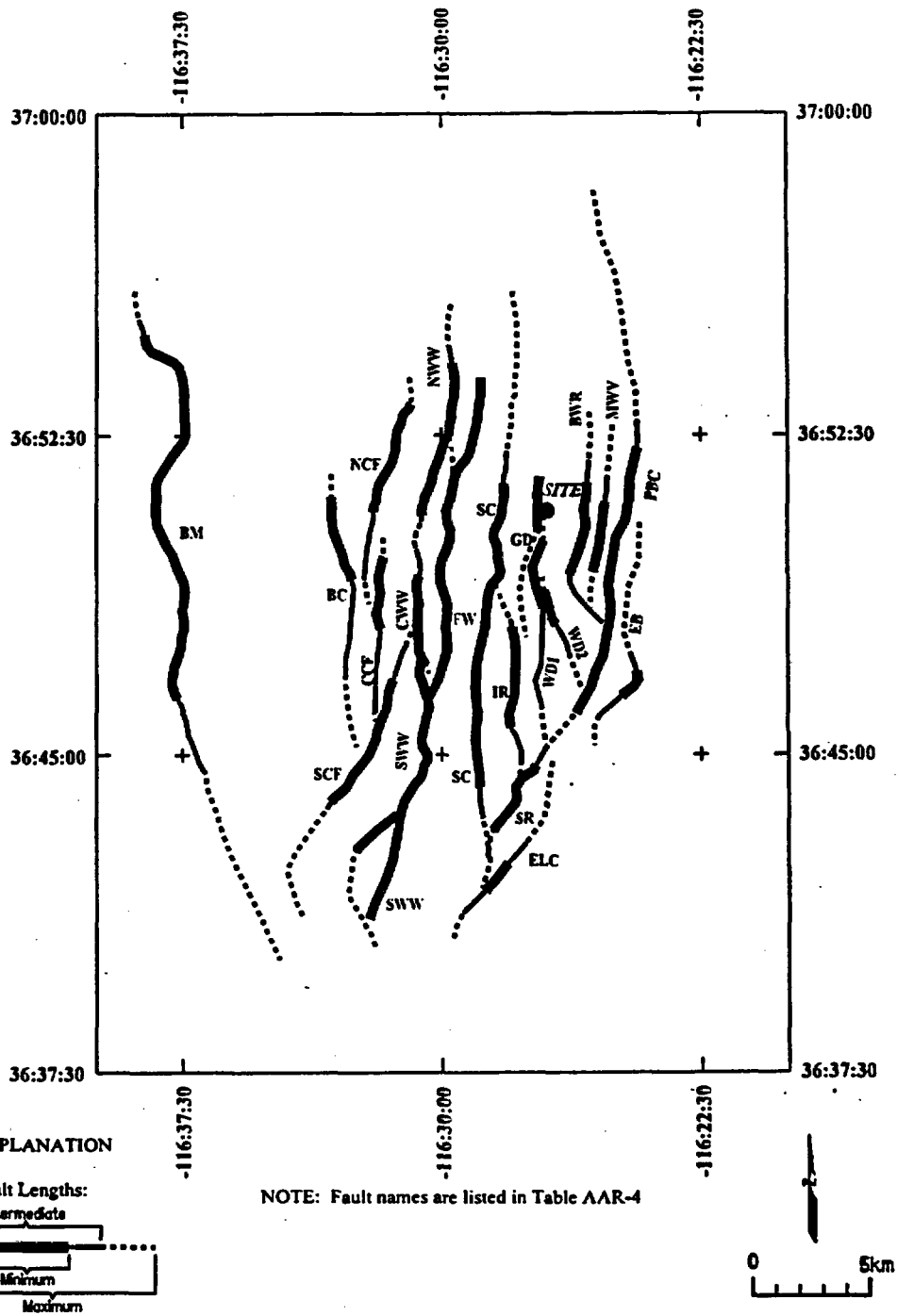


Figure AAR-3 Map showing local fault sources included in the independent model

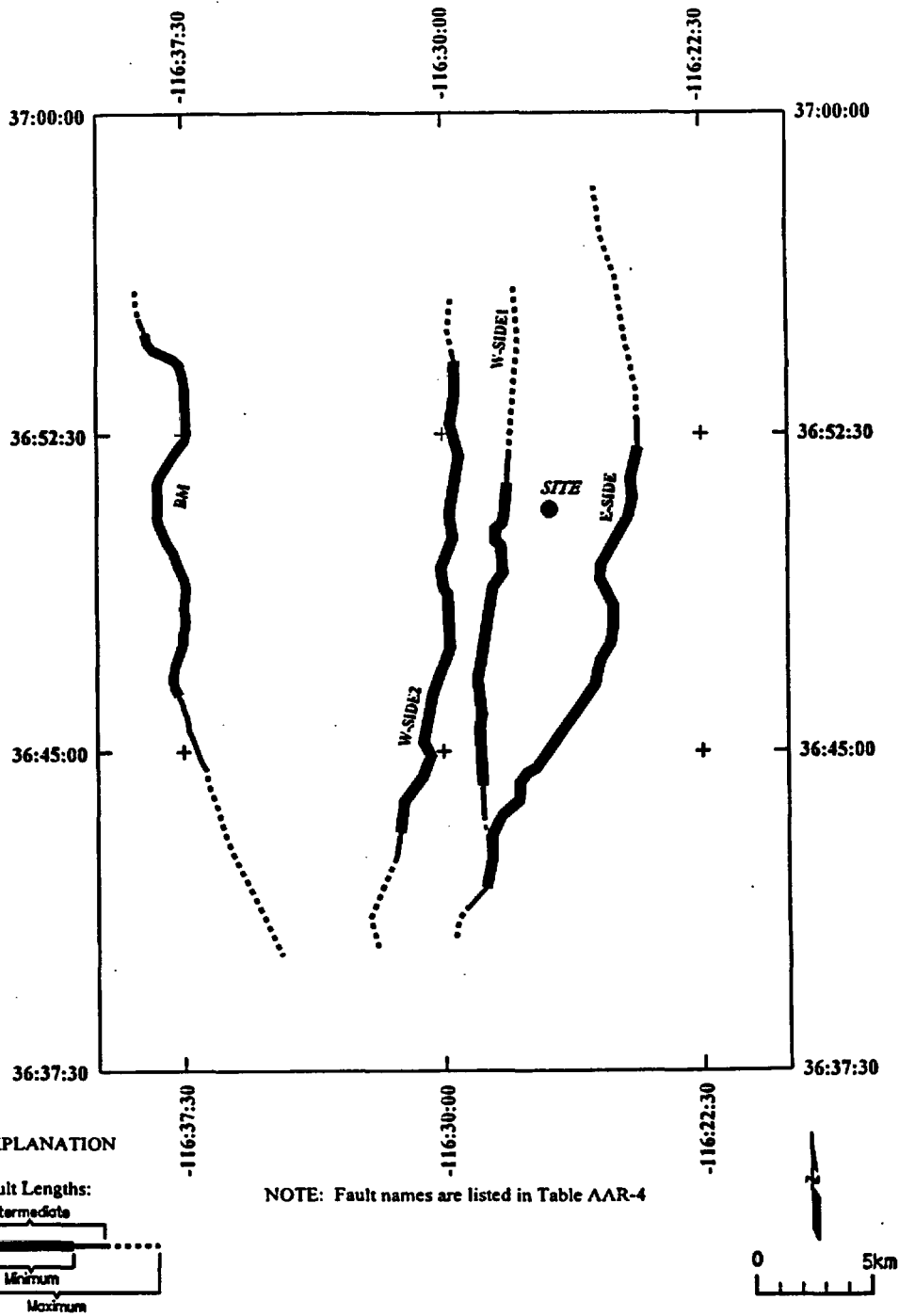


Figure AAR-4 Map showing local faults included in the coalesced model

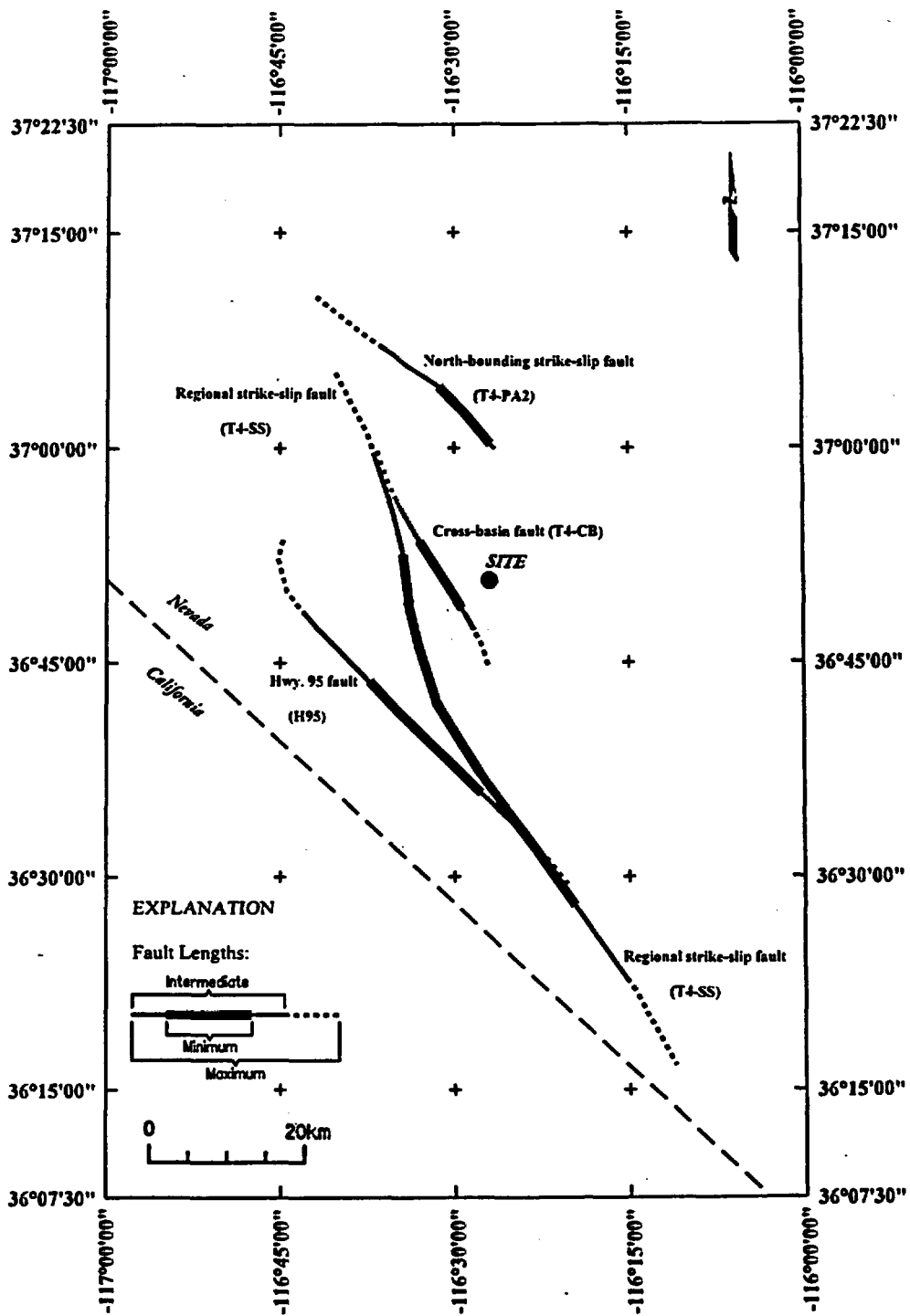


Figure AAR-5 Map showing hypothetical fault sources included in the seismic source model

<i>Model</i>	<i>Behavior</i>	<i>Coalesced Behavior</i>	<i>Source List</i>	<i>Independent Linked Behavior</i>	<i>Source List</i>
--------------	-----------------	---------------------------	--------------------	------------------------------------	--------------------

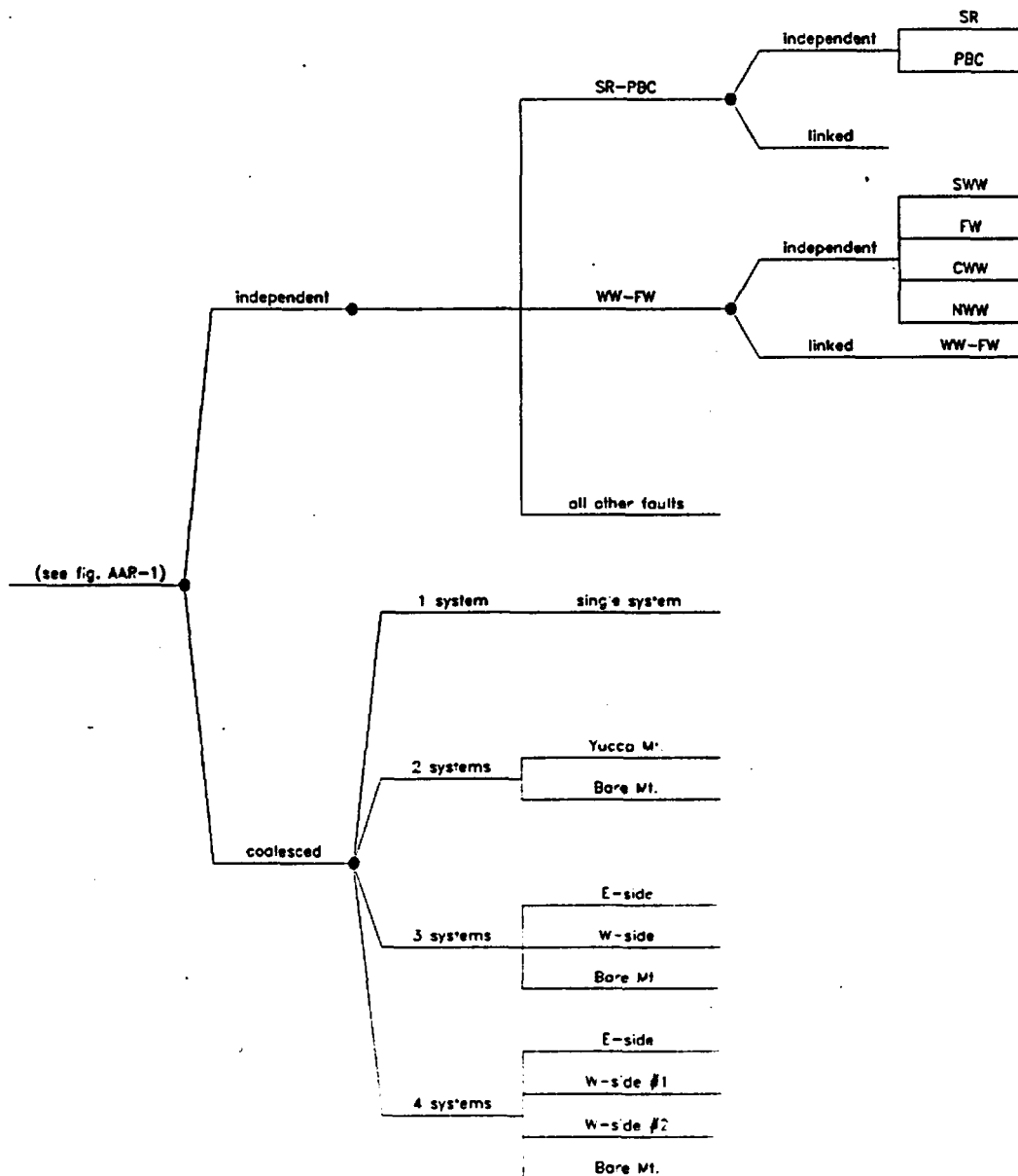


Figure AAR-6 Logic tree: behavior branches for Crater Flat domain

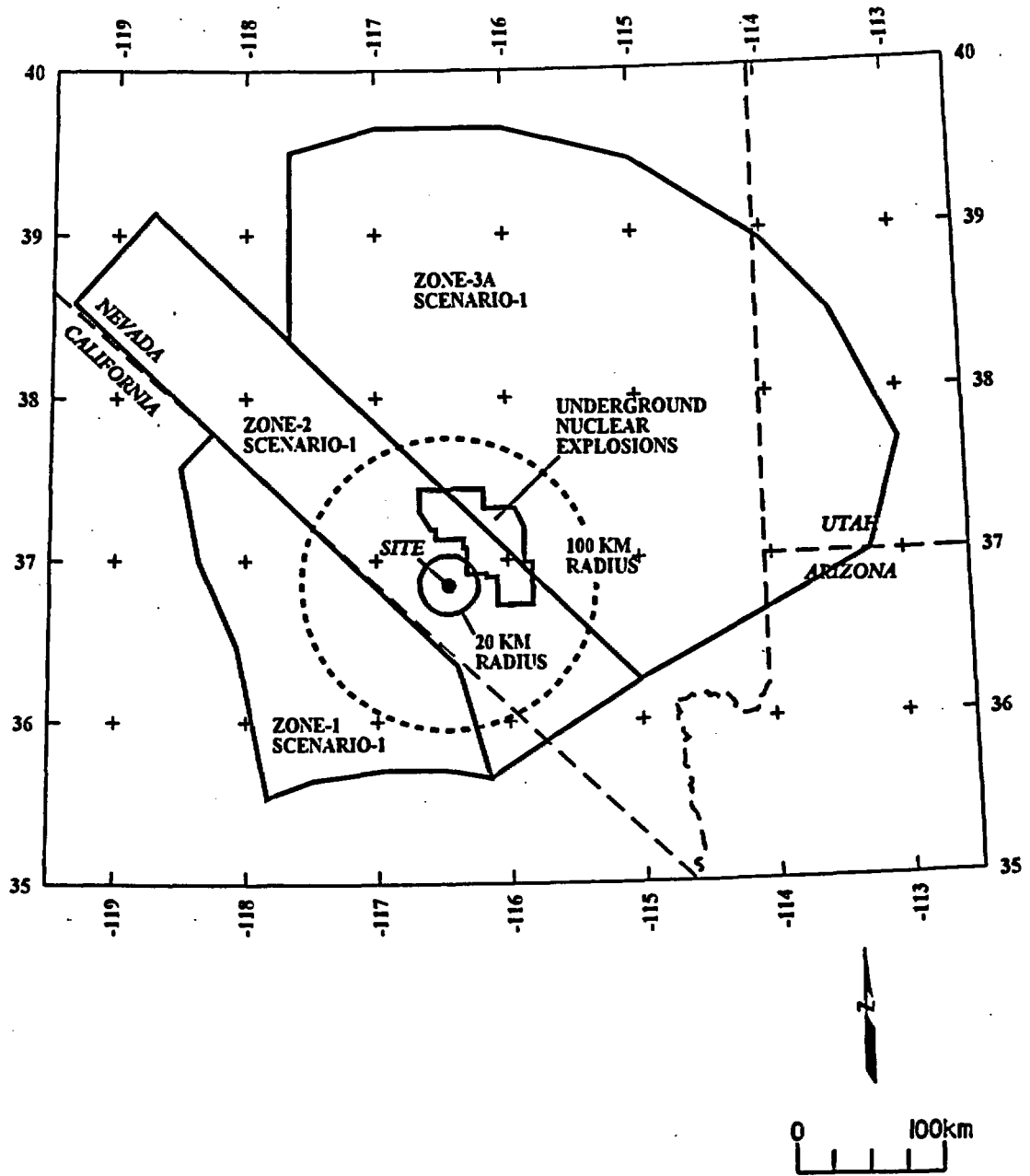


Figure AAR-7 Map showing the boundaries of seismic source zones, Scenario 1.

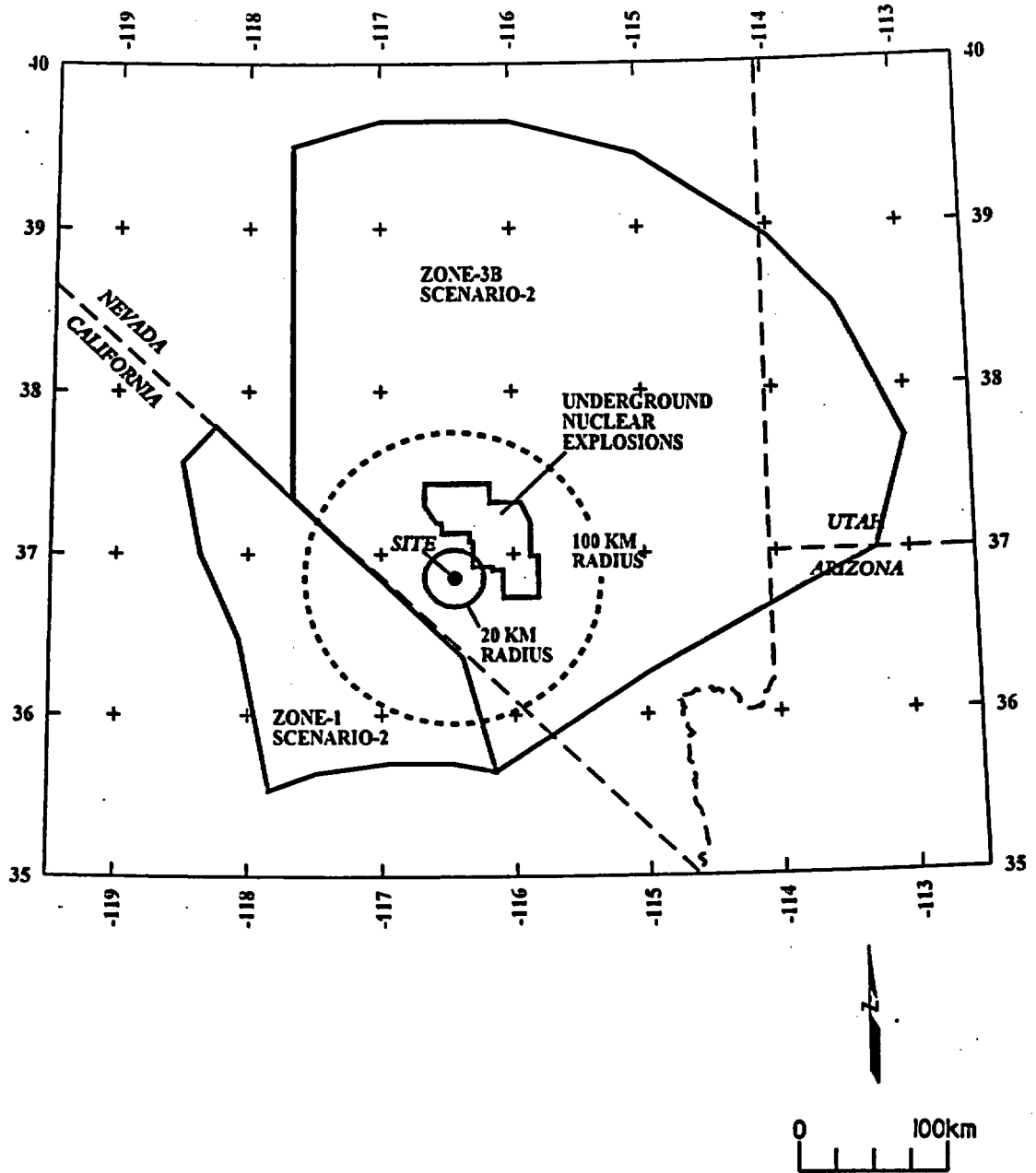


Figure AAR-8 Map showing the boundaries of seismic source zones, Scenario 2.

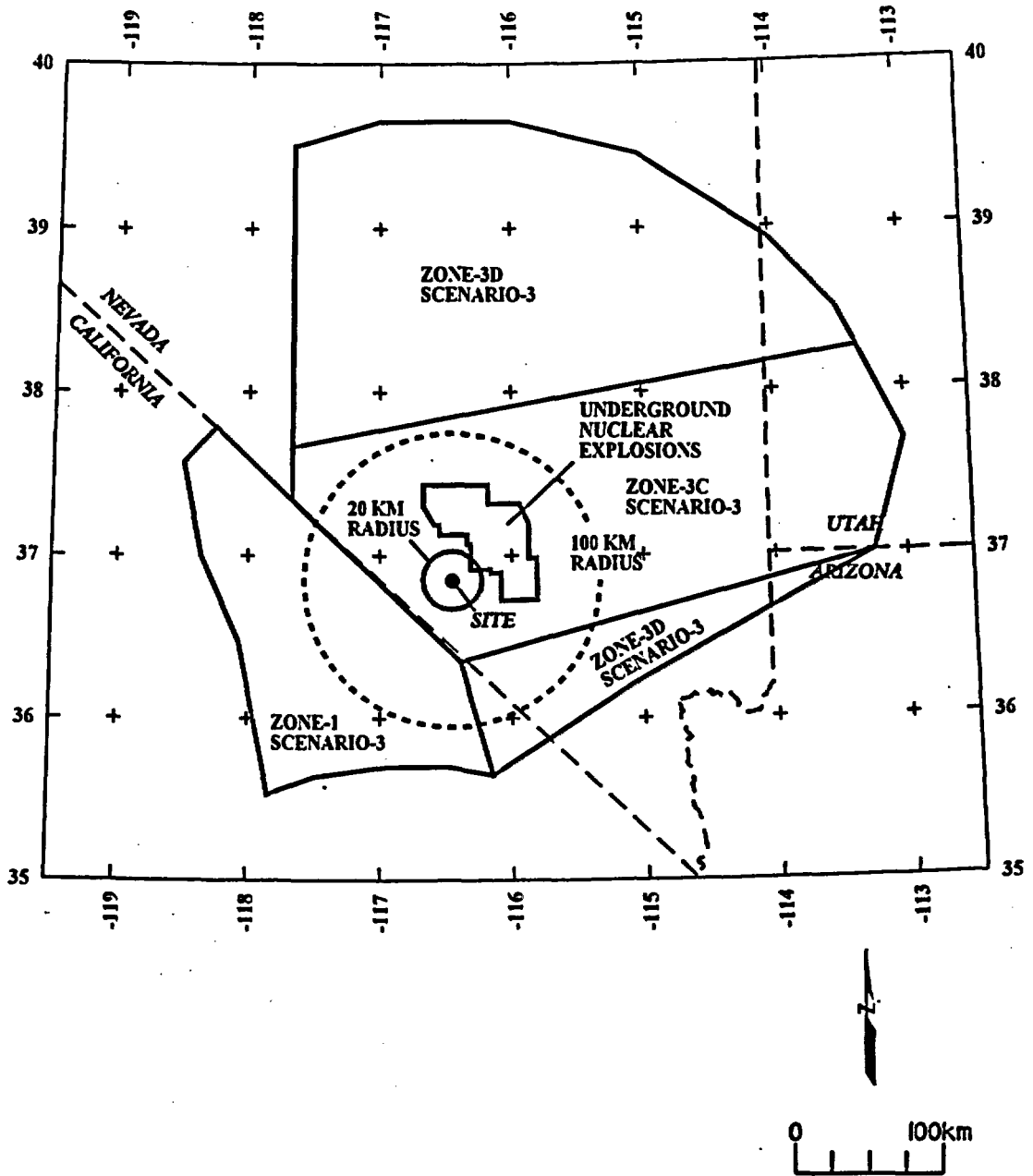


Figure AAR-9 Map showing the boundaries of seismic source zones, Scenario 3.

Declassified Catalog	Source Zonation	Spatial Variability	Sources	Maximum Magnitude	Recurrence Calculation Minimum Magnitude
----------------------	-----------------	---------------------	---------	-------------------	--

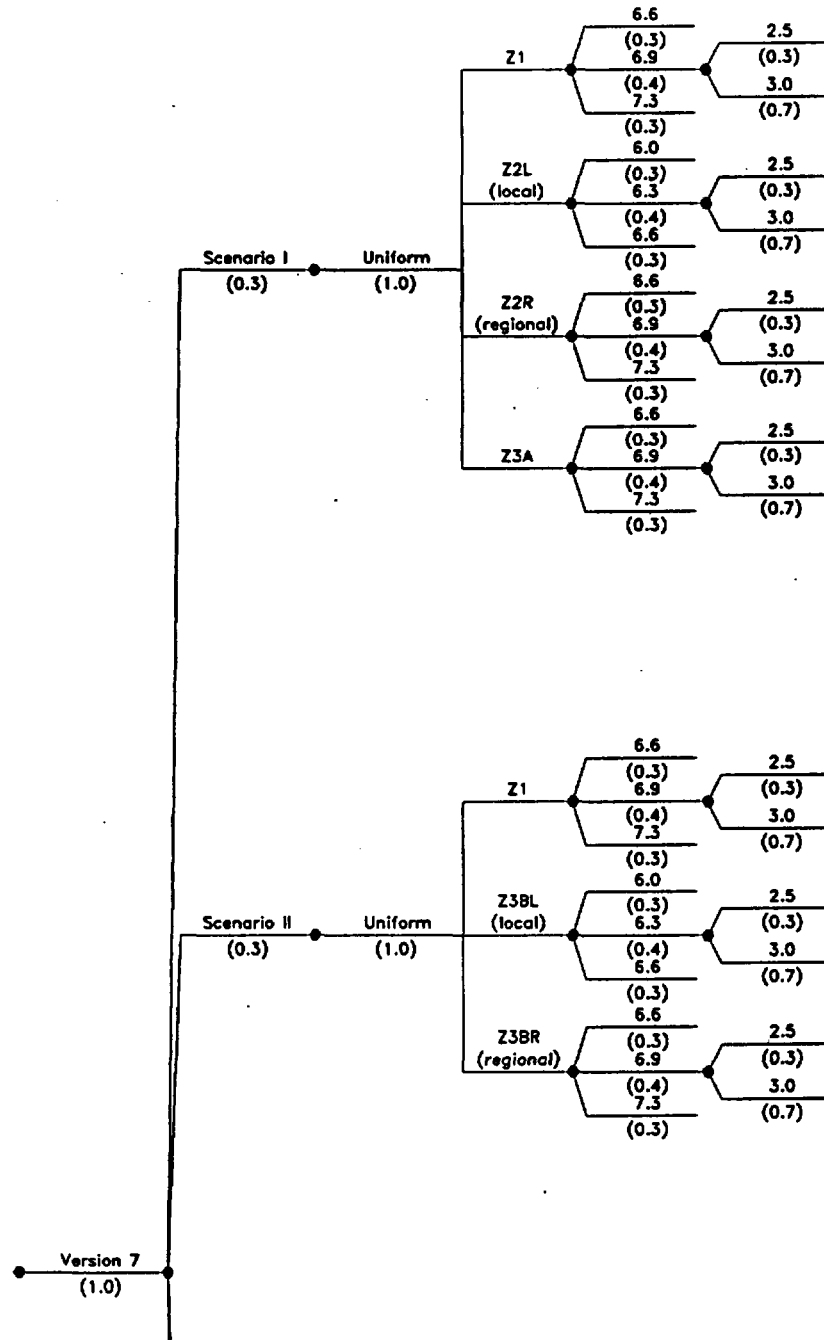


Figure AAR-10a Logic tree for source zones (top)

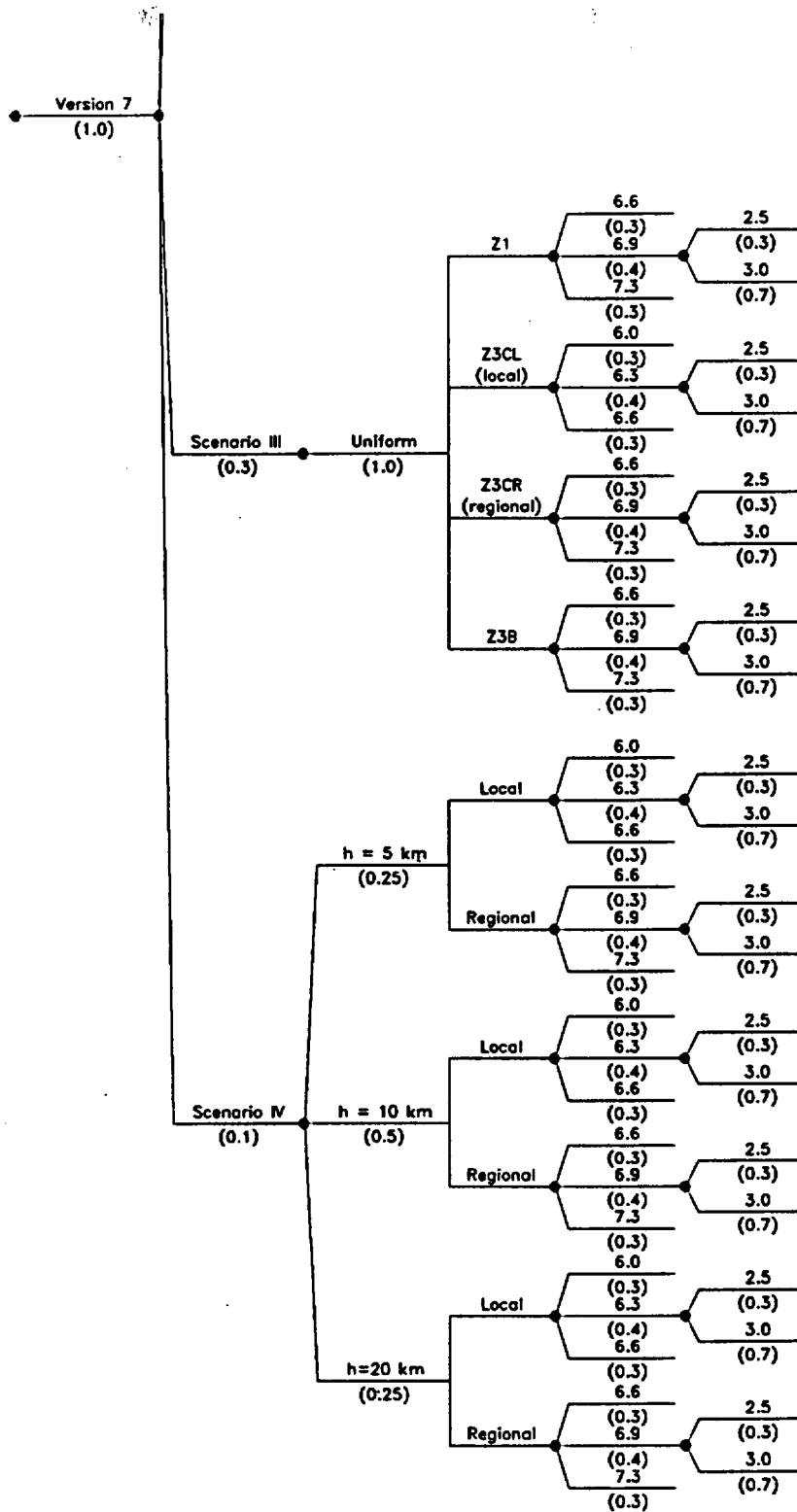
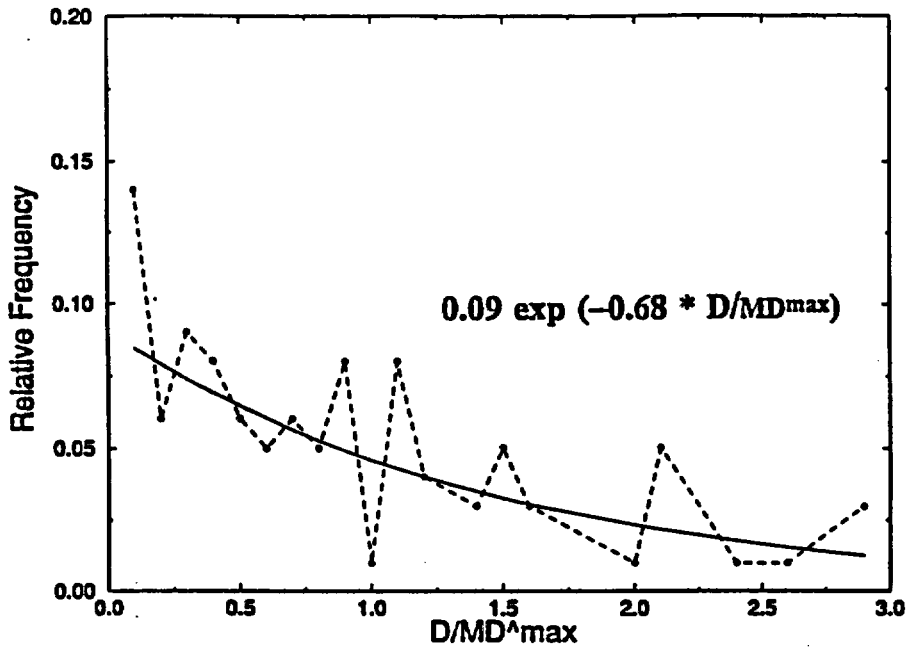


Figure AAR-10b Logic tree for source zones (bottom)

Variability of Displacement at a Point PDF



CDF

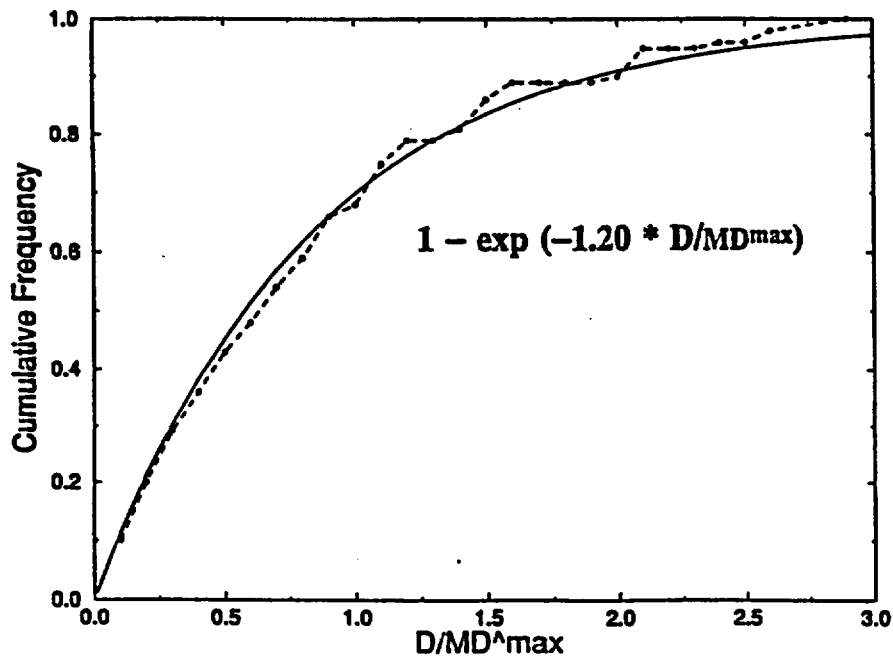
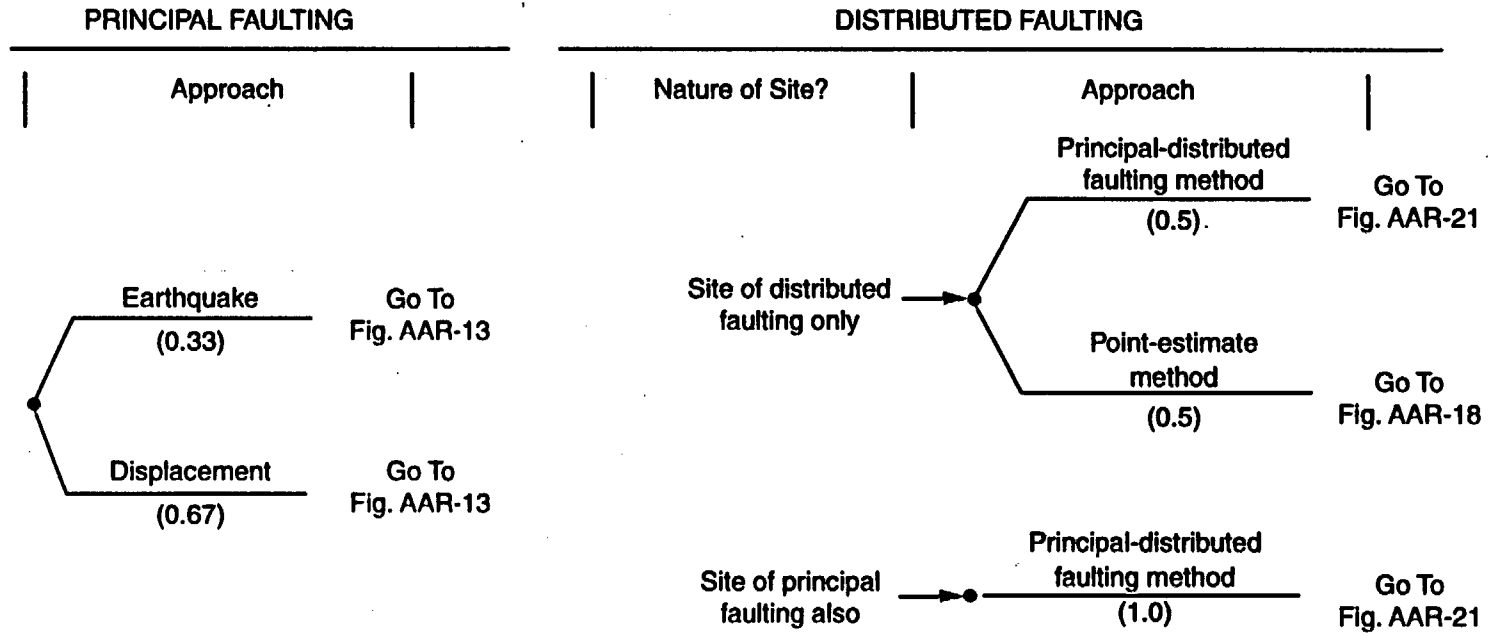


Figure AAR-11 Probability density function (PDF) and cumulative distribution function (CDF) for 80 measurements of single-event displacement, normalized to MD^{\max} for the corresponding fault, from 19 trenches in the Yucca Mountain area

**INITIAL BRANCHES OF SEPARATE LOGIC TREES
FOR PRINCIPAL AND DISTRIBUTED FAULTING**



(Conditional on using earthquake approach for principal faulting;
displacement approach for principal faulting simultaneously
accounts for distributed faulting at same site)

Figure AAR-12 Initial branches of separate logic trees for principal and distributed faulting.

PRINCIPAL FAULTING

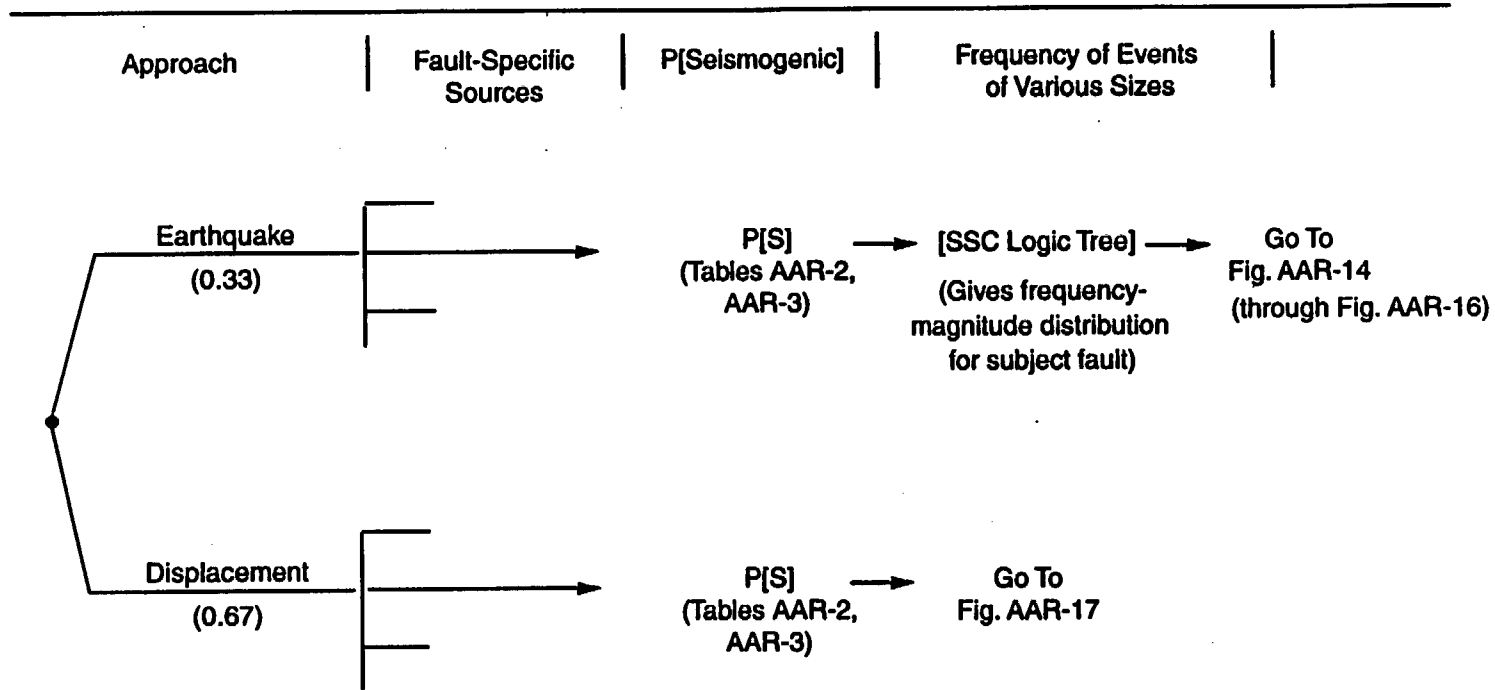


Figure AAR-13 Logic tree for principal faulting

		<i>Approach for Estimating Potential Rupture Length, Given M</i>	<i>Aspect Ratio</i>
--	--	---	-------------------------

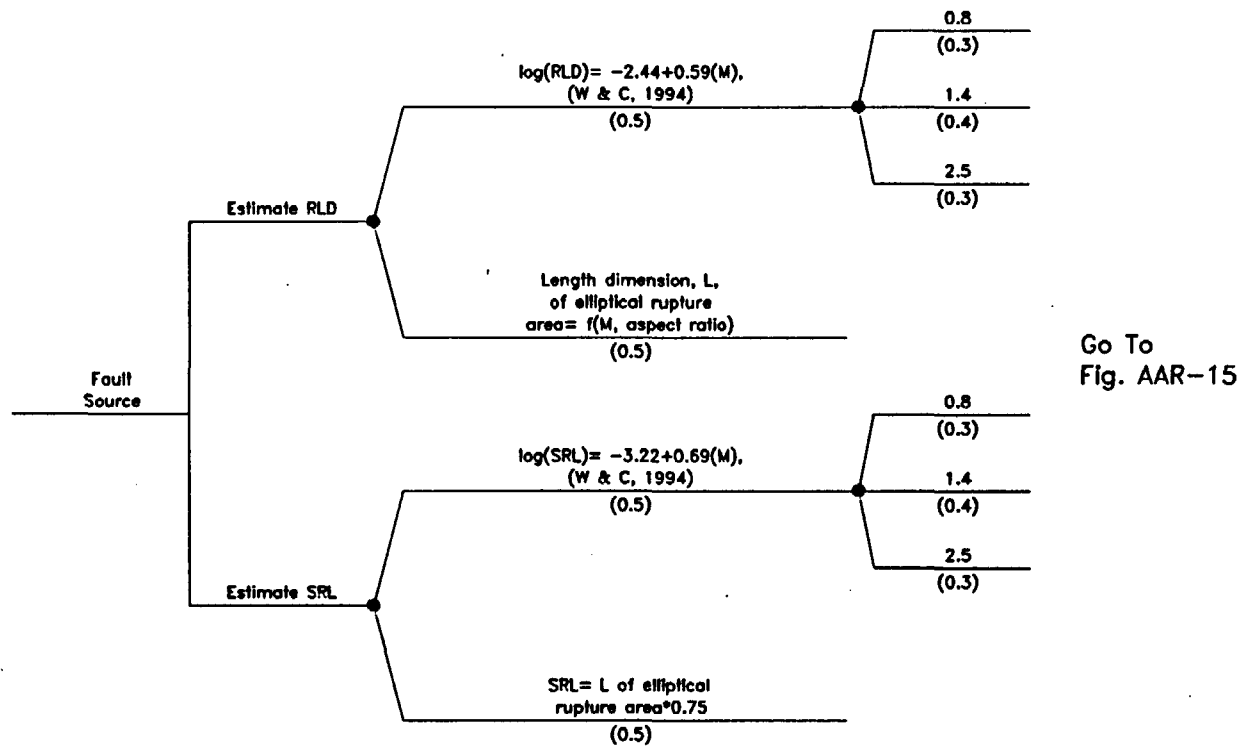


Figure AAR-14 Logic tree for principal faulting — earthquake approach (cont'd): estimating potential rupture length, given M

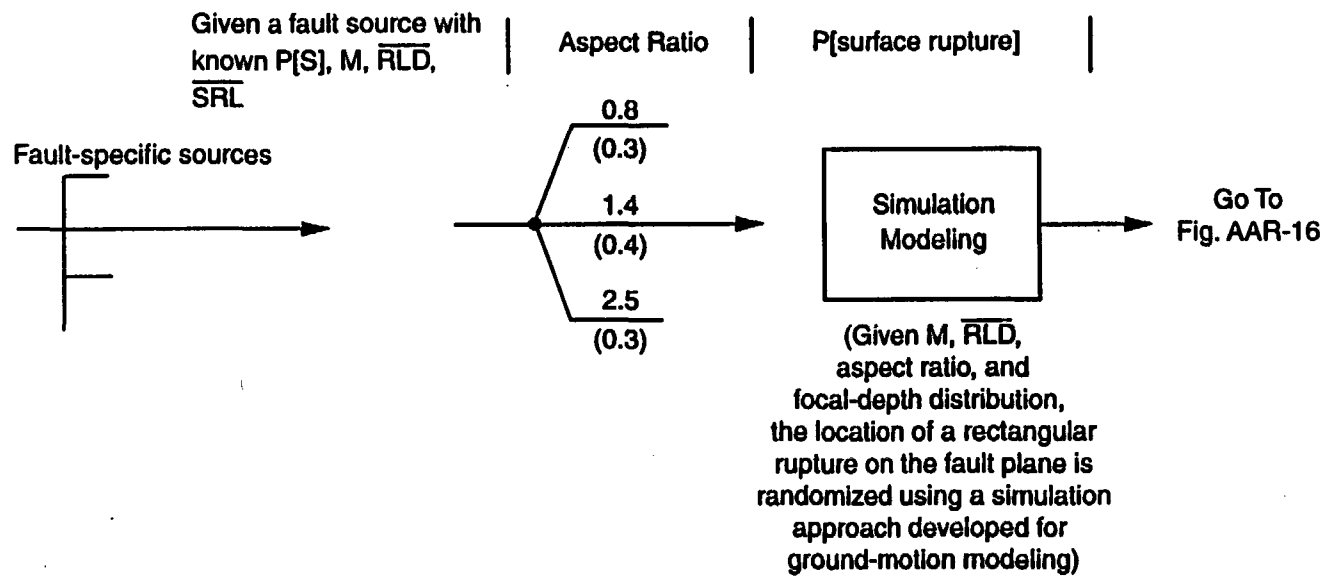


Figure AAR-15 Logic tree for principal faulting — earthquake approach, cont'd

<p>Given a rupture event on a fault source with known M, $P[S]$, \overline{RLD}, \overline{SRL}, and $P[\text{surface rupture}]$</p>	<p>Approach for Estimating Principal Fault Displacement, MD</p>	<p>Variability of Slip Along Strike</p>
---	--	---

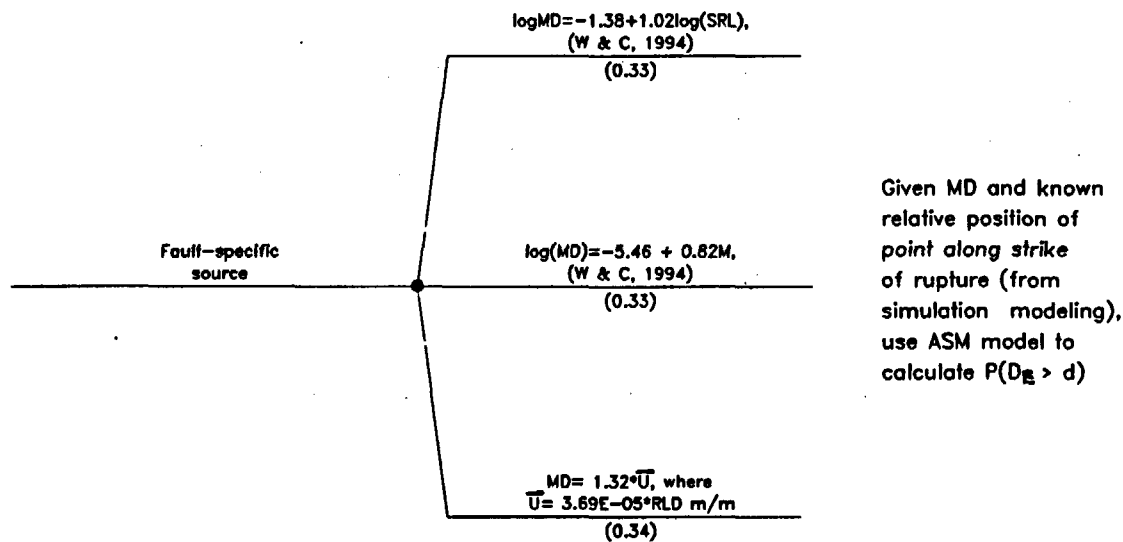


Figure AAR-16 Logic tree for earthquake approach to principal faulting (cont'd): estimating principal fault displacement, MD

PRINCIPAL FAULTING – DISPLACEMENT APPROACH

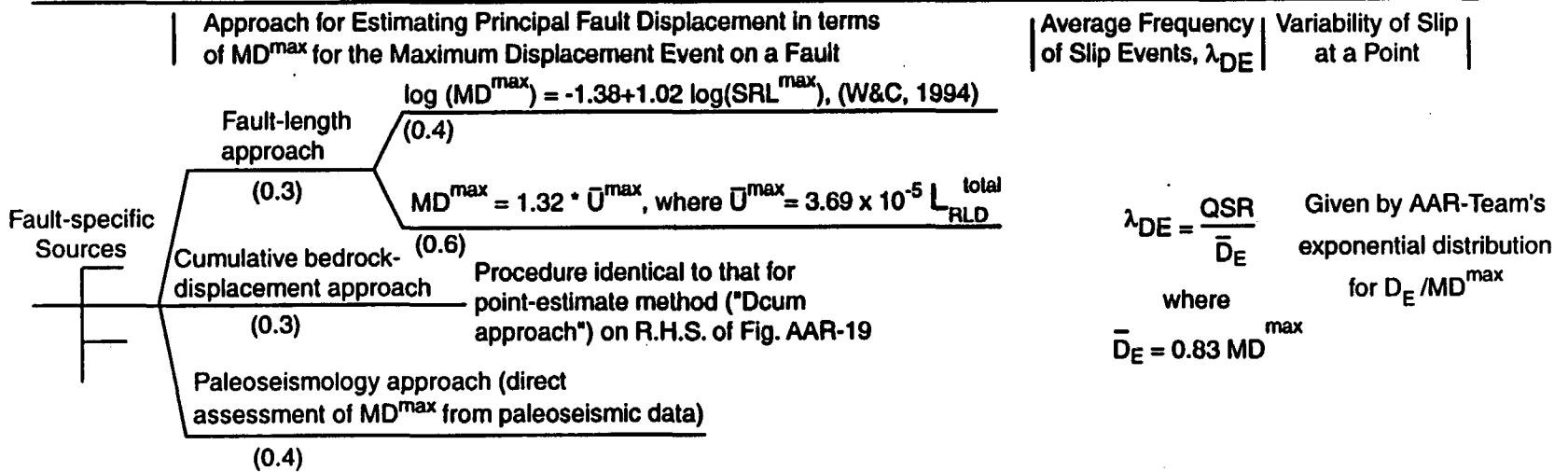
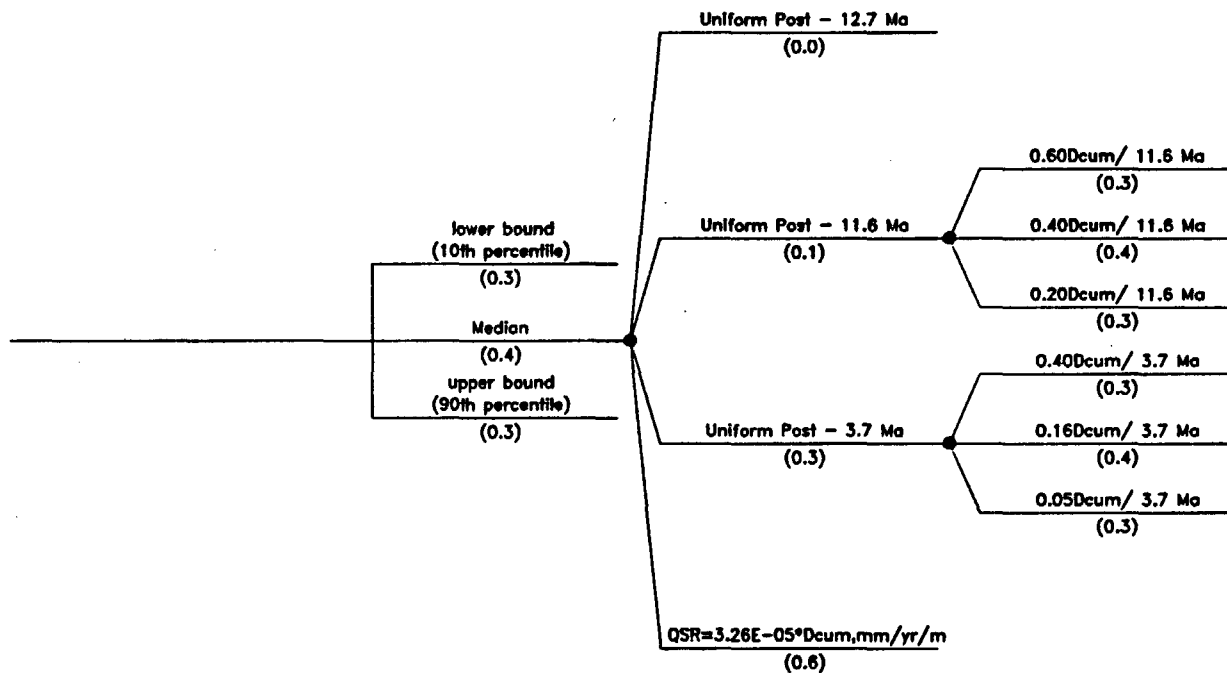


Figure AAR-17 Logic tree for principal faulting — displacement approach

<i>Secondary Fault or Fracture</i>	<i>P[C] (susceptibility to slip)</i>	<i>Total Post-Tiva Canyon Displacement, Dcum</i>	<i>Approach for Estimating Avg. Quaternary Slip Rate QSR</i>	<i>Portion of Dcum contributing to QSR</i>
------------------------------------	--------------------------------------	--	--	--



Go To
Fig. AAR-19
(through Fig. AAR-20)

Figure AAR-18 Logic tree for distributed faulting — point-estimate method

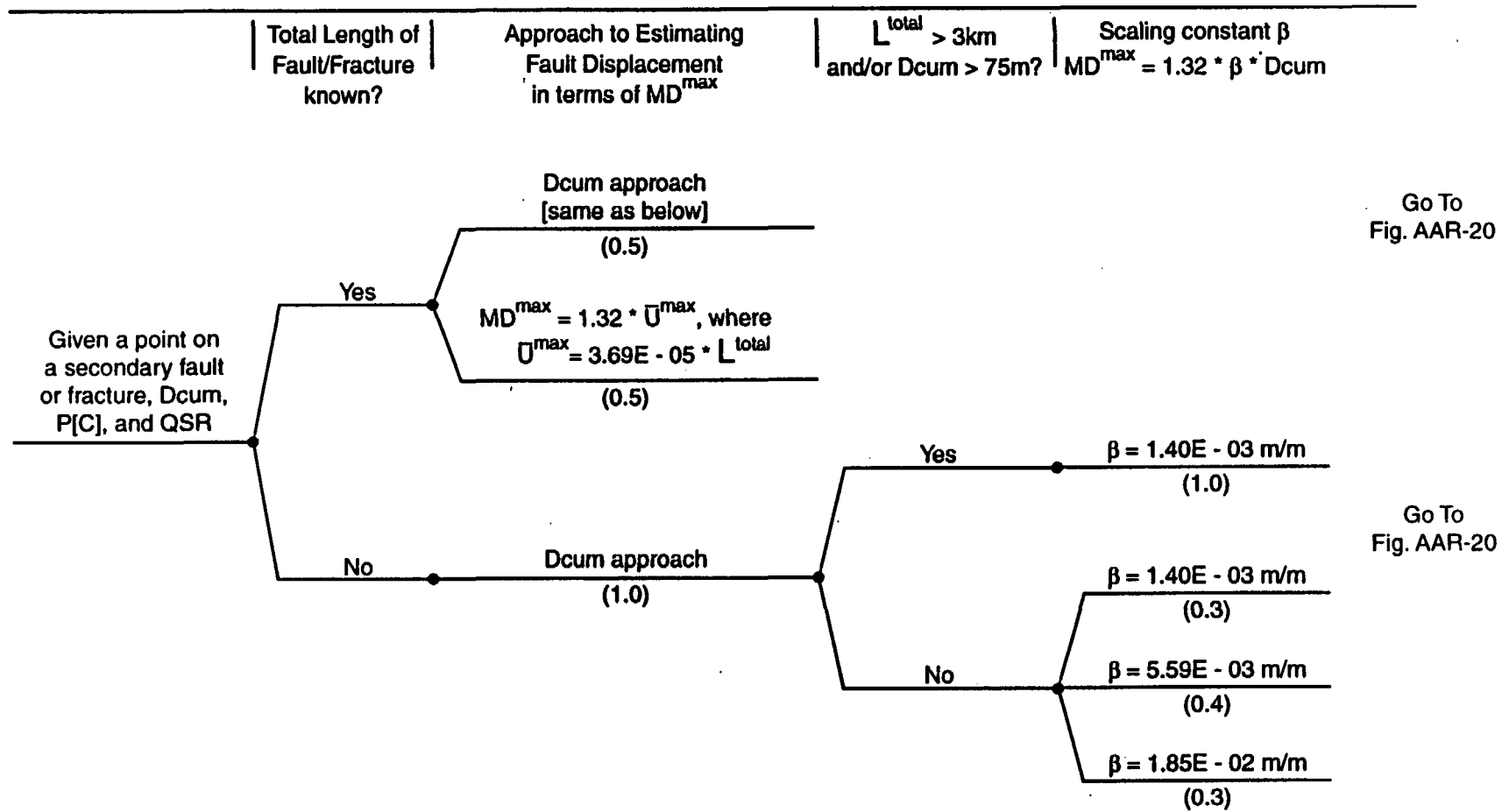


Figure AAR-19 Logic tree for distributed faulting — point-estimate method, cont'd

Average Frequency of Slip
Events, λ_{DE}

Variability of Slip at a Point

Given a point on a secondary
fault or fracture, D_{cum} ,
 $P[C]$, QSR , and MD^{max}

$$\lambda_{DE} = \frac{QSR}{\bar{D}_E}$$

where

$$\bar{D}_E = 0.83 MD^{max}$$

Given by AAR-Team's
exponential distribution
for D_E / MD^{max}

Figure AAR-20 Logic tree for distributed faulting — point-estimate method, cont'd

DISTRIBUTED FAULTING – PRINCIPAL-DISTRIBUTED FAULTING METHOD

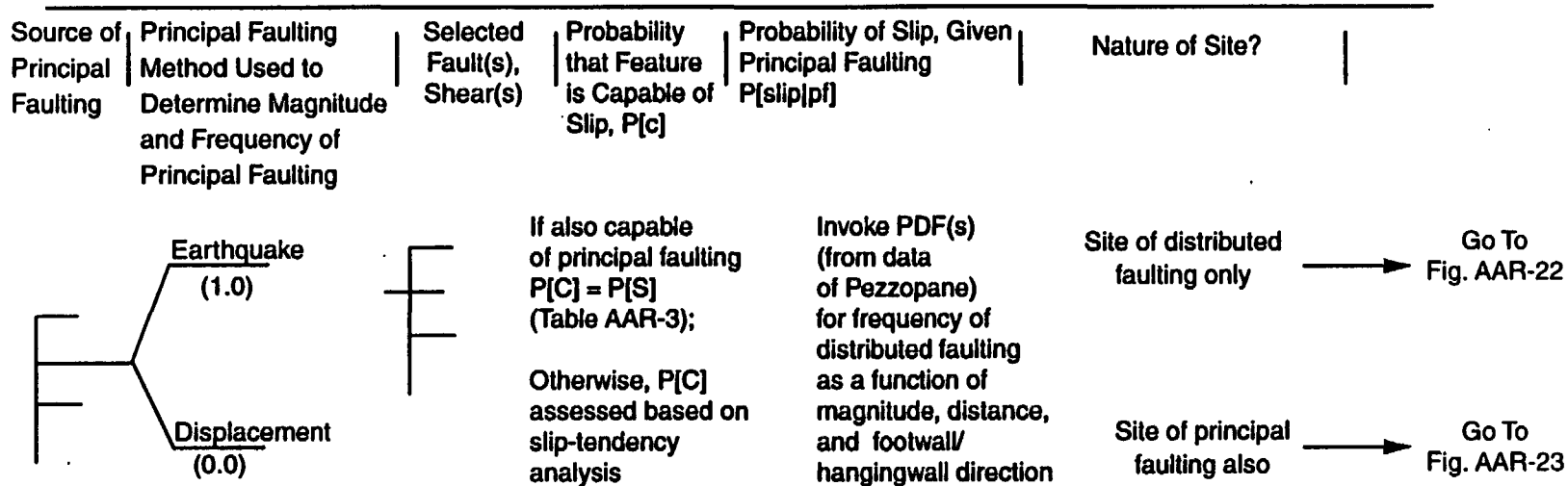


Figure AAR-21 Logic tree for distributed faulting — principal-distributed faulting method

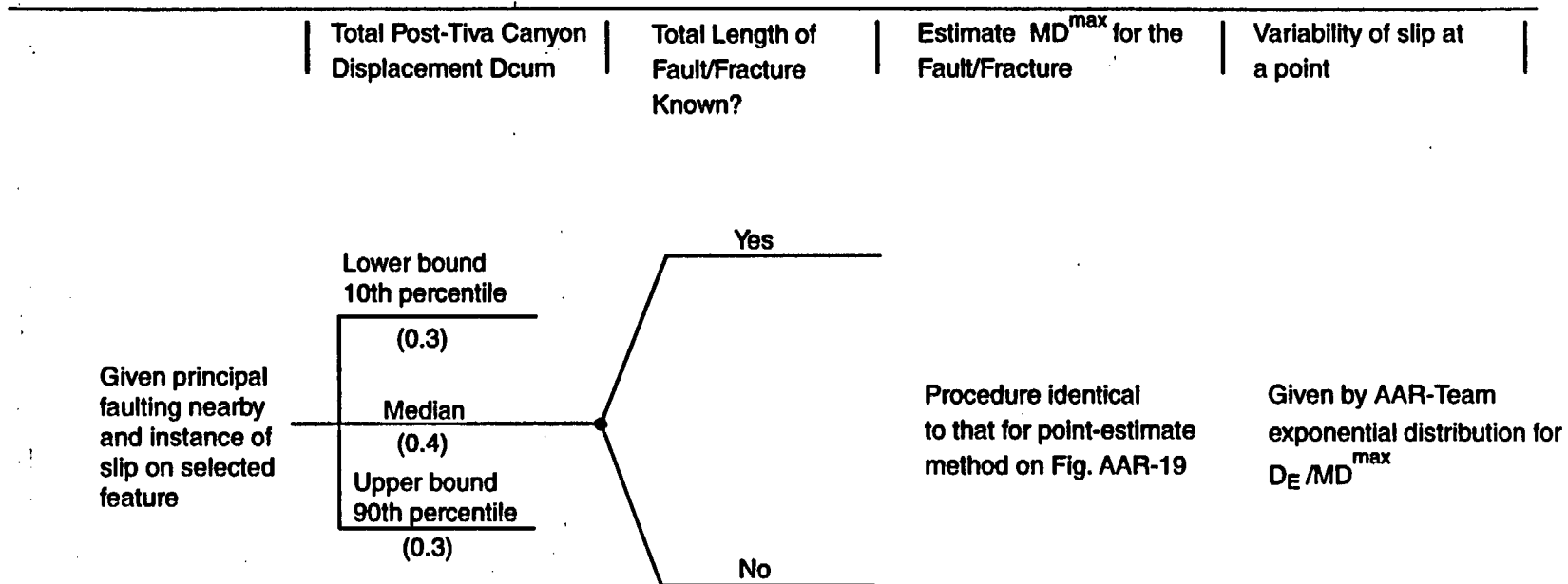


Figure AAR-22 Logic tree for distributed faulting — principal-distributed faulting method, cont'd (for site of distributed faulting only)

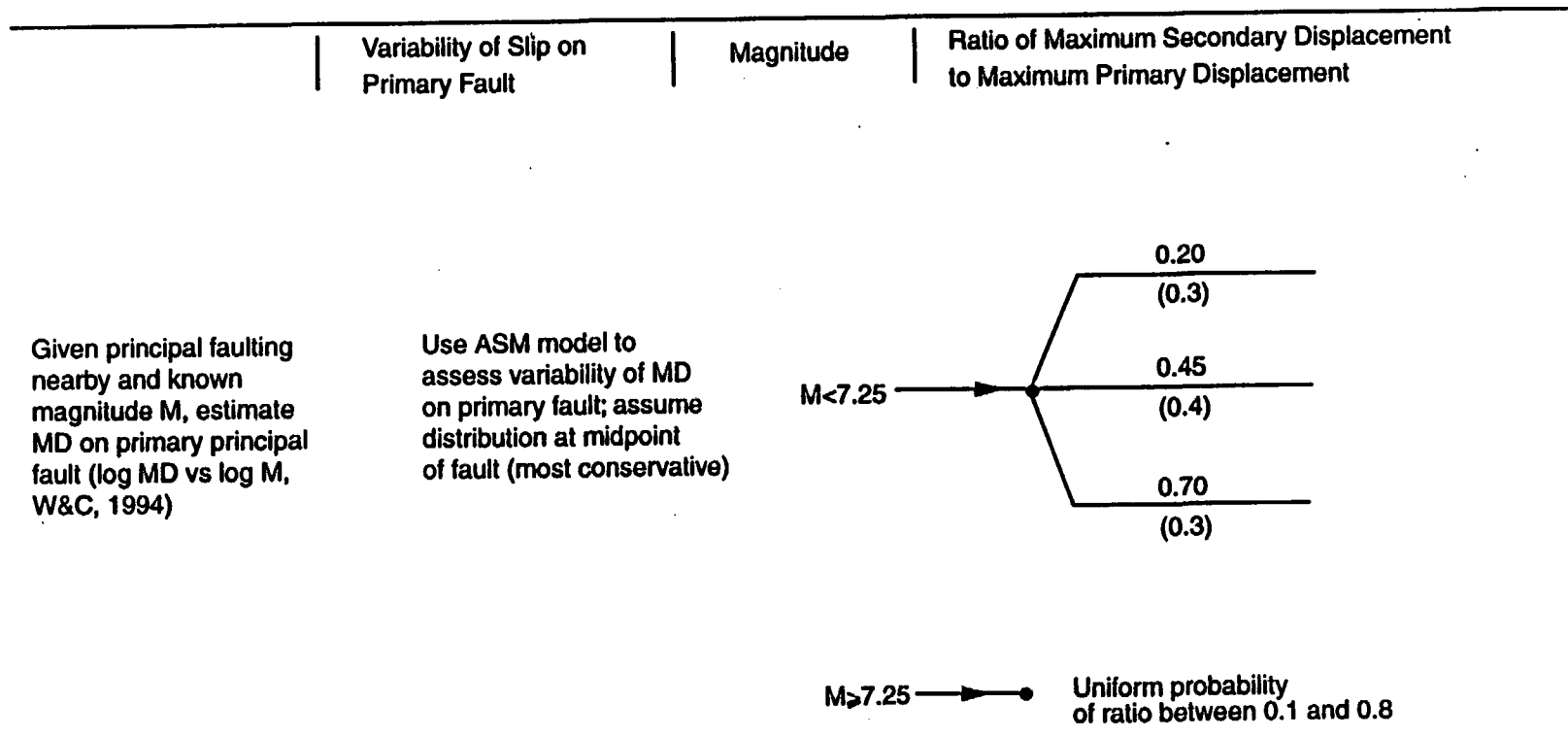


Figure AAR-23 Logic tree for distributed faulting — principal-distributed faulting method cont'd (for site of principal faulting also)

ELICITATION SUMMARY

JON AKE, BURT SLEMMONS, AND JIM McCALPIN

TABLE OF CONTENTS

	<u>Page</u>
1.0 INTRODUCTION	ASM-1
2.0 TECTONIC MODELS.....	ASM-2
2.1 COMPARISON OF TECTONIC MODELS	ASM-2
2.1.1 Caldera Model.....	ASM-2
2.1.2 Volcanic-Tectonic Model	ASM-3
2.1.3 Detachment Model	ASM-4
2.1.4 Planar Fault Blocks Model (Pure Shear)	ASM-5
2.1.5 Lateral Shear Models.....	ASM-7
2.2 PREFERRED TECTONIC MODEL	ASM-8
3.0 SEISMIC SOURCES.....	ASM-11
3.1 THICKNESS OF THE SEISMOGENIC CRUST.....	ASM-11
3.2 DETACHMENT AS SEISMIC SOURCE	ASM-11
3.2.1 Seismogenic Potential.....	ASM-12
3.2.2 Geometry	ASM-15
3.2.3 Maximum Magnitude.....	ASM-15
3.2.4 Recurrence	ASM-16
3.3 BURIED STRIKE-SLIP FAULT SOURCE	ASM-17
3.3.1 Seismogenic Potential.....	ASM-18
3.3.2 Maximum Magnitude.....	ASM-18
3.3.3 Recurrence	ASM-18
3.4 LOCAL FAULT SOURCES.....	ASM-19
3.4.1 Seismogenic Potential.....	ASM-20
3.4.2 Geometry Models.....	ASM-21
3.4.3 Behavioral Models.....	ASM-24
3.4.4 Maximum Magnitude.....	ASM-26
3.4.5 Recurrence	ASM-27
3.5 REGIONAL FAULT SOURCES.....	ASM-30
3.5.1 Estimation of Quaternary Ages.....	ASM-31
3.5.2 Maximum Magnitude.....	ASM-32
3.5.3 Slip Rate	ASM-32
3.5.4 Recurrence Intervals.....	ASM-33
3.5.5 Recurrence Models.....	ASM-35
3.6 REGIONAL SOURCE ZONES.....	ASM-35
3.6.1 Recurrence	ASM-36
3.6.2 Maximum Magnitude.....	ASM-37
3.6.3 Stationarity of Seismicity.....	ASM-38

TABLE OF CONTENTS

4.1	INTRODUCTION	ASM-40
4.2	METHOD OF CHARACTERIZING THE POTENTIAL FOR FAULT DISPLACEMENT	ASM-43
4.2.1	Method for Principal Faulting	ASM-43
4.2.1.1	Frequency of Potential Principal Faulting Events.....	ASM-43
4.2.1.2	Probability of Principal Faulting Surface Displacement During Earthquakes	ASM-43
4.2.1.3	Characterization of Displacement at a Point	ASM-44
4.2.2	Method for Distributed Faulting.....	ASM-44
4.2.2.1	Probability Feature Can Slip.....	ASM-45
4.2.2.2	Frequency of Potential Distributed Faulting Events.....	ASM-46
4.2.2.3	Probability of Distributed Displacement on a Feature .	ASM-47
4.2.2.4	Characterization of Distributed Displacement.....	ASM-49
5.0	FAULT DISPLACEMENT	ASM-55

TABLES

Table ASM-1	Average and maximum displacements for Yucca Mountain faults
Table ASM-2	Surface rupture lengths for Yucca Mountain faults
Table ASM-3	Weighting criteria for maximum magnitudes for Yucca Mountain faults
Table ASM-4	Slip rates for Yucca Mountain faults
Table ASM-5	Recurrence for Yucca Mountain faults
Table ASM-6	Regional fault data
Table ASM-7	Ratio of average to maximum displacement
Table ASM-8	Inferred number of events

FIGURES

Figure ASM-1	Logic tree for local sources
Figure ASM-2	Details of logic tree for detachment model
Figure ASM-3	Map showing hypothetical buried strike-slip fault and detachment fault in the vicinity of Yucca Mountain included in the seismic source model
Figure ASM-4	Map showing local fault sources included in the seismic source model

TABLE OF CONTENTS

Figure ASM-5	Logic tree for Crater Flat group (CFG) behavior
Figure ASM-6	Schematic of method used to develop downdip geometries of local faults
Figure ASM-7a	Schematic cross section of preferred merging geometry, northern transect
Figure ASM-7b	Schematic cross-section of deep, merging geometry. Depth of secondary faults constrained by aspect ratio
Figure ASM-7c	Schematic cross-section of shallow, merging geometry, northern transect. Depth of secondary faults constrained by aspect ratio
Figure ASM-7d	Schematic cross-section of non-merging geometry. Depth of secondary faults constrained by aspect ratio
Figure ASM-8	Simultaneous rupture scenarios and relative frequencies
Figure ASM-9	Map showing regional faults included in the seismic source model
Figure ASM-10	Map of regional seismic source zones within 300 km
Figure ASM-11	Map showing boundaries of zones used in the seismic source model
Figure ASM-12	Space-time comparing Youngs and Reasenberg declustering methods
Figure ASM-13	Annual frequency of earthquake recurrence as a function of time before Jan. 1, 1997, based on the catalog declustered by approach of Youngs et al.
Figure ASM-14	Logic tree used to characterize seismic source zones
Figure ASM-15	<i>Deleted</i>
Figure ASM-16a	Logic tree for principal faulting hazard
Figure ASM-16b	Logic tree for distributed faulting hazard
Figure ASM-17	Relationships between earthquake magnitude and probability of surface rupture
Figure ASM-18	Normalized "Wheeler" curve (adapted from Wheeler, 1989)
Figure ASM-19	Probability (frequency) of distributed slip as a function of distance from rupture
Figure ASM-20	Schematic illustration of ASSD method
Figure ASM-21	Borah Peak geodetic curve.

TABLE OF CONTENTS

APPENDICES

- APPENDIX ASM-1 GRAPHS SHOWING THE CUMULATIVE FREQUENCY OF LONG-TERM SLIP RATES FOR 10 LOCAL YUCCA MOUNTAIN FAULTS
- APPENDIX ASM-2 GRAPHS SHOWING THE CUMULATIVE FREQUENCY OF INTERVAL SLIP RATES FOR 10 LOCAL YUCCA MOUNTAIN FAULTS
- APPENDIX ASM-3 GRAPHS SHOWING FREQUENCY HISTOGRAMS OF LONG-TERM MEAN RECURRENCE INTERVAL FOR 10 LOCAL YUCCA MOUNTAIN FAULTS.
- APPENDIX ASM-4 GRAPHS SHOWING CUMULATIVE FREQUENCY DISTRIBUTIONS OF LONG-TERM MEAN RECURRENCE INTERVAL FOR 10 LOCAL YUCCA MOUNTAIN FAULTS
- APPENDIX ASM-5 GRAPHS SHOWING CUMULATIVE FREQUENCY DISTRIBUTIONS OF INDIVIDUAL RECURRENCE INTERVALS FOR 10 LOCAL YUCCA MOUNTAIN FAULTS
- APPENDIX ASM-6 REGIONAL SEISMIC SOURCE CHARACTERIZATION

ELICITATION SUMMARY
JON AKE, BURT SLEMMONS, JIM McCALPIN

1.0

INTRODUCTION

This document describes the authors' seismic sources for seismic hazard assessment and characterization of fault displacement hazard at the Yucca Mountain site. These evaluations relied on available data (either provided by the Yucca Mountain hazards management team or literature known and available to us). No additional data were gathered and only limited analyses were performed as part of this assessment.

The evaluations incorporate uncertainties through the use of logic trees. Some elements of the logic trees portray objective, statistical weights. However, for many elements of the tree no objective data were available, and subjective weights had to be applied. We attempted to follow a simple set of rules to aid in applying weights to those more subjective elements. If we considered a model or parameter was virtually certain, we applied a weight of 0.99 (or 0.01 if virtually unbelievable). If we considered a model or parameter strongly supported or strongly unsupported, we applied a subjective weight of 0.9 or 0.1. If we evaluated two competing models to be equally likely or we had a high degree of uncertainty between them, we applied a weight of 0.5 to each. Likewise, if three models or parameters were considered equally likely, we applied a weight of 0.333 to each. For regional seismic sources where the likelihood of the preferred interpretation was greater than the maximum and minimum values, the preferred interpretation was assigned a value of 0.6 and the extreme values were weighted as 0.2. If uncertainties were available in the form of standard deviations (usually assumed as Gaussian), we weighted the results of median \pm one standard deviation as 0.15, 0.7, and 0.15. For a few elements we attempted to capture the uncertainty by defining a preferred value and then ninetieth and tenth percentile values.

This summary begins with a discussion of tectonic models, followed by a description of the local seismic sources implied by the permissible tectonic models and then a summary of the

regional and areal sources considered in this evaluation. The final part of the summary describes the team's characterization of fault displacement hazard.

2.0

TECTONIC MODELS

We considered several alternative tectonic models (as we presented in SSC Workshop 4) to explain the observations and data of the Yucca Mountain region. Our interpretations are summarized in this section. Of the seven tectonic models proposed by others in SSC Workshops 1 through 3, we assigned the greatest credibility to the planar fault blocks model, followed by the detachment model, the lateral shear model, and the volcanic-tectonic model.

In Section 2.1, we discuss each tectonic model in turn, first defining what we mean by the model, then listing the strengths and weaknesses of the model compared to available field evidence (both from Yucca Mountain and from similar extensional provinces worldwide) and theoretical considerations of seismicity and tectonics. Based on the ratio of strengths to weaknesses, we assign each model a subjective degree of belief. This rating expresses our consensus that the model correctly explains the seismotectonic setting of the Yucca Mountain region. These subjective probabilities form our basis for weighting the existence of critical structures (e.g., the detachment fault, buried strike-slip fault, planar faults) that appear in our logic tree for seismic source characterization. In Section 2.2 we discuss our preferred model that incorporates those aspects of the alternative tectonic models that we feel best explain the seismotectonic setting of the Yucca Mountain region.

2.1 COMPARISON OF TECTONIC MODELS

2.1.1 Caldera Model

Definition: Crustal blocks are sliding into a structural depression beneath Crater Flat. This depression was made by Tertiary caldera collapse or by westward detachment faulting. This model includes the caldera-detachment model of Carr (1990).

Strengths:

- (1) The caldera complex is centered on a deep north-south trough or rift (Amargosa Desert rift); however, it is not clear whether the calderas are a result of the rift, or the reverse.
- (2) Crater Flat/Yucca Mountain faults make a distributed fault system that mirrors the faults north of the caldera complex. This symmetry about the calderas suggests a causal connection.

Weaknesses: (from p. 8-61 of Whitney, 1996)

- (1) The calderas have been inactive since 14 Ma, so how could they affect current faulting?
- (2) The calderas don't explain the change from rhyolitic to basaltic eruptions in Crater Flat in the past 3 Ma.
- (3) The model doesn't explain vertical axis rotations.
- (4) The model doesn't explain post-10 Ma uplift of Bare Mountain block.

Conclusion: Weaknesses much more compelling than strengths, model unlikely.

2.1.2 Volcanic-Tectonic Model

Definition: Surface-rupturing earthquakes in Crater Flat are accompanied by dike injection.

Strengths:

- (1) With continuing Quaternary eruptions in Crater Flat and south, some connection between volcanic and tectonic processes is likely.
- (2) Yucca Mountain faulting is widely distributed, like faulting in other volcanic-tectonic areas such as Mammoth Lakes. If USGS scenario earthquakes (Whitney, 1996, chapter 5) are single events, then such distributed rupture is also characteristic of volcanic-tectonic events.
- (3) The ash event at 70 ka (see Whitney, 1996, chapter 5) appears to be connected with basaltic eruptions.

Weaknesses:

- (1) Most of the 12 large (or 35 total) paleoearthquakes in the past 500 ka at Yucca Mountain are not associated with episodes of volcanic eruption.
- (2) There is no direct evidence that the rift beneath Crater Flat was formed by volcanic action. Other possible origins: (1) a deep graben created by east-west tectonic extension, (2) a more northerly trending part of an Amargosa Desert rift, which thinned the crust until subcrustal magma was tapped, or (3) a northerly jog in the N50W-trending Amargosa River-Pahump-Stewart Valley strike-slip fault zone.

Conclusion: Some volcanic-tectonic connection may operate some of the time, the calderas do not appear to control currently active faulting.

2.1.3 Detachment Model

Definition: A major low-angle, west-dipping detachment fault underlies Yucca Mountain and Crater Flat, at a mid- to low-crustal position. This detachment truncates all high-angle faults observed at the surface.

Strengths:

- (1) A detachment fault would explain the many narrow, parallel fault blocks as domino-style blocks above a detachment.
- (2) Tertiary detachment faults exist in the region surrounding Yucca Mountain.
- (3) Normal faults may utilize parts of older detachments, as in the Overthrust Belt (Smith and Arabasz, 1992).

Weaknesses: (from p. 8-74 of Whitney, 1996)

- (1) General:
 - (a) Historical earthquakes show planar faulting (e.g., the Little Skull Mountain event of 1992); no evidence of low-angle seismicity has been recorded, either in southwest Nevada, or in any other extensional terranes of the western US.
 - (b) The known detachments to the east and west are old (> 6 Ma).

- (c) Basaltic volcanism requires deeply penetrating structures.
- (2) Applies to shallow detachments:
- (a) No shallow (< 5 to 6 km) reflectors that could be interpreted to be a detachment are seen on the seismic line (T. Brocher, SSC Workshop 2).
 - (b) Elsewhere in the region, there is no detachment at the boundary between Tertiary and Paleozoic rocks (that contact is an unconformity).
 - (c) Movement on the Bare Mountain Fault would have truncated any detachment.
- (3) Applies to deep detachments:
- (a) A deep (6 to 15 km) detachment could not produce the observed dip rollovers and opposed slip on some faults.
 - (b) A deep detachment requires tensile behavior at the base of the individual dominos, which is unlikely.

Conclusion: Weaknesses are compelling, however, a deep (>6 km) detachment cannot be ruled out by geophysics.

2.1.4 Planar Fault Blocks Model (Pure Shear)

Definition No. 1: East-west Basin and Range-type extension, with diffuse dextral shear in the south part of Crater Flat.

Strengths:

- (1) The Amargosa Desert rift and all north-south-trending parallel faults suggest an east-west horst and graben system.
- (2) The largest historical earthquakes in the local area (e.g., Little Skull Mountain) show planar faulting to depth.
- (3) Seismic lines show no detachments within the upper 5 to 6 km.
- (4) Rifting can explain basaltic volcanism.

- (5) Boundary element modeling can replicate the seismic section using planar faults.
- (6) Diffuse dextral shear can explain the increasing vertical axis rotation of fault blocks in southern Crater Flat.

Weaknesses:

- (1) Pure horizontal extension does not explain the vertical axis rotations.
- (2) Net slip (and slip rate) on the Bare Mountain fault (the supposed master fault to which Yucca Mountain faults are antithetic) must be greater than the sum of all the slips (and slip rates) on all the antithetic (Yucca Mountain) faults. This does not appear to be the case. However, some of the faults in the Bare Mountain fault zone may be buried by Holocene and late Quaternary alluvium up to 150k years old.
- (3) Boundary element models show that, to produce a slip event on antithetic faults, multiple slip events on the main (Bare Mountain) fault are required. This does not appear to be the case.
- (4) Planar faulting doesn't explain the ash event, which may have involved coeval rupture on six to seven parallel faults.

Conclusion: Strengths more compelling than weaknesses, model plausible.

Definition.No. 2: Crater Flat is a transtensional rhombochasm (pull-apart) due to a right step in the Walker Lane. The east, south, west, and north boundaries of the rhombochasm are the Paintbrush Canyon/Stagecoach Road fault, the Carrara feature, the Bare Mountain fault, and a fault near Yucca Wash, respectively.

Strengths:

- (1) The model explains the inferred oblique component of normal faulting in/near Yucca Mountain.
- (2) The model explains the oblique nature of focal mechanisms observed in the instrumental seismicity (Rogers et al., 1992 and K. Smith, SSC Workshop 2).
- (3) The model may explain why fault behavior in the past 500 ka does not match the results of boundary element models, which assume pure east-west extension.

- (4) The extreme northern limit on the main Yucca Mountain faults is at or near the linear northwest-trending Yucca Wash on the north. The faults have displacements that decrease toward this geophysical lineament, which has no known fault origin in the shallower units, and does not appear to be a seismic source. [Only the Paintbrush Canyon fault clearly crosses this feature, and it may change in character across Yucca Wash.] The extreme southern limit to Crater Flat and Yucca Mountain faults is near the linear northeast-trending inferred fault shown by Fridrich and Price (1992). The orientation of N45W suggests that it may be a right-lateral oblique fault.

Weaknesses:

- (1) There is ambiguity about the existence of the required dextral faults at the north and south ends of the rhomboid.

Conclusion: Strengths more compelling than weaknesses, model plausible.

2.1.5 Lateral Shear Models

Definition No. 1: The transtensional nappe model applies (Hardyman and Oldrow, 1991).

Strengths:

- (1) The model explains how Walker Lane shear could produce observed fault blocks.
- (2) The Cedar Mountain earthquake of 1932 displayed distributed faulting having a high oblique component.

Weaknesses: (from p. 8-80 in Whitney, 1996)

- (1) "None of the criteria or geometry required for Hardyman's model exist at Yucca Mountain." Hardyman originally proposed this model for the Gillis Range-Cedar Mountain area, for a well-bedded pyroclastic sequence above a sheared unconformity with Mesozoic rocks that is cut by a lateral fault. We find no evidence for this type of mechanism at Yucca Mountain.

Conclusion: Compelling weaknesses, questionable applicability of model to Yucca Mountain area, model unlikely.

Definition No. 2: There is a buried, 250-km-long strike-slip fault beneath Yucca Mountain; it is a buried subvertical dextral fault, such as that proposed by R. Schweickert at SSC Workshop 3.

Strengths:

- (1) The model would explain the observed vertical axis rotations in southern Crater Flat.

Weaknesses: (from p. 8-84 in Whitney, 1996)

- (1) There is no surface evidence of strike-slip faults at Yucca Mountain/Crater Flat, nor of any single, continuous strike-slip fault southeast of Crater Flat along the state line.
- (2) Vertical axis rotations in the area are variable in time and space. They would be expected to be uniform if there was only one, long strike-slip fault.
- (3) There is no evidence for a 25-km dextral offset of volcanics in Crater Flat.

Conclusion: Weaknesses more compelling than strengths, model unlikely.

2.2 PREFERRED TECTONIC MODEL

Our preferred tectonic model for Yucca Mountain is a composite based primarily on the Planar Fault Model, which has the following characteristics.

- (1) Generally, the fault azimuth may be a first-order control on the type of fault, with conjugate relationships (a la Wright, 1976). Regionally northwest-trending faults are right-lateral; northerly-trending faults are normal; and northeast-trending are left-lateral. By far the most active faults are the strike-slip faults; normal faults have slip rates of 1% to 10% of the strike-slip faults. Most of the Yucca Mountain faults expressed at the surface are northerly-trending, normal faults.
- (2) Major, block-bounding faults are planar (or weakly curved) to seismogenic depths.
- (3) Faults that are closely spaced in plan view may merge above seismogenic depths. For those that are so closely spaced that they may merge above 15 km,

we calculate maximum magnitudes as if they were separate faults with aspect ratios consistent with their lengths. (Further discussion in sections on maximum magnitudes and synchronous rupture). Alternative dips and aspect ratios are considered for Yucca Mountain faults in the assessment of their downdip extent.

- (4) Given the local faults may have merging geometries, for multi-fault-rupture scenarios we compute the fault area as the sum of areas for all faults that ruptured. Note, however, that unless the separate faults ruptured simultaneously (i.e., within about 30 seconds of each other in our definition), we interpret that these scenario earthquakes to be separate earthquakes spaced a few hours to decades apart, with correspondingly lower magnitudes than a large simultaneous rupture.
- (5) Fault slip is dominantly dip slip in the northern part of the area; southward, the horizontal component increases via vertical axis rotation. It is not known whether this is due to a local effect at the southeast edge of Crater Flat, or to a subordinate tectonic rotation induced by a right-lateral fault zone in Amargosa Valley.

In addition to the above, our model must include the following elements from the Detachment and Lateral Shear Models:

- (6) The possibility of a deep detachment (>6 km) cannot be ruled out by the existing geophysics. Therefore, we allow some probability to the existence of such a detachment ($P=0.15$) and an even lower weight to it being seismogenic. The likelihood that faults merge at depth is dependent, in part, on the depth of the inferred detachment.
- (7) The oblique component of slip on Yucca Mountain faults and the clockwise vertical axis rotation are related to dextral strain (bending) transmitted from the Walker Lane. However, it is unclear whether discrete northwest-striking dextral faults exist north and south of Yucca Mountain (defining a rhombochasm), or whether lateral strain is diffuse. This model utilizes recognized faults as the eastern and western margins of the rhombochasm (Bare Mountain fault, Paintbrush Canyon/Stagecoach Road fault) and an inferred fault (Carrara feature) as the southern margin. These three faults are already characterized on the SSC logic tree, so no further additions to the logic tree are required for this tectonic model. The northern margin of the rhombochasm is approximately coincident with the Yucca Wash fault, to which we assign a 0% probability of being seismogenic, based on its lack of evidence for Quaternary displacement.

- (8) The probability that a buried, strike-slip fault exists is dependent on the probability of a detachment. If a detachment fault exists (probability = 15%), then we consider that there is a 20% probability that a buried strike-slip fault exists (net probability = 3%). If no detachment exists (probability = 85%), then there is only a 5% chance that the buried strike-slip fault exists (net probability = 4%). The sum of the two net probabilities that the buried fault exists is thus 7%. The probability that the buried strike-slip fault is seismogenic is dependent on the depth of the detachment.

Although a volcano-tectonic source is not explicitly included as a separate source model, we include one element from the Volcanic-Tectonic Model. This element does not require a caldera source, but depends on the simultaneous basaltic volcanic eruption and the extensive tectonic, seismogenic rupturing of several faults that extend northward from a Lathrop Cone volcanic source. The possibility of such a scenario is accounted for in the simultaneous rupture portion of the local fault model.

- (1) Some surface-rupturing paleoearthquakes (e.g., Scenario U) probably have accompanied episodes of basalt eruption and dike injection.
- (2) Although there may be some volcanic-tectonic connection, the possibility of volcanic earthquakes does not affect our estimates of earthquake magnitude and recurrence. Therefore, we do not include a separate volcanic earthquake branch on our seismic source characterization logic tree, for two reasons. First, the maximum magnitude of volcanic earthquakes associated with dike injection ($M = 5.5$) and calderas ($M = 4.5 \pm 1.2$) (Hackett et al., 1996) are much smaller than our estimated maximum magnitudes for tectonic earthquakes, either on individual faults or for background seismic zones. Second, the recurrence interval of volcanic eruptive events is estimated to be ca. 200 to 300 ka by the experts in volcanic hazards assessment for Yucca Mountain. Thus, any volcanic contribution to earthquake hazard is insignificant compared to the rates of background seismicity in and near Yucca Mountain (see Section 3.6).

Behavioral aspects such as distributed, multi-fault earthquakes, could occur in any of the tectonic models. However, simultaneous faulting on parallel normal faults may be more easily explained by the Volcanic-Tectonic Model (which we have not included as a separate source model) than by the Lateral Shear Model (a variant of which we weight at 20%), and least by the Planar Block Model (which we give the highest weight at 80%). Thus, our weighting of

tectonic models reflects our interpretation that simultaneous multi-fault ruptures (i.e., within a ~30- second time span) have a low probability.

3.0

SEISMIC SOURCES

The characterization of fault-specific sources in the Yucca Mountain region is based on our preferred tectonic model as summarized on Figure ASM-1. In addition to these fault sources, our seismic source model also includes more regional faults (i.e., those outside the immediate vicinity of Yucca Mountain/Crater Flat) and areal source zones.

The seismogenic potential of potential sources in the Yucca Mountain region is partly a function of the depth of the brittle (seismogenic) crust. Therefore, we first consider the assessment of the thickness of the seismogenic crust.

3.1 THICKNESS OF THE SEISMOGENIC CRUST

The depth of the brittle/seismogenic crust is assessed to be 12 km (0.1), 15 km (0.6), and 17 km (0.3). These depths and their relative weights are based on the distribution of focal depths for instrumental earthquakes in the southern Great Basin, as given in von Seggern and Brune (1997), and Harmsen and Bufe (1991), the focal depths in the Yucca Mountain region summarized by K. Smith at SSC Workshop 2, and discussions presented by Robert Smith at SSC Workshop 5. The nucleation depths of $M > 6$ earthquakes in the Basin and Range province in general (Rogers et al., 1991), and in southwestern Nevada in particular (e.g., the Little Skull Mountain earthquake; Smith et al., in press) are near the base of the seismogenic crust. This fact will be important in evaluating the existence of detachments deep in the crust.

3.2 DETACHMENT AS SEISMIC SOURCE

For this analysis, a detachment fault is defined as a regionally extensive, low-angle (< 15 - 20 degree) surface that truncates high-angle faults and lies within the brittle crust. A detachment would lie within the upper 6 to 15 km of the crust. A subhorizontal surface lying beneath the brittle-ductile transition would not be considered a detachment within this terminology. The

assessment of a detachment as a seismic source will evaluate seismogenic potential, depth of the structure, geometry, maximum magnitude and recurrence. Figure ASM-2 contains the logic tree detailing our assessment of this source.

3.2.1 Seismogenic Potential

The seismogenic potential for a detachment is judged to be a function of its existence, geometry and extent. This dependency is shown in the following logic tree (Figure ASM-2).

The first assessment is whether a detachment exists. The weight assigned to the existence of a detachment is 0.15 and to no detachment is 0.85. The following evidence supports the existence of a detachment: a detachment would explain the many narrow, parallel fault blocks as dominos above a detachment; Tertiary detachment faults exist in the region surrounding Yucca Mountain; and normal faults may utilize parts of old detachments, such as those in the Overthrust Belt (Smith and Arabasz, 1992; Arabasz et al., 1992). The arguments against a detachment are: a lack of evidence for low-angle faulting from the seismicity, including the Little Skull Mountain earthquake; the known detachments east and west of Yucca Mountain are old (> 6 Ma); basaltic volcanism requires deep penetrating structures; elsewhere in the region, there is no detachment at the Tertiary/Paleozoic boundary; movement on the Bare Mountain fault would have truncated the detachment; and, a deep detachment could not produce the observed dip rollovers and opposed slip on some faults (C. Fridrich, SSC Workshop 3).

The second assessment is the depth of the detachment, conditional on its existence. Three depths are considered, which depend on the depth of the brittle crust. The minimum depth is 6 km, which is below the depth observed in the seismic reflection profile presented by T. Brocher (SSC Workshop 2). There is no evidence for a low-angle detachment fault on the seismic reflection profile, although such a structure should have been obvious if it existed. Therefore, if a detachment fault exists beneath Crater Flat, it must lie at or below 6 km. The maximum depth for a detachment beneath Crater Flat is the depth of the brittle-ductile transition (which, as discussed above, is assumed to lie between 12 and 17 km depth). An intermediate depth of the detachment is considered, halfway between the depth of the brittle-ductile transition and 6 km. This would place the detachment toward the base of the seismogenic crust, which is the most common nucleation point for large earthquakes in the

region (Rogers et al., 1991). The relative weights assigned to the three alternative depths are 6 km (0.25), $(BD-6)/2 + 6$ (0.5), and BD (0.25), where BD is the depth of the brittle-ductile transition. The weights assigned to the three interpretations are based on the following observations: (1) A shallow depth for the detachment conflicts with the geometry of the Bare Mountain fault. The Bare Mountain fault would be truncated at a shallow depth that is a significant fraction of the total offset on the fault; lack of analogs to this situation suggest a low weight for this interpretation. (2) The observed opposed dips on some of the Crater Flat faults are inconsistent with normal faulting caused by extension above a subjacent detachment. This scenario also receives a low weight.

The next conditional assessment is whether the detachment is seismogenic, that is, capable of generating significant ($M > 5$) earthquakes in the present tectonic regime. This assessment is independent of the depth of the detachment. The possibility that a detachment (if it exists) is seismogenic is given a very low weight (0.01) based on both theoretical reasoning and empirical data. First, according to Mohr-Coulomb theory of brittle failure, given a horizontal least-principal stress and rocks having internal friction angles of 30 ± 10 degrees, the most likely dip for active normal faults is 60 ± 10 degrees (see extended discussion by Sibson, 1985). A fault dipping only 10 to 20 degrees would be in a very unfavorable orientation for slip, compared to the multitude of faults having dips closer to 60 degrees at Yucca Mountain. [Forsyth (1992) rebuts this argument, saying that if the low-angle fault had sufficiently lower strength than the high-angle faults, slip might be accommodated.] These higher-angle faults have demonstrated Quaternary slip, proving that they have accommodated Quaternary extension, as would be predicted by theory. The existence of a low-angle detachment beneath Crater Flat is merely conjectural; there is no evidence that it exists, much less that it has accommodated any Quaternary slip.

Second, although low-angle detachments have been widely described in the southwest United States (e.g., Wernicke, 1995), even after 15 years of research only one of these detachments shows evidence of Quaternary activity. The sole exception (Johnson and Loy, 1992) is a case where Quaternary fault scarps exist on the trace of the Santa Rita (Arizona) fault, which has a dip determined from seismic reflection data of 19 degrees to a depth of at least 6 km. To our knowledge this is the only documented instance of Quaternary fault scarps overlying a low-angle normal fault; although in other areas (e.g., the Overthrust Belt of Wyoming)

Quaternary fault scarps commonly overlie faults interpreted as having listric geometry (McCalpin, 1991).

Third, published summaries of focal mechanisms of earthquakes in extensional regimes show few or no cases of seismogenic rupture on low-angle normal faults (Jackson, 1987; Jackson and White, 1989; Doser and Smith, 1989; Wernicke, 1995). We estimate that there are several hundred documented focal mechanisms of significant ($M > 4$) normal-faulting earthquakes worldwide. Only two of those events (the Papua New Guinea earthquake [Abers, 1991], and the 1946 Ancash, Peru earthquake [Doser, 1987]) appear to have possibly occurred on low-angle faults. [As in any double-couple energy release, inversion for a focal mechanism can only resolve two nodal planes, one of which is the true nodal plane]. The interpretation of the true nodal plane in the New Guinea event is equivocal, and the Ancash event probably occurred on a reactivated thrust. Thus, despite the acknowledged existence of low-angle detachment faults in many extensional terranes, there are only two instances of those faults possibly generating earthquakes, compared to hundreds of instances of high-angle normal faults generating earthquakes. In the Yucca Mountain region, the historical record shows earthquakes only on higher-angle faults (e.g., the Little Skull Mountain earthquake and focal mechanism compilations of Gomberg et al., 1991; Rogers et al., 1991).

Based on the scarcity (or absence) of earthquakes generated by detachment faults, we weight the probability that a sub-Yucca Mountain detachment is seismogenic as 0.01. The possibility for a seismogenic detachment is included in the analysis, despite its very low weight, to allow for the slight chance that the hypothesis proposed by Wernicke (1995) might apply to the Yucca Mountain region. Wernicke proposes that the paucity of earthquakes on low-angle normal faults is caused by long recurrence intervals on this type of fault, compared to recurrence intervals on high-angle normal faults that have the same strain rate. Given the short period for which we have reliable focal mechanism data (roughly since 1960), Wernicke (1995) argued that the period of observation is too short to capture many earthquakes on detachments that have very long recurrence intervals.

Hypotheses that claim the period of observation is too short to capture a particular observation usually are tested through the ergodic substitution of space for time (Hunter and Mann, 1995). However, in this case we are already analyzing a worldwide data set, so

expanding the area over which data were collected is not possible. Given that Wernicke's (1995) hypothesis is not directly testable, but claims very large earthquake magnitudes for long-recurrence detachment faults, we decided to assign a nonzero (but small) probability for the seismic potential of a sub-Yucca Mountain detachment fault.

3.2.2 Geometry

Typical dimensions of detachment faults elsewhere in the world (summarized by Wernicke, 1995, p. 20,170) are: strike lengths of 60 to 180 km and downdip lengths of 60 to 70 km. Based on these dimensions, a detachment, if it were to exist, would underlie the entire Crater Flat/Yucca Mountain region, which is only about 20 x 20 km. The break-away for the detachment (its eastern extent) would be in the middle of Jackass Flat and would extend beneath Bare Mountain on the west. By analogy to the Bullfrog Hills (the nearest detachment fault to the site), and to the typical dips of detachment faults cited by Wernicke (1995), the detachment is assumed to dip 15 to 20 degrees to the west. The north-south extent of the detachment underlying the Crater Flat region is assumed to be the same as the extent of the north-south normal faults. This extent (about 25 km) is considerably smaller than that cited by Wernicke. Our reasoning is as follows. First, if the north-south-trending normal faults around Crater Flat are the surface expressions of an underlying detachment, then the detachment should not extend far beyond that surface expression. It is possible that the Timber Mountain caldera north of Crater Flat, and the Walker Lane south of Crater Flat, could somewhat obscure this structural relationship. Thus, the north-south extent of normal faults near Yucca Mountain (25 km; probability 0.25) sets a minimum along-strike distance for a detachment, with a preferred value of 60 km (0.5) and a maximum value of 120 km (probability 0.25). Downdip extent (based on a dip of 10 to 20 degrees and a crustal thickness of 12 to 17 km; all values equally likely) ranges from 35 km (probability 0.25) to 48 km (0.25), 69 km (0.25), or 98 km (0.25). The resulting area of the hypothesized detachment thus would average about 4000 km², with a standard deviation of about 2000 km².

3.2.3 Maximum Magnitude

The maximum magnitude of a detachment-fault earthquake would arise from rupture of the entire 4000 ± 2000 km² surface area estimated for the detachment. A rupture of this dimension, using the empirical relationship between rupture area and magnitude for all slip types of Wells and Coppersmith (1994) results in a mean estimated earthquake magnitude of

7.6 (+0.2, -0.3). Adding the uncertainty from the Wells and Coppersmith (1994) empirical regression (0.24 magnitude unit), our estimated magnitude for the maximum detachment earthquake is 7.6 (+ 0.4, -0.5) at a 1-sigma range. We assign weights of 0.15, 0.7, and 0.15 to these values.

3.2.4 Recurrence

Because of the absence of earthquakes having low-angle focal mechanisms in the historical record in this area, it is impossible to associate earthquakes with a detachment and use the rate of those events to constrain recurrence rates. A method for constraining recurrence is to resolve the Quaternary slip rates (using the weights arrived at for the those values as discussed in a later section) of all Yucca Mountain faults along three equally spaced east-west transects. We use the same transects as shown in L. Anderson's presentation at SSC Workshop 3. We then consider the largest of those three values to be equal to the slip rate of the detachment. Our reasoning is thus: If the surface faults are expressions of extension on the underlying detachment, their combined slip rate cannot be greater than the slip rate on the detachment. However, the combined surface slip rate could be smaller than that on the detachment, if there is any component of nonelastic deformation above the detachment, or if there is any elastic deformation on faults that do not reach the surface. Therefore, the surface slip rate is a minimum value for the detachment slip rate.

The results are:

- Slip Rate = 0.05 mm/yr; Probability = 0.6
- Slip Rate = 0.013 mm/yr; Probability = 0.2
- Slip Rate = 0.12 mm/yr; Probability = 0.2

Displacement per event is calculated from the magnitude-vs -average displacement regression of Wells and Coppersmith (1994, all fault types), assuming that $M_{max} = 7.6 (+ 0.4, - 0.5)$. This yields mean values for average displacement of 1.3 m (0.2), 2.8 m (0.6), and 5.2 m (0.2). Mean recurrence is then calculated as mean displacement per event divided by mean slip rate. This procedure yields a mean recurrence of 75 kyr for the maximum earthquake, with 1-sigma limits of about +125 kyr and -50 kyr. The recurrence model we prefer is characteristic (weighted 100%).

3.3 BURIED STRIKE-SLIP FAULT SOURCE

Two lateral shear models were considered in our analysis of tectonic models, neither model is given much credibility based on data from the Yucca Mountain region. For the reasons discussed in Section 2, we give no weight to the transtensional nappe model. We apply a low, but non-zero, weight to the buried strike-slip fault (definition #2 in Section 2.1.5) as a seismic source. In general, the arguments in favor of a buried strike-slip fault include being in the region of the Walker Lane and invoking buried strike-slip faulting to explain the lateral component of slip on Yucca Mountain area faults. Arguments against such a fault include: lack of surface evidence for strike slip faults in the Yucca Mountain region, nor of any single, continuous strike-slip fault southeast of Crater Flat along the state line; vertical axis rotations in the area are variable in time and space and can be explained by normal faulting without any strike slip (C. Fridrich, SSC Workshop 3); and there is no evidence for large-scale offset (e.g., 25 km as suggested by Schweikert, at SSC Workshop 3) of volcanic rocks in Crater Flat.

Based on the above arguments, we consider it unlikely that a buried strike-slip fault exists. As shown in the logic tree in Figure ASM-1, whether such a fault exists is evaluated conditional on whether a detachment exists (as assessed previously). This is because, if a detachment exists, it would be more difficult to identify a strike-slip fault at depth. The detachment could serve to decouple the deeper lateral deformation from that occurring above the detachment. Assuming that a detachment does exist, the probability that a buried strike-slip fault exists is assessed to be 0.2; assuming that a detachment does not exist, the probability that a buried strike-slip fault exists is assessed to be only 0.05. This is because it is judged very unlikely that surface evidence for such a fault would have escaped detection during the field investigations in the region, especially assuming there is no detachment. Assuming that such a buried strike-slip fault exists, it could follow down-on-the-east segments along the west side of Crater Flat shown by John Bell (SSC Workshop 3) as part of a regional wrench system, or it could follow the location R. Schweikert designates—from Timber Mountain caldera to the south end of Crater Flat down the center of Crater Flat (Schweikert, SSC Workshop 3). The hypothesized location of the buried strike-slip fault is shown on Figure ASM-3.

3.3.1 Seismogenic Potential

The next assessment is whether a buried strike-slip fault is seismogenic, given that it does exist. This assessment is judged to be conditional on the depth of the detachment lying structurally above the assumed strike-slip fault. (See discussion in Section 3.2.1 for the range of detachment depths as a function of the depth of the brittle crust). If the detachment is shallow, the probability that the strike-slip fault is seismogenic is relatively high (0.8); if the detachment is at moderate depth, the probability is 0.6; and if it is deep, the probability is 0. This assessment is based primarily on the observation that significant earthquakes on very long, thin (high aspect ratio) faults are not observed unless those faults penetrate the entire seismogenic crust.

3.3.2 Maximum Magnitude

Two estimates of rupture length are proposed to estimate maximum magnitude for a potential buried strike-slip fault. For the first approach, a 1932 Cedar Mountain earthquake-type rupture is assumed. The length of this rupture was about 60 km (Gianella and Callahan, 1934). Second, the length of Bell's down-to-the-east faults is assumed to represent a possible rupture segment for a strike-slip fault that is about 25 km long. Because the 25-km rupture length is based on local observations rather than a regional analogy, it is given higher weight (0.7) than the 60-km estimate (0.3). The magnitude associated with the 60-km rupture is 7.1 and with the 25-km rupture is 6.7, using the empirical relations between rupture length and magnitude of Wells and Coppersmith (1994).

Fault area also has an effect on maximum magnitude. Down-dip width of the buried strike-slip fault is conditional on the existence of the detachment. If the detachment exists, the range of possible widths of the buried strike-slip fault is based on combinations of estimated values of the detachment depth and thickness of the seismogenic crust. If no detachment exists, the upper limit of the buried strike-slip fault is assumed to be 7 km (just below the depth imaged on the seismic reflection profiles).

3.3.3 Recurrence

Earthquake recurrence is assessed based on the assumption that, if a buried strike-slip fault exists, its strain rate would be reflected at the surface by slip on the observed Yucca Mountain faults. Thus, we assumed the slip on this fault can be evaluated (or at least constrained) by

using a geometrical relationship to the east-west extension associated with the Yucca Mountain faults. We resolve the total east-west extension (slip rates) for the faults of Yucca Mountain (i.e., Solitario Canyon, Windy Wash, Northern and Southern Crater Flat, Paintbrush Canyon/Stagecoach Road) onto a northwest-trending plane that has a pure lateral sense of motion. We assume three possible strike values for this plane (N20W, N35W, and N50W) with equal probability. A strike of approximately N35W appears to be the value indicated in Schweikert and Lahren (1997). There is uncertainty in this strike value. Hence we allowed a ± 15 -degree variation in the strike of this source and assigned equal weights. This variation seemed permissible when compared to the somewhat general figures presented by Schweikert. The resulting values are:

Slip Rate = 0.1 mm/yr; Probability = 0.6
Slip Rate = 0.025 mm/yr; Probability = 0.2
Slip Rate = 0.24 mm/yr; Probability = 0.2

Given no constraints based on data for the behavior of this source, the characteristic recurrence model (Schwartz and Coppersmith, 1984; Youngs and Coppersmith, 1985) was assumed to be appropriate. This model has been shown to be appropriate for many individual faults.

3.4 LOCAL FAULT SOURCES

This section describes the local (i.e. within Crater Flat/Yucca Mountain/Bare Mountain area) fault sources considered in our preferred seismic source model (see discussion in Section 2.4). The description and characterization of the more regional faults (those outside the Crater Flat/Yucca Mountain/Bare Mountain area) is independent of the choice of local tectonic model. The more regional sources are described in Sections 3.5 and 3.6. The faults included in our evaluation (regional and local) are a subset of those identified in Piety (1995) and McKague et al. (1996). Some faults in those compilations were omitted from consideration based on a lack of Quaternary activity in Chapter 11 of the summary report (Whitney, 1996), or those more regional faults that Anderson et al. (1995a,b) considered to lack evidence for Quaternary activity.

The regional and local faults are evaluated according to the probability that they are seismogenic. Given that they have some probability of being seismogenic, their location and extent are evaluated, behavioral aspects assessed, maximum magnitudes defined and recurrence evaluated.

3.4.1 Seismogenic Potential

The evaluation of which mapped faults to include as seismic sources is a function of the interpretation of the seismogenic potential (probability of activity) of each fault. The criteria we used to evaluate whether a fault is seismogenic are: (1) the recency of slip on the fault; this is the strongest criterion but is difficult to determine in this area because of long recurrence intervals; and (2) the length of the fault, which should be long enough to generate magnitude 5 to 5½ earthquakes (approximate length of 5 km); and (3) the interpreted average late Quaternary displacement. Other observations that are potentially important include evidence of brittle slip in the geologic past and involvement in development of throughgoing structures. If a fault was active in the geologic past but is truncated downdip, we consider it will not become active as an independent source again.

Northwest-Trending Faults. The mapped northwest-trending faults in the site area (i.e., Drillhole Wash fault, Sever Wash fault, Pagany Wash fault, and Yucca Wash fault) are assessed to be nonseismogenic based on their short lengths (3 to 5 km), no evidence for Quaternary displacement, and a slip tendency that is not favorable within the present stress regime (Stamatokos and Ferrill, SSC Workshops 3 and 4; McKague et al., 1996). We consider the regional seismic source zone to incorporate the hazard from small faults of these dimensions.

Ghost Dance Fault. The Ghost Dance fault is oriented favorably for slip but there is no evidence that it is active or seismogenic. Within a resolution of less than 0.5 m, slip in the past approximately 300 ka is precluded by the lack of displacement of a bedrock paleosurface (Taylor et al., 1996). During the same time, multiple paleoearthquakes are recorded along the nearby Solitario Canyon fault. The northern terminus of the fault is identified from detailed mapping, and it appears to be truncated by a structure to the south. Therefore, the length of the fault is comparable to that of the northwest-trending faults. Further, its geologic history does not suggest that it was a zone of significant localized slip. On the basis of these

arguments, the Ghost Dance fault is assessed to have a probability of zero that it is seismogenic.

Sundance Fault. The 700-m-long Sundance fault is too short to be an independent seismic source. There is also no evidence for Quaternary slip.

North-Trending Faults. We have identified nine local faults as seismic sources near Yucca Mountain (Figure ASM-4). Four of these faults (Bare Mountain, Windy Wash, Solitario Canyon, and Paintbrush Canyon/Stagecoach Road) are termed major, block-bounding faults and are interpreted to penetrate the entire seismogenic crust. {Note: we characterize the Paintbrush Canyon/Stagecoach Road faults as a single fault.} The remaining north trending faults (Northern and Southern Crater Flat, Fatigue Wash, Iron Ridge, Bow Ridge) are termed minor or secondary faults; they likely merge with the major, block-bounding faults within the seismogenic crust. Our characterization of the local Crater Flat Group (CFG) faults is summarized on Figure ASM-5. We interpreted all the major, block-bounding faults listed above to be seismogenic (probability = 1.0). The probabilities that minor faults are seismogenic are based on the sizes of per-event displacements inferred from trenches (see Section 3.4.3.1 and Table ASM-1). The mean and maximum of $D_{\text{preferred}}$ values and the probability that the fault is NOT seismogenic are as follows: Bow Ridge fault (24, 44 cm, and 0.3); Northern Crater Flat fault (47, 50 cm, and 0.2); Southern Crater Flat fault (20, 20 cm, and 0.5); Fatigue Wash fault (61, 105 cm, and 0.1); and Iron Ridge fault (80, 100 cm, and 0.1).

3.4.2 Geometry Models

Fault Rupture Lengths. For the nine local faults that we characterized in detail, we made three estimates of maximum surface rupture length to evaluate the maximum earthquakes (Table ASM-2). The minimum length equals the along-strike distance between the farthest-apart points on the fault that display Quaternary displacement indicated on the map of Simonds et al. (1995). The preferred length is the along-strike distance between the ends of the obvious mapped fault (irrespective of age of displacement) as shown on the fault map of Simonds et al. (1995). The maximum length is the along strike distance between the maximum inferred limits of mapped bedrock fault(s), as shown on the Simonds et al. (1995)

map. On the north, most of the faults are interpreted to be truncated by the northwest-trending faults (Yucca Wash, etc.).

Because we want the length of surface rupture during the maximum earthquake, we considered it unlikely that such a rupture would be limited to a minimum length defined by distance between trenches as postulated in Table 5.1 of the synthesis report (Whitney, 1996), for two reasons: (1) the distance between trenches showing Quaternary offset is a minimum estimate for the length of Quaternary faulting, and the maximum earthquake should have a maximum (rather than a minimum) rupture length; and (2) depending on how the trenches were sited (e.g., some are clustered near roads), their spacing may show only a small extent of the Quaternary surface rupture. We give this interpretation a zero weight. We consider that the maximum earthquake would cause rupture at least equivalent to the extent of faulted Quaternary deposits. The longest possible surface rupture length in the maximum earthquake is constrained by the mapped length of the fault in bedrock. We estimate a 30 percent probability that the maximum earthquake could rupture the entire mapped extent of the fault and at least some distance beyond on along-strike structures inferred as faults on the Simonds et al. (1995) map.

Downdip Extent of Faults. To compute downdip width (and hence fault area), dips on the major, block-bounding local faults were interpreted to range from 45 to 70 degrees. These values are based on observed surface dips in the Basin and Range, theoretical considerations for normal faulting (Sibson, 1985), surface dips in the Yucca Mountain area (C. Fridrich, SSC Workshop 2), the seismic reflection profiles (presented by T. Brocher, SSC Workshop 2), and the observations of seismicity from the Little Skull Mountain sequence (K. Smith, SSC Workshop 2).

As described above, our assessment divides the local faults into two categories: major, block-bounding faults (which include the Bare Mountain, Solitario Canyon, Paintbrush Canyon/Stagecoach Road, and Windy Wash faults), and secondary faults (which include the Northern and Southern Crater Flat, Fatigue Wash, Iron Ridge, and Bow Ridge faults). The block-bounding faults are of sufficient length that they may fully penetrate the seismogenic crust. This interpretation is based on the overall length of the block-bounding faults, reasonable aspect ratios given those lengths, and total displacement across the faults. Hence

the area for these faults is conditional on the seismogenic crustal thickness or existence of a detachment, fault dip, and maximum rupture length. For the secondary faults, downdip width was assessed assuming an aspect ratio (AR) for the fault (horizontal/vertical) in the range of 0.91 to 2.2 based on data presented in Nicol et al. (1996). Dip values for the secondary local faults were assumed to be in the range of 65 to 75 degrees. These values for dip of the secondary faults are based simply on the observation from structural cross sections and seismic reflection data from normal faulting terranes that secondary faults that merge with more significant faults (in terms of structural offset) commonly have steeper dips than the associated major fault. Hence we characterize a slightly steeper dip for the secondary faults.

Our evaluation of the downdip geometry considers two basic alternatives, one with many of the faults merging at depths above the brittle-ductile transition and one with individual, planar faults that do not intersect (Figure ASM-5). Based upon the spatial proximity and anastomosing pattern of the local faults in map view, we assign a high probability (0.95) that the faults merge within the seismogenic crust. Conditional on the existence of a detachment we assign 1.0 probability that the faults merge down dip. Note that for the interpretation that a detachment exists, then all of the local faults are limited in their depth extent by the detachment depth.

A number of geometries are considered possible for the merging case, the major, block-bounding faults (Bare Mountain, Paintbrush Canyon/Stagecoach Road, Solitario Canyon, and Windy Wash) are evaluated for likelihood of interrelationships with the secondary faults and with each other based on aspect ratio and geometry (as discussed by C. Fridrich in SSC Workshops 2 and 6). As indicated on Figure ASM-6, a large number of possible geometries were considered based on ranges of dip and aspect ratio for the secondary faults and dips for the primary faults. Cross-sections for both northern and southern transects were constructed with weights for aspect ratios and dips as described above.

The result was the development of four representative cross-sections that define the uncertainty in downdip geometry of the block bounding and secondary faults (Figures ASM-5 and ASM-7). If the faults merge down dip, then three alternative geometries are defined: a shallow model, a preferred model, and a deep model. These models reflect the depth at which merging takes place. The dip of the faults is assumed to increase as the depth of merging

increases (see Figure ASM-7). Based on the weights assigned to fault dips and aspect ratios, the weights assigned to the shallow, preferred and deep merging models are 0.1, 0.6, and 0.3 respectively. For the nonmerging case, only one model is considered because steep fault dips are required to maintain fault separation throughout the seismogenic crust. In the nonmerging case, the downdip extent of the secondary faults is limited by the preferred AR value of 1.55 (the central value of the range quoted earlier).

3.4.3 Behavioral Models

Our evaluation of the behavioral aspects of the Yucca Mountain faults focused on displacement and temporal attributes.

Maximum and Average Displacements in the Maximum Earthquake. Several procedures were utilized to estimate average and maximum displacements for each local fault source from the Yucca Mountain trench data. (Note: All data to develop these parameters is from Table 5.1 of the synthesis report (Whitney, 1996)). By using the several methods we intend to capture the uncertainty in models (methods) as well as sampling and interpretation uncertainties.

Average Displacement- One method to estimate the average displacement, D_{avg} , is simply to average the preferred values of displacement, D_{pref} , from all events in all trenches along each fault. An alternative is to average the D_{pref} values from the largest event on each fault. We have computed true D_{avg} using each of these techniques and assigned a weight of 0.5 to each result. The results are contained in Table ASM-1.

Maximum Displacement- One technique is to simply take the largest value of D_{pref} in any trench on the fault to represent the maximum displacement in the earthquake, true D_{max} (we distinguish true D_{max} from the maximum estimates of displacement for each event in each trench). However, based on the Borah Peak results, only 2-3% of the fault trace exhibits displacements within 80-90% of the true maximum displacement value. Hence, it is unlikely that even three randomly placed trenches would sample within 80-90% of the true maximum displacement. We give this technique for estimating true D_{max} a weight of 0.25. An

alternative method to estimate true D_{max} is to consider choose the largest displacement value from Table 5.1 for each fault. This incorporates the uncertainty in interpretation/evaluation of displacements within the trenches. We have assigned a weight of 0.5 to this technique. Another way to estimate true D_{max} is to consider it a multiple of true D_{avg} . This is a technique suggested by Mason (1996). At Borah Peak, the ratio of true D_{max}/D_{avg} is ~ 3.37 for the entire 33.8 km of the surface rupture, for the central portion of the fault it is ~ 2.59 . Our alternative technique is then to take each of the true D_{avg} values described above and multiply them by 2.59 to arrive at values for D_{max} . We have assigned a subjective weight of 0.125 to each of the resulting values. Using this procedure we attempt to reduce the uncertainty due to sampling bias (i.e. trench location). The results for true D_{max} also are contained in Table ASM-1.

Simultaneous Rupture of Fault Sources. For this analysis, "simultaneous rupture" is defined as ruptures on two or more faults occurring within 30 seconds of each other. Hence, simultaneous rupture increases the magnitude of the earthquake. In effect, the *areas* of the faults involved are combined to contribute to a larger magnitude. We take this rather strict definition because the purpose of this characterization is to evaluate vibratory ground motion hazard. If two or more faults rupture more than ~ 30 seconds apart (i.e. strong motion from the second fault begins arriving at the site after shaking from the first event has stopped) the two earthquakes (occurrence) can be characterized as independent events. The logic tree that defines the structure and uncertainties in this assessment is given on Figure ASM-5 and is described below.

The potential for simultaneous rupture is dependent upon whether or not the faults merge down dip. If the faults do not merge, then it is assumed that simultaneous ruptures do not occur (Figure ASM-5). In addition, the probability that simultaneous ruptures occur is assessed based on the likelihood of temporal overlap during past events. Based on the results presented in the synthesis report (as presented by Pezzopane and Whitney, SSC Workshop 3) and as summarized by L. Anderson (in SSC Workshop 4) the potential simultaneous ruptures considered are listed on Figure ASM-8. We assigned probabilities to the scenarios listed in Table 5-3 of the synthesis report as follows: high confidence cited in Table 5-3 received a $P=0.9$, moderate confidence received a weight of 0.5, and low-moderate confidence received

a weight of 0.25. Then for each fault pair, these values were multiplied times the fractional number of total events on the two faults that were inferred to be in common to compute a probability of temporal overlap for the fault pair. The ultimate probability of simultaneous rupture (under our definition) is then the linked probability of the geometry and temporal overlap branches. This result is a probability of 0.3 that simultaneous ruptures occur, given that the faults merge down dip (Figure ASM-5).

3.4.4 Maximum Magnitude

Maximum earthquake magnitudes for the independent fault sources were assessed using maximum rupture dimensions (surface rupture length, displacement, area) for individual maximum events, as discussed above. Our parameters included surface rupture length, maximum and average displacement per event, rupture area, and displacement times length vs. magnitude (Mason (1996); see Table ASM-3). For the local faults, the subjective weights for each of the above methods used to compute magnitude estimates was applied individually, i.e., was given a fault-specific set of weights. We gave the highest weights to the surface rupture length (SRL) relationship of Wells and Coppersmith (1994) and SRLxD method of Mason (1996), each assigned a weight of 0.3. Weights of 0.15 were applied to the average and maximum displacement methods, and a weight of 0.1 was applied to the rupture area method (all from Wells and Coppersmith, 1994).

These general rules were modified on a fault-specific basis (Table ASM-3) for several reasons. First, on some faults no average displacement values could be calculated, because there was only one trench for which displacements were reported. In such a case, we could not estimate magnitude based on average displacement. Second, if the displacements in individual trenches ranged greatly from event to event, we had a low confidence that a computed average displacement was meaningful. Given the large variability of displacement along strike in historical normal surface ruptures (e.g., Wheeler, 1989; McCalpin, 1996), we generally had low confidence that a few randomly sited trenches would fortuitously sample either the maximum or average displacement for each paleoearthquake. Thus, magnitude estimates based on displacements usually were assigned lower weights than estimates derived by other methods. Third, if faults were so proximal at the surface that they could merge downdip within the crust, we acknowledged greater uncertainty in their downdip extent, and thus lowered the weight on estimates based on rupture area. Finally, for faults that possess short

lengths with respect to their observed per-event displacements, we generally assumed that: (1) the faults must fully penetrate the crust to explain such large coseismic displacements; (2) if the faults fully penetrate the crust, they must have a downdip dimension of 14 to 20 km (assuming a 60-degree dip and 12 to 17 km depth); (3) it would be very unusual for a fault having a 14- to 20-km downdip extent to be shorter than 14 km, because that would imply an aspect ratio of less than 1.0; therefore, (4) those faults were considered to have longer ruptures than the mapped fault length, by linking with other mapped faults; and thus (5) the large displacements considered were more representative of the maximum earthquake than the short lengths of the mapped faults. [We note that the definition and naming of separate faults in an anastomosing network of faults, such as exists at Yucca Mountain, is somewhat arbitrary. This is the reason we have chosen to consider the Stagecoach Road/Paintbrush Canyon system as a single fault. Based on the large reported displacements, short length and along strike geometry of the Stagecoach Road fault we infer it to be connected at depth with the Paintbrush Canyon fault].

For each fault, we evaluated the quality of the data on fault dimensions and then altered the weighting outlined above to reflect our assessment of believability in the measurements.

3.4.5 Recurrence

Fault Slip Rates. Slip rates were assessed using data in Table 5.1 of Whitney (1996). First, the long-term mean slip rate for each fault was computed (including data uncertainties), and a normalized-grouped cumulative density function (CDF) was generated, after the technique of McCalpin (1995). Examples of this technique are provided in Appendices ASM-1 and ASM-2. This technique considers the variation of slip rates among many faults over a short period to mimic the variation on a single fault over a longer period. The mean long-term slip rate is applied to the CDF to produce a fault-specific CDF of slip rate. Values of the 20-percentile, median, and 80-percentile are listed in Table ASM-4. The full CDF was used in the analysis.

Earthquake Recurrence. Two alternative approaches were used to characterize earthquake recurrence relationships for independent fault sources. In the first approach, the inter-event times from Table 5.1 of the Whitney (1996) are used, along with the errors cited for the "preferred, maximum, and minimum" estimates, to calculate the times between characteristic

paleoearthquakes. The cited values are considered to represent only measurement error for a given interval, and not the stochastic variability between successive events in a given trench.

To account for the stochastic variability, we again used the McCalpin (1995) approach. Normalizing all recurrence data by setting the long-term mean recurrence of each fault to 100 ka. We then grouped all normalized recurrence intervals for all faults and plotted the cumulative density function (CDF). Probability density functions and cumulative distributions for this technique are contained in Appendices ASM-3 and ASM-4, respectively. (This same approach was used for slip rate; see McCalpin, 1995 for explanation of the technique.) We then input the long-term interevent time for each fault (which contains only measurement errors) into the CDF to produce a new CDF that incorporates both measurement error and stochastic variability, as contained within the normalized-grouped data set (Appendix ASM-5). These values are listed in Table ASM-5. This approach is given a weight of 0.5, which reflects our evaluation that it is an equally valid approach to the slip rate approach described below. This approach yields only the recurrence times between maximum (or characteristic) earthquakes; frequency of smaller earthquakes is derived from the recurrence models described below.

In the second approach, the slip rate distributions described above are used to develop recurrence relationships using a moment rate approach (e.g. Youngs and Coppersmith, 1985). This approach was also given a weight of 0.5.

The application of the slip rates and recurrence intervals to develop recurrence rates for the local faults depended upon the behavior model. Under the condition that simultaneous ruptures do not occur, the individual faults are assumed to act independently, and the assessed slip rates and recurrence intervals for each fault are used to define the recurrence relationship for the fault. Under the condition that simultaneous ruptures can occur, then the slip rates and recurrence intervals are partitioned between individual fault ruptures and simultaneous fault ruptures as follows.

Listed on Figure ASM-8 are the assessed percentage of fault ruptures on the individual block-bounding faults that are considered to be simultaneous ruptures with other faults and the relative frequency of various fault rupture combinations. The slip rate that is released in

multiple-fault rupture is set equal to the assessed fault slip rate times the percentage of times the fault ruptures simultaneously with other faults. This slip rate is further partitioned among the various multiple-fault rupture scenarios by the relative frequencies listed on Figure ASM-8. For example, under the condition that simultaneous ruptures occur, 90% of major ruptures on the Bare Mountain fault are assumed to be simultaneous ruptures and 1/3 of these are in combination with the Solitario Canyon fault. Similarly, 70% of ruptures on the Solitario Canyon fault are assumed to be simultaneous ruptures and 1/2 of these are in combination with the Bare Mountain fault. The assessed slip rate used to define the recurrence of simultaneous ruptures of the Bare Mountain and Solitario Canyon faults is set equal to 30% of the Bare Mountain slip rate plus 35% of the Solitario Canyon slip rate.

The assessed recurrence rates for individual faults are similarly partitioned; 30% of the rate for Bare Mountain events are assumed to be simultaneous ruptures with Solitario Canyon and 35% of the rate for Solitario Canyon events are assumed to be simultaneous ruptures with Bare Mountain. Because these assessments are approximate, the computed frequencies were not identical, and an average of the two values was used to define the recurrence rate for the simultaneous ruptures.

Under the condition that simultaneous ruptures can occur, the slip rates and recurrence intervals for individual fault ruptures are set equal to the assessed values for the individual faults times the percentage of times that individual fault ruptures occur (e.g. for Bare Mountain 10% of the ruptures are assessed to be independent ruptures of the Bare Mountain fault).

For the local faults, three recurrence models were used. The highest weight was given to the characteristic model of Schwartz and Coppersmith (1984) (as described by Youngs and Coppersmith, 1985), weight = 0.7; the exponential recurrence model was assigned a weight of 0.2; and the "maximum magnitude" model (similar to Wesnousky et al., 1983) was assigned a weight of 0.1

In constructing the recurrence relationships we assume that the maximum magnitude assessments described in Section 3.4.4 are the central value for the characteristic magnitude interval (e.g. Youngs and others, 1987). For the characteristic and maximum moment

recurrence models, the characteristic events are uniformly distributed in the magnitude range $M_{\max} \pm 1/4$, such that the upper limit of the recurrence relationship is $M_{\max} + 1/4$. For the exponential recurrence model the upper limit is also set at $M_{\max} + 1/4$. When the recurrence relationship is specified by the recurrence interval of surface-rupturing earthquakes, this recurrence rate was assumed to apply to earthquakes of magnitude greater than or equal to $M_{\max} - 1/4$.

Under the condition that simultaneous ruptures can occur, the above three recurrence models were used to assess the relative frequency of various magnitude earthquakes for individual fault ruptures only. Multiple fault ruptures were assumed to be additional, larger events and the assessed maximum magnitude earthquakes were assumed to be the only events occurring.

3.5 REGIONAL FAULT SOURCES

Regional fault sources include regional faults (i.e., those outside the immediate Yucca Mountain/Bare Mountain/Crater Flat area) within 15 to 100 km from the site that are judged to be relevant earthquake sources. The locations of these regional fault sources are shown on Figure ASM-9. Most of the faults are listed in Table 11-1 in chapter 11 of Whitney (1996). We include, in addition:

- (1) Carrara (or U. S. Highway 95) fault,
- (2) East Specter Range fault,
- (3) a 12 km northern extension of the West Spring Mountains fault,
- (4) Middle Death Valley fault, and
- (5) West Death Valley fault.

Regional geologic, seismologic, and geophysical studies, and evaluation of these faults suggest that they are steeply- to moderately-dipping faults and exhibit conjugate relationships as discussed in Section 2.2. The northwest-trending faults are generally right-lateral and lie within the Walker Lane (Stewart, 1987) west of Yucca Mountain. Regional fault sources in the Basin and Range province east of the Death Valley-Furnace Creek-Fish Lake Valley fault zone have slip rates that are about one or more orders of magnitude lower than the faults within the Walker Lane.

Several other regional faults were excluded from our analysis based on: (1) data presented by Anderson et al. (1995a) that showed little evidence for middle to late Quaternary activity (e.g., Keane Wonder, Oasis Valley, Rocket Wash/Beatty Wash, and the Toliche Peak faults); or (2) sparse documentation of Quaternary activity (e.g., the Tin Mountain, Tikaboo, Stonewall Mountain, and Racetrack faults). The Kawich Range fault was excluded based on the discussion in Anderson et al. (1995a) and consideration of the short length of known Quaternary faulting. An estimated Mw 6.82 earthquake (based on SO = 1.5 m displacement at profile KRW-3) on this fault at about 72 km from the site would not be a relevant event on Figure 11-3 of Pezzopane in Whitney (1996).

Table ASM-6 summarizes the earthquake source characteristics for the 24 active regional faults that are included in our source model. This table is revised from the table in the memorandum from the ASM team of 13 May 1997, titled A Revised Source Data for Regional Faults (ASM Team). With the exception of the Carrara fault, all sources are assigned a probability of 1.0 of being seismogenic based mainly from paleoseismic evidence summarized in Anderson et al. (1995a and 1995b), Klinger and Piety (1996), Piety (1995), and various chapters of Whitney (1996). The Carrara fault is judged to be seismogenic with a high probability (0.85) for the reasons cited in Appendix ASM-6, but because the fault has not been fully characterized, some probability (0.15) is given to the possibility that it is not seismogenic. A generalized planar fault geometry to seismogenic depth was assumed for all the regional fault sources. Predominantly strike-slip faults are modeled as having a dip of 90 degrees. Predominantly normal or dip-slip faults are modeled as having dips of 60 degrees.

3.5.1 Estimation of Quaternary Ages

The ages of fault activity of Table 2 in Anderson et al. (1995a and 1995b) were used as a starting point. Our evaluation considered that: (1) the Pleistocene/Holocene boundary may be nearer 12 than 10 ka; (2) many references use 125 or 130 ka for the boundary between late and middle Pleistocene (128-770 ka); (3) the boundary between middle and early Pleistocene is 770 ka, and early Pleistocene is 770 to 1650 ka, which strongly skews the middle Pleistocene toward the present, and the middle Pleistocene is already skewed toward the present based on a start at 1650 ka bp, or more than 2000 to 2400 ka based on some recent dating. The terminology may be misleading as the middle Pleistocene includes the most recent 8-47 percent of the Pleistocene (using 1650 ka), and does not include even the middle of the

Pleistocene. It is however, the most widely used classification, and is required for comparative purposes. Accordingly, the following approximate dates are used in our analysis:

(1) Holocene/late Pleistocene boundary =	10 ka
(2) latest Pleistocene (avg. of 10 ka and 28 ka) =	19 ka
(3) latest Pleistocene (avg. of 10 ka and 69 ka) =	39 ka
(4) mid-late Pleistocene (avg. of 10 ka and 128 ka) =	69 ka
(5) late Pleistocene/middle Pleistocene boundary =	128 ka
(6) middle Pleistocene = (avg. of 128 and 770 ka) =	449 ka
(7) middle Pleistocene/early Pleistocene boundary =	770 ka
(8) beginning of Pleistocene =	1650 ka

3.5.2 Maximum Magnitude

Maximum magnitudes were calculated using an empirical relation that relates surface rupture length (SRL) to magnitude (Wells and Coppersmith, 1994 for all fault types). The relationship for all fault types was used because the data base is more robust, has a lower standard deviation, and higher correlation coefficient than for normal faults, and the relationship for strike slip, normal slip, and all fault types are almost coincident as shown on Figure 9 (b), and Table 2A of Wells and Coppersmith (1994). The uncertainty in maximum magnitudes is represented by the range of minimum, preferred, and maximum SRL. This uncertainty is approximately +/- 0.2-0.4 magnitude unit for 9 of 26 faults, and is lower for the other faults where SRL is constrained by intersection or connecting faults, or consistent magnitude values are obtained from maximum displacement or average displacement values.

3.5.3 Slip Rate

Two approaches were used to estimate slip rates for regional faults. For well- to moderately well-studied faults (designated by italic font in Table ASM-6) reported slip rates were used, with most preferred values assigned a weighting of 0.6 to 0.8, and maximum or minimum values of 0.1 to 0.2. For faults that have poor or incomplete characterization data (designated by normal font in Table ASM-6), slip rate was estimated from surface rupture length as described below. The weightings for these values have greater uncertainty than for the relatively well-studied cases. We thus assigned equal weight (approximately 0.33) to the preferred, maximum, and minimum values.

Slip Rate Estimated From Surface Rupture Length. The average slip rate for the faults that have relatively good SRL or length estimates and the approximate age of disturbed geomorphic surfaces as summarized in Piety (1995) were made as follows:

1. Maximum displacement (MD) for each event is estimated from surface rupture length (SRL) using the following relationship from Wells and Coppersmith (1994): $\log(\text{MD}) = -1.38 + 1.02 \log(\text{SRL})$. This relationship is based on a robust worldwide database of 95 events, and has a good coefficient of correlation of 0.75 and a standard deviation of 0.41. The regressions in Wells and Coppersmith (1994) generally are based on the maximum observed horizontal, oblique, and/or vertical surface displacement.
2. MD is multiplied by 0.38 to obtain AD, the average displacement (in mm). The multiplier value used is based on the average of values presented in Mason (1996) for Basin and Range normal faulting events, Slemmons (unpublished data for all fault types, and Basin and Range events), and Strom and Nikonov (unpublished data for normal faulting events) as summarized in Table ASM-7.
3. An assumed number of surface rupture events is inferred. Based on field data and observations for better studied regional faults (Table ASM-8) a value of 3 events is used in the analysis for the average number of surface faulting events.
4. Cumulative displacement is estimated by multiplying the estimated AD by 3 (the inferred number of surface rupture events).
5. An estimated slip rate is calculated using the cumulative displacement divided by the estimated ages for the geomorphic surfaces that are displaced by the fault. The displaced surfaces generally are assumed to be late to middle Pleistocene and equal weight is assigned three ages (69 ka, 128 ka, and 449 ka) (see Section 3.5.1 for discussion of estimated ages). The interval of time used is truncated at 10 ka, since mid-Holocene events appear to be absent from the faults, but early Holocene, or late Pleistocene events are present on some of the faults. Therefore, values of 59, 118, and 449 years were used to calculate maximum, preferred, and minimum slip rates.

3.5.4 Recurrence Intervals

dePolo and Slemmons (in review) previously examined the ten largest surface rupture areas in the Basin and Range province for earthquakes of $M_w = 6.3$ to 7.5, including (Owens Valley; Sonora, Mexico; Pleasant Valley; Hansel Valley; Cedar Mountain; Rainbow Mountain; Fairview Peak; Dixie Valley; and Borah Peak earthquakes. All areas showed prominent

Holocene and late Pleistocene paleoseismologic features along most scarps. Approximately 90 percent of the historical surface faults coincided with paleoscarps. This recurrent activity also is reported for most of the Yucca Mountain Quaternary faults, with all of the larger fault scarps showing geomorphic evidence for multiple events on at least parts of the fault zone. This multi-event relationship is better expressed in the exploratory trenches, and for the higher slip rate, most recently active faults, than by faults that have low slip rates and extremely long recurrence intervals (e.g., $> \sim 100$ kyr). Based on these observations, we assumed multiple events in our assessment of recurrence intervals for regional fault sources.

Two approaches were used to estimate recurrence intervals for regional faults: (1) for well-studied faults (designated by italic font in Table ASM-6) estimates of recurrence interval were obtained from paleoseismic data reported in the references provided and from personal observations by D. B. Slemmons as discussed in Appendix ASM-6; and (2) for faults with little or no paleoseismic data (designated by normal font) the recurrence intervals were estimated as follows.

The scarps observed in middle to late Pleistocene surfaces (based on data in Piety, 1995 and observations of D. B. Slemmons as discussed in Appendix ASM-6) are assumed to result from multiple surface faulting earthquakes. An assumed number of surface rupture events is inferred. Based on field data and observations for better studied regional faults (Table ASM-8) a value of 3 is used in the analysis for the average number of surface faulting events.

Three values (69 ka, 128 ka, and 449 ka) are used for the estimated age of the displaced geomorphic surfaces. As noted in the previous section, 10 kyr have been subtracted from these ages to estimate the pre-Holocene duration of time during which the inferred three events occurred.

The estimated duration periods of 59, 118, and 439 years are divided by 3 (the assumed number of surface rupture events) to provide the following estimated values and weights for recurrence interval: 20 kyr (0.33), 39 kyr (0.34), and 146 kyr (0.33).

In some cases (e.g., the Emigrant/Towne Pass and Grapevine faults) additional data that are available to constrain the timing of the most recent event, or possibility of connecting with

other fault extensions, also were incorporated into the assessment of recurrence interval as described in Appendix ASM-6.

3.5.5 Recurrence Models

Two recurrence relations were used to characterize the regional fault sources: the maximum moment recurrence model (Wesnousky, 1986) and the characteristic earthquake recurrence model (Youngs and Coppersmith, 1985). The maximum moment recurrence model was derived by Wesnousky (1986) from paleoseismic data for faults in southern California region, and this method, which was deemed most appropriate for our regional fault evaluations, was given a weighting of 0.8. The Youngs and Coppersmith model is widely used, but is more appropriate for earthquake catalog data. Since it is a widely used method, we felt it should be considered but assigned it a lower weighting of 0.2. The recurrence models are applied in the same manner as was done for the local sources.

The characteristic model requires estimates of the b-value associated with specific faults. The b-values used varied from fault to fault depending on the values assigned to the areal source zone in which the individual fault lies (see below).

3.6 REGIONAL SOURCE ZONES

Six regional source zones were defined within 300 km of the Yucca Mountain site for this evaluation: a Basin and Range zone, a Walker Lane zone (which contains the Yucca Mountain site), a Colorado Plateau zone, a Mojave block zone, a San Andreas zone, and a Sierra Nevada/Basin and Range zone (see Figure ASM-10). These zones are based on tectonic characteristics, style of faulting, and observed seismicity rates. From west to east the 300 km radius of the Yucca Mountain site) is divided into the following source zones:

Sierra Nevada/Basin and Range Boundary Zone. This en echelon zone includes the Mw=7.5 Owens Valley earthquake of 1872 (Beanland and Clark, 1994), that accommodates a significant fraction of the inferred activity of the Eastern California Shear Zone (Savage et al., 1990) and high seismic activity rate of the southern portion of the Central Nevada Seismic Zone (Rogers et al., 1992).

Walker Lane. This zone, defined by (Stewart, 1987), includes the Basin and Range Province of highest activity from Owens Valley to Death Valley, and a narrow eastern Walker Lane of lower tectonic and seismic activity from Death Valley to Yucca Mountain.

Yucca Mountain Subzone. A subzone of 50 km radius within the Walker Lane surrounding the Yucca Mountain site. Defined on the basis of enhanced geological investigations.

Basin and Range Province. The Basin and Range Province northeast of Walker Lane, which at the Yucca Mountain latitude has a much lower rate of activity than the Walker Lane. Dominated by north-trending normal faults and moderate to high seismic activity rate.

Colorado Plateau. The relatively stable block along the southeast boundary of the Basin and Range Province, more than 200 km east-southeast of Yucca Mountain.

Mojave Block. A relatively stable block generally south of the Garlock fault (about 100 km south of Yucca Mountain), which forms a boundary between the Walker Lane and Sierra Nevada/Basin and Range Province, and the Colorado Plateau Zone.

San Andreas Fault System. The highly active right-lateral fault system, which accommodates about 75 percent of the differential movement between the North American and North Pacific plates.

For characterization of seismic sources we used those source zones that extend within 100 km of the site as shown on Figure ASM-11 (these are the Walker Lane and Basin and Range Province).

3.6.1 Recurrence

For each zone, the recurrence is assessed to follow a truncated exponential form with probability of one. Although individual faults may follow a characteristic or maximum moment recurrence relationship, regions (i.e., source zones) generally are well represented by the truncated exponential model of earthquake recurrence (Youngs and Coppersmith, 1985; Richter, 1958).

The recurrence for each zone is computed using the appropriate subset of the 300-km catalog, declustered using the Veneziano and van Dyke (1985) (as described in McGuire, 1985) (weight =0.7) and Youngs et al. (1987) (weight=0.3) techniques (see Appendix D of the main report). The catalog declustered using the Veneziano and van Dyke approach is referred to as Version 7, the catalog declustered using the Youngs et al. approach is referred to as Version 5. Based on comparisons of the space-time plots, the Veneziano and Van Dyke (1985) technique appears to be more successful at declustering the catalog and has been weighted higher. Additional attempts at declustering were made using the technique of Reasenber (1985). This technique was significantly less successful at declustering the catalog (see example space-time diagrams in Figure ASM-12). As a result, the Reasenber algorithm was not utilized to develop recurrence statistics for the source zones. Data after 1950 from the region within the Nuclear Test Site (Figure ASM-11) where nuclear testing was performed was removed from the recurrence computations to remove the influence of induced events. Completeness intervals were estimated using existing literature (Gomberg, 1991a), comparisons of "Stepp-plots" (Stepp, 1972) (example shown in Figure ASM-13) from the catalog along with consideration of the operational history and sensitivity of instrumentation in the area (pers. comm, 1997; A. Rogers, J. Brune, K. Smith). The assessed completeness intervals for the 100 km radius around Yucca Mountain are summarized below.

M 2.0-2.5	1983-present
M 2.5-3.0	1979-present
M 3.0-3.5	1961-present
M 3.5-5.0	1932-present
M 5.0-6.0	1900-present
M 6.0-6.5	1880-present

3.6.2 Maximum Magnitude

Within the broader Walker Lane zone, a subzone (the Yucca Mountain subzone) is defined by a 50-km radius around the Yucca Mountain site. Given the extensive investigations in this area, it seems unlikely that any significant (in terms of slip rate), young, potentially surface rupturing faults have escaped detection within this zone. Hence we assign a lower maximum magnitude to this part of the Walker Lane zone. We assign a maximum magnitude of 6.3 +/- 0.3 to this source. We consider this value to represent the approximate upper limit magnitude for non-surfacing rupturing earthquakes in this sub-zone. Based upon the work of dePolo (1996, and as presented in SSC Workshop 4) and considerations of physically reasonable fault

area/displacement/stress drop considerations (as presented by J. Ake at SSC Workshop 4). The logic tree used to characterize the regional source zones that lie within a 100-km radius of the site is shown on Figure ASM-14.

Estimates of maximum magnitudes for source zones (other than the Yucca Mountain source subzone) were assigned based either on the inferred surface rupture length of the largest fault not explicitly characterized with the regional faults or the maximum magnitude event inferred to have occurred historically in that zone. It is our assessment that some potentially seismogenic faults are not represented in the list of regional faults specifically included in the source model (Table ASM-6 and discussed in Section 3.5). Some of these faults lack recurrence information. We used the maximum magnitude suggested by either: the approximate maximum length of those faults or the largest earthquake in the zone, to constrain the maximum magnitude for the zone in question. The maximum magnitudes for each of the seven source zones are summarized below:

Basin and Range	Mmax = 7.2
Walker Lane	Mmax = 6.8
Yucca Mountain subzone	Mmax = 6.3
Colorado Plateau	Mmax = 7
Mojave Block	Mmax = 7.7
San Andreas	Mmax = 8
Sierra Nevada/Basin and Range	Mmax = 7.6

Uncertainty in the maximum magnitude was assumed to be ± 0.3 units at the 90 percent confidence interval.

3.6.3 Stationarity of Seismicity

When characterizing the seismic hazard within a source zone, two alternative hypotheses are commonly used. One considers earthquake occurrence to be equally likely at each point within the zone and frequency is determined by the recurrence statistics developed for the zone as a whole. This is the Poisson spatial model. Alternatively, non-uniform patterns of seismicity observed in the historical record may be considered the best predictor for future earthquake occurrence within the broader zone (McGuire and Barnhard, 1981). To represent this interpretation, various types of spatial smoothing models may be applied, such as kernel

density estimation. A procedure of this type has been applied to construct the recent generation of national earthquake hazard maps (Frankel, 1995). This procedure results in a heterogeneous hazard function within any given zone. It is our view that the choice between the algorithms described above (or weighting) depends on the purpose of the hazard evaluation. If the goal is to characterize the hazard for an important facility with a relatively short economic life (say 150 years) for which a very low annual probability of exceedence for design parameters (say 10^{-4}) is desired, then a source zone characterization that mimics the observed patterns of historical seismicity should be given substantial weight in the hazard calculation. However, if the goal is to characterize seismic hazard for a much longer time span (say 10,000 years) with a reasonably low probability of exceedence, then the patterns of seismicity in the historical record may have little predictive value for occurrences on those time scales. In this case it would be appropriate to use a Poisson spatial model. It is our understanding that the performance assessors will be using results from the PSHA to judge the probability of occurrence of scenarios over 10,000-year, to 100,000-year, to multiple 100,000-year periods (SSC Workshop 5 discussion). Hence we have given a weight of 1.0 to the Poisson spatial algorithm for computation of hazard at this site.

4.0

FAULT DISPLACEMENT

4.1 INTRODUCTION

We characterize the potential for both principal and distributed fault displacement on seismogenic (block-bounding or primary) faults, and distributed faulting on five classes of secondary, nonseismogenic faults or fractures. We use generalized displacement patterns for normal faults derived from observed historical displacements. We apply the approach to characterize the potential for displacement at nine designated points within the Controlled Area at Yucca Mountain, but it can be used to evaluate the potential for displacements at any point. We do not specifically incorporate large-scale displacement patterns on the Yucca Mountain faults, specifically the Solitario Canyon fault (SC) or the Bow Ridge fault (BWR), the faults that bound the repository block. Instead, we rely on observed historical surface-rupturing on range-front faults larger than those at Yucca Mountain, related to earthquakes of $M \sim 7$.

There are two basic approaches for estimating the amount and timing of potential displacement on secondary faults (SSC Workshop 6). One approach is to derive all estimates from the secondary fault itself, based on its cumulative displacement, length, slip rate, or other parameters. This approach does not directly address the setting of the secondary fault, i.e., its distance to primary faults, whether it is one of many similar faults or exists alone in an otherwise unfractured block of rock, and so on; but rather assumes that these influences are reflected adequately in the fault parameters. The other approach is to examine the observed pattern of rupture in fault-bounded blocks and use this information to estimate potential displacement on distributed faults based on their position relative to principal fault rupture. This is the approach we adopted.

We consider the probability of fault displacement to be independent of depth. That is, we consider the displacement gradient between the repository level and the ground surface to be zero. Where the repository is near the surface, there is little error induced by this interpretation, because the distance over which slip would be attenuated is small. Where the repository is as much as 300 m below the surface, there is a possibility of displacement attenuation upward from the repository level to the ground surface. Whereas some data are available on slip gradients along strike in historical surface ruptures (e.g., McCalpin, 1996, p. 278, 289), few direct observations have been made on slip gradients in the dip direction during coseismic events. The observations of displacements in tunnels and mines beneath surface ruptures are too few on which to rely. Given this lack of data, our characterization of the potential for displacement applies equally to the ground surface and to the repository level (i.e., no attenuation in the dip direction).

Our approach for characterizing principal faulting hazard on seismogenic faults is based on the empirical distributions of along-strike displacement by Wheeler (1989) from the analysis of large Basin and Range earthquakes. We note that the displacement-along-strike curve for the SC fault (as described by A. Ramelli at SSC Workshop 5) is anomalous compared to historical Basin and Range ruptures, in that displacement is very high in the central 20 percent of the fault and very low elsewhere. We infer that the curve is so irregular because it only contains displacements from two faulting events; with additional

events, the curve should smooth out to more resemble the Wheeler curve, or the smooth, quasi-parabolic curve of cumulative displacement along strike (J.C. Yount, SSC Workshop 6). We also note that the most critical part of the curve is that closest to the repository, i.e., the northernmost 30 percent of the fault. In that reach the SC fault curve is almost identical to the Wheeler curve, both in mean value and upper and lower confidence limits. The rapid decrease in SC slip south of the maximum is inconsistent with other faults at Yucca Mountain, which generally increase in displacement southward. This clearly is not the case with the SC fault. The highest displacements on the SC fault occur after the Iron Ridge fault has branched off, rather than before, as one would expect if fault displacements were additive after two fault strands merged. If the SC fault displacement curve were typical of the long-term trend, Yucca Mountain would be three times higher in the vicinity of Trenches T1-T3 than elsewhere. However, the crest of Yucca Mountain does not show anomalously high elevations in the 2-km-long reach in the center. For all of these reasons, we do not use the displacements curve for the SC fault to predict the magnitude of future coseismic displacements along strike, but rather the Wheeler (1989) relationship.

Our characterization of distributed faulting rests on several interpretations about the mechanics of faulting. First, we assume that all distributed (induced) slip occurs during surface-rupturing earthquakes on primary (seismogenic) faults. It does not occur during the interseismic part of the cycle when strain is accumulating. We make this assumption because distributed faulting has been observed to occur during surface-rupturing earthquakes on normal faults. Conversely, distributed surface faulting (such as surface faulting on an intrabasin fault) without surface faulting on the adjacent primary basin-bounding fault is rare.

Secondly, we assume that during the interseismic part of the cycle, a crustal slab containing one (or more) secondary (nonseismogenic) faults in the hanging wall is strained elastically (the same is true for the foot wall). At the end of the seismic cycle, when the primary fault ruptures, the crustal rocks on either side of the fault recover through a combination of elastic rebound and inelastic deformation (fault slip) on secondary faults and discontinuities. We use the measured ground displacement profile from the 1983 Borah Peak, Idaho earthquake to characterize the variation of this displacement as a

function of distance from the principal fault rupture and location in the hanging wall or foot wall of the rupture. We utilize the amplitude of this displacement profile to represent the maximum potential for ground displacement, either through elastic rebound of the rocks, or slip on secondary features, or a combination of the two. The amount of displacement that occurs on a secondary fault, if it slips, is characterized as some fraction of this potential.

4.2 METHOD OF CHARACTERIZING THE POTENTIAL FOR FAULT DISPLACEMENT

Our method of characterizing potential fault displacement is described graphically by the logic trees shown on Figures ASM-16a and ASM-16b. We use slightly different methods for estimating the frequency and amount of slip on faults, depending on whether the fault is primary or secondary. Primary faults can experience displacement within 300 meters of the surface as principal fault rupture or as distributed fault rupture in response to principal rupture on other faults. Secondary faults can only experience distributed fault rupture.

4.2.1 Method for Principal Faulting

Figure ASM-16a shows the logic tree for characterizing the potential displacement on block-bounding, (primary) faults due to the occurrence of earthquakes on these faults. The characterization consists of the following steps.

4.2.1.1 Frequency of Potential Principal Faulting Events. The frequency of displacements occurring on a fault is estimated using the seismic source characterization developed in Section 3.0. The probability that principal faulting can occur is equal to the probability that the fault is seismogenic (see Section 3.4.1).

4.2.1.2 Probability of Principal Faulting Surface Displacement During Earthquakes. The probability that displacement will occur at or near the surface during an earthquake is computed using an empirical relationship between magnitude and the probability of surface rupture developed from the data presented in Pezzopane and Dawson (1996). Figure ASM-17 shows these empirical relationships presented in SSC Workshop

5. Of the three regression curves in Figure ASM-17, we weight the leftmost curve (labeled 32 GB events) 0.5 and the rightmost curve (labeled 105 events EC) 0.5. (The equations defining these relationships are presented in Appendix H, Section H.4.1.) These weights reflect the fact that we have no clear preference for one extreme curve over another, and we wish to capture the full range of uncertainty. The probability that slip occurs at a point of interest on a fault, given that slip occurs near the surface, is computed by randomizing the rupture along the fault. The length of the rupture is specified by the magnitude-rupture length relationships used in the ground motion hazard calculation.

4.2.1.3 Characterization of Displacement at a Point. The probability distribution for displacement occurring at a point of interest is computed in two steps. First, the maximum displacement on the primary fault is estimated using the Wells and Coppersmith (1994) relationship for maximum displacement (MD) as a function of earthquake magnitude. The variability in maximum displacement from event to event also is computed using the standard error for $\log(MD)$ found by Wells and Coppersmith (1994). The selected relationship is

$$\log(MD) = -5.46 + 0.82M, \quad \sigma_{\log(MD)} = 0.42$$

Given a maximum displacement, we use the normalized relationships shown on Figure ASM-18 to obtain the distribution for displacement at any point on the fault rupture. Figure ASM-18 was developed using the normalized displacement distributions developed by Wheeler (1989). The data were smoothed by hand to produce curves symmetric about the midpoint of the rupture. The minimum and maximum curves on Figure ASM-18 are intended to represent low (~5%) and high (~95%) cumulative probabilities for the ratio of the displacement at a point to the maximum displacement. (Appendix H, Section H.3.1 presents a statistical distribution fit to these data.)

4.2.2 Method for Distributed Faulting

Figure ASM-16b shows the logic tree that characterizes the potential for distributed faulting on both primary and secondary faults and fractures. The approach consists of the following steps.

4.2.2.1 Probability Feature Can Slip. The first step in the characterization potential of the potential for distributed faulting is an evaluation of the likelihood faulting can occur on the feature of interest. This is the product of two probabilities, one based on the cumulative displacement category of the feature and one based on the strike of the feature.

Probability of distributed displacement as a function of fault displacement category. The probability of displacement depends on the cumulative displacement of the target feature. This interpretation is based on a conceptual model in which faults in extending crust evolve through time (e.g., *Journal of Structural Geology, Special Issue on Fault Populations*, 1996, v. 18, no. 2/3). In this model, many small faults are created during the initial phases of extension. As extension continues, some small faults coalesce to form larger faults. The larger faults become preferred loci of extension (due to their size and continuity), and thus accommodate larger displacements. With larger displacements, the fault gouge zone becomes better developed, lowering fault strength and encouraging an even greater concentration of displacement on these faults. In this progression, small-displacement faults are abandoned and larger-displacement faults accommodate more and more of the extensional strain budget.

Applying this model to Yucca Mountain implies that the smaller the displacement on a fault or fracture, the higher chance that it was abandoned in the early stages of Neogene extension and no longer experiences displacement. This concept accords with field observations by Day and others (1996) that many fractures and small-displacement faults ceased to experience displacement between the deposition of the Tiva Canyon and Rainier Mesa tuffs. A corollary to this concept is that intact rock has a negligible probability of experiencing future fault displacement. From a mechanics standpoint, there are so many pre-existing fractures and faults in the Controlled Area that the formation of new fractures to accommodate extensional strain is not considered necessary.

We characterize the potential for distributed displacement on faults or fractures within six predefined classes of cumulative displacement (Table ASM-9). Listed in Table ASM-9 is the assessed probability that distributed faulting can occur for each class of feature. The

probabilities in Table ASM-9 reflect our judgment that on the one hand, block-bounding faults (class 0) are certain to experience distributed displacement (having by definition experienced principal displacement), whereas fractures have a very small chance ($P = 0.01$) of experiencing future distributed displacement. The intermediate probability values for class 1-4 reflect our approximate linear subdivision between extreme probabilities of 0.01 and 1.0. These probabilities express the likelihood that there will ever be any future distributed displacement on this structure. This meaning of probability is meant to cover our estimates that progressively smaller faults were created in an earlier stage of mechanical evolution of the crustal slab, and could be permanently abandoned now that larger, more continuous faults exist to accommodate displacement.

Probability as a function of fault/fracture orientation. Yucca Mountain faults that display evidence of Quaternary displacement all strike roughly north-south, an orientation that is compatible with the observed extension direction of approximately east-west (Day et al., 1996). Given this extension direction, distributed faults and fractures having north-south strikes are most favorably oriented to accommodate induced extension. McKague et al. (1996) quantified the favorability of slip in the present stress field, termed slip tendency. We use slip tendency to make an estimate of the probability that induced slip can occur on a distributed fault or fracture. Based on the diminishing east-west component of displacement on faults having successively more east-west strikes, we define the probability of induced slip on a fault as the sine of the angle between its strike and east-west. Thus, for north-south-striking faults, the angle is 90 degrees, so $P = 1$; for N45W-striking faults, $P = 0.87$; and for east-west-striking faults, $P = 0$.

4.2.2.2 Frequency of Potential Distributed Faulting Events. Earthquakes that may induce distributed faulting can occur on any of the primary, block-bounding faults, or can be background earthquakes within the local areal source zone. Because seismicity rates for the areal source are considerably higher than for any specific fault source (see Section 3.4), we consider it critical to incorporate the effects from areal sources. Earthquake recurrence relationship for all of the sources are defined in Section 3.0.

4.2.2.3 Probability of Distributed Displacement on a Feature. The next step in the characterization of the potential for distributed faulting is an evaluation of the likelihood of faulting on the feature of interest due to the occurrence of an earthquake. This is the product of two probabilities, one based on whether the earthquake ruptures the surface on the primary fault and one based on the distance of the feature from the primary fault and the feature's location in the hanging wall or foot wall of the rupture.

Probability of secondary displacement as a function of whether surface rupture occurs. It is our interpretation that secondary faulting is only induced by surface-rupturing earthquakes. We make this assumption because: 1) most historical secondary faulting has been accompanied by surface rupture on the primary fault, and 2) the ground surface deformation data from the Borah Peak earthquake, which we use as a basis for estimating distributed faulting displacements reflects a surface-rupturing event.

The probability that an earthquake ruptures the surface, regardless of whether it occurs on a known primary fault, or on an unknown fault as a background earthquake, is a function of its magnitude. Therefore, we use the 32-event and 105-event curves from Pezzopane (as described in Sec. 4.2.1.2) to calculate the probability that a given primary earthquake will rupture the surface, and thus be able to induce distributed displacement.

Probability of distributed displacement as a function of distance to primary fault. The probability that distributed displacement will occur at a given distance from the principal rupture is assessed using an empirical relationship based on the density of distributed faulting observed for Basin and Range earthquakes. Figure ASM-19 shows the results of analysis by R.R. Youngs (presented at SSC Workshop 6) of distributed rupture patterns based on data presented in Pezzopane and Dawson (1996). This figure shows the decreasing density of distributed faulting for historical normal faulting earthquakes with increasing distance from the primary fault. We believe that the ergodic substitution applies in this case, so that the probability of fault displacement through time on a distributed fault at a given distance from a primary fault is the same as the ratio of the area containing distributed faulting to the area containing no distributed faulting at that same distance. In other words, given enough time, the percentage of time that a given secondary fault

ruptured in distributed slip would converge on the percentage of area that ruptures at that distance from the primary fault.

We use two assessments of the frequency of distributed rupture as a function of distance from the primary rupture, as shown on Figure ASM-19. The leftmost curve is an envelope of maximum frequency for earthquakes in the range of M 6.0 to 6.9; we weight this curve 0.6. Our slight preference for this curve over the other one is based on two considerations: (1) most of the estimated maximum earthquakes on Yucca Mountain faults are in the range of M 6.0 to 6.9 range, so we consider that magnitude range to be most appropriate; and (2) the maximum frequency values for this magnitude range define a relatively smooth trend that decreases with increasing distance from the primary rupture. We believe that the frequency of distributed displacement on a secondary fault should decrease with increasing distance to the seismogenic fault, based on our ergodic assumption described earlier, and the fact that for historical earthquakes, distributed faulting increases in density toward the primary fault (Pezzopane and Dawson, 1996).

We weight the right-most curve on Figure ASM-19 at 0.4, for the following reasons. First, Pezzopane (pers. comm., 1997) indicates that all the frequency values in his plot are minima, because: (1) the older points in the data set represent field reconnaissances that may have underestimated the extent of distributed faulting; and (2) although more recent investigations may be more thorough, they only record distributed faulting that broke to the surface, which is a minimum value for distributed faulting at depths as great as 300 m. Second, we wish this curve to represent the fact that the other curve is a minimum value. We accomplish this by drawing a curve parallel to the leftmost curve, through the maximum values plotted for M 7.0 to 7.9 earthquakes. We do not use the logistic regression fits of R.R. Youngs (presented at SSC Workshop 6), because they do not represent our interpretation that all plotted points are minimum values.

The relationships shown on Figure ASM-19 are dependent on the location of a feature within the hanging wall or foot wall of the principal rupture. This geometry is not known for earthquakes occurring within the regional source zone. Therefore, we consider it is

equally likely that the point at which an assessment is made lies within the hanging wall or foot wall of the rupture.

4.2.2.4 Characterization of Distributed Displacement. The characterization of distributed displacement at a point on a feature is based on D/D_{max} defined for the principal rupture times a reduction factor (RF) that depends upon the distance and class of feature being considered. The approach is illustrated schematically on Figure ASM-20. Given the location of a point at which fault displacement hazard is being assessed with respect to a primary rupture, the distance to the rupture, x , and the location of the nearest point on the rupture, y , are defined. The distribution for displacement on the primary fault at location y , $[D(y)]$ is given by the smoothed Wheeler curve (Figure ASM-18) once D_{max} has been specified. Two alternative approaches are used to define the values for RF , one based on what we term the across-strike secondary deformation (ASSD) method and one based on the relative cumulative offset on the earthquake source compared to the feature of interest.

Description of the ASSD Method. During historical normal faulting events, distributed faulting is larger and more frequent on the hanging wall near the seismogenic fault, and decreases away from the fault (Pezzopane and Dawson, 1996). The density of distributed faulting at a given distance from the fault is greater on the hanging wall than on the foot wall (Bob Smith presentation at SSC Workshop 6). This pattern is similar to the pattern of coseismic geodetic ground displacement observed following a normal faulting earthquake. We consider the amount of potential displacement on a distributed fault to be related to the amount of accumulated interseismic strain in the nearby crustal slab. This potential displacement is interpreted to have its maximum at the primary fault, where it is realized as the principal faulting displacement, and to decrease with distance from the principal rupture. This assumption lies at the heart of the ASSD method.

We first characterize the potential displacement, $DP(x)$, on secondary faults based on their distance perpendicular to the primary fault. This defines potential displacement along transects perpendicular to the seismogenic faults. $DP(x)$ is considered to be equal to or less than the predicted vertical coseismic geodetic displacement of the ground surface, which reflects the displacement of the strained crustal slab within 10 to 20 km of a seismogenic

normal fault. We consider that potential (vertical) slip on any secondary fault must be equal to or smaller than the predicted vertical geodetic displacement, in order to avoid overcompensation of the elastic shape change accumulated during the previous earthquake deformation cycle.

To assess $DP(x)$ we use the geodetic profile from the 1983 Borah Peak earthquake, Figure ASM-21. We rescale the Borah Peak geodetic curve in both the vertical (z) and horizontal (x) directions. The vertical dimension is normalized by 1.44 m (the principal faulting displacement at the point of intersection of the Borah Peak geodetic profile with the fault trace). We expect the horizontal extent of distributed rupture to increase with increasing penetration of the principal fault into the crust. Thus, the horizontal dimension is rescaled by the inverse of the ratio of the downdip extent of the primary earthquake compared to 16 km (downdip extent of the Borah Peak event). As a result, earthquakes larger than the Borah Peak earthquake will produce the same displacement potential at a greater distance from the principal rupture; earthquakes smaller than the Borah Peak earthquake will produce the same displacement potential at a smaller distance from the principal rupture.

The proportion of $DP(x)$ that is realized as distributed fault slip is difficult to estimate, thus we consider a wide distribution for defining the fraction of $DP(x)$ that is realized in distributed rupture on a single feature at the point of interest. This distribution is expressed as four discrete alternatives that are based on two considerations.

First, we consider it likely that better-developed faults accommodate a higher percentage of $DP(x)$ than less-developed faults, because they are more continuous, longer, and wider. As such, they have more cumulative displacement and better-developed fault gouge, thus weaker material properties in the fault zone, and less resistance to shear.

Secondly, there is a logarithmic increase in the number of progressively less-developed faults in any volume of rock (Nicol et al., 1996). Most papers in the 1996 Journal of Structural Geology, Special Issue (v. 19, no. 2/3) cite a power law relationship between N (number of faults) and D_{cum} (the cumulative displacement on a fault), with an exponent of -0.7 to -0.8, or $\log(N) = C - 0.7 \times \log(D_{cum})$, where C is a constant. Thus, coseismic

distributed faulting in the crustal slab can be accommodated by displacement on one well-developed fault, or on several less-developed faults.

Using the power law relationship given by Nicol et al. (1996), we compute the number of faults in all six fault classes when the number in any one class is known. For example, fault classes 0, 1, and 2 are typically mapped at the surface, but 3 through 5 are not. Thus, if we know that in a certain area there is one class 1 fault ($D_{cum} = 35$ m), we may predict that there are 2.2 faults that have $D_{cum} = 11$ m (class 2); 10.3 faults having $D_{cum} = 1.25$ m (class 3); and 28 faults having $D_{cum} = 0.3$ m (class 4). We then consider that $DP(x)$ can be partitioned among the classes of faults. We list in Table ASM-9 the expected number of faults in each class compared to one fault in class 0 with a cumulative displacement of ~100 m.

We define four possibilities for the partition of $DP(x)$ to define the displacement on an individual feature. These several approaches are necessary due to the way in which the problem of fault displacement characterization was posed by the Facilitation Team. They specified the existence and fault displacement class of the feature of interest at nine test points, but did not specify what displacement class or how many faults/fractures were in the near vicinity of the feature of interest. Our method assumes that if secondary displacement does in fact occur on the feature of interest (as determined by the preceding probability branches in the fault displacement logic tree), that it is likely that secondary displacement also occurs on some or all of the nearby faults. Thus, we desire to partition $DP(x)$ between the feature of interest and some/all of the surrounding faults, without knowing what class those other faults fall in, how many of them exist, and how far from the feature of interest they lie.

The first partition assumes that all of $DP(x)$ occurs on the fault/fracture of interest, $RF = DP(x)$. This partition defines the maximum possible distributed displacement that can occur on a feature in our method, because it assumes that: 1) 100% of $DP(x)$ is realized as distributed fault displacement, which is the limiting case, and 2) this entire displacement occurs only on the feature of interest, despite the fact that other faults and fractures may exist nearby. Given the limiting nature of this scenario we consider that it is an unlikely occurrence and assign it a probability of 5% that it occurs in an event.

The second partition assumes that 100% of $DP(x)$ occurs as distributed displacement in the vicinity of the feature of interest, but that $DP(x)$ is partitioned equally among the five classes of secondary faults. In other words, $RF = 0.2 \times DP(x)$ for each fault class. We consider this scenario to have a 20% likelihood of occurring in an event.

The third partition assumes that 100% of $DP(x)$ occurs as distributed displacement in the vicinity of the feature of interest, and that this displacement is partitioned among all faults in the same displacement class as the feature of interest. This assumption is made for the case that only faults similar to the feature of interest exist in the vicinity, so that other classes of faults may not share the displacement. Based on our examination of faults and fractures in the ESF, there are certainly some zones in the tunnel where most or all of the faults/fractures belong to the same displacement class. The number of faults in a particular class, N , is listed in Table ASM-9. Thus, $RF = DP(x)/N$. We consider this scenario to have a 30% likelihood of occurring in an event.

The fourth partition assumes that 100% of $DP(x)$ occurs as distributed displacement, but the displacement is partitioned as 20% to each of the five secondary fault classes, and within each class, equally distributed among all faults in that class. Thus, $RF = 0.2 \times DP(x)/N$. We consider that is scenario is the most likely to occur (40%) because we consider it most plausible that, if distributed displacement does occur on the feature of interest, it would also occur on all of the nearly-identical faults/fractures nearby within the same fault displacement class.

The secondary displacement calculated for the feature of interest during a principal faulting event cannot exceed the cumulative displacement (D_{cum}) on that feature, but it may equal D_{cum} . The latter situation would arise if D_{cum} was all created in a single event, i.e., distributed faulting occurred only once during the lifetime of the secondary fault. Such a possibility cannot be ruled out. Therefore, we place an upper limit on the distributed displacement equal to D_{cum} of the feature.

The ASSD method utilizes the Borah Peak geodetic curve, which distinguishes between the hanging wall and foot wall consider to define $DP(x)$. When assessing the hazard from

earthquakes occurring in the local source zone, we consider that it is equally likely that the feature of interest is located in the hanging wall or in the foot wall. We also consider that the assessment point is located normal to the midpoint of the earthquake rupture ($y/L = 0.5$).

Ratio of Cumulative Slips Approach. The alternative approach for assessing RF utilizes the ratio of the cumulative slip on the feature of interest to that on the fault where the principal rupture occurs. The concept of this approach is best explained in an simplified manner.

We consider the distributed faulting hazard at point 3 located on the Drill Hole Wash fault and assume for the moment that all of the cumulative displacement at point 3 resulted from the occurrence of characteristic earthquakes on only the Solitario canyon (SC) or Bow Ridge (BWR) faults. Because point 3 is located in the hanging wall of the BWR fault, it is likely that most of the distributed displacement resulted from earthquakes occurring on the BWR fault because of the higher frequency of distributed rupture in the hanging wall (Figure ASM-19) and a larger displacement potential (Figure ASM-21). For the sake of illustration, we assume that 75 % of the cumulative slip at point 3 occurred as a result of earthquakes occurring on the BWR fault and 25 % occurred as a result of earthquakes occurring on the SC fault. Over the lifetime of the BWR fault, n characteristic earthquakes have occurred, where $n = D_{cum}(BWR)/D_{ct}(BWR)$, where $D_{ct}(BWR)$ is the displacement of the principal rupture of characteristic events on the fault. The fraction of these events that also produced distributed rupture at point 3 is $n \times P(\text{slip on 3} | \text{event on BWR})$, where $P(\text{slip on 3} | \text{event on BWR})$ is the probability of distributed slip at point 3 due to a characteristic earthquake on the BWR fault. Therefore, the expected displacement in a distributed slip at point 3 induced by a BWR characteristic earthquake is defined as the cumulative slip at point 3 due to earthquakes occurring on the BWR fault divided by the number of BWR events that induce distributed slip:

$$D(\text{point 3}) = 0.75 \times D_{cum}(\text{point 3}) / [n \times P(\text{slip} | \text{event})]$$

The ratio of displacement on the feature at point 3 to displacement on the BWR fault defines the reduction factor, RF , and is given by:

$$RF(BWR) = \frac{D(\text{point 3})}{D_{ch}(BWR)} = \frac{0.75 \times D_{cum}(\text{point 3})}{D_{cum}(BWR) \times P(\text{slip on 3} | \text{event on BWR})}$$

Similarly, the reduction factor for earthquakes occurring on the SC fault is given by:

$$RF(SC) = \frac{D(\text{point 3})}{D_{ch}(SC)} = \frac{0.25 \times D_{cum}(\text{point 3})}{D_{cum}(SC) \times P(\text{slip on 3} | \text{event on SC})}$$

To apply this approach to the assessment of fault displacement hazard we must account for the distribution of earthquake magnitude that may occur on a seismic source and the contributions of multiple sources to the cumulative displacement at a point. To do this, we assume that the results of applying the ASSD approach provide a good assessment of the relative contribution of individual seismic sources to the distributed faulting displacement at the point of interest. As described in Section 4.2.2 of the main text, the displacement hazard curve can be used to compute an effective slip rate that integrates the effects of all earthquakes occurring on all sources, designated as $TESR$. If a displacement hazard curve is computed for each source, then it can be used to compute the effective slip rate, ESR , due to earthquakes occurring on that source. Thus, the fraction of the cumulative slip induced by earthquakes on a particular source is estimated by the ratio of the effective slip rate for earthquakes on that source to the total effective slip rate. The result is that the reduction factor to apply to displacement on the BWR fault to estimated distributed displacement on the feature at point 3 is given by:

$$RF(BWR) = \frac{ESR(BWR)}{TESR} \times \frac{D_{cum}(\text{point 3})}{D_{cum}(BWR) \times P(\text{slip on 3} | \text{event on BWR})}$$

The calculation of the effective slip rate using this approach still requires an evaluation of the probability that an earthquake on the primary fault will induce distributed rupture on the secondary fault. We assess this probability for the maximum event on the primary fault using

the factors described in Section 4.2.2.3 because the maximum events on the various earthquake sources are expected to produce most of the distributed slip on any secondary feature.

Application of this method requires an assessment of the cumulative displacement on each of the seismic sources in the Yucca Mountain region. These values are as follows:

Fault	D_{cum}^* (m)
BARE MOUNTAIN	
Bow Ridge	125
N. Crater Flat	00
S. Crater Flat	50
Fatigue Wash	72
Iron Ridge	215
Paintbrush Canyon	500
Solitario Canyon	700
Stagecoach Road	600
Windy Wash	500

*data from Table 4.2.1 in Menges and Whitney, 1996 and Chris Potter, Pers. comm., 1997

As indicated in the logic tree shown on Figure ASM-16b, we assign a weights of 0.7 to the ASSD approach and 0.3 to the relative cumulative displacement approach. We favor the ASSD approach because it explicitly accounts for the effect of distance in the assessment of *RF* for each earthquake and does not assume that all of the faults have evolved in a parallel manner through time. It should be noted that only the ASSD approach can be used to assess the distributed faulting hazard from earthquakes occurring in the regional source zone because the cumulative slip on the sources is unknown. However, we do not believe that this is a significant detriment because these earthquakes are generally smaller than those occurring on the faults and are unlikely to produce principal faulting surface rupture. Thus their contribution to the total displacement hazard on a feature should be a small fraction of the total.

- Abers, G.A., 1991, Possible seismogenic shallow-dipping normal faults in the Woodlark-D'Entrecasteaux extensional province, Papua, New Guinea, *Geology*, v. 19, p.1205-1208.
- Anderson, R.E., Bucknam, R.C. Crone, A.J., Haller, K.M., Machette, M.N., Personius, S.F., Barnhard, T.P., Cecil, M.J. and Dart, R.L., 1995a, Characterization of Quaternary and suspected Quaternary faults, regional studies, Nevada and California: U. S. Geological Survey Open-File Report 95-599, 56 p.
- Anderson, R.E., Crone, A.J., Machette, M.N., Bradley, L., and Diehl, S.F., 1995b, Characterization of Quaternary and suspected Quaternary faults, Amargosa Area, Nevada and California: U. S. Geological Survey Open-File Report 95-613, 41 p.
- Arabasz, W.J., Pechmann, J.C., and Brown, E.D., 1992, Observational seismology and evaluation of earthquake hazards and risk in the Wasatch Front area, Utah, in Gori, P.L., and Hays, W.W. (eds.), *Assessment of regional and earthquake hazards and risk along the Wasatch Front, Utah*: U.S. Geological Survey Professional Paper 1500-D, p. D1-D36.
- Beanland, S., and Clark, M.M., 1994, The Owens Valley Fault Zone, eastern California, and surface faulting associated with the 1872 earthquake: U. S. Geological Survey Bulletin, 1994, 29 p. and 4 pls.
- Brogan, G.E., Kellogg, L.S., Slemmons, D.B., and Terhune, C.L., Late Quaternary faulting along the Death Valley-Furnace Creek fault system, California and Nevada: U. S. Geological Survey Bulletin 1991, map scale 1:62,500, 23 p. 4 pls.
- Carr, W.J., 1990, Styles of extension in the Nevada test Site region, southern Walker Lane Belt; an integration of volcano-tectonic and detachment fault models, *in* Wernicke, B.P. (ed.), *Basin and Range extensional tectonics at the latitude of Las Vegas, Nevada*: Geological Society of America Memoir 176, p. 283-303.
- Caskey, S.J., 1996, Surface faulting of the 1954 Fairview Peak (Ms 7.2) and Dixie Valley (M_s 6.8) earthquakes, central Nevada: *Bulletin of the Seismological Society of America*, v. 86, No. 3, p. 761-787.
- Crowe, B., and 9 others, 1995, Status of volcanism studies for the Yucca Mountain site characterization project: Los Alamos National Laboratory report LA-12908-Ms, UC-802, revised March 1995, variously paginated.

- Day, W.C., Potter, C.J., Sweetkind, D.S. and Keefer, W.R., 1996, Structural geology of the central block of Yucca Mountain, in Whitney, J.W. (coord.), 1996, Seismotectonic framework and characterization of faulting at Yucca Mountain, Nevada: A report to the U.S. Dept. of Energy that fulfills Level 3 Milestone 3GSH100M, WBS, Number 1.2.3.2.8.3.6, Chapter 2.
- dePolo, C.M., 1994, The maximum background earthquake for the Basin and Range Province, western North America, *Bulletin of the Seismological Society of America*, v. 84, p. 466-472.
- dePolo, C.M., and Slemmons, D.B., in review, 1997, Age criteria for active faults: Utah Geological Survey Special Publication Proceedings of the Basin and Range Seismic Hazard Summit.
- Dohrenwend, J.C., Menges, C.M., Schell, B.A., and Morning, B.C., 1992, Reconnaissance photogeologic map of young faults in the Las Vegas 1 x 2 quadrangle, Nevada, California, and Arizona: U. S. Geological Survey Miscellaneous Field Studies Map MF-2182, scale 1:250,000.
- Dohrenwend, J. C., Schell, B. A., McKittrick, M. A., and Morning, B. C., 1992, Reconnaissance photogeologic map of young faults in the Goldfield 1 x 2 degree quadrangle, Nevada and California: U. S. Geological Survey Miscellaneous Field Studies Map MF- 2183, scale 1:250,000.
- Doser, D.I., 1987, The Ancash, Peru earthquake of 1946 November 10: evidence for low-angle normal faulting in the High Andes of Peru, *Geophysical Journal of the Royal Astronomical Society*, v. 91, p. 57-71.
- Doser, D.I., and Smith, R.B., 1989, An assessment of source parameters of earthquakes in the Cordillera of the western United States: *Bulletin of the Seismological Society of America*, v. 79, p. 1393-1409.
- Forsyth, D.W., 1992, Finite extension and low-angle normal faulting: *Geology*, v. 20, p. 27-30.
- Frankel, A., 1995, Mapping seismic hazard in the central and eastern United States, *Bulletin of the Seismological Society of America*, v. 66, p. 8-21.
- Fridrich, C., and Price, J., 1992, Tectonic framework of Crater Flat Basin, adjacent to Yucca Mountain, Nevada: A preliminary report: *Geological Society of America, Abstracts with Programs*, v. 24, no. 7, p. 189-190.

- Gianella, V.P. and Callaghan, E., 1934, The earthquake of December 20, 1934 at Cedar Mountain, Nevada and its bearing on the genesis of Basin and Range structure: *Journal of Geology*, 42:1-22.
- Gomberg, J., 1991a, Seismicity and shear strain in the southern Great Basin of Nevada and California, *Journal of Geophysical Research*, 96, p. 16,383-16,399.
- Gomberg, J., 1991b, Seismicity and detection/location threshold in the southern Great Basin Seismic Network, *Journal Geophysical Research*, v. 96, No. B10, P. 16401-16414.
- Hardyman, R.F. and Oldow, J.S., 1991, Tertiary tectonic framework and Cenozoic history of the central Walker Lane, Nevada, in Raines, G.L., Lisle, R.E., Schafer, R.W., and Wilkinson, W.H. (eds.), *Geology and ore deposits of the Great Basin: Geological Society of America, Nevada Symposium Proceedings*, v. 1, p. 279-301.
- Harmsen, S.C., and Bufe, C., 1991, Seismicity and focal mechanisms for the southern Great Basin of Nevada and California: 1987-1989, U.S. Geol. Survey. Open-File Report No. 91-572, 208 p.
- Hoffard, J.L., 1991, Quaternary tectonics and basin history of Pahrump and Stewart valleys, Nevada and California: Reno, University of Nevada, M. S. thesis, map scales 1:100,000 and 1:24,000, 138 p. 5 pls., 50 figs.
- Hunter, R.L., and Mann, C.J. (eds.), 1992, Techniques for determining probabilities of geologic events and processes: *International Association for Mathematical Geology, Studies in Mathematical Geology*, no. 4, Oxford University Press, Oxford, UK, 364 p.
- Jackson, J.A., 1987, Active normal faulting and crustal extension, in Coward, M.P., Dewey, J.F., and Hancock, P.L. (eds.), *Continental Extensional Tectonics: Geological Society of London, Special Publication 28*, p. 3-17.
- Jackson, J.A., and White, N.J., 1989, Normal faulting in the upper continental crust; observations from regions of active extension: *Journal of Structural Geology*, v. 11, p. 15-36.
- Johnson, R.A., and Loy, K.L., 1992, Seismic reflection evidence for seismogenic low-angle faulting in southeastern Arizona: *Geology*, v. 20, p. 597-600.
- Klinger, R.E., and Piety, L.A., 1996, Evaluation and characterization of Quaternary faulting on the Death Valley and Furnace Creek faults, Death Valley, California: U. S. Bureau of Reclamation Seismotectonic Report 96-10, Denver, CO, prepared for the U. S. Geological Survey for Yucca Mountain Project Activity 8.31.17.4.3.2, 98 p.

- Louie, John, Shields, G., Ichinose, M., Hasting, G., Plank, G., and Bowman, S., 1997, Shallow geophysical constraints on displacement and segmentation of the Pahump Valley fault zone: Proceedings of the Nov. 14-15, 1996 Seismic Hazards in the Las Vegas Region Conference, in press.
- Mason, D.B. 1996, Earthquake magnitude potential of the intermountain seismic belt, USA, from surface-parameter scaling of late Quaternary faults: Bulletin of the Seismological Society of America, v. 86, no. 5, p. 1,487-1,506.
- McCalpin, J.P., 1991, Quaternary surface-faulting earthquakes in the Overthrust Belt; did they occur on listric faults?: Geological Society of America, Abstracts with Programs, v.23, no. 7, p.140.
- McCalpin, J.P., 1995, Frequency distribution of geologically-determined slip rates for normal faults in the western USA: Bulletin of the Seismological Society of America, v. 85, no. 6, p. 1867-1872.
- McCalpin, J.P. (ed.), 1996, Paleoseismology: Academic Press, New York, 583 p.
- McGuire, R.K., 1985, Seismic hazard methodology for nuclear facilities in the eastern United States, EPRI Research Project Number P101-29, Dames and Moore, Golden, Colorado, Vol. 2, Appendix A.
- McGuire, R.K., and Barnhard, T.P., 1981, Effects of temporal variations in seismicity on seismic hazard: Bulletin of the Seismological Society of America, v. 71, p. 321-334.
- McKague, H.L., Stamatakos, J.A. and Ferrill, D.A., 1996, Type I faults in the Yucca Mountain region: Center for Nuclear Waste Regulatory Analysis, report CNWRA 96-007, revision 1, Nov. 1996, variously paginated.
- Menges, C.M., and Whitney, J.W., 1996, Distribution of Quaternary faults at Yucca Mountain, *in* Whitney, J.W. (coord.), Seismotectonic framework and characterization of faulting at Yucca Mountain, Nevada: Report submitted to U.S. Department of Energy by the U.S. Geological Survey, Denver, Colorado, Contract DE-AC04-94AL85000, p. 4.2-1-4.2-30.
- Nichol, A., Watterson, J., Walsh, J. J., and Childs, C., 1996, The shapes, major axis orientations and displacement patterns of fault surfaces: Journal of Structural Geology, v. 18, no. 2/3, p. 235-248.
- Nicols, A., Walsh, J.J., Watterson, J., and Gillespie, P.A., 1996, Fault size distributions—are they really power-law?: Journal of Structural Geology, v. 18, no. 2/3, p. 191-198.

- Nichols, W.D., 1987, Geohydrology of the unsaturated zone at the burial site for Low-Level Radioactive Waste near Beatty, Nye County, Nevada: U. S. Geological Survey Water-Supply Paper 2312.
- Pezzopane, S.K., and Dawson, T.E., 1996, Fault displacement hazard; a summary of issues and information, *in* Whitney, J.W. (coord.), 1996, Seismotectonic framework and characterization of faulting at Yucca Mountain, Nevada: A report to the U.S. Department of Energy that fulfills Level 3 Milestone 3GSH100M, WBS Number 1.2.3.2.8.3.6, Chapter 9.
- Piety, L.A., 1995, Compilation of known and suspected Quaternary faults within 100 km of Yucca Mountain, Nevada and California: U. S. Geological Survey Open-File Report Number 94-112, 404 p.
- Quade, J., Mifflin, M.D., Pratt, W.L., and Burkle, L., 1995, Fossil spring deposits in the southern Great Basin and their implications for changes in water-table levels near Yucca Mountain, Nevada during Quaternary time: Bulletin of the Geological Society of America, v. 107, No. 2, p. 213-230.
- Reasenber, P., 1985, Second order moment of central California seismicity, 1969-1982, Journal of Geophysical Research, v. 90, p. 5479-5495.
- Reasenber, P.A., and Jones, L.M., 1989, Earthquake hazard after a main shock in California, Science, v. 243, p. 1173-1176.
- Reheis, M.C., 1992, Aerial photographic interpretation of lineaments and faults in late Cenozoic deposits in the Cactus Flat and Pahute Mesa 1:100,000 quadrangles and the western parts of the Timpahute Range, Pahrnagat Range, Indian Springs and Las Vegas 1:100,000 quadrangles, Nevada: U. S. Geological Survey-Open File Report 92-193, scale 1:100,000, 14 p., 3 pls.
- Reheis, M.C., and Noller, J.S., 1991, Aerial photographic interpretation of lineaments and faults in late Cenozoic deposits in the eastern part of Benton Range 1:100,000 quadrangle and the Goldfield, Last Chance Range, Beatty, and Death Valley Junction 1:100,000 quadrangles, Nevada and California: U. S. Geological Survey-Open File Report 90-41, scale 1:100,000, 9 p., 4 pls.
- Reheis, M.C., and Sawyer, T.L., 1997, Late Cenozoic history and slip rates of the Fish Lake Valley, Emigrant Peak, and Deep Springs fault zones, Nevada and California: Geological Society of America Bulletin, v. 109, no. 3, p. 280-299.
- Reiter, L., 1990, Earthquake Hazard Analysis: Columbia University Press, 250 p.

- Richter, C.F., 1958, *Elementary Seismology*: William Freeman and Co., San Francisco, California, 300 p.
- Rogers, A.M., Harmsen, S.C., Corbett, E.J., Priestly, K. and dePolo, D., 1991, The seismicity of Nevada and some adjacent parts of the Great Basin, in Slemmons, D.B. et al. (eds.), *Neotectonics of North America: Geological Society of America, Decade Map Volume*, p. 153-184.
- Savage, J.C., Lisowski, M., and Prescott, W.H., 1990, An apparent shear zone trending north-northwest across the Mojave Desert into Owens Valley, eastern California: *Geophysical Research Letters*, v. 17, p. 2113-2116.
- Schwartz, D.P., and Coppersmith, K. J., 1984, Fault behavior and characteristic earthquakes: Examples from the Wasatch and San Andreas faults: *Journal of Geophysical Research*, v. 89, 5681-5698.
- Sibson, R.H., 1985, A note on fault reactivation: *Journal of Structural Geology*, v. 7, p. 751-754
- Simonds, F.W., and 8 others, 1995, Map showing fault activity in the Yucca Mountain area, Nye County, Nevada: U.S. Geological Survey Map I-2520, scale 1:24,000.
- Smith, K.D., Brune, J.N., Savage, M.K., Anooshepoor, R. and Sheehan, A.F., in press, Main shock parameters and aftershock relocations of the 29 June 1992 Little Skull Mountain earthquake sequence: Accepted for publication in the U.S. Geological Survey Circular on Yucca Mountain Tectonics, 42 p.
- Smith, R. B., and Arabasz, W. J., 1992, Seismicity of the Intermountain Seismic Belt, in Slemmons, D. B., Engdahl, E.R., Zoback, M.D., and Blackwell, D.D. (eds.), *Neotectonics of North America, Geological Society of America Decade Map Volume 1*, Boulder, Colorado.
- Stepp, C., 1972, Analysis of completeness of the earthquake sample in the Puget Sound area and its effects on statistical estimates of earthquake hazard, in *Proceedings-First Microzonation Conference*, Seattle, Washington, p. 987-909.
- Stewart, J.H., 1987, Tectonics of the Walker Lane belt, western Great Basin—Mesozoic and Cenozoic deformation in a zone of shear, in Ernst, W.G., ed., *Metamorphism and Crustal Evolution of the Western United States: Rubey Volume VII*, Prentice-Hall Inc., New Jersey, p. 683-713.

- Swadley, W.C., and Hoover, D.L., 1990, Geologic map of the surficial deposits of the Yucca Flat area, Nye County, Nevada: U. S. Geological Survey Open-File Map No. I-2047, scale 1:48000.
- Taylor, E.M., Menges, C.M., de Fontaine, C.S., Buesch, D.C., Mundo, B.O. and Murray, M., 1996, Preliminary results of paleoseismic investigations on the Ghost Dance fault, *in* Whitney, J.W. (coord.), 1996, Seismotectonic framework and characterization of faulting at Yucca Mountain, Nevada: A report to the U.S. Department of Energy that fulfills Level 3 Milestone 3GSH100M, WBS Number 1.2.3.2.8.3.6, 4 vols.
- Veniziano, D., and van Dyck, J., 1985, Statistical discrimination of "aftershocks" and their contribution to seismic hazard, Appendix A-4, in Seismic Hazard Methodology for Nuclear Facilities in the Eastern United States, EPRI Research Project No. P101-29, p. A121-A186.
- von Seggern, D.H., and Brune, J.N., 1997, Seismicity in the southern Great Basin, 1868-1992, *in* Tectonic Characterization of Yucca Mountain—a Potential Geologic Repository for Nuclear Waste: Geological Society of America Special Volume, in preparation.
- Wells, D.L., and Coppersmith, K.J., 1994, New empirical relationships among magnitude, rupture length, rupture width, rupture area, and surface displacement: Bulletin of the Seismological Society of America, v. 84, no. 4, p. 974-1002.
- Wernicke, B., 1995, Low-angle normal faults and seismicity; a review: *Journal of Geophysical Research*, v. 100 (B10): 20,159-20,174.
- Wesnousky, S.G., 1986, Quaternary faults and seismic hazards in California: *Journal of Geophysical Research*, v. 91, p. 12587-12632.
- Wesnousky, S.G., Scholz, C.H., Shimazaki, K., and Matsuda, T., 1983, Earthquake frequency distribution and the mechanics of faulting: *Journal of Geophysical Research*, v. 88, p. 9331-9340.
- Wheeler, R.L., 1989, Persistent segment boundaries on basin-range normal faults, in Schwartz, D.P. and Sibson, R.H. (eds.), Fault segmentation and controls of rupture initiation and termination: U.S. Geological Survey Open File Report 89-315, p.432-444.

- Whitney, J.W. (coord.), 1996, Seismotectonic framework and characterization of faulting at Yucca Mountain, Nevada: A report to the U.S. Department of Energy that fulfills Level 3 Milestone 3GSH100M, WBS Number 1.2.3.2.8.3.6, 4 vols.
- Wright, L.A., 1976, Late Cenozoic fault patterns and stress fields in the Great Basin and westward displacement of the Sierra Nevada block: *Geology*, v. 4, p. 489-494.
- Youngs, R.R., and Coppersmith, K.J., 1985, Implications of fault slip rates and earthquake recurrence models to probabilistic seismic hazard estimates: *Bulletin of the Seismological Society of America*, v. 75, no. 4, p. 939-964.
- Youngs, R.R., Swan, F.H. III, Power, M.S., Schwartz, D.P., and Green, R.K., 1987, Probabilistic analysis of earthquake ground shaking along the Wasatch Front, Utah, in W.W. Hays, and P.L. Gori, (eds.), *Assessment of Regional Earthquake Hazards and Risk along the Wasatch Front*, U. S. Geological Survey Open-File Report No. 87-585, v. II, p. 1-110.
- Zhang, P., Ellis, M., Slemmons, D.B., and Mao, F., 1990, Right-lateral displacements and Holocene slip rate associated with prehistoric earthquakes along the southern Panamint Valley fault zone: implications for southern Basin and Range tectonics and coastal California deformation: *Journal of Geophysical Research*, v. 95, p. 4857-4872.

**TABLE ASM-1
AVERAGE AND MAXIMUM DISPLACEMENTS FOR YUCCA MOUNTAIN FAULTS**

Fault	Davg : Dpref Largest Event	Davg : Dpref All Events	Dmax : Largest Dpref	Dmax : Largest Dmax	Dmax : 2.59* Dpref Largest Event	Dmax : 2.59* Dpref All Events
Weights:	0.5	0.5	0.25	0.5	0.125	0.125
Bare Mountain (BM)	150	127	150	300	389	329
Bow Ridge (BWR)	44	24	44	80	114	62
N. Crater Flat (NCF)	50	47	50	50	130	122
S. Crater Flat (SCF)	13	20	20	32	34	52
Fatigue Wash (FW)	105	61	105	105	272	158
Iron Ridge (IR)	100	80	100	130	260	208
Paintbrush Canyon/ Stagecoach Road (SR-PBC)	167	51	167	205	433	132
Solitario Canyon (SC)	75	54	120	140	195	140
Windy Wash (WW)	58	44	88	98	150	114
Rock Valley (RV)	362	291	362	451	940	755

* Data was taken from all trenches, displacements are in cm.

**TABLE ASM-2
SURFACE RUPTURE LENGTHS FOR YUCCA MOUNTAIN FAULTS**

Fault	Minimum Length (km)	Preferred Length (km)	Maximum Length (km)
Weights:	0.1	0.6	0.3
Bare Mountain	17.5	20.6	24
Bow Ridge	6.7	7.6	9.4
N. Crater Flat	10.6	11.6	15.1
S. Crater Flat	6.1	7.8	8.8
Fatigue Wash	6.6	12.5	15.2
Iron Ridge	5.5	8.5	9.2
Paintbrush Canyon/ Stagecoach Road	18.0	24.0	28.5
Solitario Canyon	11.3	18.7	20.9
Windy Wash	15.6	21.6	24.6

**TABLE ASM-3
WEIGHTING CRITERIA FOR MAXIMUM MAGNITUDES FOR
YUCCA MOUNTAIN FAULTS**

Fault	Msrl	Mra	Mmas	Mdmax	Mdavg
Bare Mountain	0.4	0.1	0.2	0.1	0.2
Bow Ridge	0.45	0.1	0.3	0.15	0
N. Crater Flat	0.3	0.2	0.3	0.2	0
S. Crater Flat	0.3	0.1	0.3	0.15	0.15
Fatigue Wash	0.35	0.25	0.3	0.1	0
Iron Ridge	0.4	0.2	0.2	0.2	0
Paintbrush Canyon/ Stagecoach Road	0.3	0.15	0.3	0.1	0.15
Solitario Canyon	0.3	0.1	0.3	0.15	0.15
Windy Wash	0.3	0.1	0.3	0.15	0.15

Methods: Msrl—surface rupture length (Wells and Coppersmith, 1994)
Mra—rupture area (Wells and Coppersmith, 1994)
Mmas—surface rupture length*displacement (Mason, 1996)
Mdmax—maximum displacement (Wells and Coppersmith, 1994)
Mdavg—average displacement (Wells and Coppersmith, 1994)

**TABLE ASM-4
SLIP RATES FOR YUCCA MOUNTAIN FAULTS**

Fault	20-percentile (mm/yr)	Median (mm/yr)	80-percentile (mm/yr)
Weights:	0.2	0.6	0.2
Bare Mountain	0.008	0.025	0.07
Bow Ridge	0.0008	0.002	0.0047
N. Crater Flat	0.0011	0.0025	0.0048
S. Crater Flat	0.001	0.0024	0.0047
Fatigue Wash	0.0038	0.009	0.0162
Iron Ridge	0.0015	0.0036	0.0068
Paintbrush Canyon/ Stagecoach Road	0.0065	0.016	0.029
Solitario Canyon	0.005	0.0125	0.024
Windy Wash	0.003	0.007	0.0128

**TABLE ASM-5
RECURRENCE FOR YUCCA MOUNTAIN FAULTS**

Fault	20-percentile (kyr)	Median (kyr)	80-percentile (kyr)
Weights:	0.2	0.6	0.2
Bare Mountain	42	87	143
Bow Ridge	71	120	188
N. Crater Flat	135	212	330
S. Crater Flat	65	107	165
Fatigue Wash	99	161	249
Iron Ridge	83	137	220
Paintbrush Canyon/ Stagecoach Road	17	27	42
Solitario Canyon	31	51	78
Windy Wash	31	50	79

**TABLE ASM-6
REGIONAL FAULT DATA
(Page 1 of 2)**

No.	FAULT ¹	MAP DESIGNATION	CLOSEST DIST. TO SITE ² (km)	SLIP RATE (SR) ³ (mm/yr)						RECURRENCE INTERVAL (RI) ⁴ (yr)			SURFACE RUPTURE LENGTH (SRL) ⁵ (km)						TYPE ⁶	DIP (DEG / DIRECTION)			
				MINIMUM	PREFERRED	MAXIMUM	MINIMUM	PREFERRED	MAXIMUM	MINIMUM	PREFERRED	MAXIMUM	MINIMUM	PREFERRED	MAXIMUM								
1	Carrara ⁷	H95	15 DBS*	0.013	(0.2)	0.05	(0.6)	0.12	(0.2)	10000	(0.2)	19000	(0.6)	69000	(0.2)	10	(0.1)	20	(0.8)	42	(0.1)	SS	60-90/SW
2	Mine Mountain	MM	19 P1	0.006	(0.33)	0.03	(0.34)	0.06	(0.33)	20000	(0.33)	39000	(0.34)	146000	(0.33)	10	(0.5)	20	(0.5)			SS	VERT/SW
3	Wahmonie	WAH	22 P1	0.01	(0.33)	0.04	(0.34)	0.08	(0.33)	20000	(0.33)	39000	(0.34)	146000	(0.33)			14.5	(1.0)			OS	7/SE
4	Ash Meadows	AM	22 DBS	0.01	(0.2)	0.02	(0.6)	0.03	(0.2)	10000	(0.2)	35000	(0.5)	128000	(0.3)	10	(0.1)	38	(0.8)	40	(0.1)	N	60W
5	Rock Valley	RV	25 Ch 4.13	0.02	(0.2)	0.06	(0.6)	0.09	(0.2)	34325	(0.2)	58333	(0.6)	175000	(0.2)	32.6	(0.2)	62.1	(0.6)	72	(0.2)	SS	VERT
6	W Specter Range	WSR	28 DBS	0.004	(0.3)	0.01	(0.4)	0.02	(0.3)	10000	(0.1)	25000	(0.6)	>128000	(0.3)	18	(0.8)			25	(0.2)	N	60W
7	Cane Spring	CS	26 P1	0.007	(0.33)	0.03	(0.34)	0.07	(0.33)	20000	(0.33)	39000	(0.34)	146000	(0.33)	21	(0.5)			26	(0.5)	SS	VERT
8	Amargosa River	AR	34 DBS	0.01	(0.2)	0.05	(0.6)	0.09	(0.2)	10000	(0.1)	69000	(0.6)	128000	(0.3)	12.4	(0.2)	24.8	(0.6)	48	(0.2)	SS	VERT
9	Yucca Lake	YCL	36 P1	0.002	(0.33)	0.02	(0.34)	0.034	(0.33)	20000	(0.33)	39000	(0.34)	146000	(0.33)	16.3	(0.5)			20.6	(0.5)	SS?	VERT/?
10	Eleana Range	ER	37 P1	0.00006	(0.33)	0.00024	(0.34)	0.0003	(0.33)	20000	(0.33)	39000	(0.34)	146000	(0.33)	10.6	(0.5)			12.7	(0.5)	N	60E
11	E Specter Range	ESR	37 DBS	0.004	(0.33)	0.012	(0.34)	0.021	(0.33)	10000	(0.33)	25000	(0.34)	128000	(0.33)	9	(0.5)			15	(0.5)	N	60E
12	Yucca Fault	YC	40 P1	0.008	(0.33)	0.04	(0.34)	0.08	(0.33)	20000	(0.33)	39000	(0.34)	146000	(0.33)	23	(0.5)			33	(0.5)	SS?	VERT/?
13	W Spring Mountains	WSM	45 DBS	0.02	(0.2)	0.05	(0.6)	0.07	(0.2)	20000	(0.2)	69000	(0.6)	128000	(0.2)	14.6	(0.2)	43.5	(0.6)	50	(0.2)	N	60W
14	Furnace Creek	FC	52 DBS	4	(0.2)	5	(0.6)	8	(0.2)	600	(0.2)	700	(0.6)	800	(0.2)	70	(0.2)	105	(0.6)	120	(0.2)	SS	VERT
15	E Death Valley	EDV	52 P1	3.46	(0.2)	4.62	(0.6)	5.77	(0.2)	500	(0.2)	875	(0.6)	1000	(0.2)	34	(0.2)	60	(0.6)	75	(0.2)	N	60W
16	Belted Range	BLR	55 P1	0.02	(0.33)	0.04	(0.34)	0.1	(0.33)	20000	(0.33)	39000	(0.34)	69000	(0.33)	21	(0.6)			49	(0.4)	N	60W
17	M Death Valley	MDV	57 DBS	1	(0.2)	2	(0.6)	3	(0.2)	1000	(0.2)	2000	(0.6)	5000	(0.2)	32	(0.2)	60	(0.6)	72	(0.2)	SS	VERT
18	Grapevine	GV	58 P1	0.003	(0.33)	0.01	(0.34)	0.02	(0.33)	20000	(0.33)	39000	(0.34)	146000	(0.33)			29	(1.0)			N	60W
19	W Death Valley	WDV	61 DBS	0.009	(0.33)	0.05	(0.34)	0.16	(0.33)	20000	(0.33)	39000	(0.34)	146000	(0.33)	25	(0.3)	39	(0.5)	62	(0.2)	N	60E
20	Emigrant/Towne Pass	EM-TP	<65 DBS	0.003	(0.33)	0.01	(0.34)	0.03	(0.33)	10000	(0.33)	20000	(0.34)	69000	(0.33)	14.6	(0.2)	17	(0.6)	47	(0.2)	N	60/NW
21	N Pahrump-Stewart Valley	PRP	69 DBS	0.03	(0.2)	0.06	(0.6)	0.14	(0.2)	10000	(0.2)	39000	(0.6)	69000	(0.2)	20	(0.5)			40	(0.5)	SS, OS?	VERT/?
22	W Pintwater Range	WPR	76 P1	0.005	(0.2)	0.01	(0.6)	0.06	(0.2)	10000	(0.33)	39000	(0.34)	69000	(0.33)	18	(0.33)	37	(0.34)	56	(0.33)	N	60W
23	Panamint Valley-Hunter Mountain	PAN-HM	95 P1	1.57	(0.1)	2.36	(0.8)	3.15	(0.1)	700	(0.1)	1610	(0.8)	2360	(0.1)	40	(0.2)	70	(0.6)	120	(0.2)	SS	VERT
24	S Pahrump-Stateline	SPRP	107 DBS	0.002	(0.33)	0.05	(0.34)	0.1	(0.33)	20000	(0.2)	39000	(0.6)	69000	(0.2)	31	(0.5)			65	(0.5)	OS	60?/W

TABLE ASM-6
(Page 2 of 2)

Notes for Table ASM-6:

- ¹ Fault number, name, and map designation (Figure ASM-9). The 15 faults with names shown in *italic font* have substantial field data, or correlate with faults that have substantial field data, for estimating slip rates (SR), recurrence intervals (RI), and approximate surface rupture length (SRL). The 9 faults with names shown with normal font have sparse characterization data. Data and observations supporting the characterization of regional fault sources are provided in Appendix ASM-6.
- ² Approximate distance from Yucca Mountain; from Piety, 1995 (P1), or observations of D.B. Slemmons (DBS).
- ³ Slip rates for well studied (*italic font*) faults generally are based on paleoseismic data as reported in available literature (see references cited on Piety, 1995). Slip rates for other faults (normal font) are estimated from SRL data using the approach described in Section 3.5.3.1.
- ⁴ Field observations of historical Basin and Range surface faulting for events of Mw > 6.2, YM trench data and personal observations of southern Nevada faults show that more than 90 percent of Quaternary scarps are formed by recurrent events, generally having similar magnitudes and displacements, so nearly all of the tabulated faults are assumed to reflect recurrent activity. Recurrence interval (RI) for well studied faults (*italic font*) are based on references in Piety (1995) or personal observations. They are considered to have fixed age values that show the range of uncertainty, for faults that have a better database, a preferred value is given. The assigned weights are 0.2 for the extreme values and 0.6 for the preferred value. Recurrence intervals for other faults are estimated using the approach described in Section 3.5.4 in which an assumed number of surface rupturing earthquakes (3) is represented by the scarps in middle to late Pleistocene surfaces that are estimated to be middle to late Pleistocene in age (equal weight assigned to ages of 69 ka, 128 ka, and 449 ka) and have recurrence intervals estimated at 20, 39, and 146 kyr, respectively.
- ⁵ Surface rupture length (SRL). The maximum SRL is generally limited by connections on strike to other faults, major irregularities at the ends of rupture zones, or to terminations or truncations by other faults. The length is approximately expressed by the minimum, preferred, and maximum SRL interpreted from the pattern of the 24 faults and character and size of the surface rupture patterns from historical events in the Basin and Range Province. The lengths include a minimum of about 10 km, and a maximum of 40-75 km, which is within the range of longer historical surface faulting events for normal faults in the Basin and Range Province. Faults with special relationships (e.g., having lengths that appear to be controlled by truncations or connections with other faults) generally have only one, preferred SRL. Only one value is given for cases in which the length is supported by one map, generally Piety (1995).
- ⁶ SS = strike slip, OS = oblique slip, N = normal.
- ⁷ A high probability (0.85) is assigned to the Carrara fault being seismogenic based on the evidence summarized in Appendix ASM-6. However, because the fault has not been thoroughly characterized, some probability (0.15) is given to the fault being non-seismogenic. Two alternative total lengths of 20 km and 42 km are given equal weight in the source model.

**TABLE ASM-7
RATIO OF AVERAGE TO MAXIMUM DISPLACEMENT**

Worker	Number Of Events	Ad/Md Ratio	Range In Values
W&C (1994)	56, all fault types	0.5	0.2-0.8
Mason (1996)	15 normal faulting events using data from W&C (1996)	0.42	0.2-0.8
Mason (1996)	3 Basin and Range events	0.33	0.3-0.6
Slemmons, in preparation	5 Basin and Range events	0.39	
Slemmons, in preparation	15, all fault types	0.37	0.2-
Strom & Nikonov, unpublished manuscript	10 normal faulting events	0.38	0.21-0.58, standard deviation = 0.11

**TABLE ASM-8
INFERRED NUMBER OF EVENTS**

Seismic Source	Inferred Number Of Events	Data
Ash Meadows	2	Anderson et al., (1995b)
Bare Mountain	Ca. 4	Whitney (1996), Anderson (SSC Workshop Presentation)
Belted Range	4 or possibly 5, using 1-1.5m maximum per event and SO up to 4.9 m. The anomalous value of 11.3 is assumed to be an older surface.	Anderson (1995a)
East Nopah	2 or 3	Anderson et al. (1995a) and DBS photographs
Kawitch Range	2, profile 2 appears to be on an older, but less than 100 ka surface.	Anderson et al. (1995a)
West Spring Mountains	3-5	
West Specter Range	2	Anderson et al. (1995a)

Average=20.7/7=3

**TABLE ASM-9
FAULT CLASSES FOR DISPLACEMENT POTENTIAL.**

Class	Description	Seismogenic ?	Cumulative Displacement	Probability of Slip	Number of Feature, N
0	block-bounding (primary)	yes	>50 m	1.0	1
1	NW-trending (secondary)	no	20-50 m	0.75	2
2	Larger Intrablock (secondary)	no	2-20 m	0.5	4.4
3	Smaller Intrablock (secondary)	no	0.5-2 m	0.25	20.6
4	Small shear (secondary)	no	0.1-0.5 m	0.05	56
5	Fracture (secondary)	no	<<0.1 m	0.01	1000

Depth of BD Transition Or Seismic Crustal Thickness	Detachment Exists	Buried SS Exists	Depth to Detachment	Detachment Seismogenic	Buried SS Seismogenic	Sources
---	-------------------	------------------	---------------------	------------------------	-----------------------	---------

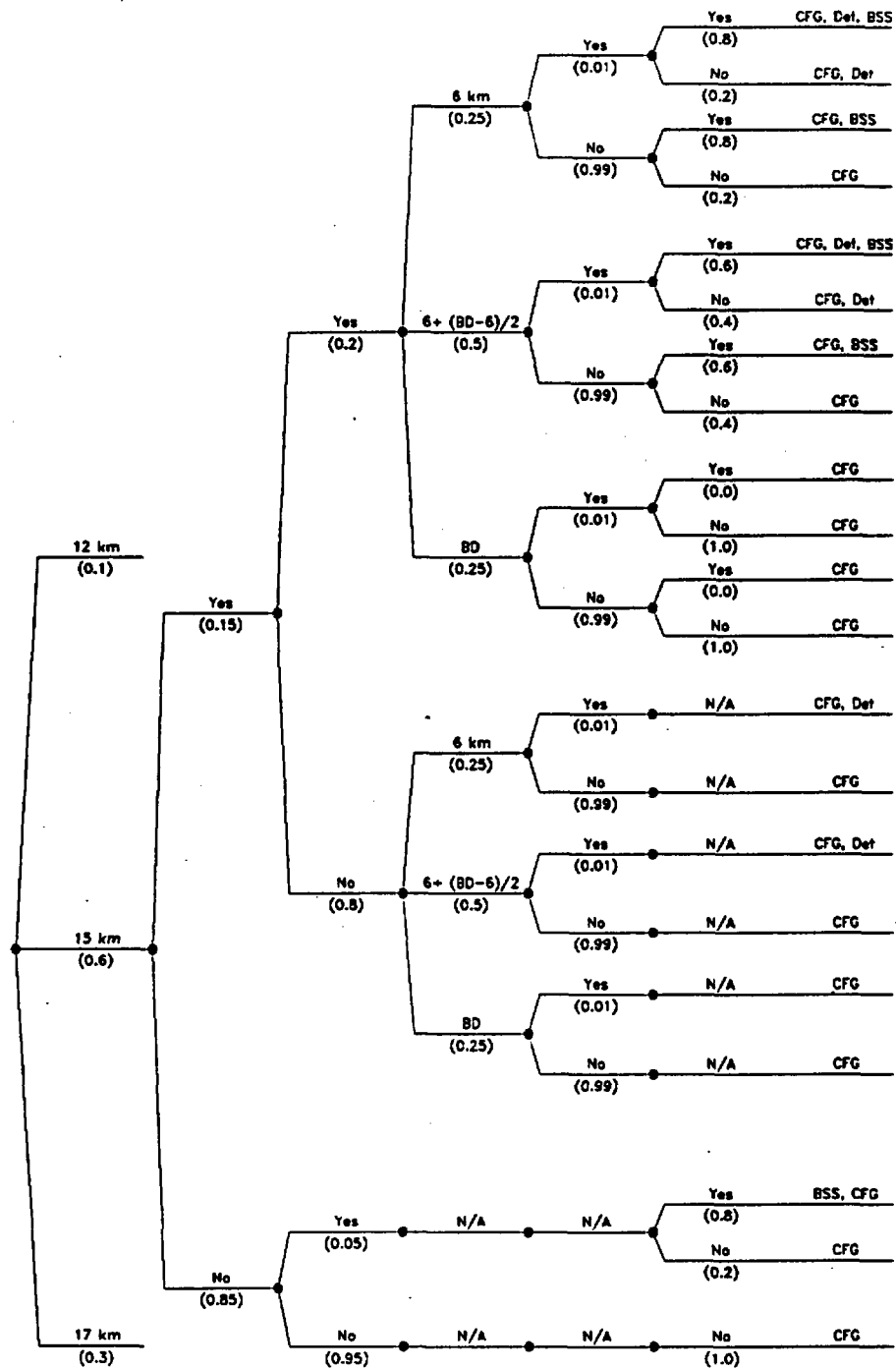


Figure ASM-1 Logic tree for local sources

<i>Depth of Brittle Crust (BDT)</i>	<i>Detachment Exists?</i>	<i>Depth of Detachment</i>	<i>Detachment Seismogenic</i>	<i>Detachment Geometry (area) (km²)</i>
-------------------------------------	---------------------------	----------------------------	-------------------------------	--

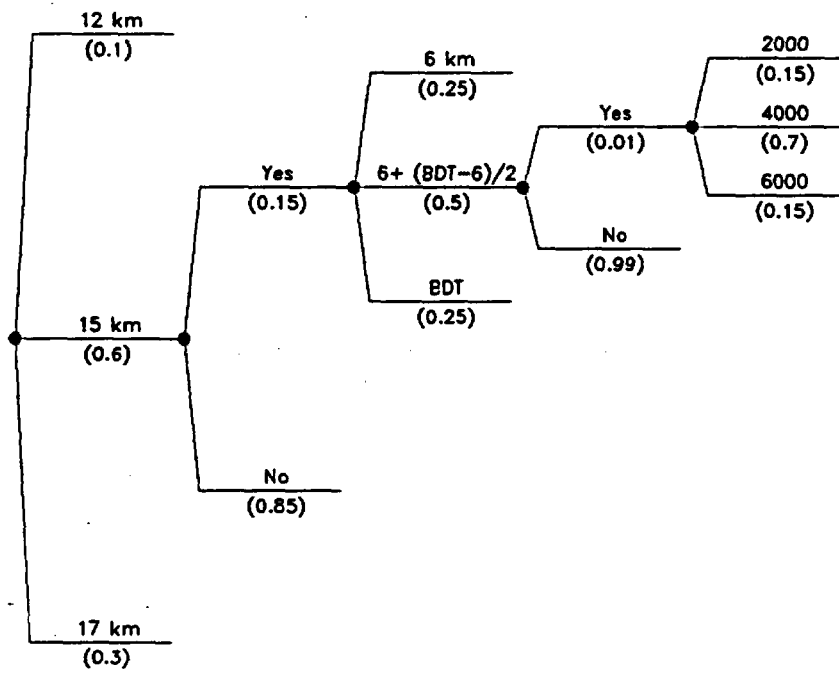


Figure ASM-2 Details of logic tree for detachment model

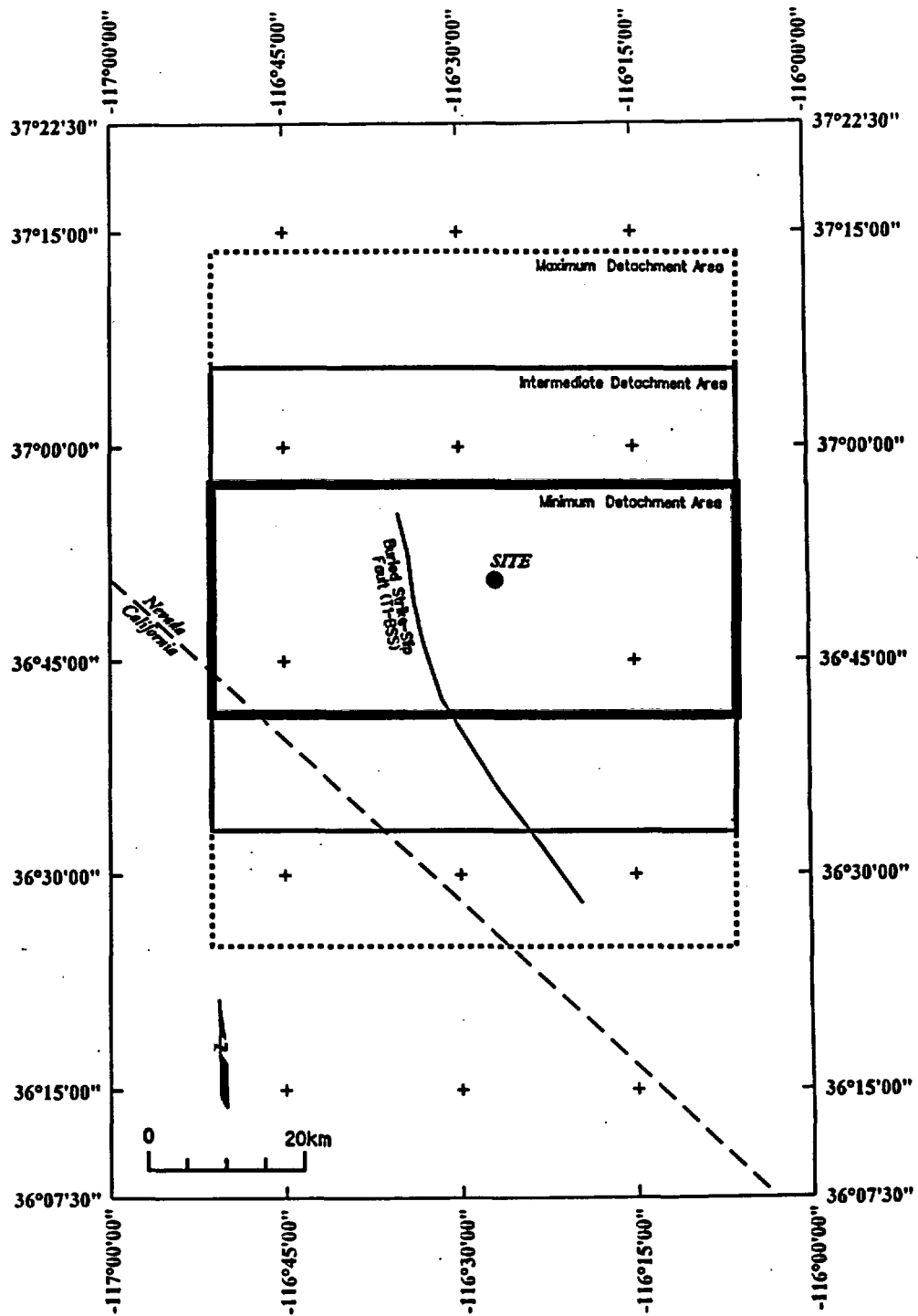


Figure ASM-3 Map showing hypothetical buried strike-slip fault and detachment fault in the vicinity of Yucca Mountain included in the seismic source model

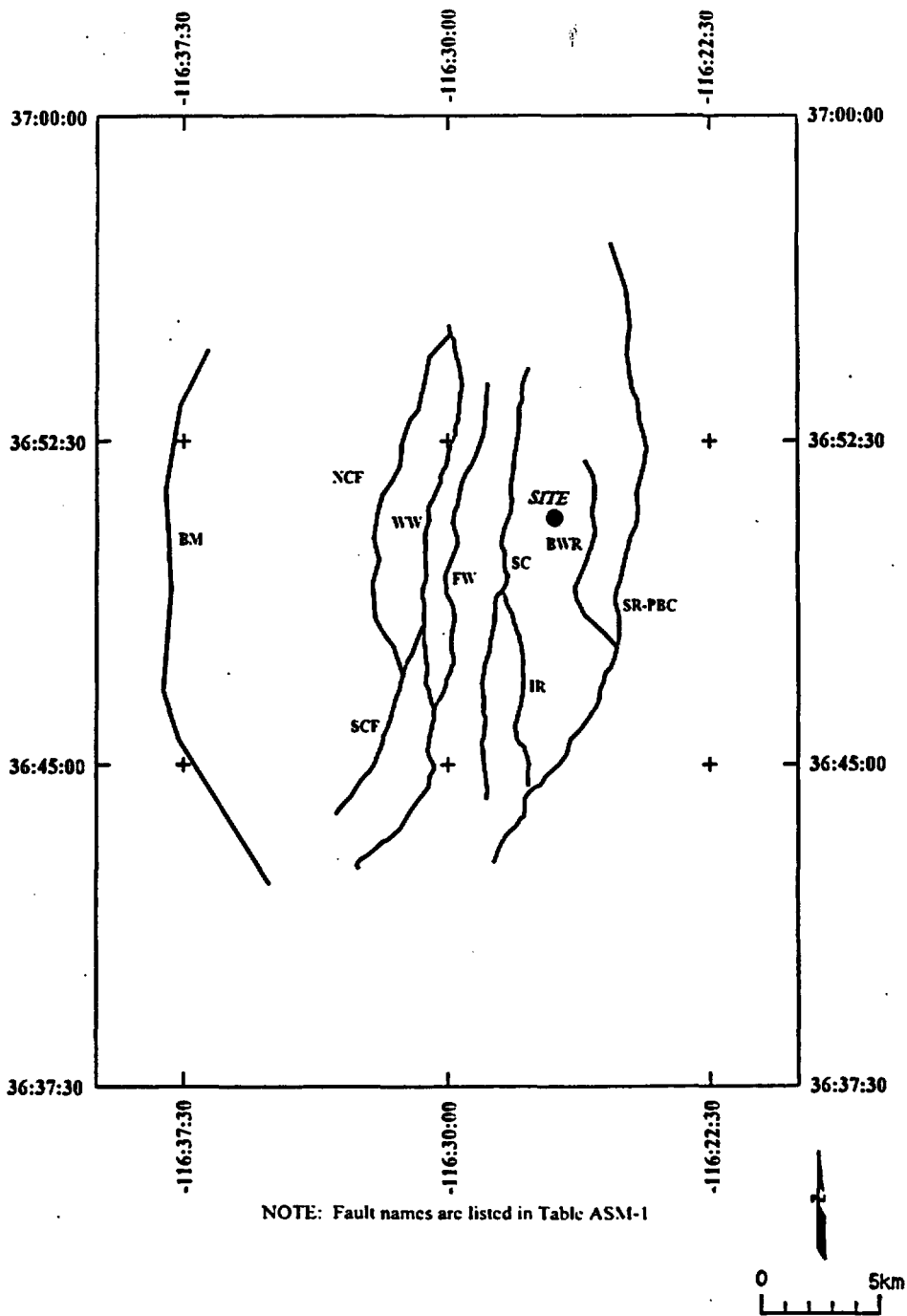


Figure ASM-4 Map showing local fault sources included in the seismic source model

<i>Detachment Exists</i>	<i>Faults Merge Downdip</i>	<i>Local Fault Geometry</i>	<i>Simultaneous Ruptures</i>
------------------------------	-------------------------------------	-------------------------------------	----------------------------------

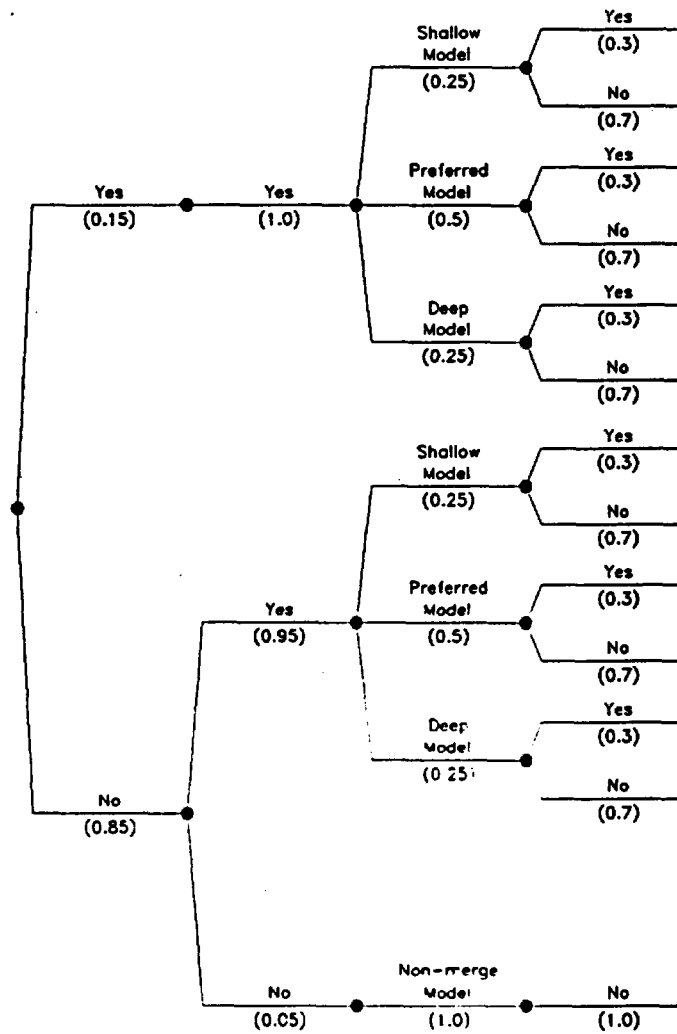


Figure ASM-5 Logic tree for Crater Flat group (CFG) behavior

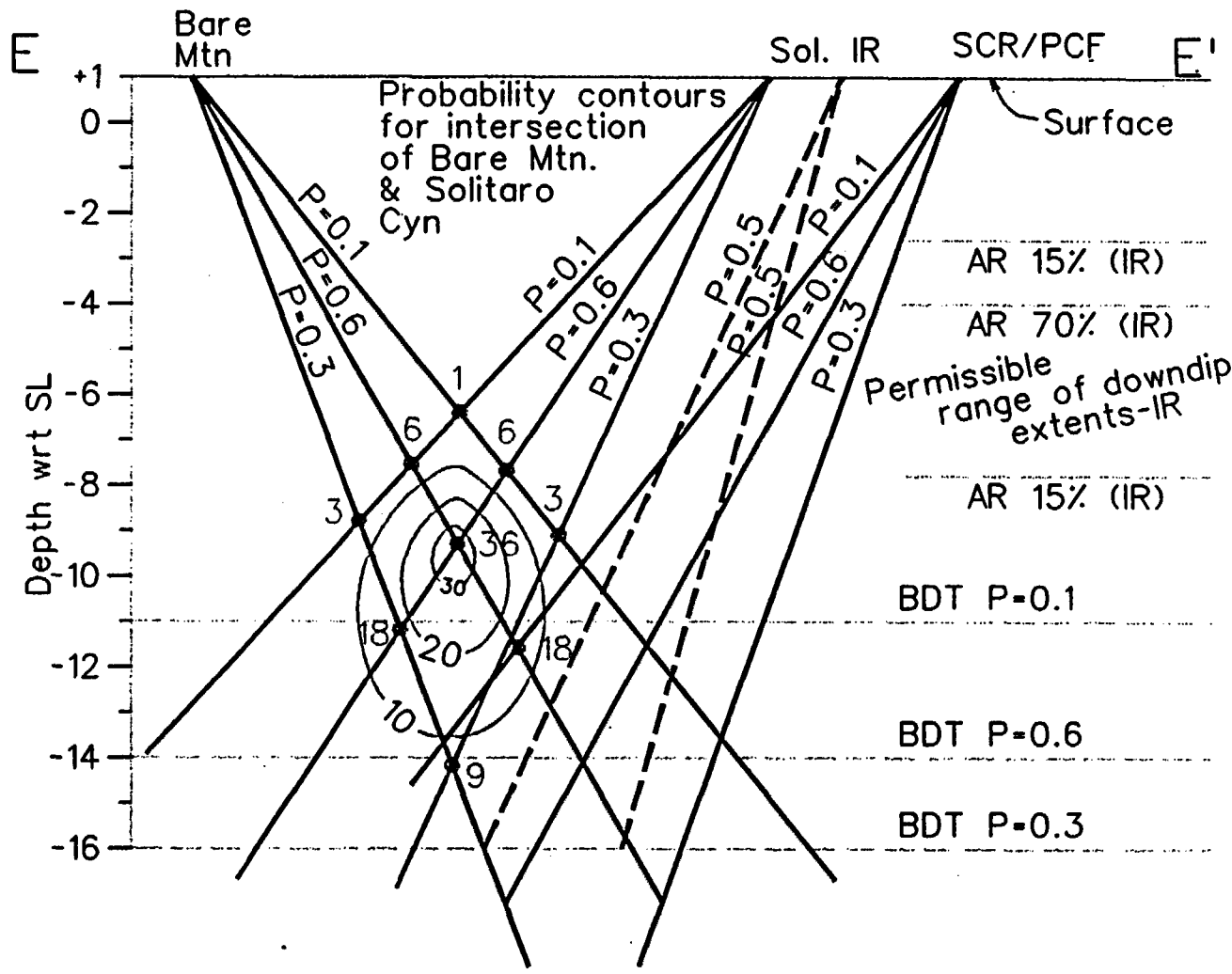


Figure ASM-6 Schematic of method used to develop downdip geometries of local faults

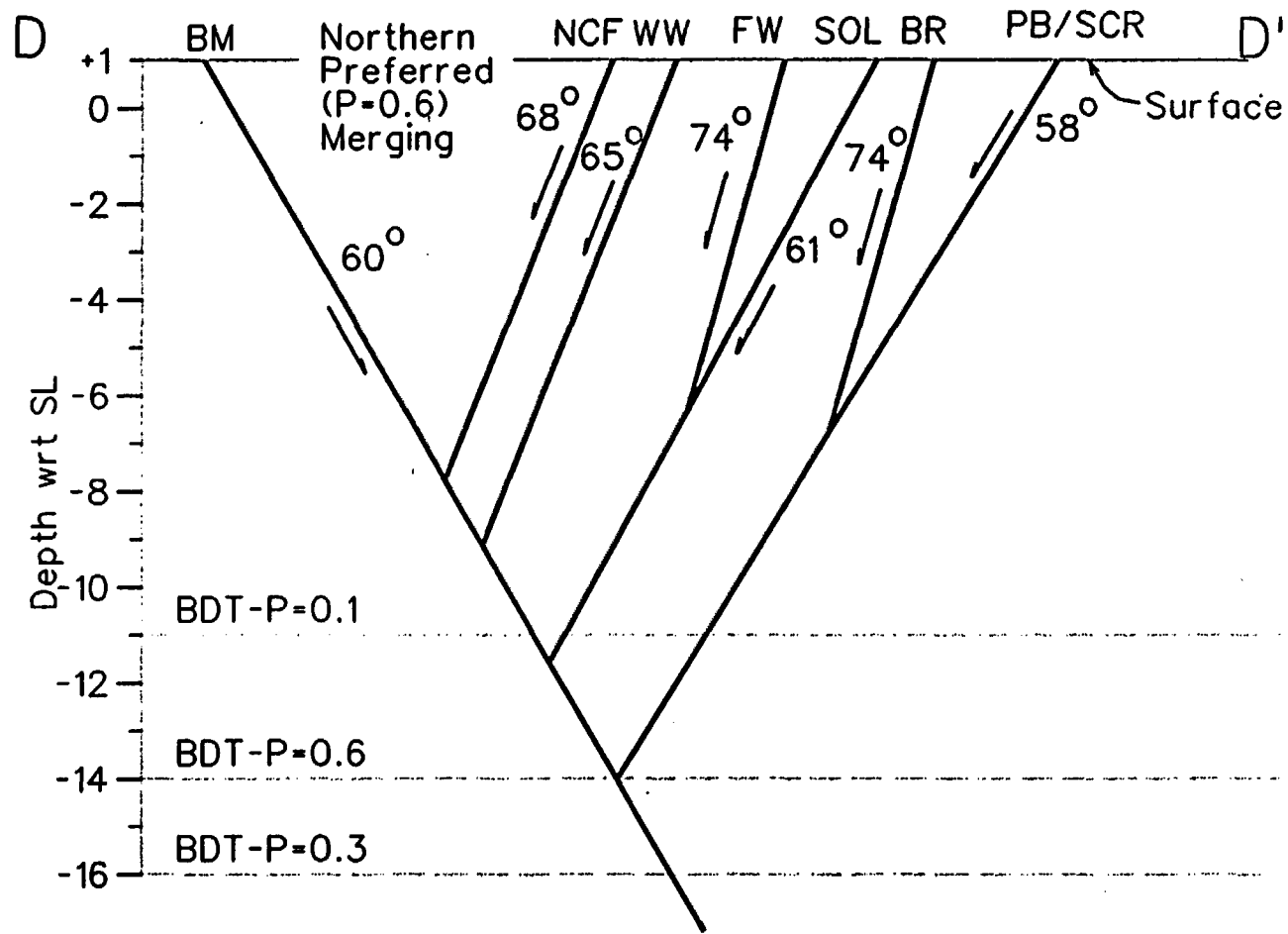


Figure ASM-7a Schematic cross section of preferred merging geometry, northern transect

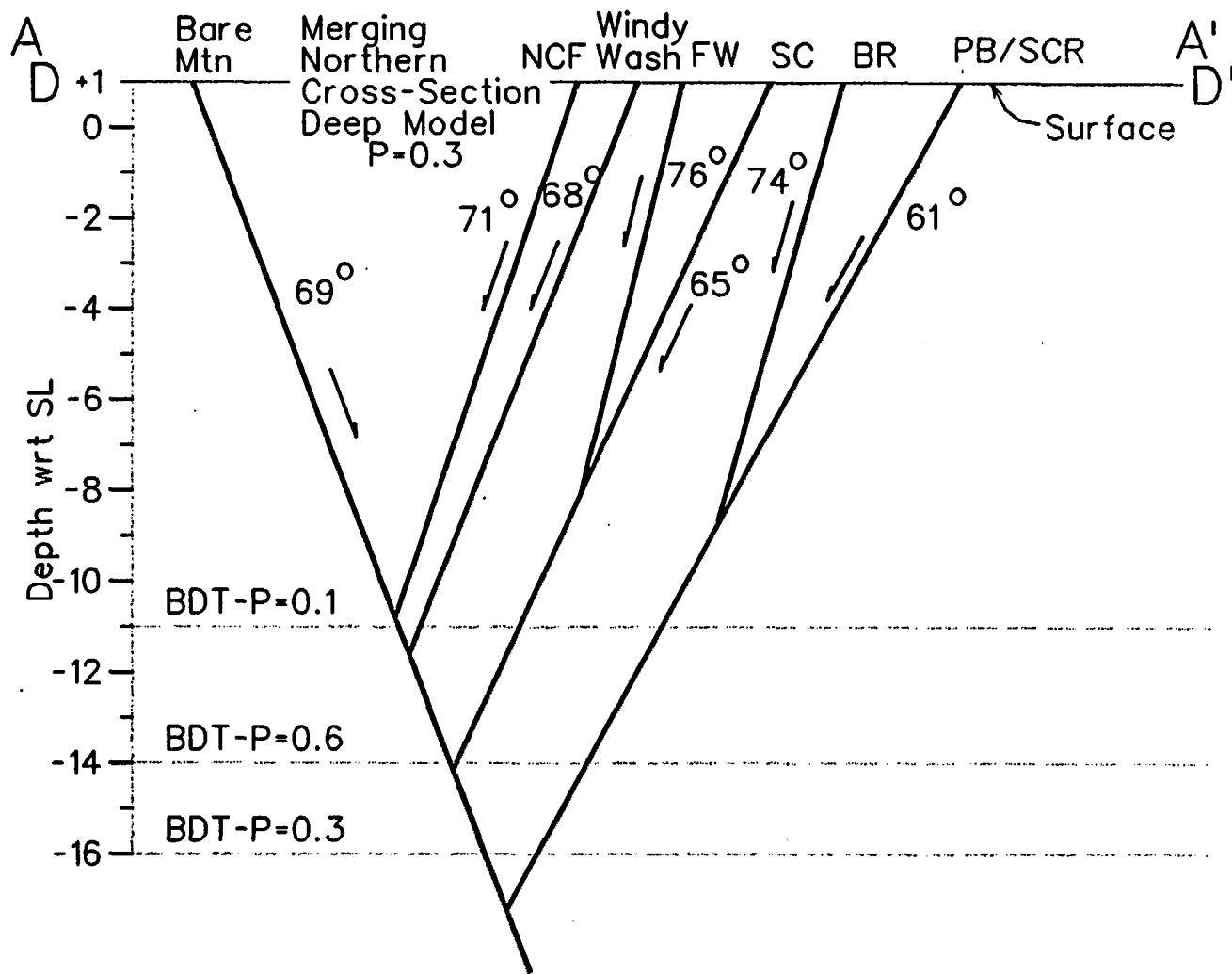


Figure ASM-7b

Schematic cross-section of deep, merging geometry. Depth of secondary faults constrained by aspect ratio

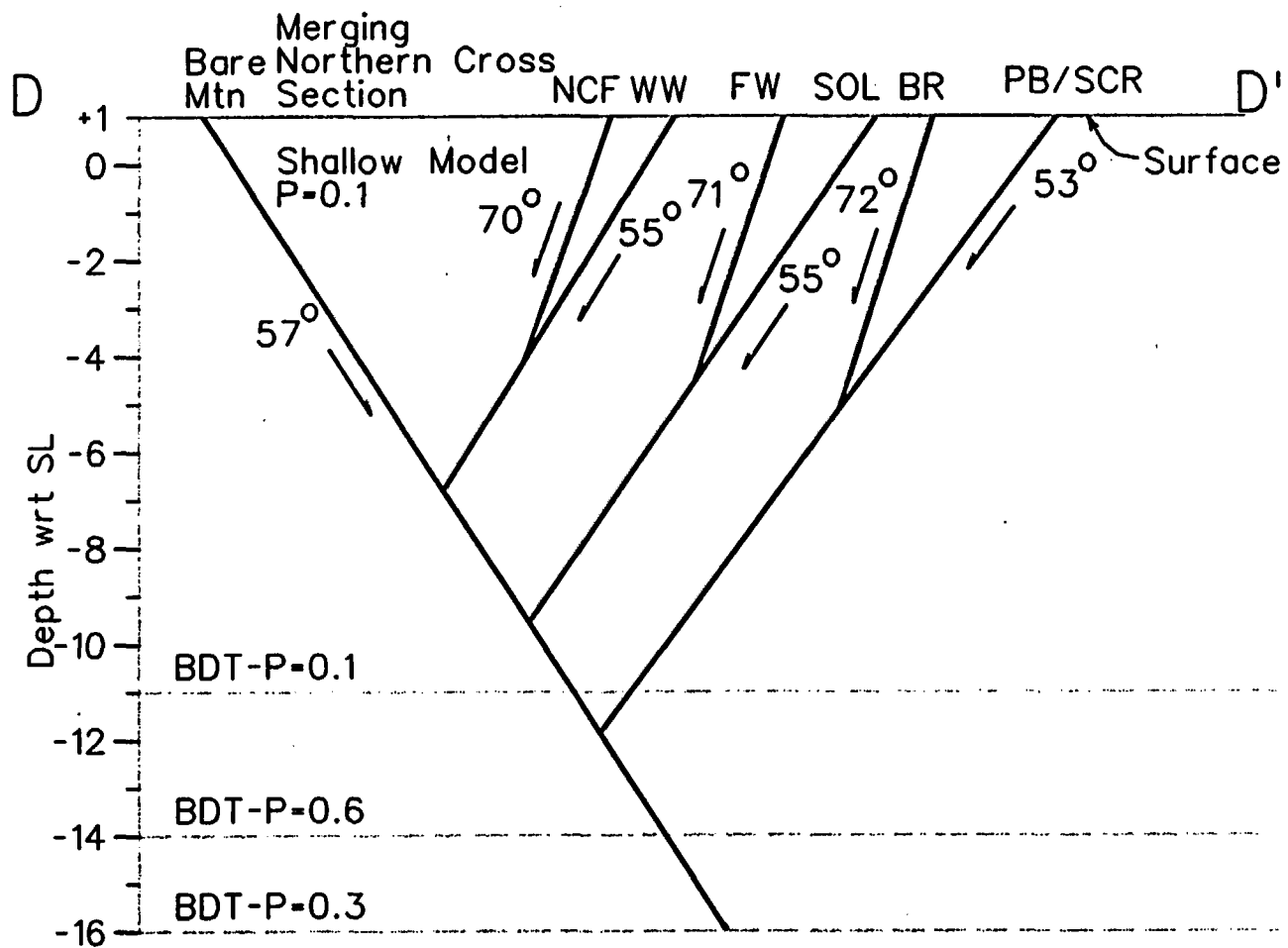


Figure ASM-7c Schematic cross-section of shallow, merging geometry, northern transect.
 Depth of secondary faults constrained by aspect ratio

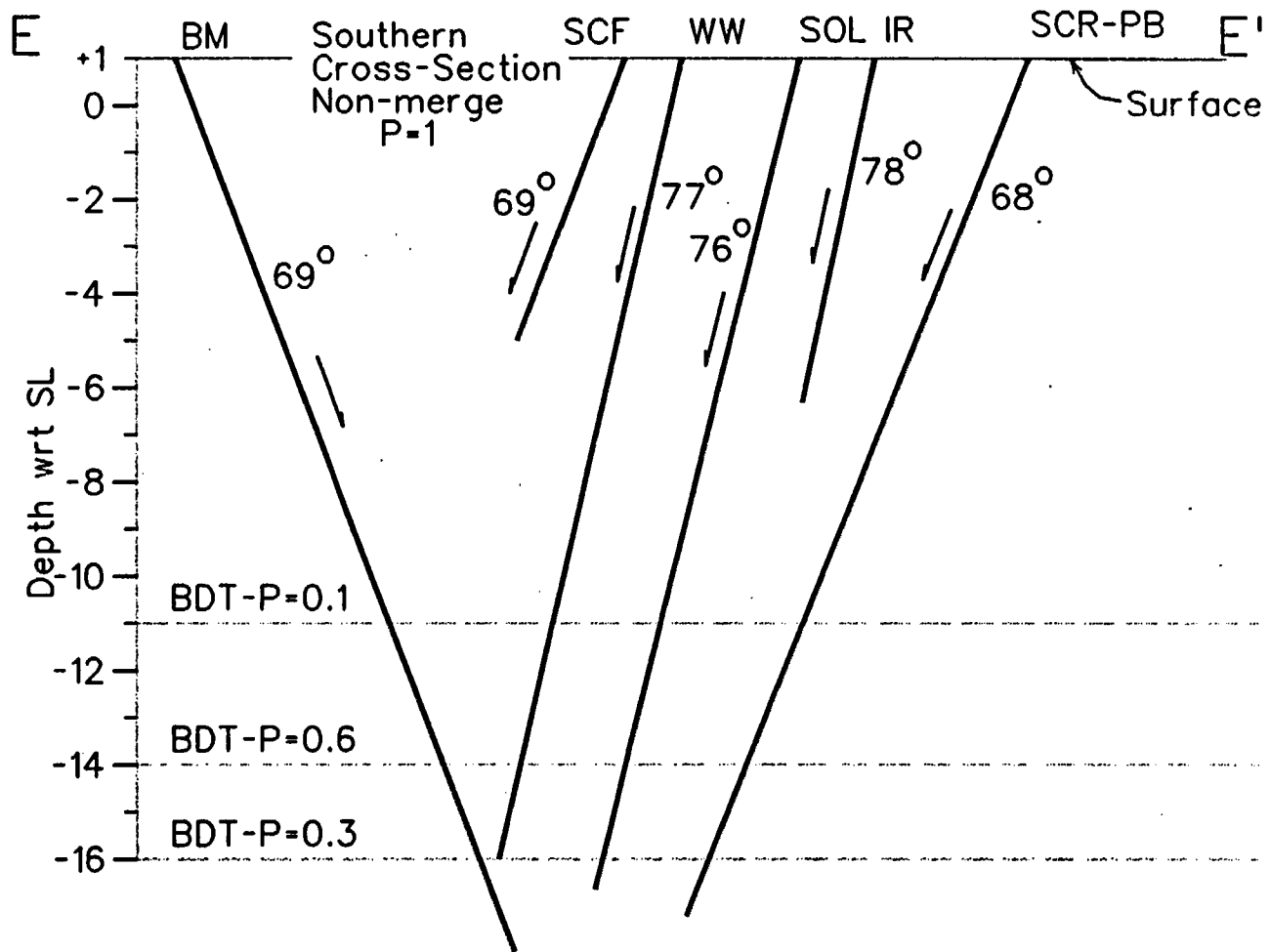
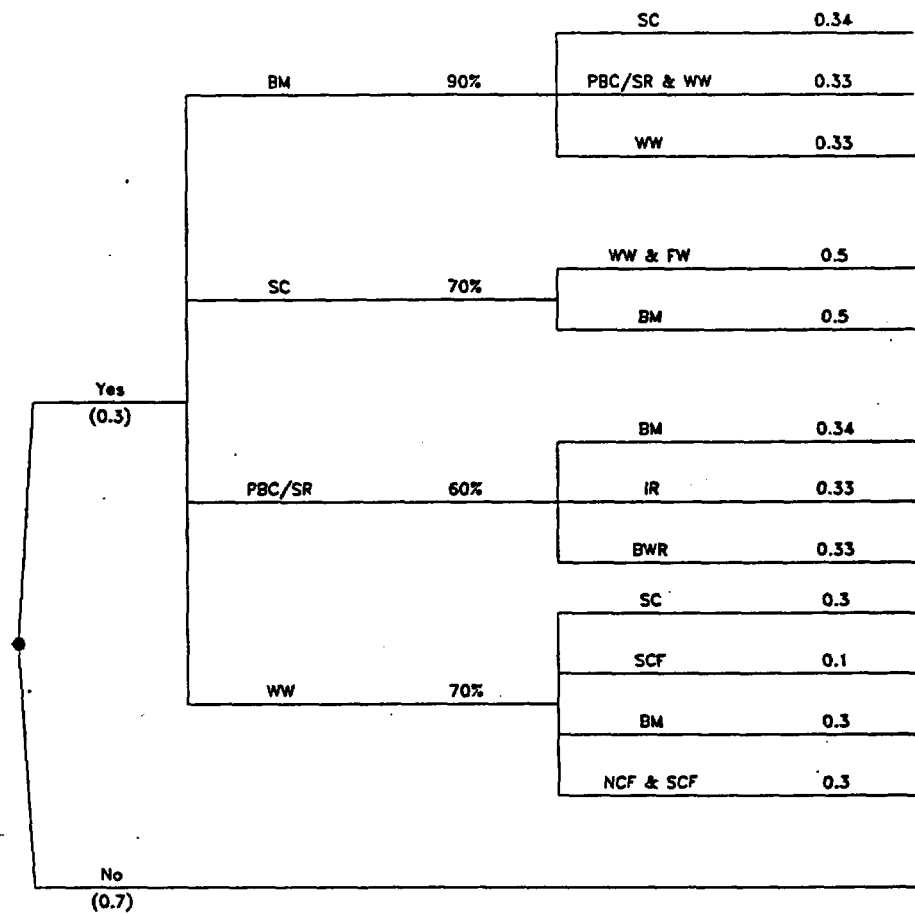


Figure ASM-7d Schematic cross-section of non-merging geometry. Depth of secondary faults constrained by aspect ratio

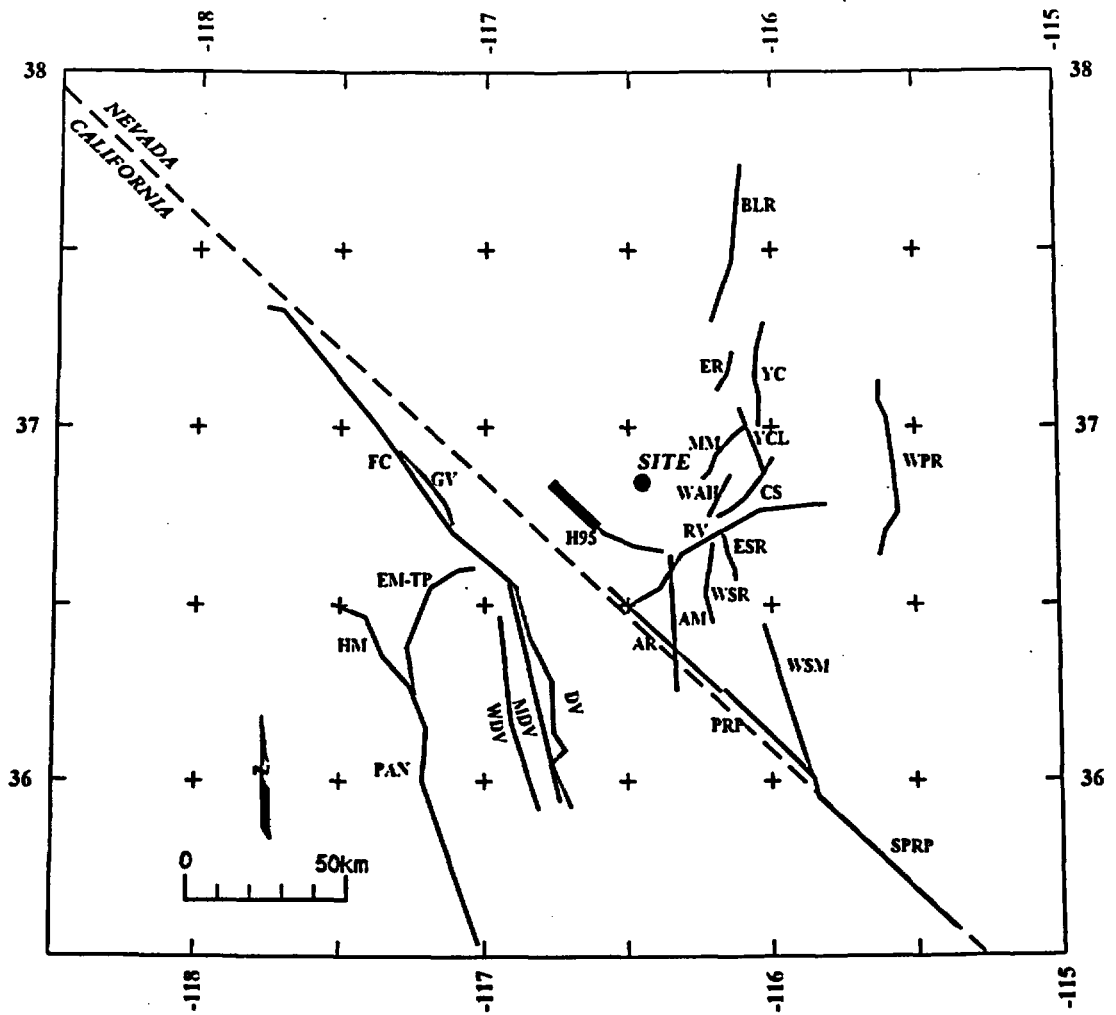
<i>Simultaneous Rupture occurs?</i>	<i>Block-bounding Fault</i>	<i>Percentage of simultaneous rupture</i>	<i>Other Faults in simultaneous rupture</i>	<i>Relative frequency for fault rupture combination</i>
-------------------------------------	-----------------------------	---	---	---



Explanation:

- BM - Bare Mountain
- SC - Solitario Canyon
- PBC/SR - Paintbrush Canyon/Stagecoach Road
- WW - Windy Wash
- FW - Fatigue Wash
- IR - Iron Ridge
- BWR - Bow Ridge
- SCF - South Crater Flat
- NCF - North Crater Flat

Figure ASM-8 Simultaneous rupture scenarios and relative frequencies



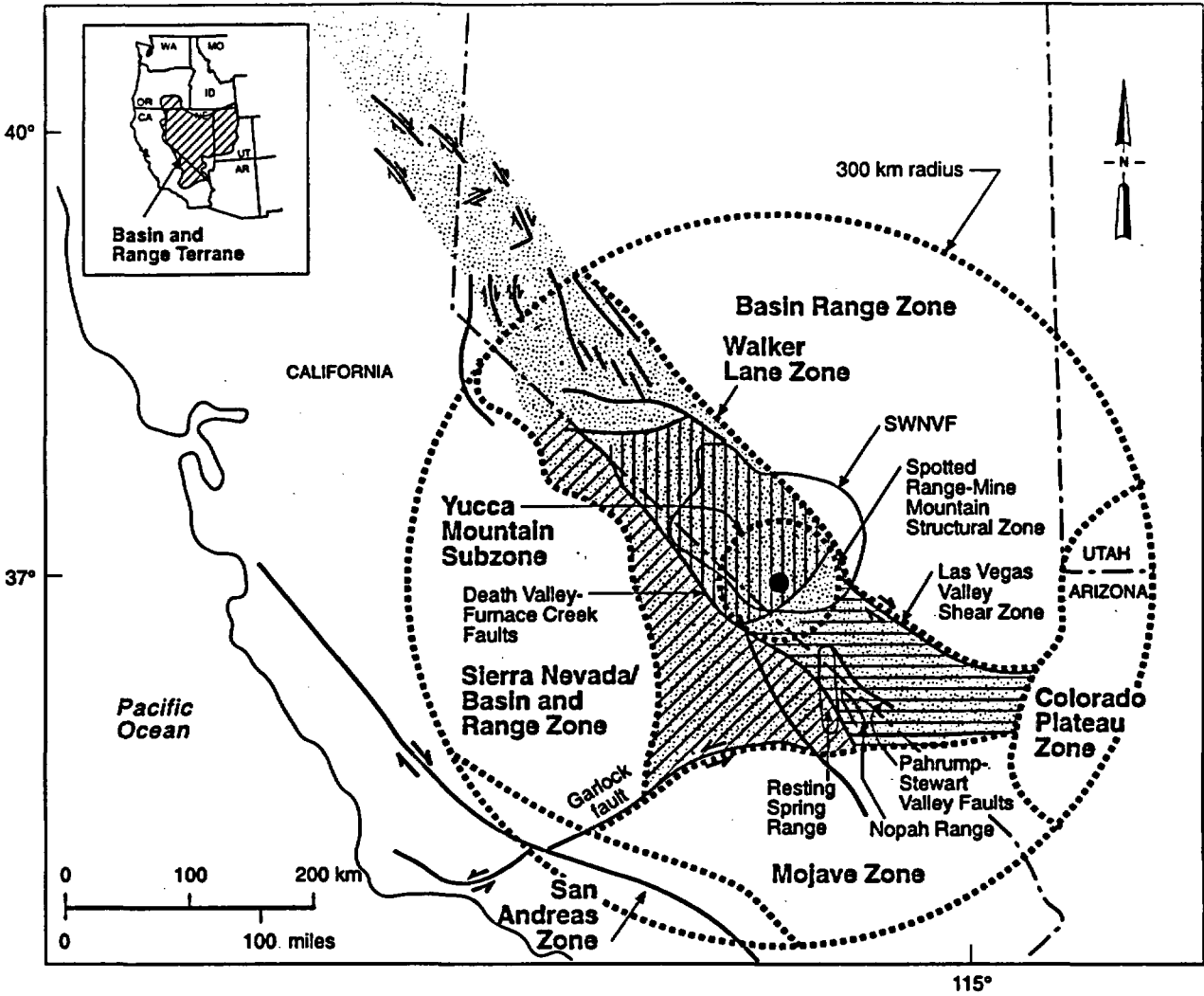
EXPLANATION

NOTE: Fault names are listed in Table ASM-6

Fault Lengths:



Figure ASM-9 Map showing regional faults included in the seismic source model



LEGEND

- Fault: arrows indicate direction of relative offset; tick on hanging wall of normal fault; dashed where inferred
- Location of Yucca Mountain
- SWNVF** Southwest Nevada volcanic field
- State boundary
- Seismic source zones
- Spring Mountains section
- Inyo-Mono Terrane
- Goldfield section
- Walker Lane

Figure ASM-10 Map of regional seismic source zones within 300 km

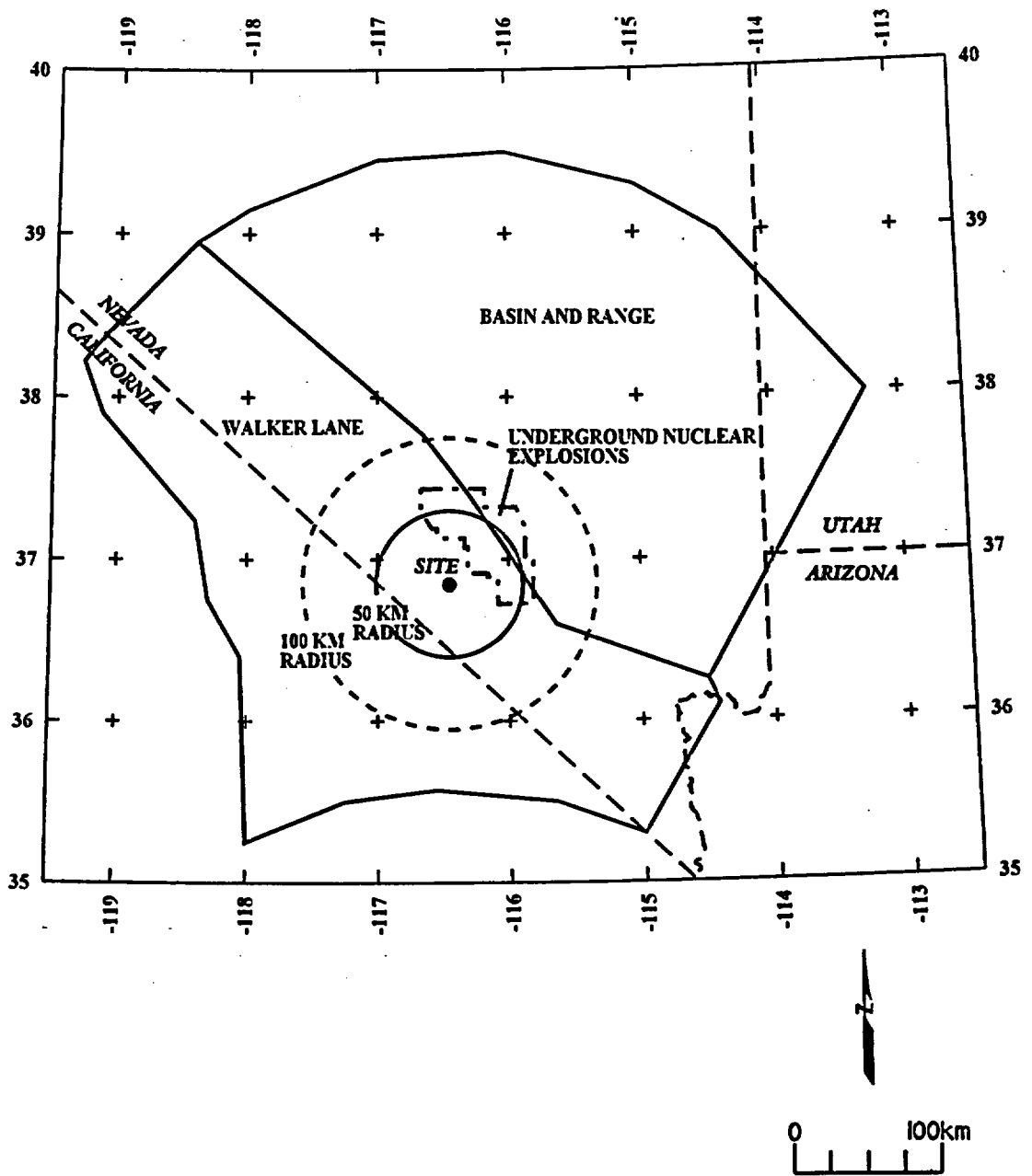
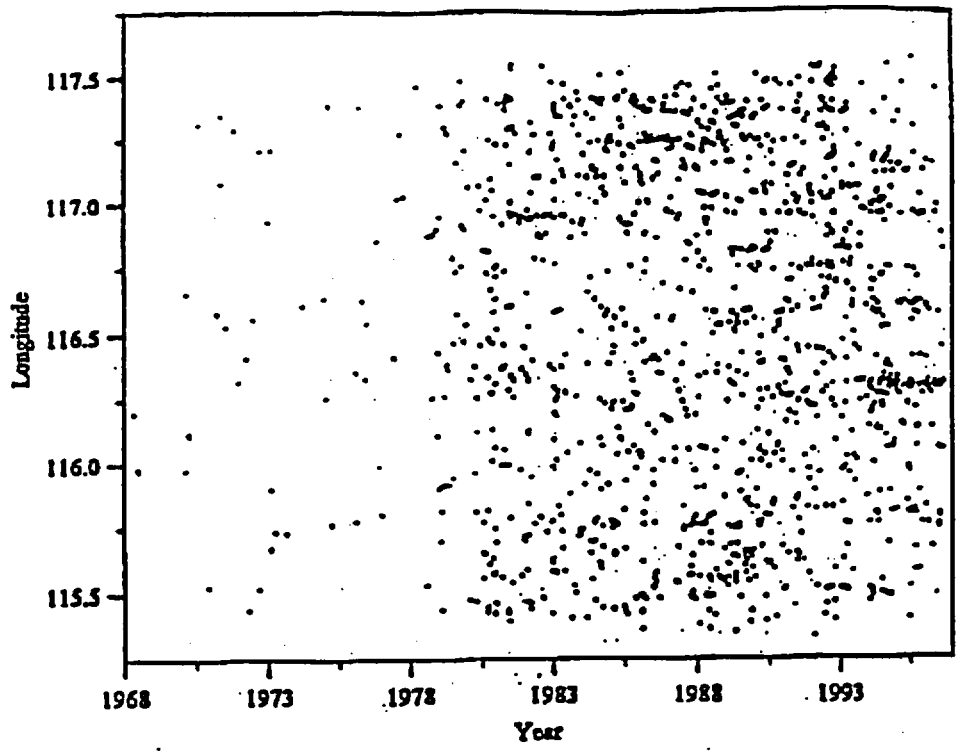
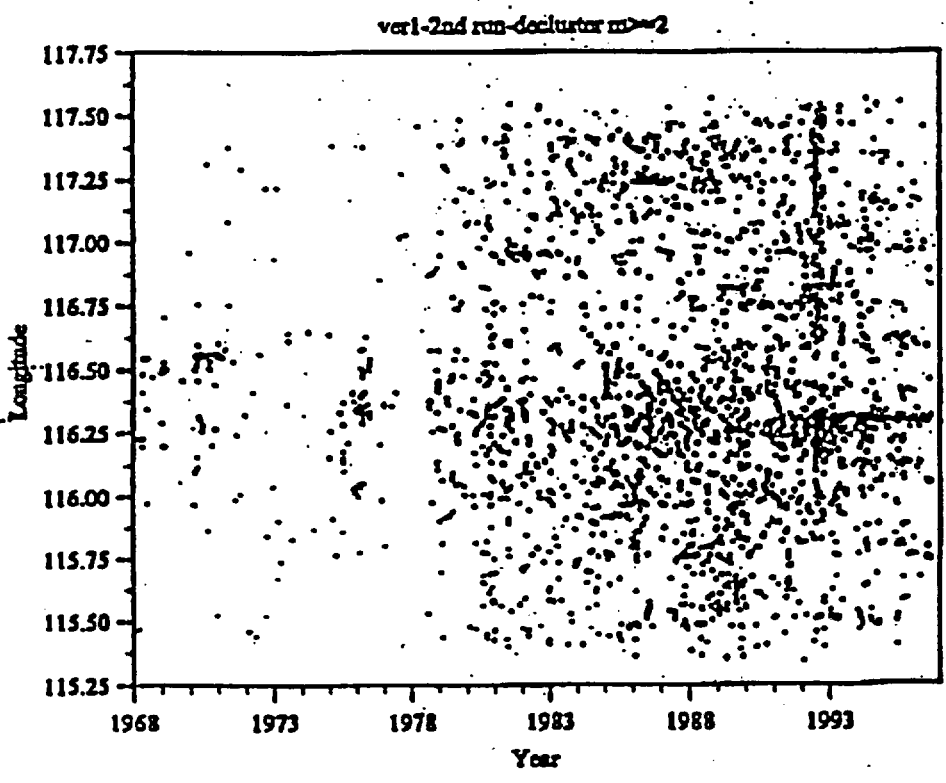


Figure ASM-11 Map showing the boundaries of zones used in the seismic source model



Youngs



Reassenberg

Figure ASM-12 Space-time diagrams comparing Youngs and Reassenberg declustering methods

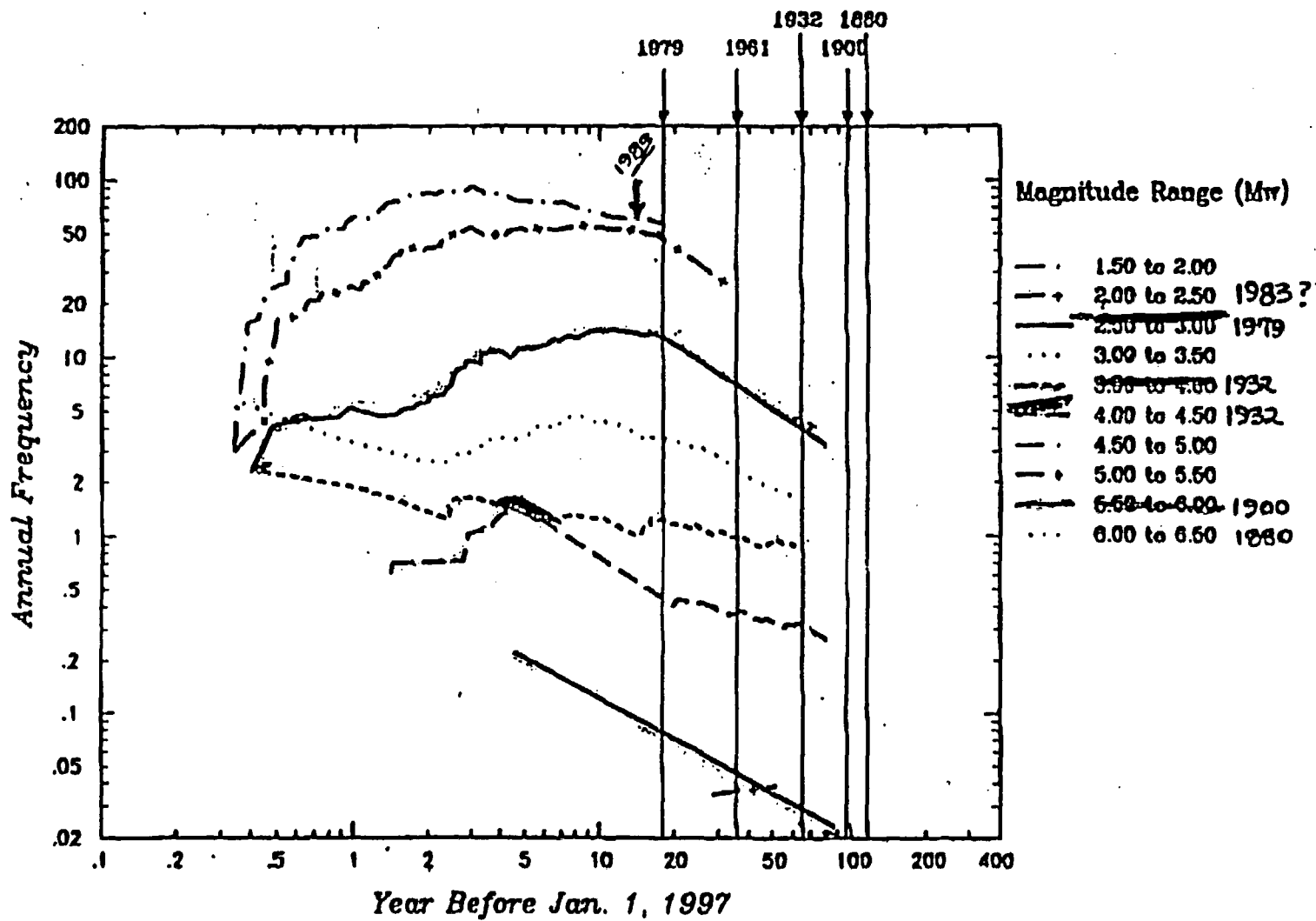


Figure ASM-13 Annual frequency of earthquake recurrence as a function of time before Jan. 1, 1997, based on the catalog declustered by approach of Youngs et al.

<i>Declassified Catalog</i>	<i>Source Zonation</i>	<i>Spatial Variability</i>	<i>Sources</i>	<i>Maximum Magnitude</i>	<i>Recurrence Calculation Minimum Magnitude</i>
-----------------------------	------------------------	----------------------------	----------------	--------------------------	---

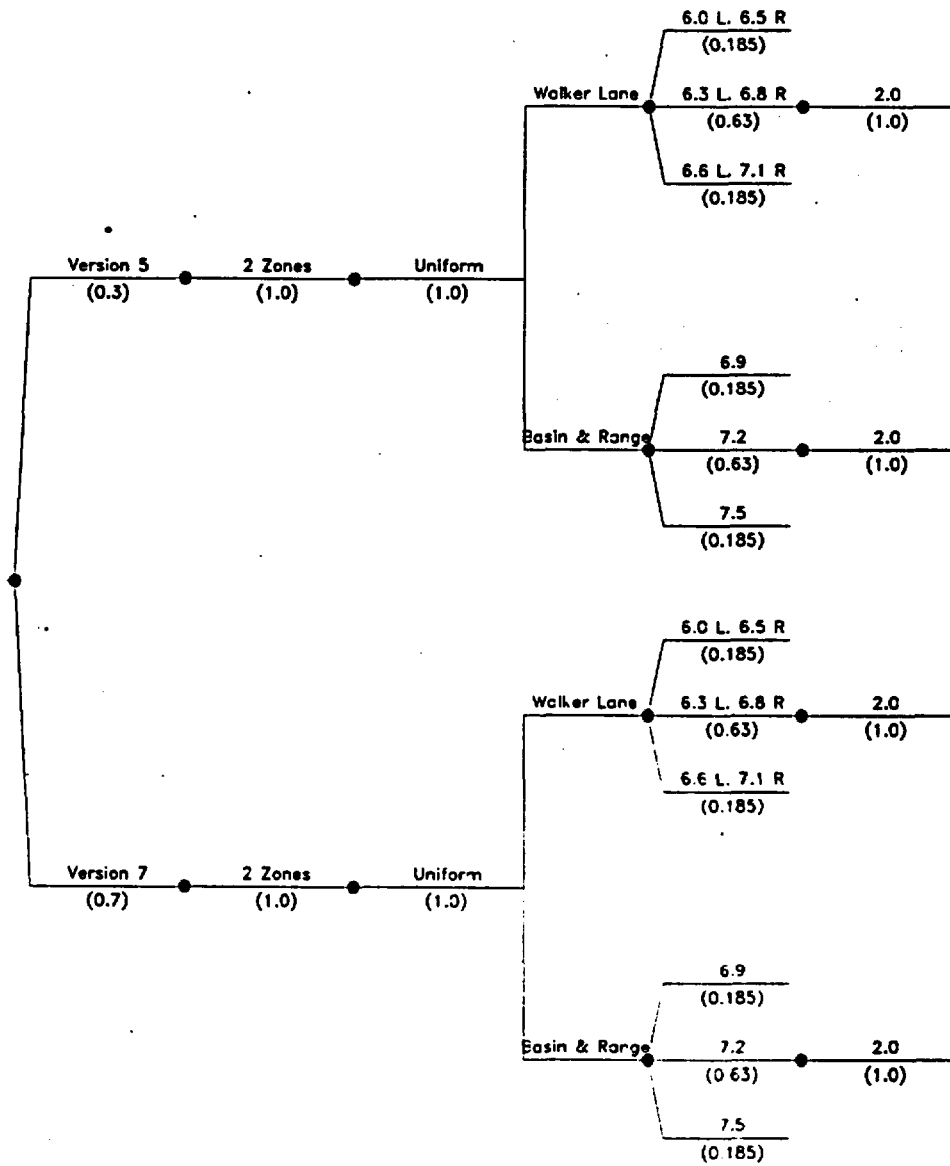


Figure ASM-14 Logic tree used to characterize seismic source zones

<i>Principal Faulting Capability</i>	<i>Earthquake Frequency</i>	<i>Probability of Surface Rupture</i>	<i>Maximum Displacement</i>	<i>Displacement Distribution</i>
--------------------------------------	-----------------------------	---------------------------------------	-----------------------------	----------------------------------

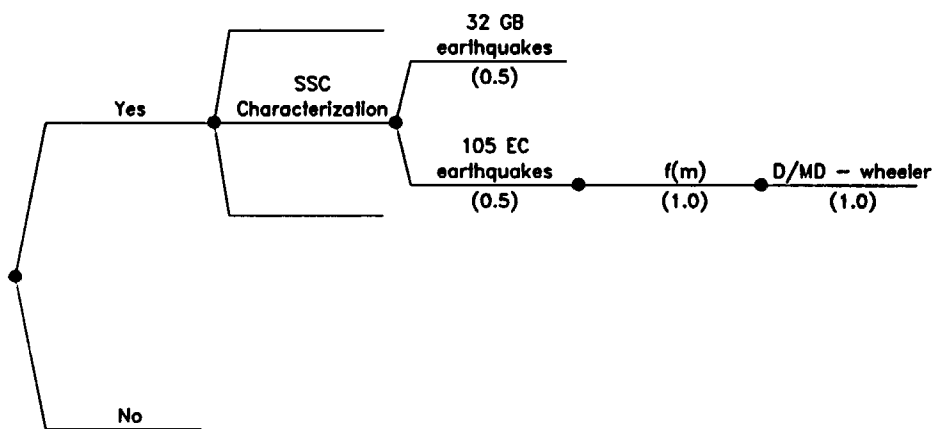


Figure ASM-16a Logic tree for principal faulting hazard

<i>Distributed Faulting Capability</i>	<i>Earthquake Frequency</i>	<i>Probability of Principal Surface Rupture</i>	<i>Probability Distributed Rupture occurs</i>	<i>Displacement Reduction Factor, RF</i>
--	-----------------------------	---	---	--

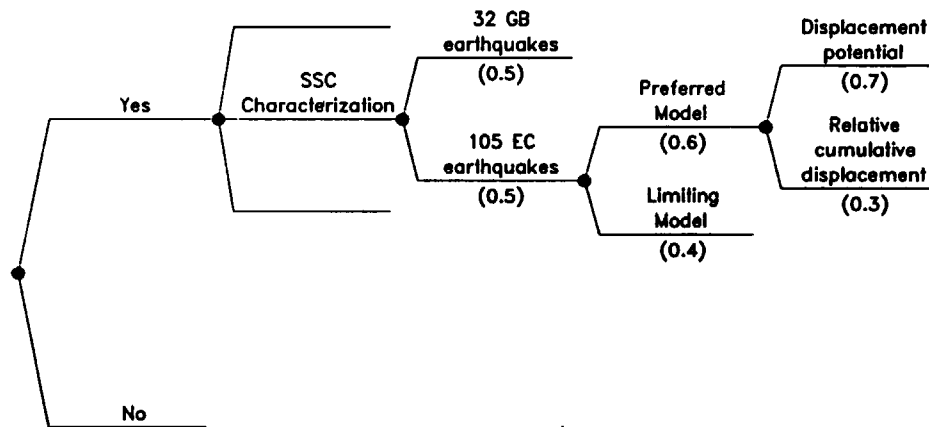


Figure ASM-16b Logic tree for distributed faulting hazard

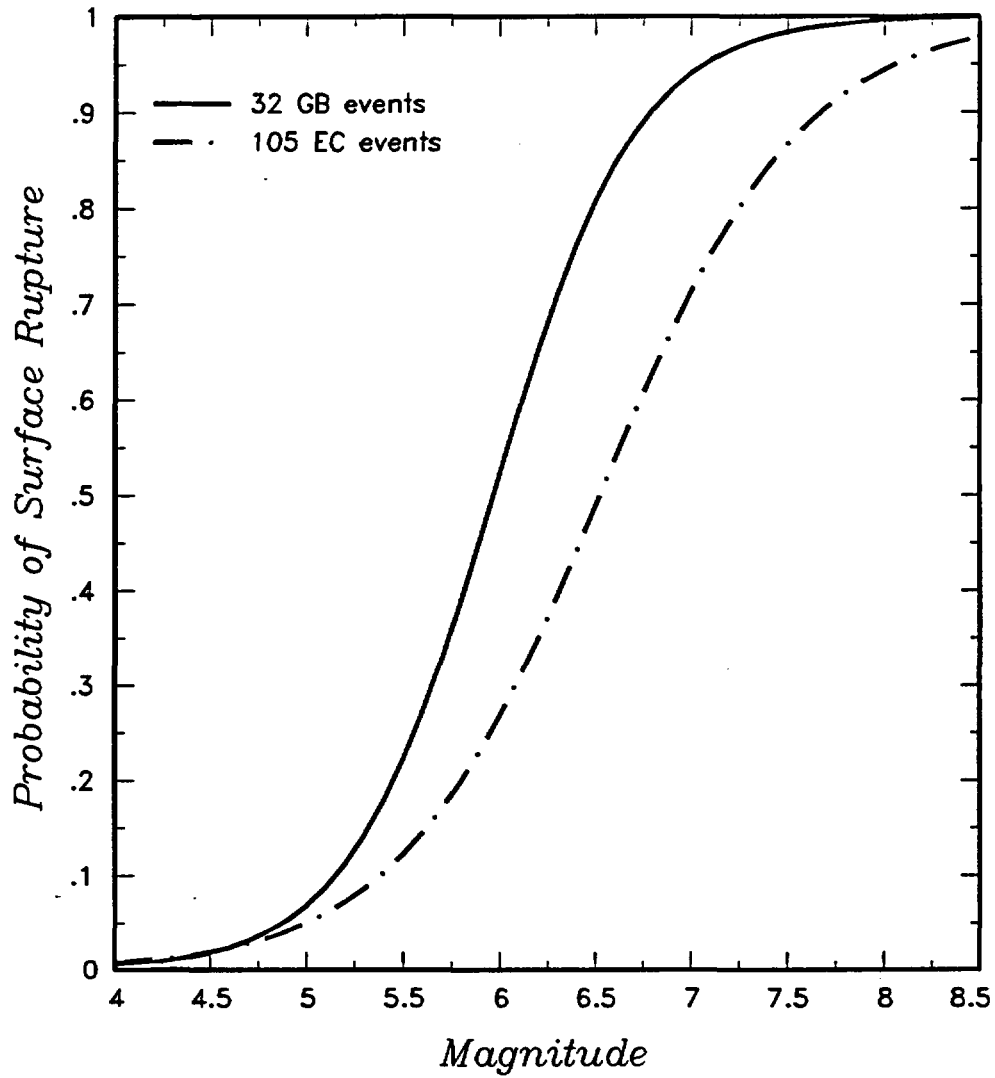


Figure ASM-17 Relationships between earthquake magnitude and probability of surface rupture

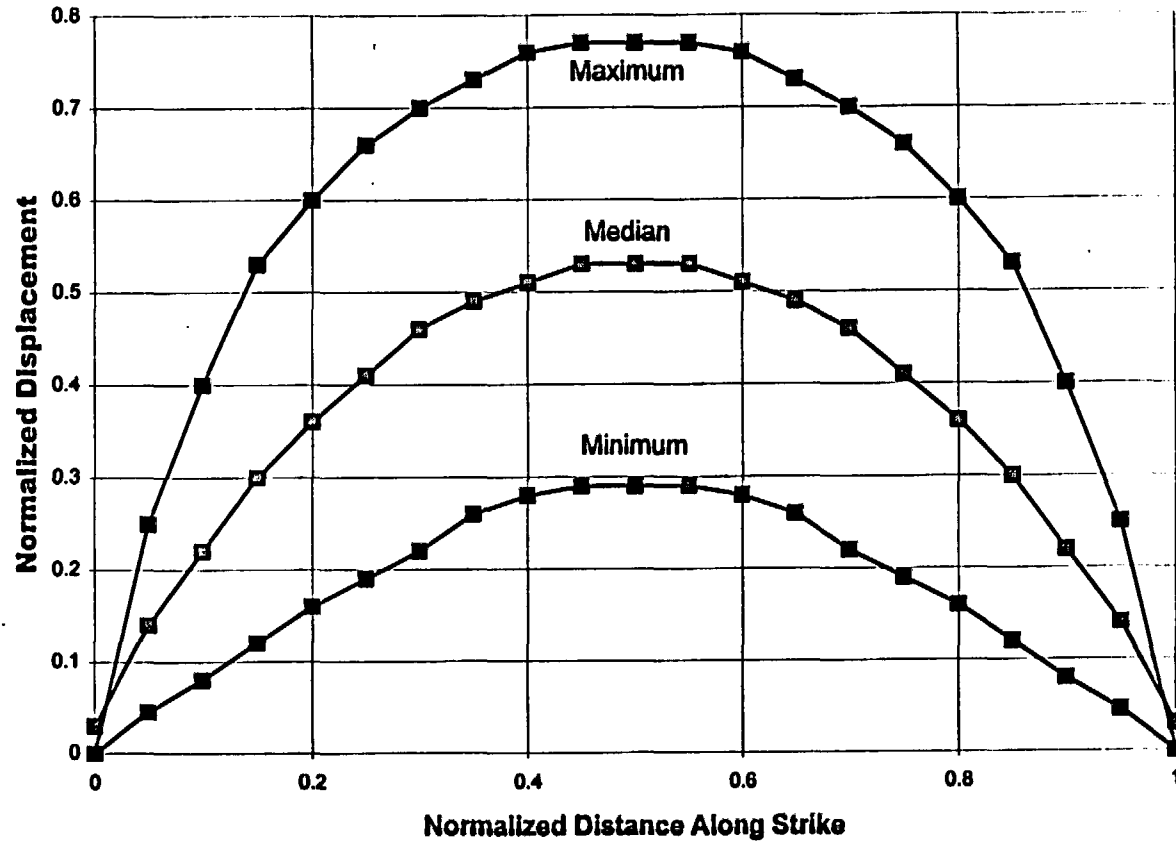


Figure ASM-18 Normalized "Wheeler" curve (adapted from Wheeler, 1989)

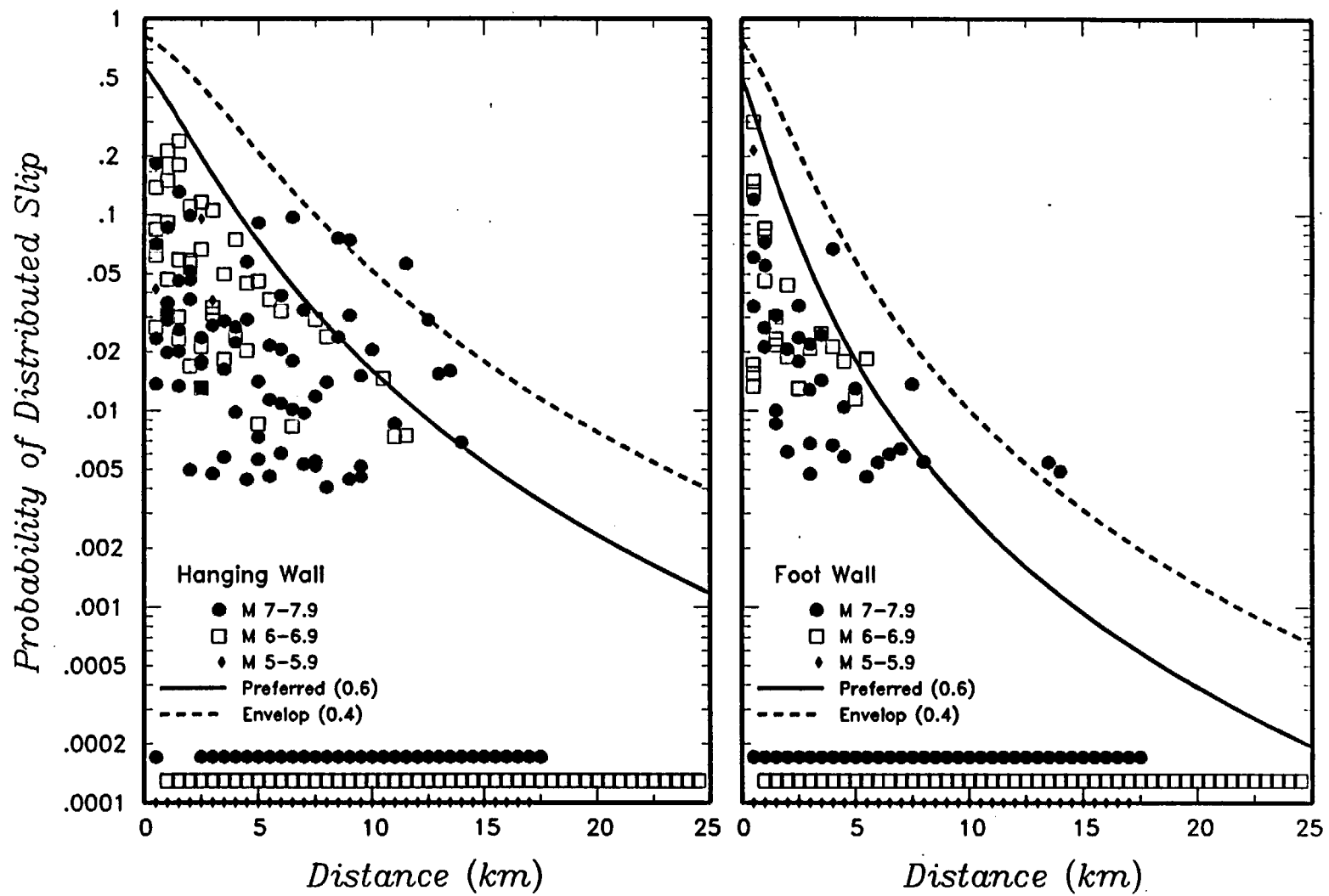
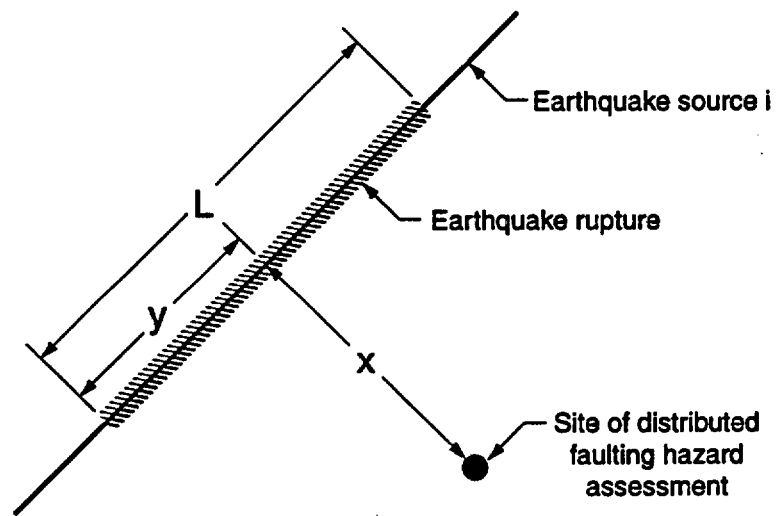


Figure ASM-19 Probability (frequency) of distributed slip as a function of distance from rupture



x = distance from rupture to site measured from fault normal point
 y = location of fault normal point within rupture
 L = length of earthquake rupture

Figure ASM-20 Schematic illustration of ASSD method

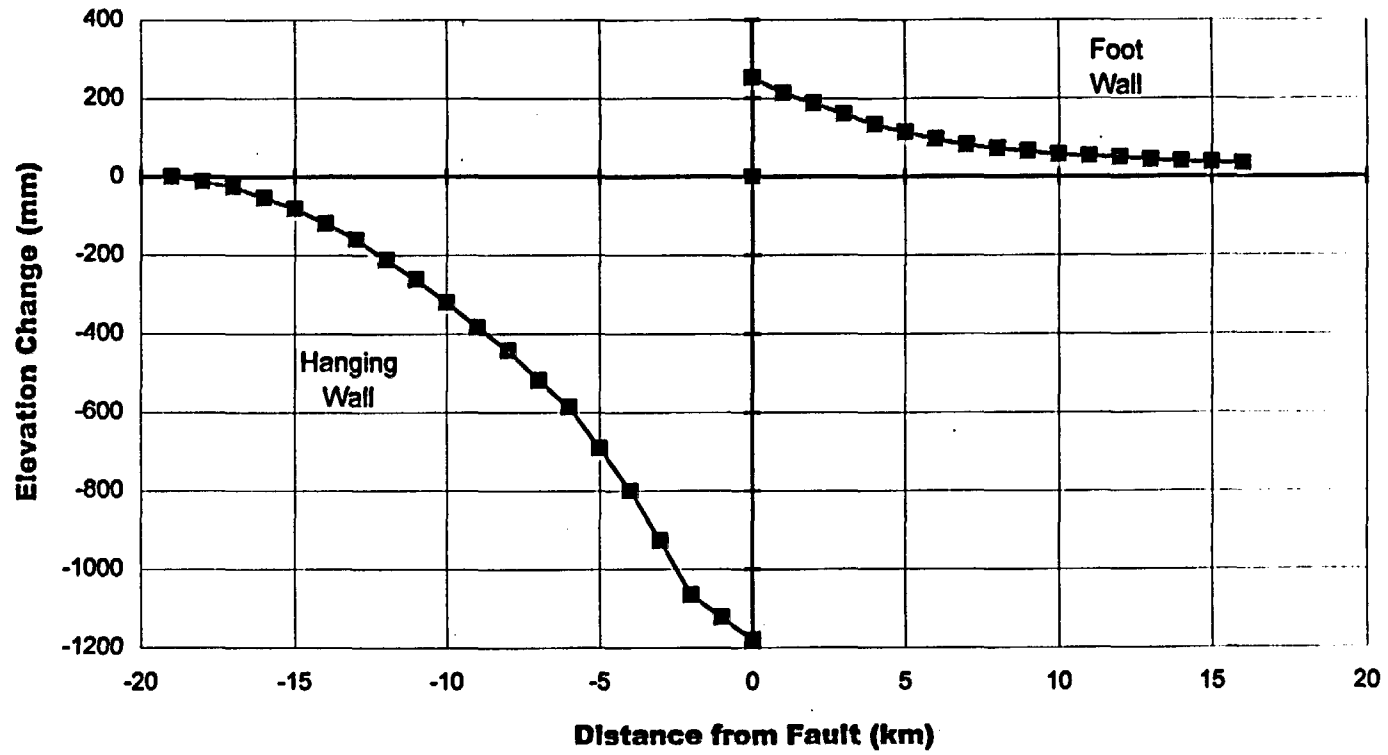


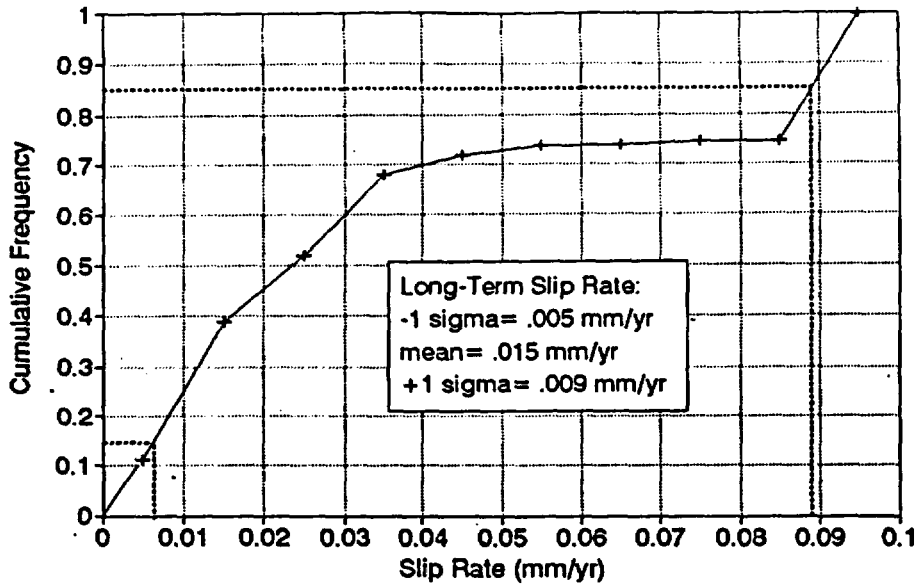
Figure ASM-21 Borah Peak geodetic curve

APPENDIX ASM-1

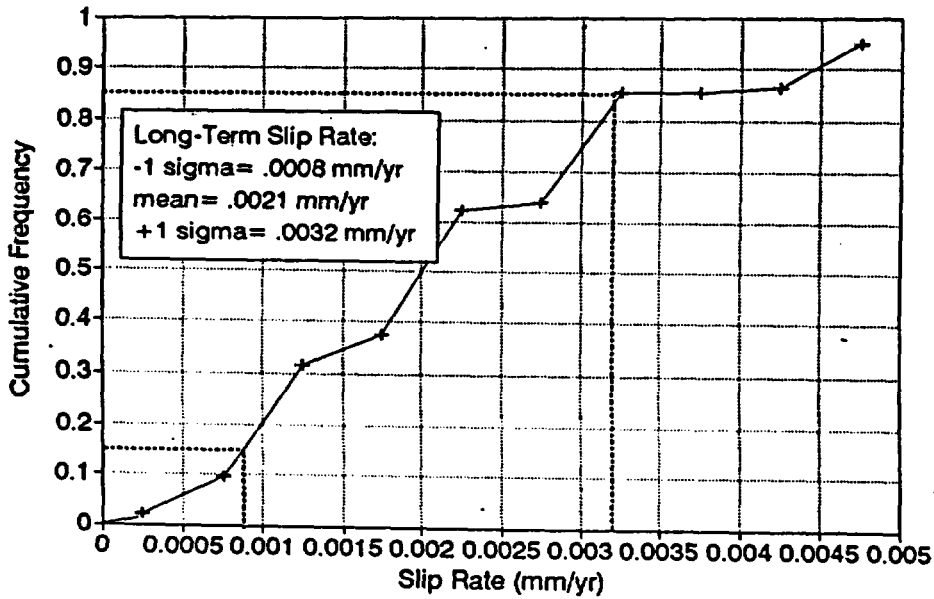
Graphs showing the cumulative frequency of long-term slip rates for 10 local Yucca Mountain faults.

Note: These CDFs were computed from permutations of cumulative displacement and age of deposits/soils from Table 5-1 in Whitney (1996).

Cumulative Frequency of Long-Term Slip Rates, Bare Mountain fault

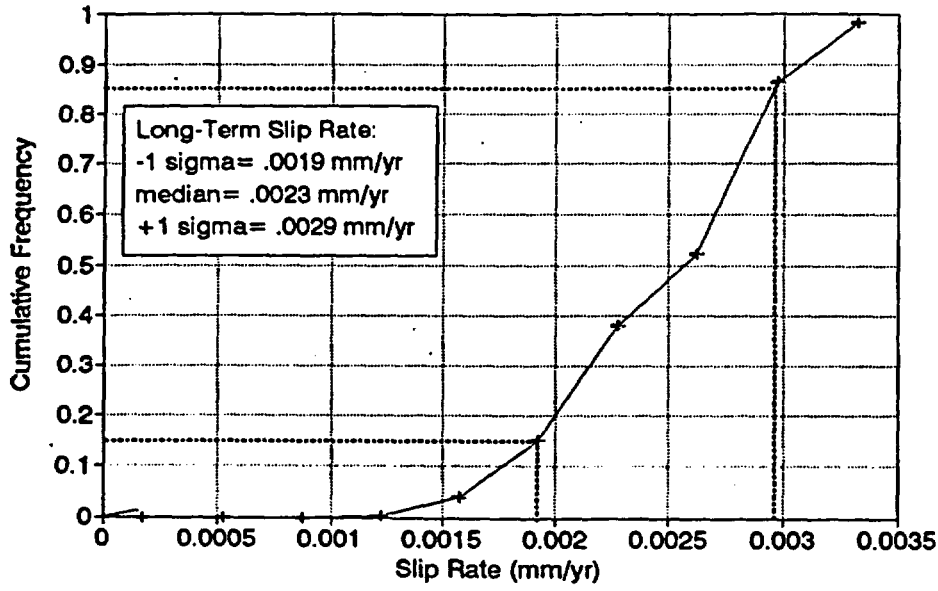


Cumulative Frequency of Long-Term Slip Rates, Bow Ridge fault

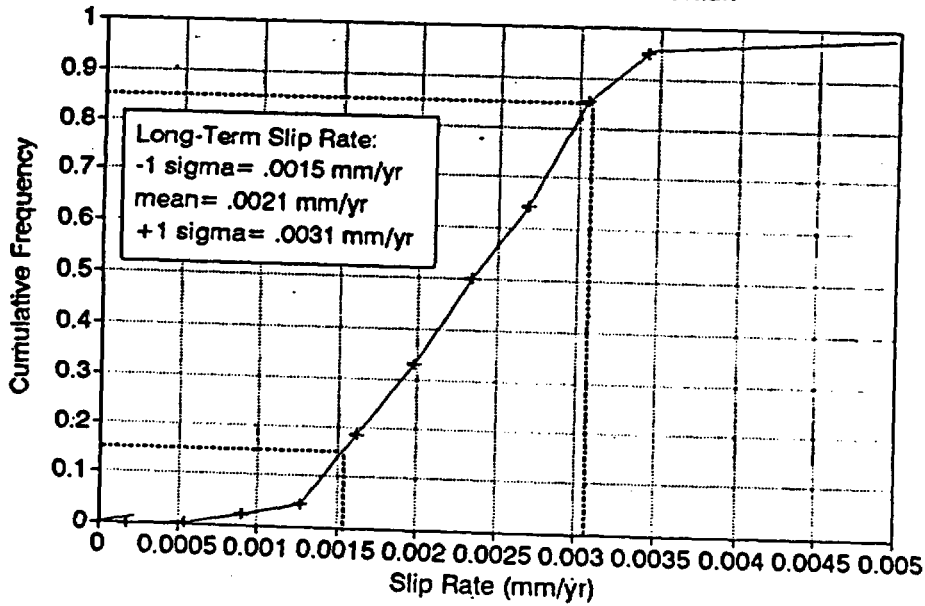


ASM-AI-2

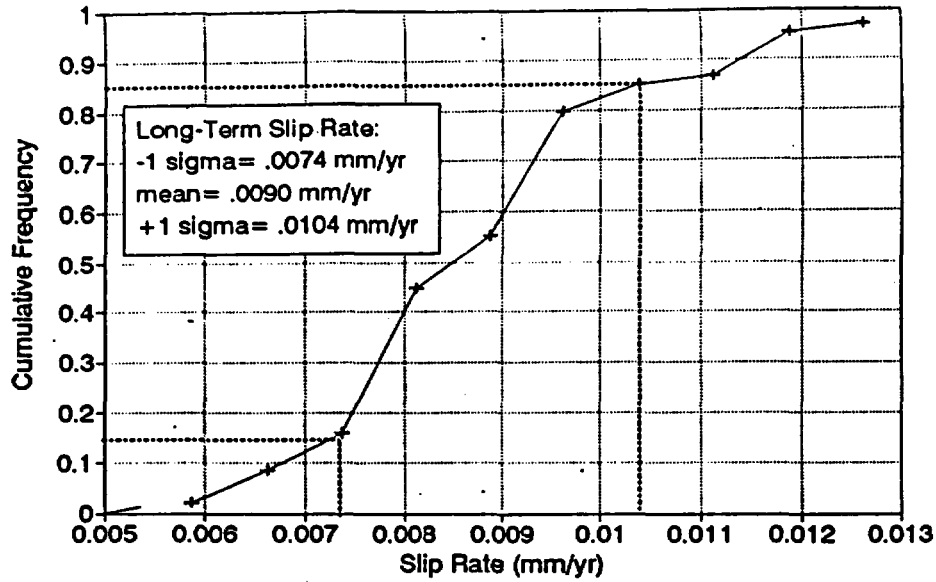
Cumulative Frequency of Long-Term Slip Rates, N. Crater Flat fault



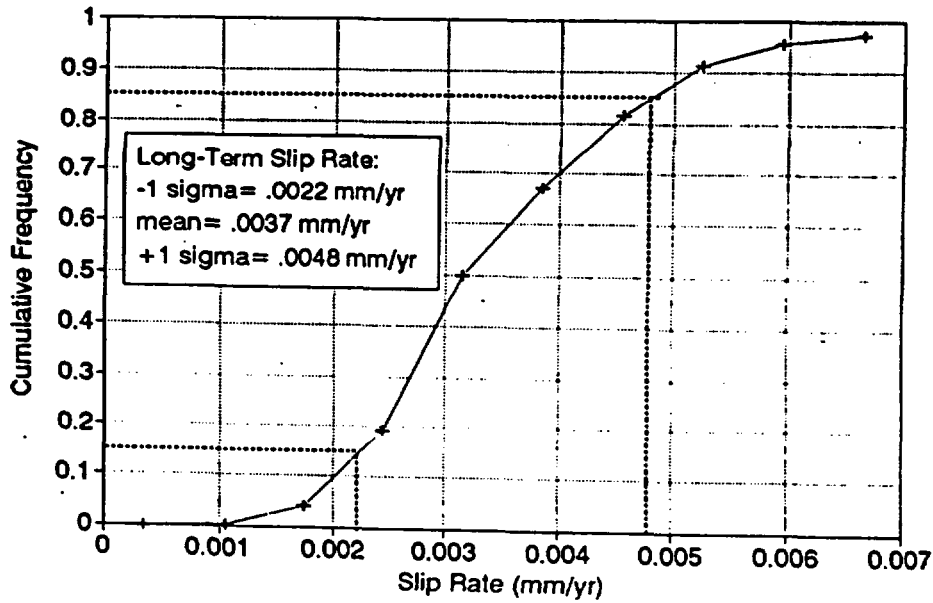
Cumulative Frequency of Long-Term Slip Rates, S. Crater Flat fault



Cumulative Frequency of Long-Term Slip Rates, Fatigue Wash fault

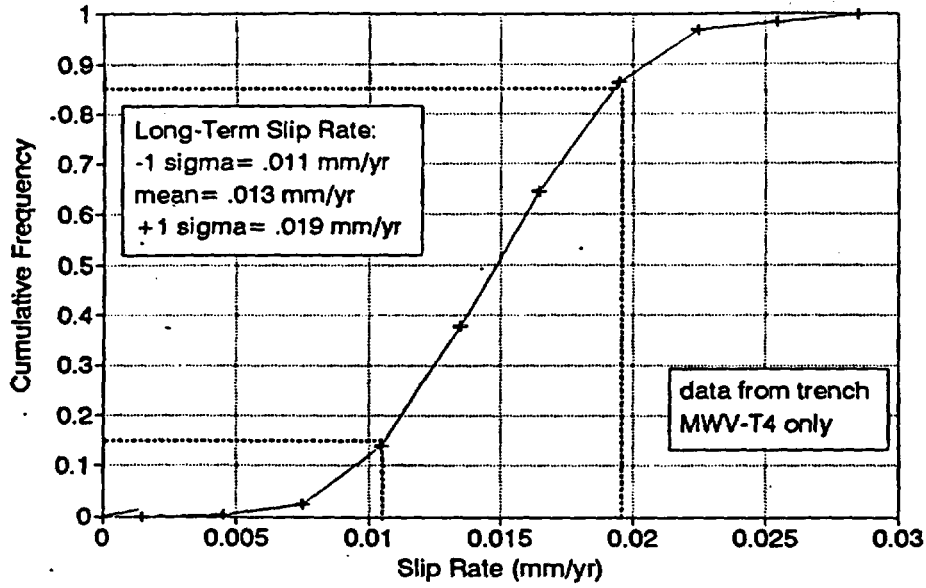


Cumulative Frequency of Long-Term Slip Rates, Iron Ridge fault

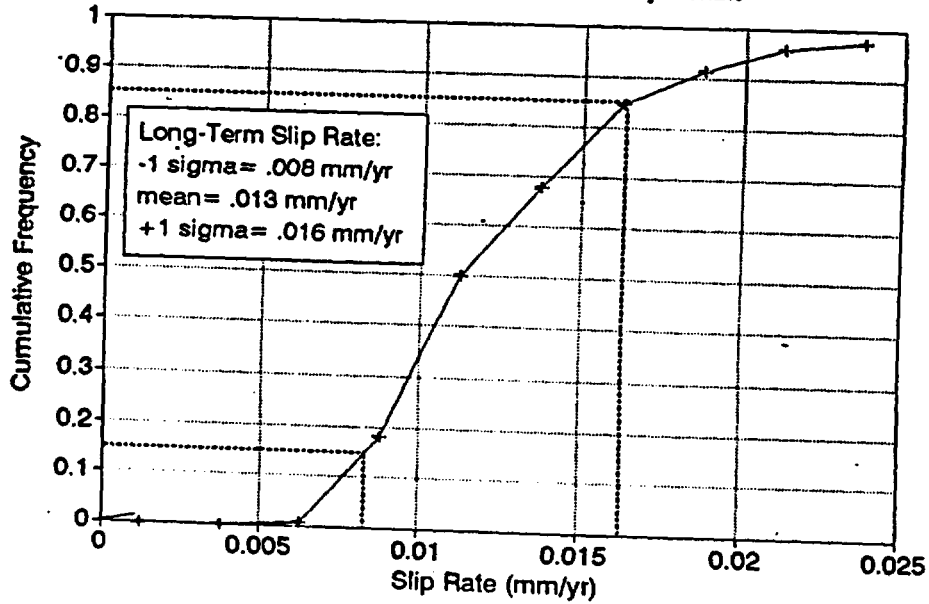


ASM - A1-4

Cumulative Frequency of Long-Term Slip Rates, Paintbrush Cyn. fault

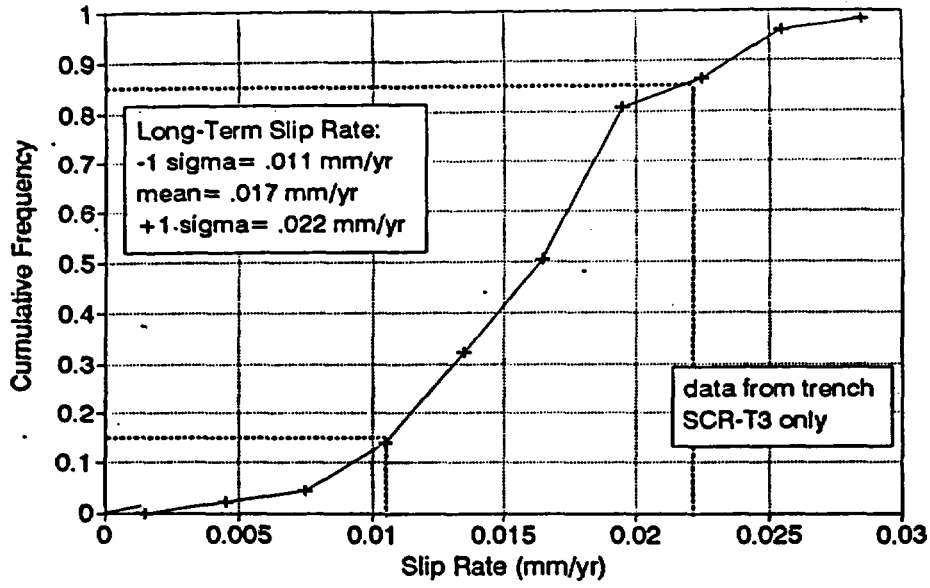


Cumulative Frequency of Long-Term Slip Rates, Solitario Cyn. fault

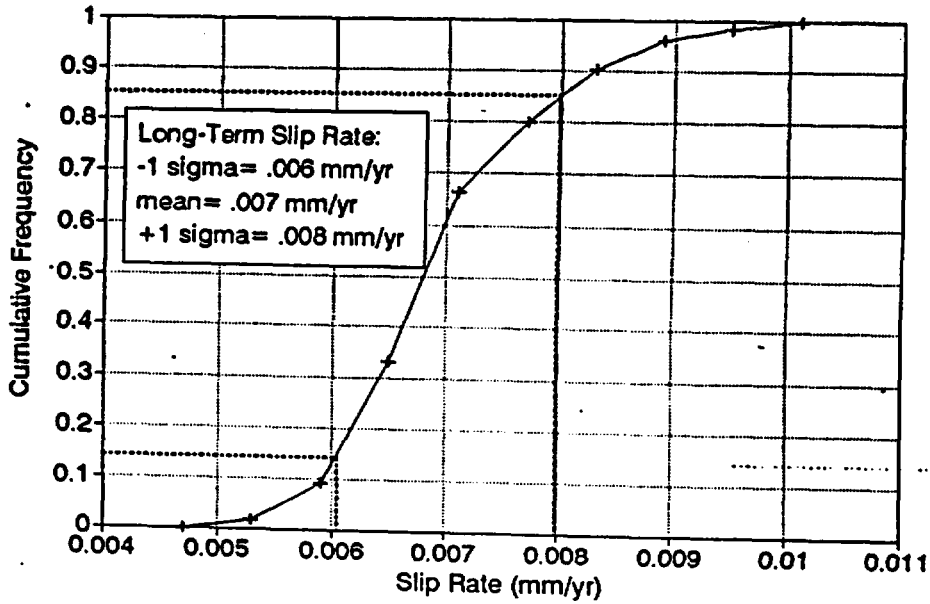


ASM-A1-5

Cumulative Frequency of Long-Term Slip Rates, Stagecoach Rd. fault



Cumulative Frequency of Long-Term Slip Rates, Windy Wash fault

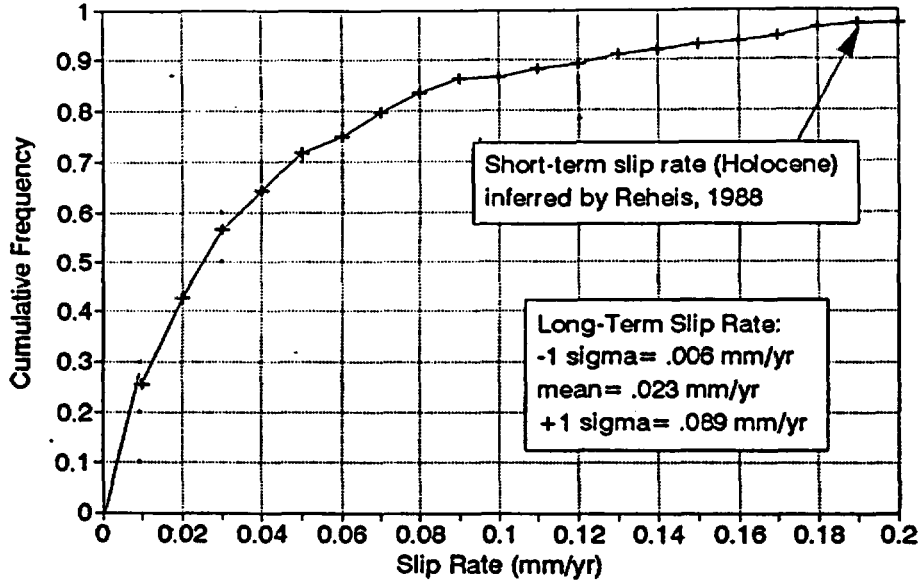


APPENDIX ASM-2

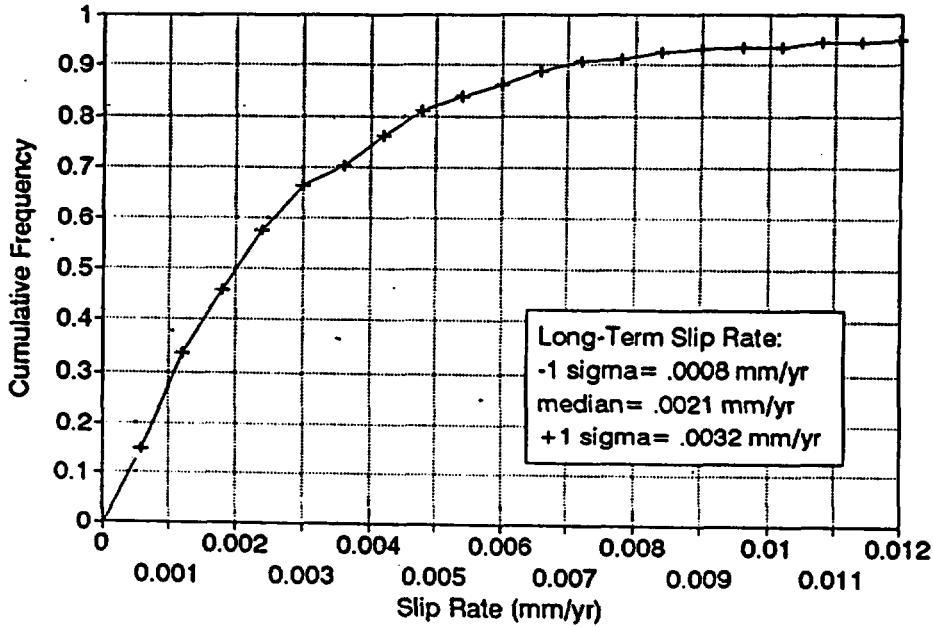
Graphs showing the cumulative frequency of interval slip rates for 10 local Yucca Mountain faults.

Note: these CDFs were computed by creating a normalized-grouped dataset of all interval slip rates on all Yucca Mountain faults, using the method of McCalpin (1995). Then for each of the 10 faults, that CDF was scaled to the long-term slip rate (from Appendix ASM-1) to yield these CDFs.

Final CDF of Slip Rates
Bare Mountain fault

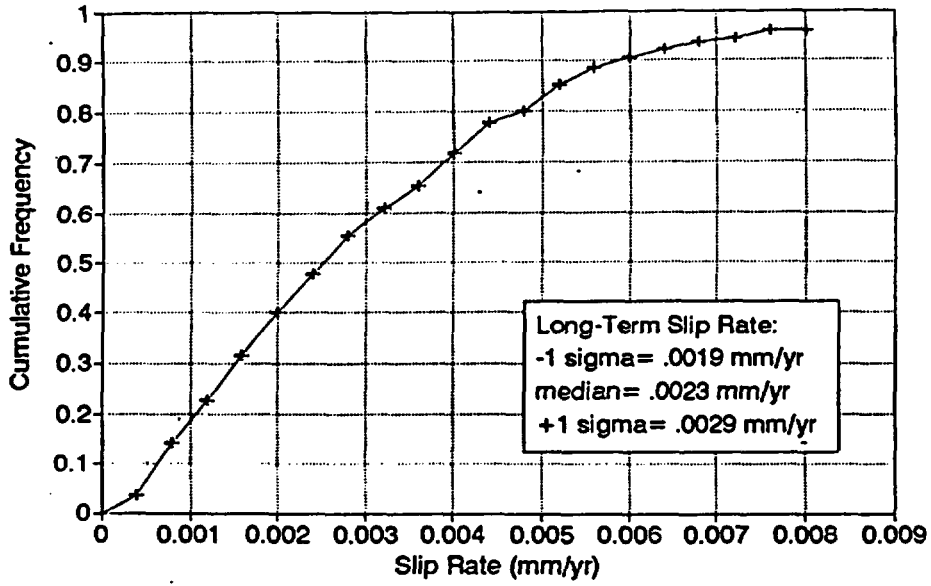


Final CDF of Slip Rates
Bow Ridge fault

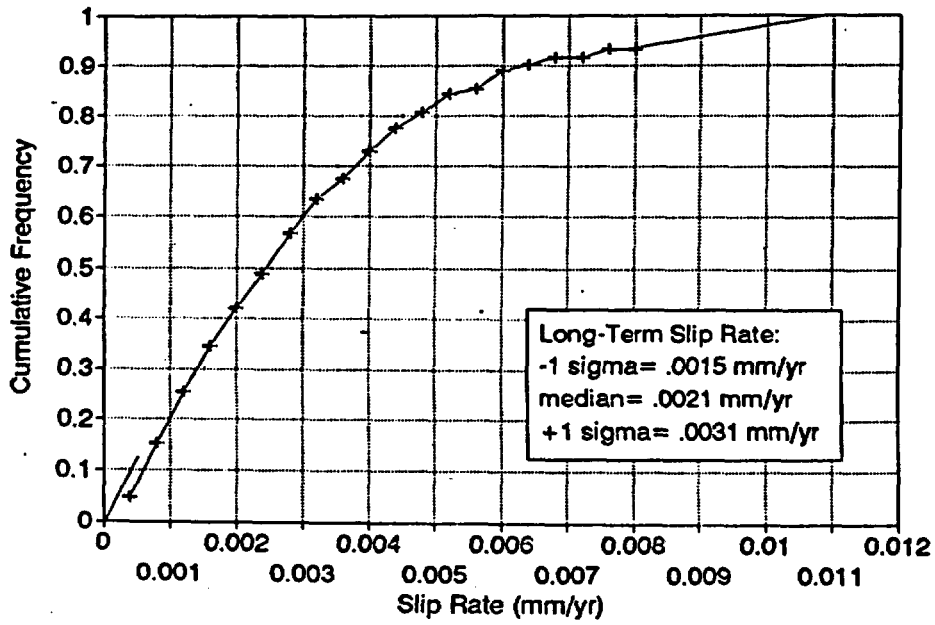


ASM-A2-2

Final CDF of Slip Rates
N. Crater Flat fault

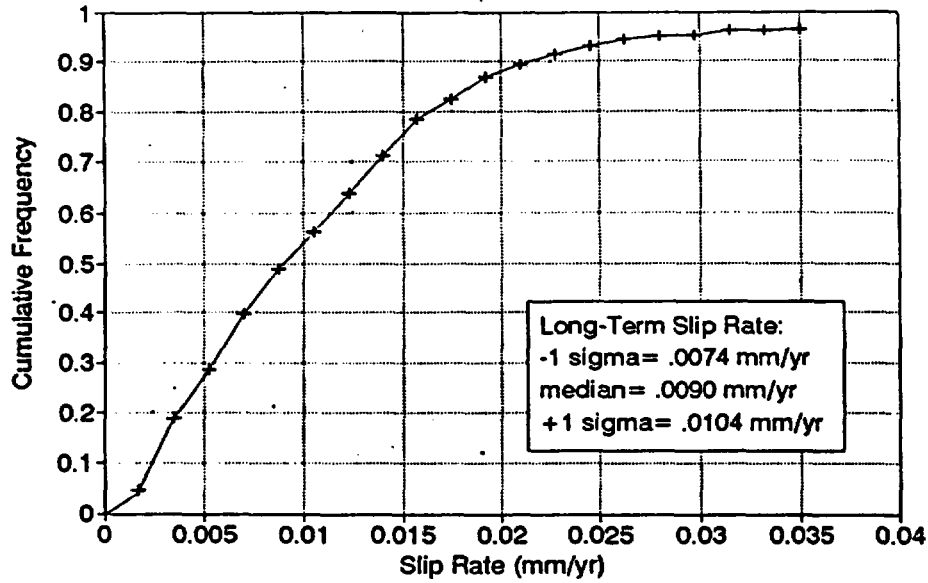


Final CDF of Slip Rates
S. Crater Flat fault

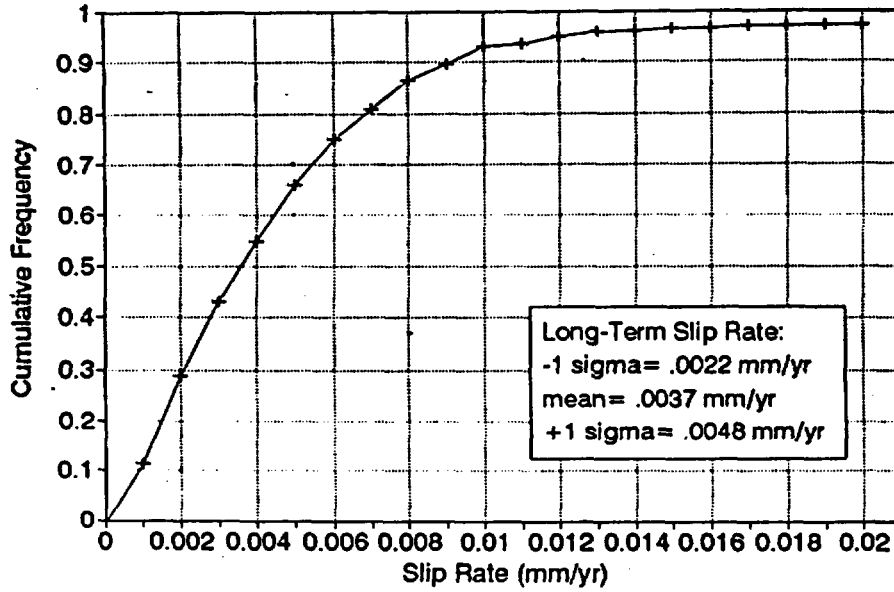


ASM-A2-3

Final CDF of Slip Rates
Fatigue Wash fault

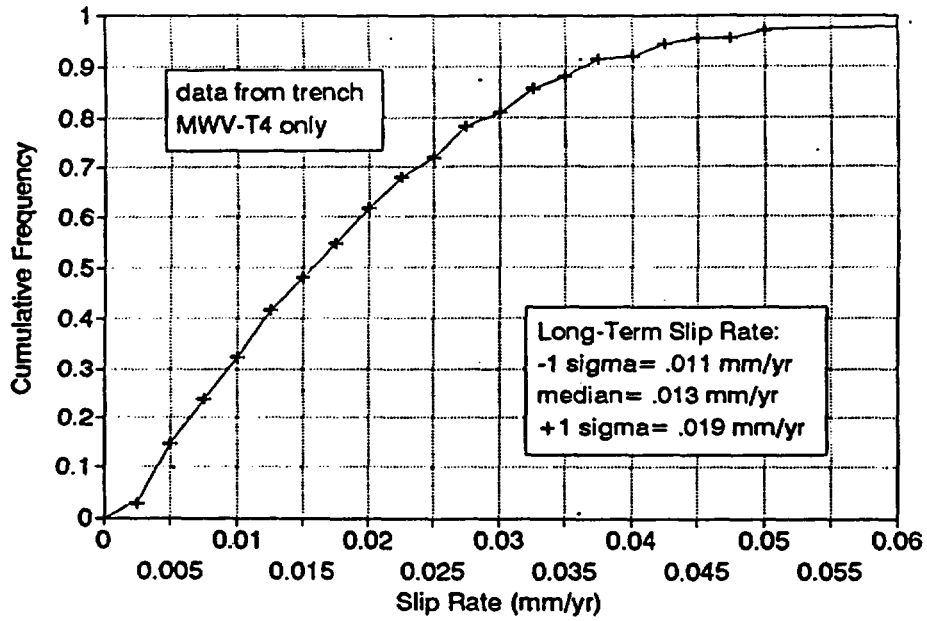


Final CDF of Slip Rates
Iron Ridge fault

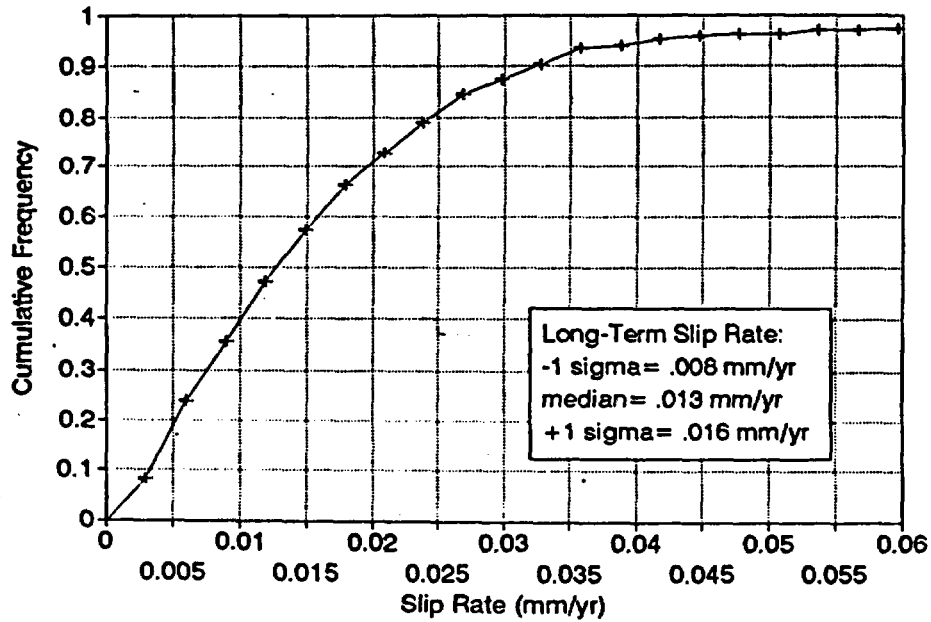


ASM-A2-4

Final CDF of Slip Rates
Paintbrush Canyon fault

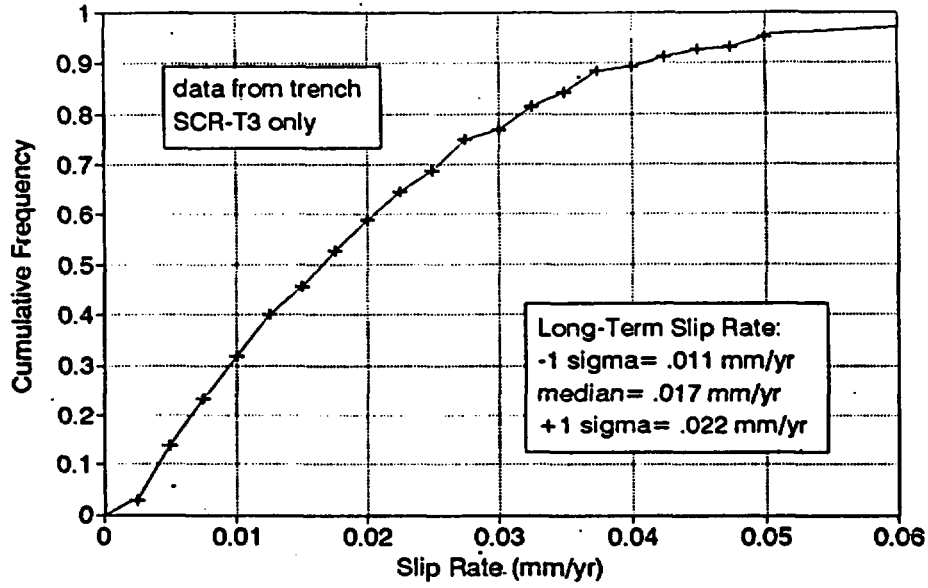


Final CDF of Slip Rates
Solitario Canyon fault

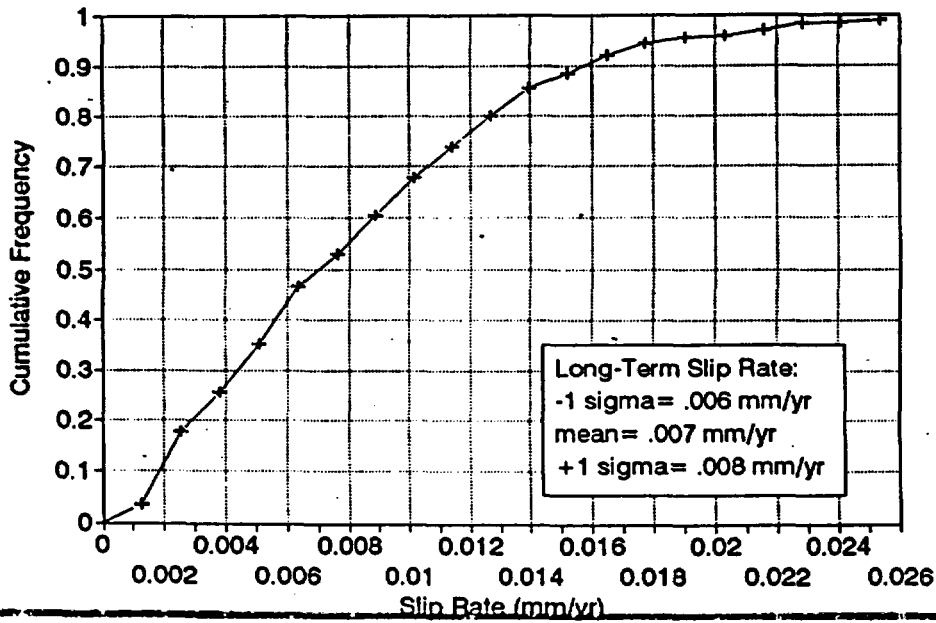


ASM-A2-5

Final CDF of Slip Rates
Stagecoach Rd. fault



Final CDF of Slip Rates
Windy Wash fault



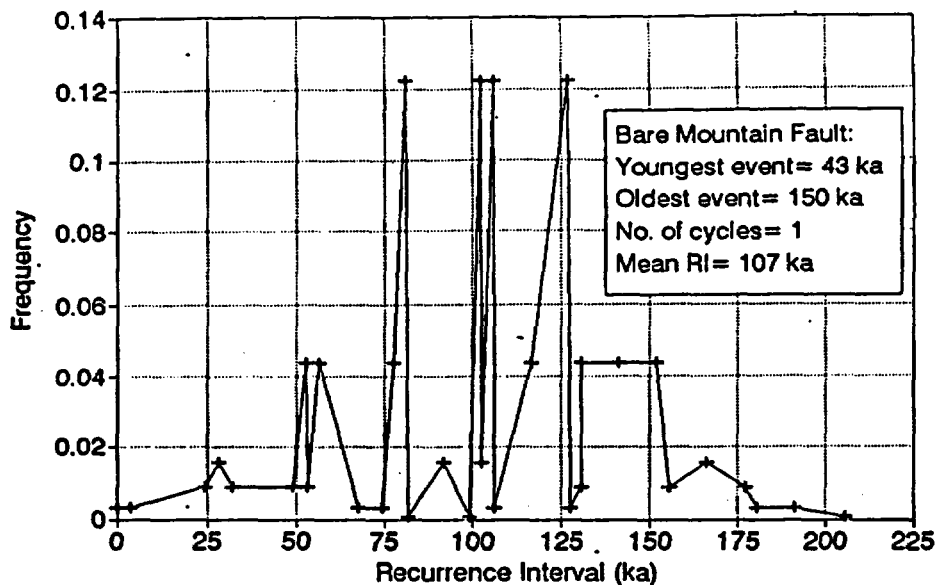
ASM-A2-6

APPENDIX ASM-3

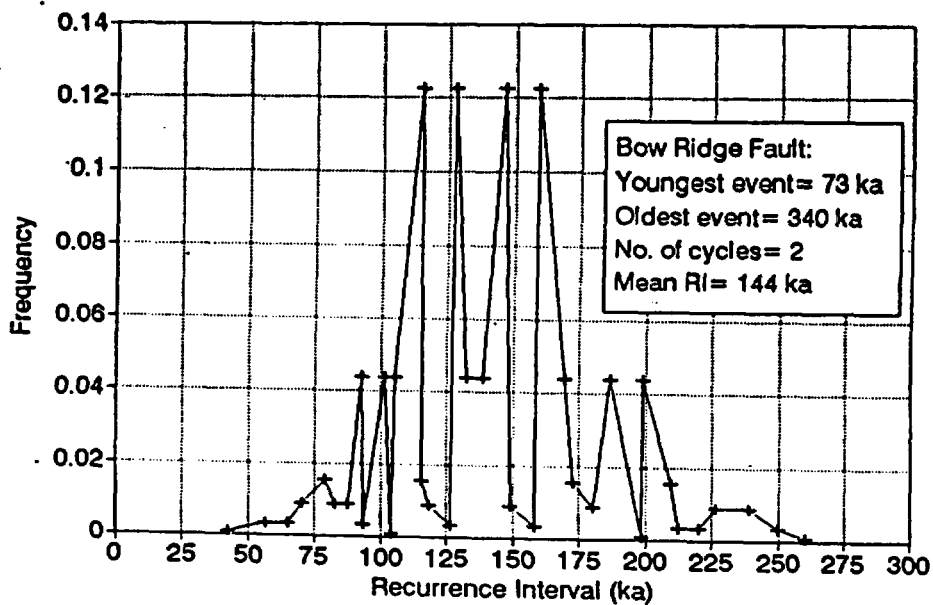
Graphs showing frequency histograms of long-term mean recurrence interval for 10 local Yucca Mountain faults.

Note: these histograms show 36 permutations of long-term mean recurrence interval, based on 6 estimates each of the age of the oldest and youngest dated paleoearthquakes, and the number of seismic cycles between those dates. We assumed that the minimum, preferred, and maximum ages for paleoearthquakes in Table 5-1 of Whitney (1996) represented ± 1 sigma limits. We then split these age values up into a six-part frequency distribution (with symmetrical probabilities of 0.025, 0.125, and 0.35) by linear interpolation (see spreadsheet RI-[fault name].WQZ for actual calculations.)

PDF of Permutations of Long Term
Mean Recurrence Interval

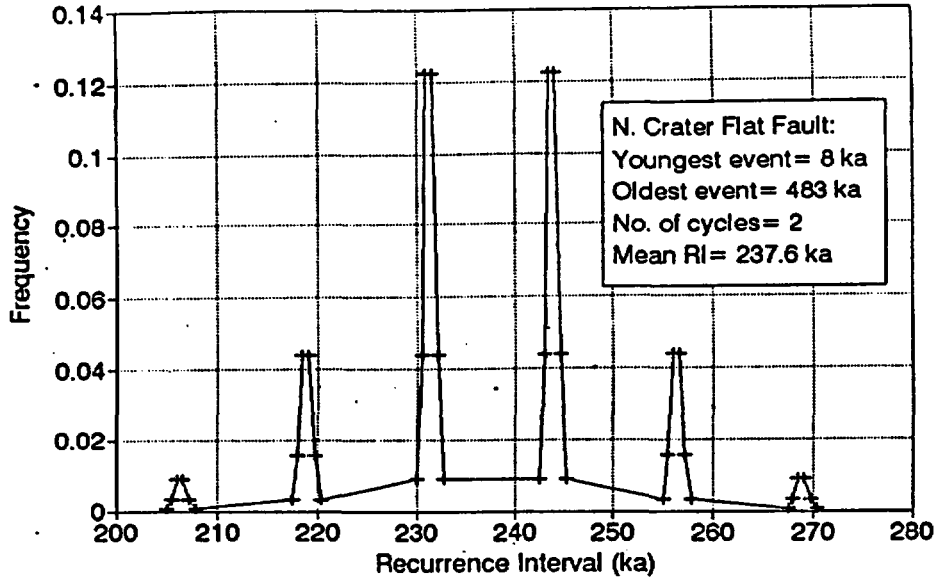


PDF of Permutations of Long Term
Mean Recurrence Interval

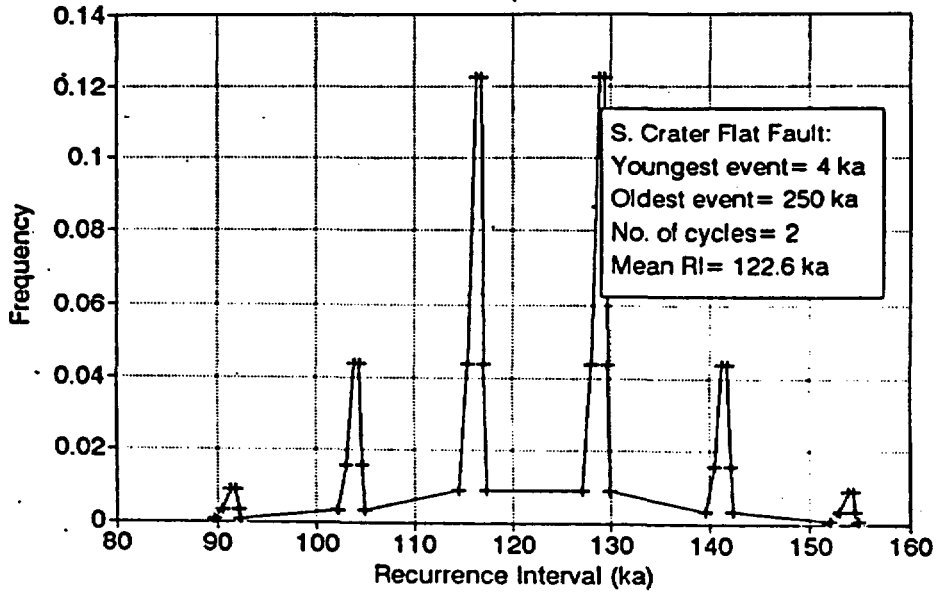


ASM - A3 - 2

PDF of Permutations of Long Term Mean Recurrence Interval

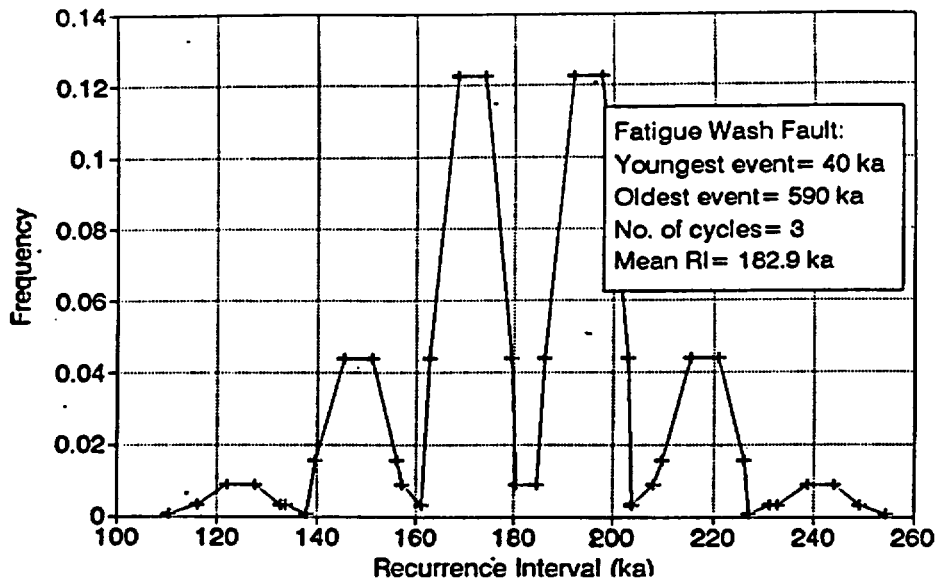


PDF of Permutations of Long Term Mean Recurrence Interval

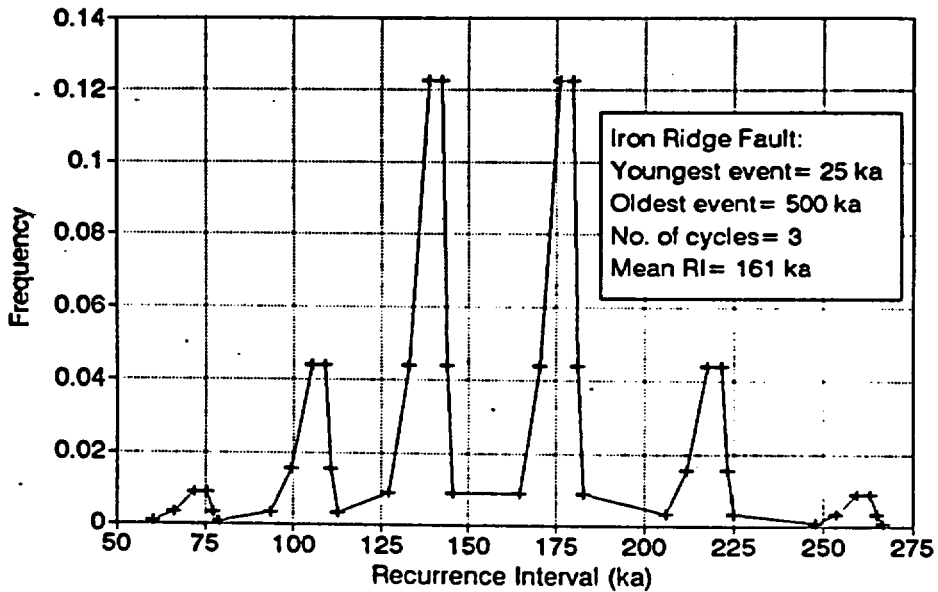


ASM-A3-3

PDF of Permutations of Long Term
Mean Recurrence Interval

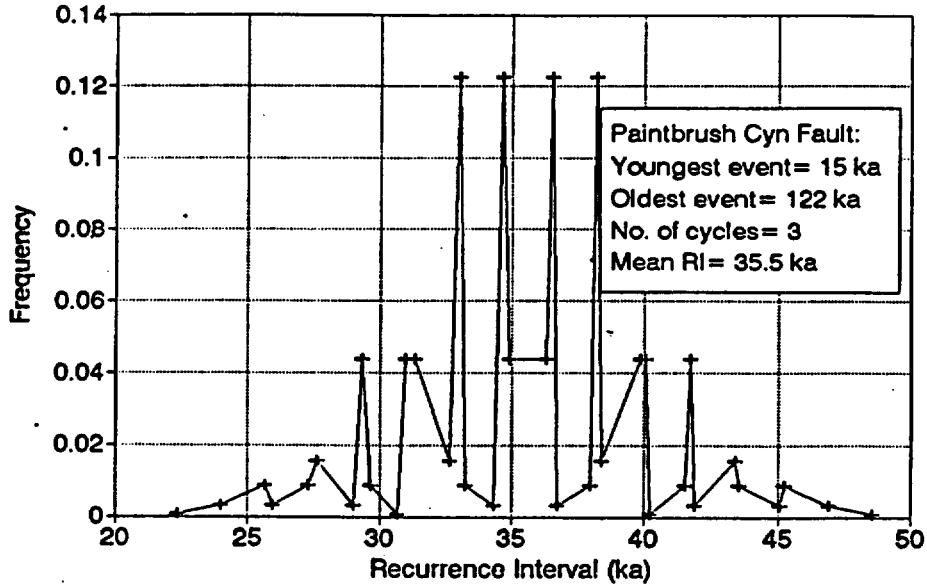


PDF of Permutations of Long Term
Mean Recurrence Interval

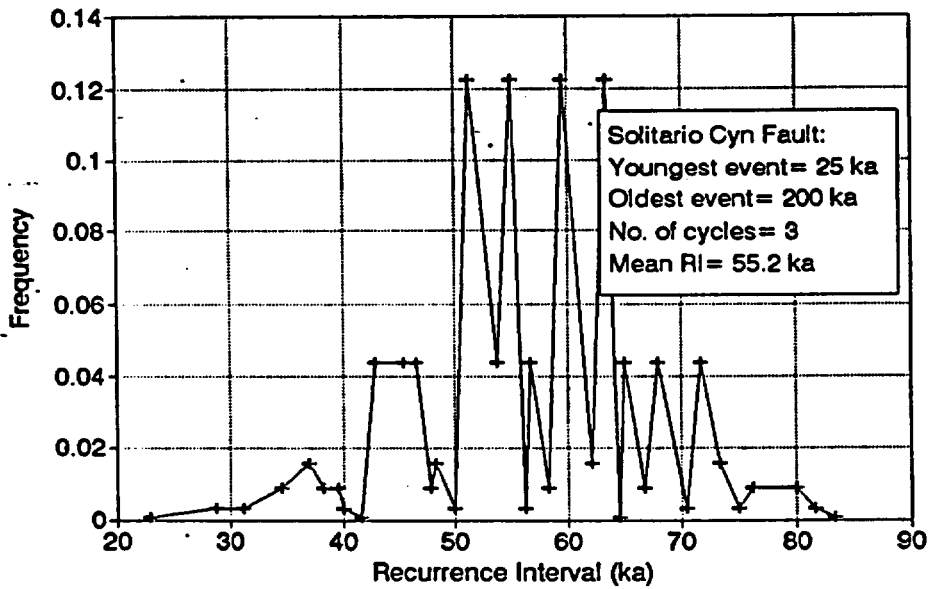


ASM-A3-4

PDF of Permutations of Long Term
Mean Recurrence Interval

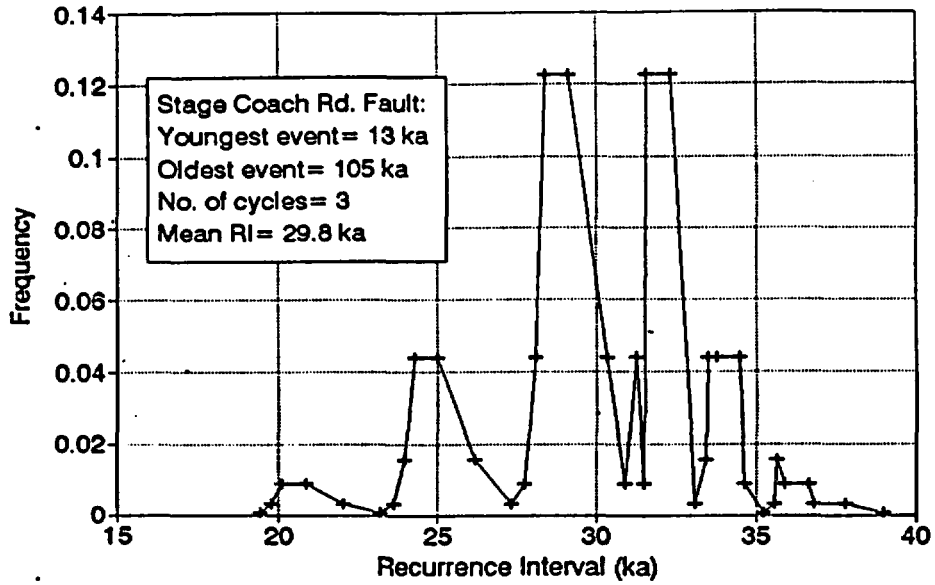


PDF of Permutations of Long Term
Mean Recurrence Interval

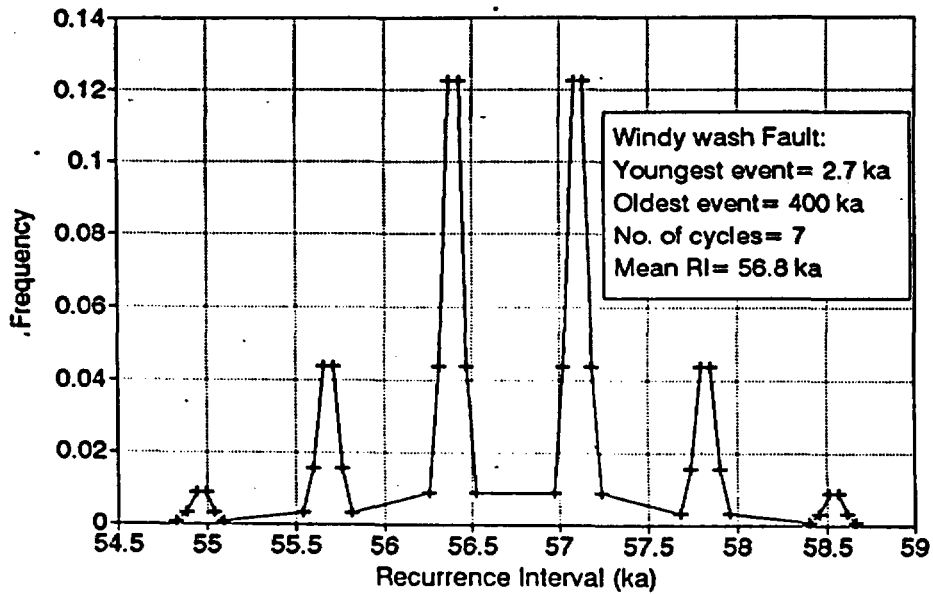


ASM-A3-5

PDF of Permutations of Long Term
Mean Recurrence Interval



PDF of Permutations of Long Term
Mean Recurrence Interval



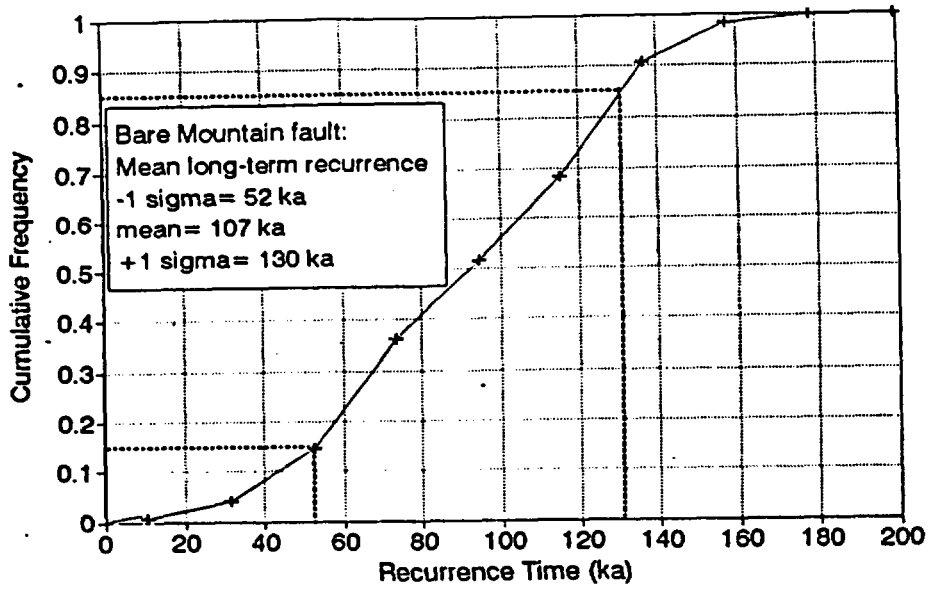
ASM-A3-6

APPENDIX ASM-4

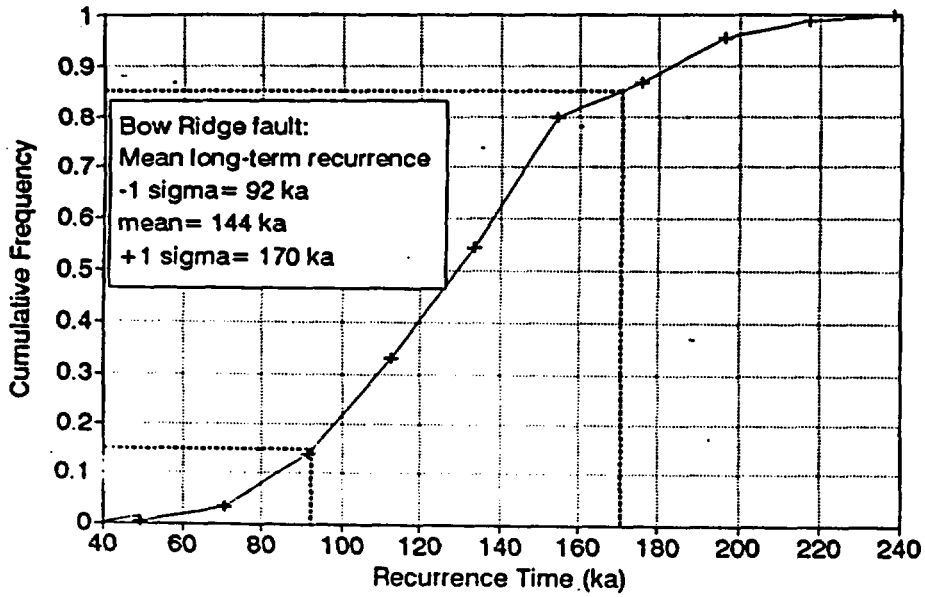
Graphs showing cumulative frequency distributions of long-term mean recurrence interval for 10 local Yucca Mountain faults.

Note: these CDFs were derived from the PDFs of Appendix ASM-3.

Cumulative Frequency of Long-Term Mean Recurrence Time

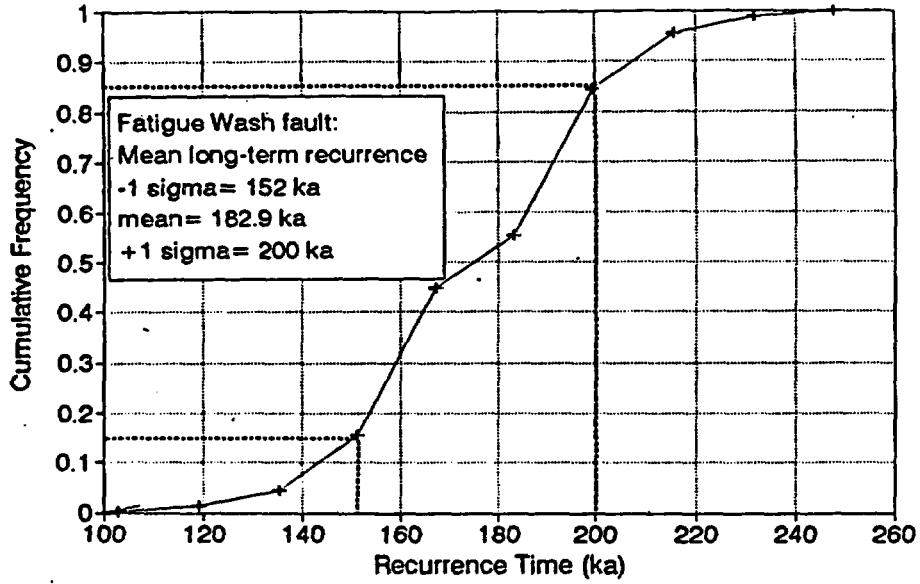


Cumulative Frequency of Long-Term Mean Recurrence Time

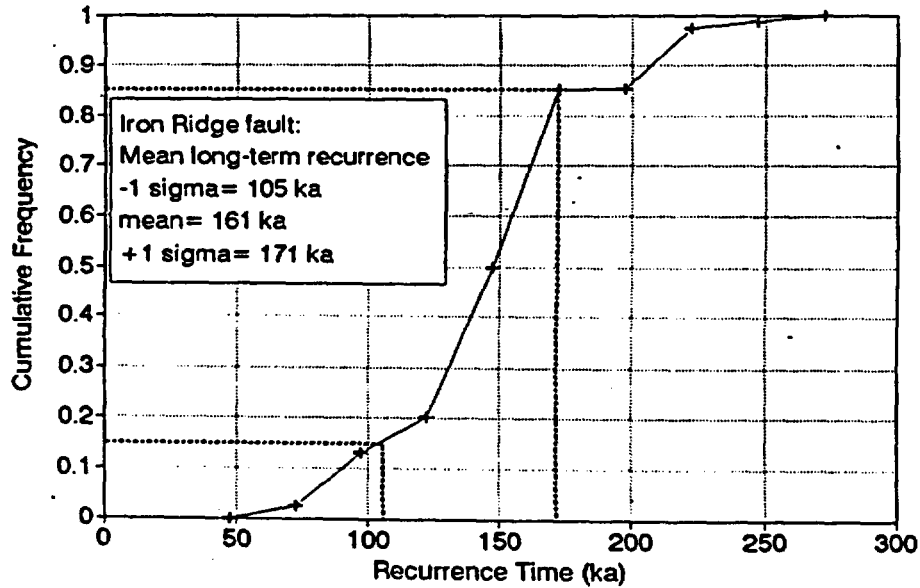


ASM-A4-2

Cumulative Frequency of Long-Term Mean Recurrence Time

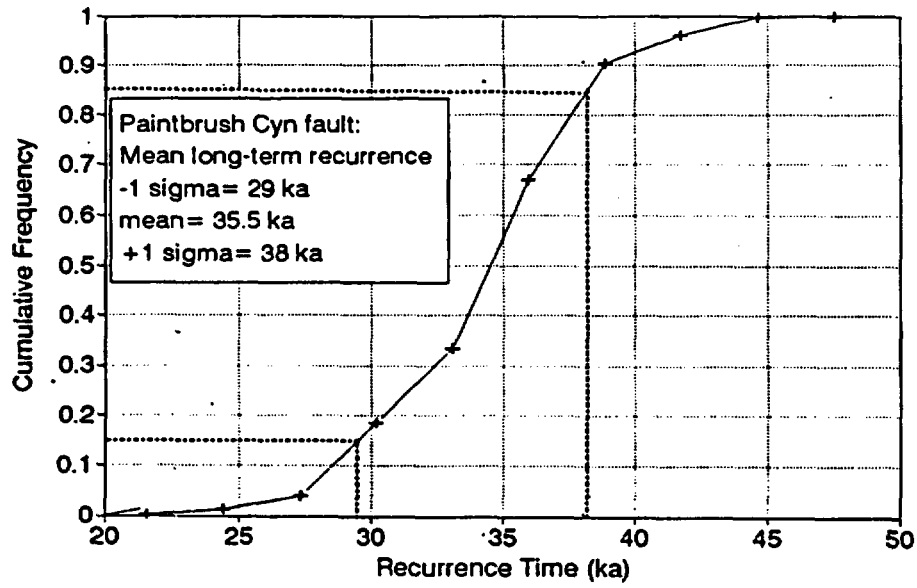


Cumulative Frequency of Long-Term Mean Recurrence Time

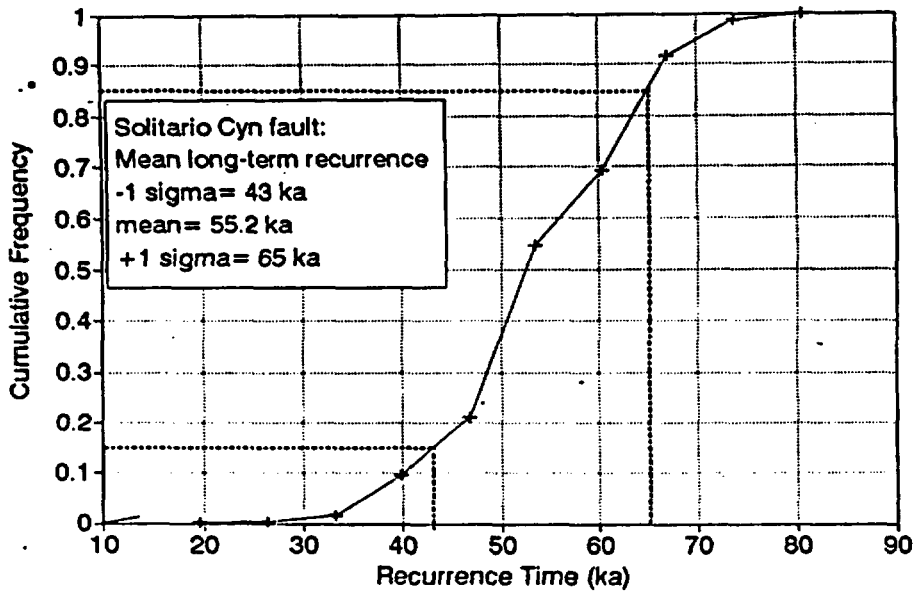


ASM-A4-3

Cumulative Frequency of Long-Term
Mean Recurrence Time

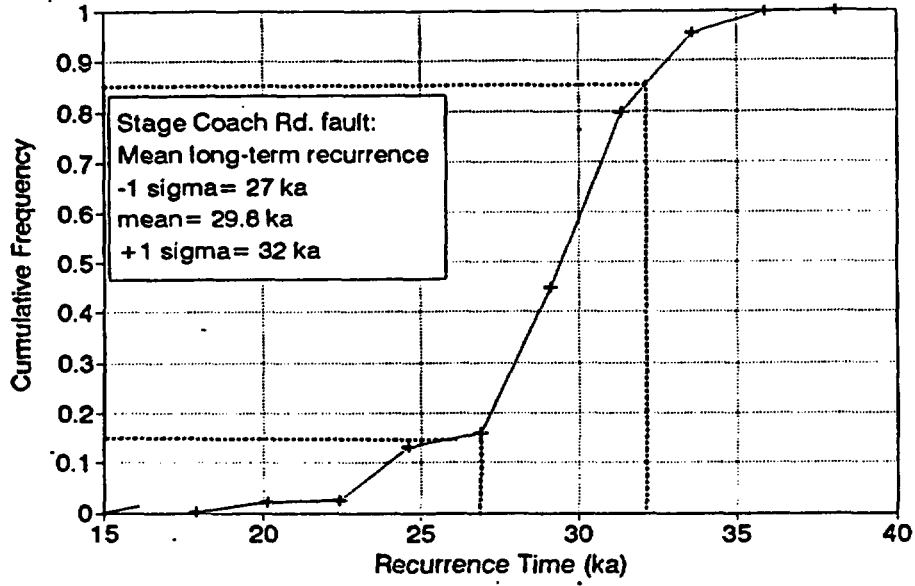


Cumulative Frequency of Long-Term
Mean Recurrence Time

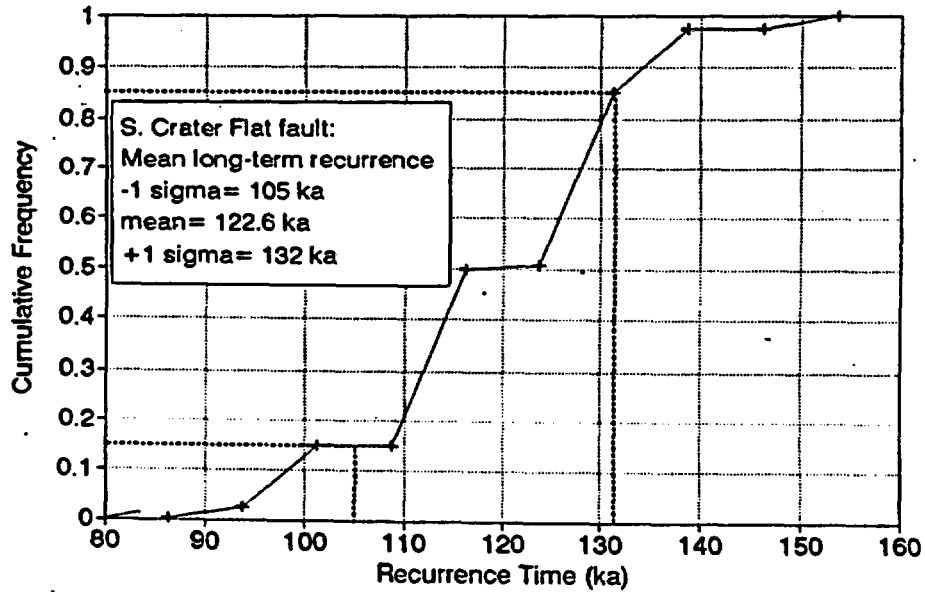


ASM-A4-4

Cumulative Frequency of Long-Term Mean Recurrence Time

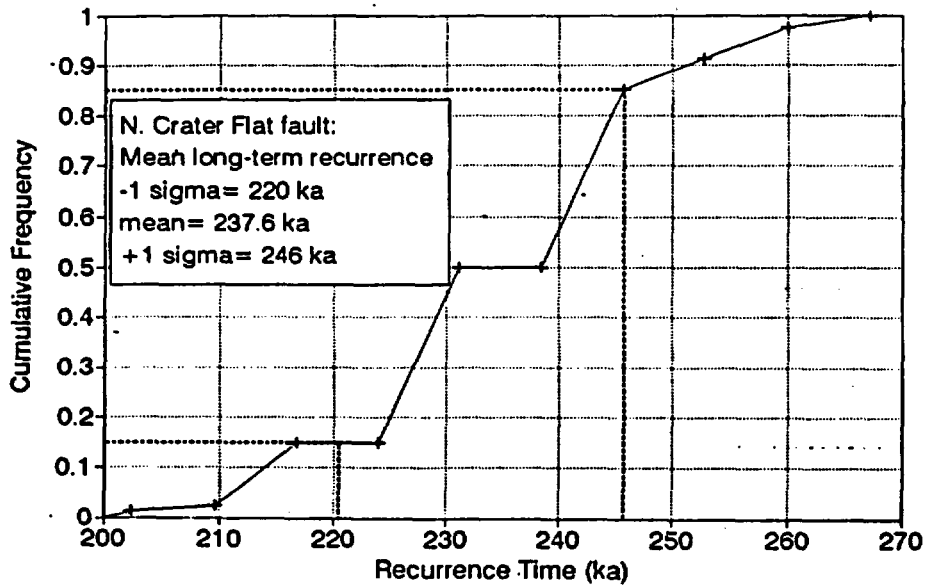


Cumulative Frequency of Long-Term Mean Recurrence Time

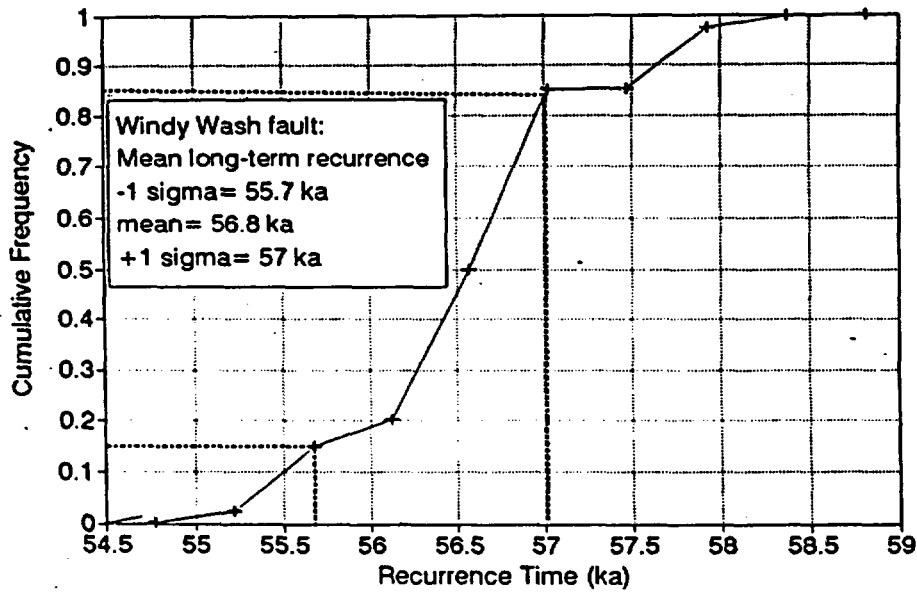


ASM-A4-5

Cumulative Frequency of Long-Term Mean Recurrence Time



Cumulative Frequency of Long-Term Mean Recurrence Time



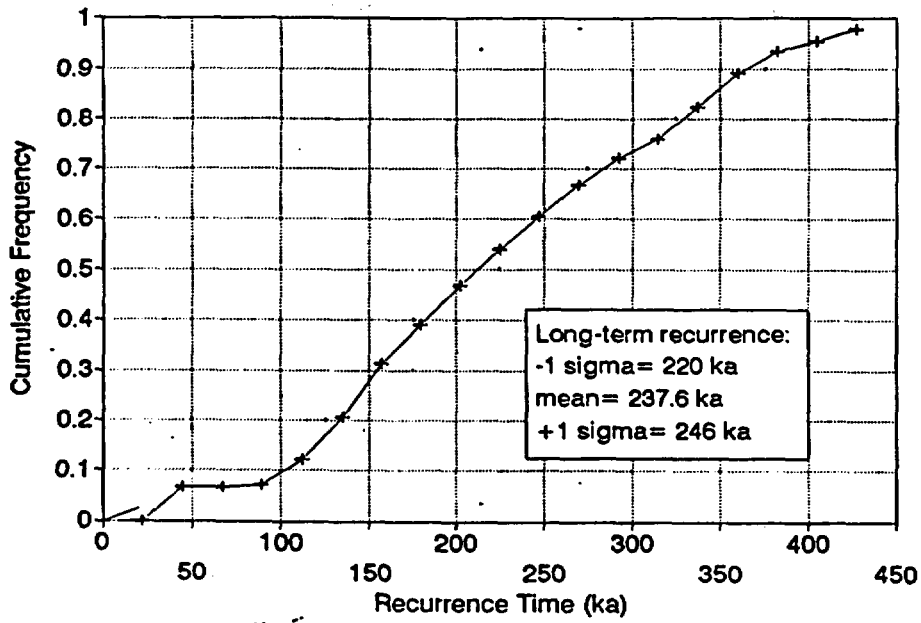
ASM-A4-6

APPENDIX ASM-5

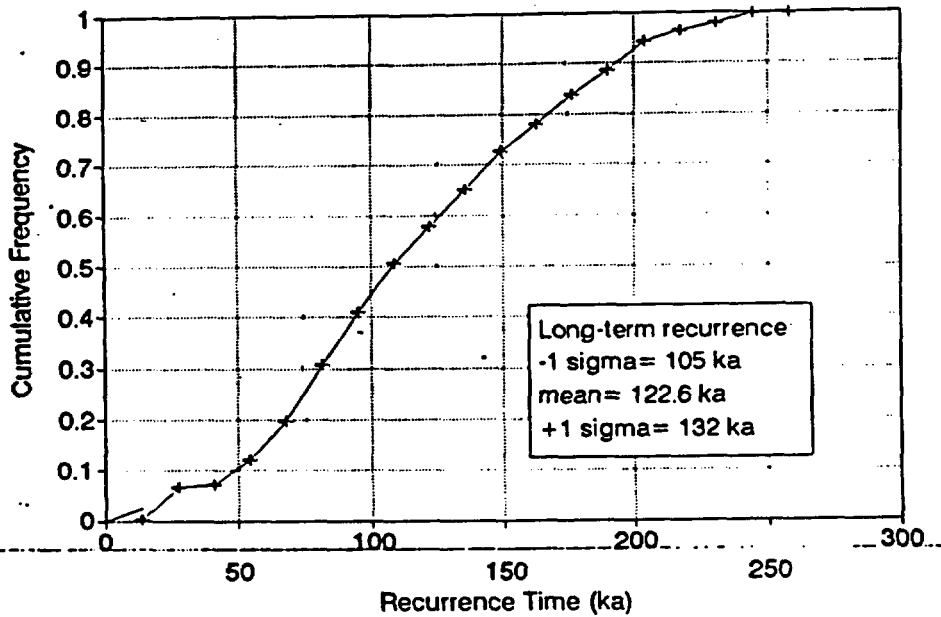
Graphs showing cumulative frequency distributions of individual recurrence intervals for 10 local Yucca Mountain faults.

Note: these CDFs were created by scaling the normalized-grouped CDF of recurrence to the long-term mean recurrence interval of each fault, in the same manner as done for slip rates (Appendix ASM-2).

Final CDF of Recurrence Times
N. Crater Flat fault

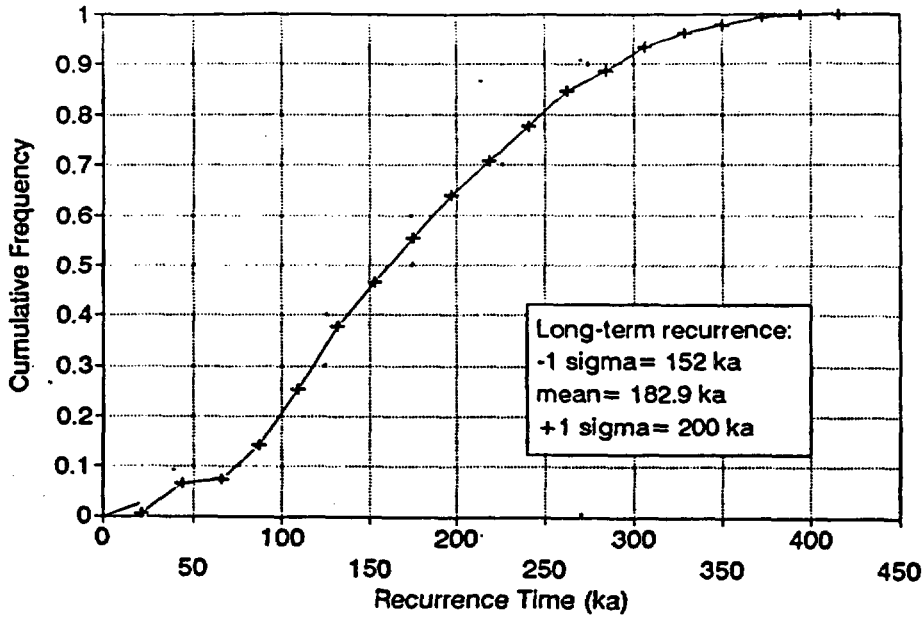


Final CDF of Recurrence Times
S. Crater Flat fault

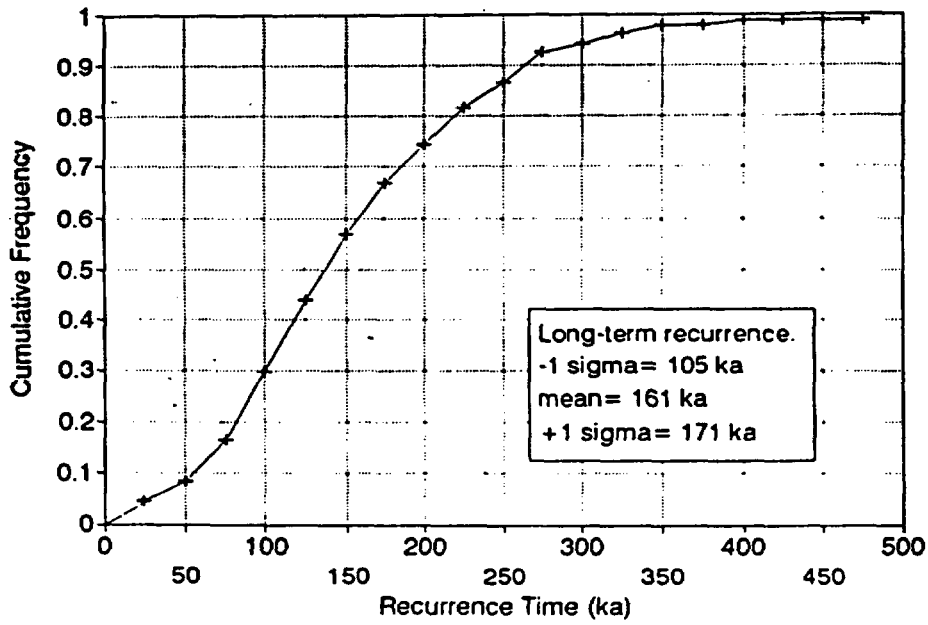


ASM-A5-3

Final CDF of Recurrence Times
Fatigue Wash fault

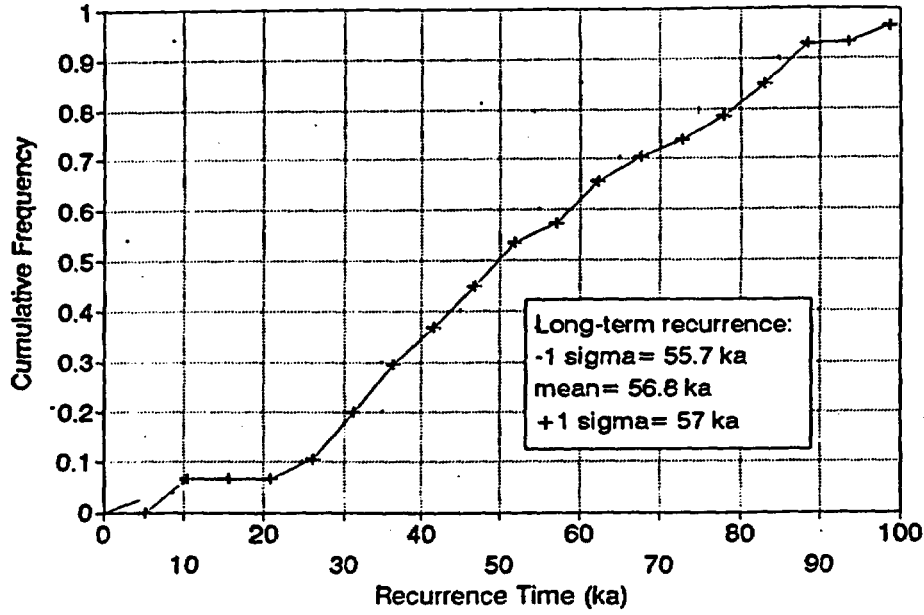


Final CDF of Recurrence Times
Iron Ridge fault

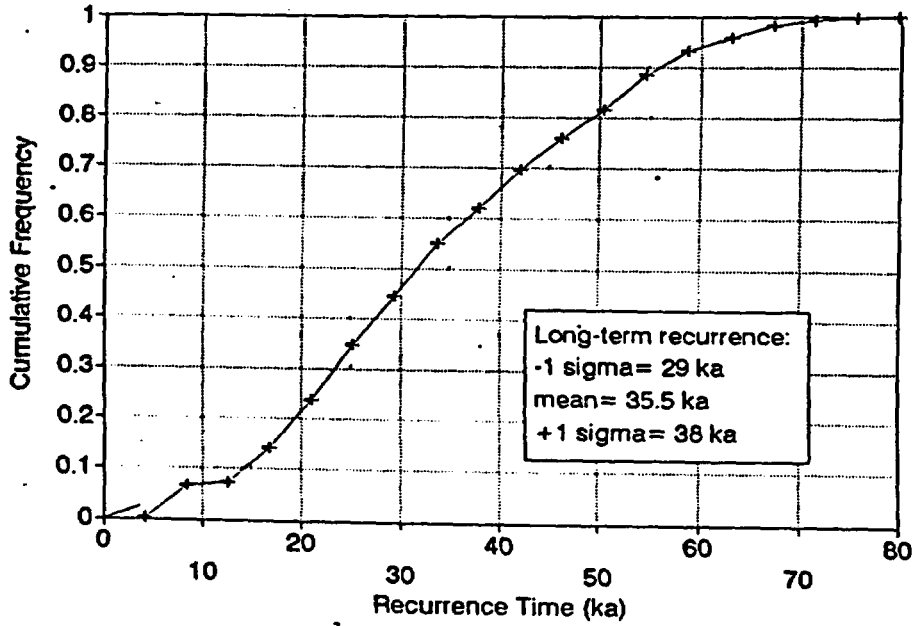


ASM-AS-4

Final CDF of Recurrence Times
Windy Wash fault



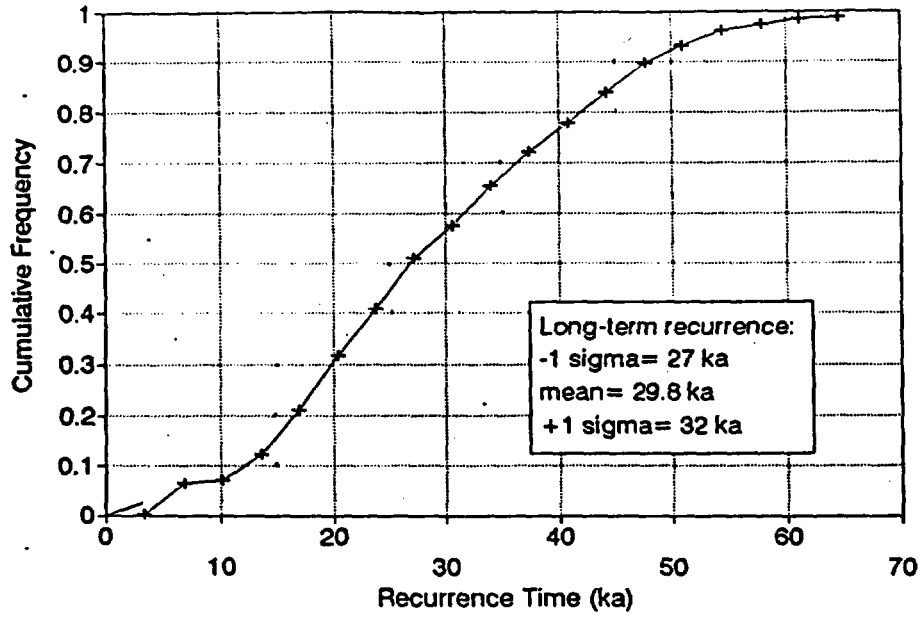
Final CDF of Recurrence Times
Paintbrush Cyn fault



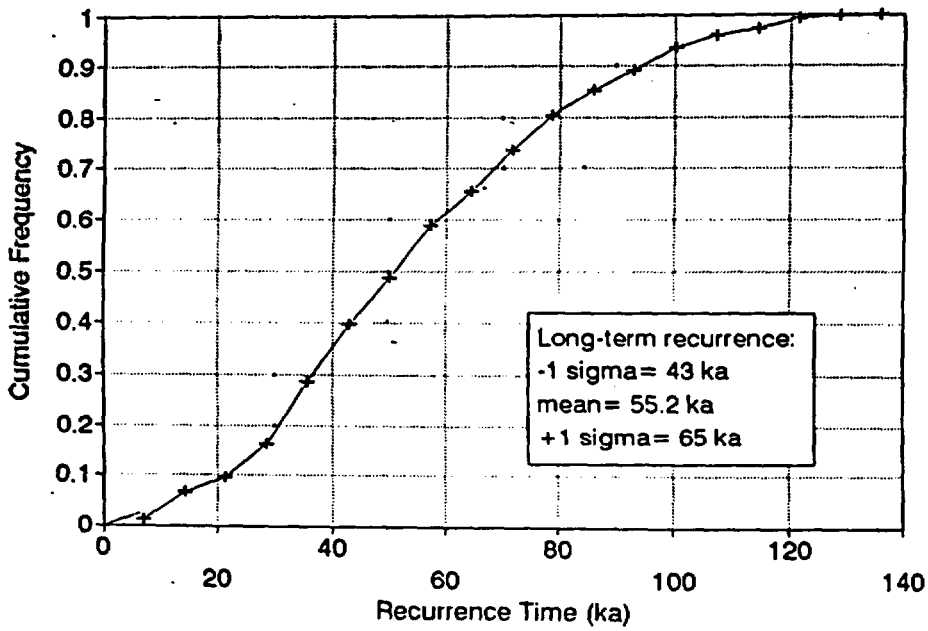
3

ASM-A5-5

Final CDF of Recurrence Times
Stage Coach Rd. fault



Final CDF of Recurrence Times
Solitario Cyn fault



2.2

ASM-AS-6

APPENDIX ASM-6

REGIONAL SEISMIC SOURCE CHARACTERIZATION

The following notes document decisions on the fault characteristics and probabilities for 24 faults listed in Table ASM-6, which summarizes the relevant regional earthquake sources for the Yucca Mountain region. The 15 faults having names shown in *italic font* have substantial field data, or correlate with faults that have substantial field data, for estimating slip rate (SR), recurrence interval (RI), and approximate surface rupture length (SRL). The 9 faults having names shown in normal font have sparse characterization data; for these we use the method described in Sections 3.5.3 and 3.5.4 to estimate SR from SRL and RI from the estimated age of the faulted geomorphic surfaces summarized in Piety (1995), Reheis (1992), Reheis and Noller (1991), and Dohrenwend et al. (1992a and 1992b).

1. H95, Carrara, or U.S. 95. The Carrara fault (also referred to as the Highway 95 fault) is informally characterized. It is not referred to in the main documentation available to the team, but is described briefly in the letter of David B. Slemmons (DBS) to Richard Quittmeyer of February 3, 1997. This document lists geologic, geomorphologic, and geophysical features that indicate that it is a Quaternary fault, including the following.
 - (1) William D. Nichols' (1987) description of drill holes and geophysical surveys indicates Pleistocene fault deformation along an unnamed northwest structure.
 - (2) Low-angle aerial reconnaissance by DBS showed many features that appeared to result from Quaternary faulting.
 - (3) The horizontal gravity gradients shown at SSC Workshop 3 exhibit a linearity that appears to be fault-controlled.
 - (4) The feature is within 2 km of the Lathrop Cone.
 - (5) The feature may explain vertical axis rotation at the south end of Yucca Mountain, and Bullfrog Hills.

- (6) Gilmore's geodetic profile as summarized by Pezzopane (SSC Workshop 2) shows an anomalous segment of the Beatty-Las Vegas geodetic level line that coincides with the Carrara feature.
- (7) Ken Smith (SSC Workshop 2) showed that it is aligned along a belt of higher seismicity.
- (8) Brocher et al. (SSC Workshop 3) showed a seismic reflection profile, aeromagnetic map, and isostatic gravity map had a NW-trending fault at U.S. Highway 95.
- (9) The M&O Geophysics Synthesis Report (1996) showed a prominent arcuate structure along the Carrara feature, which appears to curve into the Rock Valley structural zone near Skull Mountain.
- (10) Fridrich and Price (1992) inferred this fault south of Bare Mountain and Yucca Mountain on the basis of geologic and geophysical data.
- (11) Quade and others (1995) and oral discussions with Quade indicate the Carrara/Highway 95 feature is at the 13,100 ¹⁴C yr (and earlier Quaternary) diatomaceous spring deposits, which appear to be from deeply circulating groundwater that emerged at a Pleistocene groundwater barrier just west of the southward extension of the Crater Flat fault.

We assign a high probability (0.85) for the Carrara fault being seismogenic based on these factors. We assign a low probability (0.15) of the fault being non-seismogenic, since the fault has not been thoroughly characterized. The abrupt truncation of all of the seismogenic, NS-trending faults between the Bare Mountain fault and the southeast end of Yucca Mountain at the Carrara fault also suggests that it is an active Quaternary fault. Two total fault lengths (20 and 42 km) are considered with equal weight. The shorter length of 20 km represents the northwest part of the fault (from the Amargosa River to U.S. Highway 95 and the southward projection of Windy Wash fault) that exhibits greater geomorphic expression. Extension of the fault an additional 22 km to east of Lathrop Wells (Amargosa Valley) is less certain. A lower probability of 0.5 is assigned to the 42-km length, which extends the fault eastward from the 20-km section that has geomorphic expression. The 10-km-long extension at the south end of Yucca Mountain lacks documented geomorphic evidence of Quaternary activity, but is marked by the abrupt truncation of Yucca Mountain. The change to a more east-west trend east of the Windy Wash intersection could indicate a decrease in rate of activity. The additional 12-km

extension east of Yucca Mountain is an assumed feature that is based on the geophysical map showing depth to bedrock. The M_{wmax} values depend on SRL and are: $M_{wmax}=6.94$ (for $SRL=42$ km), $M_{wpref}=6.64$ ($SRL=20$ km, with a high probability of 0.7), and $M_{wmin}=6.24$ ($SRL=10$ km, with a low probability of 0.2). Although there is a component of vertical slip, the Carrara fault is characterized as a strike-slip fault. The uplifted block has a relief of about 22 m at U.S. Ecology, where Jim Yount reports that the upper surface appears to have a late Pleistocene soil (128 ka), which corresponds to a vertical separation rate >0.1 mm/yr. The estimates for the horizontal component of SR of 0.013 (0.2), 0.05 (0.6), and 0.12 (0.2) mm/yr are from the Crater Flat subparallel extension rate used for our detachment model.

2. MM, Mine Mountain. This fault is characterized as a strike-slip fault. This fault is truncated by Yucca Lake fault (YCL) and possibly by a fault at the boundary with Jackass Flat. $M_w=6.64$ for $SRL=20$ km (based on Plate 1 of Piety (1995)). Based on the northern truncation by YCL and an inferred fault along the northern edge of Jackass Flat, a total fault length of 20 km is used. Two SRL values (10 and 20 km) are given equal weight. Reheis and Noller (Y-238) list the 3-km segment as "a weakly to moderately expressed lineament or scarp on surfaces of Quaternary deposits and as a topographic lineament along a range front or in bedrock." SR and RI are inferred from SRL and assumption of three pre-Holocene surface rupturing earthquakes.
3. WAH, Wahmonie. This fault is characterized as an oblique-slip fault. $M_w=6.42$ for $SRL=14.5$, based on Plates 1 and 2 in Piety (1995). Data primarily from Plate 1. Based on the truncation by the Cane Springs fault (CS), a single value of SRL (14.5) is used (weight 1.0). Reheis and Noller (1991) report "weakly expressed to prominent scarps and lineaments." Oral discussions with Jim Yount indicate late Pleistocene activity at the north end of the fault. SR and RI are inferred from SRL and assumption of three pre-Holocene surface rupturing earthquakes.
4. AM, Ash Meadow. This fault is characterized as a west-dipping normal fault. $M_w=6.24$, 6.91, and 6.94, respectively for $SRLs=10, 38, \text{ and } 40$ km. This fault was at a shallow water table during Pleistocene, and the surface effects may be by partly plastic behavior.

Revised on Figure 13 of Anderson et al. (1995b). Preferred length is 38 km from north end near Amargosa River (AR); scarp about 14 km SE of Nevada Highway 373 and Stateline, which Anderson et al. (1995b) notes may be a northern extension of West Resting Spring Range (WRSR) fault. The fault has fair, but incomplete, characterization data. Although the original mapping of Donovan shows three segments, the displacement values tabulated in Anderson et al. (1995b) suggest that there is no segmentation. The average surface offset values from Table 5 of Anderson et al. (1995b) for the three fault segments are similar, which suggests that average displacement (AD) = 0.8 m; MS = 2 m; and for 35,000 years the average slip rate = 0.02 mm/yr. This corresponds to $M = 6.91$. The report of Anderson et al., includes a series of more active ruptures along the west side of Resting Springs Range, which could make the length too long, the slip rate too high, and recurrence interval too short for the entire zone. On the other hand, the late Quaternary surface fault shown by Anderson et al. (1995b) north of U.S. Highway 95 was verified by observations of DBS during a recent aerial flight, which is suggested by the surface scarp pattern. Their data do not clearly show whether there was one or more than one event.

5. *RV, Rock Valley*. This appears to be one of the most important strike-slip faults near Yucca Mountain. This fault appears to be truncated on the west end by the Amargosa River fault, and on the east end by the Buried Hills and/or Spotted Range faults, and to the southeast by distributed northeast-trending short faults. Data were derived from Piety (1995) and chapter 4.13 of Whitney (1996). The maximum earthquake is $M_w = 7.1 \pm 0.4$ from $M_w = 6.69 + 0.74$ MD, or $M_w = 7.23$ from $M_w = 5.08 + \log 72$. Exploratory Studies Facility (ESF) dip is 70, 80, or 90 with left oblique. SRL is based on Plate 1 of Piety (1995); SR and RI are from chapter 6.12 of Whitney (1996).
6. *WSR, West Specter Range*. This fault is characterized as a west-dipping normal fault. Based on shadows observed along this fault during low-sun-angle (LSA) aerial reconnaissance in early morning and late afternoon illumination, D.B. Slemmons (DBS) estimated that the maximum slope of the scarps in alluvium are approximately 15 to 18 degrees. Scarps with similar slopes normally indicate that the most recent displacement was early Holocene or late Pleistocene. The activity rates observed by Anderson et al.

(1995b) appear to be correct, although DBS observations at Amargosa Flat indicate that there may be one or two Holocene to late Quaternary events. The fault probably is truncated by the Rock Valley fault and may cross the valley on the west side of West Specter Range. No surface trace is visible toward the Last Chance Range fault. The fault appeared to connect northward with ESR (Anderson et al., 1995b), and may extend northward to join or terminate against the Rock Valley fault zone for a maximum length of 25 km. DBS observed that the scarp extends south for a total length of about 18 km from north of Highway 95 to the south edge of Amargosa Flat. Several aerial observations with low-sun angle illumination did not show any offsets in active alluvial fans to the south toward Last Chance. DBS observed this zone several times with LSA, and observed a 15-km gap in late Quaternary faulting south of Amargosa Flat in bedrock and recent alluvium. There also is a possibility that it connects southward under young alluvium and bedrock units to the Last Chance Range fault discussed in Anderson et al. (1995a), to Y- 938, and to the North Pahrump fault zone at the northeast end of the Stewart Valley Playa. The ASM team did not characterize the Last Chance fault because it has a low rate of activity, is a short segment with a low rate of activity, and an interconnection to the West Specter Range fault would require faulting across a 20-km gap with no known Quaternary faulting. Anderson et al. (1995) estimate a slip rate of 0.004 mm/yr and a recurrence interval of at least 113 ka, based on one event. Their descriptions suggest two events, which concurs with an observation of DBS for the scarp in Amargosa Flat. The observation of DBS of about 2 m of Holocene and late Quaternary offset led to higher SR estimates of 0.004, 0.01, and 0.02 mm/yr.

7. CS. Cane Springs. This fault is characterized as a strike-slip fault. $M_w=6.61$ for $SRL=21$ and $M_w=6.68$ for 26 km based on interpretation of Plate 1 of Piety (1995). The fault appears to merge with three splays at the southwest end, and truncates against the curving end of Yucca Lake fault at the northeast end; accordingly, the length has a small uncertainty range. SR and RI are inferred from SRL and assumption of three pre-Holocene surface rupturing earthquakes.
8. AR, Amargosa River. This fault is characterized as a strike-slip fault. This fault has unresolved relations to other faults. Map revised from Fig. 8 of Anderson et al. (1995)

and Piety (1995), $M_w=6.34$ for $SRL=12.4$ km (Anderson et al., 1995a), and $M_w=6.70$ for $SRL=24.8$ km (Anderson et al., 1995a) and D.B. Slemmons field and LSA aerial observations of a late Quaternary fault scarp at location noted on map, and $L=48$ km from north end of Y-238 to NE corner of Stewart Valley playa. DBS observations of two other unmapped Quaternary scarps between the scarp noted above and Stewart playa. SR is poorly constrained from the small 1.1-m surface offset (Anderson et al., 1995b) /12 to 128 ka, with preferred value at 0.05 mm/yr. The values, higher than those implied in Anderson et al. (1995b), are based on aerial reconnaissance. The RIs are estimated at >10 ka, 128 ka, and preferred value at a mid-value of 69 ka. Most of the fault zone is at or near the water-table level, and the surface deformation appears to be partly from warping. RI data are not available. The proposed maximum length of 48 km is from the northeast end of Stewart Valley playa to Y-238 on Plate 2 of Piety (1995) to the southeast of Big Dune, but a more likely scenario is segmentation into two segments. The latter possibility could include the activation of the northwest edge of Montgomery Range and springs including Devil's Hole. DBS has several LSA Ektachrome slides, and the 1:24,000 scale quadrangle map suggests that there are at least three active Quaternary faults in the 10- to 20-km gap between Stewart Valley and the south end of AR as suggested in Anderson et al. (1995b). However, the faults are distributed over a width of several kilometers, which appears to preclude a simple throughgoing fault. These short (2- to 3-km-long) oblique fault scarps are between the east edge of Stewart Valley, the Devil's Hole spring area, and the Grapevine Spring area. Their presence suggests that there is no gap between Amargosa River (AR) and Ash Meadow (AM) and N Pahrump-Stateline fault zones, and that the two zones may be connected by a complex, segmented zone.

9. YCL, Yucca Lake. This fault is characterized as a strike-slip fault. $M_w=6.49$ from $SRL=16.3$ km based on extension to the south as mentioned in Piety (1995); $M_w=6.63$ from $SRL=20.6$ includes Y-238 (Plate 1, Piety, 1995) near CS. Comment in Piety (1995), "only youthful-appearing...fault." SR and RI are inferred from SRL and assumption of three pre-Holocene surface rupturing earthquakes.

10. ER, Eleana Range. This fault is characterized as an east-dipping normal fault. Length=10.6 and 12.7, based on Piety (1995, Plate 1). The database has ambiguous late to mid-Pleistocene dating and no displacement data. Piety (1995) reports that one unit with scarps is 160 to 800 ka, and one date suggests that the faulting is post-128 ka. SR and RI are inferred from SRL and assumption of three pre-Holocene surface rupturing earthquakes.
11. ESR, East Specter Range. This fault is characterized as an east-dipping normal fault. SRL=9 km (minimum) and 15 km (maximum) based on Plate 2 of Piety (1995). The length is defined by scattered scarps in alluvium and by the topography. Anderson et al. (1995a) and observations noted in the letter of DBS to Richard Quittmeyer of February 3, 1997, suggested similar characteristics to West Specter Range fault (WSR) when viewed with LSA. The appearance is similar, and the West Specter Range does not appear to be tilted from long-term paleoseismic activity, so parameters similar to WSR are used. SR and RI are inferred from SRL and assumption of three pre-Holocene surface rupturing earthquakes.
12. YC, Yucca. This fault is characterized as a strike-slip fault. $M_w=6.66$ and 6.83 for SRL=23 and 33 km, respectively. SR lengths are based on the estimated total length of distributed surface rupture. No significant measurements of displacement from multiple events is reported. Oblique slip is suggested by an echelon pattern. SR and RI are inferred from SRL and assumption of three pre-Holocene surface rupturing earthquakes.
13. WSM, West Spring Mountains. This fault is characterized as a west-dipping normal fault. Fault extends northward from Hidden Hills Ranch to scarp near Grapevine Springs, and probably to near U.S. Highway 95 at the northwest corner of Spring Mountains (LSA aerial reconnaissance and tilted Pliocene/Pleistocene surfaces). Slip rate and recurrence interval data are from Anderson et al. (1995a). The Wells and Coppersmith (1994) regressions suggest that the large displacements noted by Anderson et al. (1995a) are from multiple offsets of >2.2 m. Smaller offsets suggest an average for 17 measurements of SO of 1.33 m, or using $AD/MD = 0.38$, the MD should be 3.5 m, and $M=7.05$. This is similar to $M=7.09$ for a rupture length from Grapevine Springs scarps to the PVFZ at

Hidden Hills along a narrow and linear N17W eastern boundary of the 3- to 4-km-thick Pahrump Tertiary half-graben. Anderson et al. (1995b) estimate of AD=1.8-2.0 may be somewhat too high (40%). Anderson et al. (1995a) estimated the RI and SR at more than 28 ka to as much as 120 ka, and less than 0.02 mm/yr to as much as 0.07 mm/yr. They suggest that there were two, or possibly three, events.

14. **FC, Furnace Creek.** This fault is characterized as a strike-slip fault. $M_w=7.49$ (based on >120 km length and similarity to $M=7.5$ Owens Valley fault scarp of 1872). The south end is defined as the abrupt change in strike at the north end of EDV, and extends northward without apparent segmentation to the north end of the Fish Lake Valley fault (Piety [1995] and Reheis and Sawyer [1996]). FC had average displacements (ADs) of about 2.5 to 3.5 m per event along several fault strands. Table 5 of Klinger and Piety (1996) indicates AD=4.5 m of strike-slip offset. Owens Valley is assumed to be an analogous event with $M=7.5$, $D_{max}=9\pm 2$ m, $D_{avg}=4-5$ m, slip rate ~ 2.0 m, 0.45 ± 0.75 . The unpublished data of Strom and Nikonov and of Slemmons show the AD = 0.38, or approximately $0.4 \times D_{max}$, which gives an AD of about 3.4 m for $M=7.5$. This is reasonably close to the 4.5 value estimated by Klinger and Piety (1996). Accordingly, the values of Klinger and Piety (1996) will be used. The slip rate is approximately two to four times higher than that of Owens Valley fault, and about two to three times higher than the 2.42 ± 0.7 m in Panamint Valley.

15. **EDV, East Death Valley.** This fault is characterized as a west-dipping normal fault. $M_w=7.21$ (based on $L=75$ km, scaled from maps of Brogan et al. [1991]). The maximum net displacement (5.0 m at mileage 38.1 of Table A1 in Klinger and Piety, 1996) corresponds to $M_w=7.21$, using the regression of Wells and Coppersmith (1994). These values are consistent with the somewhat higher magnitude 1872 Owens Valley earthquake of $M_w=7.5$, which had a length of 100 to 108 km and $MD=9.1 \pm 2$ m (Beanland and Clark [1994]). The north end of the fault zone is shown on Plate 2 of Piety (1995) as an abrupt strike change of Holocene scarps at California Highway 190 near Salt Springs in the middle of Section 21 of T28E, R1E. The south end is truncated by the Southern Death Valley (SDV) fault system at Shoreline Butte. The vertical component for surface fault slip rate and RI data are based on Klinger and Piety (1996).

Klinger and Piety, Tables 4 and 5, indicate a mainly vertical separation of 3 to 5 mm/yr, which should be increased by 15.5% for a 60-degree dip for use of the Wells and Coppersmith (1994) regressions. The Tertiary extension direction is about N60W in a N12S-trending Death Valley graben, as suggested by striae on fault surfaces in the bedrock (oral communication by Martin Miller, University of Wisconsin-Eau Claire). Only a few strike-slip offsets are shown in Figure 5 of Klinger and Piety (1996); their report did not include deformation at Cinder Hill. Accordingly, our analysis characterizes the EDV as a normal fault that is assumed to dip 60 degrees westward, and places the strike-slip component to a subparallel outboard fault, the inferred MDV, which is assumed to be a vertical strike-slip fault about 3 to 5 km west of EDV. A vector analysis of EDV of N12W orientation, and a vertical slip rate of 4 mm/yr for N50W extension (parallel to the FC and SDV right-slip faults), would be 4.62 mm/yr net normal-slip component on a frontal fault dipping 60 degrees. The dip-slip component for a normal fault dipping 60 degrees (EDV) would have net components 3.46, 4.62, and 5.77 mm/yr, for vertical separation rates of 3, 4, and 5 mm/yr, respectively. The AD (average displacement) from Klinger and Piety (1996) is 2.5 to 3.5 m; using a $1/0.38=2.63$ multiplier suggests AD=3.0 m, MD=7.9 m, or from Wells and Coppersmith (1994), Mw=7.35.

16. BLR, Belted Range. This fault is characterized as a west-dipping normal fault. Mw=7.04 for SRLmax=49 km and Mw=6.61 for SRLmin=21 km as reported in Anderson et al. (1995a) and Piety (1995). The scarps that Anderson et al. (1995a) studied are in the middle segment of BLR (Piety, 1995) opposite the highest part of the range; they did not evaluate the activity rates of the other parts of the fault. Anderson et al. (Table 3, 1995a) infer an AD=0.675 m based on profiles of single-event scarps at four data points; this corresponds to MD=1.8, which is close to the 1.5 m observed value. Multiple-event scarps average 2.7 m in height, which suggests four events in 118 ka. Displacements are as great as 2.5 m; they estimated SR of 0.01-0.1 mm/yr on a fault with a long-term SR of about 0.05 since 12.5 to 11.5 Ma. Examination of the data in Figures 7 and 8 (Anderson et al., 1995a) indicates steep scarp slopes of 11 to 19 degrees, which suggests that for all but one profile, there were two, three, or four faulting events, with MD= 1 to 2 m and Mw=6.6-6.9 during the last 128 ka. Anderson et al. (1995a) report that the RI is poorly

constrained. They suggest that it is greater than 10 ka, but with multiple events in less than 100 ka, perhaps much less than 100 ka. Based on multiple events (2 to 4) during the past approximately 128 ka, a range of RI (20 to 69 kyr) is used in this analysis.

17. **MDV, Mid Death Valley.** This fault is characterized as a strike-slip fault. The fault length is assumed to be 72 km from near Cinder Hill to an intersection with the southern segment of the Furnace Creek fault zone (DBS): $M_{max}=7.23$ (based on $L=72$ km, and the regression for all fault types of Wells and Coppersmith, 1994). A mid-valley fault zone includes all of the strike-slip component of EDV as shown by vector diagrams from the striation direction shown in places along the frontal fault plane, the extension direction shown in bedrock by the Miocene and Pliocene extension in Black Mountains, and geometry of extension from the valley opening, which is subparallel to the N50W Furnace Creek and Southern Death Valley strike-slip faults. MDV is demonstrated geologically by the Cinder Hill right-lateral offset, which is variously reported to be 80 m and 100 to 200 m (as reported by Larry Anderson at Stop 5 in DOE/Participant Management Field Trip Guide Book, dated January 28-31, 1992). The earlier radiometric date of Cinder Hill is 680 ka, but a new radiometric date is reported to be 100 ka to no more than 200 ka. This suggests a geologic strike-slip rate at Cinder Hill that is about 0.15 to 2 mm/yr, with a preferred rate of about 1 mm/yr, which is the minimum value in Table ASM-6. At the north end of the EDV near Salt Creek, a strike-slip fault with associated folded Quaternary to Pliocene sediments was mapped by Lauren Wright and Bennie Troxel. Martin Miller (telephone conversation of 4/24/97) reports that the Miocene (~15 Ma) to Pliocene direction of extension for the basement rocks of Black Mountains was N60W. The slip vector diagrams indicate that the strike-slip component is about 40 percent of the rate observed for the frontal fault. The minimum slip rate is based on the ca. 1 mm/yr rate observed at Cinder Hill; the maximum rate of 3 mm/yr is based on a vector diagram for the N50W extension of the valley noted under discussion of the East Death Valley fault (EDV); and the preferred slip rate is the average of the minimum and maximum values.

18. **GV, Grapevine.** This fault is characterized as a strike-slip fault. $M_w=6.72$ for $SRL=29$ km, which is similar to the 23 km estimated by Reheis (1992). It appears to

extend 8 km on Piety (1995), Plate 1, and 17 km on Plate 2 to a possible connection with FC, or a similar distance on strike to Y-239. The low uncertainty in length is the apparent connection at both ends to the more active Furnace Creek fault zone. Quaternary displacements are implied by topographic lineaments (subtle to prominent) on surfaces of Quaternary deposits. SR and RI are inferred from SRL and assumption of three pre-Holocene surface rupturing earthquakes.

19. WDV, West Death Valley. This fault is characterized as an east-dipping normal fault. $M_w=7.13$ (based on $L=62$ km as mapped by Brogan et al. [1991] in Death Valley). The minimum and preferred SRLs of 25 and 39 km are based on the two shorter groupings. This zone appears to have a very low slip rate, demonstrated by tilted fans that appear to be middle to early Pleistocene (oral comments at SSC Workshop 5 by Charles D. Harrington) along the Panamint Mountains and that have a thin veneer of younger Quaternary alluvium. Brogan (telephone conversation) reported that the scarps are only a few meters high, and the longest continuous zone is only about 3 km long. SR and RI are inferred from SRL and assumption of three pre-Holocene surface rupturing earthquakes.
20. EM-TP, Emigrant/Towne Passe. This fault is characterized as a northwest-dipping normal fault. $M_w=7.02$ for the maximum $SRL=47$. These values are revised from Plate 2 and discussion in Piety (1995). The Stovepipe Wells fault is included with EM. One early Holocene to latest Pleistocene offset of about 1 m, observed in the field by USGS staff, is also suggested in an oblique aerial photo by D.B. Slemmons (DBS), which shows about 1 to 2 m offset of a large Pleistocene or Holocene alluvial cone at Tucki Mountain. The date of the most recent event appears to be >10 ka, approximately $RI=19$ ka for latest Pleistocene, or 69 ka for late Pleistocene. The fault is not relevant unless it is coupled with the Towne Pass fault, which is shown in the longest fault option.
21. PRP, North Pahrump-Stewart Valley. This fault is characterized as a strike-slip fault. $M_w=6.94$ (based on $SRL=40$ km): Piety (1995) map. The 40-km-long fault joins the south end of the Amargosa River fault (AR) or Ash Meadows fault (AM) and the north end of the South Pahrump-Stateline fault system (SPRP); the earthquake scenarios include possibilities of either a single 40-km rupture, or two segments with half that

length. Our interpretation is based partly on the conclusions of Hoffard (1991) and observations by DBS during many low-sun-angle aerial reconnaissance flights over the area. Hoffard showed the North Pahrump fault extending into the Stewart Valley half-graben, and observations and photographs by DBS indicate a distributed pattern of at least three Quaternary faults extending into Amargosa Valley. The irregularities of faulting between Stewart Valley and the Amargosa River fault suggest that they may be strongly segmented and can be considered separate sources. The assessment partly is based on the prevalence of surface warping along faults that cross areas of shallow water table and late Pleistocene activity at paleosprings. There are Holocene scarps and vegetation lineaments. The youngest scarp of early Holocene age is 5 m high (just south of Highway 52). Aerial examination with LSA shows discontinuous Holocene or late Pleistocene scarps in the valley, partly from concealment by the extensive sand dunes along the fault escarpment; deformed terraces (late Wisconsin?) and tilted spring deposits also are observed along the fault traces. The activity includes an early Holocene event and two or three events assumed since 128 ka. If the fault is primarily strike-slip or oblique-slip, as would be expected from this orientation, the horizontal component should be greater than the vertical. Louie et al. (in press) obtained geophysical data that suggest a lateral offset of 18 m at 24 m depth, having no more than 1 m of vertical offset. They estimate a horizontal slip rate of 0.1 mm/yr for 100 to 150 ka, and a possible higher 1.8 mm/yr rate if the offset is 10 ka old. We judge the latter rate as too high, but the relationships strongly indicate that the fault is a strike-slip fault, with a high ratio of 10:1 or 20:1 for strike-slip to vertical-slip component.

22. WPR, West Pintwater. This fault is characterized as a west-dipping normal fault. $M=71$ based on $L=56$ km (Piety, 1995). Piety (1995) reports that Reheis (1992) notes "weakly expressed to prominent lineaments and scarps on surface of Quaternary (primarily) and Tertiary deposits and as faults that are in Quaternary and Tertiary (primarily) deposits and that were identified from previous mapping." The source model assumes that the 56-km-long fault can be subdivided into three segments; there is equal likelihood of rupturing as one, two, or three segments; and rupture is equally likely to occur at any part of the zone. We have no displacement data. Fault may extend north from the tectonically active Las Vegas Valley at Indian Springs.

23. PAN-HM, Panamint Valley-Hunter Mountain. This fault is characterized as a strike-slip fault. PAN fault zone is truncated on the south end by the Garlock fault (which has SR of about 8 mm/yr) and continues north to the Hunter Mountain fault zone and Saline fault zone: Note the interconnection with Hunter Pass fault, which makes it a relevant source, and frontal faults along the west side of Saline Valley. The seismic source parameters used in our model are based on Zhang et al. (1990), as summarized in Piety (1995).
24. SPRP, South Pahrump-Stateline. This fault is characterized as a strike-slip fault. Total fault length of ca. 65 km is from U.S. I-15 to Hidden Hills Ranch near the intersection of California Valley and Pahrump Valley. The north end connects with the south end of North Pahrump-Stateline and West Spring Mountains fault (WSM). The south end appears to terminate near U.S. I-15, since the adjoining Ivanpah fault does not appear to displace middle Pleistocene alluvial deposits. A full rupture length leads to $M_w=7.18$ and $AD=1.127$ m (based on MD determined from Wells and Coppersmith [1994] regression; MD, multiplied by 0.38, determines AD). The preferred $RI=39$ ka and $SR=0.05$ mm/yr, as the fault appears to be nearly linear and unsegmented. Aerial reconnaissance suggests that this section is less active than the North Pahrump/West Spring Mountains fault zones. However, the weak geomorphic expression may be due to mainly strike-slip offsets, and there may be two or more events in the past 128 ka. If the fault is primarily strike-slip or oblique-slip, as would be expected from this orientation, the horizontal component should be greater than the vertical. This fault was considered to have a low rate of activity in our first assessment, but the recent study by Louie et al. (in press) shows "almost purely strike-slip motion at scarp 1" near the Old Spanish Trail Highway, south of Hidden Hills Ranch. The weightings of one-third each include a high SR model, based on about 0.1 mm/yr (Louie et al., in press), a 0.05 mm/yr rate that is intermediate, and a very low rate of 0.002 mm/yr.

ELICITATION SUMMARY

DIANE DOSER, C.J. FRIDRICH, AND FRANK H. SWAN

TABLE OF CONTENTS

Page: i

1.0	INTRODUCTION.....	DFS-1
2.0	GEOLOGIC AND TECTONIC SETTING	DFS-1
3.0	HISTORICAL SEISMICITY DATA.....	DFS-5
4.0	CHARACTERIZATION OF SEISMIC SOURCES FOR GROUND MOTION ANALYSIS	DFS-6
4.1	SEISMIC SOURCE ZONES	DFS-6
4.1.1	Definition.....	DFS-6
4.1.2	Maximum Depth of Seismicity.....	DFS-10
4.1.3	Maximum Earthquakes.....	DFS-10
4.2	REGIONAL FAULT SOURCES.....	DFS-11
4.2.1	Guidelines for Modeling.....	DFS-12
4.2.2	Parameters.....	DFS-14
4.3	LOCAL FAULT SOURCES.....	DFS-25
4.3.1	Activity	DFS-25
4.3.2	Distributed Faulting Versus Independent Fault Sources	DFS-26
4.3.3	Total Length.....	DFS-27
4.3.4	Maximum Fault Rupture Length	DFS-31
4.3.5	Downdip Fault Geometry (Dip and Width).....	DFS-34
4.3.6	Quaternary Slip Rates (Seismic Moment Rates)	DFS-40
4.3.7	Maximum Magnitude	DFS-41
4.3.8	Recurrence Models	DFS-41
4.4	HYPOTHETICAL FAULT SOURCES.....	DFS-42
4.4.1	Proposed Highway 95 Fault.....	DFS-42
4.4.2	Postulated Hidden Strike-Slip Fault Beneath Crater Flat Basin.....	DFS-43
5.0	FAULT DISPLACEMENT.....	DFS-45
5.1	GENERAL APPROACH FOR CHARACTERIZING FAULT DISPLACEMENTS	DFS-46
5.2	POTENTIAL FOR DISPLACEMENT ON IDENTIFIED FAULTS.....	DFS-47
5.2.1	Fault Activity	DFS-48
5.2.2	Cumulative Displacement and Age of the Tiva Canyon Tuff	DFS-51
5.2.3	Average Quaternary Slip Rate	DFS-52
5.2.4	Potential for Fault Rupture	DFS-55
5.2.5	Event-to-Event Variability.....	DFS-61

TABLE OF CONTENTS

Page: ii

5.3	POTENTIAL FOR DISPLACEMENT ON FRACTURES AND UNBROKEN ROCK.....	DFS-62
5.3.1	Potential for Activity	DFS-63
5.3.2	Probability of an Event Associated with Different Deformation History Models	DFS-63
5.3.3	Threshold of Detection	DFS-64
5.4	ESTIMATION OF FAULT DISPLACEMENT	DFS-65
6.0	REFERENCES.....	DFS-67

TABLE OF CONTENTS

Page: iii

TABLES

Table DFS-1	Seismic source parameters for regional fault sources
Table DFS-2	Total fault lengths for local fault sources assuming independent behavior
Table DFS-3	Total fault lengths for local fault sources assuming distributive behavior
Table DFS-4	Maximum fault rupture lengths for local fault sources assuming independent behavior
Table DFS-5	Downdip geometry of local fault sources
Table DFS-6	Quaternary slip rates on local fault sources
Table DFS-7	Seismic source parameters for hypothetical faults
Table DFS-8	Fault activity and cumulative displacement, post-Tiva Canyon Tuff, at test calculation sites for fault displacement hazard assessment.
Table DFS-9	Quaternary slip rates based on paleoseismic data.
Table DFS-10	Slip rates calculated using decreasing slip rate model with different reduction factors (RF) compared to slip rates based on paleoseismic data.
Table DFS-11	Displacement per event and recurrence parameters. Fault displacement hazard assessment.
Table DFS-12	Summary of displacement per event data from Yucca Mountain paleoseismic investigations.
Table DFS-13	Relationship between average displacement and maximum displacement at a point along a fault (event-to-event variability)
Table DFS-14	Potential for activity on fractures and in intact bedrock.
Table DFS-15	Probability of displacement "events" (P_e) across fractures in unbroken rock given different models of deformation history.

TABLE OF CONTENTS

Page: iv

FIGURES

- Figure DFS-1 Map showing location of Yucca Mountain (star) in the southwest Nevada volcanic field (Broxton et al., 1989, of the western Great Basin, with schematic representations of faults of the Walker Lane Belt that have strike-slip components of offset (dip-slip offsets not shown). Modified from Stewart (1988)
- Figure DFS-2 Generalized map of the Yucca Mountain region showing major physiographic features and faults. Compiled from Jenkins, 1962; Longwell et al., 1965; Cornwall, 1972; Streitz and Stinson, 1974; Ekren et al., 1977, Burchfield et al., 1983; Wright, 1989; Frizzell and Schulters, 1990; Piety, 1993; Sawyer et al., 1994
- Figure DFS-3 Logic tree defining seismic source zones associated with two alternative models
- Figure DFS-3 Logic tree defining seismic source zones associated with two (Cont'd.) alternative models
- Figure DFS-4 Map showing boundaries of seismic source zones, Model A (one zone plus site vicinity)
- Figure DFS-5 Map showing boundaries of seismic source zones, Model B (three zones plus site vicinity)
- Figure DFS-6 Map showing identified late Quaternary faults included as regional fault sources in the seismic source model
- Figure DFS-7 Example of the logic tree used to characterize regional fault sources
- Figure DFS-8 Map showing local fault sources included in the seismic source model
- Figure DFS-9 Logic tree showing dependence of local fault model on distributive versus independent fault-behavior models
- Figure DFS-10 Example logic tree used to characterize local fault sources given distributed fault behavior
- Figure DFS-11 Example logic tree used to characterize local fault sources given independent fault behavior
- Figure DFS-12 Logic tree for conditional probability weights assigned to earthquake recurrence models
- Figure DFS-13 Map showing hypothetical fault sources included in the seismic source model

TABLE OF CONTENTS

Page: v

- Figure DFS-14 Map showing fault displacement hazard test calculation sites.
- Figure DFS-15 Logic tree used to characterize the fault displacement hazard based on fault slip rates.
- Figure DFS-16 Graph showing displacement versus age of displaced unit for the Paintbrush Canyon and Bow Ridge faults (From Gibson et al., 1993)
- Figure DFS-17 Graph of estimated extension rates in Crater Fault basin from middle Miocene to the present (From: Fridrich et al., 1996).
- Figure DFS-18 Logic tree showing probability weights assigned to the different Quaternary-slip-rate-estimation techniques depending on the availability of site-specific paleoseismic information.
- Figure DFS-19 Plots showing event-to-event variability in displacement relative to average displacement per event at a location along a fault based on data from paleoseismic investigations in the Yucca Mountain area.
- Figure DFS-20 Logic tree for assessing potential fault displacement hazard across a fracture or in unbroken rock.

ELICITATION SUMMARY
DIANE DOSER, C. J. FRIDRICH, AND FRANK H. SWAN

1.0

INTRODUCTION

Available seismic, geologic, and geophysical data are used to characterize potential earthquake hazards at Yucca Mountain. The approaches and source parameters presented here will be used by the Yucca Mountain project to develop probability functions that relate: (1) values of strong ground shaking (peak acceleration or spectral acceleration) to annual probability of exceedance; and (2) the likelihood of fault displacement at selected sites in the vicinity of the proposed underground repository.

The geologic and tectonic setting of the Yucca Mountain region and the seismicity data used in this analysis are described in Sections 2 and 3, respectively. The characterization of seismic sources for the ground motion analysis is presented in Section 4. The methods for assessing the potential for fault displacement and the characterization of tectonic features at selected localities within the controlled area at Yucca Mountain are presented in Section 5.

2.0

GEOLOGIC AND TECTONIC SETTING

Yucca Mountain is located in southwest Nevada in the eastern part of the Walker Lane belt, a 100- to 300-km-wide by 700-km-long zone of irregular topography and discontinuous strike-slip structures between the Sierra Nevada and the northern Basin and Range province (Stewart, 1988) (Figure DFS-1). Together, the northern Basin and Range and the Walker Lane belt make up the Great Basin, a region of dominantly extensional tectonism that began with back-arc spreading, at about 45 Ma, associated with subduction of the Farallon plate under the North American plate (Scholz et al., 1971). During northward migration of the Mendocino triple junction, subduction along the southwest coast of North America ceased as the North American plate became juxtaposed against the Pacific plate along a strike-slip boundary, the San Andreas fault (Atwater, 1989; Oldow et al., 1989). West of Yucca

Mountain. this transition occurred at about 10 Ma. Since this transition, extension in the Great Basin has been driven by the northwestward movement of the Pacific plate relative to the North American plate.

Within this framework, Yucca Mountain is a multiple-fault-block ridge in the eastern part of the Crater Flat basin, an extensional basin that formed primarily between 12.7 and 10 Ma, before the tectonic transition discussed above. The Crater Flat basin is a subbasin of the Amargosa trough, a long graben-like feature bounded on the west by the Bare Mountain range-front fault and on the east by the largely buried gravity fault (Figure DFS-2). The domain west of the Bare Mountain fault is characterized by extreme extension and by detachment faulting that terminates eastward in the vicinity of the Bare Mountain fault. The areas east of Bare Mountain fault, including the Amargosa trough, are characterized by minor to moderate extension. The domains east of the Amargosa trough are dominated by northeast-striking, left-lateral strike-slip faults and northwest-striking, right-lateral strike-slip faults. (Only the major ones are shown on Figure DFS-2.)

The Crater Flat basin lies on the south flank of the Timber Mountain caldera complex, the central eruptive source area of the southwest Nevada volcanic field. This volcanic field straddles the structural transition between the Walker Lane belt and the northern Basin and Range Province. The caldera complex has influenced the development of structures within the northernmost part of the Crater Flat basin by local modification of the stress regime associated with doming of the area around the calderas (Fridrich, in press).

Yucca Mountain is composed of a 1.5- to 3.0-km-thick sequence of variably welded Miocene ash-flow tuffs and lesser ashfall tuffs and lavas of the southwest Nevada volcanic field overlying a complexly deformed Paleozoic and late Precambrian sequence of marine carbonates, quartzites, and argillites. The Tertiary section thickens westward within the Crater Flat basin to a maximum thickness of about 4 km, and is truncated on the western margin of the basin by the Bare Mountain fault. The Tertiary strata in the basin are tilted dominantly eastward to southeastward along a closely spaced system of mostly west- to northwest-dipping faults. Most of the intrabasin faults are thus antithetical to the range-front

fault at the western margin of the basin in that they face into the range-front fault and formed coevally with it (Fridrich, in press).

Deformation in the Crater Flat basin is dominantly extensional but includes a significant component of northwest-directed right-lateral strike-slip strain. On the surface at least, the strike-slip deformation is diffuse rather than discrete—the basin evidently opened in an oblique manner, with the least extension (about 7-15 percent) and the least vertical-axis rotation (less than 5 degrees) in the northeast corner of the basin, on northern Yucca Mountain. From there, the magnitude of deformation increases to the west and south, to maximum values of 50 to 100 percent extension and at least 45 degrees clockwise rotation in the southwest corner of the basin (Fridrich et al., in press). The vertical-axis rotation in the basin is accommodated by left slip on the closely spaced north- to northeast-striking normal faults that comprise the internal structure of the basin. The structural geometry of the Crater Flat basin thus resembles that of some strike-slip pull-apart basins; however, detailed mapping has failed to uncover any evidence of master strike-slip faults anywhere in, or at the margins of, this basin. As in most of the eastern Walker Lane belt, the strike-slip deformation is diffuse rather than discrete.

In the Yucca Mountain region, the 10 Ma transition in the driving force of tectonism, discussed above, coincided with a shift in the style of volcanism to much lower eruptive volumes, and a shift from dominantly silicic volcanism before 10 Ma to dominantly basaltic volcanism afterward. A significant shift in tectonic style also may have occurred during this transition; however, because of the large decrease in silicic volcanism around 10 Ma, there is poor stratigraphic constraint on the tectonic evolution of this region between 10 Ma and present.

The evidence indicates that, after 10 Ma, the locus of both volcanism and tectonism continued to migrate westward out of the Yucca Mountain vicinity toward Death Valley, as it had been doing since 12.7 Ma. In the wake of this westward migration of the focus of tectonism, tectonism rates in the Yucca Mountain region declined strongly after 10 Ma. Quaternary tectonism in the Yucca Mountain region has consisted of selective reactivation of certain faults that formed during the middle Miocene or earlier, including some of the major

faults in Crater Flat basin, as well as faults in the Rock Valley fault system to the east (Figure DFS-2).

During the Quaternary, tectonism and volcanism in the Great Basin has been localized primarily along the eastern limit of the extensional province—at the Wasatch Front, and along the western limit of the province—in Death and Owen's valleys. In addition, a third and significantly lesser area of tectonism has been a north-trending zone in the center of the province. Yucca Mountain is located outside all three of these zones of major Quaternary seismic activity, and the rates of recent tectonism at Yucca Mountain are much lower than in any other part of the Great Basin where studies of Quaternary tectonism have been conducted.

In the Crater Flat basin, eight major faults show evidence of offset during the past 500,000 years, with rates of slip ranging from less than 0.001 to about 0.03 mm/yr. All of these faults formed around 12.7 Ma, and the current level of activity along these faults is very low relative to slip rates on the same structures between 12.7 and 10 Ma (Fridrich et al., in press). The three largest Quaternary faults on Yucca Mountain show late Quaternary slip rates that increase southward, indicating that the oblique style of extension in the Crater Flat basin, established during the middle to late Miocene, has continued to the present.

Basalts have erupted in Crater Flat basin in four episodes, at about 10 Ma, 3.7 Ma, 1 Ma, and 70 ka, that together define a trend of progressively declining volume of magma (Crowe et al., 1995). The latest eruption formed the Lathrop Wells center, a small cinder cone with associated lavas on the southern end of Yucca Mountain. The fact that ash from this eruptive center fills cracks formed during late Quaternary faulting events on Yucca Mountain has been interpreted by some workers as evidence that there may be a relationship between faulting and volcanic activity in the Crater Flat basin (Whitney et al., 1996).

HISTORICAL SEISMICITY DATA

Historical seismicity catalogs available to the panel members describe seismicity within a 100- and a 300-km radius of the site, as collated by Woodward-Clyde personnel. Our calculations of recurrence parameters made exclusive use of the 300-km radius catalog, as we believe this catalog enables us to obtain better spatial averages than the smaller catalog. Catalog magnitudes have been converted to a common moment-magnitude scale (Appendix D). We used the catalog completeness intervals defined by Woodward-Clyde Federal Services (Wong et al, 1997; I. Wong, SSC Workshop 3). Known nuclear explosions have been deleted from the catalog. Also, earthquakes that appear to be associated with regional fault sources have been subtracted from the catalog when estimating recurrence for the seismic source zones. These earthquakes were identified by drawing areas around each regional fault source (Section 4.2) and laying seismicity plots over the fault area map. The areas around the faults were drawn to include the area above the inclined fault plane (estimated dip projected to the base of the seismogenic zone) plus a nominal distance to allow for inaccuracies in epicentral locations.

The catalog was declustered using the algorithms of both Veneziano and van Dyck (1985) and Youngs et al. (1987). The two declustered catalogs were given equal weight for calculating recurrence parameters.

A minimum magnitude of 2.5 was used to compute the recurrence parameters after considering maximum likelihood rates and b-values calculated as a function of minimum magnitude (Section 3.1 contains a description of the methods used to calculate seismicity parameters). Spatially varying a-values were included in the analysis through use of a Gaussian kernel. Details of the smoothing are discussed in Section 4.1.1

Focal mechanism data compiled by Pezzopane et al. (1996a, Table 7-3) were used for analysis of variations in focal depth and focal mechanism within the study area. Results of this analysis are discussed in Section 4.1.2.

CHARACTERIZATION OF SEISMIC SOURCES FOR GROUND MOTION ANALYSIS

Our model includes four categories of seismic sources: (1) *seismic source zones* to account for seismicity that cannot be attributed to fault-specific sources included in the model; (2) *regional fault sources*, which include mapped late Quaternary faults within about 100 km of Yucca Mountain, but not including the faults in the site vicinity; (3) *local fault sources* in the vicinity of Yucca Mountain; and (4) *hypothetical faults* near the site. Different approaches are used to characterize each of these categories. Seismic sources that might make a significant contribution to the seismic hazard at Yucca Mountain (either because they have a relatively high rate of activity and/or because they are close to the site) are characterized in greater detail than are sources far from the site.

4.1 SEISMIC SOURCE ZONES

Seismic source zones are used to characterize volumes of the Earth's crust that are inferred to exhibit similar characteristics with respect to the magnitude and frequency of occurrence of earthquakes that cannot be attributed to fault-specific seismic sources (i.e., background seismicity). The seismicity within a given zone may be uniformly or non-uniformly distributed.

Uncertainties in the source zone geometry are incorporated in this analysis by considering different source zone models and a range of values for the depth of the seismogenic crust. Uncertainties in the magnitude frequency distribution within each zone are incorporated in the analysis by considering a range of values for the upper-bound earthquake and by considering different smoothing algorithms that provide for different levels of spatial smoothing of the earthquake epicenters in the seismicity catalog.

4.1.1 Definition

The region around Yucca Mountain commonly is divided into three major tectonic zones: the northern Basin and Range, the southwestern part of the Walker Lane belt, and the

northeastern part of the Walker Lane belt. The northern Basin and Range extends from the western limit of the Colorado Plateau westward to the eastern side of the Walker Lane belt, as defined below, and from the southern boundary of the Snake River Plain southward to the gravity gradient, just north of the Hoover Dam, that separates the northern and southern parts of the Basin and Range (Saltus and Thompson, 1996). The southwestern part of the Walker Lane belt extends from the Sierra Nevada, at its western boundary, eastward to the Furnace Creek and Pahrump fault systems, and extends from the northern boundary of the Mohave Desert, namely the Garlock fault at its southern limit, about 700 km to the north-northwest. The northeastern part of the Walker Lane belt extends from the Furnace Creek and Pahrump fault systems eastward to a line across which the topography changes from being very irregular to showing the regular N20°E pattern of basins and ranges that characterizes the northern Basin and Range.

All three provinces have been characterized by extensional tectonics from the Eocene to the present. In the northern Basin and Range, extensional structures dominate the tectonic pattern. Relatively little strike-slip deformation has occurred in this province relative to the two parts of the Walker Lane belt. The southwestern part of the Walker Lane belt is characterized by a strong northwest structural grain created by several major northwest-striking, right-slip and oblique slip faults. The northeastern part of the Walker Lane belt, in which Yucca Mountain is located, is a structural province characterized by numerous short, discontinuous strike-slip structures and by distributed strike-slip strain, including both northwest-striking right-slip structures and northeast-striking left-slip structures. This diverse structural pattern creates a very irregular topography in the northeastern Walker Lane belt.

The three provinces are structurally distinct and yet much more similar to one another than they are to any of the bordering provinces, including the Colorado Plateau to the east, the Mohave Desert to the south, and the Sierra Nevada to the west. The seismic characteristics of the Yucca Mountain region can be characterized based on the historical record of seismicity in the northern Basin and Range and the two parts of the Walker Lane belt. However, because of the structural differences between these three provinces, an even better characterization may be derived by studying the seismicity of these three provinces

individually to see if they have distinct seismic characteristics. Accordingly, two seismic source zone models are considered in the logic tree (Figure DFS-3): *Model A*, which consists of one regional zone plus a site-vicinity zone (Figure DSF-4); and *Model B*, which has three regional zones plus a site-vicinity zone (Figure DFS-5). The one-zone model, three-zone model, and the site-vicinity seismic source zone are described below.

Model A - One Zone Plus Site-Vicinity Zone. In this model recurrence parameters are estimated for a single regional zone outside the local site zone (see Figure DFS-4) based on the 300-km radius historical catalog and the estimated upper-bound magnitude. This model, which is assigned a weight of 0.2, assumes that over a long period (million years), regional differences in tectonics are minimized because the region as a whole is undergoing roughly the same rate of extension. Smoothing of the historical catalog was conducted using Gaussian kernels having different half-widths. The half-widths included in the analysis and their associated probability weights (in parentheses) are: 10 km (0.25), which is comparable to the location uncertainty for the better-located events in the region; 25 km (0.6), which is comparable to the value used by Frankel et al. (1996); and infinity (0.15), which corresponds to no smoothing.

Model B - Three Zones Plus Site Vicinity. In this model the recurrence parameters were estimated by dividing the region into three distinct zones (Figure DFS-5) in addition to a local site-vicinity zone. The zones reflect differences in fault style and orientation as well as differences in focal mechanisms and focal depths (Bellier and Zoback, 1995). The three zones are: (1) a Basin and Range zone; (2) an eastern Walker Lane zone; and (3) a western Walker Lane zone. The Basin and Range zone is characterized by extension along predominantly normal faults that trend north-south to NNE-SSW. The eastern Walker Lane zone is characterized by a mixture of normal (still dominant) and strike-slip faulting along NNW-SSE to NE-SW trending faults. In the western Walker Lane zone, strike-slip faulting predominates along NW-SE trending faults, and focal depths appear to be about 2 to 4 km shallower than surrounding regions, perhaps due to the increased regional heat flow. The three-zone model is assigned a higher weight (0.8) than the one-zone model, because in the short term (thousands of years), differences in the stress regimes in the three regions appear to have led to different styles of faulting.

Smoothing of the historical catalog was conducted in the same manner as for model A after removing earthquakes associated with specific fault sources. Half-widths for smoothing also were selected at 10 km, 25 km, and infinity, but weights were selected as 0.22, 0.53, and 0.25, respectively. Slightly more weight was given to infinity (as compared to Model A) because, if there are smaller regional zones, the spatial distribution of seismicity is more likely to be uniform within them.

Site-Vicinity Zone. The boundaries of the site-vicinity zone were drawn to include only the well-investigated part of the Yucca Mountain area that was the focus of the detailed USGS/DOE site-characterization studies. The earthquake recurrence parameters for the site-vicinity zone are estimated the same way as for Models A and B, except that a lower range of values is considered for the upper-bound earthquake magnitude because the active faults capable of producing larger magnitude earthquakes have been identified and are included in the model as fault-specific (local) sources.

This rationale does not necessarily apply to the seismogenic part of the crust below a detachment layer, if one exists. Given a detachment zone, the potential for larger magnitude, deep events is considered by including in the hazard model a postulated hidden strike-slip fault (Section 4.4.2).

The background earthquake for the site-vicinity zone includes a potential earthquake produced by volcanic processes. Quaternary volcanic activity in the site zone has included five basaltic eruptions that formed small cinder cones and associated lava flows; four of these occurred at about 1 Ma, and the other at about 70 ka. The calculated probability of recurrence of this type of volcanic activity in the site area has been estimated at about $10E-7$ per year (Crowe et al., 1995). Whereas volcanic activity sometimes generates earthquakes having magnitudes > 6.0 , the likely maximum magnitude earthquake associated with the formation of small cinder cones, such as formed in Crater Flat, is considerably smaller than magnitude 6.0. Given the low probability of a volcanic earthquake in Crater Flat as well as the small maximum magnitude, the upper bound earthquake for the site area source zone adequately covers this type of event.

4.1.2 Maximum Depth of Seismicity

Depth to the base of the seismogenic zone for all our models was based on studies of focal depth distributions of catalog (A quality) events and depths associated with focal mechanisms tabulated by Pezzopane et al. (1996a), which also should represent high-quality hypocenters. Only 4 percent of A quality catalog events had depths ≥ 12 km; 2 percent of the events with focal mechanisms had depths ≥ 12 km. Few events had depths of greater than 16 km. The values for the depth of the seismogenic crust that were included in the analysis and their associated weights are: 12 km (0.6), 14 km (0.3), and 16 km (0.1).

4.1.3 Maximum Earthquakes

Model A (one regional source zone excluding the site-vicinity zone) regards the maximum earthquake magnitude as the largest earthquake that could occur in the region. This event could occur randomly and/or on a geologic structure that is not explicitly included in the seismic source model. For example, several Quaternary faults shown on Piety's map (1995, plates 1 and 2) but for which there is no reported evidence of late Quaternary displacement are not included in the seismic source model. These faults presumably have low slip rates; nonetheless, they could be the source of large events. Estimates of the maximum earthquake range from Mw 7.7, which corresponds to the largest earthquake considered for any of the regional fault sources (Section 4.2), down to magnitude Mw 7.0, which is believed to be a conservative estimate for the largest event that could occur without surface fault rupture. The values included in the seismic hazard analysis and their associated probability weights (in parentheses) are: Mw 7.0 (0.2), Mw 7.3 (0.6), and Mw 7.7 (0.2).

In Model B (three regional source zones excluding the site-vicinity zone), the maximum earthquake magnitude varies with the zone. The values considered for the western Walker Lane zone are the same as for Model A [i.e., Mw 7.0 (0.2), Mw 7.3 (0.6), and Mw 7.7 (0.2)]. A slightly smaller range of values is considered for the eastern Walker Lane zone and the Basin and Range zone because these zones seem to lack the major continuous structures (e.g., the Death Valley/Furnace Creek fault system) that characterize the western Walker Lane zone. The values for these zones included in the seismic hazard analysis and their associated

probability weights (in parentheses) are: Mw 7.0 (0.2), Mw 7.25 (0.6), and Mw 7.5 (0.2).

Estimates of the maximum earthquake magnitude for the site-vicinity zone range from Mw 5.6 (about the size of the Little Skull Mountain earthquake) to about Mw 6, which corresponds to a rupture area of about 100 km² (Wells and Coppersmith, 1994). Clearly larger events have occurred in the Basin and Range that were not associated with surface fault rupture; however, given the close spacing of the local fault sources, we believe that larger events are best represented in the hazard model as occurring on the mapped faults. Selecting a cutoff magnitude of about Mw 6 also mitigates the problem of "double accounting" that can result by combining predictions of the number of large events based on observed seismicity with predictions of the number of small- to moderate-size events from paleoseismic evidence of past surface faulting events. The values included in the seismic hazard analysis and their associated probability weights are: Mw 5.6 (0.2), Mw 5.8 (0.6), and Mw 6.0 (0.2).

4.2 REGIONAL FAULT SOURCES

Regional fault sources include the mapped late Quaternary faults that extend to within about 100 km of the site but lie outside the site vicinity (Figure DFS-6). These faults were identified based on information presented in the USGS analysis to identify relevant earthquake sources (Pezzopane, 1996), Piety's (1995) report on Quaternary faults within 100 km of Yucca Mountain, and discussions during the Seismic Source Characterization Workshops with personnel who have examined some of these faults in the field. Faults included as regional seismic sources are judged to be capable of generating magnitude 5 or larger earthquakes and, based on published reports, are inferred to have had multiple late Quaternary displacements. The regional fault sources and the seismic source parameters (and associated uncertainties) used to characterize the seismic potential of these structures are summarized in Table DFS-1.

Several faults that are known or suspected to have had Quaternary displacement, but are not reported to exhibit evidence of late Quaternary displacement, are not included as fault-specific seismic sources. The rate of slip on these faults is too low to have a significant effect

on the ground motion hazard at the site, which is demonstrated by the results of previous analyses (Stepp et al., 1995; Wong et al., 1997), which show that most of the regional fault sources have no significant effect on the overall hazard at the site. Earthquakes that occur on Quaternary faults that are not included as regional fault sources are modeled as part of the seismic source zone activity (Section 4.1).

4.2.1 Guidelines for Modeling

The logic tree used to characterize the regional fault sources is shown on Figure DFS-7. A more simplified approach is used to characterize the regional faults than is used to model the local faults (Section 4.3), particularly if the faults are more than about 50 km from the site. Generalizing the fault geometry does not have a significant effect on the source-to-site distance. It could have an effect on the calculated maximum magnitudes, but this is factored into the analysis by increasing the range of uncertainty on the estimated maximum magnitude values. Except where noted in subsequent sections, the following guidelines were used in modeling regional fault sources.

Total Fault Length and Plan View Geometry. Discontinuous faults are generalized as a single continuous trace consisting of one or more straight line segments, so that the average source-to-site distance and total length of the modeled fault are consistent with the mapped fault. The total fault length is taken as the combined length of the straight line segments. A single, somewhat conservative, estimate of the total length is considered for most faults more than about 50 km from the site. For faults longer than about 25 km that extend to within about 50 km of the site, a range of values is assigned to account for uncertainties in total fault length.

Activity. The reported evidence for Quaternary displacement on all the regional fault sources described in this section is assumed to be associated with past seismogenic fault displacements (probability of activity = 1.0). Non-tectonic origins for some of the scarps may be possible, but are deemed to be sufficiently unlikely that their inclusion in this assessment would not significantly affect the hazard results.

Fault Dip and Downdip Width. Predominantly strike-slip faults are modeled as having a dip of 90 degrees. Predominantly dip-slip faults are modeled as having an average dip of 60 degrees. The faults are modeled as extending down to the base of the seismogenic crust, which is estimated to be between 12 and 16 km deep based on earthquake focal depths (see Section 4.1.2). The range of values for the maximum depth of faulting included in the analysis and their associated probability weights (in parentheses) are: 12 km (0.6), 14 km (0.3), and 16 km (0.1).

Maximum Earthquake Magnitude (M_{MAX}). Maximum magnitudes were calculated using an empirical relation that relates fault rupture length to magnitude (Wells and Coppersmith, 1994, relation for all fault types). Values were calculated by assuming 100 percent rupture of the longest geometrically defined fault segment and/or 100 percent rupture of the total fault length. The resulting values were considered to select a range of values for M_{MAX} . In most cases, the uncertainty associated with the preferred value for M_{max} is chosen to be about $\frac{1}{4}$ of a magnitude unit (i.e., plus or minus 0.2 to 0.3 Mw); however, as described below, somewhat wider and narrower ranges were considered in some cases.

Slip Rate: To the extent possible, estimated slip rates were based on published slip rates. Where reported rates were not available, slip rates were estimated (with wider uncertainty) based on analogy with other mapped faults and/or by inferring the likely ages and amount of displacement based on reported descriptions of the faults.

Earthquake Recurrence Models. The slip rate reflects the rate at which strain energy (seismic moment) is accumulating along a fault. The geologically derived seismic moment rate is used to translate slip rate into earthquake recurrence rate by partitioning the moment rate into earthquakes of various magnitudes according to a recurrence relationship (Cornell and Winterstein, 1986). Three general types of relationships have been proposed: (1) truncated exponential relations that mimic the behavior of recorded earthquakes in a region (e.g., Gutenberg and Richter, 1954); (2) a characteristic earthquake recurrence model (Youngs and Coppersmith, 1985) in which there is a greater tendency for earthquakes close to the maximum to occur than is predicted by seismicity-based exponential relations; and (3) relations that attribute all of the moment release on faults to earthquakes close to the

maximum (Wesnousky, 1986). All three recurrence relations are considered in this hazard analysis (Figure DSF-7). The greatest weight (0.6) is assigned to the characteristic earthquake model. The results of detailed paleoseismic studies along active faults have shown repeatedly that the characteristic model is more representative of the seismicity of an individual fault than are exponential models that represent the seismicity of regions, which contain faults of various sizes. Maximum moment models assume that independent events on faults (i.e., excluding aftershocks and/or foreshocks) are always close to the maximum earthquake. This model is given less weight (0.3) than the characteristic model, but more weight than the exponential model, which is given the least weight (0.1).

The exponential and characteristic recurrence models require estimates of the b-value associated with specific faults. We used a b-value of 1.0 ± 0.1 , which is based on the median value obtained for the seismic source zones plus or minus the 90-percent confidence interval. This uncertainty is about three times the uncertainty used to characterize the seismic source zones. Greater uncertainty is warranted because there is more uncertainty in the magnitude frequency distribution associated with individual faults.

4.2.2 Parameters

Eighteen regional fault sources are included in the seismic hazard analysis (not including the hypothetical faults described in Section 4.4). The fault parameters used to characterize these sources are summarized in Table DFS-1 and described below.

Hunter Mountain/Panamint Fault Zone. The Hunter Mountain/Panamint fault zone is characterized by strike slip. Individual rupture segments are estimated to range from a minimum of about 16 km to a maximum of about 74 km. Considering the possibility of rupture along multiple segments, our preferred estimate for the maximum rupture length in the range of 45 to 98 km, suggesting a M_{MAX} in the range of Mw 7.0 to 7.4. Rupture of 146 km (the total fault length included in the model) suggests an upper bound of Mw 7.6. The values included in the analysis and their associated probability weights (in parentheses) are Mw 7.0 (0.2), Mw 7.4 (0.6), and Mw 7.6 (0.2).

The Quaternary slip rate on the Panamint Valley section of the fault is better constrained than is the rate along the Hunter Mountain section. Piety (1995, p. 383) reports that the Holocene/late Pleistocene slip rate on the Panamint Valley section is between about 1.1 and 3.2 mm per year, with a preferred estimate of about 2.5 mm per year. This range of values is used to characterize the entire fault. The values included in the analysis and their associated probability weights are 1.1 mm per year (0.2), 2.5 mm per year (0.6), and 3.2 mm per year (0.2).

Furnace Creek/Fish Lake Valley Fault Zone. This system of faults, which is characterized by strike slip, has a total combined length of at least 125 km (Piety, 1995, plates 1 and 2). Individual rupture segments are estimated to range from about 26 km to a maximum of about 87 km, with a preferred estimate for the maximum rupture length in the range of 38 to 87 km, suggesting a M_{MAX} in the range of Mw 6.9 to 7.3. Rupture of 149 km (the total fault length as shown on Figure DSF-6) suggests an upper bound of about Mw 7.6. The values included in the analysis and their associated probability weights are Mw 7.0 (0.2), Mw 7.3 (0.6), and Mw 7.6 (0.2).

There is obvious evidence of late Quaternary displacement along this fault trend, but the ages of the displaced units are not well constrained. Bryant (as cited in Piety, 1995) reports 46 m of late Pleistocene offset (right slip) along the fault. If late Pleistocene is interpreted to mean older than Holocene (10 ka) and younger than or about equal to latest Pleistocene (approximately 35 ka), the likely slip rate is in the range of ≥ 1.3 mm to < 4.6 mm per year. The values included in the analysis and their associated probability weights are 1.3 mm per year (0.2), 2.3 mm per year (0.6), and 4.6 mm per year (0.2).

Death Valley Fault Zone. The Death Valley fault zone has a mapped length of 71 km and is reported to be predominantly dip-slip (Piety, 1995). Rupture of the longest geometrically defined segment (51 km) yields an expected magnitude of Mw 7.1; rupture of the entire mapped fault suggests a magnitude of about Mw 7.2. The uncertainty associated with M_{MAX} , however, is assumed to be greater than this narrow range of values. The values included in the analysis and their associated probability weights are Mw 7.0 (0.2), Mw 7.2 (0.6), and Mw 7.5 (0.2).

Piety (1995) cites slip rates on the Death Valley fault zone ranging from as little as 0.08 mm per year to as high as 11.5 mm per year, with a best estimate of about 2.5 mm per year for the late Holocene slip rate. Klinger and Piety (1996) report a vertical separation rate of 3 to 5 mm/yr. The values included in the analysis and their associated probability weights are 0.08 mm per year (0.2), 2.5 mm per year (0.6), and 11.5 mm per year (0.2), which gives a weighted average value of 3.96 mm/yr.

Pahrump/Stewart Valley Fault. This fault is composed of a discontinuous alignment of Quaternary fault scarps having a total length of about 41 km (Piety, 1995, plate 2). The total length of known Quaternary fault scarps is 18.5 km. The sense of Quaternary slip is inferred to be right-slip (Anderson et al., 1995a). The fault can be divided into two roughly equivalent segments of about 20 km based on an apparent left step in the fault trend, suggesting a magnitude of Mw 6.6. Rupture of the entire fault suggests a magnitude of about Mw 7.0. These rupture models were considered equally likely; the values included in the analysis and their associated probability weights are Mw 6.6 (0.5) and Mw 7.0 (0.5).

The Quaternary slip rate on the Pahrump/Stewart Valley fault is poorly constrained. Piety (1995) reports that the slip rate is "low," which is interpreted to mean that it is less than 1 mm per year, because faults having slip rates equivalent to or faster than this typically are well expressed geomorphically. Anderson et al. (1995a, p. 12) report that the long-term vertical slip rate is "less than a few hundredths of a millimeter per year and is most likely on the order of thousandths of a millimeter per year" (less than 0.009 to 0.02 mm per year). Even allowing for a significant lateral component to the net slip, the Quaternary slip rate probably is on the order of 0.005 to 0.05 mm per year. Given the large uncertainties in the ages of the reported displacements, any slip rate within this wide range is considered to be equally likely. The values included in the analysis and their associated probability weights are 0.005 mm per year (0.5) and 0.05 mm per year (0.5).

West Spring Mountain Fault. A nearly continuous fault trace is mapped along the west flank of the Spring Mountains for about 29 km. The southern limit of the fault is uncertain; discontinuous traces (Piety, 1995, plate 2) suggest the fault might extend to its projected

intersection with the Pahrump/Stewart Valley fault, for a total fault length of 51 km. Both of these options for the total length are included in the hazard analysis with equal weight. The fault may have a small oblique slip component, but is predominantly a dip-slip fault (Piety, 1995, p. 334). Values for M_{\max} depend on the total fault length (Figure DFS-6). In both cases, we assumed that rupture length was equal to total fault length. The resulting values (using Wells and Coppersmith's 1994 relation for all fault types) were taken as the preferred values for M_{\max} the associated uncertainty is estimated to be plus or minus about $\frac{1}{4}$ of a magnitude unit (Table DFS-1).

Hoffard (1991, as cited in Piety, 1995, p. 354) reports a preferred value for the late Quaternary slip rate on the West Spring Mountains fault of 0.06 mm per year near Wheeler Wash. His maximum and minimum rates at this locality, given the uncertainty in the age of the displaced surface, are 0.2 and 0.02 mm per year, respectively. The values included in the analysis and their associated probability weights are 0.02 mm per year (0.2), 0.06 mm per year (0.6), and 0.2 mm per year (0.2).

West Pintwater Range Fault. Piety (1995, plates 1 and 2) shows a series of mapped fault traces extending nearly continuously along the west flank of the Pintwater Range for about 55 km. The faults are interpreted to be down-to-the-west normal faults. Rupture of the longest geometrically defined segment (about 41 km) suggests a magnitude of M_w 6.9; rupture of the entire fault suggests a magnitude of M_w 7.1. Accordingly, M_{\max} is estimated to be $M_w 7 \pm \frac{1}{4}$. The values included in the analysis and their associated probability weights are M_w 6.7 (0.2), M_w 7.0 (0.6), and M_w 7.3 (0.2).

No reported slip rates were found for the West Pintwater Range fault. Piety (1995, p. 349) describes the fault as having weak geomorphic expression in late Quaternary deposits. Based on analogy to the Paintbrush Canyon fault, which is also characterized by weak geomorphic expression in late Quaternary deposits, the slip rate on the West Pintwater fault is estimated to be in the range of 0.02 to 0.2 mm per year. Having no basis for selecting a preferred value, we assumed that the actual rate is equally likely anywhere within this range. The values included in the analysis and their associated probability weights are 0.02 mm per year (0.5) and 0.2 mm per year (0.5).

Yucca Fault. The Yucca fault is predominantly dip slip (normal down-to-the-east) and has a mapped length of 25 km (Piety, 1995, plate 1). Given its short overall length, we assumed that the entire fault could rupture during the maximum earthquake, suggesting a M_{\max} of $6.7 (\pm 1/4)$. The values included in the analysis and their associated probability weights are Mw 6.5 (0.2), Mw 6.7 (0.6), and Mw 7.0 (0.2).

No reported slip rates were found for the Yucca fault. The basis for assigning a slip rate to this fault is the same as for the West Pintwater fault. The values included in the analysis and their associated probability weights are 0.02 mm per year (0.5) and 0.2 mm per year (0.5).

Emigrant Valley North Fault. The Emigrant Valley North fault consists of a diffuse zone of north-northeast-trending fault traces having an overall length of about 27 km (Piety, 1995, plate 1). The style of faulting is uncertain. In this analysis, it is modeled as a 60 degree west-dipping normal fault having a linear surface trace centered along the zone of mapped faults. Given its short overall length, we assumed that the entire fault could rupture during the maximum earthquake, suggesting a M_{\max} of $6.7 (\pm 1/4)$. The values included in the analysis and their associated probability weights are Mw 6.5 (0.2), Mw 6.7 (0.6), and Mw 7.0 (0.2).

No reported slip rates were found for the Emigrant Valley North fault. The basis for assigning a slip rate to this fault is the same as for the West Pintwater fault. The values included in the analysis and their associated probability weights are 0.02 mm per year (0.5) and 0.2 mm per year (0.5).

Oaks Spring Butte Fault. The Oak Springs Butte fault consists of a generally north-south zone of fault traces having an overall length of about 22 km (Piety, 1995, plate 1). Both down-to-the-east and down-to-the-west displacements occur within the zone, but the predominant displacement appears to be down-to-the east. In this analysis, it is modeled as a 60 degree east-dipping normal fault having a linear surface trace centered along the zone of mapped faults. Given its short overall length, we assumed that the entire fault could rupture during the maximum earthquake, suggesting a M_{\max} of $6.7 (\pm 1/4)$. The values included in the

analysis and their associated probability weights are Mw 6.5 (0.2), Mw 6.7 (0.6), and Mw 7.0 (0.2).

No reported slip rates were found for the Oak Springs Butte fault. Based on published reports (Dohrenwend et al., 1991, as cited in Piety, 1995, p. 256), there are "visible scarps" across surfaces that are estimated to be between 10 and 130 ka. Assuming that "visible scarps" means they are less than 1 to 2 m high, we estimated a slip rate less than about 0.01 to 0.2 mm per year. Having no basis for selecting a preferred value, we assumed that the actual rate is equally likely within this range. The values included in the analysis and their associated probability weights are 0.01 mm per year (0.5) and 0.2 mm per year (0.5).

Belted Range Fault. The Belted Range fault is a normal down-to-the-east fault that lies along the west foot of the Belted Range (eastern side of Kawich Valley). The total length of the fault is about 49 km (Piety, 1995, plate 1). Anderson et al. (1995b) report that scarps in Quaternary alluvium extend for only about 22 km of this length. Assuming rupture lengths of between 22 and 49 km suggests a M_{MAX} in the range of Mw 6.6 to 7.0 (or about $6\frac{3}{4} \pm \frac{1}{4}$). The values included in the analysis and their associated probability weights are Mw 6.5 (0.2), Mw 6.8 (0.6), and Mw 7.1 (0.2).

Anderson et al. (1995b, p. 13) report 11.3 m of displacement in surfaces that they estimate to be between 0.13 and 0.78 Ma, suggesting a slip rate between 0.01 and 0.09 mm per year. Having no basis for selecting a preferred value, we assumed that the actual rate is equally likely within this range. The values included in the analysis and their associated probability weights are 0.01 mm per year (0.5) and 0.1 mm per year (0.5).

Kawich Range Fault. The Kawich Range fault consists of numerous subparallel normal faults and lineaments on the west side of the Kawich Range (Piety, 1995, plate 1; and Anderson et al., 1995b). Most of the mapped faults occur in bedrock or at the bedrock-alluvial contact; the total length of Quaternary faulting is uncertain. The fault is divided into three line segments (Figure DFS-6), and four options are considered for the total length of the Quaternary active part of the Kawich Range fault. Most of the weight (0.68) is assigned to line segment A-B, because this is the only part of the fault having demonstrated

displacements of alluvial surfaces (Anderson et al., 1995b). The balance of the weight was assigned to the remaining options (Table DFS-1) based on the relative geomorphic expression of the adjacent sections of the fault. Values for M_{\max} depend on total fault length (Figure DFS-6). For all four options, we assumed that the rupture length is equal to the total fault length. The resulting values (using Wells and Coppersmith's 1994 relation for all fault types) were taken as the preferred values for M_{\max} and the associated uncertainty is estimated to be plus or minus about $\frac{1}{4}$ of a magnitude unit (Table DFS-1).

Based on the subdued geomorphic expression of the fault and an inferred rate of scarp degradation, Anderson et al. (1995b, p. 18) infer that the Quaternary slip rate on the Kawich Range fault is less than 0.01 mm per year. The values included in the analysis and their associated probability weights are 0.01 mm per year (0.5) and 0.001 mm per year (0.5).

Rock Valley Fault. The Rock Valley fault, which is inferred to be primarily a left-slip fault (Anderson et al., 1995a), trends north-northeastward across alluvial fan deposits on the southeast flank of Little Skull Mountain. The continuity of this faulting with fault traces along its southwestern projection is uncertain. Three options were considered to account for uncertainty in the total length of the Rock Valley fault (Figure DFS-6 and Table DFS-1). Most of the weight (0.6) is assigned to the well-defined section of the fault (segment A-B) adjacent to Little Skull Mountain. The balance of the weight is assigned to the remaining options. The least weight (0.1) is assigned to option A-D because it seems less likely that the fault would continue west of its projected intersection with the north-south trending Amargosa/Gravity (Ash Meadows) fault system. Values for M_{\max} depend on the total fault length (Figure DFS-7). For all three options, we assumed that the rupture length is equal to the total fault length. The resulting values (using Wells and Coppersmith's 1994 relation for all fault types) were taken as the preferred values for M_{\max} and the associated uncertainty is estimated to be plus or minus about $\frac{1}{4}$ of a magnitude unit (Table DFS-1).

Piety (1995, table 6) reports vertical slip rates on the order of 0.003 to 0.01 mm per year based on observed surface displacements ranging from less than 1 m to 1.1 m. No estimate of the amount of lateral slip is presented. D. O'Leary et al. (1996) estimate the maximum vertical displacement across the Rock Valley fault to be 0.054 mm per year (the sum across

three stands of the fault). Assuming a major strike-slip component (e.g., a rake of 20 degrees) suggests that the net slip could be about three times the vertical slip, or about 0.16 mm per year. O'Leary (1996, pers. comm.) suggests the minimum slip rate (net slip) might be an order of magnitude less than the maximum. The values included in the analysis and their associated probability weights are 0.02 mm per year (0.5) and 0.16 mm per year (0.5).

Wahmonie Fault. The Wahmonie fault, which strikes northeast, has a mapped length of 14 km (Piety, 1995). The style of faulting is uncertain. The fault scarps are predominantly down-to-the-northwest according to Piety (1995, p. 346, and plate 1). In this analysis, it is modeled as a 60-degree northwest-dipping normal fault. Given its short overall length, we assumed that the entire fault could rupture during the maximum earthquake, suggesting a M_{max} of 6.4 ($\pm 1/4$). However, an upper-bound earthquake (M_{MAX}) of less than about 6.5 is considered unlikely for surface faulting events. The values included in the analysis and their associated probability weights are Mw 6.5 (0.8) and Mw 6.8 (0.2).

Reported scarp heights of < 1 m to 3 m on surfaces that are interpreted to be between 270 and 740 ka (Swadley and Huckins, 1990, as cited in Piety, 1995, p. 346) suggest slip rates on the order of 0.01 to 0.001 mm per year. The values included in the analysis and their associated probability weights are 0.01 mm per year (0.5) and 0.001 mm per year (0.5).

Yucca Lake Fault. The surface trace of the Yucca Lake fault measures 14 km (Piety, 1995, plate 1). The fault, which strikes northwest, appears to have predominately down-to-the-northeast dip slip. Given its short overall length, we assumed that the entire fault could rupture during the maximum earthquake, suggesting a M_{max} of 6.4 ($\pm 1/4$). However, an upper bound earthquake of less than about 6.5 is considered unlikely for surface faulting events. The values included in the analysis and their associated probability weights are Mw 6.5 (0.8) Mw and Mw 6.8 (0.2).

No reported slip rates were found for the Yucca Lake fault. Based on reported recognizable scarps on late Quaternary surfaces, the fault is assumed to have a slip rate on the order of 0.02 to 0.2 mm per year (see discussion for West Pintwater Range fault above). The values

included in the analysis and their associated probability weights are 0.02 mm per year (0.5) and 0.2 mm per year (0.5).

Eleana Range Fault. The Eleana Range fault is a north-northeast-striking down-to-the-east normal fault having a total length of about 11 km (Piety, 1995, plate 1). Given its short overall length, we assumed that the entire fault could rupture during the maximum earthquake, suggesting an M_{\max} of 6.3 ($\pm 1/4$). However, an upper-bound earthquake of less than about 6.5 is considered unlikely for surface faulting events. The values included in the analysis and their associated probability weights are Mw 6.5 (0.8) and Mw 6.8 (0.2).

No reported slip rates were found for the Eleana Range fault. The basis for assigning slip rate values was the same as for the West Pintwater Range and Yucca Lake faults. The values included in the analysis and their associated probability weights are 0.02 mm per year (0.5) and 0.2 mm per year (0.5).

Peace Camp Fault. A series of discontinuous fault scarps have been mapped in alluvial deposits south and southwest of Mercury that are informally referred to as the Peace Camp fault (J. Yount, SSC Workshop 4). Based on its trend subparallel to the Rock Valley fault, the Peace Camp fault probably has a significant left-lateral component to the net slip. The total length of Quaternary faulting is uncertain. Estimates range from about 19 km, which includes the fairly well-expressed eastern section of the fault (segment A-B on Figure DFS-6), up to about 31 km (segment A-C) (J. Yount, SSC Workshop 4). More weight (0.7) is assigned to the better-expressed section of the fault (Table DFS-1). M_{\max} depends on the total fault length. For both options, we assumed that the rupture length is equal to the total fault length. The resulting values (using Wells and Coppersmith's 1994 relation for all fault types) were taken as the preferred values for M_{\max} and the associated uncertainty is estimated to be plus or minus about $1/4$ of a magnitude unit (Table DFS-1).

Half-meter-high scarps have been observed on late Pleistocene alluvial surfaces that are estimated to be between 20 ka and 130 ka (J. Yount, SSC Workshop 4), indicating vertical slip rates in the range of 0.004 to 0.025 mm per year. Allowing for a major strike-slip component, net slip might be several times vertical slip, which would be consistent with

estimated slip rates on the Rock Valley fault. The values included in the analysis and their associated probability weights are the same as those assigned to the Rock Valley fault, 0.02 mm per year (0.5) and 0.16 mm per year (0.5).

Amargosa/Gravity (Ash Meadows) Fault. This fault consists of a discontinuous zone of Quaternary fault scarps and lineaments that trends north-south along the east side of Amargosa Valley. The total length of the zone is uncertain. Four options are considered, depending on how far the zone might extend to the north and/or the south. The most weight (0.56) is assigned to the 27-km-long central part of the fault (segment A-B on Figure DFS-6). It is considered equally likely that the fault extends to the north or to the south (i.e., segments B-C and A-D both have assigned weights of 0.2). The likelihood that the fault extends in both directions is equal to the products of the probabilities that it extends in either direction (0.04). M_{MAX} depends on the total fault length. For all four options, we assumed that the rupture length is equal to the total fault length. The resulting values (using Wells and Coppersmith's 1994 relation for all fault types) were taken as the preferred values for M_{max} and the associated uncertainty is estimated to be plus or minus about $\frac{1}{4}$ of a magnitude unit (Table DFS-1).

Based on 155 cm vertical displacement observed in a trench across a trace of the Ash Meadows fault and an inferred age of about 40 ka, the slip rate is 0.04 mm per year (data from Donovan, 1991, as cited in Piety, 1995, p. 87). Assuming that the displaced late Pleistocene deposits could be as young as about 20 ka or as old as about 89 ka suggests that the actual slip rate is probably within the range of 0.02 to 0.08 mm per year. Based on surfaces that are displaced as much as 3.4 m and an inferred minimum age of 40 ka, Anderson et al. (1995a, p. 32) estimate that the slip rate on the Ash Meadows section of the fault is no more than 0.1 mm per year and that it is likely to be an "order of magnitude less." The values included in the analysis and their associated probability weights are 0.01 mm per year (0.2), 0.04 mm per year (0.6), and 0.1 (0.2).

Bare Mountain Fault. The Bare Mountain fault is the major down-to-the-east normal fault that forms the west side of Crater Flat basin. Along the west side of Crater Flat basin, the fault is well expressed geomorphically for approximately 16 km, which is taken as the

minimum total fault length. Near the southern end of the basin, the fault may bend to the southeast and continue for another 6 km. Based on the gravity data, we believe that the fault does not continue farther south as a single structure. The southernmost limit of the fault is mapped at its projected intersection with geophysical anomalies that are coincident with the proposed Highway 95 fault. M_{MAX} depends on the total fault length. A maximum rupture length of 16 km corresponds to Mw 6.5 ($\pm 1/4$). However, Mw 6.5 is assumed to be the minimum upper-bound magnitude for surface faulting earthquakes. Therefore, given a rupture length of 16 km, the values included in the analysis and their associated probability weights are Mw 6.5 (0.8) and Mw 6.8 (0.2) (Table DFS-1). Similarly, a maximum rupture length of 22 km corresponds to Mw 6.6 ($\pm 1/4$) and, in this case, the values included in the analysis and their associated probability weights are Mw 6.5 (0.2), Mw 6.7 (0.6), and Mw 7.0 (0.2).

Various slip rates have been reported for the Bare Mountain fault. Reheis (1988) reports 1.75 m of vertical displacement in deposits estimated to be 9 ka, suggesting a slip rate of 0.19 mm per year (Piety, 1995). However, if this represents displacement from a single event, the slip rate is unconstrained. Based on the results of mapping and of trench investigations at three locations along the Bare Mountain fault, Anderson and Klinger (1995) conclude that the slip rate is "quite low," about 0.01 mm per year or less. Based on uplift rates calculated from apatite fission-track thermochronometry and interpretation of alluvial fan sedimentation, Ferrill et al. (1996, p. 2-28 to 2-30) argue that the slip rate increases toward the south and suggest that it could be as high as 0.28 mm per year. Structural cross sections of the faults in the site vicinity (Section 4.3.5) indicate that the local west-dipping faults intersect the Bare Mountain fault at depth and, presumably, are truncated by the Bare Mountain fault because it has a much greater throw than the local faults. In this model, the slip rate on the Bare Mountain fault should be equal to or greater than the sum of the slip rates on the west-dipping (antithetic) faults (i.e., \geq approximately 0.05 mm per year). Clearly, there is still considerable uncertainty in the slip rate on the Bare Mountain fault. In our judgment, the most likely value is in the range of 0.05 to 0.1 mm per year. The values included in the analysis and their associated probability weights are 0.01 mm per year (0.1), 0.05 mm per year (0.4), 0.1 mm per year (0.4), and 0.28 mm per year (0.1).

4.3 LOCAL FAULT SOURCES

Local faults having recognized Quaternary displacement are included as fault-specific seismic sources in the seismic source model. The Ghost Dance fault also is included because it is the largest fault within the footprint of the proposed repository. The locations of the principal Quaternary faults included in this analysis are based primarily on the mapping of Simonds et al. (1995). The principal local faults included in the seismic source model are shown on Figure DFS-8.

Other mapped faults in the site vicinity (e.g., the Exile Hill fault, the Midway Valley fault, the Iron Ridge fault, and the northwest-trending faults such as the Yucca Wash, Sever Wash, and Pagany Wash faults) are not included as seismic sources because there is no evidence of Quaternary displacement along any of these bedrock faults. Structural models (e.g., the vertical axis block-rotation model) suggest that these faults might move in response to movements along the principal block-bounding faults. However, with the possible exception of minor fractures in calcite-silica-cemented regolith at the bedrock/alluvial-colluvial contact, the available information (USGS, 1996) indicates there have been no displacements on any of these faults younger than middle to late Quaternary. Data from numerous trenches indicate there have been repeated surface faulting events on the block-bounding faults during this same interval. The cumulative displacements on these faults in the Tertiary bedrock are small, not more than a few tens of meters. These small intrablock faults represent secondary accommodation structures that probably are related primarily to late Miocene deformation. If the intrablock faults can produce earthquakes, we assumed they would be small, having magnitudes less than or equal to the maximum random earthquake for the site-vicinity source zone (see Section 4.1).

4.3.1 Activity

There is documented Quaternary displacement on all the local fault sources except for the Ghost Dance fault (USGS, 1996; Simonds et al., 1995). The Quaternary offsets are assumed to be associated with past seismogenic fault displacements, so the probability of activity is assumed to be 1.0. Non-seismogenic mechanisms might account for some of the "paleoseismic events" identified in the fault trenches. For example, a mudflow layer due to a

storm event might be misinterpreted as a scarp-derived colluvial wedge from a faulting event. Alternatively, paleoseismic events may be missing from the record because of erosion or the absence of diagnostic characteristics for recognizing individual events. Regardless of the problems associated with the interpretation of individual events, we believe that the Quaternary slip rates derived from the Yucca Mountain trenches provide a reliable indicator of the seismic potential of the faults (assuming that the uncertainties in the amount, sense, and age of the displacement have been correctly factored into the assessment).

In contrast to the other local fault sources, no direct evidence of Quaternary displacement has been observed on the Ghost Dance fault, and the available evidence suggests that there has been no displacement since at least the middle Pleistocene (Taylor et al., 1996). Analogies to other north-south-trending intrablock faults such as the Midway Valley fault and the Exile Hill fault indicate that Quaternary displacements on the block-bounding faults have created only minor adjustments such as fracturing on the larger intrablock faults (Wesling et al., 1993; Swan et al., 1995; and Taylor et al., 1996). Therefore, we consider it unlikely that the fault is active and capable of generating significant earthquakes; the assigned probability weights are "active" (0.05), and "not active" (0.95). The potential for fault displacement on the Ghost Dance fault is addressed separately in Section 5.

4.3.2 Distributed Faulting Versus Independent Fault Sources

A Quaternary volcanic ash deposit occurs as infilling in fractures and/or along the fault plane in several fault exploration trenches in the Yucca Mountain vicinity. Based on the occurrence of this ash, it has been suggested that there may have been simultaneous rupture on subparallel faults, including faults on either side of Yucca Mountain (Pezzopane et al., 1996b). Because of the limitations in geologic dating techniques, it cannot be demonstrated that the displacements associated with the so-called "ash event" occurred during a single earthquake. Nonetheless, the physical evidence is sufficiently compelling to warrant consideration in the hazard model.

Simultaneous rupture on two faults does not require that they be physically connected at depth. Distributed fault behavior could occur with both of the structural (end-member) models that are considered in this assessment (Section 4.3.5). Accordingly, whether the

faults exhibit distributive fault behavior or behave independently has no major effect on the overall geometry of the local fault sources. It does, however, affect the assessment of the length of the maximum single-event fault rupture. Given distributed fault behavior, the maximum rupture length is not constrained by the length of an individual fault.

Figure DFS-9 is a logic tree showing the dependence of the local fault model on distributive versus independent fault behavior. Relatively low weight is assigned to the distributive fault behavior model (0.05) because of the lack of convincing historical analogs for the postulated "ash-event."

Figures DSF-10 and DSF-11 are logic trees that outline the approaches used to characterize the local fault sources given independent and distributive fault behavior, respectively. The components of the logic tree are described in the following sections.

4.3.3 Total Length

The Quaternary fault scarps are short, rarely more than a kilometer or two long, and discontinuous (Simonds et al., 1995). This may, in part, be due to the character of the fault displacements, but it is largely due to the effects of erosion and deposition since the scarps were formed. In this assessment, we assumed that the generally north-south-trending faults are linked together along strike. For example, the Paintbrush Canyon and Stage Coach Road faults are modeled as a single 20- to 30-km-long fault. The uncertainty in the overall length is due to uncertainties in how far the Quaternary faulting extends to the north and/or the south. The total length of faulting is considered two ways. First, given that the local faults are independent seismic sources, uncertainties in the total length of the individual faults are considered. Second, given the possibility of distributive faulting, the uncertainty in the total combined length of the local faults that could be involved in a distributive faulting event is considered.

Total Fault Length (Independent Fault Behavior). Figure DFS-8 and Table DFS-2 present alternatives for the total fault length and the assigned probability weights for each of the local fault sources.

Paintbrush Canyon/Stagecoach Road Fault. Four alternatives are considered, as follows.

1. Quaternary faulting is limited to the reach of the fault having evidence of Quaternary displacement, as shown on Simonds et al. (1995), i.e., fault segment B-E on Figure DFS-8. This option is given the greatest weight (0.68).
2. Quaternary faulting extends about 1.5 km farther north along the mapped bedrock fault splay that has the same strike as the fault south of Yucca Wash. This option corresponds to fault segment A-E on Figure DFS-8. This is given a low weight (0.2) because: the observed Quaternary displacements die out at the north end of Alice Ridge; no evidence for Quaternary displacement has been found on the Paintbrush Canyon fault north of Yucca Wash; and the projected intersection between the buried Yucca Wash fault would be a reasonable place for the Quaternary faulting to terminate.
3. Quaternary faulting extends about 7.5 km farther south to the projected intersection between the Stagecoach Road and proposed Highway 95 faults. This alternative, which corresponds to fault segment B-F on Figure DFS-8, is also given low weight (0.1) because there is no evidence for Quaternary displacement.
4. Quaternary faulting extends both north and south (fault segment A-F on Figure DFS-8). The probability of this is equal to the combined probability of options 2 and 3 above (0.02).

Bow Ridge Fault. The southern end of the Bow Ridge fault is taken at its projected intersection with the Paintbrush Canyon fault (location K on Figure DSF-8). Two alternatives are considered for the northern extent of Quaternary faulting; either the north end of Exile Hill (location H on Figure DFS-8), or its projected intersection with the Yucca Wash fault (location G). It is unlikely that Quaternary faulting extends much beyond the northern end of Exile Hill. Alluvial surfaces have been mapped across the northward projection of the fault that are equivalent to and older than the youngest faulted colluvial deposits on the west side of Exile Hill (Wesling et al., 1992; Swan et al., 1995). Therefore, the greatest weight (0.8) is assigned to segment KH (Table DSF-2).

Solitario Canyon Fault. The northern end of the Solitario Canyon fault is well constrained by bedrock mapping. It is unlikely that the fault extends any farther north than its projected intersection with the Yucca Wash fault (Scott and Bonk, 1984; Day et al., 1996). The

southern end of the fault is less certain, and two alternatives are considered (Table DFS-2). It is likely that the limit of Quaternary faulting coincides with the southernmost extent of the mapped Quaternary traces, as shown on the fault activity map by Simonds et al. (1995). This alternative (segment L-M on Figure DFS-8) is assigned a weight of 0.7. It is unlikely that the Solitario Canyon fault extends farther south than its projected intersection with the Stagecoach Road fault. This alternative (segment L-N on Figure DFS-8) is assigned a weight of 0.3 (Table DFS-2).

Windy Wash/Fatigue Wash Faults. The Northern Windy Wash, Fatigue Wash, and Southern Windy Wash faults are assumed to be linked along strike and are treated as a single fault zone. The Quaternary faulting is discontinuous, and the total length of the fault system is uncertain. Four alternatives are considered in the model (Table DFS-2).

1. Quaternary faulting is limited to the reach of the fault having evidence of Quaternary displacement, as shown on Simonds et al. (1995), i.e., fault segment P-R on Figure DFS-8. This option is given the greatest weight (0.57).
2. Quaternary faulting extends about 1.5 km farther north, ending at the projected intersection of the Northern Windy Wash fault with the Yucca Wash fault. This option corresponds to fault segment O-R on Figure DFS-8. This is given a relatively low weight (0.3) because no evidence for Quaternary displacement has been found along section O-P.
3. Quaternary faulting extends about 3.5 km farther south to the projected intersection between the Southern Windy Wash fault and the proposed Highway 95 fault. This alternative, which corresponds to fault segment P-S on Figure DFS-8, is also given low weight (0.1) because there is no evidence for Quaternary displacement.
4. Quaternary faulting extends both north and south (fault segment O-S on Figure DFS-8). The probability of this is equal to the combined probability of options 2 and 3 above (0.03).

Northern and Southern Crater Flat Faults. Based on the geologic cross sections and structure contour maps described in Section 4.3.5, the Northern and Southern Crater Flat faults intersect the Bare Mountain fault at a relatively shallow depth, and it is unlikely that they are linked along strike. The narrow down-dip width of the fault is consistent with the

short mapped surface traces. Therefore, the total fault lengths are taken as the mapped fault lengths shown on the fault activity map by Simonds et al. (1995).

Ghost Dance Fault. Based on the detailed mapping within the controlled area (Simonds et al., 1995; Day et al., 1996), the Ghost Dance fault is well defined for a distance of about 3 km (segment Y-Z, Figure DSF-8). Bedrock mapping indicates that the fault dies out at its northern end and that it does not extend north of location YY on Figure DSF-8. The southern termination of the fault is less distinct. The maximum length of the Ghost Dance fault is about 9 km if one assumes that the fault extends from location YY southward and includes the Abandoned Wash fault (i.e., segment YY-ZZ on Figure DSF-8). The geologic evidence for a continuous 9-km-long fault is not strong. Nonetheless, we assign a relatively high weight to a total fault length of 9 km because this assessment is conditional on the fault being an active seismogenic feature. A 3-km-long fault extending to seismogenic depths and acting as an independent seismic source is not very likely. A total fault length of 3 km (segment X-Y on Figure DSF-8) is assigned a weight of 0.3; a total length of 9 km (segment XX-ZZ) is given a weight of 0.7 (Table DSF-2).

Total Fault Length (Distributive Fault Behavior). Given the uncertainty in the total lengths of the individual faults described above, the sum of their lengths (total combined length) could be as long as 101.2 km, or as short as 84.5 km.¹ If the Northern and Southern Crater Flat faults are only minor features, the minimum combined total length is 69.9 km. Three scenarios are defined to account for the uncertainty in the total length of faulting given the distributed fault model (Figure DSF-10). These are:

Scenario A - the minimum value for the total length, minus the Northern and Southern Crater Flat faults, which in this scenario are inferred to represent minor secondary features;

Scenario B - the maximum value for the total fault length minus the Northern and Southern Crater Flat faults; and

¹ NOTE: These totals were calculated based on the distributed fault model, so that fault segment M-N of the Solitario Canyon fault was assumed to exist. The Ghost Dance fault was not included because, unlike the other local fault sources, there is a very low probability that it is an active fault.

Scenario C - the maximum value for the total fault length including the Northern and Southern Crater Flat faults.

The fault segments as shown on Figure DFS-8, total length, and assigned probability weight for each of these scenarios are presented in Table DFS-3.

4.3.4 Maximum Fault Rupture Length

Estimates of the rupture length associated with the maximum earthquake depend on whether the local faults behave independently or whether multiple traces rupture simultaneously (distributive faulting) (Figure DSF-9). The maximum rupture length per event on the local faults is discussed below for each type of fault behavior.

Maximum Rupture Length for Independent Fault Behavior. If the local faults behave independently, the maximum rupture length depends on the total fault length and on the length of the longest part of the fault that is expected to rupture during a single event. Given the range of total fault lengths presented in Table DFS-2, the following alternatives were considered:

- Rupture of 100 percent of the total fault length. For long faults, such as the Paintbrush Canyon/Stagecoach Road fault, this was given a low weight. For short faults such as the Northern Crater Flat and Southern Crater Flat faults, 100 percent rupture of the total fault length is assigned a probability of 1.
- Rupture of the longest geometrically defined fault segment. Depending on the strength of the evidence for defining fault segments, this approach was generally given the most weight.
- Rupture of two or more geometrically defined fault segments.

The basis for the alternative maximum rupture lengths considered for each of the local fault sources (assuming independent fault behavior) and the assigned probability weights are given in Table DSF-4.

Maximum Rupture Length for Distributive Fault Behavior. Based primarily on paleoseismic data from trenches, Pezzopane et al. (1996b) propose nine rupture scenarios, Z

through R, that are consistent with our distributed fault model. That is, the inferred rupture scenarios suggest the possibility of simultaneous rupture on multiple fault traces in the vicinity of Yucca Mountain. These rupture scenarios are used to evaluate the range of values for single-event fault ruptures associated with the distributed fault model. We used a somewhat different approach to define the rupture lengths associated with each scenario. Pezzopane et al. (1996b) constrain the minimum and maximum rupture length for each scenario based on the spatial distribution of the trenches. We used the trench data and geometrically defined fault segments to assess the length of surface fault rupture associated with each scenario. If the trench data suggest that two fault segments could have ruptured at the same time, we assumed that 100 percent of each segment ruptured unless trench data suggest otherwise. Our approach also incorporates the uncertainty in the total mapped length of the site-vicinity faults. Therefore, in some cases, we derive rupture lengths longer than the maximum values interpreted by Pezzopane et al. (1996b). Given below are the rupture length estimates—both ours and those of Pezzopane et al.—associated with each rupture scenario.

RUPTURE SCENARIO	RUPTURE LENGTH IN KM (PEZZOPANE, ET AL., 1996B, TABLE 5-3)	RUPTURE LENGTH IN KM (THIS STUDY)
Z	8.5 to 22	23.4 to 36.4
Y	18.5 to 25.5	25
X	15 to 24	18.9 to 24.9
W	10 to 22	30.6
V	9 to 15.5	14.8
U	10.5 to 23	55.5 to 59
T	14 to 20	< 15
S	9.5 to 19.5	< 15
R	8.5 to 22	< 15

The ranges indicated above are permitted by the data. The timing of paleoseismic events is imprecise, and the data do not necessarily indicate that single-event ruptures that are this long have occurred. Given a distributed faulting event, there is a great deal of uncertainty in the rupture length that would be associated with the maximum earthquake. The scenario earthquakes summarized above suggest values from less than 15 km up to about 60 km. Fifteen km is judged to be the minimum value that should be considered for the maximum rupture length given the distributed fault model. Using our approach to define the rupture lengths associated with the scenario earthquakes, and considering only those events having

values greater than about 15 km. the average rupture is about 30 km. Using values proposed by Pezzopane et al. (1996b, Table 5-3), the average is closer to 20 km.

The range of values for the surface fault rupture length associated with the maximum earthquake (given the distributed fault model) and the assigned probability weights are:

Maximum Rupture Length (Distributed Fault Model)	
15 km	(0.2)
20 km	(0.35)
30 km	(0.35)
60 km	(0.1)

Pattern of Fault Rupture for Distributive Fault Behavior. The following procedures were used to model the pattern of fault rupture based on the distributive fault behavior model.

- Earthquakes associated with ruptures ≤ 10 km long are assumed to occur as a single rupture randomly distributed on the mapped Quaternary faults (i.e., the local fault sources).
- Earthquakes associated with ruptures > 10 km and ≤ 25 km long are assumed to occur as two parallel ruptures of equal length that occur randomly on local fault sources. Earthquakes associated with ruptures > 25 km and ≤ 45 km long are assumed to occur as three parallel ruptures of equal length that occur randomly on local fault sources.
- Earthquakes associated with ruptures > 45 km long are assumed to occur as four parallel ruptures of equal length that occur randomly on local fault sources.

The selection of the cutoff points (10 km, 25 km, and 45 km) between single, double, triple, and quadruple parallel ruptures was somewhat arbitrary. They were chosen to minimize unreasonably short ruptures while permitting simultaneous rupture on all four principal local faults during the largest events. Alternative values could be used to test the sensitivity of the results to these postulated values. We did not propose alternative values because we believe they will have no significant impact on the overall hazard results.

4.3.5 Downdip Fault Geometry (Dip and Width)

Structural models were used to estimate the down-dip geometry of the local faults. Our understanding of the tectonics of the Yucca Mountain region is influenced by the tectonic interpretations of this region developed during the past 30 years of detailed studies. The first generation of these studies led to the proposal that Crater Flat basin formed as a caldera complex (Carr et al., 1986). Carr's work was followed by more detailed mapping of the east side of Crater Flat basin (Yucca Mountain) by Scott (1990), who proposed that the faults exposed on the surface in Crater Flat basin sole into a shallow detachment fault at the Paleozoic-Tertiary contact. At about the same time, Schweickert (1989) proposed that a regional, northwest-striking, right-slip fault extends under Crater Flat basin and is concealed under a detachment fault. In the latest generation of work, the detailed mapping started by Scott has been extended across the western half of the basin and beyond (Faulds et al., 1994; Fridrich, in press), and the surface geology and trench exposures of the Quaternary faults in the basin have been mapped (Simonds et al., 1995; Whitney et al., 1996). This latest work has led to a proposal that Crater Flat is a pull-apart basin that formed in response to the combined extensional and strike-slip strain regime of the Walker Lane belt (Fridrich, in press), as originally advocated by Wright (1989).

The latest generation of tectonic studies at Yucca Mountain (e.g., Whitney et al., 1996) largely have rejected the detachment fault hypothesis proposed by Scott (1990). Southwest Research Institute scientists (Young et al., 1993) suggested that the Paleozoic-Tertiary contact is too shallow for a detachment fault under Yucca Mountain, based on computer modeling of the proposed structure in balanced cross sections. Gravity and reflection surveys (Snyder and Carr, 1984; Brocher et al., 1996) across Crater Flat basin provide evidence that the Paleozoic-Tertiary contact is offset by several large, high-angle features, which is difficult to reconcile with this contact being a detachment fault of the sort invoked by Scott. Scott's model predicts that the Tertiary rocks were transported westward relative to the underlying Paleozoic rocks before the uplift of Bare Mountain. However, recent mapping has shown that the uplift of Bare Mountain was roughly coeval with formation of the extensional faults in Crater Flat basin and that a linear swarm of 14 Ma dikes is not offset significantly (if at all), as predicted at the Tertiary/Paleozoic contacts at the northeast and southeast corners of Bare Mountain (Fridrich, in press). Scott invoked the widely accepted

model in which the detachment fault allows lateral translation of extensional strain between the zone of brittle extensional faulting in the upper plate and the zone of ductile extension in the lower plate. Because any detachment fault under the Crater Flat basin would be truncated by the Bare Mountain range-front fault, it would be a rootless structure that would lack any kinematic impetus to move in Scott's model. For these reasons, our analysis gives Scott's detachment model a very low weight (Figures DSF-10 and DSF-11).

Carr and other's (1986) hypothesis, that the Crater Flat basin formed as a caldera complex, has been rejected by nearly all ensuing workers for the following reasons. (1) The structures of the Crater Flat basin are products of northwest-directed extension and right-slip strain (Scott, 1990; Minor et al., 1996; Fridrich, in press). They thus are consistent with patterns of late Cenozoic tectonism in the Great Basin as a whole. In contrast, the structures formed by calderas accommodate principally vertical strain (tumescence, collapse, and resurgence) over the subcaldera magma body and radial and concentric strain peripheral to the magma chamber (Smith and Bailey, 1968). (2) If a caldera complex is buried under Crater Flat basin, it must be older than 13.1 Ma because the sources for all of the younger major ash-flow sheets of the southwest Nevada volcanic field have been identified (Sawyer et al., 1994). In that the Crater Flat basin formed at about 12.7 Ma, any buried caldera under the basin was a fossil structure when the basin formed and, therefore, is irrelevant to the formation of this basin. We give the caldera model zero weight in our analysis for the reasons stated above and because this model provides no explanation for the Quaternary faulting in this basin.

The rapid succession of different tectonic interpretations of the Crater Flat basin during the past 30 years is an indication of the level of scientific uncertainty involved. Because of the large uncertainty, we consider a range of hypotheses. The strongest weight is assigned to the simplest, most conventional approach. The alternative models, which are assigned relatively low weights, are included primarily to facilitate assessment of the effect these models have on the overall seismic hazard at Yucca Mountain.

Domino Model. Our preferred model assumes that the faults exposed at the surface in Crater Flat basin extend as high-angle, planar faults to seismogenic basement (12 to 16 km), except where the geometry dictates that they run into another, larger-throw fault before they reach

that depth, as discussed below. We call this the Domino model. The theoretical basis and supporting evidence for the Domino model consists of the following points.

- (1) The 1992 Little Skull Mountain earthquake (Mw 5.7), which had its epicenter about 10 km east of Yucca Mountain, provides the only ground-truth evidence on the subsurface geometry of faults and on the relationship between faulting and earthquakes in the Yucca Mountain region.
- (2) The foci of the main Little Skull Mountain shock and aftershocks defined a planar, high-angle fault that extends from the upper crust down to at least 12 km (Harmsen, 1994; Smith et al., 1996, in press).
- (3) The nature of this earthquake is consistent with the majority of data on historical earthquakes in the Great Basin in that most significant (greater or equal to magnitude 5) earthquakes in this province are due to movement on normal faults that are high-angle, planar, and extend to depths of 10 to 15 km (the brittle-ductile transition).
- (4) Moreover, the lack of evident ground breakage associated with the Little Skull Mountain quake is consistent with the fact that most quakes in this province having a magnitude of less than 6 have no associated ground breakage.
- (5) If we can use the Little Skull Mountain quake as an analogue for what to expect at Yucca Mountain, then the Quaternary ground breakage along distances of several kilometers and more on Yucca Mountain faults having slips in individual events of as much as 1 m suggests that the Quaternary faulting events on Yucca Mountain were associated with large earthquakes (greater than magnitude 6). By inference, we believe it is valid to take the relationship of earthquake magnitude to fault rupture length (and other parameters) developed using the historical data from the Great Basin as a whole and use them to predict the potential magnitude of earthquakes at Yucca Mountain, based on the Quaternary record of surface fault rupture there.

The Domino model represents the simplest, most conventional approach because it assumes that Yucca Mountain is not seismically anomalous relative to the rest of the Great Basin. This is our preferred model because, although it is possible that Yucca Mountain may be seismically anomalous relative to the rest of the Great Basin, we believe that arguments suggesting that it is are scientifically weak. Therefore, the Domino model is assigned a very

high weight (0.8) relative to the Detachment model (0.2) in the hazard analysis (Figures DSF-10 and DSF-11).

An optional feature we placed within our Domino model is the Highway 95 fault (discussed below), based on an interpretation of Slemmons (pers. comm., 1997). Slemmons invoked this fault, based on airphoto lineament patterns, to explain a structural geometry problem. The Quaternary faults in Crater Flat basin show a pattern of southward increase in slip rates, with maximum rates documented near the southern terminations of recent activity. This geometric pattern is highly anomalous and suggests that the faults may be abruptly terminating against another structure, such as a northwest-striking right-slip fault along the southern boundary of the basin.

Detachment Model. A detachment layer at depths of 5 to 8 km below the surface may be used to satisfy the geometry arguments advanced by Southwest Research Institute (Young et al., 1993) and to be consistent with gravity and reflection data. We used this basic fault geometry to characterize the proposed detachment models, which include:

- Scott's model in which the detachment acts as the master fault in the basin that all of the intrabasin faults sole into;
- Wernicke's model in which a master detachment fault is considered a separate seismic source; and
- Schweickert's model in which a regional-scale strike-slip fault that is a potential seismic source extends under Crater Flat basin under a shallow detachment fault.

Also considered were the ideas advanced principally by O'Leary (pers. comm., November 20, 1996 Workshop), who proposed that the large difference in the mechanical behavior of the Tertiary volcanic and Paleozoic sedimentary rocks under Yucca Mountain may result in an abrupt, downward change in the style of faulting across the Paleozoic-Tertiary contact. This contact would be a passive zone of detachment that accommodates an upward change in structural behavior in the rocks. The predominantly northeast-striking, left-oblique normal faults that cut the volcanic rocks have allowed a large component of distributed right-slip strain across the basin (Fridrich et al., in press). The major point of this passive detachment

model is that the distributed strike-slip strain in the volcanic surface rocks could reflect motion along a discrete strike-slip fault at seismogenic depths under Crater Flat basin. Unlike the model proposed by Schweickert, the concealed strike-slip fault would be confined to Crater Flat basin. Such a fault has been postulated beneath the Crater Flat basin, and was informally referred to as the cross-basin fault (I. Stamatakos, SSC Workshop 2). The potential for a hidden strike-slip fault beneath Crater Flat basin is addressed in Section 4.4.2.

Estimated Downdip Geometry of Local Faults. To develop defensible interpretations of subsurface fault geometry under Crater Flat basin, we constructed a suite of cross sections and structural contour maps of the exposed Quaternary faults using two geometric styles, which we view as end-member geometries: (1) a planar fault geometry, and (2) a strongly listric geometry that merges with a detachment layer. We then used these maps and sections to develop the downdip widths of the faults, listed below. For this exercise, we used the measurements of fault attitudes of Simonds et al. (1995) as a starting constraint and assumed that the fault planes exposed on the surface represented the steepest parts of the faults. In theory, normal faults form at an angle of 50 to 70 degrees in most rocks because this is the angle of maximum shear stress, assuming that the principal compressive stress is vertical. As these faults approach the surface, however, they tend to steepen to attitudes approaching vertical because there is no shear stress at the surface of the Earth. Another assumption we made is that fault dip decreases smoothly with depth. In our planar sections and maps, the decrease in fault dip with depth is very small; in the listric model, the faults sole into a subhorizontal detachment fault at about 6 km below the surface.

We used a trial-and-error approach in constructing our maps and sections to arrive at subsurface geometries that we consider most credible. For example, we joined the two segments of the Paintbrush fault and the Stagecoach Road fault as a single fault at shallow depths because: (1) these three mapped fault segments are roughly coplanar; (2) if not joined, these three fault segments had length-to-width ratios in the planar model that are inconsistent with established aspect ratios of faults in the Great Basin based on historical seismic and paleoseismic data; and (3) the documented single-event slip on the Stagecoach Road fault segment is too large for a fault as short as this, based on historical fault data, suggesting that this segment is part of a longer fault. We joined the northern and southern segments of the

Windy Wash fault with the Fatigue Wash fault at shallow depth for the same reasons. The two other major faults in our maps and sections are the Solitario Canyon and Bare Mountain faults, both of which were mapped as single segments.

Having made the above assumptions, we found that the Paintbrush Canyon/Stagecoach Road fault, the Solitario Canyon fault, and the Windy Wash/Fatigue Wash fault cannot come together at shallow depth; the most credible geometry appears to be that they are independent faults. The projections of the other faults in the basin (i.e., the Bow Ridge and Northern and Southern Crater Flat faults) all intersect one of the four major faults at depths much shallower than the brittle-ductile transition. These faults thus either may be splays of the Paintbrush Canyon/Stagecoach Road or Solitario Canyon faults, or, in the case of the Northern and Southern Crater Flat faults, may be minor faults that are antithetic to the Bare Mountain fault. In the Domino (planar) model, the three major intrabasin faults (the Paintbrush Canyon/Stagecoach Road fault, the Solitario Canyon fault and the Windy Wash/Fatigue Wash fault) are antithetic faults to the Bare Mountain fault because they project into the Bare Mountain fault at depths that are near or above the brittle-ductile transition. In the Detachment (listric) model, the Paintbrush Canyon/Stagecoach Road fault is the master detachment fault of the basin at depth, and the other faults sole into it, except for the two Crater Flat faults, which run into the Bare Mountain fault first. In the hazard analysis, given the Detachment model, the Paintbrush Canyon/Stagecoach Road fault is modeled as a shallow-dipping, seismogenic source that extends beneath the Crater Flat Basin (Table DSF-5).

In the Domino (planar) fault model, the faults probably are not truly planar. They probably are slightly curved, which would explain the observed regions of roll-over in stratal dips in the hanging walls of these faults. Minimal curvature was used in constructing the cross sections. However, in the hazard analysis, the faults are modeled as planar features, and the average dip was used. To account for uncertainties in the actual dip and downdip width of the faults, the analysis includes a range of values represented by the alternative geometries (Alternatives A and B) shown on Table DSF-5 for the Domino model.

4.3.6 Quaternary Slip Rates (Seismic Moment Rates)

Quaternary slip rates are used in conjunction with fault areas (including the uncertainties in total fault lengths and down-dip fault widths) to compute a range of values for the average seismic moment rate for each local fault source. Except for the Ghost Dance fault, the Quaternary slip rates for the local faults are based on the reported results of detailed paleoseismic investigations. In general, these reported slip rates are reasonably well constrained by the available data; nonetheless, there are uncertainties in the amount of cumulative displacement, the age of the displaced units and, in some cases, the relation between the apparent vertical displacements measured in the trenches to the net slip on the fault (i.e., where there may be a significant component of lateral slip). To account for these uncertainties, a range of values is considered for each local fault. In most cases, the range is represented by three values: the maximum and minimum slip rates indicated by the data, and a preferred value, which were assigned subjective probability weights of 0.2, 0.2, and 0.6, respectively. Where preferred values were not reported, maximum and minimum slip rates are given, and a subjective probability weight of 0.5 is assigned to both values.

The range of values assigned to the Ghost Dance fault is based on the amount of post-Tiva Canyon displacement, using the procedures described in Section 5.0 (Fault Displacement Hazard). The preferred value, which we assigned a subjective probability of 0.6, is the weighted average from the three approaches used in the fault displacement assessment. The minimum and maximum values calculated using these techniques are each assigned a subjective probability of 0.2.

Table DFS-6 presents the range in values, assigned weights, and sources of data for the reported slip rates. In several cases the slip rates presented in Table DFS-6 indicate a greater range of uncertainty than the reported slip rates either because data from several closely spaced trenches have been generalized and/or we believe that there is greater uncertainty than represented by the reported values (e.g., in some case we made allowances for a greater amount of lateral slip).

There appears to be a systematic increase from north to south in both the amount of cumulative bedrock displacement and in the Quaternary slip rates on the local faults. To

preserve this spatial variability in the rate of seismic moment release, the longer faults are divided into segments characterized by different slip rates. These fault segments do not necessarily represent rupture boundaries. We assumed that single-event ruptures may extend across these boundaries.

4.3.7 Maximum Magnitude

Given the range of fault geometries, we used two methods to calculate earthquake magnitude. We used empirical relations that relate maximum rupture length to magnitude and similar relations that relate maximum rupture area to magnitude (Wells and Coppersmith, 1994, relations for all fault types). In addition to the uncertainty in the fault rupture parameters (length and downdip width), which is addressed by the range of values included in the logic trees, there also is uncertainty associated with the data sets used in formulating the empirical relations themselves. This uncertainty was included in the analysis by calculating $M_{MAX} \pm 1\sigma$.

Several other approaches and empirical relations are available for estimating earthquake magnitudes (e.g., Slemmons, 1982; Bonilla et al., 1984; Wyss, 1979; dePolo and Slemmons, 1990). We concluded that by incorporating the uncertainty ($\pm 1\sigma$) in the Wells and Coppersmith (1994) relations, we would adequately capture the uncertainty associated with estimation techniques in general.

The rupture-area-versus-magnitude approach is given more weight than the rupture-length-versus-magnitude approach because it incorporates more of the parameters that affect the size of an earthquake and because the rupture-length-versus-magnitude relation is insensitive to significant variations in possible downdip geometries. The rupture area approach is assigned a weight of (0.6), the rupture length approach is assigned a weight of (0.4).

4.3.8 Recurrence Models

The same earthquake recurrence models used to characterize the regional fault sources also were used to characterize the local fault sources (i.e., an exponential recurrence model, a characteristic earthquake recurrence model, and a maximum moment model; see Section 4.2). However, we believe that there is greater potential for variability in the size of earthquakes

based on distributed fault behavior than there would be if the faults behave independently. Therefore, the probability weights assigned to each earthquake recurrence model depend on the fault behavior model for the local fault sources (Figure DFS-12). Regardless of the fault behavior model, the greatest weight (0.6) was assigned to the characteristic earthquake model because the results of detailed paleoseismic studies along active faults have shown that the characteristic model is more representative of the seismicity of an individual fault than are exponential models that represent the seismicity of regions, which contain faults of various sizes. Given distributive fault behavior, more emphasis is given to the exponential model (Figure DFS-12).

4.4 HYPOTHETICAL FAULT SOURCES

In addition to the known regional and local fault sources, we included two hypothetical fault sources in the seismic hazard model. These are: the Highway 95 fault that has been proposed by Slemmons (1977), and a buried strike slip-fault that has been postulated based on proposed tectonic models (Schweikert, 1989). The existence of these faults and rate of Quaternary activity, if they exist, are uncertain. The locations of these features (as modeled in this analysis) are shown on Figure DFS-13. The seismic source parameters used to characterize the hypothetical fault sources are presented in Table DFS-7.

4.4.1 Proposed Highway 95 Fault

Slemmons (1977) proposes a fault zone, which he refers to as the "Carrara feature," along U.S. Highway 95 between the fluvial Beatty scarp near the Amargosa River to the south end of Yucca Mountain. Based on its strike (subparallel to the Furnace Creek fault), the predominant sense of slip would likely be left-lateral strike-slip.

The approach used to model the proposed Highway 95 fault is the same as the approach used to model the regional fault sources except that a low weight (0.1) is assigned to the probability that this feature is an active structure. We assigned a low probability of activity because no evidence has been found for faulting along this trend. The suspected fault-related features that have been investigated (e.g., the Beatty scarp) were found to be erosional/depositional in origin and not due to Quaternary faulting.

Because of the lack of evidence for faulting, the total length of the feature is uncertain. Two lengths are considered in the analysis: 11 km, which corresponds to the section of the lineament adjacent to the southwest flank of Bare Mountain; and 27 km, which assumes that faulting could extend southeastward to its projected intersection with the north-south-trending Amargosa/Gravity (Ash Meadows) fault. Based on the gravity data, we believe it unlikely that strike-slip faulting extends any farther southeast. The two values for the total fault length are given equal weight (maximum uncertainty). M_{MAX} depends on total fault length. A maximum rupture length of 11 km corresponds to Mw 6.3 ($\pm 1/4$). However, Mw 6.5 is considered the minimum upper-bound magnitude for surface faulting earthquakes. Therefore, given a rupture length of 11 km, the values included in the analysis and their associated probability weights are Mw 6.5 (0.7) and Mw 6.8 (0.3) (Table DFS-7). Similarly, a maximum rupture length of 27 km corresponds to Mw 6.7 ($\pm 1/4$). In this case, the values included in the analysis and their associated probability weights are Mw 6.5 (0.2), Mw 6.7 (0.6), and Mw 7.0 (0.2).

There are no reported slip rates for the proposed Highway 95 fault. Slip rates are estimated here based on the inferred rate of extension in the southern part of the Crater Flat basin. The sum of the vertical slip rates on the Quaternary faults in the southern part of the basin is approximately 0.05 to 0.1 mm per year (Fridrich et al., 1996, Figure 2-9). Depending on the average dip of the north-south faults, the rate of extension could be equivalent to, or about half of, the vertical rate (i.e., 45 degrees versus about 65 degrees). By assuming that all the extension is being taken up on the proposed Highway 95 fault, we estimated the slip rate to be in the range of 0.01 to 0.05 mm per year, with a preferred value of about 0.027 mm per year (based on preferred dips of 55 to 60 degrees). The values and associated probability weights included in the analysis are: 0.01 mm per year (0.3), 0.03 mm per year (0.4), and 0.05 mm per year (0.3). Nearly equal weights were given to all three values to reflect the high degree of uncertainty in the slip rate.

4.4.2 Postulated Hidden Strike-Slip Fault Beneath Crater Flat Basin

Given a detachment zone model, there could be hidden strike-slip faults below the detachment layer (e.g., Schweickert, 1989). The hidden strike-slip faulting could be local

(restricted to Crater Flat basin) or regional. There is little physical evidence to support the existence of a hidden strike-slip fault (Section 1.0). The probability that there is an active hidden strike-slip source is given even less weight than the activity assessment for the Highway 95 fault (0.05 versus 0.1). The primary reason for including a postulated strike-slip fault in the analysis (given the detachment model) is to enable us to test the sensitivity of the results to this hypothesis.

The location of such a fault is unknown. For this analysis, we assumed that the fault strikes parallel to, and lies 40 to 50 km east of, the Death Valley/Furnace Creek fault system. To model uncertainty in location, equal weight was given to a strike-slip fault having a 90 degree dip that is either along the northeastern margin, southwestern margin, or down the center of the zone shown on Figure DFS-13. To model uncertainty in the length of the zone, two alternatives were considered. If the fault is restricted to Crater Flat basin, it has a total length of about 30 km (segment A-B on Figure DFS-13). If the fault is regional, it was assumed to extend about 100 km in either direction from Crater Flat basin and to have a total length of about 200 km (segment C-D). These alternatives were given equal weight (i.e., maximum uncertainty).

We used different approaches to estimate the maximum earthquake magnitude depending on the structural model (local strike-slip faulting restricted to Crater Flat basin versus regional strike-slip faulting). Given the local strike-slip model, the maximum rupture dimensions are constrained by the length of the basin, the depth of the detachment zone, and the maximum depth of the seismogenic crust. The same methods used to calculate earthquake magnitudes for the local fault sources (Section 4.3.7) were used for the hypothetical buried strike-slip faults, except that more weight was given the area-versus-magnitude relation, because the structural model significantly restricts the fault width and the length-versus-magnitude relation is insensitive to this parameter. Given the local strike-slip model, the area-versus-magnitude technique is assigned a weight of 0.8, and the length-versus-magnitude technique is assigned a weight of 0.2 (Table DFS-7).

Given the regional strike-slip model, the maximum fault rupture length is unconstrained. In this case, the maximum earthquake magnitude is based on our judgment regarding the largest

events that would be consistent with the lack of surface evidence for a throughgoing strike-slip fault. The threshold for surface fault rupture is generally in the range of magnitude 6 to 6½, but larger historical events have occurred without producing surface fault rupture. It is unlikely that repeated events larger than about magnitude 7 could occur without producing surface evidence. Given the regional strike-slip model, the values included in the analysis and their associated probability weights are Mw 6.0 (0.3), Mw 6.5 (0.5), and Mw 7.0 (0.2).

There are no reported slip rates for a postulated hidden strike-slip fault beneath Crater Flat basin. For this analysis, we assumed that all the horizontal extension on the Quaternary faults at the surface occurs as strike slip on a northwest-trending fault at depth. Accordingly, the range of slip rates estimated for the Highway 95 fault also was used for the postulated hidden strike-slip fault (Table DFS-7).

5.0

FAULT DISPLACEMENT

The objective of the fault displacement characterization is to develop general procedures and perform evaluations for input to assess the probability of fault displacement (hazard curves that relate annual probability to amount of displacement) for any location within the controlled area at Yucca Mountain, given the structural characteristics at the specified location. Nine test calculation sites were identified during Seismic Source Characterization (SSC) Workshop 4 to represent the range of expected fault conditions within the Controlled Area. At two locations, four alternative fault conditions are considered. The locations of the nine test calculation sites are shown on Figure DFS-14. They include:

- (1) the Bow Ridge fault where it crosses the Exploratory Studies Facility (ESF);
- (2) the Solitario Canyon fault where it trends toward the repository block;
- (3) the Drill Hole Wash fault where it crosses the ESF;
- (4) a point along the Ghost Dance fault near the center of the controlled area;
- (5) a point along the Sundance fault west of the ESF;

- (6) a minor unnamed fault west of Dune Wash;
- (7) a point 100 m east of the Solitario Canyon fault that has:
 - (a) a small fault having 0.5 to 2 m cumulative displacement,
 - (b) a shear having about 10 cm cumulative displacement,
 - (c) a fracture having no measurable displacement, or
 - (d) intact rock;
- 8) a point midway between the Solitario Canyon and Ghost Dance faults that has:
 - (a) a small fault having 0.5 to 2 m cumulative displacement,
 - (b) a shear having about 10 cm cumulative displacement,
 - (c) a fracture having no measurable displacement, or
 - (d) intact rock;
- 9) a point along the Exile Hill fault in Midway Valley where fractures having no measurable offset have been observed in Quaternary alluvium.

5.1 GENERAL APPROACH FOR CHARACTERIZING FAULT DISPLACEMENTS

The underlying basis for assessments of fault displacement hazard is that future fault slip will recur at the same locations and in the same manner as geologically recent displacements (ASCE, 1997). Future fault displacements are most likely to occur on pre-existing faults, and the likelihood of future displacements is related to the frequency of most recent displacements. Accordingly, the most reliable assessments of the potential for fault displacement are based on direct geologic evidence regarding the recent history (Quaternary) of past displacements.

Quaternary deposits that would enable direct assessment of recent faulting are not present over most of the Controlled Area. Also, many of the features encountered at the level of the proposed repository cannot be related directly to observed surface faults. Therefore, the analysis must rely on indirect methods that relate the character of the displacements observed in the repository host rock (late Miocene Tiva Canyon Tuff) to the probable Quaternary displacement history on these features based on our knowledge of the geologic evolution of Yucca Mountain. The methods used are calibrated using data from selected locations for

which we have data on fault displacement in both the Tiva Canyon Tuff and the overlying Quaternary deposits.

Fault slip rate is the basic parameter used in this analysis to characterize the potential for the fault displacement. It is a useful parameter for: (1) assessing the fault displacement history (e.g., for comparing late Miocene faulting to Quaternary faulting on a given structure); (2) for comparing the relative hazard posed by different faults; and (3) for constraining the recurrence and/or the slip per event on a given fault. The following relation between slip rate (SR), average recurrence interval (RI), and average displacement per event (D) is important because the slip rate effectively constrains the hazard (amount of displacement and likelihood of occurrence):

$$SR = \frac{D}{RI}$$

Given the low slip rates on faults at Yucca Mountain, the average displacements must be small, or the average recurrence intervals must be long. Based on estimates of slip rate, one can use information on the average recurrence interval to calculate the average displacement per event. Alternatively, one can use information on displacement per event to calculate recurrence interval. Both approaches are used in this analysis to assess the fault displacement hazard on features for which we have slip rates (i.e., features having a measurable cumulative displacement). If the features have no detectable cumulative offset (no slip and, therefore, no slip rate), a different approach is required. The displacement characterization based on fault-slip rate are presented in Section 5.2. The potential for displacement along fractures and in unbroken rock is discussed in Section 5.3.

5.2 POTENTIAL FOR DISPLACEMENT ON IDENTIFIED FAULTS

The logic tree used to characterize the fault displacement on the identified faults in the controlled area is shown on Figure DFS-15. The parameters used to characterize the fault displacement include:

- fault activity,
- the cumulative displacement on post-Tiva Canyon Tuff,
- the average Quaternary slip rate.
- the average displacement per event,
- the average recurrence interval, and
- the event-to-event variability in the displacement per event at a point along a fault.

Each of these factors is discussed below.

5.2.1 Fault Activity

In the context of assessing fault displacement hazard, the activity of a fault is the likelihood that the feature has undergone movement (slip) in response to tectonic forces during the present tectonic regime (the Quaternary). It includes all types of fault slip (primary and secondary faulting), except displacements due to near-surface gravitational effects such as landslides, effects of liquefaction, and effects of differential compaction.

If the fault at a test calculation site has had Quaternary displacement, we assigned it a probability of activity of 1.0 (unless there is evidence that suggests the displacements were not tectonic). Only the north-south block-bounding faults at Yucca Mountain have demonstrated evidence of Quaternary displacement. These include the Bow Ridge fault (Test Calculation Site #1) and the Solitario Canyon fault (Test Calculation Site #2). These faults are assigned a probability of activity of 1.0 (Table DFS-8).

Two zones of fractures having no detectable slip have appeared at least twice in the Quaternary alluvial and colluvial deposits that overlie north-northeast-trending bedrock faults along the east side of Exile Hill in Midway Valley (Test Calculation Site #9; Swan et al., 1995; Keefer and Whitney, 1996). The fracturing occurred repeatedly (at least twice) during stratigraphically distinct episodes. Non-tectonic mechanisms for the formation of these fractures cannot be ruled out, but it seems unlikely given the consistent orientation of the fractures, the continuity of the zones along strike, the coincidence of the western zone of Quaternary fractures with the Exile Hill fault, and the fact that individual fractures in the Quaternary deposits can be traced into faults in the underlying Tertiary bedrock. The Exile Hill fault is assigned a probability of activity of 0.8.

In Section 4.3.1, we assigned a very low probability (0.05) that the Ghost Dance fault (Test Calculation Site #4) is active and capable of generating significant earthquakes. In addition to the lack of evidence for Quaternary displacement, the low weight reflects our interpretation that the small-displacement intrablock faults probably represent secondary accommodation structures rather than primary, earthquake-generating structures. Because the fault displacement hazard assessment includes the effects of both primary and secondary faulting, the probability that a fault can move is not necessarily the same as the probability that it can generate significant earthquakes. The evidence suggests there has been no displacement on the Ghost Dance fault since at least the middle Pleistocene (Taylor et al., 1996). However, very small movements similar to the fractures observed along the Exile Hill fault cannot be precluded. Based on analogy to the Exile Hill fault and consideration of structural models that suggest that the Ghost Dance fault could move in response to displacements on the block-bounding faults, we give a low but significant probability that the Ghost Dance fault has experienced a small amount of Quaternary displacement. That the fault is active and capable of displacement is assigned a probability of 0.4.

There is no evidence that any of the northwest-trending faults in the vicinity of Yucca Mountain have experienced Quaternary displacement. These include the Drill Hole Wash fault (Test Calculation Site #3) and the Sundance fault (Test Calculation Site #5). Middle Pleistocene and older deposits overlie northwest-trending faults exposed in trenches on the east side of Exile Hill, providing direct evidence of no displacement during the period of repeated displacements along the north-south block-bounding faults (Swan et al., 1996). This strongly suggests that the faults are not kinematically linked under the present tectonic regime. However, Quaternary displacement cannot be precluded at Test Calculation Sites #3 and #5. Right-slip movement on northwest-striking faults is compatible with some structural models for Yucca Mountain (e.g., vertical axis rotation of the structural blocks). Day et al. (1996, p. 2-6) present evidence that the north-striking and northwest-striking faults have been kinematically linked sometime during their displacement history. Movement on the northwest-striking faults is compatible with the inferred orientation of the present stress field. Considering these factors, we assign a very low probability that there has been Quaternary displacement on Drill Hole Wash and Sundance faults. The probability of activity assigned to these structures is 0.01.

The activity of the unnamed fault west of Dune Wash is more uncertain. Its north-south trend and position relative to the block-bounding faults suggest a potential for slip similar to that of the Ghost Dance fault. We assigned it the same probability of activity (0.4).

Test Calculation Sites #7 and #8 contain very small faults, fractures, or unbroken rock at two locations within the proposed repository area: one 100 m east of the Solitario Canyon fault, the other midway between the Solitario Canyon and Ghost Dance faults. The activity of fractures and unbroken rock is addressed in Section 5.3.1. Small-displacement faults (less than about 3 m) are common throughout the Controlled Area. The following factors should be considered when assessing the activity of these features.

- **Orientation.** Paleoseismic evidence of Quaternary displacement has been found only along the north-south-trending faults. Faults having other trends presumably have a much lower probability of being active (perhaps an order of magnitude or more).
- **Faults that die out during the Miocene.** Many of the small-displacement faults die out upward within the Tertiary section and are pre-latest Miocene in age, precluding any Quaternary displacement. Where this can be demonstrated, the probability of future displacement should be assessed using the approach outlined in Section 5.3.
- **Position relative to active block-bounding faults.** Secondary deformation is more likely to occur on the hanging wall than on the footwall; the zone of deformation typically is much narrower on the footwall of normal faults.
- **Distance from the active block-bounding faults.** Secondary deformation typically is most concentrated immediately adjacent to and within a few meters of a fault. It can, however, occur tens, hundreds, and even thousands of meters from the primary fault trace. There is no relation that reliably predicts the amount or likelihood of secondary faulting related to distance from a primary fault trace. Nonetheless, based on historical earthquakes, it is reasonable to infer that the probability of secondary faulting decreases significantly (by an order of magnitude or greater) at distances more than a few meters to a few tens of meters from a primary fault.

The only information given about Test Calculation Sites #7 and #8 is their location (distance from the active block-bounding faults) and the cumulative displacement of the Tertiary bedrock. Both locations are thousands of meters from the Bow Ridge fault. Secondary (hanging wall) deformation at these locations caused by slip on the Bow Ridge fault is unlikely. Test Calculation Site #7 is 100 m east of the main trace of the Solitario Canyon fault (i.e., in the footwall), but it is about the same distance west of a northeast-trending splay of the Solitario Canyon fault. Test Calculation Site #8 is more than 800 m east of the Solitario Canyon fault. The probability that there has been Quaternary displacement at either of these locations is judged to be extremely low. Based on its closer proximity to one of the active block-bounding faults, Test Calculation Site #7 is assigned a higher probability of activity than site #8. The probability of activity assigned to small faults (either 10 cm or 2 m cumulative slip) at sites #7 and #8 are 0.05 and 0.01, respectively.

5.2.2 Cumulative Displacement and Age of the Tiva Canyon Tuff

At most of the test calculation sites, the only basis for estimating fault slip rate is the cumulative net slip of the faulted bedrock. At the proposed repository level, this is the 12.7 ± 1.3 Ma Tiva Canyon Tuff. Table DFS-8 gives the cumulative net slip of the Tiva Canyon Tuff at the nine test calculation sites. The reported values are specific to the individual sites and do not represent average values along the length of the fault. The cumulative displacements are based on: geologic maps and geologic cross sections of Yucca Mountain (Scott and Bonk, 1984; Day et al., 1996a; and Day et al., 1996b), and geologic reports (Gibson et al., 1992, Tables 4-1 and 4-2; Swan et al., 1995, Table 9). Values shown may differ somewhat from previously published values because, in some cases, adjustments were made for a lateral component to net slip, and/or allowances were made for more uncertainty in the range of values.

Except for test calculation sites 7b, 7c, 8b, and 8c, where the displacements are inferred to be known based on direct observation, the displacements are reported as a range of values to include uncertainties related to:

- measurement errors (associated with measurement of dip slip from geologic cross sections and measurement of stratigraphic throw across the fault from geologic maps having 10- to 20-foot contour intervals);

- extrapolations of the dip slip along the strike of the fault in cases where the measured bedrock displacements are not coincident with the test calculation site; and/or
- uncertainties in the lateral slip component of the net slip.

The range of values and assigned probability weights for the cumulative displacement of the Tiva Canyon Tuff are presented in Table DFS-8.

The age of the Tiva Canyon Tuff used in this analysis, 12.7 ± 1.3 Ma, is based on the range of values presented in tables compiled by Gibson et al. (1990, and 1992, Table 4-1).

5.2.3 Average Quaternary Slip Rate

Four approaches were used to estimate the average Quaternary slip rate. Where paleoseismic data are available on the amount and timing of Quaternary displacements, these data were used to calculate the slip rate directly. In most cases, however, there is little or no geologic information to directly assess the Quaternary slip rate. Therefore, estimates also are made based on site-specific assessments of cumulative net slip of the Tiva Canyon Tuff and three different structural/historical interpretations of the late Cenozoic evolution of faulting at Yucca Mountain. Locations for which there are data on both the post-late Miocene and Quaternary displacements (e.g., Test Calculation Sites #1, #2, and #9) provide a means for calibrating the reliability of the methods based on the post-Tiva Canyon Tuff cumulative net slip. The basis for each approach is described below.

Quaternary Slip Rates Based on Paleoseismic Data. Where possible, the rate of deformation is based on the amount of displacement and ages of Quaternary deposits, soils, and/or geomorphic features overlying the faults. The Quaternary slip rates (and the associated uncertainty) for the Bow Ridge and Solitario Canyon faults are based on the results of detailed paleoseismic investigations at or near Test Calculation Sites #1 and #2. The Quaternary slip rate on the Ghost Dance fault is based on the absence of evidence for Quaternary displacement, inferences about the threshold of detection and analogy to the Exile Hill fault (Swan et al., 1995). The range of values and the corresponding probability weights used in the fault displacement hazard analysis are presented in Table DFS-9.

Uniform Slip Rate, Post-Tiva Canyon Tuff. In this interpretation, the average post-Tiva Canyon slip rate is assumed to be approximately equal to the average late Quaternary slip rate. Slip rates are calculated by dividing the post-Tiva Canyon Tuff cumulative net slip by 12.7 ± 1.3 Ma.

Uniform Slip Rate, Post-Rainier Mesa. Gibson et al. (1992, p. 72) suggest that an abrupt decrease in the slip rate on the block-bounding faults at Yucca Mountain may have occurred prior to 7 Ma (dashed line on Figure DFS-16). This abrupt decrease in slip rate may correlate to the marked decrease in silicic volcanic activity. Structural data (Scott and Bonk, 1984) indicate that most (70 to 80 percent) of the displacement on the Bow Ridge and Paintbrush Canyon faults predates the deposition of the Rainier Mesa member of the Timber Mountain Tuff (11.6 ± 1 Ma). In this interpretation, 80 percent of the post-Tiva Canyon displacement is interpreted to have occurred prior to deposition of the Rainier Mesa, and the average post-Rainier Mesa slip rate is inferred to be approximately equal to the average late Quaternary slip rate. Slip rates are calculated by dividing 20 percent of the post-Tiva Canyon Tuff cumulative displacement by 11.6 ± 1 Ma.

Decreasing Slip Rate Model. Gibson et al. (1990 and 1992) suggest an alternative interpretation of the slip rates on the Bow Ridge and Paintbrush Canyon faults in which the slip rates have decreased continuously since the late Cenozoic (solid line on Figure DFS-16). Day et al. (1996c) present data that indicate that the rate of crustal extension in the Crater Flat basin has been decreasing since the middle Miocene, when the rate of extension is estimated to have been between 18 and 40 percent, to the Quaternary (Figure DFS-17). Their estimates of the Quaternary rate of extension range from 0.1 percent to 0.7 percent. This suggests that Quaternary slip rates could be between 0.3 percent and 3.9 percent of the late Miocene rate.

In this interpretation, the Quaternary slip rate is estimated by multiplying the late Miocene slip rate by a reduction factor. The late Miocene (i.e., post-Tiva Canyon, pre-Rainier Mesa) slip rate is calculated by dividing 80 percent of the post-Tiva Canyon displacement by the interval between the deposition of these units. The duration of this interval is uncertain. The difference between the preferred ages for the two units (i.e., 12.7 Ma and 11.6 Ma) suggests

an interval of 1.1 Ma. Considering the reported uncertainties in the ages of the two units yields a maximum age of 4.4 Ma, which is unreasonably long, and a minimum age difference of - 0.5 Ma, which is geologically impossible because the Rainier Mesa is not older than the Tiva Canyon Tuff. The interval between the deposition of the Tiva Canyon Tuff and the deposition of the Rainier Mesa member of the Timber Mountain Tuff is probably within the range of 1.1 ± 0.6 Ma.

Accordingly, the average Quaternary slip rate (SR) is:

$$SR = \frac{0.8 Dtc}{1.1 \pm 0.6 Ma} RF$$

where *Dtc* is the cumulative net slip on the Tiva Canyon Tuff and RF is the reduction factor, which is in the range of 0.3% to 3.9%.

Slip rates calculated using this approach are compared to rates based on paleoseismic information in Table DFS-10 to assess the reliability of the interpretation. Reduction factors of 2.1 % (the midpoint of the range) to 3.9% (the minimum reduction based on Fridrich et al. data; Figure DFS-17) yield rates that are in general accord with the estimates based on paleoseismic information. A reduction factor of 0.3 % (the maximum reduction suggested by Fridrich et al. data) yielded values that are considered too low (Table DFS-10). Based on this comparison, the probability weights assigned to the values for the reduction factor are: 0.3 % (0.04), 2.1 % (0.48), and 3.9 % (0.48) (Figure DFS-18).

Relative Weights Assigned to Techniques for Estimating Slip Rate. Quaternary slip rates based on paleoseismic data are not available for all the test calculation sites. Therefore, the relative weights assigned to the four techniques described above are dependent on the availability of paleoseismic data (Figure DFS-18). Slip rates based on the amount of displacement and ages of faulted Quaternary units provide the most reliable indication of the current slip rate and are given the greatest weight (0.7) if these data are available. There is not a strong consensus among geologists as to which of the three models for the late Cenozoic evolution of faulting at Yucca Mountain is most likely. Therefore, the three slip

rate models based on the cumulative net slip of the Tiva Canyon Tuff are assigned equal weights.

5.2.4 Potential for Fault Rupture

The approaches described above are used to calculate the probability distribution for the Quaternary slip rate at each of the nine test calculation sites. Given the slip rate, the average interval between displacement events can be calculated by dividing the average displacement per event by the slip rate. Alternatively, the average displacement per event can be calculated by multiplying the slip rate times the average recurrence interval. Both methods are given equal weight in the fault displacement hazard analysis (Figure DFS-15).

Site-specific assessments of the average displacement per event and the average recurrence interval are made for each of the faults at the nine test calculation sites based on the available information (Table DFS-11). To the extent possible, these assessments are based on fault specific data on the size and timing of Quaternary faulting events. Where there are no data on the size and/or timing of Quaternary displacements (e.g., due to the absence of evidence of displacement, or due to the lack of suitable Quaternary strata), the displacement per event and recurrence interval are characterized based on analogy to similar faults.

#1 Bow Ridge Fault

Average Displacement Per Event. Menges and Whitney (1996b, table 4.4.3) report a maximum range of from 1 to 80 cm for the net slip associated with past surface faulting events on the Bow Ridge fault at Trench 14D, which is at the same latitude as the ESF-Bow Ridge fault crossing. If 80 cm is taken as the upperbound displacement, this suggests an average slip per event of about 46 cm (i.e., 80 cm/1.73; see Table DFS-13).¹ Menges and Whitney's preferred values for individual events identified in this trench are: 13 cm, 14 cm, and 44 cm. If 44 cm represents the maximum displacement at this location, one would expect the average displacement to be about 25 cm (44 cm/1.73), which is close to the numerical average of their preferred values (i.e., 24 cm). Based on these observations, the

¹ The relation between maximum and average displacement used here is based on analysis of the variability in the single event displacements observed in the Yucca Mountain trenches. (See Section 5.2.5 for details.)

range of values for the average slip per event where the Bow Ridge fault crosses the ESF is considered to be 10 cm (0.15); 20 cm (0.7); and 40 cm (0.15).

Average Recurrence Interval. Menges and Whitney (1996b, table 4.4.5) report a range of 70 ka to 215 ka for the average recurrence interval on the Bow Ridge fault at this location (Trench 14D). Their preferred range is between 100 ka and 140 ka. Based on these data, we considered the following range of values for the average slip rate: 70 ka (0.1); 100 ka (0.4); 140 ka (0.4); and 215 ka (0.1).

#2 Solitario Canyon Fault

Average Displacement Per Event. Site #2 is located on the Solitario Canyon fault approximately midway between trenches SCF-T4 and T8. The Quaternary fault displacement data reported by Ramelli et al. (1996, table 4.7.3) indicate that the cumulative displacement and the average displacement per event increase to the south. Accordingly, one would expect the average displacement at site #2 to be greater than the values obtained at trench SCF-T4 and less than those at T8.

The values reported from trench SCF-T4 (Ramelli et al., 1996, table 4.7.3) range from fractures having no movement up to 40 cm. If 40 cm is the maximum at this location, it suggests an average displacement per event of about 23 cm (40 cm/1.73). The average displacement for the three most recent events is about 20 cm.

The maximum values reported from trench T-8 range from 10 cm to 130 cm. If 130 cm is the upperbound displacement for a single event at this location, it suggests an average displacement per event of ≤ 75 cm (i.e., 130 cm/1.73). Averaging the reported values from the four most recent events yields an average displacement per event of about 50 cm.

Extrapolating these data suggests the average displacement per event at site #2 probably is in the range of 35 to 45 cm. Because of the uncertainty inherent in such an extrapolation, a wider range of values is considered. The range of values considered in the fault displacement hazard analysis for the average displacement per event at site #2 on the Solitario Canyon fault is: 20 cm (0.2); 40 cm (0.6); and 60 cm (0.2).

Average Recurrence Interval. Based on the results of paleoseismic investigations, Ramelli et al. (1996, p. 4.7-48) suggest that the minimum recurrence interval on the Solitario Canyon fault is about 35 ka and the maximum is about 100 ka. Based on the occurrence of three or four events during about the past 200 ka, they estimate that the average recurrence interval ranges from 50 to 70 ka. The values included in the fault displacement hazard analysis and the assigned probability weights are: 35 ka (0.2); 50 ka (0.3); 70 ka (0.3); and 100 ka (0.2).

#4 Ghost Dance Fault

Average Displacement Per Event. With the possible exception of fractures, there is no evidence of Quaternary movement on the Ghost Dance fault (Taylor et al., 1996). However, we assign a low probability that movement can occur in the future. Three approaches were used to characterize the possible average displacement per event.

- (1) If the Ghost Dance fault is considered to be an independent seismogenic source, which is judged to be very unlikely (see Section 4.3.1), the Wells and Coppersmith (1984) relation between average displacement and fault rupture length can be used to calculate the average displacement along strike associated with rupture of the entire length of the fault. The data set of historical earthquakes on which this relation is based is only marginally applicable to faults as short as the Ghost Dance fault, which has a mapped length of about 3 km (Day et al., 1996, p. 2-6). If the Ghost Dance fault is combined with the Abandoned Wash fault, the total fault length is about 9 km. Using this approach, rupture lengths of 3 to 9 km suggest a maximum value for the average displacement in the range of 8 to 22 cm.
- (2) If displacement on the Ghost Dance fault occurs as secondary deformation in the hanging wall of either the Bow Ridge or Paintbrush Canyon faults, the maximum displacement on the Ghost Dance fault would be significantly less than the slip per event on either of these faults. Based on displacement per event data summarized by Pezzopane et al. (1996b, table 5-1), the average displacement per event on the Bow Ridge and Paintbrush Canyon faults (i.e., at about the same latitude as Test Calculation Site #4 on the Ghost Dance fault) is about 24 cm and 55 cm, respectively. If the secondary displacements scale in proportion to the cumulative bedrock displacement on these faults, the average slip per event on the Ghost Dance fault is about 5 cm (25m/130m x 24 cm per event for the Bow Ridge fault; or 25m/300m x 55 cm per event for the Paintbrush Canyon fault).

- (3) Considering the Quaternary displacement history on the Ghost Dance fault to be similar to the small north-south intrablock faults in Midway Valley, suggests that Quaternary movements have been limited to fractures having slip amounts that are less than the threshold of detection. The threshold of detection on the fracturing events in Midway Valley ranges from a few millimeters or less (essentially zero displacement) to not more than 5 cm (Swan et al., 1995).
- (4) Considering all three approaches, the range of values included in the hazard characterization for the average displacement per event at site #4 on the Ghost Dance fault is: 0.05 cm (almost zero displacement) (0.3); 1 cm (0.25); 3 cm (0.2); 5 cm (0.15); 10 cm (0.07); and 15 cm (0.03).

Average Recurrence Interval. The available data indicate there has been no displacement on the Ghost Dance fault for approximately the past 100 ka (no displacements since the late Pleistocene). If the Ghost Dance fault can move in the present tectonic regime, the recurrence interval is presumably longer than about 100 ka. In the context of neotectonic studies, average recurrence intervals longer than half a million years probably are not meaningful. Given the lack of any evidence suggesting a particular recurrence interval, we assumed that, if the fault can move, the average recurrence interval is essentially equally likely to be anywhere in the range of 100 to 500 ka with a slight chance that the recurrence interval could be as short as 50 ka. The range of values included in the fault displacement hazard analysis and the assigned probability weights are: 50 (0.005); 100 ka (0.1); 200 ka (0.25); 300 ka (0.25); 400 ka (0.25); and 500 ka (0.145).

#3 Drill Hole Wash Fault and #5 Sundance Fault

No evidence of Quaternary displacement has been discovered along any of the northwest-striking faults in the Yucca Mountain area. If the faults are capable of movement in the present tectonic regime, the movement probably occurs in response to movement on the more active north-striking Quaternary faults. The average displacement per event is certainly less than that along the north-south block-bounding faults and probably is less than the Ghost Dance fault. For the purpose of the fault displacement hazard analysis, the same displacement and recurrence parameters used to characterize the average displacement per event and average recurrence interval on the Ghost Dance fault also were used to characterize the Drill Hole Wash and Sundance faults.

#6 Unnamed Fault West of Dune Wash

There are no data on the Quaternary displacement history of this fault. Its orientation and location within the Yucca Mountain block are similar to the Ghost Dance fault, but it has a shorter total fault length and smaller cumulative displacement. Except for the difference in slip rate, site #6 is considered to have a potential for displacement that is similar to that of site #4 on the Ghost Dance fault (Table DFS-8). The same parameters used to characterize the average displacement per event and average recurrence interval on the Ghost Dance fault also were used to characterize the unnamed fault at Test Calculation Site #6.

Test Calculation Sites #7a, #7b, #8a, and #8b

The fault displacement hazard at these sites was treated the same except that sites #7b and #8b have lower slip rates due to their smaller cumulative displacement (10 cm versus 2 m), and site #7 is assigned a higher potential for activity (Table DFS-8) than site #8 because it is closer to an active block-bounding fault (Section 5.2.1).

Average Displacement Per Event. If movement can occur on these small intrablock faults, the average displacement per event would be less than or similar to that of Exile Hill fault (see below). The same range of values included in the analysis for the Exile Hill fault is used to characterize the 2-m faults. In characterizing the 10-cm faults, the range is extended to include a minimum value of 0.05 cm and more weight is assigned to the low end of the range (Table DFS-11).

Average Recurrence Interval. There are no data that suggest how these short, small-displacement faults and shears behave during repeated faulting events. Therefore, a wide range of behavior is considered. If these features are capable of movement, the minimum recurrence is a single event during the present tectonic regime. For the purpose of this analysis, the period of the present tectonic regime is considered to be the Quaternary, or approximately the past 1.6 ma. The maximum recurrence rate would occur if minute displacements occurred every time there is a large-magnitude local earthquake in the immediate vicinity (e.g., on the block-bounding faults). The results of paleoseismic investigations (USGS, 1996) suggest that surface faulting events on the block-bounding faults might occur as frequently as about once every 50,000 years. This is judged to be an

upper bound for the average recurrence interval for events large enough to produce secondary displacement within the Yucca Mountain block. Given the lack of evidence for a particular recurrence interval, we judge that the average recurrence interval is more or less equally likely to be anywhere in the range of 100 to 500 ka (the same as for the Ghost Dance fault) and that there is a small chance that the recurrence interval could be as long as 1.6 ma or as short as 50 ka. The range of values included in the fault displacement hazard analysis and the assigned probability weights are: 50 ka (0.05); 100 ka (0.18); 200 ka (0.18); 300 ka (0.18); 400 ka (0.18); 500 ka (0.18); and 1600 ka (0.05).

#9 Exile Hill Fault in Midway Valley

Average Displacement Per Event. Except for two zones of fractures identified in trenches, the evidence indicates that there has been no Quaternary displacement (within the limits of detection) on the Exile Hill fault in Midway Valley (Swan et al., 1995; Keefer and Whitney, 1996). Considering the resolution for detecting displacements, some small displacement can not be ruled out. Three approaches were used to characterize the average displacement per event.

1. The total length of the Exile Hill fault is between < 2 km and 4.4 km. Using these values and the Wells and Coppersmith (1984) relation between average displacement and fault rupture length, we obtained displacements of < 5 cm to 11 cm.
2. If the Exile Hill fault represents secondary deformation in the footwall of the Bow Ridge fault or in the hanging wall of the Paintbrush Canyon fault, the maximum displacement on the Exile Hill fault would be significantly less than the slip per event on either of these faults. Based on displacement per event data summarized by Pezzopane et al. (1996b, table 5-1), the average displacement per event on the Bow Ridge and Paintbrush Canyon faults is about 24 cm and 55 cm, respectively. Scaling the secondary displacements in proportion to the cumulative bedrock displacement on these faults, suggests the average slip per event on the Exile Hill fault is about 2 cm (10m/130m x 24 cm per event for the Bow Ridge fault, or 10m/300m x 55 cm per event for the Paintbrush Canyon fault).
3. The results of the fault exploration trenches on the east side of Exile Hill indicate that the Quaternary displacements have been less than the threshold of detection. The threshold of detection on the fracturing events in Midway Valley ranges from

a few millimeters or less (essentially zero displacement) to not more than 5 cm (Swan et al., 1995).

Considering these approaches, the range of values included in the hazard analysis for the average displacement per event at site #9 on the Exile Hill fault is: 0.05 cm (almost zero displacement) (0.35); 1 cm (0.3); 3 cm (0.2); 5 cm (0.1); and 10 cm (0.05).

Average Recurrence Interval. The data indicate there has been no detectable displacement on the Exile Hill fault since the Middle Pleistocene or longer. Given the lack of evidence suggesting a particular recurrence interval, we consider that, if the fault can move, the average recurrence interval is more or less equally likely (i.e., maximum uncertainty) to be anywhere in the range of 100 to 500 ka. The range of values included in the fault displacement hazard analysis and the assigned probability weights are: 100 ka (0.1); 200 ka (0.25); 300 ka (0.25); 400 ka (0.25); and 500 ka (0.15).

5.2.5 Event-to-Event Variability

The procedures described above provide a means for assessing the probability of average displacements at a specified fault crossing. It is also important to know how much displacements are likely to vary from the average displacement. The event displacement data from Yucca Mountain paleoseismic investigations were compiled to assess: (1) the relationship between average displacement and the maximum displacement during successive events at a point along the fault; and (2) the variability in the amount of displacement during successive events at a point along the fault (not to be confused with the variability in displacement along strike during a single event).

Pezzopane et al. (1996b, table 5-1) compiled the event displacement data from the Yucca Mountain paleoseismic investigations. Table DFS-12 is a summary of the event displacement data for all localities where displacements for three or more events were reported. The average of the reported events is calculated for each locality. The ratio between the size of each event and the average displacement at that locality is also calculated. The maximum reported displacement at each locality ranges from 1.03 to 2.63 times the average displacement; on average (based on 19 localities), the maximum displacement is 1.73 times the average displacement (Table DFS-13).

Figure DFS-19 is a frequency plot showing event-to-event variability in displacement based on the displacement data (ratio of the reported displacement for an event, D , to the average displacement at the same location, AD) presented on Table DFS-12. A generalization of this frequency distribution (i.e., the dashed line on Figure DFS-19) was used to define a triangular distribution for the ratio D/AD . The Facilities Team analyzed the data in Table DFS-12 and found that a better fit is obtained with a gamma distribution (see Appendix H, Section H.2.1). We adopt the distribution given in Appendix H for characterizing the distribution of displacement at a point.

5.3 POTENTIAL FOR DISPLACEMENT ON FRACTURES AND UNBROKEN ROCK

Fractures and unbroken rock have no cumulative displacement and, therefore, no slip rate. Consequently, the slip-rate approach used above to assess the potential for displacement on faults must be modified to assess the potential for displacement on fractures or in unbroken rock. The approach adopted for this analysis is based on the premise that, given the non-occurrence of an event and a long observation period, the annual probability of the event occurring must be less than 1 divided by the duration of the observation period.

The logic tree for characterizing the displacement hazard on fractures and unbroken rock is presented in Figure DFS-20. The elements considered in assessing displacement hazard at Test Calculation Sites #7c, #7d, #8c, and #8d include:

- the potential for activity,
- relative probabilities associated with the different deformation history models,
- age of the host rock, and
- constraints on the size of an event based on the threshold of detection for fault displacement.

Uncertainties in the age of the host rock were discussed in Section 5.2.2. The other elements are discussed below.

5.3.1 Potential for Activity

If one applies the definition of activity as used to characterize faults (Section 5.2.1), fractures and unbroken rock would be classified as not active (i.e., they have had no displacement during the present tectonic regime), which implies that they have no potential for displacement during future periods of concern for repository performance. From a practical standpoint, this is true. Experience based on observations of historical surface faulting events and on detailed paleoseismic investigations of Quaternary fault movements shows that future fault movements can best be defined by recent past history and that the likelihood of new faulting is negligible (ASCE, 1997, p. 99). However, new faults must form some time. In the context of assessing fault displacement at locations where there has been no detectable displacement, the concept of activity, or potential for activity, is used to mean the relative likelihood that there could be displacement in the future. It is a relative approach whereby faults having known recent displacements would be assigned the highest weight (probability of 1), and intact rock far from active faults would have the lowest potential for activity (at least two or three orders of magnitude less likely). The factors for evaluating fault activity described in Section 5.2.1 were considered in our assessment of the potential for activity on fractures and in unbroken rock. In addition, information on the morphology of the fracture itself, such as degassing tracks that indicate formation during lithification of the tuff, may provide clues to the origin and potential activity of a fracture. Table DFS-14 gives the subjective probability weights for potential for activity assigned to fractures and unbroken rock at Test Calculation Sites #7 and #8 and describes the basis for the assigned weights.

5.3.2 Probability of an Event Associated with Different Deformation History Models

In Section 5.2.3, three models were presented for characterizing the deformation history at Yucca Mountain. In one model, the rate of deformation has been uniform since deposition of the Tiva Canyon Tuff. In this interpretation, the annual probability of a displacement event, given no prior displacement, is less than 1 over the age of the host rock, which at the repository level is the Tiva Canyon Tuff. This corresponds to an annual probability of $<1 \times 10^{-7}$ (Table DFS-15).

In the other two models, the present rate of deformation is significantly less than the average long-term (post-Tiva Canyon Tuff) rate. If other factors such as the stress field have

remained the same, the potential for deformation (movement on existing faults and/or formation of new faults) should be less now than they were during the late Miocene, when the rate is interpreted to have been much higher.

Considering the potential for displacement to be directly proportional to the rate of deformation, the probability of an event relative to the uniform deformation model can be expressed as the ratio between the inferred present rate and the average long-term post-Tiva Canyon rate times the probability of an event for the uniform deformation model. The range of probability values for the different deformation history models is given in Table DFS-15.

As discussed in Section 5.2.3, the three deformation history models are assigned equal weight (Figure DFS-20).

5.3.3 Threshold of Detection

Where there is no apparent displacement, it could be assumed that there has been a displacement too small to be detected. The size of the displacement is constrained by (less than) the threshold of detection. What is, the largest displacement that could have occurred at the location under consideration that could have gone undetected?

The threshold of detection depends on location-specific conditions. Are there sharp, well-defined marker horizons that record/preclude offsets? Is the rock massive or extensively fractured and/or sheared? What is the quality of the exposure? How extensive and detailed were the investigations to detect offsets? For the purpose of this analysis, we infer that the conditions would be typical of those parts of the ESF where the Tiva Canyon Tuff is well exposed and has been mapped in detail. Conditions may vary locally.

Investigations can more confidently preclude small displacements in unbroken rock than along a fracture. Therefore, the threshold of displacement detection is conditional on whether the rock is fractured or unbroken (Figure DFS-20).

Given the characteristics of the Tiva Canyon Tuff, we consider offsets larger than about 10 cm to be recognizable as observable stratigraphic offsets. Displacements smaller than a

millimeter would be difficult to preclude, but smaller displacements obviously can occur; nominally we selected half a millimeter as the lower bound displacement. 10 cm and 0.05 cm were taken as the end members for the displacements on fractures. More commonly displacements in the range of 1 to 5 cm can be precluded. The range of values and assigned weights included in the fault displacement hazard analysis for the threshold of detection on well exposed fractures in the Tiva Canyon Tuff are: 0.05 cm (0.145); 0.1 cm, (0.2); 0.5 cm, (0.3); 1.0 cm, (0.2); 3 cm, (0.1); 5 cm, (0.05); and 10 cm, (0.005). The range of values for unbroken rock are: 0.05 cm (0.195); 0.1 cm, (0.3); 0.5 cm (0.25); 1.0 cm, (0.1); 3 cm, (0.1); 5 cm, (0.05); and 10 cm (0.005).

5.4 ESTIMATION OF FAULT DISPLACEMENT

The approach and hazard parameters described above are used to quantitatively assess the probability of fault displacement (hazard curves that relate annual probability to amount of displacement) for the nine test calculations sites. Because the approach used to characterize the hazard on faults is different from the approach used for fractures and unbroken rock, caution should be used when comparing or combining the results. If the input parameters and their uncertainties have been appropriately characterized, the slip-rate based approach used to assess the potential for displacement on faults should yield a realistic assessment of the actual hazard. However, the approach used to assess the displacement hazard on fractures or in unbroken rock only constrains the upper bound for the hazard; it does not necessarily define the actual hazard. The actual hazard is likely to be less than the resultant values. The threshold of detection parameter gives maximum displacement values and the age of the host rock gives the minimum period for the non-occurrence of an event. The potential for activity parameter may compensate for the conservatism that is inherent in the other parameters, but we suspect the probability of future displacement may be much lower than indicated. This parameter is largely subjective and we have probably been overly conservative in assigning probability weights to potential for activity on fractures and in unbroken rock. Despite these limitations, we feel the results are useful because they indicate the hazard is extremely low.

The nine Test Calculation Sites that were selected to represent the range of conditions expected within the control area. Application of the evaluations of these sites to other parts

of the control area is straightforward. However, one important substitution may need to be made depending on the application. Here we have used the displacement data that are location-specific to characterize the potential for displacement at that location. To characterize the potential for fault displacement along the length of a fault, one should use the average post-Tiva Canyon Tuff displacement (or average Quaternary slip rate) along the plane of the fault that intersects the Control Area instead of the average displacement at a specific location along the fault.

REFERENCES

- American Society of Civil Engineers (ASCE), 1997, Seismic and dynamic analysis and design considerations for high level nuclear waste repositories : A report by the Subcommittee on Dynamic Analysis and Design of High Level Nuclear Waste Repositories of the TA Committee on Dynamic Effects of the Technical Activities Division of the Structural Engineering Institute , J. Carl Stepp (ed.), ASCE, New York, 185 pp., plus appendices A through F.
- Anderson, R.E., Bucknam, R.C., Crone, A.J., Haller, K.M., Machette, M.N., Personius, S.F., Barnhard, T.P., Cecil, M.J., and Dart, R.L., 1995b, Characterization of Quaternary and suspected Quaternary faults, regional studies, Nevada and California: U.S. Geological Survey, Open-File Report 95-599.
- Anderson, R.E., Crone, A.J., Machette, M.N., Bradley, L., and Diehl, S.F., 1995a, Characterization of Quaternary and suspected Quaternary faults, Amargosa area, Nevada and California: U.S. Geological Survey Open File Report 95-613, 41 p.
- Anderson, L.W., and Klinger, R.E., 1996, Quaternary faulting on the Bare Mountain Fault: Chapter 4.12, *in* U.S. Geological Survey (Whitney, J.W., Coordinator), Seismotectonic Framework and Characterization of Faulting at Yucca Mountain, Nevada: U.S. Geological Survey report to the Department of Energy that fulfills Level 3 Milestone 3GSH100M WBS Number 1.2.3.2.8.3.6, variously paginated.
- Atwater, T., 1989, Plate tectonic history of the northeast Pacific and western North America: Geological Society of America, *The Geology of North America*, v. N, p. 21-72.
- Bellier, O., and Zoback, M.L., 1995, Recent state of stress in the Walker Lane zone, western Basin and Range provinces, United States: *Tectonics*, v. 14, n. 3, p. 564-593.
- Bonilla, M.G., Mark, R.K., and Lienkaemper, J.J., 1984, Statistical relations among earthquake magnitude, surface rupture length, and surface fault displacement: *Bulletin Seismological Society of America*, v. 74, p. 2379-2411.
- Brocher, T. M., Hart, P. E., Hunter, W. C., and Langenheim, V. E., 1996, Hybrid-source seismic reflection profiling across Yucca Mountain, Nevada: regional lines 2 and 3: U. S. Geological Survey Open-File Report 96-28.

- Broxton, D.E., Warren, R.G., Byers, F.M., Jr., and Scott, R.B., 1989, Chemical and mineralogical trends within Timber Mountain-Oasis Valley caldera complex, Nevada: Evidence for multiple cycles of chemical evolution in a long-lived silicic magma system: *Journal of Geophysical Research*, v. 94, no. B5, p. 5961-5986.
- Burchfiel, B.C., Hamill, G.S., IV, and Wilhelms, D.E., 1983, Structural geology of the Montgomery Mountains and the northern half of the Nopah and Resting Springs ranges, Nevada and California: *Geological Society of America Bulletin*, v. 94, p. 1359-1376.
- Carr, W. J., Byers, F. M., Jr., and Orkild, P.P., 1986, Stratigraphic and volcano-tectonic relations of Crater Flat Tuff and some older volcanic units, Nye County, Nevada: U. S. Geological Survey Open-File Report 82-457, 23 p.
- Cornell, C.A., and Wintestein, S.R., 1986, Seismic hazard assessment: Chapter 5, *in* Hunter, R.L., and Mann, C.J. (eds.), *Techniques for Determining Probabilities of Events and Processes Affecting the Performance of Geologic Repositories*, NUREG/CR-3964, 1, P. 127-172, U.S. Nuclear Regulatory Commission, Washington, D.C.
- Cornwall, H.R., 1972, *Geology and mineral deposits of southern Nye County, Nevada*: Nevada Bureau of Mines and Geology Bulletin 77, 49 pp., 1 plate.
- Crowe, B. M., Perry, F. V., Geissman, J., McFadden, L. D., Wells, S. G., Murrell, M., Poths, J., Valentine, G. A., Bowker, L., and Finnegan, K., 1995, Status of volcanism studies for the Yucca Mountain Site Characterization Project: Los Alamos National Laboratories report LA-12908-MS, Los Alamos, New Mexico, 363 p.
- Day, W.C., Dickerson, R.P., Potter, C.J., Sweetkind, D.S., San Juan, C.A., and Scott, R.B., 1996a, *in* review, Preliminary Geologic Map of the Yucca Mountain Area, Nye County, Nevada: U.S. Geological Survey, Draft Version 1.1 (9/96), scale 1:24,000.
- Day, W.C., Potter, C.J., Sweetkind, D.S., Dickerson, R.P., and San Juan, C.A., 1996b, Geologic sections of the central block area, Yucca Mountain, Nye County, Nevada: Plate 2, *in* Bedrock Geologic Map of the Central Block Area, Yucca Mountain, Nye County, Nevada: U.S. Geological Survey Administrative Report.
- Day W.C., Potter, C.J., Sweetkind, D.S., and Keefer, W.R., 1996c, Structural Geology of the central block of Yucca Mountain: p. 2-1 to 2-12 of Chapter 2, *in* U.S. Geological Survey (Whitney, J.W., Coordinator), *Seismotectonic Framework and Characterization of Faulting at Yucca Mountain, Nevada*: U.S. Geological Survey report to the Department of Energy that fulfills Level 3 Milestone 3GSH100M WBS Number 1.2.3.2.8.3.6, variously paginated.

- Dohrenwend, J.C., Menges, C.M., Schell, B.A., and Morning, B.C., 1991, Reconnaissance photogeologic map of young faults in the Las Vegas 1° X 2° quadrangle, Nevada, California, and Arizona: U.S. Geological Survey Miscellaneous Field Studies map MF-2182, scale 1:250,000.
- Donovan, D.E., 1991, Neotectonics of the southern Amargosa Desert, Nye County, Nevada, and Inyo County, California: Reno, University of Nevada, M.S. thesis, map scale 1:48,000, 151 pp.
- Ekren, E.B., Orkild, P.P., Sargent, K.A., and Dixon, G.L., 1977, Geologic map of the Tertiary rocks, Lincoln County, Nevada: U.S. Geological Survey Miscellaneous Investigations Series Map I-1041, scale 1:250,000.
- Faulds, J. E., Bell, J. W., Feuerbach, and Ramelli, A. R., 1994, Geologic map of the Crater Flat area, Nye County, Nevada: Nevada Bureau of Mines and Geology Map 101, 1:24,000 scale.
- Ferrill, D.A., Stirewalt, G.L., Henderson, D.B., Stamatakos, J.A., Morris, A.P., Spivey, K.H.C., and Wernicke, B.P.C., 1996, Faulting in the Yucca Mountain region: Critical review and analyses of tectonic data from the central Basin and Range: Center for Nuclear Waste Regulatory Analyses Report CNWRA 96-007 or NUREG/CR-6401, San Antonio, Texas, Rev. 01, variously paginated.
- Frankel, A., Mueller, C., Barnhard, T., Perkins, D., Leyendecker, E.V., Dickman, N., Hanson, S., and Hopper, M., 1996, National seismic-hazard maps; documentation June: U.S. Geological Survey Open-File Report 96-532, June, 110 p.
- Fridrich, C. J., in press, Tectonic evolution of the Crater Flat basin, Yucca Mountain region, Nevada, *in* Wright, L. A. and Troxel B. W. (eds.), Cenozoic Basins of the Death Valley Region, California and Nevada: Geological Society of America Special Paper.
- Fridrich, C. J., Whitney, J. W., Hudson, M. R., and Crowe, B. M., in press, Space-time patterns of late Cenozoic extension, vertical-axis rotation, and volcanism in the Crater Flat basin, Nevada, *in* Wright, L. A. and Troxel B. W. (eds.) Cenozoic Basins of the Death Valley Region, California and Nevada: Geological Society of America Special Paper.

Fridrich, C.J., Whitney, J.W., Hudson, M.R., and Keefer, W.R., 1996, Space-time patterns of extension, vertical axis rotation, and volcanism in the Crater Flat Basin: p. 2-12 to 2-41, *in* U.S. Geological Survey (Whitney, J.W., Coordinator), Seismotectonic Framework and Characterization of Faulting at Yucca Mountain, Nevada: U.S. Geological Survey report to the Department of Energy that fulfills Level 3 Milestone 3GSH100M WBS Number 1.2.3.2.8.3.6, variously paginated.

Frizzel, V.A., Jr., and Schulters, J., 1990, Geologic map of the Nevada Test Site, southern Nevada: U.S. Geological Survey Miscellaneous Investigations Series Map I-2046, scale 1:100,000.

Gibson, J.D., Shephard, L.E., Swan, F.H., Wesling, J.R., and Kerl, F.A., 1990, Synthesis of studies for potential for fault rupture at the proposed surface facilities, Yucca Mountain, Nevada: Proceedings of International Topical Meeting, High Level Radioactive Waste Management, April 8-12, v. 1, p. 109-116.

Gibson, J.D., Swan, F.H., Wesling, J.R., Bullard, T.F., Perman, R.C., Angell, M.M., and DiSilvestro, L.A., 1992, Summary and evaluation of existing geological and geophysical data near prospective surface facilities in Midway Valley, Yucca Mountain project, Nye County, Nevada: Sandia Report SAND90-2492 UC-814, Sandia National Laboratories, Albuquerque, New Mexico.

Gutenberg, B., and Richter, C.F., 1954, Seismicity of the Earth: Princeton University Press, 2nd edition.

Harmsen, S. C., 1994, The Little Skull Mountain earthquake of 29 June, 1992: Aftershock focal mechanisms and tectonic stress field implications: Bulletin of Seismological Society of America, v. 84, no. 5, p. 1484-1505.

Jenkins, O.P., 1962, Geologic map of California, Trona Sheet: California Division of Mines and Geology, scale 1:250,000.

Keefer, W.R., and Fridrich, C.J., 1996, Geologic setting of Yucca Mountain, Chapter 1, *in* U.S. Geological Survey (Whitney, J.W., Coordinator), Seismotectonic Framework and Characterization of Faulting at Yucca Mountain, Nevada: U.S. Geological Survey report to the Department of Energy that fulfills Level 3 Milestone 3GSH100M WBS Number 1.2.3.2.8.3.6, variously paginated.

Keefer, W.R., and Pezzopane, S.K., 1996, Quaternary faults in the Yucca Mountain region: Chapter 3, *in* U.S. Geological Survey (Whitney, J.W., Coordinator), Seismotectonic Framework and Characterization of Faulting at Yucca Mountain, Nevada: U.S. Geological Survey report to the Department of Energy that fulfills Level 3 Milestone 3GSH100M WBS Number 1.2.3.2.8.3.6, variously paginated.

Keefer, R., and Whitney, J.W., 1996, Summary of Midway Valley studies: Chapter 4.3, *in* U.S. Geological Survey (Whitney, J.W., Coordinator), Seismotectonic Framework and Characterization of Faulting at Yucca Mountain, Nevada: U.S. Geological Survey report to the Department of Energy that fulfills Level 3 Milestone 3GSH100M WBS Number 1.2.3.2.8.3.6, variously paginated.

Klinger, R.E. and Piety, L.A., 1996, Evaluation and characterization of Quaternary faulting on the Death Valley and Furnace Creek faults, Death Valley, California: U.S. Bureau of Reclamation, Seismotectonic Report 96-10, 98 p.

Longwell, C.R., Pampeyan, E.H., Bowyer, B., and Roberts, R.J., 1965, Geology and mineral deposits of Clark County, Nevada: Nevada Bureau of Mines and Geology Bulletin 62, 218 p., 16 plates.

Menges, C.M., and Whitney, J.W., 1996a, Distribution of Quaternary faults at Yucca Mountain: Chapter 4.2, *in* U.S. Geological Survey (Whitney, J.W., Coordinator), Seismotectonic Framework and Characterization of Faulting at Yucca Mountain, Nevada," U.S. Geological Survey report to the Department of Energy that fulfills Level 3 Milestone 3GSH100M WBS Number 1.2.3.2.8.3.6, variously paginated.

Menges, C.M., and Whitney, J.W., 1996b, Summary of Quaternary faulting on the Paintbrush Canyon, Stagecoach Road, and Bow Ridge faults: Chapter 4.4, *in* U.S. Geological Survey (Whitney, J.W., Coordinator), Seismotectonic Framework and Characterization of Faulting at Yucca Mountain, Nevada: U.S. Geological Survey report to the Department of Energy that fulfills Level 3 Milestone 3GSH100M WBS Number 1.2.3.2.8.3.6, variously paginated.

Minor, S. A., Hudson, M. R., and Fridrich, C. J., 1996, Fault-slip data bearing on the tectonic development of northern Crater Flat basin, southern Nevada [abs.]: Geological Society of America Abstracts with Programs, v. 28, no. 7., p. A192.

Oldow, J.S., Bally, A.W., Av'e Lallmont, H.G., and Leeman, W.P., 1989, Phanuajoic evolution of the North American Cordillera—United States and Canada: Chapter 8 in the geology of North America: Geological Society of America, v. A., p. 139-232.

- O'Leary, D.W., 1996, Synthesis of tectonic models for the Yucca Mountain area: Chapter 8, *in* U.S. Geological Survey (Whitney, J.W., Coordinator), Seismotectonic Framework and Characterization of Faulting at Yucca Mountain, Nevada: U.S. Geological Survey report to the Department of Energy that fulfills Level 3 Milestone 3GSH100M WBS Number 1.2.3.2.8.3.6, variously paginated.
- O'Leary, D.W., Coe, J., and Yount, J., 1996, Characterization of Quaternary faulting within the Cane Spring and Rock Valley fault zones: U.S. Geological Survey, Administration report to U.S. Department of Energy.
- Pezzopane, S.K., 1996, Relevant earthquake sources: Chapter 11, *in* U.S. Geological Survey (Whitney, J.W., Coordinator), Seismotectonic Framework and Characterization of Faulting at Yucca Mountain, Nevada: U.S. Geological Survey report to the Department of Energy that fulfills Level 3 Milestone 3GSH100M WBS Number 1.2.3.2.8.3.6, variously paginated.
- Pezzopane, S.K., Bufe, C.G., Dawson, T.E., Wong, I.G., and Bott, J.D.J., 1996a, Historical seismicity in the Yucca Mountain region: Chapter 7, *in* U.S. Geological Survey (Whitney, J.W., Coordinator), Seismotectonic Framework and Characterization of Faulting at Yucca Mountain, Nevada: U.S. Geological Survey report to the Department of Energy that fulfills Level 3 Milestone 3GSH100M WBS Number 1.2.3.2.8.3.6, variously paginated.
- Pezzopane, S.K., and Dawson, T.E., 1996, Fault displacement hazard—A summary of issues and information: Chapter 9, *in* U.S. Geological Survey (Whitney, J.W., Coordinator), Seismotectonic Framework and Characterization of Faulting at Yucca Mountain, Nevada," U.S. Geological Survey report to the Department of Energy that fulfills Level 3 Milestone 3GSH100M WBS Number 1.2.3.2.8.3.6, variously paginated.
- Pezzopane, S.K., Whitney, J.W., and Dawson, T.E., 1996b, Models of earthquake recurrence and preliminary paleoearthquake magnitudes at Yucca Mountain: Chapter 5, *in* U.S. Geological Survey (Whitney, J.W., Coordinator), 1996, "Seismotectonic Framework and Characterization of Faulting at Yucca Mountain, Nevada," U.S. Geological Survey report to the Department of Energy that fulfills Level 3 Milestone 3GSH100M WBS Number 1.2.3.2.8.3.6, variously paginated.
- Piety, L.A., 1993, Compilation of known and suspected Quaternary faults within 100 km of Yucca Mountain: U.S. Geological Survey Open-File Report 94-112, 404 pp., 2 plates.

- Piety, L.A., 1995, Compilation of known and suspected Quaternary faults within 100 km of Yucca Mountain: Technical Report prepared by U.S. Bureau of Reclamation in cooperation with the Nevada Operations Office, U.S. Department of Energy under Interagency Agreement DE-A108-92NV10874; U.S. Geological Survey Open-File Report 94-112.
- Ramelli, A.R., Oswald, J.A., Vadurro, G., Menges, C.M., and Pares, J.B., 1996, Quaternary faulting on the Solitario Canyon fault: Chapter 4.7, *in* U.S. Geological Survey (Whitney, J.W., Coordinator), 1996, "Seismotectonic Framework and Characterization of Faulting at Yucca Mountain, Nevada," U.S. Geological Survey report to the Department of Energy that fulfills Level 3 Milestone 3GSH100M WBS Number 1.2.3.2.8.3.6, variously paginated.
- Reheis, M.C., 1988, Preliminary study of Quaternary faulting on the east side of Bare Mountain, Nye County, Nevada, *in* Carr, M.D., and Yount, J.C. (eds.), Geologic and hydrologic investigations of a potential nuclear waste disposal site at Yucca Mountain, southern Nevada: U.S. Geological Survey Bulletin 1790, p. 103-111.
- Saltus, R. W., and Thompson, G. A., 1996, Why is it downhill from Tonopah to Las Vegas: A case for mantle plume support of the high northern Basin and Range: *Tectonics*, v. 14, no. 6, p. 1235-1244.
- Sawyer, D.A., Fleck, R.J., Lanphere, M.A., Warren, R.G., Broxton, D.E., and Hudson, M.R., 1994, Episodic caldera volcanism in the Miocene southwest Nevada volcanic field: Revised stratigraphic framework, $^{40}\text{Ar}/^{39}\text{Ar}$ geochronologic framework, and implications for magmatism and extension: *Geological Society of America Bulletin*, v. 106, no. 10, p. 1304-1318.
- Scholz, C.H., Barazangi, M., and Sbar, M.L., 1971, Late Cenozoic evolution of the Great Basin, western United States, as an ensialic interarc basin: *Geological Society of America Bulletin*, v. 82, p. 2979-2990.
- Schweickert, R. A., 1989, Evidence for a concealed strike-slip fault beneath Crater Flat, Nevada: *Geological Society of America Abstracts with Programs*, v. 21, no. 9, p. A90.
- Scott, R. B., 1990, Tectonic setting of Yucca Mountain, southwest Nevada, *in* Wernicke, B. P. (ed.), Basin and Range tectonics at the latitude of Las Vegas, Nevada: *Geological Society of America Memoir* 176, p. 251-282.
- Scott, R.B., and Bonk, J., 1984, Preliminary geologic map of Yucca Mountain, with geologic sections: U.S. Geological Survey Open-File Report 84-494, scale 1:12,000.

Seismic Source Characterization Facilitation Team (SSC), 1997, Memorandum on "Fault Displacement Hazard Guidance" from the SSC Facilitation Team to the SSC Expert Teams, 16 January 1997, 4 pp. plus 1 figure.

Simonds, F.W., Whitney, J.W., Fox, K.F., Ramelli, A.R., Yount, J.C., Carr, M.D., Menges, C.M., Dickerson, R.P., and Scott, R.B., 1995, Map showing fault activity in the Yucca Mountain area, Nye County, Nevada: U.S. Geological Survey, Miscellaneous Investigations Series, Map I-2520, scale 1:24,000.

Slemmons, 1982, Determination of design earthquake magnitudes for microzonation: Proceedings Third International Earthquake Microzonation Conference, Seattle, Washington, Earthquake Engineering Research Institute, v. 1, p. 110-130.

Smith, K.D., Brune, J.N., Savage, M.K., Anoshehpour, R., dePolo, D, and Sheehan, A.F., 1996, in press, The 1992 Little Skull Mountain earthquake sequence, Southern Nevada Test Site: Bulletin of the Seismological Society of America.

Smith, R. L., and Bailey, R. A., 1968, Resurgent cauldrons: Geological Society of America Memoir 116, p. 613-662.

Snyder, D. B., and Carr, W J., 1984, Interpretation of gravity in a complex volcano-tectonic setting, southwestern Nevada: U. S. Geological Survey Open-File Report 81-1349, 50 p.

Stepp, C., Whitney, J., Wong, I.G., Savy, J., Coppersmith, K., Abrahamson, N., Quittmeyer, R., and Sullivan, T., 1995, A probabilistic analysis of fault displacement and vibratory ground motion and the development of seismic design criteria for Yucca Mountain, Nevada, *in* Topical Meeting on Methods of Seismic Hazards Evaluation Focus '95, Las Vegas, Nevada, American Nuclear Society, p. 35-42.

Stewart, J.H., 1988, Tectonics of the Walker Lane belt, western Great Basin-Mesozoic and Tertiary deformation in a zone of shear, *in* Ernst, W.G. (ed.), Metamorphism and crustal evolution of the western United States, Rubey Volume VII: Englewood Cliffs, New Jersey, Prentice Hall, p. 683-713.

Streitz, R., and Stinson, M.C., 1974, Geologic map of California, Death Valley Sheet: California Division of Mines and Geology, scale 1:250,000.

Swadley, W.C., and Huckins, H.E., 1990, Geologic map of the surficial deposits of the Skull Mountain quadrangle, Nye County, Nevada: U.S. Geological Survey Miscellaneous Investigations Series Map I [1972, scale 1:24,000.

Swan, F.H., Wesling, J.R., Angell, M.M., Thomas, A.P., Whitney, J.W., and Gibson, J.D., 1995 (in review), Evaluation of the location and recency of faulting near prospective surface facilities in Midway Valley, Yucca Mountain Project, Nye County, Nevada: Technical report prepared by Geomatrix Consultants, Inc., San Francisco, in cooperation with the U.S. Geological Survey.

Taylor, E.M., Menges, C.M., de Fontaine, C.S., Buesch, D.C., Mundo, B.O., and Murray, M., 1996, Preliminary results of paleoseismic investigation on the Ghost Dance Fault: Chapter 4.5, *in* U.S. Geological Survey (Whitney, J.W., Coordinator), 1996, Seismotectonic Framework and Characterization of Faulting at Yucca Mountain, Nevada: U.S. Geological Survey report to the Department of Energy that fulfills Level 3 Milestone 3GSH100M WBS Number 1.2.3.2.8.3.6, variously paginated.

U.S. Geological Survey (Whitney, J.W., Coordinator), 1996, Seismotectonic Framework and Characterization of Faulting at Yucca Mountain, Nevada: U.S. Geological Survey report to the Department of Energy that fulfills Level 3 Milestone 3GSH100M WBS Number 1.2.3.2.8.3.6, variously paginated.

Veneziano, D., and Van Dyck, J., 1985, Statistical discrimination of "aftershocks" and their contribution to seismic hazard: Seismic Hazard Methodology for Nuclear Facilities in the Eastern United States: EPRI Res. Project No. P101-29, EPRI/SOG Draft 85-1, v. 2, Appendix A-4.

Wells, D.L., and Coppersmith, K.J., 1994, New empirical relationships among magnitude, rupture length, rupture width, rupture area, and surface displacement: Bulletin of the Seismological Society of America, v. 84, p. 974-1002.

Wernicke, B., 1995, Low-angle normal faults and seismicity—A review: Journal of Geophysical Research, v. 10, p. 201,159-20,174.

Wesling, J.R., Bullard, T.F., Swan, F.H., Perman, R.C., Angell, M.M., and Gibson, J.D., 1992, Preliminary mapping of surficial geology of Midway Valley, Yucca Mountain, Nye County, Nevada: Sandia National Laboratory Report SAND91-0607, Albuquerque, New Mexico, 56 p.

Wesling, J.R., Swan, F.H., Thomas, A.P., and Angell, M.M., 1993, Preliminary results of trench mapping at the site of prospective surface facilities for the potential Yucca Mountain repository, Nevada [abs.]: Geological Society of America, Abstracts with Programs, v. 25, no. 5, p. 162.

Wesnousky, S.G., 1986. Earthquakes. Quaternary faults. and seismic hazard in California: Journal Geophysical Research, v. 91, p. 12,587-12,631.

Whitney, J.W., and Taylor, E.M., 1996, Quaternary paleoseimology and stratigraphy of the Yucca Mountain site area: Chapter 4.0, *in* U.S. Geological Survey (Whitney, J.W., Coordinator), Seismotectonic Framework and Characterization of Faulting at Yucca Mountain, Nevada: U.S. Geological Survey report to the Department of Energy that fulfills Level 3 Milestone 3GSH100M WBS Number 1.2.3.2.8.3.6, variously paginated.

Whitney, J.W., Taylor, E.M., and Wesling, J.R., 1996, Quaternary mapping and stratigraph: Chapter 4.1, *in* U.S. Geological Survey (Whitney, J.W., Coordinator), Seismotectonic Framework and Characterization of Faulting at Yucca Mountain, Nevada: U.S. Geological Survey report to the Department of Energy that fulfills Level 3 Milestone 3GSH100M WBS Number 1.2.3.2.8.3.6, variously paginated.

Wong, I., Pezzopane, S., Abrahamson, N., Green, R., Sun, J., and Quittmeyer, R., 1997, Development of seismic design criteria for the Waste Handling Building at Yucca Mountain, Nevada, unpublished report prepared for DOE by Woodward-Clyde Federal Services.

Wright, L. A., 1989, Overview of the role of strike-slip and normal faulting in the Neogene history of the region northeast of Death Valley, California-Nevada, *in*, Ellis, M. A. (ed.), Late Tertiary evolution of the southern Great Basin, Nevada: Nevada Bureau of Mines and Geology Open-File Report 89-1, p. 1-11.

Wyss, M., 1979, Estimating maximum expectable magnitude of earthquakes from fault dimensions: *Geology*, v. 7, p. 336-340.

Young, S.R., Morris, A.P., and Stirewalt, G., 1993, Geometric analysis of alternative models of faulting at Yucca Mountain, Nevada, *in* High level radioactive waste management: Proceedings of the Fourth Annual International Conference. Las Vegas, Nevada, American Nuclear Society, La Grange Park, Illinois. v. 2. p. 1,818-1,825.

Youngs, R.R., and Coppersmith, K.J., 1985. Implications of fault slip rates and earthquake recurrence models to probabilistic seismic hazard estimates: *Seismological Society of America Bulletin*, v. 75, p. 939-964.

Youngs, R.R., Swan, F.H., III, Power, M.S., Schwartz, D.P., and Green, R.K., 1987.
Probabilistic analysis of earthquake and ground shaking hazard along the Wasatch
Front, Utah, *in* Gori, P.O., and Hays, W.W. (eds.), Assessment of Regional
Earthquake Hazards and Risk Along the Wasatch Front, Utah: U.S. Geological
Survey Open File Report 87-585, M-1 to M-100.

TABLE DSF-1
SEISMIC SOURCE PARAMETERS FOR REGIONAL FAULT SOURCES
 (Page 1 of 2)

Fault (Designation on Fig. DSF-6)	Activity	Length (km)	Dip	Slip Rate (mm/yr)			Maximum Magnitude
				Preferred	Maximum	Minimum	
1 Hunter Mt./Panamint (HM-PAN)	1	148 [1]	90	2.5 [.6]	3.2 [.2]	1.1 [.2]	7.0 7.4 7.6 [.2] [.6] [.2]
2 Furnace Creek/Fish Lake Valley (FC-FLV)	1	149 [1]	90	2.3 [.6]	4.6 [.2]	1.3 [.2]	7.0 7.3 7.6 [.2] [.6] [.2]
3 Death Valley (DV)	1	71 [1]	60W	2.5 [.6]	11.5 [.2]	0.08 [.2]	7.0 7.2 7.5 [.2] [.6] [.2]
4 Pahrump/Stewart Valley (PRP)	1	41 [1]	90		0.05 [.5]	0.005 [.5]	6.6 7.0 [.5] [.5]
5 West Springs Mt. (WSM)	1	AB-29 km [5] AC-51 km [5]	60W	0.06 [.6] . .	0.2 [.2] . .	0.02 [.2] . .	6.6 6.8 7.0 [.2] [.6] [.2] 6.7 7.0 7.3 [.2] [.6] [.2]
6 West Pintwater Range (WPR)	1	55 [1]	60W		0.2 [.5]	0.02 [.5]	6.7 7.0 7.3 [.2] [.6] [.2]
7 Yucca (YC)	1	25 [1]	60E		0.2 [.5]	0.02 [.5]	6.5 6.7 7.0 [.2] [.6] [.2]
8 Emigrant Valley North (?) (EVN)	1	27 [1]	60W		0.2 [.5]	0.02 [.5]	6.5 6.7 7.0 [.2] [.6] [.2]
9 Oaks Spring Butte (OAK)	1	22 [1]	60E		0.2 [.5]	0.01 [.5]	6.5 6.7 7.0 [.2] [.6] [.2]
10 Belled Range (BLR)	1	50 [1]	60E		0.1 [.5]	0.01 [.5]	6.5 6.8 7.1 [.2] [.6] [.2]
11 Kawitch Range (KR)	1	AB-24 km [0.68] BC-33 km [0.1] AD-65 km [0.2] CD-74 km [0.02]	60W		0.01 [.5] . . .	0.001 [.5] . . .	6.5 6.7 7.0 [.2] [.6] [.2] 6.5 6.8 7.1 [.2] [.6] [.2] 6.9 7.2 7.5 [.2] [.6] [.2] 6.9 7.2 7.5 [.2] [.6] [.2]
12 Rock Valley (RV)	1	AB-33 km [.6] AC-47 km [.3] AD-64 km [.1]	90		0.16 [.5] . .	0.02 [.5] . .	6.5 6.8 7.1 [.2] [.6] [.2] 6.7 7.0 7.3 [.2] [.6] [.2] 6.9 7.2 7.5 [.2] [.6] [.2]
13 Wahmonie (WAH)	1	15 [1]	60NW		0.01 [.5]	0.001 [.5]	6.5 6.8 [.6] - [.2]

TABLE DSF-1
SEISMIC SOURCE PARAMETERS FOR REGIONAL FAULT SOURCES
 (Page 2 of 2)

Fault (Designation on Fig. DSF-6)	Activity	Length (km)	Dip	Slip Rate (mm/yr)			Maximum Magnitude	
				Preferred	Maximum	Minimum		
14 Yucca Lake (YCL)	1	13 [1]	60NE		0.2 [.5]	0.02 [.5]	6.5 [.8]	6.8 [.2]
15 Eleana Range (ER)	1	11 [1]	60NE		0.2 [.5]	0.02 [.5]	6.5 [.8]	6.8 [.2]
16 Peace Camp (PC)	1	AB-19 km [7]	90		0.16 [.5]	0.02 [.5]	6.5 [.2]	6.6 [.6]
		AC-31 km [3]			-	-	6.8 [.2]	7.1 [.2]
17 Amargosa/Gravity (Ash Meadows) (AM)	1	AB-27 km [0.56]	60W	0.04 [.6]	0.1 [.2]	0.01 [.2]	6.5 [.2]	6.7 [.6]
		BC-43 km [0.2]		-	-	-	6.7 [.2]	7.0 [.6]
		AD-34 km [0.2]		-	-	-	6.6 [.2]	6.9 [.6]
		DC-51 km [0.04]		-	-	-	6.8 [.2]	7.1 [.6]
18 Bare Mountain (BM)	1	AB-16 km [3]	60E	0.1 [.4]	0.05 [.4]	0.28 [.1]	0.01 [.1]	6.5 [.8]
		AC-22 km [7]		-	-	-	6.7 [.2]	7.0 [.6]
19 Highway 95 (H95)	0.1	AB-11 km [5]	90	0.03 [.4]	0.05 [.3]	0.01 [.3]	6.8 [.3]	6.5 [.7]
		AC-27 km [5]		-	-	-	7.0 [.2]	6.7 [.6]

MAXIMUM DEPTH OF FAULTING = 12 km, [.6]; 14 km, [.3]; 16 km, [.1]

**TABLE DFS-2
TOTAL FAULT LENGTHS FOR LOCAL FAULT SOURCES
ASSUMING INDEPENDENT FAULT BEHAVIOR**

FAULT (Map Designation, Fig. DFS-8)	Alternative Lengths (Figure DFS-8)	Total Fault Length (km)	Probability
Paintbrush Canyon/Stagecoach Road (PBC)	BE	19.4	(0.68)
	AE	20.9	(0.2)
	BF	26.9	(0.1)
	AF	28.4	(0.02)
Bow Ridge (BWR)	KH	7.6	(0.8)
	GK	10.3	(0.2)
Solitario Canyon (SC)	LM	16.5	(0.7)
	LN	20.6	(0.3)
Windy Wash/Fatigue Wash (WWF)	PR	22.3	(0.57)
	OR	23.8	(0.3)
	PS	25.8	(0.1)
	OS	27.3	(0.03)
Northern Crater Flat (NCF)	LU	6.5	(1)
Southern Crater Flat (SCF)	VX	8.1	(1)
Ghost Dance (GD)	YZ	3.0	(0.3)
	YY-ZZ	9.0	(0.7)

**TABLE DFS-3
TOTAL FAULT LENGTHS FOR LOCAL FAULT SOURCES
ASSUMING DISTRIBUTIVE FAULT BEHAVIOR**

RUPTURE SCENARIO ¹	TOTAL LENGTH	PROBABILITY
Scenario A = BE + HK + LN + PR	69.9 km	(0.2)
Scenario B = AF + GK + LN + OS	86.6 km	(0.6)
Scenario C = AF + GK + LN + OS + TU + VX	101.2 km	(0.2)

¹ Fault segments correspond to the line segments shown on Figure DFS-8

**TABLE DFS-4
 MAXIMUM FAULT RUPTURE LENGTHS FOR LOCAL FAULT SOURCES
 ASSUMING INDEPENDENT BEHAVIOR**

(Page 1 of 2)

FAULT TOTAL LENGTH (km/PROBABILITY)	MAXIMUM RUPTURE LENGTH (km)	PROBABILITY
Paintbrush Canyon/Stagecoach Road		
19.4 / 0.7	19.4 (1)	0.1
	11.1 (2)	0.7
	6.7 (3)	0.2
20.9 / 0.2	20.9 (1)	0.1
	11.1 (2)	0.7
	6.7 (3)	0.2
26.9 / 0.05	26.9 (1)	0.05
	19.7 (4)	0.4
	11.1 (2)	0.4
	6.7 (3)	0.1
28.4 / 0.05	28.4 (1)	0.05
	19.7 (4)	0.5
	11.1 (2)	0.3
	6.7 (3)	0.1
Bow Ridge		
7.6 / 0.8	7.6 (1)	0.7
	4.9 (5)	0.3
10.3 / 0.2	10.3 (1)	0.7
	4.9 (5)	0.3
Solitario Canyon		
16.5 / 0.7	16.5 (1)	0.8
	8.2 (6)	0.2
20.6 / 0.3	20.6 (1)	0.2
	15.4 (7)	0.6
	10.3 (6)	0.2

TABLE DFS-4
MAXIMUM FAULT RUPTURE LENGTHS FOR LOCAL FAULT SOURCES
ASSUMING INDEPENDENT BEHAVIOR
 (Page 2 of 2)

FAULT TOTAL LENGTH (km/PROBABILITY)	MAXIMUM RUPTURE LENGTH (km)	PROBABILITY
Windy Wash/Fatigue Wash		
22.3 / 0.7	22.3 (1)	0.2
	10 (6,8)	0.8
23.8 / 0.2	23.8 (1)	0.2
	10. (6,8)	0.8
25.8 / 0.05	25.8 (1)	0.1
	17.8 (9)	0.2
	10 (8)	0.7
27.3 / 0.05	27.3 (1)	0.1
	17.8 (9)	0.2
	10. (8)	0.7
Northern Crater Flat		
6.5 / 1	6.5 (1)	1.0
Southern Crater Flat		
8.1 / 1	8.1 (1)	1.0
Ghost Dance		
3.0 / 0.3	3.0 (1)	1.0
9.0 / 0.7	9.0 (1)	1.0

NOTES: (1) 100% of total fault length; (2) combined length of Alice Ridge and Fran Ridge segments; (3) length of longest segment, the Alice Ridge segment; (4) combined length of Alice Ridge, Fran Ridge, and Busted Butte segments; (5) length of well-defined north-south section of Bow Ridge fault; (6) approximately 50% of total fault length; (7) length of well-defined north-south section of Solitario Canyon fault adjacent to Yucca Crest; (8) approximate length of either the southern Windy Wash segment or the Fatigue Wash segment; (9) length of the north-south-trending section of the Windy Wash/Fatigue Wash fault system.

**TABLE DFS-5
DOWNDIP GEOMETRY OF LOCAL FAULT SOURCES**

FAULT	DOMINO (PLANAR) FAULT MODEL (0.8)		DETACHMENT FAULT MODEL (0.2)
	ALTERNATIVE A DIP / WIDTH (0.5)	ALTERNATIVE B DIP / WIDTH (0.5)	DIP / WIDTH (1.0)
① Paintbrush Canyon/Stagecoach Road Fault: Northern Segment, Paintbrush Canyon Fault	60° / 15 km	50° / 17 km	20° / 18 km
Central Segment, Paintbrush Canyon Fault	60° / 15 km	50° / 17 km	20° / 18 km
Southern Segment, Paintbrush Canyon Fault	60° / 15 km	50° / 17 km	20° / 18 km
Stagecoach Road Fault	60° / 15 km	50° / 17 km	20° / 13 km
② Bow Ridge Fault	70° / 8 km	60° / 9 km	48° / 7 km
③ Solitario Canyon Fault	55° / 13 km	50° / 14 km	42° / 9 km
④ Windy Wash/Fatigue Wash Fault: Northern Windy Wash Fault	60° / 12 km	55° / 13 km	° / 8.5 km
Fatigue Wash Fault	60° / 12 km	55° / 13 km	45° / 8.5 km
Southern Windy Wash Fault	55° / 10 km	55° / 13 km	45° / 8.5 km
⑤ Northern Crater Flat Fault	60° / 9 km	55° / 9.5 km	47° / 8.6 km
⑥ Southern Crater Flat Fault	71° / 10 km	60° / 11 km	52° / 8 km
⑦ Ghost Dance Fault	90° / 10 km	70° / 11 km	45° / 8 km

TABLE DFS-6
QUATERNARY SLIP RATES ON LOCAL FAULT SOURCES
 (Page 1 of 2)

FAULT	FAULT SEGMENT	SLIP RATE —mm/yr (PROBABILITY)			SOURCES OF DATA
		PREFERRED	MINIMUM	MAXIMUM	
Paintbrush Canyon/Stagecoach Road Fault	Northern Segment PCF	0.002 (0.6)	0.001 (0.2)	0.004 (0.2)	Modified from: Menges and Whitney, 1996, Tables 4.4.5 and 4.4.6 (Trench A1). Swan et al., 1995, Table C-8 (Trench MWV-T4). Modified from: Menges and Whitney, 1996, Tables 4.4.5 and 4.4.6 (Busted Butte exposures). Modified from: Menges and Whitney, 1996, Tables 4.4.5 and 4.4.6 (Trenches SCR-T1 and SCR-T3).
	Central Segment PCF	0.017 (0.6)	0.013 (0.2)	0.025 (0.2)	
	Southern Segment PCF	0.01 (0.6)	0.004 (0.2)	0.016 (0.2)	
	Stagecoach Road	0.04 (0.6)	0.01 (0.2)	0.07 (0.2)	
Bow Ridge Fault	G-K	0.003 (0.6)	0.002 (0.2)	0.007 (0.2)	Menges and Whitney, 1996, Tables 4.4.6.
Solitario Canyon Fault	L-N	0.01 to 0.03 (0.3) (0.3)	0.002 (0.2)	0.04 (0.2)	Ramelli et al., 1995, p. 4.7-49.

TABLE DFS-6
QUATERNARY SLIP RATES ON LOCAL FAULT SOURCES
 (Page 2 of 2)

FAULT	FAULT SEGMENT	SLIP RATE—mm/yr (PROBABILITY)			SOURCES OF DATA
		PREFERRED	MINIMUM	MAXIMUM	
Windy Wash/Fatigue Wash Fault					
Northern Windy Wash	O-P1	0.003 (0.45)	0.001 (0.45)	0.03 (0.1)	Assumed to be similar to Southern Windy Wash segment, but with greater uncertainty. Coe et al., 1996, p. 4.8-24.
Fatigue Wash	P1-Q	0.002 (0.6)	0.001 (0.2)	0.015 (0.2)	
Southern Windy Wash	Q-S	0.011 (0.6)	0.009 (0.2)	0.027 (0.2)	
Northern Crater Flat Fault	T-U		0.001 (0.5)	0.002 (0.5)	Maximum rate reported to be less than 0.002 mm/yr, Coe, 1996, P.4.11-12 (Trench TR CFF T-2).
Southern Crater Flat Fault	V-X		0.001 (0.5)	0.002 (0.5)	Maximum rate reported to be less than 0.002 mm/yr, Taylor, 1996, P.4.10-12 (trenches TR CFF T-1 and TR CFF T-1a).
Ghost Dance Fault	YY-ZZ	0.001 (0.6)	0.0001 (0.2)	0.0024 (0.2)	Preferred value equals the weighted average from all these displacement history models described in Section 5.2.3.

**TABLE DFS-7
SEISMIC SOURCE PARAMETERS FOR HYPOTHETICAL FAULTS**

Hypothetical Fault Source	ACTIVITY	LENGTH (km)	DIP (deg.)	DEPTH TO DETACHMENT (km)	SLIP RATE (mm/yr)			MAXIMUM MAGNITUDE		
					PREFERRED	MAXIMUM	MINIMUM			
Highway 95 Fault (H-95)	(0.1)	11 (0.5)	90	na	0.03 (0.4)	0.05 (0.3)	0.01 (0.3)	6.5 (0.7)	6.8 (0.3)	
		27 (0.5)	90	na	• •	• •	• •	6.5 (0.2)	6.7 (0.6)	7.0 (0.2)
Postulated Hidden Strike-Slip Fault (T2-HSS)	(0.05)	30 (0.5)	90	5 to 16 (0.2)	• •	• •	• •	L vs. M (0.2)		A vs. M (0.8)
				6.5 to 14 (0.6)						
		8 to 12 (0.2)	• •	• •	• •					
		200 (0.5)		5 to 16 (0.2)	• •	• •	• •	6.0 (0.3)	6.5 (0.5)	7.0 (0.2)
				6.5 to 14 (0.6)				• •	• •	• •
				8 to 12 (0.2)				• •	• •	• •

Maximum depth of faulting same as for regional fault sources [12 km (0.6), 14 km (0.3), 16 km < (0.1)].

**TABLE DFS-8
 FAULT ACTIVITY AND CUMULATIVE DISPLACEMENT, POST-TIVA CANYON TUFF,
 AT TEST CALCULATION SITES FOR FAULT DISPLACEMENT HAZARD
 ASSESSMENT**

TEST CALCULATION SITE	PROBABILITY OF ACTIVITY	CUMULATIVE DISPLACEMENT POST-TIVA CANYON TUFF (NET SLIP IN M)		
1) Bow Ridge Fault	1.0	125 (0.2)	130 (0.6)	135 (0.2)
2) Solitario Canyon Fault	1.0	350 (0.2)	500 (0.6)	580 (0.2)
3) Drill Hole Wash Fault	0.01	5 (0.2)	15 (0.6)	25 (0.2)
4) Ghost Dance Fault	0.4	20 (0.2)	25 (0.6)	30 (0.2)
5) Sundance Fault	0.01	6 (0.2)	8.5 (0.6)	11 (0.2)
6) Unnamed Fault West of Dune Wash	0.4	3 (0.2)	5 (0.6)	7 (0.2)
7) 100 M East of Solitario Canyon Fault				
a) Small fault	0.05	0.5 (0.2)	0.85 (0.6)	2.0 (0.2)
b) Shear	0.05	0.1 (1.0)	--	--
8) Midway Between Solitario Canyon and Ghost Dance Faults				
a) Small fault	0.01	0.5 (0.2)	0.85 (0.6)	2.0 (0.2)
b) Shear	0.01	0.1 (1.0)	--	--
9) Exile Hill Fault (Midway Valley)	0.8	5 (0.2)	10 (0.6)	15 (0.2)

**TABLE DFS-9
QUATERNARY SLIP RATES
BASED ON PALEOSEISMIC DATA**

Test Calculation Site	Slip Rate (mm per yr)			Basis
1) Bow Ridge Fault	0.002 (0.2)	0.003 (0.6)	0.007 (0.2)	Menges and Whitney, 1996, Table 4.4.6
2) Solitario Canyon Fault	0.01 (0.2)	0.02 (0.6)	0.04 (0.2)	Data from trenches SCF-T4 and T8, Ramelli et al., 1996 Table 4.7.3
3) Drill Hole Wash Fault	not available			
4) Ghost Dance Fault	less than 0.0005			(See text, Section 5.2.3)
5) Sundance Fault	not available			
6) Unnamed Fault West of Dune Wash	not available			
7) 100 M East of Solitario Canyon Fault	not available			
8) Midway Between Solitario Canyon and Ghost Dance Faults	not available			
9) Exile Hill Fault (Midway Valley)	less than 0.0005			Swan et al., 1995

**TABLE DFS-10
SLIP RATES CALCULATED USING
DECREASING SLIP RATE MODEL WITH DIFFERENT
REDUCTION FACTORS (RF) COMPARED TO SLIP RATES BASED ON
PALEOSEISMIC DATA**

FAULT	SLIP RATE (mm PER YR) ^{*1}			
	DECREASING SLIP RATE MODEL (REDUCTION FACTORS AS A PERCENT OF THE LATE MIOCENE SLIP RATE)			SLIP RATE BASED ON PALEOSEISMIC DATA
	2.1 %	3.9 %	0.3 %	
Paintbrush Canyon Fault (Trench MWV T4)	0.0057±	0.011±	0.0008±	0.017±
Bow Ridge Fault (Test Calculation Site #1)	0.0025±	0.0046±	0.0004±	0.003±
Solitario Canyon Fault (Test Calculation Site #2)	0.0095±	0.0177±	0.0014	0.02±
Ghost Dance Fault (Test Calculation Site #4)	0.0005±	0.0009±	0.0001	<0.0005
Exile Hill Fault (Test Calculation Site #9)	0.0002±	0.0004±	0.0003±	<0.0005

^{*1} Slip rates shown here are based on preferred values for displacement and age; the uncertainties in these values were incorporated in the fault displacement hazard analysis.

TABLE DSF-11 (Page 1 of 2)
DISPLACEMENT PER EVENT AND RECURRENCE PARAMETERS FOR
FAULT DISPLACEMENT HAZARD ASSESSMENT

Displacement Approach		Recurrence Approach	
Average Displacement Per Event (cm)	Probability	Average Recurrence Interval (X 1000 Years)	Probability
#1 BOW RIDGE FAULT			
40	0.15	215	0.1
20	0.7	140	0.4
10	0.15	100	0.4
		70	0.1
#2 SOLITARIO CANYON FAULT			
60	0.2	100	0.2
40	0.8	70	0.3
20	0.2	50	0.3
		35	0.2
#3 DRILLHOLE WASH FAULT			
15	0.03	500	0.145
10	0.07	400	0.25
5	0.15	300	0.25
3	0.2	200	0.25
1	0.25	100	0.1
0.05	0.3	50	0.005
#4 GHOST DANCE FAULT			
15	0.03	500	0.145
10	0.07	400	0.25
5	0.15	300	0.25
3	0.2	200	0.25
1	0.25	100	0.1
0.05	0.3	50	0.005
#5 SUNDANCE FAULT			
15	0.03	500	0.145
10	0.07	400	0.25
5	0.15	300	0.25
3	0.2	200	0.25
1	0.25	100	0.1
0.05	0.3	50	0.005

**TABLE DSF-11 -(Page 2 of 2)
DISPLACEMENT PER EVENT AND RECURRENCE PARAMETERS FOR ASSESSMENT OF
FAULT DISPLACEMENT HAZARD**

Displacement Approach		Recurrence Approach	
Average Displacement Per Event (cm)	Probability	Average Recurrence Interval (X 1000 Years)	Probability
#6 UNNAMED FAULT WEST OF DUNE WASH			
15	0.03	500	0.145
10	0.07	400	0.25
5	0.15	300	0.25
3	0.2	200	0.25
1	0.25	100	0.1
0.05	0.3	50	0.005
#7 100 M EAST OF SOLITARIO CANYON FAULT			
(A) 2 m Displacement			
10	0.05	1600	0.05
5	0.1	500	0.18
3	0.2	400	0.18
1	0.3	300	0.18
0.5	0.35	200	0.18
		100	0.18
		50	0.05
(B) 10 cm Displacement			
10	0.005	1600	0.05
5	0.05	500	0.18
3	0.2	400	0.18
1	0.35	300	0.18
0.5	0.3	200	0.18
0.05	0.095	100	0.18
		50	0.05
#8 MIDWAY BETWEEN SOLITARIO CANYON AND GHOST DANCE FAULTS			
(A) 2 m Displacement			
10	0.05	1600	0.05
5	0.1	500	0.18
3	0.2	400	0.18
1	0.3	300	0.18
0.5	0.35	200	0.18
		100	0.18
		50	0.05
(B) 10 cm Displacement			
10	0.005	1600	0.05
5	0.05	500	0.18
3	0.2	400	0.18
1	0.35	300	0.18
0.5	0.3	200	0.18
0.05	0.095	100	0.18
		50	0.05
#9 MIDWAY VALLEY (EXILE HILL FAULT)			
10	0.05	500	0.15
5	0.1	400	0.25
3	0.2	300	0.25
1	0.3	200	0.25
0.5	0.35	100	0.1

TABLE DSF-12
SUMMARY OF DISPLACEMENT PER EVENT DATA FROM
YUCCA MOUNTAIN PALEOSEISMIC INVESTIGATIONS
 (Page 1 of 2)

Locality Site	Average Displacement	EVENT (Reported Displacement in cm – Pezzopane et al. 1995, Table 5-1) [Ratio: Event Displacement / Average Displacement]							
		Z	Y	X	W	V	U	T	S
Tr 14D	23.67	44 1.88	13 0.55	14 0.59	0.00	0.00			
Tr CFF-T2A	29.60	3 0.10	5 0.17	40 1.35	50 1.69	50 1.69			
Tr CFF-T1A	19.33	18 0.93	20 1.03	20 1.03	0.00	0.00			
Tr CF 1	61.33	0.00	25 0.41	105 1.71	54 0.88	0.00			
Tr SCF-T2	61.25	5 0.08	70 1.14	100 1.63	70 1.14	0.00			
Tr A1	38.00	6 0.16	39 1.03	7 0.18	100 2.63	0.00			
BB4	89.57	44 0.49	28 0.31	47 0.52	167 1.86	142 1.59	105 1.17	94 1.05	
MWV-T4	55.00	20 0.36	62 1.13	98 1.78	40 0.73	0.00	0.00	0.00	
RV3	290.75	267 0.92	362 1.25	204 0.70	330 1.13	0.00	0.00	0.00	

TABLE DSF-12
SUMMARY OF DISPLACEMENT PER EVENT DATA FROM
YUCCA MOUNTAIN PALEOSEISMIC INVESTIGATIONS
 (Page 2 of 2)

Locality Site	Average Displacement	EVENT (Reported Displacement in cm – Pezzopane et al. 1995, Table S-1) [Ratio: Event Displacement / Average Displacement]							
		Z	Y	X	W	V	U	T	S
SCF-T3	41.67	10 0.24	80 1.92	35 0.84	0.00	0.00	0.00	0.00	
SCF-T4	18.33	5 0.27	0.00	30 1.64	20 1.09	0.00	0.00	0.00	
SCF-T8	52.50	10 0.19	120 2.29	30 0.57	50 0.95	0.00	0.00	0.00	
SCR-T1	45.00	40 0.89	42 0.93	47 1.04	51 1.13	0.00	0.00	0.00	
SCR-T3	52.20	43 0.82	59 1.13	57 1.09	67 1.28	35 0.67	0.00	0.00	
Tr CF-2 [north wall]	39.38	4 0.10	20 0.51	23 0.58	20 0.51	73 1.85	45 1.14	50 1.27	80 2.03
Tr CF-2 [south wall]	34.63	4 0.12	12 0.35	50 1.44	42 1.21	28 0.81	16 0.46	60 1.73	65 1.88
Tr CF2.5	20.75	6 0.29	20 0.96	42 2.02	15 0.72	0.00	0.00	0.00	
Tr CF-3 [north wall]	44.80	4 0.09	33 0.74	87 1.94	35 0.78	65 1.45	0.00	0.00	
Tr CF-3 [south wall]	42.00	3 0.07	35 0.83	88 2.10	0.00	0.00	0.00	0.00	

TABLE DSF-13
RELATIONSHIP BETWEEN AVERAGE DISPLACEMENT
AND MAXIMUM DISPLACEMENT AT A POINT ALONG A FAULT
(Event -to-Event Variability)

LOCALITY	$D_{max}/D_{average}^{**}$
Tr 14D	1.86
Tr CFF-T2A	1.69
Tr CFF-T1A	1.03
Tr CF 1	1.71
Tr SCF-T2	1.63
Tr A1	2.63
BB4	1.86
MWV-T4	1.78
RV3	1.13
SCF-T3	1.92
SCF-T4	1.64
SCF-T8	2.29
SCR-T1	1.13
SCR-T3	1.28
Tr CF-2	1.85
[north wall]	
Tr CF-2	1.44
[south wall]	
Tr CF2.5	2.02
Tr CF-3	1.94
[north wall]	
Tr CF-3	2.1
[south wall]	
RANGE	1.03 to 2.63
AVERAGE	1.73

** From Table DSF-12

**TABLE DFS-14
POTENTIAL FOR ACTIVITY
ON FRACTURES AND IN INTACT BEDROCK**

Test Calculation Site	Potential Activity	Basis
<p>#7 100 m East of Solitario Canyon Fault</p> <p>c) Fracture</p> <p>d) Intact Bedrock</p>	<p>< 0.05</p> <p>< 0.005</p>	<p>Likelihood of occurrence judged to be less than the probability of activity on a fault that has displacement at the same location (Table 7.2-1)</p> <p>Likelihood of occurrence judged to be at least an order of magnitude less than the probability of activity on a fault or fracture at the same location.</p>
<p>#8 Midway Between Solitario Canyon and Ghost Dance Faults</p> <p>c) Fracture</p> <p>d) Intact Bedrock</p>	<p>< 0.01</p> <p>< 0.001</p>	<p>Likelihood of occurrence judged to be less than the probability of activity on a fault that has displacement at the same location (Table 7.2-1)</p> <p>Likelihood of occurrence judged to be an order of magnitude less than the probability of activity on a fault or fracture at the same location.</p>

TABLE DFS-15
PROBABILITY OF DISPLACEMENT "EVENTS" (Pe)
ACROSS FRACTURES IN UNBROKEN ROCK
GIVEN DIFFERENT MODELS OF DEFORMATION HISTORY

- (A) Uniform Deformation Post Tiva-Canyon (Ttc).

$$\text{Probability of "Event"} \leq \frac{1}{\text{Age of Host Rock}}$$

$$Pe \leq \frac{1}{(127 \pm 13) \times 10^6}$$

$$Pe \leq 1 \times 10^{-7}$$

- (B) Uniform Deformation Rate Post-Rainier Mesa.

$$Pe \leq \frac{\text{post - Rainier Mesa deformation rate}}{\text{post - Tiva Canyon deformation rate}} (Pe \text{ Model A})$$

$$Pe \leq \left(\frac{0.2 / 11.6 \pm 1.0 \text{ Ma}}{1 / 12.7 \pm 1.3 \text{ Ma}} \right) (1 \times 10^{-7})$$

$$Pe \leq 1.8 \times 10^{-8} \text{ to } \leq 2.6 \times 10^{-8}$$

- (C) Decreasing Deformation Rate.

$$Pe \leq \frac{(\text{late Miocene deformation rate})(\text{reduction factor})}{\text{post - Tiva Canyon deformation rate}} (Pe \text{ Model A})$$

$$Pe \leq \left(\frac{(0.8 / 1.1 \pm 0.6 \text{ ma})(0.021 \pm 0.018)}{1 / 12.7 \pm 1.3 \text{ Ma}} \right) (1 \times 10^{-7})$$

$$Pe \leq 2.1 \times 10^{-9} \text{ to } \leq 5.9 \times 10^{-8}$$

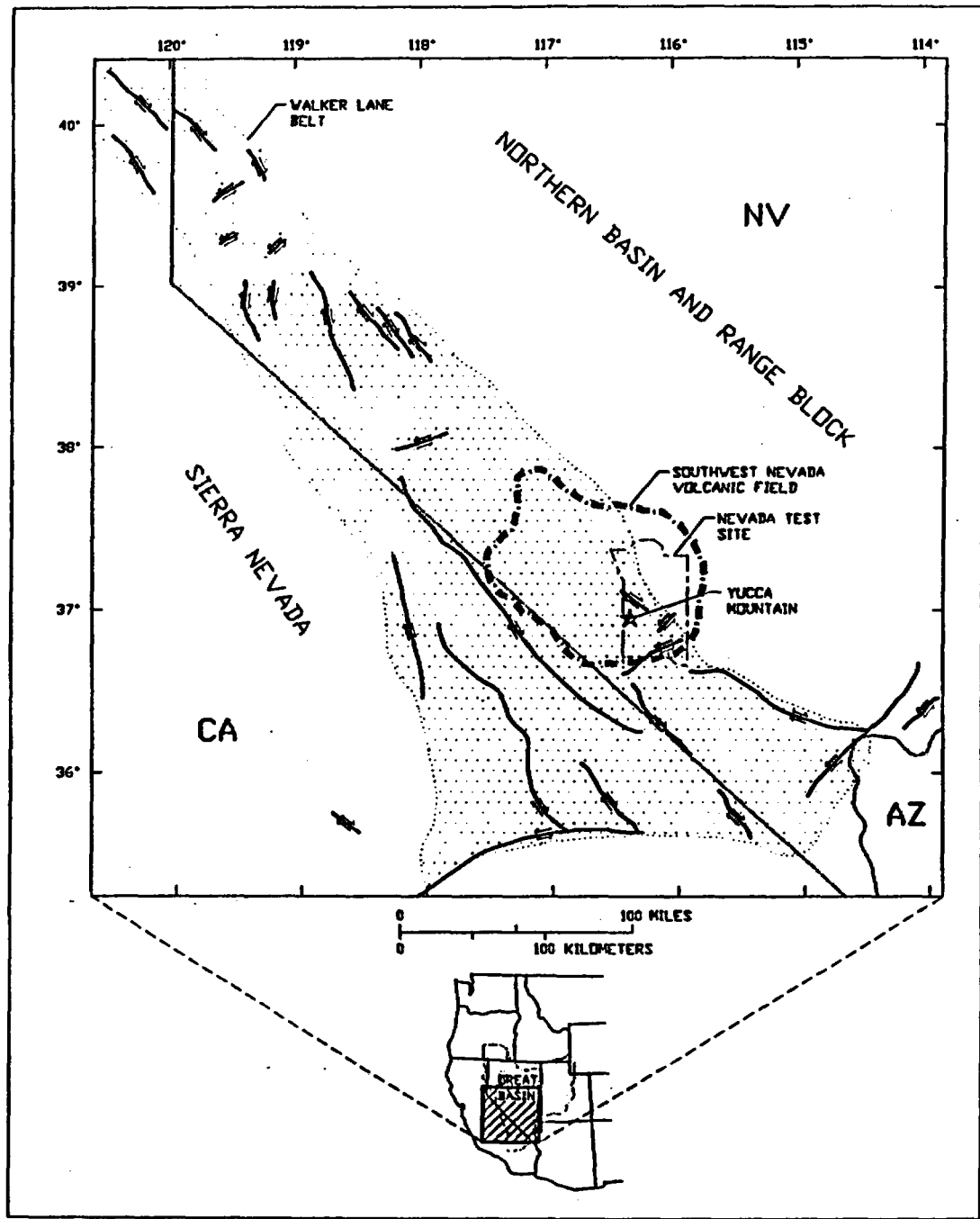


Figure DFS-1 Map showing location of Yucca Mountain (star) in the southwest Nevada volcanic field (Broxton et al., 1989, of the western Great Basin, with schematic representations of faults of the Walker Lane Belt that have strike-slip components of offset (dip-slip offsets not shown). Modified from Stewart (1988)

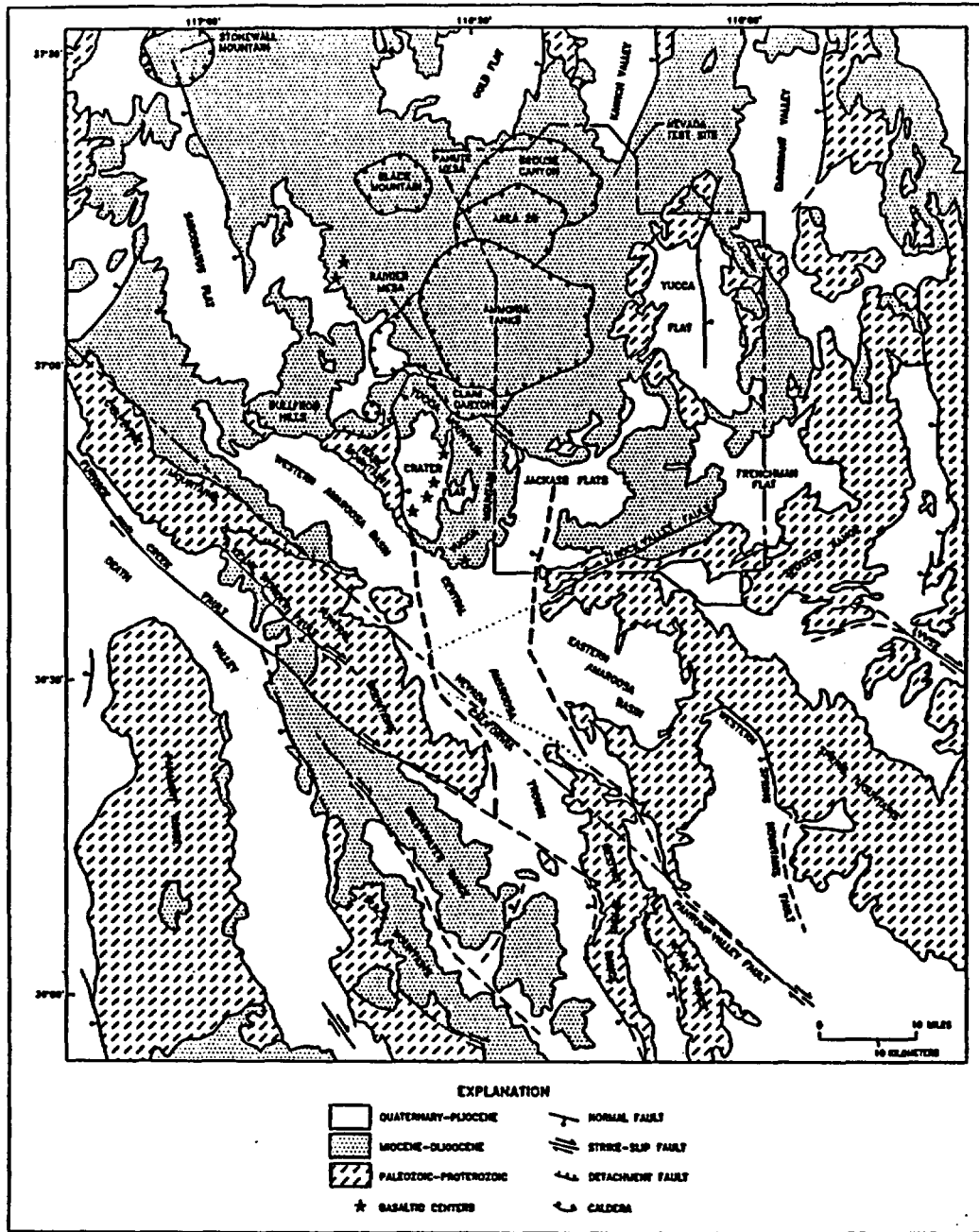


Figure DFS-2 Generalized map of the Yucca Mountain region showing major physiographic features and faults. Compiled from Jenkins, 1962; Longwell et al., 1965; Cornwall, 1972; Streitz and Stinson, 1974; Ekren et al., 1977, Burchfield et al., 1983; Wright, 1989; Frizzell and Schulters, 1990; Piety, 1993; Sawyer et al., 1994

<i>Declustered Catalog</i>	<i>Source Zonation</i>	<i>Spatial Variability</i>	<i>Sources</i>	<i>Maximum Magnitude</i>
----------------------------	------------------------	----------------------------	----------------	--------------------------

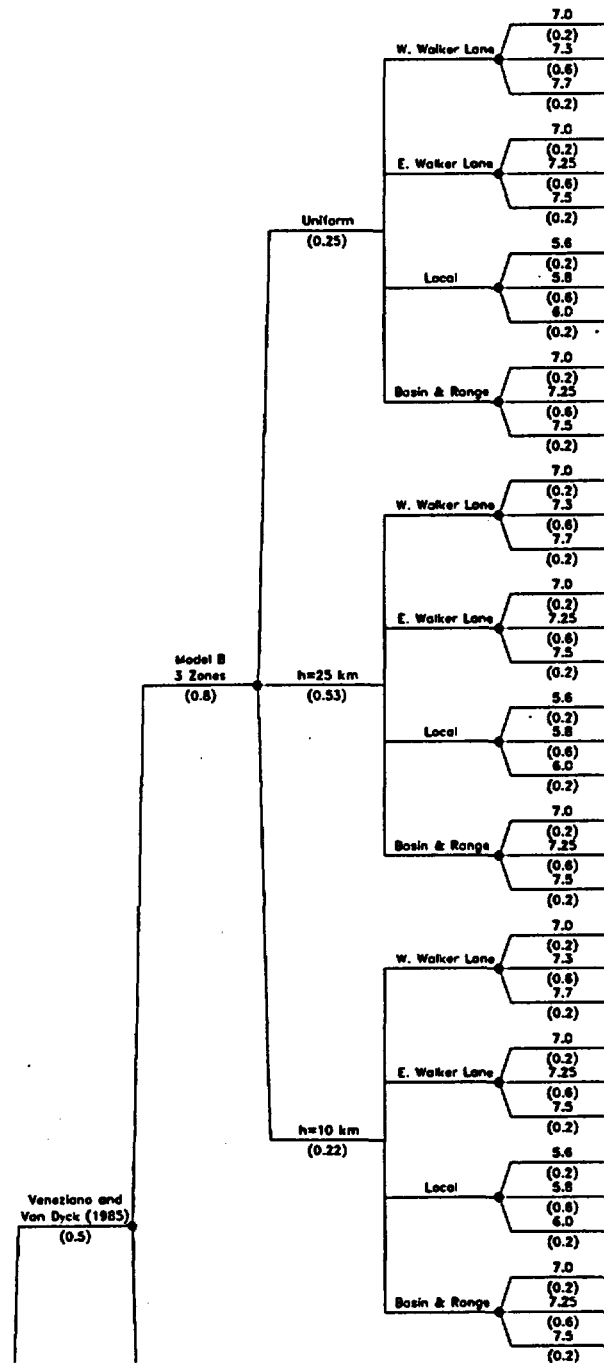


Figure DFS-3 Logic tree defining seismic source zones associated with two alternative models

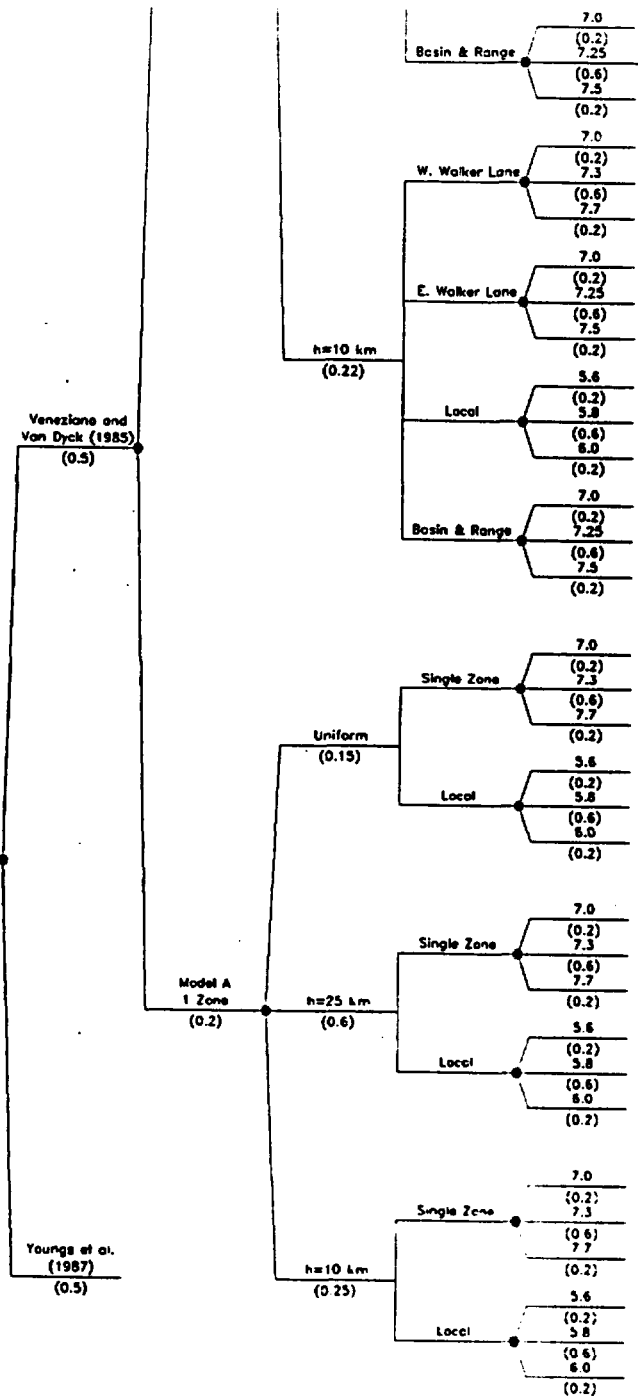


Figure DFS-3 (Cont'd) Logic tree defining seismic source zones associated with two alternative models

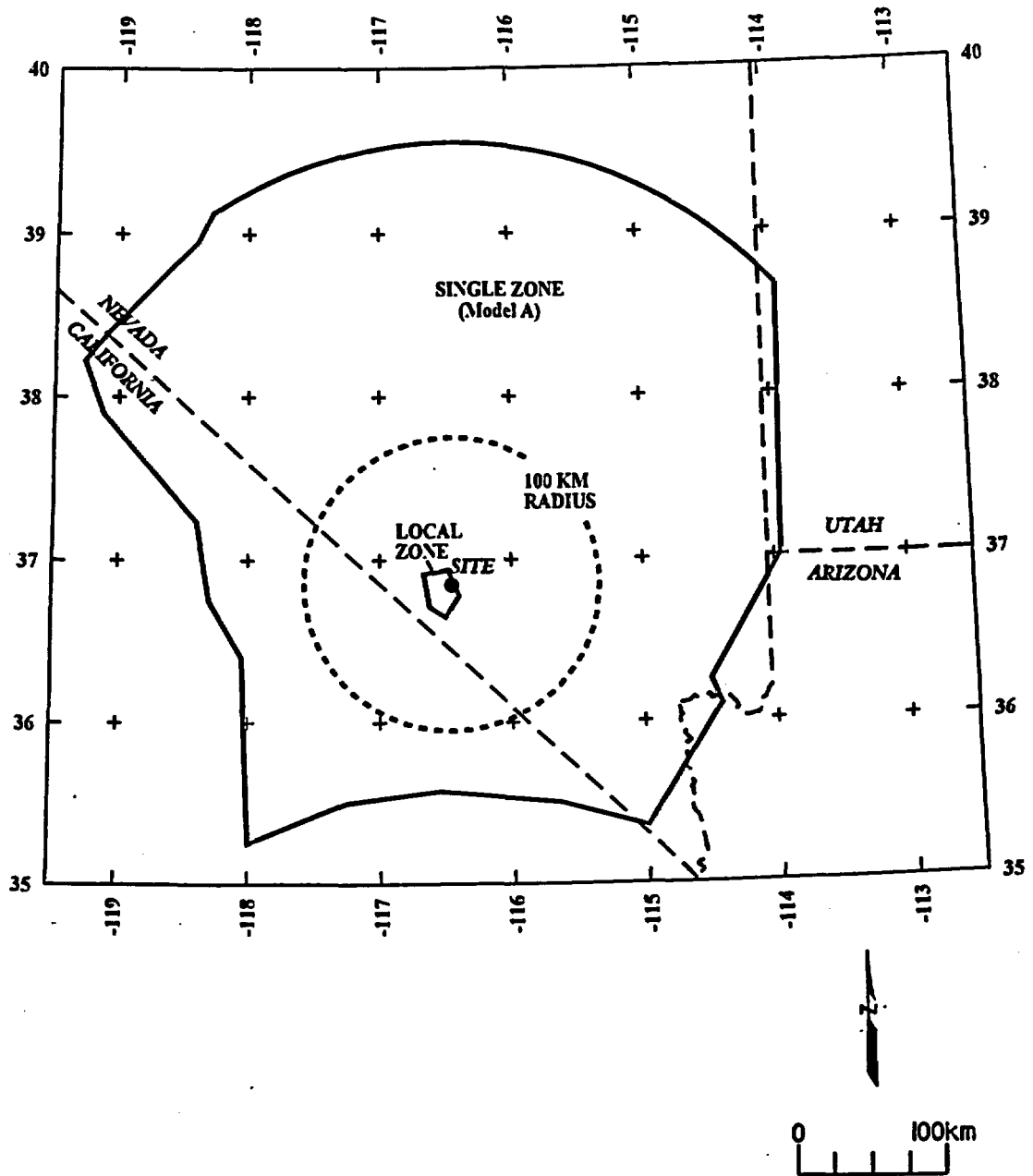


Figure DFS-4 Map showing boundaries of seismic source zones, Model A (one zones plus site vicinity).

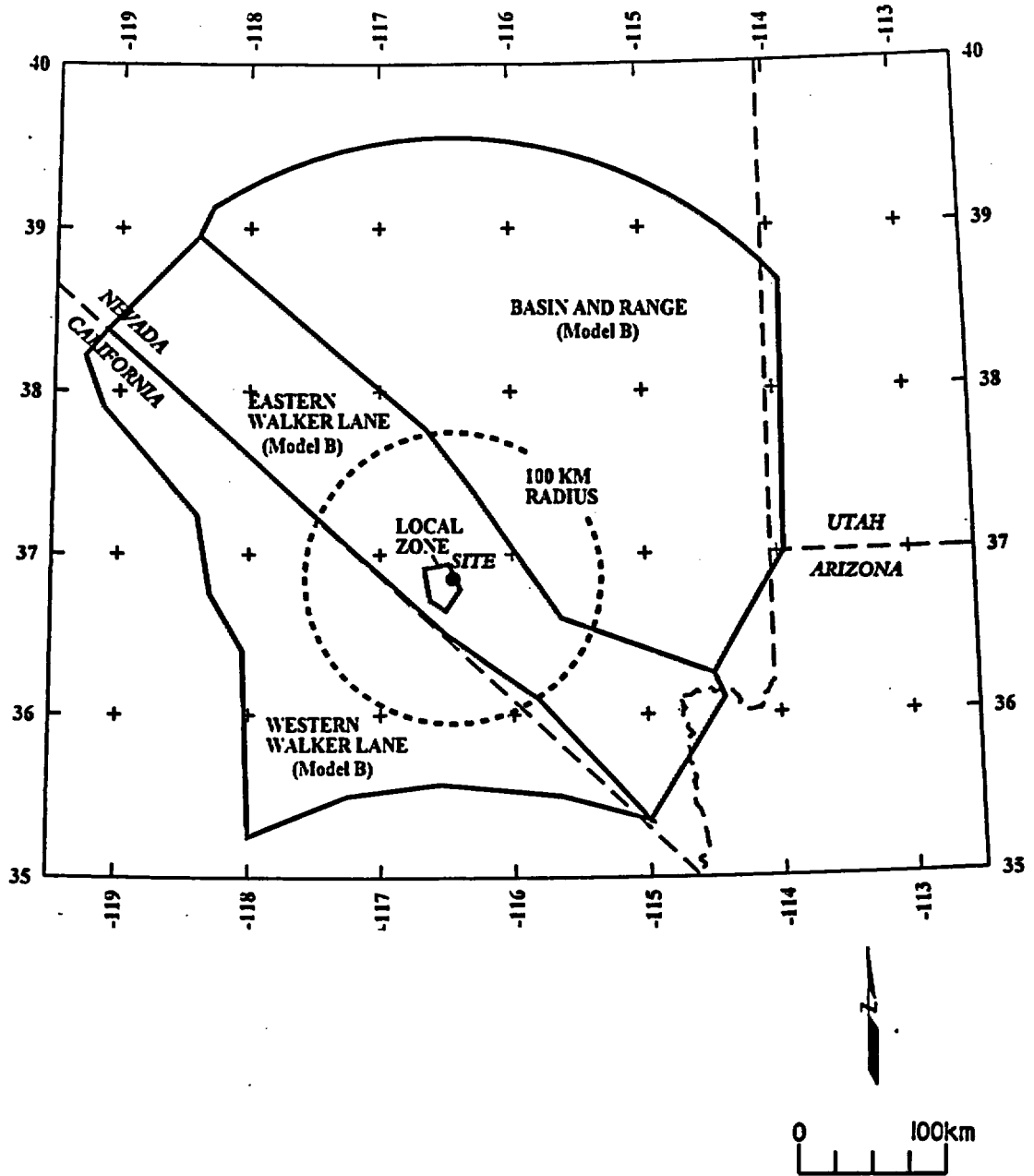
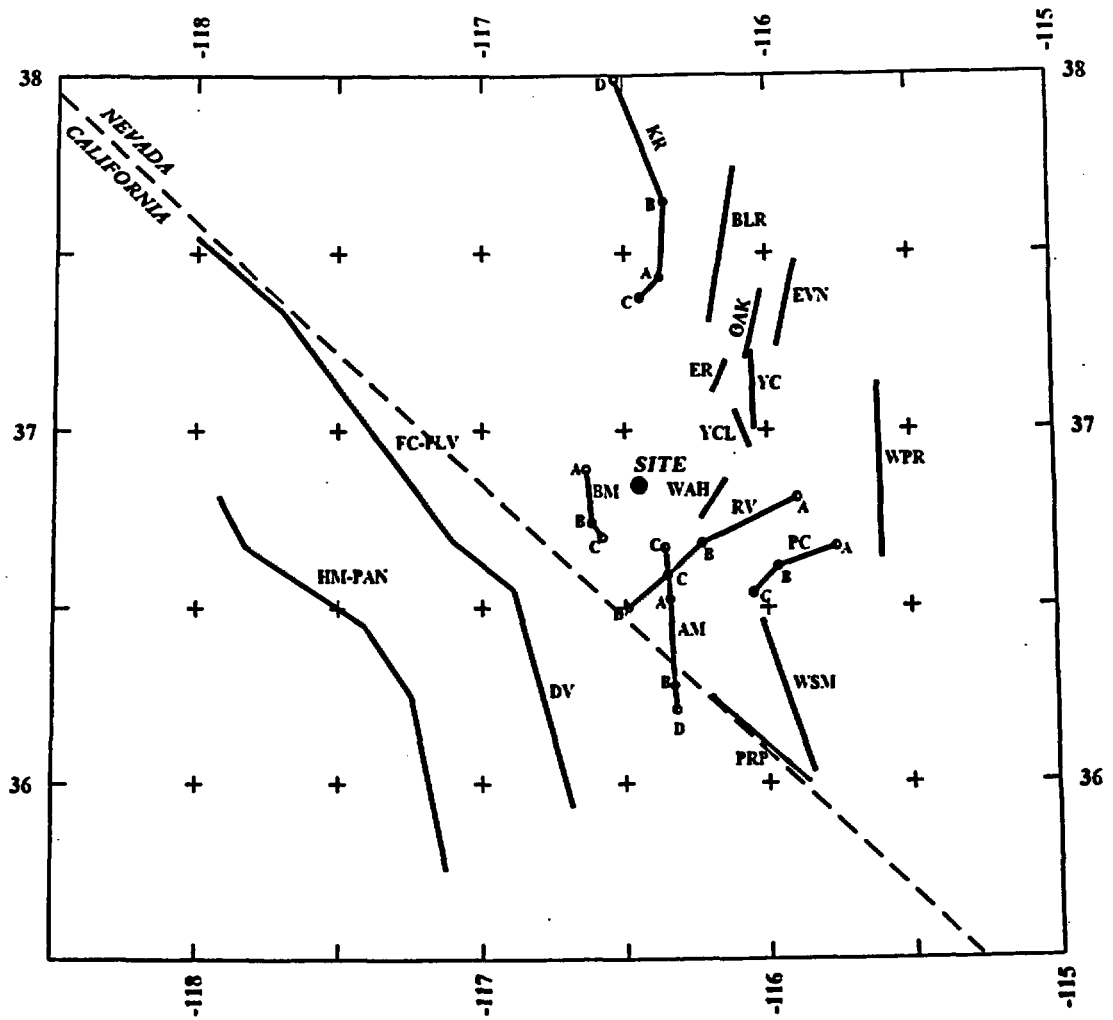


Figure DFS-5 Map showing boundaries of seismic source zones, Model B (three zones plus site vicinity).



EXPLANATION

Fault Lengths:



NOTES: Fault names are listed in Table DFS-1
Fault segments described in text

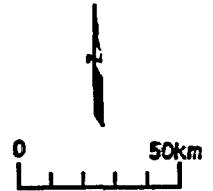


Figure DFS-6 Map showing identified late Quaternary faults included as regional fault sources in the seismic source model

<i>Regional Fault Source</i>	<i>Fault Dip</i>	<i>Maximum Depth Of Faulting</i>	<i>Total Fault Length</i>	<i>Maximum Magnitude (Mw)</i>	<i>Slip Rate (mm/yr)</i>	<i>Earthquake Recurrence Model</i>
------------------------------	------------------	----------------------------------	---------------------------	-------------------------------	--------------------------	------------------------------------

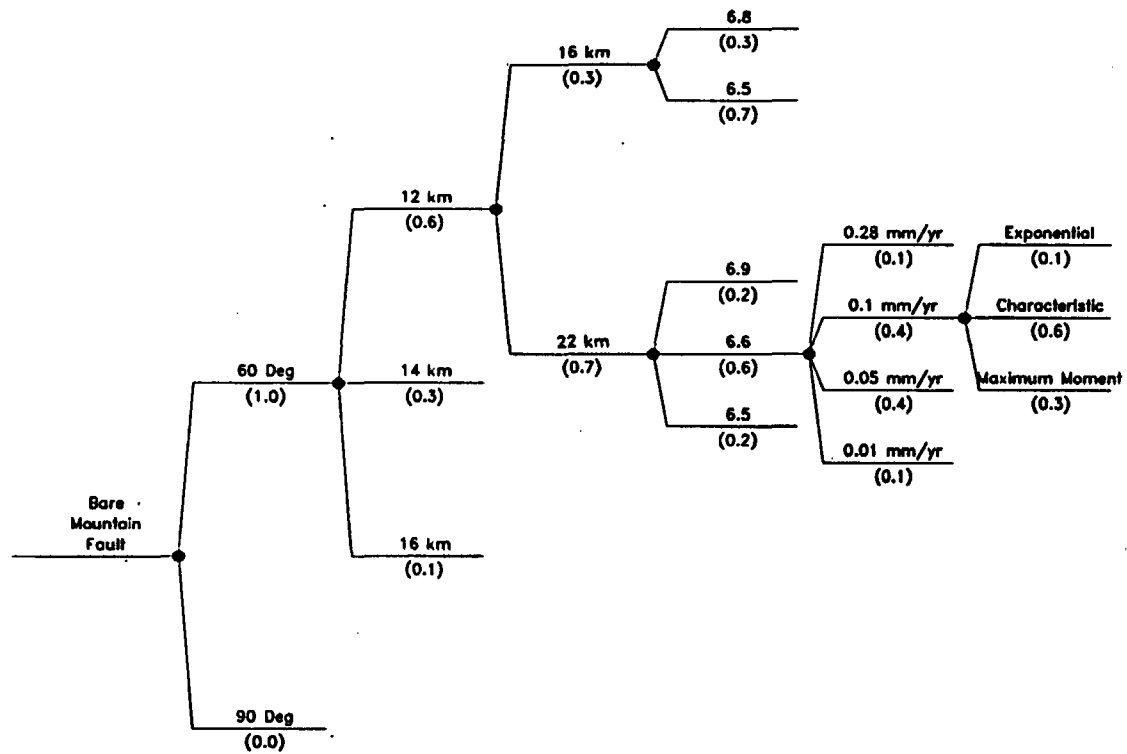


Figure DFS-7 Example of the logic tree used to characterize regional fault sources

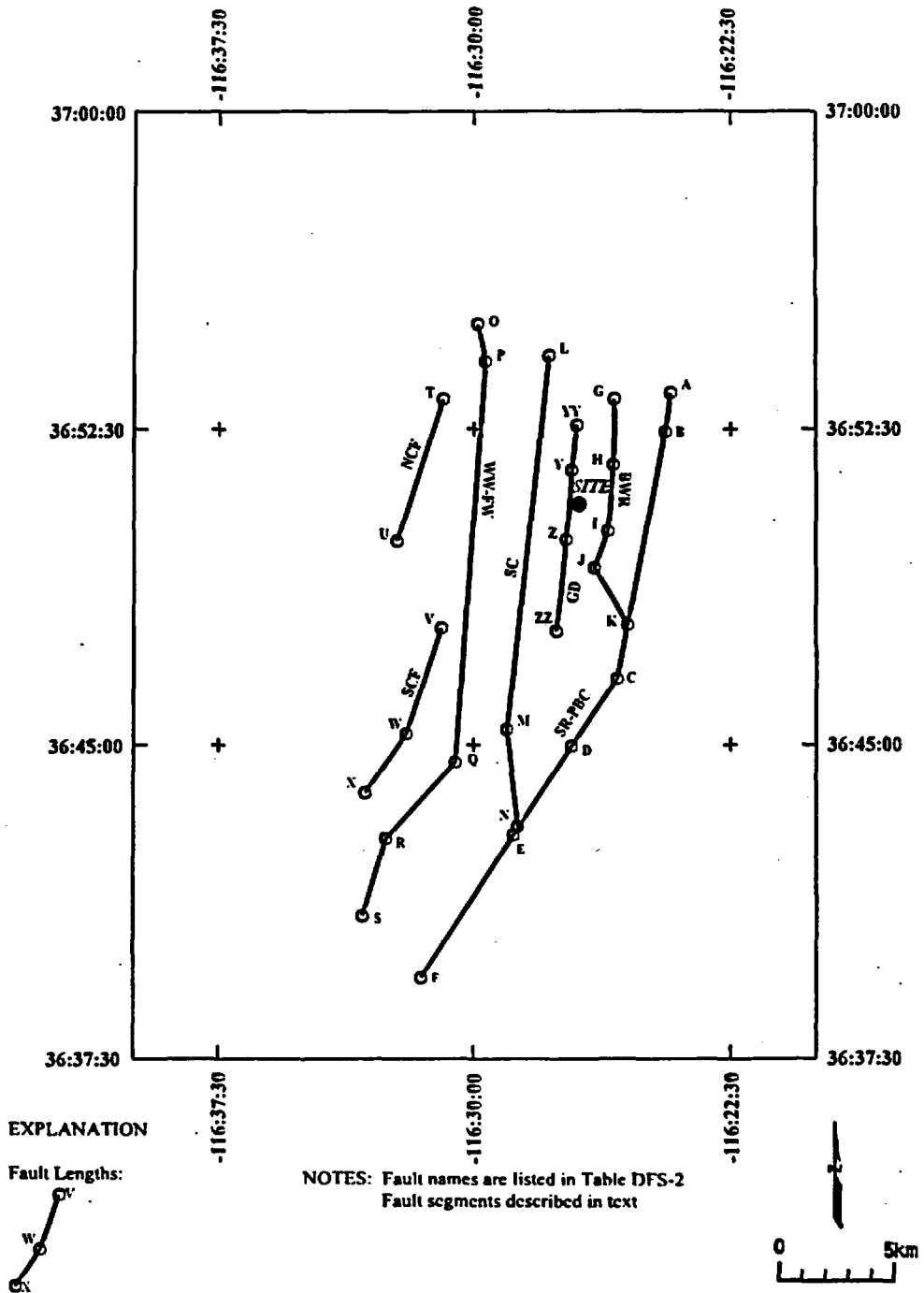
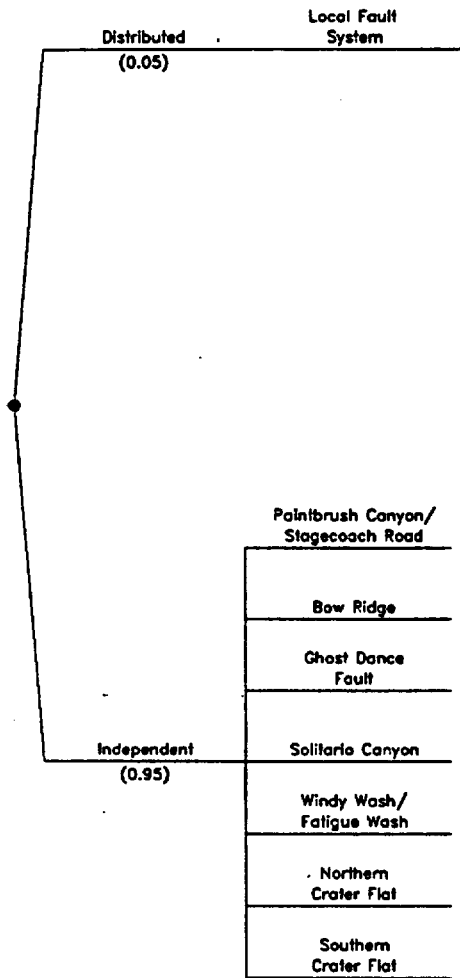


Figure DFS-8 Map showing local fault sources included in the seismic source model

<i>Fault Behavior</i>	<i>Sources</i>
-----------------------	----------------



same geometry as INDEPENDENT BEHAVIOR, but M-max is not constrained by total length of any one fault.

M-max on individual faults is constrained, in part, by the total length of the faults.

Figure DFS-9 Logic tree showing dependence of local fault model on distributive versus independent fault-behavior models

<i>Seismic Source</i>	<i>Total Fault Length Scenarios</i>	<i>Maximum Rupture Length</i>	<i>Structural Model</i>	<i>Dip/Width</i>	<i>Slip Rate (mm/yr)</i>	<i>Maximum Earthquake Method</i>	<i>Earthquake Recurrence Model</i>
-----------------------	-------------------------------------	-------------------------------	-------------------------	------------------	--------------------------	----------------------------------	------------------------------------

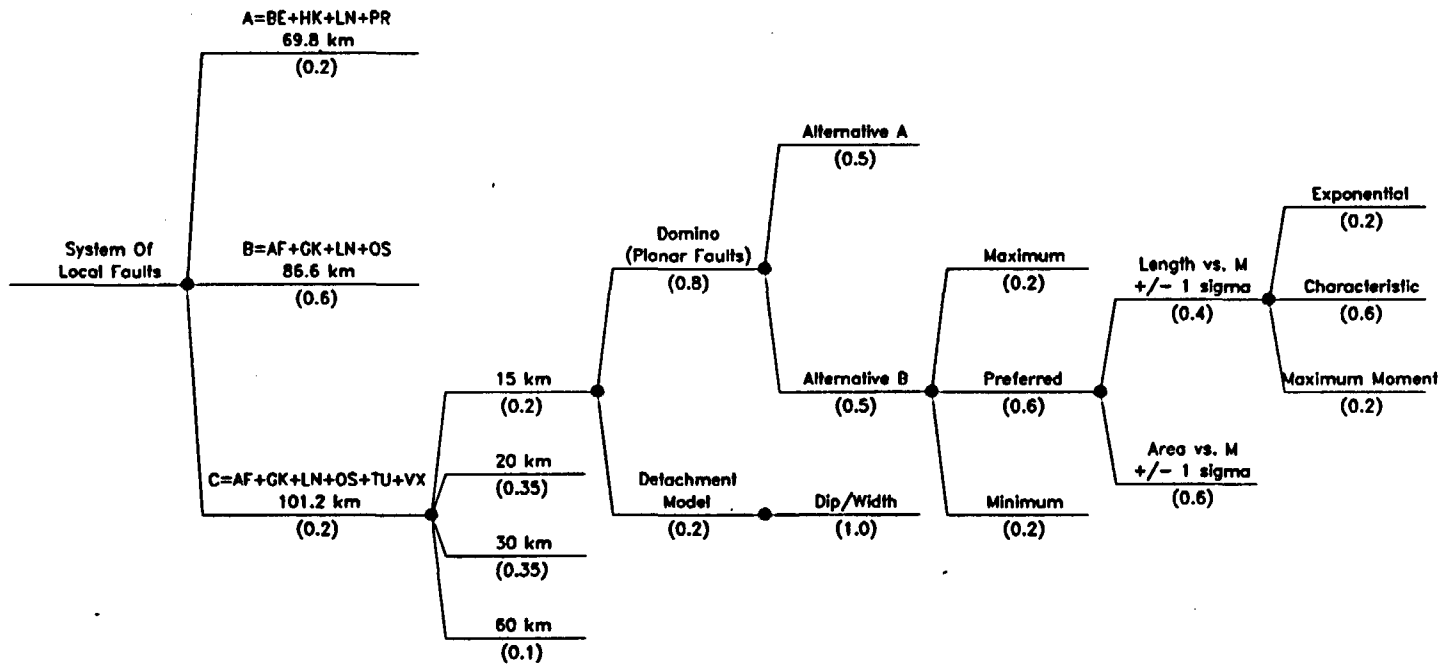


Figure DFS-10 Example logic tree used to characterize fault sources given distributed fault behavior

<i>Seismic Source</i>	<i>Total Fault Length (Table 4.3-3)</i>	<i>Maximum Rupture Length (Table 4.3-3)</i>	<i>Structural Model (Table 4.3-4)</i>	<i>Dip/Width (Table 4.3-4)</i>	<i>Slip Rate (mm/yr) (Table 4.3-5)</i>	<i>Maximum Earthquake Method</i>	<i>Earthquake Recurrence Model</i>
-----------------------	---	---	---	------------------------------------	--	----------------------------------	------------------------------------

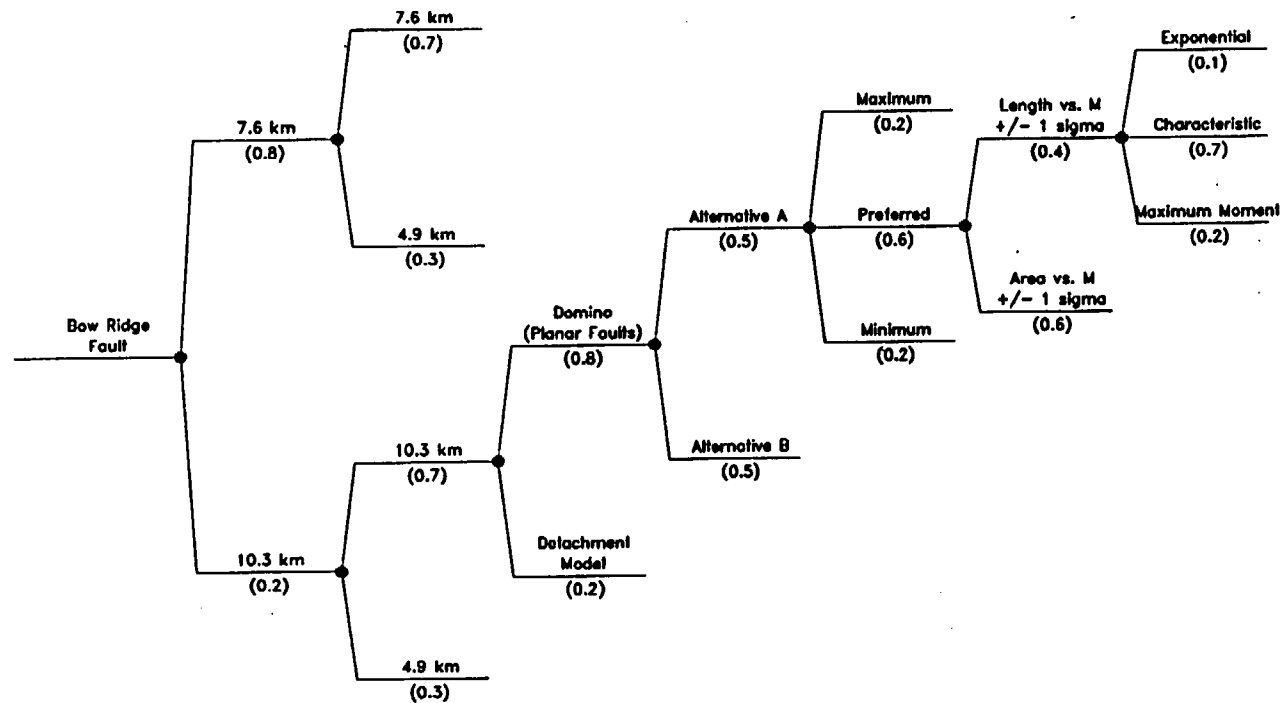


Figure DFS-11 Example logic tree used to characterize local fault sources given independent fault behavior

<i>Fault Behavior Model</i>	<i>Earthquake Recurrence Model</i>
-----------------------------	------------------------------------

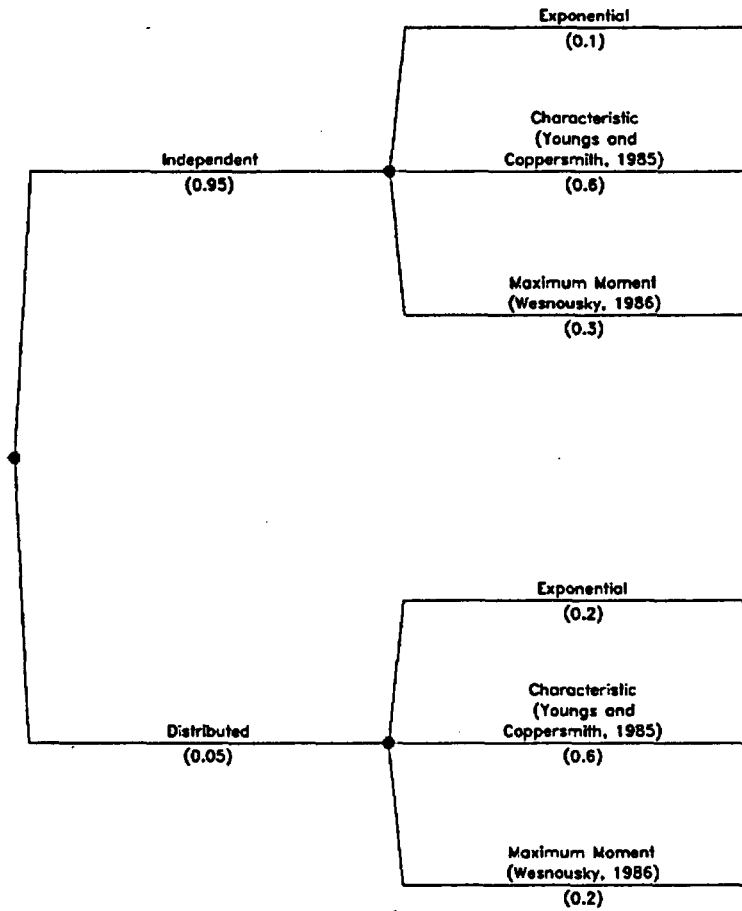
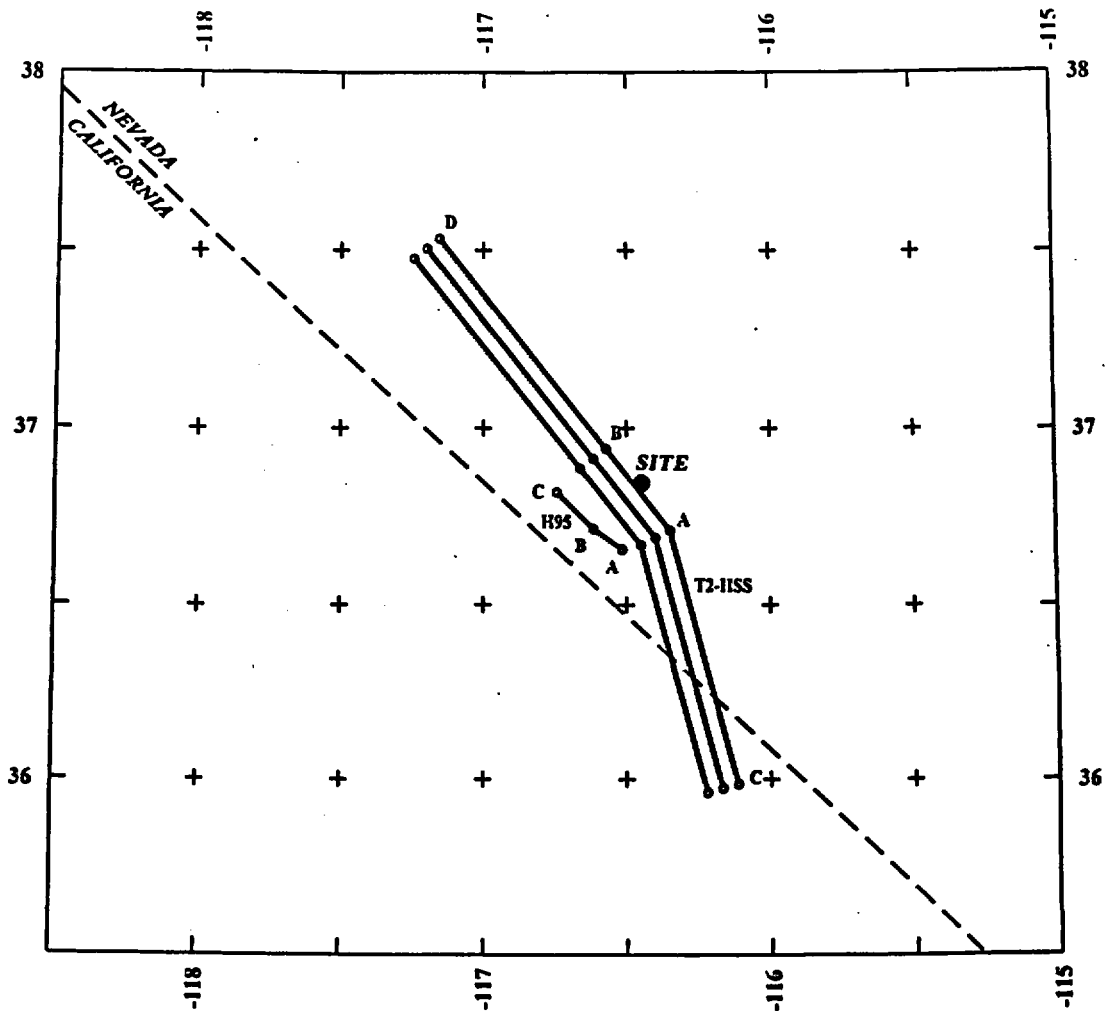
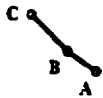


Figure DFS-12 Logic tree for conditional probability weights assigned to earthquake recurrence models



EXPLANATION

Fault Lengths:



NOTES: Fault names are listed in Table DFS-7
 Fault segments described in text

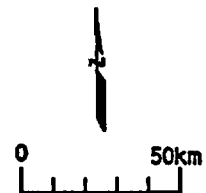
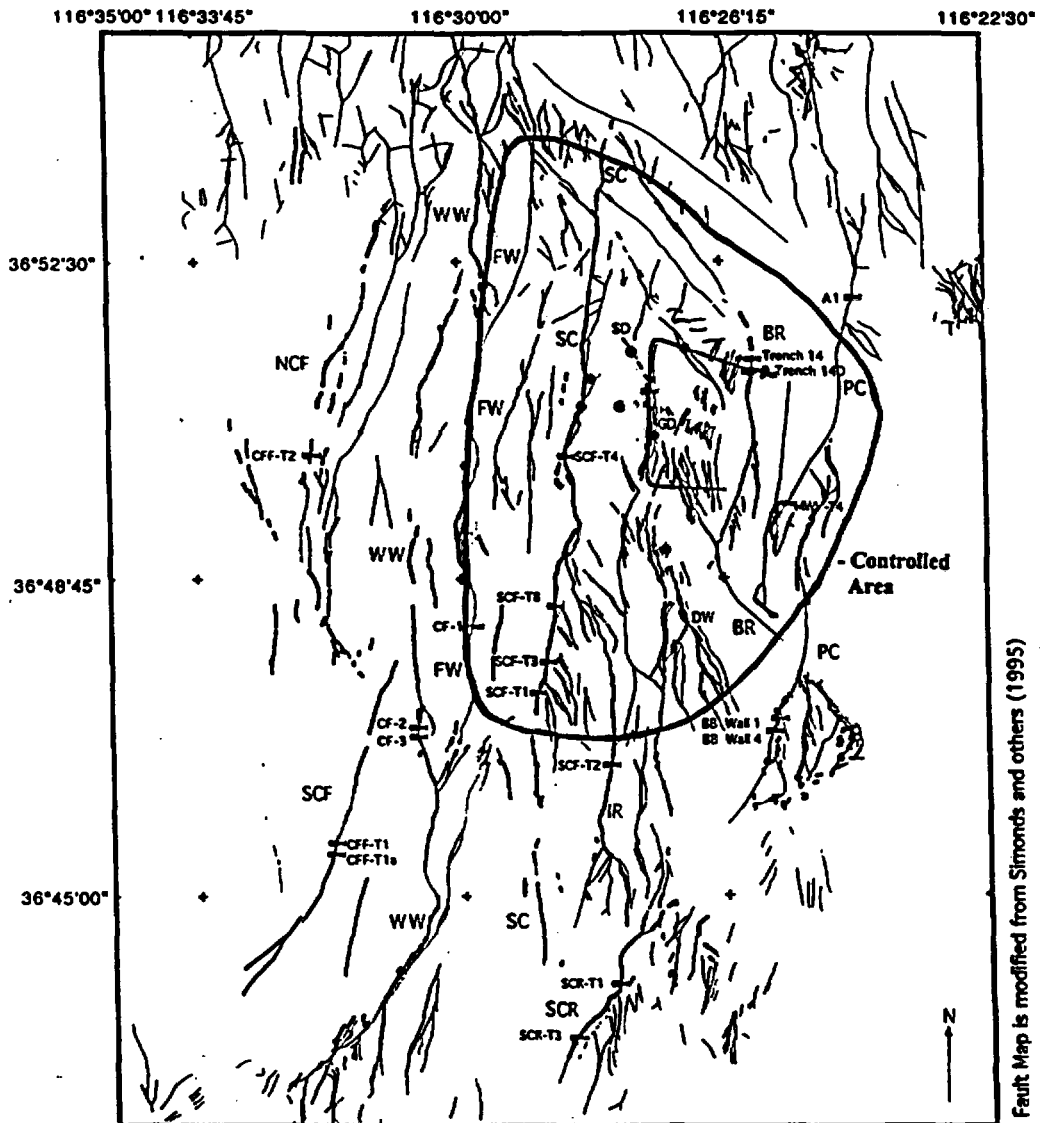


Figure DFS-13 Map showing hypothetical fault sources included in the seismic source model



Fault Map is modified from Simonds and others (1995)

EXPLANATION

- Fault Displacement Hazard Test Calculation Sites
- Approximate Controlled Area Boundary
- Approximate Potential Repository Area and Exploratory Studies Facility
- Paleoseismic Trench Locations
- Faults; Quaternary and suspected Quaternary age of last movement
- Faults; pre-Quaternary or undetermined age of last movement

0 kilometers 5

Fault Abbreviations	
BR	Bow Ridge
DW	Dune Wash
FW	Fatigue Wash
GO	Ghost Dance
IR	Iron Ridge
NCF	Northern Crater Flat
PC	Paintbrush Canyon
SD	Sundance
SC	Soltario Canyon
SCF	Southern Crater Flat
SCR	Stagecoach Road
WW	Windy Wash

USGS-YMP Pezzopane Jan 97

Figure DFS-14 Map showing fault displacement hazard test calculation sites.

Test Calculation Site	Activity	Cumulative Displacement Tiva Canyon Tuff	Age: Tiva Canyon Tuff	SLIP RATE Estimation Technique	Quaternary Slip Rate	Assessment Method	Average Displacement per event (cm)	Average Recurrence Interval (Ka)
-----------------------	----------	--	-----------------------	--------------------------------	----------------------	-------------------	-------------------------------------	----------------------------------

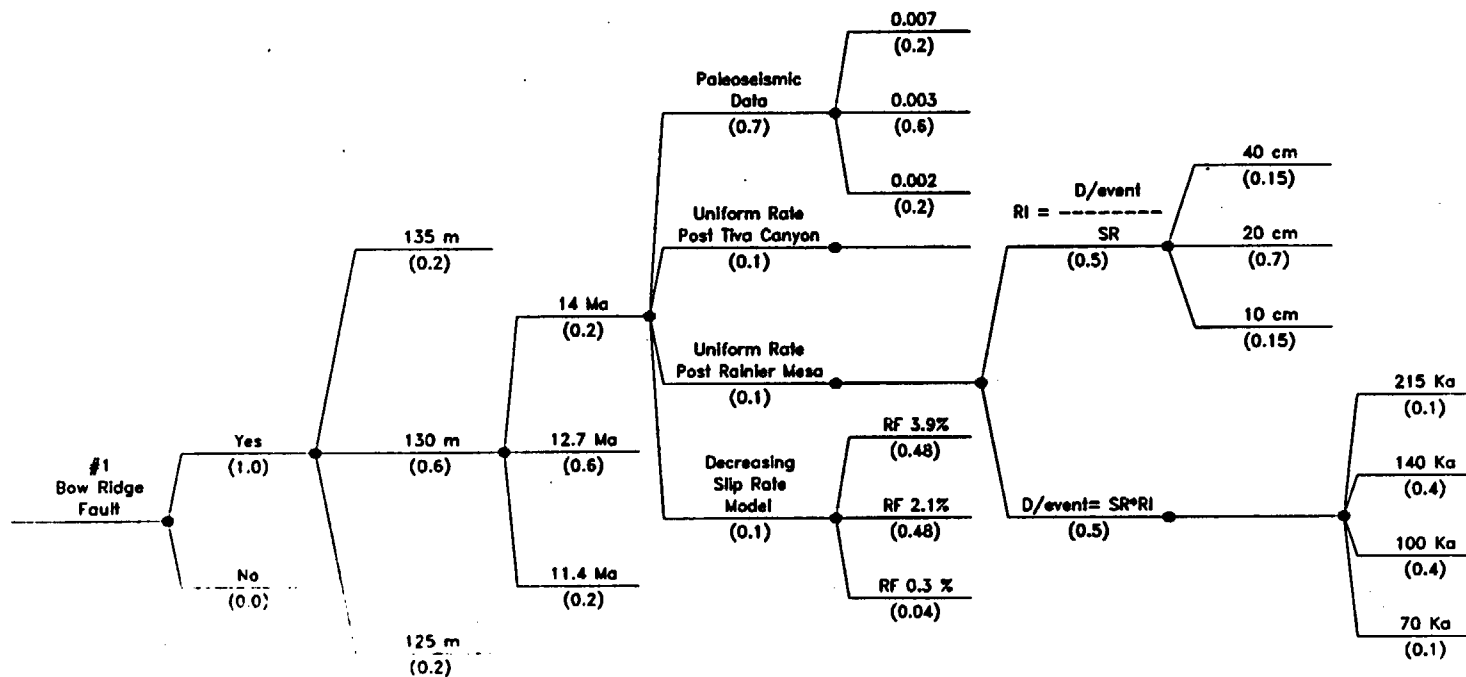
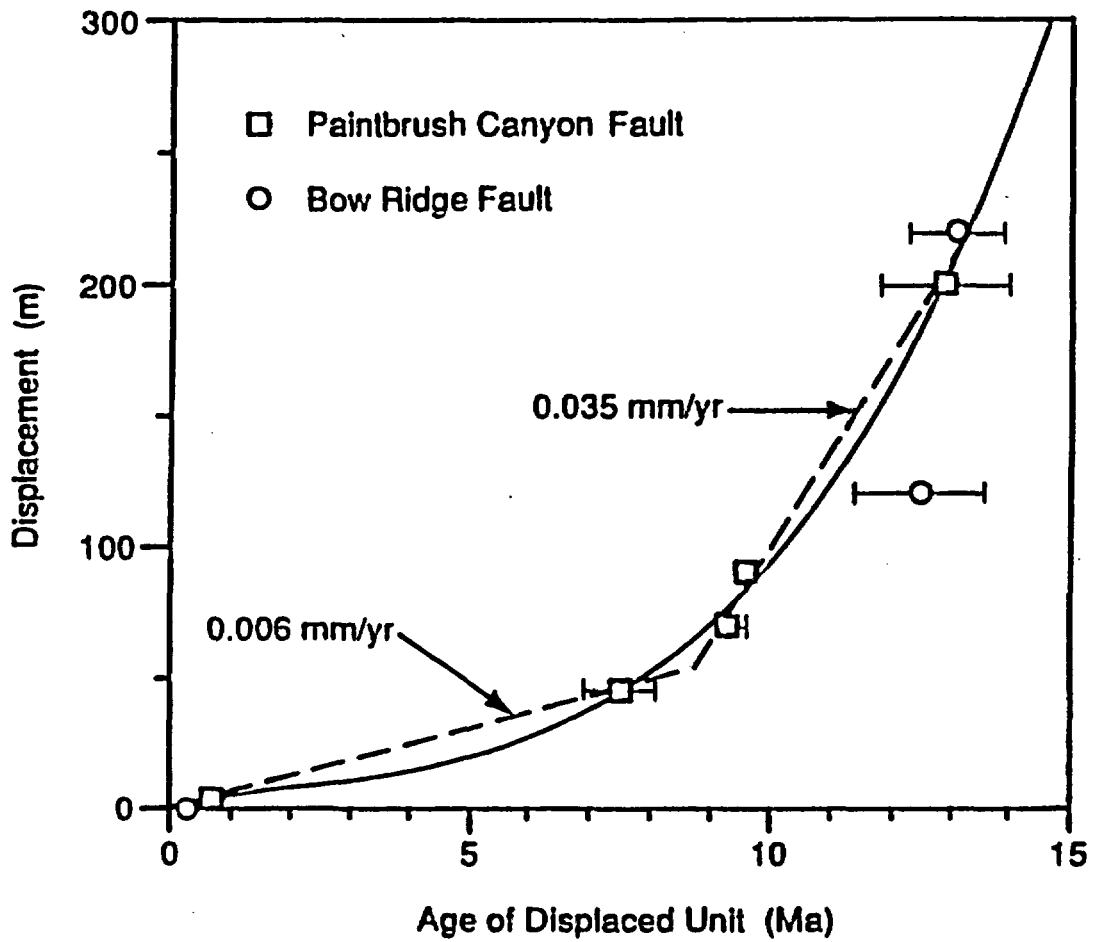


Figure DFS-15 Logic tree used to characterize the fault displacement hazard based on fault slip rates



Source: Gibson and others (1990)

Figure DFS-16

Graph showing displacement versus age of displaced unit for the Paintbrush Canyon and Bow Ridge faults (From: Gibson et al., 1993)

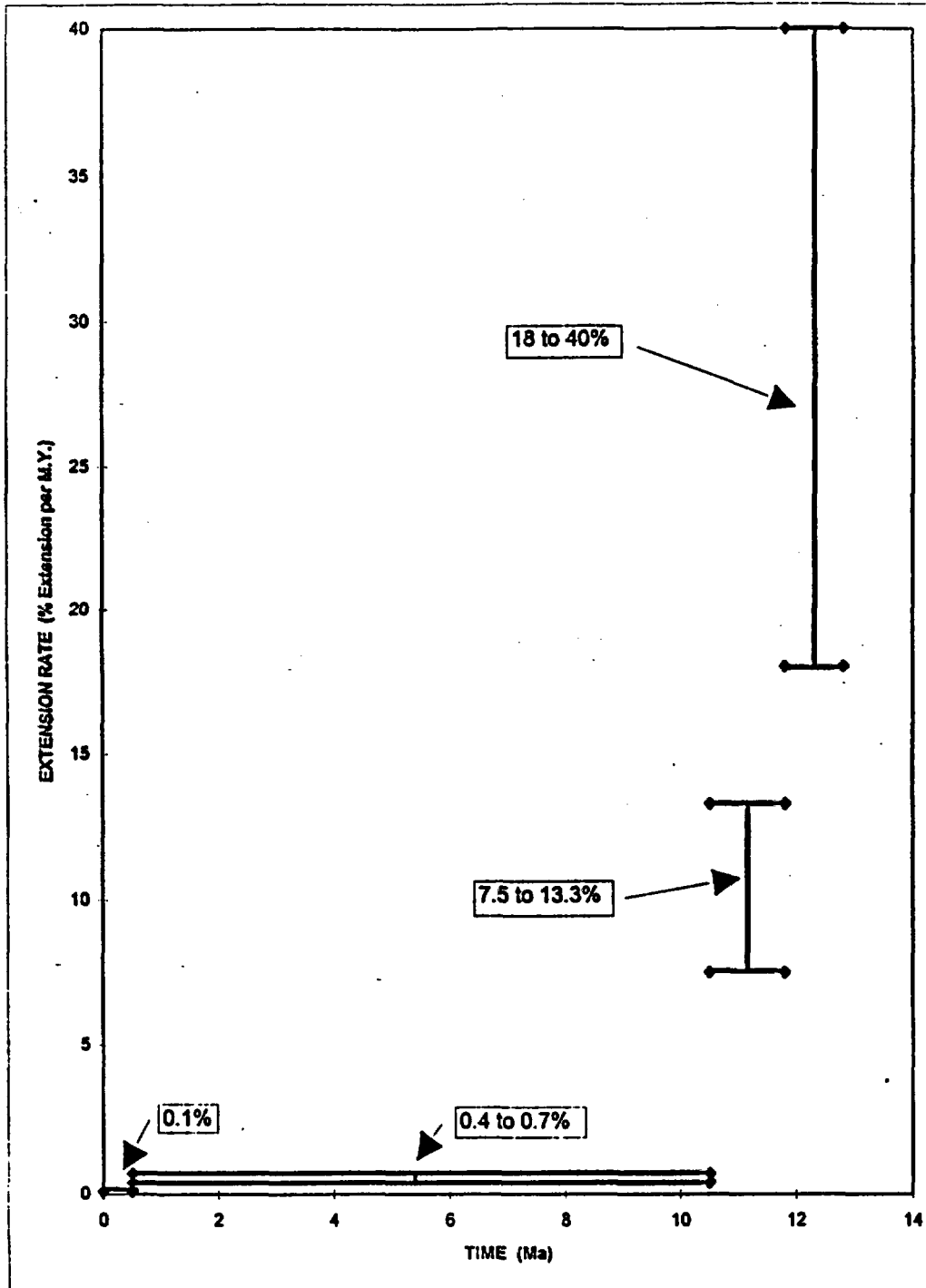


Figure DFS-17 Graph of estimated extension rates in Crater Fault basin from middle Miocene to the present (From: Fridrich et al., 1996)

Available Paleoseismic Data	Quaternary Slip Rate Estimation Technique	Reduction Factor
-----------------------------	---	------------------

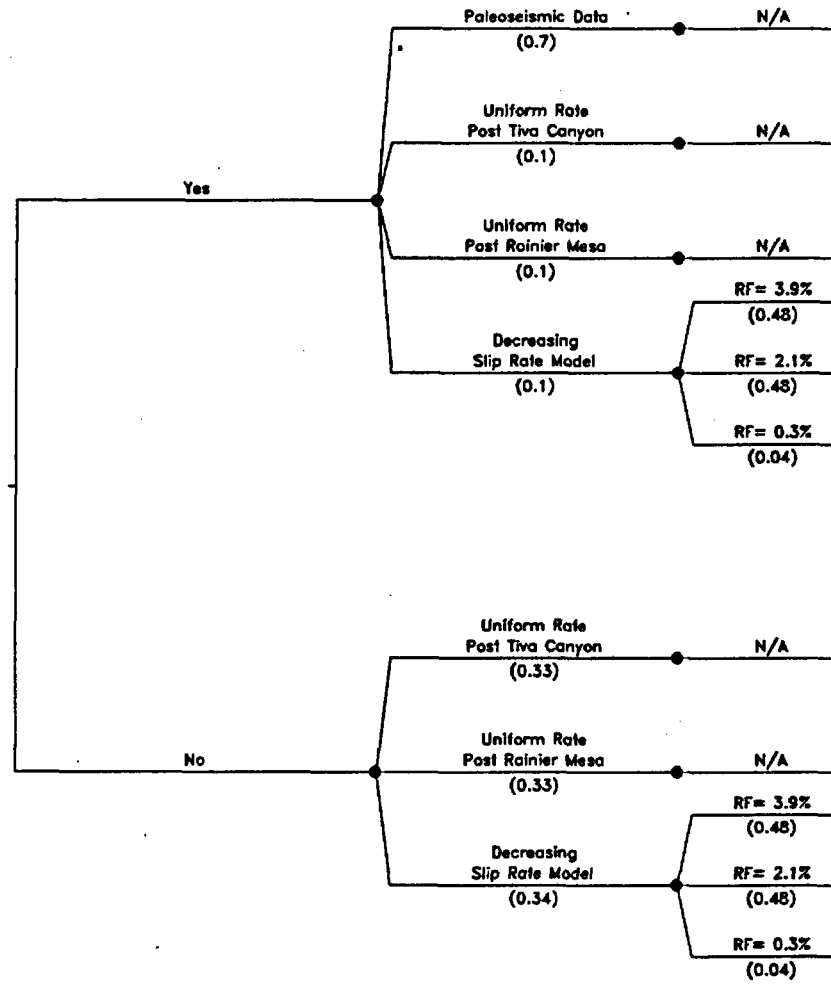


Figure DFS-18 Logic tree showing probability weights assigned to the different Quaternary-slip-rate-estimation techniques depending on the availability of site-specific paleoseismic information.

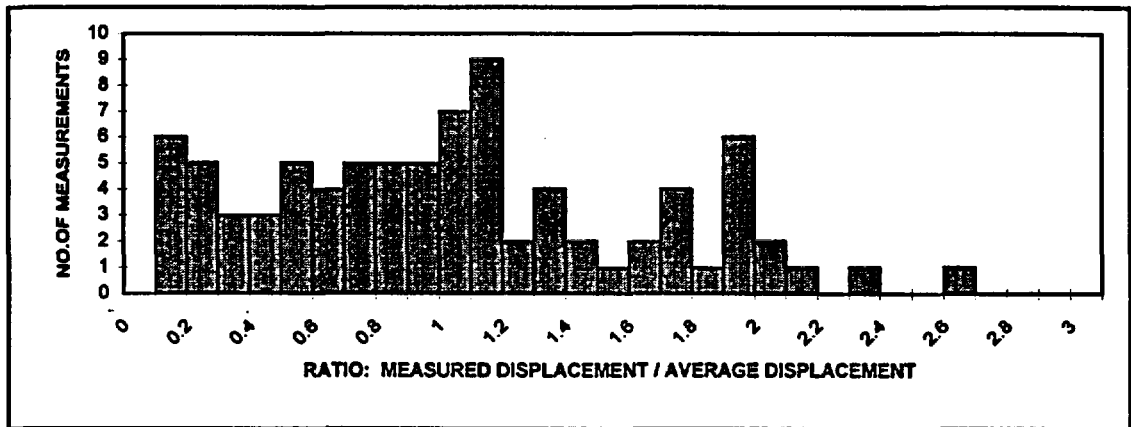
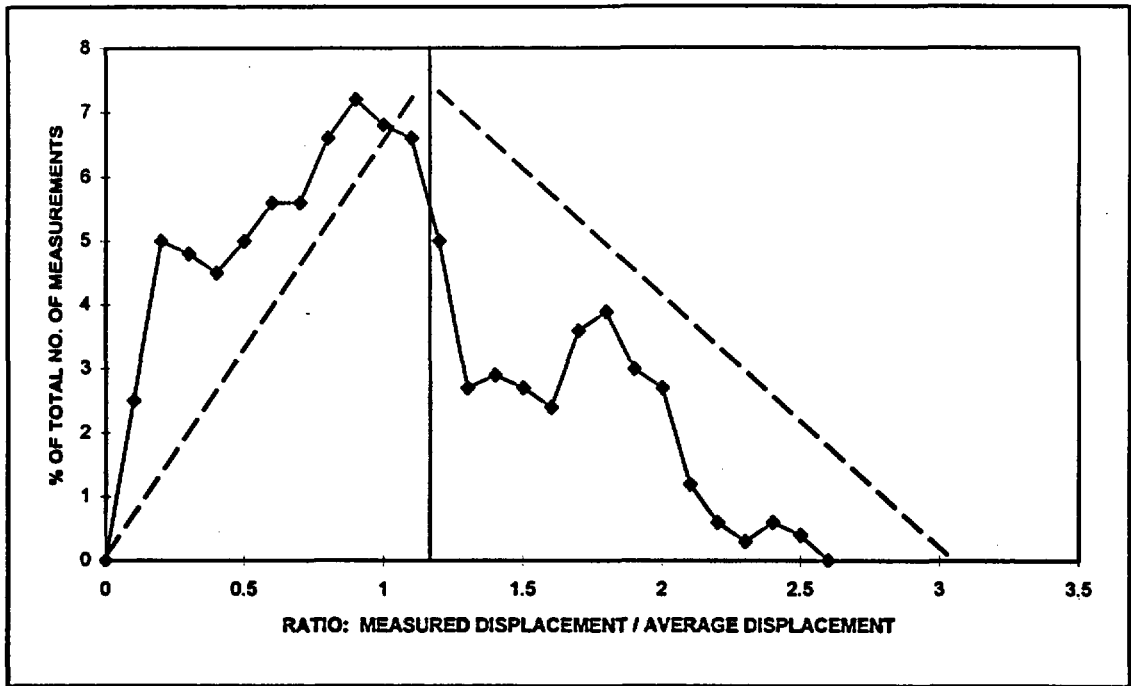


Figure DFS-19 Plots showing event-to-event variability in displacement relative to average displacement per event at a location along a fault based on data from paleoseismic investigations in the Yucca Mountain area.

Test Calculation Site	Potential for Activity Table DFS-14	Deformation History Model	Reduction Factor	Age of the Host Rock (Tiva Canyon Tuff)	Probability of an "Event" (Pe) Table DFS-15	"Event" defined as Threshold of Detection of Fault Displacement (Section 8.3)
-----------------------	-------------------------------------	---------------------------	------------------	---	---	---

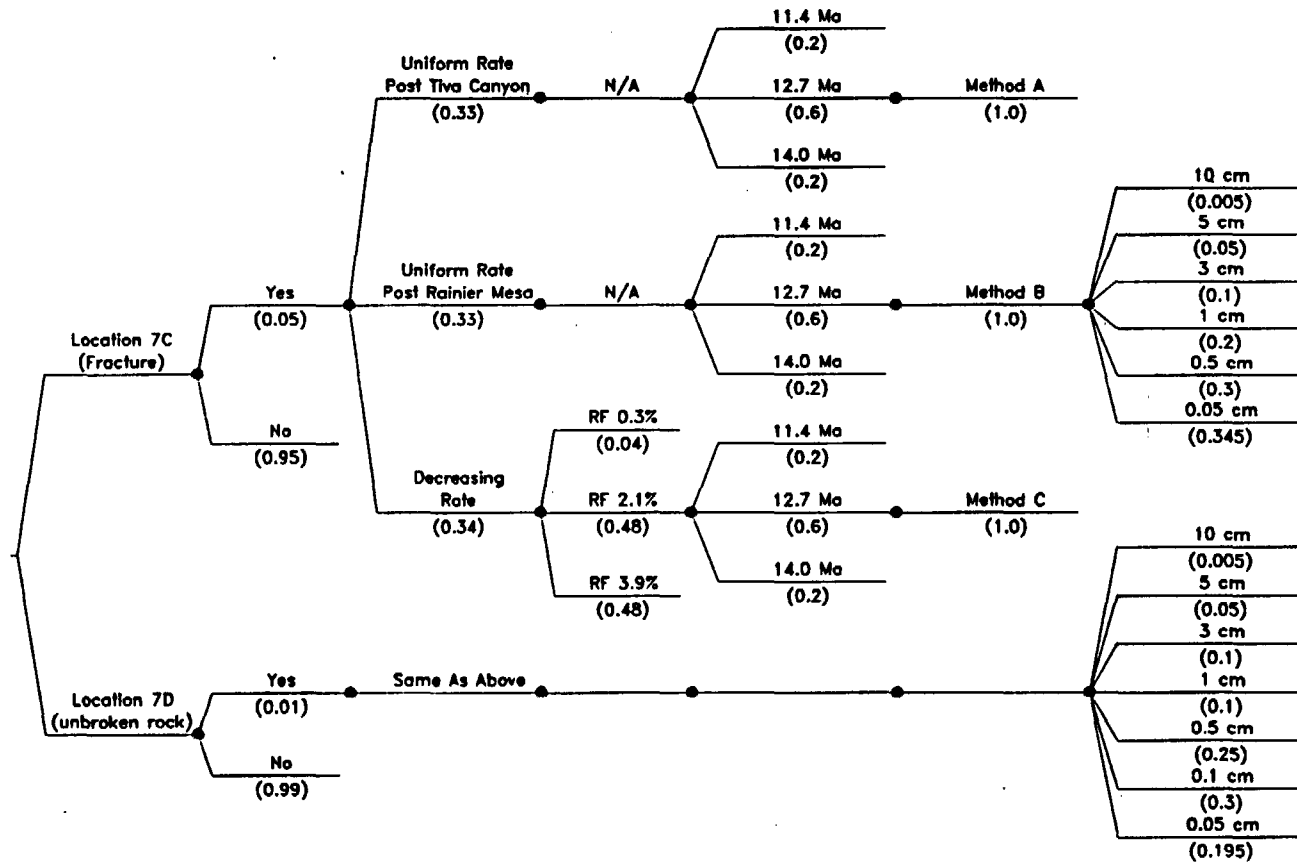


Figure DFS-20 Logic tree for assessing potential fault displacement hazard across a fracture or in unbroken rock.

ELICITATION SUMMARY

ALBERT M. ROGERS, JAMES C. YOUNT, AND LARRY W. ANDERSON

TABLE OF CONTENTS

Page: i

1.0	INTRODUCTION	RYA-1
2.0	SEISMIC SOURCES.....	RYA-2
2.1	THICKNESS OF THE SEISMOGENIC CRUST	RYA-3
2.2	AREAL OR BACKGROUND SOURCES.....	RYA-3
2.2.1	Recurrence.....	RYA-3
2.2.2	Maximum Magnitude	RYA-6
2.3	LOCAL FAULT SOURCES.....	RYA-6
2.3.1	Coalescing Fault Structure.....	RYA-7
2.3.2	Maximum Magnitude Approach	RYA-9
2.3.3	Recurrence Approach.....	RYA-10
2.4	POSSIBILITY OF A BURIED SEISMIC SOURCE	RYA-11
2.5	VOLCANIC SOURCE.....	RYA-13
2.6	REGIONAL FAULT SOURCES.....	RYA-13
2.6.1	Maximum Magnitude Approach	RYA-14
2.6.2	Recurrence Approach.....	RYA-14
3.0	FAULT DISPLACEMENT CHARACTERIZATION.....	RYA-14
3.1	INTRODUCTION.....	RYA-14
3.2	APPROACH	RYA-17
3.2.1	Probability Slip can Occur	RYA-17
3.2.2	Frequency of Displacement Events	RYA-17
3.2.3	Estimation of Slip Rate.....	RYA-18
3.2.4	Estimation of Average Slip Per Event.....	RYA-19
3.2.5	Distribution for Displacement Per Event.....	RYA-20
3.3	DATA FOR CHARACTERIZATION OF DISPLACEMENT HAZARD AT THE NINE TEST CALCULATION SITES	RYA-21
4.0	REFERENCES	RYA-27

TABLES

Table RYA-1	Completeness times
Table RYA-2	Interval recurrence parameters
Table RYA-3	Fault source parameters, Area A

Table RYA-4	Coalescing fault source model, Area A—Three Yucca Mountain fault systems
Table RYA-5	Coalescing fault source model, Area A—Two Yucca Mountain fault systems
Table RYA-6	Coalescing source model, Area A—One fault system
Table RYA-7	M_{\max} for hypothesized buried seismic source 30 km long (M_{\max} derived from $M = 4.04 + 0.98 \log [\text{rupture area}]$) (Wells and Coppersmith, 1994)
Table RYA-8	Significant regional fault source parameters, Areas B and C

FIGURES

Figure RYA-1a	Logic tree for background source zones
Figure RYA-1b	Logic tree for local fault sources
Figure RYA-2	Map showing boundaries of zones used in the seismic source model
Figure RYA-3	Map showing earthquakes from the version 5 catalog and the background source zones
Figure RYA-4	Map showing earthquakes from the version 7 catalog and the background source zones
Figure RYA-5	Stepp plot of annual frequency versus years before 9/1996 for individual magnitude bins and the version 5 catalog
Figure RYA-6	Stepp plot of annual frequency versus years before 9/1996 for individual magnitude bins and the version 7 catalog
Figure RYA-7	Histogram showing b-values obtained for the version 5 catalog given uniform sampling of completeness times
Figure RYA-8	Histogram showing b-values obtained for the version 5 catalog given normal sampling of completeness times
Figure RYA-9	Histogram showing b-values obtained for the version 7 catalog given uniform sampling of completeness times
Figure RYA-10	Histogram showing b-values obtained for the version 7 catalog given normal sampling of completeness times
Figure RYA-11	Interval rates for the version 5 catalog that produced the modal b-value 1.09 (Figure RYA-7) and the fit to these data using the Weichert maximum likelihood method

- Figure RYA-12** Interval rates for the version 7 catalog that produced the modal b-value 1.17 (Figure RYA-9) and the fit to the data using the Weichert maximum likelihood method
- Figure RYA-13** Earthquake recurrence parameters. The paired a- and b-values calculated by uniform sampling from the range of likely completeness times and associated annual rates in the version 5 catalog. This plot shows the correlation between a- and b-values.
- Figure RYA-14** Earthquake recurrence parameters. The paired a- and b-values calculated by uniform sampling from the range of likely completeness times and associated annual rates in the version 7 catalog. This plot shows the correlation between a- and b-values.
- Figure RYA-15** Estimated age and amount (in cm) of late Quaternary displacement for faults in the Yucca Mountain area based on data in USGS (1996). Faults are arranged from west to east; trench numbers under each fault are arranged from north to south. Bars and arrows show full uncertainties in estimated age of faulting event at each trench. "w" represents fracturing event (displacement < 20 cm). Age on far right of chart shows our best estimate for age of grouped event. See text and tables for fault abbreviations.
- Figure RYA-16** Map showing local fault sources included in the seismic source model
- Figure RYA-17** Map showing regional faults included in the seismic source model
- Figure RYA-18** Logic tree used to characterize fault displacement at sites with Quaternary data
- Figure RYA-19** Logic tree used to characterize fault displacement at sites without Quaternary data
- Figure RYA-20** Plots developed by DFS showing event-to-event variability in displacement relative to average displacement per event at a location along a fault based on data from paleoseismic investigations in the Yucca Mountain area
- Figure RYA-21** Probability density function (PDF) and cumulative distribution function (CDF) for 80 measurements single-event displacement, normalized to MD^{max} for the corresponding fault, from 19 trenches in the Yucca Mountain area as developed by the AAR team

ELICITATION SUMMARY
ALBERT M. ROGERS, JAMES C. YOUNT, LARRY W. ANDERSON

1.0

INTRODUCTION

Yucca Mountain is located in the southern Great Basin of Nevada. The physiography and tectonic setting of this area are the product of late Cenozoic crustal extension and silicic volcanism that occurred primarily between 17 and 9 million years ago. This deformation created a complex structural setting that presents significant interpretational difficulties. A number of tectonic models, developed to explain this structural diversity, were presented and discussed at the Yucca Mountain Workshops held between October 1996 and April 1997. For example, see Carr (1982, 1990); Carr et al. (1986); Scott (1990); and Hamilton (1988). O'Leary (1996) provides an extensive review of models and references, as well as a preferred interpretation. These models each have unique merit in explaining certain aspects of the structural evolution and present-day seismotectonic setting of the Yucca Mountain area. Although tectonic models can be useful tools, none of the models presented provide a complete, unified explanation of all the seismic, geologic, and geophysical data for Yucca Mountain and the larger Walker Lane-western Great Basin-Death Valley regions. Therefore, our approach was first to examine what appear to be the primary potential seismogenic sources, and then to use geologic and geophysical constraints to define the source properties. We find that a coalescing fault model best fits the Yucca Mountain structural domain. A question raised at several workshops was whether the Yucca Mountain faults are capable of generating earthquakes. For our assessment, faults in the Bare Mountain-Yucca Mountain area are treated as potential seismic sources. We include the following seismic sources in our assessment of the earthquake hazard at Yucca Mountain: (1) background seismicity not associated with mapped faults; (2) Yucca Mountain faults, which we interpret to have varying degrees of lateral and vertical coalescence; (3) the Bare Mountain fault; (4) volcanic activity; and (5) large, regional, late Quaternary faults.

Our analysis is based on the following fundamental interpretations: (1) the Bare Mountain fault is a planar seismogenic fault that penetrates to mid-crustal depths; (2) the faults at Yucca

Mountain are planar to listric and coalesce into one, two, or three master faults at unknown depths above or at the Bare Mountain fault; the depth at which this coalescence occurs is considered an uncertain variable (see O'Leary, 1996, for a summary of the geologic and geophysical data that support these assumptions; theoretical modeling also provides support for steeply dipping and coalescing faults); and (3) other faults, not mapped at the surface, exist in the region that can produce earthquakes below the threshold magnitude for surface rupture.

Yucca Mountain faults are considered to behave independently and/or truncate downdip in a detachment fault or a zone of decoupling. Our evaluation of Yucca Mountain faults as coalescing at variable depths implicitly includes independent rupture and truncation, although we believe that the data exclude the possibility of a seismic detachment. Because no earthquakes have been observed on detachments faults worldwide (e.g., Jackson, 1987), we do not consider them to be seismically active structures; we remain unconvinced by arguments that the historical record is too short to include earthquakes on such faults worldwide (Wernicke, 1995).

Our analysis considers regional faults that are interpreted to be steeply dipping planar faults penetrating to mid-crustal depths. Because of their distance from the site and low contribution to the hazard, these faults are modeled more simply, with little variation in downdip width. In general, we model only the larger regional faults within 100 km of Yucca Mountain, as explained below; however, we do consider background seismicity, either as uniformly distributed faults or as a smoothed historical seismicity.

2.0

SEISMIC SOURCES

The logic tree that defines our interpretations of potential seismic sources for the Yucca Mountain area is given on Figures RYA-1a and b. Various aspects of these seismic sources are discussed below. We indicate the weights assigned to the branches of the tree on the figures or in the tables that follow.

2.1 THICKNESS OF THE SEISMOGENIC CRUST

The maximum thickness of the brittle crust (with assigned probability) is interpreted to be: 12 km (0.2), 15 km (0.7), and 20 km (0.1) (Figure RYA-1b). These depths represent the limits observed for both small- and large-magnitude earthquakes (e.g., Rogers et al., 1987; K. Smith, SSC Workshop 2; Harmsen and Bufe, 1991; Doser and Smith, 1989; Rogers et al., 1991). The largest earthquakes in the southern Great Basin occur to depths of 20 km; smaller earthquakes tend to occur above about 10 and 12 km (with some exceptions). The assessment of seismogenic crustal depth is independent of the other source interpretations, and the ensuing source characteristics for the Yucca Mountain area depend on this quantity; therefore, the depth of the brittle crustal is the first assessment on the logic tree.

2.2 AREAL OR BACKGROUND SOURCES

The region within a 100-km radius surrounding the Yucca Mountain site has been divided into three zones, which are defined by different rates of seismicity and structural characteristics (Figure RYA-2). Zone A encloses the local Yucca Mountain area. It is characterized by low seismicity; Quaternary volcanism; northerly trending, anastomosing, and branching faults that appear to belong to the same structural domain; and a basement graben structure illuminated by a gravity low that may extend south into the Amargosa trough. Zone B, which surrounds Zone A, includes the Basin and Range and parts of the Walker Lane tectonic provinces. Seismic rates in Zone B are higher than those in Zone A. Structurally, Zone B is highly complex, consisting of mixed zones of volcanism; northerly trending, block-bounding faults; and northeast-trending, left-lateral and northwest-trending, right-lateral faults. Zone C consists of the Death Valley-Furnace Creek fault zone and faults to the west, such as the Hunter Mountain and Panamint fault zones. It is characterized by long faults having higher rates of slip than the faults of Zones A or B.

2.2.1 Recurrence

In our analysis, background seismicity was interpreted to be non-uniform or uniform. In the non-uniform case, the observed seismicity was smoothed in a manner similar to that described by Frankel (1995). This method was applied to preserve the observed spatial characteristics of the historical earthquake record while including a degree of geographical variation through

spatial smoothing. Spatial seismicity smoothing is assigned a weight of 0.6, because short-term seismicity patterns are considered good predictors of future short-term seismicity (McGuire and Barnhard, 1981). A Gaussian smoothing function was applied to the cumulative gridded earthquake counts for two correlation distances: 5 and 15 km. The relatively shorter h-values were used to retain the spatial concentrations of seismicity. We assign the highest weight to the short-wavelength smoother on the basis that the accuracy of earthquake location is closer to ± 5 km than to ± 15 km, on average (K. Smith, SSC Workshop 2; Rogers et al., 1987). Smoothing was conducted within the boundaries of each source zone shown on Figure RYA-2, considered a hard boundary for the spatial smoothing model. The derived rates were used with a truncated Gutenberg-Richter recurrence relationship for earthquakes below the threshold magnitude of surface faulting, discussed below.

In the uniform smoothing interpretation (weight 0.4), Zones A, B, and C are modeled as equivalent to having faults that are distributed uniformly throughout each zone. This interpretation smooths the observed seismic rate uniformly across each zone. Hence, historical seismicity is interpreted to be spatially stationary only on a zonal basis, and individual seismic clusters are assumed to be possible anywhere within the zone. The modeled faults are distributed with a uniform 1-km spacing within Zone A so that fault spacing does not artificially induce geographic variation in the computed hazard. The faults can have any length, although the rupture areas depend on the magnitude. The square rupture patches are distributed randomly on the faults. The rupture areas are constrained below the near-surface Tertiary rocks, because we assume that faults penetrating these rocks do not store significant shear strain when slip propagates from the deeper parts of the fault toward the surface; fault segments in the Tertiary sedimentary section are modeled as passive slip without significant energy release through shaking. Hence, in the model the faults are constrained below a depth of 2 km.

The seismicity rates on faults within zones A, B, and C were calculated by fitting truncated exponential relationships (e.g., Youngs and Coppersmith, 1985) to declustered catalog versions 5 and 7 within 100 km of Yucca Mountain. In this analysis, we used the Weichert maximum likelihood method (Weichert, 1980). Earthquake aftershocks were removed from the version 5 catalog using a declustering routine developed by Youngs et. al, 1987;

aftershocks also were removed from the version 7 catalog using a declustering technique, termed the Veneziano method, developed for EPRI (McGuire, 1985). We give equal weight to the catalogs, because we have no basis for preferring one to the other. We determined a- and b-values from the catalogs using these techniques and the following procedures. Figures RYA-3 and RYA-4 show maps of the declustered catalogs used in our analyses. Figures RYA-5 and RYA-6 show modified Stepp plots (Stepp, 1972) used to calculate the period of complete detection and reporting of earthquakes as a function of magnitude bin. If the rate of earthquake occurrence is constant over the long term, then, as the historical period increases, these curves should approach a constant annual rate; however, if detection and reporting of earthquakes becomes incomplete as the historical period increases, these curves will show a negative slope. The point at which the slope of these curves changes from zero to negative is termed the completeness time. Based on the spacing of these curves, we judged that the earthquake magnitude range of 1.5 to 2.0 is incompletely reported for all times. Although this bin could be complete for the Yucca Mountain region, it likely is incomplete for the 100-km circle. We exclude it from our calculations for this reason. Table RYA-1 shows the preferred completeness times and the ranges we inferred from these plots. We randomly selected from within these completeness ranges the corresponding annual earthquake rate from the Stepp plots. In separate trials, we used either uniform sampling or truncated normal distributions having a mean at the preferred values and a standard deviation of five years. The randomly selected annual rates were fit with a truncated Gutenberg-Richter relationship to obtain a- and b-values for each random selection. This procedure was repeated for 200 trials. Histograms of the resulting b-values are shown on Figures RYA-7, -8, -9, and -10. These figures show that the b-values have narrow distributions; modal values for catalog 5 range from 1.08 (normal distribution) to 1.09 (uniform distribution). For catalog 7, b-values of about 1.16 (normal distribution) to 1.17 (uniform distribution) were determined. We used the uniform distribution because it expresses the greatest uncertainty, as might be expected.

The consistently higher b-values for catalog 7 may be related to less complete removal of aftershocks. Typical recurrence curves for the modal b-value are shown on Figures RYA-11 (catalog 5) and RYA-12 (catalog 7). These figures show that the fitting technique weights the low- to mid-magnitude range most heavily; the largest-magnitude bin has little influence, but it also has the fewest earthquakes and, consequently, the largest expected error in the annual rate. For each b-value bin, we can assign a corresponding a-value based on the correlation

between a- and b-values observed in the Monte Carlo simulation. This correlation is shown on Figures RYA-13 and RYA-14. Based on this analysis, we used the b- and a-value pairs and their respective probabilities shown in Table RYA-2. (Note that the bin probabilities were determined using larger bins than shown on the figures.)

A proportioning process was applied to the a- and b-value pairs for the 100-km circle in each distribution above to compute corresponding distributions for each subzone. The total number of earthquakes greater than or equal to magnitude 3 in each subzone were counted in each magnitude bin over the preferred completeness time for that bin. These binned earthquake counts were summed separately for each zone and for the 100-km circle to obtain the cumulative number of earthquakes above this magnitude for the entire zone and its subzones. The ratio of counts in each zone to the total count in the 100-km circle then was computed. These ratios were used to proportion the anti-logarithm of the a-values, given above, to obtain cumulative earthquake counts for each subzone. The corresponding b-values and probability levels are carried along with their proportioned a-values. These proportioned counts and corresponding b-values were used to compute truncated recurrence relationships for each subzone.

2.2.2 Maximum Magnitude

We interpret background earthquakes to be caused by ruptures that do not intersect the Earth's surface. Based on the work of Pezzopane and Dawson (1996), Pezzopane (SSC Workshop 3), and dePolo (1994), we consider the maximum background earthquake magnitude to be $M_w = 6.3 \pm 0.3$. We use weights (0.185, 0.63, and 0.185) to simulate the 5th percentile, mean, and 95th percentile in a normal distribution.

2.3 LOCAL FAULT SOURCES

Within Zone A (the local Yucca Mountain area), we consider three alternative structural models: pure planar faults that behave independently, faults that lie above a detachment or zone of decoupling and respond passively to slip on a buried fault, and faults that are planar to listric but that coalesce downdip. In the planar fault model, each fault identified at Yucca Mountain is considered seismogenic and is modeled as an independent seismic source that exists from the surface downdip through the entire seismogenic crust. In the detachment or decoupled model, the surface faults could be seismic sources, but they more likely represent a

relatively passive response to earthquakes occurring on buried sources below the detachment. In the coalescing fault model for Yucca Mountain, individual faults mapped at the surface are assumed to merge or coalesce downdip and along strike and, as such, to operate as a group or groups of faults in generating earthquakes. Various groups of faults, therefore, are considered synchronous seismic sources (Figure RYA-1b).

The coalescing model is our preferred model because it is the only one that appears to account for most of the spatial and temporal fault characteristics at Yucca Mountain; that is, the close fault spacing, the merging and bifurcating of faults, and the very short mapped length for some faults that have large single-event displacements. Further, the coalescing fault model explains the apparent synchronicity of faulting on multiple Yucca Mountain faults at about 70 ka (i.e., the ash event; Pezzopane et al., 1996; Figure RYA-15). In the planar fault model, this apparently synchronous event would be considered the result of the coincidental rupture of multiple, independent faults, some of which are relatively short. We do not consider this interpretation to be geologically plausible. Some investigators have discussed the possible presence in the Yucca Mountain area of a buried strike-slip fault or a seismogenic detachment fault (e.g., Wernicke, 1995; Scott, 1990; Schweickert and Lahren, 1997; J. Bell and R. Schweickert, SSC Workshop 3; Wernicke, SSC Workshop 4). In these models the faults above a detachment or zone of decoupling may be seismogenic or nonseismogenic, and the primary seismogenic source(s) lie below the detachment or zone of decoupling. Such models commonly require unlikely fault geometry, such as a long but narrow fault, produced because the fault is constrained below a detachment and above the brittle-ductile boundary. Furthermore, our coalescing sources include as end members both the independent fault treatment and the fault truncation-detachment model. Hence, we eliminated these models and included only the coalescing sources in our logic tree.

2.3.1 Coalescing Fault Structure

Seismogenic fault sources are defined as faults capable of generating earthquakes of magnitude ≥ 5 . Criteria for evaluating whether a fault is seismogenic include evidence for Quaternary displacement, a minimum length of 5 km measured along scarps of equivalent age, paleoseismic displacements of at least tens of centimeters (i.e., not a cracking event), and a possible spatial association of the fault with observed seismicity. The primary independent seismogenic sources considered for Yucca Mountain are the Windy Wash, Solitario Canyon,

and Paintbrush Canyon faults (Table RYA-3). The Fatigue Wash, Iron Ridge, Bow Ridge, and Stagecoach Road faults are not considered independent sources because of their short lengths and spatial association to other nearby faults. The maximum northern extent of the Paintbrush Canyon fault is taken from the map of Frizzell and Shulters (1990). For the Solitario Canyon and Windy Wash faults, the northern extent is taken to be the bedrock ridge south of Yucca Wash (Simonds et al., 1995; Ramelli and Bell, 1997). The maximum southern extent of the Windy Wash and Stagecoach Road faults is taken from Ramelli and Bell (1997). The lack of Quaternary geomorphic expression in Amargosa Valley suggests that the Yucca Mountain faults do not extend south of the Lathrop Wells cone.

The Crater Flat fault system is not considered a seismic source because of the short lengths of its features and the absence of significant mid- to late Quaternary displacement on those features (see Pezzopane et al., 1996). Further, the short distance between the Crater Flat faults and the faults of the Windy Wash system suggest that the Crater Flat faults are antithetic to the Windy Wash system.

Except for the Bare Mountain (BM) fault, all the faults near Yucca Mountain are interpreted to merge downdip at relatively shallow depths (2 to 5 km) and to rupture in groups of two or more faults during individual earthquakes. The groups of faults therefore are considered to represent individual seismic sources, with the Paintbrush Canyon (PBC), Solitario Canyon (SC), and Windy Wash (WW) faults representing the primary seismogenic structures in the three-fault system (Figure RYA-16). The combinations of faults in each group are shown in the logic tree and in Tables RYA-4, RYA-5, and RYA-6.

The Bare Mountain fault always behaves independently in this model, although synchronous, secondary fault rupture could occur on some of the westernmost faults at Yucca Mountain, such as the Windy Wash. Faults in the Yucca Mountain site vicinity are considered to coalesce at depth, forming one to three groups. The branch in the logic tree that represents only one group of faults is assigned a relatively low weight (0.1 to 0.3 depending on crustal thickness) because of the large spacing between the faults (10 km across all of the mapped faults). Given their steep dips at the surface, it appears unlikely that all the faults coalesce downdip into a single structure within the 12 to 20 km thickness of the seismogenic crust. If they did, the Paintbrush Canyon fault (PBC) would be the primary rupture source in this

interpretation. The principal evidence favoring a single group of faults is the apparent contemporaneous surface rupture among several faults, which is represented by the 70-ka ash event. On the branch that has two fault groups, the east group is composed of the Paintbrush Canyon (PBC)-Stagecoach Road (SR)-Bow Ridge (BWR) faults (Paintbrush Canyon fault is primary rupture source); the west group consists of the Windy Wash (WW)-Fatigue Wash (FW)-Solitario Canyon (SC)-Iron Ridge (IR) fault systems (Solitario Canyon fault being the primary rupture source). On the branch that is composed of three groups, the east group is PBC-SR-BWR, and the west side of Yucca Mountain comprises two groups, WW-FW and SC-IR.

We consider the faults at Yucca Mountain to coalesce at variable depths. This assessment is based on the pattern of fault spacing shown on maps and geologic cross sections that suggests that many of the Yucca Mountain fault systems intersect at some depth. Coalescing faults can be modeled by allowing each mapped fault trace to intersect the master fault(s) at some depth. We assume that for magnitudes smaller than the maximum, the rupture patch is distributed uniformly on each individual fault combination. For example, a magnitude 6 rupture patch on the east fault group could occur on the Paintbrush Canyon-Stagecoach Road combination or the Paintbrush Canyon-Bow Ridge combination with equal probability; however, for the maximum magnitude ($M_{max} \pm 1/4$), we consider that all faults in a group undergo slip.

The Ghost Dance fault has no record of displacement in the past approximately 400 ka. Because of its location within the Yucca Mountain block, its short length, and its lack of Quaternary geomorphic expression, it is not considered a seismogenic source; however, the fault may experience secondary faulting or fracturing. This is discussed in Section 3.

2.3.2 Maximum Magnitude Approach

Several alternative approaches and data sets were considered to assess the maximum magnitude of each local fault source (Wells and Coppersmith, 1994; Mason, 1996; Anderson et al., 1996). We used the Wells and Coppersmith regressions because: (1) the Mason data are considered more appropriate to the longer faults of the northern Basin and Range (30 to 50 km); and (2) the approach of Anderson et al. is untested. In addition, many of the low slip-rate faults used in the analysis of Anderson et al. (1996) are thrust faults in Japan. We evaluated maximum magnitudes using rupture length (RL) and rupture area (RA) from the

regressions of Wells and Coppersmith (all fault slip styles; the difference between magnitudes for all slip styles versus normal slip faults is small, and more data are used in the regressions for all slip styles), as these are the parameters that have been or can be measured with some confidence. The regressions for RA and RL have smaller standard deviations than the relationships for maximum and average displacement; the range in magnitude value for any measured displacement is approximately ± 1.0 magnitude unit. The displacement relationships also tended to produce unreasonably high stress drops for the shorter faults. For these reasons, we did not use magnitudes based on maximum and average displacement. We give weights of 0.5 each to RA and RL magnitude estimates, because we have no basis for preferring one relationship over the other.

Computation of the maximum magnitude from the fault area relationship of Wells and Coppersmith (1994) was complicated by variability in downdip fault width. Fault width is dependent on the depth of the seismogenic crust, fault dip, and the depth of intersection with the Bare Mountain fault. We calculated the extreme and preferred fault widths based on the extreme and preferred fault dips both for Bare Mountain faults (55, 60, and 65 degrees) and Yucca Mountain faults (60, 67.5, and 75 degrees), and the extreme and preferred depths for the seismogenic crust (12, 15, and 20 km). The middle of each range is the preferred value. Fault width was taken as the downdip distance to the seismogenic zone or the Bare Mountain fault, whichever was shortest. The extreme and preferred magnitudes computed from these widths are shown in Tables RYA-3, 4, and 5. (Note that the PSHA analysis uses the full distribution for fault dip, crustal thickness, and maximum rupture length to develop the distribution for maximum magnitude). Because of the uncertainties in assessing maximum magnitude, we consider the magnitudes computed from the various empirical relationships to be uncertain by ± 0.5 magnitude units. The ± 0.5 magnitude values are considered to represent 5- and 95-percentile values. The assigned weights are 0.63 assigned to the estimate from the empirical relationships and 0.185 assigned to the ± 0.5 magnitude values, which are the appropriate weights for a three-point representation of a normal distribution (Keefer and Bodily, 1983).

2.3.3 Recurrence Approach

We assessed earthquake recurrence rates for each local fault source based on trench data (time between events) (Figure RYA-15) and on fault slip rate information and average

displacement values from USGS (1996). We give a higher weight to the slip rate (0.7) than to recurrence interval (0.3) because use of recurrence alone appears to overestimate the total slip in the Yucca Mountain area. Slip rates and their associated uncertainties are provided in Tables RYA-3, -4, -5, and -6. We consider slip of greater than 20 cm to represent earthquake occurrence at or above the threshold magnitude for surface faulting. The seismicity on mapped faults was modeled separately with both truncated-exponential (e.g., Anderson, 1979; Youngs and Coppersmith, 1985) and characteristic recurrence relationships (Schwartz and Coppersmith, 1984). The relative weights given to the two recurrence models depend on the degree to which we consider the faults to coalesce; i.e., greater coalescence suggests that the faults behave in a more exponential manner. Thus, for the one-fault system model the exponential model was given a weight of 0.9, whereas it was given 0.1 for the characteristic model. More weight was given the characteristic model in the two-fault system (0.3) and three-fault system (0.5) models. For the characteristic model, the maximum magnitude is considered to lie uniformly in the range $M_{\max} - 1/2$ to M_{\max} .

2.4 POSSIBILITY OF A BURIED SEISMIC SOURCE

Within the resolution of the data, we consider it possible that a seismic source (possibly strike-slip), buried beneath cover rocks and with no direct surface manifestation, exists within Zone A; however, we conclude that this source is incapable of generating an earthquake larger than the background earthquake, or an earthquake larger than that produced by any other source considered. Such a buried source, if it exists, is decoupled from surface faults, in that faults at depth may behave differently from faults near the surface, and the boundary between these different faulting styles may be anything from a simple low-angle fault to a zone of transition between passive and active faulting. This region of decoupling, whether a simple plane or a thicker zone, is not considered a seismic source. The surface faults above the decoupled boundary, thought to be seismic sources in the coalescing model discussed above, here are considered nonseismogenic, responding passively to earthquakes generated along a buried, near-vertical source.

The principal evidence for the decoupled structural model is the discrepancy between the earthquakes recorded in the Yucca Mountain region that have normal focal mechanisms at shallow crustal levels and those that have the more common strike-slip mechanisms recorded at depth. Further, megaton nuclear tests at Pahute Mesa produced normal faulting at the

ground surface (Bucknam, 1969; McKeown and Dickey, 1969; Maldonado, 1977a, b; Orkild et al., 1969; Snyder, 1971 and 1973; Morris, 1971), but modeling of the ground motions from these tests (Aki and Tsai, 1972; Aki et al., 1969; Lay et al., 1984; Wallace et al., 1983 and 1985; Wallace et al., 1986) indicated energy release consistent with right-lateral slip on north-trending faults at depth. Additional evidence is provided by geologic mapping in the Specter Range east of Yucca Mountain (Burchfiel, 1965), which shows a structural style in the Paleozoic cover that is interpreted as deformation above a buried strike-slip fault.

Two depths of decoupling (5 and 10 km) are considered. The shallower depth is considered a minimum for decoupling, because the seismic reflection data indicate that upper crustal, high-angle faults penetrate beneath the Paleozoic-Tertiary contact at least to this level. Also, the upper depth limit of aftershocks from the Little Skull Mountain earthquake was approximately 5 km (K. Smith, SSC Workshop 2). The greater decoupling depth is considered the maximum that might produce a significant buried earthquake, given the thicknesses considered for the seismogenic crust.

Estimates of M_{max} for the buried source are derived from the rupture area versus maximum magnitude relationship developed by Wells and Coppersmith (1994). Length of the buried source is considered to be 30 km. Thirty kilometers, which is slightly greater than the maximum fault lengths for the main faults at Yucca Mountain, is approximately the length of the north-trending gravity gradients that bound either side of the Amargosa trough. Fault width is estimated by the limits set by the various combinations of seismogenic crustal thickness at depth of decoupling (Table RYA-7). The buried source is considered to have vertical dip.

A 30-km-long buried source would produce an earthquake having a magnitude at or above the background magnitude of 6.3 ± 0.3 only for a decoupling depth of 5 km and a thick (20-km) seismogenic crust. We conclude, therefore, that a buried source is adequately included in our interpretation of the background source and the coalescing fault sources.

2.5 VOLCANIC SOURCE

The eruption of basaltic volcanoes in the site vicinity may be associated with seismicity. Based on observed eruptions within similar volcanic fields, we assess the probability that a volcanic source exists to be 0.7. This seismic source is assessed to be independent of the other seismic sources. The spatial location of future volcanic seismic sources and the recurrence rate are taken from the results of Crowe et al. (1995). Of the numerous results described by Crowe et al. (1995), return periods of 2×10^5 to 2×10^6 are preferred. The maximum magnitude associated with a volcanic eruption is assessed based on the studies by Jackson (1994), which consider the largest observed earthquakes associated with the intrusion and eruption of small- to moderate-volume basaltic magmas. An upper limit of $M_{\max} = 5.5$ is used based on this work.

2.6 REGIONAL FAULT SOURCES

Eleven regional fault sources in Zones B and C (Figure RYA-17) are identified primarily through our analysis of the data in Piety (1994) and Anderson et al. (1995a, b; See Table RYA-8). The eleven sources we identified are considered relevant due to their distance to Yucca Mountain, their length, high slip rates, evidence for late Quaternary surface rupturing earthquakes, or because they have not been studied in enough detail to preclude or adequately characterize their Quaternary activity (i.e., Wahmonie or Cane Spring faults). Several of the faults that McKague et al. (1996) consider Type I faults (for example, Keane Wonder, Oasis Valley, Rocket Wash-Beatty Wash, Sarcobatus Flat, and Kawich Range) are not considered relevant to our analysis because of their short length, distance from Yucca Mountain, and studies such as those by Anderson et al. (1995a, b) that show that some of these faults either have no significant Quaternary displacement or are much shorter than previously thought. In addition, the so-called Carrara fault (memoranda from D.B. Slemmons, February 3 and 16, 1997, to R. Quittmeyer) is not considered a potential seismic source. Interpretation of aerial photographs and reconnaissance geologic mapping by L.W. Anderson (unpub. mapping) found no evidence of late Quaternary fault activity in the area of the suspected fault. Our interpretation is that the features cited as evidence for Quaternary fault activity are instead normal fluvial terraces and terrace scarps produced by the southeast-flowing streams that drain the south flank of Bare Mountain (also see mapping of Swadley and Carr, 1987).

Faults within Zones B and C are considered to have the simple planar shape, with downdip widths that penetrate to mid-crust. The faults are assumed to be either near vertical (faults that display primarily strike-slip displacement) or steeply dipping ($\sim 60^\circ$; faults that display primarily normal or dip-slip displacement). For computing fault rupture areas, we have assumed a 15 km thick seismogenic crust. Estimates of surface rupture length, maximum displacement per event (if available), and slip rate are from the work of Piety (1994), Anderson et al. (1995a, b), Klinger and Piety (1996), and Coe et al. (1996).

2.6.1 Maximum Magnitude Approach

Empirical relationships developed by Wells and Coppersmith (1994) between magnitude and fault length, fault area, and maximum fault displacement (if available) were used to estimate the maximum magnitudes for the regional faults (Table RYA-8). Equal weights were applied to the computed magnitudes. That is, when three magnitudes were computed, weights of about 1/3 were used and when two magnitudes were computed, weights of 1/2 were used. As was done for the local faults, we consider the magnitudes computed from the various empirical relationships to be uncertain by ± 0.5 magnitude units, representing 5- and 95-percentile values.

2.6.2 Recurrence Approach

The slip rates in Table RYA-8 were converted to estimated seismic recurrence rates using estimated displacement per event [the methods indicated by Anderson (1979) and Youngs and Coppersmith (1985)], and using an average b-value from the two catalogs of 1.12 (0.63), with 5 percent and 95 percent distribution values of 1.07 (0.185) and 1.20 (0.185), respectively, based on the distributions developed above.

3.0

FAULT DISPLACEMENT CHARACTERIZATION

3.1 INTRODUCTION

Two types of fault displacement are of potential concern to the Yucca Mountain Controlled Area (the proposed repository block and the associated access and waste handling facilities):

(1) **principal** (or primary) faulting and (2) **distributed** (or secondary) faulting. Principal faulting is defined as the displacement along the main fault plane (or planes) responsible for the release of seismic energy during an earthquake. When the fault rupture extends to or near the ground surface, displacement may be represented by a zone of deformation up to several meters wide with measured amounts of fault offset (slip) ranging from several tens of centimeters to several meters. The amount of slip is dependent on the location along the fault and the magnitude of the earthquake. Within the site area, two possible sources of primary faulting have been identified, the Solitario Canyon-Iron Ridge fault system and the Paintbrush Canyon-Stagecoach Road-Bow Ridge fault system (Figure RYA-16 and Table RYA-4).

Distributed faulting is defined as displacement (measured slip as opposed to fracturing; based on our personal experience in the Yucca Mountain area, with the presence of suitable stratigraphic horizons, the uncertainty in the measurement of displacement or non-displacement is about ± 2.5 cm - anything less than that is essentially zero) that occurs on adjacent or nearby faults (or fractures) in response to an earthquake on another fault. If it occurs at all, distributed faulting is by nature discontinuous and can occur up to several kilometers from the principal fault rupture. Several factors influence the occurrence or non-occurrence of secondary faulting along a pre-existing fault or fracture (Pezzopane and Dawson in USGS, 1996; McKague et al., 1996). Among them are: (1) location with respect to the principal fault rupture (hanging wall verses foot wall; (2) fault orientation; (3) sense of previous slip; and, (4) distance to the principal fault rupture or earthquake epicenter. A primary fault also can undergo distributed displacement or fracturing in response to a nearby earthquake. Paleoseismic trench data probably cannot differentiate between principal and distributed faulting except by size of the measured displacement. However, we believe that displacement from a distributed event will always be smaller than that from a primary event. In our team's review of the Yucca Mountain paleoseismic data (Figure RYA-15), we considered all events in the trenches with less than 20 cm of displacement to represent "cracking" events.

Thus, our interpretation is that most of these cracking events are the probable surface representation of distributed faulting events due to strong ground shaking.

The teams were asked to characterize fault displacement potential at nine sites within the controlled area of Yucca Mountain. The nine sites are located:

- (1) Along the Bow Ridge fault where it crosses the ESF;
- (2) Along the Solitario Canyon fault near the proposed repository block;
- (3) Along the Drill Hole Wash fault where it crosses the ESF;
- (4) Along the Ghost Dance fault;
- (5) Along the Sundance fault west of the ESF;
- (6) On a minor unnamed fault west of Dune Wash;
- (7) 100 m east of the Solitario Canyon fault that has:
 - a. a small fault with 2.0 m cumulative slip;
 - b. a shear with about 10 cm of cumulative displacement;
 - c. a fracture having no measurable displacement; and
 - d. intact rock;
- (8) Midway between the Solitario Canyon and Ghost Dance faults that has:
 - a. a small fault with 2.0 m cumulative slip;
 - b. a shear with about 10 cm of cumulative displacement;
 - c. a fracture having no measurable displacement; and
 - d. intact rock; and
- (9) Along the Exile Hill fault in Midway Valley.

Two of the study sites (1 and 2) are on faults which are considered to be primary fault sources in our assessment of seismic sources. For the other 7 sites, all are considered to be potential sites for secondary displacement because of their location within an area of Quaternary faulting. However, the relative probability of activity is weighted depending on whether there is evidence for Quaternary (past 1.6 million years) activity associated with the feature, the

known length of the feature, amount of total post-Tiva Canyon bedrock displacement, the orientation of the feature, whether there is an existing fault or fracture, or whether the site is on intact bedrock.

3.2 APPROACH

For either primary or secondary displacement, an assessment of the probability of fault displacement requires an assessment of the frequency of occurrence and the amount of displacement if it occurs. The fault displacement hazard at any location can be characterized in terms of the expression:

$$v(d) = P(C) \cdot \lambda_{DE} \cdot P(D_E > d) \quad (1)$$

where $P(C)$ is the probability that the feature can slip in the present tectonic regime, λ_{DE} is the frequency of occurrence of displacement events on the feature, and $P(D_E > d)$ is the probability that a displacement event will exceed a slip of d . The general logic structure for characterizing the parameters of Equation (1) is shown on Figures RYA-18 and RYA-19. Figure RYA-18 shows the approaches appropriate for sites where Quaternary data are available for frequency and size of displacement events and Figure RYA-19 shows the approaches appropriate for sites where paleoseismic data are absent. The components of these approaches are discussed below.

3.2.1 Probability Slip can Occur

The probability that slip can occur on a feature in the present tectonic regime is assessed based on the evidence for recency of slip on the feature and its relationship to the structural elements of Yucca Mountain.

3.2.2 Frequency of Displacement Events

Two approaches are considered for the assessment of the frequency of displacement events: the paleoseismic recurrence intervals and the long-term fault slip rate. For sites where paleoseismic data are available, we believe that the displacement hazard at any of the various sites within the Controlled Area can best be assessed using paleoseismic data for recurrence

rates (intervals) (Figure RYA-18). The alternative approach for such locations is to use the estimates of Quaternary slip rates and compute the frequency of displacement events using the expression:

$$\lambda_{DE} = SR / \bar{D}_E \quad (2)$$

where SR is slip rate and \bar{D}_E is the average displacement per event. This approach is given a weight of 0.2. The procedures used to assess the average displacement per event are described below in Section 3.2.4.

For those sites where direct paleoseismic data is lacking, a slip rate approach is used with a weight of 1.0 (Figure RYA-19). The slip rates are estimated from the total slip of the fault since eruption of the Tiva Canyon Tuff (12.7 ± 1.3 Ma).

Without paleoseismic data or total slip information; i.e., for sites located on fractures showing no displacement or for sites located in unfractured rock, a negligibly low probability of displacement is considered. We consider that: (1) displacement from a future earthquake will be in the same sense as shown by slip indicators from the last displacement event; and (2) displacement on a fault will be confined to the fault's present length; that is, faults do not generally increase in length with each new event.

3.2.3 Estimation of Slip Rate

For those locations where data are available to estimate Quaternary slip rates, these rate estimates are used to assess displacement event frequency (Figure RYA-18). For bedrock faults that either lack specific evidence for Quaternary slip or have no specific paleoseismic data, but that show post-Miocene (post-Tiva Canyon Tuff) displacement, three alternative approaches are considered for assessing the fault slip rate (Figure RYA-19). In the first approach, the total measured cumulative post-Miocene slip is divided by the age of the Miocene rocks (12.7 Ma). This assumes a uniform slip rate through time. However, the tectonic history of the region suggests that the assumption of uniform rate over time is

incorrect. Many data indicate that extensional deformation in the region has waned with time. Therefore, the assumption of uniform slip rate is given a low weight of 0.1. A second alternative is to develop a slip history that follows Fridrich et al.'s (in press) regional extensional history. Their analysis suggests that nearly all the regional extension was accomplished in the Crater Flat region by 11 Ma, leaving only small additional extension during Quaternary time. We estimate that 2 percent of the regional extension occurred during the past 1.6 Ma, which is consistent with Fridrich et al.'s interpretation. Using this approach, a slip rate for the Quaternary period is calculated on representative faults, applying 2 percent of the observed cumulative slip to estimate the Quaternary rates. This approach is given a weight of 0.6, because it accounts for what appears to be the waning tectonic activity in the region. In a third approach, the time history of Fridrich et al. is modified to account for the onset of volcanism in Crater Flat beginning at about 3.7 Ma. This volcanic episode may indicate an increase in tectonic rates in the region since mid-Pliocene. We allow for 20 percent of the measured fault slip to occur within the past 3.7 Ma (weight of 0.3).

3.2.4 Estimation of Average Slip Per Event

For sites where paleoseismic data are available, the average slip per event is estimated from these data (Figure RYA-18). For faults without direct paleoseismic data, analogies to other faults both locally and world wide must be made. The AAR Team at Workshop 6 (June 1997) presented data relating average displacement, \bar{D}_E , to total fault length, L or cumulative fault displacement D_{cum} . The AAR Team reanalyzed the data and developed new relations in their draft summary in terms of parameter MD^{max} (the expected maximum displacement in a maximum event). These relationships are:

$$MD^{max} = 1.32 \times 3.69 \times 10^{-5} \times L \text{ (in m)} \quad (3)$$

and

$$MD^{max} = 1.32 \times \beta \times D_{cum} \text{ (m)} \quad (4)$$

where β is a constant that varies for smaller faults ($L < 3$ km and $D_{cum} < 75$ m) between 1.40×10^{-3} (weight of 0.3) and 1.85×10^{-2} (weight of 0.3) with their preferred value of 5.59×10^{-3} (weight of 0.4). For faults with $L > 3$ km and $D_{cum} > 75$ m, $B = 1.40 \times 10^{-3}$. We find these results to be reasonable and adopt them to characterize the uncertainty in estimating MD^{max} . They also find that the mean value of $\bar{D}_E / MD^{max} = 0.83$. Thus, to find an estimate of \bar{D}_E simply multiply relations (3) and (4) by 0.83.

$$\bar{D}_E = 0.83 \times 1.32 \times 3.69 \times 10^{-5} \times L \text{ (in m)} \quad (5)$$

and

$$\bar{D}_E = 0.83 \times 1.32 \times \beta \times D_{cum} \text{ (m)} \quad (6)$$

We adopt these approaches for our assessment of sites without paleoseismic data (Figure RYA-19) and give equal weight to the assessments based on the length of the fault, (5) and the cumulative offset (6).

3.2.5 Distribution for Displacement Per Event

Trenching data from Yucca Mountain indicate that displacement per event on a fault varies greatly both at individual sites and along strike (see Figure RYA-15). Recurrence intervals between earthquakes or displacement events also vary greatly. We consider two approaches for assessing the distribution for slip per event. Both approaches are based on analyses of data from trenching studies at Yucca Mountain.

The Doser-Fridrich-Swan (DFS) team developed a distribution for the ratio of D/\bar{D}_E by normalizing data from each trenching site by the average displacement at that location. Figure RYA-20 shows the resulting empirical distribution. The Facilitation Team analyzed these data and indicate that a good fit is obtained by a gamma distribution (see Appendix H, Section

H.2.1). We adopt the distribution given in Appendix H for D/\bar{D}_E . The Arabasz-Andreson-Ramelli (AAR) team normalized the displacement data by the estimate of MD^{max} for each fault and observed that the ratio of D/MD^{max} could be represented by the exponential distribution shown on Figure RYA-21. We consider these two approaches to be equally applicable to assessing the variability in displacement from event to event and give them equal weight (Figures RYA-18 and RYA-19).

3.3 DATA FOR CHARACTERIZATION OF DISPLACEMENT HAZARD AT THE NINE TEST CALCULATION SITES

Site 1 - Bow Ridge fault where it crosses the ESF

The Bow Ridge fault is about 7 km long and is both a site for primary and secondary faulting as the fault is interpreted to be a splay of the Paintbrush Canyon- Stagecoach Road fault system. Given the evidence for Quaternary displacement, the probability of activity is considered 1.0. Cumulative slip estimated at site 1 is about 100 m (USGS, 1996, chapter 2). Paleoseismic information (Figure RYA-15) from trenches near site 1 indicate that the average recurrence for surface rupturing, displacement events is about 75 ka (Table RYA-3) and the Quaternary slip rate for the fault is estimated to be 0.003 mm/yr. Using the Quaternary slip rate and recurrence information yields a average displacement value of 22.5 cm which is just larger than the 20 cm value we use as a break between faulting and cracking events (Table RYA-5). The trench data also indicate that the average displacement is about 21 cm, but the largest measured displacement is 44 cm in one trench (T-14D) and there was only fracturing observed in another nearby trench (T-14). The 44 cm value is our preferred maximum displacement from paleoseismic data. Relation (4) suggests that the maximum displacement for the Bow ridge fault could be about 18 cm whereas relation (3) indicates 34 cm. Relation (7) using the 1.73 factor indicates 49 cm, and relation (6) using the 1.73 factor suggests 26 cm for maximum displacement. The resulting parameters are

$$P(C) = 1.0$$

$$SR = \{0.001 \text{ mm/yr (0.15)}, 0.003 \text{ mm/yr (0.7)}, 0.006 \text{ mm/yr (0.15)}\}$$

$$RI_{DE} = \{25 \text{ ka (0.15)}, 75 \text{ ka (0.7)}, 140 \text{ ka (0.15)}\}$$

$$\bar{D}_E = \{21 \text{ cm (1.0)}\}$$

$$MD^{max} = \{44 \text{ cm (1.0)}\}$$

Site 2 - Solitario Canyon fault near the proposed repository block

The Solitario Canyon fault is one of the major block bounding faults at Yucca Mountain and is both a primary and a secondary fault displacement source because of the evidence for Quaternary displacement events. Therefore, the probability of activity is considered 1.0. Paleoseismic information (Figure RYA-15) indicates that the recurrence for surface rupturing events (displacement > 20 cm) ranges between 50-130 ka with a preferred value of 75 ka (Table RYA-3). However, a fracturing event that could be the result of secondary faulting apparently occurred on the fault about 25 ka. The paleoseismic Quaternary slip rate for the fault is estimated to be 0.01 mm/yr, and the post-Tiva Canyon cumulative slip estimated at site 2 is 230 m (estimated from cross section of Day and others, 1996). Although we generally prefer the 2% rule for calculating the Quaternary slip rate, the Solitario Canyon fault is the one fault we know of for which a large difference exists between the paleoseismic Quaternary slip rate estimate and the calculated Quaternary rate. This suggests, at least for the Solitario Canyon fault, that there has been an increase in activity in the last 2-4 Ma. Be that as it may, we have used the paleoseismic Quaternary slip rate and recurrence information to calculate an average displacement value of 75 cm. Also, our analysis of data in U.S. Geological Survey (1996) and shown in Figure RYA-15 indicates that the average displacement is about 75 cm from four trenches. However, at T-4, just to the south of the test site, the displacement during the last event was 30 cm. Since site 2 is near the northern end of the fault where displacement appears to be dying out, one would expect the average slip per event to be less than it is to the south. In addition, the slip rate also is probably less than the 0.01 mm/yr used in the calculations. Relation (4) suggests a maximum displacement of 43 cm, and relation (3) suggests 88 cm. The resulting parameters are:

$$P(C) = 1.0$$

$$SR = \{0.005 \text{ mm/yr (0.15)}, 0.01 \text{ mm/yr (0.7)}, 0.02 \text{ mm/yr (0.15)}\}$$

$$RI_{DE} = \{50 \text{ ka } (0.15), 75 \text{ ka } (0.7), 130 \text{ ka } (0.15)\}$$

$$\bar{D}_E = \{30 \text{ cm } (1.0)\}$$

$$MD^{max} = \{75 \text{ cm } (1.0)\}$$

Site 3 - Drill Hole Wash fault where it crosses the ESF

The Drill hole Wash fault is considered a possible source for secondary fault displacement only. Although there is no direct paleoseismic information for the fault, given the apparent lack of evidence for Quaternary activity and the northwest strike, the probability of future slip is considered low (0.1). Available information (Day et al., 1996) indicates that the fault is about 4 km long with maximum displacement of 15 m. Thus, the estimated Quaternary (2%) slip rate is about 0.0002 mm/yr. Using relations (5) and (6) suggests that the average displacement per event could be in the range of 9 to 17 cm. These values appear large in comparison to those for other short faults. However, using these displacement values and the slip estimate of 0.0002, the recurrence for such displacement events is on the order of 650 ka. Maximum displacement values are 11 and 20 cm using relations (3) and (4) and they increase to 16 and 29 cm using relations (7) and (8) and the 1.73 factor. The resulting parameters are:

$$P(C) = 0.1$$

$$D_{cum} = \{5 \text{ m } (0.15), 15 \text{ m } (0.7), 25 \text{ m } (0.15)\}$$

$$L = \{3 \text{ km } (0.15), 4.2 \text{ km } (0.7), 5.5 \text{ km } (0.15)\}$$

Site 4 - Ghost Dance fault

The Ghost Dance fault is considered a source for secondary fault displacement only. Although paleoseismic data indicates that the fault has not experienced unequivocal (>5 cm) surface rupture since the middle Quaternary, the north-south strike of the fault, the same as active faults in the site area indicates that the fault could have potential for future slip. We believe the probability of activity is 0.5. Total length of the fault is about 3 km (Day et al., 1997) and the total displacement at the site is about 25 m. The Quaternary paleoseismic slip rate for the fault has been estimated to be <0.0005 mm/yr, which agrees well with the Quaternary (2%) bedrock slip estimate of 0.0003. The age of the last displacement event appears to be at least 200 ka and may be over 1 Ma (Taylor et al., in USGS, 1996). Using the 200 ka age as an

average recurrence and a slip rate of 0.0005 suggests average displacements of about 10 cm and 20 cm for maximum displacement (weight of 0.8; figure RYA-18). Using relations (3) and (4) suggests slightly higher displacement values. The resulting parameters are:

$$\begin{aligned}P(C) &= 0.5 \\D_{cum} &= \{20 \text{ m (0.15)}, 25 \text{ m (0.7)}, 30 \text{ m (0.15)}\} \\L &= \{2.5 \text{ km (0.15)}, 3 \text{ km (0.7)}, 5 \text{ km (0.15)}\}\end{aligned}$$

Site 5 - Sundance fault west of the ESF

The Sundance fault is a source for secondary fault displacement only. However, given its northwest strike, short length, and the lack of evidence for Quaternary activity the probability of activity is considered low (0.1). Total mapped length of the fault is only about 600 m (Day and others, 1996) and total displacement is about 8.5 m (Taylor et al., in USGS, 1996). Use of relations (5) and (6) suggests that the average displacement for this fault should be on the order of 2-5 cm. This value, in conjunction with an estimated Quaternary (2%) slip rate of 0.00001 yields a recurrence of 3.5 Ma. The resulting parameters are:

$$\begin{aligned}P(C) &= 0.1 \\D_{cum} &= \{6 \text{ m (0.15)}, 8.8 \text{ m (0.7)}, 11 \text{ m (0.15)}\} \\L &= \{0.2 \text{ km (0.15)}, 0.6 \text{ km (0.7)}, 1.0 \text{ km (0.15)}\}\end{aligned}$$

Site 6 - Minor unnamed fault west of Dune Wash

Any unnamed fault west of Dune Wash is considered a source for secondary fault displacement only. Without site specific paleoseismic data and without knowing the strike, sense of slip for the fault, and length, the probability of activity is considered to be 0.2. We have assumed total slip at the site to be about 4 m (slightly less than the tunnel diameter) and an unknown length of about 1 km. Our preferred slip rate for the fault is 0.00005 mm/yr. Using relations (5) and (6) suggest an average displacement of 2-4 cm. This yields a recurrence of about 600 ka. The resulting parameters are:

$$\begin{aligned}P(C) &= 0.2 \\D_{cum} &= \{2 \text{ m (0.15)}, 4 \text{ m (0.7)}, 6 \text{ m (0.15)}\} \\L &= \{0.5 \text{ km (0.15)}, 1.0 \text{ km (0.7)}, 1.5 \text{ km (0.15)}\}\end{aligned}$$

Site 7 - 100 m east of the Solitario Canyon fault

Four situations or conditions are evaluated for site 7. (a) A small fault with 2.0 m cumulative slip, (b) a shear with about 10 cm of cumulative displacement, (c) a fracture having no measurable displacement, and (d) intact rock. For example 7a adjacent to the Solitario Canyon fault, the potential for activity is considered higher than for site 8a (0.5 verses 0.3). For example 7a and the purpose of our analysis, we have assumed that the total displacement at the site is 1.25 m, yielding a preferred Quaternary (2%) slip rate of 0.00002 mm/yr. We do not know the length of the fault but comparison to site 6 and the Ghost Dance fault suggests the length is probably less than 1 km. From this, we estimate the average displacement to be about 1cm. This would equate to a recurrence of 500 ka. For example 7b, the fault length is probably insignificant given a total displacement of 10 cm. The Quaternary (2%) slip rate for this feature would be 0.000001 mm/yr. We assume displacement per event of 1 cm (essentially at or below the level of detection). This would indicate a recurrence of 1 Ma. For examples (c) and (d) there is an essentially 0 probability of displacement. The resulting parameters are:

Point 7a: cumulative offset 2 m

$$P(C) = 0.5$$

$$D_{cum} = \{2 \text{ m (1.0)}\}$$

L not known

Point 7b: cumulative offset 10 cm

$$P(C) = 0.3$$

$$D_{cum} = \{0.1 \text{ m (1.0)}\}$$

L not known

Point 7c: fracture with no measurable cumulative offset

$$P(C) = 0$$

Point 7d: intact rock

$$P(C) = 0$$

Site 8 - Midway between the Solitario Canyon and Ghost Dance faults

The same four situations used for site 7 were evaluated for site 8. The only difference between this site and site 7 is the increased distance to a potentially active fault. Thus, we have given this fault a low activity weight. The resulting parameters are:

Point 8a: cumulative offset 2 m

$$P(C) = 0.3$$

$$D_{cum} = \{2 \text{ m (1.0)}\}$$

L not known

Point 8b: cumulative offset 10 cm

$$P(C) = 0.1$$

$$D_{cum} = \{0.1 \text{ m (1.0)}\}$$

L not known

Point 8c: fracture with no measurable cumulative offset

$$P(C) = 0$$

Point 8d: intact rock

$$P(C) = 0$$

Site 9 - Along the Exile Hill fault in Midway Valley

The Exile Hill fault is an approximately 3 km long, north-south striking fault in Midway Valley. Work by Swan and others (1995) indicates that essentially no detectable displacement has occurred on the fault in the middle to late Quaternary (limits of detection essentially 0-5 cm) although at least two fracturing events may have occurred. Because Quaternary fracturing may have been associated with this fault, the probability of activity is considered 0.7. Slip rate has been estimated to be similar to the Ghost Dance fault, <0.0005 , although total slip is less than half that of the Ghost Dance (10 m). Considering the evidence for no measurable displacement in at least the last several hundred thousand years and the limited amount of total slip, the average slip per event must be small. Thus, the estimate of about 5 cm for average slip per event which is near the detection level. This leads to an estimate of >100 ka for displacement events. Using relations (5) and (6) suggests 6 and 13 cm for average displacements. Relations (3) and (4) suggest 7 and 16 cm for maximum displacement and (5) and (6) and the 1.73 factor suggest 10 and 22 cm for maximum displacement. The resulting parameters are:

$$P(C) = 0.7$$

$$D_{cum} = \{5 \text{ m (0.15)}, 10 \text{ m (0.7)}, 15 \text{ m (0.15)}\}$$

$$L = \{2 \text{ km (0.15)}, 3.2 \text{ km (0.7)}, 4.4 \text{ km (0.15)}\}$$

REFERENCES

- Aki, K., Reasenber, P., DeFazio, T., and Tsai, Y., 1969, Near-field and far-field seismic evidences for triggering of an earthquake by the Benham explosion: *Seismological Society of America Bulletin*, v. 59, p. 2197-2207.
- Aki, K., and Tsai, Y., 1972, Mechanism of long-wave excitation by explosive sources: *Journal of Geophysical Research*, v. 77, p. 1452-1475.
- Anderson, J.G., 1979, Estimating the seismicity from geological structure for seismic risk studies: *Bulletin of the Seismological Society of America*, v. 69, p. 135-158.
- Anderson, L.W. and Klinger, R.E., 1996, Evaluation and characterization of Quaternary faulting—Bare Mountain fault, Nye County, Nevada: U.S. Bureau of Reclamation Seismotectonic Report 96-5, Denver, Colorado, 78 p.
- Anderson, R.E., Bucknam, R.C., Crone, A.J., Haller, K.M., Machette, M.N., Personius, S.F., Barnhard, T.P., Cecil, M.J., and Dart, R.L., 1995a, Characterization of Quaternary and suspected Quaternary faults, regional studies, Nevada and California: U.S. Geological Survey Open File Report 95-599, 56 p.
- Anderson, R.E., Crone, A.J., Machette, M.N., Bradley, L., and Diehl, S.F., 1995b, Characterization of Quaternary and suspected Quaternary faults, Amargosa area, Nevada and California: U.S. Geological Survey Open File Report 95-613, 41 p.
- Anderson, J.G., Wesnousky, S.G., and Stirling, M.W., 1996, Earthquake size as a function of fault slip rate: *Bulletin of the Seismological Society of America*, v. 86, p. 683-690.
- Bucknam, R.C., 1969, Geologic effects of the Benham underground nuclear explosion: *Bulletin of the Seismological Society of America*, v. 59, p. 2209-2220.
- Burchfiel, B.C., 1965, Structural geology of the Specter Range quadrangle, Nevada, and its regional significance: *Geological Society of America Bulletin*, v. 76, p. 175-192.
- Carr, W.J., 1982, Volcano-tectonic history of Crater Flat, southwestern Nevada, as suggested by new evidence from Drill Hole USW-VH-1: U.S. Geological Survey Open-File Report 82-457, 53 p.

- Carr, W.J., 1990, Styles of extension in the Nevada Test Site region, southern Walker Lane Belt—an integration of volcano-tectonic and detachment fault models, *in* Wernicke, B.P., ed., Basin and Range Extensional Tectonics Near the Latitude of Las Vegas, Nevada: Geological Society of America Memoir 176, p. 283-303.
- Carr, W.J., Byers, F.M.J., and Orkild, P.P., 1986, Stratigraphic and volcano-tectonic relations of Crater Flat tuff and some older volcanic units: U.S. Geological Survey Professional Paper 1321, 23 p.
- Coe, J.A., Yount, J.C., and O'Leary, D.W., 1996, Preliminary results of paleoseismic investigations of the Rock Valley fault system, chapter 4.13, *in* Seismotectonic framework and characterization of faulting at Yucca Mountain, Nevada: U.S. Geological Survey, Yucca Mountain Project.
- Crowe, B., Perry, F., Geissman, J., McFadden, L., Wells, S., Murrell, M., Poths, J., Valentine, G.A., Bowker, L., and Finnegan, K., 1995, Status of volcanism studies for the Yucca Mountain Site Characterization Project: Los Alamos National Laboratory Report LA-12908-MS.
- Day, W.C., Potter, C.J., Sweetkind, D.S., Dickerson, R.P., and San Juan, C.A., 1996, Bedrock geologic map of the central block area, Yucca Mountain, Nye County, Nevada: U.S. Geological Survey Administrative Report, Prepared in Cooperation with the Nevada Operations Office, U.S. Department of Energy, Plate 2.
- DePolo, C.M., 1994, The maximum background earthquake for the Basin and Range province, western North America: Bulletin of the Seismological Society of America, v. 84, p. 466-472.
- Doser, D.I., and Smith, R.B., 1989, An assessment of source parameters of earthquakes in the Cordillera of the Western United States: Bulletin of the Seismological Society of America, v. 79, p. 1383-1409.
- Frankel, A., 1995, Mapping seismic hazard in the Central and Eastern United States: Bulletin of the Seismological Society of America, v. 66, p. 8-21.
- Fridrich, C. J., Whitney, J. W., Hudson, M. R., and Crowe, B. M., in press, Space-time patterns of late Cenozoic extension, vertical-axis rotation, and volcanism in the Crater Flat basin, Nevada, *in* Wright, L. A. and Troxel B. W. (eds.) Cenozoic Basins of the Death Valley Region, California and Nevada: Geological Society of America Special Paper.

- Frizzell, V.A. Jr., and Shulters, J., 1990, Geologic map of the Nevada Test Site, southern Nevada: U.S. Geological Survey Miscellaneous Investigations Map I-2046, scale 1:100,000.
- Hamilton, W.B., 1988, Detachment faulting in the Death Valley region: U.S. Geological Survey Bulletin 1790, p. 51-85.
- Harmsen, S.C., and Bufe, C., 1991, Seismicity and focal mechanisms for the southern Great Basin of Nevada and California, 1987 through 1989: U.S. Geological Survey Open-File Report 91-572, 208 p.
- Jackson, J.A., 1987, Active normal faulting and crustal extension, *in* Coward, M.P., Dewey, J.F., and Hancock, P.L., eds., Continental-Extensional Tectonics: Geological Society of London Special Publication No. 28, p. 3-17.
- Jackson, S.M., 1994, Magnitudes of earthquakes associated with basalt dike intrusion for use in INEL seismic hazards evaluations: Idaho National Engineering Laboratory Report INEL-94/0132.
- Keefer, D.L., and S.E. Bodily, 1983, Three-point approximations for continuous random variables: *Management Science*, v 29, p 595-609.
- Klinger, R.E., and Piety, L.A., 1996, Evaluation and characterization of Quaternary faulting on the Death Valley and Furnace Creek faults, Death Valley, California: U.S. Bureau of Reclamation Seismotectonic Report 96-10.
- Lay, T., Wallace, T.C., and Helmberger, D.V., 1984, The effects of tectonic release on short-period P-waves from NTS nuclear explosions: *Bulletin of the Seismological Society of America*, v. 74, p. 819-842.
- Maldonado, F., 1977a, Composite postshot fracture map of Pahute Mesa, Nevada Test Site, June 1973 through March 1976, Nevada Operations Office, U.S. Energy Research and Development Administration: U.S. Geological Survey, Denver, USGS-474-243, 11 p.
- Maldonado, F., 1977b, Results from fault-monitoring stations on Pahute Mesa, Nevada Test Site, from July 1973 through December 1976, Nevada Operations Office, U.S. Energy Research and Development Administration: U.S. Geological Survey, Denver, USGS-474-242, 32 p.
- Mason, D.B., 1996, Earthquake magnitude potential of the Intermountain seismic belt, USA, from surface-parameter scaling of late Quaternary faults: *Bulletin of the Seismological Society of America*, v. 86, p. 1487-1506.

- McGuire, R.K., 1985, Seismic hazard methodology for nuclear facilities in the Eastern United States: Dames and Moore, Golden, Vol. 2, Appendix A, EPRI Research Project Number P101-29.
- McGuire, R.K., and Barnhard, T.P., 1981, Effects of temporal variations in seismicity on seismic hazard: *Bulletin of the Seismological Society of America*, v. 71, p. 321-334.
- McKague, H.L., Stamatakos, J.A., and Ferrill, D.A., 1996, Type I faults in the Yucca Mountain region: Center for Nuclear Waste Regulatory Analyses CNWRA 96-007, Rev. 01, variously paginated.
- McKeown, F.A., and Dickey, D.D., 1969, Fault displacements and motion related to nuclear explosions: *Bulletin of the Seismological Society of America*, v. 59, p. 2253-2269.
- Morris, R.H., 1971, Geologic effects, *in* *Geologic and Hydrologic Effects of the Handley Event, Pahute Mesa, Nevada Test Site*: U.S. Geologic Survey USGS-474-95, Denver, Colorado, p. 7-26.
- O'Leary, D.W., 1996, Synthesis of tectonic models for the Yucca Mountain area, *in* *Seismotectonic Framework and Characterization of Faulting at Yucca Mountain, Nevada*: U.S. Geological Survey, Denver, p. 8.1-8.153.
- Orkild, P.P., Sargent, K.A., and Snyder, R.P., 1969, Geologic map of Pahute Mesa, Nevada Test Site and vicinity, Nye County, Nevada: U.S. Geological Survey Miscellaneous Geologic Investigations Map I-567, scale 1:48,000.
- Pezzopane, S.K., and Dawson, T.E., 1996, Fault displacement hazard—a summary of issues and information, *in* *Seismotectonic Framework and Characterization of Faulting at Yucca Mountain*: U.S. Geological Survey, Denver, p. 9-1 to 9-160.
- Pezzopane, S.K., Whitney, J.W., and Dawson, T.E., 1996, Models of earthquake recurrence and preliminary paleoearthquake magnitudes at Yucca Mountain, *in* *Seismotectonic Framework and Characterization of Faulting at Yucca Mountain*: U.S. Geological Survey, Denver, p. 5-1 to 5-100.
- Piety, L.A., 1994, Compilation of known and suspected Quaternary faults within 100 km of Yucca Mountain, Nevada and California: U.S. Geological Survey Open-File Report 94-112.
- Ramelli, A.R., and Bell, J.W., in prep., Known and suspected Quaternary faults, Yucca Mountain-Bare Mountain, scale 1:62,500 (preliminary).

- Rogers, A.M., Harmsen, S.C., Corbett, E.J., Priestley, K., and dePolo, D., 1991, The seismicity of Nevada and some adjacent parts of the Great Basin, *in* Slemmons, D.B., Engdahl, E.R., Zoback, M.D., and Blackwell, D.D., eds., *Neotectonics of North America*: Geological Society of America, p. 153-184.
- Rogers, A.M., Harmsen, S.C., and Meremonte, M.E., 1987, Evaluation of the seismicity of the southern Great Basin and its relationship to the tectonic framework of the region: U.S. Geological Survey Open-File Report 87-408, 196 p.
- Schwartz, D.P., and Coppersmith, K.J., 1984, Fault behavior and characteristic earthquakes—examples from the Wasatch and San Andreas fault zones: *Journal of Geophysical Research*, v. 89, p. 5681-5698.
- Schweickert, R.A., and Lahren, M.M., 1997, Strike-slip fault system in Amargosa Valley and Yucca Mountain, Nevada: *Tectonophysics*, v. 272, p. 25-41.
- Scott, R.B., 1990, Tectonic setting of Yucca Mountain, southwest Nevada, in *Basin and Range extensional tectonics near the latitude of Las Vegas, Nevada*: Geological Society of America Memoir 176, p. 251-282.
- Simonds, F.W., Fridrich, C.J., Hoisch, T.D., and Hamilton, W.B., 1995, A synthesis of detachment fault studies in the Yucca Mountain region, *in* *Topical Meeting on Methods of Seismic Hazards Evaluation—Focus '95*, Las Vegas, Nevada: American Nuclear Society, p. 107-114.
- Snyder, R.P., 1971, Composite postshot fracture map of Pahute Mesa, Nevada Test Site; Energy Research Development Administration, U.S. Geologic Survey, Denver, USGS-474-100, 17 p.
- Snyder, R.P., 1973, Recent fault movement on Pahute Mesa, Nevada Test Site, from May 1970 through June 1973: Energy Research and Development Administration, U.S. Geological Survey, Denver, USGS-474-137, 32 p.
- Stepp, J.C., 1972, Analysis of completeness of the earthquake sample in the Puget Sound area and its effects on statistical estimates of earthquake hazard: *Proceedings, First Microzonation Conference*, Seattle, Washington, p. 897-909.

- Swadley, W.C., and Carr, W.J., 1987, Geologic map of the Quaternary and Tertiary deposits of the Big Dune quadrangle, Nye County, Nevada, and Inyo County, California: U.S. Geological Survey Miscellaneous Investigations Series Map I-1767.
- Swan, F.H., Wesling, J.R., Angell, M.M., Thomas, A.P., Whitney, J.W., and Gibson, J.D., 1995 (in review), Evaluation of the location and recency of faulting near prospective surface facilities in Midway Valley, Yucca Mountain Project, Nye County, Nevada: Technical report prepared by Geomatrix Consultants, Inc., San Francisco, in cooperation with the U.S. Geological Survey.
- Taylor, E.M., Menges, C.M., de Fontaine, C.S., Buesch, D.C., Mundo, B.O., and Murray, M., 1996, Preliminary results of paleoseismic investigation on the Ghost Dance Fault: Chapter 4.5, *in* U.S. Geological Survey (Whitney, J.W., Coordinator), 1996, Seismotectonic Framework and Characterization of Faulting at Yucca Mountain, Nevada: U.S. Geological Survey report to the Department of Energy that fulfills Level 3 Milestone 3GSH100M WBS Number 1.2.3.2.8.3.6, variously paginated.
- U.S. Geological Survey, 1996, Seismotectonic framework and characterization of faulting at Yucca Mountain, Nevada, U.S. Department of Energy: U.S. Geological Survey, Denver.
- Wallace, T.C., Helmberger, D.V., and Engen, G.R., 1983, Evidence of tectonic release from underground nuclear explosions in long-period P-waves: *Bulletin of the Seismological Society of America*, v. 73, p. 593-613.
- Wallace, T.C., Helmberger, D.V., and Engen, G.R., 1985, Evidence of tectonic release from underground nuclear explosions in long-period S-waves: *Bulletin of the Seismological Society of America*, v. 75, p. 157-174.
- Wallace, T.C., Helmberger, D.V., and Lay, J., 1986, Reply to comments by A. Douglas, J.B. Yalong, and N.S. Lyman and a note on the revised moments for Pahute Mesa tectonic release: *Bulletin of the Seismological Society of America*, v. 76, p. 313-318.
- Weichert, D.H., 1980, Estimation of the earthquake recurrence parameters for unequal observation period for different magnitudes: *Bulletin of the Seismological Society of America*, v. 70, p. 1337-1346.
- Wells, D.L., and Coppersmith, K.J., 1994, New empirical relationships among magnitude, rupture length, rupture width, rupture area, and surface displacement: *Bulletin of the Seismological Society of America*, v. 84, p. 974-1002.
- Wernicke, B., 1995, Low-angle normal faults and seismicity—a review: *Journal of Geophysical Research*, v. 100, p. 20,159-20,174.

Youngs, R.R., and Coppersmith, K.J., 1985, Implications of fault slip rates and earthquake recurrence models for probabilistic seismic hazard estimates: *Bulletin of the Seismological Society of America*, v. 75, p. 939-964.

Youngs, R.R., Swan, F.H., III, Power, M.S., Schwartz, D.P., and Green, R.K., 1987, Probabilistic analysis of earthquake and ground shaking hazard along the Wasatch Front, Utah, *in* Gori, P.O., and Hays, W.W. (eds.), *Assessment of Regional Earthquake Hazards and Risk Along the Wasatch Front, Utah*: U.S. Geological Survey Open File Report 87-585, M-1 to M-100.

**TABLE RYA-1
COMPLETENESS TIMES**

VERSION 5 CATALOG (YEARS)			
MW Magnitude Bin	Lower Limit	Preferred Value	Upper Limit
1.5-2.0	2.6	2.8	7.7
2.0-2.5	1.4	8.3	12.0
2.5-3.0	9.3	11.2	18.9
3.0-3.5	7.4	8.2	12.9
3.5-4.0	8.2	16.6	29.7
4.0-4.5	19.6	28.1	44.6
4.5-5.0	empty	Empty	Empty
5.0-5.5	51.2	85.8	85.8
5.5-6.0	85.8	85.8	85.8
VERSION 7 CATALOG (YEARS)			
1.5-2.0	3.0	6.0	6.0
2.0-2.5	6.0	8.0	16.0
2.5-3.0	6.5	11.0	17.0
3.0-3.5	9.5	25.0	37.0
3.5-4.0	15.7	37.0	40.0
4.0-4.5	35.4	47.0	55.0
4.5-5.0	57.2	62.0	62.0
5.0-5.5	empty	Empty	empty
5.5-6.0	85.6	85.6	85.6

**TABLE RYA-2
INTERVAL RECURRENCE PARAMETERS**

VERSION 5 CATALOG		
b-Value	a-Value	Probability
-1.088	4.13	0.020
-1.065	4.15	0.065
-1.075	4.17	0.215
-1.085	4.22	0.215
-1.095	4.24	0.285
-1.105	4.26	0.155
-1.115	4.28	0.040
-1.125	4.32	0.005
VERSION 7 CATALOG		
-1.125	4.24	0.010
-1.135	4.36	0.020
-1.145	4.38	0.060
-1.155	4.41	0.125
-1.165	4.44	0.175
-1.175	4.46	0.167
-1.185	4.48	0.167
-1.195	4.51	0.125
-1.205	4.53	0.075
-1.215	4.56	0.075
-1.225	4.58	0.005

**TABLE RYA-3
FAULT SOURCES PARAMETERS, AREA A**

Fault ¹	Fault Length (km) ²	Max.; Average Disp./Event (cm) ³	Maximum Magnitude (M _w) ⁴	Age Most Recent Event (ka) ⁵	Estimated Recurrence (kyr) ⁶	Late Quaternary Slip Rate (mm/yr) ⁷
BM	11-40; 23	150; 100	(6.3, 6.6., 6.9) (RL) (6.2, 6.6, 7.1) (RA)	40 ± 20	80-150 100	0.01
PBC	13-28; 13	100; 50	(6.4, 6.4, 6.8) (RL) (6.2, 6.4, 6.8) (RA)	13 ± 3 (c)	37-75 50	0.005-0.013
SR	4-9; 7	67; 55	(5.8, 6.1, 6.2) (RL) (5.7, 6.1, 6.3) (RA)	13 ± 3	15-40; 25	0.02
BWR	4-10; 7	44; 217	(5.8, 6.1, 6.2) (RL) (5.7, 6.1, 6.4) (RA)	75 ± 10	75?	0.003
WW	12-26; 23	88; 50	(6.3, 6.7, 6.7) (RL) (6.1, 6.5, 6.6) (RA)	6 ± 4 (c) 40 + 20	30-100; 48	0.01
FW	7-16; 11	105; 61	(6.1, 6.3, 6.5) (RL) (6.0, 6.3, 6.6) (RA)	40 ± 20 (c) 75 ± 10	30-100; 48	0.002
SC	12-21; 18	120; 75	(6.3, 6.5, 6.6) (RL) (6.2, 6.5, 6.7) (RA)	25 ± 10	50-130; 90	0.01
IR	6-9; 8	130; 100	(6.0, 6.1, 6.2) (RL) (5.9, 6.1, 6.3) (RA)	25 ± 10	?	?

¹ Named faults that comprise the fault systems are: BM, Bare Mountain; PBC, Paintbrush Canyon; SR, Stagecoach Road; BWR, Bow Ridge; WW, Windy Wash; FW, Fatigue Wash; SC, Solitario Canyon; and IR, Iron Ridge. Bare Mountain fault data from Anderson and Klinger (1996), all other fault data (displacement, age of most recent event, recurrence, and slip rate) based on review and analysis of data in USGS (1996). Bare Mountain fault assumed to dip 55, 60, or 65 degrees to the east; Yucca Mountain faults assumed to dip 60, 67.5, or 75 degrees to the west. Faults are assumed to have pure normal to normal-oblique slip.

² Minimum and maximum fault lengths; preferred estimate. Distance measured along strike of fault system, primarily from Simonds et al. (1995). Maximum lengths from Ramelli and Bell (1997) and Frizzell and Shulters (1990). Maximum fault areas can be calculated by multiplying fault length by fault width (fault width calculated using dip of fault and seismogenic depth of 12, 15, or 20 km).

³ Maximum displacement is largest single-event displacement measured or calculated from trench exposure. Average displacement represents average of all displacement values from the various trenches on the specific fault.

⁴ (RL) indicates magnitudes calculated from the "all faults" M_w-fault length relationship of Wells and Coppersmith (1994). The three magnitudes given are computed from the minimum, preferred, and maximum fault length values. (RA) indicates magnitudes calculated from the "all faults" M_w-fault area relationship of Wells and Coppersmith (1994). The three magnitudes given are computed from the smallest, preferred, and largest areas for a fault given that the Yucca Mountain faults may dip between 60 and 75 degrees; Bare Mountain may dip between 55 and 65 degrees; and the thickness of the seismogenic crust is 12, 15, or 20 km (see text for a discussion of the magnitudes and weights used in the PSHA). Relative weights are 0.5 for RL and 0.5 for RA.

⁵ "Cracking" event (displacement less than 20 cm) indicated by (c).

⁶ Upper numbers represent elapsed time between faulting events as interpreted from trench data (USGS, 1996; Figure RYA-15). Lower number is an estimate of average recurrence using slip rate and average displacement per event. Preferred recurrence model is the "characteristic model" of Schwartz and Coppersmith (1984), assigned a relative weight of 0.9, and applied to the estimate of average recurrence only.

⁷ Uncertainty probably ± 0.005 mm/yr.

**TABLE RYA-4
COALESCING FAULT SOURCE MODEL, AREA A
THREE YUCCA MOUNTAIN FAULT SYSTEMS**

Fault System ¹	Max. Fault Length (km) ²	Max. Combined Disp/Event (m) ³	Maximum Magnitude (M _w) ⁴	Age Most Recent Event (ka)	Estimated Avg. Recurrence (kyr) ⁶	Late Quaternary Slip Rate (mm/yr) ⁷
BM (planar)	11-40; 23	1.5; 1.0	(6.3, 6.6, 6.9) (RL) (6.2, 6.6, 7.1) (RA)	40 ± 20	80-150; 100	0.01
PBC-SR-BWR	7-35; 20	1.0; 0.5	(6.1, 6.5, 6.8) (RL) (6.0, 6.5, 6.9) (RA)	13 ± 3	15-75; 25	0.005-0.02; 0.01
WW-FW	11-25; 23	1.13; 0.46	(6.3, 6.7, 6.7) (RL) (6.0, 6.5, 6.6) (RA)	6 ± 4; ⁵ 40 ± 20	30-100; 46	0.01
SC-IR	8-21; 20	1.2; 0.75	(6.1, 6.6, 6.6) (RL) (6.0, 6.5, 6.7) (RA)	25 ± 10	50-130; 75	0.01

**TABLE RYA-5
COALESCING FAULT SOURCE MODEL, AREA A
TWO YUCCA MOUNTAIN FAULT SYSTEMS**

Fault System ¹	Max. Fault Length (km) ²	Max. Combined Disp/Event (m) ³	Maximum Magnitude (M _w) ⁴	Age Most Recent Event (ka)	Estimated Avg. Recurrence (ka) ⁶	Late Quaternary Slip Rate (mm/yr) ⁷
BM (planar)	11-40; 23	1.5; 1.0	(6.3, 6.6, 6.9) (RL) (6.2, 6.6, 7.1) (RA)	40 ± 20	80-150; 100	0.01
East Side (SR-PBC-BWR)	7-35; 20	1.0; 0.5	(6.1, 6.5, 6.8) (RL) (6.0, 6.5, 6.9) (RA)	13 ± 3	15-75 50	0.005-0.02; 0.01
West Side (WW-FW-SC-IR)	8-26; 23	2.3; 1.8	(6.1, 6.7, 6.7) (RL) (5.9, 6.5, 6.6) (RA)	6 ± 4; ⁵ 40 ± 20	30-130 90	0.02-0.03; 0.025

¹ Named faults that comprise the fault systems are: BM, Bare Mountain; SR, Stagecoach Road; PBC, Paintbrush Canyon; BWR, Bow Ridge; WW, Windy Wash; FW, Fatigue Wash; SC, Solitario Canyon; and IR, Iron Ridge. Bare Mountain fault data from Anderson and Klinger (1996); all other fault data (displacement, age of most recent event, recurrence, and slip rate) based on review and analysis of data in USGS (1996). Bare Mountain fault assumed to dip 55, 60, or 65 degrees to the east; Yucca Mountain faults assumed to dip 60, 67.5, or 75 degrees to the west. In this model, all sources are considered seismogenic. Bare Mountain fault is always an independent source. Faults are assumed to have pure normal to normal-oblique slip.

Notes for Tables RYA-4 and RYA-5 (Cont'd.):

- ² Minimum and maximum rupture lengths; preferred estimate. Distance measured along strike of fault system, primarily from Simonds et al. (1995). Minimum rupture length assumes rupture only of preferred length of shortest part of fault system. Maximum rupture includes possible southern projections from Ramelli and Bell (1997) and northern bedrock projections from Frizzell and Shulters (1990). Probabilities for each rupture scenario are minimum (0.15), maximum (0.15), and preferred (0.7).
- ³ Maximum displacement is largest single-event displacement measured or calculated from trench exposure. Because the Windy Wash and Fatigue Wash fault systems are parallel, the maximum is the sum of the maximum displacement values for each fault. Average displacement represents the average of all displacement values from the various trenches on the specific fault.
- ⁴ (RL) indicates magnitudes calculated from the "all faults" Mw-fault length relationship of Wells and Coppersmith (1994). The three magnitudes given are computed from the minimum, preferred, and maximum fault length values. (RA) indicates magnitudes calculated from the "all faults" Mw-fault area relationship of Wells and Coppersmith (1994). The three magnitudes given are computed from the smallest, preferred, and largest areas for a fault given that the Yucca Mountain faults may dip between 60 and 75 degrees; Bare Mountain may dip between 55 and 65 degrees; and the thickness of the seismogenic crust is 12, 15, or 20 km (see text for a discussion of the magnitudes and weights used in the PSHA). Relative weights are 0.5 for RL and 0.5 for RA.
- ⁵ 6 ± 4 ka age is for 6-cm "cracking" event on Windy Wash fault. 40 ± 20 ka age is for penultimate 35-cm displacement event also on Windy Wash fault.
- ⁶ Upper numbers represent time between faulting events as interpreted from trench data (USGS, 1996; Figure RYA-15). Lower number is an estimate of average recurrence for maximum magnitude events using slip rate and average displacement per event. No preferred recurrence model. The "characteristic model" of Schwartz and Coppersmith (1984) is given a weight of 0.5, and the exponential magnitude distribution model also is given a weight of 0.5. This applies to the average recurrence only.
- ⁷ Ranges and preferred slip rate. Relative weights are 0.15 for maximum and minimum and 0.7 for preferred estimate. Uncertainty in slip rate estimates probably ± 0.005 mm/yr.
- ⁸ Upper numbers represent elapsed time between faulting events as interpreted from trench data. Lower number is an estimate of average recurrence for maximum magnitude events using slip rate and average displacement per event. Preferred recurrence model is the exponential magnitude distribution, using the average recurrence estimates, and is assigned a weight of 0.7.

**TABLE RYA-6
COALESCING SOURCE MODEL, AREA A
ONE FAULT SYSTEM¹**

Fault System ¹	Maximum Fault Length (km) ²	Maximum Combined Disp./Event (m) ³	Age Most Recent Event (ka)	Estimated Average Recurrence (kyr) ⁴	Slip Rate (mm/yr) ⁵	Maximum Magnitude (M _w) ⁶
BM (planar)	11-40; 23	1.5; 1.0	40 ± 20	80-150; 100	0.01	(6.3, 6.6, 6.9) (RL) (6.2, 6.6, 7.1) (RA)
PBC/SR (master fault)	25	3.3	75 ± 10	73.3-94.3; 82.5	0.35- 0.45; 0.4	6.7 (RL) (6.1, 6.6, 6.9) (RA)

- ¹ Bare Mountain fault remains independent source. (See Table RYA-3 or RYA-4.) The Paintbrush Canyon/Stagecoach Road (PBC/SR), fault is the master fault. Other named faults within the fault system are the Bow Ridge, Windy Wash, Fatigue Wash, Solitario Canyon, and Iron Ridge. All fault data (displacement, age of most recent event, recurrence, and slip rate) based on review and analysis of data in USGS (1996). Faults are assumed to have pure normal to normal-oblique slip.
- ² Distance measured along strike of Windy Wash-Solitario Canyon fault system, primarily from Simonds et al. (1995). Maximum rupture includes possible southern projections from Ramelli and Bell (1997).
- ³ Maximum displacement for the fault system is the sum of the largest single-event displacements measured or calculated from all the trench exposures of all the faults.
- ⁴ Recurrence estimate (range and preferred) for maximum magnitude events calculated from maximum displacement and slip rate estimates. Preferred recurrence model is the exponential magnitude distribution, assigned a weight of 0.9. The characteristic earthquake recurrence model is given a weight of 0.1.
- ⁵ Range and preferred slip rates. Based on the sum of late Quaternary slip rates for the major parallel faults; uncertainty probably ±0.02 mm/yr.
- ⁶ (RL) indicates magnitudes calculated from the "all faults" M_w-fault length relationship of Wells and Coppersmith (1994). The three magnitudes given are computed from the minimum, preferred, and maximum fault length values. (RA) indicates magnitudes calculated from the "all faults" M_w-fault area relationship of Wells and Coppersmith (1994). The three magnitudes given are computed from the smallest, preferred, and largest areas for a fault given that the Yucca Mountain faults may dip between 60 and 75 degrees; Bare Mountain may dip between 55 and 65 degrees; and the thickness of the seismogenic crust is 12, 15, or 20 km (see text for a discussion of the magnitudes and weights used in the PSHA). Relative weights are 0.5 for RL and 0.5 for RA. Historical analogs may be the 1932 Cedar Mountain earthquake of M7.2 and the 1959 Hebgen Lake earthquake of M7.4.

TABLE RYA-7
M_{max} FOR HYPOTHESIZED BURIED SEISMIC SOURCE 30 KM LONG
(M_{max} DERIVED FROM $M = 4.04 + 0.98 \text{ LOG [RUPTURE AREA]}$)
(WELLS AND COPPERSMITH, 1994)

Decoupled Depth (km)	Thickness of Seismic Crust (km)	Rupture Area (km ²)	M _{max}
5	12	210	6.3
5	15	300	6.5
5	20	450	6.7
10	12	60	5.8
10	15	150	6.2
10	20	300	6.5

**TABLE RYA-8
SIGNIFICANT REGIONAL FAULT SOURCE PARAMETERS, AREAS B and C**

FAULT¹	Fault Rupture Length (km); Max. Disp/Event (m)² Dip (deg.) & Direction	Maximum Magnitude (M_w)³	Age Most Recent Event (ka)	Estimated Recurrence (ka)^{4,5}	Slip Rate (mm/yr)⁶	Reference⁴
Wahmonie (WAH; 22)	15; ? 90	6.4 (RL) 6.3 (RA)	<180	907	0.02	1, 6
Rock Valley (RV; 25)	30 (20-40); 2.5-3.9 90	6.8 (RL) 7.3 (MD) 6.7 (RA)	<10	25-195	0.02-0.1	1, 5
Cane Spring (CS; 28)	20 (14-27); ? 90	6.6 (RL) 6.5 (RA)	<1.8 Ma ?	?	0.02	1
Ash Meadows (AM; 30)	40 (34-47); 1.8 90	6.9 (RL) 6.9 (MD) 6.8 (RA)	>10	>120-180	<0.01	1, 3
Yucca Flat (YC; 40)	25; ? 90	6.7 (RL) 6.6 (RA)	<10	?	0.08	1, 6
Furnace Creek (FC; 52) ⁷	105 (100-111); 4.5 90	7.4 (RL) 7.2 (MD) 7.2 (RA)	>0.2	0.6 - 0.8	4-8	4
Death Valley (DV; 54) ⁷	60 (45-76); 3.5 60 W	7.2 (RL) 7.1 (MD) 7.0 (RA)	>0.2	0.5-1.0	3-5	4
West Spring Mts (WSM; 56)	36 (30-56); 2.0 60 W	6.9 (RL) 6.9 (MD) 6.8 (RA)	10	28-124	0.02-0.07	1, 2
Belted Range (BLR; 64)	30 (20-51); 0.9 60 W	6.8 (RL) 6.7 (MD) 6.7 (RA)	<10	9-90	0.01-0.1	1, 2
Pahrump-Stewart Valley (PSV; 65)	35 (18-42); 2.0 90	6.9 (RL) 6.9 (MD) 6.7 (RA)	<10	100-167	0.009-0.02	1, 3
West Pintwater (WPR; 76)	55 (55-60); ? 60 W	7.1 (RL) 7.0 (RA)	>10	?	0.01-0.1	1

Notes for Table RYA-8

- ¹ Letters and numbers in parentheses are fault abbreviations and distance in kilometers to Yucca Mountain; distance measured from Piety (1994).
- ² Preferred estimate of surface fault rupture length based on review and analysis of mapped scarp and fault length from cited references (weight 0.7). Numbers in parentheses indicate minimum and maximum values (weight 0.15 each). Where no range given, assumes rupture of entire mapped trace. Displacement estimates are from profile or trench data in cited reference. 90 degree dip assumes sense of displacement primarily strike-slip, 60 degree assumes displacement primarily dip-slip.
- ³ Magnitudes estimated from regressions of Wells and Coppersmith (1994) for all faults using preferred estimated surface rupture length (RL), maximum displacement (MD), and rupture area (RA). Relative weights are 0.35 for SRL, 0.35 for RA, and 0.3 for MD or 0.5 for RL and 0.5 for RA depending on available data. Magnitudes estimated to be ± 0.5 magnitude units for RL and RA.
- ⁴ Recurrence estimates calculated from displacement and slip rate estimates. Characteristic recurrence model given weight of 0.9; truncated exponential recurrence model is given weight of 0.1.
- ⁵ Where a range of values is given, equal weight is assigned to end member values.
- ⁶ References
 - (1) Piety, L.A., 1994, Compilation of known and suspected Quaternary faults within 100 km of Yucca Mountain, Nevada and California: U.S. Geological Survey Open-file Report 94-112.
 - (2) Anderson, R.E., et al., 1995a, Characterization of Quaternary and suspected Quaternary faults, regional studies, Nevada and California: U.S. Geological Survey Open-file Report 95-599.
 - (3) Anderson, R.E., et al., 1995b, Characterization of Quaternary and suspected Quaternary faults, Amargosa area, Nevada and California: U.S. Geological Survey Open-file Report 95-613.
 - (4) Klinger, R.E., and Piety, L.A., 1996, Evaluation and characterization of Quaternary faulting on the Death Valley and Furnace Creek faults, Death Valley, California: U.S. Bureau of Reclamation Seismotectonic Report 96-10.
 - (5) Coe, J.A., Yount, J.C., and O'Leary, D.W., 1996, Preliminary results of paleoseismic investigations of the Rock Valley fault system, Chapter 4.13; in Seismotectonic framework and characterization of faulting at Yucca Mountain, Nevada: U.S. Geological Survey, Yucca Mountain Project.
 - (6) Yount, J.C., unpub. mapping.
- ⁷ Simultaneous rupture of Death Valley and Furnace Creek faults would result in M_w 7.7 earthquake; however, the probability of this event is low, 10%.

Declustered Catalog	Source Zonation	Spatial Variability	Rate Allocations	Maximum Magnitude
---------------------	-----------------	---------------------	------------------	-------------------

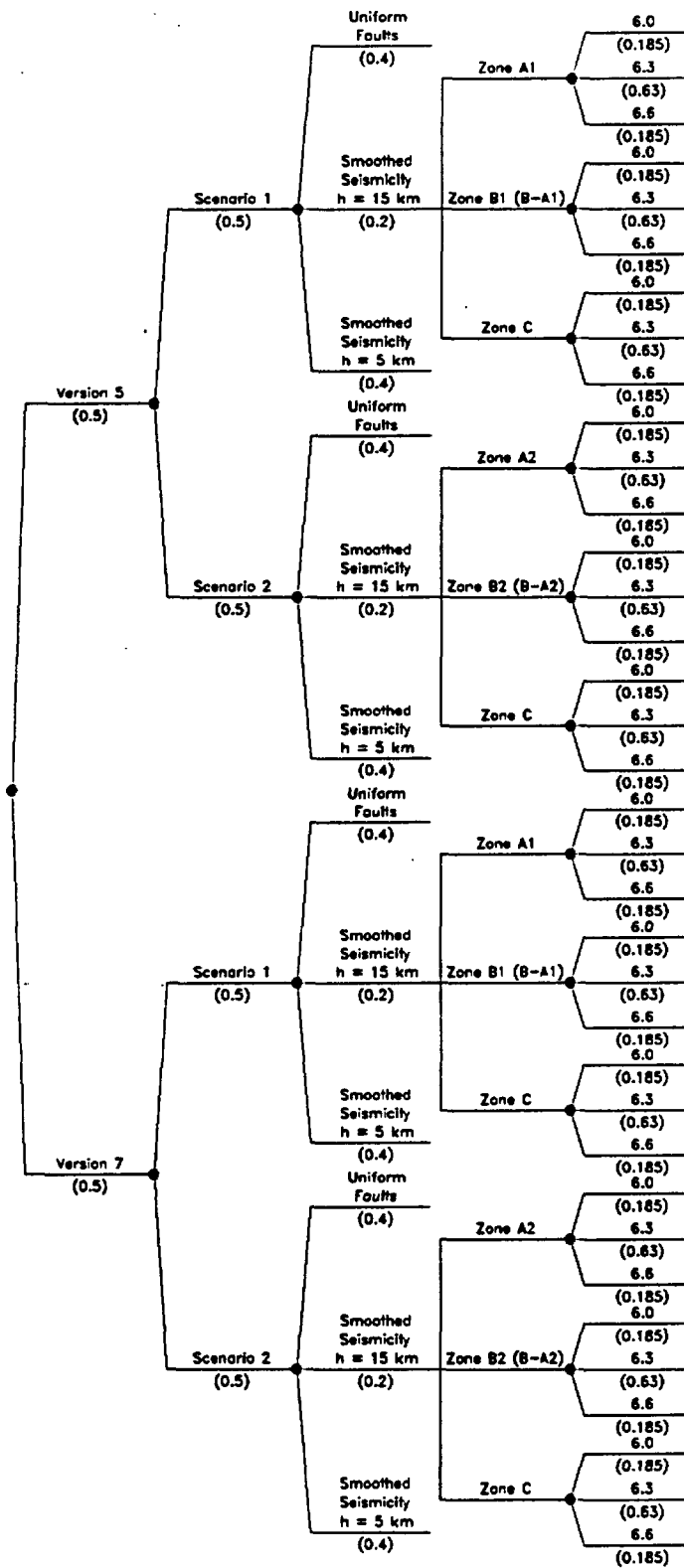


Figure RYA-1a Logic tree for background source zones

Seismogenic Crustal Thickness	Coalescing Model	Sources	P(Actual)
-------------------------------------	---------------------	---------	-----------

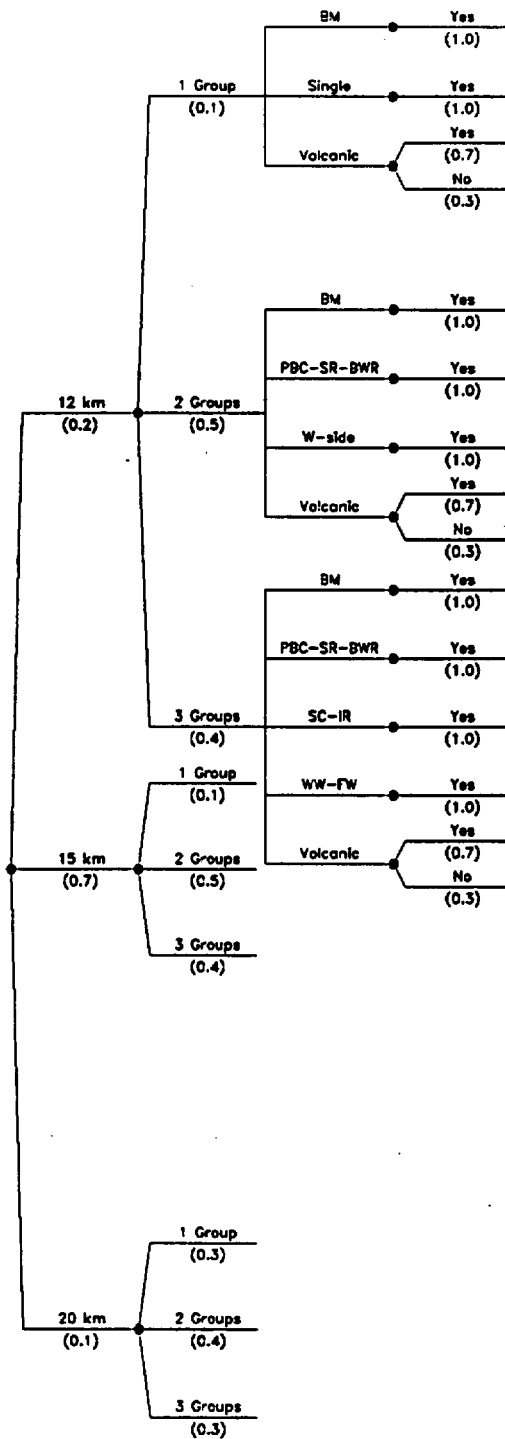


Figure RYA-1b Logic tree for local fault sources

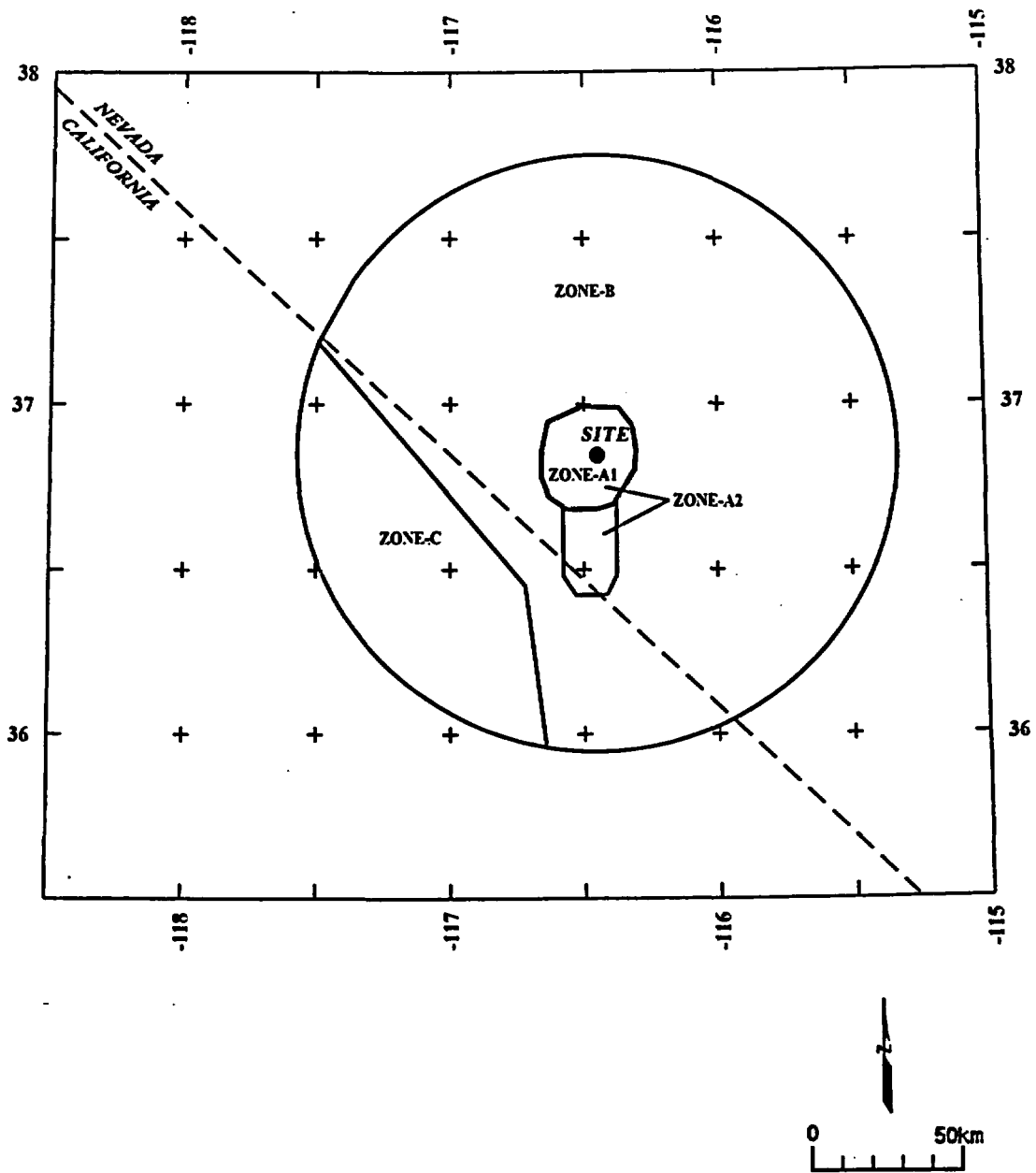


Figure RYA-2 Map showing boundaries of zones used in the seismic source model

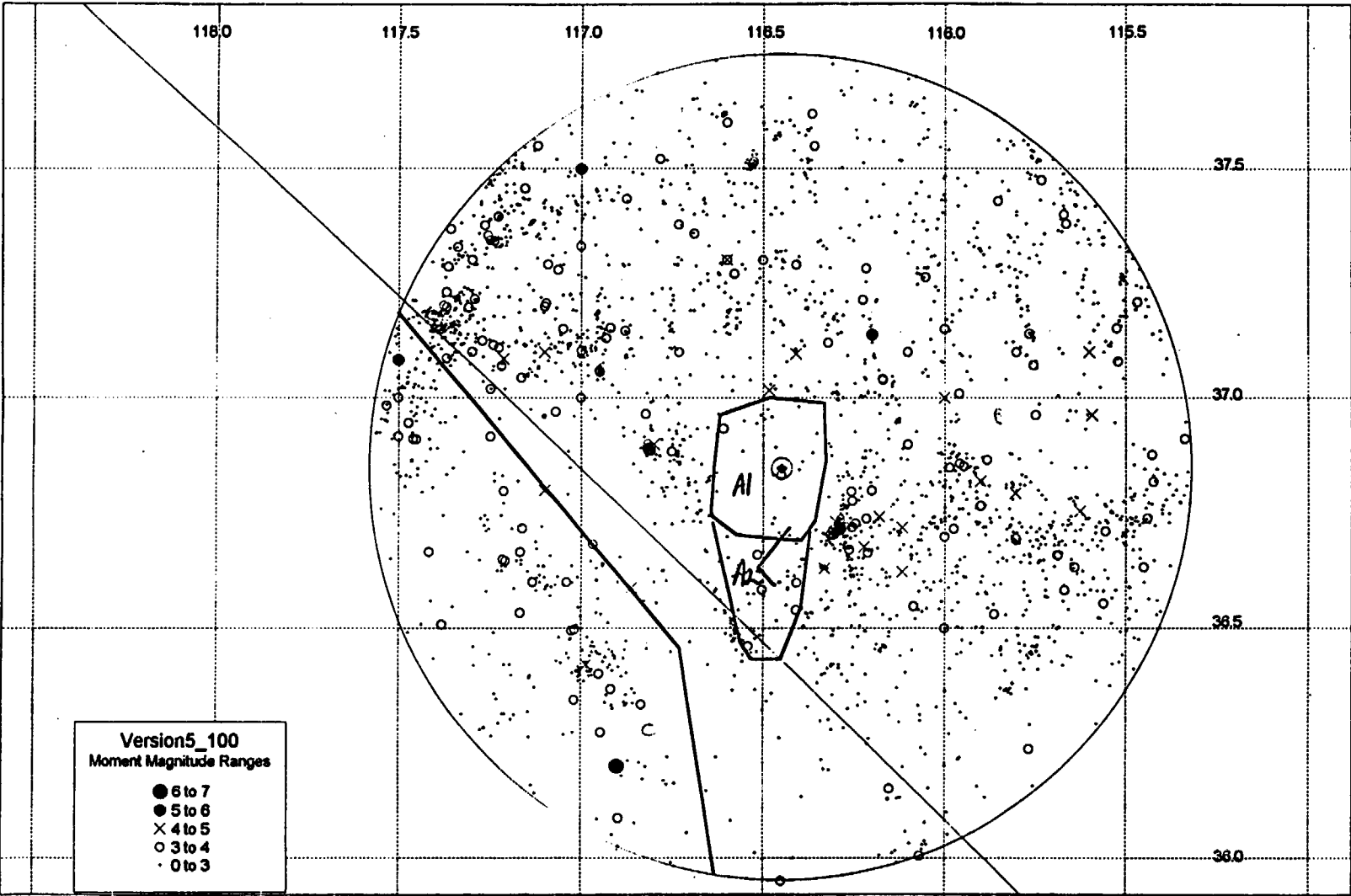


Figure RYA-3 Map showing earthquakes from the version 5 catalog and the background source zones

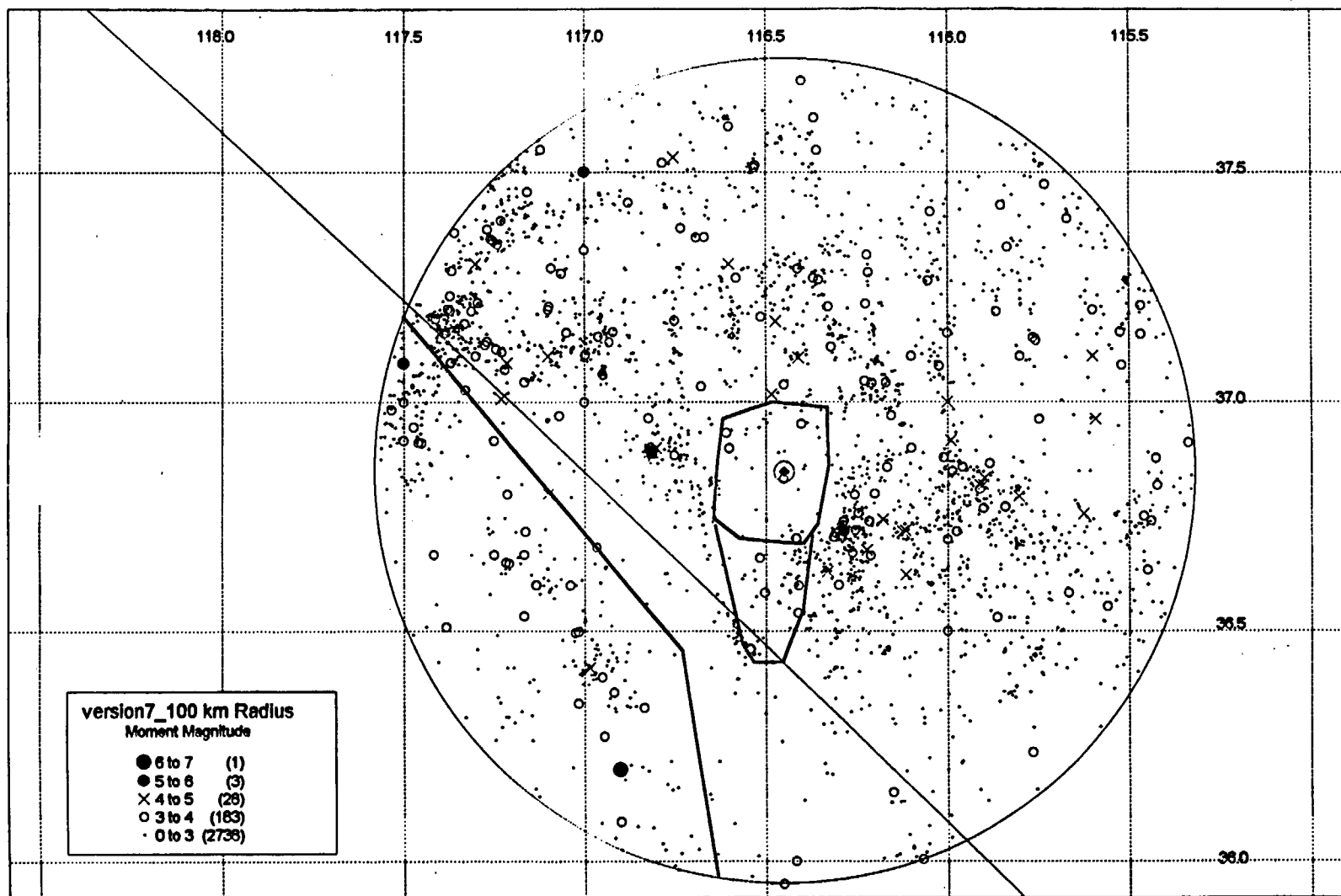


Figure RYA-4 Map showing earthquakes from the version 7 catalog and the background source zones

Version 5 100 km Radius

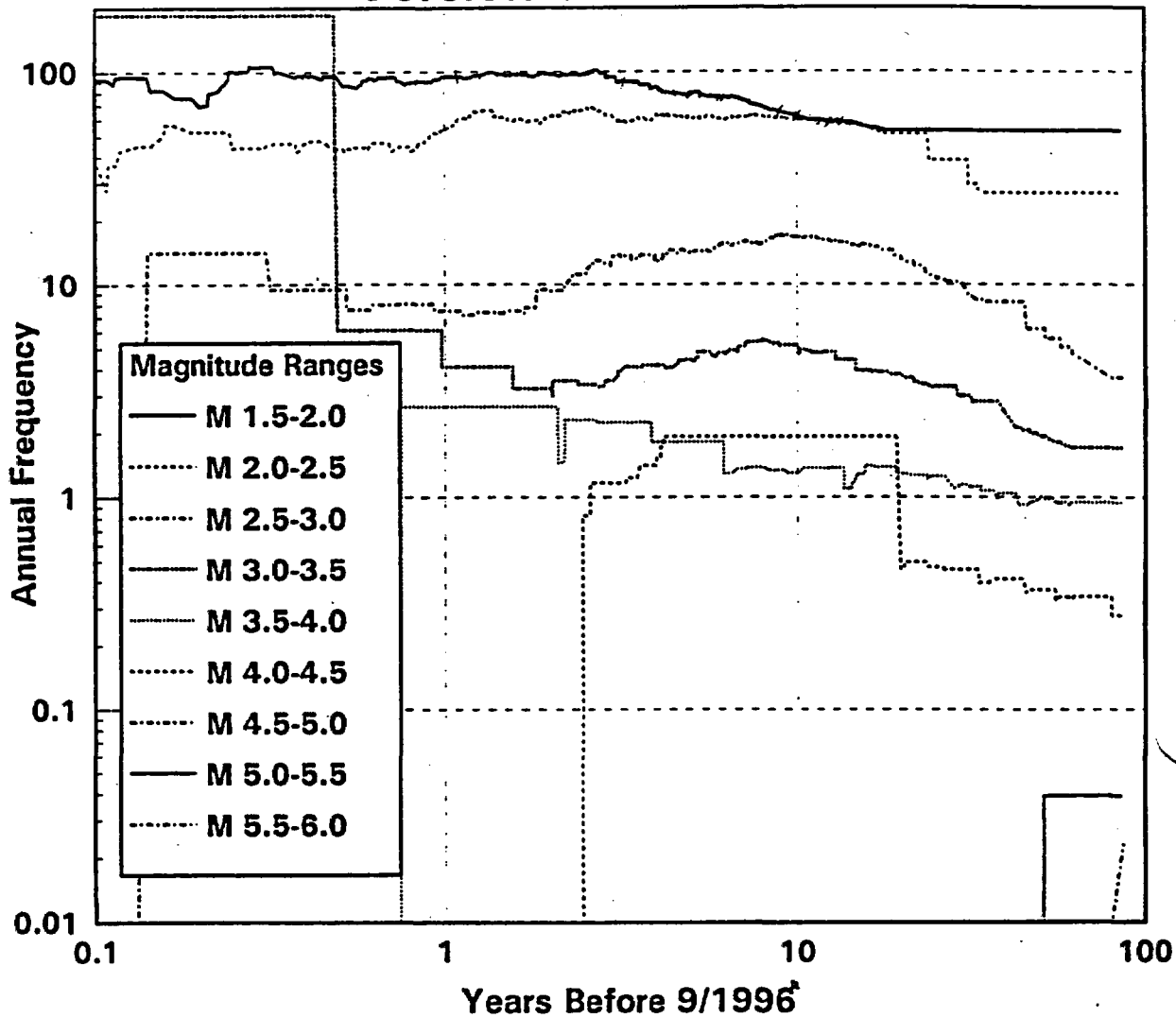


Figure RYA-5 Stepp plot of annual frequency versus years before 9/1996 for individual magnitude bins and the version 5 catalog

Version 7 100 km Radius

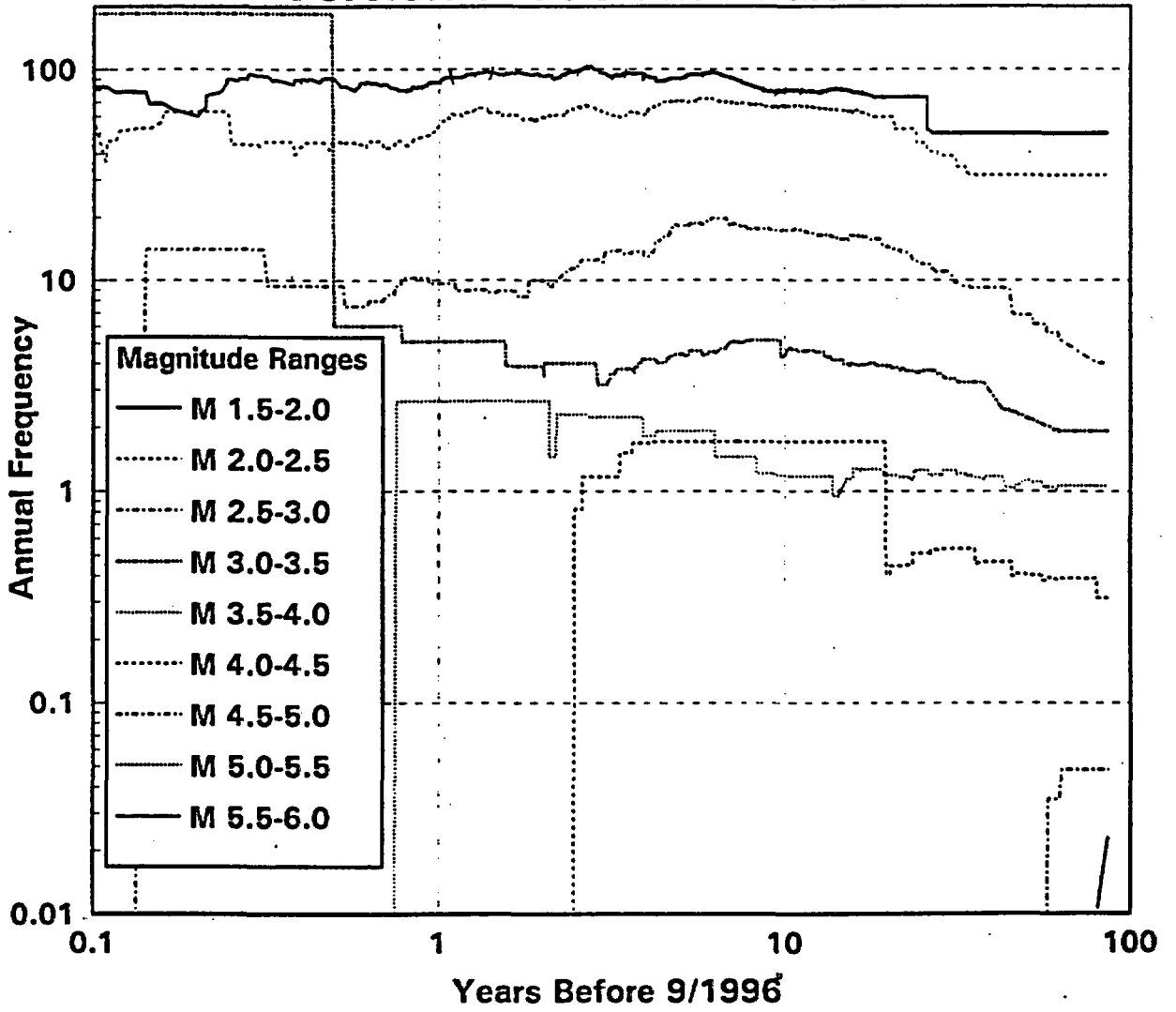


Figure RYA-6 Stepp plot of annual frequency versus years before 9/1996 for individual magnitude bins and the version 7 catalog

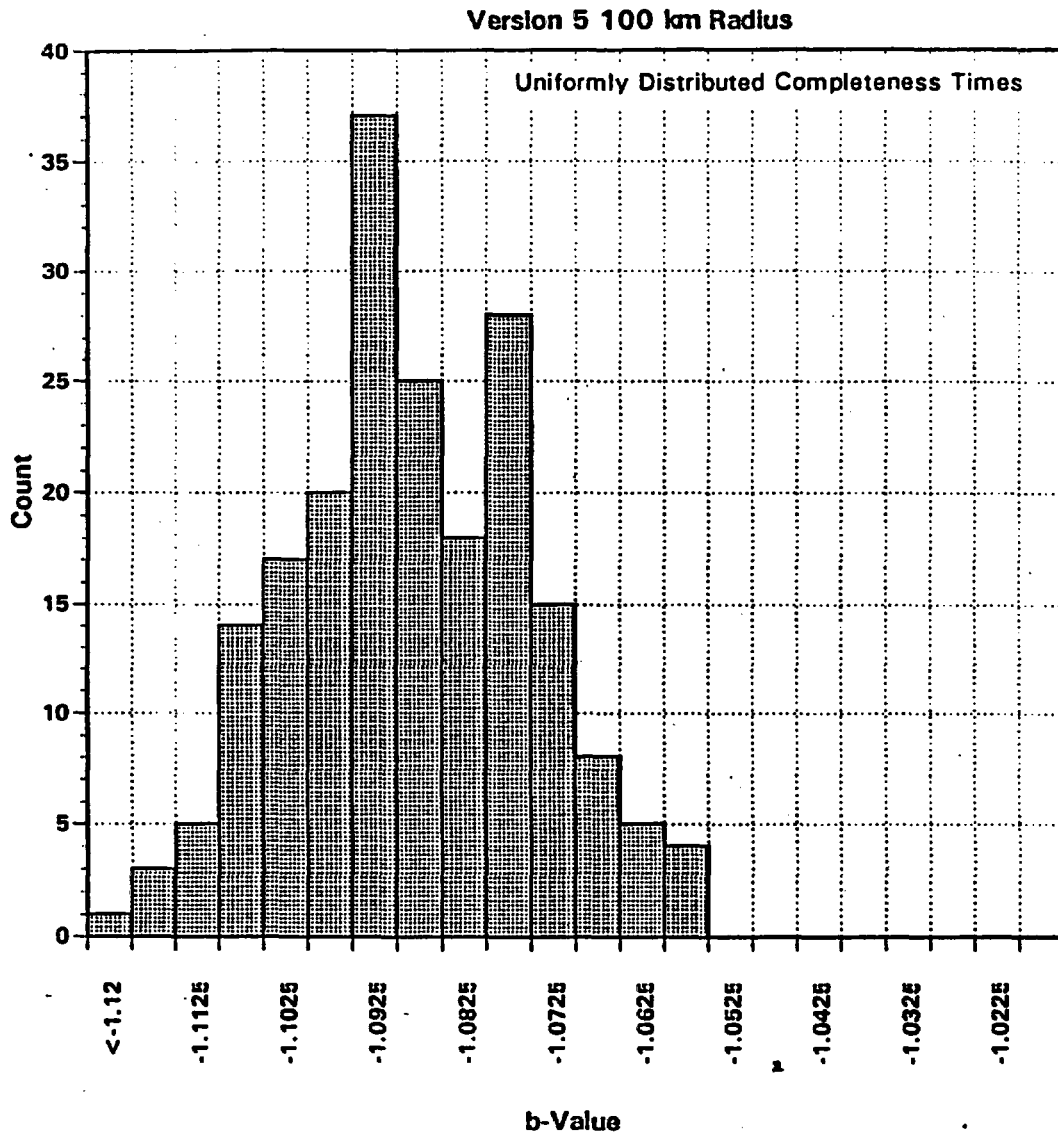


Figure RYA-7 Histogram showing b-values obtained for the version 5 catalog given uniform sampling of completeness times

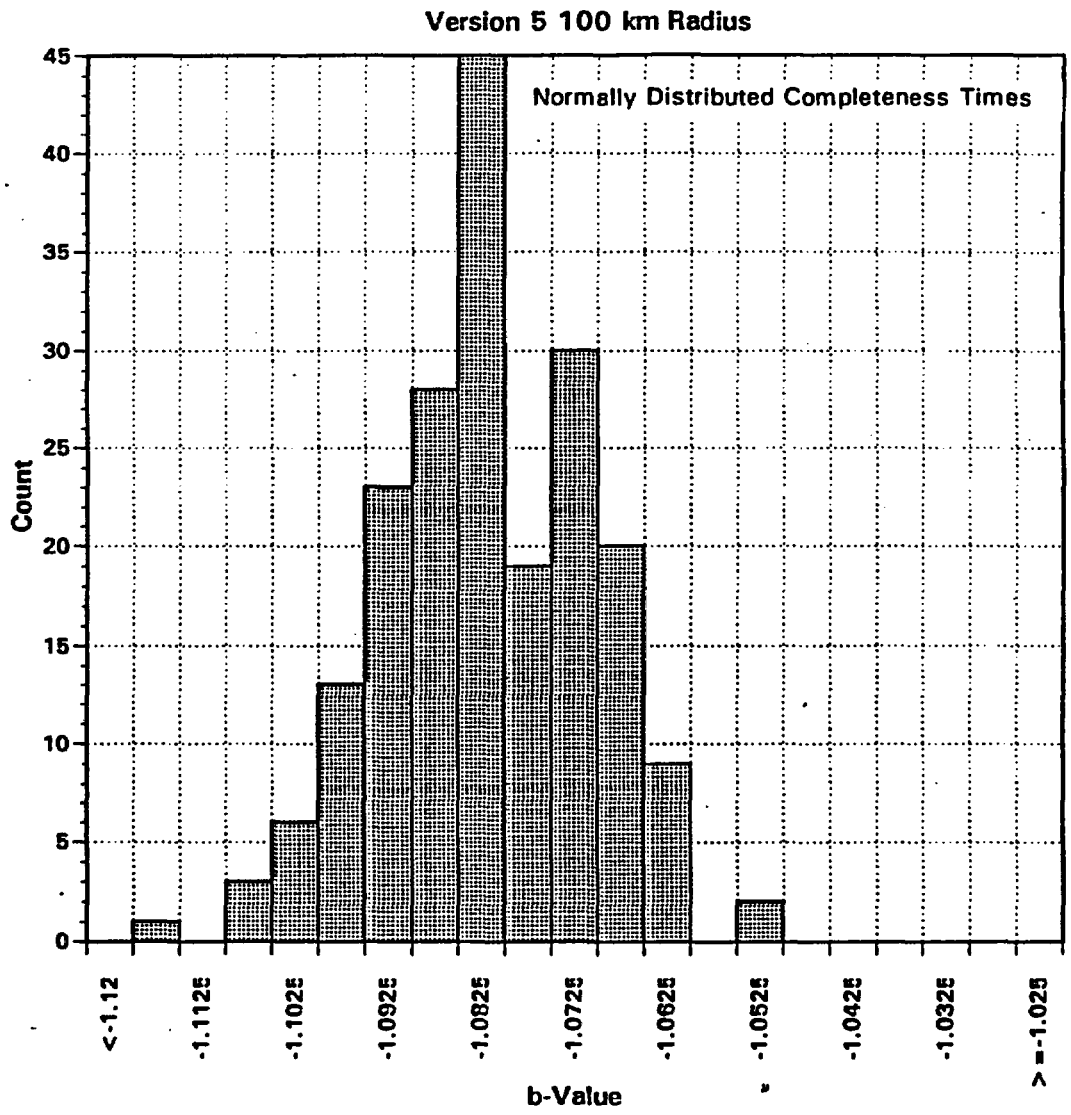


Figure RYA-8 Histogram showing b-values obtained for the version 5 catalog given normal sampling of completeness times

Version 7 100 km Radius
Uniformly Distributed Completeness Times

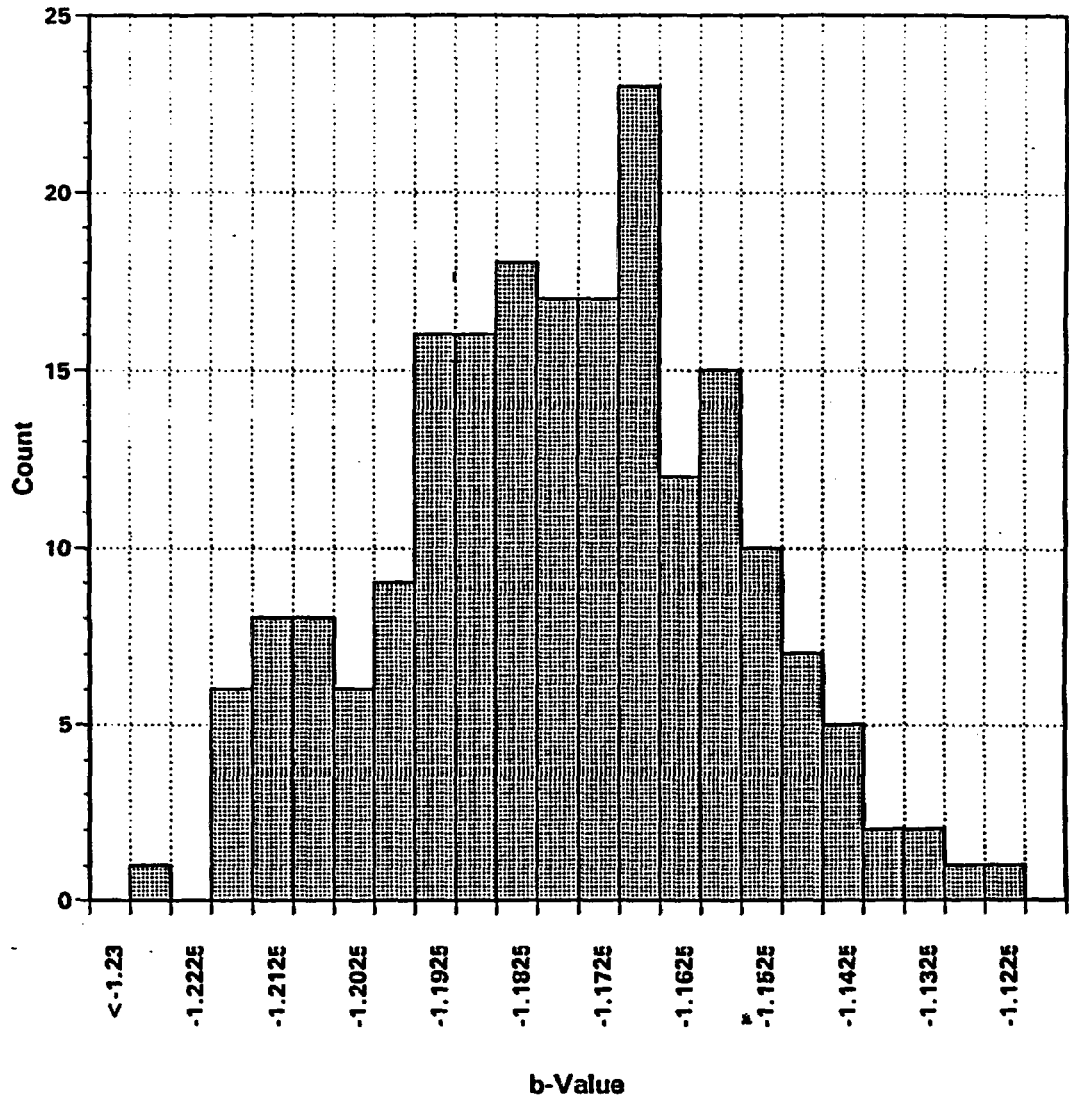


Figure RYA-9 Histogram showing b-values obtained for the version 7 catalog given uniform sampling of completeness times

Version 7 100 km Radius
Normally Distributed Completeness Times

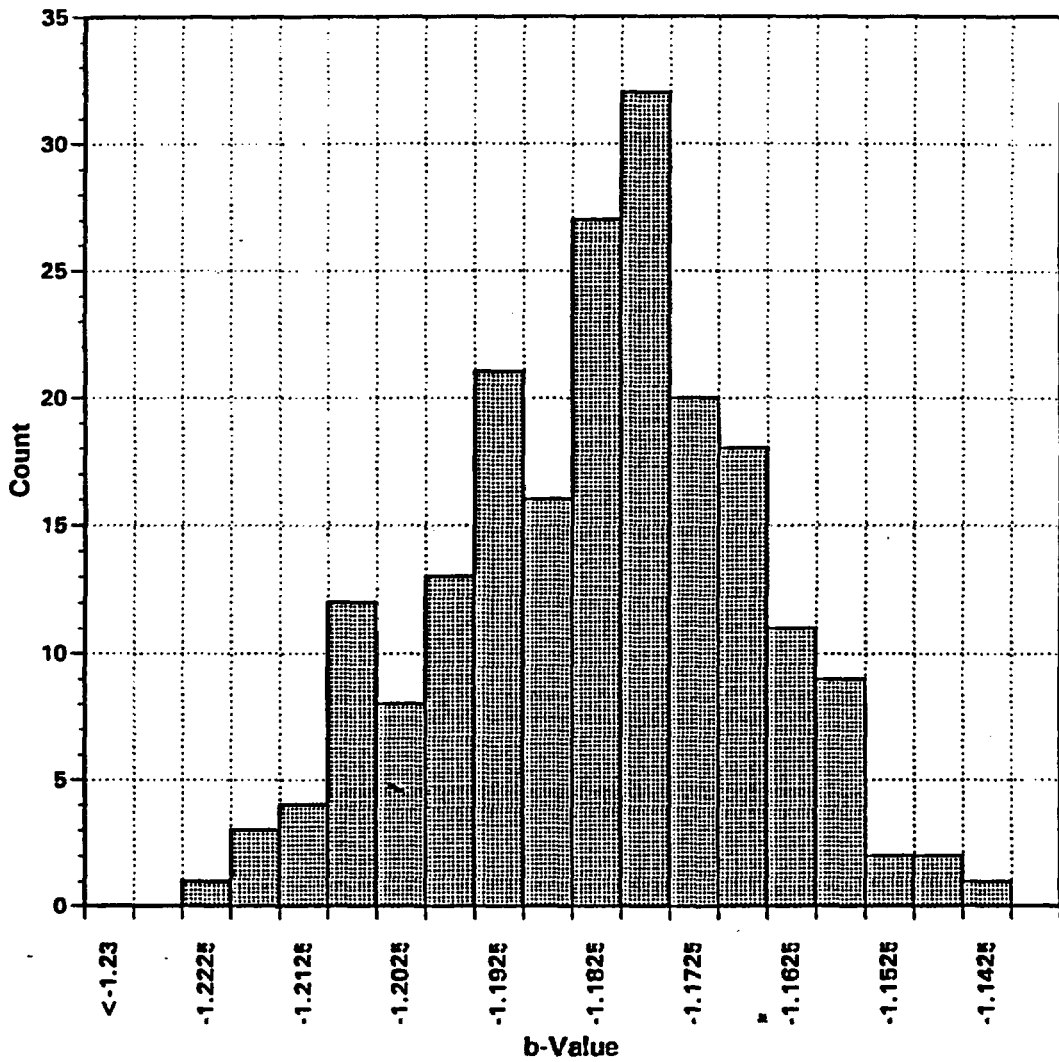


Figure RYA-10 Histogram showing b-values obtained for the version 7 catalog given normal sampling of completeness times

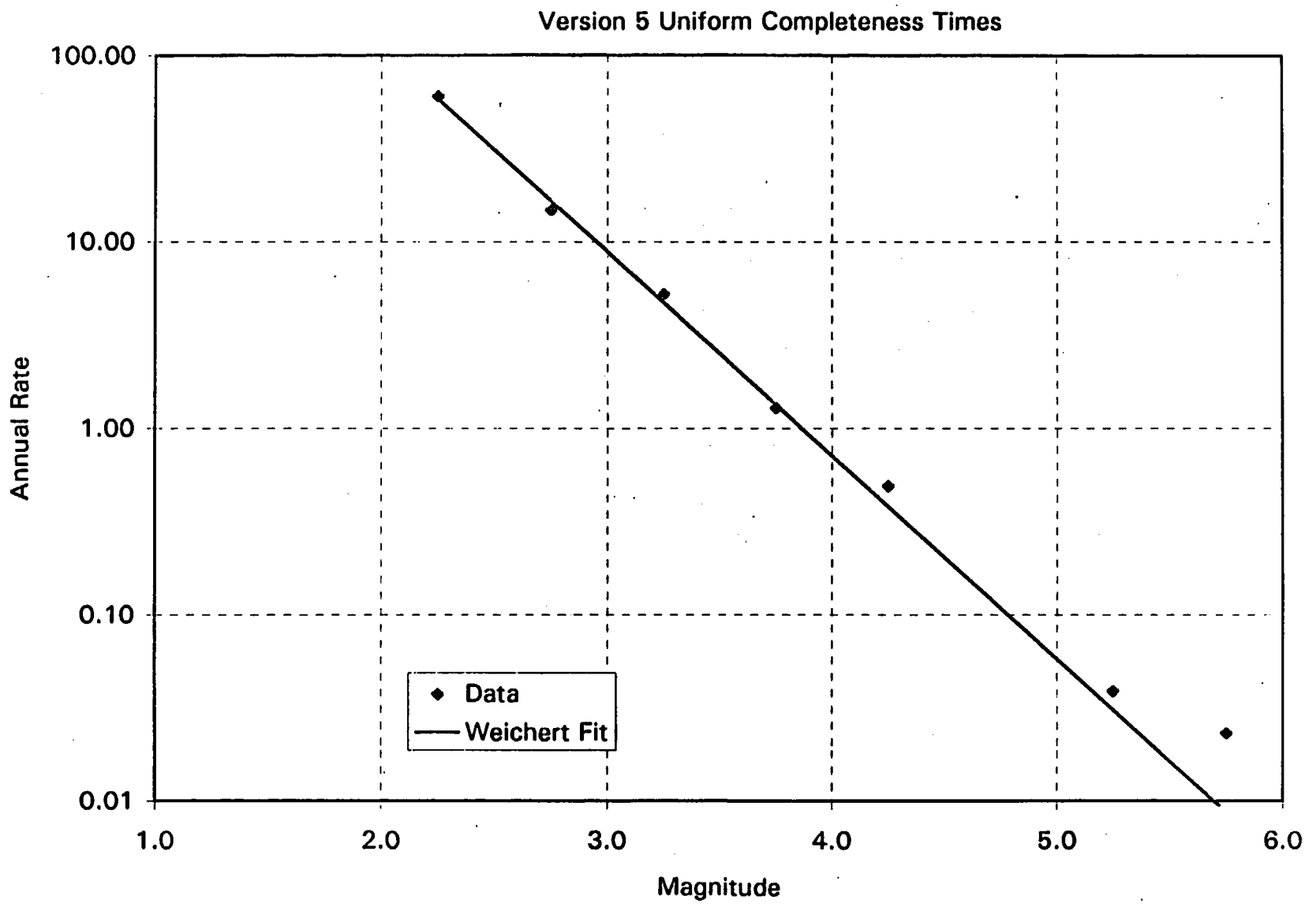


Figure RYA-11 Interval rates for the version 5 catalog that produced the modal b-value 1.09 (Figure RYA-7) and the fit to these data using the Weichert maximum likelihood method

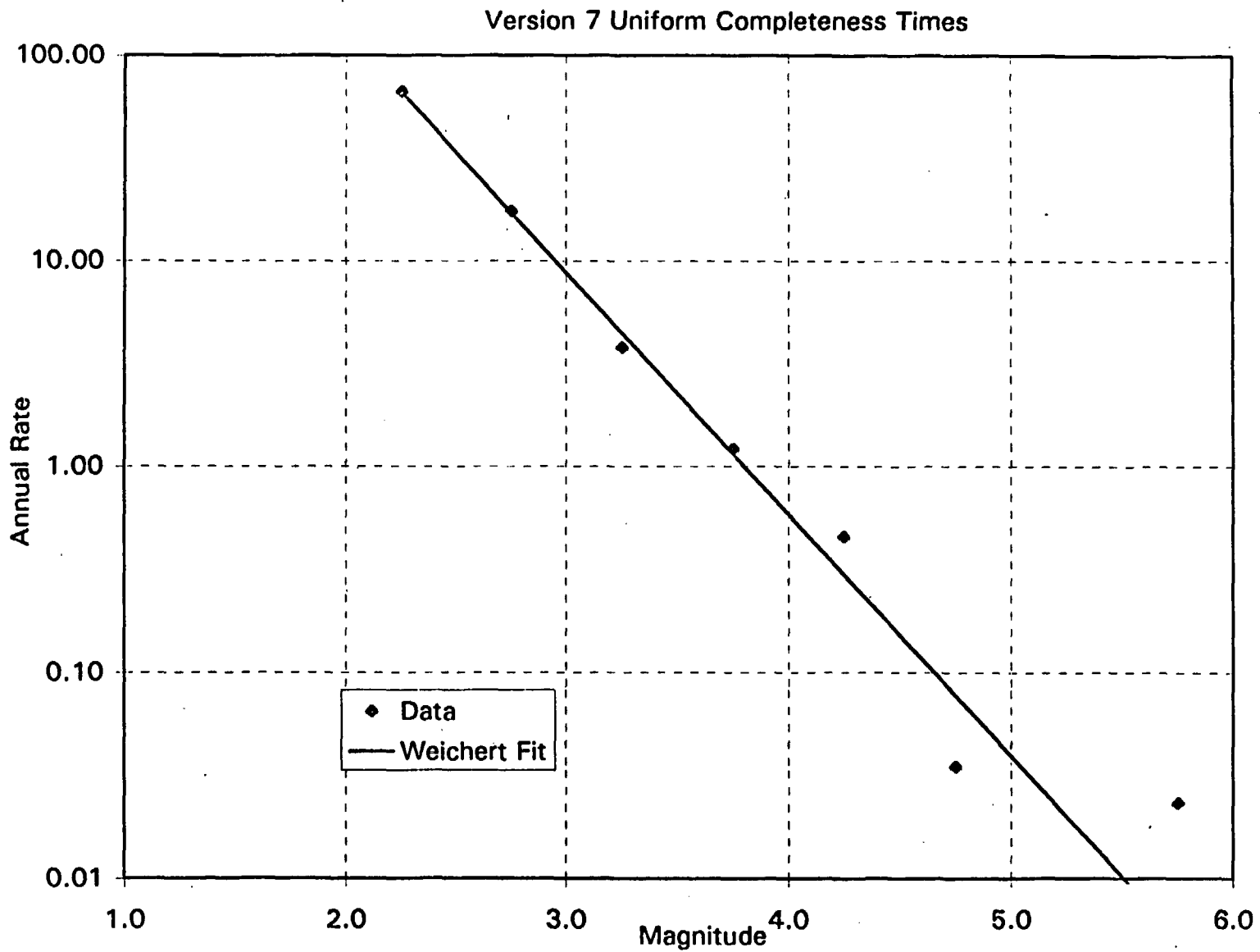


Figure RYA-12 Interval rates for the version 7 catalog that produced the modal b-value 1.17 (Figure RYA-9) and the fit to the data using the Weichert maximum likelihood method

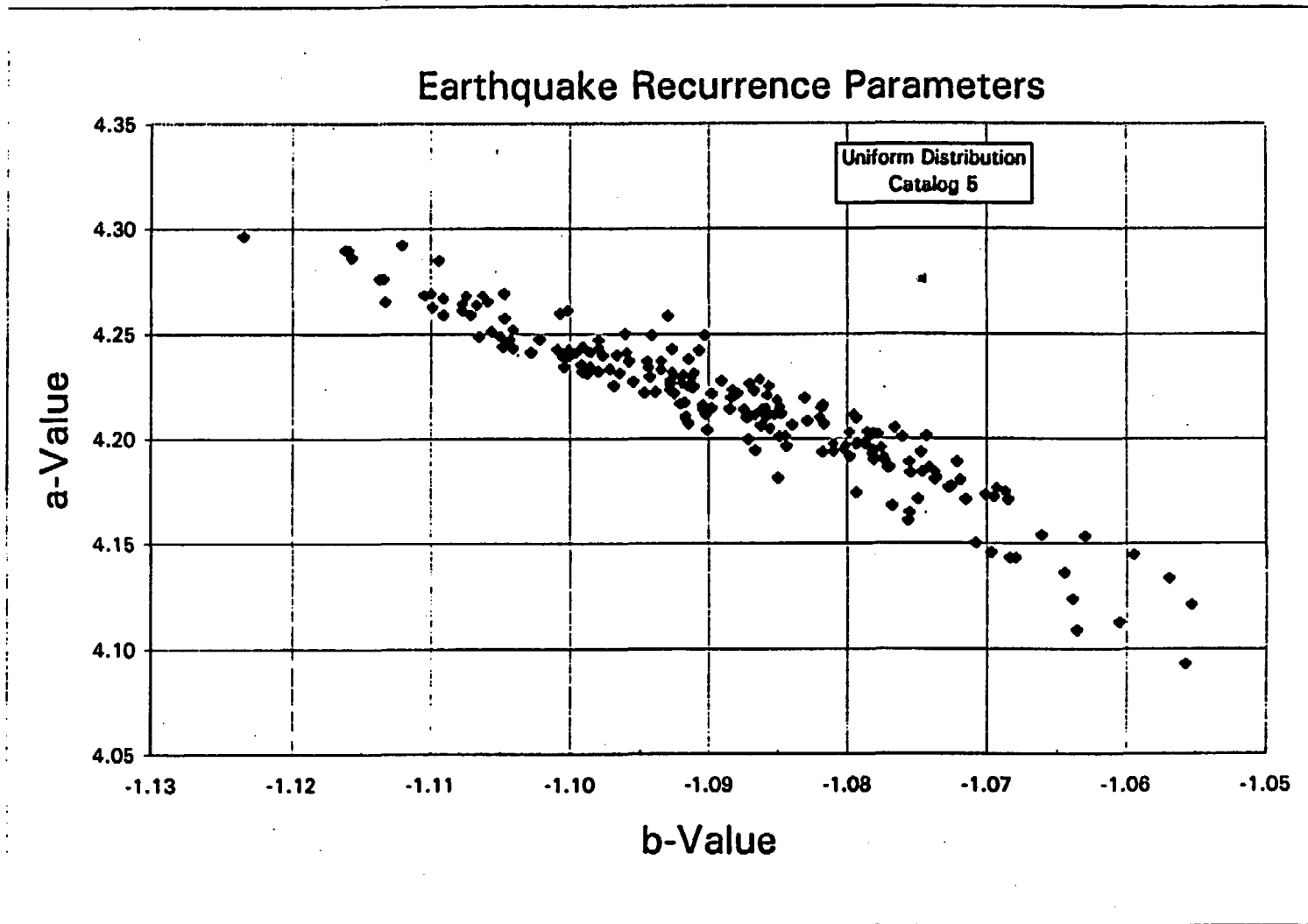


Figure RYA-13 Earthquake recurrence parameters. The paired a- and b-values calculated by uniform sampling from the range of likely completeness times and associated annual rates in the version 5 catalog. This plot shows the correlation between a- and b-values.

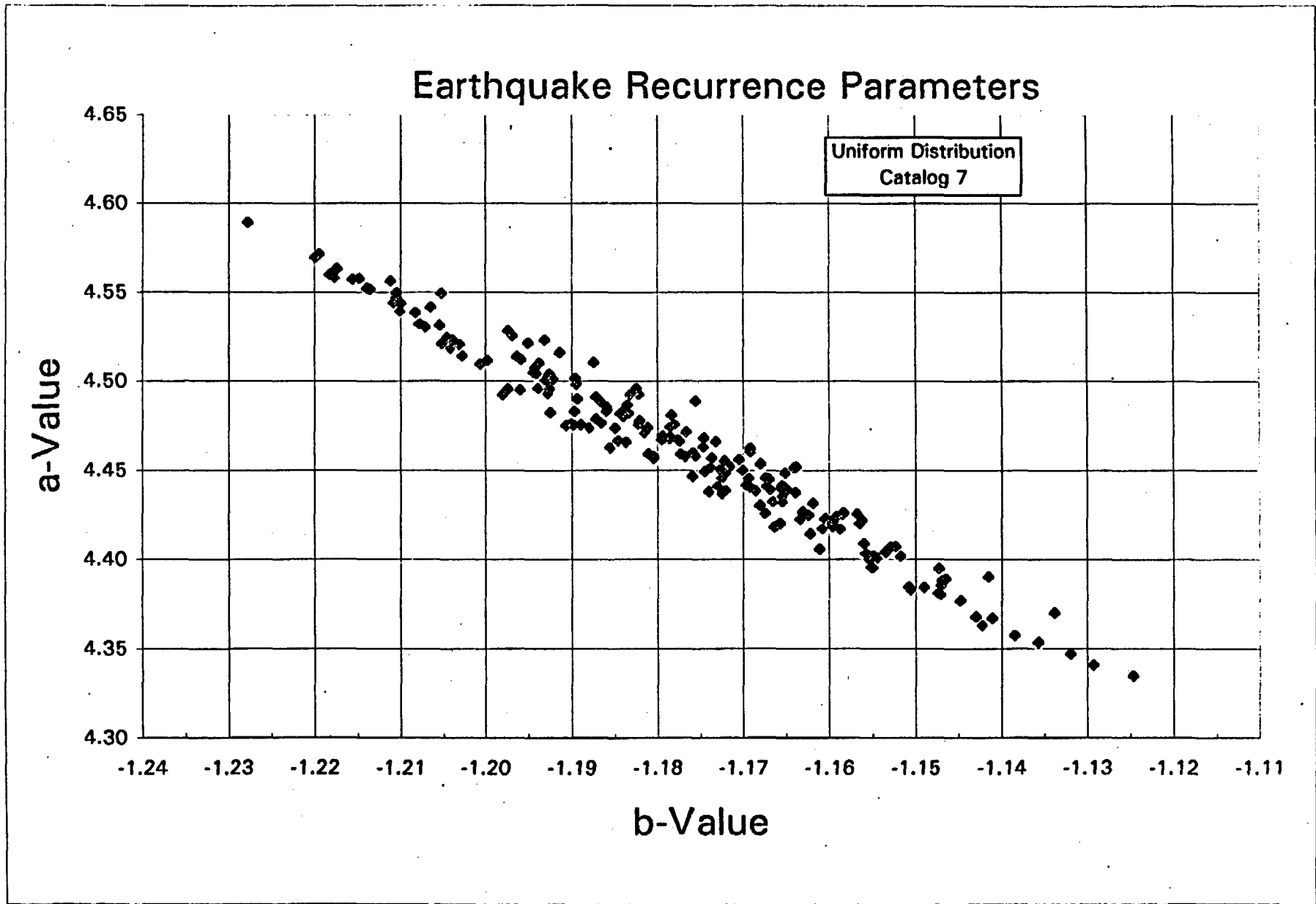


Figure RYA-14 Earthquake recurrence parameters. The paired a- and b-values calculated by uniform sampling from the range of likely completeness times and associated annual rates in the version 7 catalog. This plot shows the correlation between a- and b-values.

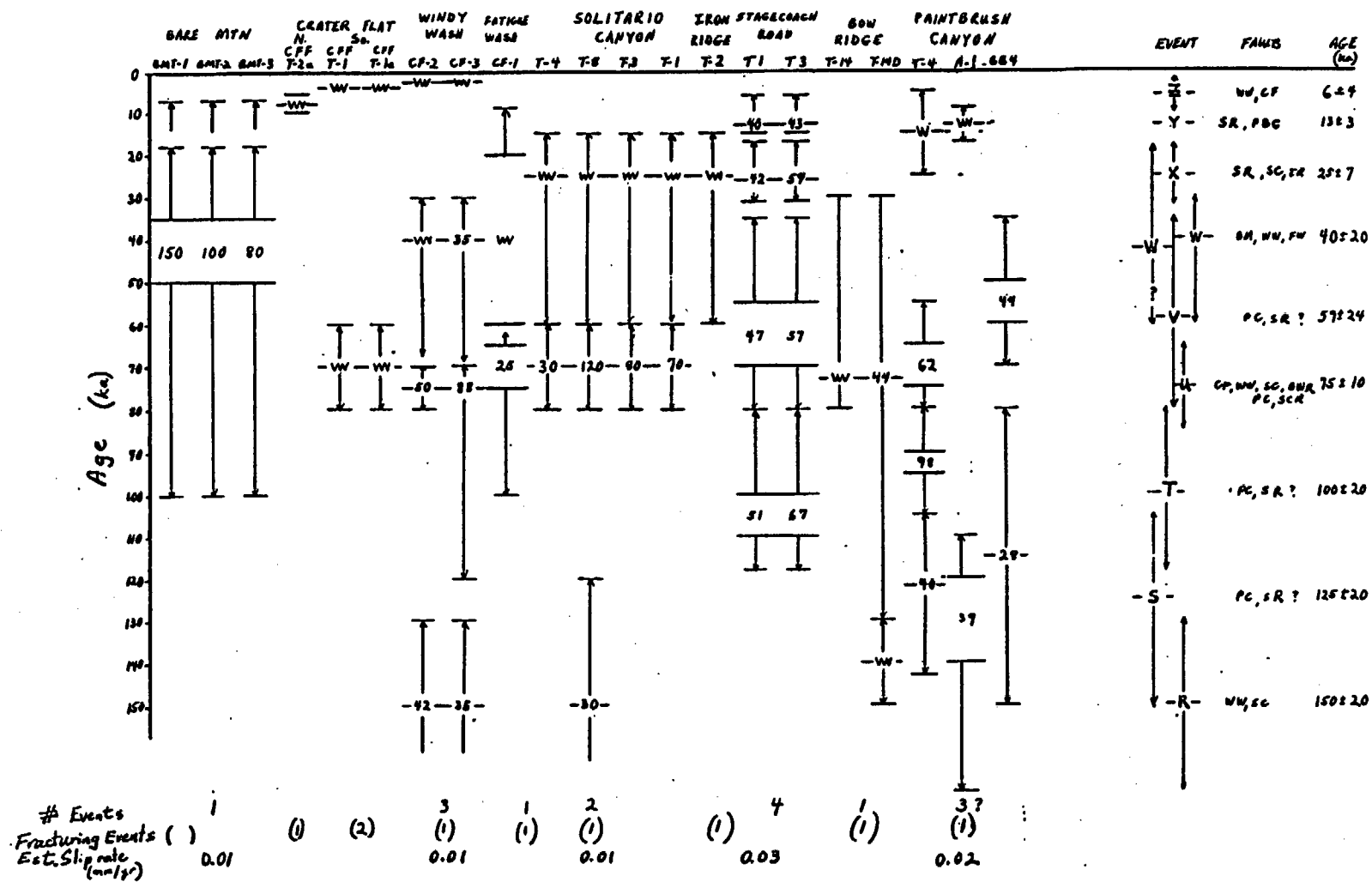


Figure RYA-15

Estimated age and amount (in cm) of late Quaternary displacement for faults in the Yucca Mountain area based on data in USGS (1996). Faults are arranged from west to east; trench numbers under each fault are arranged from north to south. Bars and arrows show full uncertainties in estimate of faulting event at each trench. "w" represents fracturing event (displacement < 20 cm). Age on far right of chart is best estimate for age of grouped event. See text and tables for fault abbreviations.

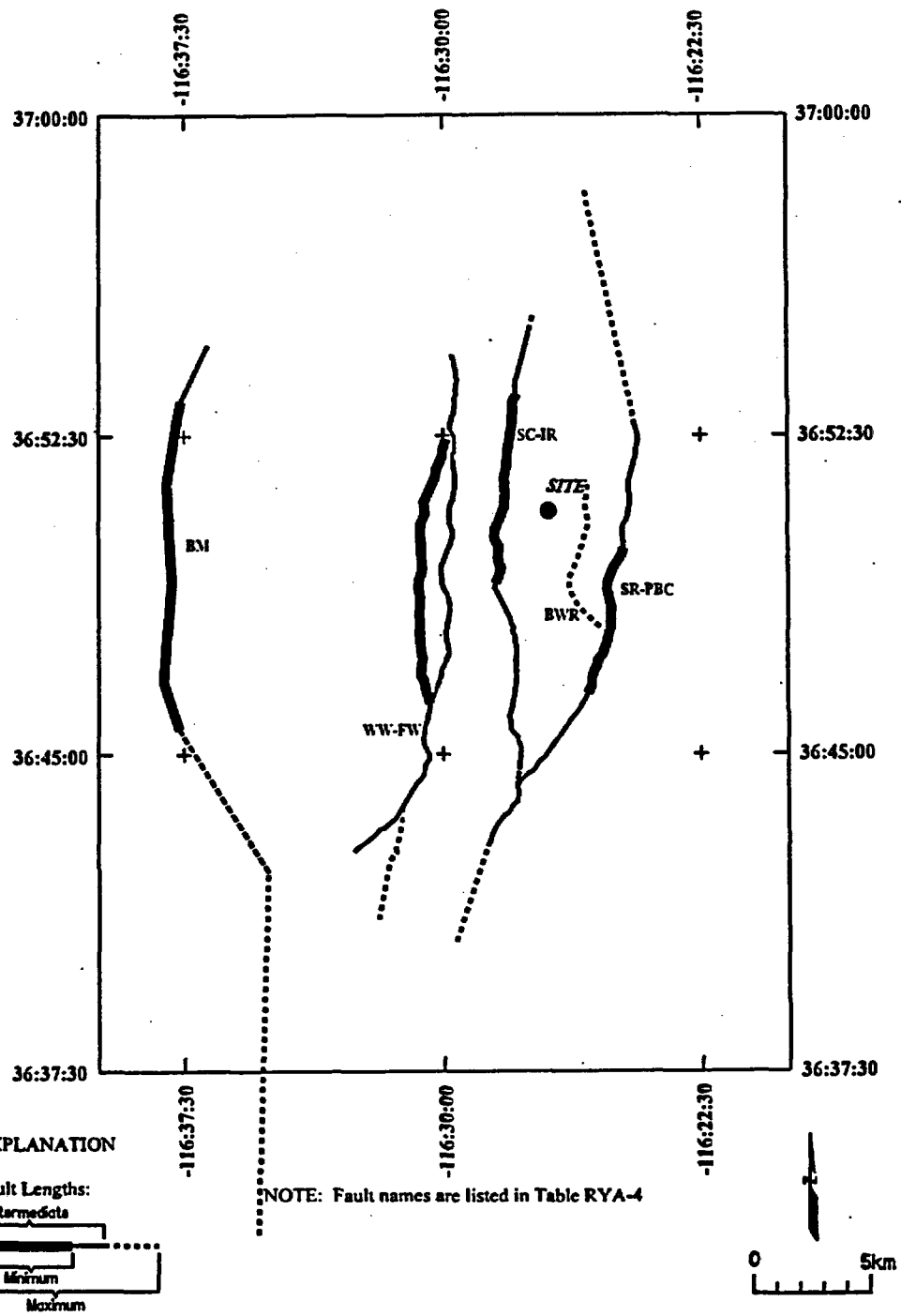
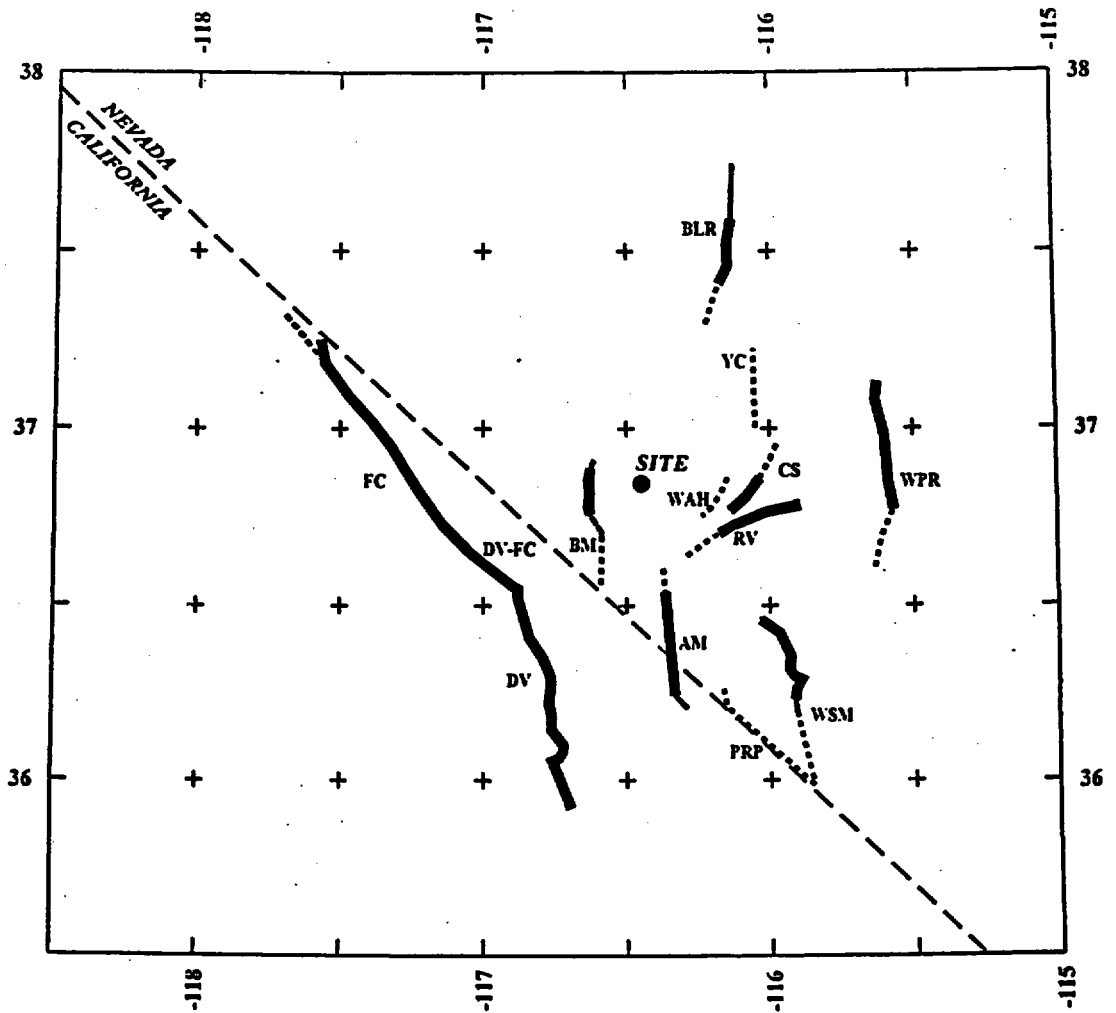


Figure RYA-16 Map showing local fault sources included in the seismic source model



EXPLANATION

NOTE: Fault names are listed in Table RYA-8

Fault Lengths:

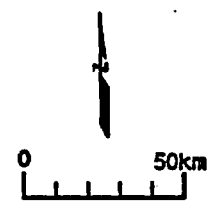
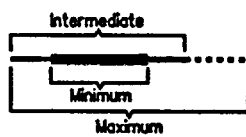


Figure RYA-17 Map showing regional faults included in the seismic source model.

<i>Displacement Capability</i>	<i>Frequency Estimation Approach</i>	<i>Rate Parameter</i>	<i>Average Displacement Per Event</i>	<i>Displacement Distribution</i>
--------------------------------	--------------------------------------	-----------------------	---------------------------------------	----------------------------------

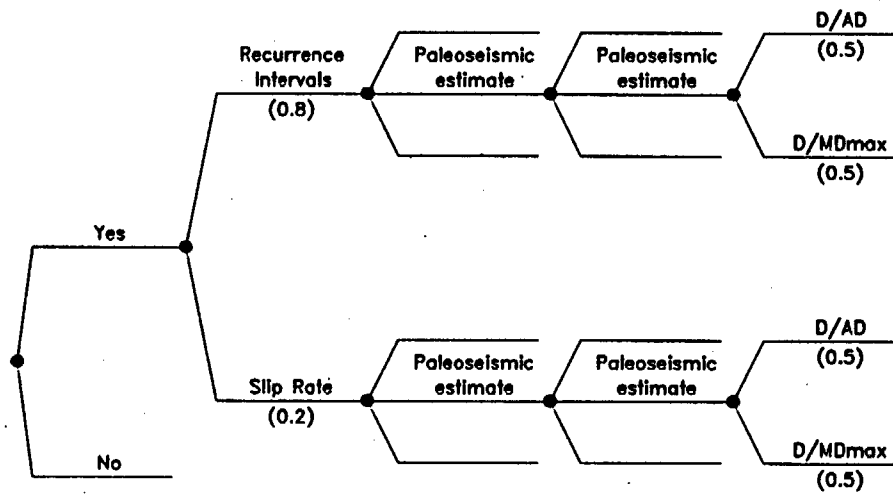


Figure RYA-18 Logic tree used to characterize fault displacement at sites with Quaternary data

<i>Displacement Capability</i>	<i>Frequency Estimation Approach</i>	<i>Dcum</i>	<i>Slip Rate Estimate</i>	<i>Average Displacement Per Event</i>	<i>Displacement Distribution</i>
--------------------------------	--------------------------------------	-------------	---------------------------	---------------------------------------	----------------------------------

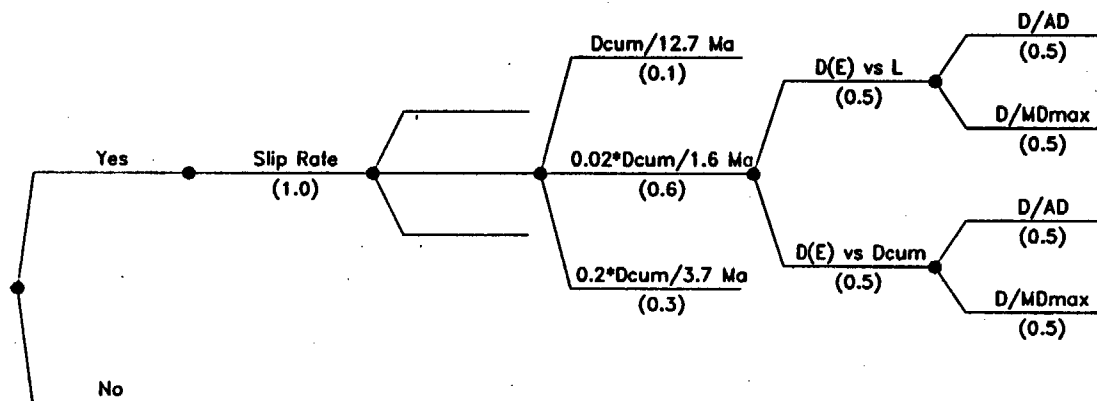


Figure RYA-19 Logic tree used to characterize fault displacement at sites without Quaternary data

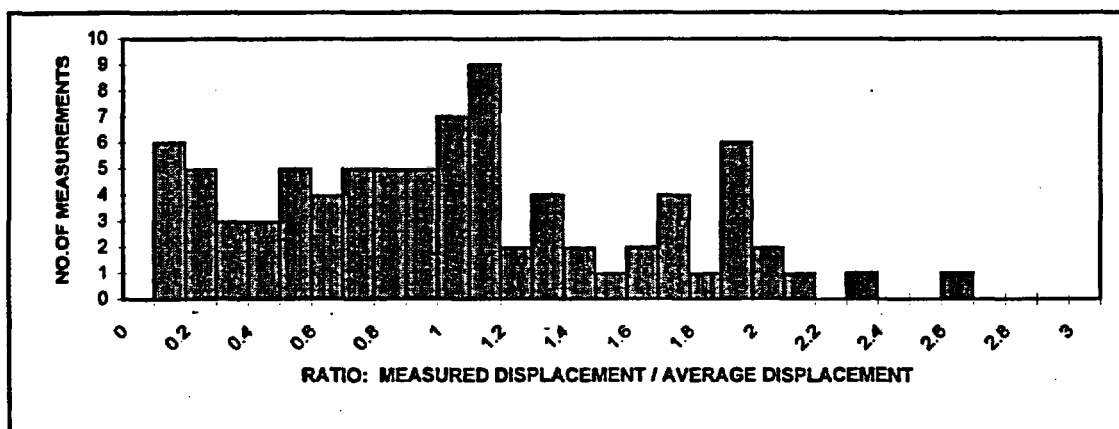
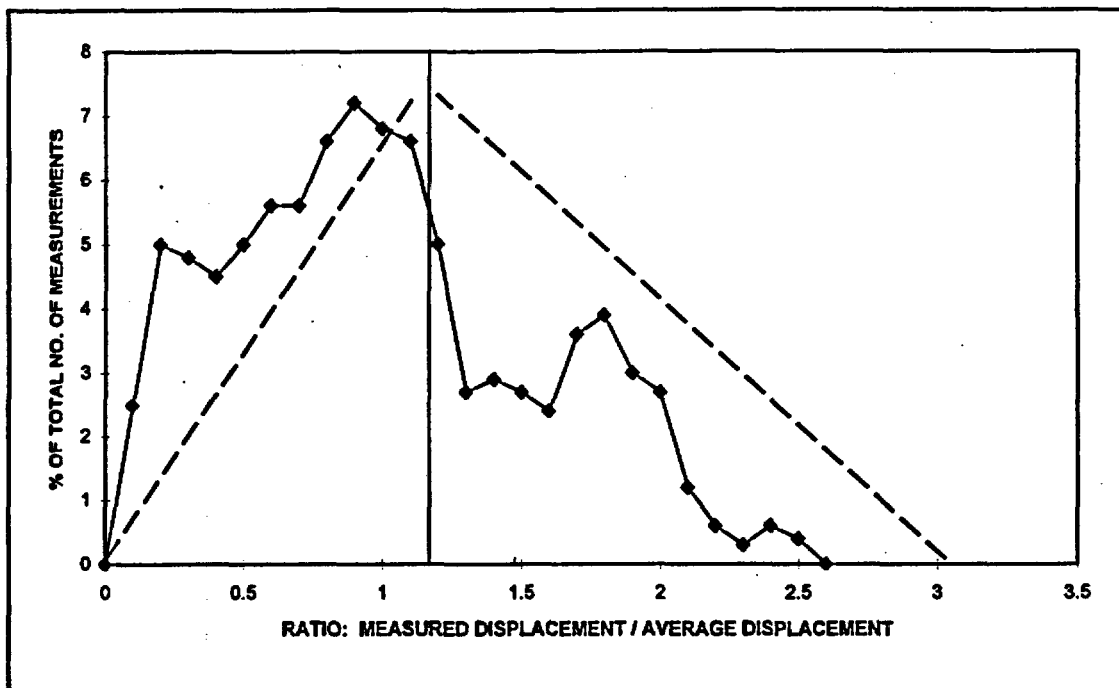
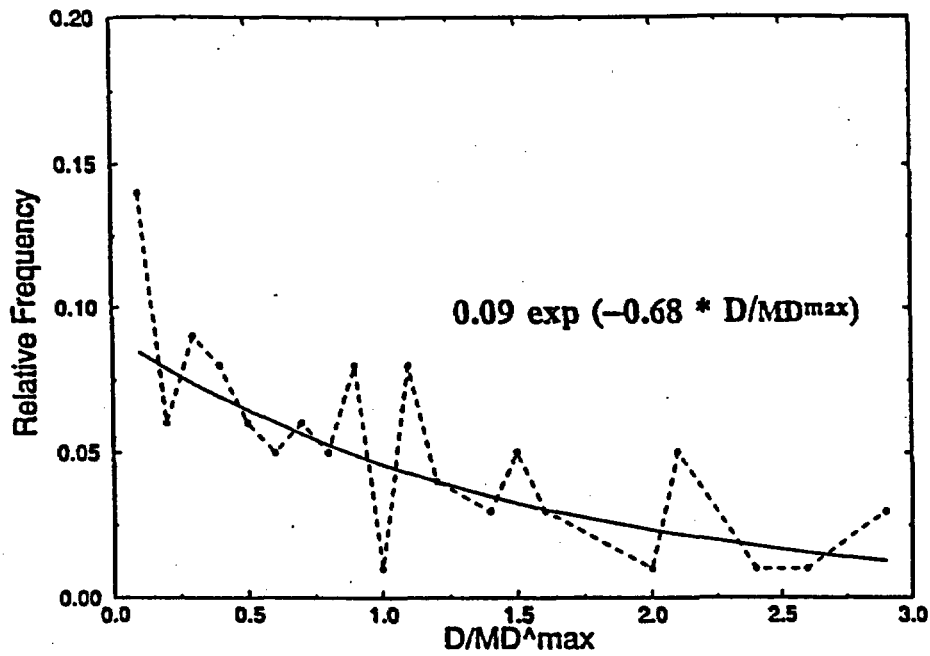


Figure RYA-20 Plots developed by DFS showing event-to-event variability in displacement relative to average displacement per event at a location along a fault based on data from paleoseismic investigations in the Yucca Mountain area

Variability of Displacement at a Point PDF



CDF

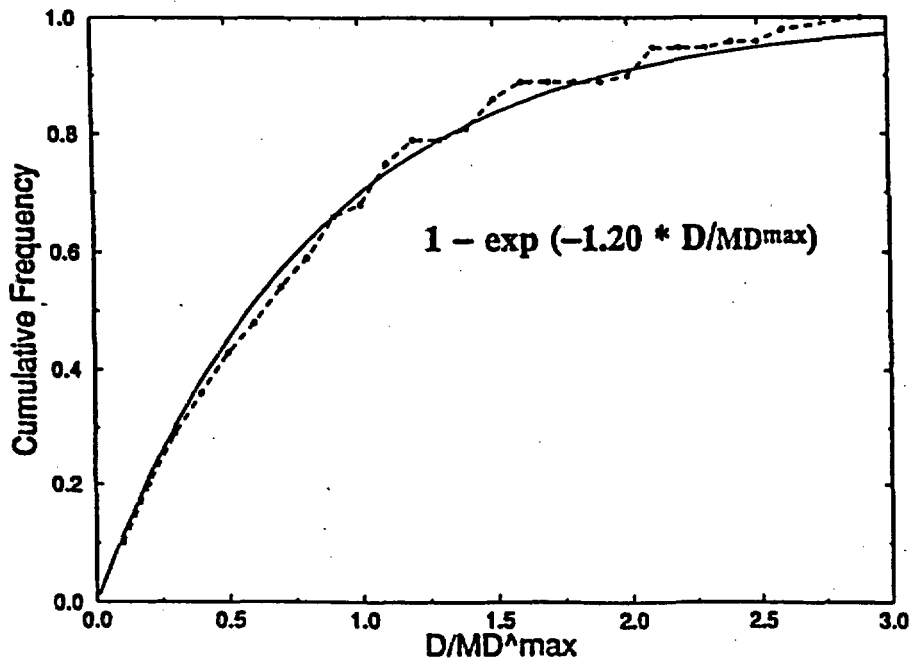


Figure RYA-21 Probability density function (PDF) and cumulative distribution function (CDF) for 80 measurements single-event displacement, normalized to Md^{\max} for the corresponding fault, from 19 trenches in the Yucca Mountain area as developed by the AAR team

ELICITATION SUMMARY

KENNETH D. SMITH, RONALD L. BRUHN, AND PETER L.K. KNUEPFER

TABLE OF CONTENTS

1.0 TECTONIC SETTING AND MODELS	SBK-1
1.1 TECTONIC SETTING	SBK-1
1.2 TECTONIC MODELS.....	SBK-3
1.2.1 Volcanic Models	SBK-3
1.2.2 Low-Angle Fault Models.....	SBK-6
1.2.3 Lateral Shear Models	SBK-7
1.2.4 High-Angle Faulting Model.....	SBK-8
1.3 EVALUATION OF TECTONIC MODELS	SBK-9
1.3.1 Oblique Rift Models.....	SBK-9
1.3.2 Regional Dextral Shear Models	SBK-9
1.3.3 Effects of Igneous Dike Injection.....	SBK-10
1.3.4 Utilization of Logic Tree for Tectonic Models.....	SBK-10
2.0 SEISMIC SOURCES	SBK-11
2.1 THICKNESS OF SEISMOGENIC CRUST	SBK-11
2.2 AREAL SOURCE ZONES	SBK-14
2.2.1 Catalogs and Declustering.....	SBK-17
2.2.2 Maximum Background Earthquake	SBK-19
2.3 REGIONAL FAULT SOURCES.....	SBK-21
2.3.1 Maximum Magnitude	SBK-23
2.3.2 Recurrence.....	SBK-24
2.4 LOCAL FAULT SOURCES	SBK-25
2.4.1 Fault Combinations and Simultaneous Ruptures	SBK-28
2.4.2 Maximum Magnitudes.....	SBK-31
2.4.3 Recurrence.....	SBK-34
3.0 FAULT DISPLACEMENT CHARACTERIZATION.....	SBK-36
3.1 INTRODUCTION.....	SBK-36
3.2 FAULTS HAVING DOCUMENTED QUATERNARY DISPLACEMENT	SBK-37
3.2.1 Earthquake Approach.....	SBK-37
3.2.1.1 Characterization of Principal Faulting Potential	SBK-37
3.2.1.2 Characterization of Distributed Faulting Potential	SBK-39
3.2.2 Displacement Approach.....	SBK-39
3.2.2.1 Frequency of Displacement Events	SBK-39
3.2.2.2 Characterization of Amount of Displacement	SBK-42
3.3 FAULTS WITHOUT DOCUMENTED QUATERNARY DISPLACEMENT	SBK-44
3.3.1 Earthquake Approach for Distributed Faulting.....	SBK-45
3.3.1.1 Fault Orientation Weighting	SBK-45

TABLE OF CONTENTS

3.3.1.2	Frequency of Distributed Faulting Events	SBK-47
3.3.1.3	Distribution of Distributed Faulting Displacement at a Point	SBK-49
3.3.2	Displacement Approach for Distributed Faulting.....	SBK-50
3.3.2.1	Frequency of Displacement Events	SBK-50
3.3.2.2	Distribution of Distributed Faulting Displacement	SBK-52
4.0	REFERENCES.....	SBK-53

TABLES

Table SBK-1	Regional fault sources
Table SBK-2	Other regional faults
Table SBK-3	Local faults
Table SBK-4	Fault Displacement Hazard Characterization Data, Points 1, 2, And 9
Table SBK-5	Fault Displacement Hazard Characterization Data, Points 3-8
Table SBK-6	Trenching Data Used To Develop Distributions For Displacement Per Event

FIGURES

Figure SBK-1	Logic tree for tectonic models
Figure SBK-2	Map showing boundaries of seismic source zones, Model A
Figure SBK-3	Map showing boundaries of seismic source zones, Model B
Figure SBK-4	Logic tree for characterizing areal source zones
Figure SBK-4	Logic tree for characterizing areal source zones (Cont'd.)
Figure SBK-5	Map showing regional faults included in the seismic source model
Figure SBK-6	Map showing local fault sources included in the seismic source model
Figure SBK 7	Logic tree for local faults
Figure SBK 7	Logic tree for local faults (Cont'd.)

TABLE OF CONTENTS

- Figure SBK-8 Logic tree to characterize site with Quaternary displacement
- Figure SBK-9 Probability of surface rupture versus magnitude computed from data presented in Pezzopane and Dawson (1996)
- Figure SBK-10 Normalized slip along strike from five normal fault ruptures developed by ASM team from data in Wheeler (1986)
- Figure SBK-11 Fractal displacement profiles developed by R. Bruhn (SBK) to predict distribution for the ratio of displacement at a point to the maximum displacement in an earthquake.
- Figure SBK-12 Distribution of U/U_{ap}
- Figure SBK-13 Distribution of U/U_a
- Figure SBK-14 Distribution of U/U_m
- Figure SBK-15 Logic tree to characterize sites without Quaternary displacement
- Figure SBK-16 Probability of induced distributed slip as a function of distance from the rupture and hanging wall/footwall location computed from the data presented in Pezzopane and Dawson (1996). Curves show logit regression fits to data.
- Figure SBK-17 Probability density function (sketched) for probability of initiating joint or fault displacement in an underground excavation. PDF is based on data summarized in Figure 2, page 2 of Brady (1990).
- Figure SBK-18 Cumulative Probability Function $P(U/D_m)$. See text Section 3.2.3 for discussion of derivation and use. Crosses represent data points from Yucca Mountain faults, solid line is a sketched fit to the data values.

APPENDICES

- APPENDIX SBK-1 SUMMARY OF SEISMICITY REPORTS
- APPENDIX SBK-2 SUMMARY OF SEISMICITY
- APPENDIX SBK-3 POTENTIAL ANALOGS TO FUTURE SITE AREA ACTIVITY

ELICITATION SUMMARY
KENNETH D. SMITH, RONALD L. BRUHN, and PETER L.K. KNUEPFER

1.0
TECTONIC SETTING AND MODELS

1.1 TECTONIC SETTING

The Yucca Mountain site lies within the Walker Lane tectonic domain (Wright, 1976, 1989; Stewart, 1988) of the southern Great Basin of the Basin and Range province. The site area is slightly more than 300 km (200 miles) from the nearest tectonic plate boundary, the San Andreas fault. The San Andreas fault is the primary structure for strain accommodation between the Pacific and North American tectonic plates. Whereas the San Andreas fault is a transform system, the Basin and Range forms an extensional tectonic regime west of the plate boundary (Wright, 1976, 1989; Stewart, 1978). The extension in the Basin and Range, which began in the late Oligocene and culminated in the Miocene, has been expressed in a variety of deformation mechanisms involving high-angle strike-slip and normal faulting and low-angle normal faulting. Along with Miocene extension came episodes of widespread ignimbrite deposition and associated basaltic volcanism. Little evidence is available in the Yucca Mountain area to evaluate whether low-angle normal faulting remains a primary mechanism for deformation; however, all large historical Basin and Range earthquakes have occurred on moderately to steeply dipping faults (R. Smith, SSC Workshop 4).

Seismogenic faulting, which is distributed throughout the western United States, partly accommodates the relative motion between the North American and Pacific Plates. Global geodetic data and kinematic models indicate that about two-thirds of the total plate motion strain budget of about 48 mm/yr is accounted for on the San Andreas fault system in California and other offshore faults (Minster and Jordan, 1987; Ward, 1990; DeMets and others, 1990; Humphreys and Weldon, 1994). The remaining one-third of the Western United States strain budget is accounted for east of the Sierra Nevada and west of the Colorado Plateau and Rocky Mountains, in the Basin and Range province.

The Sierra Nevada block moves northwestward at a rate of about 12.1 ± 1.2 mm/yr relative to fixed North America east of the Rocky Mountains (Minster and Jordan, 1987; Argus and Gordon, 1991; Dixon and others, 1995). Movements on active faults in the Basin and Range province accommodate this portion of the overall strain budget through a variety of mechanisms. A significant component of lateral slip on faults in the eastern California shear zone is required in these kinematic models and has been measured in geologic and geodetic studies (e.g., Minster and Jordan, 1987; Argus and Gordon, 1991; Dixon and others, 1995). This strain is also accounted for from faulting in the Central Nevada and Intermountain seismic belts (Minster and Jordan, 1987; Argus and Gordon, 1991; Dixon and others, 1995; Smith and Sbar, 1974). Some of these estimates, especially geodetic and Quaternary fault studies, are based on very recent deformation and may not be representative of the total Cenozoic deformation.

The most active fault zones in the Holocene within a 300-km radius of Yucca Mountain mostly are farther than 100 km from the site itself. These faults are located within the Eastern California shear zone (Dokka and Travis, 1990). The Eastern California shear zone is a northwest-trending zone of faults that accommodate right-lateral motion along a north-northwest-trending zone through the Mojave Desert that connects with right-lateral and normal faults along the eastern Sierra Nevada. Geologic and geodetic data from the Mojave Desert indicate a rate of from 5 to more than 8 mm/yr of regional dextral shear that has been active since middle Miocene time (Dokka and Travis, 1990; Savage and others, 1990; Richard, 1992).

East of the Sierra Nevada and north of the Mojave block, the Eastern California shear zone is defined by three major northwest-trending right-lateral fault zones: the Death Valley-Furnace Creek-Fish Lake Valley, the Hunter Mountain-Panamint Valley, and the Owens Valley fault zones. Geologic studies indicate an average late Quaternary slip rate of 1 to 4 mm/yr on the Hunter Mountain-Panamint Valley and Owens Valley fault zones (Burchfiel and others, 1987; Lubetkin and Clark, 1988; Zhang and others, 1990; Beanland and Clark, 1994), and as much as 4 to 8 mm/yr for the Death Valley-Furnace Creek-Fish Lake Valley fault zones (Klinger and Piety, 1996; Reheis and Dixon, 1996; Reheis and Sawyer, 1997). Thus, the Eastern California shear zone accounts for most of the strain budget of the plate boundary system east

of the Sierra Nevada, leaving a small portion to be allocated to faults in central Nevada and western Utah. Known and suspected Quaternary faults east of the Death Valley-Furnace Creek-Fish Lake Valley fault zone and in the Yucca Mountain vicinity have slip rates on the order of 0.001 to 0.01 mm/yr (Whitney and others, 1996); this is as much as three orders of magnitude less than slip rates on the faults in the Eastern California shear zone (Piety, 1995; Keefer and Pezzopane, 1996).

1.2 TECTONIC MODELS

Tectonic models are used to constrain fault geometry and behavior and to estimate the characteristics of buried seismogenic sources. First the tectonic model classification scheme of O'Leary (1996) is discussed and evaluated for completeness. We then modify O'Leary's approach and evaluate the likelihood that each model exists and controls the behavior of active seismic sources. We evaluate the potential for activity of known and inferred faults, and the manner in which the dimensions of these seismic sources may be controlled by structures inherited from geologic history, or formed under the current tectonic regime. We partly follow the terminology of O'Leary (1996) for clarity and convenience. However, the terms 'pure shear' and 'simple shear' as used by O'Leary to classify tectonic models do not accurately describe the regional tectonics, because these terms are restricted to descriptions of two-dimensional strain fields whereas the strain field at Yucca Mountain is three-dimensional.

1.2.1 Volcanic Models

Several models have been proposed in the literature that relate the development and continuing activity of faults in the Yucca Mountain area (the site fault area discussed later) to volcanic processes. We review the completeness of these models in the following sections. However, we conclude that none of these models explains the nature of active tectonism in the study area.

Caldera Model. Calderas in the Yucca Mountain region formed during Miocene tectonism. Their principal importance today could be in providing insight into the relationship between the current stress field and the orientation of Miocene structures, which could influence geometry of active faults or help localize background seismicity. Many of these structures

that formed in the Miocene also display evidence of Quaternary movement (Fridrich, 1997). The Timber Mountain-Oasis Valley caldera complex in the northern Nevada Test Site (NTS) is the primary source area for the volcanic tuffs that form Yucca Mountain (O'Leary, 1996; Day and others, 1996b). Carr (1990) proposed that these Miocene calderas extended south of the Timber Mountain complex into Crater Flat. His interpretation was based in part on the presence of basaltic volcanism in Crater Flat, but this volcanism has been shown since to have occurred much later than the Miocene (CRWMS-MOC, 1996). Also, faults at Yucca Mountain interpreted by Carr (1990) as caldera ring fracture systems have since been identified as tectonic faults rather than volcanic features (Fridrich, 1997; O'Leary, 1996). Furthermore, Crater Flat has been interpreted from gravity profiling (Langenheim, SSC Workshop 1), magnetic studies (Stamatakos and others, 1997), and geologic investigation (Fridrich, 1997) to be a pull-apart basin filled with interbedded volcanics and sediments. Given this history, we conclude that calderas do not control the active structures in the Yucca Mountain area and assign zero weight to this caldera model.

Rift Model. The north-south-trending Kawich-Greenwater trough (Carr, 1984, 1990) is an older (originated pre-10 Ma) rift structure that likely established most of the regional faulting patterns and may provide the tectonic framework for current activity (Carr, 1990, Figure 8). As proposed by Carr (1984), this rift zone is identified by a nearly north-south-striking gravity low that extends from the northern NTS and the calderas of the Timber Mountain-Black Mountain-Oasis Valley complex, through Yucca Mountain and eastern Amargosa Valley, to end southwest of Death Valley in the Greenwater volcanic center of the Greenwater Range. This rift includes a number of older (15 Ma) silicic volcanic centers as well as younger basaltic cones and flows, including the Crater Flat basalts of Pliocene and Quaternary age. Aeromagnetic data (Majer, SSC Workshop 4) show several additional buried basaltic sources in the proposed rift south of Yucca Mountain near Highway 395 and near Lathrop Wells (CRWMS-MOC, 1996; Langenheim and others, 1993; Stamatakos and others, 1997). Other buried volcanic sources south of Lathrop Wells may also be interpreted from the aeromagnetic data (Langenheim and others, 1993). Evidence for a throughgoing structure associated with these potential field anomalies is also shown by the near similarity in behavior of north to east-northeast faults mapped in Miocene tuffs in the Pahute Mesa area north of Timber Mountain and the faults at Yucca Mountain south of the Miocene caldera complex.

The isostatic gravity data (Ponce, 1993; Majer, SSC Workshop 4; O'Leary, 1996) show a north-south-striking, buried graben structure extending south of Yucca Mountain into Amargosa Valley. This southern part of the Kawich-Greenwater rift zone is named the Amargosa trough by O'Leary (1996). This graben, which is about 40 km long and about 20 km wide, forms a boundary between regional tectonic domains in southern Nevada (O'Leary, 1996). Quaternary scarps of the Ash Meadows fault system (Piety, 1995) define the east side of the graben. The west edge extends north along the east margin of Bare Mountain and western Crater Flat. The southwest end of the graben parallels the Death Valley fault system, and the southeast end abuts the northern Pahrump Valley fault system near Stewart Valley. The Rock Valley fault zone appears to be truncated along the east margin of the graben, where the north-trending gravity gradient (the so-called Gravity fault) extends into Jackass Flat. The concentration of recent and historical seismicity that parallels the Rock Valley fault zone also is interrupted at this locality (K. Smith, SSC Workshop 2). However, additional northeast-trending scarps in Amargosa Valley to the southwest may be related to the Rock Valley fault (R. Anderson and others, 1995b). We suggest that in the Miocene the graben structure accommodated strain transferred from the Las Vegas Valley shear, to the east, through the southern Great Basin. From this evidence it can be interpreted to represent a failed rift system. This is one in a family of oblique rift models that we consider to be an integral part of the Yucca Mountain tectonic setting (Figure SBK-1).

Dike Injection. As an alternative to faulting, injection of basaltic dikes may accommodate extension and strain in Crater Flat (Parsons and Thompson, 1991a, 1991b). Thus, periods of volcanism may retard normal faulting in Crater Flat. Given this mechanism of accommodating extension, the strain rates estimated from the fault slip data would tend to underestimate the total local tectonic strain rate. Alternatively, volcanic processes may trigger faulting. For the Scenario U (ash event) of Pezzopane and others (1996a), several faults in the Crater Flat basin and at Yucca Mountain have been interpreted to have ruptured concurrently with volcanic activity at about 70 ka. Evidence includes volcanic ash in several trench sites on the Solitario Canyon, Windy Wash, Fatigue Wash, South Crater Flat, and Bow Ridge faults. Elsewhere, subsurface movement of volcanic material has been associated with a series of moderate-sized earthquakes in the Mammoth Lakes-Bishop area of California (Appendix SBK-3). These earthquakes have generated secondary and possibly primary surface faulting and most likely local ground motions on the order of 0.5 g. The presence of Pliocene and Quaternary

volcanics in Crater Flat indicates that dike injection accommodates some of the extensional strain in the Yucca Mountain area. A dike injection model may be a mechanism to passively account for strain through emplacement of basaltic material in the lower crust, and it may further trigger, or at least be associated with, earthquakes by movement of volcanics into the shallow (brittle) crust. In our evaluation of tectonic models, we consider it very likely that dike injection affects strain rates (Figure SBK-1); the principal effect of this on seismic source characterization is our treatment of volcanically related sources separately from primary faulting on local sources, as discussed in Section 2.4.1.

1.2.2 Low-Angle Fault Models

All of the low-angle fault models suggested for the Yucca Mountain region include a detachment of some kind. It is possible that an old (Oligocene-Miocene?), currently inactive and deformed, detachment structure underlies the region, with the Bare Mountain fault offsetting it beneath Crater Flat (Scott, 1990; Fridrich, 1997). Large detachments structures most likely operated in the Miocene, as evidenced by the Florspar Canyon fault system (Hamilton, SSC Workshop 3); the evidence of the unroofing of Bare Mountain (Ferrill and others, 1996a); and the presence of middle to lower crustal rocks in metamorphic core complexes. Possible locations of detachments could occur beneath Crater Flat and Yucca Mountain at the Paleozoic-Tertiary contact, the Precambrian-Paleozoic contact, or the mid-crustal brittle-ductile transition (i.e., base of the seismogenic crust).

Wernicke (1995) suggests that detachment faults may be independent seismogenic sources of large lateral extent, and are capable of generating significant earthquakes. However, we do not consider detachment faults to be independent seismic sources at Yucca Mountain because: (1) geologic mapping indicates that the Paleozoic-Tertiary contact in the Yucca Mountain vicinity is not a regional detachment (Fridrich, 1997; Simonds and others, 1995); (2) there is no evidence for shallow detachments on seismic lines (Brocher, SSC Workshops 2 and 3) or in drill holes; (3) background seismicity in the vicinity shows no evidence for activity on low-angle faults; (4) although detachments occur in the surrounding regions and throughout the Basin and Range, most of these are old (Tertiary); (5) evidence shows that large normal-faulting earthquakes in continental crust occur only on high-angle faults throughout the world (Jackson and White, 1989); and (6) the Little Skull Mountain earthquake occurred on a

steeply dipping (60 to 65 degrees) structure (Appendix SBK-2). The evidence indicates that even if a detachment exists under Yucca Mountain, it has a negligible probability of being seismogenic. Thus, we do not model a detachment as a seismogenic source capable of producing earthquakes above the background. In considering the possibility that one or more detachments exist, we use such structures only to constrain down-dip width and fault areas. Specific detachment geometries are discussed in the context of the assessment of dip and area of local faults.

1.2.3 Lateral Shear Models

Lateral shear models propose regional dextral shear along either a buried throughgoing shear zone in the crust or discrete, transcurrent fault populations that are characteristic of the Walker Lane belt (Wright 1976, 1989; Stewart, 1988). In this model, the primary deformation in the southern Great Basin is ultimately driven by the large throughgoing right-slip faults of the Death Valley-Furnace Creek-Fish Lake Valley, Hunter Mountain-Panamint Valley, and Owens Valley fault systems. These latter faults account for most of the approximately 12 mm/yr of the plate motion strain budget in the western Basin and Range of southern Nevada and eastern California. Slip rates on structures east of the Eastern California shear zone are significantly less than those on the primary transcurrent faults. Indeed, the small strain budget east of the high-angle faults of the Eastern California shear zone can be accommodated readily by a combination of high-angle transcurrent, normal, and oblique-normal slip faults, as supported by paleoseismic and seismicity data. This provides further evidence that it is not necessary to invoke low-angle faulting to support our conclusion that no large-area, low-angle normal faults or detachments are active.

Schweickert (SSC Workshop 3) proposed a buried regional shear zone in the Crater Flat area that had some components of the transtensional nappe model of Hardyman and Oldow (1991). This model is given an extremely low weight because: (1) conclusive evidence for offset geologic features along the postulated shear zone is lacking; (2) a 240-km-long shear zone with kilometers of offset should have scarps or other direct evidence at the surface for most of its length, and no such evidence exists.

1.2.4 High-Angle Faulting Model

The tectonic model that we consider best explains present tectonism in the Yucca Mountain region includes a component of lateral shear related to deformation through the Walker Lane belt (Stewart, 1988). The Death Valley-Furnace Creek-Fish Lake Valley fault system accommodates most of the regional strain through a slip rate of 4 to 8 mm per year (Klinger and Piety, 1996; Reheis and Sawyer, 1997). Slip rates on faults east of the Furnace Creek fault system are 2 to 3 orders of magnitude less. Short-period focal mechanisms (Rogers and others, 1991) show a predominance of high-angle strike-slip faulting (Pezzopane and others, 1996b), although normal mechanisms form a significant percentage of the database. The best evidence for high-angle faulting from a moderate-sized event in which the causative fault plane can be isolated is the 1992 M 5.6 Little Skull Mountain earthquake. It occurred on a steeply dipping structure (60 to 65 degrees; K. Smith, SSC Workshop 2), which is consistent with teleseismic, short-period, and regional faulting mechanisms for the event (K. Smith, SSC Workshop 2). Also, detailed aftershock relocations support the interpretation of faulting on a high-angle structure (K. Smith, SSC Workshop 2). Well-constrained short-period focal mechanisms for earthquakes in the Rock Valley fault zone in 1993, which incorporated supplemental portable instrument data, show high-angle strike-slip faulting, which is consistent with mapping and trenching studies of Coe and others (1996b). Mapping of faults and dips of surface exposures for faults in the Yucca Mountain area also suggest that these are high-angle structures (Simonds and others, 1995).

In the high-angle fault model, structures in the vicinity of Yucca Mountain are interpreted to be planar, and the Rock Valley fault and a buried structure near Highway 95 within the Amargosa trough to the west act as an accommodation zone, which truncates the local Yucca Mountain faults at their south ends. The Yucca Mountain faults in this model are part of a half-graben, which is bound on the west side by the Bare Mountain fault. The faults are predominantly normal-slip structures having a left-lateral component of displacement that accommodates transtensional strain.

1.3 EVALUATION OF TECTONIC MODELS

The logic tree (Figure SBK-1) simplifies the tectonic models described above, focusing on those elements that may affect the geometric characteristics of other faults or may act as independent seismic sources. We categorize the models of O'Leary (as discussed above) into two classes: (1) oblique rifting and (2) regional dextral shear. The oblique rifting class is preferred (probability 0.99; Figure SBK-1), because it is more encompassing of volcano-tectonic structures in the Yucca Mountain region and includes the possibility of discrete strike-slip faults in addition to oblique-normal-slip and normal-slip faults.

1.3.1 Oblique Rift Models

Oblique rift models focus on the inferred presence or absence of low-angle faults (detachments, and the possibility of rolling-hinge tectonism [Hamilton, SSC Workshop 3]). All of these models include steeply to moderately dipping faults. The logic tree is structured to consider the presence of a detachment fault in two ways: (1) as a structural discontinuity that may control the depth, extent, or geometry (listric or planar) of steeply dipping faults; and (2) as a separate seismic source (active or inactive) to be considered in the seismic sources analysis. Given the lack of evidence for one or more detachment faults acting as a controlling structure in the present tectonic environment, as noted above, we apply extremely low weights (total of 0.01 to the three) to the likelihood of single or multiple detachments or Hamilton's rolling hinge model. In addition, as discussed above, we assign a likelihood of zero that a detachment structure can behave as an independent seismic source.

1.3.2 Regional Dextral Shear Models

These models are divided into two types: those with and those without a low-angle transtensional detachment. Steeply dipping faults are included in both types, but in the former model (transtensional nappe) there is a large-area, horizontal to subhorizontal detachment fault that transfers strike-slip movement into the middle to upper crust. Given the lack of evidence for the transtensional nappe model of Schweickert (SSC Workshop 3), we assign an extremely low weight (0.01) to this possibility.

1.3.3 Effects of Igneous Dike Injection

Quaternary volcanism may accommodate some of the extension in Crater Flat, and therefore decrease the slip rates on the Bare Mountain and other faults (Parsons and Thompson, 1991a, 1991b). Thus we include dike injection as an element in tectonic models. We do not consider the dike injection model as a separate branch on the logic tree for tectonic models (Figure SBK-1); instead, it is included as an option in both the oblique rift and dextral shear zone models. Given that dike injection has occurred in the Crater Flat area during the Quaternary, it clearly plays a role in any tectonic model. We assign a high likelihood (0.95) that dike injection affects slip rates on the local faults, as we discuss further when considering the seismic potential of volcanic sources. We further consider the significance of volcanic dikes in explaining the low late Quaternary slip rates on the Bare Mountain and possibly the local Yucca Mountain faults as well as acting as a trigger for simultaneous fault ruptures. We also address the question of whether fractures that produce aligned dikes, such as the Crater Flat cones, are also separate seismic sources, perhaps capable of generating earthquakes during magma injection at depth (see discussion of Mammoth Lakes area sequence Appendix SBK-3).

1.3.4 Utilization of Logic Tree for Tectonic Models

We have interpreted a most likely tectonic model—steep to moderately dipping faults in an oblique rift system—consistent with the tectonic history of the Yucca Mountain area and the kinematics of currently active structures. Most other models are given negligible or extremely low weights as descriptors of the active tectonic regime. Furthermore, we consider that the tectonic models principally control down-dip geometry of the local faults. For example, all of the detachment models (single detachment, multiple detachment, rolling hinge) imply that site faults merge at shallow or intermediate crustal depths; the interpretation affects the likelihood that faults coalesce down dip, as well as the width of individual and coalesced faults. Given that this is the only kind of effect we consider credible for the nonplanar-fault tectonic models (i.e., we do not add additional seismic sources for different models, as discussed below), we do not explicitly incorporate different tectonic models as branches of a logic tree. Instead, our weighting of tectonic models provides a framework for our evaluation of the geometry of local fault sources.

Seismic source zones are identified throughout the 100-km-radius surrounding the site, as shown on Figures SBK-2 and -3. Regional and local fault sources are identified (Figures SBK-5 and -6); areal seismic source zones (Figures SBK-2 and -3) serve as background zones to these fault sources. The maximum magnitude associated with each seismic source zone is a function of several variables. Within 100 km, the regional and local fault sources that can produce potential maximum earthquakes above the maximum background were identified and are characterized separately. Assigning the maximum background magnitudes for the areal source zones is based on the observations of the largest earthquakes in the Basin and Range that did not have reported primary surface faulting. The largest of these events occurred in Montana in 1925. This event is less relevant to the Yucca Mountain area because of the thinner seismogenic crust in southern Nevada. In the local site vicinity, extensive geologic mapping has identified small-displacement events—as small as cracking events. Because of the enhanced resolution in the local site area (including Yucca Mountain and Bare Mountain), it is interpreted that a fault source comparable to those mapped has not remained undetected. Therefore, a smaller maximum magnitude is assessed for the areal source zone in the local site vicinity. Earthquake recurrence relationships were developed for each areal source zone based on observed seismicity data. For areal sources containing regional and local fault sources, seismicity associated with these fault sources was removed before calculating recurrence parameters for the source zone. Recurrence relationships for regional and local fault sources were developed from fault-specific geologic data.

2.1 THICKNESS OF SEISMOGENIC CRUST

The thickness of the seismogenic crust in the southern Great Basin is assessed both on the depth distribution of seismicity from the earthquake catalog and the record of estimated hypocentral depths for main shocks in the Basin and Range Province (SDO Team, SSC Workshop 4). We use the depth distribution of main shocks in the Basin and Range, an extensional environment, rather than considering California analogs because of the clear difference between the tectonic regimes. We also recognize that there is some variation in the tectonic styles and crustal thickness within the Basin and Range itself (Smith and Sbar, 1974).

For example, deformation in the southern Great Basin, dominated by the strike-slip systems of the Death Valley-Furnace Creek-Fish Lake Valley, Hunter Mountain-Panamint Valley, and Owens Valley fault zones (Dixon and others, 1995; Piety, 1995), may be quite different from the tectonics of the Central Nevada Seismic Belt in north-central Nevada and the extension associated with the basaltic volcanics of the Eastern Snake River Plain in the northern Basin and Range. Also, there is some evidence that large main shocks in the Basin and Range ($M > 6.8$) may initiate at greater depth than may be indicated purely by analyzing the depth distribution of earthquakes in the recent period of seismic monitoring (SDO Team, SSC Workshop 5).

Doser and Smith (1989), Doser (1986, 1988), and the SDO Team (SSC Workshops 4 and 5) analyzed the depth of initiation and rupture of the historical, $M > 6.5$ earthquakes in the Basin and Range. These analyses show that earthquakes in this magnitude range may initiate as deep as 20 km. For example, modeling the rupture processes of the Borah Peak earthquake from teleseismic and regional seismograms indicates seismic energy radiating from the fault plane at depths as great as 22 km, whereas the Borah Peak hypocenter has been determined to be at about 16 ± 4 km (R. Smith, SSC Workshop 4). Many of the hypocentral depths for Basin and Range events were calculated from teleseismic recordings (exclusively for the older events), using techniques that require good velocity information in the middle crust to reduce uncertainties in the estimate. Clearly, of the large events in the Basin and Range, the Borah Peak event of October 1983 would provide the best data for evaluating the depth distribution of faulting, yet there were no near-source recordings (< 20 km) for this earthquake.

In contrast, recent moderate-sized earthquakes in the Basin and Range, in particular in the central and southern Great Basin, have shown a shallower depth distribution of aftershock activity and initiation of main shock rupture. The resolution of the estimates of hypocenter depth for many of these sequences is provided by high-quality regional and local data that were not available for the large historical Basin and Range events. Recent moderate-sized earthquakes in the central and southern Basin and Range include the June 1992, M 5.6 Little Skull Mountain, Nevada (Harmsen, 1993b; K. Smith, SSC Workshop 3); May 1993, M 6.1 Eureka Valley, California (Peltzer and Rosen, 1995; Massonnet and Feigl, 1995); and July 1986, M 6.3 Chalfant Valley, California, earthquakes (Appendix SBK-3). A sequence of moderate-sized earthquakes in the Mammoth Lakes area of California in the 1980s was well

recorded, but its association with the active Long Valley caldera makes it questionable with respect to evaluating seismogenic depth estimates in nonvolcanic areas. The refined hypocentral depths for these moderate sized earthquakes are: Little Skull Mountain, 11.7 km (K. Smith, SSC Workshop 3; Harmsen, 1993b; Meremonte and others, 1995); Eureka Valley, 11.8 km (Loper and others, 1993); Chalfant Valley, 12 km (Smith and Priestley, 1997). All of these earthquakes initiated near the base of the local seismogenic zone. This conclusion is based on the assumption that the maximum depth of the well-located aftershock activity defines the local base of the seismogenic zone in these areas.

Earthquakes in the southern Great Basin occur primarily between 5 and 15 km in depth (Appendix SBK-1). The distribution is dominated by the Little Skull Mountain sequence, which represents about 20 to 30 percent of the seismicity catalog for the southern Great Basin in the NTS area (Appendix SBK-1). This sequence was confined primarily between 12 and 6 km depth; the deep distribution peaks near the lower edge of the seismogenic zone. The sequence was particularly well recorded, and depth constraints are good. Rogers and others (1987a) showed that seismicity in the southern Great Basin was distributed between about 15 and 2 km, with a gap in activity at about 4 km. This observation has not continued through the period of digital data recording, 1995 through 1997, and may represent mislocations resulting from the misidentification of S-wave arrivals on vertical-component records. Shallow activity has been rare in the recent period but has been observed. The 1993 Rock Valley sequence, an unusually shallow cluster of earthquakes (K. Smith, SSC Workshop 3; Smith and Brune, 1997), generally was confined to less than 3 km depth. These shallow hypocentral depths were confirmed with the installation of near-source (less than one focal depth), three-component digital recorders. Hypocentral depths of about 2 km from the surface were identified in the Shields and others (1995) study for the 1993 Rock Valley sequence.

Rogers and others (1987a) show that most of the seismic energy released in the southern Great Basin occurs at depths less than 12 km, but this observation is based on data from a period (1978-1987) when there was minimal moment release throughout the southern Great Basin. Occasional larger-magnitude earthquakes reportedly nucleated deeper than 15 km; however, many of these events occurred early in the instrumental record, and their hypocenters probably are not well constrained. Nucleation depths of about 16 km have been

reported for several major earthquakes in the Basin and Range province: the 1954 Dixie Valley, Nevada; 1959 Hebgen Lake, Montana; and 1983 Borah Peak, Idaho (all from R. Smith, SSC Workshop 4); all were M 7+ range-bounding, normal-faulting events. Critical to the estimation of maximum moment from a structure is whether rupture can propagate to these depths, which would not necessarily have to correlate with hypocentral depth. Also, slip at these depths may not contribute significant ground motion at the surface.

Our weighting of maximum seismogenic thickness allows us to account for the possibility that larger earthquakes may rupture below the depths indicated by the distribution of well-located regional seismicity and the maximum depth of the seismogenic thickness indicated for the three central and southern Great Basin earthquake sequences listed above. Rupture may extend below the brittle seismogenic zone, because the dynamic strain rate during rupture propagation may be high enough to overcome the frictional conditions in the brittle-to-ductile transition zone that exists in the mid-crust near the base of the seismogenic zone. Under these conditions, rupture propagation may be acceptable in dynamic rheologies that physically do not allow for the initiation of the small- to moderate- sized earthquakes ($M < 6$), which comprise the bulk of the regional seismic catalogs.

The ranges and weightings of seismogenic thickness are interpreted to be the same for all source zones throughout the study area. We define the base of the seismogenic zone as: 12 km, wt. 0.3; 15 km, wt. 0.6; and 17 km, wt. 0.1.

2.2 AREAL SOURCE ZONES

Four primary source zones were delineated for non-fault-specific seismic sources within 100 km of the site (Model A - Figure SBK-2). These are the West Walker Lane, the East Walker Lane the Basin and Range, and a Local Zone within the site area that was not characterized by local faults. These source zones were chosen based on a review of the seismicity reports for the southern Great Basin (Appendix SBK-1) and an interpretation of the seismotectonic implications of the distribution of seismicity in the historical catalog (Appendix SBK-2). These seismotectonic interpretations also affected our evaluation of tectonic models, particularly with regard to neotectonic deformation (Appendix SBK-2). These zones

represent those areas that remain after the areas of regional fault sources have been removed. These areas include the location of potential maximum background and other earthquakes not associated with particular fault sources. The maximum background earthquake and the rate of recurrence for this event are assessed from the activity rates estimated from the recurrence rates of the declustered seismicity in these areas.

In addition, a subregion in the East Walker Lane (Rock Valley) is defined to account for regional variability in seismicity (Model B - Figure SBK-3). The region is defined on the bases of tectonic, geologic, and seismicity rate criteria, as described below. The branch of the logic tree that includes this subregion is assigned a weight of 0.3 (Figure SBK-4), with 0.7 assigned with the interpretation of no subregion.

The Death Valley-Furnace Creek-Fish Lake Valley fault zone defines the boundary between the West Walker Lane and East Walker Lane areal source zones. Defining the western zone as the West Walker Lane is not strictly correct, as it is more appropriately termed the Eastern California shear zone, but we use this terminology. This area includes the active faults and deformation west of the Furnace Creek system. Given that seismic network coverage in this region has been sparse throughout the history of seismic monitoring, we cannot rely on the quality of earthquake locations and hypocentral depth estimates as much as we can for other areas that have denser network coverage and thereby more accurate hypocenter locations.

The East Walker Lane zone is defined on the west by the Furnace Creek system and on the east by a change in tectonic style to a dominantly range-bounding, normal-fault environment (Figures SBK-2 and -5). We include the generally northeast-striking faults of the Sarcobatus Flat region within this source zone, although this particular fault is characterized separately (Figure SBK-5). We attribute the high level of seismicity in this zone to deformation associated with the high slip rate on the Death Valley-Furnace Creek-Fish Lake Valley fault system. Also included in this source zone is the seismicity and northeast-striking faults in the southern and central NTS region, as well as the extension of the Rock Valley fault zone east into the Spotted Range east of NTS. This zone continues south in a general northwest-southeast orientation, with its eastern border defined by the Las Vegas Valley shear zone. We also defined this zone to include only tectonic, or tectonically triggered, earthquakes, avoiding the seismicity catalog problems related to the Basin and Range source zone to the east, where

nuclear testing has been isolated. The East Walker Lane zone accounts for much of the seismicity that trends outboard, to the east, from the Furnace Creek system, as well as most of the northeast-striking fault systems that we interpret to represent neotectonic deformation most likely driven by the strain in the Eastern California shear zone. The most prominent concentration of seismicity in this zone is that associated with the Rock Valley fault zone (Appendix SBK-2). We have also defined the Death Valley area as a subzone within the East Walker Lane zone in our optional configuration (Figure SBK-3). We believe that this subzone may be more likely to produce earthquakes that may cause ground motion on the order of 0.1 g at Yucca Mountain; this is evidenced by the 1992 Little Skull Mountain earthquake. Also, several $M > 3.5$ events have taken place in the Rock Valley fault zone during the past several years, and a general concentration of seismicity is associated with the fault zone. Given this difference in activity during the past tens of years in this subzone as compared to the East Walker Lane zone as a whole, the separation as a subzone enables us to address the possible stationarity of seismicity, although we cannot establish whether this subzone will be a persistent source of activity during a 10,000-year interval.

The Basin and Range zone was established to capture the north- to north-northeast-striking, predominantly low strain rate, range-bounding fault systems within 100 km of the site. We also included the nuclear testing areas of the northern and eastern NTS in this areal source in order to contain explosion-triggered recurrence bias exclusively to the Basin and Range source zone. A subzone was established around Pahute Mesa and Yucca Flat to account for the fundamental problem of separating tectonic earthquakes from explosion-triggered seismicity. These nuclear testing areas may tend to overestimate the hazard by including seismicity that is directly triggered by explosions. Although the triggered earthquakes ultimately may have occurred without underground testing, including them could overestimate the long-term activity rate. That is, the seismicity in this subzone during the period of nuclear testing may not be representative of the long-term tectonic strain rate in the area. To account for this interpretation, we computed activity and b-values only for the periods that preceded nuclear testing. We consider any increase in seismicity in this region during the recent period of testing to be directly related to the testing, but we also recognize that any attempt to remove all of the dependent events would not be representative of the activity rate. Indeed, attempts were made to separate natural from explosion-triggered seismicity in the catalog compilation, yet we are unconvinced that this can be done adequately. Furthermore, the

explosion-triggered seismicity could be a manifestation of tectonic strain, with the explosions representing a triggering stress just as the Landers earthquake was a trigger for the Little Skull Mountain earthquake. To address the uncertainty of adequately accounting for the effect of explosion-triggered seismicity in the NTS we consider two options. The first option is that the aftershock removal process has adequately removed seismicity triggered by the NTS explosions and no adjustment is necessary. This option is assigned a weight of 0.6 (Figure SBK-4). The second alternative is to adjust for the effect of the NTS explosions by removing seismicity within the NTS region post 1950 from the calculation of seismicity rates within the Basin and Range Province. A Pahute Mesa-Yucca zone was defined (Figure SBK-3) that encompasses the area of NTS explosions. All seismicity post 1950 was removed from this area in the calculation of the seismicity rate. This option was assigned a weight of 0.4 (Figure SBK-4).

We also consider the possibility of a background earthquake within the local (site) area. This Local Zone includes the volume not characterized by the recurrence estimates for the local faults themselves: central Crater Flat and the footwalls of the Bare Mountain and Paintbrush Canyon faults. Because the local faults account for most of this volume, we consider the size of the maximum background earthquake in the Local Zone to be less than that for the other areal source zones. This is based simply on the observation, particularly from the distribution of faulting and aftershock activity for the 1986 M 6.3 Chalfant earthquake (our model background earthquake; Appendix SBK-3), that earthquakes of only a limited size could occur in the remaining volume without being accounted for in the recurrence estimates for the local faults. It would be double counting to apply the same magnitude distribution for the maximum background earthquake from the other areal source zones. The weighting for the maximum background earthquake for the Local Zone is: M 6.2, wt. 0.2; M 6.0, wt. 0.6; M 5.6, wt. 0.2.

2.2.1 Catalogs and Declustering

We have used the 100-km catalog developed for this project to assess recurrence (a- and b-values) for areal source zones. Two declustering algorithms were applied to the 100-km combined catalog. Weighting was applied relevant to the stability of the b-value estimates for the subregions. The algorithms, from Veneziano and van Dyck (1985) and Youngs and others

(1987), apply different assumptions in determining the definition of a foreshock or aftershock and therefore behave differently for different regions. The Veneziano and van Dyck (1985) method establishes a baseline activity rate within a given distance from a main shock, then uses this baseline activity to define the local rate. The Youngs and others (1987) method removes dependent events based on several time and distance criteria. The activity rates and completeness levels range significantly within the 100-km region. We consider that earthquakes within the 100-km region follow a power-law distribution in magnitude. The declustering algorithm that returned a distribution that better represented this power-law scaling was considered more efficient in removing dependent events for that region. The Veneziano and van Dyck algorithm appeared to be more stable when applied to the Little Skull Mountain aftershock zone and therefore was weighted higher in the East Walker Lane zone, whereas the Youngs and others method generated smoother recurrence curves when applied to sparse background regions. The weighting listed below and shown in Figure SBK-4 reflects our assessment of the b-value estimates. For the West Walker Lane zone, we weight the Youngs and others declustering algorithm at 0.7, assigning 0.3 weight to the Veneziano and van Dyck algorithm. Our weighting is the opposite for the East Walker Lane zone, for reasons noted above. However, we weight the Youngs and others approach more heavily for the Rock Valley subzone (Youngs and others, 0.7; Veneziano and van Dyck, 0.3). The Basin and Range zone receives weights of 0.4 for the Youngs and others algorithm and 0.6 for the Veneziano and van Dyck approach; identical weights are assigned in the Pahute Mesa-Yucca Flat subzone.

The catalog completeness intervals that we have adopted for assessing earthquake recurrence parameters are based on review of those developed by I.G. Wong (handout to team seismologists at SSC Workshop 4) and on examining the seismicity of the region. The adopted intervals are: M 2.5 to <3.5, 1979 to date; M 3.5 to <4, 1961 to date; M 4 to <5, 1934 to date; M 5 to <6, 1900 to date; M \geq 6, 1880 to date. Furthermore, we considered earthquakes that occurred in close proximity to the regional faults to be associated with those faults. These events were not counted in computing the seismicity rate for the regional zones.

A truncated exponential fit using the maximum likelihood method of Wiechert (1980) was applied to all magnitude distributions. A minimum magnitude of 2.5, where this magnitude

was above the completeness level, was used to determine the b-values and activity rates, otherwise the minimum completeness level was applied.

2.2.2 Maximum Background Earthquake

We define a background earthquake as any earthquake in a non-fault-specific zone that does not display primary surface rupture. Primary surface rupture is defined as surface faulting taking place on the actual fault plane that radiated the seismic energy at depth. DePolo (1994) reported on the maximum background earthquake for the Basin and Range. There is a range of earthquake magnitudes over which primary fault rupture has been observed in the Basin and Range (Pezzopane and Dawson, 1996). Distinguishing primary from secondary faulting from the historical data base (Pezzopane and Dawson, 1996) is difficult because of the variability of instrumental seismicity throughout the historical period and the details of the observations following many of these earthquakes. Actually, isolating the fault plane at depth may require a detailed analysis of the aftershock zone. Also, some interpretation is involved in distinguishing primary from secondary surface faulting based on field data.

The principal factor that affects the development of primary surface faulting is the distribution of seismic moment release with depth. For example, primary surface displacement was observed for the 1950 M 5.6 Fort Sage, California, earthquake, but no primary or secondary surface faulting was mapped following the 1992 M 5.6 Little Skull Mountain earthquake; events of the same magnitude. Although no instrumental record of sufficient quality to resolve the moment release at depth was available for the Fort Sage event, we consider that faulting must have been shallow, based on its surface expression. This is in contrast to the 1992 Little Skull Mountain earthquake, for which faulting was confined to between 12 and 6 km depth (K. Smith, SSC Workshop 2). It is not surprising for such depth ranges that there was no expression of surface faulting for this earthquake. Therefore, there is a range of earthquake magnitudes over which primary faulting may occur, but above which primary faulting will always be seen. If primary rupture has occurred on faults of Quaternary age, then we assume that these structures have been identified in our assessment of specific fault sources described below, and listed in Tables SBK-2 and -4. Our weighting of the magnitude of the maximum background event is developed to account for the distribution of magnitudes

over which no primary surface rupture is observed and for the incompleteness of the historical record and the subjectivity in the interpretation of primary versus secondary surface faulting.

The largest earthquake exhibiting no primary surface faulting in the historical record in the Western United States was the 1925 M 6.6 Clarkston, Montana, event (dePolo, 1994). This earthquake, which occurred in an area having a greater crustal thickness than does the southern Great Basin, is anomalous in the compiled record of background earthquakes (dePolo, 1994). We have taken the possibility for this event into account by assigning a low probability for an M 6.6 maximum event for our areal source zones, although we consider the tectonic and structural environment of the Montana area to be quite different from that of the southern Great Basin. We further consider that the 1986 M 6.3 Chalfant Valley earthquake is a better analog for a maximum background earthquake in the southern Great Basin (Appendix SBK-3). This earthquake produced significant surface faulting, but none that can be considered to have occurred on an extension of the causative fault plane from seismogenic depth to the surface; we interpret that no primary faulting occurred. Although right-lateral offsets of as much as 10 cm were observed along the White Mountains fault zone, a major Holocene fault zone (Lienkaemper and others, 1987), the Chalfant main shock rupture did not occur on this fault. Some of the fault slip, particularly small-event slip, seen in trench data for the local site faults at Yucca Mountain, may represent this type of secondary faulting.

Another moderate-sized earthquake in the southern Great Basin that we consider an analog for the background earthquake is the M 6.1 May 1993 Eureka Valley, California, earthquake. Although smaller than the Chalfant event, it also produced surface displacements that were most likely not primary surface faulting. In contrast to strike-slip faulting during the Chalfant earthquake, the Eureka Valley earthquake showed nearly pure normal slip on a structure oriented north-south (Peltzer and Rosen, 1995; Massonnet and Feigl, 1995). Given the similarity in faulting style, this earthquake is considered more representative of the surface expression of moderate-sized, normal-faulting earthquakes ($M < 6.5$) that may occur in the site area.

The maximum background earthquakes for the West Walker Lane, East Walker Lane, Basin and Range, Rock Valley, and Pahute Mesa-Yucca Flat zones and subzones are: M 6.6, wt.

0.1; M 6.4, wt. 0.2; M 6.3, wt. 0.5; and M 6.2, wt. 0.2. The maximum background earthquake for the Local Zone is: M 6.2, wt. 0.2; M 6.0, wt. 0.6; M 5.6, wt. 0.2.

2.3 REGIONAL FAULT SOURCES

Fault sources within 100 km of Yucca Mountain were identified based on Piety (1995), R. Anderson and others (1995a; 1995b), McKague and others (1996), Keefer and Pezzopane (1996), and Pezzopane (1996). Of the faults identified as relevant to ground shaking hazard (Pezzopane, 1996), potentially seismogenic faults were identified as those showing evidence of displacement since mid-Quaternary time (730 ka) or associated with historical seismicity (Table SBK-1). In many cases, only a small part of a potentially seismogenic fault is identified as having middle or late Quaternary slip; however, in assessing maximum magnitude, we treat the entire mapped fault as a seismogenic zone. We did not characterize as seismic fault sources a number of structures identified as Type I faults (McKague and others, 1996). These are summarized in Table SBK-2, along with our bases for not including them. The areal extent of a fault source was estimated based on the uncertainties of the fault dip (see below) and the potential combinations of related local structures that may be included in the recurrence for that source. For example, we combined the Buried Hills and Emigrant Valley South faults for analysis. We also consider multiple combinations of behavior of the Death Valley-Furnace Creek-Fish Lake Valley faults, as discussed below. The uncertainty in the length and down-dip width of the regional fault sources was established to account for any uncertainty in the locations of small-magnitude earthquakes in the regional catalog, which could be removed before estimating the background seismicity rates.

The location and extent of each fault source are given on Figure SBK-5; data on each fault source are compiled in Table SBK-1, with sources and annotations to clarify the bases for interpretations included in the table. Uncertainties in fault extent are included in the fault lengths in Table SBK-1. One example of a fault length that involves considerable uncertainty is the northern extent of the Ash Meadows fault zone. The fault is shown by Piety (1995) as extending north to the vicinity of the Rock Valley fault. However, the Ash Meadows fault is collinear with the so-called Gravity fault (Fridrich, 1997) to the north, and the inferred sense of downthrow is consistent, suggesting continuity of the structures. North of the Rock Valley

fault the gravity anomaly continues, but the scarps that characterize the Ash Meadows fault are not present. Therefore, two alternative models for the northern extent of the Ash Meadows fault are considered in the analysis, with the longer fault (100 km) incorporating the Gravity fault north of the Rock Valley fault. Given the lack of evidence for Quaternary slip on this part of the possible fault, we assign a low weight (0.1) to this total fault length.

Approaches to evaluating maximum magnitude and recurrence for these regional fault sources follow. Detailed notes regarding individual faults are included with Table SBK-1. Many long faults, such as the Death Valley and Furnace Creek sources, probably rupture only in part during individual earthquakes (i.e., are segmented, either in a persistent or non-persistent manner). However, we find insufficient data to adequately characterize or model segmentation explicitly on these structures. The Southern Death Valley, Death Valley, Furnace Creek, and Fish Lake Valley faults form a nearly continuous zone of right-lateral shear with a total length on the order of 300 km. It is possible that the fault system behaves as a coherent unit, comparable to portions of the San Andreas fault, although it is much more likely that the constituent faults rupture independently. In considering the combined faults, we recognize the Death Valley normal fault as a pull-apart structure within a right-lateral shear system (which we will call the Death Valley system for simplicity). We assess possible combinations of faults explicitly in our analysis. Although there is mapped continuity among all of the faults of the Death Valley system (e.g. Jennings, 1994), it is extremely unlikely that they rupture together (Klinger and Piety, 1996). First, the faults have distinct structural and geomorphic signatures (Klinger and Piety, 1996); second, the connection between the Furnace Creek and Fish Lake Valley faults has not ruptured in the Holocene (Reheis and Sawyer, 1997), suggesting these two faults have not ruptured continuously; and third, there is no historical analog where a strike-slip fault has ruptured through a major pull-apart of the dimensions of Death Valley. Thus we assign a probability of 0.01 to a single linked fault system. We next consider possible sub-linkages, including the Death Valley-Southern Death Valley fault (0.05 likelihood the faults rupture together, again because of lack of historical analogs and distinct geomorphic signature) and the Furnace Creek-Fish Lake Valley system (0.05 likelihood they rupture together, given the large step-over between them and the apparent difference in timing of paleoseismic events, from studies of Reheis and Sawyer, 1997, and Klinger and Piety, 1996). These two linked fault zones are not conditional; that is, Death Valley and Southern Death Valley can behave as linked faults in our model regardless

of the behavior of the Furnace Creek and Fish Lake Valley faults, and vice versa. Most weight (0.94 for each fault), however, is assigned to the faults rupturing independently. Details of assessments for each fault are shown in Table SBK-1.

2.3.1 Maximum Magnitude

For regional fault sources, we used various approaches for estimating maximum magnitudes based on various fault rupture parameters (Table SBK-1). These included regression relations based on surface rupture length, surface rupture area, maximum displacement, and average displacement (Wells and Coppersmith, 1994). Approaches were weighted on a fault-specific basis depending on the input needed and the data available for each fault.

Fault length is based principally on the total mapped length of a fault. In many cases, only part of the fault has documented Quaternary slip (e.g., Pahrump fault has Quaternary slip on about 18.5 km of a 50- to 65-km-long fault; Table SBK-1). We treat these faults by placing a low weight on the Quaternary section and a higher weight on the total fault length, reasoning that the *maximum* magnitude would be produced by a rupture of the entire fault, even if that apparently has not happened in the middle to late Quaternary. For the Pahrump fault, then, we assign a weight of 0.3 to the short, Quaternary fault length, and a weight of 0.7 to the longer, total fault length (which is uncertain between 50 and 65 km).

Fault area is computed by multiplying fault length by down-dip width. We compute down-dip width from the fault dip and the thickness of the seismogenic zone. We lack specific information on dip for most of the regional faults. Thus, we assign fault dip based on type of faulting: normal faults (45 degrees weighted 0.1, 60 degrees weighted 0.8, and 70 degrees weighted 0.1); strike-slip faults (70 degrees weighted 0.2, 90 degrees weighted 0.8); and oblique-slip faults (60 degrees weighted 0.2, 70 degrees weighted 0.6, and 90 degrees weighted 0.2). Our assessment of the thickness of the seismogenic crust was discussed in section 2.1.

We obtain displacement values from surface fault studies appropriate to the individual faults. In general, we use data from paleoseismic studies (trenches, mapping) to identify the largest single-event displacement reported along a fault in estimating maximum (surface)

displacement. Given that the regressions used to compute magnitude from displacement are based on surface observations (Wells and Coppersmith, 1994), use of surface data is appropriate. Although one cannot be certain that trenches have identified the true maximum coseismic surface displacement on a fault, the fact that trenches generally are sited at locations that show evidence of large displacement supports our use of these data. Average displacement is obtained from the along-fault variations in slip during a particular event, rather than from measurement of average displacement during repeated ruptures at a site, because it is the former that is the basis of the regression equations. We require at least 5 points, preferably more, along a fault to estimate average displacement, following the observations of Hemphill-Haley and Weldon (1996).

2.3.2 Recurrence

Earthquake recurrence for fault sources is assessed based on the slip rate on the fault as converted to seismic moment rate using fault area and from estimates of paleoseismic return times when available. The slip rate approach generally is preferred because of significant uncertainties in interval data, both because of dating uncertainties and because the paleoseismic events documented on each of the faults for which we can adequately assess return periods are not all equal in size. For example, one event may have an interpreted displacement of 1.5 m, whereas others at the same trench site show 0.2 to 0.5 m. It is quite likely that not all of these paleoseismic events are the size of the maximum earthquake (*characteristic earthquakes* in the sense of Schwartz and Coppersmith, 1984). In particular, the return periods may overestimate the frequency of occurrence of maximum earthquakes. Quaternary slip rates are preferred over longer-term Tertiary slip rates because the stress regime has changed for many of the structures, especially at and near Yucca Mountain. However, even slip-rate data are unavailable for some of the faults, such as the Buried Hills-Emigrant Valley South fault. In these cases, we constrain the order of magnitude of the slip rate by comparing the topography of the range along which the fault is found with the topography of other ranges in the Basin and Range for which slip rates of bounding faults are known. We further constrain the slip rate if information is available that alluvial geomorphic surfaces of a certain age (for example, middle Quaternary) are or are not displaced. All slip rate estimates are applied to the fault as a whole, even if the estimate comes from a single point; in general, we have insufficient data to characterize the regional faults in more detail.

Both the characteristic (Youngs and Coppersmith, 1985) and truncated exponential (Berrill and Davis, 1980) recurrence models are used to model the relative frequency of various size earthquakes for a given slip rate. We assign a higher weighting to the characteristic type of distribution for range-bounding faults, reasoning that these faults are most analogous to the Wasatch fault and other major faults that fit characteristic distributions. We apply a higher weighting to the truncated exponential distribution for faults that comprise numerous, discontinuous surface traces, reasoning that these are not the continuous kinds of structures on which characteristic earthquakes generally have been recognized. We assign the weighted average b-value obtained for the areal source in which a fault is located to the recurrence curves derived for faults, as there are insufficient earthquakes associated with individual regional fault sources to compute meaningful local b-values. These assessments are listed in Table SBK-1.

In developing recurrence relationship for the local sources we assume that the maximum magnitude assessments described in Section 2.3.1 are the central value for the characteristic magnitude interval (e.g. Youngs and others, 1987). The characteristic events are assumed to be uniformly distributed in the magnitude range $M_{\max} \pm 1/4$, such that the upper limit of the recurrence relationship is $M_{\max} + 1/4$. For the exponential recurrence model the upper limit is also set at $M_{\max} + 1/4$. When the overall rate of earthquake occurrence is specified by the recurrence interval of surface-rupturing earthquakes, this recurrence rate was assumed to apply to earthquakes of magnitude greater than or equal to $M_{\max} - 1/4$.

2.4 LOCAL FAULT SOURCES

We consider faults within the Crater Flat domain of O'Leary (1996) separately. Data are summarized in Table SBK-3 for all faults and fault combinations to which we assign non-zero weights as being independent seismogenic structures. These include Bare Mountain, North Crater Flat, South Crater Flat, Windy Wash, Fatigue Wash, Solitario Canyon, Iron Ridge, Bow Ridge, Paintbrush Canyon, and Stagecoach Road faults as well as the hypothesized Highway 95 fault (we refer to all but the Bare Mountain and hypothesized Highway 95 faults as the Yucca Mountain—YM—faults).

One issue concerning the Bare Mountain fault that emerged during the PSHA workshops is that the late Quaternary slip rate is less than the summed slip rates across the YM faults. If the Bare Mountain fault is the master structure, and the YM faults are antithetic or secondary, then the slip rate on the Bare Mountain fault should equal or exceed the sum of slip rates on the YM faults. This is a paradox only if one assumes that the 120-kyr of record on the Bare Mountain fault is representative of the average slip rate during the 500 kyr or more of record on the YM faults. However, additional events on the Bare Mountain fault during a 100-kyr period would increase its slip rate to a level comparable to or even greater than the YM faults. With faults such as these, which have extremely long recurrence intervals, one may need 500 kyr or more of paleoseismic record to represent the average slip rate; this is not available for the Bare Mountain fault. Second, some percentage of the extension across the master fault in this area may be accommodated by volcanism and dike injection in the lower crust in Crater Flat, which we consider a very likely scenario (as discussed in the section on tectonic models). This would reduce the slip rate across the master fault, although it may not reduce the slip rate across the antithetic faults. Clearly, several Quaternary volcanic events have accommodated extension in this area. Third, much of the slip on the YM faults occurred during the "ash event," which apparently did not rupture the Bare Mountain fault. If it was, indeed, tied to volcanism, which we interpret as the most likely explanation, then perhaps this unique event should be subtracted from the tectonic strain rate represented by the YM faults for comparison with the Bare Mountain fault. In that case, the slip rates are comparable.

We also evaluated the following mapped faults in terms of the likelihood they generate independent seismic events: Abandoned Wash (no Quaternary displacement, although some secondary cracking possible); Drill Hole Wash (no Quaternary slip); Dune Wash (no Quaternary slip); Ghost Dance (no primary Quaternary slip); Midway Valley (no primary Quaternary slip); Sundance (no Quaternary slip); and Yucca Wash (no evidence for existence). In several cases we interpret faults as having produced no primary Quaternary slip. The Ghost Dance fault is particularly important in this regard. Taylor and others (1996a) describe paleoseismic studies along the Ghost Dance fault, and additional information was made available to us during SSC Workshops 2, 3, and 4. We interpret the results of these studies as follows: evidence for ground cracking during the Quaternary is equivocal along the Ghost Dance fault: if there has been ground cracking, it produced minimal or zero surface

displacement; net displacement across the fault in the middle and late Quaternary has been undetectable, based on the detailed mapping by Day and others (1996a), which shows no surface scarps or offsets, and the evidence from surface-exposure dating of Whaleback Ridge that indicates exceptionally low rates of surface erosion. Thus we believe that the likelihood is negligible that the Ghost Dance fault produces independent seismic events above the maximum magnitude assigned to the Local Zone. Our arguments regarding other mapped faults not included in Table SBK-3 are similar.

Several other structures are hypothesized to exist in the Yucca Mountain vicinity; these were discussed by various experts during SSC Workshop 5. We evaluated each of these possible structures, and concluded either that the hypothesized structure does not exist, or that the maximum earthquake would be within the range of activity defined for the areal source zones. These include a volcanic seismic source (except for the possible link between volcanism and the ash event, considered below); a buried fault that aligns along the cones of Crater Flat; and a cross fault trending northwest across Crater Flat. The former involves earthquakes directly caused by basaltic fissure development and extensional events. We use the evidence of R. Smith and others (1996) to argue that such volcanic sources produce maximum earthquakes ($M \sim 5.5$) below the maximum magnitude we have assigned to the Local Zone. There is no evidence that a buried fault controls the alignment of Black, Red, and Little Cones in Crater Flat. Given the detailed mapping that has been carried out to describe tectonic activity and identify Quaternary fault scarps in Crater Flat, we would expect that if a north-northeast-trending fault existed and were active it would be recognized. No such fault has been recognized, although it is hypothesized in the Rift Model discussed above. We conclude that it cannot be any more active than the cones themselves, indicating no activity in middle or late Quaternary (post the ca. 1 Ma age of the cones). Finally, no evidence supports a hidden or buried strike-slip fault trending northwest across Crater Flat. Little space is available for this or any other structure to be hidden among or beneath the Yucca Mountain faults. Lacking surface expression, such a fault, if it exists, must produce earthquakes below the threshold of surface faulting. We conclude that we have captured all such earthquakes within the magnitude distribution for the Local Zone, and by including a smaller maximum background earthquake to account for such an event in the site area.

2.4.1 Fault Combinations and Simultaneous Ruptures

The possibility that some faults are linked or coalesce at depth and could rupture together during individual earthquakes is considered for the local fault sources based on similarities in rupture behavior or deformation patterns and possible along-strike or down-dip linkages. These are shown on Figure SBK-6 (Table SBK-3). The possible ruptures of the Yucca Mountain faults with each other and with the Bare Mountain fault constitute one group of such linkages. The chance that all local faults (Bare Mountain and YM faults) rupture together is considered, but given a negligible weight, because there is no paleoseismic evidence for simultaneous events involving the Yucca Mountain faults and the Bare Mountain fault. Indeed, the available stratigraphic and geochronologic evidence is inconsistent with simultaneous ruptures on Bare Mountain and all the other faults. Because of likely down-dip structural linkages among the faults, a rupture linkage cannot be precluded, and we note that at least one Bare Mountain rupture also may have involved minor movement on two or more of the block-bounding faults (event W of Pezzopane and others, 1996a). However, combinations of Bare Mountain and other faults are not explicitly assessed in our analysis, because the rupture of other faults appears to have been secondary, and we consider the simultaneous rupture of all local faults to be a negligible possibility.

We define terms as follows.

- A. **Coalesced faults.** These are faults that branch upward from a common master fault at seismogenic depths. The geometries of coalescence were summarized by Fridrich during SSC Workshop 5; we adopt his approach with minor modifications. We consider a single coalesced master fault for simplicity; we deal with other combinations through our analysis of down-dip area.
- B. **Linked faults.** These are faults mapped as independent structures (with distinct names) and separated by generally short intervals without mapped surface traces, yet having sufficient geometric continuity to make it reasonable to infer that they are linked below the surface as throughgoing structures. We consider three combinations: Paintbrush Canyon + Stagecoach Road + Bow Ridge; Solitario Canyon + Iron Ridge; and South Crater Flat + Windy Wash + Fatigue Wash. Another interpretation of the Solitario Canyon fault is that it can be linked with the Stagecoach Road fault for a few events (within Pezzopane and others' (1996a) scenarios), but the potential seismic contribution already is encompassed by other combinations considered explicitly.

- C. Simultaneous rupture. This is a rupture on more than one fault (as mapped at the surface) that occurs either as the result of a single earthquake or, more likely, as subevents during an earthquake that teleseismically would be considered a single event. In effect, a simultaneous event is one in which ground motion is contributed by the subevents, but they are spaced so closely in time as to be contained within the same seismogram. In our analysis this concept is applied principally to the so-called ash event, Scenario U.

Having resolved that all the YM faults and Bare Mountain fault do not rupture simultaneously in an earthquake, we next address fault coalescence and simultaneous ruptures. First, we consider whether all local faults (except Bare Mountain) are cut off by an active detachment. The evaluation is dependent on the tectonic model. We assign zero weight to the possibility of a shallow detachment as an active seismogenic structure and to a deeper detachment as an active seismogenic structure, even though one or both of these may exist within the present tectonic regime. Our reasoning is that, Wernicke's (1995) argument notwithstanding, all major earthquakes in the Basin and Range have occurred on crustal-penetrating faults, even if shallow structures were inferred in the vicinity from seismic reflection profiling. Thus, in our evaluation, these hypothesized detachment structures affect only down-dip fault extent, which we address separately.

Next we evaluate the likelihoods that all the YM block-bounding faults are coalesced, linked, or independent (Figure SBK-7). The first possibility is that all sole into a detachment between 5 km and the base of the seismogenic crust, a model-driven possibility to which we assign a likelihood of 0.01, in keeping with our evaluation of tectonic models discussed above. Although the seismic reflection data of lines YMP-1 and -2 do not resolve structure at that depth (Brocher and others, 1996), and the best substantiation for a moderate-depth detachment comes from the cross sections produced by Ferrill and others (1996a), the geophysical data provide little evidence to support such a structure.

The second possibility is that all of the YM block-bounding faults are planar or near-planar but coalesce at depth, in either one or two master faults. This is more allowable than the detachment models, given surface fault geometries and dips. However, lacking any direct evidence of fault coalescence, we consider this possibility still very unlikely; we assign it a weight of 0.09.

We distribute the remaining likelihood between two end members--four linked block-bounding planar faults (assigned a weight of 0.4) and planar faults behaving independently (assigned a weight of 0.5). For each fault considered individually, we further assess whether the fault acts as an independent primary source. We assign likelihoods less than 1 for both the Iron Ridge (assigned a weight of 0.1 as an independent seismic source) and Bow Ridge (assigned a weight of 0.4 as an independent seismic source) faults, as discussed in Table SBK-3. In evaluating the alternatives of linked or independent faults, our preferred approaches were to consider fault geometries and the history of linked ruptures (i.e., is it possible that two colinear faults, such as Paintbrush Canyon and Stagecoach Road, have ruptured together some or all of the time?). Most of the scenarios described by Pezzopane and others (1996a) argue for complex interactions among faults in terms of overlapping ages of rupture events. Many combinations of behavior are possible, and independent activity is the most likely behavior (although complex linkages are considered). We simplify the possibilities by restricting ourselves to the two end members and assigning a slightly higher weight to independent fault ruptures. The front part of the logic tree for our local fault models is shown on Figure SBK-7; remaining steps follow from the data in Table SBK-3.

Finally, we consider the likelihood that ruptures on all the faults or combinations of faults have been simultaneous. Given the uncertainties in the dating available from the paleoseismic studies (an inherent aspect of working with infrequent surface faulting events in an arid environment), it is possible to use the rupture scenarios of Pezzopane and others (1996a) as one extreme, and independence of every paleoseismic event as the other extreme. The intimate stratigraphic association of Scenario Event U with ash, apparently derived from an eruption of the Lathrop Wells Cone, perhaps about 70 ka, suggests one possible simultaneous rupture that is tied to volcanic eruptions in the Crater Flat area. We find it unlikely that even this "ash event" represents a true simultaneous rupture: some exposures show reworked ash, whereas others seem to have direct airfall, which suggests that not all ash-filled fractures opened simultaneously; even if events are closely spaced in time sufficiently to appear simultaneous from a stratigraphic point of view, it is highly unlikely that the events were simultaneous from a seismic point of view, given numerous examples such as the Mammoth Lakes earthquakes of 1980 or the Dixie Valley and Fairview Peak earthquakes of 1954. It nonetheless is a possibility for the maximum-magnitude earthquake that has been (and could

be) experienced within the site area. We apply low weighting to this possibility and tie recurrence of such an event principally to the recurrence of Crater Flat volcanism as described in the Probabilistic Volcanic Hazard Analysis (CRWMS-MOC, 1996). We also apply an unusual recurrence curve to this event, as explained further below. Given these unique circumstances, we treat this kind of simultaneous event in the logic tree as an additional source. Thus, we add a maximum magnitude event to the data on maximum magnitude otherwise developed for the faults (independent, linked, or coalesced).

We believe that a simultaneous rupture is more likely to occur on faults that are coalesced than on faults that are linked or independent. Accordingly, our weighting of such an event differs depending on the branch of the logic tree. For the branch in which all faults sole into a detachment, we assign a weight of 0.5 to a combination of simultaneous ruptures tied principally to volcanic events in the Crater Flat area and non-simultaneous events on the faults, and a weight of 0.5 to having all events be non-simultaneous. For the model in which all faults coalesce at depth, we apply the same weights to simultaneous and non-simultaneous events. However, for the models of linked or independent faults, we apply a weight of 0.1 to the combination of simultaneous and non-simultaneous events, with a weight of 0.9 to having all events be non-simultaneous.

2.4.2 Maximum Magnitudes

Our approach to calculating maximum magnitude for the local faults is similar to that taken for the regional faults. However, we add another branch by using stress drops to constrain average displacement, and the fault areas are more sensitive to the details of the down-dip width as estimated from fault intersection analysis and combinations of coalesced and linked faults.

We evaluated fault length based on mapped surface traces. Some teams discussed the possibility that the local faults continue south of their mapped surface traces into the subsurface beneath the Amargosa Valley (SSC Workshop 5), but we conclude that data do not support this interpretation. The Highway 95 fault provides a termination to the YM faults as well as the Bare Mountain fault. Given the lack of evidence and a model for fault termination, we see no reason to speculate that the faults extend any farther south than they

are mapped at the surface. The northern extent of some faults is less certain. Faults have been mapped north of the main Yucca Mountain block into bedrock, but without Quaternary displacement. We use the maximum mapped fault length, from Simonds and others (1995), and consider that these pre-Quaternary fault extensions have a lower likelihood of contributing to the maximum magnitude earthquake than do the Quaternary sections of the faults (Figure SBK-6).

Treatment of fault length for coalesced and linked faults is an important consideration. For the models in which faults sole into a detachment and for coalesced faults, we interpret the fault length as that of the longest fault involved in coalescence: the combined South Crater Flat + Windy Wash + Fatigue Wash fault for the shorter length of 27 km (wt. 0.6), and the combined Paintbrush Canyon + Stagecoach Road fault for the longer length of 35 km (wt. 0.4).

Fault coalescence in the subsurface, the maximum depth of penetration of faults into the crust, and fault area were evaluated using a combination of structure contour maps and trigonometric calculations. Structure contour maps were constructed as overlays to the Quaternary fault map of Ramelli and Bell (1996). The structure contour overlay maps were drawn for the local fault sources (YM faults and Bare Mountain fault), as well as for the Ghost Dance fault. Fault strike was constrained by the surface trace on the map of Ramelli and Bell (1996), and the angle of fault dip was constrained primarily by outcrop measurements annotated on the map of Simonds and others (1995). We investigated a range of fault dips, considering the common observation that the dip angle of normal faults often is steeper at the surface than at depth. Average fault dip angles between 45 and 75 degrees were considered, with subsurface dip angles between 45 and 70 degrees considered most likely. The Bare Mountain fault was assumed to be the master structure, with other faults either intersecting one another above the Bare Mountain fault, or being truncated against the Bare Mountain fault surface at depth. We do not consider it credible that one of the YM faults truncates the Bare Mountain fault at depth. The depth and orientations of fault intersections were found either by connecting points of equal depth on structure contour maps of two fault surfaces, or by direct trigonometric calculation of the depth of intersection. The trigonometric calculation was done using the dip angle of the two faults of interest and the horizontal distance between the fault surface traces as measured normal to strike. The calculated intersection depths in

combination with fault lengths were used to constrain the down-dip widths of faults to estimate area for computing the maximum earthquake magnitude. The maximum seismogenic width was limited by the intersection of a fault either with the Bare Mountain fault surface or with the base of the seismogenic crust, whichever was shallower.

The following is a summary of the weighting for down-dip width for the local faults based on a Bare Mountain/YM fault dip scenario. Using minimum dip combinations for Bare Mountain and YM faults of 45 degrees/50 degrees preferred, 60 degrees/60 degrees, and a steep limit (70 degrees/70 degrees) for both, the down-dip width in km is listed for each independent YM fault. The first dip in the (aa/bb) pair is that on the Bare Mountain fault (aa); the second is the dip on the YM fault (bb). To capture all uncertainty, the base of the seismogenic crust is interpreted to be at 17 km. The only scenario controlled by a 17-km seismogenic thickness is the case of 70 degrees/70 degrees.

	BM/YM DIPS (°)	BM/YM DIPS (°)	BM/YM DIPS (°)
	45 /50	60 /60	70 /70
Weight	0.2	0.7	0.1
DOWN-DIP WIDTH OF FAULTS IN KM			
Paintbrush Canyon	14	17	18
Bow Ridge	14	17	18
Stagecoach Road	10	15	18
Solitario Canyon	10	14	18
Windy Wash	8	11	17
Fatigue Wash	8	11	17
N Crater Flat	6	9	13
S Crater Flat	5	6	7

These estimates of down-dip fault width are multiplied by fault lengths to compute areas of individual faults. For the coalescing faults model, we compute fault area for a simultaneous rupture by summing all the contributing fault areas; we compute fault area for non-simultaneous ruptures by considering the maximum fault area for an individual contributor to the coalescing faults (i.e., the Stagecoach Road + Paintbrush Canyon combination). A similar approach is used with the model in which faults sole into a detachment.

These estimates of down-dip width also are used to compute average slip from static stress-drop weighting to establish another estimate of maximum magnitude. Stress-drop weighting

was established by taking into account the distribution of static stress drops for the normal faulting regimes (Becker and Abrahamson, 1997; GMC Workshop 3), and the stress-drop estimates for the Little Skull Mountain earthquake (Becker and Abrahamson, 1997).

Weight	0.2	0.5	0.25	0.05
σ (bars)	30	35	50	100

Stress drop is calculated from (Kanamori and Anderson, 1975)

$$\sigma = 8/(3 * \pi) * \mu * [u/ W]$$

where, $\mu = 3 \times 10^{11}$ dyne-cm (rigidity), u = average fault slip (cm), W = down-dip fault width (cm).

For the local faults, then, we use five methods to compute maximum magnitude. These are: fault length, fault area, maximum displacement from surface studies, average displacement from surface studies, and average displacement from stress-drop analysis. These are weighted for individual faults and combinations (Table SBK-3) based on availability and quality of data.

2.4.3 Recurrence

Calculation of earthquake recurrence parameters for the local faults followed the guidelines discussed for the regional fault sources. Considerably more data are available to constrain fault slip rate for the local faults than for most of the regional fault sources. In addition, we have repeat-time information available from paleoseismic trench studies for all of the local fault sources. These repeat times are defined in the field for events having different displacements, however, so they probably do not all represent the repeat time of the maximum earthquake for that source. Accordingly, we weight paleoseismic repeat-time data much lower (generally weighted 0.2 to 0.3) than slip-rate information.

Again, special consideration must be given to assessing repeat times for coalesced faults and the model of faults that sole into a detachment. In both cases, we summed slip rates computed at the surface on east-west transects across the faults (e.g., slip rate for coalesced

faults = slip rate on Paintbrush Canyon + slip rate on Solitario Canyon + slip rate on Windy Wash + slip rate on North Crater Flat). We use these slip rate calculations exclusively to define recurrence for non-simultaneous ruptures for these fault models. Our model of simultaneous ruptures ties these events closely to the recurrence of volcanic eruptions in the Crater Flat tectonic domain. Thus, we weight the recurrence of simultaneous events heavily by recurrence of volcanic eruptions (0.75 weight) and less by fault slip rate (0.25 weight), regardless of fault model (same weighting for soling faults, coalesced faults, linked faults, and individual faults when they rupture simultaneously).

We weight the choice between characteristic and truncated exponential recurrence models differently for the local faults, depending on whether we consider individual faults or combinations. The Bare Mountain fault is a range-bounding fault, so we weight the characteristic model more strongly (0.6 weight). The YM faults are not, so we weight the truncated exponential model more strongly (0.7 weight). The behavior of the fault combinations is less well resolved, so we weight the two models equally.

Finally, we consider the case of simultaneous ruptures, as represented by the "ash event," the recurrence of which we tie strongly to volcanic eruptions in the Crater Flat area. We consider these to be unusual events, whose frequency is not as much related to conventional fault models as it is tied to volcanic eruptions. Therefore, we treat these events as single contributors to moment release within the study area, reasoning that all other earthquakes are captured either by the distributions otherwise assigned to the faults or by the maximum earthquake and distribution of seismicity for the Local Zone. They are added events, which contribute only their own moment, not a full range of moment distribution as occurs with a characteristic or truncated exponential model. Thus we assign a maximum moment distribution to this kind of event, with the recurrence constrained by a combination of fault slip rate and volcanic-event rate (Table SBK-3), and the only magnitudes given by the range of the maximum magnitude distribution (i.e., all $M < M_{\max}$ give no contribution to moment for this source).

As described in Section 2.3.2 for regional faults, we assume that the characteristic and maximum moment events are uniformly distributed in the magnitude range $M_{\max} \pm 1/4$, such that the upper limit of the recurrence relationship is $M_{\max} + 1/4$. For the exponential recurrence

model the upper limit is also set at $M_{\max}+1/4$. When the overall rate of earthquake occurrence is specified by the recurrence interval of surface-rupturing earthquakes, this recurrence rate was assumed to apply to earthquakes of magnitude greater than or equal to $M_{\max}-1/4$.

3.0

FAULT DISPLACEMENT CHARACTERIZATION

3.1 INTRODUCTION

Our characterization of fault displacement is designed to permit estimates of fault displacement potential on two general classes of faults in the Yucca Mountain Controlled Area: (1) those for which we have specific data concerning the Quaternary rupture history; and (2) those faults and fractures for which data indicate no Quaternary rupture, or for which no data on Quaternary displacement are available. The first class of faults includes the major block-bounding faults, particularly the Solitario Canyon and Bow Ridge faults, that are considered potential earthquake sources (demonstration points 1 and 2); we also include structures such as the fractures in Midway Valley that have no measurable displacement in Quaternary alluvium (demonstration point 9). The second class of faults includes intrablock faults (such as the Drill Hole Wash, Ghost Dance, Sundance, and Dune Wash faults, demonstration points 3-6) as well as small faults, shears, and fractures (demonstration points 7-8). Potential fault displacement in intact rock can be assessed using the characterizations applied to this second group.

For either class of faults, we address two questions: (1) How often might displacement events occur? and (2) How large might these events be? Responding to the first question involves assessing event frequency. Our assessment involves two approaches. In the first, frequency is estimated from analysis of fault slip rate. The second uses direct (fault- or site-specific) information on frequency of displacement or cracking events. Response to the second question involves assessing the range of displacements that might characterize the events defined during the first part of the analysis. This may include fault- or site-specific data regarding prehistoric displacement events, information on variability of displacement along a fault (which may be general or fault-specific), scaling relationships for fault displacements, and data on secondary fault ruptures.

The procedures and methods for characterizing fault displacement presumably will change with improvements in our understanding of the mechanical and statistical characteristics of fault displacement on both individual faults and fault systems. Our approach is to use several alternative procedures for estimating the frequency and magnitude of fault displacement, which we consider in combination make the best use of available data and capture the uncertainty in characterization of fault displacement at this time. We discuss our general approaches for the two classes of faults, then apply the approaches to the demonstration points.

3.2 FAULTS HAVING DOCUMENTED QUATERNARY DISPLACEMENT

Our characterization of fault displacement potential for faults within the Controlled Area for which data on Quaternary displacement are available incorporates two approaches: one based on the frequency of earthquake occurrence, the earthquake approach; and the other based on assessments of the frequency and size of events from trenching data, the displacement approach (Figure SBK-8). The relative weights assigned to these two approaches depend on the data available for the site of interest.

3.2.1 Earthquake Approach

The earthquake approach to the assessment of fault displacement hazard considers two sources of earthquake induced displacements: principal faulting from earthquakes occurring on the feature of interest, and distributed faulting induced by earthquakes centered on other sources.

3.2.1.1 Characterization of Principal Faulting Potential. The steps involved in characterizing potential displacement due to principal faulting on a fault are shown on Figure SBK-8.

Frequency of Principal Faulting Events. Section 2.0 presents our characterization of the frequency of occurrence of earthquakes as a function of magnitude, $\lambda(m)$, on each seismic source. The frequency of displacement events, λ_{DE} at a point of interest is given by

$$\lambda_{DE} = \lambda(m) \cdot P_R(m) \cdot P(\text{intersection}) \quad (1)$$

where $P_R(m)$ is the probability that an earthquake of magnitude m will rupture the surface and $P(\text{intersection})$ is the probability that the along-strike location of the rupture will pass through the site of interest. The probability of surface rupture is assessed using the logistic probability model presented by R.R Youngs (Appendix H, Section H.4.1) in SSC Workshop 5 based on data presented in Pezzopane and Dawson (1996). We chose to use the assessment based on recent western Basin and Range earthquake ruptures (Figure SBK-9). The assessment of the probability that the along strike location of the rupture will pass through the site is obtained by randomizing the location of the rupture along the fault in the same manner as is done for ground motion hazard assessment.

Distribution of Principal Faulting Displacement at a Point. The probability distribution for the amount of displacement at a point is defined based on the concept presented by the ASM team in SSC Workshop 5. The first step is an estimate of the maximum displacement, MD , in the earthquake. We use the empirical relationship between MD and moment magnitude developed by Wells and Coppersmith (1994) to define a lognormal distribution for MD in each earthquake.

Given a maximum displacement, we assess the distribution for displacement at a point using normalized distributions for D/MD as a function of location along the rupture. We use two approaches, one based on the ASM evaluation of historical rupture patterns presented in Wheeler (1989) (Figure SBK-10; Appendix H, Section H.3.1) and one based on our fractal model of fault surface roughness presented in SSC Workshop 5 (Figure SBK-11; Appendix H, Section H.3.2). We give equal weight to the historical rupture and fractal interpolation approaches.

The fractal model is based on the assumption that variability in displacement along the length of a fault rupture scales with the roughness of the rupture surface. This variability is modeled using a two-dimensional fractal interpolation function in which an arbitrary displacement is located at random within the length of a synthetic rupture (length = -1 to +1). Displacement at 99 additional points are then interpolated between the initial displacement point and the end points of the rupture using fractal interpolation (Barnsley, 1988). The variability in displacement between points is controlled by the fractal dimension (D_f) of the interpolation

function, which is set at $Df = 1.3$, a value determined by Lee and Bruhn (1996) for natural fault surfaces with Quaternary and older rupturing history. One hundred ruptures were simulated using the fractal interpolation algorithm of Barnsley (1988). The displacements at 100 points along the length of the simulated ruptures were then normalized to the maximum displacement in each simulated rupture, and then collected as an ensemble from which the average and variability in displacement at each point was calculated to produce the results presented in Figure SBK-11. More details of the simulation procedure are included in documentation presented by the SBK team at Workshop 5.

3.2.1.2 Characterization of Distributed Faulting Potential. The steps involved in characterizing the potential for distributed faulting from earthquakes on other sources are the same regardless of whether the fault has documented Quaternary displacement or not. These methods are discussed below in Section 3.2.2.

3.2.2 Displacement Approach

The displacement approach to the characterizing fault displacement potential combines the effects of principal and distributed faulting into a single assessment. The steps involved in this approach are shown on Figure SBK-8.

3.2.2.1 Frequency of Displacement Events. The frequency of displacement events is computed using two approaches: one involving estimates of fault slip rate and average displacement per event; and the other involving event frequency estimated from trenching data. In general, the slip-rate approach is weighted higher than the event-frequency approach for the demonstration points consistent with our weighting of these types of data in the assessment of local fault seismic sources (Table SBK-3). However, weights will differ for other faults depending on the type and quality of information available concerning their Quaternary rupture history.

Slip Rate Evaluation. Slip rate is either determined directly at the point of interest or interpolated along the strike of the fault between trenches or other survey localities, where fault offsets and the age of offset horizons are known from measurements and dating. We consider these two conditions in structuring our logic tree for fault displacement hazard (Figure SBK-8).

Detailed mapping of Quaternary geomorphic surfaces and faults, along with the large number of paleoseismic trenches excavated across Yucca Mountain faults, has yielded considerable information about slip rate, and its variability, along major faults such as the Solitario Canyon and Paintbrush Canyon faults. Thus, slip rate can be estimated directly at numerous locations. The slip rate at a point of interest can be estimated by measuring the cumulative offset of a Quaternary horizon of known age, which may be measured in a trench or on a geomorphic surface in the landscape. Slip rate (*SR*) is estimated from the equation:

$$SR = \text{Offset} / (\text{Horizon Age}) \quad (2)$$

Minimum, preferred, and maximum slip rates are calculated using the estimated range of minimum, maximum, and preferred magnitude of offset of a geologic horizon and its age. No along-strike interpolation is necessary in these cases. At demonstration point #1 on the Bow Ridge fault, for instance, slip rate can be estimated directly.

More commonly, the point of interest is located between trenches or other points along a fault where the slip rate has been calculated from site-specific geologic data. One or more methods of slip rate interpolation must be applied. We apply two methods, the first using data on Quaternary displacements along the fault of interest, the second using cumulative displacement along the fault. The slip rate at a point of interest is scaled between two points of known displacement; we use linear interpolation unless sufficient data are available to more accurately characterize the variation in displacement along strike. The first method requires data on Quaternary displacement at two points that bracket (along strike) a point of interest. For example, this approach is used for the Solitario Canyon fault at demonstration point #2, because along-strike changes in the offset of middle to late Quaternary geomorphic surfaces are known from detailed mapping and trenching (Ramelli, SSC Workshop 6). The slip rate at the point of interest is interpolated from those obtained at trench SC-T4 and the north end of Quaternary faulting using Ramelli's curve of along-strike variability in the offset of mid- to late-Quaternary geomorphic surfaces. Such an approach can be used for any point on a fault that is between two locations of known Quaternary displacement (even if one of those is a location of known zero displacement).

Along-strike variation in fault displacement also may be measured using displaced bedrock horizons of known age. Yount (SSC Workshop 6) presented curves estimating the along-strike variability in cumulative bedrock offset along both the Solitario Canyon and Bow Ridge faults, for example. We apply a linear interpolation for this method also, unless a sufficiently large data set is available to more accurately characterize the along-strike variation in fault slip.

Given an assessment of slip rate, SR on a feature, the frequency of displacement events, λ_{DE} , is given by the expression:

$$\lambda_{DE} = SR / \bar{D}_E \quad (3)$$

where \bar{D}_E is the average displacement per event. The approaches used to assess \bar{D}_E are discussed below.

Direct Evaluation of Event Frequency. Our interpretation of the frequency of events from fault trenching data includes both those events for which we have measured shear offset and fracturing events having no measured shear offset, as both kinds of events have broken the surface. The number of events divided by the age of the youngest horizon that predates the oldest faulting or fracturing event is an estimate of the frequency (number of events / annum). Event frequency is expressed as minimum, preferred, and maximum values based on the range of estimated ages of geologic horizons and uncertainty in the number of events interpreted from the trench logs. We use the compilation (Table 5.1) of Pezzopane and others (1996a) as our principal source in estimating event frequency.

Some faults have near-surface or surface fractures that developed by cracking in Quaternary soils, but across which there is no measurable shear offset to prove Quaternary surface faulting; a good example is the Midway Valley structure at demonstration point #9. These fractures may have undergone only opening or may have been sheared less than can be detected in the paleoseismic studies (we estimate up to 10 cm). Alternatively, opening-mode or mixed shear- and opening-mode cracks may have developed at or near the surface in response to shear displacement on the fault at depth. Bruhn and Schultz (1996) provided theoretical support for this kind of surface-crack development. They investigated the nature of near-surface fracturing caused by sliding on part of a normal fault patch at depth and found

that mixed opening- and shear-mode cracking is expected at or near the Earth's surface. These features could also develop during strong ground shaking, as discussed below. Thus, surface cracking could be indicative of fault displacement at depth, even at shallow crustal depths such as those at the potential repository.

The maximum frequency of occurrence of cracking events is estimated by dividing the number of cracking events by the age of the youngest soil that is affected by the oldest cracks; the minimum is estimated by dividing the number of events by the age of the oldest deposits. The amount of displacement is estimated from the thickness of calcite or silica laminae filling the cracks following each event. Data on these events is summarized by Pezzopane and others (1996a) and recorded in detailed trench logs. We assess a 50% chance that surface cracking having no measurable shear offset reflects deformation above a slip patch on the fault at depth. This implies that not all surface cracking is directly related to shearing on the fault at depth, even if the cracks are located directly on a fault that extends to the surface.

3.2.2.2 Characterization of Amount of Displacement. Characterizing the amount of fault displacement, given a displacement event, involves estimating maximum or average displacement per event on the fault. These values can be computed from paleoseismic data (preferred, given that we have data available) or from regressions of displacement versus magnitude from historical ruptures elsewhere (Wells and Coppersmith, 1994). Paleoseismic values are obtained from Pezzopane and others (1996a) and Table SBK-3; weighting is fault-specific. As with computation of slip rate, displacement data may be available at a particular site, or it may have to be interpolated from nearby locations along the fault. Again, we use linear interpolation, and we assign greatest weighting to Quaternary displacement data.

Three approaches are used to compute the average displacement at the point of interest, two based on empirical relationships between rupture length and maximum and average displacements. Each of these, in turn, is used to characterize the variability in displacement per event.

Paleoseismic Estimates of Average Displacement. We calculate the variability of displacement about an assessment of the average displacement from paleoseismic data through

three steps. Step 1: For each trench for which we have three or more offset measurements, compute the average slip, U_{ap} .

$$U_{ap} = 1/n \sum U_i \quad (4)$$

where U_i is a single event fault slip (offset) at a site with three or more offsets, and n is the number of measurements at the site. This assessment is then used as an estimate of the average displacement per event, \bar{D}_E . Step 2: Divide each offset measurement (U_i) by U_{ap} . Step 3: Accumulate the U/U_{ap} samples from all trenches on all local faults, except the Rock Valley and Bare Mountain faults in Table 5.1 of Pezzopane and others (1996a). This provides an estimate of $P(U/U_{ap})$, the probability density function of a displacement U given an average displacement U_{ap} at a site. This approach is applicable directly at trench sites where at least three events have been recorded, and we interpolate between known points to calculate $P(U/U_{ap})$ when the site of interest is not at a trench location. Figure SBK-13 shows the resulting data and the fitted gamma distribution (Appendix H, Section H.2.2) used to characterize the probability distribution for U/U_{ap} . The data for this distribution is listed in Table SBK-6.

Empirical Estimates of Average Displacement. We apply a slightly different approach to estimate the distribution of displacement events about the average slip from the Wells and Coppersmith (1994) empirical relationships between rupture length and average displacement. Here, our approach involves four steps. Step 1: Determine the maximum, preferred, and minimum fault lengths for all local faults with trench data for Quaternary offset (Table 5.1 of Pezzopane and others, 1996a), except the Rock Valley and Bare Mountain faults. We use the values we assessed in the seismic source characterization (Table SBK-3). Step 2: Calculate the average slip, U_s , for each fault:

$$\log(U_s) = -1.99 + 1.24 \log(FL) \quad (5)$$

where FL is the fault length used to estimate the maximum magnitude earthquake in Section 3.0. This assessment is then used as an estimate of the average displacement per event, \bar{D}_E . Equation (5) is from Table C2 of Wells and Coppersmith (1994). Step 3: Divide the offset

measurement U_i from each trench on a fault by U_s for that fault. Do this for each local fault except the Rock Valley and Bare Mountain faults listed in Table 5.1 of Pezzopane and others (1996a). Step 4: Plot the frequency histogram of U/U_s as an estimator of $P(U/U_s)$. Figure SBK-13 shows the resulting data and the fitted gamma distribution (Appendix H, Section H.2.3) used to characterize the probability distribution for U/U_s . The data for this distribution is listed in Table SBK-6.

Empirical Estimates of Maximum Displacement. The alternative is to compute U_m from the Wells and Coppersmith (1994) regression for maximum displacement from fault length:

$$\log(U_m) = -1.98 + 1.51(\text{FL}) \quad (6)$$

where appropriate ranges of fault length are obtained from Table SBK-3. The estimate of average displacement per event, \bar{D}_F , is set equal to $0.69 \times U_m$. We divide each offset measurement (U_i) from the trenches on each Yucca Mountain fault by U_m for that fault. The result is a frequency histogram of U/U_m as an estimator of $P(U/U_m)$, the probability distribution of displacement U given U_m for a site. Figure SBK-14 shows the resulting data and the fitted gamma distribution (Appendix H, Section H.2.4) used to characterize the probability distribution for U/U_m . The data for this distribution is listed in Table SBK-6.

In each case we compute a cumulative probability density function from the integrals of the probability density functions. The results are expressed as the probability of exceeding a normalized displacement if fault rupture occurs at a site of interest.

3.3 FAULTS WITHOUT DOCUMENTED QUATERNARY DISPLACEMENT

Many faults in the Controlled Area lack evidence for Quaternary displacement because they are inactive, have exceedingly long recurrence intervals, are located in areas that lack Quaternary cover, or are embedded in the rock mass beneath the surface. Our approach to characterize potential displacement on these faults follows the same principles as described above, using either an earthquake approach to estimate the frequency of induced slip events or the displacement approach using direct assessment of slip rate and event size based on data for the feature. However, these are modified to account for the types of data available for the

characterization. The generalized logic tree for this class of faults is diagrammed on Figure SBK-15.

3.3.1 Earthquake Approach for Distributed Faulting

The steps involved are assessment of the probability that slip can occur, evaluation of the frequency of distributed ruptures, and evaluation of the distribution of displacements.

3.3.1.1 Fault Orientation Weighting. Maps of distributed ruptures formed during historical earthquakes and nuclear test blasts (Covington, 1987; Pezzopane and Dawson, 1996), and simple rock mechanics theory (e.g., Ferrill and others, 1996a), suggest that the likelihood of fault activation is a strong function of the orientation (strike and dip) of a fault surface with respect to the principal stresses. We develop an orientation index for evaluating the likelihood of fault activation. This index is based either on stress ratios between a most favorably oriented reference fault and the fault of interest, or by comparison to the orientations of distributed rupturing generated by historical, surface faulting earthquakes (based on diagrams in Pezzopane and others, 1996a). By most favorably oriented fault, we mean that fault which would have the greatest slip tendency, or ratio of shear to normal traction, in the ambient stress field within the Controlled Area.

Use of Fault Slip Tendency. The orientation (strike and dip) of a fault surface relative to the contemporary stress field is an important measure of the likelihood of fault activation (Ferrill and others, 1996a). Faults most likely to be active and slip in the contemporary stress field have the largest ratio of shear (T_s) to normal stress (T_n), which defines their slip tendency. Faults having lower shear-to-normal stress ratios are less likely to be active and slip as distributed or secondary ruptures under dynamic and static stress perturbations caused by an earthquake in the surrounding area. We extend this analysis by defining the fault activation factor (AF) as the ratio of the slip tendency on the fault of interest to that on the most favorably oriented fault in the contemporary stress field. The activation factor (AF) will range between 1.0 and 0. AF is a weight that reduces the expectation of failure on less favorably oriented faults.

The shear stress state on a fault or fracture is defined as:

$$Ts = \text{magnitude}(T - Tn) \quad (7)$$

where T is the traction vector across the fault of interest induced by the ambient stress tensor, Tn is the normal stress acting across the fault surface, and the bracketed term implies vector subtraction. We assume that the orientation of the fault is known to within ± 10 degrees, an angular variation that captures uncertainty in measurement by the geologist or mapper, and accounts for most natural undulations of the fault surfaces. Traction vector components of T and Tn are found using standard vector and tensor operations:

$$T_i = S_{ij} n_j \quad \text{and} \quad Tn_i = [S_{ij} n_i n_j] n_i \quad (8)$$

where $n = \langle n_1, n_2, n_3 \rangle$ is the unit vector parallel to the pole of the fault surface, S is the stress tensor, and summation is implied over repeated indices in the equations (Einstein Summation Convention).

The ambient stress in the ESF was determined by hydrofracture measurements in Testhole ESF-AOD-HDFR#1 at a depth of 244 m (Sandia National Laboratories, 1997). The three principal stresses are: $S_v = 4.69$ MPa, vertical; $SH = 2.9 \pm 0.4$ MPa, $N15^\circ \pm 14^\circ E$; and $Sh = 1.7 \pm 0.1$ MPa, $N75^\circ \pm 14^\circ W$, where S_v is the vertical compressive stress, SH is the maximum horizontal compressive stress, and Sh is the minimum horizontal compressive stress. The ESF stress tensor may originate partly by tectonic and partly by topographically induced loading. Regardless of its origin, this stress tensor indicates a normal faulting stress regime in the ESF facility, with vertical maximum compressive stress, and least horizontal compressive stress oriented approximately normal to the block-bounding faults. Notably, the orientation and magnitude of the stress tensor are compatible with other hydrofracture measurements in the Yucca Mountain block and at the Nevada Test Site, which indicate a normal faulting regime and similar horizontal stress orientations to depths of approximately 1 km (e.g. Stock and Healy, 1988).

We conclude that the most favorably oriented fault dips between 60 and 65 degrees and strikes parallel to SH . The ratio $|Ts/Tn|$ on this fault is 0.54. We use this value to normalize the ratio $|Ts/Tn|$ on faults of interest that have different orientations. The ratio of the

orientation of the fault of interest to the most favorably oriented fault defines the AF factor, which we multiply by the slip rate or event frequency to compute a revised rate or frequency.

This method neglects the role of fault interactions, which may rotate and concentrate the local stress field to cause slip on adjacent faults that are not favorably oriented for failure in the ambient stress field. We acknowledge this limitation, but we consider it of secondary importance in the evaluation of displacement hazard.

Use of Orientation Histogram. An activation factor (weight) can also be derived from empirical data on the pattern of distributed rupturing generated during historical earthquakes (Pezzopane and Dawson, 1996). This method requires construction of an azimuth (fault trend) frequency distribution of secondary ruptures generated during historical earthquakes (Appendix H, Section H.4.3; Pezzopane and Dawson, 1996; diagram presented by Pezzopane, SSC Workshop 4) and following nuclear test blasts at the Nevada Test Site (Covington, 1987). The objective is to estimate the chance that secondary rupturing will occur on faults orientated at various angles to the primary rupture zone. We expect secondary rupturing to be most common on faults that parallel the primary rupture, and least common on other faults. The underlying physical principle is that secondary rupturing is most likely on those faults favorably oriented for failure under the ambient stress field, and that other, less favorably oriented faults are less likely to rupture. Visual inspection of rupture maps in Pezzopane and Dawson's (1996) compilation shows that secondary ruptures are concentrated along the azimuth of the primary rupture trace in most earthquakes, and that the frequency and length of secondary rupturing decrease significantly for other orientations.

3.3.1.2 Frequency of Distributed Faulting Events. Section 2.0 presents our characterization of the frequency of occurrence of earthquakes as a function of magnitude, $\lambda_n(m)$, on each seismic source, n . The frequency of distributed faulting ruptures, λ_{DE} , is computed by the relationship

$$\lambda_{DE} = \lambda_n(m)P_n(\text{Slip}|\text{Event}) \quad (9)$$

where $P_n(\text{Slip}|\text{Event})$ is the probability that an earthquake on source n will induce slip on the feature of interest. We employ two approaches to characterize the frequency of events by earthquake triggering (Figure SBK-15). The first approach uses the earthquake recurrence on independent seismic sources, along with empirical functional relationships for distributed ruptures on hanging and foot wall (Pezzopane and Dawson, 1996; Pezzopane, SSC Workshops 2 and 3; R.R. Youngs, SSC Workshop 6). The second approach uses empirical observations of secondary fracturing and faulting in underground workings caused by strong ground shaking (Brady, 1990).

Historical Rupture Approach. The probability that a secondary or distributed displacement event will occur on a fault away from the seismic source is computed based on distance from the source (Appendix H, Section H.4.2). Pezzopane (SSC Workshop 3) showed the relationship between width of secondary or distributed rupture zone and earthquake magnitude derived from the Pezzopane and Dawson (1996) database of historical Basin and Range earthquakes. R.R. Youngs (SSC Workshop 6) showed the frequency of occurrence of displacement events with distance from the fault as a function of magnitude in both hanging-wall and foot wall positions. Figure SBK-16 shows the resulting relationship for the probability that distributed rupture will occur at a point as a function of earthquake magnitude, distance to rupture, and location in the hanging wall and foot wall. For earthquakes occurring in the local areal source, we consider that it is equally likely the point of interest lies in the hanging wall or the foot wall. We assign a weight of 0.5 to this approach.

Ground Shaking Approach. This approach makes use of peak particle velocity (PPV) induced by strong ground motion and transient seismic strain (Hanks and McGuire, 1981; McGarr, 1984) to estimate the probability of triggering displacement on faults and fractures in the Yucca Mountain block. The method is based on observations of damage in underground tunnels and openings (Brady, 1990), and is only applied if the point under consideration is located within an underground excavation (See Excavated Fault, or Excavation Site decision columns in Figures SBK-9 and SBK-17).

The approach is applicable for evaluating displacement on fractures that are either located adjacent to, or intersect, an underground working. Rock excavations create stress

concentrations that can either destabilize or stabilize faults and joints in the vicinity of an underground excavation. Displacements may occur, but the likelihood depends on the geometry of the excavation, the orientation of the fractures, and the ambient principal stresses (Brady, 1990; Galybin, 1997). The approach presented here reflects our evaluation that, although it is important to incorporate the effects of strong ground motion on fault displacement hazard, techniques for implementing such an analysis are not well established.

The annual probability of exceedance of a specified peak particle velocity (PPV) at the surface is a ground motion parameter that is calculated as part of the PSHA analysis. $F(PPV)$ is the annual frequency of exceedance of a PPV at the surface above a point of interest. This is computed directly from the PSHA parameters. We define $P(\text{Damage}|PPV)$ as the probability that joint or fault movement (damage) will occur in a subsurface excavation given a specified PPV. The function is based on the correlation between observed damage in underground excavations in jointed rock, and the PPV measured at the surface (Brady, 1990). Figure SBK-17 shows our evaluation of the probability function $P(\text{Damage}|PPV)$. We weight this approach 0.5.

3.3.1.3 Distribution of Distributed Faulting Displacement at a Point. We lack information about average or maximum displacement during individual rupture events on faults that lack Quaternary displacement. However, cumulative (late Cenozoic) displacement generally is known on faults for which we can measure offset of marker horizons in excavations or at the surface.

Our preferred approach for estimating displacement variability on a fault where only cumulative slip is known involves comparing the cumulative slip on the fault of interest with the cumulative slips on all Yucca Mountain faults. First, we use the maximum, preferred, and minimum estimates of cumulative fault displacement, D_m , for each Yucca Mountain fault (principally from Simonds and others, 1995). For each trench site on the Yucca Mountain faults, we divide the single-event displacement by the total to develop a frequency histogram of U/D_m , which specifies a probability density function $P(U/D_m)$ (Appendix H, Section H.3.2; U/D_m , Figure SBK-18). The cumulative slip at the site or fault of interest is then multiplied by this function to obtain the distribution of single-event displacements for the fault of interest.

3.3.2 Displacement Approach for Distributed Faulting

The steps involved are assessment of the probability that slip can occur, evaluation of the frequency of displacement events, and evaluation of the distribution of displacements.

3.3.2.1 Frequency of Displacement Events. The frequency of displacement events is evaluated using Equation (3). This assessment requires estimating the slip rate and average displacement per event.

Evaluation of Slip Rate. In the absence of data to characterize the Quaternary slip history of a fault, our use of slip rate relies on long-term, fault-specific slip data and/or on scaling of slip on one fault based on slip rates for better-studied faults in the Yucca Mountain area. We describe first the geohistorical approach, which is our preferred method because it takes into account the history of slip on a particular fault (although the weighting varies from point to point). Then we describe the fault scaling approach.

Geohistorical Method. This approach provides estimates of fault slip rate based on the cumulative displacement of a horizon of known age. The approach, which was outlined in detail by the DFS Team during SSC Workshop 5, involves not only the assessment of total displacement at a point on the fault, but also weighting of three models of slip history. The approach is applicable only to those points for which total displacement can be measured.

In the first model, we compute an average long-term slip rate. Displacement of the Tiva Canyon tuff (Ttc), with an estimated age of 12.5 Ma, is used to determine the long-term slip rate. In this model we assume that slip has been uniform during the past 12.5 Ma. Given the arguments summarized below that slip has not been uniform in the Yucca Mountain area during the past 12.5 Ma, we assign a weight of 0.1 to slip rates calculated using this model.

The second model assumes a change in slip rate at the close of tuff deposition. Fridrich (1997) suggests that approximately 80 percent of the post-Tiva Canyon tuff displacement on faults in the Yucca Mountain area occurred prior to deposition of the Rainier Mesa tuff (Trm) at 11.6 Ma. With this model, we calculate slip rates by dividing 20 percent of the post-Ttc displacement by 11.6 Ma. Here we assume that slip has been uniform during the past 11.6 Ma, although it was much more rapid from 12.5 to 11.6 Ma. We consider that this model

accounts for the geologic evidence for changes in late Cenozoic slip better than the first model, so we weight it higher (0.3).

The third model is based on geologic observations and interpretation by Day and others (1996b, Fig. 2-10) that the rate of crustal extension in the region encompassing Yucca Mountain has continued to decrease since the middle Miocene. The late Miocene slip rate is calculated by dividing 80 percent of the post-Tiva Canyon displacement by the estimated age difference between the Rainier Mesa and Tiva Canyon tuffs (about 900 ka). Then we compute the Quaternary slip rate by multiplying this late Miocene rate by a reduction factor of 0.021 ± 0.018 , which is the ratio of Quaternary to late Miocene extension estimated by Day and others (1996b). This model most fully incorporates evidence for the changes in late Cenozoic slip history; thus we weight it the highest of the three methods for computing Quaternary slip rate from long-term slip (0.6). We note that an estimate of a long-term slip rate can be defined in principle by dividing the age of any geologic horizon into the cumulative fault offset of that horizon, so one is not restricted to offsets of the Tiva Canyon or Rainier Mesa tuff horizons. However, the displacements of Ttc or Trm are the most common measurements available on the Yucca Mountain faults.

Fault Scaling Methods. Fault scaling methods are based on the observation that the slip rates on two different faults scale with their relative surface areas (Cowie and Scholz, 1992b). That is, the larger fault presumably has the higher slip rate. If fault area is not known, then ratios of cumulative displacement or fault length may be substituted for surface area based on the scaling relationships between cumulative fault displacement and fault length, and between fault length and fault surface area (Walsh and Watterson, 1987, 1992; Cowie and Scholz, 1992a, 1992b; Clark and Cox, 1996). Because cumulative displacement either is known or can be estimated from geologic mapping on block-bounding faults at Yucca Mountain, and this is the most likely data available for fractures and shears mapped in the subsurface, we give highest weight to the use of the cumulative displacement ratio (however, weighting varies with each case). The displacement ratio method proposed here is supported by both observational (Nicol et al., 1997) and mechanical modeling (P.A. Cowie, unpublished manuscript, 1998) studies which indicate that the slip rates of normal faults with larger cumulative displacement are consistently greater than those of smaller faults with less cumulative displacement in the same region. Nicol's (1997) study is based on observations of normal faulting from six rift

basins located in different parts of the world, and is applicable to terrains like those in the Controlled Area. We therefore consider the slip rates of two faults to be proportional to the ratio of their cumulative displacement:

$$Sr_i = [Dcum_i / Dcum_r] \times SR_r \quad (10)$$

where *Dcum* is cumulative displacement and *SR* is slip rate. Index "i" refers to the fault of interest, and index "r" refers to a fault with known slip rate. One or more of the block-bounding faults at Yucca Mountain with known *SR*, may be used as the reference fault. If more than one fault is used to calibrate slip rate, then the slip rate for the reference fault must be expressed as an average value, and the reference cumulative displacement must also be averaged over the reference faults. The fault of interest may be located in the repository block or elsewhere in the Controlled Area; it has known cumulative displacement at one or more points but no definitive geologic evidence for Quaternary slip rate.

Average Displacement Per Event. We use three probability distributions ($P(U/D_m)$, $P(U/U_s)$, and $P(U/U_m)$) for displacement per event at points on faults where both fault length and cumulative displacement are known (Figure SBK-15, displacement logic tree branch). However, for those points where only cumulative fault displacement is known we use just one function, $P(U/D_m)$.

3.3.2.2 Distribution of Distributed Faulting Displacement. The distribution function described in Section 3.3.1.3 and shown on Figure SBK-18 is used to characterize the distribution of displacements in faulting events.

REFERENCES

- Aki, K., 1984, Evidence for magma intrusion during the Mammoth Lakes earthquakes of May 1980 and implications of the absence of volcanic (harmonic) tremor: *Journal of Geophysical Research*, v. 89, p. 7689-7696.
- Aki, K., Reasenburg, P., DeFazio, T., and Tsai, Y.-B., 1969, Near-field and far-field seismic evidences for triggering of an earthquake by the Benham explosion: *Bulletin of the Seismological Society of America*, v. 59, p. 2197-2207.
- Anderson, J.G., Brune, J.N., Louie, J.N., Zeng, Y., Savage, M., Yu, G., Chen, Q., and dePolo, D., 1994, Seismicity in the Western Great Basin apparently triggered by the Landers, California, earthquake, 28 June 1992: *Bulletin of the Seismological Society of America* v. 84, p. 863-891.
- Anderson, J.G., Brune, J.N., dePolo, D., Gomberg, J., Harmsen, S.C., Savage, M.K., Sheehan, A.K., and Smith, K.D., 1993a, Preliminary report: The Little Skull Mountain earthquake, June 29, 1992: *Dynamic Analysis and Design Considerations for High-Level Nuclear Waste Repositories*, Structural Division of the American Society of Civil Engineers, p. 162-175.
- Anderson, J.G., Louie, J., Zeng, Y., Yu, G., Savage, M., dePolo, D., and Brune, J.N., 1993b, Earthquakes in Nevada triggered by the Landers, California earthquake, June 28, 1992 [abs.]: *Geological Society of America Abstracts with Programs*, v. 25, no. 5, p. 3.
- Anderson, L.W., and O'Connell, D.R., 1993, Late Quaternary faulting and historic seismicity in the western Lake Mead area, Nevada, Arizona, and California [abs.]: *Geological Society of America, Abstracts with Programs*, v. 25, no. 5, p. 3.
- Anderson, L.W., and Klinger, R.E., 1996a, The Beatty scarp in Nye County, Nevada—an important Late Quaternary morphologic datum: *Bulletin of the Seismological Society of America*, v. 86, p. 1650-1654.
- Anderson, L.W., and Klinger, R.E., 1996b, Quaternary faulting on the Bare Mountain fault; Chapter 4.12, *Seismotectonic Framework and Characterization of Faulting at Yucca Mountain, Nevada*. U.S. Geological Survey, Report to U.S. Department of Energy, p. 4.12-1 - 4.12-75.

- Anderson, R.E., Bucknam, R.C., Crone, A.J., Haller, K.M., Machette, M.N., Personius, S.F., Barnhard, T.P., Cecil, M.J., and Dart, R.L., 1995a, Characterization of Quaternary and suspected Quaternary faults, regional studies, Nevada and California: U.S. Geological Survey Open-file Report 95-599, 56 p. plus app.
- Anderson, R.E., Crone, A.J., Machette, M.N., Bradley, L.A., and Diehl, S.F., 1995b, Characterization of Quaternary and suspected Quaternary faults, Amargosa area, Nevada and California: U.S. Geological Survey Open-file Report 95-613, 41 p. plus appendices.
- Argus, D.F., and Gordon, R.G., 1991, No-net-rotation model of current plate velocities incorporating plate motion model NUVEL-1: Geophysical Research Letters, v. 18, p. 2038-2042.
- Bailey, R.A., Dalrymple, G.B., and Lanphere, M.A., 1976, Volcanism, structure, and geochronology of Long Valley caldera, Mono County, California: Journal of Geophysical Research, v. 81, p. 125-144.
- Barnsley, M.F., 1988, Fractals Everywhere, Academic Press (Boston), 394 p.
- Bayer, K., 1973, A preliminary seismicity study of the southern Nevada region, quarterly report January-March 1973: Earth Sciences Laboratories, NOAA, NV0-746-12.
- Beanland, S., and Clark, M.M., 1994, The Owens Valley fault zone, eastern California, and surface faulting associated with the 1872 earthquake: U.S. Geological Survey Bulletin 1982, 29 p.
- Becker, A., and Abrahamson, N., 1997, Stress drops in normal faulting earthquakes [abs.]: Seismological Research Letters, v. 68, p. 322.
- Bellier, O., and Zoback, M.L., 1995, Recent state of stress change in the Walker Lane zone, western Basin and Range Province, United States: Tectonics, v. 14, p. 564-593.
- Berrill, J.B., and Davis, R.D., 1980, Maximum entropy and the magnitude distribution: Bulletin of the Seismological Society of America, v. 70, p. 1823-1831.
- Bodin, P., and Gomberg, J., 1994, Triggered seismicity and deformation between the Landers, California, and Little Skull Mountain, Nevada, earthquake: Bulletin of the Seismological Society of America v. 84, p. 835-843.

- Brady, B.H., 1990, Dynamic performance and design of underground excavations in jointed rock, *in* Brummer, R. (ed.), *Static and Dynamic Considerations in Rock Engineering*: A.A. Balkema, Rotterdam, p. 1-11.
- Brocher, T.M., Hart, P.E., Hunter, C.W., and Langenheim, V.E., 1996, Hybrid-source reflection profiling across Yucca Mountain, Nevada: regional lines 2 and 3: U.S. Geological Survey Open-file Report 96-28, 110 p.
- Bruhn, R.L., and Schultz, R.A., 1996, Geometry and slip distribution in normal fault systems; implications for mechanics and fault-related hazards: *Journal of Geophysical Research*, v. 101, p. 3401-3412.
- Brune, J.N., and Anooshehpour, R., 1996, Task 4 Final Report: State of Nevada Nuclear Waste Projects Office, Carson City, Nevada.
- Brune, J.N., and Smith, K.D., 1996, Precarious rocks and seismic shaking during and before the 1992 Little Skull Mountain earthquake [abs.]: *Geological Society of America Abstracts with Programs*, v. 28, no 6, p. A-193.
- Brune, J.N., Nicks, W., and Aburto, A., 1992, Microearthquakes at Yucca Mountain, Nevada: *Bulletin of the Seismological Society of America*, v. 82, p. 164-174.
- Bryant, W.A., 1984, Evidence of recent faulting along the Owens Valley, Round Valley, and White Mountains fault zones, Inyo and Mono Counties, California: *California Division of Mines and Geology, Open-file Report 84-54 SAC*.
- Bucknam, R.C., 1969, Geologic effects of the Benham underground nuclear explosion, Nevada Test Site: *Bulletin of the Seismological Society of America*, v. 59, no. 6, p. 2209-2220.
- Bufe, G.G., and Topozada, T.R., 1981, California earthquakes; end to seismic quiescence: *California Geology*, v. 34, p. 111-114.
- Burchfiel, B.C., Hodges, D.V., and Royden, L.M., 1987, Geology of Panamint Valley-Saline Valley pull apart system, California; palinspastic evidence for low-angle geometry of a Neogene range-bounding fault: *Journal of Geophysical Research*, v. 92, p. 10,422-10,426.
- Carder, D.S., 1945, Seismic investigations in the Boulder Dam area, 1940-1945, and the influence of reservoir loading on local earthquake activity: *Bulletin of the Seismological Society of America*, v. 35, p. 175-192.

- Carr, W. J., 1990, Styles of extension in the Nevada Test Site region, Southern Walker Lane Belt; An integration of volcano-tectonic and detachment fault models, in Wernicke, B.P. (ed.), Basin and Range Extensional Tectonics near the Latitude of Las Vegas, Nevada: Geological Society of America Memoir 176, p. 283-303.
- Carr, W. J., 1984, Regional structural setting of Yucca Mountain, Southwestern Nevada, and late Cenozoic rates of tectonic activity in part of the Southwestern Great Basin, Nevada and California: U. S. Geological Survey, Open-File Report 84-854, 114 p.
- Chavez, D.E., and Priestley, K.F., 1985, ML observations in the Great Basin and Mo of the 1980 Mammoth Lakes, California, earthquake sequence: Bulletin of the Seismological Society of America, v. 75, p. 1583-1598.
- Civilian Radioactive Waste Management System Management and Operating Contractor (CRWMS-MOC), 1996, Probabilistic Volcanic Hazard Analysis for Yucca Mountain, Nevada (prepared by Geomatrix Consultants): Document BA0000000-01717-2200-00082, Rev 00, variously paginated.
- Clark, R.M, and Cox, S.J.D., 1996, A modern regression approach to determining fault displacement-length scaling relationships: Journal of Structural Geology, v. 16, p. 147-152.
- Cockerham, R.S., and Pitt, A.M., 1984, Seismic activity in the Long Valley caldera, eastern California, U.S.A.: June 1982 through July 1984: U.S. Geological Survey Open-file Report 84-939, p. 493-526.
- Coe, J.A., Oswald, J., Vadurro, G., and Lundstrom, S.C., 1996a, Quaternary faulting on the Fatigue Wash fault; chapter 4.8, seismotectonic framework and characterization of faulting at Yucca Mountain, Nevada: U.S. Geological Survey Report to U.S. Department of Energy, p. 4.8-1 - 4.8-32.
- Coe, J.A., Yount, J.C., and O Leary, D.W., 1996b, Preliminary results of paleoseismic investigations of the Rock Valley fault system; chapter 4.13, seismotectonic framework and characterization of faulting at Yucca Mountain, Nevada: U.S. Geological Survey Report to U.S. Department of Energy, p. 4.13-1 - 4.13-37.
- Cowie, P.A., A healing-reloading feedback control on the growth of seismogenic faults. (manuscript submitted to Journal of Structural Geology, 1998).

- Cowie, P.A., and Scholz, C.H., 1992a, Physical explanation for the displacement - length relationship of faults using a post-yield fracture mechanics model: *Journal of Structural Geology*, v. 14, p. 1133-1148.
- Cowie, P.A., and Scholz, C.H., 1992b, Displacement-length scaling relationship for faults: data synthesis and discussion: *Journal of Structural Geology*, v. 14, p. 1149-1156.
- Covington, H.R., 1987, Map showing surface features induced by underground nuclear explosions at Pahute Mesa, Nevada Test Site, Nye County, Nevada, April 1976 through November 1983: U.S. Geological Survey Miscellaneous Investigations Series Map I-1872, scale 1:48,000.
- Cramer, C.H., and Toppazada, T.R., 1980, A seismological study of the May 1980 and earlier earthquake activity near Mammoth Lakes, California: *California Division of Mines and Geology Special Report 150*, p. 91-130.
- Day, W.C., Potter, C.J., Sweetkind, D.S., Dickerson, R.P., and San Juan, C.A., 1996a, Bedrock geologic map of the Central Block area, Yucca Mountain, Nye County, Nevada: U.S. Geological Survey Administrative Report, prepared in cooperation with the Nevada Operations Office, U.S. Department of Energy.
- Day, W.C., Potter, C.J., Sweetkind, D.S., and Keefer, W.R., 1996b, Neogene tectonic evolution of Yucca Mountain; chapter 2, seismotectonic framework and characterization of faulting at Yucca Mountain, Nevada: U.S. Geological Survey Report to U.S. Department of Energy, p. 2-1 - 2-47 plus figures.
- Denlinger, R.P., and Bailey, F.S., 1984, Deformation of Long Valley caldera, Mono County, California, from 1975 to 1982: *Journal of Geophysical Research*, v. 89, p. 8303-8314.
- DeMets, C., Gordon, R.G., Argus, D.F. and Stein, S., 1990, Current plate motions: *Geophysical Journal International*, v. 101, p. 425-478.
- dePolo, C.M., 1994, The maximum background earthquake in the Basin and Range: *Bulletin of the Seismological Society of America*, v. 84, p. 466-472.
- dePolo, C.M., and Ramelli, A.R., 1987, Preliminary report on surface fractures along the White Mountains fault zone associated with the July 1986 Chalfant Valley earthquake sequence: *Bulletin of the Seismological Society of America*, v. 77, p. 290-296.
- Dickey, D.D., 1971, Strain accompanying the Jorum underground nuclear explosion and its relation to geology: *Bulletin of the Seismological Society of America*, v. 61, p. 1571-1581.

- Dickey, D.D., 1969, Strain associated with the Benham underground nuclear explosion: *Bulletin of the Seismological Society of America*, v. 59, p. 2221-2230.
- Dickey, D.D., 1968, Fault displacement as a result of underground nuclear explosions, in Eckel, E.B., ed., *Nevada Test Site: Geological Society of America Memoir 110*, p. 219-232.
- Dickey, D.D., McKeown, F.A., and Bucknam, R.C., 1972, Preliminary results of ground deformation measurements near the Cannikin explosion: *Bulletin of the Seismological Society of America*, v. 62, p. 1505-1518.
- Dixon, T.H., Robaudo, S., Lee, J., and Reheis, M., 1995, Constraints on present-day Basin and Range deformation from space geodesy: *Tectonics*, v. 14, p. 755-772.
- Dokka, R.K., and Travis, C.J., 1990, Role of the Eastern California shear zone in accommodating Pacific-North American plate motion: *Geophysical Research Letters*, v. 17, p. 1323-1326.
- Doser, D.I., 1988, Source parameters of earthquakes in the Nevada seismic zone (1915-1943): *Journal of Geophysical Research*, v. 93, p. 15,001-15,016.
- Doser, D.I., 1986, Earthquake processes in the Rainbow Mountain-Fairview Peak-Dixie Valley, Nevada, region (1954-1959): *Journal of Geophysical Research*, v. 91, p. 12,572-12,586.
- Doser, D.L., and Smith, R.B., 1989, An assessment of source parameters of earthquakes in the Cordillera of the western United States: *Bulletin of the Seismological Society of America*, v. 79, p. 1383-1409.
- Ferrill, D.A., Stirewalt, G.L., Henderson, D.B., Stamatakos, J.A., Morris, A.P., Spivey, K.H., and Wernicke, B.P., 1996a, Faulting in the Yucca Mountain region: NUREG/CR-6401, CNWRA 95-017, variously paginated.
- Ferrill, D.A., Stamatakos, J.A., Jones, S.M., Rahe, B., McKague, H.L., Martin, R.H., and Morris, A.P., 1996b, Quaternary slip history of the Bare Mountain fault (Nevada) from the morphology and distribution of alluvial fan deposits: *Geology*, v. 24, p. 559-562.
- Fridrich, C.J., 1997, Tectonic evolution of the Crater Flat basin, in Wright, L., and Troxel, B. (eds.) *Cenozoic Basins of the Death Valley Region: Geological Society of America Special Paper*, in press.

- Frizzell, V.A. Jr., and Shulters, J., 1990, Geologic map of the Nevada Test Site, southern Nevada: U.S. Geological Survey Miscellaneous Investigations Series Map I-2046, scale 1:100,000.
- Galybin, A.N., 1997, A model of mining induced fault sliding: Proceedings of the 36th U.S. Rock Mechanics Symposium, Columbia University, June 29 - July 2, 1997.
- Gomberg, J. S., 1991a, Seismicity and detection/location threshold in the southern Great Basin seismic network: *Journal of Geophysical Research*, v. 96, p. 16,401-16,414.
- Gomberg, J. S., 1991b, Seismicity and shear strain in the southern Great Basin of Nevada and California: *Journal of Geophysical Research*, v. 96, p. 16,383-16,399.
- Gomberg, J., and Bodin, P., 1994, Triggering of the $M_s = 5.4$ Little Skull Mountain, Nevada, earthquake with dynamic strains: *Bulletin of the Seismological Society of America*, v. 84, p. 844-853.
- Gross, S., and Jaume, S., 1995, Historical seismicity in the southern Great Basin: U.S. Geological Survey Administrative Report for the Yucca Mountain Project, 144 p.
- Gumper, F.J., and Scholz, C., 1971, Microseismicity and tectonics of the Nevada seismic zone: *Bulletin of the Seismological Society of America*, v. 61, p. 1413-1432.
- Hamilton, R.M., and Healy, J.H., 1969, Aftershocks of the Benham nuclear explosion: *Bulletin of the Seismological Society of America*, v. 59, p. 2271-2281.
- Hamilton, R.M., Smith, B.E., Fischer, F.G., and Papanek, P.J., 1972, Earthquakes caused by underground nuclear explosions on Pahute Mesa, Nevada Test Site: *Bulletin of the Seismological Society of America*, v. 62, p. 1319-1341.
- Hamilton, R.M., Smith, B.E., Fisher, F.G., and Papanek, P.J., 1971, Seismicity of the Pahute Mesa area, Nevada Test Site, 8 December 1968 through 31 December 1970: U.S. Geological Survey Special Studies-89 474-138.
- Hamilton, R.M., McKeown, F.A., and Healy, J.H., 1969, Seismic activity and faulting associated with a large underground explosion: *Science*, v. 166, p. 601-604.
- Hanks, T.C., and McGuire, R.K., 1981, The character of high frequency strong ground motion: *Bulletin of the Seismological Society of America*, v. 71, p. 2071-2095.

- Hardyman, R.F., and Oldow, J.S., 1991, Tertiary tectonic framework and Cenozoic history of the central Walker Lane, Nevada, in Raines, G.L., Lisle, R.E., Schafer, R.W., and Wilkinson, W.H., eds, *Geology and Ore Deposits of the Great Basin: Geological Society of Nevada Symposium Proceedings*, v. 1, p. 279-301.
- Harmsen, S.C., 1994, The Little Skull Mountain Nevada, earthquake of 29 June 1992: aftershock focal mechanisms and tectonic stress field implications: *Bulletin of the Seismological Society of America*, v. 84, p. 1484-1505.
- Harmsen, S.C., 1993a, Seismicity and focal mechanisms for the southern Great Basin of Nevada and California in 1991: U.S. Geological Survey Open-file Report 92-340, 100 p.
- Harmsen, S.C., 1993b, Preliminary seismicity and focal mechanisms for the southern Great Basin of Nevada and California-January 1992 through September 1992: U.S. Geological Survey Open-file Report 93-369, 213 p.
- Harmsen, S.C., 1991, Seismicity and focal mechanisms for the southern Great Basin of Nevada and California in 1990: U.S. Geological Survey Open-file Report 91-367, 103 p.
- Harmsen, S.C., and Bufe, C.G., 1992, Seismicity and focal mechanisms for the southern Great Basin of Nevada and California: 1987 through 1989: U.S. Geological Survey Open-file Report 91-572, 208 p.
- Harmsen, S.C., and Rogers, A.M., 1986, Inferences about the local stress field from focal mechanisms: Applications to earthquakes in the southern Great Basin of Nevada: *Bulletin of the Seismological Society of America*, v. 76, p. 1560-1572.
- Harmsen, S.C., and Rogers, A.M., 1987, Earthquake location data for the southern Great Basin of Nevada and California, 1984 through 1986: U.S. Geological Survey Open-file Report 87-596, 92 p.
- Hemphill-Haley, M.A., and Weldon, R.J. II, 1996, Estimating prehistoric earthquake magnitude from point displacements instead of surface rupture length [abs.]: *EOS, Transactions of the American Geophysical Union*, v. 77, no. 46 supplement, p. F512.
- Hill, D.P., Bailey, R.A., and Ryall, A.S., 1985, Active tectonic and magmatic processes beneath Long Valley caldera, eastern California: an overview: *Journal of Geophysical Research*, v. 90, p. 11,111-11,120.
- Hill, D. P., and 30 others, 1993, Seismicity remotely triggered by the magnitude 7.3 Landers, California earthquake: *Science*, v. 260, p. 1617-1623.

- Hill, D.P., Ellsworth, W.L., Johnston, M.L.S., Langbein, J.O., Oppenheimer, D.H. Pitt, A.M., Reasenber, P.A., Sorey, S.L., and McNutt, S., 1990, The 1989 swarm beneath Mammoth Mountain, California: an initial look at the 4 May through 30 September activity: *Bulletin of the Seismological Society of America*, v. 80, p. 325-339.
- Humphreys, E.D., and Weldon, R.J., 1994, Deformation across the western United States: a local estimate of Pacific-North America transform deformation: *Journal of Geophysical Research*, v. 99, p. 19,975-20,010.
- Jackson, J.A., and White, N.J., 1989, Normal faulting in the upper continental crust: observations from regions of active extension: *Journal of Structural Geology*, v. 11, p. 15-36.
- Jennings, C.W., 1994, Fault activity map of California and adjacent areas with locations and ages of recent volcanic eruptions: California Division of Mines and Geology, California Geologic Data Map Series, Map No. 6, scale 1:750,000.
- Johnston, M.J.S., Hill, D.P., Linde, A.T., Langbein, G., and Bilham, R., 1995, Transient deformation during triggered seismicity from the 28 June 1992 Mw = 7.3 Landers earthquake at Long Valley volcanic caldera, California: *Bulletin of the Seismological Society of America*, v. 85, 787-795.
- Julian, B.R., 1983, Evidence for dike intrusion earthquake mechanisms near Long Valley caldera, California: *Nature* v. 303, p. 323-325.
- Julian, B.R., and Sipken, S.A., 1985, Earthquake processes in the Long Valley caldera area, California: *Journal of Geophysical Research*, v. 90, p. 11,155-11,169.
- Kanamori, H., and Anderson, D.L., 1975, Theoretical basis of some empirical relations in seismology: *Bulletin of the Seismological Society of America*, v. 65, p. 1073-1095.
- Keefer, W.R., and Pezzopane, S.K., 1996, Quaternary faults in the Yucca Mountain region; chapter 3, seismotectonic framework and characterization of faulting at Yucca Mountain, Nevada: U.S. Geological Survey Report to U.S. Department of Energy, p. 3-1 - 3-34.
- King, K.W., Bayer, K.C., and Brockman S.R., 1971, Earthquakes on and around the Nevada Test Site 1950-1971: U.S. Department of Commerce NOAA Earth Sciences Laboratory, CGS-746-12.

- Klinger, R.E., and Piety, L.A., 1996, Evaluation and characterization of Quaternary faulting on the Death Valley and Furnace Creek faults, Death Valley, California: Bureau of Reclamation Seismotectonic Report 96-10, 98 p.
- Langbein, J.O., Hill, D.P., Paker, T.N., and Wilkinson, S.K., 1993, A episode of reinflation of the Long Valley Caldera, eastern California, 1989-1991: *Journal of Geophysical Research*, v. 98, p. 15, 851-15,870.
- Langenheim, V.E., Kirchoff-Stein, K.S., and Oliver, H.W., 1993, Geophysical investigations of buried volcanic centers near Yucca Mountain, southwestern Nevada, in Fourth International Conference on High-Level Radioactive Waste Management: La Grange Park, Illinois, American Nuclear Society, p. 1840-1846.
- Lee, J-J., and Bruhn, R.L., 1996, Characterization of the structural anisotropy of normal fault surfaces, *J. Structural Geology*, V. 18, p. 1043 - 1059.
- Lide, C.S., and Ryall, A.R., 1985, Aftershock distribution related to the controversy regarding mechanisms of the May 1980, Mammoth Lakes, California, earthquakes: *Journal of Geophysical Research*, v. 90, p. 11,151-11,154.
- Lienkaemper, J.J., Pezzopane, S.K., Clark, M., and Rymer, M.J., 1987, Fault fractures formed in association with the 1986 Chalfant Valley, California, earthquake sequence; preliminary report: *Bulletin of the Seismological Society of America*, v. 77, p. 297-305.
- Loper, S., Pasyanos, M., Dreger, D., and Romanowicz, B., 1993, Broadband source study of the 1993 Eureka Valley, California, earthquake sequence [abs.]: *EOS, Transactions of the American Geophysical Union*, v. 74, no. 43 supplement, p. 397.
- Lubetkin, L.D.C., and Clark, M., 1988, Late Quaternary activity along the Lone Pine fault, eastern California: *Geological Society of America Bulletin*, v. 100, p. 755-766.
- Lum, P.K., and Honda, K.K., 1992, Processed seismic motion records from Little Skull Mountain, Nevada, earthquake of June 29, 1992, recorded at stations in southern Nevada: Report #JAB-10733-TM6 UC-703; National Technical Information Service.
- Massonnet, D., and Feigl, F.L., 1995, Satellite radar interferometric map of the coseismic deformation field of the M 6.1 Eureka Valley, California earthquake of May 17, 1993: *Geophysical Research Letters*, v. 22, p. 1541-1544.

- McGarr, A., 1984, Some applications of seismic source mechanism studies to assessing underground hazard, in Gay, N.C., and Wainwright (eds.), Proceedings of the First International Congress on Rock Bursts and Seismicity in Mines: South African Institute of Mining and Metallurgy, Johannesburg, p. 198-208.
- McKague, H.L., Stamatakos, J.A., and Ferrill, D.A., 1996, Type I faults in the Yucca Mountain region: Report CNWRA 96-007, prepared by Center for Nuclear Waste Regulatory Analyses for Nuclear Regulatory Commission, variously paginated.
- McKeown, F.A., and Dickey, D.D., 1969, Fault displacements and motion related to nuclear explosions: Bulletin of the Seismological Society of America, v. 59, p. 2253-2269.
- Menges, C.M., and Whitney, J.W., 1996, Summary of Quaternary faulting on the Paintbrush Canyon, Stagecoach Road, and Bow Ridge faults; Chapter 4.4, Seismotectonic Framework and Characterization of Faulting at Yucca Mountain, Nevada: U.S. Geological Survey, Report to U.S. Department of Energy, p. 4.4-1 - 4.4-35.
- Meremonte, M.E., and Rogers, A.M., 1987, Historical catalog of Southern Great Basin earthquakes 1868-1978: U.S. Geological Survey Open-file Report 87-80, 203 p.
- Meremonte, M. E., Gomberg, J., and Cranswick, E., 1995, Constraints on the 29 June 1992 Little Skull Mountain sequence provided by robust hypocentral estimates: Bulletin of the Seismological Society of America, v. 85, p. 1039-1049.
- Meremonte, M., Cranswick, E., Gomberg, J., Worley, D., Carver, D., Brooks, J., Banfill, R., Overturf, D., and Bice, T., 1993, Report on the seismological field investigations of the 29 June 1992 Little Skull Mountain earthquake: U.S. Geological Survey Open-file Report 93-555.
- Minster, J.B., and Jordan, T.H., 1987, Vector constraints on western U.S. deformation from space geodesy, neotectonics and plate motions: Journal of Geophysical Research, v. 92, p. 4798-4804.
- Nicol, A., Walsh, J.J., Waterson, J., and Underhill, J., 1997, Displacement rates of normal faults. Nature (in press).
- O'Leary, D.W., 1996, Synthesis of tectonic models for the Yucca Mountain area; Chapter 8, Seismotectonic Framework and Characterization of Faulting at Yucca Mountain, Nevada: U.S. Geological Survey, Report to U.S. Department of Energy, p. 8-1 - 8-153.

- Parsons, T., and Thompson, G.A., 1991a, Coupled processes of normal faulting and dike intrusion in tectonically extended regions [abs.]: *Seismological Research Letters*, v. 62, p. 26.
- Parsons, T., and Thompson, G.A., 1991b, The role of magma overpressure in suppressing earthquakes and topography: worldwide examples: *Science*, v. 253, p. 1399-1402.
- Peltzer, G., and Rosen, P., 1995, Surface displacement of the 17 May 1993 Eureka Valley, California earthquake observed by SAR interferometry: *Science*, v. 268, p. 1333-1336.
- Pezzopane, S.K., 1996, Relevant earthquake sources; chapter 11, seismotectonic framework and characterization of faulting at Yucca Mountain, Nevada: U.S. Geological Survey Report to U.S. Department of Energy, p. 11-1 - 11-44.
- Pezzopane, S.K., and Dawson, T.E., 1996, Fault displacement hazard: a summary of issues and information; chapter 9, seismotectonic framework and characterization of faulting at Yucca Mountain, Nevada: U.S. Geological Survey Report to U.S. Department of Energy, p. 9-1 - 9-160.
- Pezzopane, S.K., Whitney, J.W., and Dawson, T.E., 1996a, Models of earthquake recurrence and preliminary paleoearthquake magnitudes at Yucca Mountain; chapter 5, seismotectonic framework and characterization of faulting at Yucca Mountain, Nevada: U.S. Geological Survey Report to U.S. Department of Energy, p. 5-1 - 5-100.
- Pezzopane, S.K., Bufe, C.G., Dawson, T.E., Wong, I.G., and Bott, J.D.J., 1996b, Historical seismicity in the Yucca Mountain region; chapter 7, seismotectonic framework and characterization of faulting at Yucca Mountain, Nevada: U.S. Geological Survey Report to U.S. Department of Energy, p. 7-1 - 7-72.
- Piety, L.A., 1995, Compilation of known and suspected Quaternary faults within 100 km of Yucca Mountain, Nevada and California: U.S. Geological Survey Open-file Report 94-112, 404 p.
- Pitt, A.M., and Hill, D.P., 1994, Long-period earthquakes in the Long Valley caldera region, eastern California: *Geophysical Research Letters*, v. 21, p. 1679-1682.
- Pitt, A.M., and Steeples, D.W., 1975, Microearthquakes in the Mono Lake-Northern Owens Valley, California region from September 28 to October 18, 1970: *Bulletin of the Seismological Society of America*, v. 65, p. 835-844.

- Ponce, D.A., 1993, Geophysical investigations of concealed faults near Yucca Mountain, southwest Nevada, *in* High Level Radioactive Waste Management: Fourth Annual International Conference, Proceedings, v. 1, p. 168-174.
- Priestley, K.F., Smith, K.D., and Cockerham, R.S., 1988, The 1984 Round Valley, California earthquake sequence: *Geophysical Journal of the Royal Astronomical Society*, v. 95, p. 215-235.
- Ramelli, A.R., and Bell, J.W., 1996, Known and suspected Quaternary faults, Yucca Mountain - Bare Mountain (preliminary): Nevada Bureau of Mines, scale 1:62,500.
- Ramelli, A.R., Oswald, J.A., Vadurro, G., Menges, C.M., and Paces, J.B., 1996, Quaternary faulting on the Solitario Canyon fault; Chapter 4.7, *Seismotectonic Framework and Characterization of Faulting at Yucca Mountain, Nevada: U.S. Geological Survey, Report to U.S. Department of Energy*, p. 4.7-1 - 4.7-56.
- Reheis, M.C., and Dixon, T.H., 1996, Kinematics of the Eastern California shear zone: evidence for slip transfer from Owens and Saline Valley fault zones to Fish Lake Valley fault zone: *Geology*, v. 24, 339-342.
- Reheis, M.C., and Sawyer, T.L., 1997, Late Cenozoic history and slip rates of the Fish Lake Valley, Emigrant Peak, and Deep Springs fault zones, Nevada and California: *Geological Society of America Bulletin*, v. 109, p. 280-299.
- Richard, S.M. (ed.), 1992, Deformation associated with the Neogene, Eastern California shear zone, southeastern California and southwestern Arizona: *Proceedings, San Bernardino County Museum Association, Special Publication 92-1*, 78 p.
- Richter, C.A., 1958, *Elementary Seismology*: W.H. Freeman, San Francisco, 768 p.
- Rogers, A.M., and Lee, W.H., 1976, Seismic study of earthquakes in the Lake Mead, Nevada-Arizona region: *Bulletin of the Seismological Society of America*, v. 66, p. 1657-1681.
- Rogers, A.M., Harmsen, S.C., Corbett, E.J., Priestly, K.F. and dePolo, D., 1991, The seismicity of Nevada and some adjacent parts of the Great Basin, in Slemmons, D.B., Engdahl, E.R., Zoback, M.D., and Blackwell, D.D., eds., *Neotectonics of North America: Geological Society of America, Decade Map Volume 1*, p. 153-184.
- Rogers, A. M., Harmsen, S.C., and Meremonte, M.E., 1987a, Evaluation of the seismicity of the Southern Great Basin and its relationship to the tectonic framework of the region: *U.S. Geological Survey Open-file Report 87-408*.

- Rogers, A.M., Harmsen, S.C., Herrmann, R.B., and Meremonte, M.E., 1987b, A study of ground motion attenuation in the southern Great Basin, Nevada-California, using several techniques for estimates of Q_s , $\log A_0$, and coda Q : *Journal of Geophysical Research*, v. 92, p. 3527-3540.
- Rogers, A.M., Harmsen, S.C., Carr, W.J., and Spence, W., 1983, Southern Great Basin seismological data report for 1981 and preliminary data analysis: U.S. Geological Survey Open-file Report 83-669, 240 p.
- Rogers, A.M., Harmsen, S.C., and Carr, W.J., 1981, Southern Great Basin seismological data report for 1980 and preliminary data analysis: U.S. Geological Survey Open-file Report 81-1086, 148 p.
- Romanowicz, B., Dreger, D., Pasyanos, M., and Uhrhammer, R., 1993, Monitoring strain release in central and northern California using broadband data: *Geophysical Research Letters*, v. 20, p. 1643-1646.
- Roquemore, G.R., and Simila, G.W., 1994, Aftershocks from the 28 June 1992 Landers earthquake: northern Mojave Desert to the Coso volcanic field, California: *Bulletin of the Seismological Society of America*, v. 84, p. 854-862.
- Rundle, J.B., and Whitcomb, J.H., 1984, A model for deformation in Long Valley, California, 1980-1983: *Journal of Geophysical Research*, v. 89, p. 9371-9380.
- Ryall A.S., and Ryall, F., 1983, Spasmodic tremor and possible magma injection in Long Valley Caldera, eastern California: *Science*, v. 219, p. 1432-1433.
- Sandia National Laboratories, 1997, Hydraulic fracturing stress measurements in Test Hole ESF-AOD-HDFR#1, Thermal Test Facility, Exploratory Studies Facility at Yucca Mountain: Report WBS 1.2.3.2.7.3.4, WA-0065, QA:L, 50 p.
- Savage, M.K., and Anderson, J.G., 1995, A local-magnitude scale for the western Great Basin-eastern California from synthetic Wood-Anderson seismograms: *Bulletin of the Seismological Society of America*, v. 85, p. 1236-1243.
- Savage, J.C., and Clark, M.M., 1982, Magmatic resurgence in Long Valley caldera, California: possible cause of the 1980 Mammoth Lakes earthquakes: *Science*, v. 217, p. 531-533.
- Savage, J.C., and Cockerham, R.S., 1984, Earthquake swarm in Long Valley caldera, California, January 1983: evidence for dike intrusion: *Journal of Geophysical Research*, v. 89, p. 8315-8324.

Savage, J.C. and Gross, W.K., 1995, Revised dislocation model of the 1986 Chalfant Valley earthquake, eastern California: *Bulletin of the Seismological Society of America*, v. 85, p. 629-631.

Savage, J.C., Lisowski, M., and Prescott, W.H., 1990, An apparent shear zone trending north-northwest across the Mojave Desert into Owens Valley, California: *Geophysical Research Letters*, v. 17, p. 2113-2136.

Schwartz, D.P., and Coppersmith, K.J., 1984, Fault behavior and characteristic earthquakes: examples from the Wasatch and San Andreas faults: *Journal of Geophysical Research*, v. 89, p. 5681-5698.

Scott, R.B., 1990, Tectonic setting of Yucca Mountain, southwest Nevada, in Wernicke, B.P. (ed.), *Basin and Range Extensional Tectonics Near the Latitude of Las Vegas, Nevada: Geological Society of America Memoir 176*, p. 251-282.

Sheehan, A.F., Gillett, S.L., Smith, K.D., and Savage, M.K., 1994, Data report on seismological field investigations of the 29 June 1992 Little Skull Mountain earthquake: *Administrative Report to the Department of Energy-USGS Yucca Mountain Project*.

Shields, G., Smith, K.D., and Brune, J.N., 1995, Source parameters of a sequence of very shallow earthquakes in the Rock Valley fault zone, southern Nevada Test Site [abs.]: *EOS, Transactions of the American Geophysical Union*, v. 76, p. F426.

Simonds, W.F., Whitney, J.W., Fox, K., Ramelli, A., Yount, J., Carr, M., Menges, C.M., Dickerson, R., and Scott, R.B., 1995, Map of fault activity of the Yucca Mountain area, Nye County, Nevada: *U.S. Geological Survey Miscellaneous Investigations Series Map I-2520*, scale 1:24,000.

Smith, B.E., Coakley, J.M., and Hamilton, R.M., 1972, Distribution, focal mechanisms, and frequency of earthquakes in the Fairview Peak area, Nevada, near the time of the Benham explosion: *Bulletin of the Seismological Society of America*, v. 62, p. 1223-1240.

Smith, K.D., and Brune, J.N., 1997, A sequence of very shallow earthquakes in the Rock Valley fault zone, southern Nevada Test Site: *U.S. Geological Survey Circular on Yucca Mountain Tectonics*, in press.

Smith, K.D., and Priestley, K.F., 1997, The 1986 Chalfant, California earthquake sequence, earthquake relocations and source parameters: *Bulletin of the Seismological Society of America*, in press.

- Smith, K.D., and Priestley, K.F., 1988, The foreshock sequence of the 1986 Chalfant, California earthquake: *Bulletin of the Seismological Society of America*, v. 78, p. 172-187.
- Smith, K.D., Brune, J.N., Savage, M.K., dePolo, D., Anooshehpour, R., and Sheehan, A.F., 1997, The 1992 Little Skull Mountain earthquake sequence, southern Nevada Test Site: in review, *Bulletin of the Seismological Society of America*.
- Smith, K.D., von Seggern, D., Biasi, G., Middlebrooks, C.L. and Brune, J.N., 1996, Performance of the Southern Great Basin Digital Seismic Network: *Proceedings, Methods of Seismic Hazards Evaluation Focus '95, American Nuclear Society*, p. 64-71.
- Smith, R.B., and Sbar, M.L., 1974, Contemporary tectonics and seismicity of the western United States with emphasis on the Intermountain seismic belt: *Geological Society of America Bulletin*, v. 85, p. 1205-1218.
- Smith, R.P., Jackson, S.M., and Hackett, W.R., 1996, Paleoseismology and seismic hazards evaluations in extensional volcanic terrains: *Journal of Geophysical Research*, v. 101, p. 6277-6292.
- Stamatakos, J.A., Connor, C.B., and Martin, R.H., 1997, Quaternary basin evolution and basaltic volcanism of Crater Flat, Nevada from detailed ground magnetic surveys of the Little Cones: *Journal of Geology*, v. 105, p. 319-330.
- Stewart, J.H., 1988, Tectonics of the Walker Lane belt, western Great Basin--Mesozoic and Cenozoic deformation in a zone of shear, in Ernst, W.G., ed., *Metamorphism and Crustal Evolution of the Western United States, Rubey Volume VII*: Prentice Hall, Englewood Cliffs, NJ, p. 683-713.
- Stewart, J.H., 1978, Basin-range structure in western North America: a review, in Smith, R.B., and Eaton, G.P., eds., *Cenozoic Tectonics and Regional Geophysics of the Western Cordillera*: *Geological Society of America Memoir* 152, p. 1-31.
- Stock, J.M., and Healy, J.H., 1988, Stress field at Yucca Mountain, Nevada: *U.S. Geological Survey Bulletin* 1790, p. 87-93.
- Taylor, E.M., 1996, Quaternary faulting on the Southern Crater Flat fault; Chapter 4.10, *Seismotectonic Framework and Characterization of Faulting at Yucca Mountain, Nevada*: U.S. Geological Survey, Report to U.S. Department of Energy, p. 4.10-1 - 4.10-13.

- Taylor, E.M., Menges, C.M., de Fontaine, C.S., Buesch, D.C., Mundo, B.O., and Murray, M., 1996a, Preliminary results of paleoseismic investigations on the Ghost Dance fault; chapter 4.5, seismotectonic framework and characterization of faulting at Yucca Mountain, Nevada: U.S. Geological Survey Report to U.S. Department of Energy, p. 4.5-1 - 4.5-41.
- Taylor, E.M., Coe, J.A., Huckins-Gang, H.E., and Levy, S., 1996b, Revised logs, including deepened exposures, of Trench 14 on the Bow Ridge fault; chapter 4.6, seismotectonic framework and characterization of faulting at Yucca Mountain, Nevada: U.S. Geological Survey Report to U.S. Department of Energy, p. 4.6-1 - 4.6-13.
- VanWormer, J. D., and Ryall, A.S., 1980, Sierra Nevada-Great Basin boundary zone: earthquake hazard related to structure, active tectonic processes, and anomalous patterns of earthquake occurrence: Bulletin of the Seismological Society of America, v. 70, p. 1557-1572.
- Veneziano, D. and van Dyck, J., 1985, Statistical discrimination of "aftershocks" and their contribution to seismic hazard, Appendix A-4, in Seismic Hazard Methodology for Nuclear Facilities in the Eastern United States, EPRI Research Project Number P101-29, p. A121-A186.
- Vortman, L.J., 1991, An evaluation of the seismicity of the Nevada Test Site and vicinity: Sandia National Laboratory SAND 86-7006, 231 p.
- von Seggern, D., and Brune, J.N, 1997, Seismicity in the SGB: what do earthquake catalogs accurately indicate?: Poster presented at the Western States Seismic Policy Council Symposium, Basin and Range Province Seismic Hazards Summit, Reno, Nevada, May 12-15, 1997, p. 70.
- von Seggern, D., and dePolo, D., 1995, Seismicity for the southern Great Basin of Nevada and California in 1993: U.S. Geological Survey Administrative Report for the Yucca Mountain Project, variously paginated.
- von Seggern, D., and Smith, K.D., 1997, Seismicity for the southern Great Basin of Nevada and California in 1996: U.S. Geological Survey Administrative Report for the Yucca Mountain Project.
- von Seggern, D., dePolo, D., and Smith, K.D., 1996, Seismicity for the Southern Great Basin of Nevada and California in 1993: U.S. Geological Survey Administrative Report for the Yucca Mountain Project, variously paginated.

- Wallace, R.E., 1987, Grouping and migration of surface faulting and variations in slip rates on faults in the Great Basin province: *Bulletin of the Seismological Society of America*, v. 77, p. 868-876.
- Wallace, T.C., 1984, A re-examination of the moment tensor solution of the 1980 Mammoth Lakes earthquake, *in* Active Tectonic and Magmatic Processes in Long Valley Caldera: U.S. Geological Survey Open-file Report 84-939, p. 409-439.
- Wallace, T.C., Helmberger, D.V., and Engen, G.R., 1985, Evidence of tectonic release from underground nuclear explosions in long-period S waves: *Bulletin of the Seismological Society of America*, v. 75, p. 157-174.
- Wallace, T.C., Helmberger, D.V., and Engen, G.R., 1983, Evidence for tectonic release from underground nuclear explosions in long-period P waves: *Bulletin of the Seismological Society of America*, v. 73, p. 326-346.
- Walsh, J.J., and Waterson, J., 1992, Populations of faults and fault displacements and their effects on estimates of fault related regional extension: *Journal of Structural Geology*, v. 14, p. 701-712.
- Walsh, J.J. and Waterson, J., 1987, Distribution of cumulative displacement and of seismic slip on a single normal fault surface: *Journal of Structural Geology*, v. 9, p. 1039-1046.
- Walter, W., 1993, Source parameters of the June 29, 1992 Little Skull Mountain earthquake from complete regional waveforms at a single station: *Geophysical Research Letters*, v. 20, p. 403-406.
- Ward, S.H., 1990, Pacific-North America plate motions: new results from very long baseline interferometry: *Journal of Geophysical Research*, v. 95, p. 21,965-21,981.
- Wells, D.L., and Coppersmith, K.J., 1994, New empirical relationships among magnitude, rupture length, rupture width, rupture area, and surface displacement: *Bulletin of the Seismological Society of America*, v. 84, p. 974-1002.
- Wernicke, B., 1995, Low-angle normal faults and seismicity: a review: *Journal of Geophysical Research*, v. 100, p. 20,159-20,174.
- Wheeler, R.L., 1989, Persistent segment boundaries on basin-range normal faults, in Schwartz, D.P. and Sibson, R.H. (eds.), *Fault segmentation and controls of rupture initiation and termination*: U.S. Geological Survey Open File Report 89-315, p.432-444.

- Whitney, J.W., Simonds, F.W., Shroba, R.R., and Murray, M., 1996, Quaternary faulting on the Windy Wash fault; Chapter 4.9, Seismotectonic Framework and Characterization of Faulting at Yucca Mountain, Nevada: U.S. Geological Survey, Report to U.S. Department of Energy, p. 4.9-1 - 4.9-39.
- Wiechert, D.H., 1980, Estimation of the earthquake recurrence parameters for unequal observation periods for different magnitudes: *Bulletin of the Seismological Society of America*, v. 70, p. 1337-1346.
- Wright, L.A., 1989, Overview of the role of strike-slip and normal faulting in the Neogene history of the region northeast of Death Valley, California-Nevada, in Ellis, M.A. (ed.), *Later Tertiary Evolution of the Southern Great Basin*: Nevada Bureau of Mines and Geology Open File 89-1, p. 1-11.
- Wright, L., 1976, Late Cenozoic fault patterns and stress fields in the Great Basin and westward displacement of the Sierra Nevada block: *Geology*, v. 4, p. 489-494.
- Youngs, R.R., and Coppersmith, K.J., 1985, Implications of fault slip rates and earthquake recurrence models to probabilistic seismic hazard estimates: *Bulletin of the Seismological Society of America*, v. 75, p. 939-964.
- Youngs, R.R., Swan, F.H., Power, M.S., Schwartz, D.P., and Green, R.K., 1987, Probabilistic analysis of earthquake ground shaking hazard along the Wasatch Front, Utah: U.S. Geological Survey Open-file Report 87-585, v. II, p. M1-M110.
- Zhang, P., Ellis, M., Slemmons, D.B., and Mao, F., 1990, Right-lateral displacements and the Holocene slip rate associated with prehistoric earthquakes along the southern Panamint Valley fault zone; implications for southern Basin and Range tectonics and coastal California deformation: *Journal of Geophysical Research*, v. 95, p. 4857-4872.
- Zhao, L.S., and Helmberger, D.V., 1994, Source estimation from broad-band regional seismograms: *Bulletin of the Seismological Society of America*, v. 84, p. 91-104.

**TABLE SBK-1
REGIONAL FAULT SOURCES**

Fault Name	Ind. Source	Type and Dip Direction	Maximum Magnitude Approach				Recurrence Approach			Recurrence Model
			Length (km)	Area	Max. Offset (m)	Av. Offset (m)	Long-term Slip Rate (m/kyr)	Quat Slip Rate (m/kyr)	Interval (kyr)	
Amargosa River	Y (0.8)	RL (0.6)	(0.35)	(0.35)	(0.3)			(0.9)	(0.1)	C (0.4)
	N (0.2)	N (0.4)	12 (0.7)		2.5 (0.2)			0.02 (0.5)	10 (1.0)	TE (0.6)
		East (1.0)	15 (0.3)		1.6 (0.8)			0.03 (0.5)		
Ash Meadows	Y (0.8)	N (1.0)	(0.35)	(0.35)	(0.3)		(0.1)	(0.9)		C (0.6)
	N (0.2)		30 (0.3)		1.4 (0.2)		0.016 (1.0)	0.01 (0.2)		TE (0.4)
		West (1.0)	40 (0.6)		1.8 (0.8)			0.04 (0.7)		
			100 (0.1)					0.1 (0.1)		
Belted Range	Y (0.9)	N (1.0)	(0.25)	(0.25)	(0.3)	(0.2)	(0.2)	(0.8)		C (0.6)
	N (0.1)		22 (0.4)		1.0 (1.0)	0.8 (1.0)	0.05 (1.0)	0.01 (0.1)		TE (0.4)
		West (1.0)	38 (0.2)					0.09 (0.7)		
			50 (0.4)					0.2 (0.2)		
Buried Hills – Emigrant Valley South	Y (0.01)	N (1.0)	(0.5)	(0.5)				(1.0)		C (0.6)
	N (0.99)		51 (0.8)					0.01 (0.5)		TE (0.4)
		West (1.0)	57 (0.2)					0.001 (0.5)		

**TABLE SBK-1
REGIONAL FAULT SOURCES
(Continued)**

Fault Name	Ind. Source	Type and Dip Direction	Maximum Magnitude Approach				Recurrence Approach			Recurrence Model
			Length (km)	Area	Max. Offset (m)	Av. Offset (m)	Long-term Slip Rate (m/kyr)	Quat Slip Rate (m/kyr)	Interval (kyr)	
Southern Death Valley - Death Valley - Furnace Creek - Fish Lake Valley	Y (0.01)	RL (1.0)	(0.25)	(0.25)		(0.5)		(0.8)	(0.2)	C (0.9)
	N (0.99)		340 (1.0)			2.5 (0.3)		4.0 (0.4)	0.40 (0.5)	TE (0.1)
		West (1.0)				3.5 (0.3)		5.0 (0.4)	0.80 (0.5)	
						4.5 (0.4)		8.0 (0.2)		
Death Valley - Southern Death Valley	Y (0.05)	N (0.2)	(0.15)	(0.15)		(0.7)	(0.2)	(0.4)	(0.4)	C (0.9)
	N (0.95)	RL (0.8)	115 (0.7)			2.5 (0.5)	2.0 (0.5)	1.5 (0.2)	0.50 (0.2)	TE (0.1)
			140 (0.3)			3.5 (0.5)	3.0 (0.5)	3.0 (0.4)	0.70 (0.3)	
		West (1.0)						5.0 (0.4)	1.00 (0.3)	
								1.30 (0.2)		
Furnace Creek - Fish Lake Valley	Y (0.05)	RL (1.0)	(0.2)	(0.2)	(0.2)	(0.4)		(0.8)	(0.2)	C (0.9)
	N (0.95)		230 (0.5)			3.0 (0.5)		2.0 (0.1)	0.60 (0.4)	TE (0.1)
		West (1.0)	240 (0.5)			6.0 (0.5)	4.5 (0.9)	4.0 (0.4)	0.80 (0.2)	
								8.0 (0.4)	1.70 (0.4)	
								10.0 (0.1)		
Fish Lake Valley	Y (0.94)	RL (1.0)	(0.5)	(0.5)			(0.4)	(0.6)		C (0.9)
	N (0.95)		50 (0.4)				3.0 (0.3)	2 (0.2)		TE (0.1)
		West (1.0)	75 (0.6)				5.0 (0.7)	3 (0.5)		
							4 (0.3)			

**TABLE SBK-1
REGIONAL FAULT SOURCES
(Continued)**

Fault Name	Ind. Source	Type and Dip Direction	Maximum Magnitude Approach				Recurrence Approach			Recurrence Model			
			Length (km)	Area	Max. Offset (m)	Av. Offset (m)	Long-term Slip Rate (m/kyr)	Quat Slip Rate (m/kyr)	Interval (kyr)				
Southern Death Valley	Y. (0.94) N (0.06)	RL (1.0)	(0.5)	(0.5)				(0.8) 2.0 (0.5) 3.0 (0.5)	(0.2) 0.3 (1.0)		C (0.9) TE (0.1)		
		West (1.0)	45 (0.2)									75 (0.7)	85 (0.1)
Death Valley	Y. (0.94) N (0.06)	N (0.5)	(0.35)	(0.35)			(0.3) 2.5 (0.5) 3.5 (0.5)	(0.6) 1.5 (0.2) 3.0 (0.4) 5.0 (0.3) 7.0 (0.1)	(0.4) 0.5 (0.2) 0.7 (0.3) 1.0 (0.3) 1.3 (0.2)		C (0.9) TE (0.1)		
		Obl (0.5)	45 (0.4)									51 (0.2)	68 (0.4)
		West (1.0)											
Furnace Creek	Y. (0.94) N (0.06)	RL (1.0)	(0.2)	(0.4)	(0.2)	(0.2)	(0.1) 4.0 (0.2) 8.0 (0.4) 10.0 (0.4)	(0.6) 4.0 (0.4) 8.0 (0.5) 10.0 (0.1)	(0.3) 0.60 (0.5) 0.80 (0.5)		C (0.9) TE (0.1)		
		West (1.0)	105 (0.7)									115 (0.1)	160 (0.2)
Kawich Range	Y (0.04) N (0.6)	N (1.0)	(0.35)	(0.35)	(0.3)	(1.0)		(1.0) 0.01 (0.3) 0.002 (0.7)			C (0.6) TE (0.4)		
		West (1.0)	74 (0.1)									78 (0.3)	84 (0.6)

**TABLE SBK-1
REGIONAL FAULT SOURCES
(Continued)**

Fault Name	Ind. Source	Type and Dip Direction	Maximum Magnitude Approach				Recurrence Approach			Recurrence Model
			Length (km)	Area	Max. Offset (m)	Av. Offset (m)	Long-term Slip Rate (m/kyr)	Quat Slip Rate (m/kyr)	Interval (kyr)	
Pahrump	Y (0.9)	Obl (0.8)	(0.45)	(0.45)	(0.1)		(0.8) (RL)	(0.2) (V)		C (0.4)
	N (0.1)	RL (0.2)	18.5 (0.33)		0.7 (1.0)		.11 (0.5)	0.009 (0.5)		TE (0.6)
		West (1.0)	50 (0.33)				.19 (0.5)	0.02 (0.5)		
Rock Valley	Y (1.0)	LL-N (0.3)	(0.2)	(0.2)	(0.3)	(0.3)		(0.8)	(0.2)	C (0.4)
		LL (0.7)	19 (0.1)		5.2 (0.2)	1.7 (0.5)		0.003 (0.1)	6 (0.1)	TE (0.6)
		SE (1.0)	32 (0.5)		5.7 (0.8)	3.9 (0.5)		0.02 (0.8)	12 (0.2)	
			65 (0.4)					0.05 (0.1)	20 (0.2)	
Sarcobatus Flat	Y (0.01)	N (1.0)	(0.5)	(0.5)				(1.0)		C (0.4)
	N (0.99)		27 (0.2)					0.01 (0.1)		TE (0.6)
		West (1.0)	49 (0.8)					0.001 (0.6)		
								0.0001 (0.3)		
West Pintwater Range	Y (0.5)	N (1.0)	(0.5)	(0.5)				(1.0)		C (0.6)
	N (0.5)		60 (0.3)					0.01 (0.6)		TE (0.4)
		West (1.0)	82 (0.7)					0.001 (0.4)		

**TABLE SBK-1
REGIONAL FAULT SOURCES
(Continued)**

Fault Name	Ind. Source	Type and Dip Direction	Maximum Magnitude Approach				Recurrence Approach			Recurrence Model	
			Length (km)	Area	Max. Offset (m)	Av. Offset (m)	Long-term Slip Rate (m/kyr)	Quat Slip Rate (m/kyr)	Interval (kyr)		
West Spring Mountains	Y (0.9)	N (1.0)	(0.3)	(0.3)		(0.4)		(0.7)	(0.3)	C	(0.6)
	N (0.1)		30 (0.2)			1.7 (0.5)		0.02 (0.5)	28 (0.2)	TE	(0.4)
		West (1.0)	47 (0.5)			2.0 (0.5)		0.07 (0.5)	120 (0.8)		
			54 (0.3)								
Yucca	Y (0.9)	N (0.8)	(0.5)	(0.5)			(0.2)	(0.8)		C	(0.4)
	N (0.1)	Obl (0.2)	20 (0.2)				0.03 (0.5)	0.03 (0.20)		TE	(0.6)
			32 (0.5)				0.07 (0.5)	0.09 (0.79)			
		East (1.0)	45 (0.3)					0.5 (0.01)			

Notes and Sources - Table SBK-1:

Each column contains a weighting in parenthesis (**bold**) for that variable within the overall grouping (e.g., weight of 0.3 for fault length as an estimator for maximum magnitude) as well as weightings of individual values for that variable (e.g., 60-km length weighted 0.3; 82-km length weighted 0.7). Ind. Source: likelihood that fault behaves as an independent source, generating a maximum magnitude earthquake that is larger than that of regional seismic source in which it is located. Type: RL - right lateral; LL - left lateral; Obl - oblique; N - normal. Area: computed from down-dip width of fault (fault dip and maximum seismogenic depth) times length; down-dip width depends on fault type, as noted in text. Seismogenic depth derived from regional source zone in which fault is embedded. Interval: average time between surface rupture events. Recurrence Model: shape of recurrence curve; C - characteristic; TE - truncated exponential.

Amargosa River R.E. Anderson and others, 1995b; Piety, 1995. Discontinuous strike-slip fault; fault length of 12 km from Anderson and others, 15 km from Piety. 100-ka scarps according to Anderson and others; single-event ruptures interpreted from their scarp data. Slip Rate from 2.5 to 3 m offset in ca. 100 ka as best data.

TABLE SBK-1
REGIONAL FAULT SOURCES
(Continued)

Notes and Sources - Table SBK-1 (Continued):

- Ash Meadows** R.E. Anderson and others, 1995b; Piety, 1995; Carr, 1990; regional gravity data. Discontinuous normal fault zone, up to 8 km wide. Longest length is obtained by including the so-called "gravity fault" recognizable in regional gravity gradient data along the east side of Fortymile Wash in Jackass Flat. Rock Valley fault, however, may terminate active fault zone at north, cutting off connection to "gravity fault." We consider this the more likely case, given lack of surface expression for "gravity fault," especially compared to expression of Ash Meadows fault in Amargosa Valley. Likely age of youngest event varies substantially along mapped fault traces; probably a segmented fault, but insufficient data to constrain segments.
- Belted Range** Piety, 1995; R.E. Anderson and others, 1995a. Relatively short length (21 km according to Anderson and others) has Quaternary offset; however, maximum length set as equal to mapped fault length, which is uncertain depending on source. Limited evidence for Quaternary slip leads to conclusion that earthquakes above those defined for regional source zone are very unlikely on this fault. Slip rate estimated by using 11.3 m in about 50 ka from scarp morphology reported by Anderson and others
- Buried Hills-Emigrant Valley South** Pezzopane, 1996; Piety, 1995. Possible fault combination; neither fault zone considered capable of producing larger earthquake than regional maximum magnitude. Slip rate based on comparison with other Basin-Range faults, thus has low certainty. No actual evidence that these faults have ruptured together; thus low weighting as independent source.
- Combined Southern Death Valley - Death Valley - Furnace Creek - Fish Lake Valley** Jennings, 1994; Klinger and Piety, 1996; Piety, 1995; Reheis and Sawyer, 1997. Formed by combining all four faults. Total length measured from Jennings map. Average offset taken from data compiled by Klinger and Piety, 1996. Slip rate based on best constrained slip rates for the four constituent faults. Treats Death Valley fault as a pull-apart along the shear zone. Little likelihood that all faults rupture together, given size of pull-apart basin and discontinuous traces.
- Combined Death Valley and Southern Death Valley** Piety, 1995; Klinger and Piety, 1996; Jennings, 1994. Rupture length reported as 45 to 60 km, although total length is 115 km if both faults are considered together. Note that Southern Death Valley fault is strike-slip, Death Valley fault normal (pull-apart). Long-term rate for Southern Death Valley, Quaternary rate for Death Valley.
- Combined Furnace Creek-Fish Lake Valley** Reheis and Sawyer, 1997; Piety, 1995; Klinger and Piety, 1996; Jennings, 1994. Some chance that Furnace Creek and Fish Lake Valley faults are continuous and can rupture together, within uncertainties of the data. However, available data are insufficient to prove (within overlaps on dating) that paleoseismic events could have been simultaneous on the two faults. Note that restraining bend between them has no Holocene slip.
- Fish Lake Valley** Reheis and Sawyer, 1997; Piety, 1995; Jennings, 1994. Northern termination of fault poorly shown on maps of Jennings or Reheis and Sawyer, producing uncertainty in maximum fault length. Slip rate data well constrained by Reheis and Sawyer.
- Southern Death Valley** Piety, 1995; Jennings, 1994. Southern extent of fault uncertain. Most likely southern termination at Garlock fault. Late Quaternary slip rate poorly constrained.
- Death Valley** Klinger and Piety, 1996; Jennings, 1994; Piety, 1995. Shorter fault length based on older scarps in northern third of fault, suggesting rupture length less than total fault length.
- Furnace Creek** Piety, 1995; Klinger and Piety, 1996; Jennings, 1994. Maximum surface rupture length reported as 105 km by Klinger and Piety, so this is considered most likely maximum rupture length. Fault shown by Jennings possibly continuing as much as 20 km farther southeast into Amargosa Valley; however, no evidence for this continuation, and remainder of southern Furnace Creek fault is well expressed along the range front. Thus we consider any greater length to the fault exceedingly unlikely, and it is given zero weight.

**TABLE SBK-1
REGIONAL FAULT SOURCES
(Continued)**

Notes and Sources - Table SBK-1 (Continued):

- Kawich Range** Pezzopane, 1996, Piety, 1995; R.E. Anderson and others, 1995a. Same as Kawich Range West fault zone of Anderson and others. Only a short section (3.6 to 7.4 km) is indicated by Anderson and others to have Quaternary slip; were this the entire source, it would produce earthquakes no larger than those accounted for in the regional source zone. Assessment is based on assuming entire fault could break in a single event, which is extremely unlikely, given evidence this apparently has not happened in Quaternary. Anderson and others argue that slip rate must be very low given lack of recurrent Quaternary slip and embayed range front. Most likely slip rate from approximately 2 m slip in alluvium of Quaternary age, possibly 1 Ma.
- Pahrump** Piety, 1995; R.E. Anderson and others, 1995b. Likely length 50 to 70 km; Quaternary activity may be only along 18.5 km. Maximum vertical offset 5 m on late Quaternary deposits; no constraints on Quaternary right-lateral displacement rate.
- Rock Valley** Piety, 1995; R.E. Anderson and others, 1995b; Coe and others, 1996b; unpubl preliminary TL ages from Mahan, 2/20/97. Main fault zone 32 km long, SS; youngest event post 2.45 ka at one site, >10 cm; prior event > 20km rupture ca. 7.2 ka. 14.2 m slip in that and two prior events from trench data constrain offset per event and Quaternary slip rate. Offsets of 3.2, 5.2, and 5.7 m if horiz:vert ratio remains constant. Maximum length taken by including southwest extension as mapped by Anderson and others, others; however, this section may be older than main Rock Valley fault zone, so is weighted less as defining maximum length.
- Sarcobatus Flat** R.E. Anderson and others, 1995a; Piety, 1995. Almost no evidence for any Quaternary displacement according to Anderson and others, so slip rate must be extremely low. Rate constrained by similar low slip-rate faults in regional and local area.
- West Pintwater Range** Piety, 1995. Longer fault length includes North Desert Range fault. Apparently there is a lack of repeated Quaternary displacement. Slip rate constrained by comparisons with other regional and local faults.
- West Spring Mountains** Piety, 1995; R.E. Anderson and others, 1995a. More than 20 m late Quaternary displacement. Possibly 12 m on 120-ka surface. Length uncertain principally based on how far south past range front fault is continued, as well as northern termination. Maximum length includes all of range front to north and a southern termination at the Pahrump fault. Minimum distance based on Anderson and others' mapping of scarps.
- Yucca** Piety, 1995. Scarp at least 20 km long; longer lengths from combining with other faults to the north, despite lack of evidence for linked ruptures. Fault shows explosion-related offsets; also reported to be youngest prehistoric scarp in test site region, as cited by Piety. 0.3-0.6 km total displacement post tuff 11 to 8.5 Ma; Quaternary slip rates computed assuming 15 m slip in middle to late Quaternary, as summarized by Piety, and the slight chance that historical explosion-related ruptures are releasing tectonic strain.

**TABLE SBK-2
OTHER REGIONAL FAULTS
(Page 1 of 2)**

FAULT NAME	SOURCES	NOTES
Area Three	Keefer and Pezzopane, 1996; Piety, 1995	Within regional source magnitudes
Bullfrog Hills	Keefer and Pezzopane, 1996; Piety, 1995	No convincing Q displ
Cane Spring	Keefer and Pezzopane, 1996; Piety, 1995	No convincing Q displ
Carpetbag	Keefer and Pezzopane, 1996; Piety, 1995	Largely concealed; no convincing late Q displacement
Checkpoint Pass	Keefer and Pezzopane, 1996; Piety, 1995	Little if any Quat offset proven
Crossgrain Valley	Keefer and Pezzopane, 1996; Piety, 1995	Little data on age; prob. Q scarps along 20% of mapped fault; within regional source magnitudes
Eleana Range	Keefer and Pezzopane, 1996; Piety, 1995	6-9 km likely length, but not all late Q; within regional source magnitudes
Emigrant Valley North	Keefer and Pezzopane, 1996; Piety, 1995	Within regional source magnitudes
Grapevine	Keefer and Pezzopane, 1996; Piety, 1995	Within regional source magnitudes
Hunter Mtn-Panamint Valley	Piety, 1995	Not a linked structure
Hunter Mtn	Piety, 1995	Within regional source magnitudes
Kawich Valley	Keefer and Pezzopane, 1996; Piety, 1995	Not likely middle-late Q displ
Keane Wonder	Piety, 1995; R.E. Anderson and others, 1995a	Not likely middle-late Q displ; within regional source magnitudes
Mercury Ridge	Keefer and Pezzopane, 1996; Piety, 1995	Within regional source magnitudes
Mine Mountain	Keefer and Pezzopane, 1996; Piety, 1995	Not likely middle-late Q displ
North Desert Range	Keefer and Pezzopane, 1996; Piety, 1995	Within regional source magnitudes
Oak Spring Butte	Keefer and Pezzopane, 1996; Piety, 1995	Combined with Yucca fault
Oasis Valley	Piety, 1995; R.E. Anderson and others, 1996a	Not likely middle-late Q displ

TABLE SBK-2
OTHER REGIONAL FAULTS
 (Page 2 of 2)

FAULT NAME	SOURCES	NOTES
Pahute Mesa	Keefer and Pezzopane, 1996; Piety, 1995	Not likely middle-late Q displ; within regional source magnitudes
Panamint Valley	Piety, 1995	Paleoseismic event 25-30 km long, so within regional source magnitudes
Plutonium Valley	Keefer and Pezzopane, 1996; Piety, 1995	Within regional source magnitudes
Ranger Mountains	Keefer and Pezzopane, 1996; Piety, 1995	Within regional source magnitudes
Rocket Wash-Beatty Wash	R.E. Anderson and others, 1995b; L. Anderson and Klinger, 1996a; Piety, 1995	Not a fault
South Ridge	Keefer and Pezzopane, 1996; Piety, 1995	Within regional source magnitudes
Spotted Range	Keefer and Pezzopane, 1996; Piety, 1995	Within regional source magnitudes
Tolicha Peak	R.E. Anderson and others, 1995a; Keefer and Pezzopane, 1996; Piety, 1995	Within regional source magnitudes
Wahmonie	Keefer and Pezzopane, 1996; Piety, 1995	Within regional source magnitudes
West Specter Range	R.E. Anderson and others, 1996b	Within regional source magnitudes
Yucca Lake	Keefer and Pezzopane, 1996; Piety, 1995	Within regional source magnitudes

Notes - Table SBK-2:

"Within regional source magnitudes" indicates that maximum magnitude on this fault would be within the range of magnitudes incorporated into the regional source zone of which this fault is a part.

**TABLE SBK-3
LOCAL FAULTS**

Fault Name	Ind. Source	Type	Maximum Magnitude Approach					Recurrence Approach			Recurrence Model	
			Length (km)	Area	Max Offset (m)	Av Offset (m)	Offset from Stress Drop	Long-term Slip Rate (m/kyr)	Quat Slip Rate (m/kyr)	Interval (kyr)		
Hwy. 95 fault (0.8 likelihood of existence)	Y (0.4)	LL (0.5)	(0.5)						(1.0)			C (0.1)
	N (0.6)	N (0.5)	30 0.5						0.002 0.9			TE (0.9)
			49 0.5						0.02 0.1			
Bare Mountain	Y (1.0)	N (1.0)	(0.2)	(0.5)	(0.3)				(0.05)	(0.65)	(0.3)	C (0.6)
			15.5 0.1		0.80 0.2			0.13 0.1	0.01 0.7	20 0.05	TE (0.4)	
			20 0.5		1.50 0.8			0.20 0.6	0.02 0.3	40 0.05		
			23 0.4				0.24 0.3		100 0.45	200 0.45		
South Crater Flat		N-LL (1.0)	(0.2)	(0.4)	(0.1)	(0.1)	(0.2)		(0.7)	(0.3)	C (0.3)	
			6.1 0.5		0.20 0.5	0.05 0.3		0.001 0.1	60 0.7	TE (0.7)		
			8.2 0.3		0.50 0.5	0.10 0.6		0.002 0.8	70 0.2			
			10 0.2			0.20 0.1		0.003 0.1	180 0.1			
North Crater Flat		N (0.5) Obi (0.5)	(0.2)	(0.5)	(0.1)		(0.2)		(0.7)	(0.3)	C (0.3)	
			10 0.3		0.40 0.4			0.002 0.5	120 0.5	TE (0.7)		
			13.3 0.7		0.60 0.6			0.003 0.5	160 0.5			
Windy Wash		N-LL (1.0)	(0.2)	(0.4)	(0.2)	(0.1)	(0.1)	(0.1)	(0.7)	(0.2)	C (0.3)	
			25 0.2		0.96 0.5	0.30 0.5		0.025 0.2	0.01 0.2	35 0.1	TE (0.7)	
			27 0.5		0.98 0.5	0.50 0.5		0.027 0.8	0.011 0.6	40 0.4		
			28 0.3					0.016 0.2	45 0.4	100 0.1		
Fatigue Wash		N (0.7) Obi (0.3)	(0.2)	(0.4)	(0.1)	(0.1)	(0.2)		(0.7)	(0.3)	C (0.3)	
			7.5 0.2		0.50 0.9	0.25 0.2		0.002 0.2	50 0.05	TE (0.7)		
			12.5 0.5		1.50 0.1	0.30 0.4		0.009 0.8	120 0.1			
			18.5 0.3			0.50 0.4			185 0.7	250 0.15		
Solitario Canyon		N-LL (1.0)	(0.2)	(0.5)	(0.2)		(0.1)	(0.05)	(0.75)	(0.2)	C (0.3)	
			13 0.2		1.10 0.1			0.002 0.5	0.007 0.2	40 0.3	TE (0.7)	
			18 0.8		1.20 0.6			0.003 0.5	0.01 0.6	60 0.3		
				1.30 0.3			0.02 0.2	100 0.1	180 0.3			

**TABLE SBK-3
LOCAL FAULTS
(Continued)**

Fault Name	Ind. Source	Type	Maximum Magnitude Approach					Recurrence Approach				Recurrence Model					
			Length (km)		Area	Max Offset (m)		Av Offset (m)		Offset from Stress Drop	Long-term Slip Rate (m/kyr)		Quat Slip Rate (m/kyr)		Interval (kyr)		
Iron Ridge	Y (0.1)	N (1.0)	(0.3)		(0.5)	(0.1)			(0.1)		(1.0)			C (0.3)			
	N (0.9)		7.2	0.8		1.00	0.7			0.002	0.5			TE (0.7)			
			8.5	0.2		1.30	0.3			0.004	0.5						
Bow Ridge	Y (0.4)	N (0.5) Obl (0.5)	(0.2)		(0.6)	(0.1)			(0.1)		(0.7)		(0.3)	C (0.3)			
	N (0.6)		6.7	0.7		0.40	0.2			0.002	0.2	40	0.05	TE (0.7)			
			12.2	0.3		0.45	0.6			0.003	0.6	70	0.1				
						0.80	0.2			0.007	0.2	100	0.35	140	0.35	215	0.1
Paintbrush Canyon		N-LL (1.0)	(0.2)		(0.4)	(0.2)	(0.1)	(0.1)	(0.1)		(0.7)		(0.3)	C (0.3)			
			12	0.5		1.42	0.1	0.20	0.1		0.002	0.1	20	0.01	TE (0.7)		
			18	0.2		1.67	0.7	0.45	0.5		0.007	0.3	50	0.19			
			23	0.3		2.05	0.19	0.5	0.4		0.015	0.5	85	0.2			
						2.57	0.01				0.02	0.09	100	0.3			
									0.03	0.01	115	0.2					
											270	0.1					
Stagecoach Road		N-LL (1.0)	(0.2)		(0.4)	(0.2)	(0.1)	(0.1)	(0.1)		(0.7)		(0.3)	C (0.3)			
			8	0.7		0.5	0.15	0.40	0.7		0.006	0.1	5	0.05	TE (0.7)		
			12	0.3		0.67	0.8	0.60	0.3		0.03	0.4	10	0.2			
						0.99	0.05				0.05	0.4	35	0.5			
									0.07	0.1	50	0.2					
											75	0.05					

**TABLE SBK-3
LOCAL FAULTS
(Continued)**

Fault Name	Ind. Source	Type	Maximum Magnitude Approach					Recurrence Approach				Recurrence Model			
			Length (km)	Area	Max Offset (m)	Av Offset (m)	Offset from Stress Drop	Long-term Slip Rate (m/kyr)	Quat Slip Rate (m/kyr)	Interval (kyr)					
Paintbrush Canyon + Stagecoach Road + Bow Ridge		N-LL (1.0)	(0.1)	(0.6)	(0.2)		(0.1)		(0.8)	(0.2)		C	(0.5)		
			23	0.7	0.79	0.29			0.015	0.2	10	0.05	TE	(0.5)	
			34	0.3	0.84	0.5			0.03	0.4	20	0.2			
					1.0	0.2			0.05	0.4	40	0.6			
					1.4	0.01					45	0.1			
So. Crater Flat + Windy Wash + Fatigue Wash		N-LL (1.0)	(0.1)	(0.6)	(0.1)	(0.1)	(0.1)		(0.8)	(0.2)		C	(0.5)		
			25.5	0.3	0.50	0.3	0.30	0.5		0.011	0.5	50	0.2	TE	(0.5)
			27.2	0.4	0.98	0.7	0.50	0.5		0.016	0.5	185	0.8		
			28.3	0.3											
Solitario Canyon + Iron Ridge		N-LL (1.0)	(0.2)	(0.5)	(0.2)		(0.1)		(1.0)			C	(0.5)		
			13	0.2	1.10	0.1				0.009	0.2		TE	(0.5)	
			18	0.8	1.20	0.6				0.012	0.3				
					1.30	0.3				0.014	0.4				
								0.024	0.2						
Simultaneous Rupture of Linked Faults		N-LL (1.0)	(0.1)	(0.6)	(0.3)				(1.0)			C	(0.5)		
			82	0.8	2.50	0.5				0.04	0.2		TE	(0.5)	
			95	0.2	3.30	0.5				0.06	0.6				
								0.09	0.2						
Coalesced Faults		N-LL (1.0)	(0.1)	(0.6)	(0.3)				(0.25 to 1.0)	(0 to 0.75)		Max Moment 1.0			
			27	0.6	2.50	0.5				0.04	0.2	Same as	for volcanic		
			34	0.4	3.30	0.5				0.06	0.6	volcanic eruption	otherwise C 0.5		
								0.09	0.2	freq.	TE 0.5				

**TABLE SBK-3
LOCAL FAULTS
(Continued)**

Notes and Sources - Table SBK-3 (Continued):

Each column contains a weighting in parenthesis (**bold**) for that variable within the overall grouping, as well as weightings of individual values for that variable. Both Hwy. 95 fault and Bare Mountain fault are treated as independent sources in analysis. Other local faults can rupture in various combinations, as detailed in text.

Unless

otherwise noted, maximum displacements obtained from trench data; average displacement used when at least four points available for a single event along strike of the

fault, from trench data and/or mapping. Southern termination of each fault taken from Ramelli and Bell, 1996, except for Hwy. 95 fault, which may truncate all of the others considered here.

Hwy. 95 fault Data interpreted from Memorandum by D.B. Slemmons, 3 February 1997. Likelihood of existence 0.8; if it exists, likelihood it ruptures as an independent seismogenic structure 0.5 (lacking any definitive evidence of offset in the Quaternary, yet there are sufficient indicators of possible activity to convince us we can't favor one conclusion over the other). Arguments in favor of existence and activity: apparent uplift of bedrock across feature, truncation of faults of Crater Flat/Yucca Mountain block, irregular subdued scarps as described by Slemmons, left-lateral deflection of gravity gradient at south end of Bare Mountain fault plus deflection of subsurface horizons as reported by Slemmons, April 1997 SSC Workshop. Arguments against existence and activity: irregular subdued scarps along regional gradient suggest fluvial activity.

Bare Mountain fault Sources of data: L. Anderson and Klinger, 1996b; Piety, 1995; Ferrill and others, 1996a, 1996b; Pezzopane and others, 1996a; Ramelli and Bell, 1996. Length of fault confined to that mapped by previous workers at surface along Bare Mountain. Although a gravity gradient is approximately aligned with Bare Mountain fault to south, no Quaternary faulting is associated with it, so we do not include it. There may be some secondary rupture on Yucca Mountain faults associated with primary events on the Bare Mountain fault, based on Pezzopane and others' compilation; however, no evidence of simultaneous ruptures, and the "ash event" is not recorded in Bare Mtn. rupture stratigraphy, thus we consider this an independent structure. Displacement data based on assuming that Anderson and Klinger's single late Quaternary event is in fact two events. Long-term slip rate from 2 to 3 km; total displacement in 15 Ma.

South Crater Flat fault Sources of data: Ramelli and Bell, 1996; Taylor, 1996; Simonds and others, 1995; Pezzopane and others, 1996a. Three-dimensional fault geometry consistent with possible linkage to Windy Wash fault. Late Quaternary slip rate estimated from total displacement from trenches divided by age of offset deposits.

North Crater Flat fault Sources of data: Ramelli and Bell, 1996; Coe, 1996; Simonds and others, 1995; Pezzopane and others, 1996a. Three-dimensional fault geometry consistent with lack of connection to South Crater Flat fault. Late Quaternary slip rate estimated from displacement in trenches, although ages of offset deposits not well constrained.

Windy Wash fault Sources of data: Ramelli and Bell, 1996; Whitney and others, 1996; Simonds and others, 1995; Pezzopane and others, 1996a. Northern extension of fault from Simonds and others; however, northernmost portion of fault has no convincing evidence of Quaternary displacement, so given lower weighting. Slip rate estimated from trench data.

**TABLE SBK-3
LOCAL FAULTS
(Continued)**

Notes and Sources - Table SBK-3.(Continued):

Fatigue Wash fault Sources of data: Ramelli and Bell, 1996; Coe and others, 1996a; Simonds and others, 1995; Pezzopane and others, 1996a. Most likely geometry is splaying from Windy Wash fault at both north and south; second possible geometry is that Fatigue Wash fault continues north, parallel to Windy Wash fault. All Fatigue Wash paleoseismic events are permissibly same timing as some of the Windy Wash events, although equally well they could be independent earthquakes. Slip rate estimated from trench data.

Solitario Canyon fault Sources of data: Ramelli and Bell, 1996; Ramelli and others, 1996; Simonds and others, 1995; Day and others, 1996a; Pezzopane and others, 1996a. Fault mapped in detail by Simonds and others and Day and others, yielding little uncertainty on fault length. Surface breakage events are extremely variable in displacement, including minor cracking events as well as a major displacement (the maximum event noted in table) as part of the "ash event." It is likely that at least some of the surface breaks are secondary in nature. South end of fault could link with Stagecoach Road fault, although we have not addressed this possibility explicitly in our analysis. Slip rate estimated from trench data.

Iron Ridge fault Sources of data: Ramelli and Bell, 1996; Ramelli and others, 1996; Simonds and others, 1995; Pezzopane and others, 1996a. Given geometry and timing of rupture event, it is very unlikely that this structure ruptures independently of the Solitario Canyon fault. Slip rate estimated from trench data.

Bow Ridge fault Sources of data: Ramelli and Bell, 1996; Taylor and others, 1996b; Menges and Whitney, 1996; Simonds and others, 1995; Pezzopane and others, 1996a. Fault may link north end of Solitario Canyon fault with Paintbrush Canyon fault, although the most likely geometry is as a splay of the Paintbrush Canyon fault. Given this geometry and the short length of the fault, we consider it less likely to behave as an independent seismogenic structure than to slip in response to other faults. Northern continuation of fault uncertain; we used the Pagany Wash fault mapped by Simonds and others as the most likely continuation, although given the lack of Quaternary displacement on this structure it is considered a less likely geometry than the Bow Ridge fault as shown by Ramelli and Bell. Slip rate based on trench data; complicated options for return periods based on uncertainties in dating from trench studies and variability in repeat times of events inferred from the trenches.

Paintbrush Canyon fault Sources of data: Ramelli and Bell, 1996; Menges and Whitney, 1996; Simonds and others, 1995; Frizzell and Shulters, 1990; Pezzopane and others, 1996a. Northern extent of fault from Frizzell and Shulters map; however, no evidence of Quaternary slip along north half of fault, so given lower weight in assessment of length. Slip rate and displacement data obtained principally from Busted Butte paleoseismic data.

Stagecoach Road fault Sources of data: Ramelli and Bell, 1996; Menges and Whitney, 1996; Simonds and others, 1995; Pezzopane and others, 1996a. Connection between Stagecoach Road fault and Paintbrush Canyon fault is uncertain, and we interpret the Stagecoach Road fault *sensu stricto* to extend as shown by Simonds and others. Displacement, slip rate, and repeat-time data all obtained from trench studies.

**TABLE SBK-3
LOCAL FAULTS
(Continued)**

Notes and Sources - Table SBK-3 (Continued):

Linked faults As discussed in text, we consider one set of models in which four "block-bounding" faults behave as either independent structures or rupture simultaneously. The former case involves three linked structures—Paintbrush Canyon + Stagecoach Road + Bow Ridge; South Crater Flat + Windy Wash + Fatigue Wash; and Solitario Canyon + Iron Ridge—along with the North Crater Flat fault. Fault lengths for each linked system are estimated by taking the longest along-strike fault zone; parallel and branch faults that are part of a linked system do not contribute to fault length. Maximum displacement and slip rate data are obtained from any part of the total linked fault system, using data from events that are in common for any given set of faults as summarized by Pezzopane and others, 1996a. The latter case assumes that all linked faults may have ruptured simultaneously during one or more surface faulting events. The principal example of this is the "ash event." For this scenario, the fault length is the sum of the various linked faults, and the maximum displacement is estimated from the maximum displacement on each constituent linked fault. The return time of the event can be estimated either from the sum of the slip rates on each fault, or (given the unique nature of the "ash event" and its apparent tie to volcanism) from the frequency of occurrence of volcanic eruptions in the Crater Flat area.

Coalesced faults As discussed in text, we consider a set of models in which all of the YM faults (excluding Hwy. 95 and Bare Mountain) coalesce at depth. Should all these faults rupture at the surface in a single event, as may have been the case for the "ash event," the fault length would be that of the longest ("master") fault, in this case the Paintbrush Canyon-Stagecoach Road linked fault or the Solitario Canyon-Iron Ridge linked fault. An alternative is that during any given event on a master fault at depth, any combination of the surface faults may rupture, depending on the pathway the rupture takes between the hypocenter and the surface. Recurrence estimate for the former case is tied strongly to volcanic eruption frequency (0.75 likelihood); recurrence for the latter case is tied exclusively to the summed slip rates determined from the surface faults.

**TABLE SBK-4
FAULT DISPLACEMENT HAZARD CHARACTERIZATION DATA, POINTS 1, 2, AND 9**

Point	Slip Rate (mm/yr) weight 0.8			Event Frequency weight 0.2		Displacement (m)			
	Site-Specific	Interpolated Quaternary	Interpolated Cumulative	Paleoseismic Data	EQ Recur.	Uave Paleo	Uave W&C	Umax Paleo	Umax W&C
1 (Bow Ridge fault)	1.0 wt. 0.002, 0.2 wt. 0.003, 0.6 wt. 0.007, 0.2 wt.			0.5 wt. Details in Table SBK-3	0.5 wt.	0.4 wt. 0.06, 0.2wt 0.27, 0.6wt 0.55, 0.2wt	0.1 wt	0.4 wt Table SBK-3	0.1 wt
2 (Solitario Canyon fault)		1.0 wt 0.0006 to 0.00355 (see notes)		0.5 wt. 4 events 0.5 wt 3 events 0.5 wt	0.5 wt.	0.25 wt.	0.25 wt	0.25 wt 0.3, 0.4 0.4, 0.6	0.25 wt
9 (Midway Valley fractures)	1.0 wt. 0.0, 0.2 wt. 6.6×10^{-5} , 0.4 1.4×10^{-4} , 0.4			Event frequency not used for point 9			0.3 wt.	0.4 wt. 0.05, .8 0, 0.2	0.3 wt.

Notes, Table SBK-4

EQ Recur.: earthquake recurrence distribution computed in ground shaking hazard analysis for SBK Team; **Uave Paleo:** average displacement per rupture event from paleoseismic data; **Uave W&C:** average displacement computed from Wells and Coppersmith regression; **Umax Paleo:** maximum displacement from trench-specific data; **Umax W&C:** maximum displacement computed from Wells and Coppersmith regression.

Bow Ridge fault: Slip rate approach given 0.7 weight for computation of occurrence frequency, event frequency approach given 0.3 weight. Site-specific data from Trench 14D, as compiled by Pezzopane and others, 1996a.

Solitario Canyon fault: Slip rate approach given 0.7 weight for computation of occurrence; event frequency approach given 0.3 weight. Slip rate calculated by interpolating slip rate from known point, Trench 4, along strike; demonstration point is between this trench and a point of known zero displacement (Ramelli, SSC Workshop 6). Slip rate at Trench 4, based on data from Ramelli and others, 1996: 0.0012 (0.2 wt.), 0.0024 (0.3 wt.), 0.004 (0.2 wt.), 0.0053 (0.3 wt.). Reduction factor, computed based on distance between points and uncertainty in interpolation: 0.67 (0.2 wt.), 0.59 (0.6 wt.), 0.5 (0.2 wt.). Final slip-rate results: 0.0006 (0.04 wt.), 0.00071 (0.12 wt.), 0.0084 (0.04 wt.), 0.0012 (0.06 wt.), 0.00142 (0.18 wt.), 0.00161 (0.06 wt.), 0.002 (0.04 wt.),

TABLE SBK-4
FAULT DISPLACEMENT HAZARD CHARACTERIZATION DATA, POINTS 1, 2, AND 9
(Continued)

0.00236 (0.12 wt.), 0.00265 (0.06 wt.) 0.00268 (0.04 wt.), 0.00313 (0.18 wt.), and 0.00355 (0.06 wt.). Data on paleoseismic event frequency from Ramelli and others, 1996: 4 events in 150 ka (0.2 wt.), 200 ka (0.6 wt.), or 250 ka (0.2 wt.) is assigned weight of 0.5; 3 events in same time periods assigned weight of 0.5. Average and maximum displacements computed by interpolating between Trench SCF-T4 and zero displacement point, the position of which was shown by Ramelli (SSC Workshop 6). Displacement values for U_{ave} are dependent on number of events (3 or 4) assumed to have occurred. For 4 events

Notes, Table SBK-4 (cont.)

(weight 0.5), U_{ave} weighted 0.075 m (0.2 wt.), 0.1375 m (0.6 wt.), and 0.2 m (0.2 wt.). For 3 events (weight 0.5), U_{ave} weighted 0.1 m (0.2 wt.), 0.183 m (0.6 wt.), and 0.267 m (0.2 wt.). U_{max} is not sensitive to number of events.

Midway Valley fractures: Data from Swan, SSC Workshop 3. Event frequency constrained only by slip rate. Fractures on the Exile Hill fault have maximum net displacement of 5 cm in deposits 350-760 ka in age, producing extremely low slip rates. Yet the displacement may be zero. Displacement amount constrained using maximum slip of 5 cm for fractures. Fault length 0.4 km for computation of maximum and average displacement from Wells and Coppersmith regressions.

**TABLE SBK-5
FAULT DISPLACEMENT HAZARD CHARACTERIZATION DATA, POINTS 3-8**

Point	Slip Rate (mm/yr) 0.8 weight		Event Frequency 0.2 weight		Activation Factor	
	Geologic History	Fault Parameter	Distributed Rupture	PPV Frequency	Slip Tendency	Angular Histogram
3 (Drill Hole Wash)	0.75 wt. <u>Model 1 (0.1)</u> 0.0041 (0.2) 0.0033 (0.6) 0.0025 (0.2) <u>Model 2 (0.3)</u> 0.0009 (0.2) 0.0007 (0.6) 0.0005 (0.2) <u>Model 3 (0.6)</u> 0.0009 (0.2) 0.0007 (0.6) 0.0006 (0.2)	0.25 wt. 0.0036 (0.2) 0.0009 (0.6) 0.0004 (0.2)	0.5 wt.	0.5 wt.	(0.4 wt.) 0.6 (0.1 weight) 0.5 (0.8) 0.4 (0.1)	(0.6 wt.)
4 (Ghost Dance fault)	0.75 wt. <u>Model 1 (0.1)</u> 0.0029 (0.2) 0.0025 (0.6) 0.0021 (0.2) <u>Model 2 (0.3)</u> 0.0006 (0.2) 0.0005 (0.6) 0.0004 (0.2) <u>Model 3 (0.6)</u> 0.0007 (0.2) 0.0006 (0.6) 0.0005 (0.2)	0.25 wt. 0.0026 (0.2) 0.00072 (0.6) 0.00034 (0.2)	0.5 wt.	0.5 wt.	(0.4 wt.) 0.8 (0.1) 0.7 (0.8) 0.3 (0.1)	(0.6 wt.)
5 (Sundance fault)	0.75 wt. <u>Model 1 (0.1)</u> 0.0017 (0.2)	0.25 wt. 0.0014 (0.2) 0.00036 (0.6)	1.0 wt.		(0.4 wt.) 0.6 (0.1) 0.56 (0.8)	(0.6 wt.)

TABLE SBK-5
FAULT DISPLACEMENT HAZARD CHARACTERIZATION DATA, POINTS 3-8
(Continued)

Point	Slip Rate (mm/yr) 0.8 weight		Event Frequency 0.2 weight		Activation Factor	
	Geologic History	Fault Parameter	Distributed Rupture	PPV Frequency	Slip Tendency	Angular Histogram
	0.0013 (0.6) 0.0005 (0.2) <u>Model 2 (0.3)</u> 0.0003 (0.2) 0.0003 (0.6) 0.0001 (0.2) <u>Model 3 (0.6)</u> 0.0004 (0.2) 0.0003 (0.6) 0.0001 (0.2)	0.00008 (0.2)			0.48 (0.1)	
6 (west of Dune Wash fault)	0.75 wt. <u>Model 1 (0.1)</u> 0.0017 (0.2) 0.0009 (0.6) 0.00017 (0.2) <u>Model 2 (0.3)</u> 0.00035 (0.2) 0.00019 (0.6) 0.00003 (0.2) <u>Model 3 (0.6)</u> 0.00037 (0.2) 0.00021 (0.4) 0.00004 (0.2)	0.25 wt. 0.0014 (0.2) 0.00027 (0.6) 0.000026 (0.2)	0.5 wt.	0.5 wt.	1.0 (1.0 weight)	(not implemented)
7a Fault (2 m)	0.75 wt. <u>Model 1 (0.1)</u> 1.7e-4 (1.0) <u>Model 2 (0.3)</u>	0.25 wt. 1.4e-4 (0.2) 4.8e-5 (0.6) 2.6e-5 (0.2)	0.5 wt.	0.5 wt.	1.0 (1.0 weight)	(not implemented)

TABLE SBK-5
FAULT DISPLACEMENT HAZARD CHARACTERIZATION DATA, POINTS 3-8
(Continued)

Point	Slip Rate (mm/yr) 0.8 weight		Event Frequency 0.2 weight		Activation Factor	
	Geologic History	Fault Parameter	Distributed Rupture	PPV Frequency	Slip Tendency	Angular Histogram
	5.2e-5 (1.0) <u>Model 3 (0.6)</u> 5.2e-5 (1.0)					
7b Shear (10 cm)	0.75 wt. <u>Model 1 (0.1)</u> 8e-6 (1.0) <u>Model 2 (0.3)</u> 2e-6 (1.0) <u>Model 3 (0.6)</u> 2e-6 (1.0)	0.25 wt. 7.0e-6 (0.2) 2.4e-6 (0.6) 1.3e-6 (0.2)	0.5 wt.	0.5 wt.	1.0 (1.0 weight)	(not implemented)
7c Fracture (<10 cm)	0.75 wt. [uniform between 0 & maximum of 7b]	0.25 wt. [uniform between 0 & maximum of 7b]	0.5 wt.	0.5 wt.	1.0 (1.0 weight)	(not implemented)
7d Intact Rock	notes below					
8a Fault (2 m)	0.75 wt. <u>Model 1 (0.1)</u> 1.7e-4 (1.0) <u>Model 2 (0.3)</u> 5.2e-5 (1.0) <u>Model 3 (0.6)</u> 5.2e-5 (1.0)	0.25 wt. 1.4e-4 (0.2) 4.8e-5 (0.6) 2.6e-5 (0.2)	0.5 wt.	0.5 wt.	1.0 (1.0 weight)	(not implemented)
8 bShear (10 cm)	0.75 wt. <u>Model 1 (0.1)</u> 8e-6 (1.0) <u>Model 2 (0.3)</u>	0.25 wt. 7.0e-6 (0.2) 2.4e-6 (0.6) 1.3e-6 (0.2)	0.5 wt.	0.5 wt.	1.0 (1.0 weight)	(not implemented)

TABLE SBK-5
FAULT DISPLACEMENT HAZARD CHARACTERIZATION DATA, POINTS 3-8
(Continued)

Point	Slip Rate (mm/yr) 0.8 weight		Event Frequency 0.2 weight		Activation Factor	
	Geologic History	Fault Parameter	Distributed Rupture	PPV Frequency	Slip Tendency	Angular Histogram
	2e-6 (1.0) Model 3 (0.6) 2e-6 (1.0)					
8c Fracture (<10 cm)	0.75 wt. [uniform between 0 & maximum of 7b]	0.25 wt. [uniform between 0 & maximum of 7b]	0.5 wt.	0,1 overall	1.0 (1.0 weight)	(not implemented)
8d Intact Rock	see notes below					

Notes, Table SBK-5:

Fault Parameter Method: Total displacement and slip rate of the Bow Ridge fault are the reference parameters for this trial set of calculations. We could use an average of the Solitario Canyon and Bow Ridge fault parameters, but the slip rates of the two faults are similar, and Bow Ridge fault slip rate is well defined by trench #4 near the entrance to the repository ESF. Bow Ridge fault displacement is estimated as 100 m minimum, 125 m preferred value, and 150 m maximum value based on Day et al. (1996) and our judgement of maximum error in estimating total slip from mapping. Slip rate estimates for the Bow Ridge fault and weights are given in Table SBK-4. We report three estimated slip rates for the fault parameter method which are the preferred, the most minimum and most maximum values estimated using all combinations of the reference fault (Bow Ridge fault) parameters (displacement and slip rate) and subject fault parameters (displacement). Application of displacement variability (probability) functions is described in Section 3.3.4.

Drill Hole Wash Fault: Slip rate methods - Geologic History weighted 0.6, Model 1,2 & 3 as described in manuscript. Fault Parameter method weighted 0.2, Event Frequency - Distributed Rupture method weighted 0.1, Peak Particle Velocity method weighted 0.1). Fault parameter slip rates found by ratio of maximum estimated displacement on Drill Hole Wash to Bow Ridge Fault. Displacement estimates are (30 m, 40m, 50 m) from Day et al., 1996. Stress activation factor computed using ESF stress tensor and orientation of Drill Hole Wash fault reported by Day et al. (1996). Fault pole trends 045°, plunges 05° with an assumed variation of ± 10° in both trend and plunge.

TABLE SBK-5
FAULT DISPLACEMENT HAZARD CHARACTERIZATION DATA, POINTS 3-8
(Continued)

Ghost Dance Fault: Slip rate methods - Geologic History weighted 0.6, Model 1,2 & 3 as described in manuscript. Fault Parameter method weighted 0.2, Event Frequency - Distributed Rupture method weighted 0.1, Peak Particle Velocity (PPV) method weighted 0.1. Fault parameter slip rates found by ratio of maximum estimated displacement on Ghost Dance to Bow Ridge Fault. Displacement estimates are (25 m, 30 m, 35 m) from Day et al., 1996). Stress activation factor computed using ESF stress tensor and orientation of Ghost Dance fault reported by Day et al. (1996). Fault pole trends 090°, plunges 15° with an assumed variation of $\pm 10^\circ$ in both trend and plunge.

Sun Dance Fault: Slip rate methods - Geologic History weighted 0.6, with application of Models 1,2 & 3 as described in manuscript. Fault Parameter method weighted 0.2., Event Frequency - Distributed Rupture method weighted 0.2. Fault parameter slip rates found by ratio of maximum estimated displacement on Sun Dance to Bow Ridge Fault multiplied. Displacement estimates are (6 m, 15 m, 20 m) from Day et al., (1996). Stress activation factor computed using ESF stress tensor and orientation of Sun Dance fault reported by Day et al. (1996). Fault pole trends 050°, plunges 00° with an assumed variation of $\pm 10^\circ$ in both trend and plunge.

Point 6 west of Dune Wash: The amount of displacement on this fault is assumed to be between 2 and 20 meters. We assume a minimum of 2 m, a maximum of 20 m and a preferred value of 11 m (the average of the minimum and maximum displacement estimates for this type of intrablock fault (SSC Facilitation Team memo of January 16, 1997 entitled 'Fault Displacement Hazard Guidance). Geohistory (0.6), Fault Parameter (0.2), Distributed Rupture (0.1) and Peak Particle Velocity (PPV) (0.1) methods are all implemented with appropriate weighting in closed brackets (wt).

Points 7 and 8: Value of 10 cm slip is used for both geohistory and fault parameter methods. No fault orientation is specified, so we assume that slip tendency is 1.0. Slip of less than 10 cm is not specified, so we assume that slip rates are less than those calculated using the geohistory and fault parameter methods for slip of 10 cm. Geohistory (0.6), Fault Parameter (0.2), Distributed Rupture (0.1) and Peak Particle Velocity (PPV) (0.1) methods are all implemented with appropriate weighting in ().

Intact Rock: We use an event frequency approach by assuming that the annual probability of fracturing is less than $1 / (\text{age of intact rock})$. Consider an unfractured wall of Tiva Canyon Tuff in the repository. The chance of fracturing is less than $1 / (1.2e7 \text{ years}) = 8.3e-8 \text{ yr}^{-1}$. We assume that if new fracturing does occur, the maximum amount of shear offset will be less than 10 cm, and use the event frequency displacement variability function $P(U/Dm)$ to estimate the probability of the amount of slip.

**TABLE SBK-6
TRENCHING DATA USED TO DEVELOP DISTRIBUTIONS FOR DISPLACEMENT PER EVENT**

Fault	Trench	Event	U (cm)			U/U _{ap} [*]			U/U _a ^{**}			U/U _m ^{***}		
			min.	pref.	max.	min	pref.	max	min	pref	max	min.	pref	max
Bow Ridge	T-14D	Z	1	1	5	0.19	0.06	0.12	0.092	0.092	0.220	0.054	0.054	0.109
		Z	15	44	80	2.86	2.44	1.88	1.386	4.066	3.516	0.810	2.377	1.749
		Y	4	13	45	0.76	0.72	1.06	0.370	1.201	1.978	0.216	0.702	0.984
		X	1	14	40	0.19	0.78	0.94	0.092	1.294	1.758	0.054	0.756	0.874
N. Crater Flat	CFFT2-a	Z	1	3	5	0.04	0.10	0.15	0.056	0.114	0.190	0.030	0.055	0.092
		Y	1	5	5	0.04	0.17	0.15	0.056	0.190	0.190	0.030	0.092	0.092
		X	35	40	45	1.38	1.35	1.36	1.968	1.522	1.713	1.033	0.734	0.826
		W	45	50	55	1.77	1.69	1.67	2.531	1.903	2.093	1.328	0.917	1.009
		V	45	50	55	1.77	1.69	1.67	2.531	1.903	2.093	1.328	0.917	1.009
S. Crater Flat	CFFT1	Z	7.5	8	10				0.795	0.575	0.562	0.479	0.319	0.295
		Y	7.5	10	10				0.795	0.719	0.562	0.479	0.398	0.295
	CFFT1-a	Z	2	18	18	0.25	1.13	0.83	0.212	1.295	1.012	0.128	0.717	0.531
		Y	5	10	15	0.63	0.63	0.69	0.530	0.719	0.844	0.319	0.398	0.443
		X	17	20	32	2.13	1.25	1.47	1.801	1.438	1.799	1.085	0.796	0.944
Fatigue Wash	CF-1	Z	0	1	5	0.00	0.02	0.10	0.000	0.043	0.131	0.000	0.021	0.058
		Y	15	25	35	0.37	0.54	0.67	1.205	1.066	0.918	0.684	0.527	0.408
		X	100	105	110	2.44	2.27	2.11	8.034	4.477	2.885	4.557	2.212	1.282
		W	49	54	59	1.20	1.17	1.13	3.937	2.303	1.547	2.233	1.138	0.688
Iron Ridge	SCF-T2	Z	1	5	10	0.02	0.08	0.13	0.085	0.423	0.688	0.048	0.242	0.377
		Y	50	70	90	1.17	1.14	1.13	4.225	5.916	6.191	2.423	3.393	3.395
		X	70	100	130	1.64	1.63	1.63	5.916	8.451	8.943	3.393	4.846	4.904
		W	50	70	90	1.17	1.14	1.13	4.225	5.916	6.191	2.423	3.393	3.395
Stagecoach Rd	SCR-T1	Z	40	40	82	1.51	0.89	1.01	2.966	2.966	3.678	1.653	1.653	1.838

TABLE SBK-6
TRENCHING DATA USED TO DEVELOP DISTRIBUTIONS FOR DISPLACEMENT PER EVENT
(Continued)

Fault	Trench	Event	U (cm)			U/Uap*			U/Ua**			U/Um***		
			min.	pref.	max.	min	pref.	max	min	pref	max	min.	pref	max
		Y	28	42	70	1.06	0.93	0.86	2.076	3.115	3.140	1.157	1.736	1.569
		X	14	47	99	0.53	1.04	1.22	1.038	3.486	4.441	0.579	1.943	2.219
		W	24	51	74	0.91	1.13	0.91	1.780	3.782	3.319	0.992	2.108	1.658
	SCR-T3	Z	25	43	66	1.04	0.76	0.84	1.854	3.189	2.960	1.033	1.777	1.479
		Y	20	59	77	0.83	1.04	0.98	1.483	4.375	3.454	0.827	2.439	1.726
		X	25	57	84	1.04	1.01	1.07	1.854	4.227	3.768	1.033	2.356	1.882
		W	26	67	87	1.08	1.19	1.11	1.928	4.969	3.902	1.075	2.770	1.950
Solitario Cyn	SCFT-1	Z	1	10	20				0.041	0.249	0.498	0.020	0.109	0.219
		Y	10	70	90				0.406	1.742	2.240	0.199	0.765	0.984
	SCFT-3	Z	1	10	20				0.041	0.249	0.498	0.020	0.109	0.219
		W	20	35	50				0.812	0.871	1.244	0.397	0.383	0.547
	SCFT-T4	Z	1	5	20	0.10	0.27	0.67	0.041	0.124	0.498	0.020	0.055	0.219
		Y	20	30	40	1.94	1.64	1.33	0.812	0.747	0.995	0.397	0.328	0.437
		W	10	20	30	0.97	1.09	1.00	0.406	0.498	0.747	0.199	0.219	0.328
	SCFT-8	Z	5	10	20	0.13	0.19	0.30	0.203	0.249	0.498	0.099	0.109	0.219
		Y	100	120	140	2.58	2.29	2.07	4.062	2.986	3.484	1.986	1.312	1.531
		X	20	30	40	0.52	0.57	0.59	0.812	0.747	0.995	0.397	0.328	0.437
		W	30	50	70	0.77	0.95	1.04	1.219	1.244	1.742	0.596	0.547	0.765
Paint Brush C.	Trench A-1	Z	5	6	10	0.43	0.35	0.41	0.224	0.157	0.200	0.112	0.070	0.084
		Y	29	39	49	2.48	2.25	2.01	1.301	1.023	0.981	0.650	0.455	0.411
		X	1	7	14	0.09	0.40	0.58	0.045	0.184	0.280	0.022	0.082	0.117
		W	100						4.486	0.000	0.000	2.241	0.000	0.000
	Trench	Z	1	44	72	0.03	0.49	0.47	0.045	1.154	1.441	0.022	0.513	0.604

TABLE SBK-6
TRENCHING DATA USED TO DEVELOP DISTRIBUTIONS FOR DISPLACEMENT PER EVENT
(Continued)

Fault	Trench	Event	U (cm)			U/Uap*			U/Ua**			U/Um***		
			min.	pref.	max.	min	pref.	max	min	pref	max	min.	pref	max
	BB4													
		Y	16	28	56	0.49	0.31	0.36	0.718	0.734	1.121	0.359	0.326	0.470
		X	35	47	69	1.07	0.52	0.45	1.570	1.233	1.381	0.784	0.548	0.579
		W	88	167	205	2.70	1.86	1.33	3.947	4.379	4.104	1.972	1.947	1.720
		V	1	142	222	0.03	1.59	1.44	0.045	3.724	4.444	0.022	1.655	1.863
		U	12	105	257	0.37	1.17	1.66	0.538	2.754	5.145	0.269	1.224	2.156
		T	75	94	201	2.30	1.05	1.30	3.364	2.465	4.024	1.681	1.096	1.687
	MWV-T4	Z	15	20	25	0.53	0.36	0.26	0.673	0.524	0.500	0.336	0.233	0.210
		Y	44	62	77	1.56	1.13	0.80	1.974	1.626	1.542	0.986	0.723	0.646
		X	53	98	143	1.88	1.78	1.49	2.377	2.570	2.863	1.188	1.142	1.200
		W	1	40	140	0.04	0.73	1.45	0.045	1.049	2.803	0.022	0.466	1.175
Windy Wash	T-CF2	Z	1	4	10	0.03	0.10	0.20	0.018	0.066	0.157	0.007	0.026	0.062
		Y	14	20	24	0.44	0.51	0.47	0.253	0.328	0.376	0.104	0.132	0.150
		X	20	23	30	0.63	0.58	0.59	0.361	0.377	0.471	0.148	0.151	0.187
		W	18	20	25	0.56	0.51	0.49	0.325	0.328	0.392	0.133	0.132	0.156
		V	70	73	83	2.19	1.85	1.62	1.264	1.198	1.302	0.518	0.481	0.517
		U	30	45	60	0.94	1.14	1.17	0.542	0.738	0.941	0.222	0.296	0.374
		T	38	50	78	1.19	1.27	1.52	0.686	0.821	1.224	0.281	0.329	0.486
		S	65	80	100	2.03	2.03	1.95	1.173	1.313	1.569	0.481	0.527	0.623
		Z	1	4	10	0.03	0.11	0.23	0.018	0.066	0.157	0.007	0.026	0.062
		Y	8	12	18	0.28	0.34	0.41	0.144	0.197	0.282	0.059	0.079	0.112
		X	45	50	53	1.56	1.43	1.22	0.812	0.821	0.831	0.333	0.329	0.330
		W	38	42	52	1.32	1.20	1.20	0.686	0.689	0.816	0.281	0.277	0.324
		V	24	28	30	0.83	0.80	0.69	0.433	0.459	0.471	0.178	0.184	0.187
		U	15	19	24	0.52	0.54	0.55	0.271	0.312	0.376	0.111	0.125	0.150

TABLE SBK-6
TRENCHING DATA USED TO DEVELOP DISTRIBUTIONS FOR DISPLACEMENT PER EVENT
(Continued)

Fault	Trench	Event	U (cm)			U/Uap*			U/Ua**			U/Um***		
			min.	pref.	max.	min	pref.	max	min	pref	max	min.	pref	max
		T	55	60	65	1.90	1.71	1.50	0.993	0.985	1.020	0.407	0.395	0.405
		S	45	65	95	1.56	1.86	2.19	0.812	1.067	1.490	0.333	0.428	0.592
	TCF-3	Z	4	6	10	0.27	0.29	0.34	0.072	0.098	0.157	0.030	0.040	0.062
		Y	10	20	32	0.68	0.96	1.10	0.181	0.328	0.502	0.074	0.132	0.199
		X	33	42	54	2.24	2.02	1.86	0.596	0.689	0.847	0.244	0.277	0.337
		W	12	15	20	0.81	0.72	0.69	0.217	0.246	0.314	0.089	0.099	0.125
		Z	1	4	6	0.03	0.10	0.12	0.018	0.066	0.094	0.007	0.026	0.037
		Y	25	33	42	0.82	0.83	0.87	0.451	0.542	0.659	0.185	0.217	0.262
		X	71	87	96	2.33	2.19	1.98	1.282	1.428	1.506	0.525	0.573	0.598
		W	25	35	50	0.82	0.88	1.03	0.451	0.574	0.784	0.185	0.231	0.312
	T?	Z	1	3	6	0.03	0.07	0.12	0.018	0.049	0.094	0.007	0.020	0.037
		Y	25	35	45	0.72	0.83	0.91	0.451	0.574	0.706	0.185	0.231	0.281
		X	78	88	98	2.25	2.10	1.97	1.408	1.444	1.537	0.577	0.580	0.611

Notes

* Uap is the average of measurements for fault. Minimum, preferred, and maximum values are obtained by averaging min., pref., and max. columns, respectively for U.

** Ua is computed using minimum, preferred, and maximum lengths of faults from Table SBK-3 and relationship

$$\log(Ua) = -1.99 + 1.24 \times \log(L)$$

*** Um is computed using minimum, preferred, and maximum lengths of faults from Table SBK-3 and relationship

$$\log(Ua) = -1.98 + 1.51 \times \log(L)$$

<i>Tectonic Model</i>	<i>Specific Models</i>	<i>Quaternary Dike Injection affects rates?</i>
-----------------------	------------------------	---

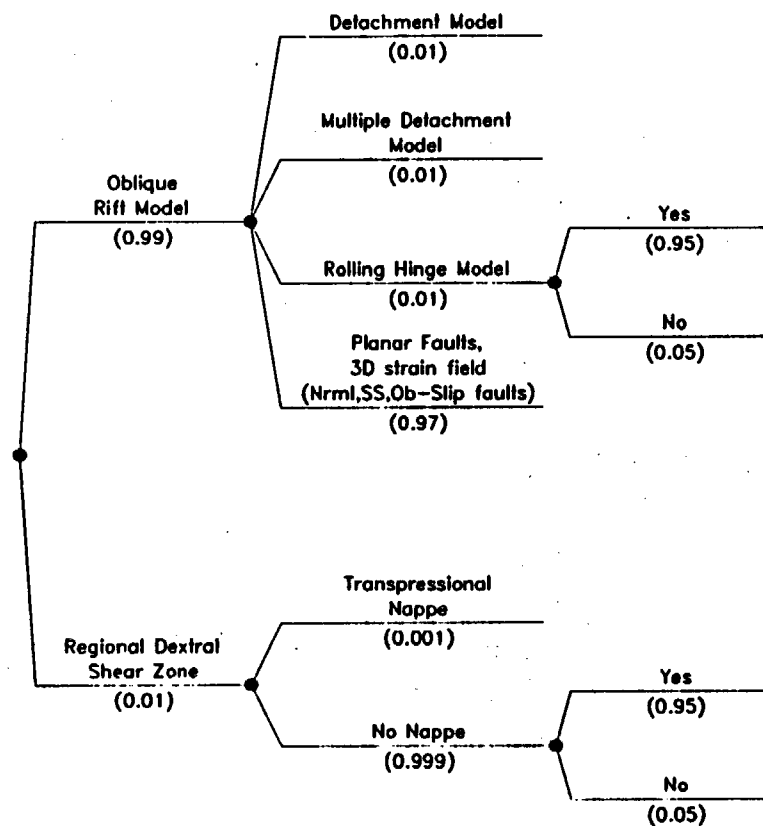


Figure SBK-1

Logic tree for tectonic models

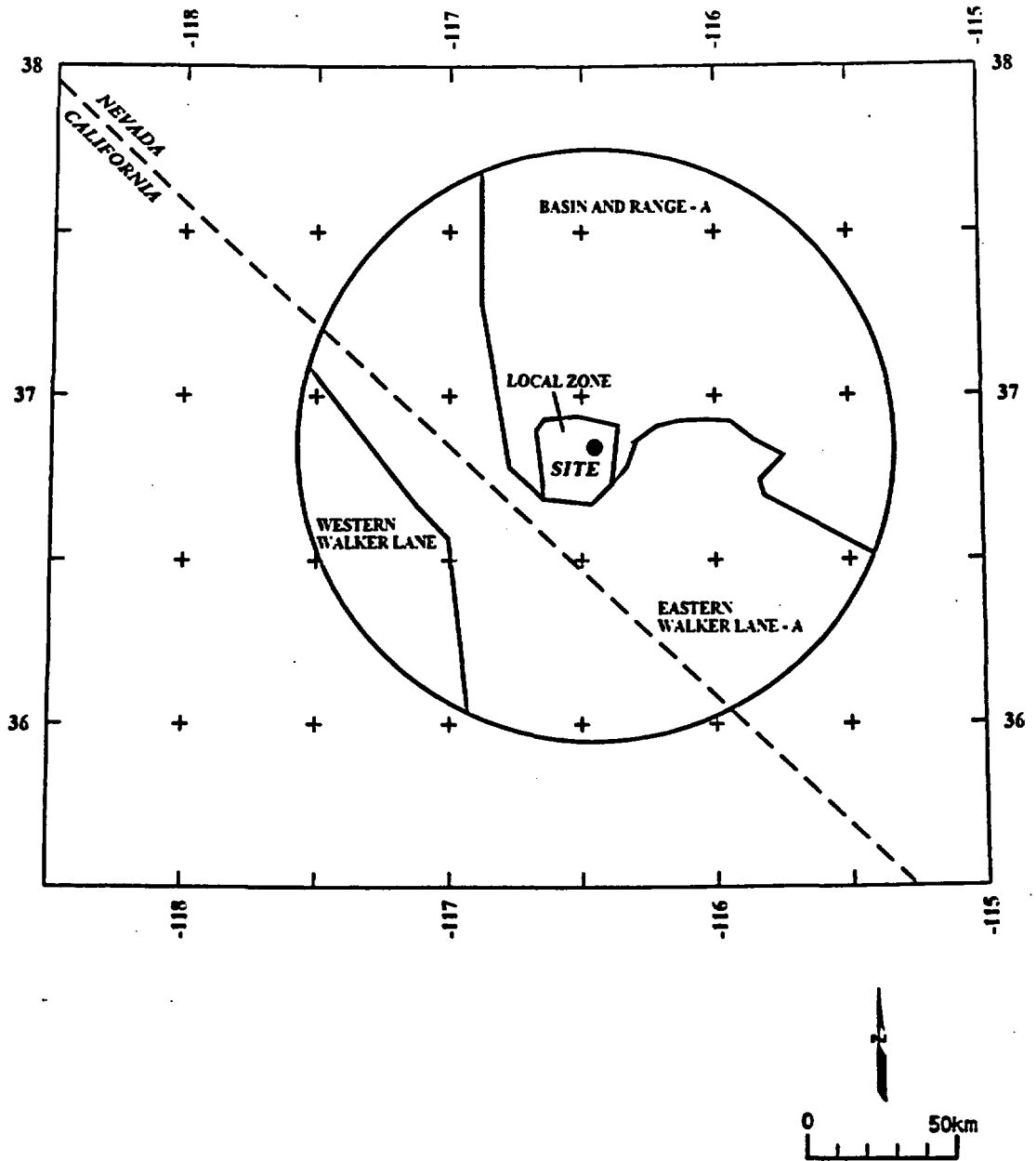


Figure SBK-2 Map showing boundaries of seismic source zones, Model A.

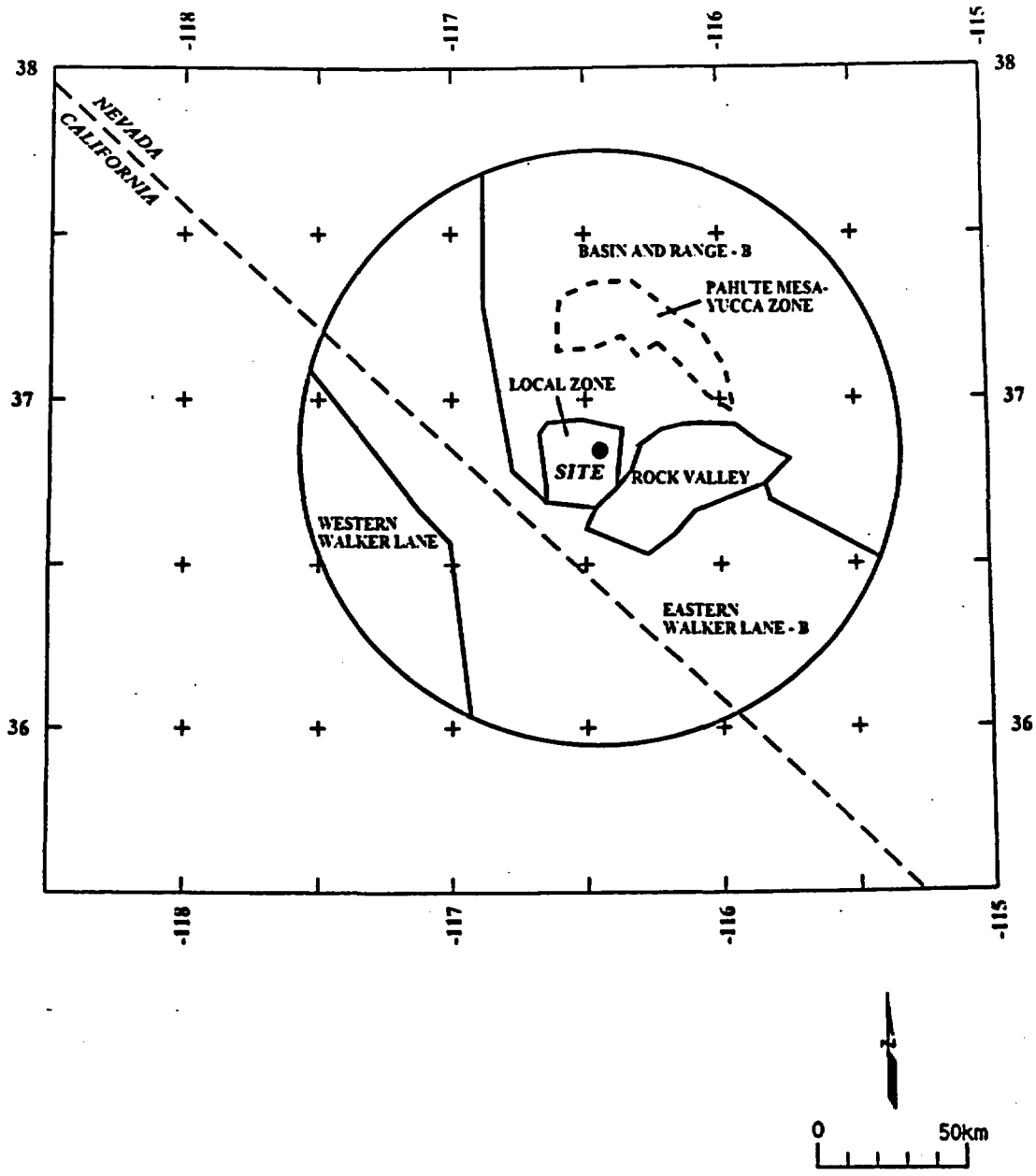


Figure SBK-3 Map showing the boundaries of seismic source zones, Model B.

Source Model	Source	Earthquake Catalog	Maximum Magnitude	Adjustment For NTS
--------------	--------	--------------------	-------------------	--------------------

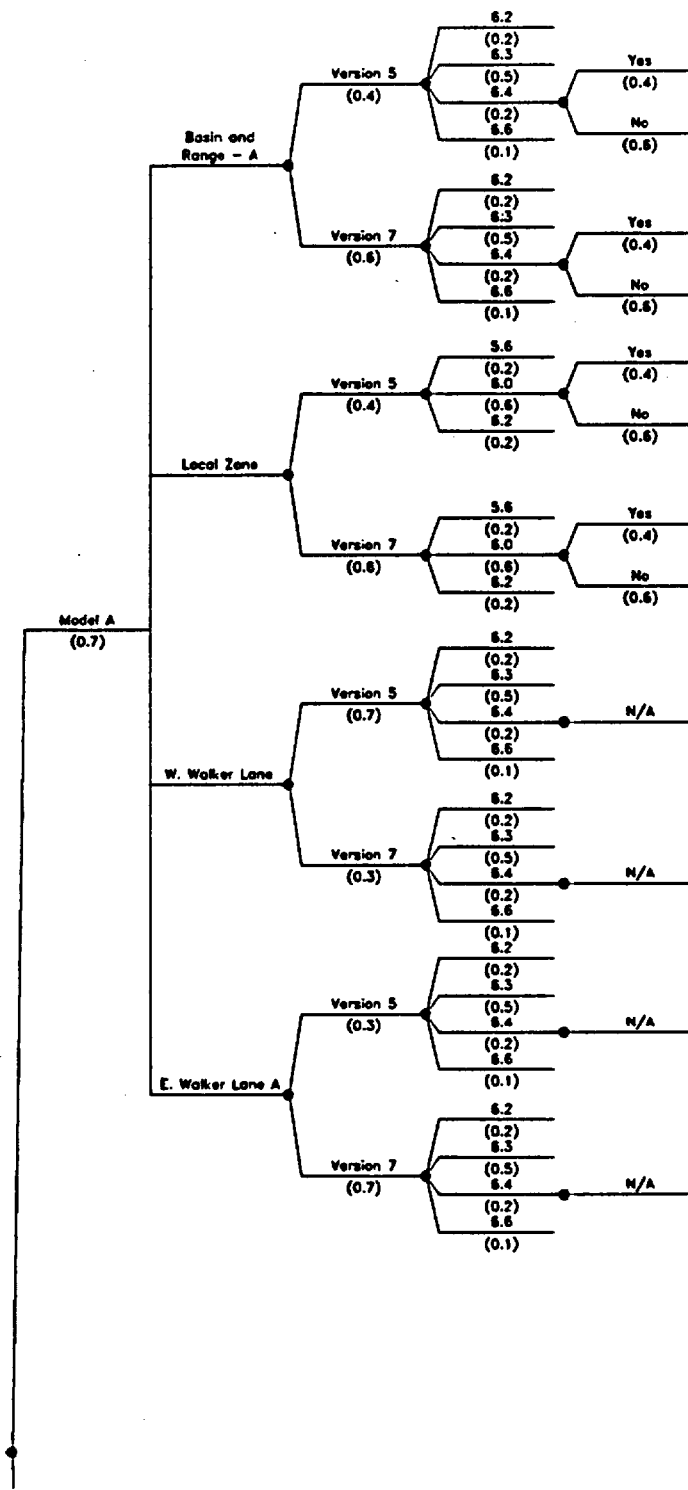


Figure SBK-4 Logic tree for characterizing areal source zones

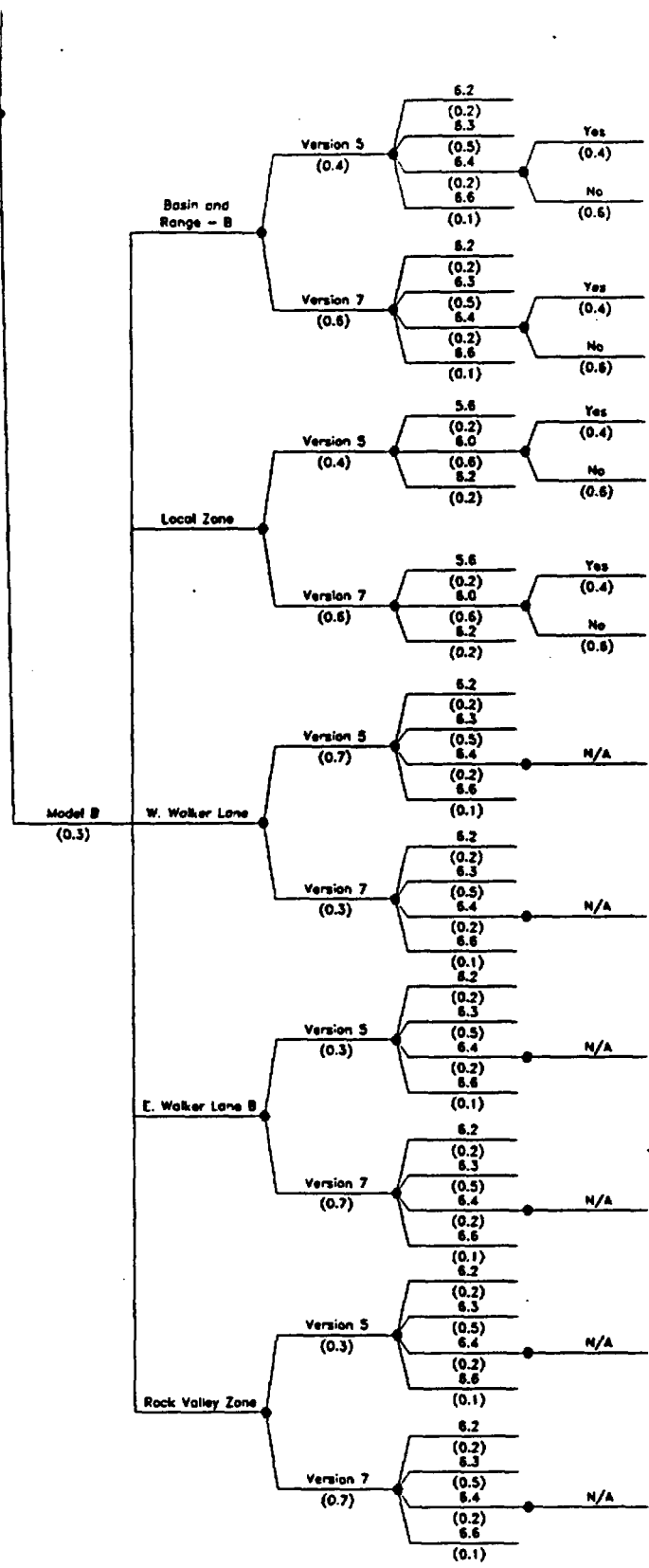
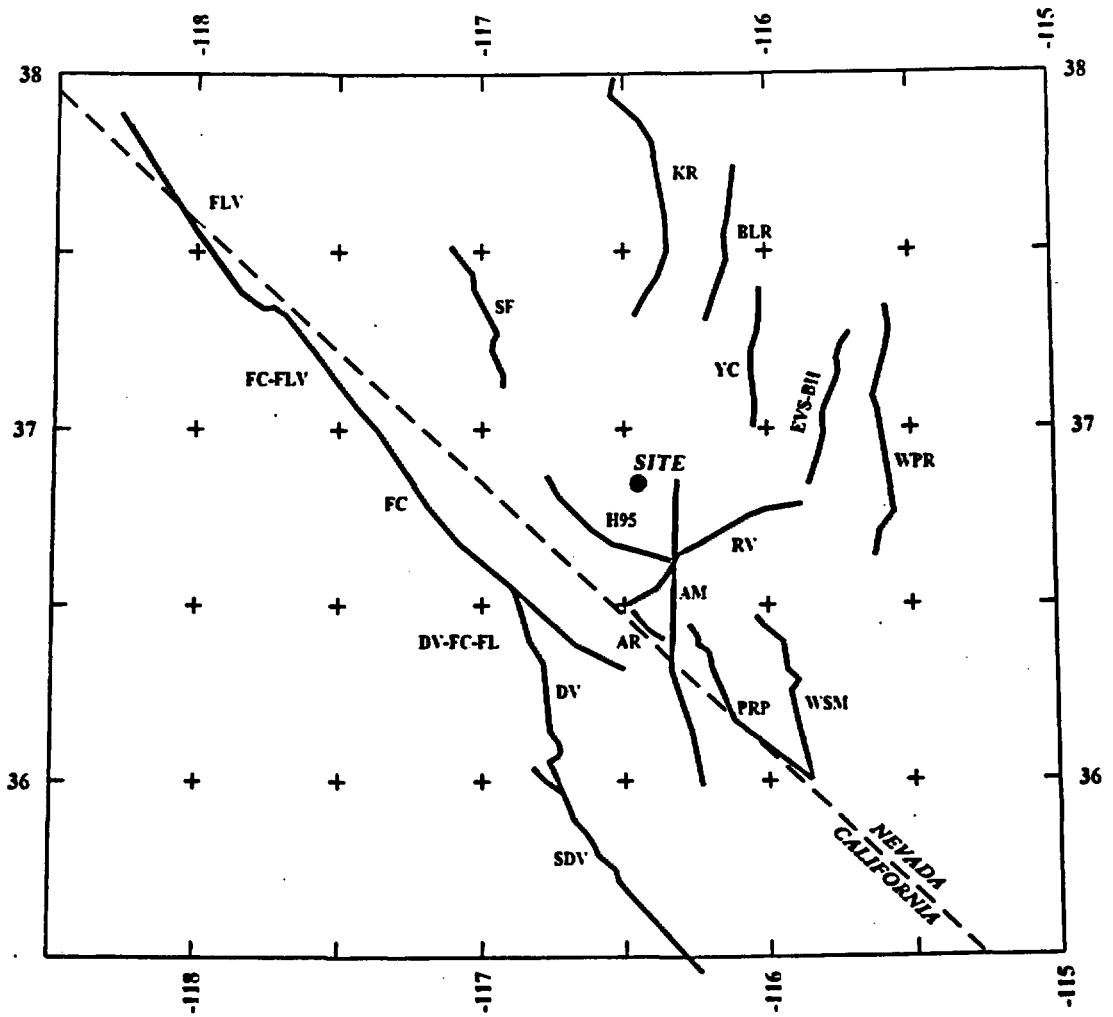


Figure SBK-4 (Cont'd.) Logic tree for characterizing areal source zones



NOTE: Fault names are listed in Table SBK-1

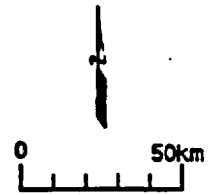


Figure SBK-5 Map showing regional faults included in the seismic source model

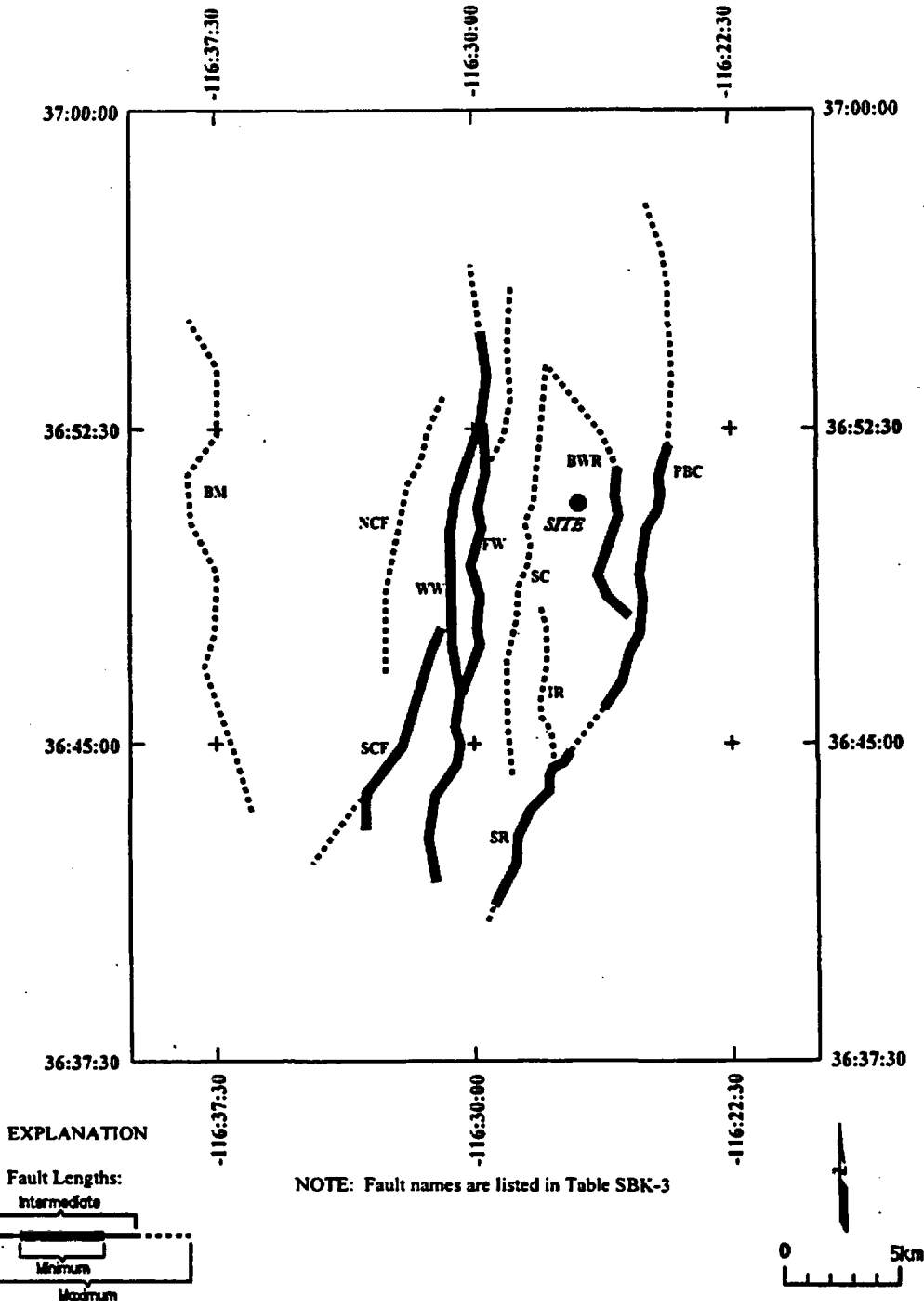


Figure SBK-6 Map showing local fault sources included in the seismic source model

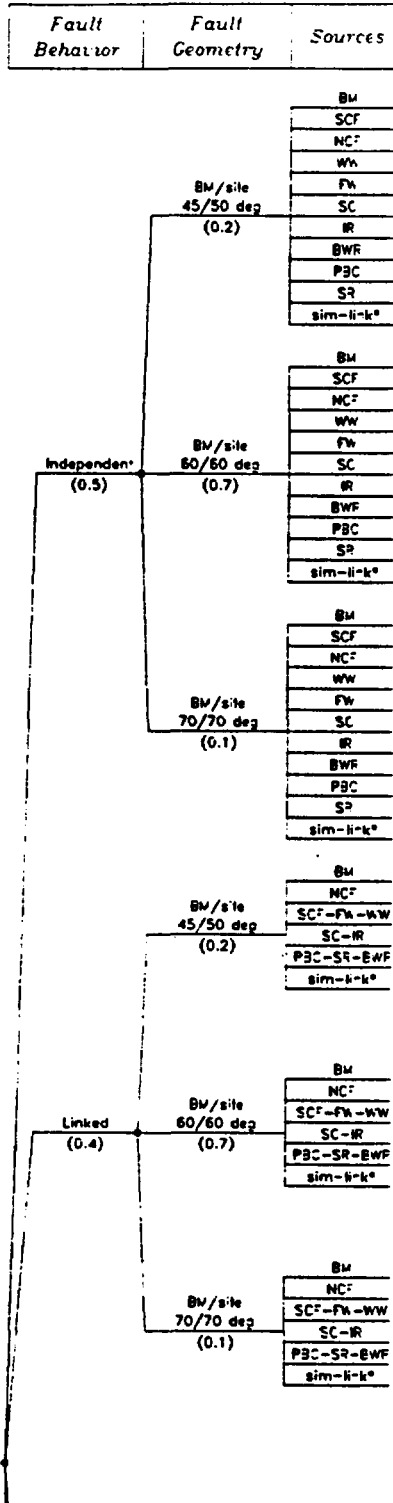
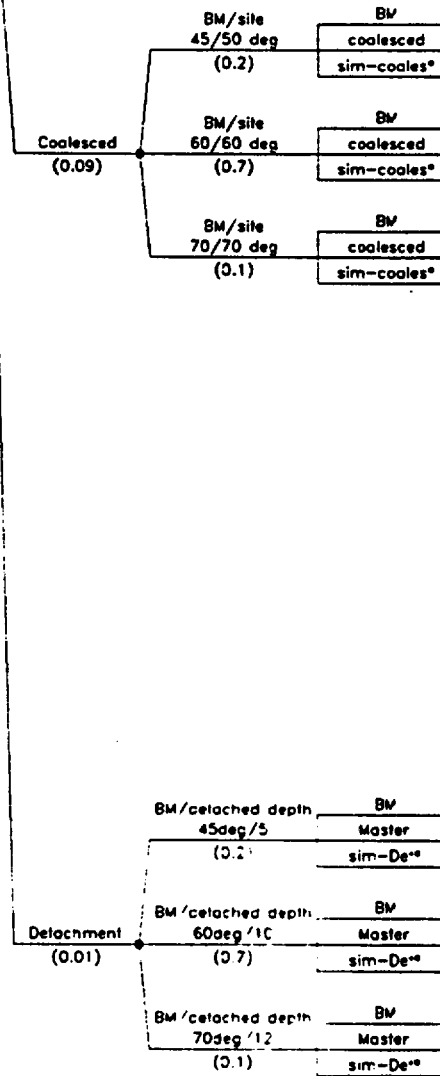


Figure SBK 7 Logic tree for local faults



* sim-link, sim-coales and sim-del are synchronous rupture scenarios that act as additional sources of large events

Figure SBK 7 (Cont'd.) Logic tree for local faults

<i>Approach</i>	<i>Hazard Source</i>	<i>Excavated Fault</i>	<i>Event Frequency</i>	<i>Event Size Measure</i>	<i>Displacement Distribution</i>
-----------------	----------------------	------------------------	------------------------	---------------------------	----------------------------------

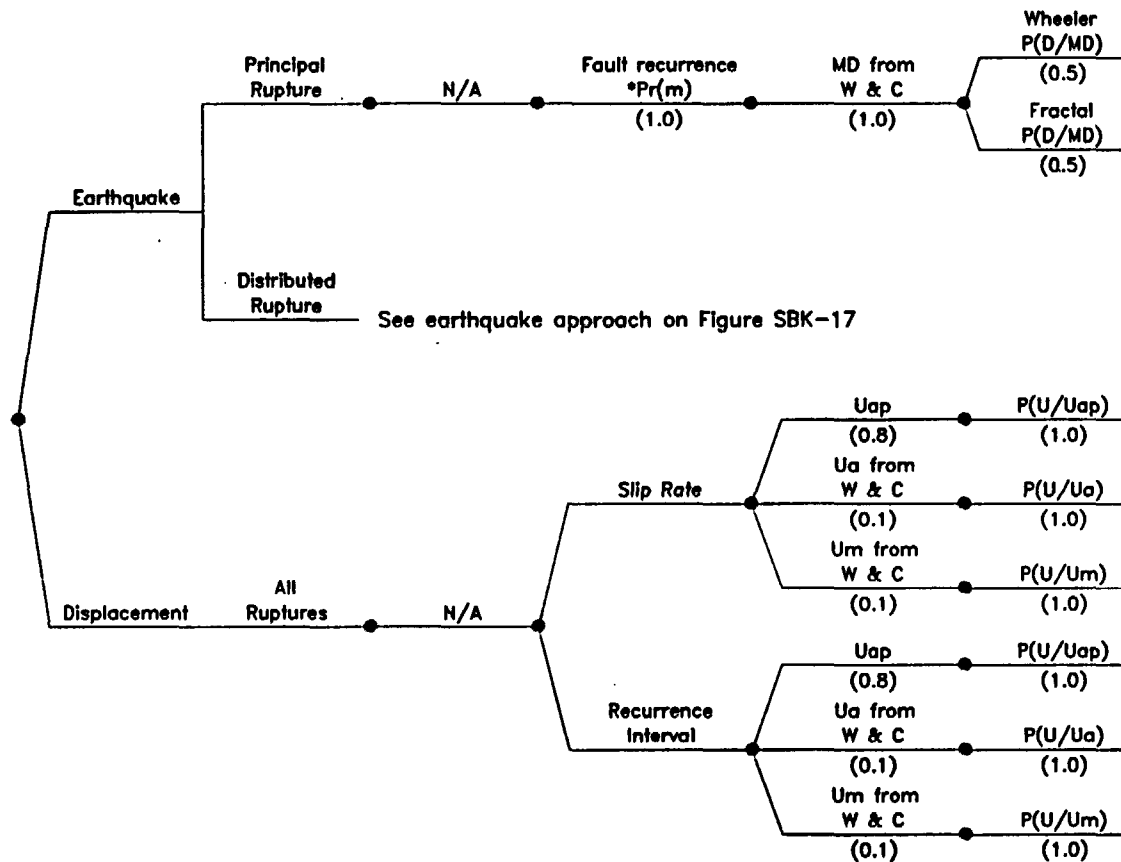


Figure SBK-8 Logic tree to characterize site with Quaternary displacement

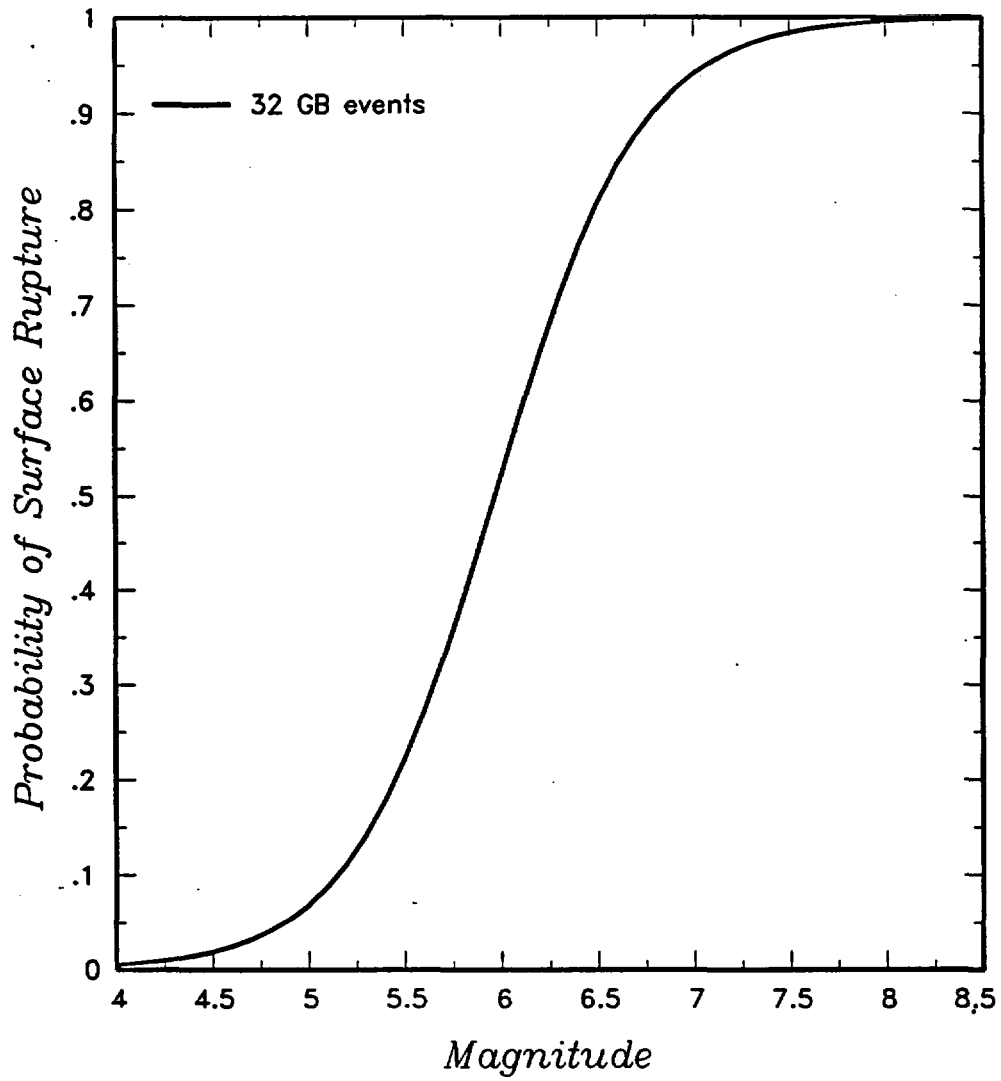


Figure SBK-9 Probability of surface rupture versus magnitude computed from data presented in Pezzopane and Dawson (1996)

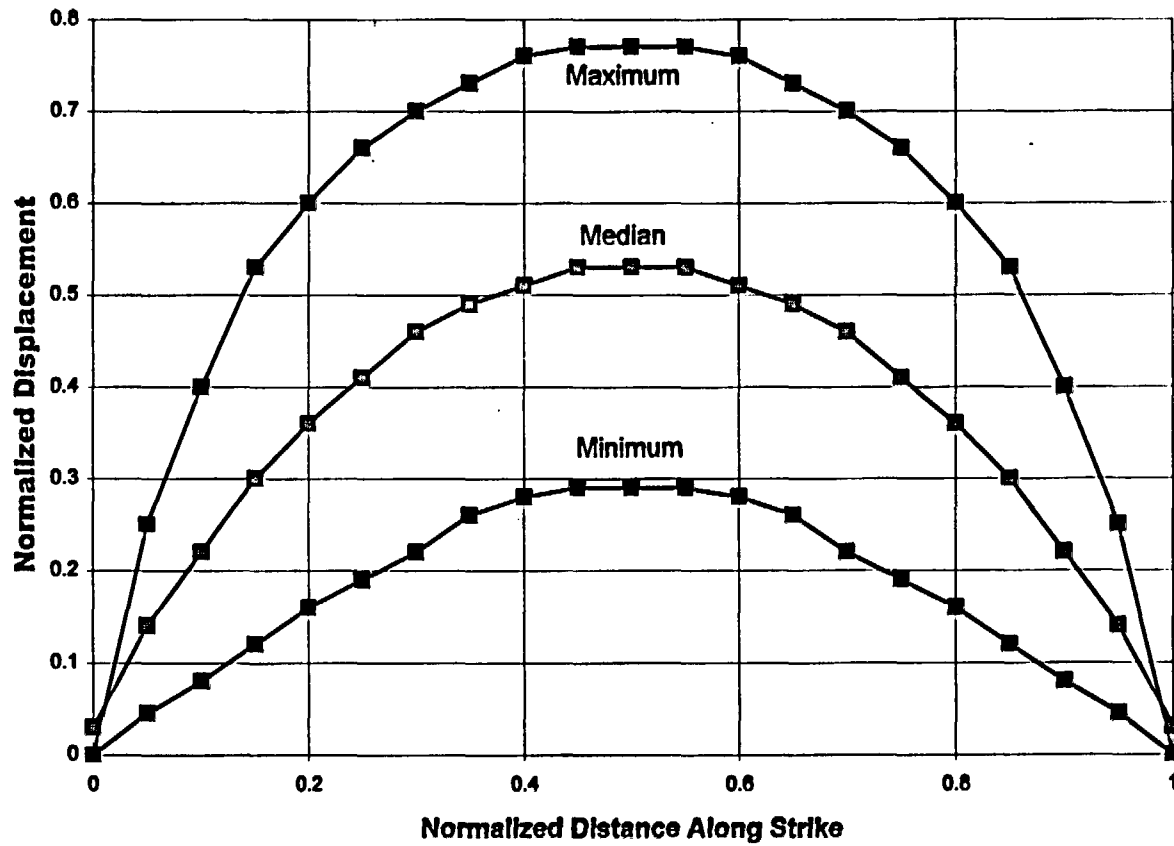


Figure SBK-10 Normalized slip along strike from five normal fault ruptures developed by ASM team from data in Wheeler (1986)

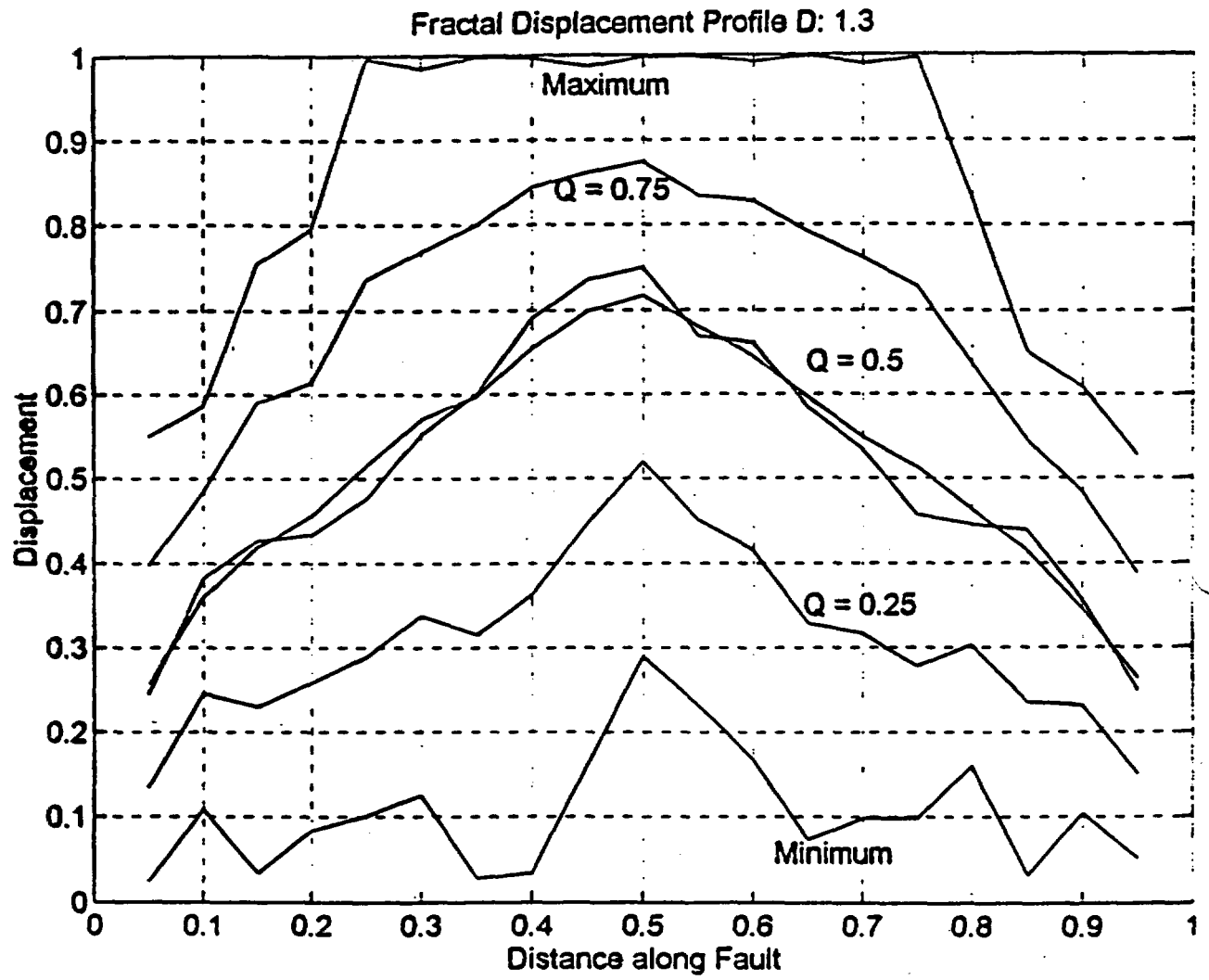


Figure SBK-11 Fractal displacement profiles developed by R. Bruhn (SBK) to predict distribution for the ratio of displacement at a point to the maximum displacement in an earthquake

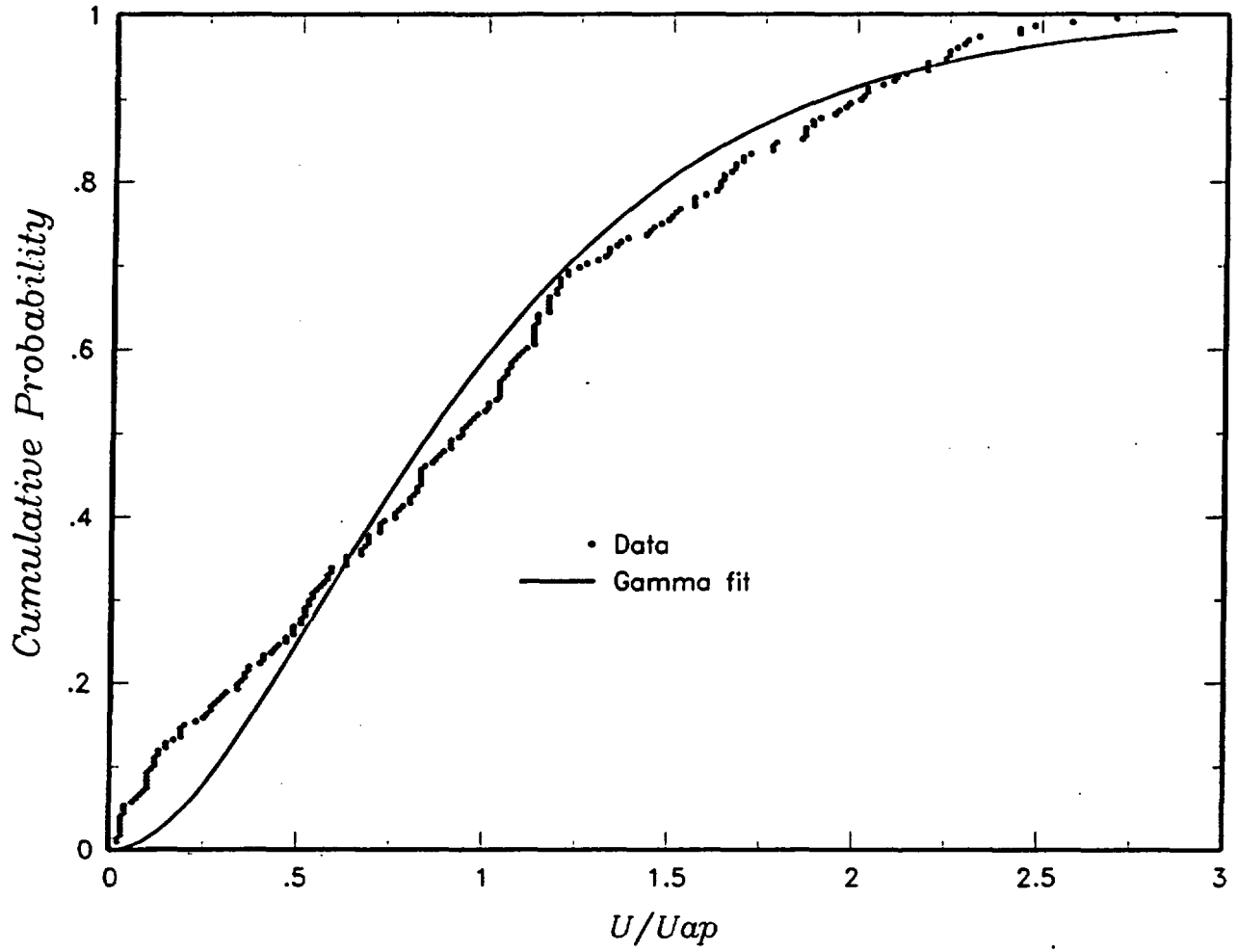


Figure SBK-12 Distribution of U/U_{ap}

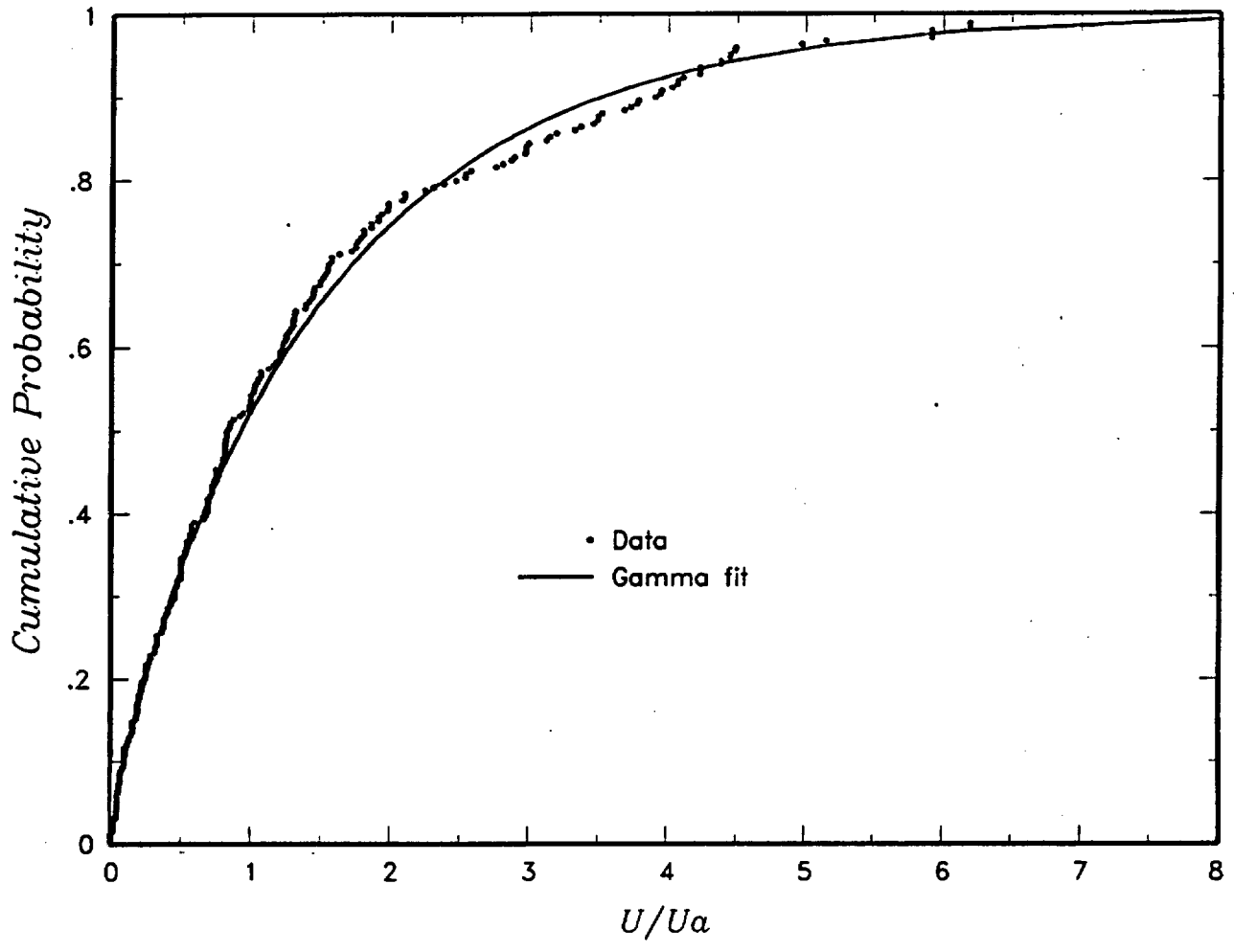


Figure SBK-13 Distribution of U/Ua

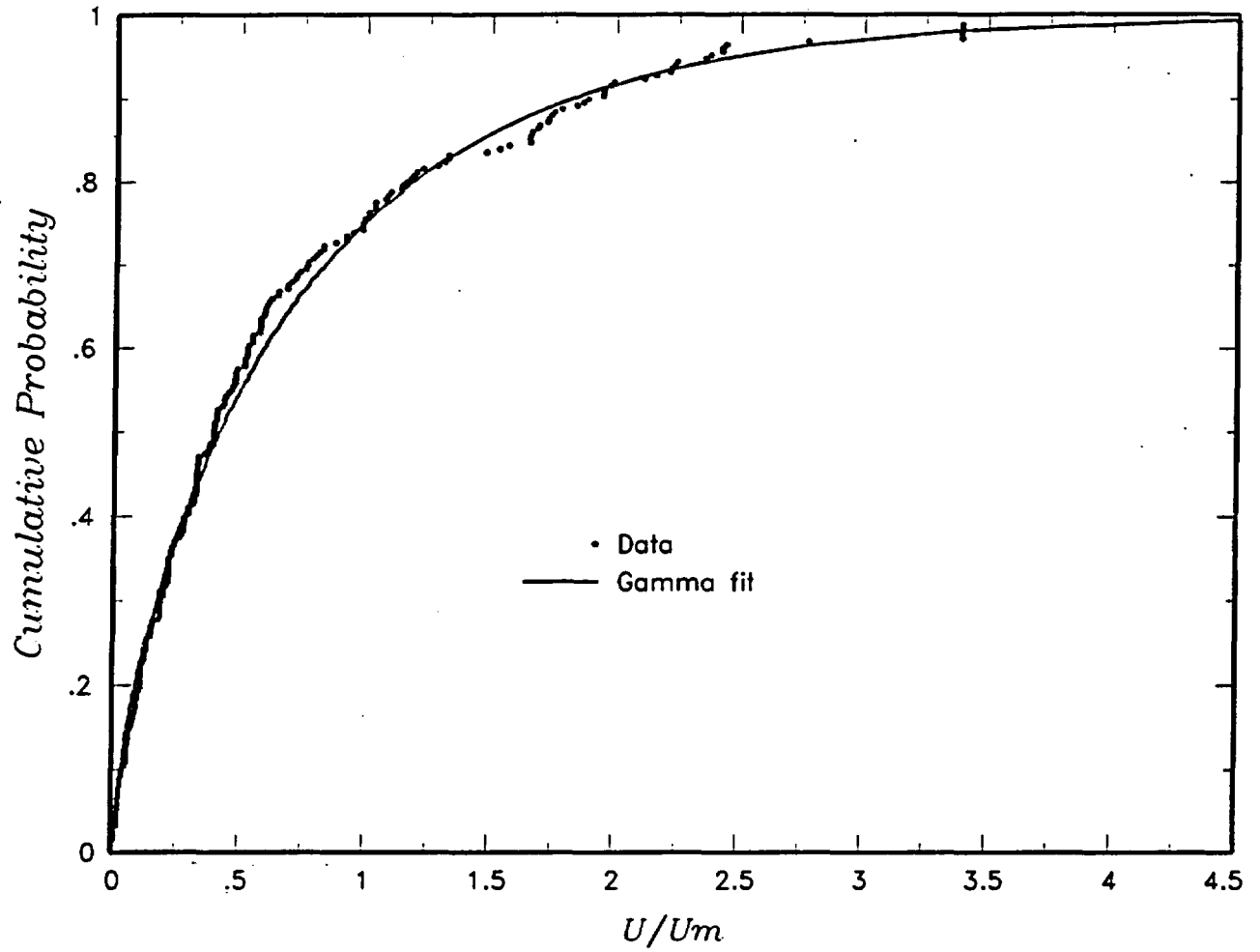


Figure SBK-14 Distribution of U/U_m

<i>Approach</i>	<i>Fault Orientation Factor</i>	<i>Excavation Site</i>	<i>Frequency of Rupture</i>	<i>Slip Rate</i>	<i>Event Size Measure</i>	<i>Displacement Distribution</i>
-----------------	---------------------------------	------------------------	-----------------------------	------------------	---------------------------	----------------------------------

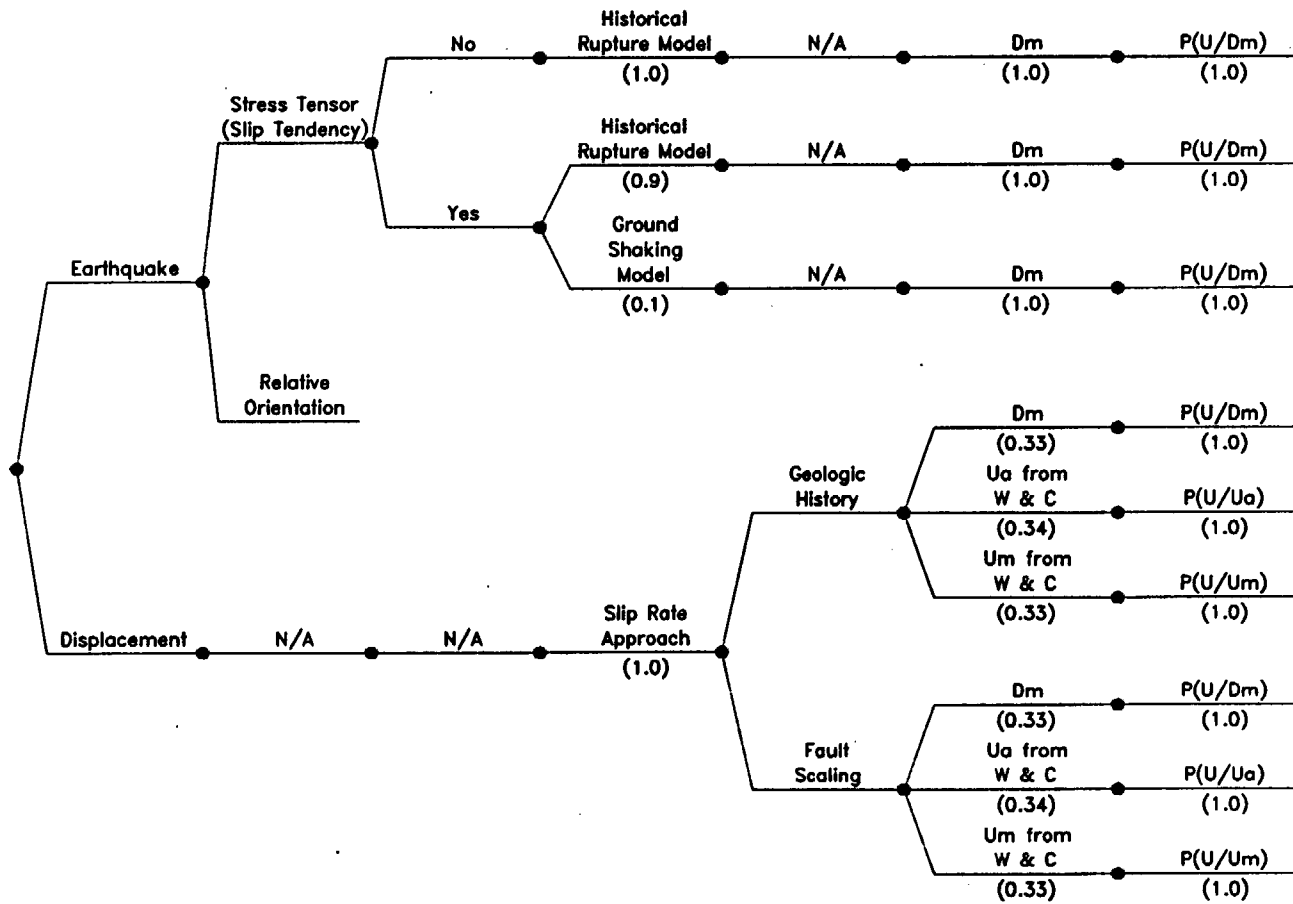


Figure SBK-15 Logic tree to characterize sites without Quaternary displacement

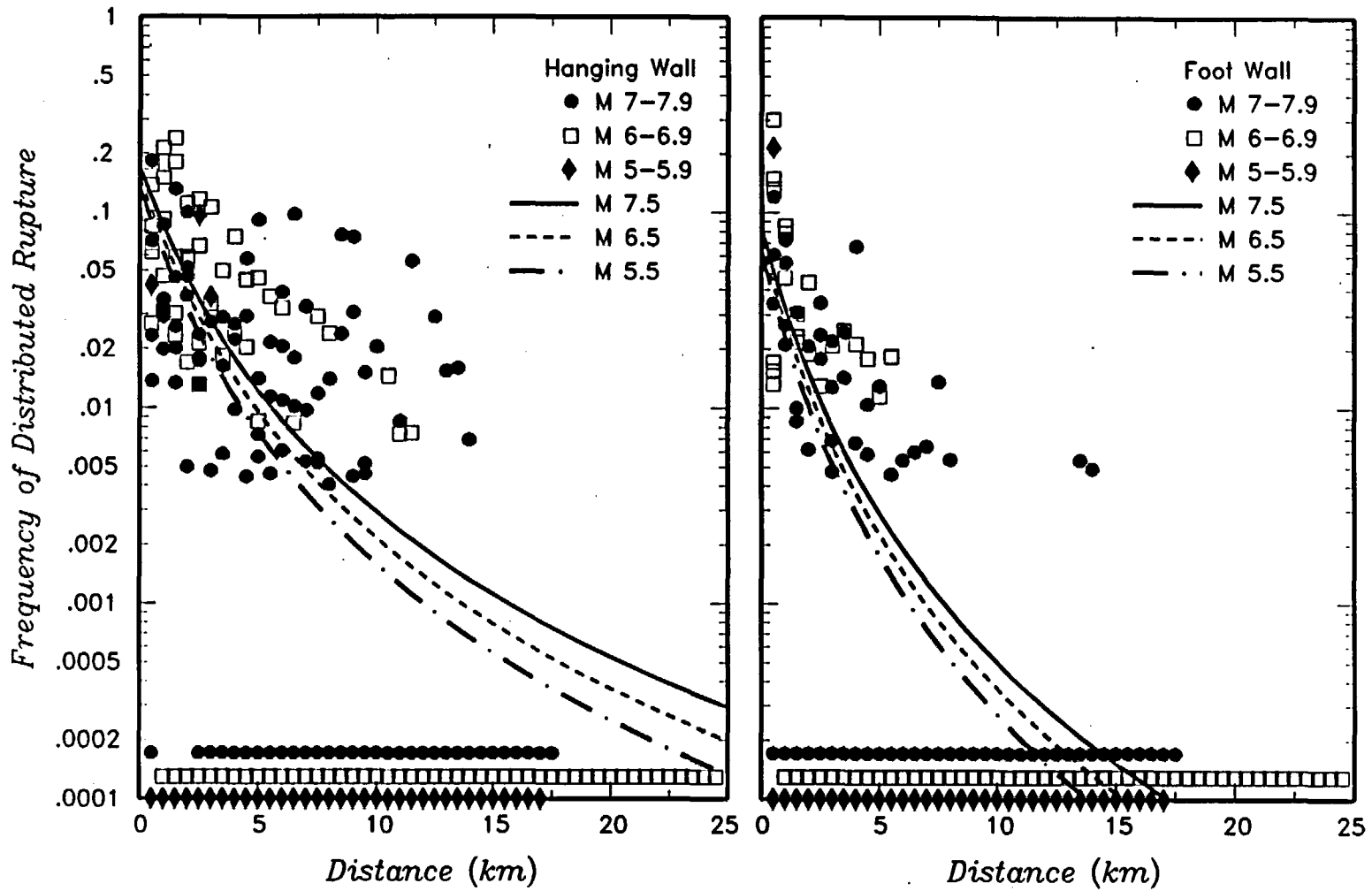


Figure SBK-16 Probability of induced distributed slip as a function of distance from the rupture and hanging wall/footwall location computed from the data presented in Pezzopane and Dawson (1996). Curves show logit regression fits to data.

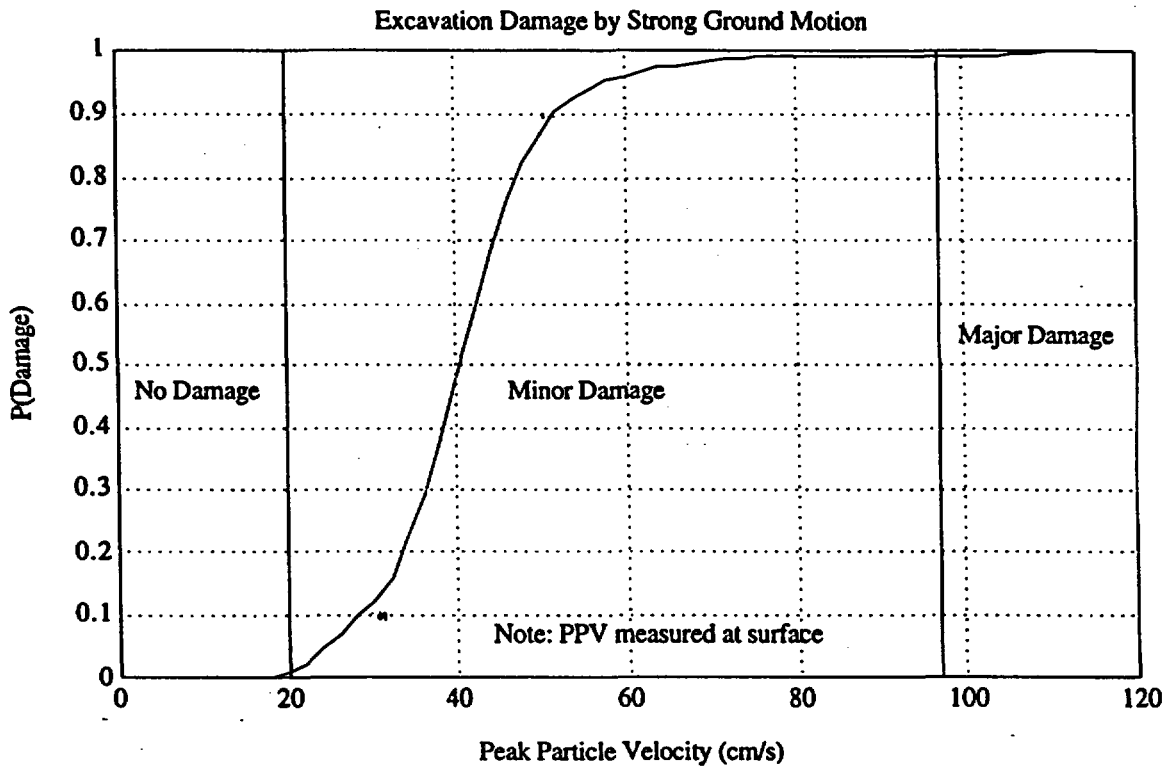


Figure SBK-17 Probability density function (sketched) for probability of initiating joint or fault displacement in an underground excavation. PDF is based on data summarized in Figure 2, page 2 of Brady (1990).

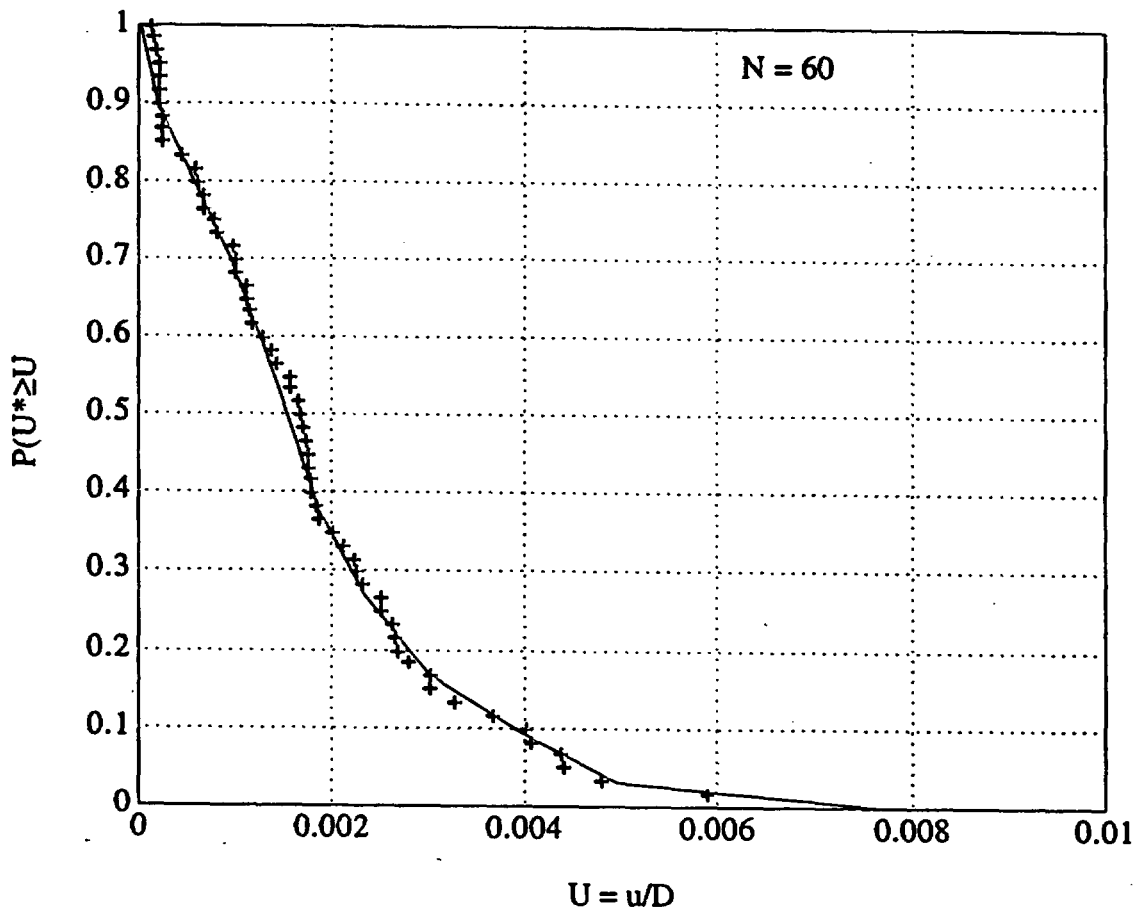


Figure SBK-18 Cumulative Probability Function $P(U/D_m)$. See text Section 3.2.3 for discussion of derivation and use. Crosses represent data points from Yucca Mountain faults, solid line is a sketched fit to the data values.

APPENDIX SBK-1 SUMMARY OF SEISMICITY REPORTS

Our decisions and weightings for the particular locations of background source regions and the behavior of seismicity were based on published reports on seismicity in the southern Great Basin. These reports have varied in their focus and scope: There are periods of time for which minor sequences are discussed in some detail, whereas other time periods are covered only by being represented in the historical earthquake catalog. Detailed reports of the seismicity in selected regions near Yucca Mountain began with the Nuclear Testing program in the 1960s, in particular, with reports on the explosion-triggered seismicity in the Pahute Mesa area (Hamilton and others, 1969a).

Meremonte and Rogers (1987) have compiled a catalog of historical earthquakes in the southern Great Basin from 1868 through 1978. This established the historical catalog to the time of the installation of the southern Great Basin regional seismic network in 1978; Meremonte and Rogers (1987) provide a full bibliography of sources for that historical compilation. In the 1930s, instrumental records of small- to moderate-sized earthquakes in the southern Great Basin were compiled for the first time by the Californian Institute of Technology; prior to that, catalog entries were primarily based on felt reports.

From 1910 through 1939, all entries in the 100 km catalog are $M > 3$, and all but one of these events is located west of Yucca Mountain. These earthquakes generally are associated with the northwest-trending Death Valley-Furnace Creek (DVFC) fault zone. From 1940 through 1949, with the increase in instrumental recording and a corresponding decrease in the magnitude detection threshold, earthquakes were located throughout the 100-km region. During this time period, the region adjacent and within DVFC fault zone is the dominant source of seismic energy release. The largest event between 1940 and 1949 was an $M 4.8$ in 1944.

King et al. (1971) provide maps and some discussion of notable earthquakes within 100 km of the central Nevada Test Site (NTS) from 1950 through 1971. Many of the earthquakes reported by King et al. (1971) are not assigned magnitudes and are considered to be smaller

than M 3. Several M 4 events are reported for the NTS, including several felt events, during this 20-year period. The most significant earthquake during this time period was the August 5, 1971, M 4.5 Massachusetts Mountain event. Portable instruments were deployed in the epicentral area of the Massachusetts Mountain sequence: 612 aftershocks were counted in the 72 hours following the earthquake (King et al., 1971). They note that the 1971 Massachusetts Mountain event took place near the location of an M 4.3 earthquake in 1957, although the locations of the two earthquakes are clearly separated in their published maps. From 1971 through the late-1970s, earthquakes were reported in monthly reports for the Atomic Energy Commission by the Earth Sciences Laboratories, a division of NOAA (Las Vegas, Nevada). The other significant earthquake sequence in the 1970s was the February, 1973, Ranger Mountains swarm. This sequence was unusual in that it produced eight earthquakes greater than M 3.5 during a three-week period, including two events greater than M 4. Also, the seismicity was distributed over a 10 x 10 km area (Earth Sciences Laboratories, 1973).

In the region south and east of the Massachusetts Mountain earthquake and within the 100-km region, approximately 75 percent of an estimated total moment release of 4.1×10^{23} dyne-cm (estimated from the historical catalog) is represented by the Massachusetts Mountain and Ranger Mountain sequences. Only 5 percent of the total moment release is from the pre-1971 period. Another 12 percent is accounted for in a cluster in January 1993. In the 10-year period 1980 through 1990, the moment release rate for this region was about 2×10^{21} dyne-cm/yr. The 1993 cluster occurred during a general increase in seismicity in the Rock Valley fault zone following the Little Skull Mountain earthquake, although this small sequence was east of the Rock Valley system.

In 1978, the USGS installed a regional analog telemetered seismic network and began reporting on the seismicity in the southern Great Basin for Yucca Mountain Site Characterization. These reports covered the years 1978 through 1991 (Rogers et al., 1981; Rogers et al., 1983; Harmsen and Rogers, 1987; Harmsen, 1991; Harmsen, 1993a). Seismicity reports from 1992 to the present have been generated by the University of Nevada Reno Seismological Laboratory (von Seggern and dePolo, 1995; von Seggern et al., 1996, von Seggern and Smith, 1997). A report by Rogers et al. (1987a) on the relationship of the

seismicity to the regional tectonic framework summarized the initial years of comprehensive seismic monitoring with the regional network. That study included detailed discussions of the seismicity and focal mechanisms of specific source regions, descriptions of the development of the various magnitude scales in use, an analysis of the regional stress field, and proposed models of regional deformation. Conclusions regarding the seismicity and tectonic framework of the Yucca Mountain region from the Rogers et al. (1987a) are summarized as follows (Priestley, 1991 written communication).

- Seismic activity in the southern Great Basin is generally expressed in clusters of earthquakes distributed in an east-west belt between latitude 36 and 38 degrees north, referred to here as the southern Nevada seismic zone (Figure 7-1). The earthquake clusters are diffusely distributed around mapped faults, covering areas larger than the surface projections of the rupture (Figure. 7-2). Most events are not readily associated with the surface traces of known faults. These clusters may align with local structural grain; composite and single-event focal mechanisms suggest that nodal planes correlate with regional stress directions.
- Earthquakes tend to distribute in vertical tubular-shaped clusters rather than along planar fault zones. Rogers et al. (1987a) interpret this geometry to represent activity at the intersections of faults. These vertically distributed, localized clusters of seismicity stretch to 10 to 15 km deep. Most seismicity is within the upper 15 km of the crust, but some earthquakes may occur below 15 km. The depth distribution of seismicity is bimodal, with maxima at 1.5 and 9 km, and a minimum of activity at 4 km.
- Focal mechanisms and hypocenter alignments indicate that right-lateral slip on northerly trending faults is the predominant mode of stress release near the site (Figures 7-3, 7-4, and 7-5). Subordinate faulting on east-northeast (left-lateral) and northeast (normal) faults has been observed, as has oblique slip on structures of intermediate orientation with the appropriate dip angles. The inferred principal stress orientations are NW for the extensional (minimum compression) axis, and angles between NE and vertical for the maximum compressional axis (Harmsen and Rogers, 1986). The style of faulting determined from the focal mechanisms is not a function of depth.
- The comparison of energy release maps for the pre-1978 and post-1978 periods show that, averaged over decades, the seismically active zones appear to be releasing moment at about the same rates. Rogers and others (1991) show that the historical rate of occurrence of the largest earthquakes (M 7) in the central Nevada seismic belt west and northwest of Yucca Mountain is larger by an order of

magnitude than would be expected from geologic evidence. Wallace (1987) notes evidence that the occurrence of active periods lasting hundreds to thousands of years is followed by quiescent periods of 10,000 to 30,000 years. On a larger distance but shorter time scale, Bufe and Topozada (1981) describe a period of relative quiescence encompassing both California and western Nevada from 1960 to 1980. The current active period for M 6 encompasses the same large region, as characterized by Bufe and Topozada (1981).

- Yucca Mountain lies within a region of relatively low historic seismic energy release.
- Focal mechanisms indicate that the maximum (P-axis) and minimum (T-axis) compressive stresses are roughly horizontal, although there is more variation in the P-axis, implying a preponderance of strike-slip faulting mechanisms. The T-axis has a consistent orientation throughout the region.
- Regional stress orientations indicate north-south and east-west orientations for high angle fault planes, with dextral slip on the north striking and sinistral slip on the east-west-striking surfaces. Normal and oblique slip are preferred on fault surfaces with orientation intermediate to these directions.

Gross and Jaume (1995) compiled a historical catalog of the southern Great Basin and discussed intensity based magnitude scales (Modified Mercalli) and levels of shaking experienced at Yucca Mountain in the historical period. After compiling a list of events within 200 km of Yucca Mountain, they concluded that the strongest shaking experienced at Yucca Mountain in historic time has been during the 1992 Little Skull Mountain earthquake. They also determined a revised location for the M 6.1, 1916 earthquake, the largest event within the 100km region, by comparing waveforms recorded during the Little Skull Mountain earthquake with a heliocorder record of the 1916 event from the Reno Seismograph Station. The revised location suggests that the event may have taken place in the Death Valley fault zone. Von Seggern and Brune (1997) relocated two M 3.5 earthquakes from 1948 that previously were reported as being located at Yucca Mountain. The initial locations of these two events were constrained by first-motion data at California seismic stations. The waveforms and S minus P times at the regional stations operating in 1948 were more consistent with a source near the Rock Valley fault zone rather than one at Yucca Mountain. By comparing waveforms from Little Skull Mountain aftershocks and heliocorder records from the Caltech station for one more well-located 1948 Rock Valley

area event, they concluded that the two 1948 events most likely occurred in the Rock Valley area and not at Yucca Mountain. Von Seggern and Brune (1997) concluded that events were most likely part of one localized earthquake sequence in the Rock Valley area. Nevertheless, the quality of locations for earthquakes in the Yucca Mountain area in the 1940s would be expected to be poor at best because of the lack of station coverage.

A report by Rogers et al. (1987b) initiated some controversy by concluding that the attenuation in the southern Great Basin was lower than that in California. Therefore, earthquake magnitudes would be lower for an equivalent amplitude recorded at the same distance in the California region. This meant that the Ao curve of Richter (1958) was not appropriate for Nevada. These conclusions have a direct effect on recurrence estimates, moment-magnitude scales, and estimates of moment release rate for the southern Great Basin. In contrast, Chavez and Priestly (1985) and Savage and Anderson (1995) concluded that the Richter curve was in fact applicable to Nevada. In support of these results, von Seggern and Smith (1997), from an analysis of three-component digital seismograms, have shown that the Richter curve is generally appropriate for the southern Great Basin, in contrast to the Rogers et al. (1987b) study. They note that the Hanks and Kanamori (1979) moment magnitude relationship is acceptable for the Basin and Range province, and that at small magnitudes, moment-magnitude relations determined from the modern three-component digital records are not consistent with the Rogers et al. (1987b) results. Chavez and Priestly (1985) also determined a moment-magnitude relationship that was different from the Hanks and Kanamori (1979) relation, at intermediate magnitudes, for the western Great Basin.

Other published reports on the seismotectonics of the southern Great Basin have applied the historical seismicity data set to constrain models of regional deformation. Gombert (1991b) developed regional strain models that incorporated slip rates on active faults and comparisons with regional seismicity, then tested these models using a boundary element method. They concluded that the seismicity is associated with the local strain field near more active faults and that Yucca Mountain was geometrically situated such that strain accumulation in the Yucca Mountain block was minimal. Also, they interpreted the general lack of seismicity at Yucca Mountain as reflecting the presence of an isolated block or zone of low strain accumulation. In another study, Harmsen and Rogers (1986) analyzed the stress field from a

set of regional focal mechanisms. The presence of both strike-slip and dip-slip mechanisms in particular localities was explained as most likely resulting from an axially symmetric stress field, in which the intermediate and maximum compressive stresses are nearly equal (Harmsen and Rogers, 1986). They suggested that because no large earthquakes were present in the data set, that movement along a variety of fault plane orientations was accommodated by an ample number of small, preferably oriented faults.

Rogers et al. (1991) proposed a model in which right-lateral strike-slip faulting on north-striking planes is indicative of north-south crustal shortening. Anderson et al. (1993) suggest a crustal shortening mechanism for deformation in the Lake Mead area, consistent with the model proposed by Rogers et al. (1991). Interpreting models of regional deformation from the focal mechanism database is problematic because of the limited number of small earthquakes that account for only a small portion of moment release; the record of historical seismicity does not span the complete seismic cycle of faults in the region, which can be on the order of 10s to 100s of thousands of years in most cases.

REFERENCES

See reference list that follows main SBK text.

APPENDIX SBK-2 SUMMARY OF SEISMICITY

This appendix presents a discussion of the seismicity in the Nevada Test Site (NTS) region. The discussion focuses on specific issues regarding the behavior of earthquake sequences, earthquake clusters, and focal mechanisms and issues related to observations of earthquake triggering. The observations of the behavior of earthquake activity contributed to the weightings we assigned to background source zones, thickness of the seismogenic crust, relationship between seismicity and mapped Quaternary faults, and the problem of discriminating between true tectonic earthquakes and earthquakes triggered or potentially triggered by underground nuclear testing. This appendix includes some of the team's interpretations of the distribution of historical seismicity.

Northern Nevada Test Site

The northern region of the NTS includes the Timber Mountain caldera, Pahute Mesa, Rainier Mesa, and Yucca Flat. These areas have been the focus of considerable seismic activity, either directly or indirectly associated with nuclear testing. In contrast, most of the seismicity that extends across the south part of the NTS, within and adjacent to the Rock Valley, Mine Mountain, and Cane Springs fault zones (including the 1992 M 5.6 Little Skull Mountain earthquake), and activity around the southern boundary of the Timber Mountain caldera is, we believe, most likely tectonic in origin. We draw this conclusion primarily because this area is somewhat distant from the testing areas.

Determining what earthquake activity is related to underground nuclear explosions (UNEs), either through cavity collapse or the stresses induced by the explosions, is problematic. A study to determine the relative number of artificial and induced seismic events in the testing area suggests that the natural seismicity of the region reflects the background activity generally found in the southern Basin and Range province (Vortman, 1991). In 1979 and 1983, several swarms of micro-seismicity apparently unrelated to the UNEs occurred in the region. Two sequences that occurred during the period of active testing took place in the vicinity of Dome Mountain and Thirsty Canyon (Rogers et al., 1981; Rogers et al., 1987a).

Focal mechanisms indicate primarily right-lateral strike-slip faulting on north-trending structures and normal faulting on northeast-trending structures (Rogers et al., 1987a).

Southern Nevada Test Site

The south part of the NTS is a seismically active region relative to some other areas in the southern Great Basin. Most of the seismicity that stretches across the south part of the NTS, within and adjacent to the Rock Valley, Mine Mountain, and Cane Springs fault zones (including the 1992 M 5.6 Little Skull Mountain earthquake), and activity around the southern boundary of the Timber Mountain caldera, is not in areas of underground nuclear testing. Some of the activity near the eastern NTS boundary, particularly the 1971 Massachusetts Mountain earthquake and 1973 Ranger Mountain swarms, may have been triggered following the initiation of testing in the Yucca Flat area; however, there seem to be considerable numbers of small earthquakes related to natural tectonic strain release (Gomberg, 1991a and b). The largest event in this region is the 1992 ML 5.6 Little Skull Mountain earthquake, which most likely was triggered by a larger regional earthquake (Anderson et al., 1993a and b).

Focal mechanisms from Rogers et al. (1987a) indicate sinistral slip on northeast structures and (or) dextral slip on northerly striking structures in the southern Great Basin. A prominent concentration of seismicity that includes the 1992 Little Skull Mountain earthquake occurs within a wide northeast-trending zone centered on the Rock Valley fault zone. This area includes the 1970 M 4.5 Massachusetts Mountain earthquake, the 1973 Range Mountains sequence, the 1992 M 5.6 Little Skull Mountain earthquake (Harmsen, 1993; Meremonte et al., 1995; Smith et al., 1997), the 1993 Rock Valley sequence (Shields et al., 1995), and other relatively minor earthquake clusters and alignments. Also, spatial patterns in the seismicity within this wider Rock Valley zone extend both north along the Mine Mountain system (Rogers et al., 1987) and south subparallel to the South Specter Range fault.

A general lack of seismicity characterizes the vicinity of Yucca Mountain. An analysis of the earthquake detection threshold for the Southern Great Basin Seismic Network (SGBSN) suggests that this zone of quiescence is real (Gomberg, 1991b). An experiment in

high-resolution monitoring of seismicity at the potential site by Brune et al. (1992) confirms the existence of the quiescent zone. Modeling of the strain field in southern Nevada by Gomberg (1991a) suggests that this area is not accumulating significant strain, and that Yucca Mountain is an isolated block within the structural framework of the southern Great Basin.

Northern Amargosa Valley-Sarcobatus Flat

The northern Amargosa Valley-Sarcobatus Flat encompasses the areas west and northwest of the Bare Mountain fault, 25 to 90 km from the site. Seismicity in the northern Amargosa Valley is diffusely distributed in the vicinity of Beatty, Nevada, and the Bullfrog Hills mining district. In Sarcobatus Flat, earthquakes have occurred in four clusters since the advent of instrumental monitoring (Rogers et al., 1983, 1987a). These clusters are spaced roughly 10 to 20 km apart in a northerly trend along the length of the valley. Focal mechanisms for the three southern clusters suggest dextral slip along north- to north-northeast-trending structures.

Northern Death Valley Region

Seismicity along the Furnace Creek fault zone in northern Death Valley is diffusely distributed over an area much larger than the mapped surface traces of the primary fault system. A concentration of activity extends northeast from northern Death Valley at the north end of the Furnace Creek fault through the Gold Mountain-Mount Dunfee region. The largest event in this area in the modern era was an ML 4 event at Gold Mountain. A cluster of events occurred in a northeast alignment near Mount Dunfee in 1983. A composite focal mechanism from several of these earthquakes suggests left-oblique normal faulting on a northeast-striking fault plane (Rogers et al., 1987a). The seismicity appears to be occurring at a low rate for such a high-slip system of faults, suggesting that the moment release in the region is concentrated on the main structures.

Explosions and Seismicity Triggered by Non-Tectonic Events

Seismicity analyses attempt to distinguish between underground nuclear explosions (UNEs), their collapses and aftershocks, chemical explosions associated with testing and mining, seismicity associated with the filling and subsequent changes in level of Lake Mead, and the

natural seismicity in the region. The historical catalog of southern Great Basin earthquakes for the period 1868 to 1978, compiled by Meremonte and Rogers (1987a), labels seismic events that are attributed to UNEs. The triggering of earthquakes by UNEs presents a difficulty in interpreting the distribution of seismicity within the context of a seismotectonic framework for the NTS area.

The most active regions within the southern Great Basin are the north and southeast sections of the NTS, the area west of the Bare Mountain fault, the region at the north end of the Death Valley-Furnace Creek fault system, and the Pahrnagat Shear Zone (Rogers et al., 1987a). The level of seismic activity may reflect tectonic release following explosions in the region surrounding the NTS. Mining-related explosions have occurred in the Bullfrog Hills west of the Bare Mountain fault and various other mining sites around the region (Vortman, 1991).

Underground Nuclear Explosions

Extensive aftershock sequences followed several UNEs in the Pahute Mesa area from 1968 through 1970 (Hamilton et al., 1971). These sequences were not confined to the test locations, but were distributed along several mapped faults as far as 15 km from the shot points. Portable instruments deployed in the late 1960s following the Benham shot recorded about 2500 earthquakes greater than M 2.0 from December 1968 through December 1970. This period included several explosions. Hamilton et al. (1971) reported that 94 percent of the events with well-constrained focal mechanisms were shallower than 5 km; some of the events were as deep as 8 km. Focal mechanisms show dominantly normal slip on northeast-to north-northeast-striking fault planes, and fault planes generally align with the fabric of mapped normal faults in the Tertiary tuffs. This correlation would imply a predominantly down-to-the-west/northwest sense of motion for most of the earthquakes.

Aftershocks of UNEs also appear in the Yucca Flat and Raineer Mesa areas in the eastern NTS, although they are not as prolific or as distributed as the triggered seismicity in the Pahute Mesa area. The earthquake locations and depth distributions of these earthquakes have not been studied in the detail Hamilton et al. (1971) applied to the Pahute Mesa area. There are also complications in resolving the relationship of UNEs to triggered earthquakes in the southeastern NTS south and east of Yucca Flat, wherein a notable increase in

seismicity occurred in the 1970s following the initiation of underground testing in that area. All UNEs in Yucca Flat were reported at or below 150 kilotons, whereas some explosions at Pahute Mesa had reported yields as great as 1 megaton (Mt).

Large UNEs (~1 Mt) have been known to trigger release of natural tectonic strain (Wallace et al., 1983, 1985). Thus, the potential exists that future testing may induce displacements on faults in the Yucca Mountain site vicinity and adjacent region; although coseismic tectonic release has not been observed far from the UNEs. The relations between UNEs and natural seismic activity near the NTS have been discussed by Aki et al. (1969); Bucknam (1969); Dickey (1968, 1969, 1971); Dickey et al. (1972); McKeown and Dickey (1969); Hamilton and Healy (1969); Hamilton et al. (1969, 1972); Smith et al. (1972); Rogers et al. (1987a); and Vortman (1991). These studies observed that strain release and related effects become difficult to find beyond 5 to 10 km from surface ground zero of even the largest events (1 Mt). The Buckboard area is the nearest historical or proposed UNE testing area to Yucca Mountain, and is approximately 25 km northeast.

The relationship between UNEs and seismicity has been discussed by Rogers et al. (1987a), Vortman (1991), and Hamilton et al. (1971). Vortman's (1991) analysis of the seismicity of the NTS and vicinity deleted those events interpreted as human-made, but considered the number and location of earthquakes triggered by UNEs. Vortman (1991) proposed that considerable numbers of small-magnitude earthquakes apparently are induced by dynamic stresses of the seismic energy generated during the explosion, whereas other small events seem to occur in response to the altered static-stress field resulting from the explosion. Some events are triggered by the arrival of the UNE phase; others appear to be in response to changes in an altered stress field caused by the explosion. A UNE may cause a stress change on the order of several bars, a fraction of the lithostatic stress in the hypocentral region. Some areas of the southern Great Basin may be in a state of critical stress, in which a small perturbation in the load on a fault, such as UNE-induced stress changes, can cause the release of accumulated tectonic strain.

Triggered Earthquakes

The triggering of aftershocks by UNEs at the Nevada Test Site near Yucca Mountain (Hamilton and Healy, 1969; Hamilton et al., 1972, Rogers et al., 1983) and the continued occurrence of induced seismicity following the impoundment of Lake Mead (Carder, 1945; Rogers and Lee, 1976) are evidence that a number of fault segments in the southern Great Basin may be near failure. There is strong evidence that the June 29, 1992, Little Skull Mountain earthquake was triggered by the June 28, 1992, Landers, California, earthquake (Ms 7.6, Mw 7.3). The Landers earthquake also apparently triggered smaller earthquakes at locations throughout a large region of the western United States, extending as far as the Yellowstone Caldera at a distance of 1250 km (Hill et al., 1993). The Little Skull Mountain earthquake occurred about 225 km north of the Landers rupture. An increase in microseismic activity in the vicinity of Little Skull Mountain was observed beginning in the coda of the Landers event (Anderson et al., 1994). This was recorded by the Yucca Mountain microearthquake array (instrumentation described in Brune et al., 1992). The activity accelerated over the next 23 hours, culminating in the M 5.6 Little Skull Mountain main shock. This pattern may indicate that the Little Skull Mountain region was near failure prior to the Landers earthquake, which in turn may have advanced the time of rupture.

The specific mechanism of triggering of the Little Skull Mountain earthquake is uncertain, but a consensus appears to be that the dynamic strains associated with the propagation of long-period surface waves from the Landers earthquake (Anderson et al., 1994; Gomberg and Bodin, 1994) initiated a failure process possibly involving fluids (Hill et al., 1993) or sympathetic slip or creep (Bodin and Gomberg, 1994). Following the Landers main shock, Johnston et al. (1995) observed a transient strain change associated with an increase in seismicity at the Long Valley Caldera. The Landers earthquake produced an unprecedented increase in seismicity in the eastern California shear zone (Roquemore and Simila, 1994) and in the Sierra Nevada-Great Basin boundary zone (Anderson et al., 1994).

Historical Seismicity near Yucca Mountain

Throughout the southern Great Basin and including the site area, seismicity generally is distributed in a broad belt that trends east-west from the Utah border to California. Earthquakes generally have strike-slip and normal faulting mechanisms and focal depths

ranging from near-surface to 12 to 15 km deep. The number of resolved focal mechanisms indicates that approximately half of the solutions are strike-slip and half are dip-slip (Rogers et al., 1992). In this region, as elsewhere in the Great Basin, there is a general lack of correlation between the distribution of epicenters and Quaternary faults.

The focal mechanisms of earthquakes closer to Yucca Mountain are strike slip to normal oblique slip along moderately to steeply dipping fault planes. The nodal planes are consistent with right-lateral faulting on north- to north-northwest-striking planes or normal-left oblique slip on northeast- to east-striking faults. These directions of inferred faulting are consistent with the style of Quaternary faulting and the orientations of principal stresses in the region. Rogers et al. (1987a, 1991) and Bellier and Zoback (1995) analyze the modern stress field in regions of Nevada near Yucca Mountain.

A zone of quiescence centered on Yucca Mountain is apparent in all studies that describe seismicity in the southern Great Basin. Brune et al. (1992) and Gomberg (1991a and b) have shown that this zone is a real feature of the seismicity and not an artifact of network design. The largest earthquake to occur under Yucca Mountain from the inception of the SGBSN in 1978 was an ML 2.1 event that occurred on November 18, 1988, located 12 km north-northwest of the proposed repository at a depth of 11 km (Harmsen and Bufe, 1992). The inferred tension axis for this event is rotated about 25 degrees counterclockwise from the average tension axis observed in the region. The observed relatively aseismic character of the site area may result because the principal faults in the Yucca Mountain block are unfavorably oriented with respect to the present stress field. In other words, in the present regional stress field, north-striking faults would be expected to accommodate a portion of right-lateral motion and not pure normal slip.

RECENT SEISMICITY

The 1992 M 5.6 Little Skull Mountain Earthquake

The largest and most significant earthquake recorded in the vicinity of Yucca Mountain since the regional seismic network was established in 1979 was the June 29, 1992, M 5.6 Little Skull Mountain (LSM) earthquake (Lum and Honda, 1992; Harmsen, 1994; Walter, 1993;

Meremonte et al., 1995; Smith et al., 1997). Origin Time: June 29, 1992; 1014 22.47 UTC; Latitude: 36 N 43.1'; Longitude: 116 W 17.16'; depth 11.8 km; ML 5.8 UNRSL; ML 5.6 NEIC. The event occurred approximately 20 km southeast of the proposed repository. The highest ground acceleration was 0.206 g recorded at a strong-motion station a Lathrop Wells, Nevada, at about 11 km epicentral distance (Blume and Honda, 1992). The earthquake caused some minor damage to the Yucca Mountain Field Operations Center in Jackass Flat, which was almost directly on the surface projection of the buried fault plane. The event was widely felt throughout the region.

The LSM earthquake initiated at a depth of 11.7 km, and nearly the entire sequence, main shock rupture surface and aftershock sequence, was confined to between 5 and 12 km depth. Fault rupture propagated unilaterally from southwest to northeast for about 6 km; the epicenter of the main shock plots near the southwest end of the aftershock zone. There was no evidence of primary or secondary surface faulting. Rockfalls along the south-facing cliffs of Little Skull Mountain were observed shortly after the earthquake. The distribution of rockfalls, which was found to be consistent with the ground shaking predicted from the source model, provided a means of calibrating the distribution of ground shaking in the epicentral region (Brune and Smith, 1996). The earthquake occurred on a northeast-striking fault plane dipping steeply to the southeast (Harmsen, 1993; Meremonte et al., 1995; Smith et al., 1997 in press) and involved nearly pure normal slip with a small left-slip component. The following table is a compilation of short-period and waveform-based focal mechanisms and reported seismic moments for the LSM earthquake.

THE 1992 LITTLE SKULL MOUNTAIN MAIN SHOCK SOURCE PARAMETERS *

Information Source	Strike	Dip	Rake	Mo x10 ²⁴ dyne-cm
Smith et al. (1997)	60±15	70±13	-70±10	-
Meremonte et al. (1995)	55	56	-72	-
Romanowicz et al. (1993)	43	66	-73	3.5
Romanowicz et al. (1993)	34	44	-70	2.6
Zhao and Helmberger (1994)	45	55	-60	3.0
Walter (1993)	35	54	-87	4.1
Harmsen (1994)	55	56	-72	-

* Source parameters strike, dip, and rake are in degrees using the convention of Aki and Richards (1980); seismic moment, Mo, is in units of 10²⁴ dyne-cm. Modified from Schneider et al. (1996).

There were three aftershocks of $M > 4$; none occurred on the main shock fault plane, but rather on adjacent "off-fault" structures that most likely accommodated the stress change from main shock rupture. These larger aftershocks also triggered near-source stations of the Blume strong motion network (Lum and Honda, 1992). The first $M 4$ aftershock occurred in the coda of the main shock; its location could be constrained only as being east of the main shock epicenter. Focal mechanisms and quality locations could be determined for the following two $M 4+$ events: $M 4.4$ July 5th, 0654 13.27 UT; Latitude: 36 N 43.55'; Longitude: 116 W 16.46'; depth 9.39 km; (Fault Plane Parameters: Strike: N75°E, Dip: 70°SE, Rake: -20°); $M 4.5$ September 13th, 1146 20.87 UT; Latitude: 36 N 43.41'; Longitude: 116 W 18.28'; depth 8.93 km (Fault Plane Parameters: Strike: N20°E, Dip: 45°SE, Rake: -80°).

The LSM earthquake could not be correlated with any mapped faults, although Harmsen (1993) and Meremonte et al. (1993) suggested that it may have taken place on a southern extension of the Mine Mountain fault zone. Smith et al. (1997) point out that the LSM sequence is situated where the Wahmonie, Caine Springs, as well as the Mine Mountain fault systems project into the Rock Valley fault zone. Some earthquakes within the LSM aftershock zone that occurred off the main shock fault plane align along a southern projection of the Wahmonie fault zone as well.

The LSM earthquake occurred in an area of persistent recent seismicity throughout the recording period of the network. This may be a zone of stress concentration, accommodating strain throughout the fault systems in the southcentral NTS area. The Rock Valley fault zone is the primary Quaternary system in this group and shows the most associated seismicity. The LSM main shock epicenter plots directly along the crest of LSM, which would place it, at hypocentral depth, at the base of the seismogenic zone, potentially near an intersection with the Rock Valley fault system. Whether the Mine Mountain fault was the causative structure for the LSM earthquake, it is clear that there is a direct relationship with the Rock Valley system.

Earthquakes in the Rock Valley Region in the Post-LSM Period

Following the Little Skull Mountain earthquake, there has been a notable increase in earthquake activity in the southern Rock Valley fault zone (Smith and Brune, 1997; Shields et al., 1995; O'Leary, 1996). Only two M 3+ earthquakes adjacent to the Rock Valley fault zone in the southern NTS region are included in the SGBSN earthquake catalog from 1979 to prior to the LSM sequence. Since LSM, three M 3.5+ earthquakes, and an unusual sequence of very shallow earthquakes in mid-1993 (Smith et al., 1997, written communication; Shields et al., 1995), have taken place in Rock Valley; these M 3.5+ earthquakes occurred at various locations in southern Rock Valley near the LSM sequence. This activity appears to be diminishing (at the time of this report - October 1997), suggesting that indeed the LSM event may have had a role in triggering the increased activity along the Rock Valley fault.

The shallow sequence of earthquakes in 1993 (main event M 3.8) was recorded on a near-source portable digital instrument. This station recorded more than 500 earthquakes, of which only 140 triggered the regional seismic network and could be located. S minus P times for the events averaged about 0.5 sec at this station; relocations of the earthquakes place them about 2 km from the surface. The largest event of the sequence, M 3.8, was also reported at a 2-km depth. Stress drops determined from modeling the S-wave spectra and using an empirical Green's function were on the order of 10 bars for all the larger events. A cluster of earthquake activity also occurred southeast of the Rock Valley fault zone in the Spotted Range in late 1993. This was the most active cluster of seismicity in the region east of the NTS since the 1973 Ranger Mountain sequence. In contrast to the Ranger Mountain and 1971 Massachusetts Mountain sequences, the 1992 cluster was confined to a small volume and included only one earthquake greater than M 3.

Micro-Earthquakes at Yucca Mountain: 1995 and 1996

From May 1995 through September 1996, 15 micro-earthquakes were located in and around the Yucca Mountain block (Smith et al., 1996; Brune and Anooshepoor, 1996). Depths ranged from 5 to 10 km; magnitudes ranged from M -0.76 to M 0.72 (Brune and Anooshepoor, 1997). Short-period focal mechanisms were determined for four of the events, and although there was not enough information from the focal mechanism data to unequivocally correlate the earthquake with mapped faults, one event may have occurred on

or near the Stage Coach Road Fault, and another three events may have taken place on or near the Paintbrush Canyon Fault. Gross and Jaume (1995) reviewed the archived waveform data to analyze a number of small events that were in the catalog and reported to be in the Yucca Mountain block after 1978 and before 1992. Their report lists some events that were incorrectly identified as earthquakes.

TABLE: SMALL-MAGNITUDE EARTHQUAKES AT YUCCA MOUNTAIN

#	Date	Origin Time	Lat	Lon	Depth	M
1.	*95 5 5	1321 33.12	36N50.66	116W24.08	6.15	0.58
2.	95 7 1	1526 56.69	36N40.84	116W30.88	8.65	
3.	95 7 7	759 -0.33	36N49.67	116W24.85	6.02	-0.27
4.	95 7 28	618 51.42	36N54.10	116W30.52	4.80	-0.48
5.	*95 9 4	1239 47.11	36N44.43	116W30.02	4.45	0.72
6.	95 11 19	2215 84.91	36N50.80	116W23.59	6.46	-0.25
7.	95 11 20	226 57.44	36N50.81	116W23.67	5.95	-0.43
8.	95 12 6	2327 15.90	36N43.74	116W29.06	7.80	0.29
9.	96 1 29	1020 32.32	36N44.23	116W29.44	9.90	
10.	96 3 30	1957 28.63	36N48.60	116W27.98	7.24	-0.59
11.	96 4 8	714 49.64	36N49.96	116W25.21	8.23	-0.58
12.	96 6 2	1645 75.18	36N49.11	116W29.44	9.61	-0.69
13.	*96 6 2	1015 33.29	36N49.23	116W29.55	9.87	0.01
14.	96 7 31	357 37.30	36N45.91	116W34.54	8.55	-0.76
15.	96 8 12	422 50.68	36N48.48	116W23.09	5.02	-0.62

- referenced on figure of Smith, SSC Workshop 3.

Origin Time: Year-Month-Day-Hour-Minute-Second (UTC). Depth: event depth referenced to surface elevation. M - ML

* - triggered; the older analog seismic network.

REFERENCES

See reference list that follows main SBK text.

POTENTIAL ANALOGS TO FUTURE SITE AREA ACTIVITY

This appendix includes a discussion of earthquakes related to volcanic activity in the Mammoth Lakes, California, area as an analog to potential volcanic earthquakes in Crater Flat and a discussion of the 1986 M 6.3 Chalfant Valley, California, earthquake and aftershock sequence, which we believe represents the most likely analog to the maximum background earthquake for the southern Great Basin.

Analog to Yucca Mountain Volcanic Earthquakes

The Mammoth Lakes, California, volcanic area, within and adjacent to the Long Valley caldera, has been the location of a recent series of moderate-sized (M 5 to 6) earthquakes, aftershock sequences, and volcanic-related earthquake swarms (1940 to the present) (Hill et al., 1985). We believe that this area may represent an analog to potential earthquake activity associated with the emplacement of volcanic materials in Crater Flat and to activity that contributed to the structural features present in the northern Nevada Test Site (NTS), which formed during emplacement of the Timber Mountain Caldera. Several late Pleistocene and younger eruptions (> 750 ka) of the Long Valley caldera have shaped the physiography of the Mammoth Lakes-Chalfant Valley-Bishop area of California (Bailey et al., 1976). Deformation in the caldera (1980 to the present) has been directly associated with most of the foreshock-mainshock-aftershock sequences (main shocks M > 6) and volcanic earthquake swarms (Hill et al., 1990). These sequences have been prolific, producing tens of thousands of earthquakes in and adjacent to the caldera.

Before the recent increase in seismicity, activity in the area had been at a low level since the 1940s (Gumper and Scholz, 1971; Pitt and Steeples, 1975; VanWormer and Ryall, 1980). But in the 1940s, two M 5 earthquakes coincided with the filling of Crowley Lake in the western part of the caldera. The recent series of moderate-sized earthquakes that began in October 1978 culminated with four M 6+ earthquakes during a 48-hour period from May 25 to May 27, 1980 (Cramer and Toppazada, 1980; Lide and Ryall, 1985). The sequence continued with the 1984 M 5.8 Round Valley earthquake (Priestley et al., 1988) and 1986 M 6.4 Chalfant Valley earthquake. Swarm-like earthquake activity (Savage and Cockerham,

1984; Cockerham and Pitt, 1984; Hill et al., 1990) and occasional tremors (Ryall and Ryall, 1983; Aki, 1984) within and adjacent to the caldera were accompanied by inflation of the caldera's resurgent dome (Savage and Clark, 1982; Rundle and Whitcomb, 1984; Denlinger and Bailey, 1984).

An energetic earthquake swarm under Mammoth Mountain near the town of Mammoth Lakes in 1989 included a number of deep, long-period earthquakes that may be associated with deep magma movement (Pitt and Hill, 1994; Langbein et al., 1993). There is some controversy regarding the possibility of non-double-couple source mechanisms, possibly associated with dike injection, determined for some of the earthquakes in and around the caldera (Julian, 1983; Julian and Sipken, 1985; Wallace, 1984). Although none of the moderate earthquakes have shown a significant component of dip-slip motion, Holocene faulting with predominantly normal offsets bound the Sierra Nevada and White Mountains (Bryant, 1984). The recent series of moderate-sized earthquakes have shown predominantly strike-slip motion.

The 1986 M 6+ Chalfant Valley Earthquake Sequence

The Chalfant Valley sequence occurred adjacent to the White Mountains beneath the volcanic Tableland, 15 km east of the Long Valley caldera (Smith and Priestly, 1988; dePolo and Ramelli, 1987; Lienkaemper and others, 1987). We believe that this sequence of earthquakes represents the best analog to the maximum background earthquake for the southern Great Basin. The sequence is a composite of three distinct faulting events (M 6.3, M 5.8, and M 5.5) that occurred over a period of 11 days (Smith and Priestly, 1988). All three earthquakes showed predominantly strike slip-motion, with the main shock occurring within the hanging wall block of the White Mountains fault zone. The main shock, M 6.3, was the largest event in the western Nevada seismic region since the 1954 Fairview Peak-Dixie Valley earthquakes.

The Chalfant sequence produced surface ruptures along the White Mountains fault zone and within the Tableland fault system west of the White Mountains (dePolo and Ramelli, 1987; Lienkaemper and others, 1987). Surface ruptures along the White Mountains fault zone stretched for a distance of 12 ± 2 km, with scattered cracks within the volcanic Tableland.

The M 6.3 Chalfant earthquake may be the model event for the maximum background earthquake (MBE) in the western Basin and Range (dePolo, 1994; Pezzopane and Dawson, 1996). The MBE is defined as the largest magnitude earthquake that does not produce primary displacement on faults at the surface. Although extensive fracturing occurred at the surface along mapped Holocene faults in the volcanic Tableland area, it is arguable whether any of that is primary rupture (Lienkaemper and others, 1987).

Smith and Priestly (1997 in press) have performed a detailed relocation of the earthquakes of the first three months of the sequence and determined the source parameters of the primary events. Static stress drops determined from the teleseismic moment and rupture areas estimated from the extent of the aftershock activity for the three primary events (M 5.8, M 6.3, and M 5.5) are 87, 26, and 23 bars, respectively. Uncertainties in these estimates are shown in that report. The primary characteristic of the sequence is the conjugate fault geometry resulting from the first two moderate-sized events: left-lateral strike-slip motion for the initial M 5.8 event, followed 24 hours later by right-lateral slip during the M 6.3 main shock (Smith and Priestley, 1997 in press; Savage and Gross, 1995). Main shock rupture extended 12 to 15 km on a northwest-striking, southwest-dipping (55 degrees) fault plane. Surface fracturing in the volcanic Tableland area was confined to the hanging wall of the main shock fault plane (Smith and Priestley, 1997 in press). A peak acceleration of 0.46 g was recorded on an accelerometer record of horizontal component at a sediment site on an alluvial fan about 12 km northeast of the main shock epicenter.

REFERENCES

See reference list that follows main SBK text.

ELICITATION SUMMARY

ROBERT SMITH, CRAIG DEPOLO, AND DENNIS O'LEARY

TABLE OF CONTENTS

	Page
1.0 INTRODUCTION	SDO-1
2.0 TECTONIC MODELS	SDO-2
2.1 DEXTRAL SHEARING AND BURIED STRIKE-SLIP FAULTS	SDO-8
2.2 DETACHMENT FAULTS	SDO-10
2.3 HALF GRABEN MODEL—CARAPACE EFFECT	SDO-15
3.0 SEISMIC SOURCES	SDO-19
3.1 FOCAL DEPTH DISTRIBUTION AND DEPTH OF THE SEISMOGENIC CRUST	SDO-20
3.2 SEISMIC SOURCE ZONES	SDO-24
3.2.1 Maximum Background Earthquake	SDO-26
3.2.2 Recurrence Rates	SDO-27
3.3 REGIONAL FAULT SOURCES	SDO-27
3.3.1 Description	SDO-29
3.3.2 Maximum Earthquake Estimates	SDO-49
3.3.3 Recurrence	SDO-49
3.3.4 Buried Strike-Slip Fault Sources	SDO-50
3.4 LOCAL FAULT SOURCES	SDO-52
3.4.1 Event Scenarios: Single Faults, Linked Faults, and Distributed Faults	SDO-62
3.4.2 Fault Source for Parameters of Maximum Magnitude	SDO-63
3.4.3 Recurrence	SDO-68
3.5 VOLCANIC SOURCES	SDO-72
4.0 HISTORICAL SEISMICITY: EVALUATION AND TREATMENT OF RECORD PARAMETERS	SDO-73
5.0 FAULT DISPLACEMENT	SDO-77
5.1 INTRODUCTION	SDO-77
5.2 PRINCIPAL FAULTING DISPLACEMENT CHARACTERIZATION	SDO-79
5.2.1 Type of Event	SDO-79
5.2.2 Frequency of Occurrence of Principal Faulting Events	SDO-79
5.2.3 Approach for Estimating Fault Displacement	SDO-80
5.2.3.1 Scaling Techniques	SDO-81
5.2.3.2 Distributions for Displacement at a Point	SDO-81
5.2.3.3 Assessment Of The Distribution For Amount Of Displacement At A Point On A Principal Rupture	SDO-83

TABLE OF CONTENTS

	Page
5.3 DISTRIBUTED FAULTING DISPLACEMENT	
CHARACTERIZATION	SDO-84
5.3.1 Earthquake Approach to Distributed Faulting Hazard.....	SDO-85
5.3.1.1 Activation Probability	SDO-85
5.3.1.2 Probability of Slip Per Event.....	SDO-85
5.3.1.3 Probability Distribution for Displacement at a Point.....	SDO-87
5.3.2 Displacement Approach to Distributed Faulting Hazard	SDO-89
5.3.2.1 Activation Probability.....	SDO-90
5.3.2.2 Assessment of Slip Rate.....	SDO-90
5.3.2.3 Assessment of Average Displacement per Event.....	SDO-90
5.3.2.4 Distribution for Displacement at a Point.....	SDO-90
5.4 DATA FOR NINE CALCULATION SITES	SDO-90
6.0 REFERENCES	SDO-93

TABLES

Table SDO-1	Maximum magnitudes for source zones
Table SDO-2	Magnitude scaling relationships used
Table SDO-3	Parameters for regional fault sources
Table SDO-4	Parameters for local fault sources
Table SDO-5	Multiple-fault event scenarios and event moments for local faults
Table SDO-6	Regressions Used for Estimating Displacement

FIGURES

Figure SDO-1	Map showing location and features of Yucca Mountain and Crater Flat
Figure SDO-2	Map showing boundaries of zones used in the seismic source model
Figure SDO-3	Depth distribution of hypocenters (focal depth distribution) of earthquakes in the southern Great Basin (SGB)
Figure SDO-4	Focal depth distribution of deep earthquakes in the area within r<100 km of Yucca Mountain
Figure SDO-5	Logic tree for regional source zones

TABLE OF CONTENTS

Figure SDO-6	Map showing regional faults included in the seismic source model
Figure SDO-7a	Map showing local fault sources included in the independent seismic source model
Figure SDO-7b	Map showing local fault sources included in the linked seismic source model
Figure SDO-8	Scaling parameters and relationships used to estimate maximum magnitudes for local faults
Figure SDO-9	Example calculation of occurrence rates for local faults
Figure SDO-10	Map showing volcanic zones included in the seismic source model
Figure SDO-11	Logic tree used to characterize principal faulting displacement hazard.
Figure SDO-12	Probability of surface rupture as a function of earthquake magnitude computed from various data sets given in Pezzopane and Dawson (1996)
Figure SDO-13	Estimated mid- to late-Quaternary displacement along the Solitario Canyon fault. Strip map depicts displacement data from trench studies (Chap. 4.7 of U.S. Geological Survey, 1996) and scarp heights from Simonds and others (1995). Graph depicts trench data (large dots) and scarp heights converted to estimated displacements (small dots). Left axis scales cumulative mid- to late-Quaternary displacement, and right axis scales <i>MD</i> based on 1/2 of the cumulative offset (a close approximation of the largest event).
Figure SDO-14	Normalized slip along strike from five Basin and Range historic normal fault earthquake ruptures developed by the ASM team from data presented in Wheeler (1989).
Figure SDO-15	Fractal displacement profiles developed by Ron Bruhn, University of Utah, to predict distribution for the ratio of displacement at a point to the maximum displacement in an earthquake.
Figure SDO-16	Plots showing event-to-event variability in displacement relative to average displacement per event at a location along a fault based on data from paleoseismic investigations in the Yucca Mountain area.
Figure SDO-17	Logic tree used to characterize distributed faulting displacement hazard.

TABLE OF CONTENTS

- Figure SDO-18 Probability of induced distributed slip as a function of distance from the rupture and hanging wall/foot wall location computed from the data presented in Pezzopane and Dawson (1996). Curves show logistic regression fits to data.
- Figure SDO-19 Observed secondary faulting distribution normalized to main fault displacement for large scarp -forming, historic normal faulting earthquakes in the Basin and Range province.
- Figure SDO-20 Cumulative probability graph of D/D_{cum} , where D is fault slip per event and D_{cum} is the cumulative displacement on the fault surface at the point of interest. Function is derived from Yucca Mountain fault data synthesis of Pezzopane and Dawson (1996) and discussions of Cowie and Scholz (1992) by SBK team.

APPENDICES

- APPENDIX SDO-1 EVENT SCENARIOS FOR LOCAL FAULTS
- APPENDIX SDO-2 ANALYSIS OF PALEOSEISMIC DATA

ELICITATION SUMMARY
ROBERT SMITH, CRAIG DEPOLO, AND DENNIS O'LEARY

1.0

INTRODUCTION

To properly represent expert epistemic uncertainty, the Yucca Mountain Probabilistic Seismic Hazard Analysis (PSHA) input evaluations were carried out by six expert teams free to choose their own methodologies, but also free to share or combine approaches. The team Smith, DePolo, O'Leary followed the evaluation structure provided to all of the teams at the PSHA workshops. We attempted to be impartial and objective in our evaluations, taking into account our different levels and areas of expertise. We amassed the data that were freely available to all participants, we attended the Yucca Mountain field trip to observe local faults and the Bare Mountain fault, and we obtained guidance from the expert presentations. We then developed our own interpretations based on the evidence, and developed our own scenarios and evaluations, then put the information and the models into a PSHA context. Team Smith, DePolo, and O'Leary shared a number of hypotheses and premises with other teams, but we adopted a fundamentally reductionist and epistemic approach to the analysis. We realized that the issue of earthquake hazard has a historical component inherent in the paleoseismic data that could not be accounted for by numerical or theory-based techniques. Accordingly, we relied as much as possible on data for Pleistocene events. Our first step was to evaluate tectonic models on the basis of field evidence or tectonic history, especially Quaternary history. The tectonic model we consider best supported by the data (a planar fault model) and its variants guided our evaluations of fundamental fault behavior, and set bounds on the key seismic parameters of magnitude and displacement. Field data from trench studies guided our estimates of recurrence and slip rates for local faults.

TECTONIC MODELS

A useful tectonic model provides an explanation for the origin, mechanical behavior, and resulting structure (deformation) of some volume of the Earth's crust. A tectonic model integrates: (1) geometry and spatial relations among structures; (2) mechanisms by which structures interact and respond to regional stress; and (3) the succession, duration, and evolution of deformation events (i.e., the history of strain). We look to tectonic models to help (1) guide understanding of present (and future) seismotectonics; (2) relate observable structure to inferences concerning fault parameters (e.g., width, distribution, extent, linkage); (3) provide bounding estimates or boundary conditions for fault behavior; and (4) identify hidden structure and behavior at seismogenic depths. Because our model must account for fault displacement hazard, it is specifically a model for Yucca Mountain. Therefore, the model incorporates Quaternary fault activity, basaltic volcanism, and other tectonic phenomena that provide evidence for seismogenic behavior at Yucca Mountain during late Pleistocene.

The model we use is conceptual and primarily kinematic. Three fundamental concepts constrain our evaluation of a model, the first of which is the domain concept. This concept holds that the crust of the southern Great Basin is an assemblage of structurally bounded slabs or blocks in various states of destruction and activity. Observed at sufficiently small scale, the domains evince regional strain patterns; taken individually they reveal local histories of deformation that complicate a regional pattern. We term the second concept "inheritance". In evaluating a tectonic model, a certain degree of idealization is necessary. However, our model does not assume pristine, ideal components; we consider that Yucca Mountain formed in a hybrid tectonic environment having a complex stress history, that the structural components reflect the processes that have varied with time and place, and that some processes are more tectonic than others. To a greater or lesser degree, present-day deformation follows ancient strain patterns. Our third concept focuses on history. The pattern and amplitude of deformation were set millions of years ago; although the style of deformation may be inherited, ancient deformation may have nothing to do with present rates and distributions of strain. Therefore, our analyses and probabilities rely on evidence of Quaternary, not Miocene, events.

An important aspect of the tectonic setting of Yucca Mountain (that is, the structural and stratigraphic assemblage of rocks within a radius of about 100 km of the mountain) is the current strain rate. Strain rate is assessed based on the moment rate of observed seismicity, geodetic data, and paleoseismology. All indications are that the current strain rate is very low--on the order of 10^{-16} /yr to 10^{-17} /yr (Eddington et al., 1987; data from Chapter 6 of the Seismotectonic Framework Report [USGS, 1996]). This is an order of magnitude lower than strain rates in the more active areas of the nearby Basin and Range province. This low rate constrains the loading rate of active faults and hence our deductions about the potential for activity and seismogenic depths.

Our preferred model for Yucca Mountain is that of an asymmetric graben, or a half graben, partly filled by a collapsed volcanic carapace. There are two fundamental components to this model. First is the half graben itself, represented by Crater Flat basin. The USGS seismic reflection profile (Brocher et al., 1996) shows clearly the structural asymmetry of the half graben, of which Bare Mountain represents the relatively uplifted footwall. Second is the volcanic carapace. Yucca Mountain is the emergent part of a faulted, extended slab of volcanic rock about 2.5 to 3 km thick that has subsided into the half graben. We call this the carapace because it forms a resistant shield that completely covers the Paleozoic bedrock beneath Yucca Mountain. Most block-bounding faults at Yucca Mountain dip westward toward Bare Mountain and show a history of extension antithetic to the Bare Mountain fault.

The half graben model requires that the Bare Mountain fault be the master fault and that the strata to the east (the hanging wall) subside against it, as a group of antithetic fault blocks. This mechanical model has two limitations which affect uncertainty in our analysis: (1) the cumulative Pleistocene dip slip on the Bare Mountain fault is less than that measured across Yucca Mountain; and (2) some faults at Yucca Mountain and in Crater Flat have a down-to-the east offset. The latter observations can be explained by local keystone faulting in the volcanic carapace, but the former observation is less readily explained. Nevertheless, the asymmetry of Crater Flat basin, the structural relief of Bare Mountain (several kilometers), the overall sense of slip on the main block-bounding faults of Yucca Mountain, the profound (about 30 mgal) gravity gradient along the Bare Mountain fault, and the evidence that the Bare Mountain front was the source of large slab slides into Crater Flat in late Miocene time

indicate that the early history of the Bare Mountain fault was that of a master, range-front fault.

The pre-Pleistocene slip history of the Bare Mountain fault lies buried beneath the pediment cover in Crater Flat. The steep part of the gravity gradient, which lies a kilometer or more east of the present range front, indicates that the fault generally dips east at less than 50 degrees. Our model, and the seismic reflection profile (Brocher et al., 1996), permit the interpretation that the Bare Mountain fault consists of an imbricate zone of several more steeply dipping fault planes, variously banked at depth by colluvial wedges or mass movement deposits. The Pleistocene fault trace sampled for this study may be the most recently active of several synthetic fault planes, and may have the least cumulative displacement (see, for example, Hancock and Barka, 1987, fig. 10).

The half graben model works well only near the central latitudinal axis of Crater Flat basin. Viewed longitudinally, the basin is plugged at its north end by the emergent caldera complex from which a population of radial faults extends through generally south-dipping strata into Crater Flat (Scott Minor, USGS, written commun., 1995). The Bare Mountain fault loses throw near the caldera rim area and transitions northward into a minor normal fault, the Tram Ridge fault, which dies out within the Rainier Mesa caldera rim zone (Fridrich, 1995). To the south, the Crater Flat basin abruptly narrows and shallows. The Bare Mountain fault has not been traced south of Steve's Pass (Figure SDO-1), and the faults of Yucca Mountain are abruptly terminated, or at least are not traceable south of a dissected escarpment along Highway 95 at the southern margin of the basin. The strata of the escarpment are the same volcanic units that form Yucca Mountain, but dip northward into the basin. The eastern margin of Crater Flat basin is well defined by an arcuate gravity gradient concave to the west, which closely parallels the trace of the combined Paintbrush Canyon-Stagecoach Road fault. On this basis, we infer that the Paintbrush Canyon-Stagecoach Road fault is a major bounding fault for Yucca Mountain, the fault that defines the basin rim and most likely descends to the base of the seismogenic crust.

The form of Crater Flat basin and its association with the caldera complex led Carr (1990) to interpret it as a sector graben, an area of subsidence caused by evacuation of an apophysis of magma from the base of the crust during or shortly following eruption of the Topopah Spring

Tuff. This interpretation accords well with the timing and magnitude of initial faulting of Yucca Mountain as well as with the shape and position of the basin. Brun et al. (1994) effectively simulated the structure, in cross section, with a sandbox model that utilized deformation of a low-density viscous mass at the base of the crust.

If the location and longitudinal axis of Crater Flat basin indicate that it originated as a sector graben, they also imply that it is a flaw within the larger rift-like Amargosa trough (i.e., the Kawich-Greenwater rift of Carr [1988, 1990] or the Amargosa Desert rift zone of Wright [1989]); that is, it is a rift within a rift. As such, crustal extension within Crater Flat basin reflects the structural orientation of the trough and perhaps is linked to basement faulting of greater extent. Carr (1990) noted the similarity between the faults at Yucca Mountain and a fault population in Pahute Mesa north of the caldera complex and on strike with Yucca Mountain (Minor et al., 1993), and surmised that both fault sets reflect extension fundamentally tied to the evolution of the Amargosa trough. Accordingly, Crater Flat basin can be understood as the southern part of a deeper, narrower flanking rift along the western flank of the Amargosa trough; or perhaps even a basin that projects from the Basin and Range terrane southward into the Walker Lane. This rift-like aspect of the model downplays the notion of the Bare Mountain fault as a conventional range-front fault. It implies that Pleistocene extensional faulting at Yucca Mountain is not a function of antithetic slip controlled by the Bare Mountain fault, but is instead controlled by axial fractures within the deepest part of the Amargosa trough.

But casting Crater Flat basin and Yucca Mountain in the context of a trough controlled (at least during its Middle Miocene phase) by dominantly east-west extension raises two questions relevant to faulting at Yucca Mountain: (1) what becomes of Bare Mountain fault at and beyond the south end of Yucca Mountain, and (2) what is the nature of the fault that bounds the east side of the Amargosa trough near Yucca Mountain?

The southward projection of the Bare Mountain fault is problematic. We infer that the fault is not traceable south of Steve's Pass (Figure SDO-1) because there it loses its identity, including its expression as a pronounced gravity gradient (Snyder and Carr, 1986), among a distributed set of small right-lateral fault segments within a shear zone that steps to the southeast for about 4 km across the dissected escarpment that marks the southern end of

Crater Flat (Fridrich, 1995). The fault then regains its identity as a unified structure, gains dip displacement, and strikes south as the boundary between the Funeral Mountains and the Amargosa trough. Although the fault is a major domain-bounding feature south of Bare Mountain, its projection along a relatively subdued gravity gradient and its weak expression as a physiographic feature indicates that the fault has played little part in the late Neogene and Quaternary history of the Amargosa trough.

The eastern margin of the Amargosa trough is bounded by faults of seismogenic significance. Especially significant for model evaluation is the so-called gravity fault (Figure SDO-1). The gravity fault was defined by Winograd and Thordarson (1975) on the basis of a gravity gradient (hence their term "gravity fault") that extends along the spring line in Ash Meadows north to Highway 95 (Figure SDO-1) and the west end of the Skeleton Hills. Down-to-the-west displacement of Paleozoic bedrock is estimated to range from about 150 m at the north end to several hundred meters at the south end. Brocher et al. (1993), on the basis of seismic profile data, confirmed that the gravity fault forms the structural boundary of the east side of the trough at about 36°35'N. Brocher et al. (1993) interpreted the gravity fault as being listric to a reflector (K) at about 2 s. (5.5 km) depth. Although Brocher et al. (1993) did not offer a preferred interpretation of reflector K, they emphasized the role of ductile flow in the lower crust at a depth of about 6 s. below the Amargosa trough. Reflector K may represent an abandoned, pre-late Oligocene detachment that controlled extension of the Specter Range.

A coincident gravity and aeromagnetic gradient aligned with the gravity fault implies that the fault can be carried northward past the west end of Little Skull Mountain (Chapter 8, Seismotectonic Framework Report [USGS, 1996])). The fault trace passes through the magnetic anomaly that marks the position of the 4.4-Ma buried volcano south of Highway 95. North of this point, a high magnetic anomaly along the gradient suggests that the hanging wall of the gravity fault contains considerable basalt or volcanoclastic sediment. There are sparse surface expressions of the gravity fault. At the west end of the Striped Hills, bedrock exposures indicate strike-slip displacement, but the western flank of Little Skull Mountain is marked by tereva blocks that indicate down-to-the-west collapse. Reheis and Noller (1991) mapped a 2.5-km-long Pleistocene scarp along the fault trace between the Striped Hills and the Skeleton Hills. The scarp is clear in large-scale aerial photos, which show that the most

recent drainage courses have been influenced by the fault. The scarp probably represents displacement within the last 10 ka.

The gravity fault is an important domain boundary; it separates dominantly east-striking structures associated with the Rock Valley fault system to the east from the north-striking structures of the Amargosa trough-Crater Flat domain to the west. North of Little Skull Mountain, the trace of the gravity fault and the eastern margin of the trough are obscure. We infer that the eastern border of the trough trends roughly due north, as expressed by a set of down-to-the west, post-12.7 Ma faults along the west side of the Calico Hills dome (Simonds and Scott, 1996).

If formation of the Bare Mountain fault and one or more crustal faults at Yucca Mountain were driven by a deep master fracture zone in the axis of Crater Flat basin, they may be largely independent of each other in terms of slip budget. This modification of our basic model is based on a mechanism proposed by Okaya and Thompson (1985) and demonstrated by boundary element modeling done for Crater Flat basin by King and Janssen (Chapter 8, Seismotectonic Framework Report [USGS, 1996]). The interpretation is consistent with the localization of basaltic volcanism near the axis of the basin: extensional stress is focused along one or more axial fractures or fault intersections at the base of the seismogenic crust. Such intersections can focus dilational strain, even at depths of 15 to 20 km, and thereby facilitate the ascent of basaltic magma to higher crustal levels. The Bare Mountain fault and the Paintbrush Canyon-Stagecoach Road fault likely would be the primary intersecting faults at the deepest crustal level; interaction of these faults at a sufficient stress threshold could be accompanied by basaltic intrusion. We consider such events would cause most faults at Yucca Mountain to slip, including those that might be antithetic to Bare Mountain fault, and that some fault crevasses might receive basaltic ash fill. G.A. Thompson (Stanford University, written commun., 1994) proposed that basaltic dike intrusion would compensate for local extensional stress and significantly reduce deviatoric stress. This would cause the stress threshold for post-intrusive faulting at Yucca Mountain to be reset to some higher level. However, as regional extensional stress continues to be applied to the mountain, small stress thresholds are exceeded and weaker faults slip from time to time. Ultimately, the maximum basal stress threshold is exceeded, at which point the basin may experience widespread faulting associated with basaltic intrusion. This aspect of the model holds that not all faulting

at Yucca Mountain is accompanied by volcanism, but that volcanism is always associated with faulting.

2.1 DEXTRAL SHEARING AND BURIED STRIKE-SLIP FAULTS

The alignment of basaltic cones and vents in Crater Flat follows a northeast trend, oblique to the axis of the basin. Volcanism is clustered in the southwest quadrant of the basin, the area of most recent subsidence and deposition. These facts indicate a distinct tectonic asymmetry linked to processes active within the past 4 m.y. Tectonic asymmetry is also indicated by paleomagnetic evidence for clockwise vertical axis rotation of fault-bounded blocks across the south end of the mountain. The rotation, which is about 30 percent, is considered to have occurred following deposition of the Tiva Canyon Tuff at about 12.7 Ma (S. Minor, written commun., 1995). These data led Fridrich (1995) to infer that Crater Flat basin has evolved as a sphenochasm, opening at its southern end but fixed at its northern end.

This motion is compatible with a northwest-oriented zone of dextral shear at the southern end of the basin, and with a general N50°W-oriented transtensional stress throughout the Walker Lane. In terms of our model, the question is whether oblique dextral shear is confined to Crater Flat basin (i.e., the basin itself is becoming distorted because of distributed, regional shear), or whether shear is imposed by a buried regional right-lateral fault that passes through Crater Flat basin. The latter case has been argued by Schweickert and Lahren (1997) and modeled as a pull-apart basin in sandbox experiments by the Center for Nuclear Waste Regulatory Analyses (presentation by D. Ferrill at Workshop 4). The question is important because a hidden throughgoing fault could generate an earthquake comparable in magnitude and mechanism to the 1932 Cedar Mountain earthquake.

Nonsystematic distributions of vertical axis rotations in time and space within the southwest Nevada volcanic field, as reported by Hudson et al. (1994), imply that individual basins have responded uniquely to distributed northwest-oriented dextral shear typical of the Walker Lane setting. This observation, plus the lack of evidence for transcurrent dextral fault offset of Pleistocene age though Crater Flat basin, supports the interpretation that dextral shear is restricted to the basin itself. The only hint of a discrete dextral shear feature within the basin is a N25°W-striking alignment known informally as the hingeline (Fridrich, written commun.,

1995). The hingeline separates paleomagnetic rotations of 10 degrees or less to its north from rotations of 20 degrees or more to its south. The boundary is more strongly indicated by the divergence of aeromagnetic gradient alignments across the mountain, and by landform terminations along the trace of the hingeline. The hingeline is considered to define a structural boundary that concentrates dextral shear between it and the southern end of the mountain. A possible second indication of a buried strike-slip fault are the scarps and lineaments along the Black Cone fault, shown on Faulds et al. (1994).

Despite painstaking investigation, researchers have identified no expression of any feature comparable to the hingeline along its strike northwest of Crater Flat. However, a strong structural alignment does exist to the southeast of Crater Flat. The structural alignment extends along Stewart Valley and along the trace of the Pahrump-Stewart Valley fault zone for a distance of about 120 km. At least 4 km of dextral offset is shown along the alignment between the Resting Spring Range and the Montgomery Mountains.

The alignment is expressed by isostatic gravity anomalies that include the gradients that form the western flank of Pahrump Valley basin and (farther north) the eastern flank of Ash Meadows basin. In general, the alignment defines the eastern margin of a large crustal block that is expressed by the Amargosa Range on the west, and by Bare Mountain, the Resting Spring Range, and the Nopah Range on the east. Structurally, the alignment is comparable to the subparallel Death Valley and Panamint faults farther west. The alignment is less well expressed by aeromagnetic anomalies except for the local gradients along the hingeline through Yucca Mountain.

We consider the structural alignment, which includes the Yucca Mountain hingeline, to be a projection of the Pahrump-Stewart Valley fault zone into, but not through, Crater Flat basin thus accounting for clockwise vertical axis rotation at Yucca Mountain, northeast alignment of basaltic volcanic centers in Crater Flat, dextral shear at the south end of Crater Flat basin, and a dextral slip component toward the southern end of Bare Mountain fault. Additionally, shear stress concentrated at the edge of the basin is considered have contributed to uplift of Bare Mountain and Calico Hills within the past 9 m.y. In light of these features, we include a buried fault source among our regional seismic fault sources and assign a 40% probability to a model that contains a strike-slip earthquake within or proximal to Crater Flat basin along the

hingeline-Pahrump-Stewart Valley fault zone alignment (Figure SDO- 1). Such an earthquake could have a magnitude as great as the 1932 Cedar Mountain earthquake. Basaltic volcanism could be associated with such an event.

2.2 DETACHMENT FAULTS

Detachment fault models of varied geometries and crustal depths have been applied to Yucca Mountain solely on the basis of the succession of rotated, west-facing normal faults that form the mountain. Each detachment mechanism invariably is referred to a single latitudinal cross section that emphasizes the rotated normal fault blocks but ignores the structural complications at the northern and southern ends of Crater Flat basin. A detachment fault model has important implications. Because all rotated normal faults of the upper plate are rooted in a common slip plane (the detachment), all faulting necessarily is distributed, and (if the detachment is deep enough) all rooted normal faults are equally seismogenic. Because the subhorizontal detachment plane is of wide lateral extent and separates structures of radically different ages and attitudes, a major seismogenic feature such as a strike-slip fault could be hidden beneath the detachment.

The most recent attempts to fit a detachment model to Yucca Mountain are provided by Ferrill et al. (1995), who describe two model variants based on syntheses of previous proposals. Model 1 of Ferrill et al. (1995) assumes that the faults of Yucca Mountain developed from the headwall of the Bullfrog Hills detachment system, which is thought to accommodate as much as 275 percent of local extension (Ferrill et al., 1995). According to this model, Yucca Mountain faults were isolated from the Bullfrog Hills system by rise of the Bare Mountain block along the Bare Mountain fault, which truncated the Yucca-Bullfrog detachment. Continued motion of the Bare Mountain fault formed a deeper, east-directed detachment plane. According to this model, the older, shallower, west-directed detachment accounts for the imbricate faulting at Yucca Mountain; the younger, deeper, east-directed detachment accounts for hanging wall collapse of the carapace into Crater Flat basin. Model 2 of Ferrill et al. (1995) accounts directly for the hanging wall rollover and imbricate faulting at Yucca Mountain by assuming that the Bare Mountain fault is the driving listric (detachment) fault and that Yucca Mountain faults are simply antithetic to the deep, master, east-directed Bare Mountain detachment. However, in this model, faults antithetic to the Bare

Mountain listric fault are simultaneously listric faults synthetic to a breakaway fault located somewhere to the east in Jackass Flats. The result is a curious "bathtub" profile having listric faults at each end that merge at a common plane of detachment (Ferrill et al., 1995). It is not clear how slip is partitioned between the two apparently competing listric faults and along the common detachment surface.

These detachments are presumed to operate in the 6 to 8 km depth range. Shallow detachment at the Tertiary/Paleozoic contact can be ruled out. Numerous exposures throughout the area, as well as the Crater Flat seismic profile (Brocher and Hunter, 1996), combine to show that the Paleozoic contact is an unconformity locally cut by high-angle faults. We leave open the question of deep detachment within the brittle-ductile lower crust transition. Much geologic evidence, such as high-grade metamorphic facies and mylonite in lower plates exposed elsewhere, indicates that detachments typically occur in the ductile transition zone, and theoretical and experimental rheological considerations (e.g., Melosh, 1990) support the mechanism in this setting. However, the occurrence of normal fault earthquakes at depths of 19 km or greater (see section 3.1) indicates that strain at these depths is not effectively assimilated by detachment. And because most of our inferences of fault behavior rely on processes that involve the brittle part of the crust, we consider whatever is meant or envisioned by "detachment" in the lower crust to be simply part of poorly understood, quasi-viscous flow deformation.

The oldest deformation that can be attributed plausibly to detachment is block faulting of the Topopah Spring Tuff at about 12.7 Ma. At that time, Bare Mountain was already an elevated range that was shedding debris into Crater Flat basin. In fact, Yucca Mountain field work revealed evidence that Bare Mountain was shedding metamorphic rock debris prior to deposition of the Crater Flat Tuff and that Crater Flat was an aggrading alluvial plain prior to 14 Ma. The Bare Mountain fault was active well before deposition of the Paintbrush Group (Fridrich, 1995). This means that uplift of Bare Mountain cannot have terminated a detachment at Yucca Mountain, and that there was no tectonic association of Yucca Mountain extension with the formation of the Bullfrog Hills. In fact, the Bullfrog Hills formed from 2 to 3 m.y. after the initial phase of Yucca Mountain faulting, in a completely different tectonic setting. The Bullfrog Hills originated from a breakaway fault along the west side of Tram Ridge beginning about 12.7 Ma (Fridrich, 1995; Hoisch et al., 1997). The transport

vector of the Bullfrog Hills projects eastward to the Rainier Mesa caldera, diverging some 20 degrees counterclockwise from the orientation of the transport vector of Yucca Mountain.

The style and direction of deformation in Crater Flat clearly are diachronous, having shifted from mountain-wide imbricate block faulting around 11.4 Ma primarily to subsidence at the southwest corner of the basin beginning around 9 Ma. Beginning around 11 Ma, sporadic basaltic volcanism became an important component of tectonism in this area. The basaltic volcanism implies that fracturing and faulting in the upper crust repeatedly connected with deep mantle sources. If a detachment plane existed in this area, it was not an effective barrier for fractures that penetrated through the crust.

Exposed detachment faults typically show slices of the upper plate resting at a high dip angle (65°) against the detachment plane. The geometric relations among the steeply dipping faults in a moderately extended domain, especially one that has no clearly identified breakaway fault, such as Yucca Mountain, are highly idealized. Detachment model 2 of Ferrill et al. (1995) requires severe curvature of the fault planes as they merge into the detachment fault at about 8 km depth. No explanation for this "special case" geometry is offered; it is a precondition of a listric model that is never seen in exposed detachment systems.

The domino mechanism of imbricate faulting is unable to resolve this geometry problem. If the block-bounding faults at Yucca Mountain are controlled by deep detachment, they cannot behave like dominos. The domino model requires rigid behavior and completely distributed simple shear; there can be no variable rollover or opposed slip. It is clear, however, that the big blocks at Yucca Mountain have some rollover and that there is local reversal of offset along strike on some of the bounding faults. Furthermore, domino rotation presumes uniform frictional slip across the entire width of the slip plane, unrealistic expectations to depths of 8 km at Yucca Mountain, even given extreme pore pressure. Nevertheless, a domino model is a more satisfactory explanation of hanging wall collapse against the Bare Mountain fault than is the quasi-listric geometry called for in model 2 of Ferrill et al. (1995), which requires a listric geometry as a consequence of a competing breakaway fault at the east side of Yucca Mountain.

A major shortcoming of the detachment model is that no breakaway zone has been identified for the imbricate faults of Yucca Mountain. For example, no such fault has been reasonably shown in the vicinity of Fortymile Wash. On the contrary, a good case can be made, both from seismic reflection profile data and stratigraphy in well UE25J#13, for a down-to-the-east fault near Fortymile Wash (Carr, 1984). The gravity fault is inferred by Ferrill et al. (1995) to be a candidate breakaway fault for Yucca Mountain. However, despite the array of small down-to-the-west normal faults (post-9 Ma) that cut Little Skull Mountain, the primary structure here is a north-dipping block, which indicates that structural rotations are referred to east-northeast-striking rotation axes. This geometry is even more pronounced in the Striped Hills, but totally absent from Yucca Mountain.

The Little Skull Mountain earthquake demonstrated that a seismogenic normal fault beneath Little Skull Mountain dips southeast and would project to the surface west of the inferred breakaway fault for Yucca Mountain. The aftershocks occurred up to nearly 5 km from the surface (Smith et al., 1995), suggesting that the hypocentral projection of this fault (cf. Meremonte et al., 1995) can be projected across a west-dipping breakaway fault. Additional constraints on the cross-sectional geometry of the detachment model are the lack of any expression of listric geometry or a detachment plane in the USGS seismic reflection profile (Brocher and Hunter, 1996). A detachment plane would have a seismic reflection in Crater Flat basin as in other areas of the Basin and Range Province (Smith et al., 1989). Another geometric constraint for any model is the elevation of Yucca Mountain. It is difficult to restore the fault blocks (W. B. Hamilton, written commun., 1995) unless the detachment plane mimics the elevation profile, or we appeal to depositional thickening or to displacements outside the plane of the section.

In fact, displacements outside the plane of the section must be factored into the model geometry because field data show that the block-bounding faults have a left-oblique component of slip. But when we consider the overall planimetric aspect of the structure of Yucca Mountain, the detachment model faces its most serious problems. Among these problems is the fact that Yucca Mountain faulting is tied exclusively to the geometry of a subjacent basin. Left-lateral bounding accommodation zones are not indicated at the margin of this basin, nor does the model offer any explanation of vertical axis rotation in the basin. Indeed, an important function of the detachment model is to isolate the upper plate

extensional structure from influence of a lower plate structure, such as a strike-slip fault that could impose a dextral torque on the surface fault pattern. To continue to operate as an extensional mechanism into Pleistocene time, a detachment plane must be a chronic locus of slip or of strain-decoupling; this is the fundamental meaning of the word detachment. It cannot behave this way and transmit shear stress from the lower crust to the upper plate. In other words, if a detachment fault were present, there could be no possibility of a 1932 Cedar Mountain type earthquake at Yucca Mountain: seismic slip below 6 to 8 km depth could never break ground.

If an inferred detachment system has operated at least intermittently for the past 12 m.y., we find it to be a contradiction that the geophysical signature of intrusive bodies such as the basalts in Crater Flat and even the calderas show no systematic offset. If the fault set at Pahute Mesa (Minor et al., 1996) were genetically related to faults of Yucca Mountain, then the detachment model must be extended north though the caldera complex. This model does not explain how a detachment could operate within or near a volume of crust subject to large-scale magma flux during nearly 7 m.y.

In terms of mechanics, the detachment model must operate on assumptions that present difficult and even intractable problems concerning dynamics. Among these is the assumption that the ductility and vertical strength profile in the crust is the same today as it was in mid-Miocene time. Models that require shifts from east-directed to west-directed detachment or invoke uplift of Bare Mountain by several kilometers during a tectonic event that terminates one episode of detachment and initiates another are unconstrained by available data and understanding of tectonic processes that have been active in the southern Great Basin.

Ofoegbu and Ferrill (1995) applied finite-element modeling to the problem of detachment-related fault slip. A five-layer linear elastic model was used, and the initial stress state included previous fault slip on simulated Yucca Mountain fault planes. For the model to work, each fault was treated as a weakly cohesive or cohesionless layer at least 150 m thick and decoupled from confining rock. Slip was forced to occur on a selected fault by reducing its coefficient of static friction. Under applicable confining stress, a friction angle of 0.93 degrees is required. The model implies also that a significant proportion of fault displacement is taken up by deformation of the hanging wall and footwall. Ofoegbu and

Ferrill (1995) found that slip rates in the detachment fault and in the steep, off-branching perturbed fault differed by six orders of magnitude. They concluded that a detachment fault is likely to slip aseismically in response to slip events that may occur at seismic rates on the off-branching steep faults. To reach this conclusion, however, the modeled mechanism appears to violate the concept of detachment faulting: steep fault perturbation is not supposed to generate strain in a detachment fault. Rather, the detachment is the master slip plane, and motion along it is supposed to generate slip along the faults of the upper plate and distribute strain among them by virtue of independent motion. In other words, the model did not demonstrate how detachment is supposed to control fault slip in the upper plate.

It is clear from the model, however, that detachment can work only along a weak layer that has an unusually low angle of friction and low cohesive strength. This is why detachments are common as slump mechanisms (undrained failure) in saturated sediments and in the marine environment (leaving apart the issue of low effective stress). It also explains why exposed detachments typically show evidence of ductile deformation in the lower plate. Given the present structure and physical conditions of the upper crust near Yucca Mountain, we consider it highly unlikely that there is a throughgoing subhorizontal weak layer having the required properties and thickness at mid-crustal levels beneath Yucca Mountain and Crater Flat. Observed focal mechanism data from the Basin and Range (Doser and Smith, 1989) do not reveal nodal plane populations that would be consistent with low-angle, listric faulting. The fact that focal mechanisms of normal to oblique slip normal faulting earthquakes in extensional regimes from a global record (Jackson and White, 1989) show no low-angle (detachment) slip further supports our conclusions. Therefore, detachment models do not figure in our analysis of local faults and they are not incorporated into the seismic source characterization model.

2.3 HALF GRABEN MODEL—CARAPACE EFFECT

The collapsed carapace model (actually a submodel, hereafter termed the *carapace effect*, of the half graben model) of Yucca Mountain defines two layers. Yucca Mountain is the morphological expression of a faulted layer about 2.5 km thick of volcanic rock (the carapace) that rests unconformably on a thicker crustal layer (15 to 20 km thick) of Paleozoic and Precambrian marine sedimentary and metasedimentary rocks. This configuration is important

because the layers differ greatly in bulk material properties and have radically different stress histories. The sub-carapace structure is revealed at Bare Mountain, the Specter Range, and the core of the Calico Hills. We emphasize that the fault characteristics, including slip history, that we measure in the carapace may have little or no relationship to seismogenic faults in the Paleozoic substrate. If we discount the carapace effect, then all of the faults we characterize at Yucca Mountain are potentially seismogenic and each can be projected as continuous fault planes to seismogenic depth as an end-member idealization of the half-graben model. If we strongly weight the carapace effect, then perhaps only one, two, or three Yucca Mountain faults project deep into the crust. The others are confined to the carapace, or link to faults having different attitudes and aspect ratios below the unconformity. According to this interpretation, the bulk of the faults in the volcanic carapace either are postseismic strain adjustments, or reflect strain that originates within or at the base of the carapace. To understand such processes we must regard the carapace as behaving like a huge, fragmented, incipient slab slide, much like an arrested slab slide or avalanche. This structure requires a basal weak layer or some form of decoupling from the substrate.

Arrested slab slides typically are broken by anastomosing faults that are broadly concave-facing downslope and have high length-to-width ratios. In cross section the fault slices show a general slump-like sense of hanging wall rotation, but along strike they are variably tilted. Much of the fault pattern at Yucca Mountain has the structural characteristics of an arrested slab slide. The abundance of toreva blocks and graben-like splays, the presence of footwall slices that are only a kilometer or two wide and that pinch out and change elevation along strike, faults that die out or fray out along strike, that are better described as breccia zones than faults (such as the Ghost Dance fault), all constitute a pattern of local tearing, spreading, and extensile damage within which the traces of deep-seated faults that span the length of the mountain are not apparent (the trace of the Solitario Canyon fault being an exception).

The closest structural analog to Yucca Mountain is the faulted volcanic carapace exposed along the south and west flanks of Mid Valley, about 22 km to the northeast. There, the faulted blocks of Timber Mountain Group and Paintbrush Group tuffs closely resemble those at Yucca Mountain, except they are about half the scale. The carapace rests unconformably on an eroded substrate of well-exposed 13-Ma Wahmonie dacite flows that do not reflect the structural attitude of the overlying tilted slices. The Wahmonie volcanic substrate is

analogous to the Paleozoic carbonate substrate beneath Yucca Mountain. Two features are important here: (1) the Mid Valley carapace has subsided and partly extended into Mid Valley basin; and (2) deep stream erosion has isolated the blocks, facilitating some local faulting and tilting. These features suggest that the fault pattern in the carapace is a local, slope-controlled phenomenon rather than one controlled by a system of deep-seated faults.

How could such a system be accounted for at Yucca Mountain? It could work only by way of a weak layer beneath the carapace. Strata beneath the volcanic carapace in Crater Flat basin are equivalent to Rocks of Pavits Spring, a pre-14-Ma unit well exposed near Pavits Spring in Rock Valley (Hinrichs, 1968). The Rocks of Pavits Spring include weakly consolidated volcanoclastic silts and fine-grained sands. Layers of the requisite compositions could include fine-grained, altered airfall tuffs. In a saturated state (normal hydrostatic stress), such sediment could be susceptible to undrained failure or abrupt loss of shear strength. The mechanism might be driven by cumulative seismic strain ("hydraulic jacking" and grain redistribution) during times of high groundwater flux (Castro and Poulos, 1977; Seed and Idriss, 1982). We emphasize that the mechanism involves transient reductions of effective stress, not wholesale grain repacking from a metastable condition as in liquefaction or quick behavior. For example, soft-sediment faults are exposed below the volcanic section at the base of the south flank of Skull Mountain. Extensive failure of this type is considered to have facilitated the collapse of the south flank of Skull Mountain into Rock Valley. Deformation of this type is well documented in the extensively collapsed Eocene lower Absaroka Volcanic Supergroup, Wyoming (Decker, 1990).

In Crater Flat, the extent of an inferred weak layer is unknown. The model assumes that the sediments form a continuous deposit that thins and perhaps pinches out against the Paleozoic rock that forms the relatively elevated eastern rim of Crater Flat basin. This distribution implies that the eastern margin of Yucca Mountain (east of the Paintbrush Canyon-Stagecoach Road fault) is anchored directly on the Paleozoic substrate, leaving the carapace to the west susceptible to deformation of the inferred weak layer.

The bulk movement we expect from weak layer failure is chiefly translational. Such motion could explain the relatively minor offset accompanied by extensive damage along some of the faults. For example, the Bow Ridge fault as seen in the Exploratory Surface Facility (ESF) is

a zone about 2 m wide that dips 60 degrees west and contains sand- and gravel-size crush material. Likewise, the Drill Hole Wash fault, as projected into the ESF, is a breccia zone about 2 m wide that contains rotated blocks as much as a meter in diameter. The characteristic breccia that defines the Ghost Dance fault could also be of oblique extensional origin. We consider an early stage of failure and collapse in which the entire volcanic carapace pulled away from the caldera rim, like a shattered ice floe on a gelid stream, the various fault blocks extending, colliding, and subsiding upon the weak layer as Crater Flat basin widened and deepened to the southwest (cf. Fossen and Gabrielsen, 1996). Such motion explains Yucca Wash as a minor extensional structure, and accounts for the odd down-to-the-east offsets along the west side of the mountain. Extension of the carapace to the west is limited by the footwall of the Bare Mountain fault. In-situ stress measurements by Stock et al. (1985) reveal that the least compressive stress at Yucca Mountain is at the limit of normal fault slip, implying that the carapace may be held together by the strength of the strata on which it rests.

The carapace effect means that most or all of the faults at Yucca Mountain are distributed. It means that Yucca Mountain is high not because of footwall uplift, but because of original deposition. It implies that any buried fault in the Paleozoic substrate could have been overridden repeatedly and broken through the carapace in more than one place, thus explaining complex fault zone structure. It also implies that some of the slip budget can be attributed to creep or postseismic adjustment to weak layer deformation. It finally implies that exogenous effects, such as high groundwater flux, may be more important here, at least locally, than tectonic effects; that unknown aspects of high pore pressure and time-dependent seismic strain weakening could be significant controls on recurrent fault slip.

The carapace effect does not explain the long, throughgoing, nearly rectilinear trace of the Solitario Canyon fault, nor the major block-bounding aspect of fault segments such as the Windy Wash fault. Accordingly, our preferred interpretation is that the large block-bounding faults (the Paintbrush Canyon-Stagecoach Road fault, the Solitario Canyon, and Windy Wash faults) are through-the-crust seismogenic faults, and that many intrablock faults such as the Ghost Dance fault, probably are confined to the carapace.

The tectonic model for Yucca Mountain best supported by the data is that of a half graben that includes both axial faults in Crater Flat basin and faults antithetic to Bare Mountain. This model posits the block-bounding faults of Yucca Mountain and the Bare Mountain fault as discrete, single plane faults that descend to the base of the seismogenic crust. It also provides a mechanism for one or more of the block bounding faults to interact with the Bare Mountain fault at the deepest seismogenic level where basaltic magma intrusion may be facilitated by fault displacement or dilation, thus providing a mechanism for coupled volcano-seismic events. All or some of the faults west of the Solitario Canyon fault may be antithetic to the Bare Mountain fault, a structural configuration that reduces the capability of large-scale faulting with widths of the scale of the seismogenic crust thickness, thereby reducing maximum magnitude. This fundamental model provides for individual fault scenarios as well as linked and distributed fault scenarios.

We do not find evidence to support an active detachment fault, which is a form of special pleading for mechanisms that are not reasonably demonstrable at Yucca Mountain. In other words, the data set do not require these models; their only purpose is to explain a "hidden" structure or some hypothetical mechanism that could act at any time but that has no manifest or unequivocal history at Yucca Mountain.

We consider two modifications to our basic model that do take into account buried faults, however: the collapsed carapace effect and a dextral strike-slip fault external to Crater Flat that projects from the southeast into Crater Flat beneath the carapace. These modifications are not exclusive and they are supported by some data. They support linked and distributed fault scenarios as well as a buried seismic source. We do not weight these modifications; their physical presence accounts for seismic sources the activity of which is assessed separately. Because specific tectonic models are not explicitly weighted, we have no tectonic models logic tree; all our local seismic structural sources are referred to in our favored model.

3.0

SEISMIC SOURCES

Three kinds of seismic sources are considered in our analysis, in order of increasing scale and specificity: seismic source zones, regional faults, and local faults. Seismic source zones are

geographic regions discriminated on the basis of tectonic style and the structural nature of the seismogenic faults contained therein. As seismic sources, these regions are noted for the maximum background earthquake each is capable of hosting. Regional faults are specific, identified structural sources within these zones that, on the evidence of past surface rupture, are capable of generating earthquakes of some estimable magnitude greater than background. We also include discussion of a possible buried strike-slip fault source with regional faults. Local faults are structural sources confined to Yucca Mountain. Because of their proximity to the potential repository, local faults are analyzed for both ground shaking and displacement hazard. The local faults are all close to each other relative to depth of the seismogenic crust so linking and distributed motion are important considerations. The potential dynamic interactions among local faults constrains estimates of earthquake magnitude and fault mechanics; for this reason, a tectonic model constitutes an important rationale for our estimates of local fault parameters.

3.1 FOCAL DEPTH DISTRIBUTION AND DEPTH OF THE SEISMOGENIC CRUST

The maximum depth distribution of earthquakes in the Yucca Mountain area was determined by analyzing focal depth data on well recorded earthquakes recorded by seismic networks within the region as well as checking this information against rheologic models of the seismogenic crust that constrain the depth to the brittle-ductile transition. We studied the focal depth distribution using filtered focal-depth plots determined by our own study employing the ZMAP (Weimer, 1996, seismicity analysis program) and by focal depth data provided by Woodward-Clyde Federal Services from the Yucca Mountain catalog filtered to our specifications.

The composite Yucca Mountain earthquake catalog, encompassing a 300 km radius sort from the Yucca Mountain site, is the same catalog that was distributed by Woodward-Clyde Federal Services to all Yucca Mountain teams after revisions for removal of multiple events and non-tectonic events. Focal depths were filtered by focal-depth accuracy, assumed to be related to the hypocenter parameter, DMN. DMN is the distance to the nearest station and is the standard statistical parameter used in the seismograph network community for analyzing focal depth accuracies. DMN is generally an indicator of the depth for which the eigenvalue

for a particular hypocenter is within a single solution space whose major and minor axes represent a source volume ellipsoid and are a measure of the error ellipse for the specified standard error of picking the appropriate phase, such as the first P wave arrival.

The Yucca Mountain earthquake catalog was first evaluated for important non-earthquake contributions such as nuclear explosions as well as mislocated epicenters. After finalizing the most complete catalog, the hypocenter files were filtered for earthquakes for most accurate focal depths in two categories: 1) with DMN equal to or less than 1, and 2) DMN equal to or less than 1.5. We finally used the focal depth constraint to be DMN equal to or less than 1.5 to constrain the depths as it gave a larger population necessary for the best statistical treatment and still retained accurately determined focal depths. We used the ZMAP seismicity analysis package (Weimer, 1996) to sort the hypocenter data for the various source areas in the 300 km wide catalog window. We used the Woodward-Clyde focal mechanism data to check against ours using the same DMN criteria.

We first considered the local Yucca Mountain area, encompassing the site and the nearby faults from the Bare Mountain fault on the west to the Gravity fault on the east and from the south edge of the Timber Mountain caldera to approximately the Highway 95 (Figure SDO-1). However using this area only provided a limited number of accurate focal depths; and we expanded our window to include the region of Source Zone 1 (Figure SDO-2).

The sorting process provided data for epicenter maps, recurrence plots for the filtered data for a given DMN value, and focal depth distributions. For completeness and to compare our data, we also asked Woodward-Clyde to provide the same data which revealed reasonably the same distributions. We then proceeded to sort the earthquake data into bins that we consider representative of the region: 1) the Yucca Mountain site, 2) a zone which included the Yucca Mountain site and extended across the California-Nevada border on the south on a NW trending line that extended across the NTS site and extended ~150 km NW and 150 km SE, 3) a zone that extended southwest from California-Nevada border ~90 km and 120 km E-W, and 4) a zone that extended ~ 200 NE into the Basin-Range. We also made epicenter plots for various depths of the distribution to examine if the distribution characteristics varied across the zones. Note these are a little different from our final three seismic source zones within 100

km of the site, but were used to assess enough good focal depth data to give statistically useful distributions.

The filtered focal depth data revealed Gaussian shaped distributions, centered at depths of ~ 8 to 10 km, with a scarcity of hypocenters from 0 to 2 km and an exponential decay to maximum depths of ~ 19 km (Figure SDO-3). We note the scarcity of data in the 0-2 km depth range, a depth range that we consider to be incapable of radiating strong ground motion because of the reduced stress state.

Alternate Evaluations--As alternate evaluations we examined focal distributions for areas around the Yucca Mountain site out to distances of 300 km, but we use data primarily from an area with a radius of 100 km from the site, because we wanted the data as representative as possible for this area which constitutes the Yucca Mountain geologic setting. We did not consider seismic sources beyond 100 km in our source models as beyond this distance the peak ground accelerations would not be significant at the site for earthquakes in this region.

We based our final maximum-depth of earthquakes on the focal depth distributions (rather than a 80 to 90% focal depth cut-off as suggested in rheological arguments) with consideration to the uncertainties in focal depth. We define a distribution for the maximum depth of earthquakes weighted as follows:

<u>Depth (km)</u>	<u>Weight</u>
14 km	0.2
17 km	0.7
19 km	0.1

We assigned the minimum focal depth as the depth with the largest (minimum) error for depth in the distribution considering ± 2 km for well resolved focal depths. The average maximum depth is near 17 km (Figure SDO-4). This depth also is consistent with the observed M 7+ normal faulting distribution of the Basin-Range (Smith and Arabasz, 1991).

A maximum focal depth of 19 km was chosen by our team as the depth of the largest well recorded earthquakes in the Basin and Range. This depth was as determined from the top of

the maximum depth source zone that was modeled to depths of 25 km for a dynamic source by Mendoza and Hartzel (1988) for the M 7.3, 1983, Borah Peak normal faulting earthquake. We recognize that it is deeper than 95% of the depths of background seismicity, but it was taken as an upper bound of depths that could plausibly occur in the Basin Range province.

Our focal depth distributions were also compared with idealized rheological models for the southern Basin-Range area considering the hypothesis that the focal depth distribution relates to the thickness of the seismogenic crust (the brittle layer). This depth has been shown to correlate with background seismicity at about the 80 percentile depth and was taken as indicator for the bottom of the background seismicity (Smith and Bruhn, 1994). It corresponds to Smith and Bruhn's (1984) model for extensional normal-faulting regimes in the Basin-Range, where the maximum focal depths of large normal-faulting earthquakes correlate approximately with the 80th percentile of focal depths for smaller background earthquakes. We followed the use of such indicators, which since the mid-1970s, have revealed that accurate hypocenter data acquired by regional and portable seismic networks in the Basin-Range region permit the construction of reliable focal-depth histograms (Sibson, 1982; Smith and Bruhn, 1984).

Seismogenic models based on theoretical depths were hypothesized for peaks in maximum shear stress at the boundary between the brittle upper crust and a quasi-plastic layer (Scholz, 1990). These models in a general way account for the maximum depths of nucleation of large normal faulting earthquakes and for the maximum depths of background seismicity, corresponding to the base of the seismogenic layer. The models involve a temperature-dependent, depth-varying power law for creep combined with a linear brittle-behavior criterion. Scholz (1990) predicts the thickness of the seismogenic layer, and hence the maximum focal depths of earthquakes, using both a similar temperature criterion as that described above and additional fault-velocity constraints.

Qualitative arguments of Sibson (1982) and Smith and Bruhn (1984) suggested that the theoretically derived transition depth from brittle to quasi-plastic flow for silica-rich rocks is controlled primarily by a critical temperature of approximately 350 °C to 450 °C and occurs at or near the depth of maximum shear stress. At this depth, short-term strain rates greater than 10^{-3} to 10^{-4} /sec are necessary to achieve brittle failure during earthquakes within the

more ductile, intermediate-depth crustal material. In theory, this is the critical depth for nucleation of the largest magnitude earthquakes. For the Yucca Mountain site the critical depth or depth to the brittle-ductile transition is taken to be 10 to 15 km for a quartz to dry quartzite composition and for the relatively low regional strain rate of 10^{-17} per second (Eddington et al., 1987).

Comparison of background focal depth data (Smith and Arabasz, 1991) for three of the best studied, scarp-forming normal faulting earthquakes of the Basin-Range (the 1959 M7.5 Hebgen Lake, the 1971 M7.1 Dixie Valley, and the 1983 M7.3 Borah Peak earthquakes) supports our evaluation of depth of nucleation of large, M7+ events at a few kilometers beneath the idealized brittle-ductile transition depth.

3.2 SEISMIC SOURCE ZONES

Seismic source zones are defined on the basis of tectonic style, structural pattern, and rates of deformation. On this basis, the source zones are equivalent to tectonic subprovinces or regional domains of the southern Great Basin. Three of these regional domains fall within a 100-km radius of Yucca Mountain and therefore qualify as source zones of potential ground shaking hazard at and near the mountain.

We determined three seismic source zones that include most, or large areas of, (1) the Walker Lane, (2) the Inyo-Mono terrane (or the Death Valley Zone), and (3) the Basin and Range Province. Figure SDO-2 shows the source zones in relation to the 100 km radius centered on Yucca Mountain.

Zone 1 comprises the Goldfield-Spring Mountain sections of the Walker Lane (Stewart 1988). It is characterized by a complex structural pattern that includes north-south-striking Basin-and-Range style normal faults, local basins, and Walker Lane style structures (northwest-striking dextral faults and northeast-striking sinistral faults). The northern part of the zone is dominated by volcanic rocks (tuffs of Miocene age); the southern part (Spring Mountains section) consists chiefly of little-extended Paleozoic rock. It is bounded on the west by the Furnace Creek-Death Valley fault zone and the Pahrump-Stewart Valley fault zone, and on the east by the Las Vegas Valley shear zone. North of Indian Springs, the eastern margin of

the zone is structurally diffuse, but generally is distinguished by northwest-striking dextral faults.

Zone 2 is the Death Valley section (or the Inyo-Mono terrane), which is characterized by active strike-slip faulting. The zone extends west from the Furnace Creek fault to the Sierra Nevada block. The Mammoth Lakes area to the north is purposely excluded from this zone because recent high levels of seismicity are associated with the Long Valley caldera and potentially localized volcano-tectonic activity. The southern boundary is marked by the Garlock fault.

Zone 3 is the central Basin and Range zone, which is bounded on the south by the Intermountain Seismic Belt that extends westward from Utah at about 36 degrees latitude and on the north by the 300-km cut-off distance from the site.

Alternative zones - Our initial categorization identified the Yucca Mountain site as a separate source zone having its own fault and seismicity characteristics. This area was bounded on the west by the Bare Mountain fault and on the east by the gravity fault. The north boundary was defined by Yucca Wash and the rim zone of the Claim Canyon caldera; the south side was at the southern termination of the Solitario and Stagecoach Road faults (Figure SDO-1). Plots of the historical seismicity from the project catalog (Appendix D of the main report) reveal only about 30 local earthquakes in this zone. Because of the sparcity of earthquakes, we chose not to identify this as a discrete seismic source zone, but included it in our regional source Zone 1 that would be characterized by its historic seismicity data.

We also considered as a separate seismic source zone an area defined by the Little Skull Mountain earthquake and its aftershock distribution. We made this interpretation based on the length of the aftershock zone (~ 30 km), which would correspond to the lower bound of our maximum background earthquake distribution for the lowest standard of error with a corresponding magnitude 6.3. However, after considering how to sort the historical data in both time and space, and considering that this location has been the site of smaller earthquakes that reflect ongoing seismicity characterized by our Zone 1 seismicity, we ultimately chose not to identify this as a discrete source area.

3.2.1 Maximum Background Earthquake

The maximum background earthquake, or MBE, is a critical parameter for the Yucca Mountain site PSHA. For our seismic source zones we consider the MBE to mean the largest earthquake that reasonably could occur in each seismic source zone without producing a distinguishable shear displacement of the ground surface (although there could be considerable ground cracks, fissures, etc. such as those that occurred with the M 6.2, 1986 Chalfant Valley, Nevada-California border earthquake). MBE was evaluated by comparing the seismicity characteristics of the Yucca Mountain area with the Quaternary tectonics (faults, fault lengths, relations to other structures, etc.) of the region and other extensional tectonic regimes. We considered that the seismic sources vary as a function of the faults that lie within them.

We used the data from Doser and Smith (1989) and the USGS fault data from Pezzopane (Seismotectonic Framework Report [USGS,1996]) to assess the maximum background earthquake distribution. We constructed our own distribution of Basin-Range earthquakes according to the following criteria: for magnitudes of $M_s > 5.5$, and for all ground breaking events.

We identified the maximum magnitude for each source zone, but also qualified that parameterization for a source radius of 100 km to ensure completeness for the Yucca Mountain site (Table SDO-1, Figure SDO-5).

Using the analogy of no tectonic fracturing associated with the Chalfant Valley earthquake and the largest earthquake in the Basin and Range province without surface rupture, the 1925 Clarkston Valley, Montana, M 6.6 (Doser and Smith, 1989, dePolo, written commun., 1997 from field mapping) a density distribution was defined from magnitude 6.2 to 6.6 for the MBE. We define a M_{max} of 6.4 ± 0.2 within 100 km with a cumulative lognormal distribution of:

<u>Magnitude (MBE)</u>	<u>Cumulative distribution</u>
6.2	0.03
6.4	0.50

Allowing for uncertainty in the magnitude of the Clarkston Valley earthquake, the maximum magnitude may be somewhat higher, as large as 6.8.

Our magnitude distribution is in accordance with a compilation of data on the occurrence of surface rupture for normal faulting earthquakes from (Doser and Smith, 1989) that revealed a similar distribution of MBE for a range of $5.3 < M < 7.5$ earthquakes. They showed that 8 events in the Doser and Smith (1989) data set revealed rupture beginning as small as M 6.1 and that all events above 7.1 experienced rupture. These data support our MBE distribution.

3.2.2 Recurrence Rates

Recurrence models describe the relative frequency of large- and small-magnitude earthquakes. The exponential model is considered to be appropriate for seismic source zones. However, for fault sources, it is not clear whether an exponential model or a characteristic earthquake model (Youngs and Coppersmith, 1985) is appropriate. We chose a truncated exponential recurrence model for our recurrence rate determination using the maximum-likelihood method of calculating the recurrence values (see Section 3.1 of the main report). We used all of the earthquake data in the catalog from the smallest to the largest magnitudes in the Yucca Mountain catalog. The choice of the entire magnitude range was made to provide as complete as possible a range of recorded earthquakes in the region. We discuss the treatment of historical seismicity for calculation of earthquake recurrence rates for the seismic source zones in section 4.0.

3.3 REGIONAL FAULT SOURCES

Regional faults within 100 km of Yucca Mountain were reviewed for inclusion in the ground motion analysis. Potential regional fault sources (Figure SDO-6) were identified first from among the following data sources: D.B. Slemmons (1966); Dohrenwend (1990); Dohrenwend et al. (1991, 1992); Piety (1995); chapters 5 and 11 of USGS Yucca Mountain Tectonic Synthesis Report, Jennings (1994); Reheis (1992); and Reheis and Noller (1991). Candidate faults were screened on the basis of evidence of Quaternary

displacement. The faults were further screened according to whether they are assessed to equal or exceed 0.05g in the analysis by Pezzopane (Seismotectonic Framework Report, Chapters 8 and 11 [USGS, 1996]). All identified and possible Quaternary faults capable of magnitudes 6.4 ± 0.2 within 50 km were included. In the range of 50 to 100 km from Yucca Mountain, only faults with lengths equal to or greater than 20 km were included. This criterion was based on the potential peak ground accelerations estimated in chapter 11 of the Seismotectonic Framework Report (USGS, 1996). A few faults having slightly lower ground motion potential also were included to account for potential uncertainties that could increase their ground motion, or because long-period ground motions from earthquakes along these faults may be important to the site. Two faults that generally lie beyond 100 km were included: the Panamint Valley fault zone and the Ash Hill fault zone (Figure SDO-6). These were included for their potential contribution to long-period ground motions. Most of the faults show clear evidence of Quaternary activity, such as fault scarps. For a few faults, the existence of Quaternary activity or the fault itself is equivocal. For these faults, a probability of Quaternary activity is assessed based on the degree of belief of fault activity (e.g., how likely the scarps observed along the Oasis Valley fault are from fault movement in the Quaternary).

In general, regional fault sources are characterized only on the basis of fault length for maximum magnitude and slip rate for earthquake recurrence, although a few have a maximum surface displacement as well. Maximum magnitudes were estimated using the scaling relations shown in Table SDO-2 and discussed further in Section 3.3.2. Each regional fault source is characterized according to the parameters in Table SDO-3.

Regional faults were compiled to a mylar overlay of Piety's (1995) map. Fault length estimates were measured on the mylar overlay. Faults were weighted as to whether or not they had Quaternary activity, by evaluating published studies of the individual faults. Maximum surface displacement measurements were taken from the published literature, such as the USGS Seismotectonic Framework report (1996). Fault dips for the regional faults are largely unknown. For the normal-slip faults, 60° was used; for strike-slip faults, 90° was used. Because the regional faults occur within three different seismic source zones, there is an implication that faults within each source zone should mirror a distinct tectonic framework, or structural geometry. However, the Gaussian distribution of

epicenters through the seismogenic crust suggests that dynamic distinctions in fault behavior throughout the region are not significant enough to require a models-based explanation. Therefore, we use a simple, universal model for all the faults: they are planar fractures that descend to seismogenic depths, the depths to a maximum of 19 km being directly proportional to fault length.

3.3.1 Description

The Gravity Fault

Because of its tectonic significance as a domain-bounding structure, the "gravity fault" (Winograd and Thordarson, 1975, p. C85) was described in the section on tectonic models. Surface expression along this fault is meager, but available data suggest chiefly normal slip. A subtle fault scarp segment on an alluvial fan was recognized by Reheis and Noller (1991); thus, there is indication of Quaternary activity along it. The lack of fault scarps suggests slip rates on the order of 0.0005 to 0.005 m/ky, but the subtle scarp may support a slip rate of 0.005 to 0.05 m/kyr (see Section 3.3.3 on recurrence justification of slip rate estimates for faults where data is lacking). Thus, the potential range of slip rate is 0.0005 to 0.05 m/kyr, with a preferred median value of 0.005 m/kyr. The minimum and preferred length is estimated to be 45 km, from the hills in the middle of Jackass Flats where the gravity anomaly diminishes, south to the end of the scarps that are on a southerly projection in the Ash Meadows area. The gravity gradient is essentially continuous along this extent. The maximum length extends south about 55 km to where many scarps are at an angle to the gravity fault. Although the Ash Meadows fault zone continues on strike to the south of the gravity fault on the basis of surficial expression, we do not extend it southward because the defining gravity gradient becomes indistinct (Winograd and Thordarson, 1975).

Amargosa River Fault

The Amargosa River fault was mapped by Donovan (1991) as a series of fault scarps and lineaments in southwest Amargosa Valley that are considered related to a strike-slip fault. Anderson et al. (1995a) confirm Quaternary activity along this fault, suggesting that it is a reactivated Miocene and Pliocene? strike-slip fault. The minimum and preferred lengths are the distance of the fault scarps mapped by Donovan. This length can be measured from the east-northeast-trending scarps in Amargosa Valley, which may be a westward

extension of the Rock Valley fault zone at the north end, to a near-intersection with the Ash Meadows fault along the south end. This is a distance of 16 km. The maximum length pushes the south end to an intersection with the Ash Meadows fault and continues north along a lineament, for a total distance of 29 km. Further extension to the north is plausible. No slip rate is reported for the Amargosa River fault; thus, a comparative methodology is employed to estimate the slip rate (see section 3.3.1.3).

Furnace Creek Fault Zone (Northern Death Valley Fault Zone)

The Furnace Creek fault zone is part of the Death Valley fault system, the largest and most active system in the Basin and Range province. The length, single-event displacements, and slip rate of this fault, as determined by Klinger and Piety (1996), support this notion. The preferred length of the Furnace Creek fault zone is given by Klinger and Piety as 105 km as measured from the intersection with the central Death Valley fault zone to the Last Chance Canyon area. They suggest that this represents a single rupture segment, an impression supported by the conspicuous scarp trace lineament seen in the USGS Death Valley 1:250,000 SLAR image composite. The minimum length for the maximum event is estimated to be 85 km based on the nearly continuous scarps represented by Piety (1995). If the Furnace Creek fault is continuous with the northern Death Valley fault the length is 120 km by our estimate, and this is our preferred value. The maximum fault length includes both the Furnace Creek and Fish Lake Valley fault zones, 195 km. Research by Sawyer and Reheis (1997) suggests that a small restraining step in the system may control the total rupture length along the Fish Lake Valley fault. The restraining step through Last Chance canyon, which lies between the Fish Lake Valley and Furnace Creek fault zones, is the basis for considering the failure of both of these faults consecutively. The Last Chance restraining step apparently has not ruptured during the Holocene, while both the Furnace Creek and Fish Lake Valley fault zones had multiple displacements. Yet, if this restraining step were to fail when both faults zones are mature in their seismic cycles, it could create a cascading double-fault zone rupture. Klinger and Piety (1996) measured the maximum single-event displacement as 6 m of lateral displacement, and an average single-event displacement of 4.5 m, but report no uncertainties for these. We infer a maximum surface displacement to range from 5.5 m to 6.5 m, with an estimated measurement uncertainty of 0.5 m. Klinger and Piety (1996) estimated two slip rates for the Furnace Creek fault zone, one near Ubehebe Crater and

one near Red Wall Canyon. The Ubehebe Crater site, located on the main strand of the Furnace Creek fault zone, is distinguished by an anticline that includes the Bishop Tuff (~ 760 ka). The anticline is offset, yielding a slip rate of 8 to 10 m/kyr. The slip rate estimate from the Red Wall Canyon site is 4 to 8 m/kyr. We use the overlapping value of the reported ranges (8 m/kyr) for the preferred rate (a decision suggested by Klinger, 1997, written commun.), and use the reported range (4 to 10 m/kyr) for the minimum and maximum values. A good analog for earthquakes along the Furnace Creek fault zone is the 1872 Owens Valley earthquake, which had average surface displacements of 6 m and was about 110 km long (dePolo et al., 1991). That earthquake had a moment magnitude of about 7.8.

Central Death Valley Fault Zone

The Central Death Valley fault zone is a right-normal, oblique-slip fault. The fault zone is part of a right step in the right-lateral Death Valley fault system. Recent work by Klinger and Piety (1996) concluded that the Central Death Valley fault zone is the most active, dominantly normal-slip fault in the Basin and Range province. Klinger and Piety measured a minimum surface rupture length of 45 km along the Central Death Valley fault zone, and a total length of about 60 km. Our estimate of 75 km extends this rupture to the south. Because of the rate and the potential size of offsets during paleoevents, we use 75 km for the preferred length, considering that the surface expression is poor along the northern part of the fault zone. The maximum and preferred values are identical, because the fault is structurally intersected at either end. For maximum surface displacement, Klinger and Piety (1996) measure surface separations (which in this case are essentially equal to vertical displacements because of steep near-surface fault dips and shallowly dipping offset surfaces) of 2.5 to 3.5 m; we adopt these values as the minimum and preferred maximum surface displacement values. Our maximum value adds 1 m to the preferred value to cover surficial noise and possible local poor preservation. Thus, the maximum surface displacement considered is 4.5 m. The minimum, preferred, and maximum slip rates are 2.6, 3.8, and 7.4 m/kyr, respectively. These are based on late Holocene offsets and age estimations of alluvial fan deposits made by Klinger and Piety (1996).

Rock Valley Fault Zone

The Rock Valley fault zone comprises at least three major strike-slip faults and numerous bridging oblique faults in a zone that extends from Frenchman Flat west through Rock Valley, and possibly to Jackass Flats south of the Striped Hills, although there is evidence that the faults veer south into the Specter Range. The major faults strike N65°-80°E, are dominantly left-slip to slightly oblique, transtensional faults expressed geomorphically as a series of intermittent fault scarps and vegetation lineaments. Late Pleistocene to possible Holocene faulting has been documented through surficial mapping and trenching studies (Chapter 4, Seismotectonic Framework Report [USGS,1996]). Fault lengths for the Rock Valley fault zone were measured from the compilation by Piety (1995). The minimum length is 32 km, based on the faults mapped in Frenchman Flat to the west end of the scarps in Rock Valley. The preferred length is 47 km, measured between the faults mapped in Frenchman Flat and faults that pass immediately south of Skeleton Hills (Chapter 4, Seismotectonic Framework Report [USGS,1996]). The maximum length, 68 km, is measured from faults east of Frenchman Flat to the west end of the north-northeast-trending scarps and lineaments that cross Amargosa Valley. Individual fault strands, as mapped and indicated by lineaments, are about 15 to 17 km long. The Rock Valley fault zone has some of the largest single-event displacements measured in the Yucca Mountain area (Chapter 4, Seismotectonic Framework Report [USGS,1996]). Paleoseismic events have produced a minimum displacement of 1.14 m to a maximum of 4.51 m. Preferred displacements range from 2.04 to 3.62 m. The second largest preferred displacement is 3.30 m. Because natural variations in surficial expression from earthquakes can be comparable to the difference between the two largest displacement values, we consider it reasonable to use the maximum value as the maximum surface displacement for maximum earthquakes along the Rock Valley fault. Slip rates along Rock Valley fault strands range from 0.05 m/kyr to < 0.002 m/kyr. Yount et al. (1987) estimate 0.02 m/kyr for the medial fault strand; we adopt this value as the preferred slip rate for the entire fault zone. The Seismotectonic Framework Report (USGS, 1996) reports a long-term lateral slip rate of 0.084 m/kyr over the past 30 Myr, but suggests that much of this activity may have occurred during the Miocene, when the rates of tectonic activity were higher.

Mine Mountain Fault

The Mine Mountain fault is defined by a 3-km-long fault contact at Mine Mountain that sets Miocene tuff against Paleozoic limestone (Maldonado, 1985). The fault can be projected 3.8 km to the northeast and 26 km to the southwest, based on scattered outcrop evidence and aeromagnetic anomalies. The maximum length is about 35 km (Maldonado, 1985; Young et al., 1992). We prefer a length of 21 km, which includes the Mine Mountain segment and the segment projected along Shoshone Mountain to near Kiwi Mesa (Maldonado, 1985). The fault strikes N35°E and dips from 90 to 60 degrees southeast; it is considered planar, based on aeromagnetic gradients and focal plane mechanisms to depths of 9 km. The fault is chiefly normal along Shoshone Mountain, but has a sinistral component along its entire length. No Quaternary offsets are mapped, but colluvium offset against caliche crust in a prospect pit at the southeast corner of Shoshone Mountain amounts to about 20 cm of dip slip. Total offset of surficial material at this site is about one meter, possibly having occurred within the past 100 ky D. O'Leary, USGS, written commun., 1996). Lineaments in old fan surfaces suggest degraded scarps of perhaps mid to early Pleistocene age. Carr (1984) reported an offset of the Paintbrush and Timber Mountain tuffs of about 1 km left-lateral on the south side of Mine Mountain. Assuming that this offset has occurred during the last 11.5 Myr, a slip rate of 0.09 km/Myr (m/kyr) can be calculated, which is considered the maximum slip rate. Because geomorphology along the Mine Mountain is more poorly expressed than along the Rock Valley fault zone, its preferred slip rate is estimated to be similar or slightly lower than for that fault zone, or about 0.01 m/kyr or less; we use a lower limit of 0.005. Recurrent clustered earthquakes beneath the hanging wall of the Mine Mountain fault and along Mine Mountain indicate overall transtension and a low strain threshold. The Mine Mountain fault is considered to be susceptible to normal-oblique, southeast-side-down slip at this time. All of these features suggest that the Little Skull Mountain earthquake was generated by the Mine Mountain fault zone. However, the Mine Mountain fault strikes consistently N35°E rather than N55°E (the strike of the Little Skull Mountain slip plane); therefore, we believe that the Little Skull Mountain earthquake was generated within the Wahmonie fault zone or represents a fault in the hanging wall of the Mine Mountain fault.

Cane Spring Fault

The Cane Spring fault is expressed as a well-defined fault-line scarp that strikes N50°-40°E along a hillslope (Poole et al., 1965). The fault is a single-plane structure that evidently controls the location and flow of Cane Spring. The fault line scarp is only about 6 km long. Frizzell and Shulters (1990) show an additional inferred 5 km extending into Barren Wash, and 2 km projected to the south side of Skull Mountain. The fault is traceable as a lineament into Skull Mountain, but is truncated by and breaks down into a complex of more northeast-striking normal faults. Field examination by O'Leary found no evidence for Quaternary offsets at Skull Mountain, and no evidence that the Cane Spring fault connects with the Rock Valley fault zone. Northeast of Cane Spring, the fault projects into an alluvial basin. Gross landforms suggest that the fault extends, buried, a considerable distance toward Yucca Flat; therefore our preferred length estimate is 26 km, following the interpretation of Cornwall (1972). The maximum cumulative lateral offset is about 1 km (Poole et al., 1965). The cumulative vertical offset, if any, is unknown because latest movement on the fault is nearly pure strike-slip. The youngest offset unit is about 9.5 Ma which gives a slip rate as high as 0.105 m/kyr. Overall geomorphic character implies very low Pleistocene activity. Thus, the minimum, preferred, and maximum slip rates assigned to the Cane Spring fault are 0.005, 0.01, and 0.05 m/kyr, respectively. In light of its tectonic isolation, lack of late Quaternary expression, and weak correlation with significant slope breaks or boundaries, we rank its probability of activity as 0.8.

Wahmonie Fault Zone

The Wahmonie fault zone is represented by degraded scarp segments in alluvial fans along the north flank of Skull Mountain, which faces Jackass Flats, and as a zone of complex faults exposed in bedrock in the divide between Little Skull Mountain and Skull Mountain (Frizzell and Shulters, 1990). The zone projects directly toward the Striped Hills, which have left-lateral offset as great as 1.4 km along the projection. The projection can be carried even farther south, across Rock Valley and along the flanks of the Specter Range. The Wahmonie fault zone either truncates or intersects the Rock Valley fault zone in a relationship not understood. The structural interaction, which is considered to be related to the recurrent, clustered seismicity at the western end of Rock Valley. Quaternary activity is indicated by fault scarps and lineaments in deposits dated 270-740 ka, and by

concealment beneath Holocene deposits (Swadley and Huckins, 1990). Possible Holocene movement is suggested by cracked and slightly offset caliche pavement (observed by O'Leary), and by a conspicuous dearth of precarious rocks at the east end of Little Skull Mountain (J. Brune, oral commun. PSHA workshop). The minimum length of the Wahmonie fault is 9 km. The preferred and maximum lengths are 15 km, which include the discontinuous series of scarps and lineaments in eastern Jackass Flats, just north of Skull Mountain (Swadley and Huckins, 1990). The minimum, preferred, and maximum slip rates assigned to the Wahmonie fault are 0.005, 0.01, and 0.05 m/kyr, respectively. Despite hints of late Pleistocene activity, evidence for significant Pleistocene offset for any appreciable distance along strike has not been noted. On this basis we rank the probability of activity as 0.8.

South Silent Canyon Fault

The South Silent Canyon fault (herein named) lies in the structural system north of the Timber Mountain caldera that is remarkably similar to the Yucca Mountain fault system (described in the section on Tectonic Models). This is only one of several faults in Pahute Mesa that are suspected to have Quaternary activity (i.e., Quaternary alluvium in fault contact with rhyolitic tuffs), but for which we have little information. Maps, such as that of Frizzell and Shulters (1990), show several of these faults bounding local Quaternary alluvial deposits. The South Silent Canyon fault ruptured following an underground nuclear explosion and/or earthquakes that occurred following the blast. The minimum length is 10 km. A preferred distance of 14 km includes the entire fault zone; a maximum distance of 17 km includes faults in the tuffs farther north. Slip rate estimates are poorly constrained; on the basis of structural similarity to the Yucca Mountain faults, minimum, preferred, and maximum slip rates are assumed to be 0.001, 0.005, and 0.01 m/kyr, respectively. These rates suggest that the South Silent Canyon fault is more active than the Bow Ridge fault, but that the minimum value might be lower. The maximum value approaches the slip rate of the Solitario Canyon fault. Little is known about the Quaternary history of the South Silent Canyon fault. Because of sparse data and uncertainty, we rank its probability of activity 0.8.

Pahute Mesa #1 Fault

The Pahute Mesa #1 fault (herein named) lies just west of the South Silent Canyon fault and is part of the same system. Also similar to the South Silent Canyon fault, the Pahute Mesa #1 fault ruptured in association with an underground nuclear explosion. This fault has a few kilometers of fault-bounded Quaternary alluvium along it (Orkild et al., 1969). The minimum length of the Pahute Mesa #1 fault is about 10 km, the distance of the fairly continuous single-plane trace. The preferred length of 13 km includes the entire fault zone. The maximum length of 16 km includes faults in tuffs farther north. The weak slip rate estimates are based on structural similarities to the Yucca Mountain faults. Thus, minimum, preferred, and maximum slip rates are interpreted to be 0.001, 0.005, and 0.01 m/kyr, respectively. These rates suggest that the Pahute Mesa #1 fault is more active than the Bow Ridge fault, but that the minimum value might be lower. The maximum value approaches the slip rate of the Solitario Canyon fault. The fault-bounded Quaternary alluvium indicates a likelihood that the Pahute Mesa #1 fault has experienced some Quaternary activity, but otherwise we rank its probability of activity the same as for the South Silent Canyon fault, for the same reasons..

Yucca-Butte Fault Zone

The Yucca-Butte fault zone is a down-to-the-east, normal-slip fault that extends across the middle of Yucca Flat (Yucca fault) into the hills north of the flat (Butte fault). Because of the continuity between the Yucca and Butte faults, they are treated here as a structurally linked fault zone. The minimum length of the Yucca-Butte fault zone is 26 km, the distance of the Yucca fault portion. The preferred value is 34 km, which includes the small range-front portion (the Butte fault) north of Yucca Flat. The maximum value, 41 km, includes scarps and lineaments north of the Butte fault. Fault scarps clearly indicate Quaternary activity (Swadley and Hoover, 1990). Fernald et al. (1968) measure a surface displacement of 15 m in the Quaternary alluvium. Using ages for surfaces mapped by Swadley and Hoover (1990) and correlations with surfaces that have been studied in the Yucca Mountain area, slip rates for the Yucca-Butte fault range from 0.015 to 0.053 m/kyr, with a preferred value of 0.026 m/kyr.

Peace Camp Fault

The Peace Camp fault has been mapped by Dohrenwend et al. (1991) as a northeast-trending, fault-controlled lineament; by Reheis (1992) as a prominent scarp or lineament in Quaternary deposits; and by Yount (unpublished mapping) as a fault in older Quaternary alluvial deposits. Its strike and location suggest that the Peace Camp fault may be a left-slip fault, part of a small system that includes the South Ridge Faults" of Piety (1995). This structural association apparently would require a left step of about 2 km. The minimum and preferred length for the Peace Camp fault, 12 km, represents its clear expression in Quaternary alluvium. The maximum length of 30 km includes the South Ridge faults. Although Dohrenwend et al. (1991) show the South Ridge faults as juxtaposing Quaternary alluvium against bedrock, lack of geomorphic expression along this eastern extension suggests that earthquakes likely are restricted to half of this maximum length (15 km). Extension of the Peace Camp fault to the west would require another left step and a change to a more northerly orientation. A westward extension would bring the Peace Camp fault into structural association with the West Spring Mountains fault.

Slip rates from the Mine Mountain fault are adopted for the Peace Camp fault, on the basis of similar geomorphic expression. Thus, the minimum, preferred, and maximum slip rates assigned to the Peace Camp fault are 0.005, 0.01, and 0.09 m/kyr, respectively.

West Spring Mountains Fault

The West Spring Mountains fault is a west-side-down, normal-slip fault that bounds the northwest side of the Spring Mountains. The fault has been mapped and studied by Hoffard (1991). Quaternary activity is evidenced by fault scarps. The minimum length of a continuous fault is 30 km. The preferred length of 37 km accounts for a south scarp that is on strike, but separated by a small gap in surficial expression. The maximum length of the West Spring Mountains fault is 56 km, which includes the Eastern Pahrump Valley fault zone southward to an intersection with the Pahrump Valley fault zone. This south reach may have a right-lateral component, given its relatively linear nature and left-stepping patterns. Based on geomorphology, the north 30 to 37 km of the West Spring Mountains fault appears to be a single earthquake segment. Hoffard (1991) measured a vertical surface separation of 12 m, which has been corrected to a vertical offset of 13.2 m

to account for the surface slope and fault dip. Different projections of the profile made by Hoffard yield potential uncertainties of - 2 and + 4 m. Hoffard estimates the age of this offset surface to be 200 ka, with a range of 130 to 500 ka. These data yield a range of slip rates from 0.02 to 0.2 m/kyr, with a preferred rate of 0.09 m/kyr.

Oasis Valley Fault Zone

The Oasis Valley fault zone is a normal-slip fault that lies along a steep north-south gravity gradient (Anderson et al., 1995b). This fault zone lacks evidence for late Quaternary faulting (Anderson et al., 1995b). A prominent lineament, however, may be evidence of minor early Pleistocene displacement (Anderson et al., 1995b). The minimum length of 5 km represents the bold faults from Piety's (1995) map. The preferred length of 8 km accounts for other faults and/or lineaments on strike. The maximum length of 20 km is the total possible expression of this fault zone, including projected faulting in Oasis Valley. Overall lack of geomorphic expression suggests that the slip rate likely is low, perhaps similar to that of the Bow Ridge fault. A range of 0.0005 to 0.003 m/kyr is assigned to the Oasis Valley fault zone, with a preferred value of 0.001 m/kyr. The very weak evidence for Quaternary activity leads us to assign a probability of activity of 0.8.

Pahrump Valley Fault Zone

The Pahrump Valley fault zone is made up of a series of discontinuous, northwest-trending scarps, spring alignments, and lineaments that indicate a right-slip fault zone (Hoffard, 1991; Anderson et al., 1995b; and Louie et al., 1996). The fault zone lies along the center of Pahrump Valley (essentially along the Nevada/California state line); it extends from Black Butte at the south end to an apparent pull-apart basin, Stewart Valley, at the north. The minimum length (25 km) is the distance of continuous geomorphic features in north Pahrump Valley, extending into south Stewart Valley. The preferred and maximum lengths (61 and 67 km, respectively) extend the zone down to Black Butte, with a maximum rupture length that traverses all of Stewart Valley. To estimate slip rate, we compare this fault zone with the Rock Valley fault zone, which has a similar, zone-like, geomorphic expression, but sharper geomorphic features. We assign a preferred slip rate of 0.01 m/kyr, with a range of 0.005 to 0.1 m/kyr.

Bare Mountain Fault

The Bare Mountain fault is poorly exposed, probably because in Quaternary time erosion and deposition have far outweighed tectonic activity along the fault. Gravity and seismic reflection data indicate that the fault plane stands at least a kilometer out from the eroded range front at the north end of the mountain, and converges more closely to the range front toward the south. Younger activity of the fault is also indicated to the south. The fault (or faults, if several planes are involved) dips east at 50 to 70 degrees; displacement is chiefly normal, with an oblique dextral component prominent to the south (Reheis, 1988; Mosen et al., 1992). The fault is at least 18 km long. At the northeast corner of Bare Mountain, the Bare Mountain fault loses throw and breaks into a group of faults that extend across tuffs of the caldera rim assemblage. The easternmost fault is the Tram Ridge fault; it extends about 10 km to the Rainier Mesa caldera. A smaller, less clearly defined fault 8 km long, east side down, bounds the tuffs and the alluvium of Crater Flat. This fault apparently is post-8 Ma (C. Fridrich, USGS, written commun.). At the south end, near Steves Pass, the Bare Mountain fault abruptly loses throw and ceases to be a range-front fault. It becomes lost in a distributed zone that includes faults traceable to Yucca Mountain itself; although a set of northwest-striking, dextral oblique faults appears to dominate the fault structure in this area. Within this plexus, the Bare Mountain fault is not a single-plane structure and probably is not a major tectonic influence. Because it surfaces within surficial deposits for most of its length, there is no direct indication of total bedrock displacement. The fault does not appear to be segmented; surface rupture has occurred along a relatively linear, narrow zone on all or most of its (preferred) 23-km length. Surface-rupturing earthquakes on the fault occur infrequently. The recurrence of moderate- to large-magnitude, surface-rupturing earthquakes appears to be on the order of tens of thousands to a hundred thousand years or more. The most recent surface-rupturing event occurred no more recently than about 14 to 24 ka and could be as old as 100 ka (Seismotectonic Framework Report [USGS, 1996]). Maximum surface displacement ranges from 1.2 m to 1.8 m; we adopt a preferred value of 1.5 m which is the value reported in the Seismotectonic Framework Report (USGS, 1996). An uncertainty of ± 0.3 m is considered to encompass a potential range of measurements (projection uncertainties or variability of datums). The minimum slip rate (0.006g m/ky) is taken from a minimum offset measured by Anderson and Klinger (1996) of 2.2 m taken over their maximum estimated age of 400 ka. The preferred value of 0.01 m/ky is the value

estimated from Anderson and Kinger (1996). Ferrill et al. (1996) suggest a higher slip (0.2 m/ky) based on indirect evidence; we adopt this as our maximum slip rate.

Keane Wonder Fault

The Keane Wonder fault is a west-side-down, normal-slip fault that bounds the southeast side of north Death Valley and part of the west side of the Grapevine Mountains. The minimum, preferred, and maximum lengths are 19, 27, and 29 km, respectively. The minimum length is the continuous central part mapped by Piety (1995); the preferred length extends this to the north and south along a range front. The maximum length extends the fault farther south along a fault trace that bounds a range front for some distance before trending into the range. Lack of a faceted range front and of fault scarps indicates a relatively low rate of activity. The preferred slip rate estimate is the approximate threshold of faults having fault scarps of 0.005 m/kyr. The fault appears to lack late Quaternary activity (Anderson et al., 1995b); but an abrupt, rectilinear range front indicates possible early to mid-Quaternary activity. Given that deposition along the range front is fairly uniform at the front, some Quaternary activity is considered likely. Thus, we consider a minimum slip rate of 0.001 m/kyr. The maximum rate is 0.05 m/kyr, just a little higher than the maximum rate of the Solitario Canyon fault. We make it slightly higher to reflect our uncertainty, because the Keane Wonder fault is untrenched.

Eleana Range Fault

The Eleana Range fault is an east-side-down, normal-slip fault that bounds the northwest side of Yucca Flat and the east side of part of the Eleana Range. This fault is about 5 km west of, and is synthetic to, the Carpetbag fault. The Eleana Range fault appears to bound a small subbasin within Yucca Flat, just west of the Carpetbag fault (Frizzell and Shulters, 1990). Fault scarps along the Eleana Range fault are indicated by Swadley and Hoover (1990) and Dohrenwend et al. (1992); the latter authors indicate some of these scarps are in late Pleistocene deposits. The Eleana Range fault is considered to be limited to its range-front expression, 15 km. This value is used for both the preferred and maximum values. A minimum value of 11 km represents the central part of the fault that has scarps. No direct slip rates are available for the Eleana Range fault, so we used comparisons. Because fault scarps are present, we assigned a minimum value of 0.003 m/kyr. The preferred value is difficult to ascertain, but we consider it be comparable to the Solitario

Canyon fault, about 0.01 m/kyr. The maximum value assigned to the Eleana Range fault is the approximate maximum value for the Yucca-Butte fault zone, 0.05 m/kyr.

Yucca Lake Fault

The Yucca Lake fault is a down-to-the-northeast, normal-slip fault that bounds a short section of the west side of Yucca Flat. The fault is shown to offset the buried upper surface of pre-Cenozoic rocks in the subsurface, and a potential right-lateral component is indicated by McKeown et al. (1976). No fault scarps are identified along the Yucca Lake fault, and Quaternary activity is uncertain, although Cornwall (1972) shows the fault in Quaternary deposits. Given the information at hand, this fault is given a 50% chance of having Quaternary activity. The minimum length is the trace portrayed by Piety (1995), 12 km. The preferred length, 20 km, considers an inferred extension to the northwest and southeast of the trace shown on Piety's map; and the maximum length, 23 km, includes an extension southward that intersects the Cane Springs fault. Slip rate estimates for the Yucca Lake fault are based on the interpretation that the fault is active and lacks scarps. The minimum rate is estimated to be 0.001 m/kyr; the preferred rate is assigned at the approximate threshold of faults that have scarps, 0.005 m/kyr. The maximum rate is similar to the preferred rate of the Solitario Canyon fault, about 0.01 m/kyr.

Carpetbag Fault

The Carpetbag fault is part of the down-to-the east system of normal faults in Yucca Flat, including the Yucca-Butte fault zone and the Eleana Range fault. At the surface, the Carpetbag fault manifested as faulting induced by nuclear testing. This exposed a fault zone that apparently has a Quaternary history of fracturing, but that had no natural surface expression prior to nuclear testing (Shroba et al., 1988). Subsurface work has further defined the extent of the Carpetbag fault by following an offset of the floor of the Yucca Flat basin (Carr, 1984). The fault is composed of two traces south of the induced surface expression; these are synthetic normal faults separated by about 1.5 km (Frizzell and Shulters, 1990). The minimum length of the Carpetbag fault, 18 km, is based on a simple geometric segment interpretation of the subsurface projection. The preferred length is the extent of the fault indicated by the extent of offset of the basin floor to the north margin of Yucca Flat and, in the south, to an intersection with the Yucca Lake fault. The maximum length, 37 km, includes some rupture along the southeast part of Quartzite Ridge, and

some rupture along the south part of the fault, parallel to the Yucca Lake faults. Slip rate estimates for the Carpetbag fault are based on assuming that the fault is active and lacks scarps. The minimum rate is estimated to be 0.001 m/kyr; the preferred rate is assigned at the approximate threshold of faults with fault scarps, 0.005 m/kyr. The maximum rate is similar to the preferred rate of the Solitario Canyon fault, about 0.01 m/kyr.

Oak Spring Butte Fault

The Oak Spring Butte fault is a down-to-the-east, normal-slip fault that bounds the easternmost part of the Belted Range and forms the west side of Emigrant Valley. The fault is expressed as a zone of scarps and lineaments. Several of the faults offset rhyolitic volcanic flows, creating expressions similar to those of the Yucca Mountain faults. Several of these faults are considered to have possible Quaternary displacement (Reheis, 1992; Dohrenwend et al., 1992). The orientation, sense-of-displacement, and position suggest that the Oak Spring Butte fault is an overlapping extension of the Yucca-Butte fault zone. The length of the Oak Spring Butte fault is difficult to assess, since it is part of a large fault swarm within the east part of the Belted Range and Emigrant Valley. The minimum length (9 km) is taken from a straight, central part of the fault. The preferred length, 16 km, extends this to the north and south, the north part along the physiographic expression of the Belted Range range front. The maximum length, 19 km, includes a small projection to the north and south. With the possible exception of some weak lineaments and/or scarps reported by Reheis (1992) along the north end, no Quaternary scarps are identified along the Oak Spring Butte fault. Slip rate estimates for the fault are based on assuming that the fault is active and lacks scarps. The minimum rate is estimated to be 0.001 m/kyr; the preferred rate is assigned at the approximate threshold of faults with fault scarps, 0.005 m/kyr. The maximum rate is similar to the preferred rate of the Solitario Canyon fault, about 0.01 m/kyr.

Belted Range Fault

The Belted Range fault is a down-to-the-west, normal-slip fault that bounds the west side of the Belted Range and the east side of Kawich Valley. This fault, which has been mapped by Reheis (1992) and Anderson et al. (1995b), shows evidence of latest Pleistocene to earliest Holocene faulting. The minimum length of the Belted Range fault is 22 km; this is the length of surface scarps mapped by Anderson et al. (1995b). The

preferred length of 35 km includes much of the topographic expression of the fault. The maximum length is 47 km, which includes projections of the fault into the mountains along the south end of the fault and a north projection along weak lineaments or fault scarps in alluvium mapped along Lava Ridge by Reheis (1992). Slip rate estimates were assigned following Anderson et al. (1995b), who estimate a Holocene slip rate of 0.1 m/kyr (1 m of offset in 10 kyr) and a Pleistocene slip rate of 0.01 to 0.09 m/kyr (11.3 m total offset in 130 to 780 kyr). From this information, we adopt minimum and maximum slip rates of 0.01 and 0.1 m/kyr. A mid-range value of 0.05 m/kyr was adopted as the preferred rate, which is the same rate as indicated by the long-term offset of the 11.5- to 12.5-Ma Timber Mountain Tuff (Anderson et al., 1995b).

Kawich Range Fault

The Kawich Range fault is a down-to-the-west, normal-slip fault that bounds the west side of the Kawich Range and the east side of Gold Flat. Anderson et al. (1995b) found latest Pleistocene fault scarps over only a small percentage of the length of this fault, but this confirms Quaternary activity. The minimum length is 23 km, as indicated by Piety (1995) and Anderson et al. (1995b). The preferred value, 33 km, includes much of the topographic expression of the fault. The maximum value, 46 km, extends the fault to the south along faults mapped by Reheis (1992) and to the north to intersect the next major strand of the Kawich fault. The total length of the Kawich Range system is not reported here. Slip rate estimates for the Kawich Range fault are based on the interpretation that the fault is active but lacks scarps. The minimum rate is estimated to be 0.001 m/kyr; the preferred rate is assigned at the approximate threshold of faults that have scarps, 0.005 m/kyr. The maximum rate is similar to the preferred rate of the Solitario Canyon fault, about 0.01 m/kyr. Although the Kawich fault is a substantial range front fault, lack of Quaternary expression leads us to assess a low probability of activity of 0.8.

Western Pintwater Range Fault

The Western Pintwater Range fault is a west-side-down, range-bounding, normal-slip fault that bounds the west side of the Pintwater Range and the east side of Indian Spring Valley. Dohrenwend et al. (1991) indicate that this fault is likely early to mid-Quaternary in age. The minimum fault length is 33 km, considering only the most prominent central part that bounds Indian Spring Valley. The preferred length, 54 km, includes the entire

western side of the Pintwater Range. The maximum length, 75 km, includes a north extension of the fault that bounds the west side of the north Desert Range. Dohrenwend et al. (1991) identify some fault scarps along the Western Pintwater Range, but they are generally short, discontinuous scarps in mid- to early Pleistocene deposits (J. Yount, 1996, written commun.). Yount finds no evidence for faulting along much of the fault, including apparently faceted portions, limiting the potential slip rate estimate. The minimum slip rate of the Western Pintwater Range is 0.005 m/kyr, near the lowest slip rate for normal faults that have fault scarps. The maximum estimated rate is 0.05 m/kyr, the approximate threshold slip rate for faults that have fault facets. The preferred slip rate is estimated to be between these two, or 0.008 m/kyr.

Grapevine Mountains Fault

The Grapevine Mountains fault is a west-side-down, normal-slip fault that bounds the north side of the Grapevine Mountains (Reheis and Noller, 1991; Dohrenwend et al., 1992). The fault is made up of two principal strands, a range-front trace and a piedmont trace that bounds some small hills along its east end. The fault is represented as a single trace for analysis purposes. The minimum and preferred lengths of the Grapevine Mountains fault are 25 km, which represents most of the easternmost part of the fault shown by Piety (1995). The maximum length, 32 km, includes a south extension of the fault that strikes into the Grapevine Mountains. Fault scarps in Quaternary alluvium are present along the piedmont trace of the Grapevine Mountains fault, but fault facets are not present. The minimum slip rate estimate, 0.003 m/kyr, is the lowest rate for a fault that has a fault scarp; the preferred slip rate, 0.01 m/kyr, is the middle of the range for faults having alluvial scarps but no fault facets; and the maximum slip rate, 0.05 m/kyr, is approaching the maximum rate of faults that lack fault facets.

Panamint Valley Fault Zone

The Panamint Valley fault zone is a major strike-slip fault that bounds the west side of the Panamint Range and the east side of Panamint Valley and has a normal-right-lateral sense of displacement. The fault zone has been discussed or mapped by several individuals (Bryant, 1989; Zhang et al., 1990). The minimum length of the Panamint Valley fault zone is 82 km, which is its extent from the south part of Panamint Valley north to a small reentrant in the range front. The preferred length, 90 km, extends the north part of the

fault to the more westerly-trending Hunter Mountain fault. The maximum length, 104 km, considers an additional extension to the southmost part of Panamint Valley. A Holocene slip rate was determined by Zhang et al. (1990) from offset alluvial features. Their slip rate estimate is 2.36 ± 0.79 m/kyr; we round this off to 2.4 ± 0.8 m/kyr.

Hunter Mountain Fault Zone

The Hunter Mountain fault zone is basically a northward extension of the Panamint Valley fault zone, but its strike is 25 degrees more westerly, and it is separated by a gap in fault scarps (see Bryant, 1989). The fault zone has a minimum length of about 46 km and a maximum length of 65 km. Our preferred length, 64 km, is close to the maximum value. The Hunter Mountain fault zone exhibits one of the finest series of right-laterally offset stream channels in the Basin and Range province, on the southwest flank of Hunter Mountain. The fault zone is a normal-right-oblique fault, with alternating downthrown sides, down-to-the-west in the south and down-to-the-east in the north. Slip rates for the Hunter Mountain fault zone are relatively high, ranging from 1.3 m/kyr to 2.7 m/kyr. Our preferred value is 2 m/kyr, comparable to the rate for the Panamint Valley fault. Slip rates for this fault were taken from Piety (1995), Schweig (1989), and Burchfiel et al. (1987).

Ash Hill Fault Zone

The Ash Hill fault zone is a right-slip fault zone that runs up the west side of Panamint Valley. Bryant (1989) provides the most detailed description of this fault. The Ash Hill fault zone appears to alternate downthrown sides along strike, being down-to-the-east along the south part and down-to-the-west along the north part. The Ash Hill fault zone appears to coincide with the western margin of Panamint Valley; if so, it apparently has a much stronger normal component than the north part. The minimum length estimated for the fault zone is 33 km, which is the minimum length of the relatively continuous "backfacing-scarp appearance." The preferred length, 55 km, extends the Ash Hill fault zone slightly on the north and substantially along the south. The south end is extended along the northeast flank of the Slate Range as a buried fault (only probable liquefaction grabens are portrayed by Bryant (1989) along this projection). A buried fault is inferred primarily because this range front is on strike with the mapped surficial expression, and some active tectonism along the range front is considered to account for its youthful appearance. The maximum length, 90 km, includes a small increase in length on the north

and, again, a substantial increase in length to the south. This is to account for the continued on-strike potential southward, along the west side of Panamint Valley, to just north of Wingate Pass. The slip rate of the Ash Hill fault has been investigated by Densmore and Anderson (1994). They map an olivine basalt K/Ar dated at 4.05 ± 0.15 Ma that is offset right laterally by 1.2 ± 0.3 km, indicating minimum, preferred, and maximum slip rates of 0.21, 0.3, and 0.38 m/kyr, respectively.

West Specter Range Fault

The West Specter Range fault is a west-side-down, normal-slip fault just west of the Specter Range (Anderson et al., 1995b). The north part of the West Specter Range fault is expressed as "small scarps and conspicuous lineaments on alluvial deposits"; the south part is made up of "discontinuous but prominent scarps on alluvial deposits and by lineations in Tertiary(?) bedrock" (Anderson et al., 1995b). Anderson et al. indicate that fault scarps have as much as 1.4 m of surface offset in deposits of probable middle Pleistocene age. Small scarps along the north part have 0.3 to 0.5 m of surface offset on deposits that likely are latest Pleistocene in age (Anderson et al., 1995b). The minimum length given to the West Specter Range fault is 10 km, which is the extent of faulting mapped by Anderson et al. (1995b). The preferred length, 19 km, extends this fault north across a small wash and south across Amargosa Valley. The maximum length, 25 km, extends the fault farther north up a crude linear valley and completely across the valley in the south. The slip rate is based on Anderson and et al.'s estimated maximum of 0.004 m/kyr. We adopt this as the preferred value and estimate 0.001 to 0.01 m/kyr for the minimum and the maximum slip rates. These values are identical to the values Anderson currently is using for his team's analysis (1997, this report).

Spotted Range Fault Zone

The Spotted Range fault zone represents a swarm of faults around the Spotted Range, the primary one of which was culled to represent the zone. This is the longest, most continuous fault of the group identified by Reheis (1992) and Piety (1995). This fault is a down-to-the-west, normal-slip fault that bounds the west side of a central ridge in the Spotted Range. Quaternary fault scarps and lineaments are indicated by Reheis (1992), supporting Quaternary activity. The minimum length of 17 km represents the central part of the fault, roughly the continuous expression mapped by Reheis. The preferred length,

30 km, extends the minimum to the south across a small wash and to the north along a series of discontinuous fault traces shown by Piety (1995). The maximum length is the same as the preferred because it is difficult to push the fault in either direction reasonably. Slip rates for this fault are difficult because of limited information. The minimum rate estimated, 0.001 m/kyr, is below the range of faults having no fault facets; the preferred value, 0.01 m/kyr, is typical of faults that have fault scarps and fault facets in the Great Basin; and the maximum value is 0.05 m/kyr.

Buried Hills Fault Zone

The Buried Hills fault zone generally bounds the west side of the Buried Hills and is a down-to-the-west, normal-slip fault (Reheis, 1992; Piety, 1995). The minimum length, 15 km, represent the central part of the fault zone as mapped by Reheis. The preferred length, 18 km, extends the minimum to the north and south along discontinuous fault traces. The maximum length, 25 km, extends the fault farther north along the southeast side of Papoose Lake flat. Slip rate estimates for this fault are difficult because of limited information. The Buried Hills themselves lack fault facets and have a relatively laid-back range front. Quaternary fault scarps and lineaments shown by Reheis (1992) are weakly to moderately expressed (Piety, 1995). The minimum slip rate estimated, 0.001 m/kyr, is below the range for faults having no fault facets; the preferred value, 0.01 m/kyr, is typical of faults that have fault scarps and fault facets in the Great Basin; and the maximum value is more than 0.05 m/kyr.

Northern Emigrant Valley Fault Zone

The Northern Emigrant Valley fault zone is made up of a swarm of more than 75 Quaternary fault scarps in the western part of an alluvial valley. The nature of the tectonism that gives rise to this pattern is uncertain, but it seems to be related or interconnected to adjacent faults in the surrounding hills. A few right-lateral offsets have been identified by Reheis (1992), suggesting that the pattern could represent the distributed expression of a lateral-slip fault. Because this system is more than 50 km from the site area, the exact mechanism of the fault is of lesser importance; thus, a right-lateral fault is assumed. The minimum length, 18 km, is the length of the main part of the fault swarm shown by Reheis (1992). The preferred length, 37 km, includes the fault scarps to the north and south. The maximum length, 45 km, considers possible extensions of the

fault in the Papoose Lake area, and a small extension to the north. Evaluating the slip rate of this swarm is difficult. The slip rate was assumed to be similar to the Rock Valley fault zone; we adopt the Rock Valley fault zone's slip rates, 0.01, 0.02, and 0.08 m/kyr, for the Northern Emigrant Valley fault zone.

Eastern Pintwater Range Fault Zone

The Eastern Pintwater Range fault zone is an east-side-down, normal-slip fault on the east side of the Pintwater Range (Dohrenwend et al., 1991; Reheis, 1992). Geomorphic expression along the Eastern Pintwater Range fault zone appears to be subtle, consisting of short fault scarps, lineaments, and abrupt alluvium/bedrock contacts. The minimum length, 28 km, is the central part of the fault zone. The preferred length of 36 km includes most of the range front that seems to be related to the fault. The maximum length, 57 km, includes the entire range front. The Eastern Pintwater Range fault zone appears to be near the threshold of geomorphic expression, specifically as regards fault scarps. The minimum slip rate, 0.001 m/kyr, is less than that for faults that have little expression. The preferred rate is 0.005 m/kyr, the middle value for faults with and without scarps. The maximum slip rate is 0.01 m/kyr, close to the rate of the Solitario Canyon fault.

Towne Pass Fault Zone

The Towne fault zone is a northwest-side-down, normal-slip fault that bounds the west side of the Panamint Range. This fault reportedly has weak Quaternary expression (Bryant, 1989; Reheis, 1991; Piety, 1995), although Bryant (1989) suggests that two beheaded drainages indicate latest Pleistocene to Holocene displacement. The Towne Pass fault locally is a prominent west-facing scarp in dolomite (Bryant, 1989) and may have some small fault facets. These, if they are facets, are highly eroded and occur only along small parts of the fault zone. The minimum length of the Towne Pass fault zone is 33 km, from the north end of the Panamint Range to the south end of the Holocene or latest Pleistocene activity indicated by Piety (1995). The preferred length of 38 km extends the fault a little farther south, to a point where the fault bifurcates, and most of the range-front expression is gone. The maximum length of 50 km includes the total mapped geologic fault, with some minor inferred faulting off the north end. There was little information for estimating slip rate, so we used a broad range, 0.005 to 0.1 m/kyr. This

rate places the fault zone between the threshold of faults that generally lack fault scarps and the point at which fault facets may be expected. The preferred value is 0.03 m/kyr.

3.3.2 Maximum Earthquake Estimates

Maximum earthquakes were estimated for the regional faults using empirical magnitude versus length, magnitude versus length and slip rate, and, in a few cases, magnitude versus maximum surface displacement relationships (Table SDO-2). All fault lengths given are the estimated maximum earthquake segment lengths for these faults. For regional faults that have multiple earthquake segments, only the closest segment was analyzed; in all these cases the other segments were too far away to have a significant impact on Yucca Mountain. A distribution of earthquake magnitudes also is considered for these faults down to the maximum background earthquake; these events are distributed randomly along the maximum earthquake segment. Different relations for magnitude versus length and magnitude versus maximum displacement were used for normal-slip versus strike-slip faults. All relationships are weighted equally, except that of Anderson et al. (1986). A concern about how well the data used by Anderson et al. compares to the southern Great Basin caused us to give this relationship a weight of one-third that of the other relations. A more extensive discussion of scaling relations for estimating maximum magnitudes and the associated input fault parameters in general is included in Section 3.4.2

The maximum magnitude evaluation assumed a similarity of structural style and expected geometry of regional faults throughout the areas within the same part of the southern Basin and Range province. Therefore, we assumed that they nucleated under similar stress field of extension. We considered, for example, unless there were contradictory data, that the faults have planar geometries from the surface to the depth of the maximum focal depths discussed earlier.

3.3.3 Recurrence

The occurrence of the maximum earthquake along regional faults is expressed by estimating the strain accumulation interval for the maximum event. The minimum, preferred, and maximum fault lengths are associated with an average surface displacement using relationships from Wells and Coppersmith (1994). This average displacement is divided by the fault slip rate, providing the slip accumulation time, which is considered to be the average recurrence

interval. This is then inverted for annual earthquake occurrence rate. Since there is significant uncertainty in making these kinds of estimations, the final weighting of the average earthquake recurrence intervals are set at the 10th and 90th percentiles for the minimum and maximum values, and hence a "0.3, 0.4, 0.3" weighting is used in a three-point discrete distribution. Slip rates were taken from or derived from the published literature where possible. Estimates generally were made by comparing faults having unknown slip rates with the structural and geomorphic characteristics of faults having known slip rates, and thereby making a comparative estimate of the potential slip rate for the former. For example, faults that have alluvial fault scarps but do not have facets tend to have rates around 0.01 m/kyr, whereas faults that have neither facets or scarps tend to have rates of 0.001 m/kyr or less (dePolo, in preparation). Although a more rigorous approach is desired, most of these faults have moderate to low slip rates and their impacts on the final ground motion values at Yucca Mountain are likely small. Slip rates are similar to the local faults at Yucca Mountain and, thus, can be compared with these relatively well-studied local faults. For the more active faults, results from field studies generally were available.

Earthquake occurrence rates for events smaller than the maximum earthquake are estimated by assuming a combination of characteristic and a truncated exponential distributions, weighted 0.7 and 0.3, respectively. For both of these models, it is assumed that the occurrence of earthquakes smaller than the MBE (magnitude 6.2) is addressed by the regional source zones. Therefore, the size of earthquakes occurring on the regional faults is limited to magnitudes greater than or equal to M 6.2.

The approaches used to evaluate maximum magnitude and recurrence for other regional fault sources were used to evaluate both the possible buried strike-slip faults and the Carrara fault. Fault parameters used to characterize these faults are provided in Table SDO-3.

3.3.4 Buried Strike-Slip Fault Sources

The question of a buried strike-slip fault in Crater Flat or beneath Yucca Mountain was introduced in Section 2.0 on Tectonic Models. Although there is direct evidence that dextral strike-slip has influenced the structural development of Yucca Mountain, there is insufficient data to characterize a single-plane strike-slip fault source, particularly one active in Quaternary time. There are two ways we dealt with the issue: one was to assume that a

strike-slip fault (after Schweickert and Lahren, 1997) passes beneath Yucca Mountain and that it will be undetectable until it generates an earthquake. We do not consider this a well-founded proposition; it precludes the use of many of the rational tools developed for the present evaluation, such as estimation of slip rate, estimation of recurrence, or parametric evaluation of magnitude. We have no means of assessing the likelihood that it could happen. Thus it cannot be treated the way we treat all the other fault sources.

A second way we deal with the issue of a buried strike-slip fault source is to build on the meager evidence we have. The pattern and history of deformation at the southern end of Crater Flat, including the alignment of basaltic volcanoes, the structure along the rampart that forms the southern end of Yucca Mountain and Crater Flat north of Highway 95, evidence of vertical axis rotation at Yucca Mountain, alignment and changes of fault and fault block geometry south of the hingeline, all suggest a zone of distributed dextral faulting. The hingeline represents a structural border to this zone, albeit a poorly defined one. It could indicate a buried fault or fault zone, or a series of linked faults of relatively small local displacement that die out to the northwest. We plausibly can characterize the hingeline as a strike-slip fault trace approximately 20 km long, having as much as a kilometer of cumulative offset. We plausibly can consider the hingeline as the northwest extension of the Pahrump Valley fault zone and, therefore, infer a maximum length of about 120 km and a cumulative lateral offset of at least 4 km for the inferred fault trace. However, our preferred length for such a fault projection is limited to its possible extent beneath Yucca Mountain and Crater Flat, 27 km.

The Pahrump Valley fault shows some evidence of Quaternary activity (Piety, 1995) but the hingeline projection does not. Therefore, we assign a slip rate to the inferred buried fault projection (0.005 m/kyr) and a probability of activity of 0.4. The important point about this buried fault is that it could generate a large earthquake external to Crater Flat that could propagate focused ground motion along strike into Crater Flat, perhaps triggering any number of faults at Yucca Mountain that are susceptible to slip. Because of the large degree of assertion and speculation involved in a multiple-fault scenario, we model only a single buried strike-slip fault. The hingeline seems to be the only candidate for a buried fault (in the sense that there is no recognized fault trace at the surface) that can be characterized by at least some of the basic fault parameters established for this analysis.

We assign a probability of 0.2 to the likelihood of a fault extending along the southwest side of Bare Mountain in Amargosa Wash (the Carrara fault proposed by D.B. Slemmons, oral commun.)(Figure SDO-6). No measurable evidence for such a fault is available; much of the area is covered by latest Quaternary alluvium. Plausible lengths range from 12 to 24 km. With no physical features on which to base an estimate of earthquake magnitude or recurrence, we have no means of arguing for either the existence of a fault or any seismogenic characteristics. We assign a provisional slip rate of 0.001 m/kyr to this hypothetical fault. This rate is so slow that surficial evidence, such as fault scarps, are generally lacking in the Great Basin.

3.4 LOCAL FAULT SOURCES

Local faults are those at Yucca Mountain and in Crater Flat. These faults are considered to be potential seismic sources on the evidence of Quaternary displacement; a number of these faults have been trenched to determine the amounts, recurrence, and ages of the Quaternary offsets. Local faults that have a history of Quaternary displacement are all normal to steeply left-lateral oblique (primarily west-dipping) faults. The faults are categorized, on the basis of length and cumulative offset, as block-bounding faults and intrablock faults. The block-bounding faults, which are the largest and most likely seismogenic, are inferred to descend through the seismogenic crust as more or less uniformly dipping, single plane faults, in keeping with our tectonic model. The intrablock faults tend to be curvilinear in plan, segmented or distributed, and only locally follow large slope breaks (i.e. have small paleo-offsets). This distinctive structural pattern is one of the primary reasons for invoking a carapace collapse effect in our preferred model. These latter faults may be confined to the volcanic carapace or linked to the block-bounding faults at relatively shallow depths. Of the numerous interconnected faults at Yucca Mountain (Figures SDO-7a, b), six are long enough to warrant consideration as penetrating the Paleozoic substrate. These six Quaternary faults are:

Paintbrush Canyon fault
Stagecoach Road fault
Solitario Canyon fault
Iron Ridge fault
Fatigue Wash fault

Windy Wash fault

Local fault parameters are listed in Table SDO-4, event scenarios are listed in Table SDO-5. All principal faults considered but the Iron Ridge and Fatigue Wash faults are considered block-bounding faults—faults that define major tilted panels of the carapace, and that are considered to penetrate to significant seismogenic depth without intersection. The Fatigue Wash and Iron Ridge faults are less confidently interpreted; the interpretations are discussed below. All local faults are considered 100 percent active, but some may be involved only in linked or distributed event scenarios (see Section 3.4.1 for further discussion of event scenarios).

Paintbrush Canyon Fault

Paintbrush Canyon fault is the easternmost block-bounding fault that cuts Yucca Mountain. It is distinguished by: (1) it coincides with the northern part of the gravity gradient that defines the eastern structural margin of Crater Flat basin; (2) it is the only Yucca Mountain fault that is continuously traceable north of Yucca Mountain, deep into the unextended caldera rim terrane (a maximum distance of about 12 km north of Yucca Wash); and (3) the footwall consists of segmented, variably tilted and dissected buttes or ridges, rather than the more or less coherent rotated panel typical of Yucca Mountain to the west, and the hanging wall is broken by horsts and graben and numerous splay faults. Despite this evidence of major fault displacement and a broad zone of fault damage, the Paintbrush Canyon fault is poorly exposed south of Paintbrush Canyon. Along Yucca Mountain, it lies buried along the east side of Midway Valley; it is questionable whether the main break has been observed or is anywhere exposed south of Yucca Wash. Estimates of down-to-the-west displacement of Tertiary volcanic strata range from 250 to 500 m (Lipman and McKay, 1965; Scott and Bonk, 1984). Average dip on the fault plane is about 70 degrees west, and slip along it has been left oblique (Simonds et al., 1995). We divide the Paintbrush Canyon fault into two segments, a segment that extends along Paintbrush Canyon north of Yucca Wash (PC(N)), and a segment that extends along the east side of Midway Valley south of Yucca Wash (PC(S)). The preferred length of PC(N) is 6 km, and of PC(S) is 12 km. We add 2 km from the south end of Busted Butte to establish linkage with the Stagecoach Road fault, for a total maximum length of 20 km (the maximum total length is 26.3 km if we carry PC(N) as far north as seems reasonable). Paleoseismic studies at three sites—natural exposures of sand ramps on the west

side of Busted Butte and one trench each at Fran Ridge and Alice Ridge--indicate that multiple Quaternary displacements have occurred. As many as five faulting episodes may have occurred during earlier Quaternary time (Seismotectonic Framework Report [USGS,1996]). Measurements of net slip displacements vary widely among individual events and from one study site to another, with values ranging from 28 to 167 cm for a single Quaternary event. Cumulative Quaternary displacement ranges from 1.7 to 7.8 m locally. Age determinations for the various events differ from one site to another, with the most recent event ranging from 5 to 90 ka and the next youngest ranging from 70 to 150 ka. Values of recurrence intervals based on the combined age data for all three study sites range from 21 to 118 ky. Our preferred slip rate for the entire fault is 0.008 m/kyr. The slip rate is a mid-Pleistocene rate inferred from the exposures at Busted butte. Menges (Seismotectonic Framework Report [USGS,1996]) estimates the offset at the base of the strata there as 5.22 m to 7.62m; an approximate mean value of 6.4 m is used for the preferred value. The age of the base of these sediments is interpreted to be about 740 ka, based on exposure of the Bishop ash.

Stagecoach Road Fault

The minimum fault length, as mapped by Simonds (1995) from Stagecoach Road south, is 4.5 km. However, if we extend it north to join the Paintbrush Canyon fault near the south end of Busted Butte, and extend it south to the dissected escarpment near Wells Cone, the maximum inferred length is 11 km. We take it to the most southerly mapped fault scarp for a preferred distance of 9 km. The minimum segment is expressed as discontinuous scarps in mid-Pleistocene alluvium; the south end of this trace is concealed by undeformed Holocene sediment. Alluvium of late Quaternary age is displaced 1.0 to 2.3 m; slickensides indicate chiefly dip slip. Bedrock displacement is estimated to be 400 to 600 m down-to-the-west (Scott, 1990). Average dip is 73 degrees west. Trench excavations display evidence for three to seven episodes of Quaternary faulting (Seismotectonic Framework Report [USGS,1996]). The two youngest events have been dated at 5 to 15 ka and 20 to 30 ka, respectively. Two earlier events may have occurred in late Pleistocene time, the oldest about 110 ka. The age relationships indicate preferred values of recurrence intervals in the range of 10 to 35 ky, and slip rates of 0.0057 to 0.028 m/kyr. The slip rates are calculated from data reported in the Seismotectonic Framework Report (USGS,1996) for trench SCR-T3. Here, our inferred

range of dip-slip offset is 0.67 m to 2.7 m, corrected for hanging wall rollover. The offset unit, G2, has a U-series date of 108 ± 10 ka.

Solitario Canyon Fault

The Solitario Canyon fault is a block-bounding fault that defines the west side of the potential repository block. Displacement along most of the fault trace is down-to-the-west, with offsets of more than 500 m. Average dip of the fault plane is 72 degrees west. At the north end, the fault dips east, and displacement is 61 m down-to-the-east (Scott and Bonk, 1984). From a north terminus on the south flank of Yucca Wash on south to the hingeline, it is a well-defined fault zone 14.8 km long. Farther south, it loses topographic definition and splays into three or more faults that distribute the total displacement (W. Day, USGS, written commun., 1997). South of the hingeline, the main fault trace may regather and strike west of south to join up with the Windy Wash fault (Day et al., unpub. map); or it may trend east of south and merge with the Stagecoach Road fault. On the basis of aeromagnetic data, we infer that it becomes a buried fault--possibly a graben-bounding fault--that continues south, parallel to the Stagecoach Road fault, for a maximum length of 21.5 km. Our preferred length is 18.5 km for Stagecoach Road fault linkage option, based on mapping by Simonds (1995). The fault appears to become more shallow in dip and more zonal in general as it extends south from the elevated area of the Prow, exposing more footwall on strike. Opposite the potential repository block, the footwall includes an attenuated slice 3.5 km long and about 200 m wide broken by complex scarps and local faults. The slice is sampled by trenches T4 and T5. The character of the main fault trace is unclear along this segment. Eleven trenches and one natural wash exposure have been excavated across or near the Solitario Canyon fault, exposing evidence that suggests as many as four paleoseismic events dated at 20 to 30, 70 to 80, 120 to 250, and 150 to 250 ka, respectively, took place along the fault (Seismotectonic Framework Report [USGS, 1996]). There is also indication that two episodes of fracturing postdate the most recent event; these fracturing episodes are interpreted as being associated with moderate-sized earthquakes on the Solitario Canyon fault or with earthquakes on nearby or regional faults. Characteristics of the affected surficial deposits suggest that the fractures developed in Holocene and/or latest Pleistocene time. A recurrence interval of 35 ky is considered a minimum (two events within the past 70 to 80 ka and four within the past 150 ka). Estimates of cumulative displacement over 150 to 250 ky range from 1.8 m (from

scarp measurements and trench logs) to 2.6 m (from trench logs). Our preferred average slip rate for the fault is 0.015 m/kyr, based on a preferred soil correlation age of 200 ka.

Iron Ridge Fault

The Iron Ridge fault is what Day et al. (written commun.) term a relay fault. Its minimum (and preferred) length of 8.3 km spans the distance between its juncture with the Solitario and Stagecoach Road faults. However, the Iron Ridge fault is well defined only along the western edge of Iron Ridge. The north and south termini are frayed out for a kilometer or more along strike; and it is possible that, at the south end, the main trace projects south to merge with the (buried) Solitario Canyon fault. If so, this gives a maximum length of 10 km. However, Iron Ridge is terminated at the hingeline, where the fault jogs east for a kilometer, around the nose of the truncated ridge, bringing the ridge-bounding fault trace within 500 m of the Stagecoach Road fault. For half its length, the Iron Ridge fault forms a bedrock-alluvial contact with prominent scarps. Displacement is chiefly dip-slip, down to the west on a fault plane that dips 70 degrees. At least one locality shows multiple late-Quaternary faulting (Simonds et al., 1995). The Iron Ridge fault is a complex and damaged zone of normal faults that have numerous splays and flare-off fractures (including the Abandoned Wash fault). As such, it simply may be the most prominent of a wide zone of linked-bridging faults that have formed in response to extension and left-lateral shear between the Solitario and Stagecoach Road faults. Its seismogenic significance is questionable; it may be confined to the carapace (minimum width of about 2 km) or at least not extend deeply into the Paleozoic substrate as a single-plane (about 5 km). Ramelli (1996, written commun.) estimates 2 m of offset has occurred since mid-Quaternary, but considering erosion over this time, the offset could range from 1.7 m to 2.2 m. Ramelli correlates the offset unit with deposits that make up the Solitario surface of Peterson et al. (1995). This surface ranges in age from 433 ka to 730 ka. To calculate our preferred slip rate (0.0033m/kyr) we chose a mid-point age of 600 ka. Smaller displacements (0.5, 0.7, 1 m; Table SDO-5) are reported from trench SCF-T2 observations (Seismotectonic Framework Report [USGS,1966]).

Fatigue Wash Fault

The Fatigue Wash fault is a north- to northeast-striking, down-to-the-west normal to steep oblique fault located about 3.5 km west of the potential repository. From its south merger with the Windy Wash fault to a possible northern merger with the Windy Wash fault at the

south end of West Ridge, it has a minimum length of 12 km. It also could be carried north along a deep notch that defines the east side of West Ridge to the Prow, where it frays out in a plexus of normal faults and graben. The longest trace through this area takes it into the caldera rim zone, for a maximum length of 22 km. We prefer 18 km because of uncertainty in the north termination. The Fatigue Wash fault is remarkably parallel to the Windy Wash fault, which lies only about a kilometer to the west, along the west flank of West Ridge. It probably is not a major fault despite its considerable length. Its geometry and association with bridge faults to the Windy Wash fault suggests that the Fatigue Wash fault is either: (1) one or more linked slices of the footwall of the Windy Wash fault, formed in response to Windy Wash faulting, or (2) a parallel subsidiary fault that merges with the Windy Wash fault beneath the carapace. The fact that Fatigue Wash fault merges with the south Windy Wash fault strongly implies that the Northern and Southern Windy Wash faults are indeed a single continuous fault, or at least linked faults, the middle (linking) part of which is buried but which apparently forms a graben in association with the Fatigue Wash fault in the vicinity of the hingeline. Average dip of the fault plane is 73 degrees, and displacement is about 72 m (Scott and Bonk, 1984). Three to six paleoseismic events (five being the preferred number) are documented by the stratigraphic and structural relations exposed in two trenches excavated in Quaternary deposits along the fault trace. Four of the preferred events occurred after 730 ka. The two most recent events probably took place between 20 to 70 ka, suggesting a late-Quaternary clustering of earthquakes. An estimate of the long-term average recurrence interval ranges from 120 to 250 ky, with a preferred value of 185 ky. Two meters of cumulative vertical displacement during the last four events indicate a Quaternary slip rate of 0.002 ± 0.0001 m/kyr. Data from measurements on scarps outside the trenches indicate a greater Quaternary slip rate of 0.009 ± 0.006 m/kyr (Seismotectonic Framework Report, [USGS, 1996]). Offsets at trench SP5 were measured by projection of intact correlative surfaces to give values of 2.8 and 3.9 m of normal displacement. A minimum value of 2.5 m of vertical separation is estimated based on uncertainties of scarp measurement and surface projection. The fault scarp is developed in the Solitario surface of Peterson et al. (1995) which is estimated to have an age range of 433 ka to 739 ka, with a preferred age of 600 ka.

Windy Wash Fault

We consider the north-striking Windy Wash fault to be a segmented or linked block-bounding fault. The north strand extends from the Prow south for 9 km. It can be carried north of the

Prow into the caldera rim zone an additional 2 km, but we prefer a length of 9 km to accommodate the uncertainties. The south strand extends south from trench CF2 for 8 km as a well-defined fault trace (Simonds et al., 1995). It can be carried farther south by linking scarp segments for a preferred length of 11.5 km. If we carry it north of trench CF2 (along an east-facing scarp; Simonds, 1995), we obtain a maximum length of 12.5 km. The total maximum length of the linked north and south segments is about 24 km. Apart from the central, down-to-the-east scarp in alluvium, the fault has down-to-the-west displacement of a few hundred meters (Scott, 1990). Average dip of the fault is 63 degrees to the west, and offset is chiefly dip slip; but locally both right and left oblique slip have occurred. Evidence of Quaternary displacement is limited to subtle scarps in alluvium and to fractures in hanging walls of fault line scarps. Three trenches were excavated across scarps in alluvium along the central part of the fault (Seismotectonic Framework Report [USGS, 1996]). One trench displays evidence of eight coseismic surface ruptures during Quaternary time; the other two display evidence of five ruptures. Mid- to late-Pleistocene gravel in one trench is displaced about a meter down-to-the-west, and Holocene silt above the main fault plane is ruptured. Dating of soils and fine silt deposits indicates that the surface faulting along the Windy Wash fault took place about 3, 40, 75, 150, 200, 240, 340, and 400 ka (preferred values or mid-points of the ranges of event timing). The recurrence interval of faulting for the last four events is about 40 to 50 ky, and between 50 to 57 ky for the longer record; the preferred recurrence interval is 40 ky. Total net displacement on the oldest hanging wall deposit is 3.67 m with an uncertainty of ± 0.3 m. U-series ages constrain the offset unit to be at least 300 ka old, and as much as 400 ka (USGS Seismotectonic Framework Report, 1996), indicating a long-term average slip rate ranging from 0.009 to 0.017 m/kyr. Displacements measured in trench CF-2 are 0.6 m to a maximum value of 0.88 m (Seismotectonic Framework Report [USGS, 1996]). A 1 m offset is proposed on the basis that the trench may not be sited at a point of maximum displacement.

In addition to the faults described above, several other faults at the site may penetrate the carapace, but in our evaluation these are capable of generating maximum earthquakes only at or below MBE levels of moment magnitude 6.4 ± 0.2 ; thus, these faults are considered to be covered by the background seismicity. Several of these faults are used in the linked and distributed event scenarios developed for this analysis. These include the Bow Ridge, Ghost Dance, Abandoned Wash, Northern Crater Flat, and Southern Crater Flat faults. Although

these faults are considered not capable of individually generating an earthquake larger than the maximum background, by virtue of linkage or distributed connections they may make a small contribution to some of the earthquake scenario parameters.

Bow Ridge Fault

The Bow Ridge fault has been called a block-bounding fault (W. C. Day, written commun.), but little is known about it except that it is a largely alluvium-covered, north-striking, west-dipping normal fault that lies along the east side of the potential repository block for a length of 7 km. It is exposed only along the west side of Bow Ridge and Exile Hill (site of trench 14) and in the ESF. Structure at Bow Ridge is complex, marked by breccia and small graben; a throughgoing fault that defines the arcuate scarp face of Bow Ridge is strongly suggested. Its shape and bounding structure imply that the Bow Ridge fault, as an inferred single-plane fault, arcs abruptly east to merge with the Paintbrush Canyon fault. However, the Bow Ridge fault may simply represent an assemblage of variously striking fault segments, all part of hanging wall damage associated with the Paintbrush fault. The fault is defined in places along the west side of Exile Hill by a fault line scarp and a bedrock-colluvium contact (Simonds et al., 1995). Here, Tertiary volcanic rocks show about 125 m of down-to-the-west displacement along a 65- to 75-degree, west-dipping, left-oblique fault plane. North of Isolation Ridge, the Bow Ridge fault has east-side- down displacement. A series of trenches has been excavated to reveal a complex fault zone developed in highly fractured Tertiary volcanic rock and Quaternary colluvial deposits. Several faulting events are evident in the surficial units, the oldest more than 700 ka and two younger events 130 to 150 ka and 30 to 130 ka, respectively. A minimum age of 48 ± 20 ka is established for the youngest displacement. Cumulative dip-slip displacement of the Quaternary deposits ranges from 30 to 45 cm (considering an oblique slip component, net slip is 33 to 70 cm). Preferred values for average recurrence intervals of faulting events range from 100 to 140 ky. Slip rates range from 0.002 to 0.007 m/kyr, with a preferred value of 0.003 m/kyr.

Ghost Dance Fault

The Ghost Dance fault strikes north through the central part of the repository block between Wren Wash on the north and Abandoned Wash on the south, a distance of 3.7 km. The fault is not exposed as a single-plane feature, but consists of three right-stepping segments. The north segment is 660 m long; it extends south to Split Wash, is 2 to 4 m wide, and has as

much as 6 m displacement down-to-the-west. The central segment is 450 m long; it extends from Live Yucca Ridge to Antler Ridge, forms a zone of breccia-filled splays from 1 to 2 m thick over a zone as much as 150 m wide, and has as much as 20 m down-to-the-west displacement. The south segment is 830 m long; it extends to Broken Limb Ridge, forms a breccia zone as much as 55 m wide, and has about 27 m of down-to-the-west displacement. Near Broken Limb Ridge, the fault bifurcates, the most prominent and continuous branch extending southwest for 1.5 km to apparently link with the Abandoned Wash fault of Scott and Bonk (1984) at Abandoned Wash. The Ghost Dance fault does not physically connect with the Abandoned Wash fault; it more or less comes into alignment with the local slip planes that comprise the north extent of the Abandoned Wash fault (W. C. Day, USGS, written commun.).

The amount of brecciation and offset along the Ghost Dance fault decrease in the vicinity of the ESF and Ghost Dance Wash (a 2- to 15-m wide breccia zone; 3 to 6 m of offset); but displacement increases with proximity to the Abandoned Wash fault (as much as 17 m). Throughout its length, the Ghost Dance fault ranges in dip from vertical to 75 degrees west and is characterized by one or more breccia zones of variable thickness. The breccia typically is uncemented or an open fretwork that shows little or no evidence of size or shape segregation or milling due to shear. The Ghost Dance fault has no aeromagnetic signature and only small, low-amplitude gravity lows along the hanging wall (Potter et al., written commun.).

Four trenches have been excavated in Quaternary sediment across projected traces of the Ghost Dance fault, but no offset of any of these deposits has been observed. In one trench, for example, 40 to 50 cm of unfaulted latest Pleistocene to early Holocene (age 82.8 ± 1.9 to 9.6 ± 0.1 ka) slope-wash colluvium and fine-grained eolian deposits can be seen to overlie faulted and fractured tuff. A discontinuous fracture, however, was observed in a highly calcified horizon draped over bedrock in one trench; but it does not extend upward through the overlying units. Age relations suggest that the fracturing must have occurred at least 82 ka; the fracture may have resulted from a seismic event on any number of faults in the area. The non-integration of the fault segments along strike; the brecciated, zonal character and the poorly defined, fayed fault terminations; and the lack of shear tooling or shear segregation within and along the fault breaks, all indicate that the rock broke with minor offset during a

single, short-lived failure event and has not undergone subsequent deformation that might have modified the initial damage.

We interpret the Ghost Dance fault as a tear fault confined to the carapace. It is considered to have resulted from clockwise torque and bending applied to the central block during the initial to peak phase of vertical axis rotation. Potter et al. (written commun.) deduce that the right steps may be controlled by pre-existing sets of closely spaced, northwest-striking cooling joints. Because the Ghost Dance fault is a relic of ancient tensile failure and has virtually no cohesive strength, it is a locus of tensile strain for overlying cohesive strata and likely will remain so as long as extension dominates the stress regime at Yucca Mountain.

Abandoned Wash Fault

The Abandoned Wash fault is essentially a 6-km-long zone of small normal faults and horsts and graben of negligible offset that connects the Ghost Dance and the Solitario Canyon faults. It probably is structurally and genetically akin to the Ghost Dance fault and is confined to the carapace. Its presence is marked by deep erosion. Where it crosses ridge divides and especially at its junction with the Solitario Canyon fault, there is little geomorphic indication of offset.

Northern Crater Flat Fault

The Northern Crater Flat fault is a poorly defined structure that appears to consist of aligned horsts and graben in a zone about 600 m wide. Dominant displacement is down-to-the-west normal or normal oblique. It trends north to northeast along the east side of Crater Flat, about 5 km west of the potential repository. As mapped (Simonds, 1995), the maximum length is about 12 km. It terminates to the south at the hingeline and frays out to the north among normal faults within the caldera rim zone. Its location implies that it is antithetic to Bare Mountain fault; hence, we infer a relatively small fault width. Only one of the two trenches excavated across the center of the projected trace of the fault intersected the fault. Stratigraphic and structural evidence for as many as five paleoearthquake events was observed in this trench. On the basis of a minimum age of 500 ka for the oldest exposed Quaternary unit and an estimate of less than 10 ka (preliminary age date of 5.46 ± 1.4 ka) for the most recent faulting event, a possible range in average recurrence interval is 120 to 160 ky.

Cumulative displacement for all five events is about 160 cm, indicating a slip rate of 0.003 m/kyr since the earliest event.

Southern Crater Flat Fault

The Southern Crater Flat fault is a north- to northeast-striking, normal fault that is down to the west, and has a left-slip component. It is defined by a basalt-alluvium contact, fractured carbonate-cemented alluvium, subtle scarps in alluvium, and a linear stream channel (Simonds et al., 1995). North of trench CFFT1, the fault trace is subtle. It projects toward convergence with the north end of the Southern Windy Wash fault. Alternatively, the north end of the Southern Crater Flat fault could be offset 1.5 km east of the Northern Crater Flat fault by slip along the hingeline. The Southern Crater Flat fault can be traced south for a maximum of about 15 km. The minimum length, as mapped by Simonds et al. (1995), is 6 km. The amount of offset is unknown; slickensides on a plane that dips 70 degrees indicate left-oblique movement. Two trenches were excavated across the Southern Crater Flat fault, exposing alluvial gravel deposits that contain accumulations of fine-grained aeolian material. There is evidence that at least three paleoseismic events occurred during the Quaternary, for a total measured offset of 24 to 65 cm. Preliminary age determinations of the alluvial materials and of opaline silica collected from the inner rinds of clasts indicate that the oldest event occurred 130 to 250 ka, the next 10 to 60 ka, and the youngest 2 to 6 ka. Minimum recurrence intervals are in the range of 5 to 60 ky, the estimated maximum vertical slip rate is 0.002 m/kyr.

3.4.1 Event Scenarios: Single Faults, Linked Faults, and Distributed Faults

For local faults, three types of maximum earthquake models, or scenarios, are considered: single fault, linked fault, and distributed fault scenarios. Single-fault scenarios are given for the six local (i.e., Yucca Mountain) faults identified for this analysis (Figure SDO-7a).

Linked-fault scenarios were developed by considering direct structural linkages and indications of potential event correlation between adjacent faults (Figure SDO-7b).

Earthquake lengths are based on the end-to-end length of the combined fault plane segments. Distributed-fault scenarios involve parallel faults that slip together. For distributed fault scenarios, maximum surface displacements are combined in a cross-strike fashion, and lengths may or may not be increased over single-fault scenarios. All event scenarios, individual fault, linked faults, and distributed faults, are presented in Appendix SDO-1. Six faults are

involved, and one (Paintbrush Canyon) has two earthquake segment alternatives. Thus, there can be seven individual fault scenarios. Nine combinations of faults are modeled for the linked scenarios (Figure SDO-7b), and eight combinations of faults are modeled for the distributed fault scenarios. The relative weighting of each scenario is expressed in the occurrence rates given in Appendix SDO-1; the generation of these occurrence rates is discussed in section 3.3.3 on earthquake recurrence.

3.4.2 Fault Source Parameters for Maximum Magnitude

Fault source parameters are the basic, quantitative components needed to estimate the maximum earthquake a mapped fault is capable of generating. We estimate maximum earthquake magnitudes on the basis of as many parameters as possible to mitigate the uncertainties inherent in any individual parameter. An attempt is made to capture the uncertainties of the input values by using minimum and maximum values along with preferred values; various observational uncertainties are considered to be accounted for in empirical relationships relating fault parameters to magnitude. We consider the fault parameters we measure at the surface to be representative of the seismogenic structure at depth. For each scaling parameter, either an empirical relationship or an equation is used to scale magnitude from the input parameters. For the final value, we averaged the results for our magnitude estimates.

Using multiple magnitude estimation techniques provides the epistemic uncertainty to the final value. To characterize some of the aleatory uncertainty that also exists, each final value is considered to have an uncertainty of ± 0.25 magnitude units. This is a comparable value to the standard deviations of the regressions used to scale earthquake magnitude.

A logic tree (Figure SDO-8) was designed on the simplest sequence of parameter decisions necessary and justified by the data. The sizes of potential maximum earthquakes were scaled using fault length, fault width, maximum surface displacement, length times maximum surface displacement, fault area, length and slip rate, and calculations of seismic moment. Measured values are ordered in our assessments (Table SDO-4) and weighted on the basis of the uncertainties we assess for each parameter. The bases of the various input parameters are discussed in the respective subsections that follow.

Geometry of Planar Normal Faulting

We recognized the sparcity of data on the geometry of active normal faults for the Yucca Mountain region and decided to use data from studies of normal faulting earthquakes from other areas of the Basin-Range province as well as the focal mechanism data provided at the YMPHSA workshops by Ken Smith (1996, 1997) of the University of Nevada and the earlier research on the seismicity of southern Great Basin, including the Yucca Mountain area (Rogers et al., 1991). We also studied the data of Doser and Smith (1989) who summarized the geometry of historic normal faults and used focal mechanism data for both short and long period arrivals, source mechanisms from seismic moments and from geologic and related geodetic information.

We also referred to published working models of large Basin and Range-type normal faulting earthquakes from Smith and Arabasz (1991). These include three of the largest earthquakes in the western U.S. that had dominantly normal-faulting slip: Ms 6.8 Dixie Valley, Nevada, earthquake of 1954; the Ms 7.5 Hebgen Lake, Montana, earthquake of 1959; and the Ms 7.3 Borah Peak, Idaho, earthquake of 1983.

The primary characteristics of these large earthquakes include rupture on planar normal faults, dipping 40° to 60° , nucleation at mid-crustal depths of about 15 km, and no evidence from the seismic data of non-planar geometries.

Estimates of fault dip are based on studies of the most modern (since 1954, when well-recorded seismic data became available) historical, scarp-forming normal-faulting earthquakes as analogs. We chose 50° , 60° and 75° as our distribution of likely dips. Our rationale for these values is based on the minimum dip of 49° for one of the 1959 Hebgen Lake, Montana, main shock segments, including an error of 10° . We assigned 60° the greatest weight because this is a typical mid-value for the dips of earthquakes in the Basin and Range province (e.g., Doser and Smith, 1989, their figure 4) and it is commonly measured surface dip throughout the province. It was determined using the most modern methodology and with the widest variety of instrumentation, short-and long-period data; several authors found a similar geometry (Richins et al., 1985; Doser and Smith, 1985; Stein and Barrientos, 1985; Nablek et al., 1990). The upper bound value of 75° was used because it is considered a bound of the steepest dips of historical earthquakes from seismic data, such as the $78 \pm 5^{\circ}$ dip of the 1954

Rainbow Mountain, Nevada, earthquake. Also, this highest value is near that for steeper normal surface faulting of these normal-faulting events of approximately 90° . The estimates of dip are also closely constrained by field measurements made during mapping of Yucca Mountain and observations made from logging the ESF. Data from fault mechanism solutions for nearby earthquakes, notably from that of the 1992 Little Skull Mountain earthquake, also guided our estimates. Our observation, supported by regional data, is that steep dips measured in outcrop tend to decrease to moderate dips at seismogenic depths.

Alternative Models

We considered low angle and listric fault geometries as possible seismogenic structures. But because of the global lack of unequivocal data on focal mechanisms of large, scarp forming normal faulting earthquakes having dips less than $\sim 40^\circ$, we did not consider the shallower fault dips for earthquake source at Yucca Mountain. That is not to say that low angle and listric faults do not exist in the Yucca Mountain region, but we consider that if they are present, they are not now seismogenic and were generated in an earlier tectonic regime. Hence, we do not appeal to detachment faulting as a tectonic model for fault behavior.

Fault width refers to the downdip dimension of a fault. Unless otherwise noted, we consider the width to be the seismogenic depth, taking into account the fault dip (i.e., the seismogenic depth divided by the sine of the fault dip).

Magnitude versus fault length. Estimating magnitudes on the basis of fault length is a conventional approach for all fault sources. Three lengths are estimated: the minimum, preferred, and maximum. Because many of the faults at Yucca Mountain are short relative to depth of the seismogenic crust, these lengths are considered to correspond to earthquake segments. Two regressions are used as scaling relations to estimate moment magnitudes: Mason (1996) and Wells and Coppersmith (1994). These relations are shown in Table SDO-2. Mason's relationship is based on earthquakes from extensional environments; Wells and Coppersmith (1994) use a worldwide data set of normal to oblique-slip earthquakes.

Magnitude versus maximum surface displacement. Because single-event surface displacements are available from the many trenches involved with this project, the opportunity exists for estimating earthquake magnitude based on surface displacement. Many of the

displacements are small (less than a meter). Several trenches appear to be located such that the maximum surface displacement would have been recorded, but this is speculation, and local situations that would diminish surface rupture could prevail. There generally were only a few points of information along any one fault, and information commonly varied at each site. Only a few faults appeared to have documentable modes of rupture that might be inferred as average surface displacements. Many of the paleoevents at the sites have displacements of a few decimeters to a meter, and surface manifestation, after such rupture works its way through the volcanic carapace, may be attenuated up dip, broken up and discontinuous at the surface, and/or widely distributed between faults. Estimates of maximum surface displacement could be made and bracketed, however, using maximum single-event displacements from the trenches, or the maximum displacements for an event from different trenches. For distributed ruptures, displacements for the same event are added in a cross-strike manner to obtain a maximum surface displacement of the event.

As with fault length, two regressions are used to scale earthquake size as a function of displacement, one by Mason (1996), and one by Wells and Coppersmith (1994). These relations are shown in Table SDO-2. Mason's relationship is based on a data set using earthquakes from extensional environments. Wells and Coppersmith use a worldwide data set. Mason's regression uses surface-wave magnitude, which is assumed to be equal to moment magnitude (see discussion in Wells and Coppersmith, 1994). Wells and Coppersmith's regression is in moment magnitude.

Magnitude versus fault length x maximum surface displacement. Mason (1996) developed a regression for magnitude versus fault length times maximum surface displacement, which provides a parameter that more closely estimates seismic moment than either of the base parameters individually. Both fault length and maximum surface displacement are determined as discussed above and simply are multiplied. Mason's regression uses surface-wave magnitude, which is assumed to be equal to moment magnitude (see discussion in Wells and Coppersmith, 1994).

Magnitude versus fault area. Fault area is estimated from two parameters, fault length and downdip width. Fault area also affords a closer estimate of seismic moment than does a single parameter. However, the fault areas used in magnitude-scaling relationships typically are

derived from aftershock data, so there is a large uncertainty in the resulting values. For example, many of the minimum downdip widths of faults are significantly limited by intersections with other faults. This limitation was added to the information constraining earthquake sizes by using the magnitude versus fault area relationship and by calculating seismic moments. Fault areas are calculated using the estimated fault lengths and downdip widths, and magnitudes are scaled using Wells and Coppersmith's (1994) regression, acknowledging the error produced by the lack of internal consistency (fault area versus aftershock area). Downdip widths were estimated considering maximum dynamic seismogenic depth, ranges in fault dips, and possible structural intersections.

Magnitude versus length and slip rate. Anderson et al. (1996) developed a magnitude-scaling relationship that includes fault slip rate and fault length. Their approach is based on observations that, for a given length, faults having lower slip rates or faults having longer recurrence intervals tend to have larger earthquakes. Although the method is controversial, it builds on the previously established observation that earthquake size has a dependency on earthquake return time (e.g., Kanamuri and Allen, 1986) and tectonic environment (Scholz et al., 1986). Wesnousky (1986) sorted magnitude versus fault length data into high and low slip-rate categories and regressed them separately to account for the potential effects on slip rate. Unfortunately, several of the faults in the Yucca Mountain area have slip rates lower than the data used in Anderson et al.; thus, the overall technique is given a third of the weight of other, more established, approaches.

Magnitude versus seismic moment. Seismic moments are estimated using fault area times average subsurface displacement times shear rigidity. Shear rigidity for the seismogenic zone is taken to be 3×10^{11} dynes/cm². Average subsurface displacements are considered to be half the maximum surface displacement. This ratio was chosen after examination of Figures 6 and 7 of Wells and Coppersmith (1994) and considerations that D.B. Slemmons articulated during the January 1997 Probabilistic Seismic Hazards Analysis Workshop. Slemmons suggested that new studies will indicate that average subsurface displacements will be found to be about 38 percent of maximum surface displacements. Wells and Coppersmith (1994) find a mode of this ratio from 44 earthquakes to be 0.76. We use the rough average of these two ratios, 50 percent.

3.4.3 Recurrence

The assessment of earthquake recurrence for the local fault sources is based on the interpretation that all three types of rupture scenarios (individual ruptures, linked ruptures, and distributed ruptures) can occur. These data are interpreted to define the frequency of maximum events for each type of rupture behavior. The recurrence rates for "maximum" earthquakes are defined using the procedure described below. In constructing the recurrence relationships we follow the convention of Youngs and others (1987) and consider that the maximum magnitude earthquake assessed above is the central estimate of a "characteristic" magnitude interval. For the characteristic and maximum moment recurrence models discussed below, the characteristic events are uniformly distributed in the magnitude range $M_{\max} \pm 1/4$, such that the upper limit of the recurrence relationship is $M_{\max} + 1/4$. For the exponential recurrence model the upper limit is also set at $M_{\max} + 1/4$. Thus, the frequency of "maximum" earthquakes is interpreted to be the frequency of earthquakes of magnitude greater than or equal to $M_{\max} - 1/4$. This frequency is interpreted to be the frequency of earthquakes within 1/2 magnitude unit of the maximum magnitude earthquake defined for each type of rupture behavior. For the individual fault rupture scenarios, the frequency of earthquakes smaller than the maximum magnitude minus 1/2 magnitude units are estimated using either a characteristic or truncated exponential recurrence model, weighted 0.7 and 0.3, respectively. Our preference for a characteristic model is based on the observation that paleoearthquake displacements exposed in the trenches at Yucca Mountain demonstrate repeated offsets of about a meter. However, we do not discount the observation that the historical seismicity of the southern Great Basin may have a truncated exponential distribution. The linked and distributed rupture scenarios are interpreted to be larger earthquakes that occur in addition to the individual rupture scenarios. Thus we allow for only these events to occur. As was the case for the regional sources, the size of earthquakes occurring on the local faults is limited to magnitudes of 6.2 and larger. The occurrence of smaller earthquakes is addressed by the regional source zones.

The relative frequency of each type of rupture behavior is estimated from the recorded paleoseismic data. If there have been n paleoearthquakes on fault x , then we have n observations of the fault's behavior. The number of times that it has ruptured as a single fault versus the number as a linked or distributed fault define the relative frequency of these types of behavior. Because of the uncertainty in assessing what type of behavior actually occurred

in each paleoevent, we assess the relative likelihood (or probability) of the various types of behavior that might have occurred for each event. Averaging these over all of the paleoevents provides an assessment of the expected relative frequency of each type of event. These relative frequencies are then multiplied by the overall frequency of events on the fault to define the actual frequency of occurrence of each type of behavior.

This type of analysis is motivated by the desire to incorporate as much of the extensive paleoseismic data set that has been developed at the Yucca Mountain site as possible. To be as clear as possible about this analysis, we have broken it up into steps, which are described individually in the following subsections, and an example is illustrated in Figure SDO-9. This analysis tracks earthquake occurrence rate (events/year) rather than recurrence intervals.

Analysis step 1 determines the occurrence rates of earthquakes along the principal local faults. Three techniques were used to determine the occurrence rates for the faults, a moment rate technique, an average earthquake recurrence interval technique, and an average interseismic interval technique.

The moment rate technique uses the various fault lengths, down-dip widths, and slip rates to generate a moment rate ($MR = LWS\mu$, where MR = moment rate, L = length, W = down-dip width, S = slip rate, and μ = shear rigidity [3×10^{11} dyne/cm²]). Slip rates were determined using total offsets from trench logs and the estimated time since those offsets ($S=O/T$; S =slip rate, O = offset, T = time). Uncertainties in slip rates are calculated by cross multiplying the range in possible offset and dating uncertainties. The seismic moment was calculated using preferred values. Using the full range in moment estimations produced unreasonable results for occurrence rate. Thus, the maximum and minimum values were obtained by use of the preferred parameters, but considering the maximum and minimum displacement values. The seismic moment estimated for the fault is divided by the moment rate to obtain the recurrence interval for events. This interval is inverted to get occurrence rate.

The average earthquake recurrence interval technique is estimated by taking the age of the oldest reported paleoseismic event and dividing the age by the number of events that have occurred since, minus the most recent event. Since the elapsed time since the last event is an

incomplete interseismic interval, the last event and the time since the last event are removed from the calculation.

The average interseismic interval technique averages the preferred interseismic intervals determined for each fault. The maximum and minimum interseismic intervals are adopted directly for the maximum and minimum values. Five of the six principal faults have at least four or more paleoseismic events to consider for interseismic intervals. The other fault (the Iron Ridge fault) has two to three events.

In general the preferred values of the average and interseismic interval techniques are similar as we might expect. The most significant difference comes from the estimation of the maximum and minimum values. For the average earthquake recurrence interval technique, the uncertainty that is translated into maximum and minimum values is determined from the uncertainty in the age of the oldest event and the number of events since. The uncertainty in the interseismic interval technique comes from the variation of the interseismic intervals themselves.

These three estimates, moment rate, average recurrence interval, and interseismic interval, are averaged for estimating the occurrence rates ascribed to the fault. We weight these three methods equally because the uncertainty in the methods is roughly the same.

Analysis step 2 is an empirical approach that uses data from the Yucca Mountain trenches to identify paleoseismic events. These are listed in Appendix SDO-2 for each fault, with a nominal age of each event listed as well. Then a single and perhaps multiple possible event histories are determined for a fault. If multiple possible event histories exist, the relative likelihood of these histories is assessed, and a relative weight is assigned to each history. For example, if there was uncertainty as to whether a particular paleoseismic event occurred, two models of paleoseismic history can be used, one with the uncertain event and one without.

Analysis step 3. Each paleoseismic event is considered an observation or sampling of a fault's behavior (whether it might behave as an individual, linked, or distributed fault during an earthquake event). Each paleoseismic event is considered an equally valuable piece of information, and is given a weight in the analysis of $1/n$, where n is the number of paleoevents

in the history. This is not a "relative weight" in the classic sense; thus we call this a relative frequency. The series of paleoevents thus define the relative frequency of different rupture patterns.

Analysis step 4 divides paleoseismic events into event scenarios and relatively weights these scenarios. Three main models of event scenarios are considered, (1) single fault, (2) linked faults, and (3) distributed faults. The potential event scenarios are determined considering potential correlations of events from trenching data on different faults and structural linkages.

Because of the small cross-strike distances, the highly interconnected nature of the faults, empirical information from historical Basin and Range province earthquakes, and the apparent similarities in age of paleoseismic events along different faults within the relatively small area of Yucca Mountain, we considered the occurrence of multiple fault scenarios to be a likelihood in some cases. The weighting between different event scenarios was based on the uncertainties in the age estimates of events, secondary correlation evidence (e.g., same volcanic ash found within the fault zone or in an event horizon), representations of event scenarios given in Chapter 5 of the Seismotectonic Framework Report (USGS, 1996). Most of the weights are 50/50 or 30/70 between the single faults and multiple fault scenarios dependent on age uncertainties and number of correlating factors, or are equal weights across all event scenarios reflecting similar uncertainties in dates and high degrees of structural connectivity.

Earthquake lengths are based on the end-to-end length of the combined faults for the linked scenarios. Distributed fault scenarios involve parallel faults that fail together. For distributed scenarios, maximum surface displacements are combined in a cross-strike fashion, and lengths may or may not be increased over single fault scenarios. All events scenarios are presented in Appendix SDO-1 as a listing of all events, and under each of the six principal faults considered.

Analysis step 5 calculates the occurrence rate of the event scenarios for each paleoseismic event. This is done by multiplying the occurrence rate from each fault times the relative weight of the paleoseismic histories times the relative frequency of a specific paleoseismic

event ($1/n$, where n is the number of events) times the relative weighting of the specific event scenario (based on age uncertainties and structural connectivity).

Analysis step 6 adds up the occurrence rates for each event scenario with that from multiple paleoseismic events along a fault. The occurrence rates for each event scenario involved in multiple paleoseismic events are added together. This now represents the occurrence rate of a specific scenario per fault. These results are displayed in the beginning of Appendix SDO-1 by principal fault. Note that there are different occurrence rates for some of the same event scenarios for different faults. These are resolved in the next step.

Analysis step 7 combines the occurrence rates from event scenarios common to multiple principal faults. A simple averaging of the occurrence rates from different faults is done to accomplish this. These final values are the occurrence rates then used for the different event scenarios.

3.5 VOLCANIC SOURCES

Our team recognized the importance of volcanic-related seismicity in light of the Quaternary basaltic volcanoes near the Yucca Mountain site. We used the data from the Yucca Mountain volcanic hazard analysis (US DOE, 1996). We considered several sources that could be activated along the northeast alignment of approximately 1-million-year-old volcanic vents across Crater Flat, as well as those that might be associated with the Lathrop Wells vent at the south end of Crater Flat.

One volcanic source (Figure SDO-10) is taken to represent volcanism along the alignment of vents within an area determined by a spatial smoothing of the average distance between volcanic vents, that average defining a perimeter around each vent to make up a northeast-aligned source zone. We assumed two to three volcanic events per million years. The potential activity of this source was weighted 0.25.

Our second volcanic source is at the south end of the vent alignment that encompasses the 70,000-year-old Lathrop Wells volcanic vent (Figure SDO-10). We weighted the potential activity of that source 0.75.

The maximum magnitude for a volcanic earthquake was assigned on the basis of Smith and Jackson (1996), a study of volcanic-related earthquakes worldwide, as well as the recently completed Yucca Mountain Probabilistic Volcanic Hazard Assessment and its documentation (Probabilistic Hazard Analysis for Yucca Mountain, Nevada, Civilian Radioactive Waste Management System, Management and Operating Contract, BA00000-01717-2200-00082, Rev.0).

We characterize the distribution for volcanic-related earthquakes magnitudes as follows.

<u>Magnitude</u>	<u>Weight</u>
6.0 ± 0.2	0.1
5.8 ± 0.4	0.6
5.5 ± 0.4	0.3

Smith and Jackson (1996) found a maximum magnitude of M 4.5 for basaltic vents. We choose a preferred Mmax of 5.8 for volcanic source zones in the Yucca Mountain area on that basis, with the most likely occurrence along our northeast alignment.

4.0

HISTORICAL SEISMICITY: EVALUATION AND TREATMENT OF RECORD PARAMETERS

Spatial Smoothing

The final earthquake catalog data were treated by a smoothing algorithm as a means of distributing the seismic moment uniformly across the source zones.

Our smoothing parameters were choosing from three zones:

- (a) Uniform smoothing with fixed boundaries of the source areas were chosen to approximate the long term windows (thousands to hundreds of thousands of years) that would encompass seismotectonic potential of our identified source areas.

Weight = 0.50

- (b) We considered shorter time frames of tectonic processes (a few hundred years), we assigned a weight to Frankel's (1995) smoothing algorithm for a 10 km radius of the Gaussian kernel (with a 1 s standard error) and with magnitude 3 and 5 cutoffs. This radius was assumed to take into account the events with a 10 km aftershock length that generally are consistent with a few tens to a few hundred year return period for the Basin-Range.

Weight = 0.25

- (c) We addressed a wider geographic window (several hundred years) by assigning a wider aperture of 20 km to Frankel's (1995) smoothing algorithm for the Gaussian kernel for a 1 s standard error for his radii specifications for magnitude 3 and 5 cutoffs. This considers aftershock distributions that correspond to larger and less frequent earthquakes of several hundred years for the Basin-Range.

Weight = 0.25

Alternate Model—We initially attempted to smooth the earthquake catalog data by developing a weighting algorithm that would have as its smoothing kernel a radius determined by first searching a grid up to 50 km, then assigning a window with a radius on the basis of the aftershock length vs. magnitude (using the relationship of Wells and Coppersmith, 1994). However, because of the low background historical seismicity of the Yucca Mountain area, this method produced a very small effective search radius of ~5 km or less and was not used.

Relationships Between Magnitude Scales

We studied the magnitude scales for various catalog contributions that were done by Woodward-Clyde Federal Services. After examining these conversions we chose to use them as described in the Woodward-Clyde Federal Services Yucca Mountain PHSA unpublished report (Wong, 1996).

Magnitude Uncertainties

We assessed magnitude uncertainties by comparing the catalog period with the Woodward-Clyde Federal Services Yucca Mountain PHSA unpublished report on the Yucca Mountain composite catalog (Wong, et al., 1996) as follows:

Time Period	Estimate of Magnitude Uncertainty
1900-1930	± 0.8
1931-1961	± 0.6
1962-1970	± 0.5
1971-1978	± 0.2
1978-present	± 0.2

Declustering Parameters

We used a distribution for declustering of our earthquake catalog as follows.

- (a) We used Youngs et al. (1987) declustering parameters (updated Geomatrix version 5) for the four weighting parameter sets.

Weight = 0.6

- (b) We used the Veneziano and van Dyke (1985) approach but downweighted the method as it is not yet fully accepted. It used a variable radius-dependent spatial smoothing window to acquire sufficient numbers of earthquakes to determine if a single event was independent either in time or space to the previous event. Parameters are dynamic and not stationary over the study area.

Weight = 0.2

- (c) Our team, SDO, also developed a modified time-distance window based upon Youngs et al.' (1987) declustering parameters. These were patterned after the Wasatch Front seismicity and are as follows:

Weight = 0.2

Mag.	Time (hours)	Distance (km)
2.5	20	20
3.5	30	30
4.5	100	40
5.5	300	60
6.5	600	200
7.25	2000	300

Catalog Completeness

Catalog completeness is a parameter that captures the idea of a minimum magnitude cutoff above which the earthquake catalog is complete such that a recurrence curve will not deviate from an exponential decay with an assumed constant slope. We estimated the completeness by examining the temporal distribution of earthquakes using the method of Stepp (1972) to each of the catalogs. Our team's estimate of the completeness from our own time-space windows are:

Magnitude Completeness	Period
M 6+	1900 present
M 5.0 - 5.9	1924 present
M 4.0 - 4.9	1934 present
M 3.5 - 3.9	1950 present
M 3.0 - 3.5	1962 present
M 2.5 - 2.9	1972 present
M 2.0 - 2.4	1979 present

The catalog completeness intervals for the catalogs declustered using the Youngs and others (1987) and the Veneziano and van Dyke (1985) approaches are based on those presented by Ivan Wong in SSC Workshop 3 and on review of the data. The completeness intervals are:

Completeness Magnitude	Period
M 7.0+	1880-present
M 6.0-6.9	1900-present
M 5.0-5.9	1914-present
M 4.0-4.9	1934-present
M 3.5-3.9	1961-present
M 2.5-3.5	1979-present

Recurrence parameters were estimated using the maximum likelihood method described in Section 3.1 of the main report. The minimum magnitude was set at 2.0 except for Zone 2. For this zone, the minimum magnitude was set at 2.5 because the catalog appeared to be incomplete at magnitude 2.

FAULT DISPLACEMENT**5.1 INTRODUCTION**

In dealing with fault displacement hazard, our team considered that the level of our scientific knowledge of the subject and technique is less certain than that applicable to seismic source characterization. There are a number of reasons for this, but a prime consideration is that idealizations that can be applied to rock behavior at seismogenic depth are not as readily applicable to the upper one or two kilometers of the earth's crust where the repository site is located. At seismogenic depths (~ 4 to 19 km) rock is under high confining stress and is assumed to behave as an elastic, isotropic medium; the strength of fractures is high ($0.6 < \mu < 0.8$) and exhibits essentially frictional behavior. At depths less than about 4 km the crustal carapace consists of a variety of rock types ranging from pristine rock, to weathered or altered rock, to consolidated and unconsolidated alluvium; here, fracture strength may be appreciably different than the shear strength of the host material.

Because of these differences in properties and conditions, strain release (stress drop) considered as seismogenic slip along deep-seated faults may not efficiently be propagated to the surface as a fault displacement. Accordingly, we followed closely working models and data presented at the Yucca Mountain Fault Displacement workshops that extend our teams concept of the problem, and gave weight to the cogency and reasoning of alternate approaches. Our basic premise, however, was to use, where possible, observational data on principal and distributed faulting appropriate for the Basin and Range extensional regime, and especially to use data from the Yucca Mountain area. This is not to say that the problems of fault displacement are not amenable to epistemic solution, though we emphasize that uncertainties in the interpretation of the data may be large. We also note that it is important to the user of our characterization to understand that we downplayed research-oriented approaches and attempted to understand the uncertainties of observational data, and hence dealt with them in a probabilistic sense.

There are three major questions that we considered:

First, there is the problem of what constitutes principal surface displacement. Ideally, principal surface displacement is systematically proportional to the source-depth displacement of the causative earthquake. In practice, the primary displacement is smaller to a greater or lesser degree for the following reasons:

- Anti-clustering and roll-over effects in the hanging wall.
- Material and fault damage differences in hanging wall versus foot wall.
- Strain diffusion associated with local fracturing, reconsolidation, and fissuring.

Second, there is the complication of secondary faulting: How can we discriminate secondary from primary faulting on a genetic basis?

- Time-dependent strain release involves reconsolidation, compaction, groundwater phenomena, foot-wall degradations, subsidence, stress history, "effective elastic thickness" phenomena, etc. These factors contribute to well-defined criteria for defining the extent of these ruptures.

Third, there is a time and spatial sampling problem.

- Degradation of sample sites with time.
- Sample technique: authoritative vs. random/systematic sampling.

To address these problems we approached the analysis at two levels: one for ruptures on the primary faults, i.e., those considered to be seismogenic (at depth), and one for distributed rupturing on secondary faults (near the ground surface). There is a general logic tree for each. The methodology for displacement along the seismogenic faults is largely an extension of our teams (SDO) approach to the seismic source characterization analysis, using the magnitudes of earthquakes and their frequency of occurrence developed in Sections 3 and 4. We considered distributed or secondary displacements to be diffusely scattered and discontinuous ruptures that mostly occur in the hanging wall of normal-slip faults. These are interpreted to result from local strain release distributed along and across the hanging wall, triggered by a nearby earthquake or by non-tectonic mechanisms such as thermal contraction, ground slumping, localized ground subsidence due to ground water withdrawal, etc.

Most of the methods we used for estimating the potential for distributed faulting lack the refinement of seismic source characterization. However, we considered them reasonable

given the relatively small data base, the precision of the data, the generally limited knowledge of the normal faulting process and the relationships of primary to secondary fault triggering. To span the variety of methodologies, we used several approaches that we judged applicable to the Yucca Mountain environment to overcome the large uncertainties or potential bias of any one approach.

5.2 PRINCIPAL FAULTING DISPLACEMENT CHARACTERIZATION

The logic tree for characterizing the potential for principal fault displacement (Figure SDO-11) is divided into five parts: (1) type of event, (2) frequency of occurrence of events, (3) approach for estimating fault displacement, (4) scaling techniques, and (5) distribution for displacement at a point. The following discussion expands these topics.

5.2.1 Type of Event

We considered two levels of principal rupture size along seismogenic faults: maximum displacement events and events smaller than the maximum earthquake. The characterization of displacement hazard from events associated with distributed displacements is described in Section 5.3. Defining the size and frequency of maximum earthquakes (those within $\frac{1}{2}$ magnitude unit of the upper bound earthquake for the fault) are a focus of the earthquake source characterization for assessment of ground motion hazard. The frequency and size distribution of smaller earthquakes down to the maximum background earthquake are assessed using the earthquake recurrence models described in Sections 3.0 and 4.0. We consider that secondary displacement is possible in response to earthquakes along other faults, including aftershock sequences. The characterization of these faults is discussed in Section 5.3. In that part of the analysis, the seismogenic fault is treated in the distributed faulting as the larger end of the fractal distribution of faults.

5.2.2 Frequency of Occurrence of Principal Faulting Events

We utilize the earthquake approach for characterizing principal faulting displacement hazard. The frequency of earthquakes along the seismogenic faults is developed in our (team SDO) earthquake source characterization study (Sections 3 and 4). This is based on three approaches: (1) averaging of moment rates; (2) using an average recurrence interval; and (3) using the interseismic time interval. Events that have magnitudes distributed between the maximum earthquake and the maximum background earthquake have their occurrence rates

developed using the characteristic and truncated exponential models. These models are weighted 0.7 and 0.3, respectively.

The probability of seismogenic rupture at or near the surface is computed using an empirical relationship between the probability of surface rupture and earthquake magnitude developed from data presented by Pezzopane and Dawson (1996). Figure SDO-12 shows the results of fitting a logistic probability model to the data sets presented by Pezzopane and Dawson (1996) for recent Basin and Range earthquakes (see Appendix H, Section H.4.1). We assign equal weight to these two treatments. The probability of surface rupture at any given point along a fault is computed by randomizing the location of the rupture along the length of the fault.

5.2.3 Approach for Estimating Fault Displacement

The approaches used for estimating fault displacement include empirical regressions of observations of faults that produce normal-faulting earthquakes, data from single-event paleoearthquake displacements, and an along-strike displacement plot for the Solitario Canyon fault determined by Allan Ramelli (1997) as part of the Yucca Mt. earthquake hazard assessment.

Four types of empirical regressions are used: (1) average displacement versus moment magnitude; (2) average displacement versus length; (3) maximum surface displacement versus moment magnitude; and (4) maximum surface displacement versus length. These are taken from Wells and Coppersmith (1994) and an analysis by the AAR Team of Yucca Mountain data. Both the average and maximum surface displacements are considered because both can be used for assessing the distribution for displacement at a point in an event.

Fault parameter data were taken from the trenching studies of Quaternary faults in the Yucca Mountain area and are the interpreted maximum surface displacements that have been reported in the earthquake seismic source characterization analysis. Average surface displacements were scaled from maximum surface displacements using scaling relationships of Wells and Coppersmith (1994) judged appropriate for an extensional, normal faulting stress regime. Wells and Coppersmith's (1994) Figure 5 plots the ratio of average surface displacement to maximum surface displacement and shows a distribution between 0.2 and 0.8.

We used the approximate average value of these data and take the ratio between average and maximum displacement to be 0.5.

The Ramelli fault displacement data for the Solitario Canyon fault is a combination of trench observations and measurements from the scarp observed along the Solitario Canyon fault trace (Figure SDO-13). It shows some of the ambiguities involved in assessing surface data from both random (field reconnaissance) and authoritative sampling (trench measurements). The curve is useful, however, because it uses direct information from the fault that is in close proximity to the Yucca Mountain site and therefore judged as a good proxy for conditions at the repository.

5.2.3.1 Scaling Techniques. The scaling techniques we used (Table SDO-6) are the regressions aforementioned and a theoretical relationship presented at the SSC workshop #4 and based on a rock mechanics approach (see Bruhn, 1997, SSC Workshop #5). The Wells and Coppersmith (1994) regressions are those for normal faults; the analysis by the AAR Team (presented at SSC workshop #4, Jan. 8, 1997) is developed using data from the Yucca Mountain area. Values from these regressions were used to scale the displacement diagrams presented in the next section.

5.2.3.2 Distributions for Displacement at a Point. Because engineered structures are designed for site specific locations, we need to be able to estimate the potential scale of local fault displacement. Typically, displacement at a surface rupture can range from large values along a single scarp, to smaller values across a broader stepped-scarp distribution. We attempt to model the distribution for the amount of displacement that occurs at a point on a principal rupture by employing a variety of displacement distributions (some named after their developers): (1) a compilation of five large Basin and Range historical earthquakes compiled by R. Wheeler (1989), called here the five-earthquake curves (Figure SDO-14); (2) a fault-roughness curve (Figure SDO-15) which is developed in more of a rock mechanics sense by R. Bruhn; (3) a Yucca Mountain site-specific, trench-displacement distribution developed by the DFS Team (Figure SDO-16); and (4) for the Solitario Canyon fault, the displacement plot (Figure SDO-13) developed by Alan Ramelli of the Nevada Geological Survey.

The Wheeler five-earthquake curves (presented at SSC Workshop #5, April 15, 1997) are based on data from five large, scarp-forming Basin and Range province earthquakes. The ASM Team smoothed the data presented in Wheeler (1989) to derive, symmetric curves that define the median and range of the ratio of displacement at a point to the maximum displacement associated with an earthquake, *DMD*, as a function of location along the principal fault rupture (Figure SDO-14). The Facilitation team developed a statistical model to represent this distribution (see Appendix H, Section H.3.1). The fault roughness curve is based on the consideration that surface roughness along a fault plane is related to amount of displacement, as noted by Ronald Bruhn (SSC Workshop #5). The SBK Team developed a model that represents the theoretical surface roughness along a fault and predicts a distribution for the ratio of displacement at a point to the maximum displacement associated with earthquake magnitude (Figure SDO-15). This distribution is analogous to the empirical distribution developed by the ASM Team (Figure SDO-14) and presented at SSC Workshop # 5, April 15, 1997. Although Bruhn's model is considered to portray real displacement variation along strike, we note that it is an untested theoretical model and should be weighted accordingly. The Facilitation team developed a statistical model to represent this distribution (see Appendix H, Section H.3.2).

The Yucca Mountain trench-displacement distribution, developed by the DFS Team and presented at SSC Workshop # 5, April 15, 1997, examines the event-to-event variability in displacement at a point on a fault about the average historical displacement (Figure SDO-16). This distribution was originally specified as a triangular distribution by the DFS team. However, the Facilitation team determined that a gamma distribution provided a better fit to the data (see Appendix H, Section H.2.1) and we adopt that distribution.

The longitudinal displacement profile for the Solitario Canyon fault offered by Ramelli (Figure SDO-13) shows a large "bump" in fault displacement created entirely by measured offsets in trenches T1 and T8. Elsewhere along the fault, displacement determined by trenching is compatible with scarp heights. Why are the T1 and T8 offsets on the fault anomalously large? The answer seems to be fault segmentation (Ramelli, SSC Workshop #5 information transmittal, May 5, 1997). But we are cautious when asked to compare scarp heights cited by Simonds and others (1995) from field reconnaissance with displacements measured in four trenches. Two of the trenches, T1 and T3, give displacement values that are twice as great as

the range of all other measurements. This leads us to ask what is actually being measured in these two trenches that returns such anomalously large mid- to late-Quaternary displacements? If we project a line through the span of displacements of all the other data sources we get a broad convex longitudinal profile along the fault, a curve similar to that obtained by Jim Yount (SSC Workshop # 6, June 1, 1997), who measured cumulative displacement with reference to a single Miocene horizon the observed length of the fault.

5.2.3.3 Assessment of the Distribution for Amount of Displacement at a Point on a Principal Rupture. The procedures to assess the distribution of potential amount of displacement at a point are shown on Figure SDO-11. There are two approaches: one based on assessment of the maximum displacement, *MD*, associated with an earthquake; and one based on an assessment of the average surface displacement, *AD*, that occurs during an earthquake. These two approaches are given equal weight in the analysis because of the uncertainties we describe in the Introduction.

The estimation of *MD* and *AD* depends upon the size of the earthquake. For magnitudes smaller than $m^U - \frac{1}{2}$ the estimation is based solely on the relationships given in Table SDO-6 for *MD* and *AD* as a function of earthquake magnitude. For the maximum events ($m^U - \frac{1}{2} \leq m \leq m^U$), we also estimate *MD* and *AD* using scaling relationships based on the assessment of rupture length using the relationships in Table SDO-6, and directly from the paleoseismic data. The weights assigned to these various approaches are 0.2 to assessment based on magnitude, 0.4 to assessments based on rupture length, and 0.4 on the paleoseismic displacement data. These weights reflect the relative importance we place on empirical data. For assessment of *AD* as a function of rupture length, equal weight is given to the Wells and Coppersmith (1994) regression and the regression developed by the AAR team (Table SDO-6).

The displacement plot for the Solitario Canyon fault (Figure SDO-13) allowed us to consider a different treatment for displacement along this fault. The displacement at any point of interest is read from the displacement curve and is taken to be the average displacement at that point during maximum earthquakes. This estimate is given a weight of 0.7 and all of the above assessments are given a combined weight of 0.3. We have not been able to determine whether the displacement peak along the Solitario Canyon fault is a segmentation

phenomenon or a sampling alias; we consider the data with due caution, in light of possible interpretations that may significantly bias analytical conclusions.

Given an assessment of MD from the various scaling relationships, the probability of exceeding a specified displacement at a point is computed as follows: The uncertainty in MD in a single event is considered to be lognormally distributed about the assessed value, with a standard deviation of $\log(MD)$ equal to that obtained by Wells and Coppersmith (1994) from regression analysis of empirical data. This lognormal distribution is used to assess the value of MD in a single earthquake. Given MD for an individual earthquake, the probability of exceeding a specified displacement is computed using the distributions for D/MD shown on Figures SDO-14 and SDO-15. The empirical distribution developed by the ASM team (Figure SDO-14) is weighted 0.8 and the theoretical distribution developed by the SBK team (Figure SDO-15) is weighted 0.2 for the reasons discussed above in Section 5.2.3.2.

Given an assessment of AD , the probability of exceeding a specified displacement at a point is computed as follows. The estimate of AD is considered to represent the average displacement over multiple earthquakes. The distribution for the ratio of the displacement in a single event to the average over multiple events, D/AD , developed by the Facilitation team from the data presented by the DFS team (Figure SDO-16), is used to assess the probability of exceeding a specified displacement.

5.3 DISTRIBUTED FAULTING DISPLACEMENT CHARACTERIZATION

Modeling the potential displacements from distributed faulting involves: (1) evaluating the characteristics of faults not directly part of the primary fault trace; (2) estimating the cumulative magnitude of the distributed fault displacements and the probability of occurrence of subsequent displacements; and (3) evaluating the affect of the free surface on fault propagation from the repository depth to the surface. Figure SDO-7 shows the logic structure used to characterize distributed faulting hazard. Two approaches were used. One is based on assessment of the frequency at which earthquakes on the various seismic sources induce distributed slip on the feature of interest. This is termed the earthquake approach. The second approach uses the cumulative slip at the point of interest to estimate the slip rate and displacement per event. This is termed the displacement approach. Both approaches are used for features that are subject to only distributed faulting hazard, with the earthquake approach

given a weight of 0.8 and the displacement approach given a weight of 0.2. The earthquake approach is given a higher weight because it has a stronger theoretical basis and a more complete database. It is also favored because it is tied to our paleoearthquake analysis. The displacement approach has not been studied in as much detail and has limited data. For those features that are also subject to principal faulting hazard, only the earthquake approach is used. Again, the large uncertainties associated with near-surface phenomena and widely variable material properties of media in the upper few hundred meters lead us to give a relatively low weight to the displacement approach.

5.3.1 Earthquake Approach to Distributed Faulting Hazard

The steps in the earthquake approach are: (1) assessment of the probability that distributed faulting can occur on the feature (activation probability); (2) an assessment of the probability of slip in an individual earthquake; and (3) an assessment of the distribution relative to the amount of potential total displacement.

5.3.1.1 Activation Probability. The probability that an individual fault can be activated among many during a distributed faulting event is estimated using an analysis of slip tendency of faults with respect to the regional stress field (Morris and others, 1996). The slip tendency technique considers the ratio of shear to normal stresses imposed on a fault within a regional stress field. Slip tendency, T_s , reduces to μ , the coefficient of static friction which, according to Byerlee's law (Byerlee, 1978), is 0.85 from ground surface to seismogenic depths (10 km). McKague and others (1996) present an analysis of the slip tendency of faults in the Yucca Mountain region. Their analysis of the local faults (their Figure 3-5b) indicates the north-south trending faults have the highest slip tendency (~ 0.7). Because most of the larger north-south trending faults show evidence of Quaternary slip, we utilize a value of T_s of 0.7 to correspond to a probability that slip can occur, $P(C)$ of 1.0. For faults and features with other orientations, we define $P(C)$ as the ratio $T_s/0.7$. For northwest-southeast trending structures, T_s read from Figure 3-5b of McKague and others (1996) is approximately 0.55, resulting in $P(C) = 0.8$.

5.3.1.2 Probability of Slip Per Event. The frequency of occurrence of earthquakes on each of the seismic sources is defined by our seismic source characterization described in Sections 3.0 and 4.0. The probability of distributed slip on a feature in an individual earthquake is

assessed using an analysis of the density of distributed rupture based on the mapped patterns of rupture presented in Pezzopane and Dawson (1996). The logistic regression model presented by R. R. Youngs (Yucca Mountain SSC Workshop #6) was adopted (Figure SDO-18) (see also Appendix H, Section H.4.2). We excluded the data for hanging wall cracking from the 1988 Chalfant Valley earthquake and data from the 1980 Mammoth earthquake because these earthquakes are considered background type earthquakes. The curves show the probability of secondary rupture occurring at a point as a function of earthquake magnitude, distance from the principal rupture, and location in the hanging wall or foot wall of the rupture. For earthquakes occurring on the regional areal source, it is considered equally likely that the point of interest lies in either the hanging wall or the foot wall of the rupture.

We further modify the probability of distributed rupture in an event by a factor related to the orientation of the feature relative to the principal fault rupture. The distribution of the orientation of distributed ruptures with respect to the principal rupture provides an assessment of the likelihood that distributed faulting occurs on a feature with a given orientation with respect to the strike of the earthquake-generating fault. Maps of historical ruptures presented in Pezzopane and Dawson (1996) were used to assess the relative frequency of distributed ruptures in increments of 5° of the angle θ between the strike of the principal rupture and the strike of the distributed rupture (see Appendix H, Section H.4.3). This relative frequency was used to define the likelihood of rupture as a function of relative strike between the principal rupture and the feature of interest. We selected the assessment based on a minimum of three points defining the distributed rupture trace because the process used to digitize the fault maps produced a distribution of two-point rupture traces with modes in the north-south and east-west directions, suggesting poor estimation of the strike azimuth distribution.

The strike azimuth for earthquakes occurring in the regional source zone is not known. Examination of the orientation of nodal planes of Yucca Mountain region earthquakes presented in Chapter 7 of U.S. Geological Survey (1996) indicates a nearly random pattern. Therefore, we assume that the strike azimuth of these earthquakes is uniformly distributed from 0° to 360° and compute an average value of the orientation probability of 0.34 to apply to these earthquakes.

5.3.1.3 Probability Distribution for Displacement at a Point. Two approaches are used to assess the distribution of possible displacements at a given point along a fault scarp induced by slip on an earthquake source: one based on the ratio of cumulative displacements; and one based on maximum potential displacement computed from earthquake magnitude.

Cumulative Displacement Ratio Approach. In this approach, we consider the ratio of displacement on the principal rupture to displacement on the secondary rupture to be equal to the ratio of their cumulative displacements. We define a factor, RF , that is used to scale the principal rupture displacement to the distributed rupture displacement. The scaling factor RF is set equal to the ratio of the cumulative displacement on the fault of interest to the cumulative displacement on the earthquake source fault. We impose an upper limit of 0.8 to RF based on the maximum ratio of secondary to primary slip reported by Coppersmith and Youngs (1992). The procedures described in Section 5.2.3.3 are used to assess the distribution for slip on the principal rupture at its closest approach and this slip is scaled by RF to the point of interest. This approach is given a weight of 0.2. The low weight takes into account the uncertainties associated with origin, mechanics, displacements, and slip histories of shallow distributed faults compared to the seismogenic faults.

The application of this approach requires an assessment of the average cumulative displacement for each of the seismic sources in the vicinity of Yucca Mountain. The assessed values are:

Source	Average Cumulative Displacement (m)
Paintbrush Canyon	380
Bow Ridge	244
Solitario Canyon	457
Fatigue Wash	396
Windy Wash	380
N. Crater Flat	244
S. Crater Flat	<244
Iron Ridge	350
Stagecoach Road	457
Bare Mountain	500-900

When simultaneous fault ruptures are considered, the largest cumulative displacement among the individual faults is used to define *RF*.

Displacement Potential Approach. As an empirical data set, secondary (or distributed) faults include numerous, difficult to discriminate strain phenomena along with true fault displacements. We consider that distributed displacement represents an upper limit of strain, i.e., failure in the rock mechanics sense, but that all the strain effects measurable as geodetic displacement normal to the rupture are consequences of main fault plane seismogenic rupture. The displacement potential approach simply acknowledges the reality that surficial materials are not classic elastic media and cannot be expected to behave (strain and fail) the same way a seismogenic fault does at depth.

For this approach we used a distribution ratio of secondary to primary slip empirically observed in historical, ground-breaking earthquakes in the Basin and Range province: (1) the M 7.1 1954 Fairview Peak, Nevada, earthquake and associated Stingaree Valley rupture; (2) the M, 7.5 1959, Hebgen Lake, Montana, earthquake; and (3) the M, 7.3 1983 Borah Peak earthquakes recognizing there are many more data points in the hanging wall than in the foot wall. Figure SDO-19 shows maximum distributed fault displacements normalized to the maximum principal fault rupture, *MD*, plotted versus distance from the principal rupture, and distinguishes displacement in the hanging wall from the foot wall side of the fault. We define an approximate envelope of the observed data on the hanging wall side of the rupture and fit an exponential curve to these data, as shown on Figure SDO-19. An exponential curve is used because it is a simple parametric model that allows for a gradual decay of amplitude with distance. The resulting curve for the hanging wall displacement potential is

$$D(\text{distributed in hanging wall})/MD(\text{principal}) = 0.35 \times \exp(-0.091r)$$

where *r* is the distance from the principal rupture. Examination of data presented in Pezzopane and Dawson (1996) and Coppersmith and Youngs (1992) indicates that the distributed faulting zones on the foot wall side of normal fault ruptures are much narrower than those on the hanging wall side of the rupture. Consequently, we assume that the rate of decay of distributed displacement amplitude is 50 percent greater on the foot wall side than on

the hanging wall side, and using the single foot wall data point define a foot wall displacement potential as:

$$D(\text{distributed in foot wall})/MD(\text{principal}) = 0.16 \times \exp(-0.137r)$$

The displacement potential is interpreted to represent the 95th-percentile of the distribution of possible displacements, with the lower limit of this distribution equal to 0. We use a distribution with a similar degree of skewness as exhibited by the distribution for D/AD shown on Figure SDO-16 and impose an upper limit to the displacement potential equal to the cumulative displacement on the feature. As described in Appendix H, the various normalized displacement data sets developed by the expert teams can be modeled by gamma distributions with the shape parameter, α , of about 2.5. For $\alpha = 2.5$, the 95th-percentile of a gamma distribution occurs at $5.535b$, where b is the normalizing parameter of the distribution. Thus, we define a gamma distribution for the distribution of $D(\text{distributed})/MD(\text{principal})$ at a distance r from a principal rupture with α equal to 2.5 and b equal to the displacement potential defined by the above relationships divided by 5.535. The computation of the distribution for the displacement is completed by utilizing a lognormal distribution for MD on the principal rupture about the values given by the various scaling relationships defined in Section 5.2.3.1.

We weight the displacement potential approach 0.8. In assessing the potential for fault displacement from earthquakes occurring in the areal source zone only the displacement potential approach can be used because the cumulative displacement on the earthquake source is not known.

5.3.2 Displacement Approach to Distributed Faulting Hazard

The steps in the displacement approach are: (1) assessment of the probability that distributed faulting can occur on a fault (activation probability); (2) assessment of the rate of slip on the feature; (3) assessment of the average slip per event; and (4) assessment of the distribution for the amount of displacement. In the displacement approach the location, size, and orientation of the faults that generate earthquakes inducing the distributed slip are unknown.

5.3.2.1 Activation Probability. The probability that an individual fault can be activated during a distributed faulting event is estimated using the analysis of slip tendency of faults with respect to the regional stress field, as discussed in Section 5.3.1.1.

5.3.2.2 Assessment of Slip Rate. The Quaternary slip rate on the feature of interest is assessed by estimating the fraction of the cumulative slip that has occurred in the past 1.6 Ma, and dividing that slip by 1.6 Ma. Based on review of the various proposed slip histories for the Yucca Mountain faults, the following distribution is assessed for the percentage of cumulative slip that has occurred in the Quaternary, 0.2% (0.3), 0.6% (0.4), 2% (0.3).

5.3.2.3 Assessment of Average Displacement per Event. We utilize two approaches for estimating the average slip per event, \bar{D}_E . The first is based on the scaling relationships between cumulative offset and average offset developed by the AAR Team (SSC Workshop # 4, Jan. 8, 1997). The second is based on an analysis of the fault offset data from Yucca Mountain normalized by the cumulative offset on the fault. This empirical distribution was developed by the SBK Team (SSC Workshop #6, June 1, 1997) (see Figure SDO-20). These two alternatives are given equal weight. The frequency of faulting events is equal to the fault slip rate divided by the average slip per event.

5.3.2.4 Distribution for Displacement at a Point. The approach for assessing the distribution for the displacement in an event is tied to the approach used for estimating the average slip per event. If the AAR scaling relationships are used, then the exponential distribution for D/MD^{max} developed by AAR is used to calculate the probability distribution for D , with $MD^{max} = \bar{D}_E / 0.83$ based on the scaling relationship developed by the AAR team. If the approach developed by the SBK team is used, then the empirical distribution shown on Figure SDO-20 is used to assess the probability distribution for displacement. This distribution was modeled by the Facilitation team by a gamma distribution (see Appendix H, Section H.2.6).

5.4 DATA FOR NINE CALCULATION SITES

The following summarizes the data required to characterize the displacement hazard at each of the nine demonstration sites.

Point 1 Bow Ridge fault

Site of potential principal faulting , use the methods described in Sections 5.2 and 5.3.1. For distributed faulting , $P(C) = 1.0$. The paleoseismic $MD = 44$ cm, with assumed lognormal distribution, and $\sigma_{\log(MD)} = 0.42$ based on empirical models. The assessed cumulative displacement at Point 1 is 200 m. The distribution for the length of the feature is {7 (0.3), 8 (0.4), 10 (0.3)} km.

Point 2 Solitario Canyon fault

Site of potential principal faulting , use the methods described in Sections 5.2 and 5.3.1. For distributed faulting , $P(C) = 1.0$. The paleoseismic $MD = 0.7$ m, with assumed lognormal distribution, and $\sigma_{\log(MD)} = 0.42$ based on empirical models. The paleoseismic AD estimated from the profile developed by Alan Ramelli is 25 cm. The assessed cumulative displacement at Point 2 is 700 m. The distribution for the length of the feature is {16 (0.3), 18.5 (0.4), 21.5 (0.3)} km

Point 3 Drill Hole Wash fault

Site of distributed faulting, use the methods described in Section 5.3. $P(C) = 0.8$ from slip tendency. The cumulative displacement is assessed to be 12 m.

Point 4 Ghost Dance fault

Site of distributed faulting, use the methods described in Section 5.3. $P(C) = 1.0$ from slip tendency. The cumulative displacement is assessed to be 40 m.

Point 5 Sundance fault

Site of distributed faulting , use the methods described in Section 5.3. $P(C) = 0.8$ from slip tendency. The cumulative displacement is assessed to be 11 m.

Point 6 Unnamed fault west of Dune Wash

Site of distributed faulting , use the methods described in Section 5.3. $P(C) = 1.0$ from slip tendency. The cumulative displacement is assessed to be 150 m.

Point 7 Point 100 m east of Solitario Canyon

Site of distributed faulting, use the methods described in Section 5.3. For point 7a, $P(C) = 1.0$ from slip tendency and the cumulative displacement is 2 m. For point 7b, $P(C) = 1.0$ from slip tendency and the cumulative displacement is 10 cm. It is judged that the probability of displacement in intact rock (point 7d) is essentially negligible because the Yucca Mountain block is highly faulted and fractured at a wide range of scales and displacement within the block will likely occur along these pre-existing zones of weakness rather than break intact rock. Fractures with no displacement (point 7c) are either small features or are on the fringe of a larger feature. In both cases, secondary displacement will probably be negligible.

Point 8 Point midway between Ghost Dance and Solitario Canyon faults

Use the same set of parameters defined above for Point 7.

Point 9 Midway Valley

Site of distributed faulting, use the methods described in Section 5.3. $P(C) = 1.0$ from slip tendency. The cumulative displacement is assessed to be 50 m.

REFERENCES

- Anderson, J.G., Wesnousky, S.G., and Stirling, M.W., 1996, Earthquake size as a function of fault slip rate: *Bulletin of the Seismological Society of America*, v. 86, no. 3, p. 683-690.
- Anderson, L.W., and Klinger, R.E., 1996, Evaluation and characterization of Quaternary faulting - Bare Mountain fault, Nye County, Nevada: Bureau of Reclamation Seismotectonic Report 96-5, Denver, Colorado, prepared for Yucca Mountain Project Activity 8.3.1.17.4.3.4, 78 p., plates and appendices.
- Anderson, R.E., Bucknam, R.C., Crone, A.J., Haller, K.M., Machette, M.N., Personius, S.F., Barnhard, T.P., Cecil, M.J., and Dart, R.L., 1995b, Characterization of Quaternary and suspected Quaternary faults, regional studies, Nevada and California: U. S. Geological Survey, Open-File Report 95-599, 56 p.
- Anderson, R.E., Crone, A.J., Machette, M.N., Bradley, L.-A., and Diehl, S.F., 1995a, Characterization of Quaternary and suspected Quaternary faults, Amargosa area, Nevada and California: U. S. Geological Survey, Open-File Report 95-613, 41 p.
- Archuleta, R., Cranswick, E., Mueller, C., and Spudich, P., 1982, Source parameters of the 1980 Mammoth Lakes, California, earthquake sequence, *Journal of Geophysical Research*, v. 87, p. 4595-4607.
- Brocher, T.M., Carr, M.D., Fox, K.F., J., and Hart, P.E., 1993, Seismic reflection profiling across Tertiary extensional structures in the eastern Amargosa Desert, southern Nevada, Basin and Range province: *Geological Society of America Bulletin*, v. 105, p. 30-46.
- Brocher, T.M., Hart, P.E., Hunter, W.C., and Langenheim, V.E., 1996, Hybrid-source seismic reflection profiling across Yucca Mountain, Nevada: regional lines 2 and 3: , U.S. Geological Survey Open File Report 96-28, 110 p.
- Brocher, T.M., and Hunter, W.C., 1996, Seismic reflection evidence against a shallow detachment beneath Yucca Mountain, Nevada: High-Level Radioactive Waste Management Proceedings of the Seventh International Conference, Las Vegas, Nevada, American Nuclear Society, La Grange Park, Illinois, p. 148-150.
- Brun, J.-P., Sokoutis, D., and Van Den Driessche, J., 1994, Analogue modeling of detachment fault systems and core complexes: *Geology*, v. 22, p. 319-322.

- Bryant, W.A., 1989, Panamint Valley fault zone and related faults, Inyo and San Bernardino Counties, California: California Division of Mines and Geology, Fault Evaluation Report FER-206, 33 p.
- Burchfiel, B.C., Hodges, D.V., and Royden, L.M., 1987, Geology of Panamint Valley-Saline Valley pull apart system, California; palinspastic evidence for low-angle geometry of a Neogene range-bounding fault: *Journal of Geophysical Research*, v. 92, p. 10,422-10,426.
- Byerlee, J. D., 1978, Friction of rocks: *Pure and Applied Geophysics*, v. 116, p. 615-626.
- Carr, W. J., 1984, Regional structural setting of Yucca Mountain, southwestern Nevada, and late Cenozoic rates of tectonic activity in part of the southwestern Great Basin, Nevada and California: U.S. Geological Survey, Open-File Report 84-854, 109 p.
- Carr, W.J., 1988, Volcano-tectonic setting of Yucca Mountain and Crater Flat, southwestern Nevada: U.S. Geological Survey Bulletin 1790, p. 35-85.
- Carr, W.J., 1990, Styles of extension in the Nevada Test Site region, southern Walker Lane Belt; an integration of volcano-tectonic and detachment fault models, *in* Wernicke, B. P. (ed.), Basin and Range extensional tectonics near the latitude of Las Vegas, Nevada: Geological Society of America Memoir 176, p. 283-303.
- Castro, G., and Poulos, S., 1977, Factors affecting liquefaction and cyclic mobility: *American Society of Civil Engineers Journal of the Geotechnical Engineering Division*, v. 103, no. GT6, p. 501-516.
- Chavez, D. E. and Priestley, K.F. 1985, ML observations in the Great Basin and MO versus ML relationships for the 1980 Mammoth Lakes, California, earthquake sequence, *Bulletin of the Seismological Society of America*, v. 75, p. 1583-1598.
- Cladouhos, T. T., and Marrett, R., 1996, Are fault growth and linkage consistent with power law distributions of fault lengths, *Journal of Structural Geology*, v. 18, 281-293.
- Coppersmith, K.J., and Youngs, R.R., 1992, Earthquakes and tectonics: in McGuire, R.K. (ed.), *Demonstration of a Risk-Based Approach to High-Level Waste Repository Evaluation: Phase 2*, Electric Power Research Institute, EPRI TR-100384, Palo Alto, California
- Cornwall, H.R., 1972, Geology and mineral deposits of southern Nye County, Nevada: Nevada Bureau of Mines and Geology, Bulletin 77, 49 p.

- Cowie, P. A., Knipe, R.J., and Main, I.G., 1996, Introduction to the Special Issue, *Journal of Structural Geology*, v. 18, p. v-x.
- Cowie, P. A., and Scholz, C.H. 1992, Growth of faults by accumulation of seismic slip, *Journal of Geophysical Research*, v. 97, p. 11085-11095.
- Cowie, P. A. and Scholz, C.H., 1996, Displacement-length relationship for faults: Data synthesis and discussion, *Journal of Structural Geology*, v. 14, 1149-1156.
- Decker, P.L., 1990, Style and mechanics of liquefaction-related deformation, lower Absaroka Volcanic Supergroup (Eocene), Wyoming: Geological Society of America Special Paper 240, 71 p., 8 plates.
- Densmore, A. L., and Anderson, R. S., 1994, Recent tectonic geomorphology of Panamint Valley, California: American Geophysical Union, EOS, Fall Meeting Abstracts with Programs, p. 296.
- dePolo, C.M., 1997, in preparation, A method using geomorphic observations to estimate slip rates for normal faults in the Great Basin: Ph.D. Dissertation, University of Nevada, Reno.
- dePolo, C.M., Clark, D.G., Slemmons, D.B., and Ramelli, A.R., 1991, Historical surface faulting in the Basin and Range province, western North America—Implications for fault segmentation: *Journal of Structural Geology*, v. 13, no. 2, p. 123-136.
- Dohrenwend, J.C., Menges, C.M., Schell, B A., and Moring, B.C., 1991, Reconnaissance photogeologic map of young faults in the Las Vegas 1° x 2° quadrangle, Nevada, California, and Arizona: U. S. Geological Survey, Miscellaneous Field Studies Map MF-2182, 1:250,000.
- Dohrenwend, J.C., Schell, B.A., McKittrick, M.A., and Moring, B.C., 1992, Reconnaissance photogeologic map of young faults in the Goldfield 1°x2° quadrangle, Nevada and California: U. S. Geological Survey Miscellaneous Field Studies Map MF-2183, 1:250,000.
- Donovan, D.E., 1991, Neotectonics of the southern Amargosa Desert, Nye County, Nevada and Inyo County, California: Masters Thesis, University of Nevada Reno, 151 p., 5 plates (1:48,000).
- Doser, D.D., and Smith, R.B., 1982, Seismic moment rates for earthquakes in the Utah region: *Bulletin of the Seismological Society of America*, v. 72, p. 525-552.

- Doser, D. D., and Smith, R. B., 1983, Seismicity of the Teton-Southern Yellowstone Region, Wyoming: *Bulletin of the Seismological Society of America*, v. 73, p. 1369-1394.
- Doser, D.D., and Smith, R.B., 1985, Source parameters of the October 28, 1983 Borah Peak, Idaho earthquake from body wave analysis: *Bulletin of the Seismological Society of America*, v. 75, p. 1041-1051.
- Doser, D.D., and Smith, R.B., 1989, An assessment of source parameters of earthquakes in the Intermontane region of the United States: *Bulletin of the Seismological Society of America*, v. 79, p. 1383-1409.
- Eddington, P.J., Smith, R.B., and Renggli, C., 1987, Kinematics of Basin-Range intraplate extension, *in* Coward, M.P., Dewey, J.F., and Hancock, P.L. (eds.), *Continental Extension: London Geological Society, Special Publication 28*, p. 371-392.
- Ekren, E.B., and Sargent, K.A., 1965, Geologic Map of the Skull Mountain Quadrangle, Nye County, Nevada: U.S. Geological Survey, Geologic Map, GQ-387, 1 plate (1:24,000).
- Fernald, A.T., Corchary, G.S., Williams, W.P., and Colton, R.B., 1968, Surficial deposits of Yucca Flat area, Nevada Test Site, *in* Eckel, E. B. (eds.), *Nevada Test Site: Geological Society of America, Memoir 110*, p. 49-55.
- Ferrill, D.A., Stirewalt, G.L., Henderson, D.B., Stamatakos, J.A., Morris, A.P., Wernicke, B.P., and Spivey, K.H., 1995, Faulting in the Yucca Mountain region: critical review and analysis of tectonic data from the central basin and range. Report CNWRA 95-017.
- Ferrill, D.A., Stamatakos, J.A., Jones, S.M., Rahe, B., McKague, H.L., Martin, R.H., and Morris, A.P., 1996, Quaternary slip history of the Bare Mountain Fault (Nevada) from the morphology and distribution of alluvial fan deposits: *Geology*, v.24, no. 6, p.559-562.
- Fossen, H., and Gabrielsen, R.H., 1996, Experimental modeling of extensional fault systems by use of plaster: *Journal of Structural Geology*, v. 18, no. 5, p. 673-687.
- Frankel, A., 1995, Mapping seismic hazard in the Central and Eastern United States: *Bulletin of the Seismological Society of America*, v. 66, p. 8-21.
- Fridrich, C.J., 1995, Tectonic evolution of the Crater Flat basin, Yucca Mountain region, Nevada: *in* Simonds, F.W. (ed.), *Characterization of detachment faults in the Yucca Mountain region*, U.S. Geological Survey Administrative Report Milestone Number 3GTD500M, p. 111-152.

- Frizzell, V.A., Jr., and Shulters, J., 1990, Geologic map of the Nevada Test Site, southern Nevada: U.S. Geological Survey, Miscellaneous Investigations Series Map I-2046, 1 plate (1:100,000).
- Hancock, P.L., and Barka, A.A., 1987, Kinematic indicators on active normal faults in western Turkey: *Journal of Structural Geology*, v. 9, no. 5/6, p. 573-584.
- Hanks, T.C., and Kanamori, H., 1979, A moment magnitude scale, *Journal of Geophysical Research*, v. 84, p. 2348-2350.
- Hill, D.P., Reasenber, P.A., Michael, A., Arabasz, W.J., Beroza, G., Brumbaugh, D., Brune, J.N., Castro, R., Davis, S., dePolo, D., Ellsworth, W.L., Gomberg, J., Harmsen, S., House, L., Jackson, S., Johnston, M., Jones, L., Keller, R., Malone, S., Munguia, L., Nava, S., Pechmann, J., Sanford, A., Simpson, R., Smith, R.B., Stark, M., Stickney, M., Vidal, A., Walter, S., Wong, V., and Zollweg, J., 1993, Seismicity remotely triggered by the M 7.3 Landers, California, earthquake, 1993: *Science*, v. 260, p. 1617-1623.
- Hinrichs, E.N., 1968, Geologic map of the Camp Desert Rock quadrangle, Nye County, Nevada: U. S. Geological Survey Geologic Quadrangle Map GQ-726, 1:24,000.
- Hoffard, J.L., 1991, Quaternary tectonics and basin history of Pahrump and Stewart valleys, Nevada and California: M.S. Thesis, University of Nevada, Reno, 138 p.
- Hoisch, T.D., Heizler, M.T., and Zartman, R.E., 1997, Timing of detachment faulting in the Bullfrog Hills and Bare Mountain area, southwest Nevada: inferences from $^{40}\text{Ar}/^{39}\text{Ar}$, K-Ar, U-Pb and fission-track thermochronology: *Journal of Geophysical Research*, v. 102, no. B2, p. 2815-2833.
- Hudson, M.R., Sawyer, D.A., and Warren, R.G., 1994, Paleomagnetism and rotation constraints for the middle Miocene southwestern Nevada volcanic field: *Tectonics*, v. 13, no. 2, p. 258-277.
- Jackson, J., and White, N., 1989, Normal faulting in the upper continental crust: observations from regions of active extension: *Journal of Structural Geology*, v. 11, p. 15-36.
- Klinger, R.E. and Piety, L.A., 1996, Evaluation and characterization of Quaternary faulting on the Death Valley and Furnace Creek faults, Death Valley, California: U.S. Bureau of Reclamation, Seismotectonic Report 96-10, 98 p.
- Lipman, P.W., and McKay, E.J., 1965, Geologic map of the Topopah Spring SW quadrangle, Nye County, Nevada: U. S. Geological Survey Quadrangle Map GQ-439, 1:24,000.

- Louie, J., Shields, G., Ichinose, G., Hasting, M., Plank, G., and Bowman, S., 1996, Shallow geophysical constraints on displacement and segmentation of the Pahrump Valley fault zone, *in* Seismic Hazards in the Las Vegas Region: Nevada Earthquake Safety Council Program and Abstracts, p. 29-30.
- Lowry, A.R. and R.B. Smith, 1994, High resolution mapping of flexural rigidity using maximum entropy coherence of gravity and topography: *Journal of Geophysical Research*, v. 99, p. 20,095-20,122.
- Lowry, A.R., and Smith, R.B., 1995, Strength and rheology of western U. S. Cordillera: *Journal of Geophysical Research*, v. 100, p. 17,947-17,964.
- Maldonado, F., 1985, Geologic map of the Jackass Flats area, Nye County, Nevada: U.S. Geological Survey, Miscellaneous Investigations, Map I-1519, 1 plate (1:48,000).
- Marrett, R., 1996, Aggregate properties of fracture populations, *Journal of Structural Geology*, v. 18, 169-178.
- Mason, D.B., 1996, Earthquake magnitude potential of the Intermountain seismic belt, USA, from surface-parameter scaling of late Quaternary faults: *Bulletin of the Seismological Society of America*, v. 86, p. 1487-1506.
- McGuire, R.K., 1985, Seismic hazard methodology for nuclear facilities in the Eastern United States: Dames and Moore, Golden, Vol. 2, Appendix A, EPRI Research Project Number P101-29. *Veneziano method, developed for EPRI (McGuire, 1985)*
- McKague, H.L., Stamatakos, J.A., and Ferrill, D.A., 1996, Type 1 faults in the Yucca Mountain region: report CNWRA 96-007 prepared by Center for Nuclear Waste Regulatory Analyses for the Nuclear Regulatory Commission, Contract NRC-02-93-005, November.
- McKeown, F.A., Healey, D.L., and Miller, C.H., 1976, Geologic map of the Yucca Lake Quadrangle, Nye County, Nevada: U. S. Geological Survey, Geologic Quadrangle Map, map GQ-1327, 1:24,000.
- Melosh, H.J., 1990, Mechanical basis for low-angle normal faulting in Basin and Range province: *Nature*, v. 343, p. 331-335.
- Mendoza, C., and Hartzell, S.H., 1988, Inversion for slip distribution using teleseismic P-waveforms: North Palm Springs, Borah Peak, and Michoacan earthquakes: *Bulletin of the Seismological Society of America*, v. 78, p. 1092-1111.

- Meremonte, M., Gomberg, J., and Cranswick, E., 1995, Constraints on the 29 June 1992 Little Skull Mountain, Nevada, earthquake sequence provided by robust hypocenter estimates: *Bulletin of the Seismological Society of America*, v. 85, no. 4, p. 1039-1049.
- Minor, S.A., et al., 1993, Preliminary geologic map of the Pahute Mesa 30'x60' quadrangle, Nevada: U.S. Geological Survey Open-File Report 93-299, 39 p.
- Monsen, S.A., Carr, M.D., Reheis, M.C., and Orkild, P.P., 1992, Geologic map of Bare Mountain, Nye County, Nevada: U.S. Geological Survey Miscellaneous Investigations Series Map I-2201, 1:24,000 scale.
- Morris, A., Ferrill, D. A., and Henderson, D. B., 1996, Slip-tendency analysis and fault reactivation: *Geology*, v. 24, p. 275-278.
- Nicol, A., Walsh, J.J., Watterson, J., and Gillespie, P.A., Fault size distributions-are they really power-law?, *Journal of Structural Geology*, v. 18, p. 191-197.
- Ofoegbu, G.I., and Ferrill, D.A., 1995, Finite element modeling of listric normal faulting. Report CNWRA 95-008.
- Okaya, D.A., and Thompson, G.A., 1985, Geometry of Cenozoic extensional faulting, Dixie Valley, Nevada: *Tectonics*, v. 4, no. 1, p. 107-125.
- Orkild, P.P., Sargent, K.A., and Snyder, R.P., 1969, Geologic map of Pahute Mesa, Nevada Test Site and vicinity, Nye County: U.S. Geological Survey, Miscellaneous Geologic Investigations Map I-567, 1 plate (1:48,000).
- Peterson, F.F., Bell, J.W., Dorn, R.I., Ramelli, A.R., and Ku, T.-L., 1995, Late Quaternary geomorphology and soils in Crater Flat, Yucca Mountain, southern Nevada: *Geological Society of America Bulletin*, v. 107, no. 4, p. 379-395.
- Pezzopane, S.K., and Dawson, T.E., 1996, Fault displacement hazard: A summary of issues and information; Chapter 9, *Seismotectonic Framework and Characterization of Faulting at Yucca Mountain, Nevada*: U.S. Geological Survey, Report to U.S. Department of Energy, p. 9-1-9-160.
- Piety, L. A., 1995, Compilation of known and suspected Quaternary faults within 100 km of Yucca Mountain, Nevada and California: U.S. Geological Survey, Open-File Report 94-112, 404 p.

- Poole, F.G., Elston, D.P., and Carr, W.J., 1965, Geologic map of the Cane Spring Quadrangle, Nye County, Nevada: U.S. Geological Survey, Geologic Map, GQ-455, 1:24,000.
- Potter, C.J., Dickerson, R.P., and Day, W.C., 1995, Nature and continuity of the Sundance fault, Yucca Mountain, Nevada, U. S. Geological Survey Administrative Report to the U. S. Department of Energy, 27 p., 4 figures, 3 plates.
- Purcaru, G., and Berckhemer, H., 1978, A magnitude scale for very large earthquakes: *Tectonophysics* v. 49, p. 189-198.
- Reheis, M.C., 1988, Preliminary study of Quaternary faulting on the east side of Bare Mountain, Nye County, Nevada, *in* Carr, M.D., and Yount, J.C. (eds.), *Geologic and hydrologic investigations of a potential nuclear waste disposal site at Yucca Mountain, southern Nevada*: U.S. Geological Survey Bulletin 1790, p. 103-111.
- Reheis, M.C., 1991, Aerial photographic interpretation of lineaments and faults in late Cenozoic deposits in the eastern parts of the Saline Valley 1:100,000 Quadrangle, Nevada and California, and the Darwin Hills 1:100,000 Quadrangle, California: U.S. Geological Survey, Open-File Report 90-500, 6 p., 2 plates.
- Reheis, M.C., 1992, Aerial photographic interpretation of lineaments and faults in late Cenozoic deposits in the Cactus Flat and Pahute Mesa 1:100,000 quadrangles and the western parts of the Timpahute Range, Pahrangat Range, Indian Springs, and Las Vegas 1:100,000 Quadrangles, Nevada: U.S. Geological Survey, Open-File Report 92-193, 14 p., 3 plates.
- Reheis, M.C. and Noller, J.S., 1991, Aerial photographic interpretation of lineaments and faults in late Cenozoic deposits in the eastern part of the Benton Range 1:100,000 Quadrangle and the Goldfield, Last Chance Range, Beatty, and Death Valley Junction 1:100,000 Quadrangles, Nevada and California: U.S. Geological Survey Open-File Report 90-41, 9 p., 4 plates.
- Renalli, G., 1995, *Rheology of the Earth*, 2nd Edition: Chapman and Hall, pp. 413.
- Richins, W.D., Pechmann, J.C., Smith, R.B., Langer, C.J., Goter, S.K., Zollweg, J.E., and King, J. J., 1987, The 1983 Borah Peak, Idaho earthquake and its aftershocks: *Bulletin of the Seismological Society of America*, 77, p. 694-723.
- Richins, W.D., Smith, R.B., Langer, C.J., Zollweg, J.E., King, J.J., and Pechmann, J.C., 1985, The 1983 Borah Peak, Idaho earthquake: Relationship of aftershocks to the mainshock, surface faulting, and regional tectonics, Workshop XXVIII on "The Borah Peak Earthquake": U.S. Geological Survey Open-File Report, 85-290, p. 285-310.

- Rogers, A. M., Corbett, E.J, Priestley, K., and dePolo, D, 1991, The seismicity of Nevada and some adjacent part of the Great Basin, *in*. Slemmons, D.B., Engdahl, E.R., Zoback, M.L. and Blackwell, D.D (eds.), Neotectonics of North America: Geological Society of America, SMV V-1, Decade Map v. 1, p. 153-184.
- Sawyer, T.L. and Reheis, M.C., 1997, Holocene paleoseismicity, segmentation, and seismic potential of the Fish Lake Valley fault zone, Nevada and California: Western States Seismic Policy Council, Basin and Range Province Seismic Hazard Summit, Program and Abstracts, p. 64.
- Scholz, C. H., 1990, The Mechanics of Earthquakes and Faulting, Cambridge University Press, New York, 439 p.
- Schweickert, R.A., and Lahren, M.M., 1997, Strike-slip fault system in Amargosa Valley and Yucca Mountain, Nevada: Tectonophysics, v. 272, no. 1, p. 25-42.
- Schweig, E.S., III, 1989, Basin-Range tectonics in Darwin Plateau, southwestern Great Basin, California: Geological Society of America Bulletin, v. 101, no. 5, p. 652-662.
- Scott, R.B., 1990, Tectonic setting of Yucca Mountain, southwest Nevada, *in* Wernicke, B. P. (ed.), Basin and Range extensional tectonics near the latitude of Las Vegas, Nevada: Geological Society of America Memoir 176, Boulder, Colorado, p. 251-282.
- Scott, R.B., and Bonk, J., 1984, Preliminary geologic map of Yucca Mountain, Nye County, Nevada with geologic sections: U. S. Geological Survey Open File Report 84-494, (map scale 1:12,000), 9 p.
- Seed, H.B., and Idriss, I.M., 1982, Ground motions and soil liquefactions during earthquakes: Berkeley, California, Earthquake Engineering Research Institute, 134 p.
- Shemeta, J., 1989, New analyses of three-component digital data for aftershocks of the 1983 Borah Peak, Idaho, earthquake: Source parameters and refined hypocenters, M.S. Thesis University of Utah, 129 p.
- Shroba, R.R., Muhs, D.R., and Rosholt, J.N., 1988, Uranium-trend and uranium-series age estimates of surficial and fracture-fill deposits on the Carpetbag fault system, Nye County, Nevada: Geological Society of America, Abstracts with Programs, v. 20, p. 231.
- Sibson, R.H., 1982, Fault zone models, heat flow, and the depth distribution of earthquakes in the continental crust of the United States: Bulletin of the Seismological Society of America, v. 72, p. 151-163.

Simonds, F.W., and Scott, R.B., 1996, Geology and hydrothermal alteration at Calico Hills, Nye County, Nevada: U.S. Geological Survey Milestone Report: 3GTD018M prepared in cooperation with the Nevada Field Office U.S. Department of Energy, Interagency Agreement DE-A108-92NV10874, 104 p. two plates, 1:12,000.

Simonds, F.W., et al., 1995, Map showing fault activity of the Yucca Mountain area, Nye County, Nevada: U.S. Geological Survey Miscellaneous Investigations Series Map I-2520, 30 p., scale 1:24,000.

Smith, K.D., Brune, J.N., Savage, M.K., and Sheehan, A.F., 1995, The 29 June 1992 Little Skull Mountain earthquake and its aftershock sequence: University of Nevada Reno - Seismological Laboratory Mackay School of Mines, Reno, Nevada, v. Special Report to the Department of Energy and United States Geological Survey, p. 20.

Smith, R.B. and Arabasz, W.J., 1991, Seismicity of the Intermountain Seismic Belt, *in* D.B. Slemmons, E.R. Engdahl, M.L. Zoback and D. D. Blackwell (eds.), Neotectonics of North America: Geological Society of America, SMV V-1, Decade Map Volume 1, p. 185-228.

Smith, R.B. and Bruhn, R.L., 1984, Intraplate extensional tectonics of the western U.S. Cordillera: Inferences on structural style from seismic reflection data, regional tectonics and thermal-mechanical models of brittle-ductile deformation: *Journal of Geophysical Research*, v. 89, p. 5733-5762.

Smith, R. B. and Eddington, P., 1984, Strain rates in Utah from seismic moments, geodetic surveys and paleoslip, Workshop XI on "Evolution of Regional and Urban Earthquake Hazards and Risk in Utah": U. S. Geological Survey Open-File Report, 84-763, p. 422-237.

Smith, R.B., Nagy, W.C., Julander, K.A., Viveiros, J.J., Barker, C.A., and Gants, D.G., 1989, Geophysical and tectonic framework of the eastern Basin and Range-Colorado Plateau-Rocky Mountain transition, in Geophysical Framework of the Continental U.S., Pakiser, L.C. and Mooney, W.C., (eds.), Geological Society of America Memoir 172, 205-233.

Smith, R.B., and Richins, W.D., 1984, Seismicity and earthquake hazards of Utah and the Wasatch front: Paradigm and Paradox Proceedings from Workshop XI on "Evaluation of Regional and Urban Earthquake Hazards and Risk in Utah", U. S. Geological Survey Open-File Report, v. 84-763, 73-112.

- Smith, R.B., Richins, W.D., and Doser, D.I., 1985, The Borah Peak earthquake: Seismicity, faulting kinematics and tectonic mechanism, Workshop XXVIII on "The Borah Peak Earthquake": U.S. Geological Survey Open-File Report, v. 85-290, p. 236-263.
- Smith, R.P., and Jackson, S.M., 1996, Paleoseismology and seismic hazards evaluations in extensional volcanic terrains: *Journal of Geophysical Research*, v. 10, p. 6,277-6,292.
- Smith, R.P., Jackson, S.M., and Hackett, W.R., 1996, Paleoseismology and seismic hazards evaluations in extensional tectonic terrains: *Journal of Geophysical Research*, v. 101, p. 6277-6292.
- Snyder, D.B., and Carr, W.J., 1984, Interpretation of gravity data in a complex volcano-tectonic setting, southwestern Nevada: *Journal of Geophysical Research*, v. 89, no. B12, p. 10,193-10,206.
- Stein, R.S., and Barrientos, S.E., 1985, Planar high-angle faulting in the Basin and Range: geodetic analysis of the 1983 Borah Peak, Idaho, earthquake: *Journal of Geophysical Research*, v. 90, no. B13, p. 11,355-11,366.
- Stewart, J.H., 1988, Tectonics of the Walker Lane Belt, western Great Basin-Mesozoic and Tertiary deformation in a zone of shear, *in* Ernst, W.G. (ed.), *Metamorphism and crustal evolution of the western United States, Rubey Volume VII*: Englewood Cliffs, New Jersey, Prentice Hall, p. 683-713.
- Stock, J.M., Healy, J.H., Hickman, S.H., and Zoback, M.D., 1985, Hydraulic fracturing stress measurements at Yucca Mountain, Nevada, and relationship to the regional stress field: *Journal of Geophysical Research*, v. 90, no. B10, p. 8691-8706.
- Swadley, W.C., and Hoover, D.L., 1990, Geologic Map of the surficial deposits of the Yucca Flat area, Nye County, Nevada: U.S. Geological Survey, Miscellaneous Investigations Series Map I-2047, 1 plate (1:48,000).
- Swadley, W.C., and Huckins, H.E., 1990, Geologic map of the surficial deposits of the Skull Mountain Quadrangle, Nye County, Nevada: U.S. Geological Survey, Miscellaneous Investigation Series, Map I-1972, 1 plate (1:24,000).
- Sweetkind, D.S., and Williams-Stroud, S., 1996, Characteristics of fractures at Yucca Mountain, Nevada: Synthesis Report, U. S. Geological Survey Administrative Report to the U. S. Department of Energy, 124 p.
- Sweetkind, D.S., Verbeek, E.R., Geslin, J.K., and Moyer, T.C., 1995a, Fracture character of the Paintbrush Tuff nonwelded hydrologic unit, Yucca Mountain, Nevada: U. S. Geological Survey Administrative Report to the U. S. Department of Energy, 202 p.

- Sweetkind, D.S., Verbeek, E.R., Singer, F.R., Byers, F.M., Jr., and Martin, L.G., 1995b, Surface fracture network at pavement p2000, Fran Ridge, near Yucca Mountain, Nye County, Nevada: U.S. Geological Survey Administrative Report to the U.S. Department of Energy, 130 p.
- Throckmorton, C.K., and Verbeek, E.R., 1995, Joint networks in the Tiva Canyon and Topopah Spring Tuffs of the Paintbrush Group, southwestern Nevada: U.S. Geological Survey Open File Report 95-2, 179 p.
- U.S. Department of Energy (DOE), 1996, Probabilistic volcanic hazards analysis for Yucca Mountain, Nevada: Civilian Radioactive Waste Management System Management and Operating Contractor BA00000000-01717-2200-00082, Rev. 0, Washington, DC: U.S. Government Printing Office.
- U.S. Geological Survey (Whitney, J.W., Coordinator), 1996, Seismotectonic framework and characterization of faulting at Yucca Mountain, Nevada: U.S. Geological Survey report to the Department of Energy that fulfills Level 3 Milestone 3GSH100M WBS Number 1.2.3.2.8.3.6, four volumes variously paginated.
- Veneziano, D., and Van Dyck, J., 1985, Statistical discrimination of *aftershocks* and their contribution to seismic hazard: Seismic Hazard Methodology for Nuclear Facilities in the Eastern United States: EPRI Res. Project No. P101-29, EPRI/SOG Draft 85-1, v. 2, Appendix A-4.
- Wells, D.L., and Coppersmith, K.J., 1994, New empirical relationships among magnitude, rupture length, rupture width, rupture area, and surface displacement: Bulletin of the Seismological Society of America, v. 84, no. 4, p. 974-1002.
- Wesnousky, S. G., Scholz, C.H., and Shimazaki, K., 1982, Deformation of an island arc: Rates of moment release and crustal shortening in intraplate Japan determined from seismicity and Quaternary fault data: Journal of Geophysical Research, v. 87, p. 6829-6852.
- Westaway, R., and Smith, R.B., 1989, Strong ground motion in normal-faulting earthquakes: Geophysical Journal of the Royal Astronomical Society, 96, p. 529-559.
- Wheeler, R.L., 1989, Persistent segment boundaries on basin-range normal faults, in Schwartz, D.P. and Sibson, R.H. (eds.), Fault segmentation and controls of rupture initiation and termination: U.S. Geological Survey Open File Report 89-315, p.432-444.

- Wiemer, S., 1996, ZMAP Users Guide Version 3.0, Geophysical Institute, University of Alaska, Fairbanks, internal publication, 109 pages.
- Winograd, I.J., and Thordarson, W., 1975, Hydrogeologic and hydrochemical framework, south-central Great Basin, Nevada-California, with special reference to the Nevada Test Site: U. S. Geological Survey Professional Paper 712-C, 126 p.
- Wong, I., 1996, Conversion to moment magnitude, A draft Woodward-Clyde Federal Consultants, distributed to the YMPHSA teams.
- Wong, I., Bott, J., and Wright, D., 1996, Historical earthquake catalog for Yucca Mountain, Yucca Mountain Seismic Source Characterization Workshop, Salt Lake City, Utah, 17 October 1996.
- Wright, L.A., 1989, Overview of the role of strike-slip and normal faulting in the Neogene history of the region northeast of Death Valley, California-Nevada, *in* Ellis, M. A. (ed.), Late Cenozoic evolution of the southern Great Basin: Nevada Bureau of Mines and Geology Open File Report 89-1, p. 1-11.
- Young, S. R., Stirewalt, G. L., and Morris, A. P., 1992, Geometric models of faulting at Yucca Mountain: Center For Nuclear Waste Regulatory Analyses, CNWRA 92-008.
- Youngs, R.R., and Coppersmith, K.J., 1985, Implications of fault slip rates and earthquake recurrence models for probabilistic seismic hazard estimates: Bulletin of the Seismological Society of America, v. 75, p. 939-964.
- Youngs, R.R., Swan, F.H., III, Power, M.S., Schwartz, D.P., and Green, R.K., 1987, Probabilistic analysis of earthquake and ground shaking hazard along the Wasatch Front, Utah, *in* Gori, P.O., and Hays, W.W. (eds.), Assessment of Regional Earthquake Hazards and Risk Along the Wasatch Front, Utah: U.S. Geological Survey Open File Report 87-585, M-1 to M-100.
- Yount, J.C., Shroba, R.R., McMasters, C.R., Huckins, H.E., and Rodriguez, E. A., 1987, Trench logs from a strand of the Rock Valley fault system, Nevada Test Site, Nye County, Nevada: U.S. Geological Survey, Miscellaneous Field Studies Map, MF-1824, 1 plate.
- Zhang, P., Ellis, M., Slemmons D. B., and Moa, F., 1990, Right-lateral displacements and the Holocene slip rate associated with prehistoric earthquakes along the southern Panamint Valley fault zone: Implications for southern basin and range tectonics and coastal California deformation: Journal of Geophysical Research, v. 95, p. 4857-4872.

**TABLE SDO-1
MAXIMUM MAGNITUDES FOR SOURCE ZONES**

Zone	Maximum Magnitude ¹	Name of Zone and Comments
1	6.4 ± 0.2 MBE $M_s 7.1 \pm 0.2$ $M_s 7.0 \pm 0.2$	Goldfield-Spring Mountain Zone including Yucca Mountain site: a) within 100 km of the site b) outside 100 km South, Frenchman Mtns. fault North, Emigrant Peak fault
2	6.4 ± 0.2 MBE $M_s 7.4 \pm 0.2$	Death Valley Zone a) within 100 km b) outside 100 km White Mountain fault system
3	6.4 ± 0.2 MBE $M_s 7.4 \pm 0.2$	Basin-Range Zone a) within 100 km b) outside 100 km Railroad Valley fault system

¹ M_s should be equivalent to M_w (Hanks and Kanamori, 1979).

TABLE SDO-2
MAGNITUDE SCALING RELATIONSHIPS USED

Magnitude versus Length	
Mason (1996)	extensional environments; all displacement types
$M_w = 5.08 + 1.16 \log L$	
Wells and Coppersmith (1994)	All environments (excl. subduction zones)
$M_w = 4.86 + 1.32 \log L$	normal-slip faults
$M_w = 5.16 + 1.12 \log L$	strike-slip faults
$M_w = 5.08 + 1.16 \log L$	all displacement types
Magnitude versus Maximum Surface Displacement	
Mason (1996)	extensional environments; all types
$M_s = 6.81 + 0.74 \log D$	
Wells and Coppersmith (1994)	All environments (excl. subduction zones)
$M_w = 6.61 + 0.71 \log D$	normal-slip faults
$M_w = 6.81 + 0.78 \log D$	strike-slip faults
$M_w = 6.69 + 0.74 \log D$	all displacement types
Magnitude versus Fault Area	
Wells and Coppersmith (1994)	all environments (excl. subduction zones)
$M_w = 3.93 + 1.02 \log A$	normal-slip faults
$M_w = 3.98 + 1.02 \log A$	strike-slip faults
$M_w = 4.07 + 0.98 \log A$	all displacement types
Magnitude versus Length x Displacement	
Mason (1996)	extensional environments; all displacement types
$M_s = 5.95 + 0.55 \log LD$	
Magnitude versus Length and Slip Rate	
Anderson et al. (1996)	15-20 km maximum seismogenic depth
$M_w = 5.12 + 1.16 \log L - 0.20 \log SR$	all displacement types
Magnitude via Seismic Moment	
Hanks and Kanamori (1979)	all environments
$M_w = 2/3 \log M_o - 10.7$	all displacement types
Average Displacement versus surface length	
Wells and Coppersmith (1994)	all environments (excl. subduction zones)
$\log (AD) = -0.99 + 1.24 \log L$	normal-slip faults
$\log (AD) = -0.70 + 1.04 \log L$	strike-slip faults
$\log (AD) = -1.43 + 0.88 \log L$	all faults

TABLE SDO-3
PARAMETERS FOR REGIONAL FAULT SOURCES
 (Page 1 of 2)

Fault (map designation)	Sense of Displacement	Length			Maximum Surface Displacement Per Event			Slip Rate			Quaternary Activity Relative Weighting	
		Minimum	Preferred	Maximum	Minimum	Preferred	Maximum	Minimum	Preferred	Maximum	Yes	No
Amaragosa River (AR)	rl	17	17	28				0.001	0.01	0.05	1	0
Ash Hill (AH)	rl	33	55	90				0.21	0.3	0.38	1	0
Bare Mountain (BM)	n	18	23	30	1.2	1.5	1.8	0.006	0.01	0.2	1	0
Belted Range (BLR)	n	22	34	46				0.01	0.05	0.1	1	0
Buried Hills (BH)	n	15	18	25				0.001	0.01	0.05	1	0
Buried Strike-slip (T6-SS)	rl	20	27	120				0.001	0.005	0.02	0.4	0.6
Cane Spring (CS)	ll	19	26	30				0.005	0.01	0.05	0.8	0.2
Carpetbag (CB)	n	17	28	39				0.001	0.005	0.01	0.8	0.2
Carrara (Highway 95) (H95)	rl	11	26	41				0.0005	0.001	0.005	0.2	0.8
Central Death Valley (DV)	m	41	61	75	2.5	3.5	4.5	2.6	3.8	7.4	1	0
E. Pintwater Range (EPR)	n	28	36	58				0.001	0.005	0.01	1	0
Eleana Range (ER)	n	11	15	15				0.003	0.01	0.05	1	0
Furnace Creek (FC)	rl	85	105	195	5.5	6	6.5	4	8	10	1	0
Grapevine Mountains (GM)	n	26	26	32				0.003	0.01	0.05	1	0
Hunter Mountain (HM)	nrl	46	64	65				1.3	2	2.7	1	0
Jackass Flats "Gravity" (JFG)	n	26	34	44				0.0005	0.005	0.05	0.9	0.1
Kawich Range (KR)	n	22	32	45				0.001	0.005	0.01	1	0
Keane Wonder (KW)	n	19	27	29				0.001	0.005	0.05	0.8	0.2
Mine Mountain (MM)	ll	21	21	35				0.005	0.01	0.09	1	0
N. Emigrant Valley (EVN)	rl?	18	37	45				0.01	0.02	0.08	1	0
Oak Spring Butte (OAK)	n	9	16	19				0.001	0.005	0.01	0.8	0.2
Oasis Valley (OSV)	n	5	8	19				0.0005	0.001	0.003	0.8	0.2
Pahrump Valley (PRP)	rl	24	61	66				0.005	0.01	0.1	1	0
Pahute Mesa #1 (PM1)	n	11	13	15				0.001	0.005	0.01	0.8	0.2
Panamint Valley (PAN)	rl	82	90	105				1.6	2.4	3.2	1	0
Peace Camp (PC)	nl	12	12	30				0.005	0.01	0.09	1	0

TABLE SDO-3
(Page 2 of 2)

Fault (map designation)	Sense of Displacement	Length			Maximum Surface Displacement Per Event			Slip Rate			Quaternary Activity Relative Weighting	
		Minimum	Preferred	Maximum	Minimum	Preferred	Maximum	Minimum	Preferred	Maximum	Yes	No
Rock Valley (RV)		33	48	68	1.1	3.6	4.5	0.01	0.02	0.08	1	0
South Silent Canyon (SSC)	n	11	14	17				0.001	0.005	0.01	0.8	0.2
Spotted Range (SPR)	n	17	30	30				0.001	0.01	0.05	1	0
Towne Pass (TP)	n	33	38	50				0.005	0.03	0.1	1	0
Wahmonie (WAH)		9	15	15				0.005	0.01	0.05	0.8	0.2
West Specter Range (WSR)	n	10	19	25				0.001	0.004	0.01	1	0
West Spring Mountains (WSM)	n	31	36	58				0.02	0.09	0.2	1	0
Western Pintwater Range (WPR)	n	33	54	76				0.005	0.008	0.05	1	0
Yucca Lake (YCL)	n	12	19	23				0.001	0.005	0.01	0.5	0.5
Yucca-Butte (YB)	n	26	34	49				0.015	0.026	0.053	1	0

**TABLE SDO-4
PARAMETERS FOR LOCAL FAULT SOURCES**

FAULT	TOTAL LENGTH	WEIGHTING	FAULT DIP	DOWNDIP WIDTH	WEIGHTING	MAXIMUM SURFACE DISPLACEMENT	WEIGHTING	SLIP RATE	WEIGHTING	MOMENT RATE	EVENT MOMENT	MOMENT MAGNITUDE
	Km		degrees	km		(m)		m/kyr		dyne-cm/yr	dyne-cm	
Solitario Canyon fault (SC)	16	0.3	55	11.1	0.2	0.7	0.3	0.009	0.3	4.436e+20	1.72494e+25	6.2
	18.5	0.4	55	13.3	0.4	1.2	0.4	0.015	0.4	1.107e+21	4.42890e+25	6.6
	21.5	0.3	55	17.6	0.4	1.5	0.3	0.022	0.3	2.497e+21	8.51400e+25	6.9
Iron Ridge fault (IR)	8.3	0.3	55	11.5	0.2	0.5	0.3	0.0023	0.3	6.586e+19	7.15875e+24	5.9
	8.3	0.4	55	14.5	0.6	0.7	0.4	0.0033	0.4	1.191e+20	1.26368e+25	6.1
Fatigue Wash fault (FW))	9	0.3	55	19	0.2	1	0.3	0.0051	0.3	2.907e+20	2.85000e+25	6.4
	16	0.3	55	9.7	0.2	1	0.3	0.003	0.3	1.048e+20	1.74600e+25	6.2
	17	0.4	55	11.6	0.6	1.25	0.4	0.005	0.4	3.132e+20	3.91500e+25	6.6
Southern Windy Wash fault (SWW)	20	0.3	75	17.6	0.2	1.5	0.3	0.009	0.3	1.045e+21	8.71200e+25	6.9
	9	0.3	45	8.5	0.2	0.6	0.3	0.009	0.3	2.066e+20	6.88500e+24	5.9
	11.5	0.4	55	10.5	0.6	0.88	0.4	0.011	0.4	3.985e+20	1.59390e+25	6.2
Paintbrush Canyon fault (PC(N) + PC(S))	15	0.3	75	17.6	0.2	1	0.3	0.017	0.3	1.122e+21	3.30000e+25	6.5
	12	0.3	55	14.5	0.3	0.4	0.3	0.007	0.3	3.654e+20	1.04400e+25	6.0
	17.5	0.4	55	17.3	0.6	1.7	0.4	0.008	0.4	7.266e+20	7.72013e+25	6.8
Paintbrush Canyon (North) (PC(N))	26.2	0.3	55	23	0.1	2.6	0.3	0.011	0.3	1.989e+21	2.35014e+26	7.3
	7	0.3	55	14.5	0.3	0.4	0.3	0.007	0.3	2.132e+20	6.09000e+24	5.8
	12.3	0.4	55	17.3	0.6	1	0.4	0.008	0.4	5.107e+20	3.19185e+25	6.5
Paintbrush Canyon (South) (PC(S))	18.7	0.3	55	23	0.1	1.45	0.3	0.011	0.3	1.419e+21	9.35468e+25	6.9
	9	0.3	55	14.5	0.3	0.3	0.3	0.007	0.3	2.436e+20	5.22000e+24	5.8
	11	0.4	55	17.3	0.6	1.7	0.4	0.008	0.4	4.567e+20	4.85265e+25	6.6
Stagecoach Road fault (SCR)	11	0.3	55	23	0.1	2.6	0.3	0.011	0.3	8.349e+20	9.86700e+25	6.9
	4.5	0.3	55	11.5	0.2	0.6	0.3	0.0057	0.3	8.849e+19	4.65750e+24	5.7
	10	0.4	55	14.5	0.6	0.8	0.4	0.017	0.4	6.656e+20	1.56600e+25	6.2
	12	0.3	55	19	0.2	1.2	0.3	0.028	0.3	1.756e+21	376200e+25	6.5

TABLE SDO-5
MULTIPLE-FAULT EVENT SCENARIOS AND EVENT MOMENTS FOR LOCAL FAULTS
 (Page 1 of 2)

FAULT ¹	TOTAL LENGTH	WEIGHTING	FAULT DIP	DOWNDIP WIDTH	WEIGHTING	MAXIMUM SURFACE DISPLACEMENT	WEIGHTING	EVENT MOMENT	MOMENT MAGNITUDE
	km		degrees	km		(cm)		dyne-cm	
PC(N) + BR	8	0.3	55	14.5	0.3	33	0.3	5.742e+24	5.8
	14	0.4	55	17.3	0.6	52	0.4	1.889e+25	6.3
	19.7	0.3	55	23.2	0.1	94	0.3	6.444e+25	6.8
PC(N) + PC(S) + BR + SCR	18.6	0.3	55	14.5	0.3	33	0.3	1.335e+25	6.1
	28.8	0.4	55	17.3	0.6	53	0.4	3.961e+25	6.6
	34.4	0.3	55	23.2	0.1	185	0.3	2.215e+26	7.2
PC(N) + PC(S) + BR	12	0.3	55	14.5	0.3	33	0.3	8.613e+24	6.0
	17.5	0.4	55	17.3	0.6	53	0.4	2.407e+25	6.4
	26.2	0.3	55	23.2	0.1	185	0.3	1.687e+26	7.1
SC + SWW	22	0.3	55	11.1	0.2	20	0.3	7.326e+24	5.9
	24.8	0.4	55	13.3	0.4	35	0.4	1.732e+25	6.2
	25	0.3	55	17.6	0.4	50	0.3	3.300e+25	6.5
FW + SWW + SCF	18.8	0.3	55	9.7	0.2	47	0.3	1.286e+25	6.1
	26	0.4	55	11.6	0.6	105	0.4	4.641e+25	6.6
	31	0.3	75	17.6	0.2	165	0.3	1.333e+26	7.0
SWW + SCF	9	0.3	45	8.5	0.2	55	0.3	6.311e+24	5.8
	12.3	0.4	55	10.5	0.6	62	0.4	1.201e+25	6.1
	14.4	0.3	75	17.6	0.2	84	0.3	3.193e+25	6.5
SWW + SCF + NCF	19.8	0.3	45	8.5	0.2	7.5	0.3	1.893e+24	5.4
	22.2	0.4	55	10.5	0.6	12	0.4	4.196e+24	5.7
	23	0.3	75	17.6	0.2	20	0.3	1.214e+25	6.1
ash event	18.6	0.3	55	14.5	0.3	115	0.3	4.652e+25	6.6
	28.8	0.4	55	17.3	0.6	145	0.4	1.084e+26	7.0
	34.4	0.3	55	23.2	0.1	175	0.3	2.095e+26	7.2
PC(N) + PC(S) + SCR	18.6	0.3	55	14.5	0.3	26	0.3	1.052e+25	6.0
	28.8	0.4	55	17.3	0.6	40	0.4	2.989e+25	6.5
	34.4	0.3	55	23.2	0.1	140	0.3	1.676e+26	7.1

¹ Fault names are given in Table SDO-4

TABLE SDO-5
(Page 2 of 2)

FAULT ¹	TOTAL LENGTH	WEIGHTING	FAULT DIP	DOWNDIP WIDTH	WEIGHTING	MAXIMUM SURFACE DISPLACEMENT	WEIGHTING	EVENT MOMENT	MOMENT MAGNITUDE
	km		degrees	km		(cm)		dyne-cm	
PC(S) + SCR	15.2	0.3	55	14.5	0.3	25	0.3	8.265e+24	5.9
	19.8	0.4	55	17.3	0.6	57	0.4	2.929e+25	6.4
	19.8	0.3	55	23.2	0.1	84	0.3	5.788e+25	6.7
PC(S) + BR	11	0.3	55	14.5	0.3	88	0.3	2.450e+25	6.4
	12.8	0.4	55	17.3	0.6	167	0.4	4.767e+25	6.6
	15.6	0.3	55	23.2	0.1	205	0.3	1.113e+26	7.0
SCR + SC	20.4	0.3	55	11.1	0.2	28	0.3	9.510e+24	6.0
	25.6	0.4	55	13.3	0.6	59	0.4	3.013e+25	6.5
	25.6	0.3	55	17.6	0.2	77	0.3	5.204e+25	6.7
IR + AW	9.7	0.3	55	11.1	0.2	50	0.3	8.075e+24	5.9
	9.7	0.4	55	13.3	0.6	70	0.4	1.355e+25	6.1
	11	0.3	55	17.6	0.2	100	0.3	2.904e+25	6.4
IR + AW + GD	13.2	0.3	55	11.1	0.2	50	0.3	1.099e+25	6.1
	13.2	0.4	55	13.3	0.6	70	0.4	1.843e+25	6.3
	13.7	0.3	55	17.6	0.2	100	0.3	3.643e+25	6.5
FW + SWW	18.8	0.3	55	9.7	0.2	30	0.3	8.206e+24	5.9
	26	0.4	55	11.6	0.6	105	0.4	4.604e+25	6.6
	31	0.3	75	17.6	0.2	165	0.3	1.307e+26	7.0
SWW + FW + NWW	22.8	0.3	55	9.7	0.2	14	0.3	4.644e+24	5.7
	26	0.4	55	11.6	0.6	20	0.4	9.048e+24	6.0
	27.4	0.3	75	17.6	0.2	24	0.3	1.736e+25	6.2
SWW + CWW	12.6	0.3	55	8.5	0.2	38	0.3	6.105e+24	5.8
	15.4	0.4	55	10.5	0.6	73	0.4	1.771e+25	6.2
	18	0.3	75	17.6	0.2	83	0.3	3.944e+25	6.6

¹ Fault names are given in Table SDO-4

Table SDO-6

Regressions Used for Estimating Displacement

Note that the regressions assumed *AD* and *MD* as the independent variable.

Regression	Reference
$\log AD = 0.63 M - 4.45$	Wells and Coppersmith (1994)
$\log AD = 1.24 \log L - 1.99$	Wells and Coppersmith (1994)
$\log AD = \log L - 1.43$	AAR Team (SSC workshop #4, Jan. 8, 1997)
$\log MD = 0.89 M - 5.90$	Wells and Coppersmith (1994)
$\log MD = 1.51 \log L - 1.98$	Wells and Coppersmith (1994)

where *AD* = average surface displacement in meters; *MD* = maximum surface displacement in meters; *M* = moment magnitude; and *L* = surface rupture length in kilometers.

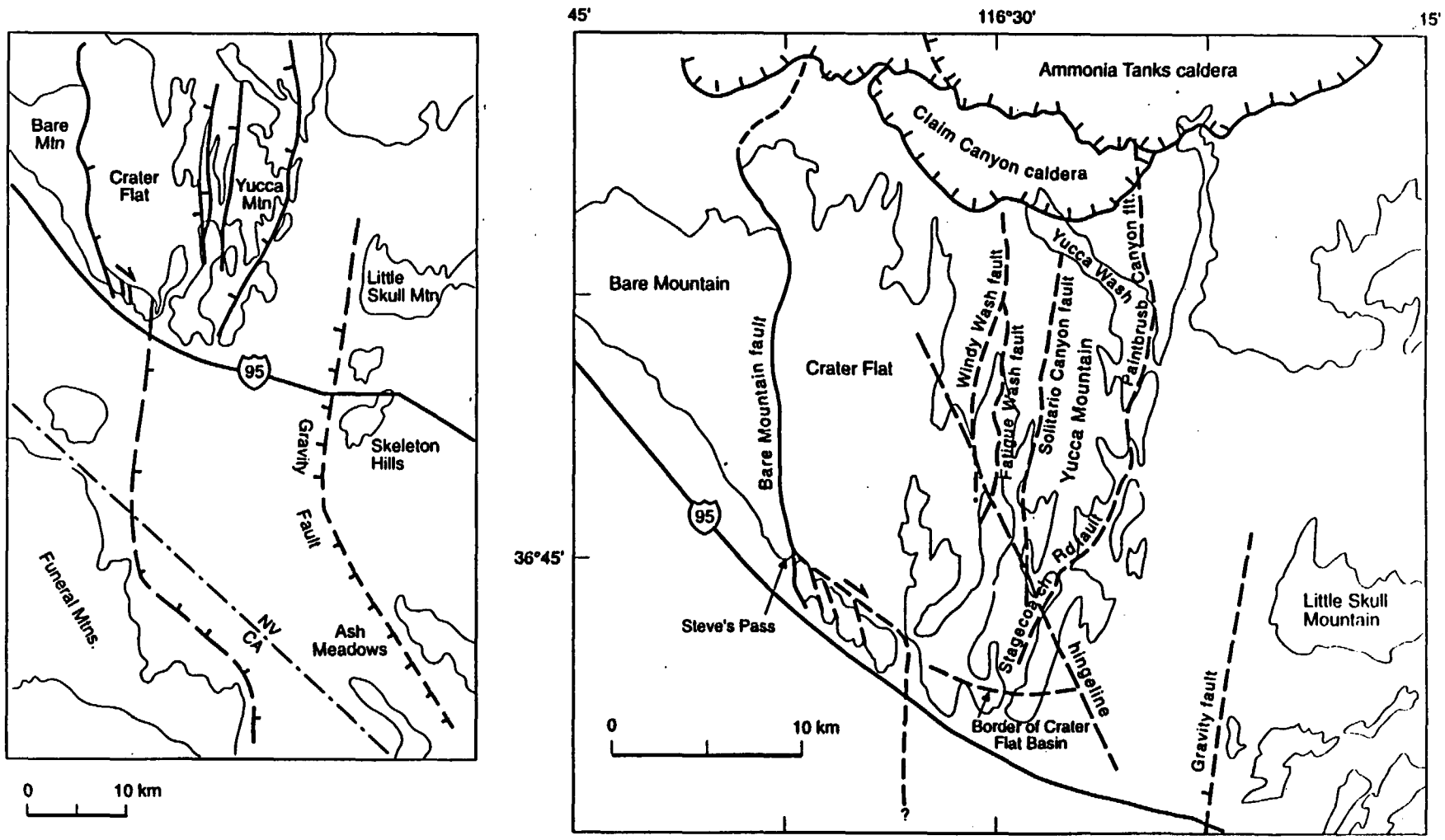


Figure SDO-1 Map showing location and features of Yucca Mountain and Crater Flat

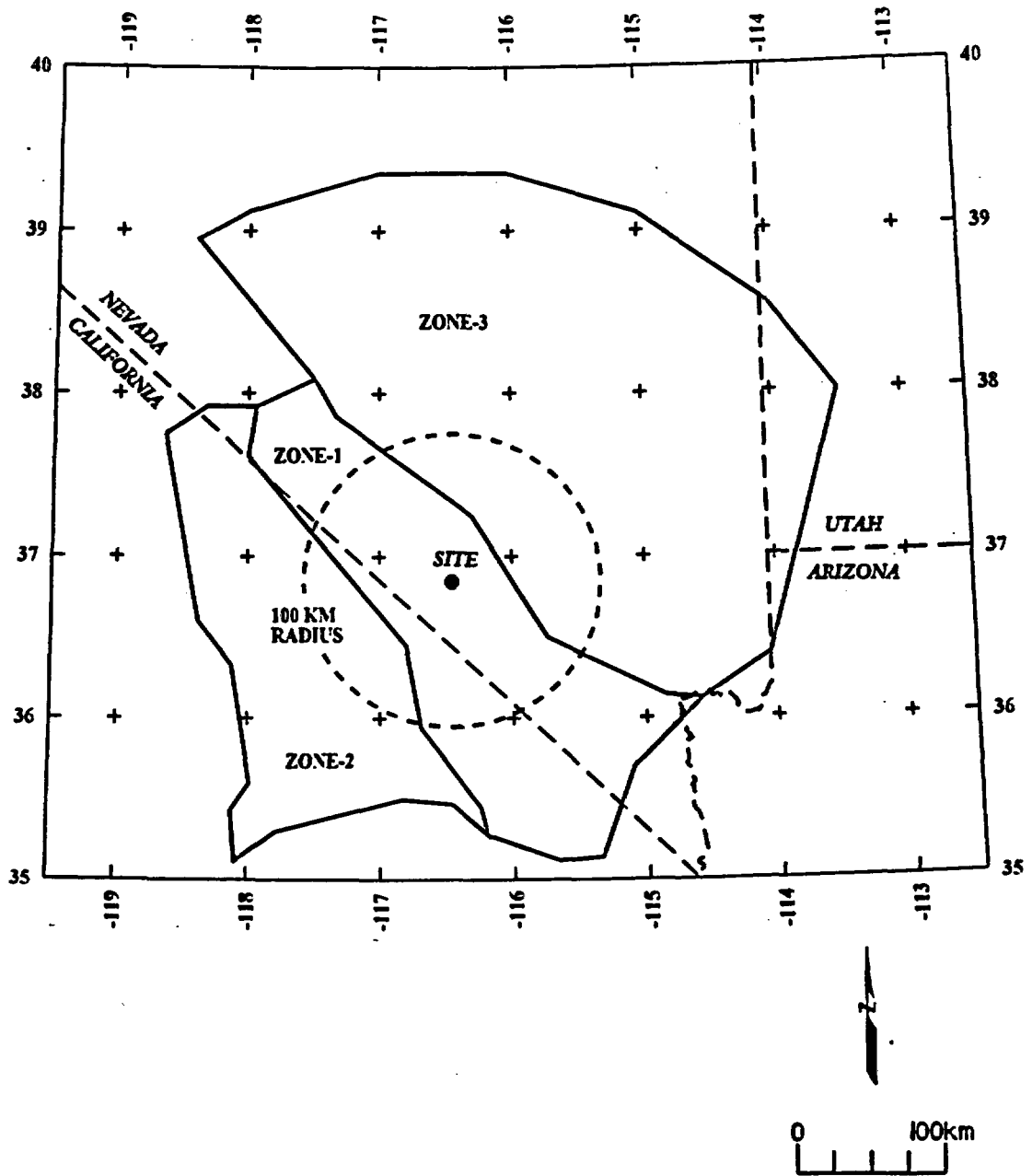


Figure SDO-2 Map showing the boundaries of zones used in the seismic source model

DEPTH DISTRIBUTION - SGB 1979-PRESENT

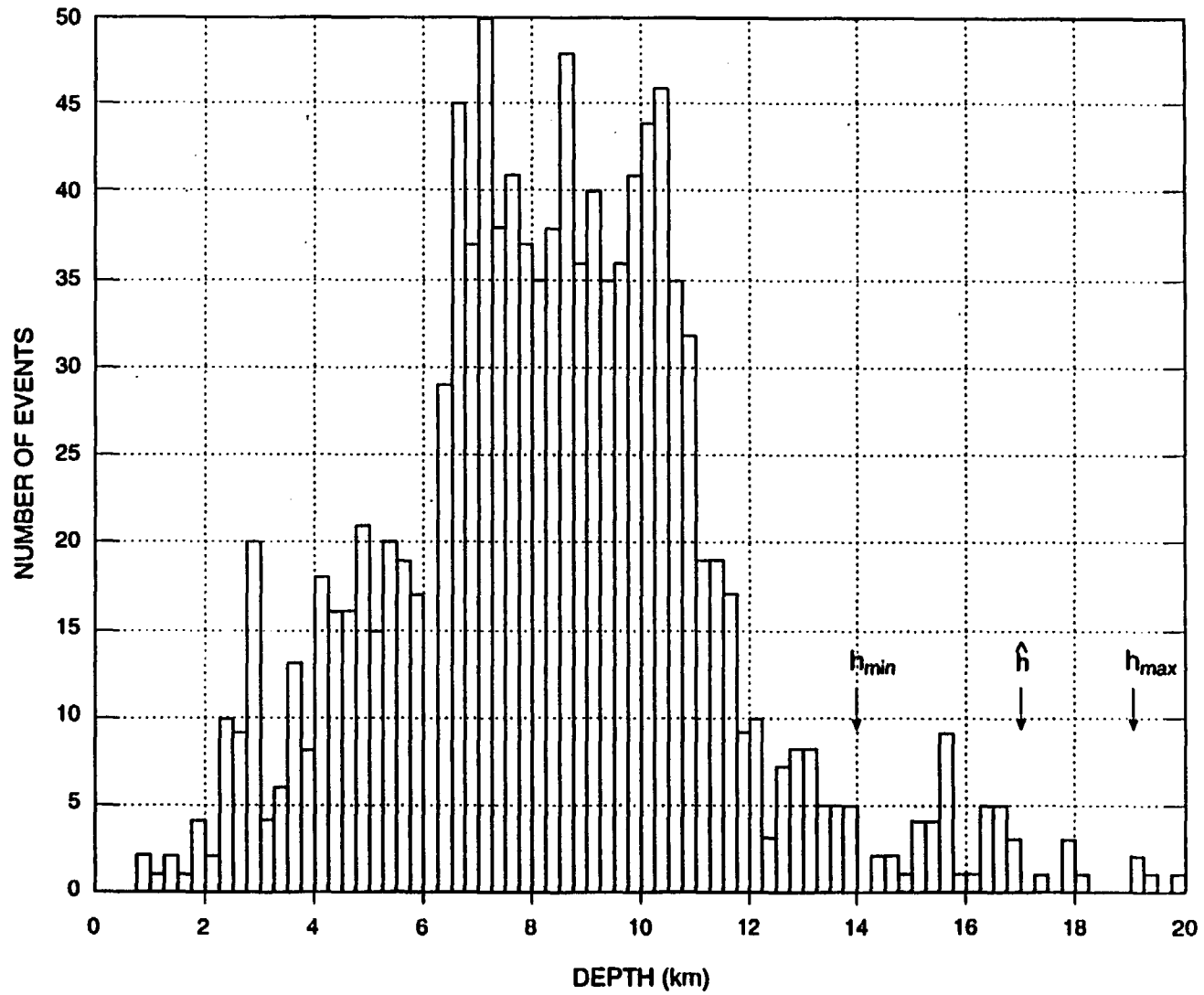


Figure SDO-3 Depth distribution of hypocenters (focal depth distribution) of earthquakes in the southern Great Basin (SGB)

DEPTH HISTOGRAM, $d_{min} \leq 1$ and $r \leq 100$ km

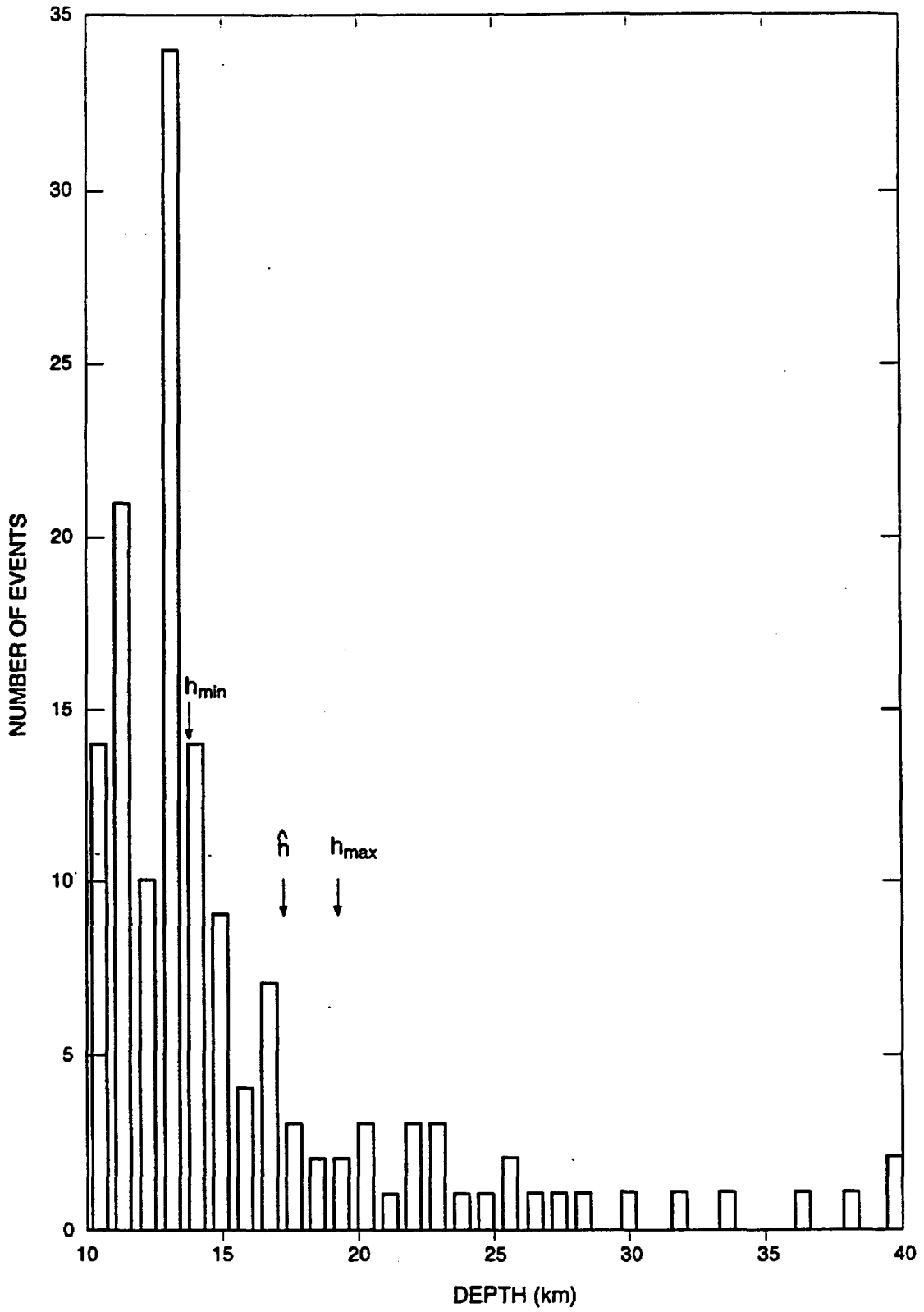


Figure SDO-4 Focal depth distribution of deep earthquakes in the area within $r < 100$ km of Yucca Mountain

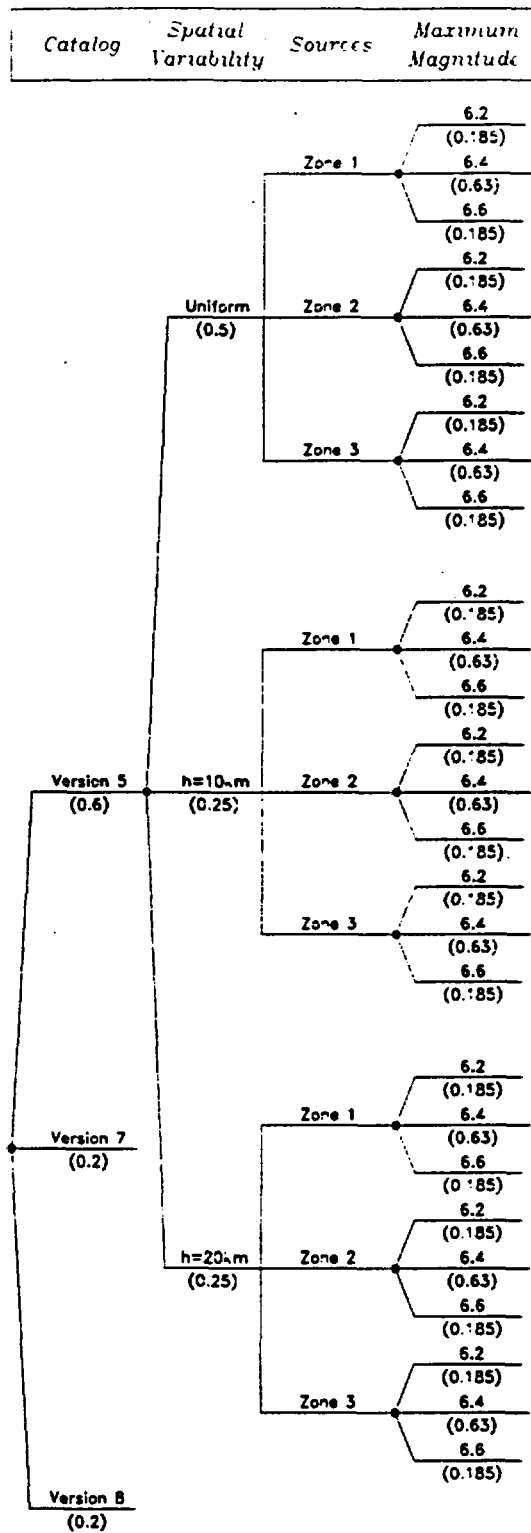
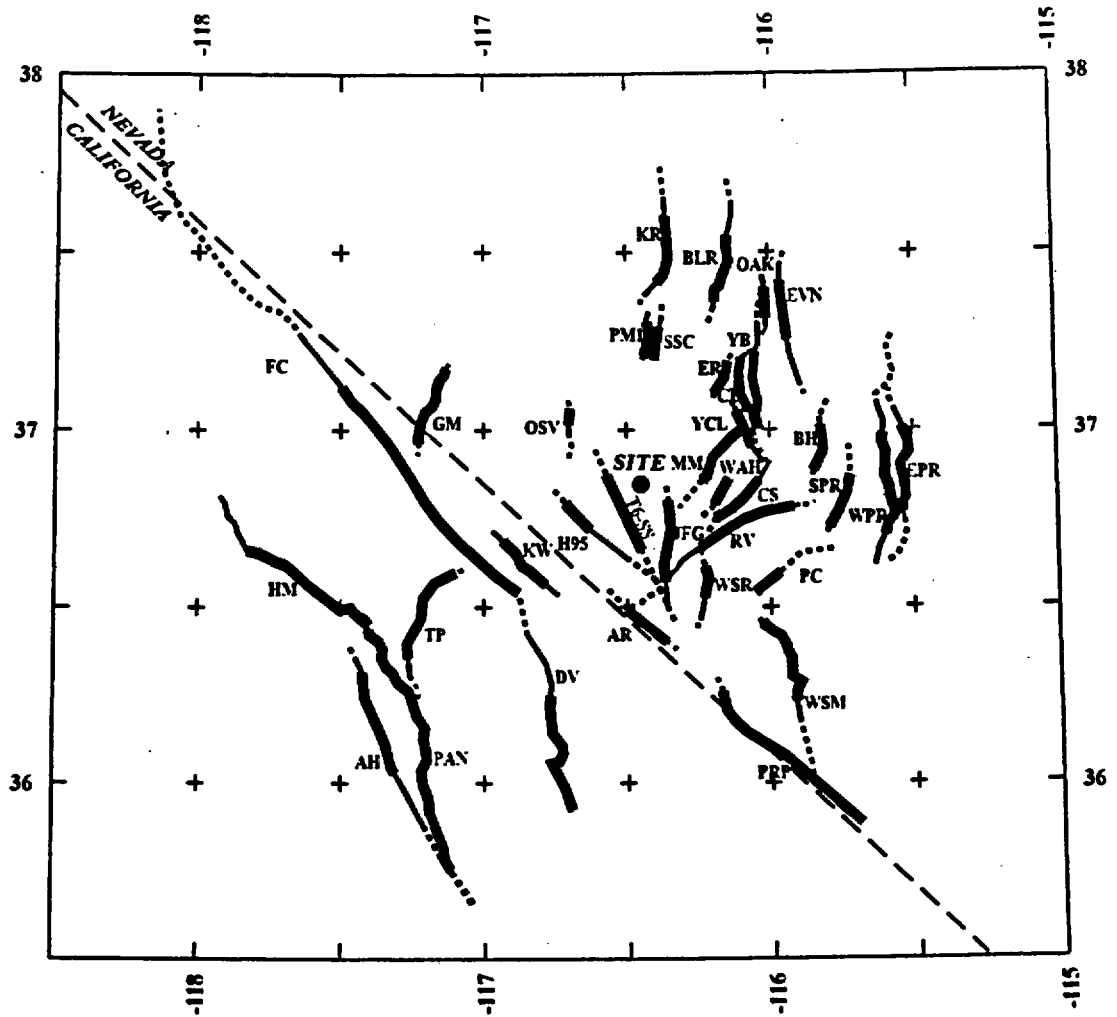


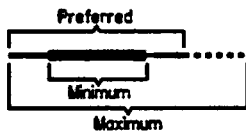
Figure SDO-5

Logic tree for regional source zones



EXPLANATION

Fault Lengths:



NOTE: Fault names are listed in Table SDO-3

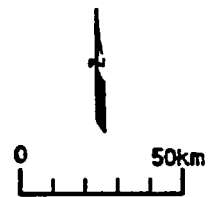
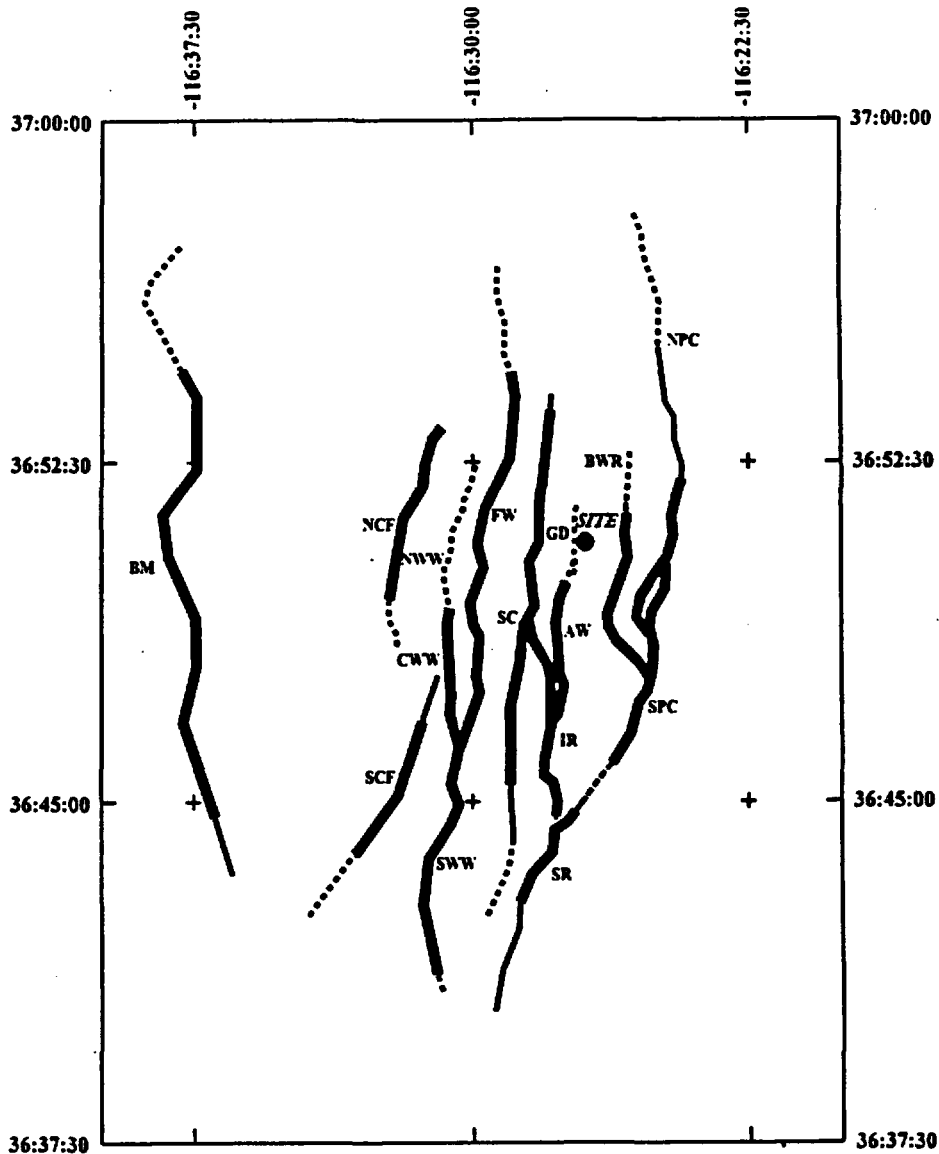
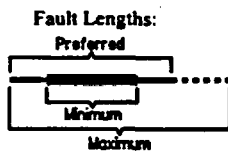


Figure SDO- 6 Map showing regional faults included in the seismic source model.



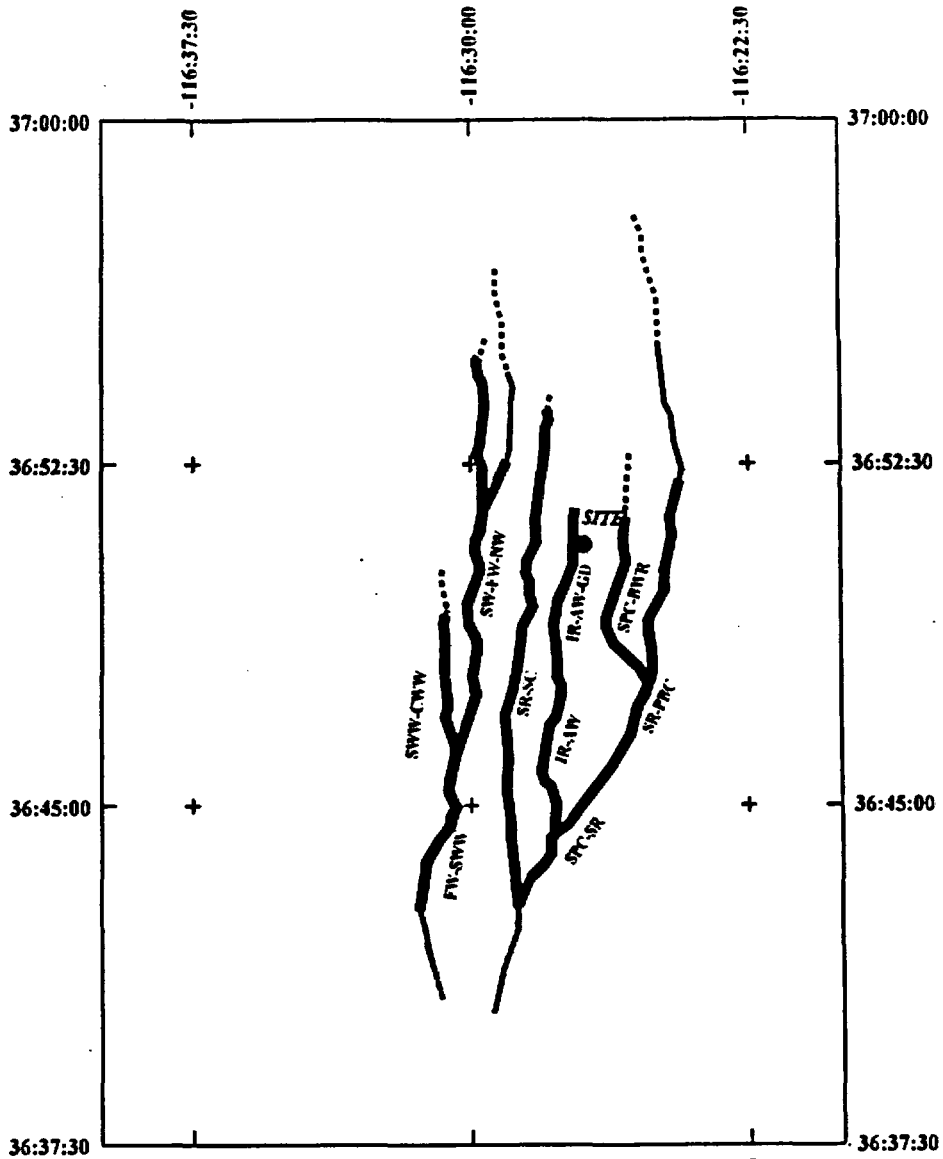
EXPLANATION



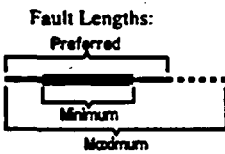
NOTE: Fault names are listed in Table SDO-4



Figure SDO- 7a Map showing local fault sources included in the independent seismic source model



EXPLANATION



NOTE: Fault names are listed in Table SDO-4

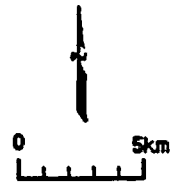


Figure SDO-7b Map showing local fault sources included in the linked seismic source model

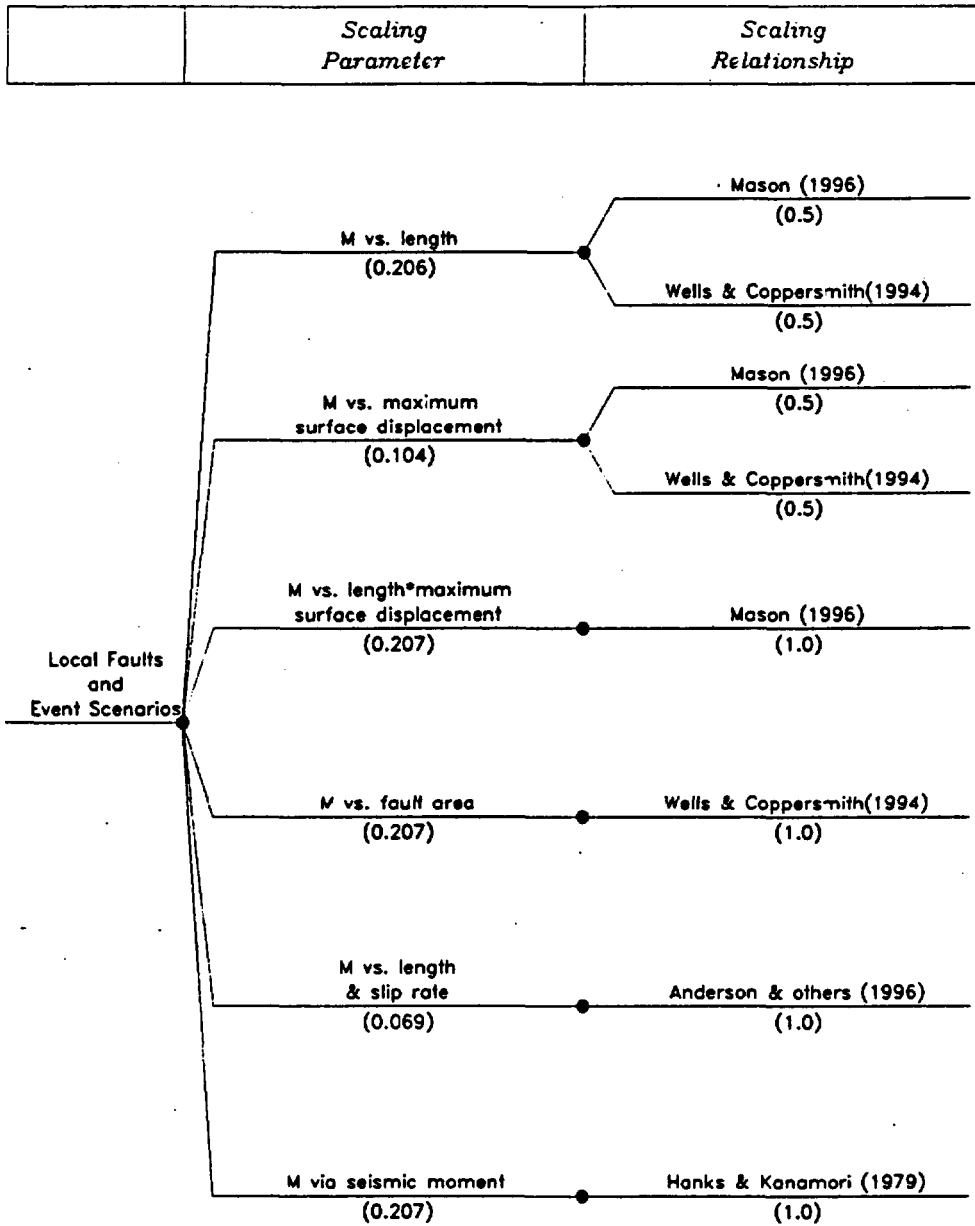


Figure SDO-8

Scaling parameters and relationships used to estimate maximum magnitudes for local faults

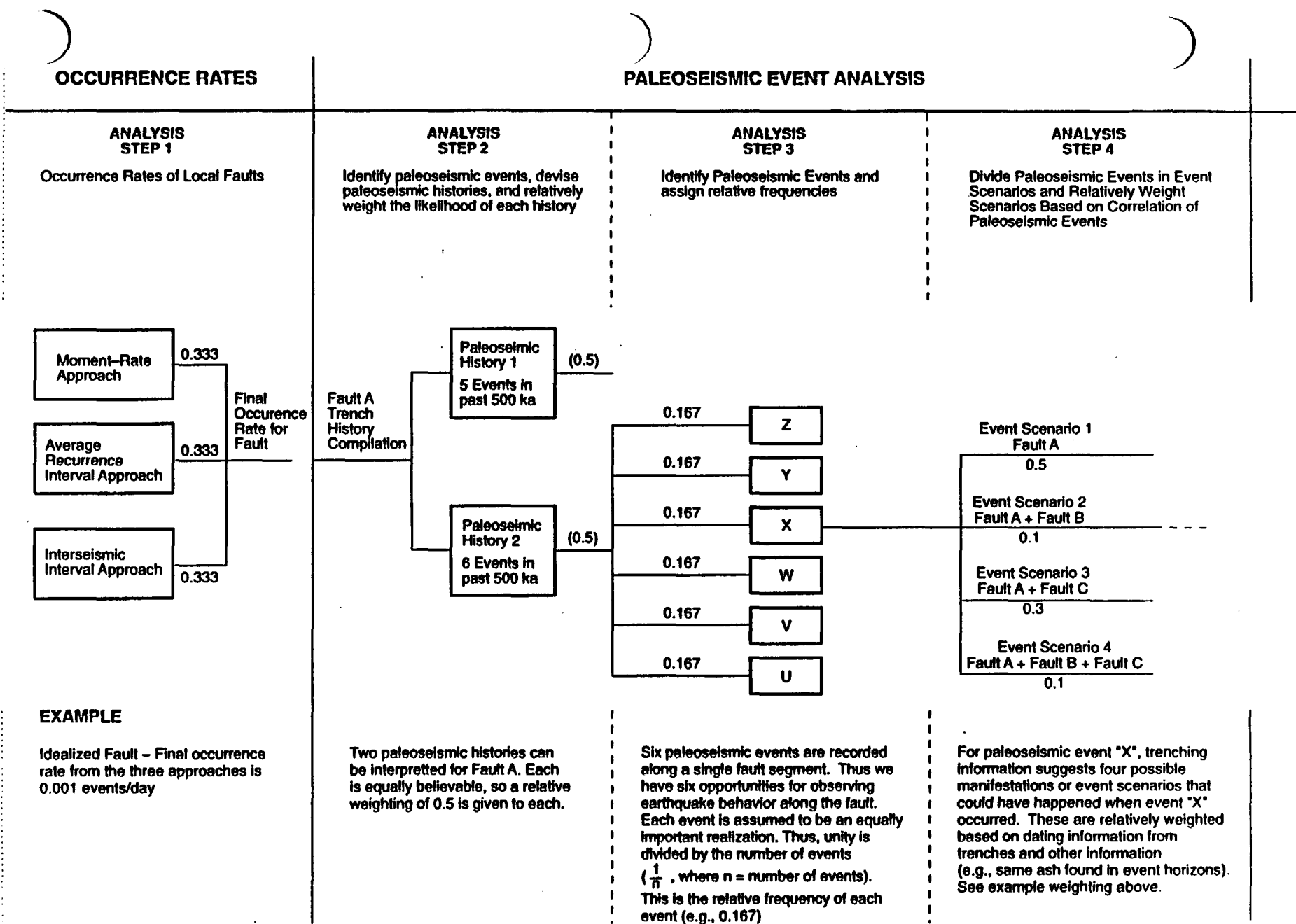


Figure SDO-9 Example calculation of occurrence rates for local faults

EVENT SCENARIO OCCURRENCE RATES

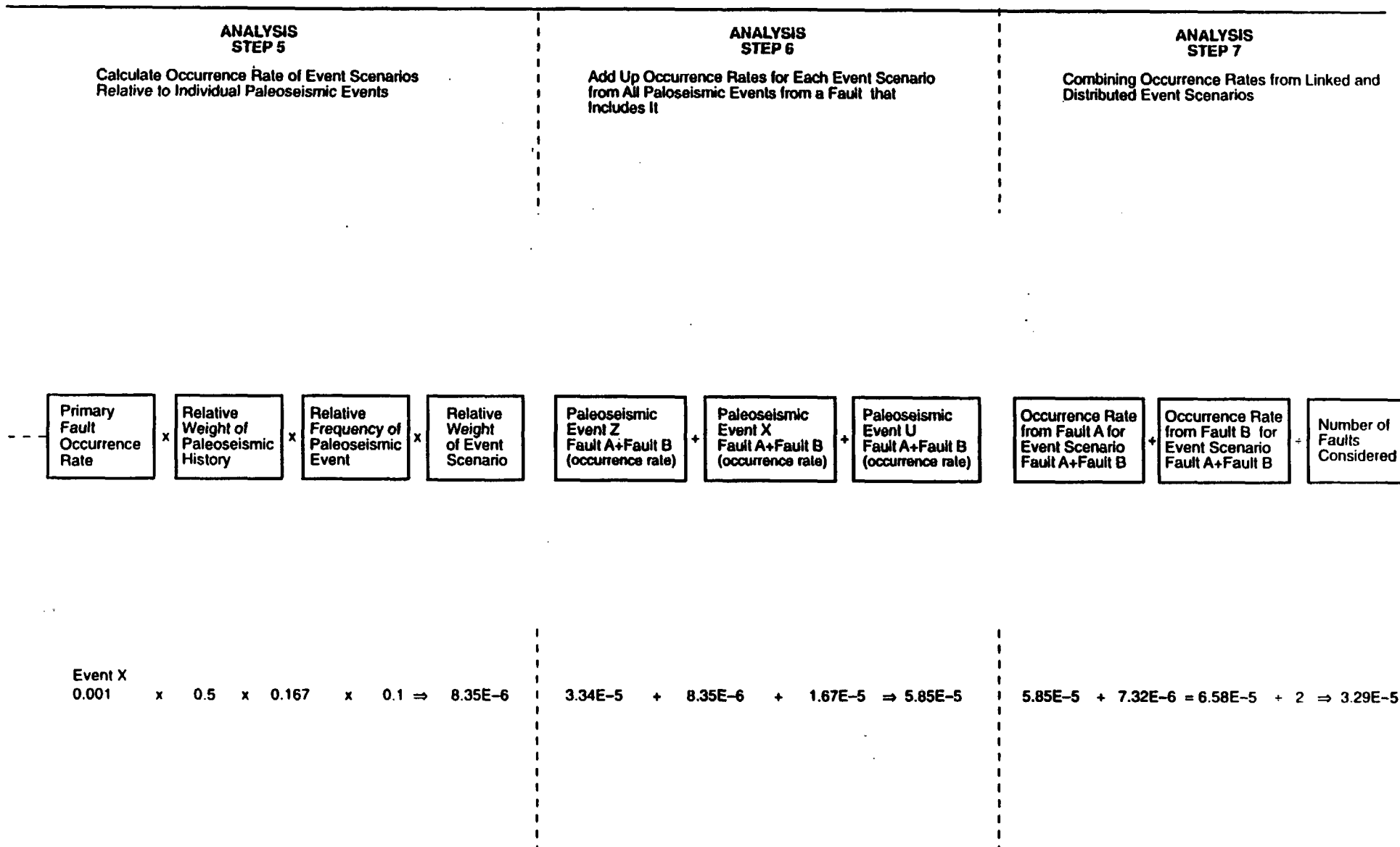


Figure SDO-9

Example calculation of occurrence rates for local faults
(continued)

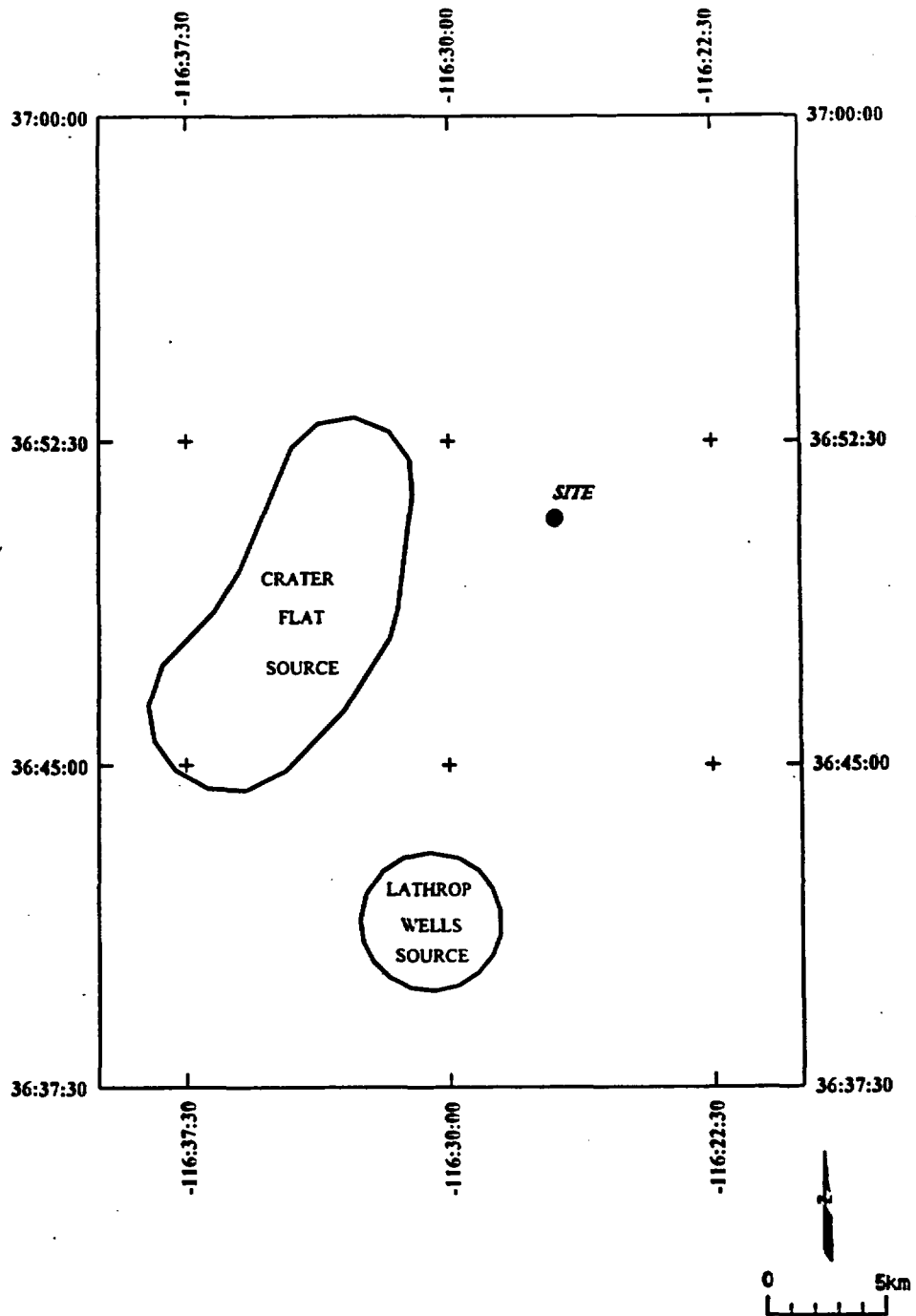


Figure SDO-10 Map showing volcanic zones included in the seismic source model

<i>Frequency of Earthquakes (from Section 3.0)</i>	<i>Probability of Surface Rupture</i>	<i>Approach for Displacement</i>	<i>Type of Event</i>	<i>Scaling Relationships</i>	<i>Displacement Distribution</i>
--	---------------------------------------	----------------------------------	----------------------	------------------------------	----------------------------------

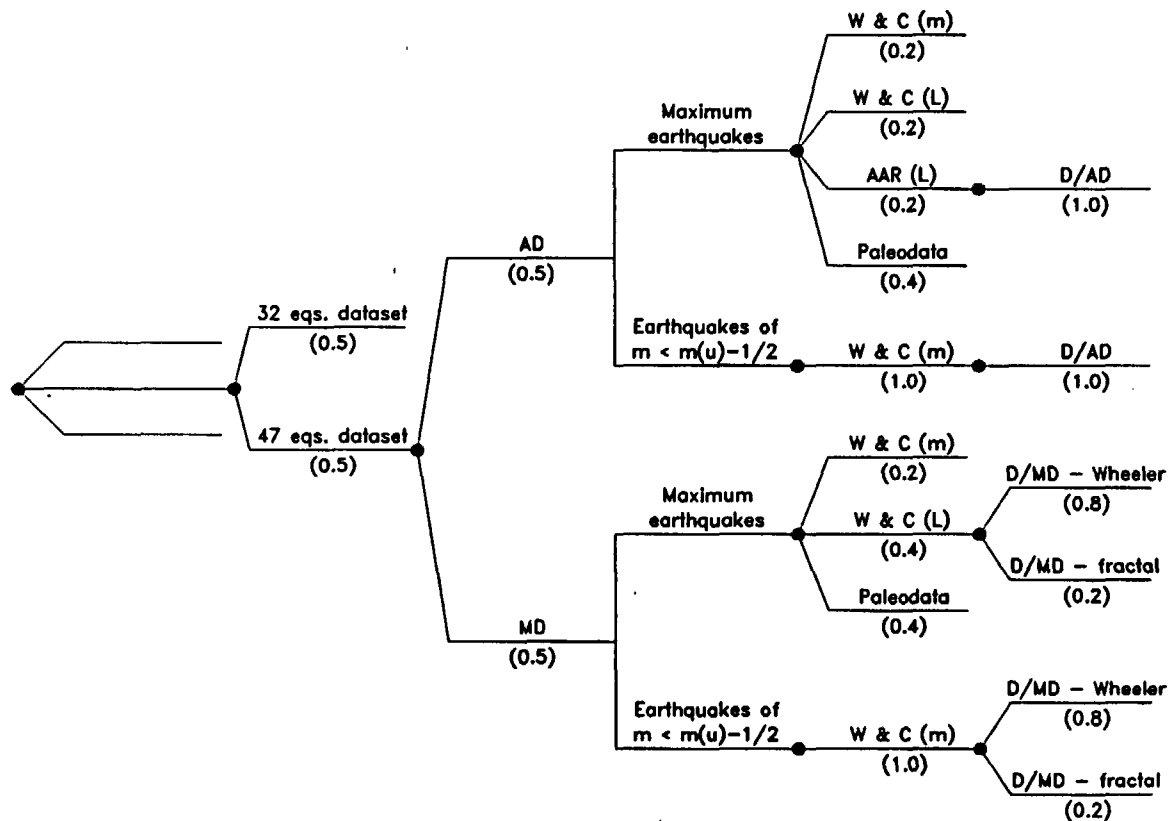


Figure SDO-11

Logic tree used to characterize principal faulting displacement hazard.

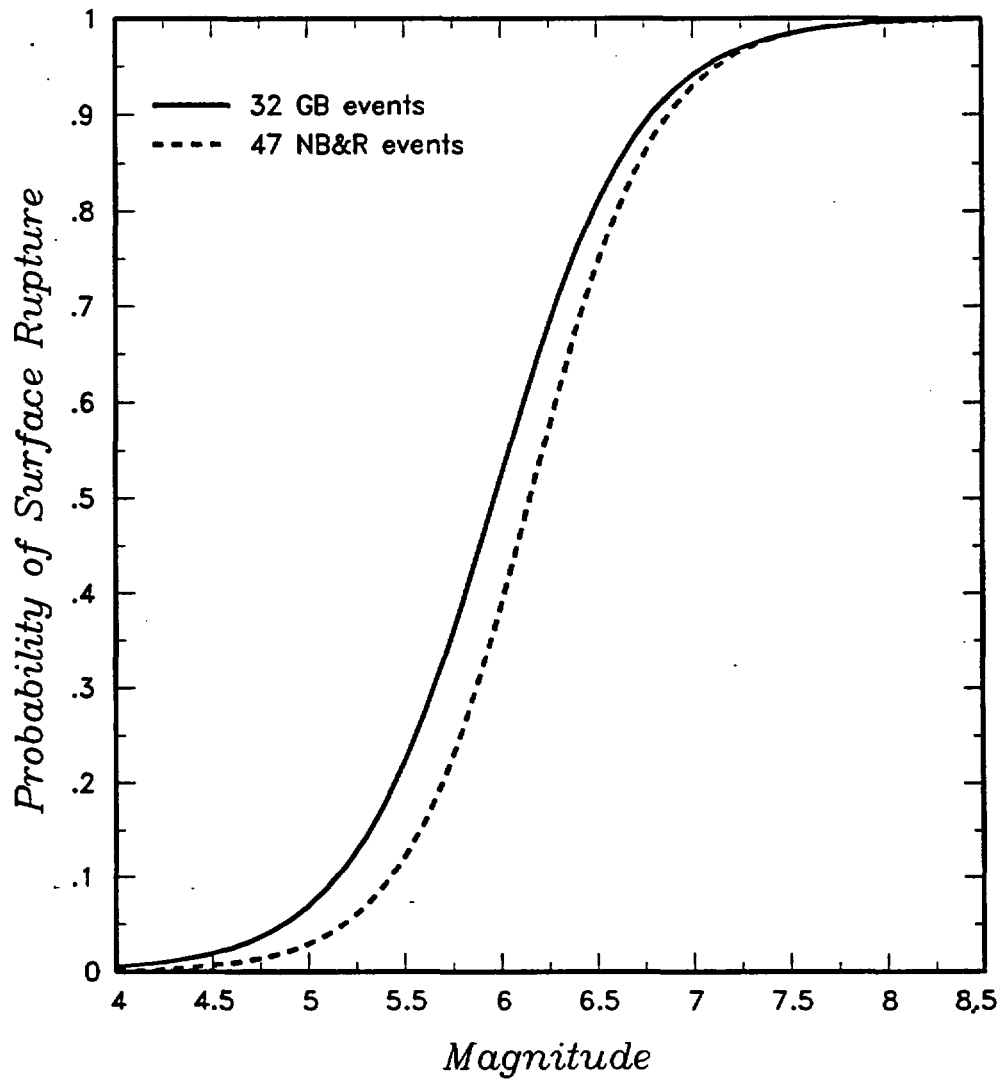


Figure SDO-12

Probability of surface rupture as a function of earthquake magnitude computed from various data sets given in Pezzopane and Dawson (1996)

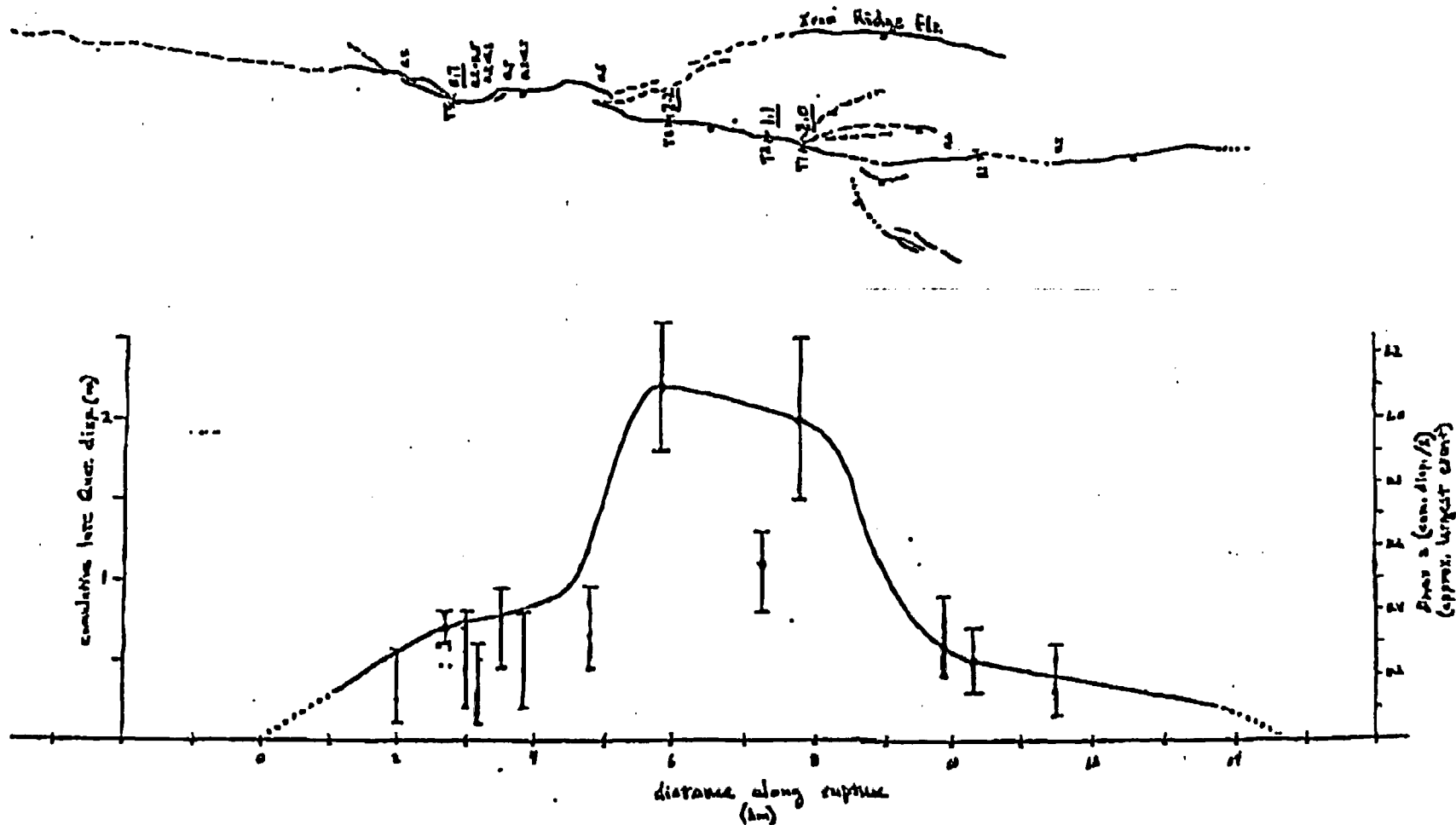


Figure SDO-13

Estimated mid- to late-Quaternary displacement along the Solitario Canyon fault. Strip map depicts displacement data from trench studies (Chap. 4.7 of U.S. Geological Survey, 1996) and scarp heights from Simonds and others (1995). Graph depicts trench data (large dots) and scarp heights converted to estimated displacements (small dots). Left axis scales cumulative mid- to late-Quaternary displacement, and right axis scales *MD* based on 1/2 of the cumulative offset (a close approximation of the largest event).

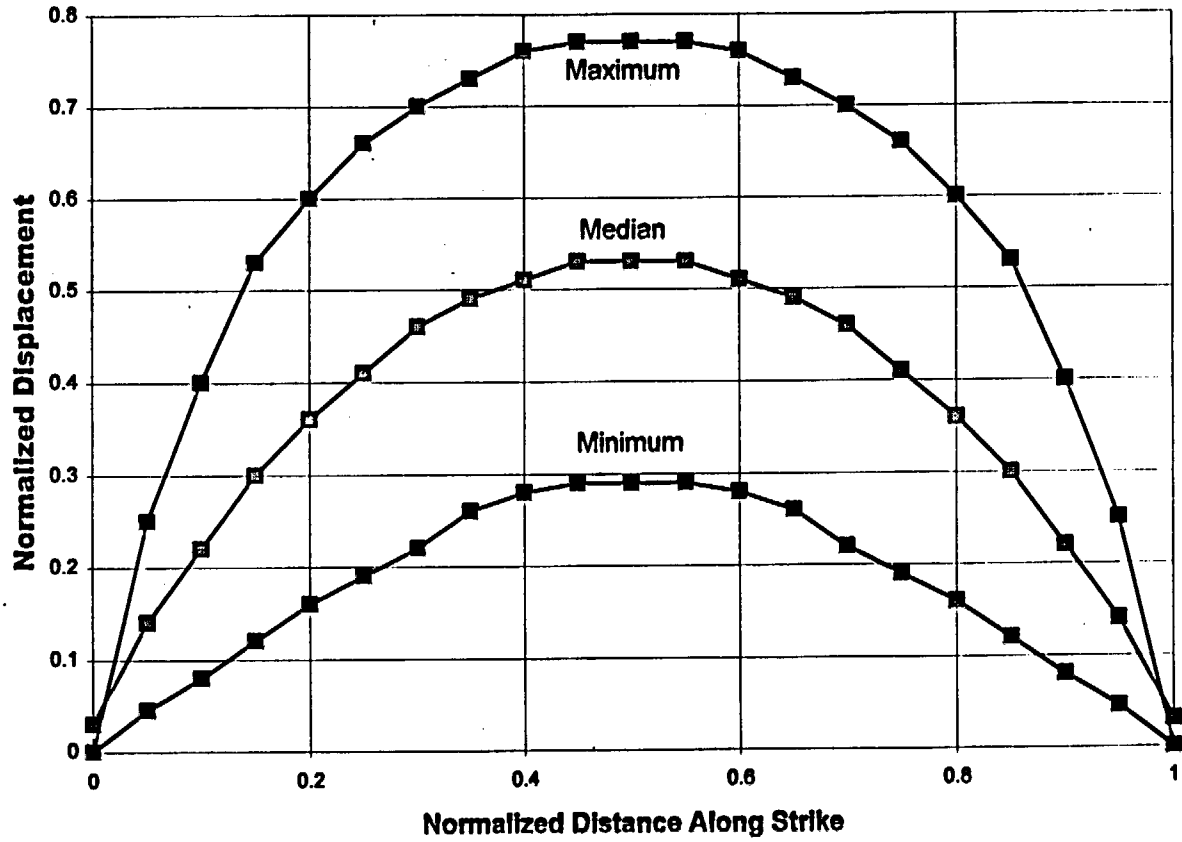


Figure SDO-14

Normalized slip along strike from five Basin and Range historic normal fault earthquake ruptures developed by the ASM team from data presented in Wheeler (1989).

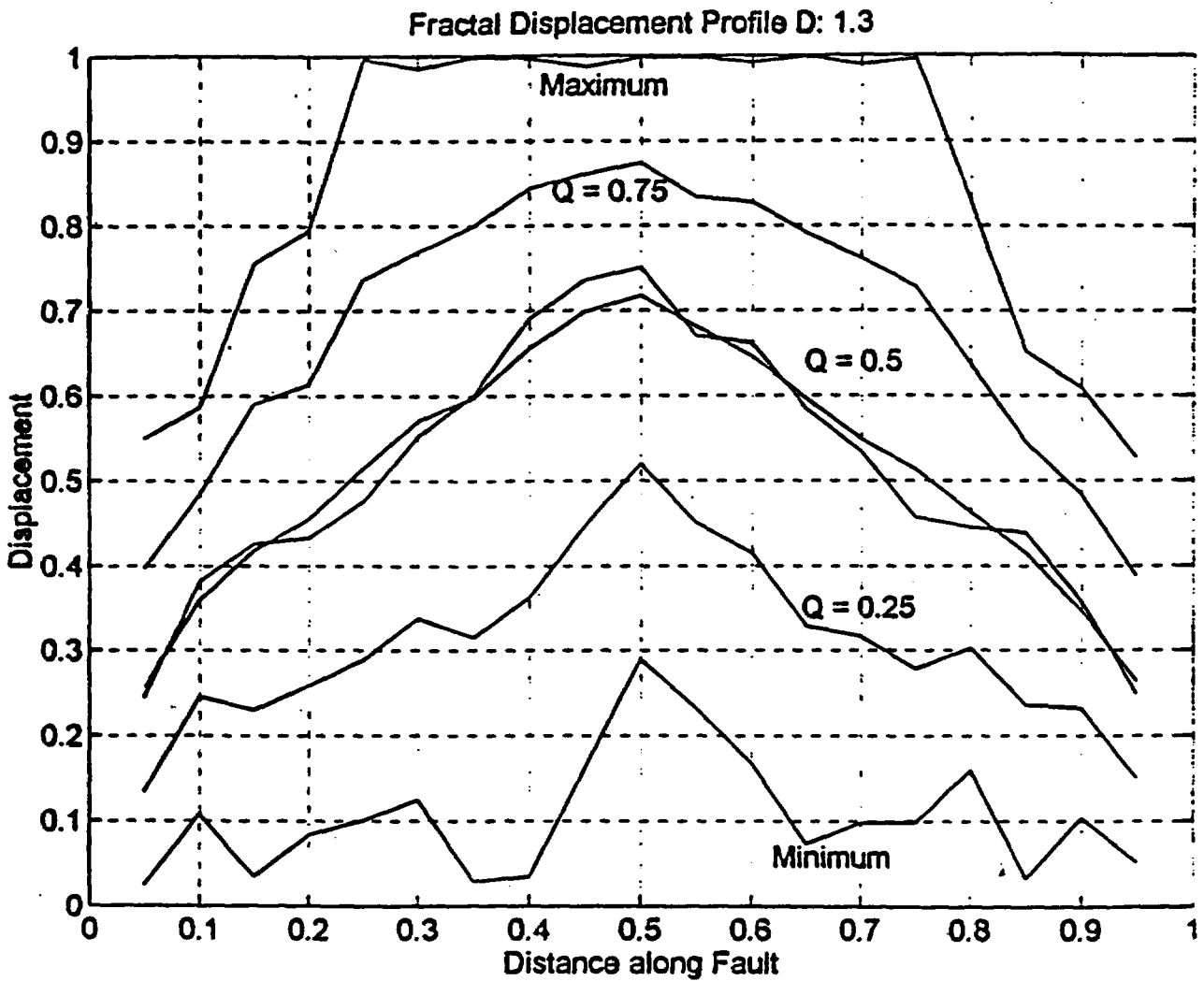


Figure SDO-15

Fractal displacement profiles developed by Ron Bruhn, University of Utah, to predict distribution for the ratio of displacement at a point to the maximum displacement in an earthquake.

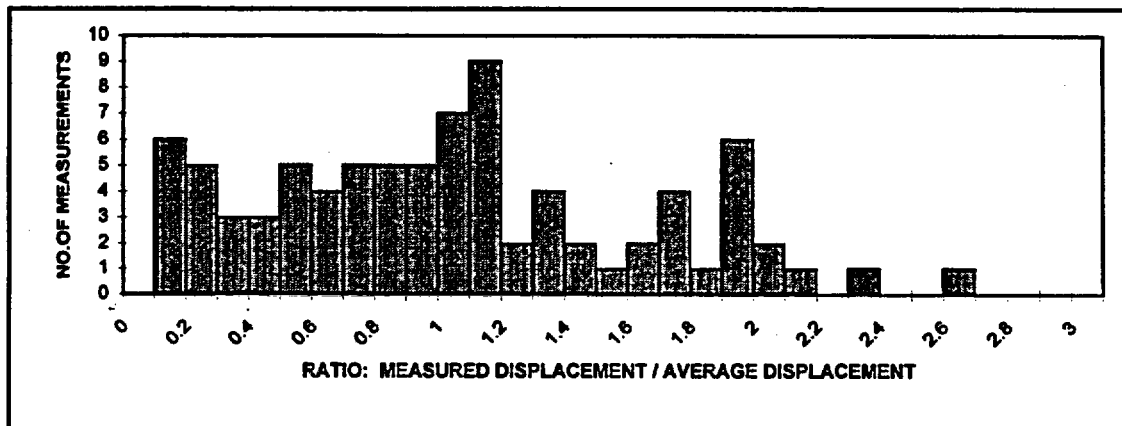
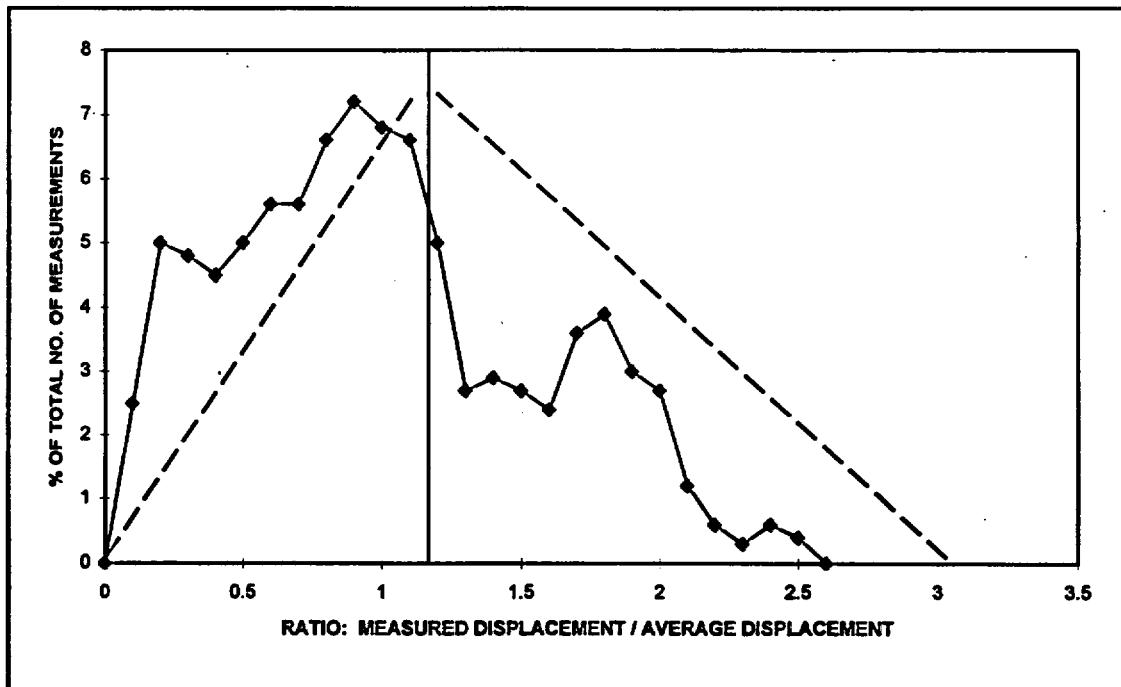


Figure SDO-16

Plots showing event-to-event variability in displacement relative to average displacement per event at a location along a fault based on data from paleoseismic investigations in the Yucca Mountain area.

<i>Distributed Faulting Approach</i>	<i>Activation Probability</i>	<i>P(Slip event)</i>	<i>Slip Rate</i>	<i>Average Displacement per Event</i>	<i>Distribution of Slip per Event</i>
--------------------------------------	-------------------------------	----------------------	------------------	---------------------------------------	---------------------------------------

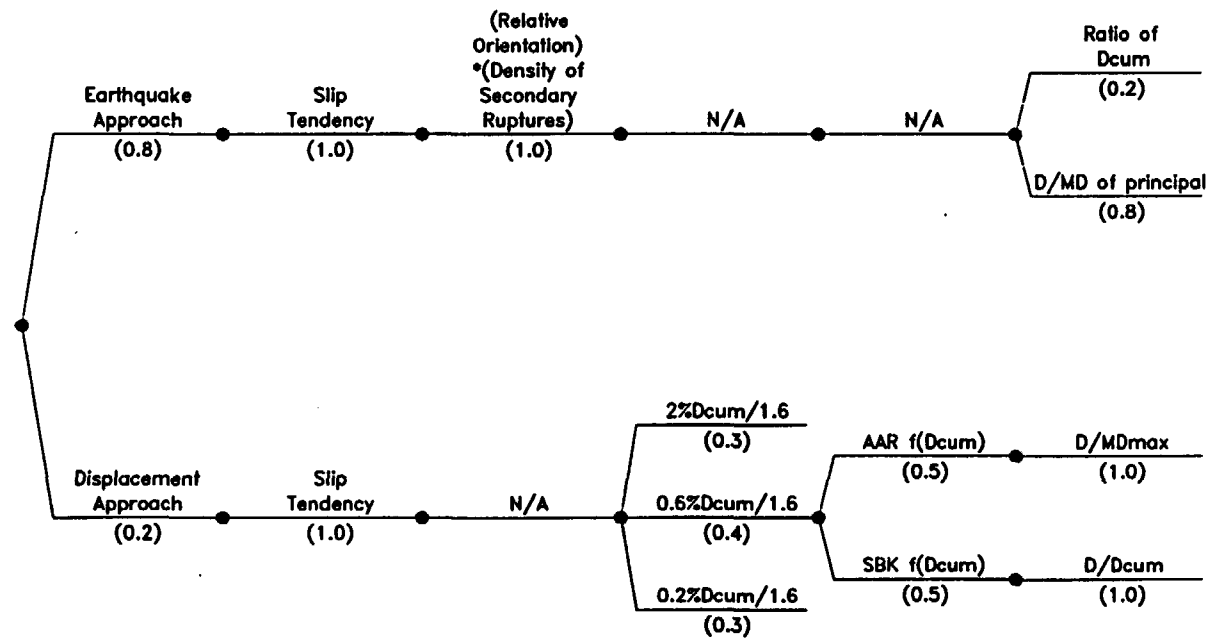


Figure SDO-17

Logic tree used to characterize distributed faulting displacement hazard.

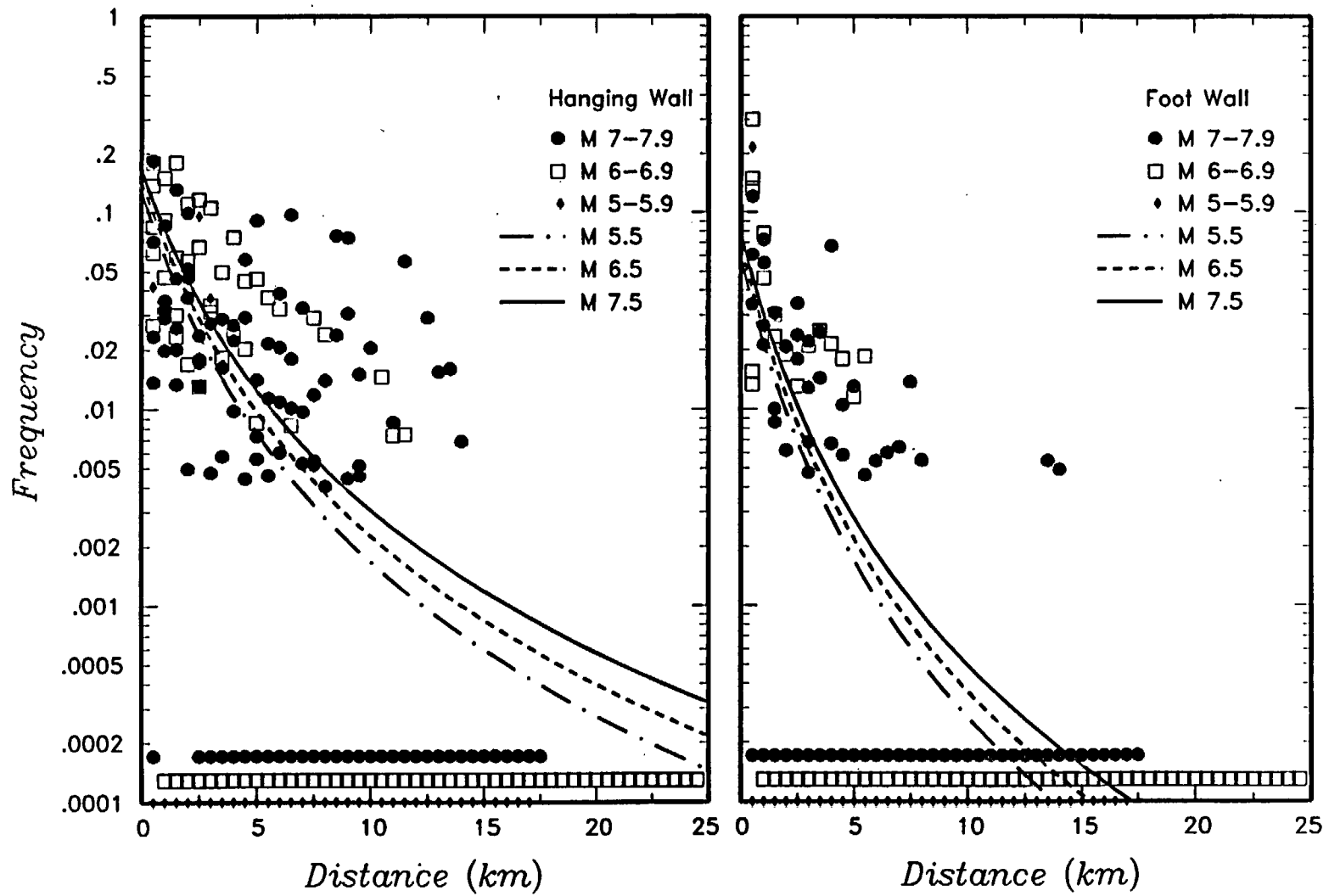


Figure SDO-18

Probability of induced distributed slip as a function of distance from the rupture and hanging wall/foot wall location computed from the data presented in Pezzopane and Dawson (1996). Curves show logistic regression fits to data.

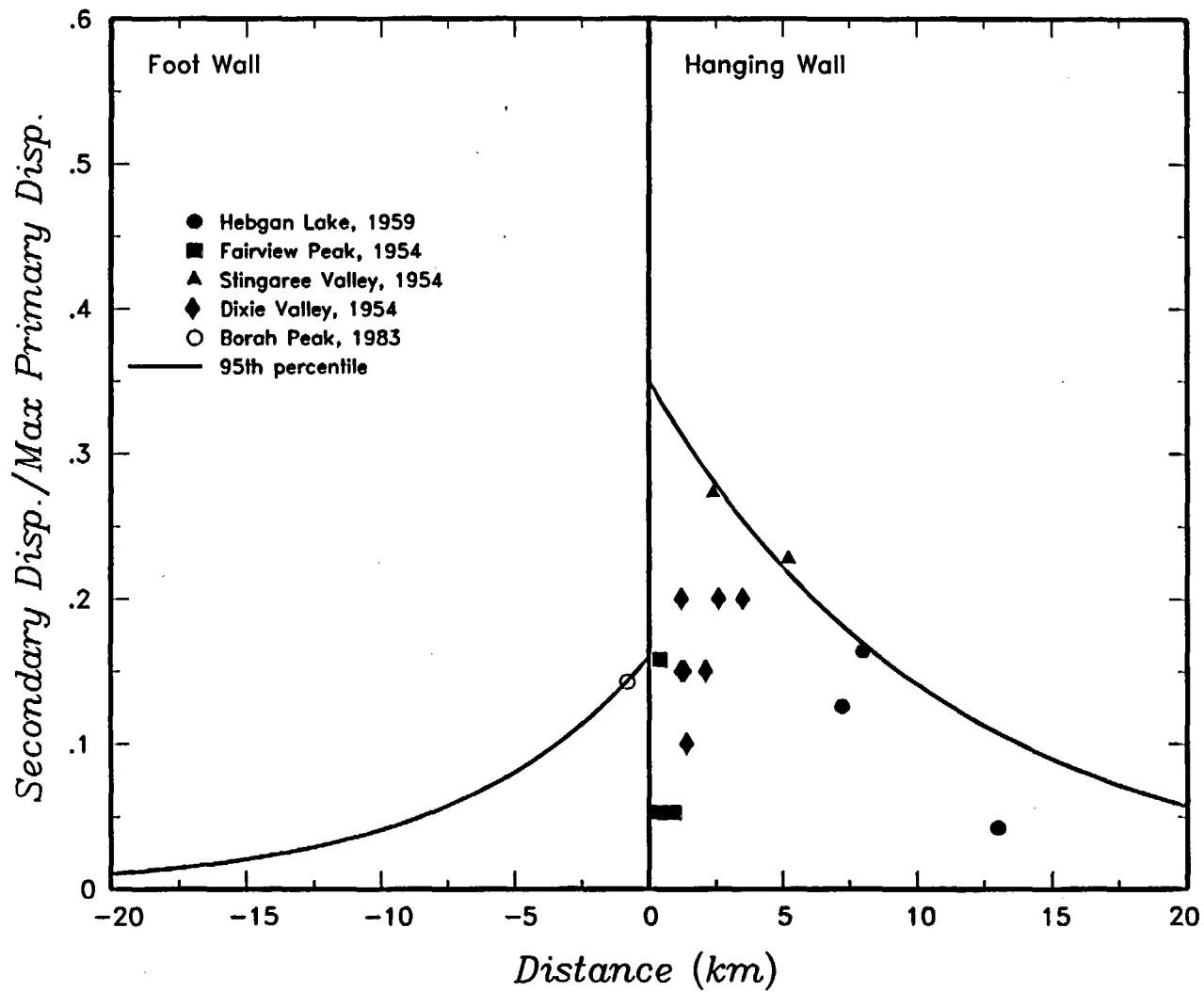


Figure SDO-19

Observed secondary faulting distribution normalized to main fault displacement for large scarp-forming, historic normal faulting earthquakes in the Basin and Range province.

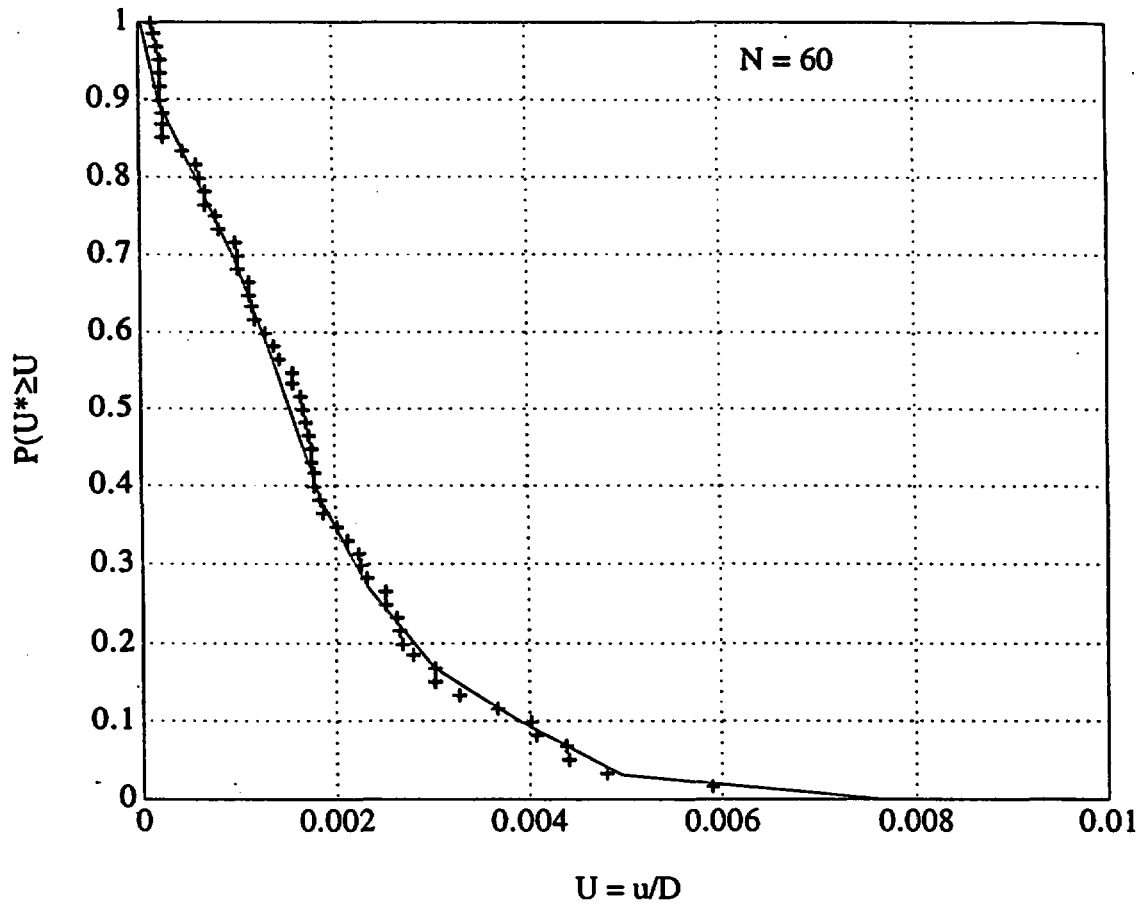


Figure SDO-20

Cumulative probability graph of D/D_{cum} , where D is fault slip per event and D_{cum} is the cumulative displacement on the fault surface at the point of interest. Function is derived from Yucca Mountain fault data synthesis of Pezzopane and Dawson (1996) and discussions of Cowie and Scholz (1992) by SBK team.

APPENDIX SDO-1
EVENT SCENARIOS FOR LOCAL FAULTS
 (Page 1 of 3)

Event Scenarios	Occurrence Rates (events/yr)		
	Minimum	Preferred	Maximum
<u>Paintbrush</u>	1.96E-005	3.13E-005	7.174E-005
PC(N)	7.98E-006	1.27E-005	2.91E-005
PC(S)	4.63E-006	7.39E-006	1.69E-005
PC(N+S)	1.88E-006	3.00E-006	6.85E-006
PCN+BR	1.76E-007	2.82E-007	6.43E-007
PC(S)+BR	1.45E-006	2.32E-006	5.28E-006
PC+BR	1.76E-007	2.82E-007	6.43E-007
PC+SCR	1.88E-006	3.00E-006	6.85E-006
PC(S)+SCR	8.23E-007	1.31E-006	3.00E-006
PC+BR+SCR	1.76E-007	2.82E-007	6.43E-007
PC+ash event	4.31E-007	6.89E-007	1.57E-006
<u>Stagecoach Road</u>	2.44E-005	3.33E-005	5.00E-005
SCR	1.22E-005	1.67E-005	2.50E-005
SCR+PC(S)	2.24E-006	3.06E-006	4.60E-006
SCR+PC	4.07E-006	5.56E-006	8.35E-006
SCR+ash event	1.83E-006	2.50E-006	3.75E-006
SCR+SC	3.05E-006	4.16E-006	6.25E-006
SCR+PC+BR	1.02E-006	1.40E-006	2.10E-006
<u>Solitario Canyon</u>	1.47E-005	1.92E-005	2.7E-005
SC	8.45E-006	1.10E-005	1.55E-005
SC+SCR	1.84E-006	2.40E-006	3.38E-006
SC+ash event	2.57E-006	3.36E-006	4.73E-006
SC+SWW	1.84E-006	2.40E-006	3.38E-006
<u>Iron Ridge</u>	3.91E-006	4.98E-006	6.99E-006
IR	3.52E-006	4.48E-006	6.29E-006
IR+AW	2.61E-007	3.32E-007	4.66E-007
IR+AW+GD	1.30E-007	1.66E-007	2.33E-007

APPENDIX SDO-1
EVENT SCENARIOS FOR LOCAL FAULTS
 (Page 2 of 3)

Event Scenarios	Occurrence Rates (events/yr)		
	Minimum	Preferred	Maximum
<u>Fatigue Wash</u>	3.46E-006	6.06E-006	1.16E-005
FW	2.22E-006	3.98E-006	7.45E-006
FW+SWW	3.71E-007	6.49E-007	1.24E-006
FW+SW+NW	1.24E-007	2.16E-007	4.14E-006
FW+SW+SCF	2.47E-007	4.33E-007	8.29E-007
FW+ash event	4.94E-007	8.66E-007	1.65E-006
<u>S. Windy Wash</u>	1.3E-005	1.96E-005	2.78E-005
SWW	8.16E-006	1.23E-005	1.75E-005
SWW+SCF	1.08E-006	1.63E-006	2.31E-006
SWW+FW	6.76E-007	1.02E-006	1.45E-006
SWW+SC	4.03E-007	6.08E-007	8.62E-007
SWW+CW	8.06E-007	1.22E-006	1.72E-006
SWW+SCF+NCF	4.03E-007	6.08E-007	8.62E-007
SWW+FW+NWW	4.03E-007	6.08E-007	8.62E-007
SWW+FW+SCF	2.73E-007	4.12E-007	5.84E-007
SWW+ash event	8.19E-007	1.23E-006	1.75E-006
<u>Individual Faults</u>			
PC (N + S)	2.24E-006	2.91E-006	8.3E-006
PC (N)	7.98E-006	1.27E-005	2.91E-005
PC (S)	4.63E-006	7.39E-006	1.69E-005
SCR	1.22E-005	1.67E-005	2.50E-005
SC	8.45E-006	1.10E-005	1.55E-005
IR	3.52E-006	4.48E-006	6.29E-006
FW	2.22E-006	3.89E-006	7.45E-006
SWW	8.16E-006	1.23E-005	1.75E-005
<u>Linked Faults</u>		<u>Scenarios:</u>	
PC+SCR	2.98E-006	4.28E-006	7.60E-006
PC(S)+SCR	1.53E-006	2.19E-006	3.80E-006
PC(S)+BR	1.45E-006	2.32E-006	5.28E-006
SCR+SC	2.45E-007	3.28E-006	4.82E-006
IR+AW	2.61E-007	3.32E-007	4.66E-007
IR+AW+GD	1.30E-007	1.66E-007	2.33E-007
FW+SWW	5.24E-007	8.35E-007	1.35E-006
SWW+FW+NWW	2.64E-007	4.12E-007	6.38E-007
SWW+CW	4.03E-007	6.08E-007	8.62E-007

APPENDIX SDO-1
EVENT SCENARIOS FOR LOCAL FAULTS
 (Page 3 of 3)

Event Scenarios	Occurrence Rates (events/yr)		
	Minimum	Preferred	Maximum
<u>Distributed Faults</u>			
PC(N)+BR	1.76E-007	2.82E-007	6.43E-007
PC+BR+SCR	5.98E-007	8.41E-007	1.37E-006
PC+BR	1.76E-007	2.82E-007	6.43E-007
SC+SWW	1.12E-006	1.50E-006	2.12E-006
FW+SWW+SCF	2.60E-007	4.23E-007	7.07E-007
SWW+SCF	1.08E-006	1.63E-006	2.31E-006
SWW+SCF+NCF	4.03E-007	6.08E-007	8.62E-007
ash event	1.22E-006	1.73E-006	2.69E-006

APPENDIX SDO-2
ANALYSIS OF PALEOSEISMIC DATA

REPRESENTATIVE AGES

Representative or nominal ages were ascribed to the paleoseismic data to make the use of this information more tractable (especially, given the time frame for the analysis) and transparent. There are, however, large uncertainties associated with these age data; we handle these in the relative weighting of event scenarios. Most of the ages and displacements used for the local faults at Yucca Mountain came from the Seismotectonic Framework Report produced by the U.S. Geological Survey. In particular, Table 5-1, "Event Displacements and Timing Data from Paleoseismic Studies of Yucca Mountain Faults", was used extensively.

PAINTBRUSH CANYON FAULT

Paleoseismic Earthquake Recurrence Information:

Six to nine events in the last 300 to 410 ka along the Paintbrush Canyon fault have been revealed by trenching. However, four to six of these events have occurred in the last 100 to 150 ka. Either paleoevents prior to 100 to 150 ka have been erased or left no record where the fault has been examined, or earthquake occurrence is becoming more frequent post 100 to 150 ka. In either case, it makes the most sense to calibrate earthquake recurrence for future predictions of the next earthquakes on the last 100 to 150 ka. The preferred number of events is five, the midpoint, and the preferred age is 120 ka. The most recent event occurred at 15 ka.

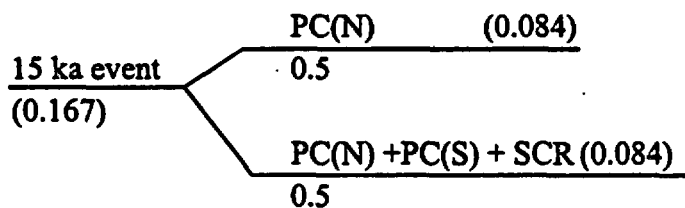
	Raw Average Earthquake Recurrence Intervals	Corrected Average Earthquake Recurrence Intervals - Most Recent Event and Elapsed Time Removed
Min.	17 kyr	17 kyr
Pref.	24 kyr	26 kyr
Max.	38 kyr	45 kyr

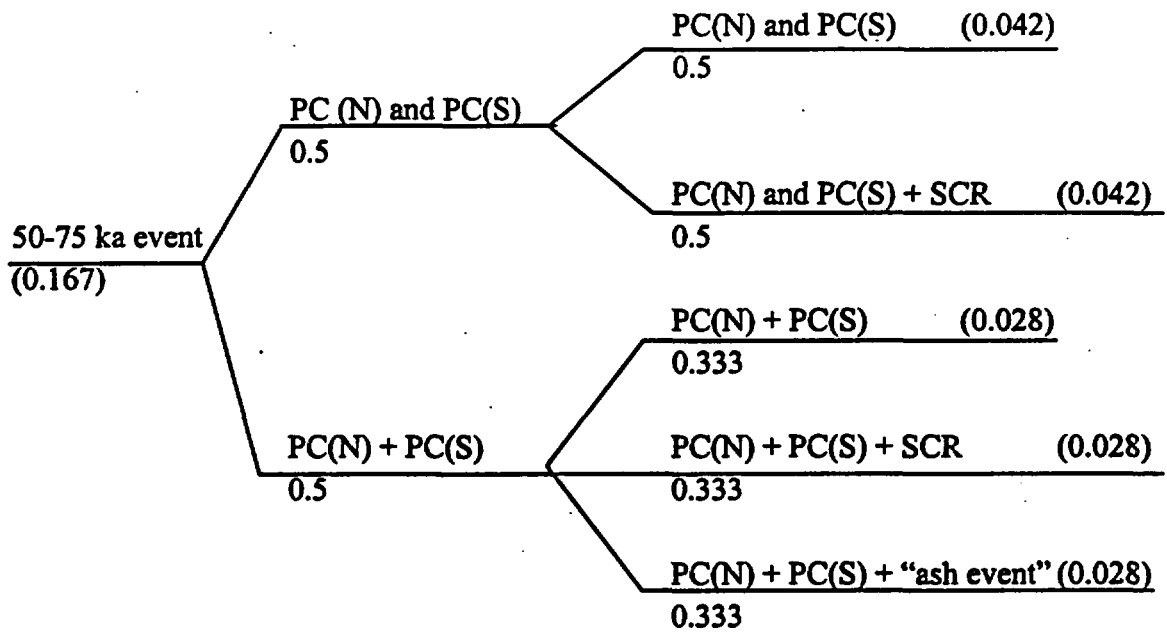
Similar to the average recurrence interval, the interseismic intervals examined are for the last 100 to 150 ka. Considering the preferred ranges presented in Chapter 5 of the U. S. Geological Survey Synthesis Report, interseismic intervals were estimated by subtracting the extreme

values. The range of values for the interseismic intervals is 15 to 60 kyr. The average of all the estimates, 38 kyr, is taken as the preferred value.

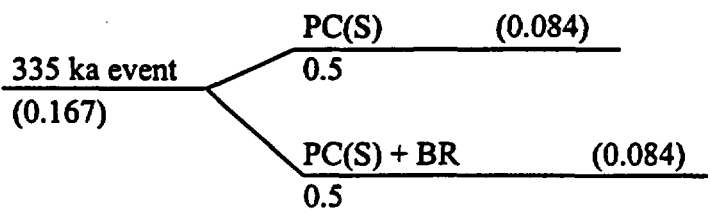
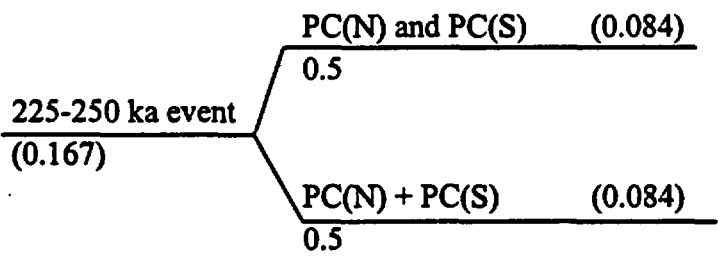
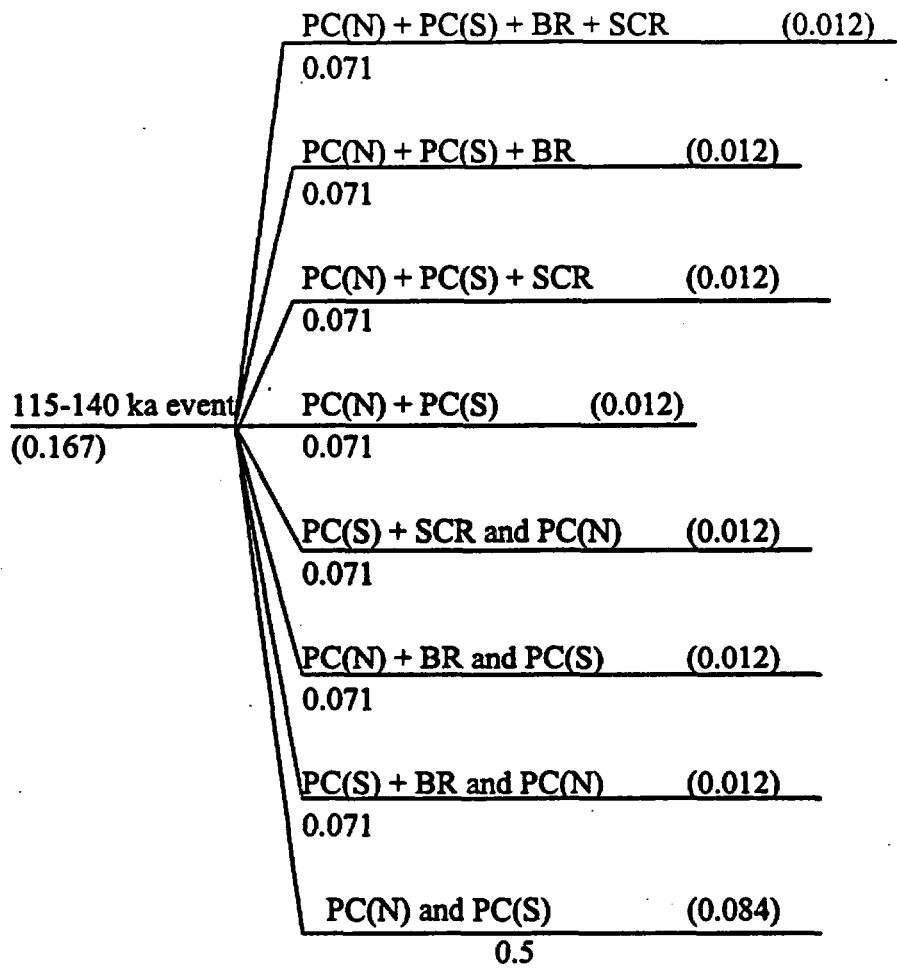
	Moment Rate Recurrence	Average Earthquake Recurrence	Preferred Interseismic Interval	Averaged Earthquake Recurrence	Maximum Earthquake Occurrence Rate (events/yr)
Min.	8.6 kyr	17 kyr	15 kyr	14 kyr	7.14×10^{-5}
Pref.	31 kyr	26 kyr	38 kyr	32 kyr	3.13×10^{-5}
Max.	47 kyr	45 kyr	60 kyr	51 kyr	1.96×10^{-5}

Relative Frequency	Nominal Age of the Event	Surface Displacement	Possible Event Scenarios
(0.167)	15 ka	0.05/0.2/0.2	PC(N) + PC(S.?, poss. erased) + SCR or PC(N)
(0.167)	50-75 ka	0.44/0.62/0.77	PC(N) + "ash event" or PC(S) + SCR or PC(N) and PC(S)
(0.167)	90-95 ka	0.53/0.98/1.43	PC(N)
(0.167)	115-140 ka	0.29/0.4/1.40	PC(N) + PC(S) + BR + SCR or PC(N) + PC(S) PC(N) + PC(S) + BR or PC(N) + PC(S) + SCR PC(N) + BR or PC(S) + BR PC(N) and PC(S)
(0.167)	225-250 ka	0.35/0.47/0.69	PC(N) + PC(S) or PC(N) and PC(S)
(0.167)	335 ka	0.88/1.67/2.05	PC(S) + BR





90-95 ka event PC(N) (0.167)
 (0.167)



Final Relative Weighting:

(0.407)	PC(N)
(0.236)	PC(S)
(0.096)	PC(N) + PC(S)
(0.009)	PC(N) + BR
(0.074)	PC(S) + BR
(0.009)	PC(N) + PC(S) + BR
(0.096)	PC(N) + PC(S) + SCR
(0.042)	PC(S) + SCR
(0.009)	PC(N) + PC(S) + BR + SCR
(0.022)	PC(N) + PC(S) + 'ash event'

STAGECOACH ROAD FAULT

Paleoseismic Earthquake Recurrence Information:

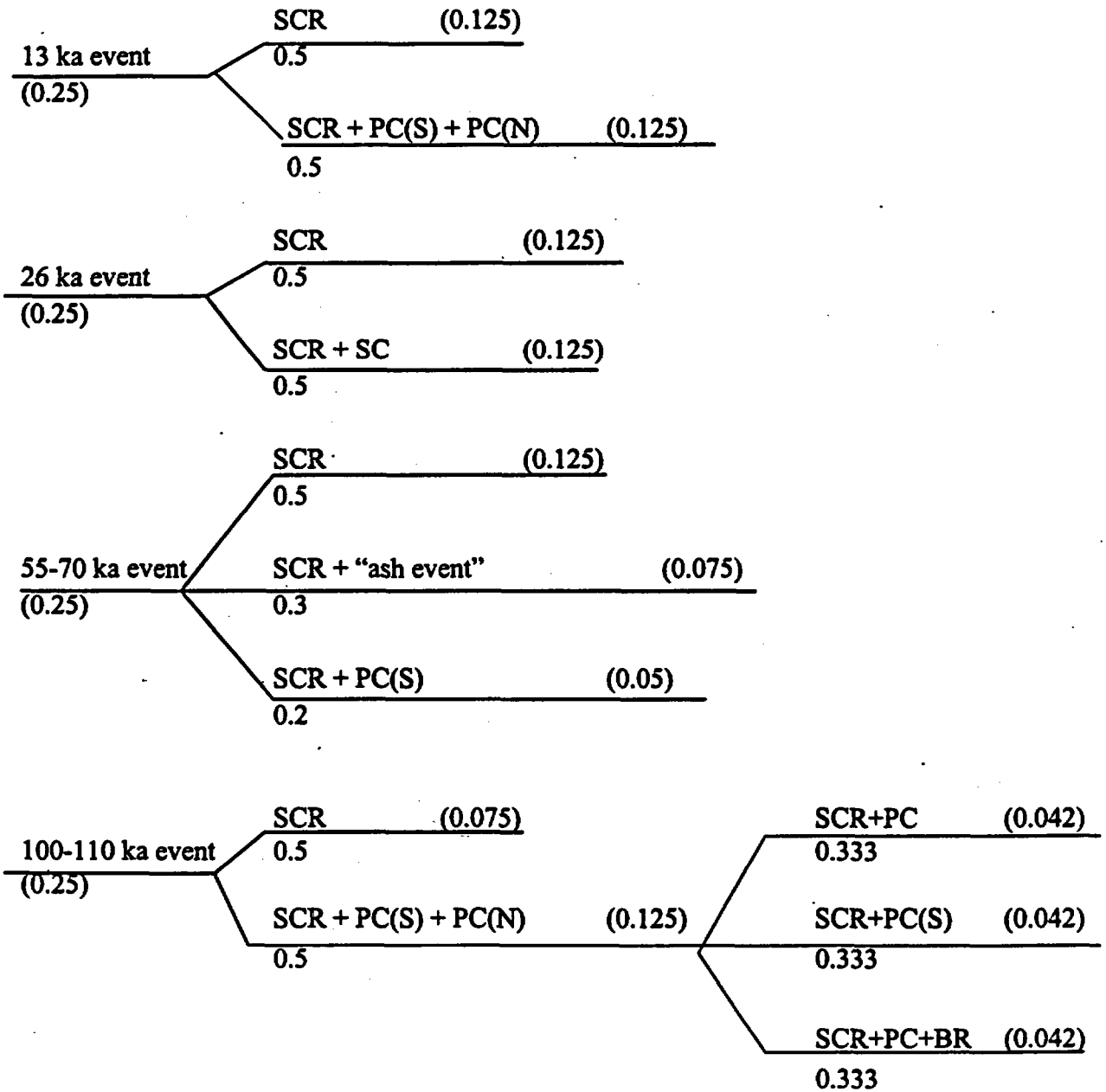
Four events have occurred in the last 98 to 118 ka, with a preferred value of 108 ka. The most recent event was 6 to 15 ka, with a preferred value of 13 ka.

	Raw Average Earthquake Recurrence Intervals	Corrected Average Earthquake Recurrence Intervals Most Recent Event and Elapsed Time Removed
Min.	25 kyr	28 kyr
Pref.	27 kyr	32 kyr
Max.	30 kyr	34 kyr

Considering the preferred ranges presented in Chapter 5 of the U. S. Geological Survey Synthesis Report, interseismic intervals were estimated by subtracting the extreme values. Preferred value interseismic intervals ranged from 13 kyr to 55 kyr; the average interseismic interval is 34 kyr.

	Moment Rate Recurrence	Average Earthquake Recurrence	Preferred Interseismic Interval	Averaged Earthquake Recurrence	Maximum Earthquake Occurrence Rate (events/yr)
Min.	18 kyr	28 kyr	13 kyr	20 kyr	5×10^{-5}
Pref.	24 kyr	32 kyr	34 kyr	30 kyr	3.33×10^{-5}
Max.	35 kyr	34 kyr	55 kyr	41 kyr	2.44×10^{-5}

Relative Frequency	Nominal Age of the event	Surface Displacement	Poss. Event Scenarios
(0.25)	13 ka	0.4/0.43/0.82 m	SCR or SCR + PC(S.?, poss erased) + PC(N)
(0.25)	26 ka	0.28/0.59/0.77 m	SCR or SCR + SC
(0.25)	55-70 ka	0.25/0.57/0.99 m	SCR + "ash event" or SCR + PC(S) or SCR
(0.25)	100-110 ka	0.26/0.67/0.87 m	SCR + PC(S) + PC(N) or SCR



Final Relative Weighting:

(0.5)	SCR
(0.092)	SCR + PC(S)
(0.167)	SCR + PC(S) + PC(N)
(0.075)	SCR + "ash event"
(0.125)	SCR + SC
(0.042)	SCR+PC+BR

SOLITARIO CANYON FAULT

Paleoseismic Information:

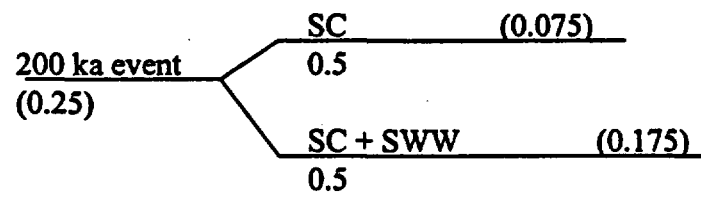
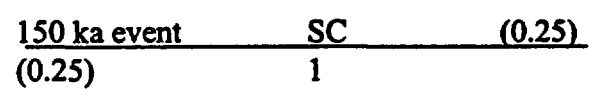
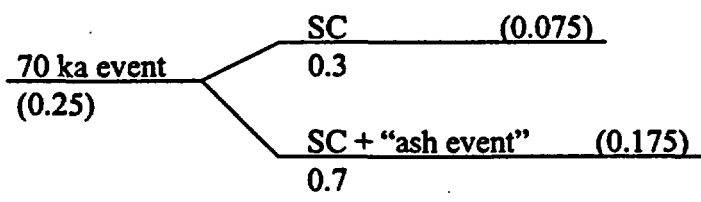
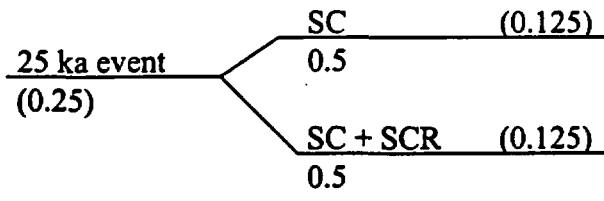
Four events have occurred over the last 150 to 250 ka (preferred 200 ka). The most recent event occurred at about 25 ka.

	Raw Average Earthquake Recurrence Intgervals	Corrected Average Earthquake Recurrence Interval Most Recent Event and Elapsed Time Removed
Min.	38 kyr	42 kyr
Pref.	50 kyr	58 kyr
Max.	63 kyr	75 kyr

Interseismic intervals of preferred values are 45, 50, and 80 kyr, with an average of 58 kyr.

	Moment Rate Recurrence	Average Earthquake Recurrence	Preferred Interseismic Recurrence	Average Earthquake Recurrence	Maximum Earthquake Occurrence Rate (EVENTS/YR)
Min.	23 kyr	42 kyr	45 kyr	37 kyr	2.7×10^{-5}
Pref.	40 kyr	58 kyr	58 kyr	52 kyr	1.92×10^{-5}
Max.	50 kyr	75 kyr	80 kyr	68 kyr	1.47×10^{-5}

Relative Frequency	Nominal Age of the event	Surface Displacement	Poss. Event Scenarios
(0.25)	25 ka	0.05/0.1/0.2 m	SC or SC + SCR
(0.25)	70 ka	1.00/1.20/1.40 m	SC + "ash event"
(0.25)	150 ka	0.2/0.3/0.4 m	SC
(0.25)	200 ka	0.3/0.5/0.7 m	SC + SWW or SC



Final Relative Weighting:

(0.575)	SC
(0.125)	SC+SCR
(0.175)	SC + "ash event"
(0.125)	SC + SWW

FATIGUE WASH FAULT

Paleoseismic Information:

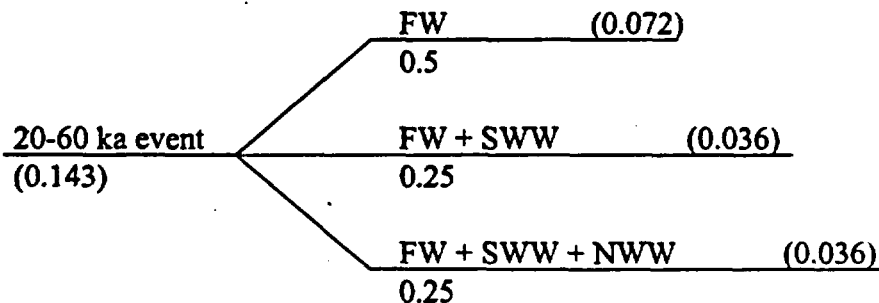
Three to four events (four preferred) have occurred within the last 450 to 730 ka (assume 600 ka for preferred value. The most recent event was 20 to 60 ka ago (the midpoint, 40 ka is used for preferred).

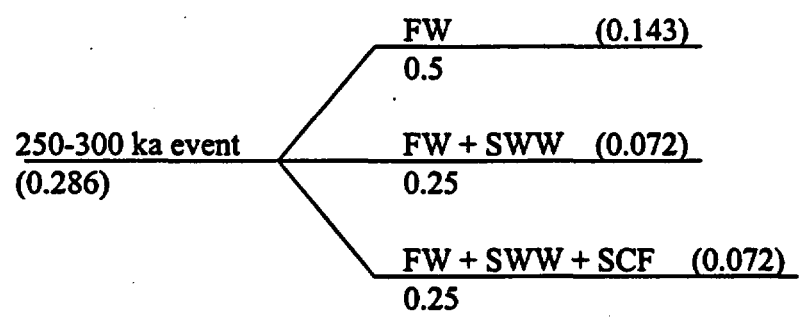
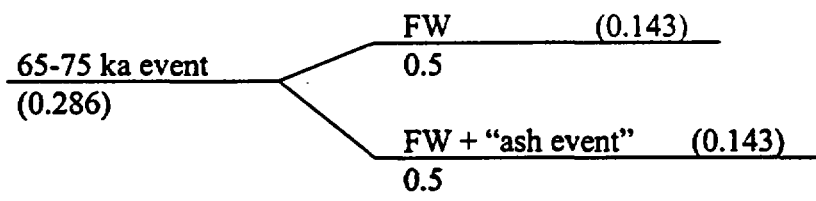
	Raw Average Earthquake Recurrence Intervals	Corrected Average Earthquake Recurrence Intervals Most Recent Event and Elapsed Time Removed
Min.	113 kyr	130 kyr
Pref.	150 kyr	187 kyr
Max.	243 kyr	237 kyr

Interseismic intervals of the preferred values range from 28 to 480 kyr, with an average of 183 kyr. A possible other minimum interseismic interval can be calculated from comparing the extremes of 65-60=5 kyr, but this is deemed wholly unreasonable given the trench information available along and geomorphic expression of the Fatigue Wash fault.

	Moment Rate Recurrence	Average Earthquake Recurrence	Preferred Interseismic Interval	Averaged Earthquake Recurrence	Maximum Earthquake Occurrence Rate (events/yr)
Min.	100 kyr	130 kyr	28 kyr	86 kyr	1.16×10^{-5}
Pref.	125 kyr	187 kyr	183 kyr	165 kyr	6.06×10^{-6}
Max.	150 kyr	237 kyr	480 kyr	289 kyr	3.46×10^{-6}

Relative Frequency	Nominal Age of the Event	Surface Displacement	Poss. Event Scenarios
(0.143)	20-60 ka	large fractures	FW + SWW + NWW or FW + SWW or FW
(0.286)	65-75 ka	0.15/0.25/0.35 m	FW + "ash event"
(0.286)	250-300 ka	/1.25/ m	FW + SWW + SCF or FW + SWW or FW
(0.286)	450-730 ka	/0.54/ m	FW





<u>450-730 ka event</u> (0.286)	FW	(0.286)
	1	

Final Relative Weighting:

- | | |
|---------|------------------|
| (0.643) | FW |
| (0.107) | FW + SWW |
| (0.036) | FW + SWW + NWW |
| (0.071) | FW + SWW + SCF |
| (0.143) | FW + "ash event" |

SOUTHERN WINDY WASH FAULT

Paleoseismic Information:

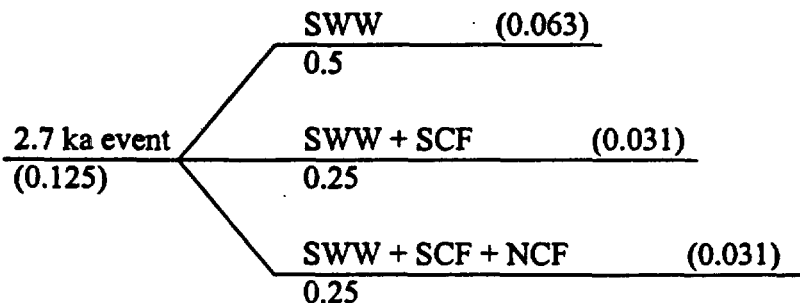
Eight events have occurred in the last 390 to 450 ka (preferred 400 ka). The most recent event occurred about 2.7 ka age.

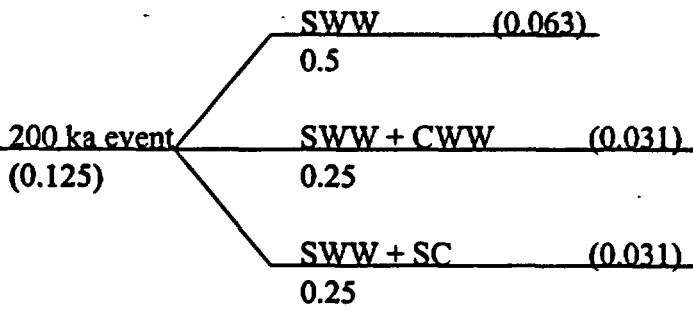
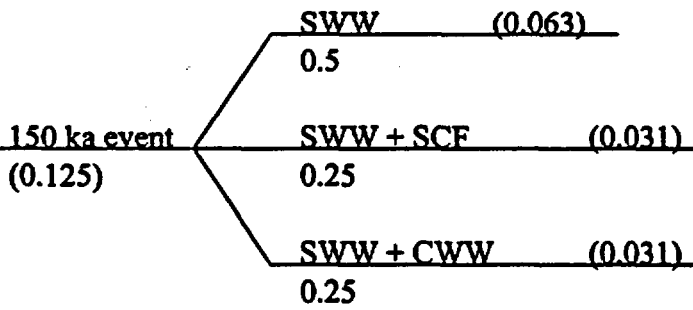
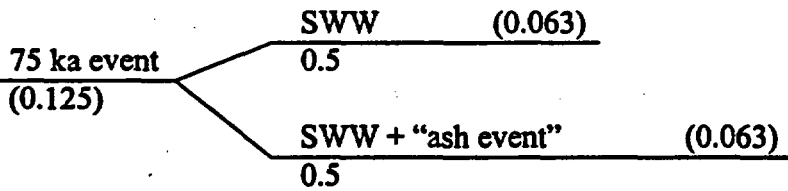
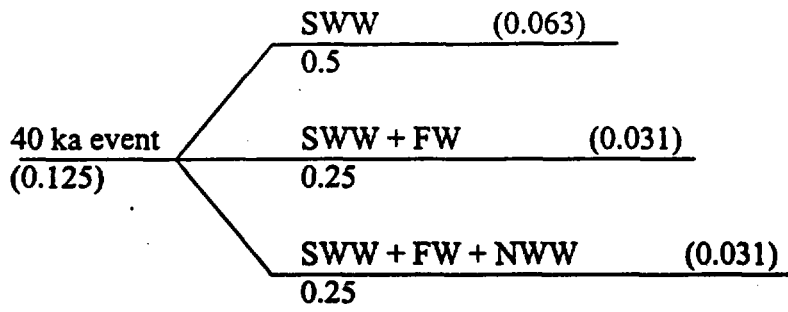
	Raw Average Earthquake Recurrence Intervals	Corrected Average Earthquake Recurrence Intervals Most Recent and Elapsed Time Removed
Min.	49 kyr	55 kyr
Pref.	50 kyr	57 kyr
Max.	56 kyr	64 kyr

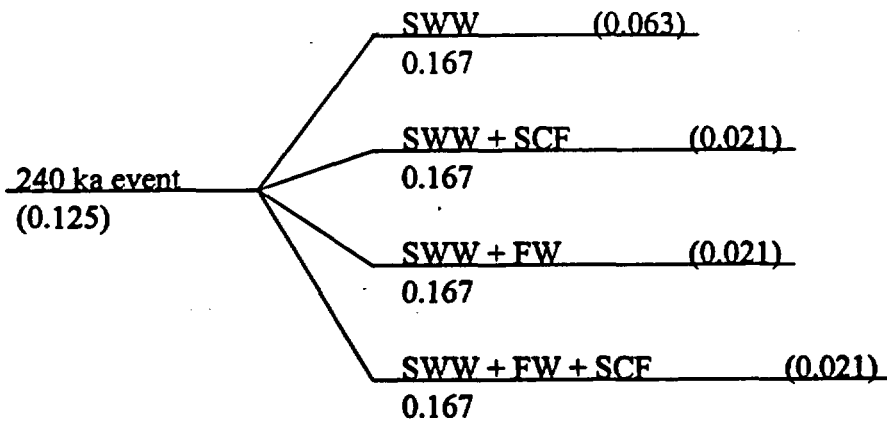
Interseismic intervals of the preferred values range from 30 kyr to 130 kyr, with an average of 62 kyr.

	Moment Rate Recurrence	Average Earthquake Recurrence	Preferred Interseismic Interval	Averaged Earthquake Recurrence	Maximum Earthquake Occurrence Rate (events/yr)
Min.	22 kyr	55 kyr	30 kyr	36 kyr	2.78×10^{-5}
Pref.	33 kyr	57 kyr	62 kyr	51 kyr	1.76×10^{-5}
Max.	37 kyr	64 kyr	130 kyr	77 kyr	1.3×10^{-5}

Relative Frequency	Nominal Age of the Event	Surface Displacement	Poss. Event Scenarios
(0.125)	2.7 ka	0.04/0.06/0.1 m	SWW + SCF + NCF or SWW + SCF or SWW
(0.125)	40 ka	0.14/0.20/0.45 m	SWW + FW + NWW or SWW + FW or SWW
(0.125)	75 ka	0.78/0.88/0.98 m	SWW + "ash event" or SWW
(0.125)	150 ka	0.38/0.42/0.52 m	SWW + CWW or SWW + SCF or SWW
(0.125)	200 ka	0.70/0.73/0.83 m	SWW + SC or SWW + CWW or SWW
(0.125)	240 ka	0.30/0.45/0.60 m	SWW + FW + SCF or SWW + FW or SWW + SCF or SWW
(0.125)	340-370 ka	0.55/0.60/0.78 m	SWW
(0.125)	400 ka	0.65/0.80?/1.00? m	SWW







340 ka event SWW (0.125)
 (0.125) 1

400 ka event SWW (0.125)
 (0.125) 1

Final Relative Weighting:

(0.625)	SWW
(0.083)	SWW + SCF
(0.052)	SWW + FW
(0.031)	SWW + SC
(0.063)	SWW + CWW
(0.031)	SWW + SCF + NCF
(0.031)	SWW + FW + NWW
(0.021)	SWW + FW + SCF
(0.063)	SWW + "ash event"

IRON RIDGE FAULT

Paleoseismic Information:

Three events have occurred along the Iron Ridge fault since 430 to 730 kyr (600 kyr pref.). The most recent event was at 5 to 10 ka and was small in offset (<0.1 m) with some question to its existence. Because of the lack of information, this event is assumed to occur for estimating corrected average earthquake recurrence intervals.

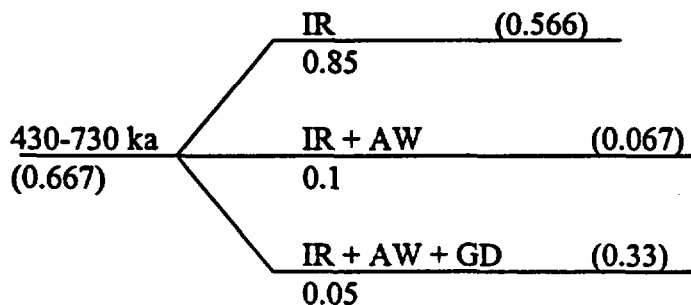
	Raw Average Earthquake Recurrence Intervals	Corrected Average Earthquake Recurrence Intervals Most Recent Event and Elapsed Time Removed
Min.	143 kyr	210 kyr
Pref.	200 kyr	295 kyr
Max.	243 kyr	360 kyr

Interseismic intervals are poorly constrained along the Iron Ridge fault.

	Moment Rate Recurrence	Average Earthquake Recurrence	Preferred Interseismic Interval	Averaged Earthquake Recurrence	Maximum Earthquake Occurrence Rate (events/yr)
Min.	76 kyr	210 kyr	none	143 kyr	6.99×10^{-6}
Pref.	106 kyr	295 kyr	none	201 kyr	4.98×10^{-6}
Max.	152 kyr	360 kyr	none	256 kyr	3.91×10^{-6}

Relative Frequency	Nominal Age of the Event	Surface Displacement	Poss. Event Scenarios
(0.333)	5-10 ka	0/0.05/0.1 m	IR
(0.333)	430-730 ka	0.5/0.7/1.0 m	IR or IR + AW or IR + AW + GD
(0.333)	430-730 ka	0.5/0.7/1.0 m	IR or IR + AW or IR + AW + GD

5-10 ka	IR	(0.333)
(0.333)	1	



Final Relative Weighting:

(0.900)	IR
(0.067)	IR + AW
(0.033)	IR + AW + GD